ПРИЛОЖЕНИЕ 1

к научному докладу на соискание ученой степени

доктора химических наук

КРЫЛОВ ВАДИМ БОРИСОВИЧ

По теме:

ГАЛАКТОФУРАНОЗИЛСОДЕРЖАЩИЕ ОЛИГОСАХАРИДЫ: СИНТЕЗ И ПРИЛОЖЕНИЕ В ИММУНОХИМИЧЕСКИХ ИССЛЕДОВАНИЯХ ГРИБКОВЫХ И БАКТЕРИАЛЬНЫХ ПАТОГЕНОВ

1.4.9. – Биоорганическая химия

Москва – 2022

Оглавление

9. Gerbst, A.G. Application of computational methods for the studies of carbohydrate reactivity / A.G. Gerbst, **V.B. Krylov**, N.E. Nifantiev // Carbohydrate Chemistry: Chemical and Biological Approaches. The Royal Society of Chemistry. – 2021. – V. 44. – P. 151–169. http://doi.org/10.1039/9781788013864-00151. **С. 68**
10. **Krylov, V.B.** Preparative synthesis of selectively substituted 1, 6-anhydro-α-D-galactofuranose derivatives/ **V.B. Krylov**, D.A. Argunov, N.E. Nifantiev // Mendeleev Communications. – 2014. – V. 6. – P. 336–337. http://doi.org/10.1016/j.mencom.2014.11.006. **С. 87**
11. Argunov, D.A. Convergent synthesis of isomeric heterosaccharides related to the fragments of galactomannan from Aspergillus fumigatus / D.A. Argunov, **V.B. Krylov**, N.E. Nifantiev // Organic & Biomolecular Chemistry. – 2015. – V. 13. – P. 3255–3267. http://doi.org/10.1039/C4OB02634A. – **Q1 (2015)***. **С. 89**
12. Argunov, D.A. The Use of Pyranoside-into-Furanoside Rearrangement and Controlled O(5)→O(6) Benzoyl Migration as the Basis of a Synthetic Strategy To Assemble (1→5)- and (1→6)-Linked Galactofuranosyl Chains / D.A. Argunov, **V.B. Krylov**, N.E. Nifantiev // Organic Letters. – 2016. – V. 18. – P. 5504–5507. http://doi.org/10.1021/acs.orglett.6b02735. **Q1 (2016)***. **С. 102**
13. **Krylov, V.B.** Synthesis of oligosaccharides related to galactomannans from Aspergillus fumigatus and their NMR spectral data / **V.B. Krylov**, D.A. Argunov, A.S. Solovev, M.I. Petruk, A.G. Gerbst, A.S. Dmitrenok, A.S. Shashkov, J.-P. Latgé, N.E. Nifantiev // Organic & Biomolecular Chemistry. – 2018. – V. 16. – P. 1188–1199. http://doi.org/10.1039/C7OB02734F. – **Q1 (2018)***. **С. 106**
14. Argunov, D.A. Convergent synthesis of oligosaccharides structurally related to galactan I and galactan II of Klebsiella pneumoniae and their use in screening of antibody specificity / D. A. Argunov, A. S. Trostianetskaia, **V. B. Krylov**, E. A. Kurbatova, N. E. Nifantiev // European Journal of Organic Chemistry. – 2019. – V. 2019. – P. 4226–4232. http://doi.org/10.1002/ejoc.201900389 – **Q2 (2019)***. **С. 118**
15. Verkhnyatskaya, S.A. Pyranoside-into-furanoside rearrangement of 4-pentenyl glycosides in the synthesis of a tetrasaccharide-related to galactan I of Klebsiella pneumoniae / S.A. Verkhnyatskaya, **V.B. Krylov**, N.E. Nifantiev // European Journal of Organic Chemistry. – 2017. – V. 2017. – P. 710–718. http://doi.org/10.1002/ejoc.201601413. – **Q2 (2017)***. **С. 125**
16. **Krylov, V.B.** Definitive structural assessment of enterococcal diheteroglycan / **V. B. Krylov**, A. G. Gerbst, D. A. Argunov, A. S. Dmitrenok, A. S. Shashkov, Z. Kaczynski, J.

Huebner, O. Holst, N. E. Nifantiev // Chemistry – A European Journal. – 2015. – V. 21. – P. 1749–1754. http://doi.org/10.1002/chem.201405857. – **Q1 (2015)***. **С. 134**

17. Laverde, D. Synthetic oligomers mimicking capsular polysaccharide diheteroglycan are potential vaccine candidates against encapsulated enterococcal infections / D. Laverde, F. Romero-Saavedra, D. A. Argunov, J. Enotarpi, **V. B. Krylov**, E. Kalfopoulou, C. Martini, R. Torelli, G. A. van der Marel, M. Sanguinetti, J. D. C. Codée, N. E. Nifantiev, J. Huebner // ACS Infectious Diseases. – 2020. – V. 6. – P. 1816–1826. http://doi.org/10.1021/acsinfecdis.0c00063. – **Q1 (2020)***. **С. 140**
18. Dorokhova, V.S. Synthesis and conformational analysis of vicinally branched trisaccharide β-d-Galf-(1→2)-[β-d-Galf-(1→3)-]-α-Galp from *Cryptococcus neoformans* galactoxylomannan / V. S. Dorokhova, A. G. Gerbst, B. S. Komarova, J. O. Previato, L. M. Previato, A. S. Dmitrenok, A. S. Shashkov, **V. B. Krylov**, N. E. Nifantiev // Organic & Biomolecular Chemistry. – 2021. – V. 19. – P. 2923–2931. http://doi.org/10.1039/D0OB02071K. – **Q1 (2021)***. **С. 151**
19. Vinnitskiy, D.Z. The synthesis of heterosaccharides related to the fucoidan from *Chordaria flagelliformis* bearing an α-L-fucofuranosyl unit / D. Z. Vinnitskiy, **V. B. Krylov**, N. E. Ustyuzhanina, A. S. Dmitrenok and N. E. Nifantiev // Organic & Biomolecular Chemistry. – 2016. – V. 14. – P. 598–611. http://doi.org/10.1039/C5OB02040A. – **Q1 (2016)***. **С. 160**
20. Gerbst, A.G. ^{13}C-NMR glycosylation effects in (1→3)-linked furanosyl-pyranosides / A. G. Gerbst, **V. B. Krylov**, D. Z. Vinnitskiy, A. S. Dmitrenok, A. S. Shashkov, N. E. Nifantiev // Carbohydrate Research. – 2015. – V. 417. – P. 1–10. http://doi.org/10.1016/j.carres.2015.08.014. **С. 174**
21. Gerbst, A.G. Ring distortion in pyranosides caused by per-O-sulfation / A. G. Gerbst, **V. B. Krylov**, D. A. Argunov, A. S. Solovev, A. S. Dmitrenok, A. S. Shashkov, N. E. Nifantiev // Carbohydrate Research. – 2016. – V. 436. – P. 20–24. http://doi.org/10.1016/j.carres.2016.10.011. **С. 184**
22. Gerbst, A.G. Conformational changes in common monosaccharides caused by per-O-sulfation / A.G. Gerbst, **V.B. Krylov**, N.E. Nifantiev // Pure and Applied Chemistry. – 2019. – V. 91. – P. 1223–1229. http://doi.org/10.1515/pac-2018-1212. – **Q2 (2019)*** **С. 189**
23. Gerbst, A.G. Influence of per-O-sulfation upon the conformation behaviour of common furanosides / A. G. Gerbst, **V. B. Krylov**, D. A. Argunov, M. I. Petruk, A. S. Solovev, A. S. Dmitrenok, N. E. Nifantiev // Beilstein Journal of Organic Chemistry. – 2019. – V. 15. – P. 685–694. – http://doi.org/10.3762/bjoc.15.63. – **Q2 (2019)***. **С. 196**

24. Gerbst, A.G. Computational and NMR conformational analysis of galactofuranoside cycles presented in bacterial and fungal polysaccharide antigens / A.G. Gerbst, **V.B. Krylov**, N.E. Nifantiev // Frontiers in Molecular Biosciences. – 2021. – V. 8. – 719396. http://doi.org/10.3389/fmolb.2021.719396. – **Q1 (2021)***. **C. 206**
25. Zhang, R. et al. Lysozyme's lectin-like characteristics facilitates its immune defense function / R. Zhang, L. Wu, T. Eckert, M. Burg-Roderfeld, M. A. Rojas-Macias, T. Lütteke, **V. B. Krylov**, D. A. Argunov, A. Datta, P. Markart, N. E. Nifantiev // Quarterly Reviews of Biophysics. – 2017. – V. 50. – P. e9. http://doi.org/10.1017/S0033583517000075. – **Q1 (2017)***. **C. 215**
26. Zhang R. Nanomedical relevance of the intermolecular interaction dynamics-examples from lysozymes and insulins / R. Zhang, N. Zhang, M. Mohri, L. Wu, T. Eckert, **V. B. Krylov**, A. Antosova, S. Ponikova, Z. Bednarikova, P. Markart, A. Günther, B. Norden, M. Billeter, R. Schauer, A. J. Scheidig, B. N. Ratha, A. Bhunia, K. Hesse, M. A. Enani, J. Steinmeyer, A. K. Petridis, T. Kozar, Z. Gazova, N. E. Nifantiev, H.-C. Siebert// ACS Omega. – 2019. – V. 4 – P. 4206–4220. http://doi.org/10.1021/acsomega.8b02471. **Q1 (2019)***. **C. 227**
27. **Krylov, V.B.** Recent advances in the synthesis of fungal antigenic oligosaccharides / **V. B. Krylov**, L. Paulovičová, E. Paulovičová, Y. E. Tsvetkov, N. E. Nifantiev // Pure and Applied Chemistry. – 2017. – V. 89. – P. 885–898. http://doi.org/10.1515/pac-2016-1011. **Q2 (2017)***. **C. 242**
28. **Krylov, V.B.** Synthetic oligosaccharides mimicking fungal cell wall polysaccharides / **V.B. Krylov**, N.E. Nifantiev // Current Topics in Microbiology and Immunology. – 2020. – V. 425. – P. 1–16. http://doi.org/10.1007/82_2019_187. **C. 256**
29. **Krylov, V.B.** Synthetic carbohydrate based anti-fungal vaccines / **V.B. Krylov**, N.E. Nifantiev // Drug Discovery Today: Technologies. – 2020. – V. 35-36. – P. 35–43. https://doi.org/10.1016/j.ddtec.2020.11.002. **Q1 (2020)***. **C. 272**
30. Wong S.S.W. Potential of chemically synthesized oligosaccharides to define the carbohydrate moieties of the fungal cell wall responsible for the human immune response, using aspergillus fumigatus galactomannan as a model / S. S. W. Wong, **V. B. Krylov**, D. A. Argunov, A. A. Karelin, J.-P. Bouchara, T. Fontaine, J.-P. Latgé, N. E. Nifantiev // mSphere. – 2020. – V. 5. – P. e5:e00688-19. http://doi.org/10.1128/mSphere.00688-19. **Q1 (2020)***. **C. 281**
31. Paulovičová, E. Immunobiological activity of synthetically prepared immunodominant galactomannosides structurally mimicking aspergillus galactomannan / E. Paulovičová, L. Paulovičová, M. Hrubiško, **V. B. Krylov**, D. A. Argunov and N. E. Nifantiev // Frontiers

in Immunology. – 2017. – V. 8. – P. 1273. http://doi.org/10.3389/fimmu.2017.01273. – **Q1 (2017)***. **С. 288**

32. Kazakova, E.D. Biotinylated oligo-α-(1→ 4)-D-galactosamines and their N-acetylated derivatives: α-stereoselective synthesis and immunology application / E. D. Kazakova, D. V. Yashunsky, **V. B. Krylov**, J.-P. Bouchara, M. Cornet, I. Valsecchi, T. Fontaine, J.-P. Latge and N. E. Nifantiev // Journal of the American Chemical Society. – 2020. – V. 142. – P. 1175–1179. http://doi.org/10.1021/jacs.9b11703. **Q1 (2020)***. **С. 302**
33. Komarova, B.S. Chemical synthesis and application of biotinylated oligo-α-(1→3)-D-glucosides to study the antibody and cytokine response against the cell wall α-(1→3)-D-glucan of Aspergillus fumigatus / B. S. Komarova, S. S. W. Wong, M. V. Orekhova, Y. E. Tsvetkov, **V. B. Krylov**, A. Beauvais, J.-P. Bouchara, J. F. Kearney, V. Aimanianda, J.-P. Latgé, N. E. Nifantiev // Journal of Organic Chemistry. – 2018. – V. 83. – P. 12965–12976. http://doi.org/10.1021/acs.joc.8b01142. **Q1 (2018)***. **С. 307**
34. Paulovičová, E. Importance of candida antigenic factors: structure-driven immunomodulation properties of synthetically prepared mannooligosaccharides in RAW264.7 macrophages / E. Paulovičová, L. Paulovičová, P. Farkaš, A. A. Karelin, Y. E. Tsvetkov, **V. B. Krylov**, N. E. Nifantiev // Frontiers in Cellular and Infection Microbiology. – 2019. – V. 9. – P. 378. http://doi.org/10.3389/fcimb.2019.00378. – **Q1 (2019)***. **С. 319**
35. **Krylov, V.B.** Reinvestigation of carbohydrate specificity of EB-A2 monoclonal antibody used in the immune detection of Aspergillus fumigatus galactomannan / **V. B. Krylov**, A. S. Solovev, D. A. Argunov, J.-P. Latgé and N. E. Nifantiev // Heliyon. – 2019. – V. 5. – P. e01173. http://doi.org/10.1016/j.heliyon.2019.e01173. **Q1 (2019)***. **С. 333**
36. **Крылов, В.Б.** Углеводная специфичность антител против *Aspergillus fumigatus*. Исследование с использованием библиотеки синтетических микоантигенов / **В.Б. Крылов,** М.И. Петрук, И.В. Григорьев, Ю.С. Лебедин, Н.И. Глушко, Е.В. Халдеева, Д.А. Аргунов, Е.А. Хатунцева, М.В. Топлишек, Б.С. Комарова, А.А. Карелин, О.Н. Юдина, В.М. Меньшов, Д.В. Яшунский, Ю.Е. Цветков, Н.Э. Нифантьев // Биоорганическая химия. – 2018. – Т. 44. – С. 78-86. http://doi.org/10.7868/S0132342318010086. **С. 342**
37. **Крылов, В.Б.** Исследование углеводной специфичности антител против препаратов условно патогенных грибов рода Aspergillus / В.Б. Крылов, М.И. Петрук, Н.И. Глушко, Е.В. Халдеева, В.Л. Мокеева, Е.Н. Биланенко, Ю.С. Лебедин, С.А. Ерёмин, Н.Э. Нифантьев // Прикладная биохимия и микробиология. – 2018. – Т. 54. – С. 525-531. http://doi.org/10.1134/S0555109918050094. **С. 351**

38. **Крылов, В.Б.** Углеводная специфичность антител против препаратов дрожжевых грибов Saccharomyces cerevisiae и Candida krusei / В.Б. Крылов, М.И. Петрук, А.А. Карелин, Д.В. Яшунский, Ю.Е. Цветков, Н.И. Глушко, Е.В. Халдеева, В.Л. Мокеева, Е.Н. Биланенко, Ю.С. Лебедин, С.А. Ерёмин, Н.Э. Нифантьев // Прикладная биохимия и микробиология. – 2018. – Т. 54. С. – 614-618**.** http://doi.org/10.1134/S0555109918060107. **С. 358**

39. **Krylov, V.B.** Reinvestigation of carbohydrate specificity of EBCA-1 monoclonal antibody used for the detection of candida mannan / **V. B. Krylov**, A. S. Solovev, I. A. Puchkin, D. V. Yashunsky, A. V. Antonets, O. Y. Kutsevalova, N. E. Nifantiev // Journal of Fungi – 2021. V. 7 – P. 504. http://doi.org/10.3390/jof7070504 – **Q1 (2021)**. **С. 365**

40. Matveev, A.L. Novel mouse monoclonal antibodies specifically recognize Aspergillus fumigatus galactomannan / A. L. Matveev, **V. B. Krylov**, L. A. Emelyanova, A. S. Solovev, Y. A. Khlusevich, I. K. Baykov, T. Fontaine, J.-P. Latgé, N. V. Tikunova, N. E. Nifantiev // PloS One. – 2018. – V. 13. – P. e0193938. http://doi.org/10.1371/journal.pone.0193938. – **Q1 (2019)***. **С. 373**

41. Schubert, M. Monoclonal antibody AP3 binds galactomannan antigens displayed by the pathogens Aspergillus flavus, A. fumigatus and A. parasiticus / M. Schubert, S. Xue, F. Ebel, A. Vaggelas, **V. Krylov**, N. Nifantiev, I. Chudobova, S. Schillberg and G. Nölke // Frontiers in Cellular and Infection Microbiology. – 2019. – V. 9. – P. 234. http://doi.org/10.3389/fcimb.2019.00234. **Q1 (2019)***. **С. 388**

42. Matveev, A.L. Novel mouse monoclonal antibodies specifically recognizing β-(1→3)-D-glucan antigen / A. L. Matveev, **V. B. Krylov**, Y. A. Khlusevich, I. K. Baykov, D. V. Yashunsky, L. A. Emelyanova, Y. E. Tsvetkov, A. A. Karelin, A. V. Bardashova, S. S. W. Wong, V. Aimanianda, J.-P. Latgé, N. V. Tikunova and N. E. Nifantiev // PloS One. – 2019. – V. 14. P. e0215535. http://doi.org/10.1371/journal.pone.0215535. **Q1 (2019)***. **С. 403**

43. **Крылов, В.Б.** Возможности поляризационного флуоресцентного иммуноанализа для определения галактоманнана Aspergillus fumigatus / **В.Б. Крылов**, М.И. Петрук, М.Р. Каримова, Л.И. Мухаметова, А.Л. Матвеев, Н.В. Тикунова, С.А. Еремин, Н.Э. Нифантьев/ Известия Академии наук. Серия химическая. – 2019 – С. 2365-2369. http://doi.org/10.1007/s11172-019-2713-y. **С. 422**

44. Alenichev, M.K. Nano-biosensor based on the combined use of the dynamic and static light scattering for Aspergillus galactomannan analysis / M. K. Alenichev, A. D. Levin, A. A. Yushina, E. S. Kostrikina, Y. S. Lebedin, I. P. Andreeva, V. G. Grigorenko, **V. B.**

Krylov, N. E. Nifantiev // Sensing and Bio-Sensing Research – 2022. – V. 35. – P. 100475. http://doi.org/10.1016/j.sbsr.2022.100475 – **Q2 (2022)*.** **C. 427**

45. Poimanova, E.Y. Biorecognition layer based on biotin-containing [1] benzothieno [3, 2-b][1] benzothiophene derivative for biosensing by electrolyte-gated organic field-effect transistors / E. Y. Poimanova, P. A. Shaposhnik, D. S. Anisimov, E. G. Zavyalova, A. A. Trul, M. S. Skorotetcky, O. V. Borshchev, D. Z. Vinnitskiy, M. S. Polinskaya, **V. B. Krylov**, N. E. Nifantiev, S.A. Ponomarenko // ACS applied materials & interfaces – 2022. – V. 14. – P. 16462–16476. https://doi.org/10.1021/acsami.1c24109. – **Q1 (2022)***.

C. 437

* 33 публикаций в журналах первого и второго квартилей (Q1, Q2) за последние 10 лет

Mar. Drugs **2013**, *11*, 2444-2458; doi:10.3390/md11072444

OPEN ACCESS

marine drugs

ISSN 1660-3397

www.mdpi.com/journal/marinedrugs

Article

Influence of Fucoidans on Hemostatic System

Nadezhda E. Ustyuzhanina [1], Natalia A. Ushakova [2], Ksenia A. Zyuzina [3], Maria I. Bilan [1], Anna L. Elizarova [4], Oksana V. Somonova [4], Albina V. Madzhuga [4], Vadim B. Krylov [1], Marina E. Preobrazhenskaya [2], Anatolii I. Usov [1], Mikhail V. Kiselevskiy [4] and Nikolay E. Nifantiev [1,*]

[1] N.D. Zelinsky Institute of Organic Chemistry, Russian Academy of Sciences, Leninsky prospect 47, 119991 Moscow, Russian Federation; E-Mails: ustnad@gmail.com (N.E.U.); bilan@ioc.ac.ru (M.I.B.); vadimkrilov@yandex.ru (V.B.K.); usov@ioc.ac.ru (A.I.U.)

[2] V.N. Orekhovich Institute of Biomedical Chemistry, Russian Academy of Medical Sciences, Pogodinskaya str. 10, 119121 Moscow, Russian Federation; E-Mails: natalia.ushakova@ibmc.msk.ru (N.A.U.); marina.preobrajenskaya@ibmc.msk.ru (M.E.P.)

[3] Department of Physics, M.V. Lomonosov Moscow State University, Leninskie gory, 119991 Moscow, Russian Federation; E-Mail: kseniazyuzina@ya.ru

[4] N.N. Blokhin Russian Cancer Research Center, Russian Academy of Medical Sciences, Kashirskoe shosse, 24, 115478 Moscow, Russian Federation; E-Mails: anna_el@rambler.ru (A.L.E.); somonova@mail.ru (O.V.S.); takustya@mail.ru (A.V.M.); kisele@inbox.ru (M.V.K.)

* Author to whom correspondence should be addressed; E-Mail: nen@ioc.ac.ru; Tel./Fax: +7-499-137-8784.

Received: 22 April 2013; in revised form: 20 May 2013 / Accepted: 25 June 2013 / Published: 12 July 2013

Abstract: Three structurally different fucoidans from the brown seaweeds *Saccharina latissima* (SL), *Fucus vesiculosus* (FV), and *Cladosiphon okamuranus* (CO), two chemically modified fucoidans with a higher degree of sulfation (SL-S, CO-S), and a synthetic totally sulfated octasaccharide (OS), related to fucoidans, were assessed on anticoagulant and antithrombotic activities in different *in vitro* experiments. The effects were shown to depend on the structural features of the compounds tested. Native fucoidan SL with a degree of sulfation (DS) of 1.3 was found to be the most active sample, fucoidan FV (DS 0.9) demonstrated moderate activity, while the polysaccharide CO (DS 0.4) was inactive in all performed experiments, even at high concentrations. Additional introduction of sulfate groups into fucoidan SL slightly decreased the anticoagulant effect of SL-S,

while sulfation of CO, giving rise to the preparation CO-S, increased the activity dramatically. The high level of anticoagulant activity of polysaccharides SL, SL-S, and CO-S was explained by their ability to form ternary complexes with ATIII-Xa and ATIII-IIa, as well as to bind directly to thrombin. Synthetic per-*O*-sulfated octasaccharide OS showed moderate anticoagulant effect, determined mainly by the interaction of OS with the factor Xa in the presence of ATIII. Comparable tendencies were observed in the antithrombotic properties of the compounds tested.

Keywords: fucoidan; anticoagulant; hemostasis; heparin; thrombin; antithrombin; factor Xa

1. Introduction

Thromboembolic disorders, such as venous thromboembolism and arterial thrombosis, are considered to be among the main reasons for cardiovascular diseases. The situation leads to increased utilization of anticoagulant and antithrombotic agents in medical practice. Heparin and its derivatives are usually recommended as support therapy [1,2], but side effects of these medicines, like hemorrhage and heparin-induced thrombocytopenia, force the search for anticoagulants of another nature.

Natural sulfated polysaccharides, such as galactans [3–7], arabinans [8], fucans [3–5,9], and fucoidans [3,6,10–13], present in seaweeds and invertebrates, are regarded as perspective inhibitors of blood coagulation and thrombosis. Influence of these biopolymers on the hemostatic system is determined by the ability of polymeric sulfates to interact with positively charged groups in proteins responsible for hemostasis, leading to the formation of stabilized complexes. The anticoagulant properties of sulfated polysaccharides are mainly connected with thrombin inhibition mediated by antithrombin III (ATIII) and/or heparin cofactor II (HCII), with different efficiencies depending on the structural features of carbohydrates. Other mechanisms, such as direct inhibition of thrombin, are also possible. Thrombin also plays an important role in thrombosis as an inducer of platelet aggregation, and this event may also be controlled by sulfated polysaccharides.

A number of studies revealed certain structure-activity relationships for these macromolecules [3,6,8,11,12,14–16]. The main structural features of sulfated polysaccharides, which should be taken into account regarding their anticoagulant and antithrombotic properties, include the monosaccharide composition, the degree and pattern of sulfation, molecular weight, and types of glycosidic bonds. The level of sulfation more than 1.0 was shown to be important for high anticoagulant activity of fucans and galactans [17,18]. High molecular weight fucans demonstrated a greater anticoagulant effect than structurally similar polysaccharides having lower molecular weight [17,19].

The pattern of *O*-sulfation together with the structure of the backbone and branches, but not only total negative charge of sulfates, has a substantial impact on the activity of the biopolymers under discussion (see for example [12]). Thus, in a series of polysaccharides from invertebrates it has been shown that 2-*O*-sulfated (1→3)-linked α-L-galactan, but not an α-L-fucan, with a similar sulfation pattern and molecular size, is a potent thrombin inhibitor mediated by ATIII or HCII [4]. In the case of HCII-mediated inhibition, the major structural requirement for the activity is the presence of selectively 4-*O*-sulfated fucose units [4]. In addition, the linear (1→3)-linked α-L-fucans, enriched in

2,4-di-*O*-sulfated units, were shown to have an amplifying effect on the ATIII-mediated anticoagulant activity [4,9].

Fucoidans from brown algae possess a significantly more complicated structure than fucans from invertebrates due to the presence of numerous branches, non-fucose monosaccharide constituents, and acetates [13]. It was found that, besides ATIII- and HCII-mediated thrombin inhibition activities, which are typical of fucans, the algal fucoidans could also be direct inhibitors of thrombin. For the first time, this behavior was shown for fucoidans from *Fucus vesiculosus* and *Laminaria brasiliensis*, which are built up of alternating (1→3)- and (1→4)-linked α-L-fucose residues sulfated at C-2 and/or C-4, and bearing fucose branches [14]. The similar mechanism of action was shown for fucoidans from the brown seaweeds *Saccharina latissima* (previous name *Laminaria saccharina*) and *Fucus distichus*, but polysaccharides from *Cladosiphon okamuranus* and *Analipus japonicus* were inactive [15]. Notably, a linear arabinan consisting of (1→3)-linked β-L-arabinose residues sulfated at C-2 and/or C-4 was also found to be the potent direct thrombin inhibitor [8].

In this paper we report the results of the study on anticoagulant and antithrombotic activities of three fucoidans from brown seaweeds differed in the monosaccharide composition, types of glycosidic bonds, sulfate content, and sulfation pattern. Chemically *O*-sulfated fucoidan derivatives and structurally related synthetic octasaccharide were studied as well.

2. Results and Discussion

2.1. Sulfated Carbohydrate Samples

Three samples of native fucoidans were used in this study (see Experimental Section). Their monosaccharide composition and sulfate content are summarized in Table 1. The dominant component of fucoidan SL from *S. latissima* (fraction "F-1.25" in [20]), which demonstrated high anti-inflammatory activity [16], contains poly-(1→3)-α-L-fucopyranosyl backbone sulfated at C-2 and/or at C-4, where approximately each fifth residue bears at C-2 a single sulfated α-L-fucopyranose residue as a branch [20] (Figure 1). The main structural feature of fucoidan FV from *F. vesiculosus* [21] is the backbone consisting of alternating (1→3)- and (1→4)-linked α-L-fucose units, which are sulfated at C-2 and/or C-4. The backbone bears some single α-L-fucose branches, but the degree of branching is lower than that of SL (Figure 1). Fucoidan CO from *C. okamuranus* contains a poly-(1→3)-α-L-fucopyranosyl backbone, sulfated at C-4 and branched at C-2. Its degree of branching is comparable with that of SL, but this fucoidan contains single α-D-glucuronic acid residues as branches instead of fucose residues [22]. It should be noted that fucoidan CO has a relatively low degree of sulfation as compared to the preparations SL and FV (Table 1).

To assess the influence of the degree of sulfation on anticoagulant and antithrombotic activities, chemically *O*-sulfated derivatives of fucoidans SL and CO, namely, samples SL-S and CO-S (Figure 1) were prepared by the reported method [23] (see Experimental Section) and used in this study. According to their enhanced degree of sulfation (Table 1), preparations SL-S and CO-S contain a great number of 2,4-di-*O*-sulfated units. Detailed structural investigation of macromolecules SL-S and CO-S will be published elsewhere.

Figure 1. The main structural features of studied samples.

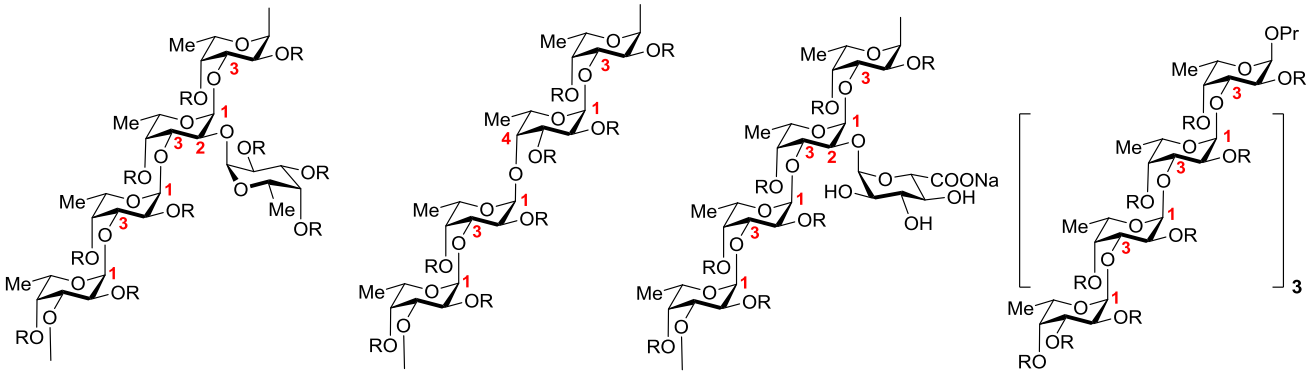

Table 1. Composition * of the samples tested.

Sample	Source	Fuc	Xyl	Man	Gal	Uronic acids	SO_3Na	Degree of Sulfation **
SL	*S. latissima*	36.7	1.8	0.7	8.4	1.9	39.8	1.3
FV	*F. vesiculosus*	28.5	5.6	2.8	2.9	7.9	26.0	0.9
CO	*C. okamuranus*	42.7	2.0	1.1	1.9	15.1	16.9	0.4
SL-S	Sulfation of SL	26.9	-	1.3	7.1	1.0	46.7	2.0
CO-S	Sulfation of CO	19.7	0.8	0.9	0.7	8.1	45.7	2.4
OS	Synthetic compound	39.4	-	-	-	-	59.1	2.1

* Content (w/w %) of monosaccharides and sulfate (the presence of acetate is not shown); ** Molar ratio SO_3Na: (Fuc + Gal + UA + Xyl).

In addition to the polymeric samples, synthetic per-*O*-sulfated linear *n*-propyl octa-(1→3)-α-L-fucoside OS (Figure 1) [24], which may be regarded as a linear backbone fragment of polysaccharides SL-S and CO-S, was used as a model to investigate the influence of the molecular weight on the biological activity of fucoidans.

2.2. Clotting Assays

General clotting assays were performed with the use of normal plasma, which was incubated with the samples. Commercially available, low-molecular-weight heparin Clexane® (enoxaparin) was chosen as a reference, as this polysaccharide is intensively used in medical practice as a heparinoid anticoagulant with low risk of side effects [2,25,26]. The profiles of anticoagulant activity of the samples and Clexane® were compared.

To evaluate the influence of the fucoidans and their derivatives on the intrinsic pathway of coagulation, the activated partial thromboplastin time (APTT) assays have been performed. The dose-depended changes in the APTT value are shown on Figure 2, and the values of 2APTT (the concentration of a sample, at which double increasing of control value of APTT was observed) are presented in Table 2.

The effect on blood coagulation was shown to depend on the structural features of the tested sample. Among parent fucoidans, the polysaccharide SL demonstrated the highest level of activity,

even exceeding that of Clexane®. Double increasing of control value of APTT was achieved at a concentration of ~1.1 μg/mL for SL and ~3.3 μg/mL for Clexane®. Fucoidan FV showed moderate activity (2APTT ~6.8 μg/mL), while polysaccharide CO was inactive even at a concentration of 100 μg/mL.

Figure 2. Anticoagulant activity measured by APTT assay.

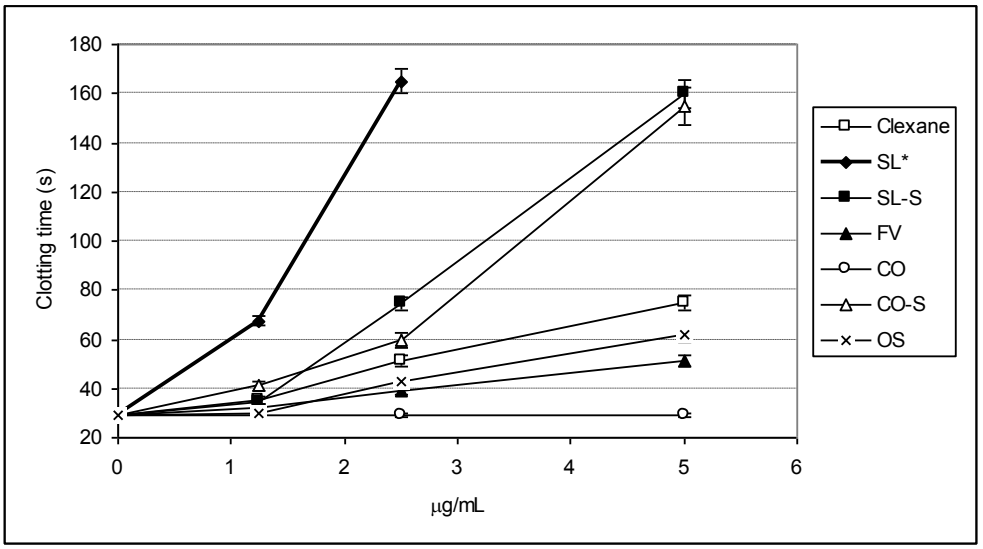

* Data for SL at a concentration of 5 μg/mL are omitted, as the APTT value significantly exceeded the upper limit of determination.

Table 2. 2APTT and 2TT values for studied compounds.

Sample	2APTT (μg/mL)	2TT (μg/mL)
Clexane®	3.32 ± 0.12	2.25 ± 0.03
SL	1.07 ± 0.05	2.43 ± 0.05
SL-S	2.01 ± 0.07	2.20 ± 0.07
FV	6.81 ± 0.03	9.15 ± 0.11
CO	>100	>100
CO-S	2.51 ± 0.09	4.28 ± 0.07
OS	5.10 ± 0.12	16.08 ± 0.23

The degree of sulfation of the polysaccharides was found, in most cases, to influence the activity to a major extent. Per-*O*-sulfation of inactive fucoidan CO gave product CO-S (degree of sulfation 2.4, Table 1) with pronounced anticoagulant properties. This sample prolonged blood coagulation by two times at a concentration of ~2.5 μg/mL. Thus, one of the possible explanations of the low activity of the fucoidan CO can be assigned to the absence of a sufficient amount of sulfate groups in its structure (degree of sulfation 0.4, Table 1).

Interestingly, an opposite situation was observed in the case of the samples SL and SL-S. Additional introduction of sulfates into the structure of SL led to a slight decrease in the anticoagulant effect; however, the sample SL-S (2APTT~2.0 μg/mL) was slightly more active than CO-S. It should be noted that synthetic per-*O*-sulfated octasaccharide OS demonstrated moderate activity

(2APTT ~5.0 μg/mL), indicating that its molecular size is not sufficient for achieving a high effect in this test.

To assess the influence of the studied compounds on the extrinsic pathway of coagulation, the value of Prothrombin time (PT) was measured. All samples, except CO, slightly increased PT in a dose-dependent manner (0.5–2 s, data not shown) within the concentration range used in the APTT test. According to literature data [15], significant changes in PT could be expected when fucoidan is applied at concentrations higher than 10 μg/mL.

The influence of the samples on thrombin-induced clot formation was also investigated. The value of Thrombin time (TT) was measured at several concentrations (see Figure 3) to again show different profiles of activity for the tested samples. The values of 2TT (the concentration of a sample, at which double increasing of control value of TT was observed) were also calculated (Table 2). The determined 2TT-values for Clexane® (~2.2 μg/mL), SL (~2.4 μg/mL), and SL-S (~2.2 μg/mL) suggested that these preparations possess comparable effects. Increasing polysaccharide concentration gave quite different responses. Thus, at a concentration of ~3.8 μg/mL Clexane® prolonged blood coagulation by eight times, while SL and SL-S gave prolongation only by four and three times, respectively. It is noticeable that, similarly to the results of the APTT test, the chemically sulfated polysaccharide SL-S exhibited slightly lower activity than parent fucoidan SL.

Figure 3. Anticoagulant activity measured by TT assay.

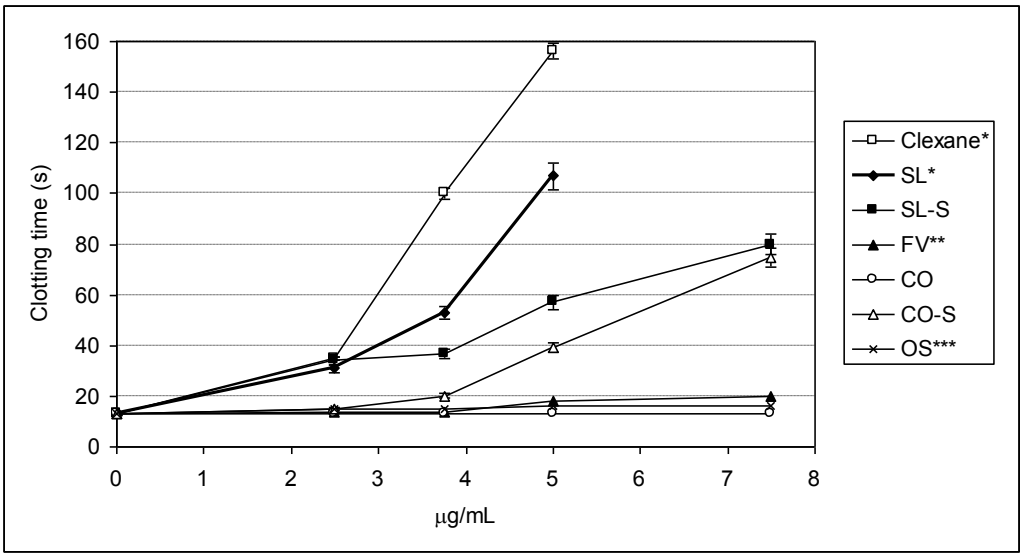

* Data for Clexane® and SL at a concentration of 7.5 μg/mL are omitted, as the TT value significantly exceeds the upper limit of determination; ** FV in a concentration of 15 μg/mL showed TT = 52 s; *** OS in a concentration of 21 μg/mL showed TT = 60 s.

The fucoidan CO was inactive in the TT assay even at a concentration of 100 μg/mL, while its sulfated derivative CO-S at a concentration of ~7.5 μg/mL demonstrated a comparable effect with preparation SL-S at the same concentration. Significant activity of the samples SL, SL-S, and CO-S in this test could be explained by their ability to interact with thrombin. Similarly to the results of the APTT test, fucoidan FV showed moderate inhibitory effect in TT assay (the 2TT value was ~9.2 μg/mL). This can be due to its slightly lower degree of sulfation (0.9, Table 1) in comparison with

SL, or to different presentations of sulfates because of another type of the backbone (Figure 1). Although the octasaccharide OS was structurally related to the backbones of SL-S and CO-S, its activity was lower (2TT ~16.1 μg/mL). This indicates again that longer and probably branched molecules are required for high anticoagulant effect.

2.3. Effect of the Compounds on the Inactivation of Thrombin and Factor Xa in the Presence and in the Absence of Antithrombin III

To investigate further the mechanism of anticoagulant action of fucoidans and their derivatives, the experiments with purified proteins were performed. These studies were based on the assay of amidolytic activity of thrombin (IIa) or factor Xa using chromogenic substrates, as described previously [8,14,15]. The ability of samples to inhibit thrombin and factor Xa was assessed in the presence and in the absence of ATIII. In addition to Clexane®, another heparin-related drug, Arixtra® (fondaparinux, based on synthetic pentasaccharide), was used as a reference. The results are shown in Table 3 and Figures 4 and 5.

Table 3. Inhibition of thrombin and factor Xa.

Sample	IC_{50} (μg/mL)		
	ATIII + thrombin	**+thrombin**	**ATIII + Xa**
SL	0.76 ± 0.04	45.86 ± 0.58	1.06 ± 0.04
SL-S	0.47 ± 0.02	55.86 ± 1.07	1.94 ± 0.08
FV	2.1 ± 0.08	No *	28.22 ± 0.95
CO	no	no	No
CO-S	0.88± 0.03	58.81 ± 1.12	2.06 ± 0.09
OS	No **	no	12.94 ± 0.98
Clexane®	0.59 ± 0.02	no	0.059 ± 0.002
Arixtra®	no	no	0.0065 ± 0.0003

* Not observed, but only 25% inhibition was observed at a concentration of 59.0 μg/mL; ** Not observed, but only 34% inhibition was observed at a concentration of 59.0 μg/mL.

Figure 4. Effect of the samples on thrombin inactivation in the presence and in the absence of ATIII. (♦) experiments with ATIII, (○) experiments without ATIII.

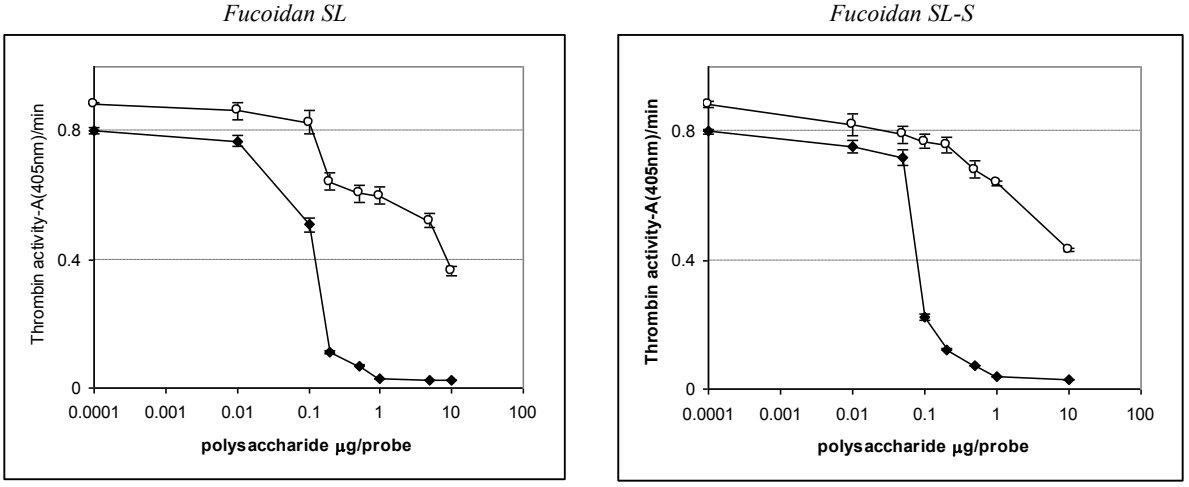

Figure 4. *Cont.*

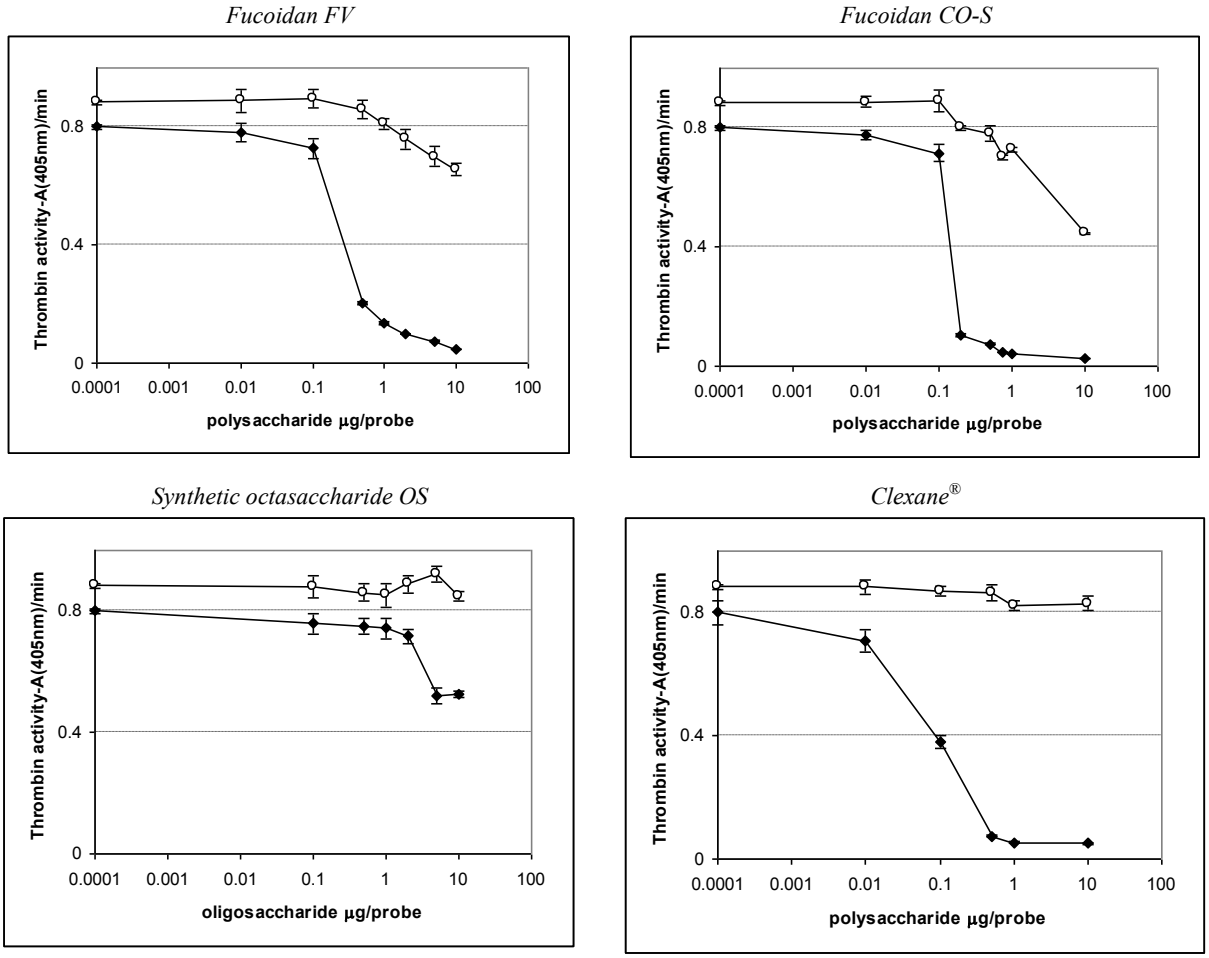

Figure 5. Effect of the samples on factor Xa inactivation in the presence of ATIII.

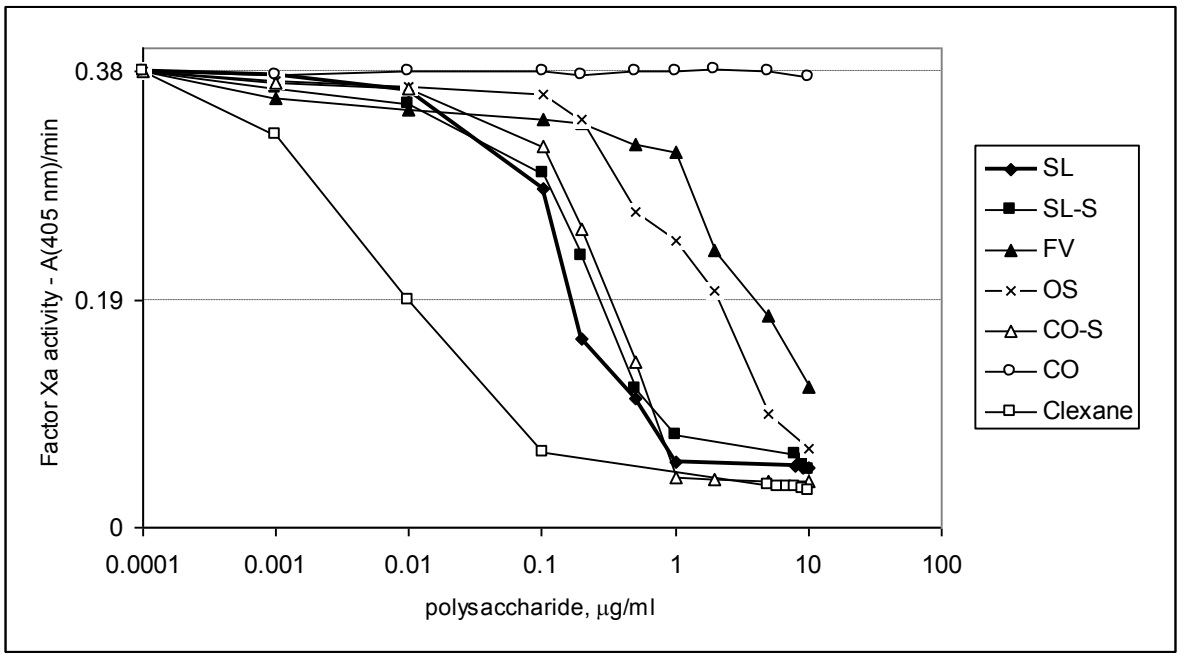

The preparations SL, SL-S, CO-S, and FV were shown to interact with thrombin both in the presence and in the absence of ATIII, while heparinoid Clexane® was active only in the presence of ATIII. Effectiveness of binding to thrombin in the presence of ATIII was high for the samples SL, SL-S, CO-S, and Clexane® (IC_{50} < 1.0 μg/mL), but it was slightly lower for the fucoidan FV (IC_{50} ~2.1 μg/mL). The fucoidan CO was inactive in all tested concentrations.

The synthetic octasaccharide OS demonstrated more than 100 times lower anti-IIa activity in the presence of ATIII than the polysaccharides SL, SL-S, and CO-S, with the same backbone. This result could be compared with known data for heparinoids. Thus, synthetic pentasaccharide Arixtra® did not inhibit thrombin activity in the presence of ATIII even at a concentration of 100 μg/mL, while the polysaccharide Clexane® demonstrated significant inhibitory effect in this experiment (IC_{50} < 1.0 μg/mL). It was established earlier [27–29] that more than 16 monosaccharide units in the chain of the heparinoid structure are required for the formation of a ternary complex with thrombin and ATIII.

For direct thrombin inhibition, higher concentrations of polysaccharides were required. Thus, the samples SL, SL-S, and CO-S showed 50% inhibition at concentrations of ~45.9, ~55.9, and ~58.9 μg/mL, respectively, while the fucoidan FV demonstrated only 25% inhibition at a concentration of 59.0 μg/mL.

The fucoidan CO, as well as the synthetic octa-(1→3)-α-L-fucoside OS, were found to be unable to interact directly with thrombin. It is interesting to mention that, according to the theoretical prediction, the high activity of linear sulfated (1→3)-β-L-arabinan was explained by the specific structure of its octasaccharide fragment [8]. The different biological properties of these two octasaccharides demonstrate, once more, the importance of the carbohydrate structure for the biological activity of sulfated polysaccharides.

The polysaccharides SL, SL-S, and CO-S efficiently bind to factor Xa only in the presence of ATIII (the values of IC_{50} were ~1.1, ~1.9, and ~2.0 μg/mL, respectively), but their activity was significantly lower than that for heparinoids Clexane® and Arixtra® (the values of IC_{50} were ~0.059 and ~0.0065 μg/mL, respectively). The fucoidan FV showed 50% inhibition only at a concentration of ~28.0 μg/mL. Surprisingly, the synthetic per-*O*-sulfated octasaccharide OS demonstrated moderate anti-Xa activity in the presence of ATIII (IC_{50} were ~13.0 μg/mL), even exceeding the effect of polysaccharide FV. Neither fucoidans, nor heparinoids, bind to factor Xa in the absence of ATIII (data not shown).

The tendencies found in amidolytic experiments (see Table 3 and Figures 4 and 5, showing anti-IIa and anti-Xa activities) for the studied samples correlated well with the results obtained in clotting assays. Thus, the polysaccharides SL, SL-S, and CO-S, enriched in 2,4-di-*O*-sulfated (1→3)-linked α-L-fucose units demonstrated high effects in clotting assays and also possessed significant anti-IIa and anti-Xa activities. These results are in good agreement with the data obtained previously for linear highly sulfated fucans from invertebrates [4,9,14]. Moreover, it is noticeable that inhibition of thrombin by these polysaccharides was performed both in the presence and in the absence of ATIII, which coincides well with the published data for other branched fucoidans from brown seaweeds [14,15].

2.4. Influence on Platelets Aggregation

The ability of the studied samples to influence on the cell-regulated hemostasis was assessed in experiments with platelets rich plasma (PRP). Two types of inducers of platelets aggregation, namely

thrombin and adenosine diphosphate (ADP), were used. All samples were tested at a concentration of 100 μg/mL, while the fucoidan SL was also studied at a concentration of 10 μg/mL (Figures 6 and 7).

Figure 6. Influence of the samples on thrombin-induced platelets aggregation *.

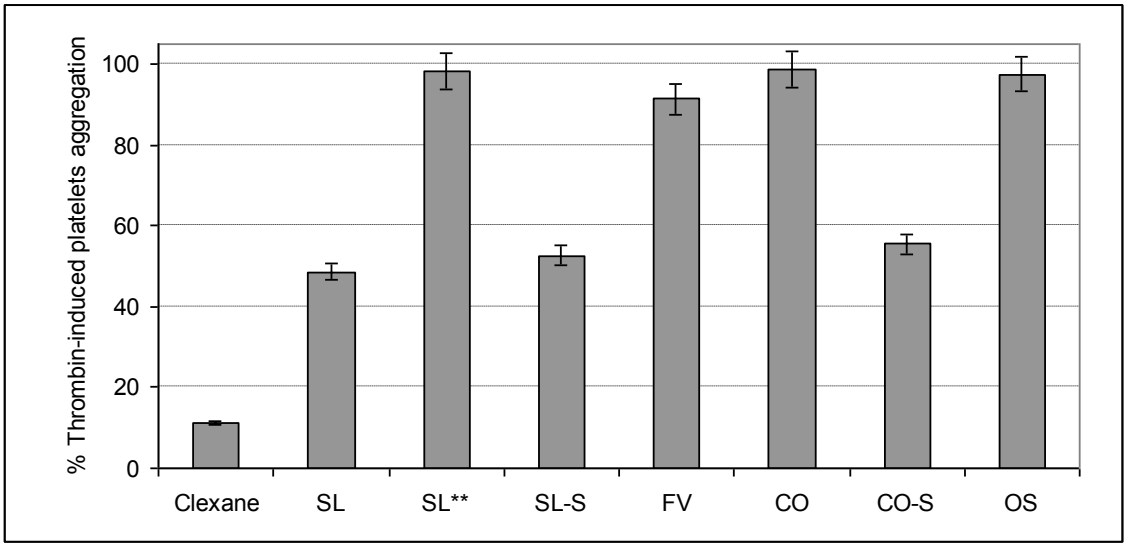

* Activities of studied samples (100 μg/mL) were tested in the presence of 0.5 U of thrombin; ** Activity of fucoidan SL at a concentration of 10 μg/mL.

Figure 7. Influence of the samples on ADP-induced platelets aggregation *.

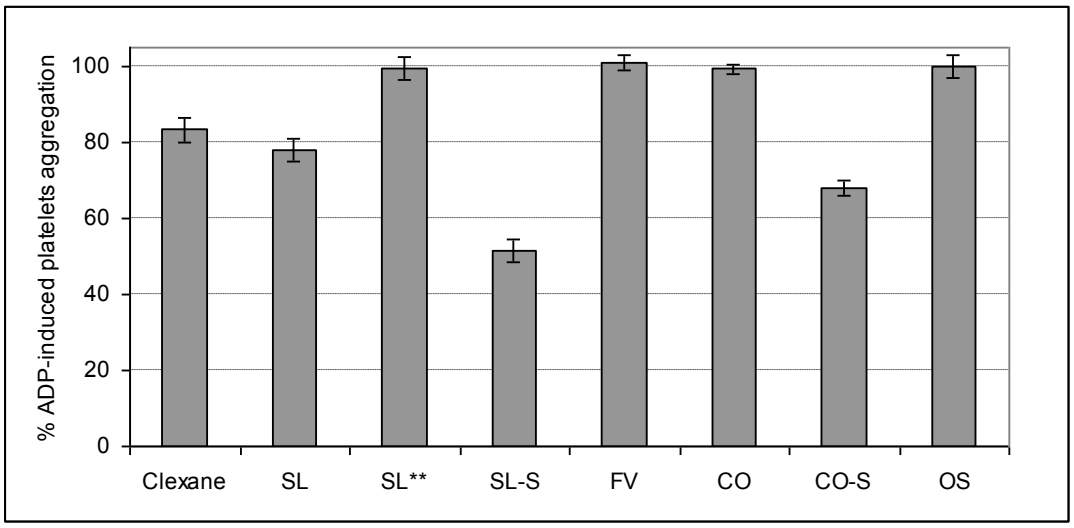

* Activities of studied samples (100 μg/mL) were tested in the presence of 10 μm of ADP; **Activity of fucoidan SL at a concentration of 10 μg/mL.

The polysaccharides SL, CO-S, and SL-S, as well as heparinoid Clexane®, efficiently inhibited thrombin-induced platelets aggregation. The 51% inhibition was observed for SL, 48% for SL-S, 42% for CO-S, and 88% for Clexan®, while the fucoidans FV and CO, the synthetic octasaccharide OS, as well as SL (at a concentration of 10 μg/mL), were inactive in this test. Thrombin is considered as the main protein target in this assay and, thus, the results obtained demonstrate comparable tendencies described above for the amidolytic assay.

The preparations SL, SL-S, and CO-S demonstrated a statistically significant effect on ADP-induced platelets aggregation exceeding that for Clexane®. Contrary to the mechanism of thrombin-induced platelets aggregation, the polysaccharide inhibitors interact directly with special receptors on the surface of platelets but not with the inducer of aggregation. That is why the observed values of inhibitory effects of the tested samples differed from those measured in the previous experiment. Inhibition of aggregate formation in PRP was 50% for SL-S, 32% for CO-S, and 22% for SL. The fucoidans FV and CO, the synthetic octasaccharide OS, as well as SL (at a concentration of 10 μg/mL) were inactive again.

3. Experimental Section

3.1. Preparation of the Samples

Preparation of the fucoidan SL ("fraction F-1.25" in [20]) from the brown seaweed *S. latissima* was described earlier [20]. A crude fucoidan preparation extracted from *F. vesiculosus* was purified by decoloration with $NaClO_2$ in dilute HCl [30] followed by precipitation with cetyltrimethylammonium bromide and transformation into sodium salt [31], giving rise to purified fucoidan FV. The polysaccharide CO was received as a gift from Dr. M. Iho (South Product Co., Suzaki, Japan).

The fucoidans SL and CO were subjected to *O*-sulfation under acid-promoted conditions [23], transformed into sodium salts and desalted by column chromatography on Sephadex G-15 (2.5 × 70 cm, elution with water) to obtain the corresponding oversulfated polysaccharides SL-S and CO-S, respectively. The octasaccharide OS was synthesized from L-fucose [24] and characterized by mass spectrometry (ESI-MS), as well as by ^{1}H and ^{13}C NMR spectroscopy.

The monosaccharide composition and sulfate content of the samples were determined as described earlier [32] and summarized in Table 1.

3.2. General Coagulation Assays

APTT and PT were determined with an SRA-R Evolution® hemostasis analyzer (Diagnostica Stago, USA) according to the established procedure and using standard reagents (Diagnostica Stago). A solution (15 μL) containing 15 μg, 7.5 μg, or 3.75 μg of a sulfated carbohydrate sample in saline solution (0.9% NaCl) was added to the normal platelet-depleted citrated plasma (3 mL). Low-molecular-weight heparin Clexane® (manufactured by Sanofi) was used for the comparison of anticoagulant activity of the samples. The saline solution was used as a control. The samples were incubated at 37 °C for 1 min.

A kit, "Thrombin test" (Renam, Russia), was used for determination of thrombin time. A saline solution with a sulfated carbohydrate sample (20 μL) was added to the normal plasma (80 μL). The mixture was incubated at 37 °C for 1 min, and a saline solution (100 μL) of stabilized thrombin (10 U/mL) was added. The saline solution was used as a control. The time of clot formation was then determined.

3.3. Amidolytic Assays

Determination of amidolytic activity of thrombin was performed using "ReaChrom ATIII test" kit (Renam, Russia) as described previously [15]. A solution of ATIII (0.2 U/mL, 50 μL) or the buffer

(50 μL) was added to a solution of a sulfated carbohydrate sample (0.001–10 μg) in buffer (0.15 μM Tris-HCl, pH 8.4, 20 μL), followed by the addition of an aqueous solution (50 μL) of human thrombin (5.0 U/mL). The mixture was incubated at 37 °C for 3 min, and 50 μL of synthetic chromogenic substrate was added. After 2 min the reaction was quenched by 220 μL of 50% acetic acid. The absorbance of *para*-nitroaniline was measured at 405 nm on an Ultospec II spectrophotometer (LKB, Switzerland).

Determination of amidolytic activity of factor Xa was performed using "ReaChrom Heparin" (Renam, Russia) kit. A solution of ATIII (0.5 U/mL, 50 μL) or the buffer (50 μL) was added to a solution of a sulfated carbohydrate sample (0.0001–10 μg) in the buffer (0.15 μM Tris-HCl, pH 8.4, 20 μL). Then an aqueous solution of the factor Xa (2.0 U/mL, 50 μL) was added. The mixture was worked-up, treated with chromogenic substrate, and analyzed as described above.

3.4. Inhibition of Platelets Aggregation

Blood with citrate buffer (9:1) was centrifuged at 1000 rpm for 5 min, and platelets rich plasma was collected from different tubes and combined. A saline solution (10 μL) containing 45 μg of a sulfated carbohydrate sample was added to 450 μL of this plasma. The saline solution was used as a control. The samples were incubated at 37 °C for 2 min, then 10 μm of ADP or 0.5 U of thrombin was added, and light transmittance was measured on a Chrono-Log aggregometer. The data were transformed to percent of platelets aggregation using the established software. The control was considered as 100% of platelets aggregation.

3.5. Statistical Analysis

All experiments were performed in quadruplicate (n = 4). The results are presented as mean ± S.D. Statistical significance was determined with Student's t test. The P values less than 0.05 were considered as significant.

4. Conclusions

The effect of the fucoidans on blood coagulation and platelets aggregation was shown to depend on their structural features. Thus, the branched polysaccharides SL, SL-S, and CO-S, enriched in 2,4-di-*O*-sulfated (1→3)-linked α-L-fucose units demonstrated high effect in clotting assays, while the fucoidan FV built up of alternating (1→3)- and (1→4)-linked α-L-fucose residues with a degree of sulfation of 0.9 was remarkably less active. The polysaccharide CO with the (1→3)-linked α-L-fucose backbone containing α-D-glucuronic acid branches at C-2 with the degree of sulfation 0.4 did not influence on blood coagulation, and this feature could be explained by the absence of a sufficient amount of sulfate groups in its structure, or by the presence of glucuronic acid side residues. The tendencies found in clotting assays correlated with the results obtained in experiments with individual proteins. High anti-IIa and anti-Xa activities were shown for the samples SL, SL-S, and CO-S in the presence of ATIII. The fucoidan FV demonstrated moderate effects under these conditions, while the fucoidan CO was inactive. It is noticeable that the branched polysaccharides with the degree of sulfation ≥0.9 (SL, SL-S, CO-S, and FV) were also shown to be direct thrombin inhibitors and, hence,

they differ from heparinoids and linear fucans from invertebrates. The synthetic per-*O*-sulfated octasaccharide OS, which was structurally related to the polysaccharides SL, SL-S, and CO-S, possessed a moderate effect on clot formation connected mainly with its moderate anti-Xa activity. This result indicated that longer, and probably branched, fucoidan fragments are required for the efficient inhibition of blood coagulation. The most active samples SL, SL-S, and CO-S also exhibited a statistically significant inhibitory effect on platelets aggregation mediated by ADP and thrombin.

Acknowledgments

This work was supported in part by the Russian Foundation for Basic Research (grants 12-04-01749 and 12-03-92703).

References

1. Galanaud, J.P.; Laroche, J.P.; Righini, M. The history and historical treatments of deep vein thrombosis. *J. Thomb. Haemost*. **2013**, *3*, 402–411.
2. Falanga, A.; Vignoli, A.; Diani, E.; Marchetti, M. Comparative assessment of low-molecular-weight heparins in cancer from the perspective of patient outcomes and survival. *Patient Related Outcome Meas.* **2011**, *2*, 175–188.
3. Pomin, V.H. Fucanomics and galactanomics: Current status in drug discovery, mechanisms of action and role of the well defined structures. *Biochim. Biopys. Acta* **2012**, *1820*, 1971–1979.
4. Pereira, M.S.; Melo, F.R.; Mourão, P.A. Is there a correlation between structure and anticoagulant action of sulfated galactans and sulfated fucans? *Glycobiology* **2002**, *12*, 573–580.
5. Melo, F.R.; Pereira, M.S.; Foguel, D.; Mourão, P.A. Antithrombin-mediated anticoagulant activity of sulfated polysaccharides: Different mechanisms for heparin and sulfated galactans. *J. Biol. Chem.* **2004**, *279*, 20824–20835.
6. Jiao, G.; Yu, G.; Zhang, J.; Ewart, S. Chemical structures and bioactivities of sulfated polysaccharides from marine algae. *Mar. Drugs* **2011**, *9*, 196–223.
7. Ciancia, M.; Quintana, I.; Cerezo, A.S. Overview of anticoagulant activity of sulfated polysaccharides from seaweeds in relation to their structures, focusing on those of green seaweeds. *Curr. Med. Chem*. **2010**, *17*, 2503–2529.
8. Fernandez, P.V.; Quintana, I.; Cerezo, A.S.; Caramelo, J.J.; Pol-Fachin, L.; Verli, H.; Estevez, J.M.; Ciancia, M. Anticoagulant activity of a unique sulfated pyranosic (1→3)-β-L-arabinan through direct interaction with thrombin. *J. Biol. Chem.* **2013**, *288*, 223–233.
9. Fonseca, R.J.; Santos, G.R.; Mourão, P.A. Effects of polysaccharides enriched in 2,4-disulfated fucose units on coagulation, thrombosis and bleeding. Practical and conceptual implications. *Thromb. Haemost*. **2009**, *102*, 829–836.
10. Fitton, J.H. Therapies from fucoidan; Multifunctional marine polymers. *Mar. Drugs* **2011**, *9*, 1731–1760.
11. Ale, M.T.; Mikkelsen, J.D.; Meyer, A.S. Important determinants for fucoidan bioactivity: A critical review of structure-function relations and extraction methods for fucose-containing sulfated polysaccharides from brown seaweeds. *Mar. Drugs* **2011**, *9*, 2106–2130.

12. Cumashi, A.; Ushakova, N.A.; Preobrazhenskaya, M.E.; D'Incecco, A.; Piccoli, A.; Totani, L.; Tinari, N.; Morozevich, G.E.; Berman, A.E.; Bilan, M.A.; *et al.* Comparative study of the anti-inflammatory, anticoagulant, antiangiogenic, and antiadhesive activities of nine different fucoidans from brown seaweeds. *Glycobiology* **2007**, *17*, 541–552.
13. Usov, A.I.; Bilan, M.I. Fucoidans—Sulfated polysaccharides of brown algae. *Russ. Chem. Rev.* **2009**, *78*, 785–799.
14. Pereira, M.S.; Mulloy, B.; Mourão, P.A. Structure and anticoagulant activity of sulfated fucans. *J. Biol. Chem.* **1999**, *274*, 7656–7667.
15. Ushakova, N.A.; Morozevich, G.E.; Ustyuzhanina, N.E.; Bilan, M.I.; Usov, A.I.; Nifantiev, N.E.; Preobrazhenskaya, M.E. Anticoagulant activity of fucoidans from brown seaweeds (in Russian). *Biomed. Chem*. **2008**, *54*, 597–606.
16. Croci, D.O.; Cumashi, A.; Ushakova, N.A.; Preobrazhenskaya, M.E.; Piccoli, A.; Totani, L.; Ustyuzhanina, N.E.; Bilan, M.I.; Usov, A.I.; Grachev, A.A.; *et al.* Fucans, but not fucomannoglucuronans, determine the biological activities of sulfated polysaccharides from *Laminaria saccharina* brown seaweed. *PLoS One* **2011**, *6*, doi:10.1371/journal.pone.0017283.
17. Nishino, T.; Nagumo, T. The sulfate-content dependence of the anticoagulant activity of a fucan sulfate from the brown seaweed *Ecklonia kurome*. *Carbohydr. Res.* **1991**, *214*, 193–197.
18. Haroun-Bouhedja, F.; Ellouali, M.; Sinquin, C.; Boisson-Vidal, C. Relationship between sulfate groups and biological activities of fucans. *Thromb. Res.* **2000**, *100*, 453–459.
19. Pomin, V.H.; Pereira, M.S.; Valente, A.P.; Tollefsen, D.M.; Pavao, M.S.G.; Mourão, P.A.S. Selective cleavage and anticoagulant activity of a sulfated fucan: Stereospecific removal of a 2-sulfate ester from the polysaccharide by mild acid hydrolysis, preparation of oligosaccharides, and heparin cofactor II-dependent anticoagulant activity. *Glycobiology* **2005**, *15*, 369–381.
20. Bilan, M.I.; Grachev, A.A.; Shashkov, A.S.; Kelly, M.; Sanderson, C.J.; Nifantiev, N.E.; Usov, A.I. Further studies on the composition and structure of a fucoidan preparation from the brown alga *Saccharina latissima*. *Carbohydr. Res*. **2010**, *345*, 2038–2047.
21. Chevolot, L.; Mulloy, B.; Ratiskol, J.; Foucault, A.; Colliec-Jouault, S. A disaccharide repeat unit is the major structure in fucoidans from two species of brown algae. *Carbohydr. Res.* **2001**, *330*, 529–535.
22. Nagaoka, M.; Shibata, H.; Kimura-Takagi, I.; Hashimoto, S.; Kimura, K.; Makino, T.; Aiyama, R.; Ueyama, S.; Yokokura, T. Structural study of fucoidan from *Cladosiphon okamuranus* TOKIDA. *Glycoconj. J*. **1999**, *16*, 19–26.
23. Krylov, V.B.; Ustyuzhanina, N.E.; Grachev, A.A.; Nifantiev, N.E. Efficient acid-promoted per-*O*-sulfation of organic polyols. *Tetrahedron Lett.* **2008**, *49*, 5877–5879.
24. Krylov, V.B.; Kaskova, Z.M.; Vinnitskiy, D.Z.; Ustyuzhanina, N.E.; Grachev, A.A.; Chizhov, A.O.; Nifantiev, N.E. Acid-promoted total sulfation of fucoidan fragments. *Carbohydr. Res.* **2011**, *346*, 540–550.
25. McGarry, L.J.; Thompson, D. Retrospective database analysis of the prevention of venous thromboembolism with low-molecular-weight heparin in acutely III medical inpatients in community practice. *Clin. Ther.* **2004**, *26*, 419–430.

26. Sobieraj, D.M.; Coleman, C.I.; Tongbram, V.; Chen, W.; Colby, J.; Lee, S.; Kluger, J.; Makanji, S.; Ashaye, A.; White, C.M. Comparative effectiveness of low-molecular-weight heparins *versus* other anticoagulants in major orthopedic surgery: A systematic review and meta-analysis. *Pharmacotherapy* **2012**, *32*, 799–808.
27. Gray, E.; Hogwood, J.; Mulloy, B. The anticoagulant and antithrombotic mechanisms of heparin. *Handb. Exp. Pharmacol*. **2012**, *207*, 43–61.
28. Imberty, A.; Lortat-Jacob, H.; Perez, S. Structural view on glycosaminoglycan-protein interactions. *Carbohydr. Res.* **2007**, *342*, 430–439.
29. Petitou, M.; Casu, B.; Lindahl, U. 1976–1983, a critical period in the history of heparin: The discovery of the antithrombin binding site. *Biochimie* **2003**, *85*, 83–89.
30. Usov, A.I.; Smirnova, G.P.; Klochkova, N.G. Polysaccharides of algae. 55. Polysaccharide composition of some brown algae from Kamchatka. *Russ. J. Bioorg. Chem.* **2001**, *27*, 395–399.
31. Usov, A.I.; Smirnova, G.P.; Bilan, M.I.; Shashkov, A.S. Polysaccharides of algae. 53. Brown alga *Laminaria saccharina* (L.) Lam. as a source of fucoidan. *Russ. J. Bioorg. Chem.* **1998**, *24*, 437–445.
32. Bilan, M.I.; Grachev, A.A.; Ustuzhanina, N.E.; Shashkov, A.S.; Nifantiev, N.E.; Usov, A.I. Structure of a fucoidan from the brown seaweed *Fucus evanescens* C. Ag. *Carbohydr. Res*. **2002**, *337*, 719–730.

Conference paper

Nadezhda E. Ustyuzhanina, Natalia A. Ushakova, Marina E. Preobrazhenskaya, Maria I. Bilan, Eugenia A. Tsvetkova, Vadim B. Krylov, Natalia A. Anisimova, Mikhail V. Kiselevskiy, Nadezhda V. Krukovskaya, Chunxia Li, Guangli Yu, Saurabh Saran, Rajendra K. Saxena, Anatolii I. Usov and Nikolay E. Nifantiev*

Fucoidans as a platform for new anticoagulant drugs discovery

Abstract: Anionic fucose-containing polysaccharides (fucoidans of brown seaweeds, sulfated fucans and fucosylated chondroitin sulfates of invertebrates) are attracting a rapidly growing research interest due to different types of their biological activity discovered in recent years. In particular, algal fucoidans are characterized by large structural variations depending on the species used for their isolation and by the lack of structural regularity due to random distribution of both carbohydrate and non-carbohydrate substituents along the polymer chains. These features make it difficult to find distinct correlations between structural elements and biological properties of polysaccharides. Nevertheless, there is expectation that systematic structural and biochemical studies of fucoidans will form a basis for the development of new drugs. Herewith we summarize our recent results on the influence of fucoidan structure on blood coagulation.

Keywords: anticoagulant; carbohydrates; drug discovery; factor Xa; fucoidan; hemostasis; ICS-27; marine chemistry; polysaccharide; thrombin.

DOI 10.1515/pac-2014-0404

Introduction

Natural sulfated polysaccharides, such as galactans [1–5], arabinans [6], and fucoidans [1, 4, 7–11], present in seaweeds, as well as sulfated fucans of invertebrates [1–3, 7, 12], are regarded as the perspective basis to

Article note: A collection of invited papers based on presentations at the 27th International Carbohydrate Symposium (ICS-27), Bangalore, India, 12–17 January 2014.

***Corresponding author: Nikolay E. Nifantiev,** Laboratory of Glycoconjugate Chemistry, N. D. Zelinsky Institute of Organic Chemistry, Russian Academy of Sciences, Leninsky Prospect 47, 119991 Moscow, Russia, e-mail: nen@ioc.ac.ru; nifantiev@gmail.com
Nadezhda E. Ustyuzhanina, Nadezhda V. Krukovskaya and Vadim B. Krylov: Laboratory of Glycoconjugate Chemistry, N. D. Zelinsky Institute of Organic Chemistry, Russian Academy of Sciences, Leninsky Prospect 47, 119991 Moscow, Russia
Natalia A. Ushakova and Marina E. Preobrazhenskaya: V.N. Orekhovich Research Institute of Biomedical Chemistry, Russian Academy of Medical Sciences, Pogodinskaya str. 10, 119121 Moscow, Russia
Maria I. Bilan, Eugenia A. Tsvetkova and Anatolii I. Usov: Laboratory of Plant Polysaccharides, N. D. Zelinsky Institute of Organic Chemistry, Russian Academy of Sciences, Leninsky Prospect 47, 119991 Moscow, Russia
Natalia A. Anisimova and Mikhail V. Kiselevskiy: N.N. Blokhin Russian Cancer Research Center, Russian Academy of Medical Sciences, Kashirskoe shosse, 24, 115478 Moscow, Russia
Chunxia Li and Guangli Yu: School of Medicine and Pharmacy, Ocean University of China, 5 Yushan Road, Qingdao, 266003 China,
Saurabh Saran and Rajendra K. Saxena: Department of Microbiology, University of Delhi South Campus, Benito Juarez Road, New Delhi-110021, India

develop drugs for different applications. Among these polysaccharides, the fucoidans raise the largest interest, as it can be concluded from the statistical records for corresponding papers summarized in Fig. 1 (comp. with ref. [9]). Great attention to fucoidans can be connected with their facile availability from brown seaweeds, lack of toxicity, great biocompatibility, as well as with broad structural variability, which stimulates their structural analysis to assess the relation between structure and biological activity.

Influence of these biopolymers on the hemostatic system depends on the ability of polymeric sulfates to interact with positively charged groups in proteins responsible for hemostasis, leading to the formation of stabilized complexes. The anticoagulant properties of sulfated polysaccharides are mainly connected with thrombin inhibition mediated by antithrombin III (ATIII) and/or heparin cofactor II (HCII), with different efficiencies depending on the structural features of carbohydrates. Other mechanisms, such as direct inhibition of thrombin, are also possible.

A number of studies revealed certain structure-activity relationships for these macromolecules [2, 5, 8, 10, 12–16]. The main structural features of sulfated polysaccharides, which should be taken into account regarding their anticoagulant properties, include the monosaccharide composition, the degree and pattern of sulfation, molecular weight, and types of glycosidic bonds. The level of sulfation exceeding one sulfate per monosaccharide residue was shown to be important for high anticoagulant activity of fucans and galactans [17, 18]. High molecular weight fucans demonstrated a greater anticoagulant effect than structurally similar polysaccharides having lower molecular weight [17, 19].

The pattern of *O*-sulfation together with the structure of the backbone and branches, but not only total negative charge of sulfates, has a substantial impact on the activity of the biopolymers under discussion (see, for example, ref. [12]). Thus, in a series of polysaccharides isolated from invertebrates it has been shown that 2-*O*-sulfated (1 → 3)-linked α-L-galactan, but not an α-L-fucan, with a similar sulfation pattern and molecular size, is a potent thrombin inhibitor mediated by ATIII or HCII [2]. In the case of HCII-mediated inhibition, the major structural requirement for the activity is the presence of selectively 4-*O*-sulfated fucose units [2]. In addition, the linear (1 → 3)-linked α-L-fucans, enriched in 2,4-di-*O*-sulfated units, were shown to have an amplifying effect on the ATIII-mediated anticoagulant activity [2, 7].

Fucoidans from brown algae possess a significantly more complicated structure than fucans from invertebrates due to the presence of numerous branches, non-fucose monosaccharide constituents, and acetates [11]. It was found that, besides ATIII- and HCII-mediated thrombin inhibition activities, which are typical of fucans, the algal fucoidans could also be direct inhibitors of thrombin. For the first time, this behavior was shown for fucoidans from *Fucus vesiculosus* and *Laminaria brasiliensis*, which are built up of alternating (1 → 3)- and (1 → 4)-linked α-L-fucose residues sulfated at C-2 and/or C-4, and bearing fucose branches [12].

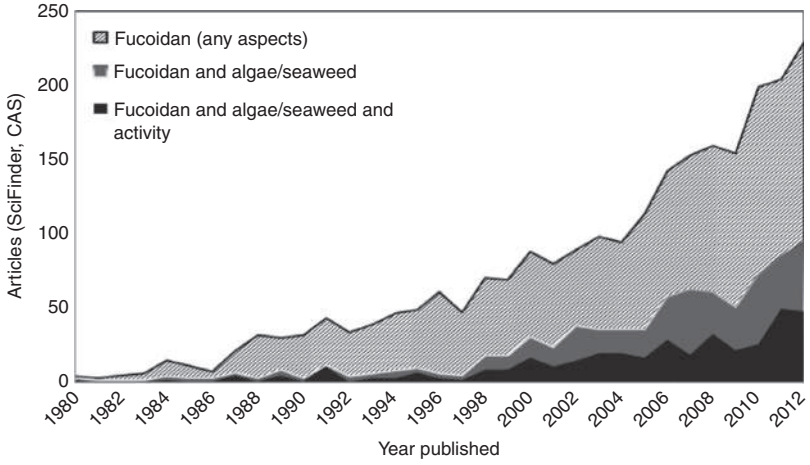

Fig. 1 Statistical data for scientific publications related to fucoidan studies. Searched in December, 2013 with SciFinder (CAS) database.

The similar mechanism of action was shown for the fucoidans from the brown seaweeds *Saccharina latissima* and *F. distichus*, but the polysaccharides from *Cladosiphon okamuranus* and *Analipus japonicus* were inactive [13]. Notably, a linear arabinan consisting of (1 → 3)-linked β-L-arabinose residues sulfated at C-2 and/or C-4 was also found to be the potent direct thrombin inhibitor [6].

Here we summarize the results of the study on anticoagulant activity of several fucoidans from brown seaweeds, their chemically modified derivatives, and synthetic oligosaccharides, related to the fucoidans. The studied compounds differed in the monosaccharide composition, types of glycosidic bonds, pattern and degree of sulfation, and molecular weight.

Stuctural diversity of brown algal fucoidans

As a rule, fucoidans present in different algal species vary not only in sulfation pattern, but also in the structures of their carbohydrate moieties. Moreover, even a crude fucoidan obtained from the single algal species may be a mixture of polysaccharides having different chemical structures. For example, it was shown by detailed chemical analysis that a mixture of sulfated polysaccharides extracted from the brown alga *S. latissima* contained at least four structurally different components [20]. Fractions enriched in the main components of this mixture, namely, in a sulfated fucan and a sulfated fucoglucuronomannan, respectively, were obtained using anion-exchange chromatography on DEAE-Sephacel. Recently it was shown that sulfated fucan, but not sulfated fucoglucuronomannan is of primary importance for the biological activity of a total fucoidan from *S. latissima* [14]. Similar approach was used for isolation of the highly sulfated fucoidan fractions from a number of other brown seaweed species, namely, *Chordaria flagelliformis* (**CF**) [21], *Cladosiphon okamuranus* (**CO**) [22], *Punctaria plantaginea* (**PP**) [23], *Fucus evanescens* (**FE**) [24], *Fucus distichus* (**FD**) [25], *Sargassum polycystum* (**SP**) [26] (Table 1). The main structural features of these polymers are shown in Fig. 2, and their monosaccharide and sulfate content is presented in Table 1. Elucidation of these structures was described elsewhere [20–26].

Several chemical modifications of the natural polysaccharides have been performed. Thus, the per-*O*-sulfated derivatives **SL-S** and **CO-S** have been prepared from the polymers **SL** and **CO**, respectively, by treatment with sulfating reagents (Scheme 1, Table 1) [18].

The polysaccharide **CF** was subjected to another chemical transformation. Reduction of carboxyl groups in its structure gave rise to the polymer **CF-R** bearing glucosyl branches instead of glucuronyl ones (Scheme 2, Table 1) [21]. Smith degradation of the branched xylofucan sulfate **PP** led to the linear sulfated fucan **PPX** devoid of xylose residues (Scheme 3, Table 1) [23].

The studied polysaccharides were different in monosaccharide content, degree of sulfation, types of glycosidic bonds, molecular weight. The homogeneity of the fucoidan fractions was evidenced by the results of electrophoresis of the samples in agarose gel (Fig. 3).

Synthesis of the oligosaccharides related to fucoidans

Besides the polymeric compounds the low molecular weight fucosides have been studied. The linear and branched oligosaccharides **OS1**–**OS5** (Fig. 4) have been synthesized [27–29]. The tetrasaccharide **OS1** and the octasaccharide **OS3** built up of (1 → 3)-linked α-L-fucopyranosyl residues could be considered as the backbone fragments of the highly sulfated polysaccharides **SL-S** and **CO-S**. The octasaccharide **OS2** has the same chain length as **OS3**, but it bears sulfate groups only at *O*-2. The compound **OS4** built up of the alternating (1 → 3)- and (1 → 4)-linked α-L-fucopyranosyl residues is the isomer of the octasaccharide **OS3**. The tetrasaccharide **OS5** is related to the branched fragment of the polysaccharide **SL-S**. Key synthetic steps are shown below (Scheme 4) and are applicable also for the preparation of much larger oligosaccharides including the 16-fucoside [28].

Table 1 Composition[1] of the polysaccharide preparations.

Sample	Source	Fuc	Xyl	Man	Gal	Glc	UA[2]	SO_3^{-2}	DS[3]
SL [20]	*S. latissima*	36.7	1.8	0.7	8.4	–	1.9	39.8	1.3
CF [21]	*C. flagelliformis*	40.1	–	–	1.7	0.7	**13.5**	26.6	0.8
CO [22]	*C. okamuranus*	42.7	2.0	1.1	1.9	0.8	**15.1**	16.9	0.4
PP [23]	*P. plantaginea*	44.3	**17.1**	–	2.6	–	2.3	19.2	0.5
FE [24]	*F. evanescens*	52.4	1.9	–	1.6	–	–	35.0	1.0
FD [25]	*F. distichus*	40.8	0.8	–	0.8	–	–	34.8	1.4
SP [26]	*S. polycystum*	36.0	1.7	–	**19.1**	0.7	1.6	33.7	1.0
SL-S [18]	Sulfation of SL	26.9	–	1.3	7.1	–	1.0	46.7	2.0
CO-S [18]	Sulfation of CO	19.7	0.8	0.9	0.7	0.7	8.1	39.7	2.0
CF-R [21]	Reduction of CF	53.9	–	–	1.2	**10.1**	–	28.5	0.8
PPX [23]	Smith degradation of PP	60.2	–	–	1.5	–	–	27.4	0.7

[1]Content (w/w%) of monosaccharides and sulfate (the presence of acetate is not shown).

[2]Uronic acid.

[3]Degree of sulfation calculated as the molar ratio of sulfate (as SO_3Na) and the sum of monosaccharide constituents (Fuc + Gal + UA + Xyl).

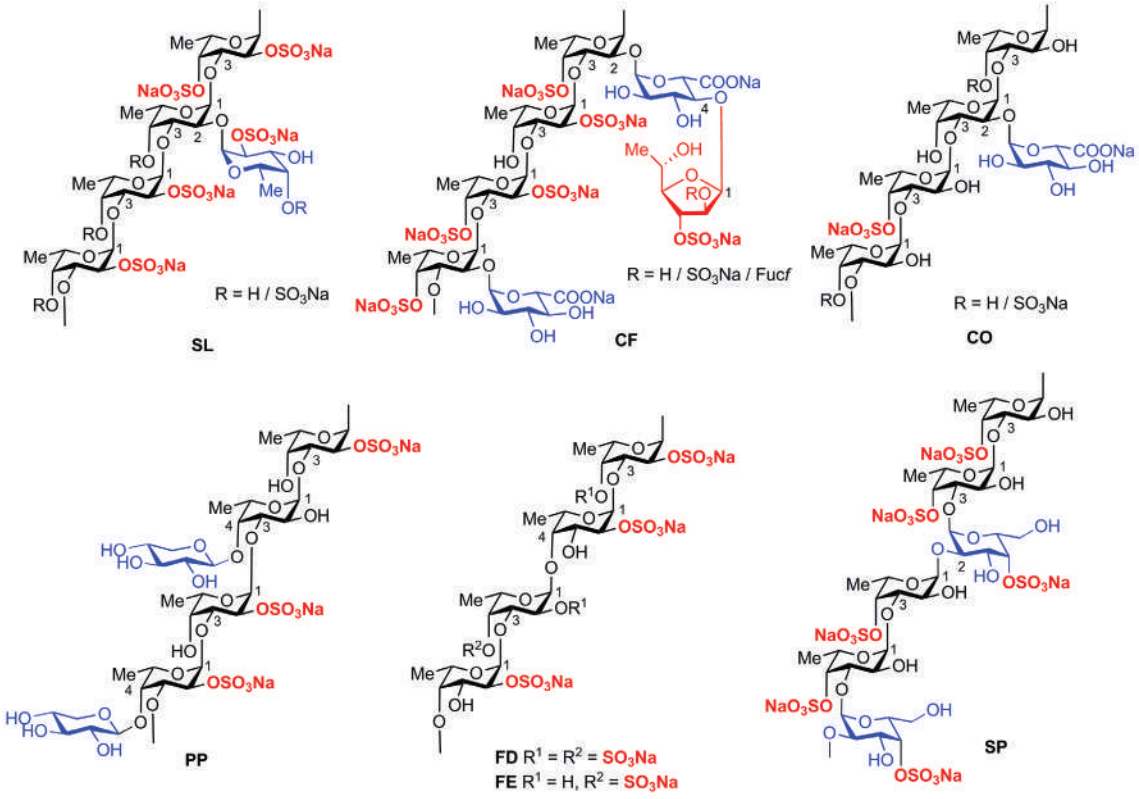

Fig. 2 The main structural features of the fucoidans isolated from the brown seaweeds *S. latissima* (**SL**) [20], *C. flagelliformis* (**CF**) [21], *C. okamuranus* (**CO**) [22], *P. plantaginea* (**PP**) [23], *F. evanescens* (**FE**) [24], *F. distichus* (**FD**) [25], *S. polycystum* (SP) [26].

For the synthesis of the compounds **OS1**–**OS5** the efficient method of the α-L-fucosylation has been developed [27, 30–32]. The stereoselectivity of the reaction is determined by the presence of acyl groups at *O*-3 and/or *O*-4 of a fucosyl donor, which stabilize the glycosyl cation in a manner favorable for the α-attack

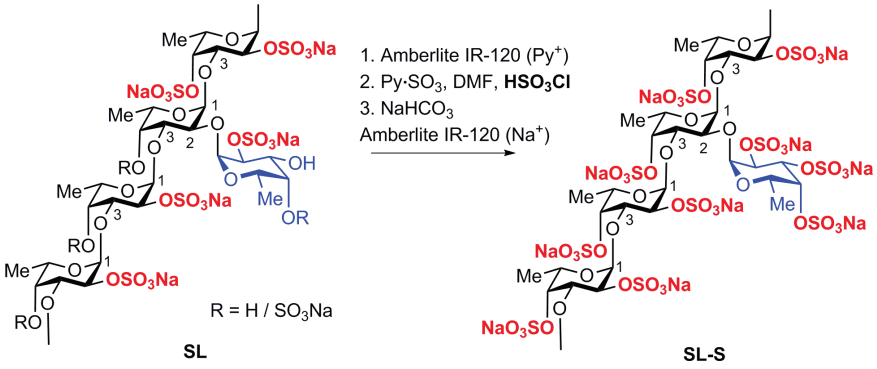

Scheme 1 Preparation of the chemically sulfated derivative **SL-S** from **SL**.

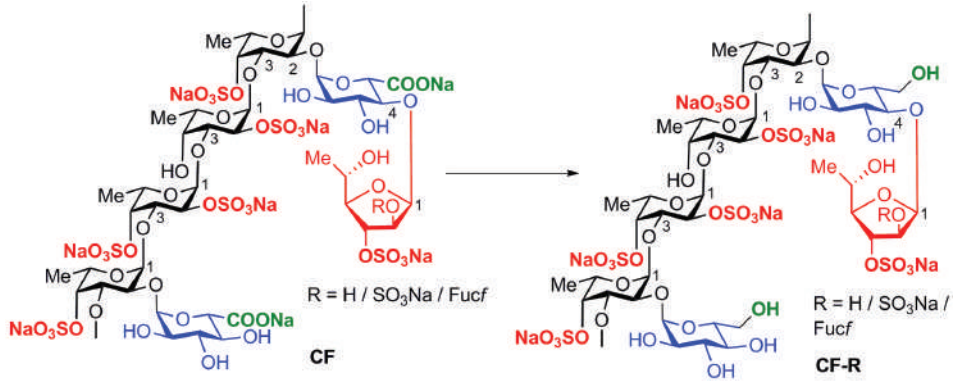

Scheme 2 Preparation of the polysaccharide **CF-R** by reduction of GlcA units in **CF**.

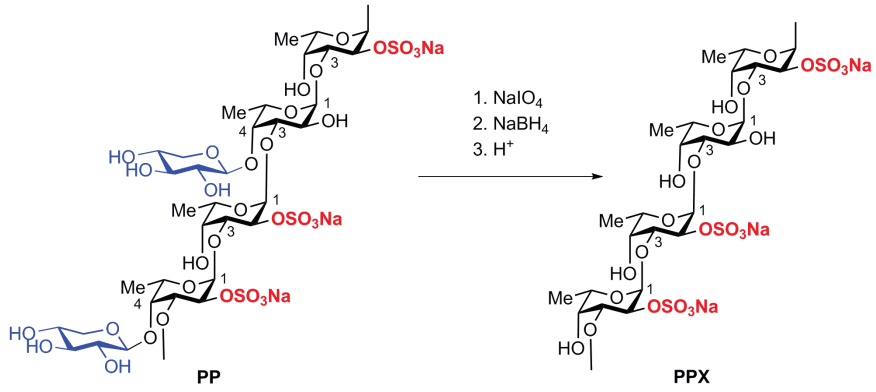

Scheme 3 Preparation of the linear sulfated fucan **PPX** by Smith degradation of **PP**.

of a glycosyl acceptor. Notably, not only monosaccharide, but also di- and tetrasaccharide glycosyl donors bearing acyl groups at *O*-3 and/or *O*-4 were successfully used for the preparation of the α-linked fucosides. This led to develop efficient blockwise strategies for large carbohydrate chains assembling.

The fragment of the convergent synthesis of the octasaccharide **OS4** is shown on Scheme 4. The presence of an allyl aglycon and an acetyl group at O-3‴ in a structure of the tetrasaccharide **1** permitted its selective transformation either to the glycosyl acceptor **2** or to the glycosyl donor **3**. Thus, acidic *O*-deacetylation of **1** gave the tetrasaccharide **2** in a yield of 82 %. Deallylation of **1** followed by trichloroacetimidation afforded the glycosyl donor **3** as a 1:1 mixture of α- and β-isomers in a total yield of 78 %. Coupling of the tetrasaccharides

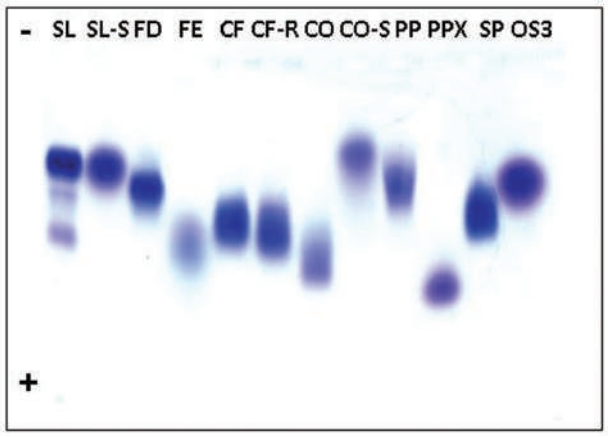

Fig. 3 Electrophoresis of the samples in agarose gel.

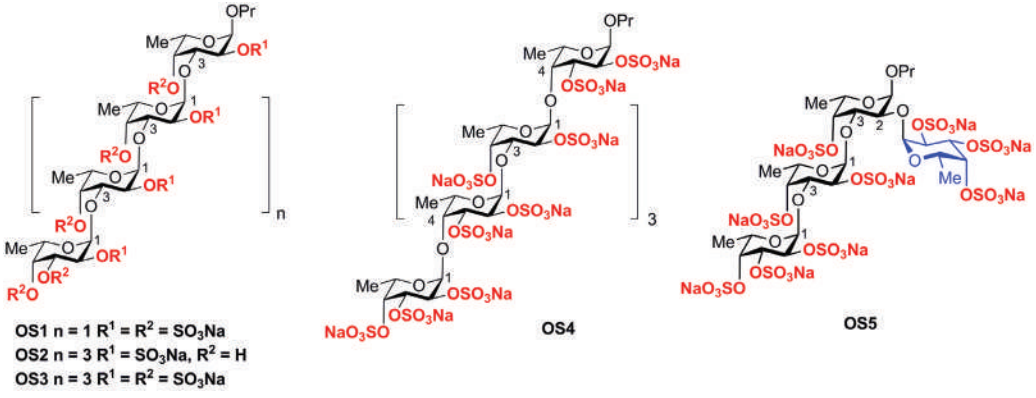

Fig. 4 The synthetic oligosaccharides related to fucoidans.

2 and **3** proceeded stereospecifically with the formation of the α-linked octafucoside **4** in a yield of 76 %. Deprotection of **4** followed by per-*O*-sulfation [33] gave the compound **OS4**.

Influence of different structural features of fucoidans on blood coagulation

Poly- and oligosaccharides described above were assessed on anticoagulant activity in different in vitro experiments. General clotting assays were performed as described previously [18] with the use of normal plasma, which was incubated with the samples. Commercially available low-molecular-weight heparin Clexane® (enoxaparin) was chosen as a reference, because this polysaccharide is intensively used in medical practice as heparinoid anticoagulant with low risk of side effects [34, 35].

The influence of the samples on the intrinsic pathway of coagulation was evaluated in the activated partial thromboplastin time (APTT) assays. The dose-depended changes in the APTT value are shown on Fig. 5, and the values 2APTT (the concentration of a sample, at which double increasing of control value of APTT is observed) are presented in Table 2.

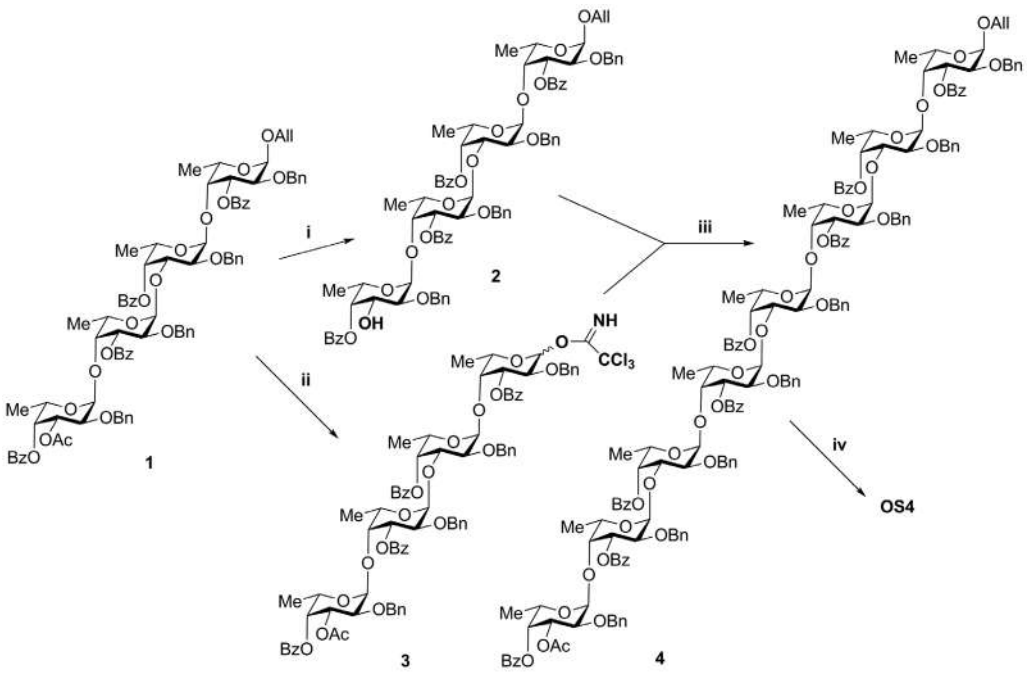

Scheme 4 The fragment of the convergent synthesis of the octasaccharide **OS4**. Regents and conditions: (i) HCl, MeOH; (ii) a) $PdCl_2$, MeOH, b) CCl_3CN, Cs_2CO_3; (iii) TMSOTf, −30 °C, CH_2Cl_2; (iv) a) H_2, Pd/C, b) MeONa, MeOH, c) Py·SO_3, DMF, HSO_3Cl, d) $NaHCO_3$, Amberlite IR-120 (Na^+).

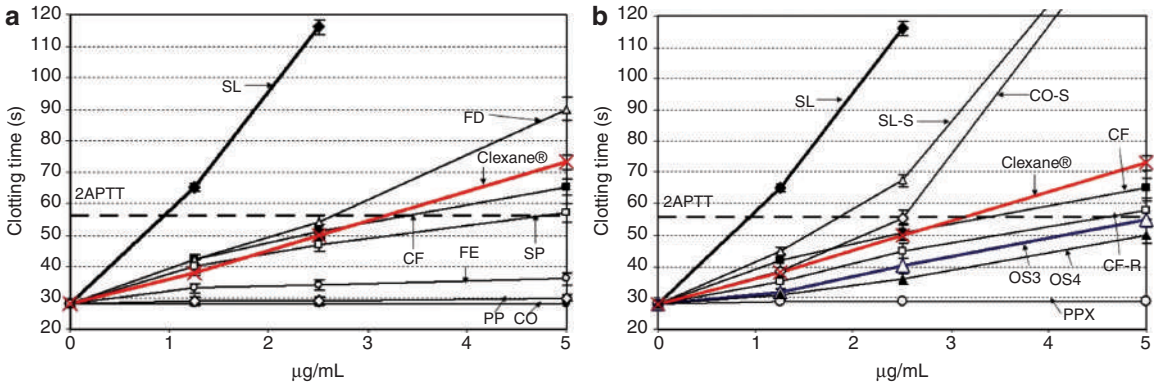

Fig. 5 Anticoagulant activity of the fucoidans, their chemically modified derivatives, the synthetic octasaccharides **OS3**, **OS4**, and the heparinoid Clexane® measured by APTT assay, n = 4, $p < 0.05$.

The biological effect was shown to depend on structural features of the tested sample. Among the parent fucoidans (Fig. 5a), the samples **SL** and **FD** demonstrated high level of activity, even exceeding that for Clexane®. The values 2APTT for **SL** and **FD** were ~1.1 μg/mL and ~2.8 μg/mL, respectively, while this value for Clexane® was ~3.3 μg/mL. Slightly lower effects were detected for CF and SP (2APTT were ~3.5 μg/mL and ~4.9 μg/mL, respectively). Moderate activity was shown for FE (~25.1 μg/mL), while the polysaccharides **CO** and **PP** were inactive even at a concentration of 100 μg/mL.

Chemical sulfation of the fucoidans **CO** and **SL** changed their properties. Thus, per-*O*-sulfation of the inactive fucoidan **CO** gave the product **CO-S** (DS is 2.0, Table 1) with pronounced anticoagulant effect. This sample prolonged blood coagulation by 2 times at a concentration of ~2.5 μg/mL. An opposite situation was

Table 2 2APTT and 2TT values for the compounds studied.

Sample	2APTT (μg/mL)	2TT (μg/mL)
SL	1.07 ± 0.05	2.43 ± 0.05
CF	3.45 ± 0.05	4.75 ± 0.06
CO	ND[a]	ND
PP	ND	ND
FE	25.05 ± 0.20	ND
FD	2.75 ± 0.09	3.40 ± 0.06
SP	4.90 ± 0.07	31.02 ± 0.15
SL-S	1.90 ± 0.05	2.20 ± 0.07
CO-S	2.51 ± 0.09	4.28 ± 0.07
CF-R	4.85 ± 0.05	18.21 ± 0.21
PPX	ND	ND
OS3	5.01 ± 0.12	16.08 ± 0.23
OS4	7.50 ± 0.11	17.11 ± 0.31
Clexane®	3.32 ± 0.12	2.25 ± 0.03

[a]Not detected at a range of concentrations 0.059–59.0 μg/mL.

observed in the case of the samples **SL** and **SL-S**. Additional introduction of sulfates into a structure of SL led to a slight decrease in the anticoagulant effect, however, the sample **SL-S** (2APTT ~1.9 μg/mL) was slightly more active than **CO-S** (Fig. 5b).

Reduction of caboxyl groups in a structure of **CF** gave the polysaccharide **CF-R**, which was less active than the parent fucoidan (2APTT were 3.5 μg/mL and 4.9 μg/mL for **CF** and **CF-R**, respectively). Dexylosylation of the sample **PP** did not influence on the anticoagulant properties of the polysaccharide. The preparation **PPX** was inactive similarly to **PP**.

Among the synthetic oligosaccharides only the per-*O*-sulfated octasaccharides **OS3** and **OS4** deserved attention because of moderate anticoagulant effect (2APTT were 5.0 μg/mL and 7.5 μg/mL for **OS3** and **OS4**, respectively). Notably, **OS3** built up of (1 → 3)-linked α-L-fucopyranosyl residues was more active, than its isomer **OS4** consisted of alternating (1 → 3)- and (1 → 4)-linked α-L-fucosyl units. Neither the per-*O*-sulfated tetrasaccharides **OS1** and **OS5**, nor the selectively 2-*O*-sulfated octasaccharide **OS2** demonstrated anticoagulant properties (data not shown).

The influence of the samples on thrombin-induced clot formation was also investigated. The values of 2TT (the concentration of a sample, at which double increasing of control value of TT was observed) are presented in Table 2. High level of activity was determined for **SL**, **CF**, **SL-S**, **FD**, **CO-S** (2TT 2.2–4.75 μg/mL), which was comparable with the effect of Clexane® (2TT ~2.2 μg/mL). Moderate effect was observed for the octasaccharides **OS3** and **OS4**, as well as for the polysaccharide **CF-R** (2TT 16.1–18.2 μg/mL). The fucoidan **SP** showed low anticoagulant activity, while **CO**, **PP**, **FE** and **PPX** were inactive in this test.

To investigate further the mechanism of anticoagulant action of the fucoidans and their derivatives, the experiments with purified proteins have been performed. These studies were based on the assay of amidolytic activity of thrombin (IIa) or factor Xa using chromogenic substrates, as described previously [18]. The ability of the samples to inhibit thrombin and factor Xa was assessed in the presence and in the absence of antithrombin III (ATIII). The results are shown on Fig. 6 and in Table 3.

Effectiveness of binding to thrombin in the presence of ATIII was high for the samples **SL**, **CF**, **FD**, **SL-S**, and **CO-S** (IC_{50} 0.4–0.9 μg/mL), which was similar to Clexane® activity (IC_{50} 0.6 μg/mL). These polysaccharides are enriched in 2,4-di-*O*-sulfated fucosyl residues, which was previously shown to be essential for the anticoagulant activity [2, 7]. Branched polysaccharides from this series, namely **SL**, **SL-S**, **CO-S** and **CF**, bear negatively charged group (sulfate or carboxyl) at a branch fragment. It is remarkable, that the preparation **CF-R** with non-charged glucosyl units as branches demonstrated low anti-IIa activity (IC_{50} 41.3 μg/mL). The polysaccharide **SP** containing sulfate groups at *O*-4 showed moderate effect (IC_{50} 6.5 μg/mL), while the 2-*O*-sulfated fucoidan **FE** with the same degree of sulfation (1.0, Table 1) was inactive in this test.

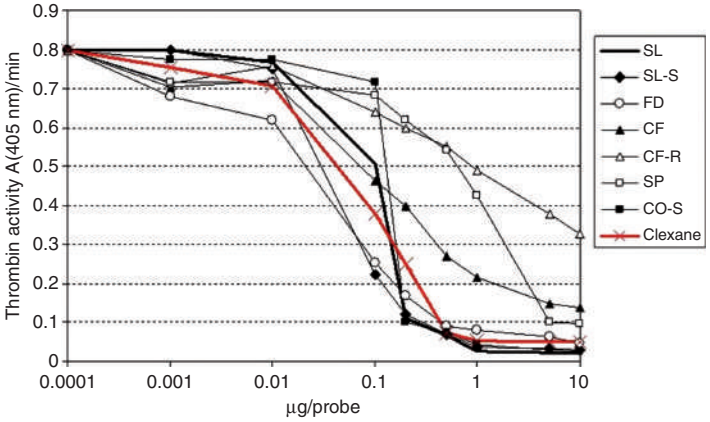

Fig. 6 Effect of the samples on thrombin inactivation in the presence of ATIII.

Table 3 Inhibition of thrombin and factor Xa.

Sample	IC_{50} (µg/mL)		
	ATIII + thrombin	**+ thrombin**	**ATIII + Xa**
SL	0.76 ± 0.04	45.86 ± 0.58	1.06 ± 0.04
CF	0.83 ± 0.02	ND[a]	ND
CO	ND	ND	ND
PP	ND	ND	ND
FE	ND	ND	ND
FD	0.40 ± 0.01	ND	10.06 ± 0.13 9
SP	6.50 ± 0.10	ND	ND
SL-S	0.47 ± 0.02	55.86 ± 1.07	1.94 ± 0.08
CO-S	0.88 ± 0.03	58.81 ± 1.12	2.06 ± 0.09
CF-R	41.30 ± 0.51	ND	ND
PPX	ND	ND	ND
OS3	ND	ND	12.94 ± 0.98
OS4	ND	ND	ND
Clexane®	0.59 ± 0.02	ND	0.059 ± 0.001

[a]Not detected at a range of concentrations 0.059–59.0 µg/mL.

Opposed to the polymeric compounds with the same backbone, the octasaccharides **OS3** and **OS4** showed no anti-IIa activity in the presence of ATIII. It could be connected with insufficient chain length, because it was established earlier [36–38] that at least 16 monosaccharide units in the chain of the heparinoid structure are required for the formation of a ternary complex with thrombin and ATIII.

The fucoidans **CO**, **PP**, and **PPX** with low degree of sulfation (0.4–0.7, Table 1) were inactive in all tested concentrations. On the contrary, three of the tested samples, namely **SL**, **SL-S**, and **CO-S**, were found to bind with thrombin in the absence of ATIII (Table 3). However, higher concentrations of the polysaccharides were required for this test. Thus, the samples **SL**, **SL-S**, and **CO-S** showed 50 % inhibition at concentrations of ~45.9, ~55.9, and ~58.9 µg/mL, respectively.

The polysaccharides **SL**, **SL-S**, and **CO-S** efficiently bind to factor Xa only in the presence of ATIII (the values of IC_{50} were ~1.1, ~1.9, and ~2.0 µg/mL, respectively), but their activity was significantly lower than that for heparinoid Clexane® (the value of IC_{50} was ~0.059 µg/mL). The linear fucoidan **FD** consisted of alternating (1 → 3)- and (1 → 4)-linked α-L-fucosyl units was less active than branched polysaccharides **SL**, **SL-S**, and **CO-S** built up of (1 → 3)-linked α-L-fucopyranosyl residues. Surprisingly, the synthetic per-*O*-sulfated octasaccharide OS3 demonstrated moderate anti-Xa activity in the presence of ATIII (IC_{50} were ~13.0 µg/mL). Neither fucoidans, nor heparinoids bind to factor Xa in the absence of ATIII (data not shown).

The trends found in amidolytic experiments (see Table 3 and Fig. 6 showing anti-IIa and anti-Xa activities) for the studied samples correlated well with the results obtained in clotting assays. Thus, the polysaccharides **SL**, **FD**, **CF**, **SL-S**, and **CO-S** enriched in 2,4-di-*O*-sulfated (1 → 3)-linked α-L-fucose units demonstrated high effects in clotting assays and also possessed significant anti-IIa activity. These results are in a good correlation with the data obtained previously for linear highly sulfated fucans from invertebrates [2, 7]. Moreover, it is noticeable that inhibition of thrombin by the polysaccharides **SL**, **SL-S**, and **CO-S** was performed both in the presence and in the absence of ATIII, which coincides well with the published data for other branched fucoidans from brown seaweeds [12, 13]. Additionally, the samples **SL**, **SL-S**, and **CO-S** demonstrated significant anti-Xa activity. The synthetic per-*O*-sulfated octasaccharide **OS3**, which was structurally related to the polysaccharides **SL**, **SL-S**, and **CO-S**, possessed a moderate effect on clot formation connected mainly with its moderate anti-Xa activity.

Conclusion

Fucoidans isolated from different brown seaweed species vary in monosaccharide content, types of glycoside bonds, degree and pattern of sulfation, presence of branches, and molecular weight. The effect of fucoidans on blood coagulation was shown to depend on their structural features. Thus, the polysaccharides **SL**, **CF**, **FD**, **SL-S**, and **CO-S** enriched in 2,4-di-*O*-sulfated (1 → 3)-linked α-L-fucose units demonstrated high effect in clotting assays. The polysaccharides **CO**, **PP**, **PPX** with the (1 → 3)-linked α-L-fucose backbone with degree of sulfation 0.4–0.7 did not influence on blood coagulation, and this behaviour could be explained by the absence of a sufficient amount of sulfate groups in their structure. The trends found in clotting assays correlated well with the results obtained in experiments with individual proteins. High anti-IIa activity was shown for the samples **SL**, **CF**, **FD**, **SL-S**, and **CO-S** in the presence of ATIII, while **CO**, **PP**, **PPX** were inactive. It is noticeable that the branched polysaccharides **SL**, **SL-S**, **CO-S** were also shown to be direct thrombin inhibitors and, hence, they differ from heparinoids and linear fucans from invertebrates. Additionally **SL**, **SL-S**, and **CO-S** demonstrated significant anti-Xa activity. The synthetic per-*O*-sulfated octasaccharide **OS3**, which was structurally related to the polysaccharides **SL**, **SL-S**, and **CO-S**, possessed a moderate effect on clot formation connected mainly with its moderate anti-Xa activity. This result indicated that longer and probably branched fucoidan fragments are required for the efficient inhibition of blood coagulation.

Acknowledgments: This work was supported in part by the Russian Foundation for Basic Research (grants 12-04-01749, 12-03-92703, 13-03-91170, KOMFI-grant 13-04-40315-K and its parts 13-04-40313-H, 13-04-40314-H, and 13-04-40315-H).

Funding: Russian Foundation for Basic Research, (Grant/Award Number: 12-04-01749, 12-03-92703, 13-04-40313-H, 13-03-91170, KOMFI-grant 13-04-40315-K, 13-04-40314-H, 13-04-40315-H).

References

[1] V. H. Pomin. *Biochim. Biophys. Acta* **1820**, 1971 (2012).
[2] M. S. Pereira, F. R. Melo, P. A. Mourão. *Glycobiology* **12**, 573 (2002).
[3] F. R. Melo, M. S. Pereira, D. Foguel, P. A. Mourão. *J. Biol. Chem.* **279**, 20824 (2004).
[4] G. Jiao, G. Yu, J. Zhang, S. Ewart. *Mar. Drugs* **9**, 196 (2011).
[5] M. Ciancia, I. Quintana, A. S. Cerezo. *Curr. Med. Chem*. **17**, 2503 (2010).
[6] P. V. Fernandez, I. Quintana, A. S. Cerezo, J. J. Caramelo, L. Pol-Fachin, H. Verli, J. M. Estevez, M. Ciancia. *J. Biol. Chem.* **288**, 223 (2013).
[7] R. J. Fonseca, G. R. Santos, P. A. Mourão. *Thromb. Haemost*. **102**, 829 (2009).
[8] J. H. Fitton. *Mar. Drugs* **9**, 1731 (2011).
[9] M. T. Ale, J. D. Mikkelsen, A. S. Meyer. *Mar. Drugs* **9**, 2106 (2011).

[10] A. Cumashi, N. A. Ushakova, M. E. Preobrazhenskaya, A. D'Incecco, A. Piccoli, L. Totani, N. Tinari, G. E. Morozevich, A. E. Berman, M. I. Bilan, A. I. Usov, N. E. Ustuzhanina, A. A. Grachev, C. J. Sanderson, M. Kelly, G. A. Rabinovich, S. Iacobelli, N. E. Nifantiev. *Glycobiology* **17**, 541 (2007).
[11] A. I. Usov, M. I. Bilan. *Russ. Chem. Rev*. **78**, 785 (2009).
[12] M. S. Pereira, B. Mulloy, P. A. Mourão. *J. Biol. Chem.* **274**, 7656 (1999).
[13] N. A. Ushakova, G. E. Morozevich, N. E. Ustyuzhanina, M. I. Bilan, A. I. Usov, N. E. Nifantiev, M. E. Preobrazhenskaya. *Biomed. Chem*. **3**, 77 (2009).
[14] D. O. Croci, A. Cumashi, N. A. Ushakova, M. E. Preobrazhenskaya, A. Piccoli, L. Totani, N. E. Ustyuzhanina, M. I. Bilan, A. I. Usov, A. A. Grachev, G. E. Morozevich, A. E. Berman, C. J. Sanderson, M. Kelly, P. Di Gregorio, C. Rossi, N. Tinari, S. Iacobelli, G. A. Rabinovich, N. E. Nifantiev. *PLoS One* **6**, e17283 (2011).
[15] T. Nishino, T. Nagumo. *Carbohydr. Res.* **214**, 193 (1991).
[16] F. Haroun-Bouhedja, M. Ellouali, C. Sinquin, C. Boisson-Vidal. *Thromb. Res.* **100**, 453 (2000).
[17] V. H. Pomin, M. S. Pereira, A. P. Valente, D. M. Tollefsen, M. S. G. Pavao, P. A. S. Mourão. *Glycobiology* **15**, 369 (2005).
[18] N. E. Ustyuzhanina, N. A. Ushakova, K. A. Zyuzina, M. I. Bilan, A. L. Elizarova, O. V. Somonova, A. V. Madzhuga, V. B. Krylov, M. E. Preobrazhenskaya, A. I. Usov, M. V. Kiselevskiy, N. E. Nifantiev. *Mar. Drugs* **11**, 2444 (2013).
[19] N. P. Chandia, B. Matsuhiro. *Int. J. Biol. Macromol*. **42**, 235 (2008).
[20] M. I. Bilan, A. A. Grachev, A. S. Shashkov, M. Kelly, C. J. Sanderson, N. E. Nifantiev, A. I. Usov. *Carbohydr. Res*. **345**, 2038 (2010).
[21] M. I. Bilan, E. V. Vinogradova, E. A. Tsvetkova, A. A. Grachev, A. S. Shashkov, N. E. Nifantiev, A. I. Usov. *Carbohydr. Res.* **343**, 2605 (2008).
[22] M. Nagaoka, H. Shibata, I. Kimura-Takagi, S. Hashimoto, K. Kimura, T. Makino, R. Aiyama, S. Ueyama, T. Yokokura. *Glycoconj. J*. **16**, 19 (1999).
[23] M. I. Bilan, A. S. Shashkov, A. I. Usov. *Carbohydr. Res*., **393**, 1 (2014).
[24] M. I. Bilan, A. A. Grachev, N. E. Ustuzhanina, A. S. Shashkov, N. E. Nifantiev, A. I. Usov. *Carbohydr. Res*. **337**, 719 (2002).
[25] M. I. Bilan, A. A. Grachev, N. E. Ustuzhanina, A. S. Shashkov, N.E. Nifantiev, A. I. Usov. *Carbohydr. Res*. **339**, 511 (2004).
[26] M. I. Bilan, A. A. Grachev, A. S. Shashkov, T. T. T. Thanh, V. T. T. Tran, L. M. Bui, N. E. Nifantiev, A. I. Usov. *Carbohydr. Res*. **377**, 48 (2013).
[27] N. E. Ustyuzhanina, V. B. Krylov, A. A. Grachev, A. G. Gerbst, N. E. Nifantiev. *Synthesis* **23**, 4017 (2006).
[28] V. B. Krylov, Z. M. Kaskova, D. Z. Vinnitskiy, N. E. Ustyuzhanina, A. A. Grachev, A. O. Chizhov, N. E. Nifantiev. *Carbohydr. Res.* **346**, 540 (2011).
[29] N. E. Ustyuzhanina, V. B. Krylov, A. I. Usov, N. E. Nifantiev. In *Progress in the Synthesis of Complex Carbohydrate Chains of Plant and Microbial Polysaccharides*, N. E. Nifantiev, (Ed.), pp. 131–154, Transworld Research Network, Kerala, India (2009).
[30] A. G. Gerbst, N. E. Ustuzhanina, A. A. Grachev, D. E. Tsvetkov, E. A. Khatuntseva, D. M. Whitefield, A. Berces, N. E. Nifantiev. *J. Carbohydr. Chem.*, **20**, 821 (2001).
[31] A. G. Gerbst, N. E. Ustuzhanina, A. A. Grachev, D. E. Tsvetkov, E. A. Khatuntseva, A. S. Shashkov, A. I. Usov, M. E. Preobrazhenskaya, N. A. Ushakova, N. E. Nifantiev. *J. Carbohydr. Chem.* **22**, 109 (2003).
[32] E. A. Khatuntseva, N. E. Ustuzhanina, G. V. Zatonskii, A. S. Shashkov, A. I. Usov, N. E. Nifant'ev. *J. Carbohydr. Chem.* **19**, 1151 (2000).
[33] V. B. Krylov, N. E. Ustyuzhanina, A. A. Grachev, N. E. Nifantiev. *Tetrahedron Lett.* **49**, 5877 (2008).
[34] L. J. McGarry, D. Thompson, *Clin. Ther.* **26**, 419 (2004).
[35] D. M. Sobieraj, C. I. Coleman, V. Tongbram, W. Chen, J. Colby, S. Lee, J. Kluger, S. Makanji, A. Ashaye, C. M. White. *Pharmacotherapy* **32**, 799 (2012).
[36] E. Gray, J. Hogwood, B. Mulloy. *Handb. Exp. Pharmacol*. **207**, 43 (2012).
[37] A. Imberty, H. Lortat-Jacob, S. Perez. *Carbohydr. Res.* **342**, 430 (2007).
[38] M. Petitou, B. Casu, U. Lindahl. *Biochimie* **85**, 83 (2003).

Tetrahedron Letters 49 (2008) 5877–5879

Contents lists available at ScienceDirect

Tetrahedron Letters

journal homepage: www.elsevier.com/locate/tetlet

Efficient acid-promoted per-O-sulfation of organic polyols

Vadim B. Krylov, Nadezhda E. Ustyuzhanina, Alexey A. Grachev, Nikolay E. Nifantiev *

N.D. Zelinsky Institute of Organic Chemistry, Russian Academy of Sciences, Leninsky prospect 47, 119991 Moscow B-334, Russia

ARTICLE INFO

Article history:
Received 2 June 2008
Revised 11 July 2008
Accepted 23 July 2008
Available online 29 July 2008

This paper is dedicated to Professor Genrikh A. Tolstikov on the occasion of his 75th birthday

Keywords:
Sulfation
Carbohydrates
Lignans
Flavonoids
Cyclitols

ABSTRACT

An efficient protocol for the preparation of per-O-sulfated organic compounds is reported. Sulfation of polyols with the $Et_3N{\cdot}SO_3$ complex in DMF in the presence of triflic acid allowed acceleration of the reaction at lower temperature. The efficiency of the developed protocol is demonstrated by the transformation of a series of organic polyols and phenols related to oligosaccharides, cyclitols, lignans and flavonoids.

The biological importance of poly-O-sulfated compounds necessitates the development of efficient methods for their preparation from the parent polyols. The most commonly used reagents for the synthesis of poly-O-sulfated derivatives include the complexes of sulfur trioxide with tertiary amines or amides, for example, $Et_3N{\cdot}SO_3$, $Py{\cdot}SO_3$ and $DMF{\cdot}SO_3$. These reagents were used in the syntheses of poly-O-sulfated organic compounds, particularly of heparin[1–3] and fucoidan[4–7] fragments, the anticancer drug PI-88,[8] oligo-O-sulfated flavonoid glycosides,[9] *myo*-inositol hexasulfate[10,11] and others.

O-Sulfation of organic compounds containing several OH-groups may require elongation of reaction times up to several days, increasing the temperature up to 95 °C and the use of a large excess of the sulfating complex. Thus, per-O-sulfation of carbohydrates with the complexes $Et_3N{\cdot}SO_3$ or $Py{\cdot}SO_3$ is usually carried out at 50–65 °C,[2,3,7,8] while $DMF{\cdot}SO_3$ appears to be more reactive

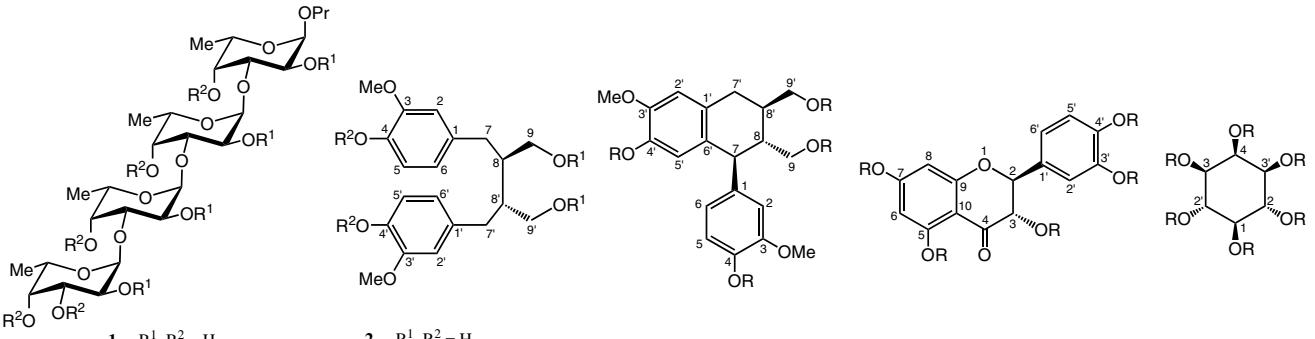

1 $R^1, R^2 = H$
1a $R^1 = SO_3Na, R^2 = H$
1b $R^1, R^2 = SO_3Na$

2 $R^1, R^2 = H$
2a $R^1 = SO_3Na, R^2 = H$
2b $R^1, R^2 = SO_3Na$

3 R = H
3a $R = SO_3Na$

4 R = H
4a $R = SO_3Na$

5 R = H
5a $R = SO_3Na$

Figure 1. Polyhydroxylated substrates **1**–**5** and their products of O-sulfation.

* Corresponding author. Tel./fax: +7 495 135 8784.
E-mail address: nen@ioc.ac.ru (N. E. Nifantiev).

0040-4039/$ - see front matter © 2008 Elsevier Ltd. All rights reserved.
doi:10.1016/j.tetlet.2008.07.135

and multiple sulfation with this reagent is performed at temperatures as low as −5 °C in good yield.[12] Also a rapid microwave-based protocol was developed for the synthesis of per-O-sulfated organic molecules.[13]

Herewith we report an improved protocol for the preparation of per-O-sulfated derivatives of polyhydroxy organic compounds, which was developed for the synthesis of highly sulfated fragments and analogues of natural polysaccharide fucoidans. These polysaccharides exhibit an interesting spectrum of important biological activities including anticoagulant, antiangiogenic and antimicrobial as well as the ability to inhibit selectin mediated inflammation.[14,15]

Our study towards the preparation of per-O-sulfated polyols was started with attempts to synthesize nonasulfate **1b** from tetrasaccharide **1** (Fig. 1).[6] Its selectively tetrasulfated derivative **1a** was recently obtained by us[6] via sulfation of the appropriate selectively substituted tetraol precursor with Py·SO_3 (5 equiv per OH-group) within 1 h in DMF at 20 °C. This protocol appeared to be inefficient for per-O-sulfation of tetrasaccharide **1** affording a mixture of partially O-sulfated products and only traces of target compound **1b** (Table 1, entry 1).

Treatment of **1** with Py·SO_3 in pyridine at elevated temperature, as was applied[7] for the per-O-sulfation of the β-octyl glycoside analogue of tetrasaccharide **1**, also produced a mixture of partially sulfated derivatives (entry 2). This result was probably connected with the low solubility of sulfated products and their precipitation from the reaction mixture. Application of DMF-Py (3:1 v/v) as a solvent system, which increases the solubility and prevents precipitation, resulted in the formation of a mixture of products with an increased degree of sulfation, but again no target completely sulfated compound **1b** was obtained (entry 3). Attempts at per-O-sulfation of **1** with Py·SO_3 in DMF were also unsuccessful (entry 4). In this case, the reaction was accompanied by cleavage of the glycoside bonds and gave a very complex mixture of products. Application of the complex $Et_3N·SO_3$ under the same conditions was free of degradation but not efficient enough to give persulfate **1b** (entry 5).

Surprisingly, we found that the addition of triflic acid (TfOH) to the reaction mixture significantly promoted O-sulfation with $Et_3N·SO_3$ and allowed the reaction to be run at 0 °C in a shorter time. This was demonstrated by NMR analysis of reaction mixtures obtained after sulfation of **1** using the $Et_3N·SO_3$ complex in DMF in the presence of different amounts of TfOH (Fig. 2) which varied from 0.3 to 1.6 equiv of TfOH per OH-group. The use of 1.6 equiv[16] of TfOH resulted in the clear formation of per-O-sulfated product **1b** (entry 6).

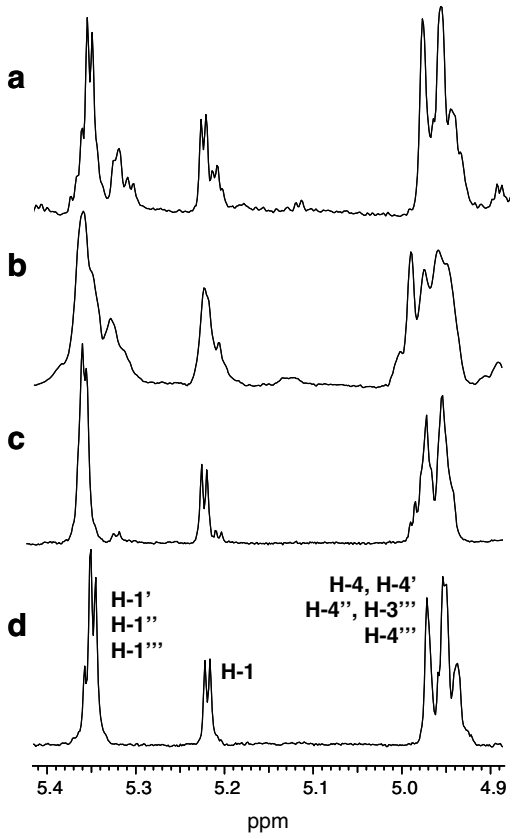

Figure 2. Anomeric regions in the ^1H NMR spectra of the products of O-sulfation of tetrasaccharide **1** by $Et_3N·SO_3$ (5 equiv/OH-group) in DMF in the absence (a) and in the presence of 0.3 (b), 1.0 (c) and 1.6 equiv (d, entry 6 in Table 1) of TfOH per OH-group.

We connect the effect of TfOH with its ability to liberate free SO_3 from the amine complex in situ, which is the most reactive sulfation agent. The TfOH promoted O-sulfation protocol was shown to be efficient for the sulfation of polyol substrates of other types. Thus, sulfation of the lignan secoisolariciresinol **2**[17] with the $SO_3·NEt_3$ complex in DMF at 0 °C in the absence of acid gave, in 40 min, selectively disulfated derivative **2a** (entry 7). Its exhaustive sulfation required both increasing the temperature up to 20 °C and elongation of the reaction time (24 h, entry 8), while per-O-sulfation in the presence of TfOH (1.0 equiv per OH-group, entry

Table 1
Per-O-sulfation of polyol substrates

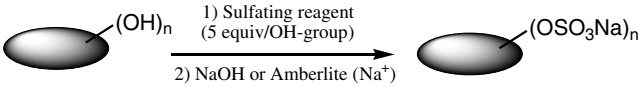

Entry	Polyol	Amount of TfOH, equiv/OH-group	Temperature (°C)	Reaction time	Sulfation agent	Reaction products	Yield (%)[14]
1	**1**	0	20	1 h	Py·SO_3, DMF	Mixture of partially sulfated products	—
2	**1**	0	55	72 h	Py·SO_3, Py	Mixture of partially sulfated products	—
3	**1**	0	55	72 h	Py·SO_3, DMF/Py (3:1 v/v)	Mixture of partially sulfated products	—
4	**1**	0	55	72 h	Py·SO_3, DMF	Mixture of partially sulfated and degradation products	—
5	**1**	0	55	72 h	$Et_3N·SO_3$, DMF	Mixture of partially sulfated products	—
6	**1**	1.6	0	24 h	$Et_3N·SO_3$, DMF	**1b**	77
7	**2**	0	0	40 min	$Et_3N·SO_3$, DMF	**2a**	57
8	**2**	0	20	24 h	$Et_3N·SO_3$, DMF	**2b**	81
9	**2**	1.0	0	90 min	$Et_3N·SO_3$, DMF	**2b**	75
10	**3**	1.0	0	90 min	$Et_3N·SO_3$, DMF	**3a**	53
11	**4**	1.0	0	24 h	$Et_3N·SO_3$, DMF	**4a**	60
12	**5**	1.6	0	24 h	$Et_3N·SO_3$, DMF	**5a**	61

9) was complete within 90 min at 0 °C. This protocol was also efficient for per-O-sulfation of isolariciresinol[17] **3** (entry 10), the flavonoid dihydroquercetin[17] **4** (entry 11) and cyclitol *myo*-inositol **5** (entry 12), and gave the corresponding per-O-sulfated products **3a**-**5a** in practical yields. The necessary amounts of TfOH to convert phenols **3** and **4** were determined by us within preliminary experiments. It should be noted that O-sulfation of flavonoid derivatives using the $SO_3{\cdot}NEt_3$ complex in dimethylacetamide at 65 °C was shown[9] to be inapplicable for exhaustive O-sulfation of all phenolic OH-groups. Compound **5a** was prepared previously by sulfation of *myo*-inositol with chlorosulfonic acid or oleum under heating (Fig. 1).[10,11]

In conclusion, an improved protocol for the synthesis of persulfated derivatives of polyols containing multiple alcoholic and phenolic OH-groups has been reported. The applicability of this method was demonstrated by the preparation of per-O-sulfated derivatives of polyols of interest for pharmacology investigations as well as examples related to lignans, flavonoids, cyclitols, and oligosaccharides.

Acknowledgements

This work was supported by the Russian Foundation for Basic Research (Grant 06-03-33080). We also thank Dr. Yu.E. Tsvetkov for critical reading of the manuscript and for helpful discussions.

References and notes

1. Petitou, M.; van Boeckel, C. A. A. *Angew. Chem., Int. Ed.* **2004**, *43*, 3118–3133.
2. Duchaussoy, P.; Jaurand, G.; Driguez, P.-A.; Lederman, I.; Gourvenec, F.; Srassel, J.-M.; Sizun, P.; Petitou, M.; Herbert, J.-M. *Carbohydr. Res.* **1999**, *317*, 85–99.
3. Petitou, M.; Imberty, A.; Duchaussoy, P.; Driguez, P.-A.; Ceccato, M.-L.; Gourvenec, F.; Sizun, P.; Hrault, J.-P.; Perez, S.; Herbert, J.-M. *Chem. Eur. J.* **2001**, *7*, 858–873.
4. Gerbst, A.; Ustyuzhanina, N.; Grachev, A.; Khatuntseva, E.; Tsvetkov, D.; Shashkov, A.; Usov, A.; Preobrazenskaya, M.; Ushakova, N.; Nifantiev, N. *J. Carbohydr. Chem.* **2003**, *22*, 109–122.
5. Gerbst, A.; Ustyuzhanina, N.; Grachev, A.; Zlotina, N.; Khatuntseva, E.; Tsvetkov, D.; Shashkov, A.; Usov, A.; Nifantiev, N. *J. Carbohydr. Chem.* **2002**, *21*, 313–324.
6. Ustyuzhanina, N.; Krylov, V.; Grachev, A.; Gerbst, A.; Nifantiev, N. *Synthesis* **2006**, *23*, 4017–4031.
7. Hua, Y.; Gu, G.; Du, Y. *Carbohydr. Res.* **2004**, *339*, 867–872.
8. Fairweather, J.; Hammond, E.; Johnstone, K.; Ferro, V. *Bioorg. Med. Chem.* **2008**, *16*, 699–709.
9. Correia-da-Silva, M.; Sousa, E.; Pinto, M.; Duarte, B.; Marques, F. *Abstracts of Papers*, 1st International Conference on Drug Design and Discovery, Dubai, UAE, Feb 4–7, 2008; p 31.
10. Fatiadi, A. J. *Carbohydr. Res.* **1970**, *12*, 293–296.
11. Takahashi, N.; Egami, F. *Nippon Kagaku Zasshi* **1959**, *80*, 1364–1366.
12. Kuszmann, J.; Medgyes, G.; Boros, S. *Carbohydr. Res.* **2004**, *339*, 1569–1579.
13. Raghuraman, A.; Riaz, M.; Hindle, M.; Desai, U. R. *Tetrahedron Lett.* **2007**, *48*, 6754–6758.
14. Berteau, O.; Mulloy, B. *Glycobiology* **2003**, *13*, 29R–40R.
15. Cumashi, A.; Ushakova, N.; Preobrazhenskaya, M.; D'Incecco, A.; Piccoli, A.; Totani, L.; Tinari, N.; Morozevich, G.; Berman, A.; Bilan, M.; Usov, A.; Ustyuzhanina, N.; Grachev, A.; Sanderson, C.; Kelly, M.; Rabinovich, G.; Iacobelli, S.; Nifantiev, N. *Glycobiology* **2007**, *17*, 541–552.
16. *General conditions for per-O-sulfation*: To a stirred solution of polyol (0.1 mmol) in DMF (5 ml) was added $SO_3{\cdot}NEt_3$ complex (5 equiv per OH). The reaction mixture was kept for 10 min at 0 °C, then the necessary amount of TfOH was added dropwise at −20 °C. The temperature was allowed to rise to 0 °C and the reaction mixture was stirred for the appropriate time and in the cases of **1a**, **2a**–**c** and **5a** was quenched with excess of 1 M aq NaOH. The aqueous phase was separated and washed with CH_2Cl_2 (2 × 1 ml), then loaded onto a Sephadex G-15 column (40 × 3 cm) and eluted with water; the fractions containing the product were combined and freeze-dried to give the persulfates as amorphous substances. Compounds **2a** and **2b** were recrystallized from EtOH to give pure compounds as white crystals. In the case of the preparation of **3a** and **4a**, the reaction mixture was quenched with excess Et_3N and MeOH, stirred for 30 min and concentrated at 30 °C. The residue was purified by flash column chromatography on silica gel 60 (40–63 μm, E. Merck) with elution by CH_2Cl_2: MeOH–Et_3N = 4:1:0.1, the fractions containing the target product were combined and concentrated at <30 °C. The residue was dissolved in water and treated with Amberlite IR-120 (Na^+) cation exchange resin for 2 h. The resin was filtered off, and the filtrate was concentrated to a volume of 1 mL, and then subjected to gel-permeation chromatography on a Sephadex G-15 gel column as described above for **1a** and **5a**. *Selected data of O-sulfated products*: *Compound* **1b**: $[\alpha]_D$ −107 (*c* 1, H_2O); ^1H NMR (500 MHz, D_2O): 5.41 (3H, s br, H-1′, H-1″, H-1‴), 5.24 (1H, d, H-1, $J_{1,2}$ = 3.4 Hz), 4.95–4.89 (5H, m, H-4, H-4′, H-4″, H-3‴, H-4‴), 4.59–4.50 (5H, m, H-2, H-2′, H-2″, H-2‴, H-5‴), 4.46–4.29 (5H, m, H-3, H-3′, H-5′, H-3″, H-5″), 4,23 (1H, q, H-5, $J_{5,6}$ = 6.7 Hz), 3.66 (1H, m, OC*H*H′), 3.58 (1H, m, OCH*H*′), 1.64 (2H, m, Pr), 1.36–1.30 (12H, m, 12 H-6), 0.93 (3H, t, Pr, *J* = 7.4 Hz); MS-ESI $C_{27}H_{39}Na_9O_{44}S_9$ $[M+H]^+$; calcd: 1562.746, found: 1562.740. *Compound* **2a**: $[\alpha]_D$ −30 (*c* 1, H_2O); ^1H NMR (500 MHz, D_2O): 6.76 (2H, d, *J* = 8.6 Hz, H-5), 6.62 (4H, s br, H-2, H-6), 4.21 (2H, dd, *J* = 5.1 Hz, *J* = 9.4 Hz, H-9a), 4.06 (2H, dd, *J* = 6.8 Hz, *J* = 10.2 Hz, H-9b), 3.70 (6H, s, CH_3), 2.72 (2H, dd, *J* = 5.1 Hz, *J* = 13.7 Hz, H-7a), 2.57 (2H, dd, *J* = 9.4 Hz, *J* = 13.7 Hz, H-7b), 2.07 (2H, m, H-8); ^{13}C NMR (125 MHz, D_2O): 149.2 (C-3), 145.9 (C-4), 133.3 (C-1), 123.7 (C-6), 116.8 (C-5), 114.5 (C-2), 70.6 (C-9), 57.1 (Me), 41.0 (C-8), 35.7 (C-7); MS-ESI $C_{20}H_{24}Na_2O_{12}S_2$ $[M+Na]^+$; calcd: 589.04, found: 589.04. *Compound* **2b**: $[\alpha]_D$ −19 (*c* 1, H_2O); ^1H NMR (500 MHz, D_2O): 7.29 (2H, d, *J* = 8.1 Hz, H-5), 6.83 (4H, m, H-2, H-6), 4.25 (2H, dd, *J* = 5.1 Hz, *J* = 10.3 Hz, H-9a), 4.13 (2H, dd, *J* = 5.9 Hz, *J* = 10.3 Hz, H-9b), 3.77 (6H, s, CH_3), 2.79 (4H, m, H-7), 2.16 (2H, m, H-8); ^{13}C NMR (125 MHz, D_2O): 151.0 (C-3), 139.5 (C-4), 138.2 (C-1), 122.3 (C-5), 121.9 (C-6), 113.8 (C-2), 68.9 (C-9), 55.9 (Me), 39.5 (C-8), 34.4 (C-7); MS-ESI $C_{20}H_{22}Na_4O_{18}S_4$ $[M+Na]^+$; calcd: 792.92, found: 792.92. *Compound* **3a**: $[\alpha]_D$ −7 (*c* 1, H_2O); ^1H NMR (500 MHz, D_2O): 7.37 (1H, d, *J* = 8.3 Hz, H-5), 7.02 (1H, s, H-2′), 6.99 (1H, s, H-2), 6.89 (1H, d, *J* = 8.3 Hz, H-6), 6.77 (1H, s, H-5′), 4.24 (2H, d, *J* = 4.6 Hz, H-9′), 4.18 (1H, d, *J* = 10.2 Hz, H-9a), 4.13 (1H, d, *J* = 10.6 Hz, H-7), 3.90–3.84 (7H, m, 2 CH_3, H-9b), 3.02 (2H, m, H-7′), 2.37 (1H, m, H-8′), 2.18 (1H, t, *J* = 10.2 Hz, H-8); ^{13}C NMR (125 MHz, D_2O): 152.7 (C-3′), 150.9 (C-3), 144.7 (C-6′), 140.2 (C-4′), 139.6 (C-4), 136.7, (C-1), 133.4 (C-1′), 125.1 (C-5′), 124.1 (C-5), 123.7 (C-6), 116.2 (C-2), 114.5 (C-2′), 71.71 (C-9′), 68.3 (C-9), 57.7 (Me), 57.6 (Me), 47.7 (C-7), 43.8 (C-8), 36.1 (C-8′), 33.3 (C-7′); MS-ESI $C_{20}H_{20}Na_4O_{18}S_4$ $[M+Na]^+$; calcd: 790.9, found: 790.8. **4a**: $[\alpha]_D$ 17 (*c* 1, H_2O); ^1H NMR (500 MHz, D_2O): 7.76 (1H, d, *J* = 1.9 Hz, H-2′), 7.62 (1H, d, *J* = 8.5 Hz, H-5′), 7.55 (1H, dd, *J* = 1.9 Hz, *J* = 8.5 Hz, H-6′), 7.20 (1H, d, *J* = 2.2 Hz, H-6), 7.00 (1H, d, *J* = 2.2 Hz, H-8), 5.68 (1H, d, *J* = 11.0 Hz, H-2), 5.44 (1H, d, *J* = 11.0 Hz, H-3); ^{13}C NMR (125 MHz, D_2O): 187.9 (C-4), 162.3 (C-9), 157.4 (C-7), 151.7 (C-5), 143.9 (C-3′), 142.9 (C-4′), 133.5 (C-1′), 126.1 (C-6′), 122.8 (C-2′), 122.7(C-5′), 110.5 (C-10), 108.7 (C-6), 106.9 (C-8), 80.8 (C-2), 77.6 (C-3); MS-ESI $C_{15}H_7Na_5O_{22}S_5$ $[M+Na]^+$; calcd: 836.7, found: 836.7. *Compound* **5a**: $[\alpha]_D$ 0 (*c* 1, H_2O); ^1H NMR (500 MHz, D_2O): 5.13 (1H, br s, H-4), 5.07 (2H, br s, H-2), 4.87 (2H, br s, H-3), 4.77 (1H, br s, H-1); ^{13}C NMR (125 MHz, D_2O): 76.1 (C-4), 75.8 (C-2, 2′), 75.1 (C-3, 3′), 74.5 (C-1). Anal. Calcd (%) for $C_6H_6Na_6O_{24}S_6{\cdot}5H_2O$: C, 8.17; H, 1.83; S, 21.80; Na, 15.63. Found: C, 8.41; H, 1.93; S, 21.63; Na, 15.72.
17. Nifantiev, N.E.; Yashunsky, D.V.; Menshov, V.M.; Tsvetkov, Y.E., Tsvetkov, D.E. PCT/RU2008/000176.

Carbohydrate Research 346 (2011) 540–550

Contents lists available at ScienceDirect

Carbohydrate Research

journal homepage: www.elsevier.com/locate/carres

Acid-promoted synthesis of per-O-sulfated fucooligosaccharides related to fucoidan fragments ☆

Vadim B. Krylov [a], Zinaida M. Kaskova [c], Dmitry Z. Vinnitskiy [c], Nadezhda E. Ustyuzhanina [a], Alexey A. Grachev [a], Alexander O. Chizhov [b], Nikolay E. Nifantiev [a,*]

[a] Laboratory of Glycoconjugate Chemistry, N.D. Zelinsky Institute of Organic Chemistry, Russian Academy of Sciences, Leninsky Prospect 47, 119991 Moscow, Russia
[b] Laboratory of NMR spectroscopy, N.D. Zelinsky Institute of Organic Chemistry, Russian Academy of Sciences, Leninsky Prospect 47, 119991 Moscow, Russia
[c] Higher Chemical College, Russian Academy of Sciences, Miusskaya sq. 9, 125047 Moscow, Russia

ARTICLE INFO

Article history:
Received 4 August 2010
Received in revised form 2 January 2011
Accepted 7 January 2011
Available online 15 January 2011

Keywords:
Fucoidans
Oligofucosides
O-Sulfation
Fucopyranoside
Fucofuranoside
Fucopyranoside-to-fucofuranoside rearrangement

ABSTRACT

The synthesis of per-O-sulfated derivatives of di-, tetra-, hexa-, octa-, dodeca-, and hexadecafucosides related to natural fucoidans of different types has been performed with the use of previously reported acid-promoted protocol for per-O-sulfation of polyols by SO_3 complexes.[2] During the treatment of (1→3)-linked oligofucosides under these conditions with the promotion by TfOH, the unusual rearrangement of the reducing pyranose residue into furanose one was observed. To avoid the formation of rearrangement by-products, the use of a series of strong acids as promoters of sulfation of large oligofucosides was studied and the improved protocol was developed based on the use of TFA instead of TfOH. The efficiency of the new method was demonstrated by the syntheses of per-O-sulfated derivatives of dodeca- and hexadecafucosides. The described method of O-sulfation opens access to the preparation of the oligosaccharides related to fucoidan fragments and their per-O-sulfated derivatives interesting for elucidation of the relationship between their structure and biological activity.

1. Introduction

Natural O-sulfated polysaccharides fucoidans from brown seaweeds and marine invertebrates exhibit a wide range of biological activities, including anticoagulant, antiangiogenic, and antimicrobial, as well as the ability to inhibit P- and L-Selectin mediated inflammation.[3–6] To determine the structure of pharmacophore fragments within the fucoidan chains, we carried out the systematic synthesis[1,7–12] (see Ref. 13 for review), conformational analysis,[8,10–12,14–16] and studies of biological activities of various oligofucosides related to natural fucoidans.

Highly sulfated oligofucosides represent special interest for biomedical investigations because of previous observations that chemically O-sulfated fucoidans exhibit enhanced anticoagulant activity and could be considered as a possible alternative to most widely used anticoagulant heparin.[6,17] The synthesis of highly and per-O-sulfated derivatives of large oligosaccharides still needs the development of preparative protocols. The known typical procedures (see Ref. 2 and papers cited therein) often result in the formation of complex mixtures of target products together with partly sulfated ones, which are difficult for preparative separation.

Recently we have described[2] the acid-promoted protocol to transform the oligosaccharides into their per-O-sulfated derivatives by the treatment with the SO_3 complexes in the presence of triflic acid (TfOH). In this communication we report the further optimization of the developed method and its application to the first synthesis of a series of per-O-sulfated derivatives of oligofucosides related to the main types of natural fucoidan chains (Scheme 1). The first series of the compounds consists of di-, tetra-, hexa-, octa-, dodeca-, and hexadecasaccharides **1b**–**6b** built up of (1→3)-linked α-L-fucopyranose residues, which correspond to polysaccharides isolated from seaweeds *Laminaria saccharina*[18,19] (new name *Saccharina latissima*[20]), *Chorda filum*,[21] and *Cladosiphon okamuranus*.[22] The second series of the compounds is presented by di-, tetra-, and hexasaccharides **7b**–**9b** built up of alternating (1→3)- and (1→4)-linked α-L-fucopyranose residues related to fucoidans from *F. evanescens*,[23] *F. distihus*,[24] and *Ascophyllum nodosum*.[25] In addition, the synthesis of per-O-sulfated trisaccharide **10b** consisted only from (1→4)-linked α-L-fucopyranose residues like in the fucoidan from *L. cichorioides* seaweed was reported and turned out to be highly sulfated and containing ca. 2 sulfo groups per fucose unit.[26] Similar fucan was also isolated from *Arabacia lixula* sea urchin.[27] Finally, disaccharides **11b** and **12b**, bearing (1→2)-linked α-L-fucopyranosyl and α-D-glucuronyl units and representing the branch points of fucoidans from

☆ Synthesis, NMR, and conformational studies of fucoidan fragments. Part 11. For Part 10, see Ref. 1.

* Corresponding author. Tel./fax: +7 499 135 8784.
E-mail address: nen@ioc.ac.ru (N.E. Nifantiev).

0008-6215/$ - see front matter © 2011 Elsevier Ltd. All rights reserved.
doi:10.1016/j.carres.2011.01.005

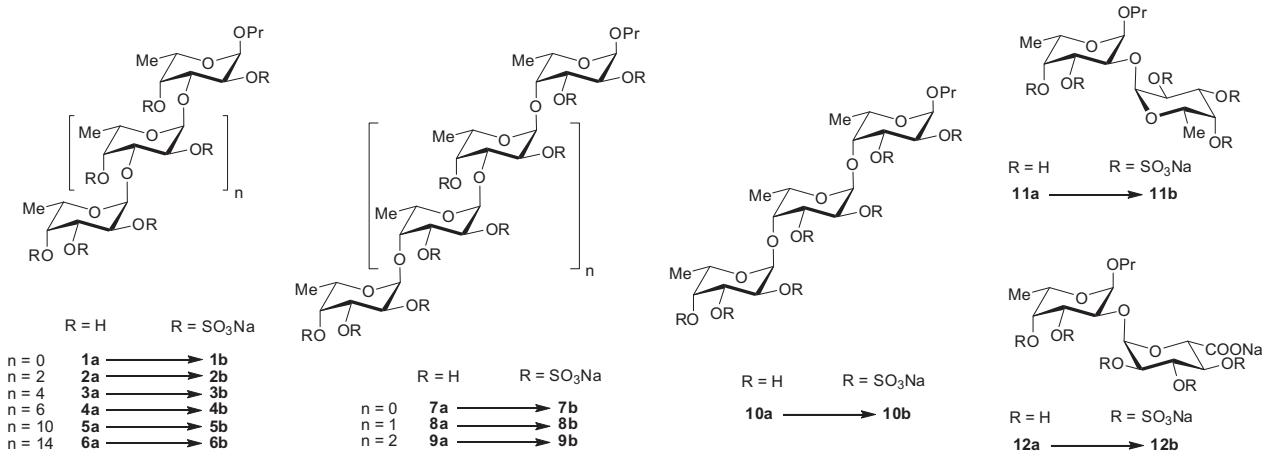

Scheme 1. Target per-O-sulfated oligosaccharides **1b**–**12b** and their precursors **1a**–**12a**.

L. saccharina[18,19] and *C. okamuranus*,[22] respectively, have also been reported.

2. Results and discussion

2.1. Synthesis of oligosaccharide substrates for per-O-sulfation studies

The synthesis of target oligosaccharides **1b**–**12b** was performed from the corresponding parent non-sulfated compounds **1a**–**12a**. Highly stereoselective syntheses of disaccharides **1a**, **7a**, **11a**, and **12a**, tetrasaccharides **2a** and **8a**, hexasaccharides **3a** and **9a**, and octasaccharide **4a** were reported in our previous communications.[1,7,24]

The synthesis of dodeca- and hexadecasaccharides **5a** and **6a** was performed from the protected precursors **13**,[28] **17**,[7] and **19**[7] (Scheme 2) according to the main procedures, which were previously used by us for the synthesis of oligofucosides.[7] Thus, monosaccharide **13**[28] was subjected to 3-O-chloroacetylation followed by bromination with *N*-bromosuccinimide (NBS) and hydrolysis in aq acetone[29] followed by the subsequent treatment with CCl_3CN to give trichloroacetimidate **14** in a overall yield of 72% (Scheme 3). The TMSOTf-catalyzed glycosylation of **13** with **14** was performed at −90 °C and gave disaccharide **15** in a moderate yield of 66%. Low temperature allowed us to increase the selectivity of the reaction and to minimize the formation of the by-product resulted from the undesirable SEt-transfer (not shown). The obtained product **15** was then transformed into acceptor **16** by the selective removal of the chloroacetyl group with NH_2CSNH_2 and 2,4,6-collidine in methanol at 60 °C with an almost quantitative yield. Coupling of disaccharides **16** and **17** was performed as described for the synthesis of compound **15** and afforded tetrasaccharide donor **18** in a yield of 55%.

The acidic methanolysis of previously obtained **19**[7] afforded octasaccharide acceptor **20**, which was further glycosylated by donor **18** to give dodecasaccharide **21** in a yield of 69%. This product was subjected to the catalytic hydrogenolysis and reduction of the allyl group into the propyl one followed by the saponification of the benzoyl and acetyl groups. Additional hydrogenolysis of the obtained product was performed to remove the residual benzyl groups, which remained in a low extent as the result of low solubility of partly debenzylated intermediates under the hydrogenolysis conditions. Finally, deprotected dodecasaccharide **5a** was obtained in a total yield of 61%.

For the synthesis of hexadecasaccharide **6a**, the O-acetyl group in dodecasaccharide **21** was selectively removed by acidic methanolysis to form acceptor **22** (72%). Its glycosylation by donor **18** in the presence of NIS-TMSOTf gave the substituted hexadecasaccharide **23** in a yield of 74%. The removal of all protective groups in **23** together with the reduction of the allyl group into the propyl one was performed as described for the preparation of dodecasaccharide **5a** to give hexadecasaccharide **6a** in a total yield of 54%.

The synthesis of trisaccharide **10a** was performed from previously reported monosaccharide acceptor **24** and disaccharide donor **25** (Scheme 3).[7] Coupling of **24** and **25** in the presence of TMSOTf yielded trisaccharide **26**, which was then subjected to hydrogenolysis and subsequent saponification to give trifucoside **10a**.

2.2. Synthesis of per-O-sulfated oligosaccharides 1b–12b

Preparation of per-O-sulfated disaccharides **1b** and **11b** from the corresponding unprotected compounds **1a** and **11a** was reported to be efficient under the treatment with the $Py{\cdot}SO_3$ complex in DMF at room temperature.[14] The same conditions were shown to be inapplicable for per-O-sulfation of tetrasaccharide **2a** and resulted in the formation only of a mixture of partially sulfated derivatives.[2] The temperature increase and the variation of the solvents and sulfation reagents afforded no per-O-sulfated tetrasaccharide **2b**.[2]

Recently, we reported a new protocol for the per-O-sulfation of polyols of different types with the use of the complex $Et_3N{\cdot}SO_3$ (5.0 equiv per OH group) in DMF at 0 °C in the presence of TfOH (1.0–1.6 equiv per OH group).[2] The addition of strong acid to the reaction mixture was assumed to deliberate unbound SO_3 and facilitate the per-O-sulfation of polyols. In particular, we demonstrated that linear tetrafucoside **2a** can be transformed into per-O-sulfated derivative **2b** in a good yield.[2] In continuation of this work, we studied the acid-promoted per-O-sulfation of larger oligosaccharides (**3a–6a**).

Contrary to the result of the per-O-sulfation of disaccharide **1a** (Table 1, entry 1, see also Fig. 1) and tetrasaccharide **2a**,[2] a similar reaction with hexa- and octasaccharides resulted in the formation of a mixture of partly O-sulfated products. Our attempts to use a larger amount of an acidic promoter gave rise to the formation of an unexpected product with the unusual set of signals in ^1H and ^{13}C NMR spectra. To assess its structure, the sulfation of di-(**1a**) and tetrasaccharide **2a** in the presence of a larger amount of TfOH were studied further.

Thus, the treatment of **1a** in the presence of TfOH in an amount of 2 equiv per OH group resulted in the formation of a 3.2:1 mixture of two disaccharide products **1b** and **27** (Scheme 4 and

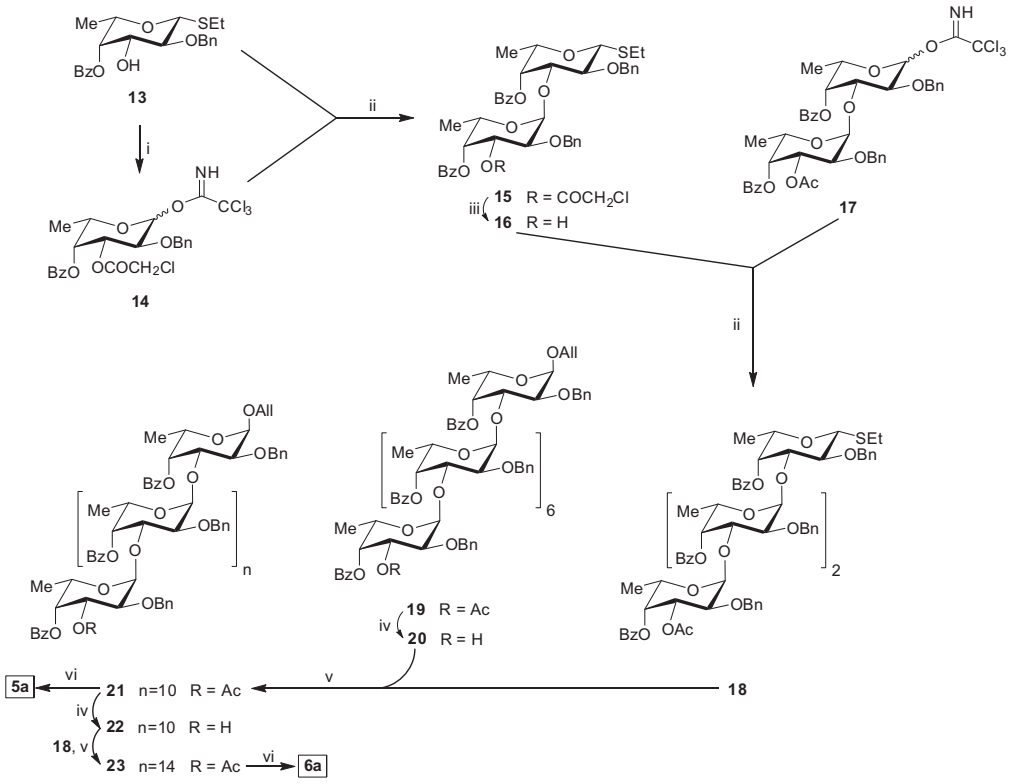

Scheme 2. Synthesis of dodeca- and hexadecasaccharides **5a** and **6a**. Reagents and conditions: (i) (1) $CH_2ClCOCl$, Py, CH_2Cl_2; (2) NBS, acetone–water; (3) CCl_3CN, DBU, CH_2Cl_2, −40 °C, 2 h, 72%; (ii) TMSOTf, −90 °C, 1 h, 66% for **15** and 55% for **18**; (iii) NH_2CSNH_2, 2,4,6-collidine, MeOH, 60 °C, 24 h, 94%, (iv) HCl, MeOH, 20 °C, 6 h, 76% for **20**, 72% for **22**; (v) NIS, TfOH, CH_2Cl_2, −40 °C, 2 h, 69% for **21** and 74% for **23**; (vi) (1) H_2, Pd/C, THF–EtOH–AcOH, 20 °C, 5 h, (2) NaOH, CH_2Cl_2–EtOH–H_2O, 60 °C, 12 h; (3) H_2, Pd/C, MeOH–AcOH, 20 °C, 5 h, 61% for **5a** and 54% for **6a**.

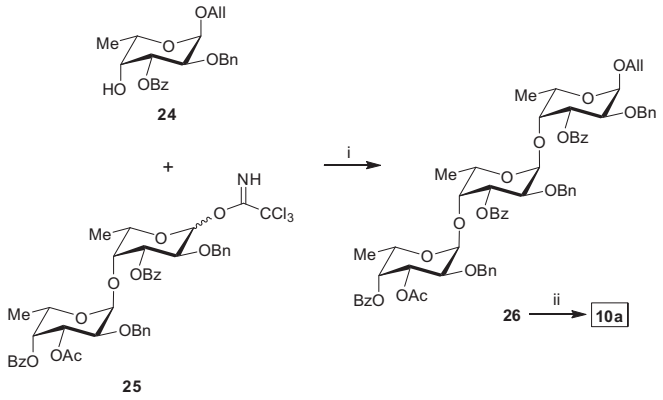

Scheme 3. Synthesis of trifucoside **10a**. Reagents and conditions: (i) TMSOTf, −40 °C, 3 h, 77%; (ii) (1) H_2, Pd/C, MeOH–EtOAc, 20 °C, 5 h, (2) NaOH, MeOH–H_2O, 20 °C, 24 h, 75%.

Table 1
Acid-promoted sulfation of disaccharide **1a** by $Et_3N{\cdot}SO_3$ (5 equiv per OH group) in DMF at 0 °C and formation of side product **27**

Entry	Amount of acid (equiv per OH group)	Time (h)	Products	Yield (%)
1	1.0	24	**1b**	77
2	2.0	24	**1b**:**27** = 3.1:1	82
3	2.0	186	**1b**:**27** = 1:2.3 + decomposition	

Table 1, entry 2). Increasing in the reaction time to 168 h (1 week) favored to accumulate side product **27** (entry 3, ratio **1**:**27** = 1:2.3) (Fig. 1) and was accompanied by the formation of decomposition products.

The formation of similar side product **28** was more intensive in the case of homologous tetrasaccharide **2a**. Thus, the acid-promoted sulfation of **2a** by the $Et_3N{\cdot}SO_3$ complex (5 equiv per OH group) in the presence of TfOH (2 equiv per OH group) during 48 h resulted in the formation of product **28** only, which was confirmed by mass spectrometry and NMR spectroscopy. Very surprisingly, their data show that compound **28** has the terminal 2,5-di-O-sulfated α-L-fucofuranose unit in the 'reducing end'. Its structure was confirmed by characteristic resonances for fucofuranose of H-4 (4.02 ppm, t) and C-4 (83.9 ppm) in the ^1H and ^{13}C NMR spectra (see Fig. 2 and Table 2).[30,31] Moreover, the presence of the five-membered ring was evidenced by a correlation of H-1–C-4 as well as C-1–H-4 in HMBC NMR experiments. Spatial proximity of H-4 with H-2 was observed from NOE NMR experiments. Signals of molecular ion in ESI-MS also confirmed that products **2b** and **28** are the isomers.

Similarly to the transformation **2a**→**28**, the treatment of hexasaccharide **3a** and octasaccharide **4a** by the $Et_3N{\cdot}SO_3$ complex (5 equiv per OH group) in the presence of TfOH (2 equiv per OH group) during 48 h at 0 °C resulted to their complete conversion into the corresponding rearranged derivatives **29** and **30** in yields of ~70%. The observed unusual rearrangement of the fucopyranoside residue into the fucofuranoside one with the cleavage of the cyclic C(1)–O(5) bond followed by the recyclization and formation of a new O(4)–C(1) bond but without affecting propyl aglycon belongs to a rare type of reactions in carbohydrate chemistry.[32–34] This transformation is contrary to the usual situation when the cleavage of the acyclic C(1)–O(1) glycoside bond proceeds more intensely than that of the cyclic C(1)–O(5) bond. It is noticeable that the described transformation proceeds selectively only with the fucopyranoside unit at the reducing end but not with other ones

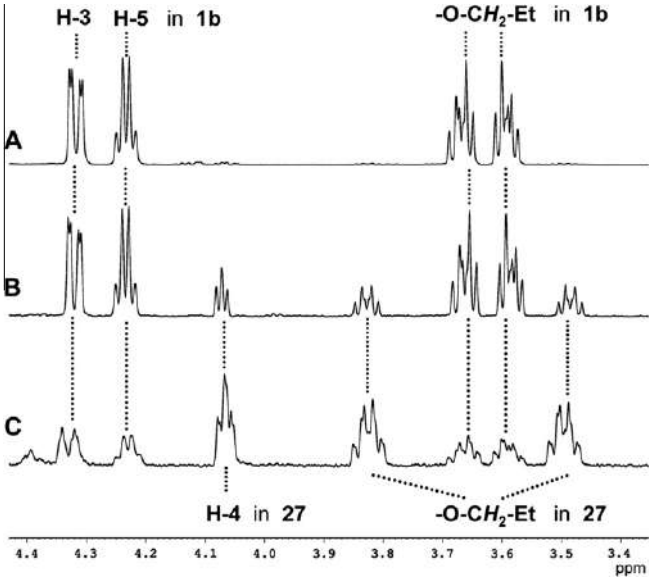

Figure 1. Parts of ^{1}H NMR spectra of the products of TfOH-promoted per-O-sulfation of disaccharide **1a** described in Table 1: (A) entry 1 (only product **1a** is formed), (B) entry 2 and (C) entry 3.

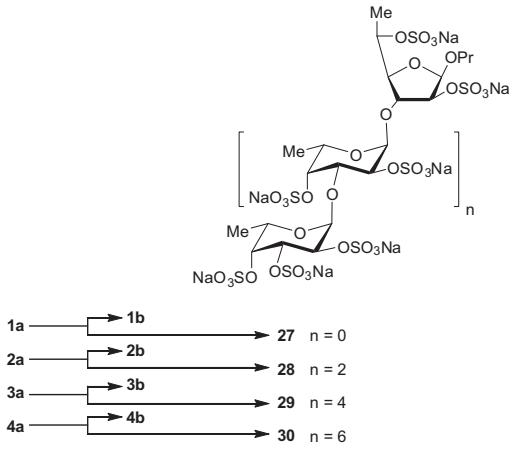

Scheme 4. Products of the TfOH-promoted per-O-sulfation of oligofucosides **1a**–**4a**.

presented in the oligosaccharide chains under investigation. The discussed process does not have direct analogy among chemical reactions, only enzymatic transformation 'fucopyranoside→fucofuranoside' without cleavage of aglycon is known.[35] Detailed investigation of the mechanism and scopes of the observed rearrangement is in progress and will be reported elsewhere.

It could be expected that the optimization of an acidic promoter used for the activation of the sulfating reagent can improve the yield of the target non-rearranged per-O-sulfated products. Using of chlorosulfonic acid (1.0 equiv per OH group) as a promoter also gave compound **29** in a yield of 83% without any significant amounts of product **3b** (Table 3, entry 1). Sulfation promoting activities of both H_2SO_4 and $BF_3{\cdot}Et_2O$ in an amount of 1.0 equiv per OH group were insufficient to perform per-O-sulfation and produced a complex mixture of partly sulfated products (Table 3, entries 2 and 3). Fortunately, the use of weaker trifluoroacetic acid (TFA) led to desired product **3b**. Thus, its use in an amount of 1.0 equiv per OH group formed a 5:1 mixture (^{1}H NMR monitoring) of **3b** and **29** (Table 3, entry 4), while a decrease in the amount of TFA down to 0.5 equiv per OH group gave 76% of desired **3b** as the only formed product (Table 3, entry 5).

Promotion with TFA, which was used in the synthesis of hexasaccharide **3b** (Table 3, entry 5), was successfully applied to the synthesis of per-O-sulfated octasaccharide **4b** (yield 78%), dodecasaccharide **5b** (yield 72%), and hexadecasaccharide **6b** (yield 75%) from parent unsubstituted oligofucosides **4a**–**6a**. Compounds **4b**, **5b**, and **6b** had one product in the ^{1}H NMR spectra with the signal groups presented in the spectra of previously synthesized α-(1→3)-linked oligofucosides **2b** and **3b**. The ratio of integral intensities of H-1 signals for 'reducing' unit (δ 5.21, d) and non-reducing units (δ 5.40, br s) corresponded well to a number of fucopyranose residues in oligosaccharides **4b**–**6b** (Fig. 3).

Per-O-sulfation of oligosaccharides **8a** and **9a** related to the second type of fucoidan backbone consisted of alternating α-(1→4)- and α-(1→3)-linked fucopyranose residues and only of α-(1→4)-linked compounds **7a** and **10a** were studied further starting first from disaccharide **7a**. Both TFA and TfOH acids were tested as promoters to give desired pentasulfate **7b** in a yield of 80% and 83%, respectively (Table 4, entries 1 and 2). No rearrangement of the terminal fucopyranose residue (at the 'reducing' end) into the fucofuranose one is possible for compounds **7a**–**10a** because of the 4-O-substitution of this unit in these compounds. Therefore, for these examples TfOH was used as the promoter of sulfation in an amount of 1 equiv per OH group to give per-O-sulfated tetra- and

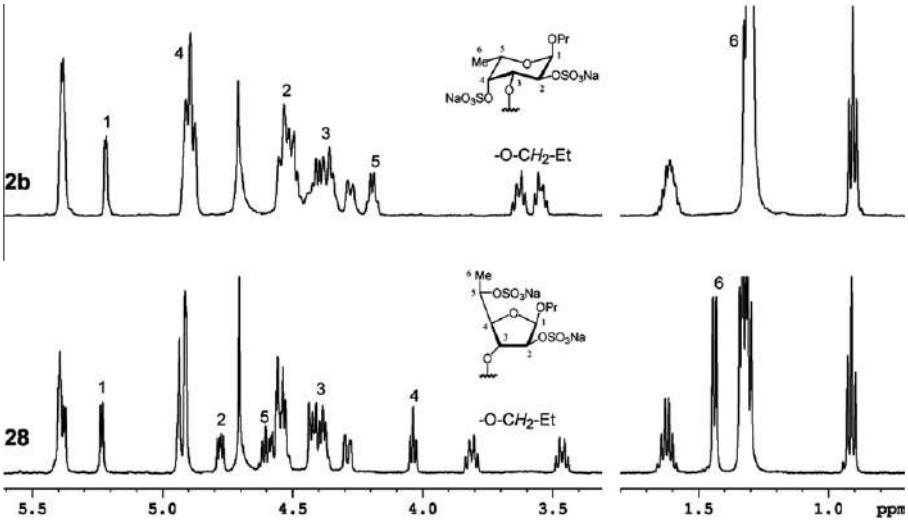

Figure 2. Comparison of ^{1}H NMR spectra of isomeric tetrasaccharides **2b** and **28**.

Table 2
Selected spectral characteristics of **2b** and **28**

Structure	Selected NMR data						
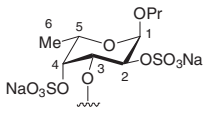 **2b**	H-1	H-2	H-3	H-4	H-5	H-6	O–CH_2–Et
	5.21	4.52	4.28	4.90	4.22	1.30	3.55; 3.63
	C-1	C-2	C-3	C-3	C-5	C-6	O–CH_2–Et
	97.4	76.2	76.1	81.3	68.3	17.0	71.9
	$J_{H-1,H-2}$	$J_{H-4,H-5}$	$J_{C-4,H-1}$	$J_{C-1,H-4}$	$J_{C-5,H-1}$	$J_{C-1,H-5}$	
	3.4 Hz	~1 Hz	—	—	6.9 Hz	—	
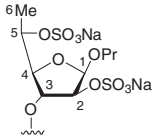 **28**	H-1	H-2	H-3	H-4	H-5	H-6	O–CH_2–Et
	5.23	4.77	4.43	4.02	4.61	1.45	3.47; 3.82
	C-1	C-2	C-3	C-3	C-5	C-6	O–CH_2–Et
	101.2	81.6	81.2	83.9	78.6	18.0	71.8
	$J_{H-1,H-2}$	$J_{H-4,H-5}$	$J_{C-4,H-1}$	$J_{C-1,H-4}$	$J_{C-5,H-1}$	$J_{C-1,H-5}$	
	4.4 Hz	6.0 Hz	7.0 Hz	3.2 Hz	—	—	

Table 3
Sulfation of hexasaccharide **3a** with $Et_3N{\cdot}SO_3$ (5 equiv per OH group) in DMF at 0 °C promoted by different acids

Entry	Acid	Amount of acid (equiv per OH group)	Products	Yield (%)
1	$ClSO_3H$	1.0	**29**	83
2	H_2SO_4	1.0	Mixture of partially sulfated products	
3	$BF_3{\cdot}Et_2O$	1.0	Mixture of partially sulfated products	
4	TFA	1.0	**3b**:**29** ~ 5:1	73
5	TFA	0.5	**3b**	76

hexasaccharides **8b**, **9b**, and **10b** in 84%, 83%, and 75% yields, respectively (Table 4, entries 3–5). Comparable results were obtained also in the preparation of per-O-sulfated disaccharides **11b** and **12b** (Table 4, entries 6 and 7).

3. Conclusion

The synthesis of per-O-sulfated oligosaccharides **1b**–**12b** related to various types of fucoidans is described. Preparation of target products is achieved by using acid-promoted sulfation suitable for oligosaccharides of different types. The described acid-promoted sulfation protocol appeared to be a powerful method for the per-O-sulfation of large oligosaccharides, which is not accessible in the preparative scale by previously known methods. The unknown rearrangement of the fucopyranose unit at the reducing end into the fucofuranose one was observed and the efficiency of this process depended on the type of the used acid promoter. The variation of the type and amount of the acidic promoter allows the direct formation of per-O-sulfated rearranged **28**–**30** or non-rearranged **1b**–**6b** oligosaccharides to access. The sulfation of oligosaccharides **7a**–**12a** with 4-O- or 2-O-substituted terminal residues was free from any side processes and gave per-O-sulfated derivatives **7b**–**12b** in a good yield. The results of conformational and biological studies of synthetic fucoidan fragments **1b**–**12b** will be published elsewhere.

4. Experimental

4.1. General methods

TLC was performed on Silica Gel 60 F_{254} (Merck) with toluene-EtOAc and with detection by charring with H_3PO_4. Liquid chromatography was performed on Silicagel 60–200 μm (Fluka) by gradient elution with toluene-EtOAc. Gel chromatography was performed on a BioBeads SX-3 (Bio Rad) column (2 × 70 cm) by elution with toluene at a flow rate of 1 mL/min and on a Sephadex G-15 column (3.5 × 50 cm) by elution with water at a flow rate of 1 mL/min. Optical rotations were determined with a Jasco DIP-360 digital polarimeter at 26–30 °C. All solvents used for the syntheses were purified according to conventional procedures.[36] NMR spectra for substituted compounds were recorded on AM-300, DRX-500, and Avance 600 Bruker spectrometers at 303 K. NMR spectra for non-protected oligosaccharides **5a** and **10a** were recorded in D_2O, for **6a** in CD_3OD on a DRX-500 Bruker spectrometer. NMR spectra for sulfated oligosaccharides **1b–12b**, **27–30** were recorded in D_2O on DRX-500 and Avance 600 Bruker spectrometers. Gradient enhanced 2D gCOSY, gNOESY, and gHSQC experiments, as well as TOCSY experiments, were used for resonance assignment. High resolution mass spectra (HR MS) were measured on a Bruker micrOTOF II instrument using electrospray ionization (ESI).[37] The measurements were done in a positive ion mode (interface capillary voltage—4500 V) or in a negative ion mode (3200 V); mass range from *m*/*z* 50 to *m*/*z* 3000 Da; external or internal calibration was done with Electrospray Calibrant Solution (Fluka). A syringe injection was used for solutions in a mixture of acetonitrile and water (50:50 v/v flow rate 3 μL/min). Nitrogen was applied as a dry gas; interface temperature was set at 180 °C. All reactions involving air- or moisture-sensitive reagents were carried out using dry solvents under dry argon.

4.2. Preparation of protected oligosaccharides

4.2.1. 4-*O*-Benzoyl-2-*O*-benzyl-3-*O*-chloroacetyl-L-fucopyranosyl trichloroacetimidate (14)

To a soln of monosaccharide **13** (400 mg, 1.00 mmol) in anhydrous CH_2Cl_2 (10 mL), Py (320 μL, 4.0 mmol) and chloroacetylchloride (160 μL, 2.0 mmol) were added. After 1 h the mixture was diluted with $CHCl_3$ and washed successively with 1 M HCl, satd $NaHCO_3$, and water. The solvent was evaporated and the residue was chromatographed (10:1 toluene–EtOAc) to give the chloroacetylated derivative as a yellowish foam. Then it was dissolved in (1:9) H_2O–acetone CH_3COCH_3 (20 mL) and *N*-bromosuccinimide (535 mg, 3.00 mmol) was added at 0 °C. The mixture was vigorously stirred for 10 min, then diluted with CH_2Cl_2 and washed with aq $NaHCO_3$ (3 × 100 mL). The organic phase was dried over anhyd Na_2SO_4 and concentrated under diminished pressure giving a white residue. To a soln of the above residue in anhyd CH_2Cl_2 (5 mL) CCl_3CN (1 mL, 10.0 mmol) and DBU (75 μL, 0.50 mmol)

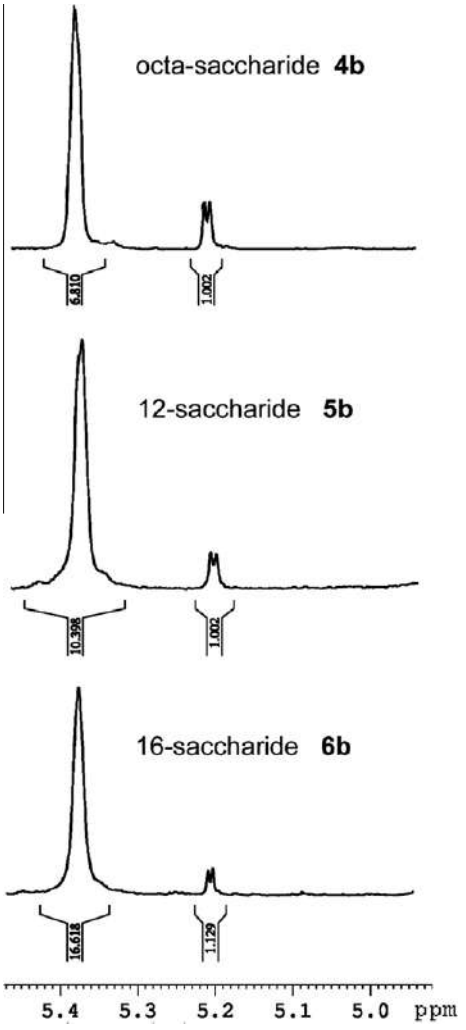

Figure 3. Parts of ^{1}H NMR spectra of per-O-sulfated octa-, dodeca-, and hexadecasaccharides **4b**–**6b** with the integration of anomeric signals of reducing and non-reducing residues.

Table 4
Acid-promoted sulfation of oligosaccharides **7a**–**12a** by the treatment with 5 equiv per OH group $Et_3N{\cdot}SO_3$ in DMF

Entry	Saccharide	Acid	Amount of acid (equiv per OH group)	Product	Yield (%)
1	**7a**	TFA	0.5	**7b**	80
2	**7a**	TfOH	1.0	**7b**	83
3	**8a**	TfOH	1.0	**8b**	84
4	**9a**	TfOH	1.0	**9b**	83
5	**10a**	TfOH	1.0	**10b**	75
6	**11a**	TfOH	1.0	**11b**	72
7	**12a**	TfOH	1.0	**12b**	85

were added under an argon atmosphere, and the mixture was then stirred for 2 h. The concentration of the reaction mixture followed by purification of the residue by column chromatography (5:1 petroleum ether–EtOAc) gave **14** (415 mg, 72% over three steps, α/β = 1.4:1) as a syrup; ^{1}H NMR (300 MHz, $CDCl_3$): α-isomer—δ 1.24 (d, 3H, $J_{5,6}$ 6.3 Hz, H-6), 3.91–3.97 (m, 2H, CH_2Cl), 4.18 (dd, 1H, $J_{1,2}$ 3.6 Hz, $J_{2,3}$ 7.9 Hz, H-2), 4.48 (q, 1H, $J_{5,6}$ 6.3 Hz, H-5), 4.63–4.76 (m, 2H, CH_2Ph), 5.55 (dd, 1H, $J_{2,3}$ 7.9 Hz, $J_{3,4}$ 3.2 Hz, H-3), 5.63 (d, 1H, $J_{3,4}$ 3.2 Hz, H-4), 6.61 (d, 1H, $J_{1,2}$ 3.6 Hz, H-1), 7.20–8.10 (m, 10H, 2Ph), 8.66 (s, 1H, =N*H*); β-isomer—δ 1.32 (d, 3H, $J_{5,6}$ 6.4 Hz, H-6), 3.75–3.90 (m, 2H, CH_2Cl), 4.02 (t, 1H, $J_{1,2}$, $J_{2,3}$ 8.1 Hz, H-2), 4.10 (q, 1H, $J_{5,6}$ 6.4 Hz, H-5), 4.65, 4.91 (2d, 2H, *J* 11.3 Hz, CH_2Ph), 5.25 (dd, 1H, $J_{2,3}$ 8.1 Hz, $J_{3,4}$ 3.3 Hz, H-3), 5.51 (d, 1H, $J_{3,4}$ 3.3 Hz, H-4), 5.91 (d, 1H, $J_{1,2}$ 8.1 Hz, H-1), 7.20–8.10 (m, 10H, 2Ph), 8.77 (s, 1H, =N*H*). Anal. Calcd for $C_{24}H_{23}Cl_4NO_7$: C, 49.76; H, 4.00; N, 2.42. Found: C, 49.52; H, 4.07; N, 2.64.

4.2.2. Ethyl 4-*O*-benzoyl-2-*O*-benzyl-3-*O*-chloroacetyl-α-L-fucopyranosyl-(1→3)-4-*O*-benzoyl-2-*O*-benzyl-1-thio-β-L-fucopyranoside (15)

A mixture of MS 4 Å (500 mg), thioglycoside acceptor **13** (300 mg, 0.75 mmol), and donor **14** (400 mg, 0.69 mmol) in CH_2Cl_2 (8 mL) was stirred for 30 min at room temperature, cooled to −90 °C, and then TMSOTf (50 μL, 0.26 mmol) was added dropwise. The resulting mixture was stirred at −90 to −80 °C until the disappearance of starting **14** (TLC monitoring), quenched with Et_3N, diluted with $CHCl_3$, and filtered through a Celite layer. Column chromatography of the residue (5:1 petroleum ether–EtOAc) afforded **15** (373 mg, 66%) as a colorless foam; $[\alpha]_D$ −214 (*c* 1.0, EtOAc). ^{1}H NMR (300 MHz, $CDCl_3$): δ 0.82 (d, 3H, $J_{5,6}$ 6.5 Hz, H-6^{II}), 1.28 (d, 3H, $J_{5,6}$ 6.8 Hz, H-6^{I}), 1.42 (t, 3H, *J* 7.4 Hz, CH_2CH_3), 2.82–2.98 (m, 2H, CH_2CH$_3$), 3.66–3.79 (m, 2H, CH_2Cl), 3.80–3.96 (m, 3H, H-2^{I}, H-5^{I}, H-2^{II}), 4.04 (dd, 1H, $J_{2,3}$ 9.4 Hz, $J_{3,4}$ 3.2 Hz, H-3^{I}), 4.27 (q, 1H, $J_{5,6}$ 6.5, H-5^{II}), 4.32, 4.50 (2d, 2H, *J* 12.5 Hz, CH_2Ph), 4.60 (d, 1H, $J_{1,2}$ 9.6 Hz, H-1^{I}), 4.71, 5.14 (2d, 2H, *J* 9.7 Hz, CH_2Ph), 5.18 (d, 1H, $J_{4,3}$ 3.4 Hz, H-4^{II}), 5.39 (d, 1H, $J_{1,2}$ 3.5 Hz, H-1^{II}), 5.48 (dd, 1H, $J_{2,3}$ 10.5 Hz, $J_{3,4}$ 3.4 Hz, H-3^{II}), 5.69 (d, 1H, $J_{3,4}$ 3.2, H-4^{I}), 7.05–8.10 (m, 20H, 4Ph). Anal. Calcd for $C_{44}H_{47}ClO_{11}S$: C, 64.50; H, 5.78. Found: C, 64.70; H, 5.90.

4.2.3. Ethyl 4-*O*-benzoyl-2-*O*-benzyl-α-L-fucopyranosyl-(1→3)-4-*O*-benzoyl-2-*O*-benzyl-1-thio–L-fucopyranoside (16)

A mixture of disaccharide **15** (170 mg, 0.21 mmol), 2,4,6-collidine (30 μL, 0.22 mmol), and thiourea (77 mg, 1.01 mmol) in MeOH (6 mL) and $CHCl_3$ (1 mL) was boiled under reflux for 24 h, cooled, and evaporated to dryness. A soln of the residue in $CHCl_3$ was washed with 1 M HCl and satd $NaHCO_3$ and concentrated. The residue was purified by column chromatography (5:1 toluene–EtOAc) to give **16** (145 mg, 94%) as a white foam; $[\alpha]_D$ −174 (*c* 1.0, EtOAc). ^{1}H NMR (500 MHz, $CDCl_3$): δ 0.91 (d, 3H, $J_{5,6}$ 6.5 Hz, H-6^{II}), 1,25 (d, 3H, $J_{5,6}$ 6.3 Hz, H-6^{I}), 1.38 (t, 3H, *J* 7.5 Hz, CH_2CH_3), 2.00 (s br, 1H, O*H*), 2.78–2.91 (m, 2H, CH_2CH$_3$), 3.75 (dd, 1H, $J_{1,2}$ 3.1 Hz, $J_{2,3}$ 10 Hz, H-2^{II}), 3.78–3.84 (m, 2H, H-2^{I}, H-5^{I}), 4.03 (dd, 1H, $J_{2,3}$ 9.4, $J_{3,4}$ 3.0 Hz, H-3^{I}), 4.09–4.14 (m br, 1H, H-3^{II}), 4.21 (q, 1H, $J_{5,6}$ 6.5 Hz, H-5^{II}), 4.35, 4.54 (2d, 2H, *J* 12.0 Hz, CH_2Ph), 4.57 (d, 1H, $J_{1,2}$ 9.6 Hz, H-1^{I}), 4.66, 5.07 (2d, 2H, *J* 10.3 Hz, CH_2Ph), 5.04 (d, 1H, $J_{3,4}$ 3.7 Hz, H-4^{II}), 5.43 (d, 1H, $J_{1,2}$ 3.1 Hz, H-1^{II}), 5.69 (d, 1H, $J_{3,4}$ 3.0 Hz, H-4^{I}), 7.10–8.10 (m, 20H, 4Ph). Anal. Calcd for $C_{42}H_{46}O_{10}S$: C, 67.91; H, 6.24. Found: C, 68.04; H, 6.49.

4.2.4. Ethyl 3-*O*-acetyl-4-*O*-benzoyl-2-*O*-benzyl-α-L-fucopyranosyl-(1→3)-4-*O*-benzoyl-2-*O*-benzyl-α-L-fucopyranosyl-(1→3)-4-*O*-benzoyl-2-*O*-benzyl-α-L-fucopyranosyl-(1→3)-4-*O*-benzoyl-2-*O*-benzyl-1-thio–L-fucopyranoside (18)

Glycosylation of difucoside **16** (130 mg, 0.175 mmol) with trichloroacetimidate **17** (170 mg, 0.192 mmol) as described for the preparation of **15** gave tetrasaccharide **18** (141 mg, 55%) as a yellowish syrup; $[\alpha]_D$ −235 (*c* 1.0, EtOAc). ^{1}H NMR (500 MHz, $CDCl_3$): δ 0.55 (d, 3H, $J_{5,6}$ 6.4 Hz, H-6^{IV}), 0.85 (d, 6H, $J_{5,6}$ 6.5 Hz, H-6$^{II–III}$), 1.24 (d, 3H, $J_{5,6}$ 6.5 Hz, H-6^{I}), 1.37 (t, 3H, *J* 7.4 Hz, CH_2CH_3), 2.02 (s, 3H, COCH_3), 2.75–2.90 (m, 2H, CH_2CH$_3$), 3.76 (dd, 1H, $J_{1,2}$ 3.4 Hz, $J_{2,3}$ 10.5, H-2^{IV}), 3.78–3.84 (m, 2H, H-2^{I}, H-5^{I}), 3.92–4.00 (m, 2H, H-2$^{II–III}$), 4.01 (dd, 1H, $J_{2,3}$ 9.4 Hz, $J_{3,4}$ 3.0 Hz, H-3^{I}), 4.12–4.21 (m, 5H, H-5$^{II–IV}$, H-3^{III}, PhC*H*H′), 4.32–4.42 (m, 4H, 3 × PhC*H*H′, H-3^{II}), 4.53–4.68 (m, 4H, 3 × PhC*H*H′, H-1^{I}), 5.00 (d, 1H, $J_{3,4}$ 3.1 Hz,

H-4[IV]), 5.07–5.11 (m, 2H, H-1[IV], PhC*H*H′), 5.16 (d, 1H, $J_{3,4}$ 2.6 Hz, H-4[III]), 5.24 (dd, 1H, $J_{2,3}$ 10.5 Hz, $J_{3,4}$ 3.1 Hz, H-3[IV]), 5.28–5.31 (m, 3H, H-1[II–III], H-4[II]), 5.67 (d, 1H, $J_{4,5}$ 3.0 Hz, H-4[I]), 7.00–8.12 (m, 40H, 8Ph). Anal. Calcd for $C_{84}H_{88}O_{21}S$: C, 68.84; H, 6.05. Found: C, 68.61; H, 5.91.

4.2.5. Allyl 4-*O*-benzoyl-2-*O*-benzyl-α-L-fucopyranosyl-(1→3)-4-*O*-benzoyl-2-*O*-benzyl-α-L-fucopyranosyl-(1→3)-4-*O*-benzoyl-2-*O*-benzyl-α-L-fucopyranosyl-(1→3)-4-*O*-benzoyl-2-*O*-benzyl-α-L-fucopyranosyl-(1→3)-4-*O*-benzoyl-2-*O*-benzyl-α-L-fucopyranosyl-(1→3)-4-*O*-benzoyl-2-*O*-benzyl-α-L-fucopyranosyl-(1→3)-4-*O*-benzoyl-2-*O*-benzyl-α-L-fucopyranosyl-(1→3)-4-*O*-benzoyl-2-*O*-benzyl-α-L-fucopyranoside (20)

Anhyd HCl in MeOH (0.5 M, 5.2 mL), obtained by adding AcCl (200 μL, 2.8 mmol) to chilled MeOH (5 mL), was added to a soln of **19** (245 mg, 0.087 mmol) in anhyd CH_2Cl_2 (2 mL). The resulting mixture was kept for 6 h at ambient temperature, diluted with $CHCl_3$, washed with satd $NaHCO_3$ and water, and concentrated. Column chromatography of the residue (10:1 toluene–EtOAc) gave **20** (184 mg, 76%) as a colorless foam; $[\alpha]_D$ −287 (*c* 1.0, EtOAc). ^{1}H NMR (500 MHz, $CDCl_3$): δ 0.52–0.65 (m, 12H, 4 × H-6), 0.68, 0,99, 1.11, 1.20 (4d, 12H, $J_{5,6}$ 6.5 Hz, 4 × H-6), 3.55–4.52 (m, 42H, 8 × H-2, 8 × H3, 8 × H-5, 8 × PhCH_2, CH_2=CH–CH_2), 4.70–5.35 (m, 16H, 8 × H-1, 6 × H-4, CH_2=CH–CH_2), 5.42 (s br, 1H, H-4), 5.63 (s br, 1H, H-4), 5.87–6.00 (m, 1H, CH_2=C*H*–CH_2), 6.90–8.00 (80H, 16 × Ph). Selected ^{13}C NMR data (125 MHz, $CDCl_3$): δ 15.6–16.0 (8 × C-6), 91.9–93.2 (7 × C-1), 96.3 (C-1), 117.7 (CH_2=CH–CH_2). Anal. Calcd for $C_{163}H_{166}O_{41}$: C, 70.40; H, 6.02. Found: C, 70.23; H, 6.09.

4.2.6. Allyl 3-*O*-acetyl-4-*O*-benzoyl-2-*O*-benzyl-α-L-fucopyranosyl-(1→3)-4-*O*-benzoyl-2-*O*-benzyl-α-L-fucopyranosyl-(1→3)-4-*O*-benzoyl-2-*O*-benzyl-α-L-fucopyranosyl-(1→3)-4-*O*-benzoyl-2-*O*-benzyl-α-L-fucopyranosyl-(1→3)-4-*O*-benzoyl-2-*O*-benzyl-α-L-fucopyranosyl-(1→3)-4-*O*-benzoyl-2-*O*-benzyl-α-L-fucopyranosyl-(1→3)-4-*O*-benzoyl-2-*O*-benzyl-α-L-fucopyranosyl-(1→3)-4-*O*-benzoyl-2-*O*-benzyl-α-L-fucopyranosyl-(1→3)-4-*O*-benzoyl-2-*O*-benzyl-α-L-fucopyranosyl-(1→3)-4-*O*-benzoyl-2-*O*-benzyl-α-L-fucopyranosyl-(1→3)-4-*O*-benzoyl-2-*O*-benzyl-α-L-fucopyranosyl-(1→3)-4-*O*-benzoyl-2-*O*-benzyl-α-L-fucopyranoside (21)

To a soln of **21** (172 mg, 0.062 mmol) and **18** (91 mg, 0.062 mmol) in CH_2Cl_2 (3 mL), MS 4 Å (300 mg) was added, and the resulting mixture was stirred for 30 min at rt. After cooling to −15 °C NIS (21 mg, 0.093 mmol) was added, and the mixture was stirred for 10 min. Then the temperature of the reaction mixture was decreased to −40 °C, and TfOH (2.7 μL, 0.03 mmol) was added. After the stirring for 2 h the reaction was quenched with a drop of pyridine, the mixture was diluted with $CHCl_3$ and filtered through a Celite layer. The filtrate was washed with 1 M aq $Na_2S_2O_3$ and water, concentrated, and was twice coevaporated with toluene. Chromatographic purification of the residue (15:1 toluene–EtOAc) produced **21** (179 mg, 69%) as a colorless syrup; $[\alpha]_D$ −288 (*c* 1.0, EtOAc). ^{1}H NMR (500 MHz, $CDCl_3$): δ 0.56 (d, 3H, $J_{5,6}$ 6.4 Hz, H-6), 0.60–0.70 (m, 24H, 8 × H-6), 0.75, 1.07, 1.17, (3d, 9H, $J_{5,6}$ 6.5 Hz, 3 × H-6), 1.74 (s, 3H, COCH_3), 3.74–4.83 (m, 61H, 12 × H-2, 11 × H3, 12 × H-5, 12 × PhCH_2, CH_2=CH–CH_2), 4.96–5.40 (m, 25H, 12 × H-1, 10 × H-4, H-3, CH_2=CH–CH_2), 5.50 (s br, 1H, H-4), 5.70 (s br, 1H, H-4), 5.95–6.04 (m, 1H, CH_2=C*H*–CH_2), 6.96–8.06 (120H, 24 × Ph). Selected ^{13}C NMR data (125 MHz, $CDCl_3$): δ 15.5–16.3 (12 × C-6), 92.5–93.3 (11 × C-1), 96.5 (C-1), 117.8 (CH_2=CH–CH_2). Anal. Calcd for $C_{245}H_{248}O_{62}$: C, 70.32; H, 5.97. Found: C, 70.31; H, 6.03.

4.2.7. Allyl 4-*O*-benzoyl-2-*O*-benzyl-α-L-fucopyranosyl-(1→3)-4-*O*-benzoyl-2-*O*-benzyl-α-L-fucopyranosyl-(1→3)-4-*O*-benzoyl-2-*O*-benzyl-α-L-fucopyranosyl-(1→3)-4-*O*-benzoyl-2-*O*-benzyl-α-L-fucopyranosyl-(1→3)-4-*O*-benzoyl-2-*O*-benzyl-α-L-fucopyranosyl-(1→3)-4-*O*-benzoyl-2-*O*-benzyl-α-L-fucopyranosyl-(1→3)-4-*O*-benzoyl-2-*O*-benzyl-α-L-fucopyranosyl-(1→3)-4-*O*-benzoyl-2-*O*-benzyl-α-L-fucopyranosyl-(1→3)-4-*O*-benzoyl-2-*O*-benzyl-α-L-fucopyranosyl-(1→3)-4-*O*-benzoyl-2-*O*-benzyl-α-L-fucopyranosyl-(1→3)-4-*O*-benzoyl-2-*O*-benzyl-α-L-fucopyranosyl-(1→3)-4-*O*-benzoyl-2-*O*-benzyl-α-L-fucopyranoside (22)

O-Deacetylation of **21** (108 mg, 0.026 mmol) was performed as described for the preparation of **20** to give dodecasaccharide **22** (77 mg, 72%); $[\alpha]_D$ −288 (*c* 1.0, EtOAc). ^{1}H NMR (600 MHz, $CDCl_3$): δ 0.63–0.73 (m, 27H, 8 × H-6), 0.78, 1.09, 1.20, (3d, 9H, $J_{5,6}$ 6.5 Hz, 3 × H-6), 3.63–4.88 (m, 62H, 12 × H-2, 12 × H3, 12 × H-5, 12 × PhCH_2, CH_2=CH–CH_2), 4.98–5.44 (m, 24H, 12 × H-1, 10 × H-4, CH_2=CH–CH_2), 5.51 (s br, 1H, H-4), 5.72 (s br, 1H, H-4), 5.96–6.04 (m, 1H, CH_2=C*H*–CH_2), 6.98–8.10 (120H, 24 × Ph). Selected ^{13}C NMR data (150 MHz, $CDCl_3$): δ 15.8–16.3 (12 × C-6), 91.6–93.3 (11 × C-1), 96.6 (C-1), 117.7 (CH_2=CH–CH_2). Anal. Calcd for $C_{243}H_{246}O_{61}$: C, 70.45; H, 5.99. Found: C, 70.35; H, 6.13.

4.2.8. Allyl 3-*O*-acetyl-4-*O*-benzoyl-2-*O*-benzyl-α-L-fucopyranosyl-(1→3)-4-*O*-benzoyl-2-*O*-benzyl-α-L-fucopyranosyl-(1→3)-4-*O*-benzoyl-2-*O*-benzyl-α-L-fucopyranosyl-(1→3)-4-*O*-benzoyl-2-*O*-benzyl-α-L-fucopyranosyl-(1→3)-4-*O*-benzoyl-2-*O*-benzyl-α-L-fucopyranosyl-(1→3)-4-*O*-benzoyl-2-*O*-benzyl-α-L-fucopyranosyl-(1→3)-4-*O*-benzoyl-2-*O*-benzyl-α-L-fucopyranosyl-(1→3)-4-*O*-benzoyl-2-*O*-benzyl-α-L-fucopyranosyl-(1→3)-4-*O*-benzoyl-2-*O*-benzyl-α-L-fucopyranosyl-(1→3)-4-*O*-benzoyl-2-*O*-benzyl-α-L-fucopyranosyl-(1→3)-4-*O*-benzoyl-2-*O*-benzyl-α-L-fucopyranosyl-(1→3)-4-*O*-benzoyl-2-*O*-benzyl-α-L-fucopyranosyl-(1→3)-4-*O*-benzoyl-2-*O*-benzyl-α-L-fucopyranosyl-(1→3)-4-*O*-benzoyl-2-*O*-benzyl-α-L-fucopyranosyl-(1→3)-4-*O*-benzoyl-2-*O*-benzyl-α-L-fucopyranosyl-(1→3)-4-*O*-benzoyl-2-*O*-benzyl-α-L-fucopyranoside (23)

Glycosylation of dodecasaccharide **22** (70 mg, 0.0169 mmol) with tetrasaccharide **18** (27 mg, 0.182 mmol) was performed as described for the preparation of **21** and gave hexadecasaccharide **23** (69 mg, 74%) as a yellowish syrup; $[\alpha]_D$ −277 (*c* 1.0, EtOAc). ^{1}H NMR (600 MHz, $CDCl_3$): δ 0.58 (d, 3H, $J_{5,6}$ 6.4 Hz, H-6), 0.62–0.73 (m, 36H, 12 × H-6), 0.78, 1.08, 1.20, (3d, 9H, $J_{5,6}$ 6.5 Hz, 3 × H-6), 1.75 (s, 3H, COCH_3), 3.74–4.85 (m, 81H, 16 × H-2, 15 × H3, 16 × H-5, 16 × PhCH_2, CH_2=CH–CH_2), 4.98–5.43 (m, 33H, 16 × H-1, 14 × H-4, H-3, CH_2=CH–CH_2), 5.51 (s br, 1H, H-4), 5.71 (s br, 1H, H-4), 5.97–6.05 (m, 1H, CH_2=C*H*–CH_2), 7.00–8.10 (160H, 32 × Ph). Selected ^{13}C NMR data (150 MHz, $CDCl_3$): δ 15.5–16.3 (16 × C-6), 92.6–93.3 (15 × C-1), 96.6 (C-1), 117.6 (CH_2=CH–CH_2). Anal. Calcd for $C_{325}H_{328}O_{82}$: C, 70.38; H, 5.96. Found: C, 70.49; H, 5.91.

4.2.9. Allyl 3-*O*-acetyl-4-*O*-benzoyl-2-*O*-benzyl-α-L-fucopyranosyl-(1→4)-3-*O*-benzoyl-2-*O*-benzyl-α-L-fucopyranosyl-(1→4)-3-*O*-benzoyl-2-*O*-benzyl-α-L-fucopyranoside (26)

A mixture of MS 4 Å (150 mg), acceptor **24** (40 mg, 0.101 mmol), and donor **25** (97 mg, 0.110 mmol) in CH_2Cl_2 (2 mL) was stirred for 30 min at room temperature, cooled to −40 °C, and then TMSOTf (4.6 μL, 0.024 mmol) was added. The resulting mixture was stirred at −40 to −30 °C until the disappearance of

starting **25** (TLC monitoring), quenched with Et_3N, diluted with $CHCl_3$, and filtered through a Celite layer. Column chromatography of the residue (5:1 petroleum ether–EtOAc) gave **26** (87 mg, 77%) as a colorless foam; $[\alpha]_D$ −168 (*c* 1.0, EtOAc). ^1H NMR (600 MHz, $CDCl_3$): δ 0.47 (d, 3H, $J_{5,6}$ 6.3, H-6^{III}), 0.77 (d, 3H, $J_{5,6}$ 6.6 Hz, H-6^{II}), 1.33 (d, 3H, $J_{5,6}$ 6.6 Hz, H-6^{I}), 1.91 (s, 3H, $COCH_3$), 3.94 (dd, 1H, $J_{1,2}$ 3.3 Hz, $J_{2,3}$ = 10.6 Hz), 4.04–4.26 (m, 7H, H-$2^{I–II}$, –$CH_2CH{=}CH_2$, H-5^{I}, H-$4^{I–II}$), 4.28 (q, 2H, $J_{5,6}$ 6.4 Hz, H-$5^{II–III}$), 4.53–4.75 (m, 6H, 3 × $PhCH_2$), 4.88 (d, 1H, $J_{1,2}$ 3.2 Hz, H-1^{I}), 5.03 (d, 1H, $J_{1,2}$ 3.3 Hz, H-1^{II}), 5.10 (d, 1H, $J_{1,2}$ 3.3 Hz, H-1^{III}), 5.23, 5.36 (2d, 2H, *J* 10.5 Hz, *J* 16.8 Hz,, $–CH_2CH{=}CH_2$), 5.43 (s br, 1H, H-4^{III}), 5.46 (dd, 1H, $J_{2,3}$ 10.8 Hz, $J_{3,4}$ 2.9 Hz, H-3^{III}), 5.55–5.61 (m, 2H, H-$3^{I–II}$), 5.92–6.00 (m, 1H, $–CH_2CH{=}CH_2$), 7.15–8.10 (m, 30H, 6Ph). Anal. Calcd for $C_{65}H_{68}O_{17}$: C, 69.63; H, 6.11. Found: C, 69.41; H, 5.97.

4.3. Preparation of unprotected oligofucosides 5a, 6a, and 10a

4.3.1. Propyl α-L-fucopyranosyl-(1→3)-α-L-fucopyranosyl-(1→3)-α-L-fucopyranosyl-(1→3)-α-L-fucopyranosyl-(1→3)-α-L-fucopyranosyl-(1→3)-α-L-fucopyranosyl-(1→3)-α-L-fucopyranosyl-(1→3)-α-L-fucopyranosyl-(1→3)-α-L-fucopyranosyl-(1→3)-α-L-fucopyranoside (5a)

To a soln of oligofucoside **21** (66 mg, 0.016 mmol) in (1:3:0.1) THF–EtOH–AcOH (3 mL) Pd/C (10%, 40 mg) was added. The mixture was stirred under H_2 (1 atm) at rt for 5 h and then filtered through a Celite layer. The catalyst was carefully washed with MeOH–CH_2Cl_2, and the combined filtrates were concentrated. The residue was dissolved in a mixture CH_2Cl_2–EtOH (1:5) (1.5 mL) and treated with 2 M aq NaOH (0.7 mL) for 12 h at 60 °C. The oligosaccharide products were isolated from the reaction mixture by column chromatography on a gel Sephadex G-15 (60 × 3 cm) with water elution. Freeze-drying of the oligosaccharide fraction, dissolution of the residue in MeOH–AcOH (20:1), and stirring of the mixture under H_2 (1 atm) in the presence of 10% Pd/C (10 mg) for 5 h led to the complete deprotection of **21**. Separation of the mixture from Pd/C by filtration, concentration of the solution, column chromatography of the residue on a gel Sephadex G-15 (60 × 3 cm) with water elution, and further lyophilization gave **5a** (18 mg, 61%) as a white amorphous powder; $[\alpha]_D$ −143 (*c* 1.0, H_2O). ^1H NMR (600 MHz, D_2O): δ 0.93 (t, 3H, *J* 7.3 Hz, $CH_2CH_2CH_3$), 1,24 (d, 36H, $J_{5,6}$ 6.2 Hz, H-$6^{I–XII}$), 1.60–1.69 (m, 2H, $CH_2CH_2CH_3$), 3.50–3.56, 3.59–3.65 (2 × m, 2H, $CH_2CH_2CH_3$), 3.79–3.85 (m, 2H, H-2^{XII}, H-4^{XII}), 3.91–4.14 (m, 35H, H-$2^{I–XI}$, H-$3^{I–XII}$, H-$4^{I–XI}$, H-5^{I}), 4.30–4.42 (m, 11H, H-$5^{II–XII}$), 4.93 (d, 1H, $J_{1,2}$ 3.6 Hz, H-1^{I}), 5.08 (d, 1H, $J_{1,2}$ 3.8, H-1^{XII}), 5.12 (br s, 10H, H-$1^{II–XI}$). ^{13}C NMR (150 MHz, D_2O): δ 11.3 ($CH_2CH_2CH_3$), 16.8 (C-$6^{I–XII}$), 23.6 ($CH_2CH_2CH_3$), 67.9 (C-$2^{I–XI}$), 68.1 (C-$5^{I–XI}$), 68.4 (C-5^{XII}), 69.5 (C-2^{XII}), 70.0 (C-$4^{I–XI}$), 71.0 (C-3^{XII}), 71.7 ($CH_2CH_2CH_3$), 73.4 (C-4^{XII}), 75.9 (C-3^{I}), 76.4 (C-$3^{II–XI}$), 96.5 (C-1^{I}), 97.0 (C-$1^{II–XI}$), 99.7 (C-1^{XII}). HRESIMS: found *m/z* 929.3672; calcd for $C_{75}H_{128}O_{49}$ $[M+2Na]^{2+}$ 929.3654.

4.3.2. Propyl α-L-fucopyranosyl-(1→3)-α-L-fucopyranosyl-(1→3)-α-L-fucopyranosyl-(1→3)-α-L-fucopyranosyl-(1→3)-α-L-fucopyranosyl-(1→3)-α-L-fucopyranosyl-(1→3)-α-L-fucopyranosyl-(1→3)-α-L-fucopyranosyl-(1→3)-α-L-fucopyranosyl-(1→3)-α-L-fucopyranoside (6a)

Deprotection of hexadecasaccharide **23** (62 mg, 0.011 mmol) as described for the preparation of compound **5a** gave hexadecasaccharide **6a** (14 mg, 54%); $[\alpha]_D$ −157 (*c* 1.0, H_2O).

^1H NMR (600 MHz, CD_3OD): δ 0.91 (t, 3H, *J* 7.6 Hz, $CH_2CH_2CH_3$), 1.22 (d, 48H, *J* 6.3 Hz, H-$6^{I–XVI}$), 1.60–1.68 (m, 2H, $CH_2CH_2CH_3$), 3.48–3.55, 3.57–3.64 (2 × m, 2H, $CH_2CH_2CH_3$), 3.78–3.83 (m, 2H, H-2^{XVI}, H-4^{XVI}), 3.88–4.09 (m, 47H, H-$2^{I–XV}$, H-$3^{I–XVI}$, H-$4^{I–XV}$, H-5^{I}), 4.28–4.39 (m, 15H, H-$5^{II–XVI}$), 4.90 (d, 1H, $J_{1,2}$ 3.2 Hz, H-1^{I}), 5.06 (d, 1H, $J_{1,2}$ 3.2, H-1^{XVI}), 5.10 (br s, 14H, H-$1^{II–XV}$). Selected ^{13}C NMR data (150 MHz, D_2O): δ 16.8 (C-$6^{I–XII}$), 67.8 (C-$2^{I–XI}$), 68.1 (C-$5^{I–XI}$), 69.9 (C-$4^{I–XI}$), 76.2 (C-$3^{II–XI}$), 97.0 (C-$1^{II–XI}$). HRESIMS: found *m/z* 1221.4794; calcd for $C_{99}H_{168}O_{65}$ $[M+2Na]^{2+}$ 1221.4812.

4.3.3. Propyl α-L-fucopyranosyl-(1→4)-α-L-fucopyranosyl-(1→4)-α-L-fucopyranoside (10a)

A mixture of trifucoside **26** (75 mg, 0.067 mmol) and the catalyst 10% Pd/C (37 mg) in MeOH–EtOAc (3:1) (4 mL) was stirred under H_2 (1 atm) at rt for 5 h and then filtered through a Celite layer. The catalyst was carefully washed with MeOH and the combined filtrates were concentrated. The residue was dissolved in MeOH (1 mL) and treated with 1 M aq NaOH (1 mL) for 24 h. Deprotected trisaccharide was isolated from the reaction mixture by column chromatography on a gel Sephadex G-15 (60 × 3 cm) with water elution followed by lyophilization to give **10a** (25 mg, 75%) as a white amorphous powder; $[\alpha]_D$ −131 (*c* 1.0, H_2O). ^1H NMR (600 MHz, D_2O): δ 0.93 (t, 3H, J 7.4 Hz, $CH_2CH_2CH_3$), 1.19 (d, 3H, $J_{5,6}$ 6.6 Hz, H-6^{III}), 1.27 (d, 3H, $J_{5,6}$ 6.7 Hz, H-6^{II}), 1.32 (d, 3H, $J_{5,6}$ 6.7 Hz, H-6^{I}), 1.60–1.67 (m, 2H, $CH_2CH_2CH_3$), 3.49–3.53, 3.63–3.68 (2 m, 2H, $CH_2CH_2CH_3$), 3.80–3.88 (m, 6H, H-$2^{I–III}$, H-$4^{I–III}$), 3.92–3.98 (m, 2H, H-$3^{I,III}$), 4.03 (dd, 1H, $J_{2,3}$ 10.3 Hz, $J_{3,4}$ 3.2 Hz, H-3^{II}), 4.14 (q, 1H, $J_{5,6}$ 6.6 Hz, H-5^{I}), 4.51–4.58 (m, 2H, H-$5^{II–III}$), 4.94 (d, 1H, $J_{1,2}$ 4.0 Hz, H-1^{I}), 4.97 (d, 1H, $J_{1,2}$ 4.0 Hz, H-1^{II}), 5.00 (d, 1H, $J_{1,2}$ 4.0 Hz, H-1^{III}). ^{13}C NMR (150 MHz, D_2O): δ 11.3 ($CH_2CH_2CH_3$), 16.7 (C-$6^{I–III}$), 23.6 ($CH_2CH_2CH_3$), 68.4, 68.5, 69.1 (C-$5^{I–III}$), 69.6 (H-2^{II}), 70.2, 70.4, 70.6, 70.9 (C-$3^{I–III}$, H-$2^{I,III}$), 71.8 ($CH_2CH_2CH_3$), 73.45 (C-4^{III}), 81.6, 81.7 (C-$4^{I–II}$), 99.83 (C-1^{I}), 101.9, 102.0 (C-$1^{II–III}$). HRESIMS: found *m/z* 521.2186; calcd for $C_{21}H_{38}O_{13}$ $[M+Na]^+$ 521.2205.

4.4. Preparation of per-*O*-sulfated oligofucosides 1b–12b and 28–30

4.4.1. General procedure of acid-promoted O-sulfation

To a vigorously stirred soln of oligosaccharide (10 mg) in anhyd DMF (1 mL) the complex $Et_3N{\cdot}SO_3$ (5 equiv per OH group) was added followed by the introduction of an appropriate promoting acid (0.5–2 equiv per OH group) at 0 °C. The mixture was stirred until the reaction was completed (TLC monitoring), and then an excess of 1 M aq NaOH was added. The aqueous phase was washed with CH_2Cl_2 (2 × 1 mL), then loaded onto a Sephadex G-15 column (60 × 3 cm), and eluted with water; the fraction containing the product was collected and freeze-dried to give the per-O-sulfated oligosaccharide as an amorphous substance.

4.4.2. Propyl 2,3,4-tri-*O*-sulfonato-α-L-fucopyranosyl-(1→3)-2,4-di-*O*-sulfonato-α-L-fucopyranoside pentasodium salt (1b)

Per-O-sulfation of **1a** (10 mg, 0.028 mmol) promoted with TfOH (12 μL, 0.14 mmol, 1.0 equiv per OH group) during 24 h gave **1b** (18.8 mg, 77%); $[\alpha]_D$ −106 (*c* 0.5, H_2O). ^1H NMR (600 MHz, D_2O): δ 0.92 (3H, t, *J* 7.5 Hz, CH_2CH_3), 1.26–1.31 (m, 6H, H-$6^{I–II}$), 1.58–1.67 (m, 2H, CH_2CH_3), 3.53–3.59 (m, 1H, O–CH*H′*-Et), 3.60–3.67 (m, 1H, O–*CH*H′-Et), 4.20 (q, 1H, $J_{5,6}$ 6.6 Hz, H-5^{I}), 4.29 (dd, 1H, $J_{2,3}$ 10.4 Hz, $J_{3,4}$ 2.6 Hz, H-3^{I}), 4.46 (q, 1H, $J_{5,6}$ 6.4 Hz, H-5^{II}), 4.57 (m, 2H, H-$2^{I–II}$), 4.91–4.96 (m, 3H, H-$4^{I–II}$, H-3^{II}), 5.23 (d, 1H, $J_{1,2}$ = 3.6 Hz, H-1^{I}), 5.39 (d, 1H, $J_{1,2}$ = 3.4 Hz, H-1^{II}). ^{13}C NMR (150 MHz, D_2O): δ 11.3 (CH_2CH_3) 17.2 (C-6^{II}), 17.3 (C-6^{I}), 23.3 (CH_2CH_3), 68.0 (C-5^{I}), 68,6 (C-5^{II}), 71.8 (O–CH_2–Et), 73.8 (C-3^{II}),

74.8 (C-2^{II}), 75.5 (C-3^{I}), 76.0 (C-2^{I}), 80.9 (C-4^{II}), 81.4 (C-4^{I}), 97.6 (C-1^{I}), 99.1 (C-1^{II}). HRESIMS: found *m/z* 884.8561; calcd for $C_{15}H_{23}Na_5O_{24}S_5$ $[M+Na]^+$ 884.8563.

4.4.3. Propyl 2,3,4-tri-*O*-sulfonato-α-L-fucopyranosyl-(1→3)-2,4-di-*O*-sulfonato-α-L-fucopyranosyl-(1→3)-2,4-di-*O*-sulfonato-α-L-fucopyranosyl-(1→3)-2,4-di-*O*-sulfonato-α-L-fucopyranoside nonasodium salt (2b)

Per-O-sulfation of **2a** (10 mg, 0.016 mmol) promoted with TFA (5.3 μL, 0.072 mmol, 0.5 equiv per OH group) during 24 h gave **2b** (17.6 mg, 75%); $[\alpha]_D$ −107 (*c* 1.0, H_2O). ^1H NMR (500 MHz, D_2O): 0.94 (t, 3H, *J* 7.4 Hz, $CH_2CH_2CH_3$), 1.29–1.35 (m, 12H, 12 H-6), 1.57–1.66 (m, 2H, $CH_2CH_2CH_3$), 3.52–3.58 (m, 1H, OC*H*H′), 3.60–3.67 (m, 1H, OCH*H*′), 4,22 (q, 1H, H-5^{I}, $J_{5,6}$ 6.7 Hz), 4.30–4.47 (m, 5H, H-3$^{I–III}$, H-5$^{II–III}$), 4.51–4.61 (m, 5H, H-2$^{I–IV}$, H-5^{IV}), 4.89–4.97 (m, 5H, H-4$^{I–IV}$, H-3^{IV}), 5.21 (d, 1H, $J_{1,2}$ 3.4 Hz, H-1^{I}), 5.42 (s br, 3H, H-1$^{II–IV}$). ^{13}C NMR (125 MHz, D_2O): δ 11.3 (CH_2CH_3), 17.0, 17.3 (C-6$^{I–IV}$), 23.3 (CH_2CH_3), 68,2, 68.3, 68.8 (C-5$^{I–IV}$), 71.9 (O–CH_2–Et), 73.8, 74.0, 75.2, 76.1, 76.2 (C-3$^{I–IV}$, C-2$^{I–IV}$), 81.2, 81.5 (C-4$^{I–IV}$), 97.4 (C-1^{I}), 98.7, 99.6 (C-1$^{II–IV}$). HRESIMS: found *m/z* 757.8796; calcd for $C_{27}H_{39}Na_9O_{44}S_9$ $[M-2Na]^{2-}$ 757.8798.

4.4.4. Propyl 2,3,4-tri-*O*-sulfonato-α-L-fucopyranosyl-(1→3)-2,4-di-*O*-sulfonato-α-L-fucopyranosyl-(1→3)-2,4-di-*O*-sulfonato-α-L-fucopyranosyl-(1→3)-2,4-di-*O*-sulfonato-α-L-fucopyranosyl-(1→3)-2,4-di-*O*-sulfonato-α-L-fucopyranosyl-(1→3)-2,4-di-*O*-sulfonato-α-L-fucopyranoside tridecasodium salt (3b)

Per-O-sulfation of **3a** (10 mg, 0.011 mmol) promoted with TFA (5.3 μL, 0.72 mmol, 0.5 equiv per OH group) during 24 h gave **3b** (18.3 mg, 76%); $[\alpha]_D$ −89 (*c* 1.0, H_2O). ^1H NMR (600 MHz, D_2O): δ 0.93 (t, 3H, *J* 7.5 Hz, CH_2CH_3), 1.29–1.38 (m, 18H, H-6$^{I–VI}$), 1.60–1.70 (m, 2H, CH_2CH_3), 3.52–3.59 (m, 1H, O–CH*H*′-Et), 3.60–3.67 (m, 1H, O–C*H*H′-Et), 4.22 (q, 1H, $J_{5,6}$ 6.7 Hz, H-5^{I}), 4.29–4.46 (m, 9H, H-3$^{I–V}$, H-5$^{II–V}$), 4.47–4.57 (m, 7H, H-2$^{I–VI}$, H-5^{VI}), 4.89–4.96 (m, 7H, H-4$^{I–VI}$, H-3^{VI}), 5.21 (d, 1H, $J_{1,2}$ 3.4 Hz, H-1^{I}), 5.41 (s br, 5H, H-1$^{II–VI}$). ^{13}C NMR (150 MHz, D_2O): δ 11.3 (CH_2CH_3), 17.1, 17.3 (C-6$^{I–VI}$), 23.3 (CH_2CH_3), 68,2, 68.3, 68.9 (C-5$^{I–VI}$), 71.9 (O–CH_2–Et), 73.8 (C-3^{VI}), 74.1 (C-2^{VI}), 75.2, 75.5, 76.1, 76.2 (C-3$^{I–V}$, C-2$^{I–V}$), 81.3, 81.5 (C-4$^{I–VI}$), 97.4 (C-1^{I}), 98.8, 100.1 (C-1$^{II–VI}$). HRESIMS: found *m/z* 1153.7926; calcd for $C_{39}H_{55}Na_{13}O_{64}S_{13}$ $[M+2Na]^{2+}$ 1153.7936.

4.4.5. Propyl 2,3,4-tri-*O*-sulfonato-α-L-fucopyranosyl-(1→3)-2,4-di-*O*-sulfonato-α-L-fucopyranosyl-(1→3)-2,4-di-*O*-sulfonato-α-L-fucopyranosyl-(1→3)-2,4-di-*O*-sulfonato-α-L-fucopyranosyl-(1→3)-2,4-di-*O*-sulfonato-α-L-fucopyranosyl-(1→3)-2,4-di-*O*-sulfonato-α-L-fucopyranosyl-(1→3)-2,4-di-*O*-sulfonato-α-L-fucopyranoside heptadecasodium salt (4b)

Per-O-sulfation of **4a** (10 mg, 0.0081 mmol) promoted with TFA (5.1 μL, 0.069 mmol, 0.5 equiv per OH group) during 24 h gave **4b** (18.8 mg, 78%). $[\alpha]_D$ −84 (*c* 1.0, H_2O). ^1H NMR (600 MHz, D_2O): δ 0.96 (t, 3H, *J* 7.6 Hz, CH_2CH_3), 1.32–1.40 (m, 24H, H-6$^{I–VI}$), 1.61–1.71 (m, 2H, CH_2CH_3), 3.54–3.61 (m, 1H, O–CH*H*′-Et), 3.62–3.69 (m, 1H, O–C*H*H′-Et), 4.25 (q, 1H, $J_{5,6}$ 6.7 Hz, H-5^{I}), 4.32–4.48 (m, 13H, H-3$^{I–VII}$, H-5$^{II–VII}$), 4.50–4.60 (m, 9H, H-2$^{I–VIII}$, H-5^{VIII}), 4.92–4.99 (m, 9H, H-4$^{I–VIII}$, H-3^{VIII}), 5.25 (d, 1H, $J_{1,2}$ 3.5 Hz, H-1^{I}), 5.44 (s br, 7H, H-1$^{II–VIII}$). ^{13}C NMR (150 MHz, D_2O): δ 11.4 (CH_2CH_3). 17.1, 17.3 (C-6$^{I–VIII}$), 23.4 (CH_2CH_3), 68.2, 68.4, 69.1 (C-5$^{I–VIII}$), 71.9 (O–CH_2–Et), 73.8 (C-3^{VIII}), 74.1 (C-2^{VIII}), 75.2, 75.7, 76.1, 76.3 (C-3$^{I–VII}$, C-2$^{I–VII}$), 81.3, 82.1 (C-4$^{I–VIII}$), 97.4 (C-1^{I}), 98.8, 100.2 (C-1$^{II–VIII}$). HRESIMS: found *m/z* 964.1730; calcd for $C_{51}H_{71}Na_{17}O_{84}S_{17}$ $[M-3Na]^{3-}$ 964.1707.

4.4.6. Propyl 2,3,4-tri-*O*-sulfonato-α-L-fucopyranosyl-(1→3)-2,4-di-*O*-sulfonato-α-L-fucopyranosyl-(1→3)-2,4-di-*O*-sulfonato-α-L-fucopyranosyl-(1→3)-2,4-di-*O*-sulfonato-α-L-fucopyranosyl-(1→3)-2,4-di-*O*-sulfonato-α-L-fucopyranosyl-(1→3)-2,4-di-*O*-sulfonato-α-L-fucopyranosyl-(1→3)-2,4-di-*O*-sulfonato-α-L-fucopyranosyl-(1→3)-2,4-di-*O*-sulfonato-α-L-fucopyranosyl-(1→3)-2,4-di-*O*-sulfonato-α-L-fucopyranosyl-(1→3)-2,4-di-*O*-sulfonato-α-L-fucopyranosyl-(1→3)-2,4-di-*O*-sulfonato-α-L-fucopyranoside sodium salt (5b)

Per-O-sulfation of **5a** (10 mg, 0.0055 mmol) promoted with TFA (5.1 μL, 0.069 mmol, 0.5 equiv per OH group) during 24 h gave **5b** (17.3 mg, 72%); $[\alpha]_D$ −116 (*c* 1.0, H_2O). ^1H NMR (600 MHz, D_2O): δ 0.93 (t, 3H, *J* 7.4 Hz, CH_2CH_3), 1.27–1.44 (m, 36H, H-6$^{I–XII}$), 1.60–1.69 (m, 2H, CH_2CH_3), 3.54–3.59 (m, 1H, O-CH*H*′-Et), 3.61–3.67 (m, 1H, O–C*H*H′-Et), 4.22 (q, 1H, $J_{5,6}$ 6.7, H-5^{I}), 4.28–4.45 (m, 21H, H-3$^{I–XI}$, H-5$^{II–XI}$), 4.47–4.56 (m, 13H, H-2$^{I–XII}$, H-5^{XII}), 4.88–4.96 (m, 13H, H-4$^{I–XII}$, H-3^{XII}), 5.24 (d, 1H, $J_{1,2}$ 3.3 Hz, H-1^{I}), 5.41 (s br, 11H, H-1$^{II–XII}$). Selected ^{13}C NMR data (150 MHz, CDC_{l3}): 17.2 (C-6$^{I–XVI}$), 68.3, (C-5$^{I–XVI}$), 75.5 76.3, (C-3$^{I–XV}$, C-2$^{I–XVI}$), 81.2, 82.1 (C-4$^{I–XVI}$), 97.4 (C-1^{I}), 100.0, 98.8 (C-1$^{II–XVI}$).

4.4.7. Propyl 2,3,4-tri-*O*-sulfonato-α-L-fucopyranosyl-(1→3)-2,4-di-*O*-sulfonato-α-L-fucopyranosyl-(1→3)-2,4-di-*O*-sulfonato-α-L-fucopyranosyl-(1→3)-2,4-di-*O*-sulfonato-α-L-fucopyranosyl-(1→3)-2,4-di-*O*-sulfonato-α-L-fucopyranosyl-(1→3)-2,4-di-*O*-sulfonato-α-L-fucopyranosyl-(1→3)-2,4-di-*O*-sulfonato-α-L-fucopyranosyl-(1→3)-2,4-di-*O*-sulfonato-α-L-fucopyranosyl-(1→3)-2,4-di-*O*-sulfonato-α-L-fucopyranosyl-(1→3)-2,4-di-*O*-sulfonato-α-L-fucopyranosyl-(1→3)-2,4-di-*O*-sulfonato-α-L-fucopyranosyl-(1→3)-2,4-di-*O*-sulfonato-α-L-fucopyranosyl-(1→3)-2,4-di-*O*-sulfonato-α-L-fucopyranosyl-(1→3)-2,4-di-*O*-sulfonato-α-L-fucopyranosyl-(1→3)-2,4-di-*O*-sulfonato-α-L-fucopyranosyl-(1→3)-2,4-di-*O*-sulfonato-α-L-fucopyranoside sodium salt (6b)

Per-O-sulfation of **6a** (10 mg, 0.0042 mmol) promoted with TFA (5.1 μL, 0.069 mmol, 0.5 equiv per OH group) during 24 h gave **6b** (18.0 mg, 75%); $[\alpha]_D$ −108 (*c* 1.0, H_2O). ^1H NMR (600 MHz, D_2O): δ 0.95 (t, 3H, *J* 7.6 Hz, CH_2CH_3), 1.37 (d, 48H, $J_{5,6}$ 6.1 Hz, H-6$^{I–XVI}$), 1.63–1.70 (m, 2H, CH_2CH_3), 3.55–3.61 (m, 1H, O–CH*H*′-Et), 3.62–3.68 (m, 1H, O–C*H*H′-Et), 4.24 (m, 1H, H-5^{I}), 4.32–4.48 (m, 29H, H-3$^{I–XV}$, H-5$^{II–XV}$), 4.49–4.59 (m, 17H, H-2$^{I–XVI}$, H-5^{XVI}), 4.90–4.97 (m, 17H, H-4$^{I–XVI}$, H-3^{XVI}), 5.26 (d, 1H, $J_{1,2}$ = 3.5 Hz, H-1^{I}), 5.43 (s br, 15H, H-1$^{II–XVI}$). Selected ^{13}C NMR data (150 MHz, D_2O): 17.1 (C-6$^{I–XVI}$), 68.3, (C-5$^{I–XVI}$), 75.5 76.2, (C-3$^{I–XV}$, C-2$^{I–XVI}$), 81.3, 82.1 (C-4$^{I–XVI}$), 97.4 (C-1^{I}), 100.2, 98.8 (C-1$^{II–XVI}$).

4.4.8. Propyl 2,3,4-tri-*O*-sulfonato-α-L-fucopyranosyl-(1→4)-2,3-di-*O*-sulfonato-α-L-fucopyranoside pentasodium salt (7b)

Per-O-sulfation of **7a** (10 mg, 0.028 mmol) promoted with TfOH (12.4 μL, 0.14 mmol 1.0 equiv per OH group) during 24 h gave **7b** (20.3 mg, 83%); $[\alpha]_D$ −96 (*c* 1.0, H_2O). ^1H NMR (600 MHz, D_2O): δ 0.97 (t, 3H, *J* 7.5 Hz, $-CH_2CH_2CH_3$), 1.35 (d, 3H, $J_{5,6}$ 6.5 Hz, H-6^{II}), 1.42 (d, 3H, $J_{5,6}$ 6.6 Hz, H-6^{I}), 1.63–1.71 (m, 2H, $CH_2CH_2CH_3$), 3.58–3.64, 3.68–3.73 (2 × m, 2H, $CH_2CH_2CH_3$), 4.24 (q, 1H, $J_{5,6}$ 6.6 Hz, H-5^{I}), 4.32 (br s, 1H, H-5^{I}), 4.57–4.62 (m, 2H, H-2^{II}, H-5^{II}), 4.67 (dd, 1H, $J_{1,2}$ 3.6 Hz, $J_{2,3}$ 10.8 Hz, H-2^{I}), 4.72 (dd, 1H, $J_{3,4}$ 2.3 Hz, $J_{2,3}$ 10.8 Hz, H-3^{I}), 4.86 (dd, 1H,, $J_{3,4}$ 2.6 Hz, $J_{2,3}$ 10.7 Hz, H-3^{II}), 5.01 (d, 1H, $J_{3,4}$ 2.6 Hz, H-4^{II}), 5.28 (d, 1H, $J_{1,2}$ 3.6 Hz, H-1^{I}), 5.35 (d, 1H, $J_{1,2}$ 3.4 Hz, H-1^{II}). ^{13}C NMR (150 MHz, D_2O): δ 11.4 ($-CH_2CH_2CH_3$), 17.0 (C-6^{I}), 17.3 (C-6^{II}), 23.4 ($-CH_2CH_2CH_3$), 68.5 (C-5^{II}), 68.7 (C-5^{I}), 71.9 ($-CH_2CH_2CH_3$), 73.8 (C-3^{II}), 74.0 (C-2^{I}), 74.2 (C-2^{II}), 75.5 (C-3^{I}), 81.2 (C-4$^{I–II}$), 97.9 (C-1^{I}), 100.3 (C-1^{II}). HRESIMS: found *m/z* 884.8569; calcd for $C_{15}H_{23}Na_5O_{24}S_5$ $[M+Na]^+$ 884.8563; found *m/z* 838.8760; calcd for $[M-Na]^-$ 838.8779.

4.4.9. Propyl 2,3,4-tri-*O*-sulfonato-α-L-fucopyranosyl-(1→4)-2,3-di-*O*-sulfonato-α-L-fucopyranosyl-(1→3)-2,4-di-*O*-sulfonato-α-L-fucopyranosyl-(1→4)-2,3-di-*O*-sulfonato-α-L-fucopyranoside nonasodium salt (8b)

Per-O-sulfation of **8a** (10 mg, 0.016 mmol) promoted with TfOH (12.8 μL, 0.14 mmol, 1.0 equiv per OH group) during 24 h gave **8b** (19.7 mg, 84%); $[\alpha]_D$ −107 (*c* 1.0, H_2O). ^{1}H NMR (600 MHz, D_2O): 0.95 (t, 3H, *J* 7.4 Hz, $CH_2CH_2CH_3$), 1.34–1.42 (m, 12H, H-6$^{I–IV}$), 1.61–1.70 (m, 2H, $CH_2CH_2CH_3$), 3.57–3.61, 3.66–3.71 (2 × m, 2H, $CH_2CH_2CH_3$), 4.23 (q, 1H, $J_{5,6}$ 6.7 Hz, H-5^{I}), 4.31 (br s, 2H, H-4^{I,III}), 4.40 (dd, 1H, $J_{2,3}$ 10.7 Hz, $J_{3,4}$ 2.2 Hz, H-3^{II}), 4.44 (q, 1H, $J_{5,6}$ 6.4 Hz, H-5), 4.53 (q, 1H, $J_{5,6}$ 6.5 Hz, H-5), 4.56–4.64 (m, 4H, H-2$^{I–II,\ IV}$, H-5), 4.68 (dd, 1H, $J_{2,3}$ 10.7 Hz, $J_{3,4}$ 2.2 Hz, H-3^{I}), 4.72 (dd, 1H, $J_{1,2}$ 3.4 Hz, $J_{2,3}$ 10.8 Hz, H-2^{III}), 4.85 (dd, 1H, $J_{2,3}$ 10.7 Hz, $J_{3,4}$ 2.8 Hz, H-3^{IV}), 4.92 (dd, 1H, $J_{2,3}$ 2.4 Hz, $J_{3,4}$ 10.7 Hz, H-3^{III}), 4.96 (d, 1H, $J_{3,4}$ 2.2 Hz, H-4^{II}), 4.99 (d, 1H, $J_{3,4}$ 2.4 Hz, H-4^{IV}), 5.25 (d, 1H, $J_{1,2}$ 3.8 Hz, H-1^{I}), 5.32 (d, 1H, $J_{1,2}$ 3.4 Hz, H-1^{IV}), 5.38 (d, 1H, $J_{1,2}$ 3.4 Hz, H-1^{II}), 5.46 (d, 1H, $J_{1,2}$ 3.4 Hz, H-1^{III}). ^{13}C NMR (150 MHz, D_2O): δ 11.4 (–$CH_2CH_2CH_3$), 17.0, 17.2, 17.3, 17.5 (C-6$^{I–IV}$), 23.4 (–$CH_2CH_2CH_3$), 68.4, 68.8, 69.0, 69.4 (C-5$^{I–IV}$), 71.9 (–$CH_2CH_2CH_3$), 73.2 (C-3^{II}), 73.9 (C-3^{IV}, C-2^{III}), 74.1, 74.2 (C-2^{I,IV}), 74.9 (C-3^{III}), 75.3 (C-2^{II}), 75.8 (C-3^{I}), 80.9 (C-4^{II}), 81.3, 81.4 (C-4$^{I,III–IV}$), 97.5 (C-1^{III}), 97.9 (C-1^{I}), 100.2 (C-1^{IV}), 100.4 (C-1^{II}). HRESIMS: found *m/z* 757.8817; calcd for $C_{27}H_{39}Na_9O_{44}S_9$ $[M-2Na]^{2-}$ 757.8798.

4.4.10. Propyl 2,3,4-tri-*O*-sulfonato-α-L-fucopyranosyl-(1→4)-2,3-di-*O*-sulfonato-α-L-fucopyranosyl-(1→3)-2,4-di-*O*-sulfonato-α-L-fucopyranosyl–(1→4)-2,3-di-*O*-sulfonato-α-L-fucopyranosyl-(1→3)-2,4-di-*O*-sulfonato-α-L-fucopyranosyl-(1→4)-2,3-di-*O*-sulfonato-α-L-fucopyranoside tridecasodium salt (9b)

Per-O-sulfation of **9a** (10 mg, 0.011 mmol) promoted with TfOH (12.7 μL, 0.14 mmol, 1.0 equiv per OH group) during 24 h gave **9b** (20.0 mg, 83%); $[\alpha]_D$ −115 (*c* 1.0, H_2O). ^{1}H NMR (600 MHz, D_2O): 0.96 (t, 3H, *J* 7.5 Hz, $CH_2CH_2CH_3$), 1.35–1.44 (m, 18H, H-6$^{I–VI}$), 1.63–1.70 (m, 2H, $CH_2CH_2CH_3$), 3.57–3.63, 3.67–3.73 (2 × m, 2H, $CH_2CH_2CH_3$), 4.24 (q, 1H, $J_{5,6}$ 6.7 Hz, H-5^{I}), 4.31–4.34 (m, 3H, H-4^{I,III,V}), 4.38–4.41 (m, 2H, H-3^{II,IV}), 4.44 (q, 1H, $J_{5,6}$ 6.6 Hz, H-5), 4.49–4.56 (m, 3H, 3 × H-5), 4.58–4.66 (m, 5H, H-2^{I,II,IV,VI}, H-5), 4.67–4.71 (m, 2H, H-3^{I}, H-2^{III}), 4.72–4.75 (m, 1H, H-2^{V}), 4.86 (dd, 1H, $J_{2,3}$ 10.7 Hz, $J_{3,4}$ 3.0 Hz, H-3^{VI}), 4.91–4.95 (m, 2H, H-3^{III,V}), 4.97–5.01 (3 × d, 3H, $J_{3,4}$ 2.5 Hz, H-4^{II,IV,VI}), 5.27 (d, 1H, $J_{1,2}$ 3.7 Hz, H-1^{I}), 5.34 (d, 1H, $J_{1,2}$ = 3.6 Hz, H-1^{VI}), 5.39, 5.43 (2 × d, 2H, $J_{1,2}$ 3.6 Hz, H-1^{II,IV}), 5.46, 5.48 (2 × d, 2H, $J_{1,2}$ 3.4 Hz, H-1^{III,V}). ^{13}C NMR (150 MHz, D_2O): δ 11.4 (–$CH_2CH_2CH_3$), 17.0, 17.3, 17.5 (C-6$^{I–VI}$), 23.4 (–$CH_2CH_2CH_3$), 68.4, 68.8, 68.9, 69.0, 69.5 (C-5$^{I–VI}$), 71.9 (–$CH_2CH_2CH_3$), 73.2 (C-3^{II}), 73.9, 74.0, 74.1 (C-2^{I,III,V,VI}, C-3^{IV,VI}) 74.9, 75.1 (C-3^{III,V}), 75.4, 75.5 (C-2^{II,IV}), 75.9 (C-3^{I}), 80.9 (C-4^{II}), 81.4, 81.5 (C-4$^{I,III–VI}$), 97.5 (C-1^{III}), 97.9 (C-1^{I}), 98.2 (C-1^{V}), 100.1 (C-1^{VI}), 100.2, 100.3 (C-1^{II,IV}). HRESIMS: found *m/z* 730.8823; calcd for $C_{39}H_{55}Na_{13}O_{64}S_{13}$ $[M-3Na]^{3-}$ 730.8804.

4.4.11. Propyl 2,3,4-tri-*O*-sulfonato-α-L-fucopyranosyl-(1→4)-2,3-di-*O*-sulfonato-α-L-fucopyranosyl-(1→4)-2,3-di-*O*-sulfonato-α-L-fucopyranoside heptasodium salt (10b)

Per-O-sulfation of **10a** (10 mg, 0.020 mmol) promoted with TfOH (12.4 μL, 0.14 mmol, 1.0 equiv per OH group) during 24 h gave **10b** (17.9 mg, 75%); $[\alpha]_D$ −102 (*c* 1.0, H_2O). ^{1}H NMR (600 MHz, D_2O): δ 0.97 (t, 3H, *J* 7.5 Hz, $CH_2CH_2CH_3$), 1.37 (d, 3H, $J_{5,6}$ 6.5 Hz, H-6), 1.42 (d, 3H, $J_{5,6}$ 6.6 Hz, H-6), 1.46 (d, 3H, $J_{5,6}$ 6.7 Hz, H-6), 1.64–1.71 (m, 2H, $CH_2CH_2CH_3$), 3.58–3.63, 3.67–3.73 (2 × m, 2H, $CH_2CH_2CH_3$), 4.23 (q, 1H, $J_{5,6}$ 6.7 Hz, H-5), 4.32 (d, 1H, $J_{3,4}$ 2.4 Hz, H-4^{I}), 4.34 (d, 1H, $J_{3,4}$ 2.5 Hz, H-4^{II}), 4.54 (q, 1H, $J_{5,6}$ 6.6 Hz, H-5), 4.58–4.63 (m, 2H, H-5, H-2^{III}), 4.66–4.72 (m, 3H, H-2$^{I–II}$, H-3^{I}), 4.83–4.87 (m, 2H, H-3$^{II–III}$), 5.00 (d, 1H, $J_{3,4}$ 3.0 Hz, H-4^{III}), 5.28 (d, 1H, $J_{1,2}$ 3.5 Hz, H-1^{I}), 5.33 (d, 1H, $J_{1,2}$ 3.5 Hz, H-1^{III}), 5.37 (d, 1H, $J_{1,2}$ 3.5 Hz, H-1^{II}). ^{13}C NMR (150 MHz, D_2O): δ 11.3 ($CH_2CH_2CH_3$), 17.0, 17.3 (C-6$^{I–III}$), 23.4 ($CH_2CH_2CH_3$), 68.5, 68.8, 69.8 (C-5$^{I–III}$), 71.9 ($CH_2CH_2CH_3$), 73.8 (C-3^{III}), 74.0, 74.2, 74.3 (C-2$^{I–III}$), 75.1 (C-3^{II}), 75.5 (C-3^{I}), 80.6 (C-4^{I}), 81.4 (C-4^{III}), 81.7 (C-4^{II}), 97.9 (C-1^{I}), 100.3 (C-1$^{II–III}$). HRESIMS: found *m/z* 582.9116; calcd for $C_{21}H_{31}Na_7O_{34}S_7$ $[M-2Na]^{2-}$ 582.9116.

4.4.12. Propyl 2,3,4-tri-*O*-sulfonato-α-L-fucopyranosyl-(1→2)-3,4-di-*O*-sulfonato-α-L-fucopyranoside pentasodium salt (11b)

Per-O-sulfation of **11a** (8 mg, 0.022 mmol) promoted with TfOH (9.8 μL, 0.11 mmol, 1.0 equiv per OH group) during 24 h gave **11b** (14.1 mg, 72%); $[\alpha]_D$ −104 (*c* 1.0, H_2O). ^{1}H and ^{13}C NMR spectra coincided with the previously reported ones.[12] HRESIMS: found *m/z* 407.9443; calcd for $C_{15}H_{23}Na_5O_{24}S_5$ $[M-2Na]^{2-}$ 407.9443.

4.4.13. Propyl 2,3,4-tri-*O*-sulfonato-α-D-glucopyranosyl uronic acid-(1→2)-2,3-di-*O*-sulfonato-α-L-fucopyranoside hexasodium salt (12b)

Per-O-sulfation of **12a** (7.3 mg, 0.018 mmol) promoted with TfOH (8.0 μL, 0.09 mmol, 1.0 equiv per OH group) during 24 h gave **12b** (14.0 mg, 85%); $[\alpha]_D$ −14 (*c* 1.0, H_2O). ^{1}H NMR (600 MHz, D_2O): δ 0.96 (t, 3H, *J* 7.5 Hz, –$CH_2CH_2CH_3$), 1.30 (d, 3H, $J_{5,6}$ 6.5 Hz, H-6^{I}), 1.65–1.72 (m, 2H, –$CH_2CH_2CH_3$), 3.60–3.68 (m, 2H, –$CH_2CH_2CH_3$), 3.21 (dd, 1H, $J_{1,2}$ 3.8 Hz, $J_{2,3}$ 10.6 Hz, H-2^{I}), 4.25 (q, 1H, $J_{5,6}$ 6.5 Hz, H-5^{I}), 4.41 (d, 1H, $J_{4,5}$ 5.5 Hz, H-5^{II}), 4.54 (dd, 1H, $J_{1,2}$ 2.3 Hz, $J_{2,3}$ 6.5 Hz, H-2^{II}), 4.73–4.78 (m, 2H, H-3^{I}, H-4^{II}), 4.94–4.98 (m, 2H, H-3^{II}, H-4^{I}), 5.09 (d, 1H, $J_{1,2}$ 3.8 Hz, H-1^{I}), 5.45 (d, 1H, $J_{1,2}$ 2.3 Hz, H-1^{II}). ^{13}C NMR (150 MHz, D_2O): δ 11.3 (–$CH_2CH_2CH_3$), 17.1 (C-6^{I}), 23.4 (–$CH_2CH_2CH_3$), 67.2 (C-5^{I}), 71.9 ($CH_2CH_2CH_3$), 74.17 (C-2^{II}), 75.3 (C-3^{II}, C-2^{I}), 75.7 (C-3^{I}, C-4^{II}), 76.2 (C-5^{II}), 80.5 (C-4^{I}), 97.8 (C-1^{II}), 99.3 (C-1^{I}). HRESIMS: found *m/z* 936.8141; calcd for $C_{15}H_{20}Na_6O_{26}S_5$ $[M+Na]^+$ 936.8125.

4.4.14. Propyl 2,3,4-tri-*O*-sulfonato-α-L-fucopyranosyl-(1→3)-2,4-di-*O*-sulfonato-α-L-fucopyranosyl-(1→3)-2,4-di-*O*-sulfonato-α-L-fucopyranosyl-(1→3)-2,5-di-*O*-sulfonato-α-L-fucofuranoside nonasodium salt (28)

Per-O-sulfation of **2a** (10 mg, 0.016 mmol) promoted with TfOH (25.6 μL, 0.29 mmol, 2.0 equiv per OH group) during 48 h gave **28** (16.7 mg, 71%); $[\alpha]_D$ −126 (*c* 1.0, H_2O). ^{1}H NMR (500 MHz, D_2O): δ 0.91 (t, 3H, *J* 7.5 Hz, CH_2CH_3), 1.32–1.40 (m, 9H, H-6$^{II–IV}$), 1.45 (d, 3H, $J_{5,6}$ 6.4 Hz, H-6^{I}), 1.58–1.67 (m, 2H, CH_2CH_3), 3.43–3.50 (m, 1H, O–CH′-Et), 3.77–3.85 (m, 1H, O–CH′-Et), 4.02 (t, 1H, $J_{3,4}$ $J_{4,5}$ 6.0 Hz, H-4^{I}), 4.28 (dd, 1H, $J_{2,3}$ 10.4 Hz, $J_{3,4}$ 2.5 Hz, H-3^{II}), 4.34–4.42 (m, 4H, H-3^{I,III}, H-5^{II,III}), 4.50–4.61 (m, 4H, H-2$^{II–IV}$, H-5^{IV}), 4.61–4.65(m, 1H, H-5^{I}), 4.77 (dd, 1H, $J_{1,2}$ 4.4 Hz, $J_{2,3}$ 7.3 Hz, H-2^{I}), 4.87–4.95 (m, 6H, H-4$^{II–IV}$, H-3^{IV}), 5.23 (d, 1H, $J_{1,2}$ 4.4 Hz, H-1^{I}), 5.39–5.44 (m, 3H, H-1$^{II–IV}$). ^{13}C NMR (125 MHz, D_2O): δ11.2 (CH_2CH_3); 17.2, 17.5 (C-6$^{II–IV}$), 18.0 (C-6^{I}), 23.3 (CH_2CH_3), 68.1 (C-5^{II}), 68.7, 69.1 (C-5$^{III–IV}$), 71.8 (O–CH_2–Et), 73.8 (C-3^{IV}), 73.9 (C-2^{IV}), 75,2, 75.5, 75.6, 75,7 (C-2^{II,III}, C-3^{II,III}), 78.6 (H-5^{I}), 81.2 (C-3^{I}), 81.3, 81.5, 81.6 (C-4$^{II–VI}$), 83.9 (C-4^{I}), 98.4, 99.5 (C-1$^{II–IV}$), 101.2 (C-1^{I}). HRESIMS: found *m/z* 757.8783; calcd for $C_{27}H_{39}Na_9O_{44}S_9$ $[M-2Na]^{2-}$ 757.8798.

4.4.15. Propyl 2,3,4-tri-*O*-sulfonato-α-L-fucopyranosyl-(1→3)-2,4-di-*O*-sulfonato-α-L-fucopyranosyl-(1→3)-2,4-di-*O*-sulfonato-α-L-fucopyranosyl-(1→3)-2,4-di-*O*-sulfonato-αα-L-fucopyranosyl-(1→3)-2,4-di-*O*-sulfonato-α-L-fucopyranosyl-(1→3)-2,5-di-*O*-sulfonato-α-L-fucofuranoside tridecasodium salt (29)

Per-O-sulfation of **3a** (10 mg, 0.011 mmol) promoted with TfOH (25.4 μL, 0.29 mmol, 2.0 equiv per OH group) during 48 h gave **29**

(17.8 mg, 74%); $[\alpha]_D$ −138 (*c* 0.5, H_2O). ^1H NMR (500 MHz, D_2O): δ 0.93 (t, 3H, *J* 7.4 Hz, CH_2CH_3), 1.30–1.38 (m, 15H, H-$6^{II–VI}$), 1.45 (d, 3H, $J_{5,6}$ 6.4 Hz, H-6^{I}), 1.58–1.67 (m, 2H, CH_2CH_3), 3.44–3.51 (m, 1H, O–CH*H*′-Et), 3.77–3.86 (m, 1H, O–C*H*H′-Et), 4.02 (t, 1H, $J_{3,4}$ $J_{4,5}$ 6.0 Hz, H-4^{I}), 4.26 (dd, 1H, $J_{2,3}$ 10.4 Hz, $J_{3,4}$ 2.5 Hz, H-3^{II}), 4.34–4.46 (m, 8H, H-$3^{I,III–V}$, H-$5^{II–V}$), 4.48–4.58 (m, 6H, H-$2^{II–VI}$, H-5^{VI}), 4.58–4.65 (m, 1H, H-5^{I}), 4.77 (dd, 1H, $J_{1,2}$ 4.4 Hz, $J_{2,3}$ 7.3 Hz, H-2^{I}), 4.90–4.97 (m, 6H, H-$4^{II–VI}$, H-3^{VI}), 5.23 (d, 1H, $J_{1,2}$ 4.4 Hz, H-1^{I}), 5.39–5.44 (m, 5H, H-$1^{II–VI}$). ^{13}C NMR (125 MHz, D_2O): δ 11.2 (CH_2CH_3); 17.3 (C-$6^{II–VI}$), 18.0 (C-6^{I}), 23.3 (CH_2CH_3), 68.2 (C-5^{II}), 68.8, 69.0, 69.3 (C-$5^{III–VI}$), 71.8 (O–CH_2–Et), 73.8 (C-3^{VI}), 74.0 (C-2^{VI}), 75.5, 75.7, 75.9 (C-$3^{III–V}$, C-$2^{II–V}$), 76.6 (H-3^{II}), 78.6 (H-5^{I}), 81.2 (C-3^{I}), 81.9, 81.5, 81.3 (C-$4^{II–VI}$), 83.9 (C-4^{I}), 100.3, 98.8, 98.4 (C-$1^{II–VI}$), 101.3 (C-1^{I}). HRESIMS: found *m/z* 1107.8149; calcd for $C_{39}H_{55}Na_{13}O_{64}S_{13}$ $[M-2Na]^{2-}$ 1107.8152.

4.4.16. Propyl 2,3,4-tri-*O*-sulfonato-α-L-fucopyranosyl-(1→3)-2,4-di-*O*-sulfonato-α-L-fucopyranosyl-(1→3)-2,4-di-*O*-sulfonato-α-L-fucopyranosyl-(1→3)-2,4-di-*O*-sulfonato-α-L-fucopyranosyl-(1→3)-2,4-di-*O*-sulfonato-α-L-fucopyranosyl-(1→3)-2,4-di-*O*-sulfonato-α-L-fucopyranosyl-(1→3)-2,4-di-*O*-sulfonato-α-L-fucopyranosyl-(1→3)-2,5-di-*O*-sulfonato-α-L-fucofuranoside heptadecasodium salt (30)

Per-O-sulfation of **4a** (10 mg, 0.0081 mmol) promoted with TfOH (24.4 μL, 0.28 mmol, 2.0 equiv per OH group) during 48 h gave **30** (16.6 mg, 69%); $[\alpha]_D$ −121 (*c* 1.0, H_2O). ^1H NMR (500 MHz, D_2O): δ 0.93 (t, 3H, *J* 7.4 Hz, CH_2CH_3), 1.30–1.40 (m, 21H, H-$6^{II–VIII}$), 1.45 (d, 3H, $J_{5,6}$ 6.5 Hz, H-6^{I}), 1.58–1.66 (m, 2H, CH_2CH_3), 3.43–3.51 (m, 1H, O–CH*H*′-Et), 3.77–3.87 (m, 1H, O–C*H*H′-Et), 4.04 (t, 1H, $J_{3,4}$ $J_{4,5}$ 5.9 Hz, H-4^{I}), 4.25 (dd, 1H, $J_{2,3}$ 10.3 Hz, $J_{3,4}$ 2.3 Hz, H-3^{II}), 4.30–4.45 (m, 12H, H-$3^{I,III–VII}$, H-$5^{II–VII}$), 4.48–4.57 (m, 8H, H-$2^{II–VIII}$, H-5^{VIII}), 4.57–4.67 (m, 1H, H-5^{I}), 4.78 (dd, 1H, $J_{1,2}$ 4.4 Hz, $J_{2,3}$ 7.3 Hz, H-2^{I}), 4.89–4.96 (m, 8H, H-$4^{II–VIII}$, H-3^{VIII}), 5.23 (d, 1H, $J_{1,2}$ = 4.4 Hz, H-1^{I}), 5.37–5.43 (m, 7H, H-$1^{II–VIII}$). ^{13}C NMR (125 MHz, D_2O): δ 11.2 (CH_2CH_3), 17.3 (C-$6^{II–VIII}$), 18.1 (C-6^{I}), 23.3 (CH_2CH_3), 68.2 (C-5^{II}), 68.8, 68.9, 69.3 (C-$5^{III–VIII}$), 71.8 (O–CH_2–Et), 73.8 (C-3^{VIII}), 74.1 (C-2^{VIII}), 75.5, 75.6, 75.9 (C-$3^{III–VII}$, C-$2^{II–VII}$), 76.5 (H-3^{II}), 78.5 (H-5^{I}), 81.1 (C-3^{I}), 81.3, 81.5, 82.0 (C-$4^{II–VI}$), 83.9 (C-4^{I}), 98.4, 98.6, 100.2 (C-$1^{II–VIII}$), 101.2 (C-1^{I}). HRESIMS: found *m/z* 1503.7348; calcd for $C_{51}H_{71}Na_{17}O_{84}S_{17}$ $[M+2Na]^{2+}$ 1503.7291.

Acknowledgments

This work was supported by the Russian Foundation for Basic Research (Grant 10-03-00980-a) and a grant from the President of the Russian Federation to Young Scientists, MK-3901.2009.4 and MK-5544.2010.3. High resolution mass spectra were recorded in the Department of Structural Studies of Zelinsky Institute of Organic Chemistry, Moscow.

Supplementary data

Supplementary data (high resolution mass spectra of non-protected and sulfated oligofucosides) associated with this article can be found, in the online version, at doi:10.1016/j.carres.2011.01.005.

References

1. Zlotina, N. S.; Ustyuzhanina, N. E.; Grachev, A.; Gerbst, A. A.; Nifantiev, N. E. *J. Carbohydr. Chem.* **2008**, *27*, 429–445.
2. Krylov, V. B.; Ustyuzhanina, N. E.; Grachev, A. E.; Nifantiev, N. *Tetrahedron Lett.* **2008**, *49*, 5877–5879.
3. Cumashi, A.; Ushakova, N. A.; Preobrazhenskaya, M. E.; D'Incecco, A.; Piccoli, A.; Totani, L.; Tinari, N.; Morozevich, G. E.; Berman, A. E.; Bilan, M. I.; Usov, A. I.; Ustyuzhanina, N. E.; Grachev, A. A.; Sanderson, C. J.; Kelly, M.; Rabinovich, G. A.; Iacobelli, S.; Nifantiev, N. E. *Glycobiology* **2007**, *17*, 541–552.
4. Pomin, V. *Biopolymers* **2009**, *91*, 601–609.
5. Berteau, O.; Mulloy, B. *Glycobiology* **2003**, *13*, 29R–40R.
6. Mourau, P. A. S. *Curr. Pharm. Des.* **2004**, *10*, 964–981.
7. Ustyuzhanina, N.; Krylov, V.; Grachev, A.; Gerbst, A.; Nifantiev, N. *Synthesis* **2006**, *23*, 4017–4031.
8. Khatuntseva, E. A.; Ustuzhanina, N. E.; Zatonskii, G. V.; Shashkov, A. S.; Usov, A. I.; Nifantiev, N. E. *J. Carbohydr. Chem.* **2004**, *19*, 1151–1173.
9. Gerbst, A. G.; Ustuzhanina, N. E.; Grachev, A. A.; Tsvetkov, D. E.; Khatuntseva, E. A.; Whitefield, D. M.; Berces, A.; Nifantiev, N. E. *J. Carbohydr. Chem.* **2001**, *20*, 821–831.
10. Gerbst, A. G.; Ustuzhanina, N. E.; Grachev, A. A.; Tsvetkov, D. E.; Khatuntseva, E. A.; Nifantiev, N. E. *J. Carbohydr. Chem.* **2002**, *21*, 313–324.
11. Gerbst, A. G.; Ustuzhanina, N. E.; Grachev, A. A.; Tsvetkov, D. E.; Khatuntseva, E. A.; Shashkov, A. S.; Usov, A. I.; Preobrazhenskaya, M. E.; Ushakova, N. A.; Nifantiev, N. E. *J. Carbohydr. Chem.* **2003**, *22*, 109–122.
12. Gerbst, A. G.; Grachev, A. A.; Ustyuzhanina, N. E.; Khatuntseva, E. A.; Tsvetkov, D. E.; Usov, A. I.; Shashkov, A. S.; Preobrazhenskaya, M. E.; Ushakova, N. A.; Nifantiev, N. E. *Russ. J. Bioorg. Chem.* **2004**, *30*, 137–147.
13. Ustyuzhanina, N. E., Krylov, V. B., Usov, A. I., Nifantiev, N. E., Eds.Progress in the synthesis of complex carbohydrate chains of plant and microbial polysaccharides; Nifantiev, N. E., Ed.; Transworld Research Network: Kerala, 2009; Vol. 6, pp 131–154.
14. Grachev, A. A.; Gerbst, A. G.; Ustuzhanina, N. E.; Khatuntseva, E. A.; Shashkov, A. S.; Usov, A. I.; Nifantiev, N. E. *J. Carbohydr. Chem.* **2005**, *24*, 85–99.
15. Grachev, A. A.; Gerbst, A. G.; Ustuzhanina, N. E.; Shashkov, A. S.; Usov, A. I.; Nifantiev, N. E. *J. Carbohydr. Chem.* **2006**, *25*, 315–330.
16. Grachev, A. A.; Gerbst, A. G.; Ustuzhanina, N. E.; Krylov, V. B.; Shashkov, A. S.; Usov, A. I.; Nifantiev, N. E. *Mendeleev Commun.* **2007**, *17*, 57–62.
17. Nishino, T.; Nagumo, T. *Carbohydr. Res.* **1992**, *229*, 355–362.
18. Usov, A. I.; Smirnova, G. P.; Bilan, M. I.; Shashkov, A. S. *Bioorg. Khim.* **1998**, *24*, 437–445.
19. Bilan, M. I.; Grachev, A. A.; Shashkov, A. S.; Kelly, M.; Sanderson, C. J.; Nifantiev, N. E.; Usov, A. I. *Carbohydr. Res.* **2010**, *345*, 2038–2047.
20. Lane, C. E.; Mayes, C.; Druehl, L. D.; Saunders, G. W. *J. Phycol.* **2006**, *42*, 493–512.
21. Chizhov, A. O.; Dell, A.; Morris, H. R.; Haslam, S. M.; McDowell, R. A.; Shashkov, A. S.; Nifantiev, N. E.; Khatuntseva, E. A.; Usov, A. I. *Carbohydr. Res.* **1999**, *320*, 108–119.
22. Nagaoka, M.; Shibata, H.; Kimura-Takagi, I.; Hashimoto, S.; Kimura, K.; Aiyama, R.; Ueyama, S.; Yokokura, T. *Glycoconjugate J.* **1999**, *16*, 19–26.
23. Bilan, M. I.; Grachev, A. A.; Ustuzhanina, N. E.; Shashkov, A. S.; Nifantiev, N. E.; Usov, A. I. *Carbohydr. Res.* **2002**, *337*, 719–730.
24. Bilan, M. I.; Grachev, A. A.; Ustuzhanina, N. E.; Shashkov, A. S.; Nifantiev, N. E.; Usov, A. I. *Carbohydr. Res.* **2004**, *339*, 511–517.
25. Chevolot, L.; Foucault, A.; Chaubet, F.; Kervarec, N.; Sinquin, C.; Fisher, A.-M.; Boisson-Vidal, C. *Carbohydr. Res.* **1999**, *319*, 154–165.
26. Yoon, S. J.; Pyun, Y. R.; Hwang, J. K.; Mourao, P. A. S. *Carbohydr. Res.* **2007**, *342*, 2326–2330.
27. Alves, A.-P.; Mulloy, B.; Diniz, J. A.; Mourao, P. A. S. *J. Biol. Chem.* **1997**, *272*, 6965–6971.
28. Ziegler, T. *Carbohydr. Res.* **1994**, *262*, 195–212.
29. Hua, Y.; Du, Y.; Yu, G.; Chu, S. *Carbohydr. Res.* **2004**, *339*, 2083–2090.
30. Gelin, M.; Ferrieres, V.; Lefeuvre, M.; Plusquellec, D. *Eur. J. Org. Chem.* **2003**, 1285–1293.
31. Breitmaier, E.; Voelter, W., Eds.; In *Carbon-13 NMR Spectroscopy,* 3rd ed.; VCH: Weinheim, 1989; p 384.
32. McPhail, D.; Lee, J.; Fraser-Reid, B. *J. Am. Chem. Soc.* **1992**, *114*, 1905–1906.
33. Liras, J.; Anslyn, E. *J. Am. Chem. Soc.* **1994**, *116*, 2645–2646.
34. Lichtenthaler, F. W.; Breunig, J.; Fischer, W. *Tetrahedron Lett.* **1971**, *12*, 2825–2828.
35. Quan, Wang; Peng, Ding; Perepelov, A. V.; Yanli, Xu; Ying, Wang; Knirel, Y. A.; Lei, Wang; Lu, Feng. *Mol. Microbiol.* **2008**, *70*, 1358–1367.
36. Armarego, W. L. F.; Chai, C. L. L. Purification of Laboratory Chemicals, 5th ed.; Butterworth: Heinemann, 2003.
37. Belyakov, P. A.; Kadentsev, V. I.; Chizhov, A. O.; Kolotyrkina, N. G.; Shashkov, A. S.; Ananikov, V. P. *Mendeleev Commun.* **2010**, *20*, 125–131.

Glycochemistry

Pyranoside-into-Furanoside Rearrangement: New Reaction in Carbohydrate Chemistry and Its Application in Oligosaccharide Synthesis

Vadim B. Krylov,[a] Dmitry A. Argunov,[a] Dmitry Z. Vinnitskiy,[a] Stella A. Verkhnyatskaya,[a] Alexey G. Gerbst,[a] Nadezhda E. Ustyuzhanina,[a] Andrey S. Dmitrenok,[a] Johannes Huebner,[b] Otto Holst,[c] Hans-Christian Siebert,[d] and Nikolay E. Nifantiev*[a]

Abstract: Great interest in natural furanoside-containing compounds has challenged the development of preparative methods for their synthesis. Herein a novel reaction in carbohydrate chemistry, namely a pyranoside-into-furanoside (PIF) rearrangement permitting the transformation of selectively O-substituted pyranosides into the corresponding furanosides is reported. The discovered process includes acid-promoted sulfation accompanied by rearrangement of the pyranoside ring into a furanoside ring followed by solvolytic O-desulfation. This process, which has no analogy in organic chemistry, was shown to be a very useful tool for the synthesis of furanoside-containing complex oligosaccharides, which was demonstrated by synthesizing disaccharide derivatives α-D-Gal*p*-(1→3)-β-D-**Gal*f***-OPr, 3-*O*-S-lactyl-β-D-**Gal*f***-(1→3)-β-D-Glc*p*-OPr, and α-L-**Fuc*f***-(1→4)-β-D-Glc*p*A-OPr related to polysaccharides from the bacteria *Klebsiella pneumoniae* and *Enterococcus faecalis* and the brown seaweed *Chordaria flagelliformis*.

Introduction

Different types of furanosyl residues are included in the structures of a variety of natural compounds, especially bacterial, plant, and fungal polysaccharides.[1,2] The synthesis of oligosaccharides related to these biopolymers, as well as glycoconjugates thereof, is often dictated by the needs of vaccine and diagnostics development.[3–6] Currently, the most widely used methods for furanoside synthesis are based on the initial transformation of unblocked monosaccharides by the Fischer reaction under kinetic control[7,8] or their high-temperature acylation.[7,9] All of these reactions proceed with the formation of a mixture of α- and β-furanosides and are contaminated by respective pyranoside isomers that may require laborious chromatography in order to separate the target products. It is also notable that further regioselective introduction of O-blocking groups into furanosides can be more difficult than in the case of related pyranoside derivatives.

The idea of pyranoside-into-furanoside (PIF) rearrangement came from our recent observation[10] that an unusual oligosaccharide impurity with a terminal (at the "reducing end") furanoside residue (e.g., disaccharide **C** on Figure 1) in addition to the expected pyranoside product (e.g., compound **B**) was formed in acid-promoted O-sulfation[11] of oligofucosides (e.g., disaccharide **A**) related to seaweed fucoidans. It was shown that per-O-sulfation by Py·SO_3 complex was accompanied by the formation of unexpected furanoside byproducts of type **C** only in the presence of a strong acid (trifluoromethanesulfonic or chlorosulfonic acid), while no formation of such compounds was observed, when a weaker acid promoter, particularly, the trifluoroacetic acid, was used.[10]

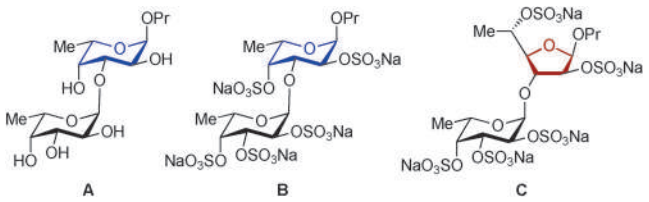

Figure 1. Difucopyranoside **A** and the products of its acid-promoted O-sulfation with pyranoside (**B**) and furanoside (**C**) terminal residues.[10]

[a] *Dr. V. B. Krylov, D. A. Argunov, D. Z. Vinnitskiy, S. A. Verkhnyatskaya, Dr. A. G. Gerbst, Dr. N. E. Ustyuzhanina, Dr. A. S. Dmitrenok, Prof. Dr. N. E. Nifantiev*
Laboratory of Glycoconjugate Chemistry
N.D. Zelinsky Institute of Organic Chemistry, Russian Academy of Sciences
Leninsky prospect 47, 119991 Moscow (Russian Federation)
E-mail: nen@ioc.ac.ru

[b] *Prof. Dr. J. Huebner*
Division of Pediatric Infectious Diseases, Hauner Children's Hospital
Ludwigs-Maximilian University, Munich (Germany)

[c] *Prof. Dr. O. Holst*
Research Center Borstel
Leibniz-Center for Medicine and Biosciences, Borstel (Germany)

[d] *Prof. Dr. H.-C. Siebert*
RI-B-NT - Research Institute of Bioinformatics and Nanotechnology
24118 Kiel (Germany)

Supporting information for this article is available on the WWW under http://dx.doi.org/10.1002/chem.201405083.

Observed PIF rearrangement has no analogy in organic chemistry and can be compared formally only with enzymatic isomerization of sugar nucleotides mediated by pyranose–furanose mutase (Scheme 1).[12] The discovered intriguing side process challenged us to study whether it can be performed in a straightforward way within the context of synthesizing oligosaccharides bearing furanoside units. Herewith we report our first results from this study.

Scheme 1. Conversion of UDP-Gal*p* into UDP Gal*f* by UDP-galactopyranose mutase.[12]

Results and Discussion

To optimize the PIF rearrangement protocol, readily available 3-*O*-benzyl-β-D-galactopyranoside (**1**)[13] was used as a model substrate (Scheme 2).

It was treated under the conditions leading to the formation of furanoside byproducts from oligofucopyranosides.[10] It appeared that its treatment with the Py·SO_3 complex in the presence of chlorosulfonic acid in DMF at room temperature (see general procedure in Experimental Section and Supporting Information) readily gave per-O-sulfated rearranged furanoside product **3** via the initial formation of per-O-sulfated derivative **2**, which was detected first by ^{1}H NMR spectroscopy on the basis of its characteristic downfield shifts of the *H*-2, *H*-4, and *H*-6 signals (see the Supporting Information). ^{13}C NMR monitoring of the reaction mixture revealed that already after 10 min all of compound **1** had been transformed into sulfate **2** (Figure 2), and after 2 h about 30% of pyranoside **2** was rearranged into furanoside **3**. Further prolongation of the treatment time up to 48 h afforded complete PIF rearrangement to give sulfated galactofuranoside **3**. Its further O-desulfation under conventional solvolysis[14,15] by Py·HCl in a dioxane/DMF mixture gave galactofuranoside **4**.

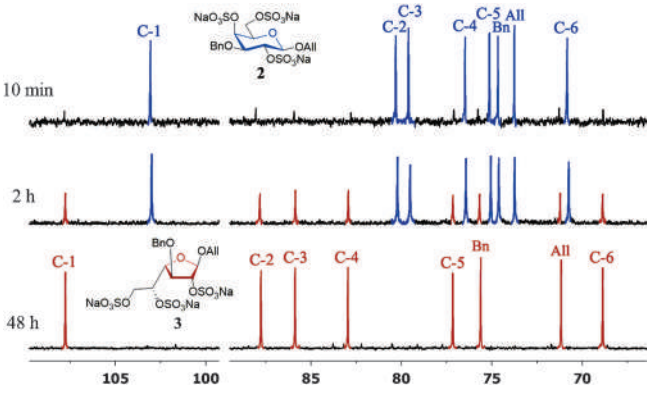

Figure 2. ^{13}C NMR spectroscopy monitoring of galactopyranoside **1** transformation into galactofuranoside **3**: after 10 min (total conversion of **1** into tri-O-sulfated intermediate **2** with minor formation of **3**), after 2 h (mixture of **2** and **3**, ~2:1), and after 48 h (complete formation of the furanoside **3**).

The structures of galactofuranoside derivatives **3** and **4** were confirmed by HR-mass and NMR spectroscopy data. Particularly, the HMBC spectrum of product **3** contained a correlation peak between *C*-4 and *H*-1, while there were no correlations between *C*-5 and *H*-1, clearly evidencing the presence of the furanoside ring. In addition, the removal of the Bn group and reduction of allyl in **4** by catalytic hydrogenolysis gave propyl β-D-galactofuranoside **5**, whose ^{1}H and ^{13}C NMR spectra coincided well with the published spectra of *n*-octyl β-galactofuranoside.[16]

It is reasonable to assume that the rearrangement starts with the protonation of *O*-5 giving pre-reaction intermediate **A** (Scheme 2). Further transformation of the pyranoside ring in **A** was studied employing ab initio RHF calculations (see the Supporting Information). It is supposed that the rate-determining step in the PIF rearrangement was the formation of open-ring intermediate **C**, which proceeded via transition state **B**. In this case, further recyclization of **C** accompanied by sulfate transfer should yield furanoside **3**. The geometry of the transition state (**B**) obtained in the calculations led us to the conclusion that the sulfate group at *O*-2 might participate in the *O*(5)–*C*(1) bond cleavage, facilitating this process and contributing to the

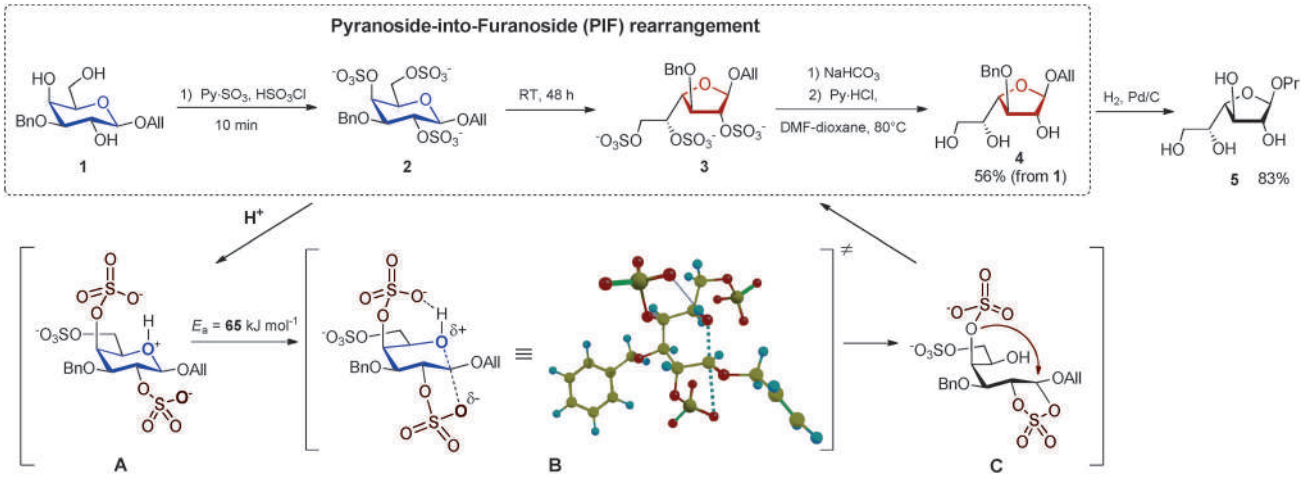

Scheme 2. The per-O-sulfation of β-D-galactopyranoside **1** followed by **2**→**3** isomerization and putative intermediate structures **A**–**C**.

fixation of the anomeric configuration during the rearrangement.

To confirm the crucial role of the sulfate group at *O*-2, we prepared 2-O-acetylated derivative **6** from galactoside **1** with intermediate 4,6-acetonation and hydrolysis steps (Scheme 3, for details see Supporting Information). As expected, the treatment of 2-O-acetylated derivative **6** under standard PIF conditions resulted only in totally sulfated pyranoside **7** without the formation of even traces of the furanoside derivative. Remarkably, the activation energy for 2-O-sulfated derivative **2** calculated as the difference between **A** and **B** was 65 kJ mol^{-1} (Scheme 2); when the substituent at *O*-2 was changed to acetate in the calculations, the activation energy (difference between **E** and **D**) was much higher, reaching 117 kJ mol^{-1} (Scheme 3). This fact supports the above discussed mechanism of the PIF rearrangement. Its further investigation is in progress and will be reported elsewhere.

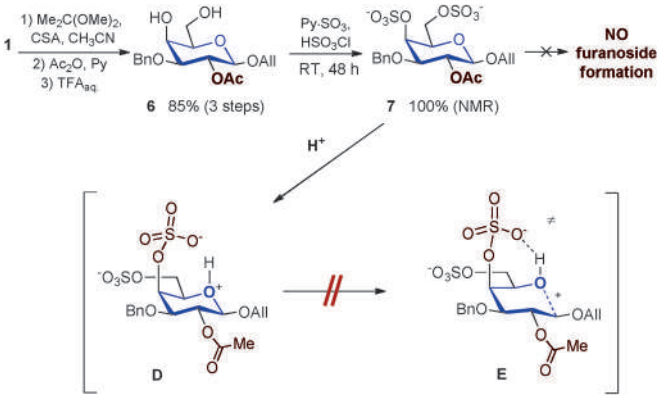

Scheme 3. The preparation of non-rearrangeable 2-O-acetylated derivative **6** and structures of putative protonated structures **D** and **E**.

3-*O*-Benzyl-β-D-galactopyranoside (**1**) was used as a model substrate to optimize the protocol for the PIF rearrangement, because its furanoside isomer **4** was regarded as a convenient precursor for the planned synthesis of disaccharide **11** representing the repeating unit of the O-specific polysaccharide (OPS) of *Klebsiella pneumonia* (Scheme 4). This bacterium causes pneumonia, bacteremia, and urinary tract infections with high incidence and mortality.[17] The OPS chain is built up of the disaccharide repeating unit [→3)-α-D-Gal*p*-(1→3)-β-D-Gal*f*-(1→].[18,19] Disaccharide **11**, representing this repeating unit, was prepared as a molecular probe to study the topology of OPS recognition by lysozyme and other proteins of the immune system.

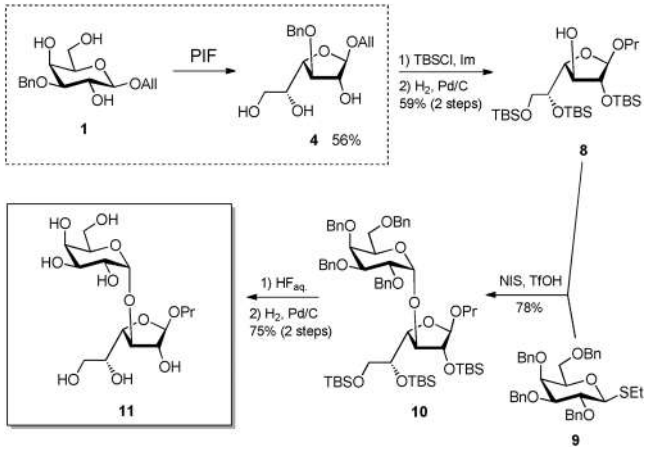

Scheme 4. The synthesis of disaccharide **11** related to OPS of *K. pneumonia*.

Silylation of compound **4** with TBSCl in DMF followed by hydrogenolysis gave monohydroxy derivative **8** (Scheme 4). Its glycosylation with ethylthio galactopyranoside **9**[20] gave α-linked disaccharide **10**, the deprotection of which afforded the target disaccharide **11** in a yield of 75%.

The applicability of PIF rearrangement was also demonstrated by the synthesis of disaccharide **20**, related to fucoidan from the brown seaweed *Chordaria flagelliformis*[21] (Scheme 5). Polysaccharide fucoidans from brown seaweeds demonstrate promising types of biological activity[22–27] that stimulate the preparation of related oligosaccharides as models for QSAR studies.

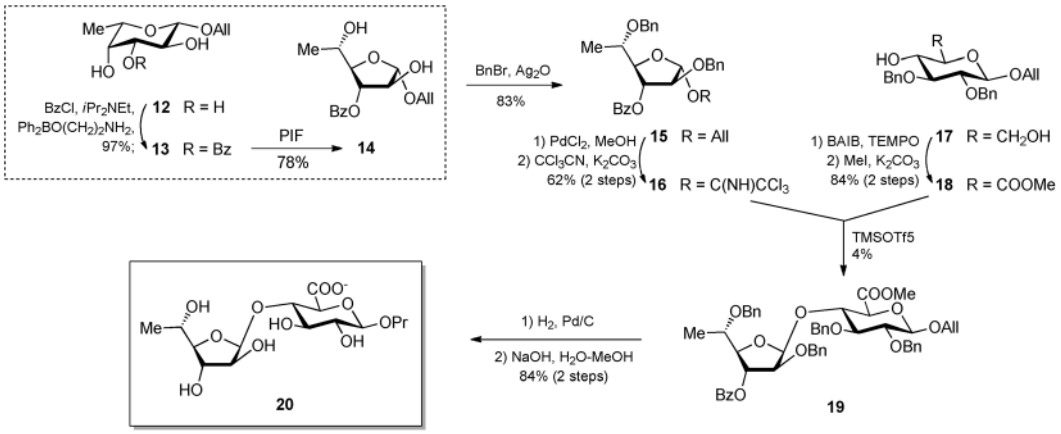

Scheme 5. The synthesis of disaccharide **20** related to fucoidan from *C. flagelliformis*.

3-*O*-Benzoylated allyl β-L-fucofuranoside (**14**) was chosen as the main precursor towards disaccharide **20** with the aim of exploring the remote stereocontrolling effect[28,29] of the 3-*O*-benzoyl group for efficient α-fucofuranosylation during disaccharide assembly (Scheme 5). Compound **13** was prepared in high yield by the regioselective benzoylation of triol **12**[30] via intermediate generation of an organoboron intermediate.[31] Further PIF rearrangement of pyranoside **13** proceeded smoothly with formation of the required furanoside **14**. Its benzylation followed by anomeric deallylation and imidate formation gave the fucofuranosyl donor **16**. Coupling of monosaccharides **16** and **18** (obtained from diol **17**[32] by regioselective oxidation of the primary OH group at *C*-6, see the Supporting Information) in the presence of TMSOTf gave stereoselectively α-linked disaccharide **19**. Deprotected disaccharide **20** was obtained by hydrogenolysis and saponification of product **19**, which can be regarded as a convenient block for the assembly of larger oligosaccharides *via* *O*-deallylation followed by transformation into glycosyl donor derivatives.

The synthetic potential of PIF rearrangement was also demonstrated by the preparation of mono- (**30**) and disaccharides (**34**) related to the diheteroglycan polysaccharide of *Enterococcus faecalis*, which is built up from repeating disaccharide units with the formula [→6)-3-*O*-lactyl-β-D-Gal*f*-(1→3)-β-D-Glc*p*-(1→].[33] *Enterococci* are currently the third most common pathogen (among Gram-positive bacteria) causing hospital-associated infections in the US, and are the second most common pathogen isolated from intensive care unit patients worldwide.[34] Oligosaccharides related to the heteroglycan chain are regarded as promising components for vaccine design.[33]

Selectively substituted galactopyranoside **25** bearing the 3-*O*-lactyl group was used as a substrate for PIF rearrangement (Scheme 6).

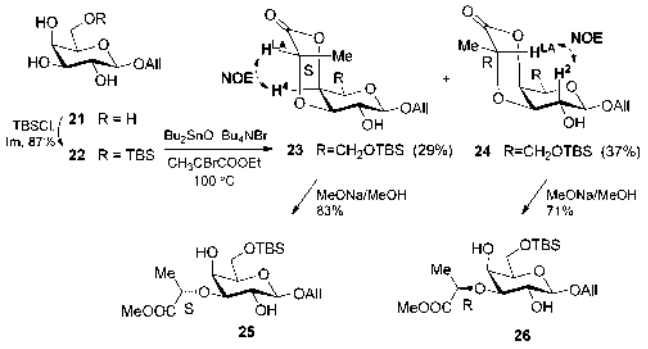

Scheme 6. The synthesis of galactopyranosides **25** and **26** bearing 3-*O*-lactyl substituent.

Its preparation was performed by regioselective 6-*O*-silylation with TBSCl of readily available allyl β-D-galactopyranoside **21**[35] followed by alkylation of triol **22** with racemic ethyl 2-bromopropionate via an organotin intermediate[36] (see the Supporting Information). These reactions gave a mixture of bicyclic lactones dominated by compounds **23** and **24**, which were isolated in their individual forms. Their structures, including the configurations of lactic units, were assessed by NMR spectroscopy with NOE experiments (shown in the Supporting Information). These demonstrated the spatial proximity of the H^{LA} and *H*-4 protons in **23** but of H^{LA} and *H*-2 in **24**. Based on these data, the *S*- and *R* configurations of lactic units were ascribed to compounds **23** and **24**, respectively. The lactones in **23** and **24** were further transformed into isomeric esters **25** and **26** under treatment with MeONa in anhydrous MeOH. Compound **25** was used for the further preparation of furanoside derivatives **30** and **34** (Scheme 7). Thus, PIF rearrangement of **25** gave intermediate product **27**, the solvolytic O-desulfation of which in a DMF/dioxane mixture in the presence of Py·HCl followed by saponification gave target monosaccharide **30**.

Alternatively to the above-described solvolytic protocol, O-desulfation can be also performed by acetolysis to give corresponding per-acetylated derivatives (see transformation **27**→**28** in Scheme 7). Acetolysis of the sulfate groups is accompanied by the cleavage of the glycoside bond with the formation of the corresponding acetate, which is a valuable precursor in the preparation of various furanosyl donors. Thus, acetolysis of **27** in the presence of $AcOH/Ac_2O/H_2SO_4$ gave tetraacetate **28** as a mixture of α- and β-isomers ($\alpha/\beta = 1{:}3$). Selective removal of the anomeric acetate in compound **28** followed by treatment with *N*-phenyltrifluoroacetimidoyl chloride afforded galactofuranoside donor **29**. The spacer-armed glycosyl acceptor **32** was prepared from the known diol **31**[37] by regioselective 2-O-benzoylation by the method of Szeja[38] as modified by Krepinsky.[39] Coupling of acceptor **32** and the galactofuranosyl donor **29** proceeded smoothly and gave disaccharide **33** in good yield. Its deprotection gave the spacer-armed disaccharide **34**. The application of compounds **30** and **34** in immunobacteriological investigations as well as in the structural assessment of diheteroglycan of *E. faecalis* will be published elsewhere.

The described examples of PIF rearrangement demonstrate its applicability for the transformation of monosaccharide derivatives with allyl, benzyl, benzoyl, and lactyl substituents. Moreover, it turned out that the discovered procedure could also be used for PIF rearrangement of oligosaccharides. Thus, the treatment of disaccharide **36** (Scheme 8) afforded the rearranged product **37** bearing the furanoside residue at the "reducing end". Its hydrogenolysis gave disaccharide **11**, revealing an alternate synthesis strategy towards this compound in addition to that shown in Scheme 4. Substrate **36** was prepared from the known disaccharide **35**[40] by acidic hydrolysis with aqueous TFA as described in Supporting Information.

It is remarkable that the PIF rearrangement proceeds with the retention of the anomeric configuration. Thus, only α-furanosides were obtained from α-pyranosides (see compounds **A** and **C** in Figure 1).[10] Similarly, all β-pyranoside substrates described above gave exclusively β-furanosides (see transformation **1**→**4** on Scheme 2, **13**→**14** on Scheme 5, **25**→**30** on Scheme 7 and **36**→**37** on Scheme 8).

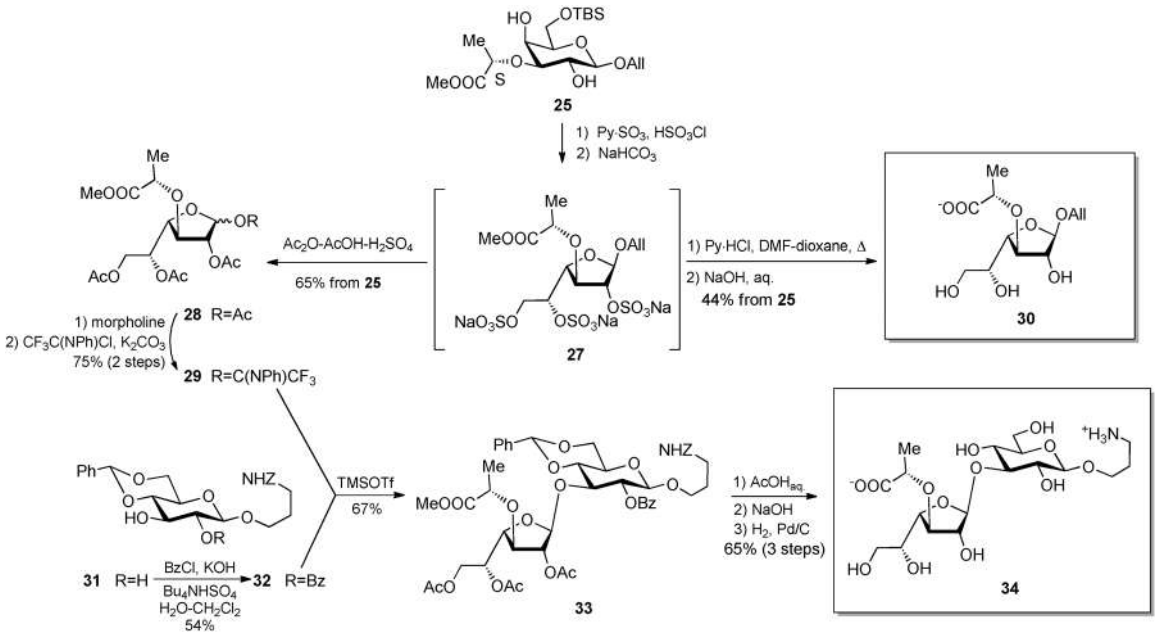

Scheme 7. The synthesis of mono- (**30**) and disaccharide (**34**) fragments related to polysaccharide from *E. faecalis*.

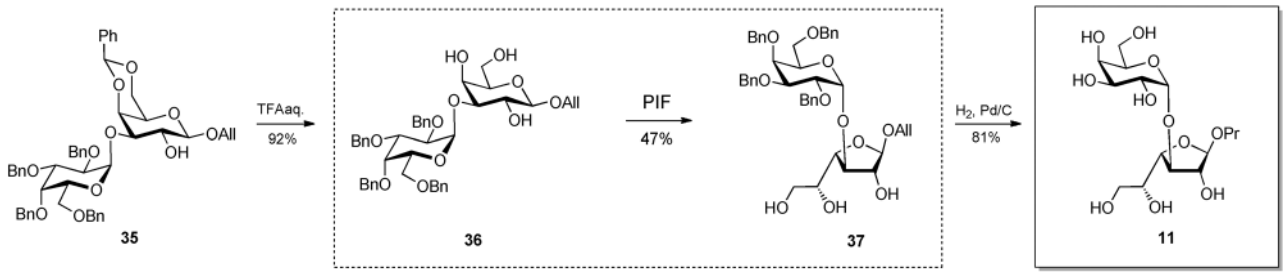

Scheme 8. The alternative synthesis of disaccharide **11**.

Conclusion

In conclusion, a new reaction, namely, PIF rearrangement, was discovered. It has no analogy in organic chemistry and can be compared only to enzymatic isomerization by action of pyranose mutases. PIF rearrangement provides a very good and advantageous alternative to known methods of furanoside oligosaccharide synthesis as demonstrated by the described examples.

Experimental Section

General methods

All solvents for reactions were dried according to conventional procedures[41] or purchased as dry. Dichloromethane (CH_2Cl_2) was distilled over CaH_2, and methanol (MeOH) was distilled over $Mg(OMe)_2$. Dimethylformamide (DMF) and acetonitrile (CH_3CN) were purchased as dry and used without further purification. Reagents for synthesis were commercial and used without further purification. All reactions involving air- or moisture-sensitive reagents were carried out using dry solvents under dry argon. Molecular sieves for glycosylation reactions were activated prior to use at 180 °C in vacuum of an oil pump during 2 h. Thin-layer chromatography (TLC) was carried out on aluminum plates coated with silica gel 60 F_{254} (Merck). Analysis TLC plates were inspected by UV light ($\lambda = 254$ nm) and developed by the treatment with a mixture of 15% H_3PO_4 and orcinol (1.8 g L^{-1}) in EtOH/H_2O (95:5, v/v) followed by heating. Silica gel column chromatography was performed with Silica Gel 60 (40–63 μm, Merck). Gel filtration was performed on a Sephadex G-15 column (35×500 mm) by elution with water at a flow rate of 1 mL min^{-1} or on a column of TSK HW-40 (S) gel (25×400 mm) in 0.1 M AcOH at a flow rate of 0.7 mL min^{-1}.

Spectroscopic methods

NMR spectra were recorded at 293–305 K using Bruker AM 300 (300 MHz), Bruker AMX400 (400 MHz), Bruker DRX-500 (500 MHz), or Bruker AV600 (600 MHz) spectrometers. Shifts are referenced relative to deuterated solvent residual peaks. NMR spectra of free oligosaccharides were measured for solutions in D_2O using acetone ($\delta_H = 2.225$ ppm, $\delta_C = 31.45$ ppm) as an internal standard. The following abbreviations are used to explain the observed multiplicities: s, singlet; d, doublet; t, triplet; m, multiplet and brt, broad triplet. Assignments were deduced from 2D experiments (COSY, HSQC, HMBC and TOCSY). Optical rotations were measured using a JASCO DIP-360 polarimeter at ambient temperature in solvents

specified. High-resolution mass spectra (HR-MS) were measured on a Bruker micrOTOF II instrument using electrospray ionization (ESI).[42] The measurements were performed in a positive ion mode (interface capillary voltage −4500 V) or in a negative ion mode (3200 V); mass range from *m/z* 50 to *m/z* 3000 Da; external or internal calibration was made with Electrospray Calibrant Solution (Fluka). A syringe injection was used for solutions in a mixture of acetonitrile and water (50:50 v/v, flow rate 3 μL min^{-1}). Nitrogen was applied as a dry gas; interface temperature was set at 180 °C.

Computational details

Calculations were carried out using the NWChem v. 6.3 software[43] and RHF approach with 6–31+G* basis set. Starting structures were obtained as stationary points after geometry optimization. Transition states were located using saddle point search as structures having exactly one negative vibrational frequency corresponding to C1–O5 bond cleavage. Activation energies were estimated as differences between full energies of the found transition states and were used uncorrected for zero-point vibrational energy. Energies of both starting and saddle point structures were converged to RMS gradient less than 10^{-4}.

General procedure for pyranoside-into-furanoside (PIF) transformation

O-Sulfation and rearrangement

HSO_3Cl (26 μL, 0.39 mmol) was added dropwise to a stirred solution of the pyranoside derivative (0.10 mmol) and Py·SO_3 complex (159 mg, 1.00 mmol) in DMF (1.2 mL). The reaction mixture was kept for 48 h at 20 °C and then quenched with aqueous $NaHCO_3$ (266 mg in 3 mL H_2O, 3.17 mmol) and evaporated twice with water. The residue was dissolved in a minimal amount of water and then an excess of MeOH was added to result in precipitation of inorganic salts, the mixture was filtrated, the solid was washed with MeOH, and the filtrate was concentrated and used for the next step without additional purification.

O-Desulfation

Crude sulfated furanoside obtained as described above and Py·HCl (51 mg, 0.5 mmol) were dissolved in DMF (1 mL), and then dioxane (5 mL) was added. The mixture was stirred at 80 °C for 30 min and then cooled to room temperature. The reaction mixture was dissolved in $CHCl_3$ (15 mL) and washed with saturated aqueous NaCl (15 mL). The organic layer was concentrated, and the residue was purified by column chromatography on silica gel to give the furanoside derivative.

NMR monitoring of PIF rearrangement

To a stirred solution of pyranoside **1** (30 mg, 0.097 mmol) in DMF (1.2 mL) Py·SO_3 complex (159 mg, 1.00 mmol) and HSO_3Cl (26 μL, 0.39 mmol) were added. The reaction mixture was kept at 20 °C. After 10 min, 2 h and 48 h the sample of the resulted solution (250 μL) was taken from the reaction mixture and quenched with an aqueous solution of $NaHCO_3$ (0.5 M, 1.32 mL). The resulting solution was concentrated in vacuo and then co-evaporated twice with H_2O and then lyophilized with D_2O. The resulting white solid residue was dissolved in D_2O and used for recording the NMR spectrum.

Full experimental procedures, characterization for all new compounds and copies of ^1H, ^{13}C NMR and HRMS spectra are provided in the Supporting Information.

Acknowledgements

This work was supported by RSF grant 14-23-00199 (NEN). We thank Dr. Y. E. Tsvetkov for reading this manuscript and valuable comments, and Dr. A. O. Chizhov for recording high resolution mass spectra at the Department of Structural Studies of the Zelinsky Institute of Organic Chemistry, Moscow.

Keywords: carbohydrates · furanoside · glycosylation · rearrangement · sulfation

[1] P. Peltier, R. Euzen, R. Daniellou, C. Nugier-Chauvin, V. Ferrieres, *Carbohydr. Res.* **2008**, *343*, 1897–1923.
[2] B. Tefsen, A. F. Ram, I. van Die, F. H. Routier, *Glycobiology* **2012**, *22*, 456–469.
[3] H. M. Zuurmond, P. A. M. van der Klein, G. H. Veeneman, J. H. van Boom, *Recl. Truv. Chiin. Pays-Bas.* **1990**, *109*, 437–441.
[4] R. A. Splain, L. L. Kiessling, *Bioorg. Med. Chem.* **2010**, *18*, 3753–3759.
[5] T. L. Lowary, *Curr. Opin. Chem. Biol.* **2003**, *7*, 749–756.
[6] L. Cattiaux, B. Sendid, M. Collot, E. Machez, D. Poulain, J. M. Mallet, *Bioorg. Med. Chem.* **2011**, *19*, 547–555.
[7] A. Imamura, T. Lowary, *Trends Glycosci. Glycotechnol.* **2011**, *23*, 134–152.
[8] V. Ferrières, J.-N. Bertho, D. A. Plusquellec, *Tetrahedron Lett.* **1995**, *36*, 2749–2752.
[9] N. B. D'Accorso, I. M. E. Thiel, M. Schüller, *Carbohydr. Res.* **1983**, *124*, 177–184.
[10] V. B. Krylov, Z. M. Kaskova, D. Z. Vinnitskiy, N. E. Ustyuzhanina, A. A. Grachev, A. O. Chizhov, N. E. Nifantiev, *Carbohydr. Res.* **2011**, *346*, 540–550.
[11] V. B. Krylov, N. E. Ustuzhanina, A. A. Grachev, N. E. Nifantiev, *Tetrahedron Lett.* **2008**, *49*, 5877–5879.
[12] I. Chlubnova, L. Legentil, R. Dureau, A. Pennec, M. Almendros, R. Daniellou, C. Nugier-Chauvin, V. Ferrières, *Carbohydr. Res.* **2012**, *356*, 44–61.
[13] Y. Zhou, J. Li, Y. Zhan, Z. Pei, H. Dong, *Tetrahedron* **2013**, *69*, 2693–2700.
[14] A. I. Usov, K. S. Adamyants, L. I. Miroshnikova, A. A. Shaposhnikova, N. K. Kochetkov, *Carbohydr. Res.* **1971**, *18*, 336–338.
[15] I. J. Miller, J. W. Blunt, *Carbohydr. Res.* **1998**, *309*, 39–43.
[16] V. Ferrières, J.-N. Bertho, D. A. Plusquellec, *Carbohydr. Res.* **1998**, *311*, 25–35.
[17] S. Shankar-Sinha, G. A. Valencia, B. K. Janes, J. K. Rosenberg, C. Whitfield, R. A. Bender, T. J. Standiford, J. G. Younger, *Infect. Immun.* **2004**, *72*, 1423–1430.
[18] O. Kol, J. Wieruszeski, G. Strecker, B. Fournet, R. Zalisz, P. Smets, *Carbohydr. Res.* **1992**, *236*, 339–344.
[19] S. Y. Zhu, J. S. Yang, *Tetrahedron* **2012**, *68*, 3795–3802.
[20] S. Basu, J. N. Pal, *Carbohydr. Res.* **1990**, *208*, 241–245.
[21] M. I. Bilan, E. V. Vinogradova, E. A. Tsvetkova, A. A. Grachev, A. S. Shashkov, N. E. Nifantiev, A. I. Usov, *Carbohydr. Res.* **2008**, *343*, 2605–2612.
[22] N. E. Ustyuzhanina, N. A. Ushakova, K. A. Zyuzina, M. I. Bilan, A. L. Elizarova, O. V. Somonova, A. V. Madzhuga, V. B. Krylov, M. E. Preobrazhenskaya, A. I. Usov, M. V. Kiselevskiy, N. E. Nifantiev, *Mar. Drugs* **2013**, *11*, 2444–2458.
[23] A. Cumashi, N. A. Ushakova, M. E. Preobrazhenskaya, A. D'Incecco, A. Piccoli, L. Totani, N. Tinari, G. E. Morozevich, A. E. Berman, M. I. Bilan, A. I. Usov, N. E. Ustyuzhanina, A. A. Grachev, C. J. Sanderson, M. Kelly, G. A. Rabinovich, S. Iacobelli, N. E. Nifantiev, *Glycobiology* **2007**, *17*, 541–552.
[24] D. O. Croci, A. Cumashi, N. A. Ushakova, M. E. Preobrazhenskaya, A. Piccoli, L. Totani, N. E. Ustyuzhanina, M. I. Bilan, A. I. Usov, A. A. Grachev, G. E. Morozevich, A. E. Berman, C. J. Sanderson, M. Kelly, P. Di Gregorio, C. Rossi, N. Tinari, S. Iacobelli, G. A. Rabinovich, N. E. Nifantiev, *PLoS One* **2011**, *6*, e17283.
[25] J. H. Fitton, *Mar. Drugs* **2011**, *9*, 1731–1760.
[26] A. I. Usov, M. I. Bilan, *Russ. Chem. Rev.* **2009**, *78*, 785–799.

[27] V. H. Pomin, *Biochim. Biopys. Acta* **2012**, *1820*, 1971 – 1979.
[28] B. S. Komarova, N. E. Ustyuzhanina, Y. E. Tsvetkov, N. E. Nifantiev, in *Modern Synthetic Methods in Carbohydrate Chemistry: From Monosaccharides to Complex Glycoconjugates* (Eds: S. Vidal, D. Wertz), Wiley-VCH, Weinheim **2013**, pp. 125 – 159.
[29] N. E. Ustyuzhanina, B. S. Komarova, N. S. Zlotina, V. B. Krylov, A. G. Gerbst, Y. E. Tsvetkov, N. E. Nifantiev, *Synlett* **2006**, *6*, 921 – 923.
[30] H. J. Vermeer, C. M. van Dijk, J. P. Kamerling, J. F. Vliegenthart, *Eur. J. Org. Chem.* **2001**, 193 – 203.
[31] D. Lee, M. S. Taylor, *J. Am. Chem. Soc.* **2011**, *133*, 3724 – 3727.
[32] F. Sugawara, H. Nakayama, G. A. Strobel, T. Ogawa, *Agric. Biol Chem.* **1986**, *50*, 2251 – 2259.
[33] C. Theilacker, Z. Kaczyński, A. Kropec, I. Sava, L. Ye, A. Bychowska, O. Holst, J. Huebner, *PLoS ONE* **2011**, *6*, e17839.
[34] J. L. Vincent, M. Norrenberg, *Crit. Care Med.* **2009**, *37*, 296 – 298.
[35] J. A. Himanen, P. M. Pihko, *Eur. J. Org. Chem.* **2012**, 3765 – 3780.
[36] W. B. Severn, J. C. Richards, *J. Am. Chem. Soc.* **1993**, *115*, 1114 – 1120.
[37] Y. Wang, Q. Yan, J. Wu, L. H. Zhang, X. S. Ye, *Tetrahedron* **2005**, *61*, 4313 – 4321.
[38] W. Szeja, *Synthesis* **1979**, 821 – 822.
[39] D. M. Whitfield, J. P. Carver, J. J. Krepinsky, *J. Carbohydr. Chem.* **1985**, *4*, 369 – 379.
[40] R. T. Lee, Y. C. Lee, *Carbohydr. Res.* **1994**, *251*, 69 – 79.
[41] W. L. F. Armarego, C. L. L. Chai, *Purification of Laboratory Chemicals*, 5edth edButterworth, Heinemann, **2003**.
[42] P. A. Belyakov, V. I. Kadentsev, A. O. Chizhov, N. G. Kolotyrkina, A. S. Shashkov, V. P. Ananikov, *Mendeleev Commun.* **2010**, *20*, 125 – 131.
[43] M. Valiev, E. J. Bylaska, N. Govind, K. Kowalski, T. P. Straatsma, H. J. J. van Dam, D. Wang, J. Nieplocha, E. Apra, T. L. Windus, W. A. de Jong, *Comput. Phys. Commun.* **2010**, *181*, 1477 – 1489.

Received: September 1, 2014
Published online on October 15, 2014

Synlett V. B. Krylov et al. Letter

The Pyranoside-*into*-Furanoside Rearrangement of Alkyl Glycosides: Scope and Limitations

Vadim B. Krylov
Dmitry A. Argunov
Dmitry Z. Vinnitskiy
Alexey G. Gerbst
Nadezhda E. Ustyuzhanina
Andrey S. Dmitrenok
Nikolay E. Nifantiev*

Laboratory of Glycoconjugate Chemistry, N.D. Zelinsky Institute of Organic Chemistry, Russian Academy of Sciences, Leninsky Prospect 47, 119991 Moscow, Russian Federation
nen@ioc.ac.ru

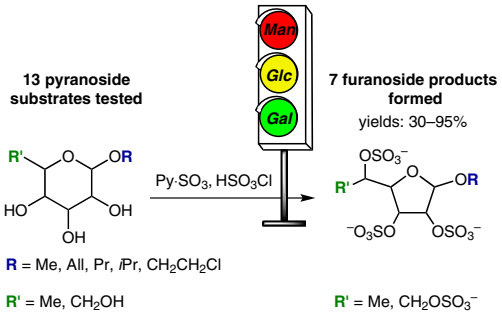

Received: 25.11.2015
Accepted after revision: 03.03.2016
Published online: 06.04.2016
DOI: 10.1055/s-0035-1561595; Art ID: st-2016-d0011-l

Abstract The pyranoside-*into*-furanoside (PIF) rearrangement was recently reported as a useful tool for the synthesis of furanoside-containing complex oligosaccharides. Until now, this transformation has only been described for some protected allyl-β-D-galactosides and one L-fucoside. In this communication its applicability is expanded. The formation of furanosides was observed under acid-promoted sulfation for a series of galactosides with varying alkyl substituents at the anomeric position as well as for several fucosides and glucosides. Meanwhile, furanoside formation was not detected in the case of mannopyranosides. The different reactivity of substrates was explained by values of activation barriers of endocyclic C1–O5 bond cleavage calculated by *ab initio* RHF methods. The reported results clarify the scope and limitations of the PIF rearrangement, which is important for its application in the synthesis of carbohydrate structures of practical meaning.

Key words pyranoside-*into*-furanoside rearrangement, per-O-sulfation, furanoside, pyranoside, ring contraction

The pyranoside-*into*-furanoside (PIF) rearrangement was recently reported[1–4] as an original and useful method for the synthesis of selectively protected furanosides directly from the corresponding pyranosides. The contraction of a pyranoside ring into furanoside proceeds under acid-promoted per-O-sulfation[5,6] of the substrate in the presence of a $Py{\cdot}SO_3$ complex and a strong acid (e.g., HSO_3Cl). In the first step, formation of a totally O-sulfated pyranoside occurs (**B** in Scheme 1) which then relatively slowly converts into a corresponding per-O-sulfated furanoside. We propose[1] that the rate-determining step in the PIF rearrangement is the formation of open-ring intermediate **III**, which proceeds *via* protonated form **I** and transition state **II** (TS **II**). Further recyclization of **III** accompanied by sulfate transfer yields furanoside **C**.

This reaction followed by solvolytic de-O-sulfation opens the way to the preparation of a variety of selectively protected building blocks for the oligosaccharide synthesis. For example, monosaccharides **1b**[1] and **4b**[1] (Scheme 2) were used for the synthesis of structures related to the O-

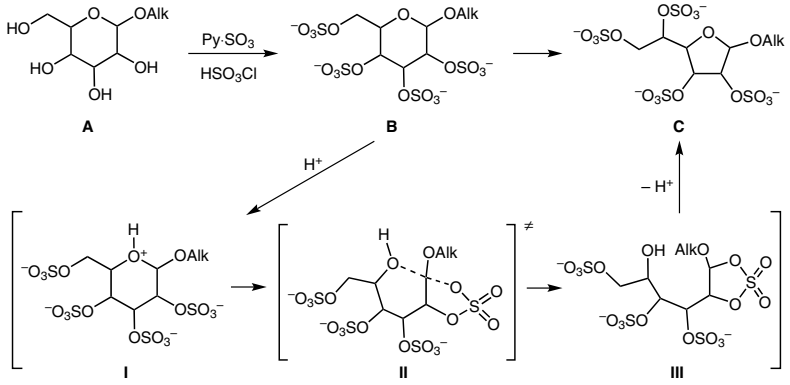

Scheme 1 The pyranoside-*into*-furanoside (PIF) rearrangement and its proposed[1] mechanism

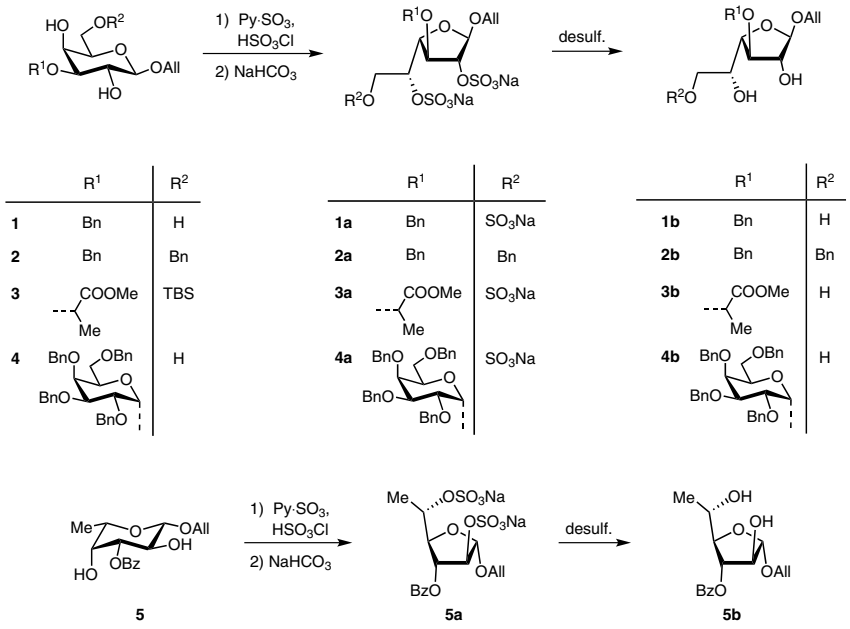

Scheme 2 Reported synthesis of selectively protected furanosides (**1b**,[1] **2b**,[3] **3b**,[1,2] **4b**[1], **5b**[1,4]) using PIF rearrangement

specific polysaccharide of *Klebsiella pneumoniae* while synthetic block **2b**[3] was used for assembling of pentasaccharide fragment of a galactomannan from *Aspergillus fumigatus*.[3]

The lactyl derivative **3b** was used for the synthesis[1,2] of fragments related to the diheteroglycan of *Enterococcus faecalis*. Additionally, the PIF protocol was successfully applied[4] in the synthesis of pentasaccharides representing unusual fragments of a fucoidan from brown seaweed *Chordaria flagelliformis*.[7]

In all the reported examples of the PIF rearrangement, only selectively substituted allyl glycosides were used as the starting pyranosides (Scheme 1). To expand the scope of this method, herein we report application of the PIF rearrangement for a series of alkyl glycosides **6**–**18** (Table 1), with varied structures of the anomeric substituent and the monosaccharide residue.

The starting pyranosides **6**–**18** were either prepared according to known methods (**7**,[8] **8**,[8] **9**,[9] **10**,[10] **11**,[11] **13**,[12] **14**,[13] **16**,[8] **17**,[10] **18**[10]) or were available commercially (**6**, **12**, **15**). The acid-promoted per-O-sulfation was performed under typical conditions for the PIF rearrangement.[1,14] After a certain period of time the reaction mixture was quenched with aqueous $NaHCO_3$, concentrated *in vacuo*, and the crude residue was analyzed using ^1H NMR, ^{13}C NMR, and 2D NMR spectroscopy without any purification. The NMR analysis of the resulted mixtures revealed the presence of per-O-sulfated pyranosides and furanosides. In some cases aglycon cleavage and formation of glycosyl sulfates were also observed. The results are summarized in Table 1. ^1H NMR and ^{13}C NMR spectra are available in the Supporting Information.

The acid-promoted per-O-sulfation[14] of β-galactopyranosides **6**–**10** bearing methyl, allyl, propyl, *iso*-propyl, and chloroethyl groups at the anomeric position resulted in the formation of β-galactofuranoside derivatives, although the reaction rates were strongly influenced by the aglycon structure. Methyl galactoside **6** (Table 1, entry 1) gave 55% of furanoside **6f** in two hours. A prolonged reaction time of 5.5 hours (Table 1, entry 2) increased the conversion into furanoside **6f**, but a significant portion of decomposition products was also observed in the NMR spectrum. A similar 60% conversion in two hours was observed for allyl galactoside **7** (Table 1, entry 3). In the case of propyl and *iso*-propyl derivatives **8** and **9** (Table 1, entries 5, 6) a reaction time of two hours was sufficient to convert all the pyranoside into the furanoside with only a trace of side products. In the case of the monochloroethyl aglycon (Table 1, entry 7) after two hours only 10% conversion into furanoside **10f** was observed and extension of the reaction time to 5.5 hours (Table 1, entry 8) afforded just 30% conversion. The electron-withdrawing trichloroethyl group in the aglycon completely blocked the formation of furanoside: No trace of the required product was observed even after 24 hours (Table 1, entry 9).

Table 1 Acid-Promoted Sulfation of Pyranosides

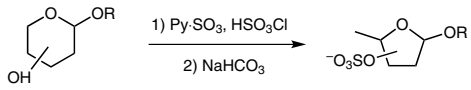

Entry	Starting pyranoside	Structure(s) of detected product(s)		Procedure[14]	Time (h)	Pyranoside to furanoside ratio[a]	Yield (%) of furanoside (NMR)[b]
D-Gal							
1	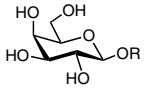	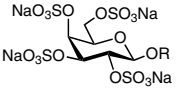	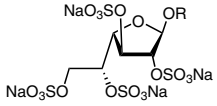	A	2	2:3	55
2				A	5.5	0:1[c]	70
	6 R = Me	**6p** R = Me	**6f** R = Me				
3	**7** R = All	**7p** R = All	**7f** R = All	A	2	2:3	60
4	**7** R = All	**7p** R = All	**7f** R = All	B	24	0:1[c]	95
5	**8** R = Pr	**8p** R = Pr	**8f** R = Pr	A	2	1:9	85
6	**9** R = *i*-Pr	–	**9f** R = *i*-Pr	A	2	0:1[c]	90
7	**10** R = CH_2CH_2Cl	**10p** R = CH_2CH_2Cl	**10f** R = CH_2CH_2Cl	A	2	7:1	10
8	**10** R = CH_2CH_2Cl	**10p** R = CH_2CH_2Cl	**10f** R = CH_2CH_2Cl	A	5.5	7:3	30
9	**11** R = CH_2CCl_3	**11p** R = CH_2CCl_3		A	24	1:0[d]	0
10	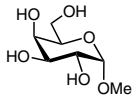	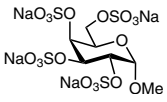		A	24	1:0[d]	0
	12	**12p**					
L-Fuc							
11	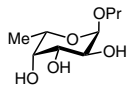	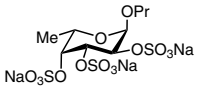		B	24	1:0[d]	0
	13	**13p**					
12	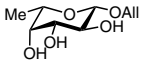		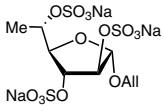	B	24	0:1[c]	85
	14		**14f**				
D-Glc							
13	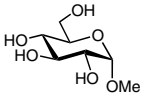	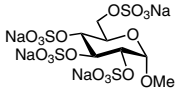		B	24	1:0[d]	0
	15	**15p**					
14	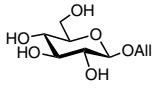	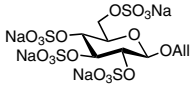	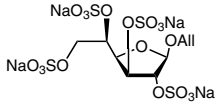	B	24	2:1	30
	16	**16p**	**16f**				
D-Man							

Table 1 (continued)

Entry	Starting pyranoside	Structure(s) of detected product(s)	Procedure[14]	Time (h)	Pyranoside to furanoside ratio[a]	Yield (%) of furanoside (NMR)[b]
15	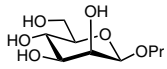	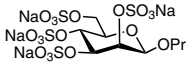	B	24	1:0[d]	0
	17	**17p**				
16	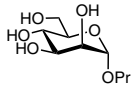	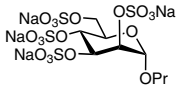	B	24	1:0[d]	0
	18	**18p**				

[a] The ratio was calculated using the average integral intensity of non-overlapping signals of pyranoside and furanoside forms in ^{1}H NMR spectrum.
[b] The yield was calculated as the ratio of average integral intensity of furanoside signals to the average integral intensity of furanoside, pyranoside, and decomposition products in the ^{1}H NMR spectrum multiplied by 100%.
[c] Pyranoside product was not detected in the NMR spectrum.
[d] Furanoside product was not detected in the NMR spectrum.

All β-galactofuranosides **6f**–**10f** had similar ^{13}C NMR spectra with an insignificant difference in chemical shifts of the anomeric carbons (see Figure 1 and Supporting information). Their structures were confirmed by characteristic ^{13}C NMR chemical shifts for sulfated β-galactofuranosides[1] (e.g., C-1, δ = 104–107 ppm; C-2, δ = 85–84 ppm; C-4, δ = 81–82 ppm) and coupling constants in ^{1}H NMR spectra[15] (see Supporting Information).

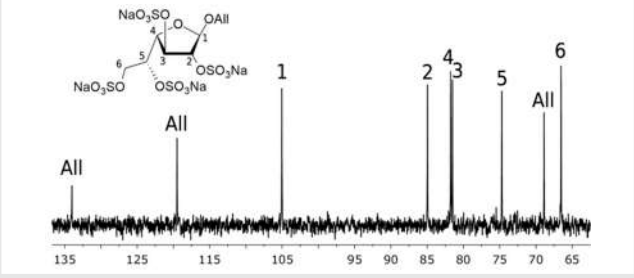

Figure 1 ^{13}C NMR spectrum of per-O-sulfated allyl-β-D-galactofuranoside **7f** (see Table 1, entry 4)

Contrary to the successful isomerization of most β-galactopyranoside derivatives, the treatment of methyl α-D-galactopyranoside **12** (Table 1, entry 10) with Py·SO_3 complex and HSO_3Cl under the described conditions did not afford any furanoside products, but only yielded the per-O-sulfated derivative of parent pyranoside **12p**. The coupling constants of the ring protons in the ^{1}H NMR spectrum of **12p** corresponded to the α-galactopyranoside ring in $^4C_1$ conformation while significant downfield shifts of H-2, H-3, H-4, and H-6 protons confirmed the presence of sulfate groups at the corresponding positions (for NMR details see Tables in Supporting Information).

To minimize the amount of inorganic salts formed after the neutralization of the reaction mixture and thus to simplify further purification of the furanoside product, in the next series of experiments a per-O-sulfation protocol with a reduced amount of sulfation reagents was applied (procedure B instead of procedure A[14]). Under these conditions allyl galactoside **7** gave complete PIF conversion in 24 hours (Table 1, entry 4, see Figure 1).

The behavior of fucopyranosides **13** and **14** under the per-O-sulfation conditions[14] was similar to that of the galactopyranosides described above. α-Propyl fucoside **13** did not undergo the PIF rearrangement at all (Table 1, entry 11), while β-allyl fucoside **14** (Table 1, entry 12) reacted smoothly with the formation of the β-furanoside derivative **14f** in a good yield, similarly to β-allyl galactoside **7** (Table 1, entry 4).

Next, glucosides were studied as substrates for the PIF rearrangement. The treatment of α-methyl glycoside **15** (Table 1, entry 13) under the PIF conditions[14] produced just totally sulfated derivative **15p** without any trace of furanosides, as was the case for α-methyl galactoside **12** (Table 1, entry 10). However, unlike β-allyl galactoside **7** (Table 1, entry 4), per-O-sulfation of β-allyl glucoside **16** during 24 hours gave only 30% conversion to furanoside derivative **16f** (Table 1, entry 14). The NMR spectra of compound **16f** had chemical shifts and coupling constants typical for a furanoside structure (see Supporting Information). Additionally, after desulfation[16] allyl-β-D-glucofuranoside **19** was obtained (Scheme 3), whose ^{1}H NMR and ^{13}C NMR spectra were essentially identical to the previously published spectra (see Supporting Information).[17]

The last examples used to study the sugar configuration influence on the PIF rearrangement were α- and β-propyl mannosides **17** and **18** (Table 1, entries 15, 16). The only

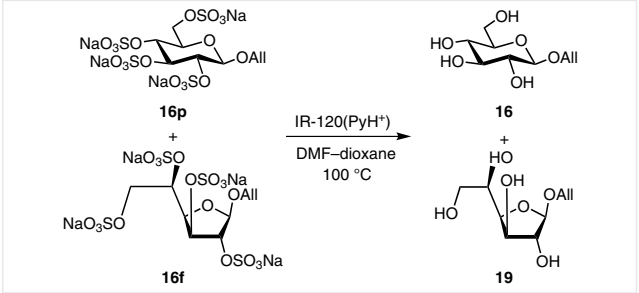

Scheme 3 Solvolytic de-O-sulfation of glucopyranoside **16p** and glucofuranoside **16f** mixture

difference between mannosides and glucosides is the configuration at C-2, and the critical role of the sulfate group at O-2 had been demonstrated previously.[1] The acid-promoted per-O-sulfation of both mannosides yielded just the corresponding pyranosides in the $^4C_1$ conformation.

To explain the observed difference in reactivity of the studied pyranosides depending on the ring configuration we calculated the activation barriers of endocyclic C(1)–O(5)-bond cleavage which is proposed to be the rate-determining step for the PIF rearrangement (Figure 2).[1] The calculations were performed for methyl glycoside models employing *ab initio* RHF calculations (see Supporting Information). It was found that, in the case of galactosides, the calculated activation energy had the lowest value for the β-isomeric form and the highest for the α-isomer. This correlated with the experimental data according to which α-galactoside did not undergo PIF rearrangement. In structural terms this could be explained by steric interactions between the axially oriented aglycon and the participating SO_3 group in the transition state. Quite expectedly, in the case of methyl mannoside, the activation energy was also rather high. In this molecule the 'participating' SO_3 group is itself in an axial position which makes its interaction with the anomeric carbon atom less effective. The activation energy for the β-glucoside was intermediate between β-galactoside and β-mannoside and the formation of the transition state was accompanied by ring distortion. This explains why the glucoside derivatives only reacted slowly under the conditions.

Furthermore, our hypothesis is in agreement with the experimentally observed critical role of the sulfate group at C-2,[1] and it could additionally provide an explanation for the retention of anomeric configuration during the rearrangement. The interaction between the sulfate at C-2 and the anomeric center in the transition state leads to the formation of a five-membered pseudocycle that restricts the C1–C2 bond from rotating and yields a product with the retained configuration.

In conclusion, the ability to form furanoside derivatives under the acid-promoted per-O-sulfation conditions has been studied for a series of 13 alkyl pyranosides. It was shown that α-isomers did not undergo this transformation. Galactosides bearing electron-donating groups (Me, Pr, All, *i*-Pr) in the aglycon rearranged faster than those with electron-withdrawing ones (CH_2CH_2Cl, CH_2CCl_3). Galactosides reacted faster than glucosides, and mannosides did not rearrange at all; which was in agreement with calculated transition-state energies. All these results are important for practical application of the PIF rearrangement in oligosaccharide synthesis as well as for the further theoretical investigation of its mechanism.

Acknowledgment

This work was supported by RSF grant 14-23-00199 (NEN).

Supporting Information

Supporting information for this article is available online at http://dx.doi.org/10.1055/s-0035-1561595.

References and Notes

(1) Krylov, V. B.; Argunov, D. A.; Vinnitskiy, D. Z.; Verkhnyatskaya, S. A.; Gerbst, A. G.; Ustyuzhanina, N. E.; Dmitrenok, A. S.; Huebner, J.; Holst, O.; Siebert, H.-Ch.; Nifantiev, N. E. *Chem. Eur. J.* **2014**, *20*, 16516.
(2) Krylov, V. B.; Gerbst, A. G.; Argunov, D. A.; Dmitrenok, A. S.; Shashkov, A. S.; Kaczynski, Z.; Huebner, J.; Holst, O.; Nifantiev, N. E. *Chem. Eur. J.* **2015**, *21*, 1749.
(3) Argunov, D. A.; Krylov, V. B.; Nifantiev, N. E. *Org. Biomol. Chem.* **2015**, *13*, 3255.

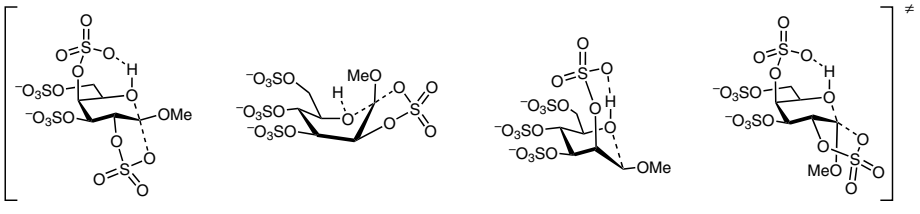

Figure 2 The calculated activation barrier and geometry of the transition state of the endocyclic C(1)→O(5) bond cleavage

(4) Vinnitskiy, D. Z.; Krylov, V. B.; Ustyuzhanina, N. E.; Dmitrenok, A. S.; Nifantiev, N. E. *Org. Biomol. Chem.* **2016**, *14*, 598.
(5) Krylov, V. B.; Kaskova, Z. M.; Vinnitskiy, D. Z.; Ustyuzhanina, N. E.; Grachev, A. A.; Chizhov, A. O.; Nifantiev, N. E. *Carbohydr. Res.* **2011**, *346*, 540.
(6) Krylov, V. B.; Ustyuzhanina, N. E.; Grachev, A. A.; Nifantiev, N. E. *Tetrahedron Lett.* **2008**, *49*, 5877.
(7) Bilan, M. I.; Vinogradova, E. V.; Tsvetkova, E. A.; Grachev, A. A.; Shashkov, A. S.; Nifantiev, N. E.; Usov, A. I. *Carbohydr. Res.* **2008**, *343*, 2605.
(8) Lee, R. T.; Lee, Y. C. *Carbohydr. Res.* **1974**, *37*, 193.
(9) Kartha, K. R.; Aloui, M.; Field, R. A. *Tetrahedron Lett.* **1996**, *37*, 5175.
(10) Yu, Y.; Ko, K. S.; Zea, C. J.; Pohl, N. L. *Org. Lett.* **2004**, *6*, 2031.
(11) Moore, C. J.; Auzanneau, F. I. *Beilstein J. Org. Chem.* **2012**, *8*, 1134.
(12) Garegg, P. J.; Norberg, T. *Carbohydr. Res.* **1976**, *52*, 235.
(13) de Souza, A. C.; Halkes, K. M.; Meeldijk, J. D.; Verkleij, A. J.; Vliegenthart, J. F.; Kamerling, J. P. *Eur. J. Org. Chem.* **2004**, 4323.
(14) **PIF Rearrangement**
Py·SO_3 (102 mg, 0.64 mmol) and HSO_3Cl (17 µL, 0.26 mmol) were added to a stirred solution of alkyl pyranoside (procedure A: 0.032 mmol of tetraols; procedure B: 0.05 mmol of tetraols, 0.067 mmol of triols) in DMF (0.7 mL). The mixture was stirred at 25 °C. After the requisite period of time the solution was neutralized with aq solution of $NaHCO_3$, concentrated *in vacuo*, and then co-evaporated with H_2O and then with D_2O. The residue was dissolved in D_2O and used for recording of NMR spectra.
(15) Gerbst, A. G.; Krylov, V. B.; Vinnitskiy, D. Z.; Dmitrenok, A. S.; Shashkov, A. S.; Nifantiev, N. E. *Carbohydr. Res.* **2015**, *417*, 1.
(16) **Solvolytic De-O-sulfation**
The solid mixture of products[14] obtained after per-O-sulfation was dissolved in a minimum amount of water, and then an excess of MeOH was added to cause precipitation of inorganic salts, the mixture was filtered, the solid was washed with MeOH, and the combined filtrates were concentrated. The residue was dissolved in DMF (1.5 mL), and IR-120(PyH^+) (250 mg) and dioxane (5 mL) were added. The mixture was stirred at 100 °C for 30 min and then cooled to room temperature. The cation-exchange resin was filtered off, and the filtrate was concentrated. The residue was purified by column chromatography on silica gel ($CHCl_3$–MeOH, gradient 5:1 → 3:1) to give the mixture of desulfated products which was analyzed by NMR spectroscopy.
(17) (a) Fang, T. T.; Zirrolli, J.; Bendiak, B. *Carbohydr. Res.* **2007**, *342*, 217. (b) Furneaux, R. H.; Martin, B.; Rendle, P. M.; Taylor, C. M. *Carbohydr. Res.* **2002**, *337*, 1999.

Available online at www.sciencedirect.com

ScienceDirect

Mendeleev Commun., 2016, **26**, 483–484

Mendeleev Communications

Pyranoside-*into*-furanoside rearrangement of D-glucuronopyranoside derivatives

Vadim B. Krylov, Dmitry A. Argunov and Nikolay E. Nifantiev*

N. D. Zelinsky Institute of Organic Chemistry, Russian Academy of Sciences, 119991 Moscow, Russian Federation. Fax: +7 499 135 8784; e-mail: nen@ioc.ac.ru

DOI: 10.1016/j.mencom.2016.11.007

The pyranoside-*into*-furanoside (PIF) rearrangement of α- and β-D-glucuronopyranosides under acid-promoted sulfation proceeded significantly faster than similar isomerization of β-D-glucopyranosides.

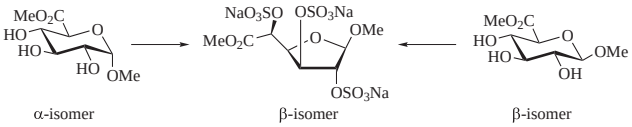

Recently discovered[1–5] pyranoside-*into*-furanoside (PIF) rearrangement is a new reaction in carbohydrate chemistry, which represents the contraction of 6-membered pyranoside ring into 5-membered furanoside one under acid-promoted sulfation conditions.[6–8] This reaction followed by solvolytic de-O-sulfation opens the synthetic way towards a variety of selectively protected furanoside blocks suitable in the assembling of higher oligosaccharides. To date PIF rearrangement was successfully applied in the synthesis of oligosaccharides which are structurally related to those of bacteria *Klebsiella pneumoniae*[1] and *Enterococcus faecalis*,[2] fungi *Aspergillus fumigatus*[3] and the brown seaweed *Chordaria flagelliformis*.[4]

However, the influence of structural characteristics of parent pyranosides on the outcome of PIF rearrangement remains to be studied in more detail. In particular, there is no information on similar rearrangement of uronic acid derivatives. To fill this gap, we have studied the PIF rearrangement of isomeric methyl α- and β-D-glucuronopyranosides **1** and **2** under typical[8] conditions for PIF rearrangement and assessed the structures of formed products.

The treatment† of β-methyl glucuronopyranoside **1**[9] (Scheme 1, Table 1, entry 1) produced in 45 min per-O-sulfated derivative **3**‡ together with the corresponding product of PIF rearrangement, β-D-glucuronofuranoside **5**§ in the ratio 7 : 3. Further prolongation of the reaction to 24 h caused complete rearrangement to give β-furanoside **5** in 65% yield (entry 2), which was contaminated with minor product **6**¶ where anomeric methyl group was replaced with sulfo one. Under the same conditions β-D-glucopyranoside gave only 30% yield of the corresponding β-glucofuranoside.[8] This observation shows that PIF rearrangement of β-glucuronopyranosides proceedes significantly faster than in the case of corresponding β-glucopyranosides.

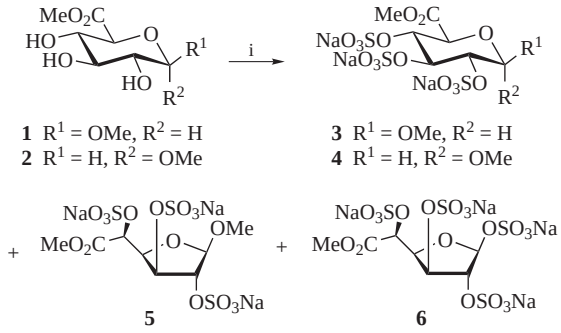

Scheme 1 *Reagents and conditions*: i, Py·SO_3, HSO_3Cl, DMF, then $NaHCO_3$.

The structure of furanoside **5** and in particular its β-anomeric configuration were confirmed by NMR data (Figure 1). Thus, ^{13}C NMR spectrum contained characteristic chemical shifts for

Table 1 The results of PIF rearrangement of pyranosides **1** and **2**.

Entry	Parent pyranoside	Reaction time/h	Reaction products and their ratios[a]	Yield of furanoside **5**[a]
1	**1**	0.75	**3** + **5** (7 : 3)	30%
2	**1**	24	**5** + **6** (2 : 1)[b]	65%
3	**2**	0.75	**4** + **5** (50 : 1)	2%
4	**2**	24	**4** + **5** (5 : 1)	17%

[a] The ratio and yields were determined by integration of non-overlapping signals for pyranoside (**3** or **4**), furanoside **5** and product **6** in ^1H NMR spectra. [b] Pyranoside product was not observed in NMR spectrum.

† *Protocol for PIF rearrangement.* The reagents Py·SO_3 (102 mg, 0.64 mmol) and HSO_3Cl (17 μl, 0.26 mmol) were added to a stirred solution of methyl pyranoside (0.058 mmol) in DMF (0.7 ml). The mixture was stirred at 25 °C for the required period of time and the solution was neutralized with aq. $NaHCO_3$, then concentrated *in vacuo* and co-evaporated with H_2O and D_2O. The residue was dissolved in D_2O and studied by NMR spectroscopy.

‡ *Selected NMR data for* **3**. ^1H NMR (600 MHz, D_2O) δ: 5.00–4.97 (m, 1H, H-4), 4.85 (d, 1H, H-1, $J_{1,2}$ 5.9 Hz), 4.79 (dd, 1H, H-3, $J_{3,4}$ 5.4 Hz, $J_{3,2}$ 4.2 Hz), 4.70 (d, 1H, H-5, $J_{5,4}$ 4.7 Hz), 4.37 (dd, 1H, H-2, $J_{2,1}$ 5.8 Hz, $J_{2,3}$ 4.2 Hz), 3.81 (s, 3H, CO_2Me), 3.55 (s, 3H, OMe). ^{13}C NMR (125 MHz, D_2O) δ: 101.7 (C-1), 77.3 (C-2), 76.0 (C-3), 75.0 (C-5), 74.2 (C-4), 58.7 (OMe), 54.5 (CO_2Me).

§ *Selected NMR data for* **5**. ^1H NMR (600 MHz, D_2O) δ: 5.19 (s, 1H, H-1), 5.07–5.05 (m, 1H, H-3), 5.06 (s, 1H, H-2), 4.97 (d, 1H, H-5, $J_{5,4}$ 8.0 Hz), 4.70 (dd, 1H, $J_{4,5}$ 8.0 Hz, $J_{4,3}$ 5.5 Hz), 3.84 (s, 3H, CO_2Me), 3.42 (s, 3H, OMe). ^{13}C NMR (125 MHz, D_2O) δ: 108.0 (C-1), 82.8 (C-2), 80.1 (C-4), 78.3 (C-3), 73.9 (C-5), 56.4 (OMe), 53.9 (CO_2Me).

¶ *Selected NMR data for* **6**. ^1H NMR (600 MHz, D_2O) δ: 5.95 (s, 1H, H-1), 5.24 (s, 1H, H-2), 5.10 (d, 1H, H-3, $J_{3,4}$ 5.0 Hz), 5.03 (d, 1H, H-5, $J_{5,4}$ 8.2 Hz), 4.72 (dd, 1H, H-4, $J_{4,5}$ 8.2 Hz, $J_{4,3}$ 5.0 Hz). ^{13}C NMR (125 MHz, D_2O) δ: 103.6 (C-1), 83.0 (C-2), 81.6 (C-4), 77.5 (C-3), 73.7 (C-5).

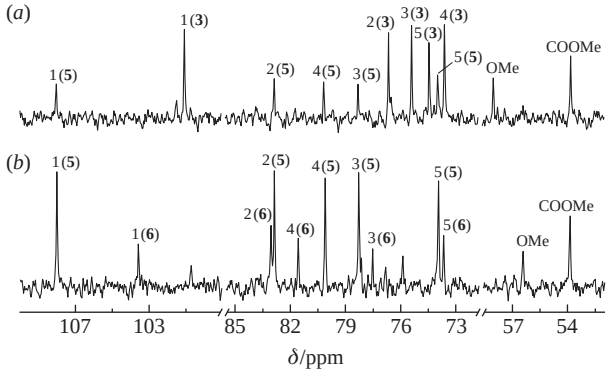

Figure 1 ^{13}C NMR spectra of β-glucuronopyranoside **1** per-O-sulfation products formed in (*a*) 45 min and (*b*) 24 h.

sulfated β-furanosides[8] (*e.g.*, C-1, 108.0 ppm; C-2, 82.8 ppm; C-4, 80.1 ppm) and ^{1}H NMR spectrum contained the right coupling constants. Moreover, the HMBC spectrum of product **5** exhibited a correlation peak between C-4/H-1 clearly evidencing the presence of the furanoside ring. The strong NOE between H-3 and H-4 also confirmed the structure of product **5** (see Figure 2). β-Configuration and the presence of anomeric sulfate in **6** was confirmed by singlet forms of H-1 and H-2 signals in ^{1}H NMR spectrum and down-field shift of H-1 signal (5.19 → 5.95 ppm) if compared with the spectrum of methyl glycoside **5**.

Surprisingly, the treatment of α-methyl pyranoside **2**[9] (entry 3) produced in 45 min the mixture of the product of its per-O-sulfation **4**†† together with traces of β-D-glucuronofuranoside **5** but not of its expected α-isomer. The prolongation of the reaction to 24 h favored to further conversion **4** → **5**, however, it proceeded slowly to give only 17% of β-furanoside **5**.

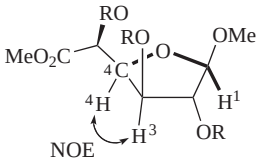

Figure 2 NMR data confirming β-glucuronofuranoside structure of product **5** (R = SO_3^-).

†† *Selected NMR data for* **4**. ^{1}H NMR (600 MHz, D_2O) δ: 5.23 (d, 1H, H-1, $J_{1,2}$ 3.3 Hz), 4.73 (dd, 1H, $J_{3,2}$ 8.6 Hz, $J_{3,4}$ 6.9 Hz), 4.58–4.54 (m, 2H, H-4, H-5), 4.46 (dd, 1H, H-2, $J_{2,3}$ 8.6 Hz, $J_{2,1}$ 3.3 Hz), 3.80 (s, 3H, CO_2Me), 3.50 (s, 3H, OMe). ^{13}C NMR (125 MHz, D_2O) δ: 97.5 (C-1), 75.1 (C-3), 74.6 (C-4), 74.4 (C-2), 71.2 (C-5), 56.9 (OMe), 54.0 (CO_2*Me*).

In conclusion, the study of capability of glucuronopyranosides to undergo PIF rearrangement under acid-promoted O-sulfation conditions showed that their reactivity was higher than that of glucopyranosides.[8] Moreover, formation of β-furanoside **5** from α-glucuronopyranoside **4** was observed, while the corresponding α-glucopyranoside did not rearrange at all under used conditions.[8] The side process of aglycon cleavage resulting in formation of glycosyl sulfate **6** also occurred intensively along with PIF rearrangement in the case of glucuronide **1**. We assume that the observed higher reactivity of glucuronides can be related to the presence of a COOMe group at C-5. The results of quantum calculations of reaction pathways in above described processes will be published elsewhere.

This work was supported by the Russian Science Foundation (grant no. 14-23-00199).

References

1 V. B. Krylov, D. A. Argunov, D. Z. Vinnitskiy, S. A. Verkhnyatskaya, A. G. Gerbst, N. E. Ustyuzhanina, A. S. Dmitrenok, J. Huebner, O. Holst, H.-C. Siebert and N. E. Nifantiev, *Chem. Eur. J.*, 2014, **20**, 16516.
2 V. B. Krylov, A. G. Gerbst, D. A. Argunov, A. S. Dmitrenok, A. S. Shashkov, Z. Kaczynski, J. Huebner, O. Holst and N. E. Nifantiev, *Chem. Eur. J.*, 2015, **21**, 1749.
3 D. A. Argunov, V. B. Krylov and N. E. Nifantiev, *Org. Biomol. Chem.*, 2015, **13**, 3255.
4 D. Z. Vinnitskiy, V. B. Krylov, N. E. Ustyuzhanina, A. S. Dmitrenok and N. E. Nifantiev, *Org. Biomol. Chem*., 2016, **14**, 598.
5 V. B. Krylov, D. A. Argunov and N. E. Nifantiev, *Mendeleev Commun.*, 2014, **24**, 336.
6 V. B. Krylov, Z. M. Kaskova, D. Z. Vinnitskiy, N. E. Ustyuzhanina, A. A. Grachev, A. O. Chizhov and N. E. Nifantiev, *Carbohydr. Res*., 2011, **346**, 540.
7 V. B. Krylov, N. E. Ustyuzhanina, A. A. Grachev and N. E. Nifantiev, *Tetrahedron Lett.*, 2008, **49**, 5877.
8 V. B. Krylov, D. A. Argunov, D. Z. Vinnitskiy, A. G. Gerbst, N. E. Ustyuzhanina, A. S. Dmitrenok and N. E. Nifantiev, *Synlett*., 2016, **27**, 1659.
9 F. C. Baines, P. M. Collins and F. Farnia, *Carbohydr. Res*., 1985, **136**, 27.

Received: 24th May 2016; Com. 16/4941

ACS OMEGA

Article

Cite This: ACS Omega 2019, 4, 1139−1143

http://pubs.acs.org/journal/acsodf

Driving Force of the Pyranoside-into-Furanoside Rearrangement

Alexey G. Gerbst, Vadim B. Krylov, Dmitry A. Argunov, Andrey S. Dmitrenok, and Nikolay E. Nifantiev*

Laboratory of Glycoconjugate Chemistry, N.D. Zelinsky Institute of Organic Chemistry, Russian Academy of Sciences, Leninsky Prospect 47, 119991 Moscow, Russia

Supporting Information

ABSTRACT: Ab initio calculations of fully O-sulfated model monosaccharides, including common hexoses (glucose, galactose, fucose, and mannose) and pentoses (arabinose and xylose), were performed to study the energetic properties of the recently discovered pyranoside-into-furanoside (PIF) rearrangement. It was shown that the per-O-sulfated derivatives of furanoside isomers generally had lower energies than the corresponding per-O-sulfated pyranosides, while nonsulfated furanosides were always less favored than nonsulfated pyranosides. Mannose, which is known to be unreactive in PIF rearrangement, was the only exception. The results of the theoretical calculations were confirmed by experimental studies of monosaccharide models and explained the driving force of such unusual ring contraction process as PIF rearrangement. The conclusions of performed investigation can be used for prediction of new substrates applicability for PIF rearrangement.

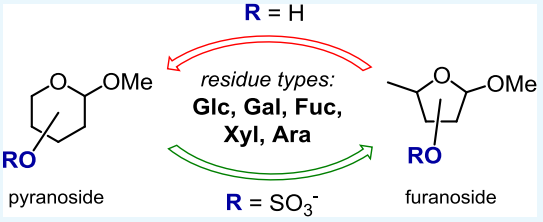

INTRODUCTION

It is well known that furanosides are generally less thermodynamically stable than the corresponding pyranosides.[1,2] In an acid-promoted Fischer reaction, furanosides are formed as the kinetic products, whereas thermodynamic equilibrium predominantly results in the formation of pyranosides.[3] The conversion between pyranosides and furanosides containing a substituent at the anomeric position is complicated; however, it is possible under enzymatic conditions. For example, mutase enzymes catalyze the transformation of uridine diphosphate galactopyranose (UDP-Galp, **1**) into the corresponding galactofuranose (UDP-Galf, **2**) (Scheme 1A). However, the equilibrium concentration in the latter process is only 5%.[4]

Certain substituents at C-2 also facilitate the acid-promoted conversion between the pyranoside and furanoside forms. For example, *N*-acetylgalactosamine (**3**) under mild acidic conditions gives 5% of isomeric furanoside **4** (Scheme 1B). The same ratio of monosaccharides **3** and **4** can be reached by acid treatment of furanoside **4**. The participation of the acetyl group was proposed as a key step in the mechanism facilitating the endocyclic cleavage of the O(5)−C(1) bond.[5]

The analogous participation of the 2-O-sulfonato group plays a key role in pyranoside-into-furanoside (PIF) rearrangement (Scheme 1C) under the acid-promoted per-O-sulfation conditions[6,7] that were discovered in 2014.[8,9] Unlike the previous examples, the PIF rearrangement gives predominantly furanoside products. This process was already successfully used in the syntheses of oligosaccharides related to *Aspergillus galactomannan*,[10−12] *Enterococcus diheteroglycan*,[13] galactan I from *Klebsiella pneumoniae*,[14] and some others.[15]

In our previous investigations, the kinetic aspects of PIF rearrangements were studied, including ab initio calculations of the activation energies of monosaccharides with gluco, galacto, fuco, and manno configurations.[8,9] Additionally, there was a study by Satoh et al. reporting the importance of the conformational strain caused by protecting groups for the endocyclic cleavage reaction.[16] In this work, we studied the energetic aspects of PIF rearrangements, which revealed for the first time the driving force of the nontrivial chemical process of ring contraction. Ab initio calculations were used to explore the relative stability of the corresponding pyranoside and furanoside forms of pentoses and hexoses depending on the presence or absence of sulfate groups on the structures.

RESULTS AND DISCUSSION

Experimentally, it was previously demonstrated[9] that in the case of β-galactosides and β-fucosides, the PIF rearrangement proceeds irreversibly until the initially formed fully O-sulfated pyranosides are completely consumed. Thus, allyl galactoside **5** and allyl fucoside **8** under PIF rearrangement conditions give corresponding furanosides **7** and **9**, and no traces of the initially formed per-O-sulfated allyl pyranosides **6** and **10** were detected in the reaction mixture after 24 h (Table 1, entries 1−2).[9] On the other hand, propyl α- and β-mannopyranosides **11** and **14** under the same conditions gave only per-O-sulfated pyranosides **12** and **15**, and no traces of proposed furanoside products **13** and **16** were found. The behavior of these mannosides is probably determined by the axial orientation of the OH group at C-2.

Received: November 23, 2018
Accepted: December 24, 2018
Published: January 14, 2019

Scheme 1. Examples of PIF Rearrangements: (A) Conversion of UDP-Galp into UDP-Galf by UDP-Galactopyranose Mutase;[4] (B) Equilibrium between Pyranoside and Furanoside in *N*-Acetylgalactosamine;[5] and (C) PIF Rearrangement under Acid-Promoted Per-O-Sulfation Conditions[8]

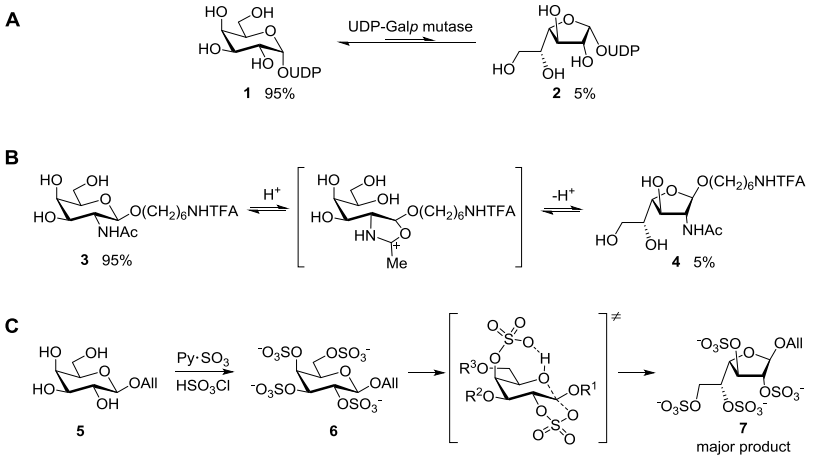

Table 1. Acid-Promoted Sulfation[a] of Galacto-, Fuco-, Manno-, Gluco-, Arabino- and Xylo-Pyranosides

Entry	Starting materials	Products and NMR yields		Reaction time, h
		furanoside	pyranoside	
1	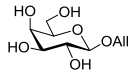 **5**	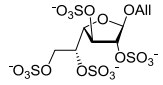 **7** - 95%	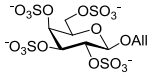 **6** - not detected	24
2	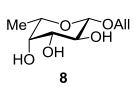 **8**	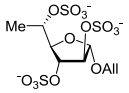 **9** - 85%	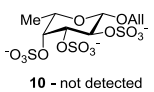 **10** - not detected	24
3	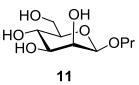 **11**	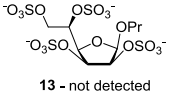 **13** - not detected	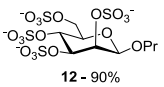 **12** - 90%	24
4	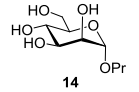 **14**	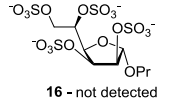 **16** - not detected	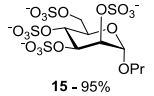 **15** - 95%	24
5	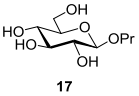 **17**	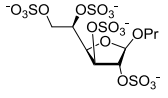 **18** - 75%	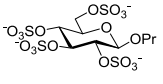 **19** - traces	24
6	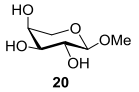 **20**	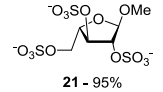 **21** - 95%	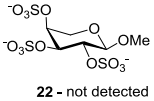 **22** - not detected	2
7	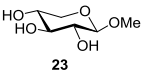 **23**	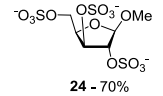 **24** - 70%	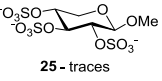 **25** - traces	5

[a]Standard conditions for PIF rearrangement were used for all experiments: (1) Py·SO_3 (5 equiv/OH-group), HSO_3Cl (2 equiv/OH-group), and dimethylformamide (DMF), 25 °C; and (2) $NaHCO_3$ (aq).

Glucose represented a rather complicated case. Previous experiments on PIF rearrangements of allyl β-D-glucopyranoside resulted in the formation of a mixture of the pyranoside and furanoside, and complete transformation of the glucopyranoside into the furanoside required a long reaction time[9] that caused the formation of undesirable degradation products. To determine if this was due to thermodynamic or kinetical reasons, in the present work, a more reactive propyl β-D-glucopyranoside (**17**) was used, as the relative rate of the PIF rearrangement of propyl glycosides was shown to be generally higher.[9] Indeed, during 24 h, the initially formed fully O-sulfated propyl β-D-glucopyranoside **19** was consumed to give furanoside **18** in 75% NMR yield.

The presence of CH_2OR or CH_3 groups at C(5) of the hexoses anchors the conformation and may significantly influence the relative stability of the monosaccharide forms.

DOI: 10.1021/acsomega.8b03274
ACS Omega 2019, 4, 1139−1143

Therefore, along with hexosides, the PIF rearrangements of pentosides **20** and **23** were also included in this study. The reactivity of pentosides was higher than that of hexosides and can be accompanied by aglycon cleavage as a side reaction. Thus, methyl α-L-arabinopyranoside **20** was completely transformed into α-L-arabinofuranoside **21** as the key product in 2 h while no pyranoside **22** was observed in the NMR spectra (Figure 1). In the case of methyl β-D-xylopyranoside **23**, the transformation into methyl β-D-xylofuranoside **24** was completed in 5 h.

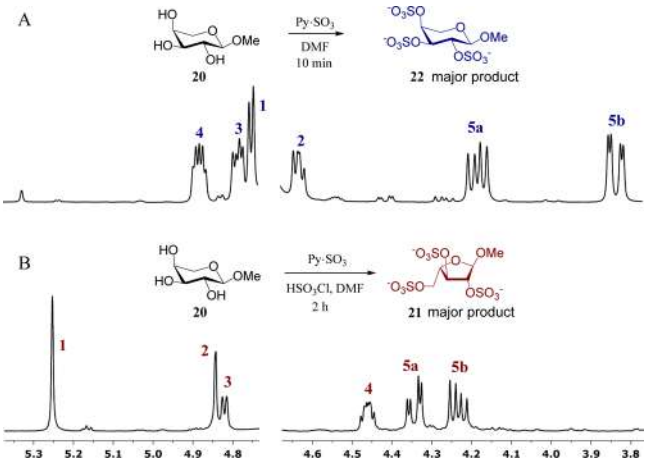

Figure 1. Part of the ^{1}H NMR spectra of the reaction mixtures: (A) per-O-sulfation of methyl α-L-arabinofuranoside **20** (10 min); (B) acid-promoted PIF rearrangement is almost complete after 2 h, and the signals of initially formed pyranoside **22** have almost disappeared.

For the α-L-arabinoside model structure (entries 1 and 2), the lowest energy conformers[17] were considered for the pyranoside form ($^4C_1$ for the nonsulfated form and $^1C_4$ for the per-O-sulfated form) and E_O for the furanoside. The complete sulfation causes the furanoside form to be 2.5 kcal/mol more preferable than α-arabinopyranoside. The same situation was observed for the β-D-xyloside model (entries 3 and 4): the pyranoside form tended to adopt an inverted chair $^1C_4$ (Figure 2) conformation upon the introduction of sulfates, and the furanoside form became dominant over the pyranoside. This,

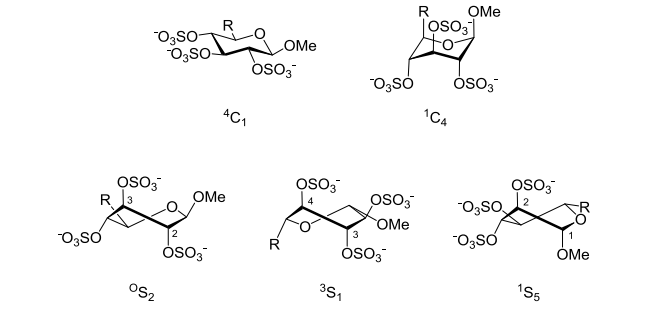

	$^4C_1$	$^1C_4$	$^OS_2$	$^3S_1$	$^1S_5$
R = H	4.2	**0**	4.7	5.1	4.5
R = $CH_2OSO_3^-$	2.9	0.2	**0**	0.9	2.1

Figure 2. Chair ($^4C_1$ and $^1C_4$) and skewed ($^0S_2$, $^3S_1$ and $^1S_5$) conformations of per-O-sulfated β-glucosides and β-xylosides and their relative energies (kcal/mol). The energies of the lowest energy conformations ($^1C_4$ for xylose and $^0S_2$ for glucose) were taken as zero.

in our opinion, is the basis for the driving force of the isomerization as the final step of the studied PIF rearrangement process.

A similar preference for the furanoside forms in the case of per-O-sulfated monosaccharides was revealed for the three studied hexosides with β-D-galacto (entries 5 and 6), β-L-fuco (entries 7 and 8), and β-D-gluco configurations (entries 9 and 10). The previous NMR studies[17] reveal that manno- and galacto-pyranosides exist mostly in normal chair configuration $^4C_1$, whereas for the per-O-sulfated β-glucosides, the skewed conformer $^0S_2$ is dominant (Figure 2). The conformers observed in the NMR spectra had the lowest energies in the ab initio calculations and were used to estimate the relative stability of the corresponding conformers.

These data clearly indicate that in the unsubstituted forms of all the studied hexoses, the pyranoside isomers are preferable by several kcal/mol. However, upon the introduction of sulfate substituents, the situation is reversed, and the furanoside isomers become more energetically stable, which provides the driving force for the isomerization of per-O-sulfated pyranosides into corresponding furanosides.

The only exceptions are the cases of α- and β-D-mannosides (entries 11−14). In these examples, the pyranoside form is the dominant form for both free and per-O-sulfated compounds, but in the β-isomers, this favorability is less pronounced. This might also account for the fact that in the course of our studies of the PIF rearrangement, we failed to find conditions under which either α- or β-mannosides could be transformed into the furanoside form.

The origin of such a change in the furanoside/pyranoside preference clearly lies in the repulsive interactions between the bulky and charged sulfate groups (Figure 3). The presence of

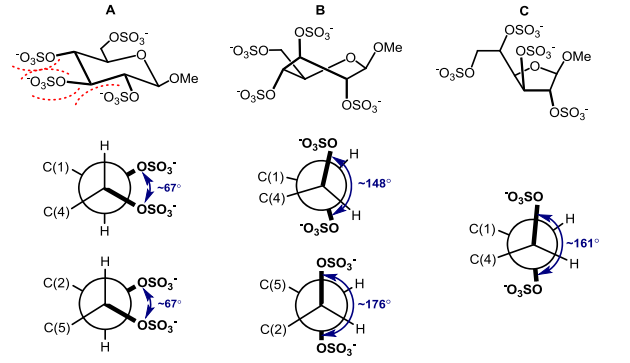

Figure 3. Spatial orientation of vicinally located O-sulfate groups in per-O-sulfated methyl β-D-gluco-pyranoside and -furanoside: repulsions in 2,3- and 3,4-pairs of equatorial O-sulfates in $^4C_1$ conformation (A), near to transorientation of 2,3- and 3,4-pairs of O-sulfates in $^0S_2$ conformation (B) and C2-exo furanoside conformation (C).

these interactions in highly sulfated carbohydrates and their ability to influence the conformation of carbohydrate rings was confirmed previously.[17−19] However, in the furanoside form, one of the sulfates is expelled from the ring and moves to the side chain, which gives it more degrees of freedom and allows it to avoid unfavorable interactions with the ring sulfates. In mannosides, these repulsions are decreased because the O-2 and O-3 sulfates are ax/eq oriented. In the α-mannosides, additionally, the ax/ax orientation of the aglycon and O-2 sulfate reduces the repulsion; thus, these sugars exhibit a stronger preference for the pyranoside form, especially their α-

DOI: 10.1021/acsomega.8b03274
ACS Omega 2019, 4, 1139−1143

Table 2. Calculated Differences between Total Energies and Natural Coulomb Electrostatic (NCE) Energies (kcal/mol) of the Furanoside and Pyranoside Forms of Different Monosaccharides

Entry	Structure, conformation: pyranoside, conformer	Structure, conformation: furanoside, conformer	ΔE_{total} (kcal/mol) ($E_{fur} - E_{pyr}$)	ΔE_{NCE} (kcal/mol) ($E_{fur} - E_{pyr}$)
1	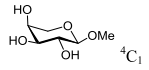 $^4C_1$	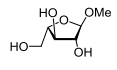 O4-*exo*	4.1	-
2	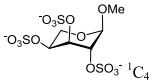 $^1C_4$	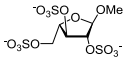 C1-*endo*	-2.5	-9.4
3	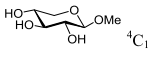 $^4C_1$	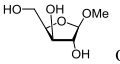 O4-*endo*	6.3	-
4	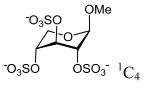 $^1C_4$	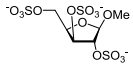 C2-*exo*	-2.6	-23.6
5	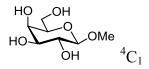 $^4C_1$	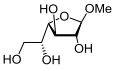 C4-*endo*	6.2	-
6	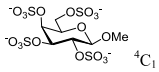 $^4C_1$	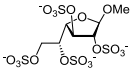 C1-*endo*	-1.8	-12.0
7	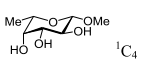 $^1C_4$	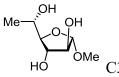 C3-*endo*	3.5	-
8	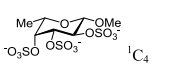 $^1C_4$	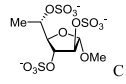 C1-*exo*	-3.9	-50.5
9	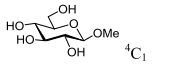 $^4C_1$	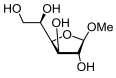 C2-*exo*	4.5	-
10	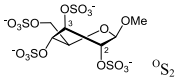 $^0S_2$	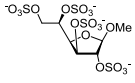 C2-*exo*	-1.7	1.6
11	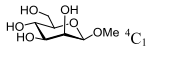 $^4C_1$	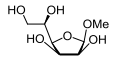 C2-*exo*	3.9	-
12	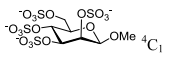 $^4C_1$	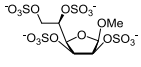 C2-*exo*	1.3	11.5
13	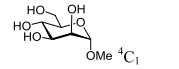 $^4C_1$	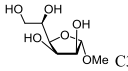 C3-*endo*	3.7	-
14	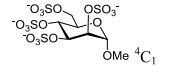 $^4C_1$	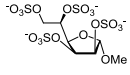 C3-*endo*	5.1	8.4

anomers. To prove this hypothesis, NCE energies were computed for all the sulfated molecules in this work using NBO 6.0 software.[20] The results given in Table 2 indicate that for the sulfated pentoses, the NCE energies of the furanosides are lower than those of the pyranosides. For the hexoses with galacto or fuco configurations, the situation is the same, whereas for the sulfated glucoside, these energies are almost equal, and for both mannosides, a strong preference for the pyranoside form is observed (as expected).

CONCLUSIONS

The described results demonstrate that for per-O-sulfated monosaccharides with galacto-, gluco-, fuco-, arabino-, and xylo-configurations, the furanoside forms are more stable than the corresponding pyranoside. The opposite situation occurs for unsulfated derivatives, which is consistent with the common knowledge that they predominantly exist as pyranosides in solution.[1,2] We suggest that this inversion of the energetic parameters serves as the driving force for the PIF rearrangement accompanied by the unexpected ring contraction process. For both α- and β-mannosides, the pyranoside forms are more stable even when all ring oxygen atoms are sulfated. The latter result suggests that mannosides do not undergo PIF rearrangement not only because of kinetics but also due to thermodynamic reasons.

EXPERIMENTAL SECTION

General Methods. ^1H and ^{13}C NMR spectra were recorded on Bruker AV-600, Bruker AV-400, or Bruker Fourier 300HD spectrometers equipped with 5 mm pulsed-field gradient probes at 298−303 K. The resonance assignments in the ^1H and ^{13}C NMR spectra were made using COSY and HSQC 2D experiments. Chemical shifts are reported in ppm and are referenced to the DMF residual peaks in D_2O (δ 3.01 for ^1H and δ 37.54 for ^{13}C).

Geometry optimization was performed using the ORCA 2.9.1 program.[21,22] RHF approximation with a 6-311++G** basis set was employed.[23] Sulfates in the studied structures were treated as anions. When the COSMO[24] model was applied, the built-in parameters for DMF were used. Geometry optimizations were performed until the RMS gradient reached a value less than 10^{-4}. The resulting energies were taken after applying outlying charge correction. For the NCE calculations, ORCA 4.0 was used, and NBO 6.0 was called directly from single-point calculations of the previously optimized structures.

PIF Rearrangement (Typical Procedure).[9] To a stirred solution of the monosaccharide substrate (0.05 mmol) in DMF (1 mL) was added the Py·SO_3 complex (5 equiv per OH). The reaction mixture was kept for 10 min at 20 °C, and then, HSO_3Cl (2 equiv per OH) was added dropwise under an inert atmosphere. The reaction mixture was stirred for the desired period of time, neutralized with aqueous NH_4HCO_3, concentrated in vacuo, and coevaporated with H_2O and then with D_2O. The residue was dissolved in D_2O and analyzed by NMR spectroscopy.

ASSOCIATED CONTENT

Supporting Information

The Supporting Information is available free of charge on the ACS Publications website at DOI: 10.1021/acsomega.8b03274.

Experimental details of PIF rearrangement, copies of $^1H-^{13}C$ HSQC spectra of reaction mixtures, ^1H and ^{13}C chemical shifts and J-constants for sulfated furanosides

DOI: 10.1021/acsomega.8b03274
ACS Omega 2019, 4, 1139−1143

18, **21** and **24**, and computational details: cartesian coordinates and total energies for all compounds from Table 2 (Tables S4−S31) (PDF)

AUTHOR INFORMATION

Corresponding Author

*E-mail: nen@ioc.ac.ru. Phone/Fax: +7-499-135-87-84.

ORCID

Nikolay E. Nifantiev: 0000-0002-0727-4050

Notes

The authors declare no competing financial interest.

ACKNOWLEDGMENTS

This work was supported by RSF grant 14-23-00199 (N.E.N.).

REFERENCES

(1) Mackie, W.; Perlin, A. S. Pyranose−Furanose and Anomeric Equilibria: Influence of Solvent and of Partial Methylation. *Can. J. Chem.* **1966**, *44*, 2039−2049.

(2) Smirnyagin, V.; Bishop, C. T. Glycosidation of Sugars. IV. Methanolysis of D-Glucose, D-Galactose, and D-Mannose. *Can. J. Chem.* **1968**, *46*, 3085−3090.

(3) Bishop, C. T.; Cooper, F. P. Glycosidation of Sugars: I. Formation of Methyl-D-Xylosides. *Can. J. Chem.* **1962**, *40*, 224−232.

(4) Sanders, D. A. R.; Staines, A. G.; McMahon, S. A.; McNeil, M. R.; Whitfield, C.; Naismith, J. H. UDP-Galactopyranose Mutase Has a Novel Structure and Mechanism. *Nat. Struct. Biol.* **2001**, *8*, 858.

(5) Lee, R. T.; Wong, T. C.; Lee, Y. C. Synthesis of 6′-Aminohexyl 2-Acetamido-2-Deoxy-D-Galactoside Isomers and a Unique Isomerization Catalyzed by Ion Exchange Resin. *J. Carbohydr. Chem.* **1986**, *5*, 343−357.

(6) Krylov, V. B.; Kaskova, Z. M.; Vinnitskiy, D. Z.; Ustyuzhanina, N. E.; Grachev, A. A.; Chizhov, A. O.; Nifantiev, N. E. Acid-promoted synthesis of per-O-sulfated fucooligosaccharides related to fucoidan fragments. *Carbohydr. Res.* **2011**, *346*, 540−550.

(7) Krylov, V. B.; Ustyuzhanina, N. E.; Grachev, A. A.; Nifantiev, N. E. Efficient acid-promoted per-O-sulfation of organic polyols. *Tetrahedron Lett.* **2008**, *49*, 5877−5879.

(8) Krylov, V. B.; Argunov, D. A.; Vinnitskiy, D. Z.; Verkhnyatskaya, S. A.; Gerbst, A. G.; Ustyuzhanina, N. E.; Dmitrenok, A. S.; Huebner, J.; Holst, O.; Siebert, H.-C.; et al. Pyranoside-into-Furanoside Rearrangement: New Reaction in Carbohydrate Chemistry and Its Application in Oligosaccharide Synthesis. *Chem.—Eur. J.* **2014**, *20*, 16516−16522.

(9) Nifantiev, N.; Krylov, V.; Argunov, D.; Vinnitskiy, D.; Gerbst, A.; Ustyuzhanina, N.; Dmitrenok, A. The Pyranoside-into-Furanoside Rearrangement of Alkyl Glycosides: Scope and Limitations. *Synlett* **2016**, *27*, 1659−1664.

(10) Argunov, D. A.; Krylov, V. B.; Nifantiev, N. E. Convergent Synthesis of Isomeric Heterosaccharides Related to the Fragments of Galactomannan from Aspergillus Fumigatus. *Org. Biomol. Chem.* **2015**, *13*, 3255−3267.

(11) Argunov, D. A.; Krylov, V. B.; Nifantiev, N. E. The Use of Pyranoside-into-Furanoside Rearrangement and Controlled O(5)→O(6) Benzoyl Migration as the Basis of a Synthetic Strategy To Assemble (1→5)-and (1→6)-Linked Galactofuranosyl Chains. *Org. Lett.* **2016**, *18*, 5504−5507.

(12) Krylov, V. B.; Argunov, D. A.; Solovev, A. S.; Petruk, M. I.; Gerbst, A. G.; Dmitrenok, A. S.; Shashkov, A. S.; Latgé, J.-P.; Nifantiev, N. E. Synthesis of Oligosaccharides Related to Galactomannans from Aspergillus Fumigatus and Their NMR Spectral Data. *Org. Biomol. Chem.* **2018**, *16*, 1188−1199.

(13) Krylov, V. B.; Gerbst, A. G.; Argunov, D. A.; Dmitrenok, A. S.; Shashkov, A. S.; Kaczynski, Z.; Huebner, J.; Holst, O.; Nifantiev, N. E. Definitive Structural Assessment of Enterococcal Diheteroglycan. *Chem.—Eur. J.* **2014**, *21*, 1749−1754.

(14) Verkhnyatskaya, S. A.; Krylov, V. B.; Nifantiev, N. E. Pyranoside-into-Furanoside Rearrangement of 4-Pentenyl Glycosides in the Synthesis of a Tetrasaccharide-Related to Galactan I of Klebsiella Pneumoniae. *Eur. J. Org. Chem.* **2017**, 710−718.

(15) Vinnitskiy, D. Z.; Krylov, V. B.; Ustyuzhanina, N. E.; Dmitrenok, A. S.; Nifantiev, N. E. The Synthesis of Heterosaccharides Related to the Fucoidan from Chordaria Flagelliformis Bearing an α-L-Fucofuranosyl. *Org. Biomol. Chem.* **2016**, *14*, 598−611.

(16) Satoh, H.; Manabe, S.; Ito, Y.; Lüthi, H. P.; Laino, T.; Hutter, J. Endocyclic Cleavage in Glycosides with 2,3-Trans Cyclic Protecting Groups. *J. Am. Chem. Soc.* **2011**, *133*, 5610−5619.

(17) Gerbst, A. G.; Krylov, V. B.; Argunov, D. A.; Solovev, A. S.; Dmitrenok, A. S.; Shashkov, A. S.; Nifantiev, N. E. Ring Distortion in Pyranosides Caused by Per-O-Sulfation. *Carbohydr. Res.* **2016**, *436*, 20−24.

(18) Wessel, H. P.; Bartsch, S. Conformational Flexibility in Highly Sulfated β-D-Glucopyranoside Derivatives. *Carbohydr. Res.* **1995**, *274*, 1−9.

(19) Gerbst, A. G.; Vinnitsky, D. Z.; Dmitrenok, A. S.; Ustyuzhanina, N. E.; Nifantiev, N. E. Conformational Study of Persulfated Propyl Glucuronide. *Carbohydr. Res.* **2018**, *455*, 81−85.

(20) Glendening, E. D., Badenhoop, J. K., Reed, A. E., Carpenter, J. E., Bohmann, J. A.; Morales, C. M., Landis, C. R., Weinhold, F. *NBO 6.0*; Theoretical Chemistry Institute; University of Wisconsin: Madison, WI, 2013; http://nbo6.chem.wisc.edu.

(21) Neese, F. The ORCA Program System. *Wiley Interdiscip. Rev.: Comput. Mol. Sci.* **2011**, *2*, 73−78.

(22) A library for the evaluation of molecular integrals of many-body operators over Gaussian functions *Libint* Version 2.3.1. http://libint.valeyev.net.

(23) Krishnan, R.; Binkley, J. S.; Seeger, R.; Pople, J. A. Self-Consistent Molecular Orbital Methods. XX. A Basis Set for Correlated Wave Functions. *J. Chem. Phys.* **1980**, *72*, 650−654.

(24) Klamt, A.; Schüürmann, G. A New Approach to Dielectric Screening in Solvents with Explicit Expressions for the Screening Energy and Its Gradient. *J. Chem. Soc., Perkin Trans. 2* **1993**, 799−80.

DOI: 10.1021/acsomega.8b03274
ACS Omega 2019, 4, 1139−1143

Application of computational methods for the studies of carbohydrate reactivity

Alexey G. Gerbst,* Vadim B. Krylov and Nikolay E. Nifantiev*

DOI: 10.1039/9781788013864-00151

This self-review covers the application of various computational methods for the investigation of carbohydrate reactivity. Since this topic cannot be investigated properly without paying attention to conformational behaviour of sugar molecules, some aspects of the theoretical conformational analysis are also discussed.

1 Introduction

Computational methods play an increasingly important role in understanding mechanisms of chemical reactions and planning syntheses of new compounds, particularly in carbohydrate chemistry. In the first part of this self-review some aspects of glycosylation stereoselectivity modelled through the remote assistance of substituents in the carbohydrate ring are discussed. Control over stereoselectivity of glycosylation is a very complex task due to the large variety of factors that can play role in these processes. They include, for example, the nature of a solvent and used promotor, the nature of the leaving group in the glycosyl donor and the structure of the acceptor. Also, besides the remote assistance hypothesis that will be surveyed herein, other stereoelectronic interactions between substituents can take place and they will be analysed in details in the second section of the review. The third part covers mechanistic investigations of the pyranoside-*into*-furanoside (PIF) rearrangement, a newly discovered reaction having no analogues in carbohydrate chemistry. In the last part some conformational aspects of oligosaccharides composed of *N*-protected glucosamine residues are discussed that lead to possibility of their cyclization forming structures that have significant practical importance for biochemical studies and drug design.

2 Possible role of remote *O*-acyl groups assistance in stereocontrol of glycosylation

Generally it is assumed that glycosylation proceed *via* formation of a carbocation like particle which is conventionally referred to as ''oxocarbenium ion''.[1] This can be formed as either a contact ion pair (CIP) or a solvent separated ion pair (SSIP) which further governs the stereochemical outcome. However, if this cation survives long enough before being attacked by a nucleophile, it can undergo several transformations that may also influence the stereoselectivity. Particularly, such transformations might result in the cation stabilization by a remote assistance of a carbonyl containing

Laboratory of Glycoconjugate Chemistry, N.D. Zelinsky Institute of Organic Chemistry, Russian Academy of Sciences, Leninsky prospect, 47, Moscow, Russia. E-mail: alger@ioc.ac.ru; nen@ioc.ac.ru

(*i.e.*, acyl) substituent in the donor moiety. The energy difference between the stabilized and non-stabilized form can be used to estimate the possibility of such stabilization. To carry out theoretical calculations of stabilization energy of glycosyl cations, we optimized the geometries and calculated energies of two conformations for each of the studied glycosyl cations. In one of the conformations, the protecting group at atom O(3) or O(4) was turned in such a way that the possible interaction with the cationic center was excluded (''non-stabilized cation''). In the case of the ''stabilized cation'', this protecting group was turned for such an interaction to appear (Fig. 1). After this, the difference between the obtained energies for non-stabilized and stabilized cations (further, the stabilization energy) was analysed.[2,3]

During our studies we encountered several situations when the stereochemical result of glycosylations could be explained with such a model. Among these were the fucosylations in order to form an α-Fuc → Fuc linkage using differently protected fucosyl bromides and trichoroacetimidates. Here we summarize computational approaches that could be employed for its verification.

Experimentally observed data showed that the substituent at O(4) influences the α-stereoselectivity of glycosylation by 2,3-di-*O*-benzylfucosyl donors. This problem was investigated using molecular mechanics approach. The results are shown in Table 1 and demonstrate good correlation between the stereochemical outcome and the calculated stabilization energies.

Moreover, our results showed that stereoselectivity of glycosylation with fucosyl bromides is strongly influenced by the presence of a single benzoyl protective group at O(3), which were shown to effectively stabilize the intermediate glycosyl cation (Fig. 2).[3]

Additionally, it was found that when two acyl groups are present in the donor structure at both at O(3) and O(4), the former substituent is more potent in the stabilization of the oxocarbenium ion according to the

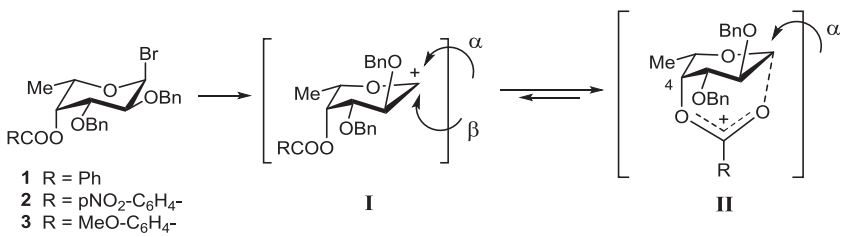

Fig. 1 The structure of the plausible oxocarbenium intermediates formed from fucosyl donors **1–3**: I – non-stabilized form; II – stabilized by participating acyl group at O(4) form.

Table 1 Stereoselectivity of glycosylation by fucosyl donors **1–3** and energies of stabilization of oxocarbenium ions by the participating of acyl group from O(4).[2]

Starting donor	α/β ratio	Δ*E* stabilization, kcal mole^{-1}
1	3.5 : 1	−3.6
2	2 : 1	−2.1
3	5 : 1	−4.7

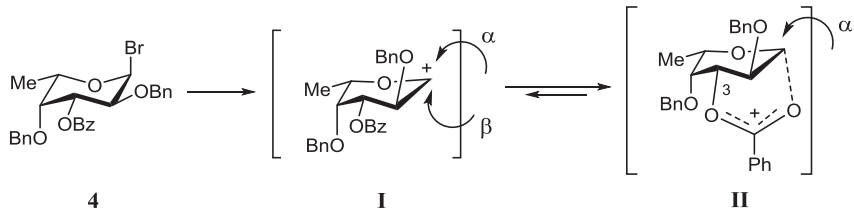

4 I II

Fig. 2 The structure of the plausible oxocarbenium intermediates formed from fucosyl donors **4**: I – non-stabilized form; II – stabilized by participating acyl group at O(3) form.

Table 2 Stereoselectivity of glycosylation and energies of stabilization of oxocarbenium ions by the participating of acyl group from O(3) and O(4).[3]

		Stabilization energy, kcal mole^{-1}, O(3)/O(4)	
Former donor	α/β ratio	MM+	DFT
4	13 : 1	−8.9	−14.3
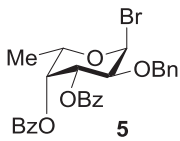 **5**	20 : 1	−9.9 (O-3)/−4.1 (O-4)	n.d.
1	3.5 : 1	−3.6	−7.3

calculations (Table 2). This time calculations were performed employing not only molecular mechanics, but also quantum chemical DFT approach. The molecular mechanics calculations showed that a cation type stabilized by an acyl group at O(3) is indeed much more stable than the open type cation (Table 2). Since molecular mechanics is designed to find structures of neutral compounds with ''normal'' bong lengths, bond angles, dihedral angles *etc.* we decided to further study these hypothetical intermediates at a higher level of calculation, namely using Density Functional Theory (DFT) calculations. Thus, the structures found by MM+ calculations were used as input and reoptimized using the Amsterdam Density Functional implementation of DFT.[4] It is expected that such calculations are as accurate as the model and therefore the differences between calculated and experimental results will reflect the neglect of solvent, counterions *etc.* in the calculations. It is readily apparent that trends observed with the MM+ forcefield are reproduced by the DFT calculations. The 3D structures of cations predicted by DFT calculations are presented in Fig. 3.

Further on, it was found that even chloroacetate groups can be used for this purpose and provide good stereoselectivity (Table 3).[5] For this kind of protecting groups the stabilization energies were additionally calculated at MP2 *ab initio* level of theory. It can be seen that, similar to MM+/DFT case described above, the tendencies revealed by molecular mechanics are generally reproduced at using MP2 approximation. Fig. 4 represents 3D structures of the differently stabilized and non-stabilized conformations of the chloroacetate containing donor.

Finally we decided to directly compare all possible methods that can be used for the prediction of the possible stabilization.[6] This was achieved

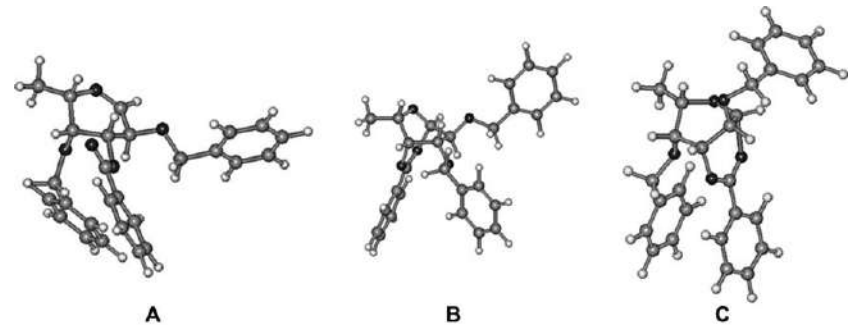

Fig. 3 3D structure of nonstabilized (A), O(4) stabilized (B) and O(3) stabilized (C) oxocarbenium ions.

Table 3 Stabilization by chloroacetates as compared to other acyl groups.

Starting donor	The stabilizing group	Stabilization energy, kcal mole^{-1}	
		MM+	SCF/MP2
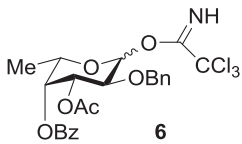 **6**	3-*O*-Ac	−11.6	−15.5
	4-*O*-Bz	−9.7	−15.5
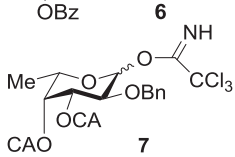 **7**	3-*O*-C(O)CH_2Cl	−11.1	−10.4
	4-*O*-C(O)CH_2Cl	−6.2	−8.6

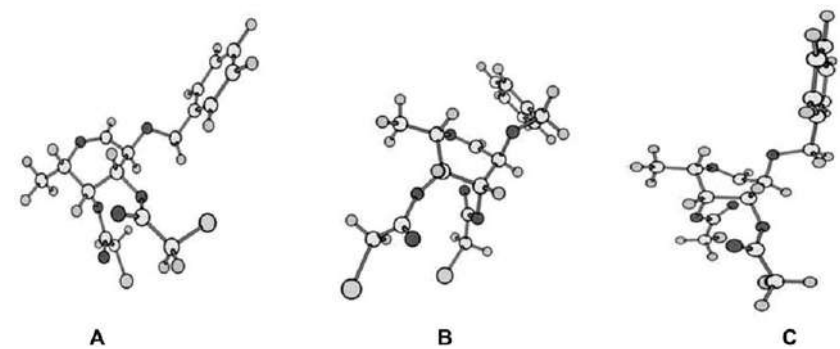

Fig. 4 Non-stabilized (**A**), O(3) stabilized (**B**) and O(4) stabilized (**C**) oxocarbenium ions containing chloroacetate protecting groups.

on the example of two furanoside donors **8** and **9** shown in Fig. 5. The approaches used included molecular mechanics, semi-empirical PM3, simple Hartree-Fock (HF), DFT and MP2 calculations.

The initial calculations by the molecular mechanics method and in the semiempirical approximation PM3 gave considerably different results. While the calculation by the MM+ method predicted substantial values

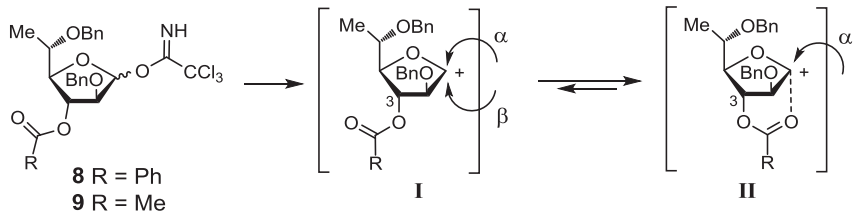

Fig. 5 The structure of the oxocarbenium ions formed from furanoside donors **8** and **9** used to compare different approaches for the prediction of the possible cation stabilization: I – non-stabilized; II – O(3) stabilized forms.

Table 4 Stabiliztion energies obtained at different levels of theory.

Starting donor	Stabilization energy, kcal mole^{-1}					α/β ratio
	MM+	PM3	HF	MP2	DFT	
8	−10.1	−0.6	−2.5	−4.5	−3.9	4 : 1
9	−8.0	−1.7	−3.4	−7.1	−7.2	4 : 1

of stabilization energies, in the PM3 approximation they were negligibly small. At the same time, the experimental data allowed us to suppose that still the stabilization occurs (Table 4).

When *ab initio* calculations in the 6-31 + G* basis were employed, the situation slightly improved, but the calculated stabilization energy values were still rather small. After the optimization of the structures in the HF/MP2 approximation, the stabilization energy values for oxocarbenium intermediates from donor **8** and **10** raised significantly. The calculations by the DFT method resulted in even more significant values of stabilization energies. It should be noted that the speed of calculation by the latter method is somewhat higher than that in the MP2 approximation. Surprisingly, the considerably differing values of stabilization obtained by MP2 and DFT methods did not agree with the similar ratios of stereo isomers (α/β), which correlated with the MM+ data. Generally, the geometries of stabilized and non-stabilized glycosyl oxocarbenium ions calculated by quantum chemical methods differed insignificantly (Fig. 6).

It should be noted that the most considerable difference was observed for the C(1)–O(5) bond distance, which, however, did not change upon ''stabilization''. In the calculations by the simple *ab initio* (HF) method, it was only 1.22 Å, while in the calculations with account for electron correlation on the MP2 level, it increased to 1.26 Å. Conversely, the distance between the carbonyl oxygen atom and the cationic center (CO–C(1)) decreased on going to the stabilized cation. Moreover, the evaluations of this distance in the stabilized cation considerably depended on the calculation method used. Thus, this distance decreased from 2.86 (HF) to 2.81 Å (MP2). At the same time, the use of semiempirical method PM3 provided that the C(1)–O(5) bond distance remained constant and equal to 1.26 Å, while the distance between the participating oxygen atom and the cationic center increased to 3.01 Å. In our opinion, this can be the reason why the semiempirical approximation does not completely account for the interaction of the participating group with the cationic

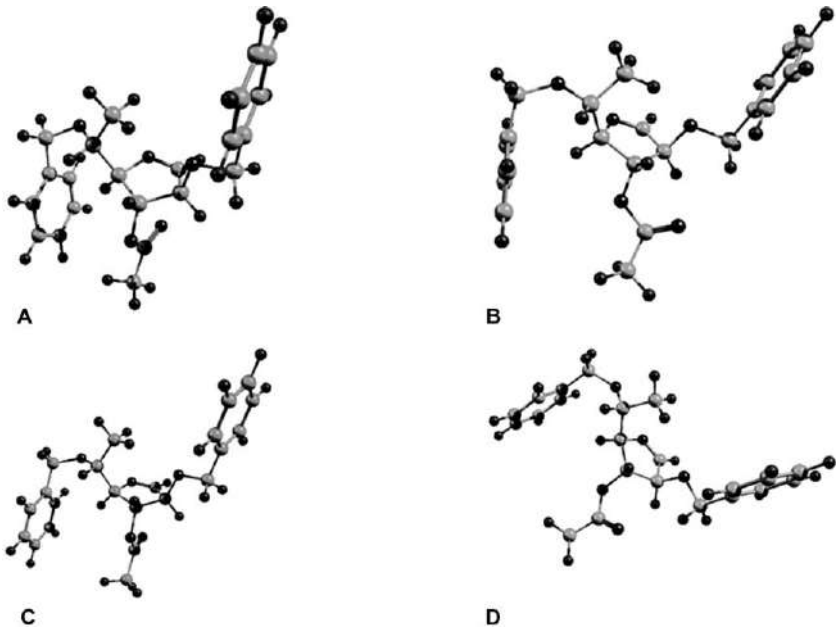

Fig. 6 3D views of the stabilized (A, C) and non-stabilized (B, D) conformations of oxocarbenium intermediates formed from fucosyl donor **9**calculated at the MP2 (A, B) and HF levels (C, D).

center and predicts too low values of stabilization energy. The values of the dihedral angles H(3)–C(3)–O(3)–C(O) changed insignificantly, within several degrees, upon optimization of the stabilized forms. However, the optimization of the unstabilized cation gave the changes reaching 40–50°. This is apparently explained by the fact that in the stabilized form of glycosyl carbocations the interaction of the carbonyl oxygen atom with the cationic center ''fixes'' the conformation.

The listed results suggest for the correct calculation of stabilization energy of hypothetical carbocations formed in the course of glycosylation reactions, it is necessary to correctly make account for the electron density redistribution. That is why the semi-empirical methods of quantum mechanics do not give a correct result. The *ab initio* methods without account for the electron correlation can also give incorrect results, namely, too low values of stabilization energies. At the same time, account for the electron correlation in the MP2 approximation gives more significant energy values. The same is true for the density functional method, since the last mentioned group of methods considers for the electron correlation, with the DFT method being much less demanding to the calculation resources. It is interesting that the use of simple molecular mechanics methods also shows the possibility of such stabilization.

Above described anchimeric effects[7–10] of remote *O*-acyl substituents can be used as efficient stereo directing instruments to control the formation of a desired configuration of anomeric centre in glycosylation reactions. They were already applied in the syntheses of complex oligosaccharides structurally related to fragments of sulphated seaweed

polysaccharides fucoidans and fucosylated chondroitin sulfates,[11–14] xylosylated notch epidermal growth factor repeats,[15] α-(1→3)-D-glucans of *Aspergillus fumigatus*[16,17] and their (1→6)-linked isomers,[18] of galactosaminogalactan of *A. fumigatus*[19] and some others.

3 Possible role of 1,3-*syn*-diaxial repulsion

Another factor that may influence the stereochemical result of the glycosylations is the possible interaction between oxygen atoms in the plausible intermediate carbocation that change its conformation as illustrated in Fig. 7.

To study the possibility of such repulsion practically, we used several model idoside structures (Fig. 8). According to the classic works,[20,21] in benzyliden-protected α-idopyranosides like **10–12**, 1,3-*syn*-diaxial repulsion between aglycon and a substituent at O-3 causes distortion of the normal $^4C_1$ conformation towards preference of $^OS_2$. Based on the work of Lemieux[22] it was suggested that the proportion of $^OS_2$ conformation in the equilibrium of a 3-O-substituted derivative of α-idopyranoside should reflect the degree of 1,3-*syn*-diaxial repulsive interaction between the O-3 substituent and aglycon. For the detection of the conformational changes in the sugar ring, vicinal proton–proton were measured to determine the conformational equilibrium of the carbohydrate rings.[23]

Assuming observable vicinal constants (^3J) to be linear combinations of the corresponding constants for separate conformers in the equilibrium, proportions of the conformers were to be calculated on the basis of experimental ^3J magnitudes and values of the corresponding constants for separate conformers calculated using quantum mechanical approach.

Geometry optimization of studied structures **10–12** and **13–15** gave the following results. Starting $^4C_1$ conformations for both α- **10–12** and β-idosides **13–15** during the optimization showed just a slight change in the ring shape producing the same conformation very slightly distorted towards $^OH_5$ or $^OH_1$ in case of α- and β-isomers respectively (Table 5). However, when starting $^OS_2$ conformations were subjected to the optimization, there was significant difference depending on the anomeric configuration. Thus, α-idosides **10–12** all retained $^OS_2$ conformation, while their β-counterparts ended up in a conformation almost exactly intermediate between $^1S_5$ and $B_{2,5}$ (Table 5). In our opinion, this suggests

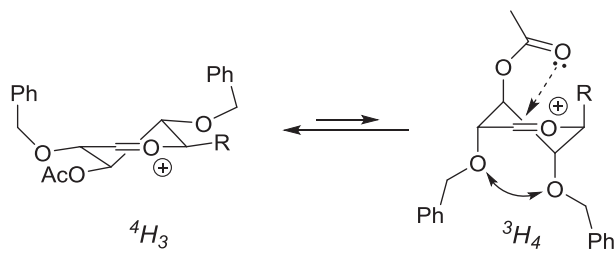

Fig. 7 1,3-*syn*-diaxial repulsion in the oxocarbenium ion.

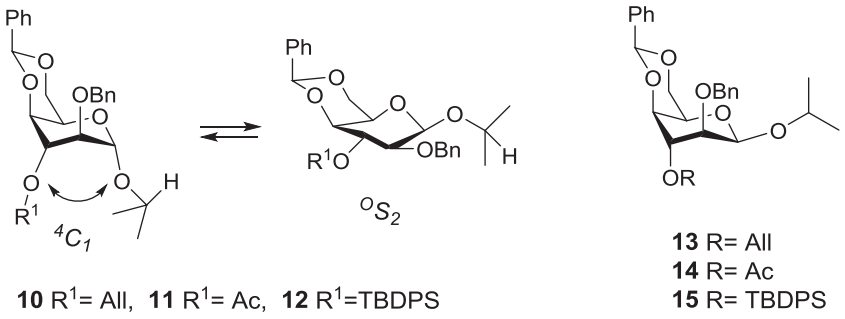

Fig. 8 The idoside structures used to explore possible 1,3-*syn*-diaxial repulsion.

Table 5 Cremer-Pople parameters of the DFT optimized structures for **10–15**.

Compound	Starting conformation	Cremer-Pople parameters			Resulting conformation
		φ	θ	Q	
10	$^4C_1$	330.25	11.48	0.48	Slightly distorted $^4C_1$ ($\rightarrow{}^OH_5$)
	$^OS_2$	326.32	86.40	0.73	$^OS_2$
11	$^4C_1$	335.56	11.13	0.48	Slightly distorted $^4C_1$ ($\rightarrow{}^OH_5$)
	$^OS_2$	325.78	87.92	0.74	$^OS_2$
12	$^4C_1$	330.69	10.65	0.48	Slightly distorted $^4C_1$ ($\rightarrow{}^OH_5$)
	$^OS_2$	324.63	86.78	0.72	$^OS_2$
13	$^4C_1$	35.68	11.01	0.54	Slightly distorted $^4C_1$ ($\rightarrow{}^OH_1$)
	$^OS_2$	284.43	97.18	0.69	$^1S_5/B_{2,5}$
14	$^4C_1$	32.11	11.96	0.53	Slightly distorted $^4C_1$ ($\rightarrow{}^OH_1$)
	$^OS_2$	283.13	97.80	0.69	$^1S_5/B_{2,5}$
15	$^4C_1$	36.48	11.19	0.54	Slightly distorted $^4C_1$ ($\rightarrow{}^OH_1$)
	$^OS_2$	285.73	97.55	0.69	$^1S_5/B_{2,5}$

that in the studied β-idosides neither pure skew, nor pure boat conformations seem to exist.

Finally, from the analysis of $^3J_{H,H}$ data for compounds **10–12** (Table 6) it can be concluded that 3-*O*-allylated idopyranoside **10** persists as mainly $^OS_2$ conformer with $^OS_2$ proportion around 73%. Acetylated idosyl derivative **11** seems to have approximately equal amount of $^OS_2$ and $^4C_1$ conformers with the range of $^OS_2$ proportion around 32%. Conformer ratio for idosyl derivative **12** bearing TBDPS protective group was found to be roughly 26%. The latter result looks like a contradiction with the tag ''bulky'' that is conventionally associated with TBDPS group. In other words, it evidences that silylated α-isoropylidoside **12** tends to assume $^4C_1$ conformation despite that in this case bulky TBDPS substituent in axial position is supposed to have a steric repulsion with the isopropyl group in the aglycon.

However, in fact there is no contradiction but rather elaboration of stereoelectronic properties of TBDPS group. In carbohydrate chemistry TBDPS, TBDMS and TIPS are used not only as protective groups but also as substituents that are capable of changing pyranoside conformation.[24–26] Main driving force for the conformational flip induced by TBDPS, TBDMS[24] or TIPS is said to be steric repulsion that emerges when these

Table 6 $^{3}J_{H,H}$ constants for **10–15**, Hz.

Compound	Coupling constants	$J_{1,2}$	$J_{2,3}$	$J_{3,4}$	$J_{4,5}$	$J_{6S,5}$	$J_{6R,5}$
10	Exp. Values	5.0	9.0	3.4	2.5	1.5	2.5
	Calculated $^{O}S_2$	6.2	11.7	3.7	2.9	1.1	3.4
	Calculated $^{4}C_1$	0.8	1.7	2.2	1.9	1.6	2.5
	Percentage of $^{O}S_2$ conformer	78	73	80	60	20	—[a]
11	Exp. Values	3.0	5.3	3.1	2.5	0.9	2.3
	Calculated $^{O}S_2$	6.1	12.6	4.7	3.0	1.1	3.5
	Calculated $^{4}C_1$	0.8	1.8	2.5	1.9	1.7	2.4
	Percentage of $^{O}S_2$ conformer	42	32	27	55	—[a]	—[a]
12	Exp. Values	2.5	4.4	2.7	2.2	1.5	2.1
	Calculated $^{O}S_2$	6.0	11.8	3.8	2.8	1.2	3.4
	Calculated $^{4}C_1$	0.8	1.8	2.3	1.9	1.6	2.4
	Percentage of $^{O}S_2$ conformer	33	26	27	33	25	—[a]
13	Exp. Values	1.4	3.4	2.8	2.0	1.2	2,1
	Calculated $^{1}S_5/B_{2,5}$	3.3	10.0	0.7	2.6	1.5	2.5
	Calculated $^{4}C_1$	1.2	2.8	2.3	2.1	1.4	2.7
	Percentage of $^{1}S_5/B_{2,5}$ conformer	10	8	—[a]	—[a]	—[a]	—[a]
14	Exp. Values	1.5	3.2	2.6	1.8	1.4	2.2
	Calculated $^{1}S_5/B_{2,5}$	2.9	10.6	0.8	2.6	1.5	2.4
	Calculated $^{4}C_1$	1.2	2.8	2.4	2.0	1.6	2.6
	Percentage of $^{1}S_5/B_{2,5}$ conformer	18	5	—[a]	—[a]	—[a]	—[a]
15	Exp. Values	0[c]	2.8	—[c]	0[b]	0[b]	1.8
	Calculated $^{1}S_5/B_{2,5}$	3.0	10.2	0.9	2.7	1.4	2.7
	Calculated $^{4}C_1$	1.3	2.8	2.3	2.1	1.5	2.6
	Percentage of $^{1}S_5/B_{2,5}$ conformer	—[a]	0	—[a]	—[a]	—[a]	—[a]

[a] Percentage of conformer cannot be calculated because experimental value falls out of the range between two corresponding constants calculated for separate conformers.
[b] Signals are so broadened that measurement of coupling constant with 0.1 Hz exactness was not possible.
[c] Coupling constant cannot be determined because of signals overlap.

groups have vicinal arrangement. As can be seen from the example of **12**, the ability of TBDPS to render a steric hindrance plays smaller role as compared to other stereoelectronic effects in the case of 1,3-*syn*-relashionship. In particular, the effect of TBDPS on the conformation of **12** is reminiscent of an observation[27,28] that in the O-TBDPS-substituted cyclohexanol TBDPS group assumes axial orientation.

Two β-isomers, **13** and **14**, were also studied in order to get an estimation of the strength of the repulsive interaction between 2-OBn and 4-OBzd substituents which also have mutual 1,3-*syn*-diaxial space relationship in $^{4}C_1$ conformation of both α- (**10–12**) and β-isopropylglycosides **13–15**. On the other hand, both chair and skew conformations of β-idosides lack O(3)–O(1) 1,3-*syn*-diaxial repulsion.

From Table 6 it is seen that values of $J_{3,4}$, $J_{4,5}$ and $J_{5,6}$ fall out of the range between two corresponding constants calculated for $^{4}C_1$ and $^{1}S_5/B_{2,5}$ conformers of **13–15**. Taking the values of $J_{2,3}$, allylated β-idopyranoside **13** as well as its acetylated analog **14**, both assume mainly $^{4}C_1$ conformation, likely having the percentage of $^{O}S_2$ between 0–15%. Therefore, it should be concluded that the interaction between 2-OBn and 4-OBzd does not contribute too much to the preference for $^{O}S_2$ conformer in **10–12**, which is thus mainly governed by the relative

instability of the $^4C_1$ conformer due to O(3)–O(1) repulsion. In this way the validity of compounds **10–12** as models for the study of 1,3-*syn*-diaxial repulsion is proved.

The destabilizing O(1)/O(3) interaction causes shift in the conformational equilibrium $^4C_1 \leftrightarrow {}^OS_2$ towards $^OS_2$. The percentage of the latter conformer reaches 73%, which shows that anomeric effect and strain resulting from the ring puckering are outweighed by 1,3-*syn*-diaxial repulsion. In accordance with assumption that electron density on oxygen atoms determines the strength of this repulsion, the 3-*O*-acetyl derivative adopts mainly $^4C_1$ conformation with the relative proportion of $^OS_2$ dropping down to 32%. The finding that in the 3-*O*-TBDPS derivative the weight of $^OS_2$ conformer is only 26%, despite presumably unfavorable spatial interactions, leads to disclosure of some peculiar properties of TBDPS group that has indisputable fame of a bulky substituent. Although the phenomenon is to be studied in-depth in later works, this probably throws some light on understanding of the stereoelectronic effects in controllable flip of pyranoside conformations with help of silyl substituents.

The repulsive interaction between 3-*O*-allyl and 1-*O*-isopropyl groups depends on polarity of solvent: namely, lower content of $^OS_2$ conformer in the equilibrium correlates with higher dielectric constant. Assuming that stereoselectivity of glycosylation is regulated by the conformational equilibrium of oxycarbenium ions, this opens the way to understanding how dielectric constant influences stereoselectivity through destabilization of conformers that have 1,3-*syn*-diaxial relationship of two alkoxy substituents. This is, for example, the case of donors with *gluco*- configuration bearing two alkyl protecting groups at O(2) and O(4) simultaneously. This suggestion does not contradict with known β-selectivity of perbenzylated glucosyl donors in acetonitrile.

Thus this piece of work demonstrate applicability of *ab initio* calculations for the conformational analysis of the pyranoside rings by means of coupling constants estimation, from which, upon their comparison with the experimentally observed values the percentage of particular conformers can be derived.

4 Investigation of the pyranoside-*into*-furanoside rearrangement

The PIF rearrangement was recently discovered[29] as an original and useful method for the synthesis of selectively protected furanosides from corresponding pyranosides under acid promoted per-*O*-sulfation. The contraction of a pyranoside ring into furanoside proceeds under acid-promoted per-*O*-sulfation in presence of a SO_3-complex and a strong acid (see example of the PIF rearrangement on Fig. 9). On the first step, formation of a totally *O*-sulfated pyranoside occurs (**16**→**17**) which then relatively slowly converts into a corresponding per-*O*-sulfated furanoside (**17**→**18**). Following step is solvolytic de-*O*-sulfation (**18**→**19**) which afforded to obtain desire furanoside building blocks. We investigated this reaction theoretically in two aspects. First, mechanistic studies were performed.[30] Then, its possible driving force was explored.[31]

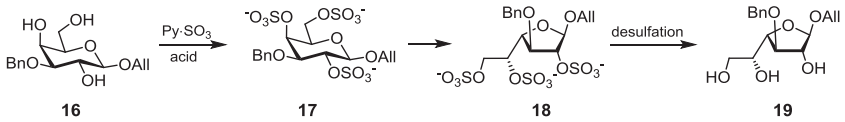

Fig. 9 Example of the PIF rearrangement.

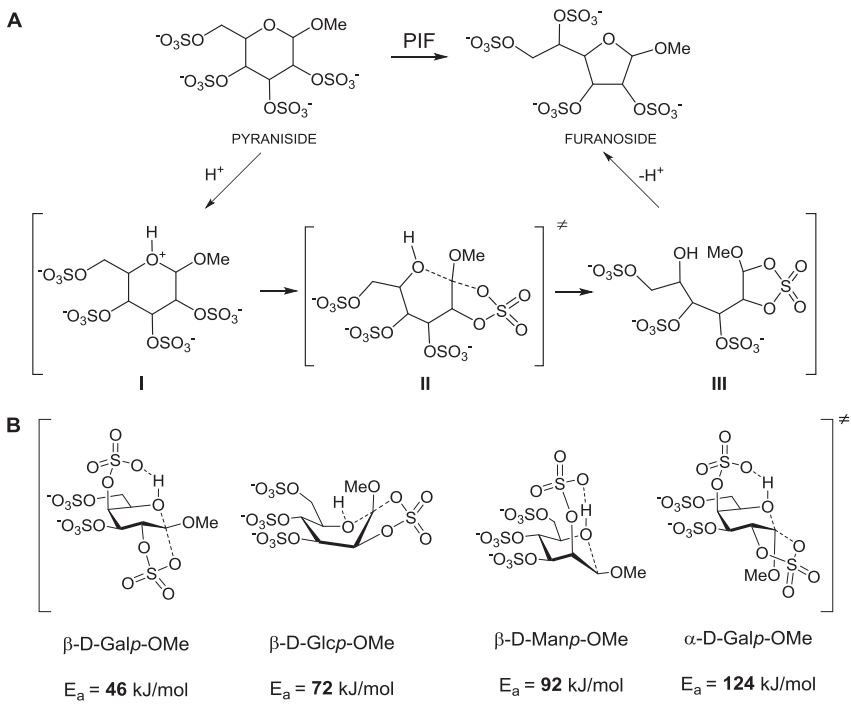

Fig. 10 Proposed mechanism (A); possible transition states and activation energies (B) for PIF rearrangement.

The theoretical mechanistic studies were performed by means of transition state search and calculation of activation energies. Since it was known that this reaction proceeds excellently in the case of galactose, worse with glucose and does not proceed at all with mannose (Fig. 10), these three sugars were used to model possible mechanism of this rearrangement.

To explain the observed difference in reactivity of the studied pyranosides depending on the ring configuration we calculated the activation barrier of *endo*-cyclic C(1)–O(5)-bond cleavage which proposed to be rate-determining step for pyranoside-*into*-furanoside rearrangement. The calculations were performed for methyl glycoside models employing *ab initio* RHF calculations. It was shown that in case of galactosides the calculated activation energy had the lowest value for the β-isomeric form and the highest for the α-isomer. This correlated with the experimental data according to which α-galactoside did not undergo PIF-rearrangement. In structural terms it could be explained by steric interactions between the axially oriented aglycon and the participating SO_3-group in the

transition state. Quite expectedly, in the case of methyl mannoside the activation energy was also rather high. In this molecule the ''participating'' SO_3-group is itself in axial position which makes its interaction with the anomer carbon atom less effective. The activation energy for the β-glucoside was intermediate between β-galactoside and β-mannoside and the formation of the transition state was accompanied by ring distortion. This explained why the glucoside derivatives only slowly reacted under the discussed conditions.

This hypothesis suggest critical role of the sulfate group at O(2), and it could additionally provide an explanation for the retention of anomeric configuration during the rearrangement. The interaction between the sulfate at O(2) and the anomeric center in TS leads to the formation of a 5-membered pseudo-cycle which restricts C(1)–C(2) bond from rotating and yields a product with the retained configuration.

The critical importance of the sulfate at O(2) was also found experimentally and proved by additional computational studies. Particularly, 2-*O*-acetylated model was studied in order to compare it with its sulphated counter-part. The calculation of activation energy (E_a) of such reaction pathway in model substrates with 2-*O*-sulfo and 2-*O*-acetyl groups respectively was performed using RHF calculations with 6-31 + G* basis. It was found that discussed reactivity is more favoured for the derivative with 2-*O*-sulfo then for that with 2-*O*-acetyl group (E_a 52.7 kJ *vs* 142.0 kJ, Fig. 11). Moreover, it can be concluded from the geometry of transition state that sulfate at O(2) in substrate ''participate'' in this reaction, while 2-*O*-Ac does not or to much smaller extent. We assume that ''participation'' of 2-*O*-sulfo-group allows for facilitation of O(5)–C(1)-bond cleavage and contributes to the fixation of configuration of anomeric centre during rearrangement process.

The driving force of the PIF rearrangement was studied by computing energy differences between furanoside and pyranoside forms for a series of pentoses and hexoses (Table 7). Thus, for the α-L-arabinoside model structure (entries 1 and 2), the lowest energy conformers were considered for the pyranoside form ($^4C_1$ for the nonsulfated form and $^1C_4$ for the per-*O*-sulfated form) and E_O for the furanoside. The complete sulfation

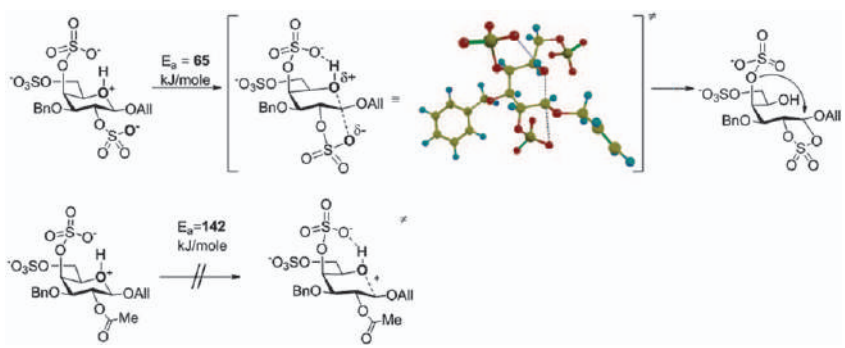

Fig. 11 Possible transition state structures for 2-*O*-sulfated and 2-*O*-acetylated galactoside models.

Table 7 The model structures used for studies of the PIF driving force and energy differences.

N	Structure, conformation				ΔE_{total} (kcal mole^{-1}) (E_{fur}–E_{pyr})	ΔE_{NCE} (kcal mole^{-1}) (E_{fur}–E_{pyr})
	Pyranoside		Furanoside			
1	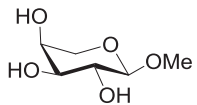	$^4C_1$	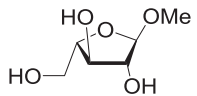	O4-*exo*	4.1	—
2	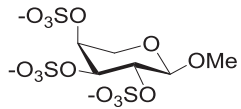	$^1C_4$	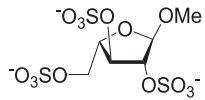	C1-*endo*	−2.5	−9.4
3	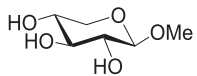	$^1C_4$	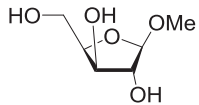	O4-*endo*	6.3	—
4	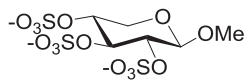	$^1C_4$	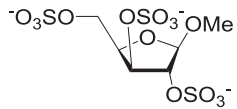	C2-*exo*	−2.6	−23.6
5	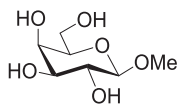	$^4C_1$	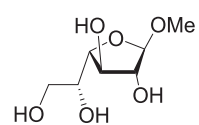	O4-*exo*	6.2	—
6	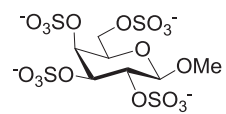	$^4C_1$	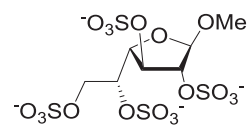	C1-*endo*	−1.8	−12.0
7	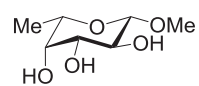	$^1C_4$	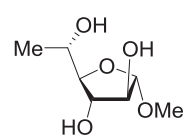	C3-*endo*	3.5	—

Table 7 (*Continued*)

N	Structure, conformation				ΔE_{total} (kcal mole^{-1}) (E_{fur}–E_{pyr})	ΔE_{NCE} (kcal mole^{-1}) (E_{fur}–E_{pyr})
	Pyranoside		Furanoside			
8	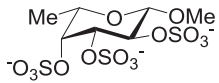	$^{1}C_{4}$	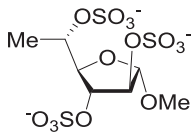	C1-*exo*	−3.9	−50.5
9	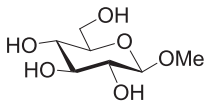	$^{4}C_{1}$	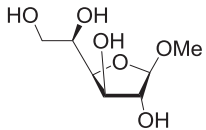	C2-*exo*	4.5	—
10	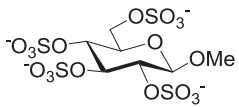	$^{O}S_{2}$	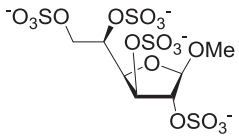	C2-*exo*	−1.7	1.6
11	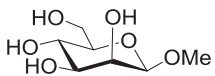	$^{4}C_{1}$	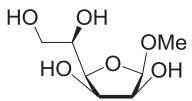	C2-*exo*	3.9	—
12	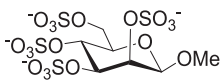	$^{4}C_{1}$	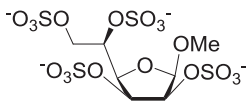	C2-*exo*	1.3	11.5
13	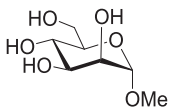	$^{4}C_{1}$	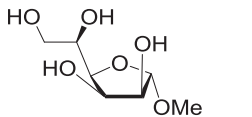	C3-*endo*	3.7	—
14	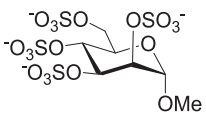	$^{4}C_{1}$	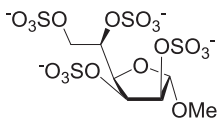	C3-*endo*	5.1	8.4

causes the furanoside form to be 2.5 kcal mole^{-1} more preferable than α-arabinopyranoside. The same situation was observed for the β-D-xyloside model (entries 3 and 4): the pyranoside form tended to adopt an inverted chair $^{1}C_{4}$ conformation upon the introduction of sulfates, and the furanoside form became dominant over the pyranoside. This, in our opinion, is the basis for the driving force of the isomerization as the final step of the studied PIF rearrangement process.

A similar preference for the furanoside forms in the case of per-*O*-sulfated monosaccharides was revealed for the three studied hexosides with β-D-*galacto*- (entries 5 and 6), β-L-*fuco*- (entries 7 and 8), and β-*gluco*-configurations (entries 9 and 10). The previous NMR studies[32] reveal that *manno*- and *galacto*pyranosides exist mostly in normal chair configuration $^{4}C_{1}$, whereas for the per-*O*-sulfated β-glucosides, the skewed conformer $^{O}S_{2}$ is dominant. The conformers observed in the NMR spectra had the lowest energies in the *ab initio* calculations and were used to estimate the relative stability of the corresponding conformers.

These data clearly indicate that in the unsubstituted forms of all the studied hexoses, the pyranoside isomers are preferable by several kcal mole^{-1}. However, upon the introduction of sulfate substituents, the situation is reversed, and the furanoside isomers become more energetically stable, which provides the driving force for the isomerization of per-*O*-sulfated pyranosides into corresponding furanosides.

The only exceptions are the cases of α- and β-D-mannosides (entries 11–14). In these examples, the pyranoside form is the dominant form for both the free and per-*O*-sulfated compounds, but in the β-isomers, this preference is less pronounced. This might also account for the fact that in the course of our studies of the PIF rearrangement, we failed to find conditions under which either α- or β-mannosides could be transformed into the furanoside form.

The origin of such a change in the furanoside/pyranoside preference clearly lies in the repulsive interactions between the bulky and charged sulfate groups. The presence of these interactions in highly sulfated carbohydrates and their ability to influence the conformation of carbohydrate rings was confirmed previously.[32–34] However, in the furanoside form, one of the sulfates is expelled from the ring and moves to the side chain, which gives it more degrees of freedom and allows it to avoid unfavorable interactions with the ring sulfates. In mannosides, these repulsions are decreased because the O-2 and O-3 sulfates are *ax*/*eq* oriented. In the α-mannosides, additionally, the *ax*/*ax* orientation of the aglycon and O-2 sulfate reduces the repulsion; thus, these sugars exhibit a stronger preference for the pyranoside form, especially their α-anomers. To prove this hypothesis, natural Coulomb electrostatic (NCE) energies were computed for all the sulfated molecules in this work using NBO 6.0 software. The results given in Table 2 indicate that for the sulfated pentoses, the NCE energies of the furanosides are lower than those of the pyranosides. For the hexoses with *galacto*- or *fuco*-configurations, the situation is the same, while for the sulfated glucoside, these energies are almost equal, and for both mannosides, a strong preference for the pyranoside form is observed (as expected).

This demonstrates that *ab initio* quantum mechanical calculations can be applied both for the studies of PIF mechanism and its driving force. The latter aspect in combination with NBO calculations reveals the reasons for the furanoside form domination over the pyranoside upon total sulfation as the result of the sulfates repulsion.

Above described pyranoside-*into*-furanoside rearrangement was applied in the syntheses of furanoside-containing complex oligosaccharides structurally related to galactomannan of *Aspergillus fumigatus*,[35–37] *O*-chains of *Klebsiella pneumoniae* LPS (namely galactan I),[38,39] Enterococcal diheteroglycan[40] and some others.

5 Investigation of self-cyclization of 6-monohydroxylated oligo-(1→6)-glucosamine glycosyl donors

Another type of reactivity was studied in the case of oligosaccharide 6-hydroxylated *N*-acylated glucosamine derivatives bearing internal (1→6)-bonds (Fig. 12). Modelling studies[41–43] with the use of molecular dynamics (MD) employing MM3 force field revealed that such compounds exhibit spiral-like conformations favouring spatial proximity of glycosylating and glycosylated parts that are needed for the intramolecular glycosidic bond formation. Cyclic oligosacharides thus synthesized contained 2 to 7 glucosamine units with the free amino group (Fig. 12, $n = 0, 1, 2, 3, 4, 5$; $R = H$) or *N*-substituted derivatives with functionalised *R* substituents. In particular, the synthesised cycloglucosamines were used as scaffolds to design oligodentate blockers of bacterial lectins,[44] building components of ionic channels[45,46] and some other high-tech applications.

In most cases β-isomers were formed during the cyclization. However, starting from the tetrasaccharide sometimes the formation of the α-linkage was observed. This result was explained by examining the most preferred conformation of the linear tetrasaccharide precursor obtained from the MD simulations. It represented one turn of a right-handed spiral (Fig. 12), in which C-1 of the glycosylating unit and 6-OH of the glycosyl acceptor residue are spatially prearranged in a way favoring α-glycosylation. However, the anchimeric participation of the phthaloyl group could impede the immediate formation of the α-linked cycle and also stabilize the glycosyl cationic intermediate, which becomes stable enough to survive until reorganization to a conformation favoring the

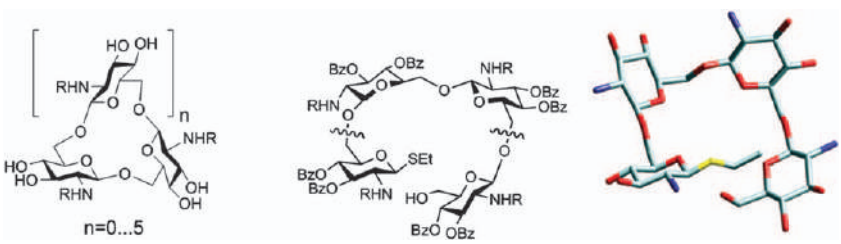

Fig. 12 Studied cycloglucosamines prepared by intramolecular cyclization of 6-hydroxylated oligoglucosamine derivatives with internal (1→6)-bonds and their conformations favouring spatial proximity of glycosylating and glycosylated parts.

β-attack. The observed stereochemical outcome of cyclization of the tetrasaccharide is apparently a result of the competition between these two processes. Similar conformational α-stereocontrol could be also expected for longer bifunctional blocks in which the terminal residues are situated on adjacent turns of the right-handed helical structure.

6 Conclusion

In recent years computational methods have become useful instruments to investigate the mechanisms and directions of new reactions in organic chemistry and even predict the possibility and efficiency of these complex processes. This is highlighted by the reviewed studies in the aspect of carbohydrate chemistry, which include different types of chemical transformations – stereoselective glycosylation, monosaccharide ring distortion in the course of pyranoside-*into*-furanoside rearrangement and intramolecular cyclisation of oligosaccharide bifunctional precursors. There is no doubt that further development of computational methods is necessitated due to emerging novel chemical approaches and methods.

Acknowledgements

Authors are supported by the Russian Science Foundation (grant 19-73-30017).

References

1 D. M. Whitfield, *Adv. Carbohydr. Chem. Biochem.*, 2009, **62**, 83.
2 A. G. Gerbst, N. E. Ustuzhanina, A. A. Grachev, D. E. Tsvetkov, E. A. Khatuntseva and N. E. Nifant'ev, *Mendeleev Commun.*, 1999, **9**, 114.
3 A. G. Gerbst, N. E. Ustuzhanina, A. A. Grachev, E. A. Khatuntseva, D. E. Tsvetkov, D. M. Whitfield, A. Berces and N. E. Nifantiev, *J. Carbohydr. Chem.*, 2001, **20**, 821.
4 T. Nukada, A. Berces, M. Z. Zgierski and D. M. Whitfield, *J. Am. Chem. Soc.*, 1998, **120**, 13291.
5 N. E. Ustyuzhanina, P. A. Fomitskaya, A. G. Gerbst, A. S. Dmitrenok and N. E. Nifantiev, *Mar. Drugs*, 2015, **13**, 770.
6 A. G. Gerbst, V. B. Krylov, D. Z. Vinnitsky, N. E. Ustyuzhanina and N. E. Nifantiev, *Russ. Chem. Bull.*, 2015, **64**, 2763.
7 B. S. Komarova, M. V. Orekhova, Y. E. Tsvetkov and N. E. Nifantiev, *Spec. Period. Rep.: Carbohydr. Chem.*, 2015, **41**, 187.
8 B. S. Komarova, Y. E. Tsvetkov and N. E. Nifantiev, *Chem. Rec.*, 2016, **16**, 488.
9 N. Ustyuzhanina, B. Komarova, N. Zlotina, V. Krylov, A. Gerbst, Y. Tsvetkov and N. Nifantiev, *Synlett*, 2006, ~~2006~~, 921.
10 B. S. Komarova, M. V. Orekhova, Y. E. Tsvetkov and N. E. Nifantiev, *Carbohydr. Res.*, 2014, **384**, 70.
11 E. A. Khatuntseva, N. E. Ustuzhanina, G. V. Zatonskii, A. S. Shashkov, A. I. Usov and N. E. Nifant'ev,
12 N. Ustyuzhanina, V. Krylov, A. Grachev, A. Gerbst and N. Nifantiev, *Synthesis*, 2006, **2006**, 4017.
13 V. B. Krylov, Z. M. Kaskova, D. Z. Vinnitskiy, N. E. Ustyuzhanina, A. A. Grachev, A. O. Chizhov and N. E. Nifantiev, *Carbohydr. Res.*, 2011, **346**, 540.

AQ:1

14 D. Z. Vinnitskiy, V. B. Krylov, N. E. Ustyuzhanina, A. S. Dmitrenok and N. E. Nifantiev, *Org. Biomol. Chem.*, 2016, **14**, 598.
15 V. Krylov, N. Ustyuzhanina, A. Grachev, H. Bakker and N. Nifantiev, *Synthesis*, 2007, **2007**, 3147.
16 B. S. Komarova, M. V. Orekhova, Y. E. Tsvetkov, R. Beau, V. Aimanianda, J.-P. Latgé and N. E. Nifantiev, *Chem. – Eur. J.*, 2015, **21**, 1029.
17 B. S. Komarova, S. S. W. Wong, M. V. Orekhova, Y. E. Tsvetkov, V. B. Krylov, A. Beauvais, J.-P. Bouchara, J. F. Kearney, V. Aimanianda, J.-P. Latgé and N. E. Nifantiev, *J. Org. Chem.*, 2018, **83**, 12965.
18 B. S. Komarova, V. S. Dorokhova, Y. E. Tsvetkov and N. E. Nifantiev, *Org. Chem. Front.*, 2018, **5**, 909.
19 E. D. Kazakova, D. V. Yashunsky, V. B. Krylov, J.-P. Bouchara, M. Cornet, I. Valsecchi, T. Fontaine, J.-P. Latge and N. E. Nifantiev, *J. Am. Chem. Soc.*, AQ:2 2020, **142**, 1175–1179.
20 S. J. Angyal and Y. Kondo, *Carbohydr. Res.*, 1980, **81**, 35.
21 H. Paulsen and M. Friedmann, *Chem. Ber.*, 1972, **105**, 718.
22 R. U. Lemieux and A. A. Pavia, *Can. J. Chem.*, 1969, **47**, 4441.
23 B. S. Komarova, A. G. Gerbst, A. M. Finogenova, A. S. Dmitrenok, Y. E. Tsvetkov and N. E. Nifantiev, *J. Org. Chem.*, 2017, **82**, 8897.
24 J. Broddefalk, K.-E. Bergquist and J. Kihlberg, *Tetrahedron*, 1998, **54**, 12047.
25 C. M. Pedersen, L. U. Nordstrøm and M. Bols, *J. Am. Chem. Soc.*, 2007, **129**, 9222.
26 Y. Okada, T. Mukae, K. Okajima, M. Taira, M. Fujita and H. Yamada, *Org. Lett.*, 2007, **9**, 1573.
27 C. H. Marzabadi, J. E. Anderson, J. Gonzalez-Outeirino, P. R. Gaffney, C. G. White, D. A. Tocher and L. J. Todaro, *J. Am. Chem. Soc.*, 2003, **125**, 15163.
28 E. L. Eliel and H. Satici, *J. Org. Chem.*, 1994, **59**, 688.
29 V. B. Krylov, D. A. Argunov, D. Z. Vinnitskiy, S. A. Verkhnyatskaya, A. G. Gerbst, N. E. Ustyuzhanina, A. S. Dmitrenok, J. Huebner, O. Holst and H.-C. Siebert, *et al.*, *Chem. – Eur. J.*, 2014, **20**, 16516.
30 V. B. Krylov, D. A. Argunov, D. Z. Vinnitskiy, A. G. Gerbst, N. E. Ustyuzhanina, A. S. Dmitrenok and N. E. Nifantiev, *Synlett*, 2016, **27**, 1659.
31 A. G. Gerbst, V. B. Krylov, D. A. Argunov, A. S. Dmitrenok and N. E. Nifantiev, *ACS Omega*, 2019, **4**, 1139.
32 A. G. Gerbst, V. B. Krylov, D. A. Argunov, A. S. Solovev, A. S. Dmitrenok, A. S. Shashkov and N. E. Nifantiev, *Carbohydr. Res.*, 2016, **436**, 20.
33 H. P. Wessel and S. Bartsch, *Carbohydr. Res.*, 1995, **274**, 1.
34 A. G. Gerbst, D. Z. Vinnitsky, A. S. Dmitrenok, N. E. Ustyuzhanina and N. E. Nifantiev, *Carbohydr. Res.*, 2018, **455**, 81.
35 D. A. Argunov, V. B. Krylov and N. E. Nifantiev, *Org. Biomol. Chem.*, 2015, **13**, 3255.
36 D. A. Argunov, V. B. Krylov and N. E. Nifantiev, *Org. Lett.*, 2016, **18**, 5504.
37 V. B. Krylov, D. A. Argunov, A. S. Solovev, M. I. Petruk, A. G. Gerbst, A. S. Dmitrenok, A. S. Shashkov, J.-P. Latgé and N. E. Nifantiev, *Org. Biomol. Chem.*, 2018, **16**, 1188.
38 S. A. Verkhnyatskaya, V. B. Krylov and N. E. Nifantiev, *Eur. J. Org. Chem.*, 2017, **2017**, 710.
39 D. A. Argunov, A. S. Trostianetskaia, V. B. Krylov, E. A. Kurbatova and N. E. Nifantiev, *Eur. J. Org. Chem.*, 2019, **2019**, 4226.
40 V. B. Krylov, A. G. Gerbst, D. A. Argunov, A. S. Dmitrenok, A. S. Shashkov, Z. Kaczynski, J. Huebner, O. Holst and N. E. Nifantiev, *Chem. – Eur. J.*, 2015, **21**, 1749.

41 M. L. Gening, D. V. Titov, A. A. Grachev, A. G. Gerbst, O. N. Yudina, A. S. Shashkov, A. O. Chizhov, Y. E. Tsvetkov and N. E. Nifantiev, *Eur. J. Org. Chem.*, 2010, **2010**, 2465.
42 A. A. Grachev, A. G. Gerbst, M. L. Gening, D. V. Titov, O. N. Yudina, Y. E. Tsvetkov, A. S. Shashkov, G. B. Pier and N. E. Nifantiev, *Carbohydr. Res.*, 2011, **346**, 2499.
43 D. V. Titov, M. L. Gening, A. G. Gerbst, A. O. Chizhov, Y. E. Tsvetkov and N. E. Nifantiev, *Carbohydr. Res.*, 2013, **381**, 161.
44 M. L. Gening, D. V. Titov, S. Cecioni, A. Audfray, A. G. Gerbst, Y. E. Tsvetkov, V. B. Krylov, A. Imberty, N. E. Nifantiev and S. Vidal, *Chem. – Eur. J.*, 2013, **19**, 9272.
45 T. Saha, A. Roy, M. L. Gening, D. V. Titov, A. G. Gerbst, Y. E. Tsvetkov, N. E. Nifantiev and P. Talukdar, *Chem. Commun.*, 2014, **50**, 5514.
46 A. Roy, T. Saha, M. L. Gening, D. V. Titov, A. G. Gerbst, Y. E. Tsvetkov, N. E. Nifantiev and P. Talukdar, *Chem. – Eur. J.*, 2015, **21**, 17445.

Available online at www.sciencedirect.com
ScienceDirect
Mendeleev Commun., 2014, **24**, 336–337
Mendeleev Communications

Preparative synthesis of selectively substituted 1,6-anhydro-α-D-galactofuranose derivatives

Vadim B. Krylov, Dmitry A. Argunov and Nikolay E. Nifantiev*

N. D. Zelinsky Institute of Organic Chemistry, Russian Academy of Sciences, 119991 Moscow, Russian Federation. Fax: +7 499 135 8784; e-mail: nen@ioc.ac.ru

DOI: 10.1016/j.mencom.2014.11.006

Heating of trisodium salt of allyl 3-*O*-benzyl-2,5,6-tri-*O*-sulfonato-β-D-galactofuranoside with pyridinium chloride in dioxane affords 1,6-anhydro-3-*O*-benzyl-α-D-galactofuranose which was regioselectively acylated to give useful precursors for oligosaccharide synthesis.

Growing biological interest to furanoside-containing natural carbohydrates of plant, bacterial and fungal origin challenges the development of new synthetic approaches to their chemical preparation. One of the convenient type of building blocks for assembling of a variety of galactofuranoside-containing oligosaccharides includes 1,6-anhydro-α-D-galactofuranose derivatives.[1,2] Recently, a simple three-step procedure for the synthesis of unprotected 1,6-anhydro-α-D-galactofuranose was reported.[3] However, this compound appeared to be inconvenient for the use in the assembling of oligosaccharides because of difficulties for further regioselective reactions through hydroxy groups at C^2, C^3 and C^5.

Here (Scheme 1) we describe a simple and convenient preparation of selectively protected 1,6-anhydro-3-*O*-benzyl-α-D-galactofuranose **4** and its derivatives **5**, **6**. Compound **4** was unexpectedly obtained during the study of solvolytic O-desulfation of trisulfate **2** – the product of the pyronaside-*into*-furanoside rearrangement[4] of allyl galactopyranoside **1**[5] under the conditions of acid promoted per-O-sulfation.[6] Particularly, O-desulfation of compound **2** upon heating in a dioxane–pyridine (10:1) mixture in the presence of Py·HCl[7,8] gave the expected triol **3**,† while the same treatment but in dioxane afforded only unexpected 1,6-anhydro product **4**.‡ The same compound was formed upon heating of triol **3** in dioxane in the presence of pyridine·HCl (Scheme 1). Evidently, compound **4** is produced in the course of acid-catalyzed transacetalyzation.

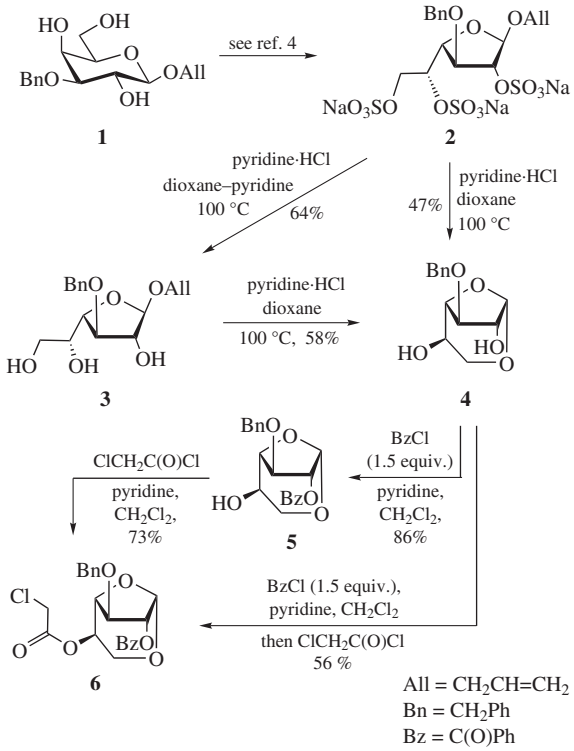

Scheme 1

The structure of product **4** was undoubtedly proved by NMR spectroscopy and mass spectrometry. In particular, the cross-peak H^1/C^6 in the HMBC spectrum (Figure 1) of **4** confirmed the presence of H^1–C^1–O^6–C^6 structural fragment in **4**, while the correlation peak between H^1 and C^4 and the absence of the cross-peak H^1/C^5 clearly indicated the presence of the five-membered

† *Allyl 3-O-benzyl-β-D-galactofuranoside* **3**. Dioxane (2.7 ml) was added to an intensively stirred suspension of trisodium salt of allyl 3-*O*-benzyl-2,5,6-tri-*O*-sulfonato-β-D-galactofuranoside **2**[4] (108 mg, 0.175 mmol) and Py·HCl (50 mg, 0.433 mmol) in pyridine (0.3 ml). The mixture was heated at 100 °C for 90 min and then cooled to room temperature. The mixture was dissolved in $CHCl_3$ (15 ml) and washed with saturated aqueous NaCl (15 ml). The organic layer was concentrated, and the residue was purified by column chromatography on silica gel in ethyl acetate–toluene (2:1) to give the furanoside derivative **3** (35 mg, 64%) identical to the previously described product.[4]

‡ *1,6-Anhydro-3-O-benzyl-α-D-galactofuranose* **4**.

Procedure 1. A suspension of **2**[4] (98 mg, 0.159 mmol) and Py·HCl (50 mg, 0.433 mmol) in dioxane (3.0 ml) was stirred at 100 °C for 30 min and then cooled to room temperature. The reaction mixture was dissolved in $CHCl_3$ (15 ml) and washed with saturated aqueous NaCl (15 ml). The organic layer was concentrated and the residue was purified by column chromatography on silica gel in ethyl acetate–toluene (2:1) to give product **4** (19 mg, 47%) as white solid, R_f = 0.69 (EtOAc), $[\alpha]_D$ = 62° (*c* = 1.0, MeOH). ^{1}H NMR (400 MHz, $CDCl_3$) δ: 7.44–7.30 (m, 5H, H_{Ph}), 5.24 (d, 1H, H^1, $J_{1,2}$ 4.6 Hz), 4.68 (d, 1H, $PhCH_aH_b$, *J* 11.8 Hz), 4.64 (d, 1H, $PhCH_aH_b$, *J* 11.8 Hz), 4.37–4.33 (m, 1H, H^2), 4.28 (d, 1H, H^4, *J* 4.3 Hz), 4.13–3.99 (m, 3H, H^5, H^3, H^{6a}), 3.57 (t, 1H, $J_{6b,6a} = J_{6b,5}$ = 10.5 Hz), 2.39 (br. s, 1H, OH), 2.20 (br. s, 1H, OH). ^{13}C NMR (100 MHz, $CDCl_3$) δ: 137.59 (q, Ph), 128.50 (Ph), 127.91 (Ph), 98.07 (C^1), 82.66 (C^3), 82.35 (C^4), 79.53 (C^2), 71.50 ($PhCH_2$), 65.39 (C^6), 62.53 (C^5). HRMS (ESI), *m/z*: 275.0882 $[M+Na]^+$ (calc. for $C_{13}H_{16}O_5$, *m/z*: 275.0890).

Procedure 2. A solution of triol **3**[4] (30 mg, 0.0967 mmol) and Py·HCl (31 mg, 0.268 mmol) in dioxane (1.5 ml) was stirred at 100 °C for 45 min and then cooled to room temperature. The mixture was dissolved in $CHCl_3$ (10 ml) and washed with saturated aqueous NaCl (10 ml). The organic layer was concentrated and the residue was purified by column chromatography on silica gel in ethyl acetate–toluene (2:1) to give product **4** (14 mg, 58%).

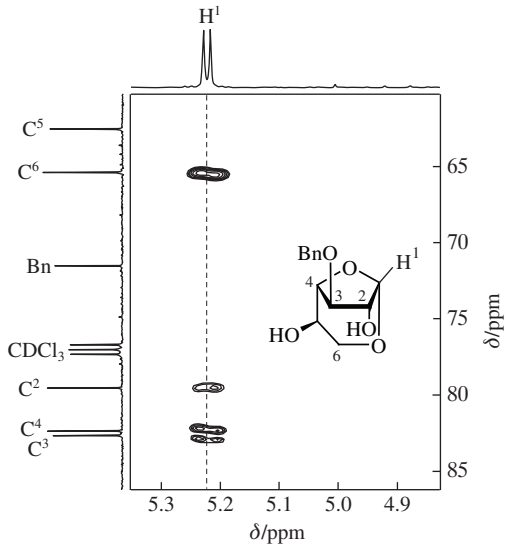

Figure 1 Part of the HMBC spectrum of 1,6-anhydrogalactofuranose **4**.

furanoside ring. Low-field resonance of C^6 in the ^{13}C NMR spectrum of **4** also confirmed the formation of the 1,6-anhydro cycle.

Compound **4** contains two OH groups of different reactivity. Thus, the treatment of diol **4** with 1.5 equiv. of BzCl in the presence of pyridine regioselectively led to 2-O-benzoylated product **5**[§] along with traces of the corresponding dibenzoate (detected by TLC). The structure of benzoate **5** was confirmed by characteristic downfield resonance of H^2 in the ^1H NMR spectrum as a result of 2-O-benzoylation (4.35 → 5.34 ppm). Further 5-O-chloroacetylation of compound **5** with 2 equiv. of $ClCH_2C(O)Cl$ gave totally protected derivative **6**.[¶] Remarkable difference in reactivity of the OH groups in diol **4** permits an easy transformation of this compound into **6** within a one-pot process by successive treatment first with BzCl and then by $ClCH_2C(O)Cl$.[††]

In conclusion, we developed the regioselective synthesis of galactofuranose derivative, which seems promising for the preparation of a variety of furanoside-containing oligosaccharides. Particularly, the galactofuranoside **6** related compounds were applied by us as key synthetic blocks for the assembling of large oligosaccharide chains related to *Aspergillus* galactomannan. These results will be published elsewhere.

This work was supported by the Russian Science Foundation grant 14-23-00199 (NEN).

Online Supplementary Materials

Supplementary data associated with this article can be found in the online version at doi:10.1016/j.mencom.2014.11.006.

References

1 M. Černý, *Adv. Carbohydr. Chem. Biochem.*, 2003, **58**, 121.
2 S. S. Kulkarni, J.-C. Lee and S.-C. Hung, *Curr. Org. Chem*., 2004, **8**, 475.
3 L. Baldoni and C. Marino, *Beilstein J. Org. Chem.*, 2014, **10**, 1651.
4 V. B. Krylov, D. A. Argunov, D. Z. Vinnitskiy, S. A. Verkhnyatskaya, A. G. Gerbst, N. E. Ustyuzhanina, A. S. Dmitrenok, J. Huebner, O. Holst, H.-C. Siebert and N. E. Nifantiev, *Chem. Eur. J*., DOI: 10.1002/chem.201405083.
5 Y. Zhou, J. Li, Y. Zhan, Z. Pei and H. Dong, *Tetrahedron*, 2013, **69**, 2693.
6 V. B. Krylov, N. E. Ustyuzhanina, A. A. Grachev and N. E. Nifantiev, *Tetrahedron Lett*., 2008, **49**, 5877.
7 A. I. Usov, K. S. Adamyants, L. I. Miroshnikova, A. A. Shaposhnikova and N. K. Kochetkov, *Carbohydr. Res*., 1971, **18**, 336.
8 I. J. Miller and J. W. Blunt, *Carbohydr. Res*., 1998, **309**, 39.

Received: 5th September 2014; Com. 14/4456

[§] *1,6-Anhydro-2*-O-*benzoyl-3*-O-*benzyl-α-D-galactofuranose* **5**. Benzoyl chloride (26 μl, 0.22 mmol) was added dropwise to a stirred solution of galactoside **4** (37 mg, 0.147 mmol) and pyridine (60 μl, 0.735 mmol) in CH_2Cl_2 (2 ml) at 0 °C. After disappearance of the starting compound (TLC control), MeOH (1 ml) was added and the mixture was co-evaporated with toluene (2×10 ml) *in vacuo*. Purification of the crude product by column chromatography on silica gel (hexane–ethyl acetate, 1.5:1) gave the 2-O-benzoylated derivative **5** (45 mg, 86%) as colorless oil. ^1H NMR (600 MHz, $CDCl_3$) δ: 8.06 (d, 2H, *o*-H_{Bz}, *J* 7.6 Hz), 7.61 (t, 1H, *p*-H_{Bz}, *J* = 7.6 Hz), 7.48 (t, 2H, *m*-H_{Bz}, *J* 7.6 Hz), 7.41–7.28 (m, 5H, H_{Ph}), 5.66 (d, 1H, H^1, $J_{1,2}$ 4.4 Hz), 5.34 (br. s, 1H, H^2), 4.70 (d, 1H, PhC$H_a$$H_b$, *J* 11.8 Hz), 4.63 (d, 1H, PhC$H_a$$H_b$, *J* 11.8 Hz), 4.47 (s, 1H, H^3), 4.36 (d, 1H, H^4, $J_{4,5}$ 4.2 Hz), 4.17–4.11 (m, 1H, H^5), 4.01 (dd, 1H, H^{6a}, $J_{6a,6b}$ 11.2 Hz, $J_{6a,5}$ 6.6 Hz), 3.60 (t, 1H, H^{6b}, $J_{6b,6a} = J_{6b,5}$ = 10.8 Hz), 2.24 (br. s, 1H, OH). ^{13}C NMR (150 MHz, $CDCl_3$) δ: 165.54 [Ph*C*(O)], 137.21 (q, $PhCH_2$), 133.47 (*p*-C_{Bz}), 129.76 (*o*-C_{Bz}), 129.19 [q, PhC(O)], 128.51 (Ph), 128.44 (Ph), 127.89 (Ph), 96.65 (C^1), 81.92 (C^4), 80.38 (C^2), 79.65 (C^3), 71.64 (Ph*C*H_2), 65.32 (C^6), 62.37 (C^5).

[¶] *1,6-Anhydro-2*-O-*benzoyl-3*-O-*benzyl-5*-O-*chloroacetyl-α-D-galactofuranose* **6**. Chloroacetyl chloride (28 μl, 0.25 mmol) was added to a stirred solution of galactoside **5** (45 mg, 0.126 mmol) and pyridine (40 μl, 0.5 mmol) in CH_2Cl_2 (2 ml). After 20 min, the mixture was diluted with $CHCl_3$ (15 ml) and washed with saturated $NaHCO_3$ (15 ml). The organic layer was concentrated, pyridine was co-evaporated with toluene (15 ml), and the residue was purified by column chromatography [silica gel, hexane–ethyl acetate (5:1)] to give product **6** (40 mg, 73%) as colorless syrup. ^1H NMR (600 MHz, $CDCl_3$) δ: 8.05 (d, 2H, *o*-H_{Bz}, *J* 7.6 Hz), 7.63 (t, 1H, *p*-H_{Bz}, *J* 7.6 Hz), 7.50 (t, 2H, *m*-H_{Bz}, *J* 7.6 Hz), 7.38–7.28 (m, 5H, Ph), 5.69 (d, 1H, H^1, $J_{1,2}$ 4.5 Hz), 5.38 (dd, 1H, H^2, $J_{2,1}$ 4.5 Hz, $J_{2,3}$ 2.3 Hz), 5.17 (ddd, 1H, H^5, *J* 10.9, 6.6 and 4.4 Hz), 4.72 (d, 1H, PhC$H_a$$H_b$, *J* 12.2 Hz), 4.62 (d, 1H, PhC$H_a$$H_b$, *J* 12.2 Hz), 4.52 (d, 1H, H^4, $J_{4,5}$ 4.4 Hz), 4.35 (d, 1H, H^3, $J_{3,2}$ 2.3 Hz), 4.17–4.12 (m, 1H, H^{6a}), 4.02 [d, 1H, C(O)C$H_a$$H_b$Cl, *J* 14.9 Hz], 3.99 [d, 1H, C(O)C$H_a$$H_b$Cl, *J* 14.8 Hz], 3.68 (t, 1H, H^{6b}, $J_{6b,6a} = J_{6b,5}$ = 10.9 Hz). ^{13}C NMR (150 MHz, $CDCl_3$) δ: 165.88 [*C*(O)CH_2Cl], 165.35 [Ph*C*(O)], 136.94 (q, $PhCH_2$), 133.59 (*p*-C_{Bz}), 129.77 (*o*-C_{Bz}), 129.07 [q, PhC(O)], 128.57 (Ph), 128.52 (Ph), 128.06 (Ph), 127.85 (Ph), 97.15 (C^1), 80.20 (C^2), 79.60 (C^3), 78.88 (C^4), 71.57 (Ph*C*H_2), 65.41 (C^5), 62.21 (C^6), 40.33 [C(O)*C*H_2Cl]. HRMS (ESI), *m/z*: 455.0859 $[M+Na]^+$ (calc. for $C_{13}H_{16}O_5$, *m/z*: 455.0868).

[††] *1,6-Anhydro-2*-O-*benzoyl-3*-O-*benzyl-5*-O-*chloroacetyl-α-D-galactofuranose* **6** *(one-pot method)*. Benzoyl chloride (12 μl, 0.100 mmol) was added to a stirred solution of galactoside **4** (17 mg, 0.067 mmol) and pyridine (22 μl, 0.27 mmol) in CH_2Cl_2 (2 ml) at 0 °C. Immediately after the disappearance of the starting compound (TLC control), chloroacetyl chloride (11 μl, 0.134 mmol) was added. After 20 min, the reaction was quenched with MeOH (0.5 ml) and co-evaporated with toluene. Purification of the crude product by column chromatography on silica gel (hexane–ethyl acetate, 7:1) gave desired product **6** (16 mg, 56%).

Organic & Biomolecular Chemistry

PAPER

View Article Online
View Journal

Cite this: DOI: 10.1039/c4ob02634a

Convergent synthesis of isomeric heterosaccharides related to the fragments of galactomannan from *Aspergillus fumigatus*†

D. A. Argunov, V. B. Krylov and N. E. Nifantiev*

Received 19th December 2014,
Accepted 22nd January 2015

DOI: 10.1039/c4ob02634a

www.rsc.org/obc

Aspergillus fumigatus is a very common fungus with high pathogenic potential for immunosuppressed hospital patients. *A. fumigatus* galactomannan, being the part of its cell wall, is considered as a promising candidate for vaccine and diagnostic test-systems. In this article we report the convergent synthesis of pentasaccharide fragments of the galactomannan containing the β-(1→5)-linked galactofuranoside chain attached to O-3 or O-6 of a spacer-armed mannopyranoside residue. The synthesis of selectively protected galactofuranoside precursors has been performed using recently developed pyranoside-*into*-furanoside (PIF) rearrangement. For assembling the target galactomannan structures the [1 + 2 + 2]-scheme was applied. This strategy was shown to be highly efficient and can easily be extended to the synthesis of longer fragments of thegalactomannan.

Introduction

Aspergillus fumigatus is the most prevalent airborne fungal pathogen, causing severe and usually fatal invasive aspergillosis (IA) in immunocompromised patients.[1] At risk are patients with cancer and patients undergoing intensive immunosuppressive therapy after receiving organ transplants. An important factor for the successful treatment of IA is its early diagnosis.

Galactomannan, built up from the α-(1→2) and α-(1→6)-linked poly-D-mannose backbone with short (4–5 units) β-(1→5)-linked galactofuranoside branches at O-3 or O-6 of some of the mannose units, is an essential cell-wall component of *A. fumigatus*.[2] The detection of this antigen in biological fluids is currently widely used for the diagnosis of aspergillosis.[1] The structurally specified oligosaccharides related to galactomannan fragments are strongly in demand for immunological studies and particularly for the development of more sensitive and selective diagnostic test systems for the detection of this dangerous pathogen.

Previously, the syntheses of different oligosaccharide fragments of galactomannan corresponding to the homogalactofuranosyl[3–5] or heterosaccharide[6] chains were described. However, a more representative series of oligosaccharides built up from both galactofuranosyl and mannopyranoside units is required as antigens for immunological investigation. Herein, we describe the first synthesis of two galactomannan related heterosaccharides **1** and **2** containing β-(1→5)-linked tetragalactofuranoside blocks attached to either O-6 or O-3 of the spacer-armed mannopyranoside residue (Fig. 1).

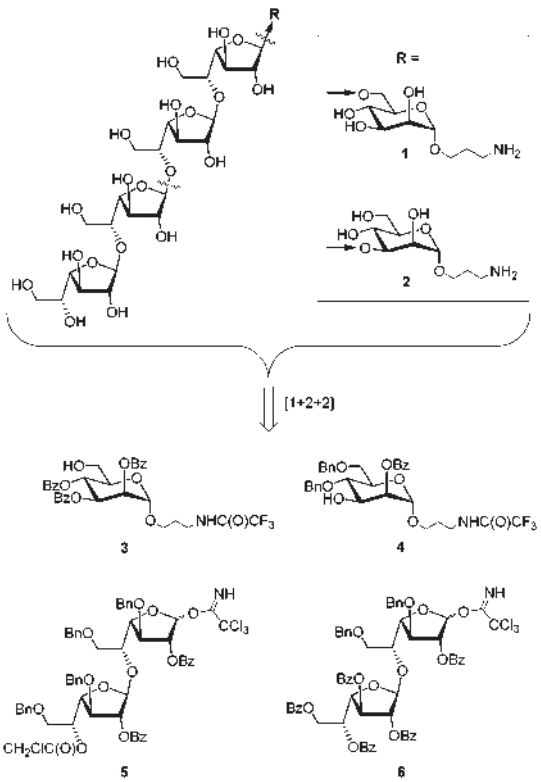

Fig. 1 Target galactomannan related pentasaccharides **1** and **2** and their key synthetic precursors **3**–**6**, as revealed by retrosynthetic analysis.

Laboratory of Glycoconjugate Chemistry, N.D. Zelinsky Institute of Organic Chemistry, Russian Academy of Sciences, Leninsky prospect 47, 119991 Moscow, Russian Federation. E-mail: nen@ioc.ac.ru; Fax: (+) 7-499-135-87-84

†Electronic supplementary information (ESI) available: Experimental procedures, characterization data, and NMR and HRMS spectra. See DOI: 10.1039/c4ob02634a

Results and discussion

The assembling of target galactomannosides **1** and **2** was performed by applying a [1 + 2 + 2]-scheme. The key synthetic blocks were spaced-armed mannosides **3** and **4** containing free OH-groups at C-6 and C-3, respectively, and disaccharide donors **5** and **6** (Fig. 1). Difuranoside **5** contained a temporary chloroacetyl group at O-5 of the "non-reducing" unit for further deprotection to the free OH-group followed by chain elongation, while donor **6** was used only at the final glycosylation step when further chain elongation was not required.

The methods for preparation of selectively *O*-substituted furanoside derivatives are poorly developed as compared to synthesis of the corresponding pyranoside analogues. Nowadays, the most widely used protocols for furanoside synthesis are based on the Fischer reaction or high-temperature acylation of unprotected sugars.[7] However, the resulting products are often difficult to use for further regioselective introduction of protective groups of required types.

Recently, we have discovered a new reaction of pyranoside-*into*-furanoside (PIF) rearrangement permitting the transformation of selectively *O*-substituted pyranosides into the corresponding furanosides.[8,9] The herein reported first syntheses of heterosaccharides related to the galactomannan from *A. fumigatus* were performed with the use of PIF-rearrangement as a key step.

According to the substrate requirements for PIF-rearrangement, the starting pyranosides should have β-configuration of the anomeric center and free OH-groups at C-2 and C-4 of the pyranose ring.[8] In order to obtain an appropriately substituted furanoside for the simplification of the final orthogonal protective group placement, galactopyranoside **8** was chosen as a substrate for the PIF-rearrangement ((Scheme 1). This compound was prepared by regioselective benzylation of allyl galactoside **7**[10] *via* the organotin intermediate.[11] Isomerization of pyranoside **8** into furanoside **10** was performed in DMF with the Py·SO_3 complex and chlorosulfonic acid followed by solvolytic O-desulfation of isolated crude per-*O*-sulfated derivative **9** in dioxane in the presence of Amberlite IR-120(H^+). NMR-monitoring of the reaction mixture (see the ESI†) permitted us to optimize the amount of the sulfating reagents and to shorten the reaction time.

The synthesis of target galactomannan pentasaccharides **1** and **2** required further regioselective protection of O-5 in diol **10**. The results of the studied acylation reactions of diol **10** are summarized in Table 1. Chloroacetylation of **10** in the presence of Py in DCM at low temperatures smoothly produced

Table 1 Regioselective acylation of diol **10**

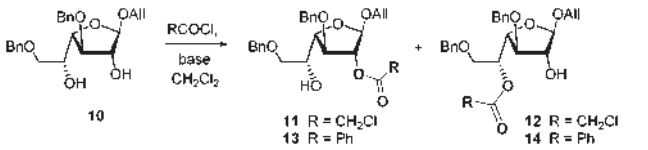

Entry	Acylation conditions	2-*O*-Acylated product, yield	5-*O*-Acylated product, yield
1	$ClCH_2C(O)Cl$ (1.3 eq.), Py (1.5 eq.), −78 to 0 °C, 1 h	**11**, <5% (TLC)	**12**, 69%
2	$ClCH_2C(O)Cl$ (1.3 eq.), Et_3N (1.5 eq.), −78 to 0 °C, 1 h	**11**, 56%[a]	**12**, 17%[a]
3	PhC(O)Cl (2.0 eq.), Et_3N (2.5 eq.), −20 to +8 °C, 16 h	**13**, 58%[a]	**14**, 16%[a]

[a] Ratio of isomers was calculated from ^{1}H-NMR spectra.

5-O-acylated product **12** (entry 1), while only traces of 2-*O*-acylated and 2,5-di-*O*-acylated derivatives were detected. This was in contrast to the result of the previously observed preferential 2-*O*-acylation of 2,5-diol on the basis of 1,6-anhydrogalactofuranose derivative.[12]

The presence of the 5-*O*-acyl group in **12** was confirmed by the downfield shift of H-5 (3.89→5.34 ppm) in the ^{1}H NMR spectrum. Surprisingly, the analogous acylation, in the presence of Et_3N instead of Py, resulted in the predominant formation of 2-*O*-substituted derivative **11** (entry 2), which was confirmed by the downfield location of the H-2 signal (4.16→5.20 ppm). In the same way, benzoylation of furanoside **10** by BzCl in the presence of Et_3N also gave 2-*O*-benzoylated derivative **13** predominantly (entry 3). The difference in regioselectivity of the acylation reaction in the presence of Et_3N or Py can be explained by the influence of steric and polar factors. It is known that the base was involved both in the activation of an acid chloride and polarization of an O–H bond.[13] Thus, the difference in basicity and spatial hindrance of the intermolecular interaction can dramatically change regioselectivity.

Chloroacetylation of diol **10** in Py (entry 1) due to its better regioselectivity was employed in the further synthesis towards pentasaccharides **1** and **2** (Scheme 2). 5-*O*-Substituted furano-

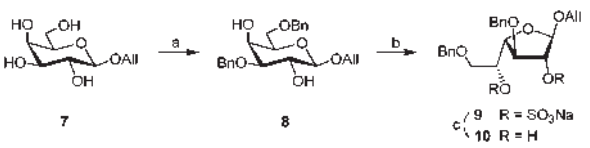

Scheme 1 Synthesis of dibenzylated galactofuranoside **10** by PIF-rearrangement of pyranoside **8**. (a) $(Bu_3Sn)_2O$, toluene, Δ, 6 h, then BnBr, TBAI, 100 °C, 70%; (b) Py·SO_3, HSO_3Cl, DMF, 40 °C, 1 h, then excess of aq. $NaHCO_3$; (c) IR-120(H^+), dioxane, Δ, 59% over two steps.

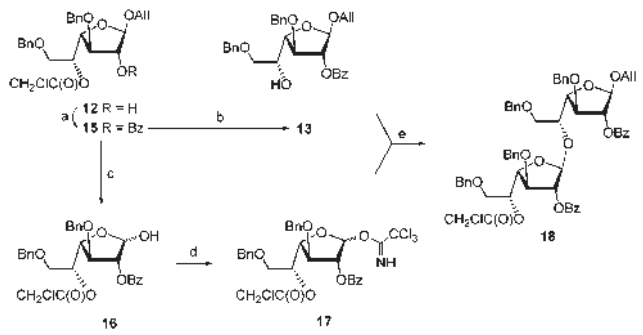

Scheme 2 Synthesis of disaccharide **18**. (a) BzCl, Py, CH_2Cl_2, 90%; (b) $H_2NC(S)NH_2$, 2,4,6-collidine, MeOH (dry), Δ, 85%; (c) $PdCl_2$, MeOH (dry), 67%; (d) CCl_3CN, DBU, CH_2Cl_2, −50 to 0 °C, 88%; (e) TMSOTf, MS 4 Å, CH_2Cl_2, −78 to −20 °C, 68%.

side **12** obtained was then benzoylated to give orthogonally protected precursor **15** (Scheme 2). A portion of compound **15** was dechloroacylated by treatment with $NH_2C(S)NH_2$ [14] to give monohydroxy compound **13**, which was further used as a glycosyl acceptor in the synthesis of β-(1→5)-linked disaccharide **18** (Scheme 2). On the other hand, O-deallylation[15–17] and subsequent trichloroacetimidation of monosaccharide **15** afforded glycosyl donor **17**. Its coupling with acceptor **13** in the presence of TMSOTf gave exclusively β-linked disaccharide **18**. The configuration of the newly formed glycoside bond was confirmed by the singlet shaped H-1′ signal in the ^{1}H NMR spectrum and characteristic downfield location of the C-1′ signal (106.2 ppm) in the ^{13}C NMR spectrum.

The excellent regioselectivity of 5-*O*-chloroacylation of diol **10** challenged us to examine the regioselectivity of its glycosylation (Scheme 3). Fortunately, coupling of diol **10** both with donors **17** and **20** resulted in predominant formation of desired β-(1→5)-linked products **19** and **21**, which were separated by chromatography from trace amounts of the (1→2)-linked isomers.

Benzoylation of derivatives **19** and **21** with BzCl in Py gave the corresponding disaccharides **18** and **22**. Thus, the strategy based on the regioselective 5-*O*-glycosylation of diol **10** (Scheme 3) also represents a highly efficient and short way for

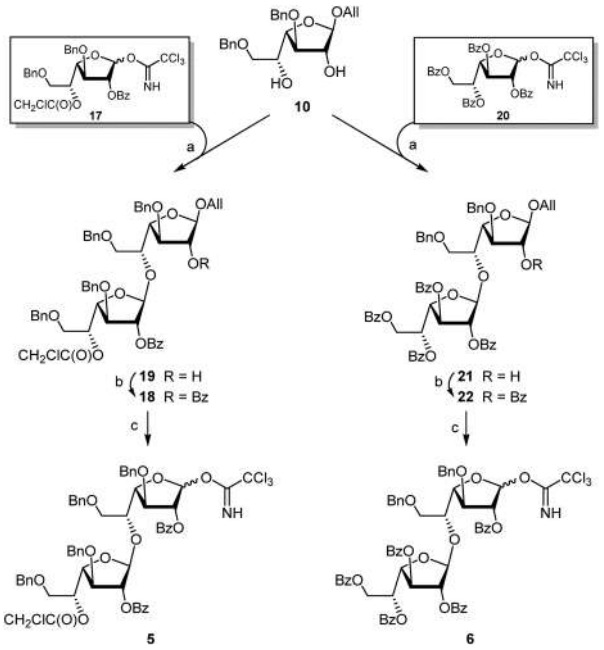

Scheme 3 Synthesis of disaccharide donors **5** and **6**. (a) TMSOTf, MS300 AW, CH_2Cl_2, −78 to −20 °C, 65% for **19**, 62% for **21**; (b) BzCl, Py, CH_2Cl_2, 87% for **18**, 84% for **22**; (c) i: $PdCl_2$, MeOH; ii: CCl_3CN, DBU, CH_2Cl_2, −50 to 0 °C, 55% on 2 steps for **5**, 59% on 2 steps for **6**.

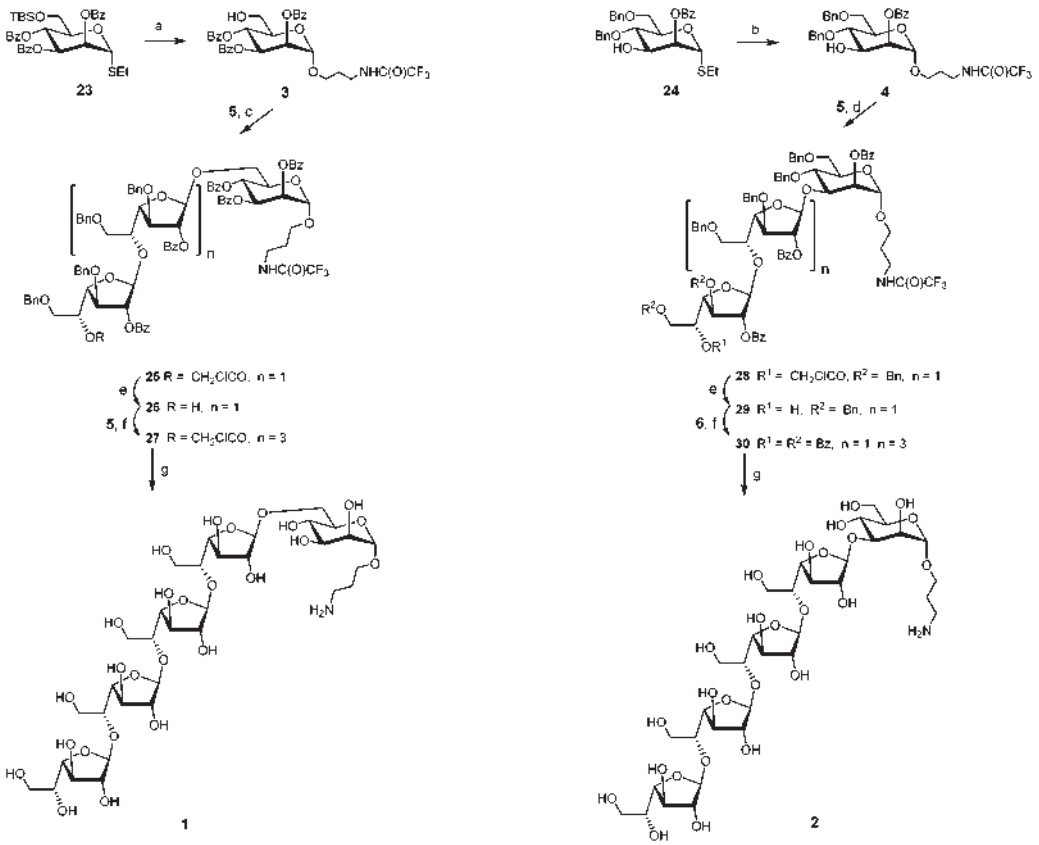

Scheme 4 Synthesis of monosaccharide acceptors **3** and **4**, their coupling with tetrasaccharide donor **5** and obtaining target pentasaccharides **1** and **2**. (a) i: $HO(CH_2)_3NHTFA$, NIS, TfOH, MS 4 Å, CH_2Cl_2, −40 to −15°; ii: 90% aq. TFA, 62% on 2 steps; (b) i: $CH_2ClC(O)Cl$, Py, CH_2Cl_2; ii: $HO(CH_2)_3NHTFA$, NIS, TfOH, MS300 AW, CH_2Cl_2, −40 to −15°; iii: $H_2NC(S)NH_2$, 2,4,6-collidine, MeOH (dry), Δ, 55% on 3 steps; (c) TMSOTf, MS 4 Å, CH_2Cl_2, −78 to −20 °C, 85%; (d) TMSOTf, MS300 AW, CH_2Cl_2, −78 to −10 °C, 60%; (e) $H_2N(S)NH_2$, 2,4,6-collidine, MeOH (dry), Δ, 86% for **26**, 80% for **29**; (f) TMSOTf, MS300 AW, CH_2Cl_2, −78 to −20 °C, 71% for **27**, 80% for **30**; (g) i: H_2, Pd/C (10% Pd), EtOAc–MeOH 1 : 1; ii: MeONa, MeOH, then H_2O, 83% for **1**, 70% for **2**.

the formation of the required β-(1→5)-linked disaccharides. Anomeric O-deallylation and subsequent trichloroacetimidation of disaccharides **18** and **22** gave desired disaccharide donors **5** and **6**.

Spacer-armed mannosides **3** and **4** were synthesized from described precursors **23**[18] and **24**[19] by mannosylation of 3-trifluoroacetamidopropanol and subsequent manipulation with blocking groups (Scheme 4). Further coupling of acceptors **3** and **4** with disaccharide donor **5** gave the corresponding trisaccharides **25** and **28** in yields of 85% and 60%. The lower yield in the latter case could be explained by the lower reactivity of acceptor **4** which required the application of a slightly higher reaction temperature.

O-Dechloroacetylation and subsequent glycosylation of trisaccharide acceptors **26** and **29** by trichloroacetimidates **5** and **6**, respectively, gave pentasaccharides **27** and **30**. Full deprotection of these compounds yielded target spacer armed pentasaccharides **1** and **2**. Their structures were unambiguously confirmed by NMR and mass-spectrometry.

Conclusions

The first synthesis of isomeric heteropentasaccharides **1** and **2** structurally related to fragments of galactomannan from *Aspergillus fumigatus* has been performed. The new strategy based on the PIF-rearrangement of the appropriately *O*-substituted galactopyranoside precursor into the corresponding furanoside block has been proved efficient and competitive to the known approaches for the synthesis of oligo-β-(1→5)-galactofuranoside chains. The developed synthetic scheme is applicable for the synthesis of oligosaccharides representing larger galactomannan fragments. The synthesis of glycoconjugates of obtained pentasaccharides **1** and **2** and their glycobiological evaluation will be published elsewhere.

Experimental

General methods

Commercial chemicals were used without purification unless noted. All solvents were distilled and dried if necessary according to standard procedures or purchased dry (DMF, Acrus). All reactions involving air- or moisture-sensitive reagents were carried out using dry solvents under an Ar-atmosphere. Thin-layer chromatography (TLC) was carried out on aluminum sheets coated with silica gel 60 F_{254} (Merck). TLC plates were inspected under UV light (λ = 254 nm) and developed by treatment with a mixture of 15% H_3PO_4 and orcinol (1.8 g l^{-1}) in EtOH–H_2O (95 : 5, v/v) followed by heating. Column chromatography was performed with Silica Gel 60 (40–63 μm, E. Merck). Solvents for column and thin layer chromatography (TLC) are listed in volume to volume ratios. Gel-filtration was performed on a TSK-40 HW(S) column (400 × 17 mm) by elution with 0.1 M AcOH in water at a flow rate of 0.5 mL min^{-1}.

NMR spectra were recorded on Bruker AMX400 (400 MHz), Bruker DRX-500 (500 MHz), or Bruker AV600 (600 MHz) spectrometers equipped with 5 mm pulsed-field-gradient (PFG) probes at temperatures denoted in the spectra in the ESI.† Microtubes (Shigemi, Inc.) were used for sensitivity enhancement of small concentration probes of compounds **1**, **2**, and **30**. The resonance assignment in ^{1}H and ^{13}C NMR spectra was performed using various 2D-experiments (*e.g.*, COSY, NOESY, HSQC, HMBC, TOCSY, HSQC-TOCSY, and ROESY). Chemical shifts are reported in ppm referenced to the solvent residual peaks as a standard (δ 7.27 for chloroform or δ 3.31 methanol for ^{1}H NMR and δ 77.0 and δ 49.0 for ^{13}C NMR). The following abbreviations are used to describe spin multiplicity: s = singlet, d = doublet, t = triplet, q = quartet, m = multiplet, br = broad, dd = doublet of doublets and dt = doublet of triplets. Monosaccharide residues in oligosaccharides are numbered by the Roman numerals starting from the reducing end. For carbohydrate numbering nomenclature in pyranoside and furanoside systems see below.

Optical rotations were measured using a JASCO DIP-360 polarimeter at an ambient temperature (22–25 °C) in ethyl acetate.

High-resolution mass spectra (HRMS) were recorded on a Bruker micrOTOF II instrument using electrospray ionization (ESI).[20] The measurements were performed in positive ion mode (interface capillary voltage −4500 V) or in negative ion mode (3200 V); mass range from *m*/*z* 50 to *m*/*z* 3000 Da; external or internal calibration was made with a electrospray calibrant solution (Fluka). A syringe injection was used for solutions in a mixture of acetonitrile and water (50 : 50 v/v, flow rate 3 μL min^{-1}). Nitrogen was applied as a dry gas; interface temperature was set at 180 °C.

Synthesis

General procedure for chloroacetyl group removal (GP I). To a stirred solution of starting sugar (1 mmol) and thiourea (10 mmol) in anhydrous MeOH (30 mL), 2,4,6-collidine (0.125 mmol) was added and the mixture was refluxed until TLC showed reaction completion. Then the mixture was filtered, the residue was washed with MeOH, and the filtrate was concentrated *in vacuo*.

General procedure for allyl group cleavage (GP II). To a stirred solution of starting sugar (1 mmol) in anhydrous MeOH (17 mL), $PdCl_2$ (0.4 mmol) was added and the mixture was stirred vigorously until TLC showed reaction completion. Then the mixture was filtered through a Celite layer, the residue washed with MeOH, 1–2 drops of Et_3N and 10 mL of toluene were added, and the filtrate was concentrated *in vacuo*.

General procedure for the preparation of trichloroacetimidates (GP III). To a stirred solution of starting hemiacetal (1 mmol) in CH_2Cl_2 (7–8 mL), trichloroacetonitrile (8 mmol) and a catalytic amount of DBU (approx. 50 μL) were added at

−50 °C. The reaction mixture was allowed to warm to 0 °C in 30 min and subjected to flash chromatography on passivated Et_3N silica gel.

Allyl 3,6-di-*O*-benzyl-β-D-galactopyranoside (8). To a stirred suspension of allyl β-D-galactopyranoside **7** [10] (1.1 g, 5 mmol) in toluene (50 mL) $(Bu_3Sn)_2O$ (3.8 mL, 7.5 mmol) was added and the mixture was refluxed for 6 h accompanied by azeotropic removal of water. Then BnBr (1.8 mL, 10 mmol) and TBAI (5.5 g, 15 mmol) were added and the mixture was stirred at 100 °C overnight. The solvents were removed *in vacuo*, the residue was diluted using CH_2Cl_2 and washed with sat. aq. $NaHCO_3$. The organic layer was concentrated and column chromatography (toluene–EtOAc 4 : 1) gave the desired product **8** (1.4 g, 70%) as a yellowish oil. $[\alpha]_D = -4°$ (c = 1, EtOAc). ^{1}H NMR (400 MHz, CD_3OD): δ 7.46–7.23 (m, 10H, PhH), 6.02–5.91 (m, 1H, OCH_2CHCH_2), 5.31 (m, 1H, OCH_2CHCH_2), 5.15 (m, 1H, OCH_2CHCH_2), 4.80–4.72 (m, 3H, $PhCH_2$), 4.66 (d, $^2J_{ab}$ = 11.8 Hz, 1H, $PhCH_2$), 4.37–4.30 (m, 1H, OCH_2CHCH_2), 4.28 (d, J_{12} = 7.8 Hz, 1H, H-1), 4.17–4.10 (m, 1H, OCH_2CHCH_2), 4.10 (dd, J_{43} = 3.3 Hz, $J_{45} \approx$ 0.9 Hz, 1H, H-4), 3.74 (dd, $^2J_{6a6b}$ = 10.2 Hz, J_{56a} = 5.8 Hz, 1H, H-6a), 3.71 (dd, J_{21} = 7.8 Hz, J_{23} = 9.7 Hz, 1H, H-2), 3.70 (dd, $^2J_{6a6b}$ = 10.2 Hz, J_{56b} = 6.4 Hz, 1H, H-6b), 3.61 (dt, $J_{54} \approx$ 0.9 Hz, $J_{56a} \approx J_{56b} \approx$ 6.0 Hz, 1H, H-5), 3.37 (dd, J_{32} = 9.7 Hz, J_{34} = 3.3 Hz, 1H, H-3). ^{13}C NMR (100 MHz, CD_3OD): δ 139.9, 139.6 (quat. Ph), 139.8 (OCH_2CHCH_2), 129.4–128.6 (Ph), 117.4 (OCH_2CHCH_2), 103.9 (C-1), 82.40 (C-3), 74.9 (C-5), 74.3 ($PhCH_2$), 72.6 ($PhCH_2$), 71.7 (C-6), 71.1 (C-2), 70.7 (C-4), 67.4 (OCH_2CHCH_2). HRMS (ESI): calcd m/z for $[M + Na]^+$ $C_{23}H_{28}O_6$ 423.1778, found 423.1770. Calcd m/z for $[M + K]^+$ $C_{23}H_{28}O_6$ 439.1517, found 439.1516.

Disodium salt of allyl 3,6-di-*O*-benzyl-2,4-di-*O*-sulfo-β-D-galactofuranoside (9). To a stirred solution of **8** (1.0 g, 2.5 mmol) and Py·SO_3 (3.2 g, 20.0 mmol) in DMF (16 mL), $ClSO_3H$ was added dropwise (550 μL, 8 mmol) and the mixture was kept at 40 °C for 1 h. Then the reaction was quenched by the addition of $NaHCO_3$ (5.6 g, 67 mmol) solution in water (160 mL) and concentrated *in vacuo*. MeOH (100 mL) was added, the suspension was filtered through cotton, the residue was washed twice with MeOH (2 × 50 mL), and the filtrate was evaporated and carefully dried. The resulting crude product **9** was analyzed and used in the next step without purification. ^{1}H NMR (400 MHz, CD_3OD): δ 7.42–7.20 (m, 10H, PhH), 6.02–5.88 (m, 1H, OCH_2CHCH_2), 5.29–5.25 (m, 1H, OCH_2CHCH_2), 5.26 (s, 1H, H-1), 5.12–5.09 (m, 1H, OCH_2CHCH_2), 4.84 (d, J_{23} = 2.0 Hz, 1H, H-2), 4.82–4.54 (m, 5H, $2PhCH_2$, H-5), 4.46 (dd, J_{32} = 2.0 Hz, J_{34} = 6.7 Hz, 1H, H-3), 4.43 (dd, J_{43} = 6.7 Hz, J_{45} = 3.0 Hz, 1H, H-4), 4.19–4.14 (m, 1H, OCH_2CHCH_2), 4.04–3.98 (m, 1H, OCH_2CHCH_2), 3.88–3.76 (m, 2H, H-6a, H-6b). ^{13}C NMR (100 MHz, CD_3OD): δ 139.6, 139.5 (quat. Ph), 135.6 (OCH_2CHCH_2), 129.3–128.5 (Ph), 117.2 (OCH_2CHCH_2), 106.8 (C-1), 87.2 (C-2), 85.1 (C-3), 81.3 (C-4), 75.7 (C-5), 74.3 ($PhCH_2$), 73.5 ($PhCH_2$), 69.6 (C-6), 68.8 (OCH_2CHCH_2). HRMS (ESI): Calcd m/z for $[M - 2Na]^{2-}$ $C_{23}H_{26}O_{12}S_2Na_2$ 279.0438, found 279.0436. Calcd m/z for $[M - Na]^-$ $C_{23}H_{26}O_{12}S_2Na_2$ 581.0769, found 581.0777. Calcd m/z for $[M - 2Na + H]^-$ $C_{23}H_{26}O_{12}S_2Na_2$ 559.0949, found 559.0928.

Allyl 3,6-di-*O*-benzyl-β-D-galactofuranoside (10). Crude product **9** was desulfated by refluxing in dioxane (100 mL) in the presence of IR-120H$^+$ (1.5 g) for 40 min. Then inorganic salts were filtered off, washed with EtOAc, and the filtrate was neutralized using Et_3N to pH 8–9. Solvents were evaporated *in vacuo* and column chromatography (toluene–EtOAc 2 : 1) gave product **10** (0.59 g, 59% over two steps) as a colorless oil. $[\alpha]_D = 62°$ (c = 1, EtOAc). ^{1}H NMR (600 MHz, CD_3OD): δ 7.36–7.23 (m, 10H, PhH), 5.96–5.89 (m, 1H, OCH_2CHCH_2), 5.28 (m, 1H, OCH_2CHCH_2), 5.14 (m, 1H, OCH_2CHCH_2), 4.94 (s, 1H, H-1), 4.69 (d, $^2J_{ab}$ = 11.8 Hz, 1H, $PhCH_2$), 4.53 (d, $^2J_{ab}$ = 12.0 Hz, 1H, $PhCH_2$), 4.52 (d, $^2J_{ab}$ = 11.8 Hz, 1H, $PhCH_2$), 4.50 (d, $^2J_{ab}$ = 12.0 Hz, 1H, $PhCH_2$), 4.21–4.15 (m, 2H, OCH_2CHCH_2, H-2), 4.09 (dd, J_{32} = 3.8 Hz, J_{34} = 6.1 Hz, 1H, H-3), 4.01–3.91 (m, 1H, OCH_2CHCH_2), 3.94 (dd, J_{43} = 6.1 Hz, J_{45} = 2.6 Hz, 1H, H-4), 3.84 (m, 1H, H-5), 3.56 (dd, $^2J_{6a6b}$ = 9.9 Hz, J_{56a} = 5.5 Hz, 1H, H-6a), 3.52 (dd, $^2J_{6a6b}$ = 9.9 Hz, J_{56b} = 6.7 Hz, 1H, H-6b). ^{13}C NMR (150 MHz, CD_3OD): δ 139.6, 139.4 (quat. Ph), 135.8 (OCH_2CHCH_2), 129.3–128.6 (Ph), 117.1 (OCH_2CHCH_2), 109.1 (C-1), 86.8 (C-3), 83.6 (C-4), 81.4 (C-2), 74.3 ($PhCH_2$), 73.1 ($PhCH_2$), 72.6 (C-6), 71.1 (C-5), 69.0 (OCH_2CHCH_2). HRMS (ESI): Calcd m/z for $[M + Na]^+$ $C_{23}H_{28}O_6$ 423.1778, found 423.1770.

Allyl 3,6-di-*O*-benzyl-5-*O*-chloroacetyl-β-D-galactofuranoside (12). To a stirred solution of **10** (700 mg, 1.75 mmol) in CH_2Cl_2 (10 mL) at −78 °C pyridine (0.31 mL, 3.85 mmol) and chloroacetyl chloride (155 μL, 0.19 mmol) were slowly added. The reaction mixture was allowed to warm to 0 °C over 1 h and diluted using CH_2Cl_2, washed with 1 M HCl and sat. aq. $NaHCO_3$ and concentrated *in vacuo*. Column chromatography (toluene–EtOAc 7 : 1) gave **12** (575 mg, 69%) as a colorless oil. R_f = 0.37 (toluene–ethyl acetate 5 : 1). $[\alpha]_D = 58°$ (c = 1, EtOAc). ^{1}H NMR (600 MHz, $CDCl_3$): δ 7.38–7.28 (m, 10H, PhH), 5.94–5.86 (m, 1H, OCH_2CHCH_2), 5.33 (m, 1H, H-5), 5.29 (m, 1H, OCH_2CHCH_2), 5.18 (m, 1H, OCH_2CHCH_2), 4.98 (s, 1H, H-1), 4.66 (d, $^2J_{ab}$ = 12.0 Hz, 1H, $PhCH_2$), 4.56 (d, $^2J_{ab}$ = 12.0 Hz, 1H, $PhCH_2$), 4.53 (d, $^2J_{ab}$ = 12.1 Hz, 1H, $PhCH_2$), 4.50 (d, $^2J_{ab}$ = 12.1 Hz, 1H, $PhCH_2$), 4.25 (dd, J_{43} = 5.8 Hz, J_{45} = 4.0 Hz, 1H, H-4), 4.21–4.17 (m, 2H, H-2, OCH_2CHCH_2), 4.02–3.96 (m, 3H, $C(O)CH_2Cl$, OCH_2CHCH_2), 3.77 (dd, J_{32} = 2.2 Hz, J_{34} = 5.8 Hz, 1H, H-3), 3.73 (dd, $^2J_{6a6b}$ = 10.7 Hz, J_{56a} = 6.5 Hz, 1H, H-6a), 3.62 (dd, $^2J_{6a6b}$ = 10.7 Hz, J_{56b} = 4.7 Hz, 1H, H-6b), 2.15 (br s, 1H, OH). ^{13}C NMR (150 MHz, $CDCl_3$): δ 166.8 ($C(O)CH_2Cl$), 137.5 (Ph), 134.0 (OCH_2CHCH_2), 128.5–127.7 (Ph), 117.4 (OCH_2CHCH_2), 107.4 (C-1), 85.0 (C-3), 80.3 (C-4), 80.2 (C-2), 73.3 ($PhCH_2$), 72.9 (C-5), 72.4 ($PhCH_2$), 68.3 (C-6), 68.2 (OCH_2CHCH_2), 40.8 ($C(O)CH_2Cl$). HRMS (ESI): Calcd m/z for $[M + Na]^+$ $C_{25}H_{29}ClO_7$ 499.1494, found 499.1486. Calcd m/z for $[M + K]^+$ $C_{25}H_{29}ClO_7$ 515.1233, found 515.1226.

Allyl 3,6-di-*O*-benzyl-2-*O*-chloroacetyl-β-D-galactofuranoside (11). To a stirred solution of **10** (20 mg, 0.05 mmol) in CH_2Cl_2 (2 mL) at −78 °C, Et_3N (20 μL, 0.15 mmol) and chloroacetyl chloride (5 μL, 0.06 mmol) were slowly added. The reaction mixture was allowed to warm to 0 °C for 1 h and diluted using CH_2Cl_2, washed with 1 M HCl and sat. aq. $NaHCO_3$ and concentrated *in vacuo*. Column chromatography (toluene–EtOAc

7 : 1) gave a mixture of **11** (13 mg, 56%) and **12** (4 mg, 17%) as a colorless oil (ratio **12**/**11** calculated from H-1 signals in NMR). Data for **11**: R_f = 0.41 (toluene–ethyl acetate 5 : 1). ^{1}H NMR (400 MHz, $CDCl_3$) δ 7.39–7.28 (m, 10H, Ph*H*), 5.96–5.84 (m, 1H, $OCH_2CH{=}CH_2$), 5.31 (dd, J = 17.3 Hz, J = 1.6 Hz, 1H, $OCH_2CH{=}CH_aH_b$), 5.21 (dd, J = 10.4 Hz, J = 1.3 Hz, 1H, $OCH_2CH{=}CH_aH_b$), 5.20 (d, $J_{2,3}$ = 1.4 Hz, 1H, H-2), 5.10 (s, 1H, H-1), 4.75 (d, J = 12.0 Hz, 1H, $PhCH_aH_b$), 4.60–4.54 (m, 3H, 3 × Ph*H*H), 4.24–4.18 (m, 1H, $OCH_aH_bCH{=}CH_2$), 4.17 (dd, $J_{4,5}$ = 5.9 Hz, $J_{4,3}$ = 3.3 Hz, 1H, H-4), 4.07–4.00 (m, 4H, H-3, CH_2Cl, $OCH_aH_bCH{=}CH_2$), 3.93–3.86 (m, 1H, H-5), 3.57 (dd, $J_{6a,6b}$ = 9.7 Hz, $J_{6a,5}$ = 7.1 Hz, 1H, H-6$_a$), 3.52 (dd, $J_{6a,6b}$ = 9.7 Hz, $J_{6b,5}$ = 5.0 Hz, 1H, H-6$_b$), 2.28 (d, J_{HOH} = 6.3 Hz, 1H, *OH*). ^{13}C NMR (100 MHz, $CDCl_3$): δ 166.33 (C=O), 137.86 (quat. Ph), 137.44 (quat. Ph), 133.64 ($OCH_2CH{=}CH_2$), 128.45, 128.03, 127.95, 127.80, 127.72 (Ph), 117.70 ($OCH_2CH{=}CH_2$), 104.69 (C-1), 83.10 (C-3), 82.97 (C-2), 82.49 (C-4), 73.48 (PhCH_2), 72.57 (PhCH_2), 71.52 (C-6), 69.63 (C-5), 67.95 ($OCH_2CH{=}CH_2$), 40.59 (CH_2Cl). HRMS (ESI): Calcd m/z for $[M + NH_4]^+$ $C_{25}H_{29}ClO_7$ 494.1940, found 494.1935. Calcd m/z for $[M + Na]^+$ $C_{25}H_{29}ClO_7$ 499.1494, found 499.1496. Calcd m/z for $[M + K]^+$ $C_{25}H_{29}ClO_7$ 515.1233, found 515.1234.

Allyl 2-*O*-benzoyl-3,6-di-*O*-benzyl-β-D-galactofuranoside (13) from diol 10. To a stirred solution of **10** (20 mg, 0.05 mmol) in CH_2Cl_2 (2 mL) at −20 °C Et_3N (40 μL, 0.3 mmol) and BzCl (9 μL, 0.075 mmol) were added. The reaction mixture was allowed to warm to 8 °C over 2 h and kept at this temperature overnight. Then it was diluted using CH_2Cl_2, washed with sat. aq. $NaHCO_3$, and concentrated *in vacuo*. Column chromatography (toluene–EtOAc 12 : 1) gave **13** (14.5 mg, 58%) and **14** (4 mg, 16%) as a colorless oil (ratio **13**/**14** calculated from H-6 signals in NMR). All data for **13** were in agreement with the same compound obtained from **15**.

Allyl 2-*O*-benzoyl-3,6-di-*O*-benzyl-5-*O*-chloroacetyl-β-D-galactofuranoside (15). To a solution of **12** (575 mg, 1.21 mmol) and pyridine (0.47 mL, 6.0 mmol) in CH_2Cl_2 (5 mL) BzCl (0.42 mL, 3.6 mmol) was added dropwise under r.t. After completion of the reaction by TLC (approx. 4 h) the mixture was diluted using CH_2Cl_2, washed with 1 M HCl and sat. aq. $NaHCO_3$, and concentrated *in vacuo*. Column chromatography (toluene–EtOAc 15 : 1) gave **15** (630 mg, 90%) as a colorless oil. R_f = 0.62 (toluene–ethyl acetate 10 : 1). $[\alpha]_D$ = −21° (c = 1, EtOAc). ^{1}H NMR (600 MHz, $CDCl_3$): δ 8.03 (d, J = 8.2 Hz, 2H, *o*-C(O)Ph), 7.61 (t, J = 7.5 Hz, 1H, *p*-C(O)Ph), 7.47 (dd, J = 8.2 Hz, J = 7.5 Hz, 2H, *m*-C(O)Ph), 7.34–7.26 (m, 10H, PhH), 5.96–5.89 (m, 1H, OCH_2CHCH_2), 5.39 (d, J_{12} = 1.6 Hz, 1H, H-2), 5.37 (m, 1H, H-5), 5.33 (m, 1H, OCH_2CHCH_2), 5.22–5.19 (m, 2H, H-1, OCH_2CHCH_2), 4.82 (d, $^2J_{ab}$ = 11.9 Hz, 1H, PhCH_2), 4.57 (d, $^2J_{ab}$ = 11.9 Hz, 1H, PhCH_2), 4.52 (d, $^2J_{ab}$ = 12.1 Hz, 1H, PhCH_2), 4.47 (d, $^2J_{ab}$ = 12.1 Hz, 1H, PhCH_2), 4.37 (dd, J_{43} = 6.0 Hz, J_{45} = 4.5 Hz, 1H, H-4), 4.23 (m, 1H, OCH_2CHCH_2), 4.06 (m, 1H, OCH_2CHCH_2), 3.97 (d, $^2J_{ab}$ = 14.7 Hz, 1H, C(O)CH_2Cl), 3.94 (br d, J_{34} = 6.0 Hz, 1H, H-3), 3.92 (d, $^2J_{ab}$ = 14.7 Hz, 1H, C(O)CH_2Cl), 3.66 (dd, $^2J_{6a6b}$ = 10.4 Hz, J_{56a} = 6.5 Hz, 1H, H-6a), 3.64 (dd, $^2J_{6a6b}$ = 10.4 Hz, J_{56b} = 4.9 Hz, 1H, H-6b). ^{13}C NMR (150 MHz, $CDCl_3$): δ 166.7 (*C*(O)CH_2Cl), 165.3 (Ph*C*O), 134.0 (OCH_2CHCH_2), 133.8–127.6 (Ph), 117.6 (OCH_2CHCH_2), 105.0 (C-1), 83.0 (C-3), 81.8 (C-4), 80.7 (C-2), 73.2 (PhCH_2), 72.7 (C-5), 72.5 (PhCH_2), 68.4 (C-6), 68.0 (OCH_2CHCH_2), 40.7 (C(O)CH_2Cl). HRMS (ESI): Calcd m/z for $[M + Na]^+$ $C_{32}H_{33}ClO_8$ 603.1756, found 603.1752. Calcd m/z for $[M + K]^+$ $C_{32}H_{33}ClO_8$ 619.1496, found 619.1494.

Allyl 3,6-di-*O*-benzyl-2-*O*-benzoyl-β-D-galactofuranoside (13). Furanoside **15** (170 mg, 0.29 mmol) was treated as described in GP I by thiourea (220 mg, 2.9 mmol) and collidine (48 μL, 0.36 mmol) in 10 mL of MeOH. Column chromatography (toluene–EtOAc 8 : 1) gave **13** (125 mg, 85%) as a colorless oil. R_f = 0.40 (toluene–ethyl acetate 8 : 1). $[\alpha]_D$ = −46° (c = 1, EtOAc). ^{1}H NMR (600 MHz, $CDCl_3$): δ 8.04 (d, J = 8.2 Hz, 2H, *o*-C(O)-Ph), 7.59 (t, J = 7.5 Hz, 1H, *p*-C(O)Ph), 7.45 (dd, J = 8.2 Hz, J = 7.5 Hz, 2H, *m*-C(O)Ph), 7.35–7.26 (m, 10H, PhH), 5.97–5.90 (m, 1H, OCH_2CHCH_2), 5.42 (d, J_{12} = 1.5 Hz, 1H, H-2), 5.34 (m, 1H, OCH_2CHCH_2), 5.22 (s, 1H, H-1), 5.21 (m, 1H, H-1, OCH_2CHCH_2), 4.83 (d, $^2J_{ab}$ = 12.0 Hz, 1H, PhCH_2), 4.61 (d, $^2J_{ab}$ = 12.0 Hz, 1H, PhCH_2), 4.57 (d, $^2J_{ab}$ = 12.0 Hz, 1H, PhCH_2), 4.53 (d, $^2J_{ab}$ = 12.0 Hz, 1H, PhCH_2), 4.27–4.23 (m, 2H, OCH_2CHCH_2, H-4), 4.17 (br d, J_{34} = 5.8 Hz, 1H, H-3), 4.08 (m, 1H, OCH_2CHCH_2), 3.94 (m, 1H, H-5), 3.58 (dd, $^2J_{6a6b}$ = 9.8 Hz, J_{56a} = 7.1 Hz, 1H, H-6a), 3.54 (dd, $^2J_{6a6b}$ = 9.8 Hz, J_{56b} = 4.9 Hz, 1H, H-6b), 2.44 (br d, J_{HOH} = 6.1 Hz, 1H, OH). ^{13}C NMR (150 MHz): δ 165.4 (Ph*C*O), 137.9, 137.5 (quat. Ph), 133.8 (OCH_2CHCH_2), 133.6, 133.3, 129.7–127.6 (Ph), 117.5 (OCH_2CHCH_2), 105.2 (C-1), 83.5 (C-3), 82.6 (C-4), 81.8 (C-2), 73.4 (PhCH_2), 72.4 (PhCH_2), 71.5 (C-6), 70.0 (C-5), 67.9 (OCH_2CHCH_2). HRMS (ESI): Calcd m/z for $[M + NH_4]^+$ $C_{30}H_{32}O_7$ 522.2486, found 522.2480. Calcd m/z for $[M + Na]^+$ $C_{30}H_{32}O_7$ 527.2040, found 527.2034. Calcd m/z for $[M + K]^+$ $C_{30}H_{32}O_7$ 543.1780, found 543.1776.

2-*O*-Benzoyl-3,6-di-*O*-benzyl-5-*O*-chloroacetyl-D-galactofuranose (16). Allyl galactoside **15** (545 mg, 0.94 mmol) in 16 mL of MeOH was treated according to GP II with $PdCl_2$ (67 mg, 0.38 mmol) for 2.5 h. Column chromatography (hexane–EtOAc 5 : 2) gave **16** (340 mg, 67%) as a white solid (β/α = 2 : 1 based on H-1 integral in NMR). R_f = 0.38 (toluene–ethyl acetate 10 : 1). ^{1}H NMR (600 MHz, $CDCl_3$): δ 8.14–8.07, 7.65–7.19 (m, 22.5H, PhH), 5.69 (d, J_{12} = 4.3 Hz, 0.5H, H-1$^\alpha$), 5.53 (d, $J_{1\text{-}1OH}$ = 6.0 Hz, 1H, H-1β), 5.43 (m, 0.5H, H-5$^\alpha$), 5.39 (br s, 1H, H-2$^\beta$), 5.34 (m, 1H, H-5$^\beta$), 5.30 (dd, J_{21} = 4.3 Hz, J_{23} = 5.7 Hz, 1H, H-2$^\beta$), 4.84 (d, J_{ab} = 11.8 Hz, 1H, PhCH_2^β), 4.76 (d, J_{ab} = 11.7 Hz, 0.5H, PhCH_2^α), 4.66 (d, J_{ab} = 11.7 Hz, 0.5H, PhCH_2^α), 4.62 (d, J_{ab} = 11.8 Hz, 1H, PhCH_2^β), 4.57 (dd, J_{43} = 4.1 Hz, J_{45} = 6.3 Hz, 1H, H-4$^\beta$), 4.55 (d, J_{ab} = 12.0 Hz, 0.5H, PhCH_2^α), 4.51 (d, J_{ab} = 12.0 Hz, 0.5H, PhCH_2^α), 4.47 (d, J_{ab} = 12.1 Hz, 1H, PhCH_2^β), 4.42 (d, J_{ab} = 12.1 Hz, 1H, PhCH_2^β), 4.41 (t, J_{32} = J_{34} = 5.7 Hz, 0.5H, H-3$^\alpha$), 4.21 (dd, J_{43} = 5.7 Hz, J_{45} = 6.3 Hz, 0.5H, H-4$^\alpha$), 4.12 (d, J_{ab} = 15.0 Hz, 0.5H, C(O)CH_2Cl^α), 4.09 (br d, J_{34} = 4.1 Hz, 1H, H-3$^\beta$), 4.09 (d, J_{ab} = 15.0 Hz, 0.5H, C(O)CH_2Cl^α), 4.02 (d, J_{ab} = 14.9 Hz, 1H, C(O)CH_2Cl^β), 3.99 (d, J_{ab} = 14.9 Hz, 1H, C(O)CH_2Cl^β), 3.69 (dd, $^2J_{6a6b}$ = 10.9 Hz, J_{56a} = 6.0 Hz, 0.5H, H-6a$^\alpha$), 3.65(dd, $^2J_{6a6b}$ = 10.9 Hz, J_{56a} = 4.5 Hz, 0.5H, H-6b$^\alpha$), 3.60 (m, 2H, H-6a, H-6b). ^{13}C NMR (150 MHz, $CDCl_3$): 166.8 (*C*(O)-CH_2Cl), 165.4 (Ph*C*O), 137.4–136.8, 133.7–127.6 (Ph), 101.1

(C-1$^{\beta}$), 95.8 (C-1$^{\alpha}$), 82.1 (C-3$^{\beta}$, C-4$^{\beta}$), 80.7 (C-2$^{\beta}$), 80.3 (C-3$^{\alpha}$), 78.9 (C-4$^{\alpha}$), 78.7 (C-2$^{\alpha}$), 74.5 (C-5$^{\alpha}$), 73.3 (Ph*C*H$_2^{\alpha}$), 73.2 (Ph*C*H$_2^{\beta}$, C-5$^{\beta}$), 72.5 (Ph*C*H$_2^{\beta}$), 72.3 (Ph*C*H$_2^{\alpha}$), 68.4 (C-6$^{\beta}$), 68.2 (C-6$^{\alpha}$), 40.9 (C(O)*C*H$_2$Cl$^{\alpha}$), 40.7 (C(O)*C*H$_2$Cl$^{\beta}$). HRMS (ESI): Calcd *m*/*z* for [M + NH$_4$]$^+$ $C_{29}H_{29}ClO_8$ 558.1889, found 558.1886. Calcd *m*/*z* for [M + Na]$^+$ $C_{29}H_{29}ClO_8$ 563.1443, found 563.1434. Calcd *m*/*z* for [M + K]$^+$ $C_{29}H_{29}ClO_8$ 579.1153, found 579.1171.

2-*O*-Benzoyl-3,6-di-*O*-benzyl-5-*O*-chloroacetyl-β-D-galactofuranoside trichloroacetimidate (17). Starting hemiacetal **16** (340 mg, 0.63 mmol) in CH_2Cl_2 (5 mL) was treated with CCl_3CN (0.35 mL, 3.5 mmol) and DBU (60 μL, cat) according to GP III. Column chromatography (toluene–EtOAc 20 : 1 + 1 vol% of Et_3N) gave product **17** (380 mg, 88%) as a colorless oil. R_f = 0.69 (toluene–ethyl acetate 10 : 1). ^{1}H NMR (600 MHz, $CDCl_3$): δ 8.63 (s, 1H, =NH), 8.07–7.16 (m, 15H, PhH), 6.50 (s, 1H, H-1), 5.64 (d, $J_{23} \approx 1.0$ Hz, 1H, H-2), 5.39 (m, 1H, H-5), 4.88 (d, J_{ab} = 11.8 Hz, 1H, PhC*H*$_2$), 4.63–4.60 (m, 2H, PhC*H*$_2$, H-4), 4.50 (d, J_{ab} = 12.1 Hz, 1H, PhC*H*$_2$), 4.46 (d, J_{ab} = 12.1 Hz, 1H, PhC*H*$_2$), 4.10 (br d, J_{34} = 5.3 Hz, 1H, H-3), 3.95 (d, J_{ab} = 14.8 Hz, 1H, C(O)C*H*$_2$Cl), 3.90 (d, J_{ab} = 14.8 Hz, 1H, C(O)C*H*$_2$Cl), 3.68 (dd, $^2J_{6a6b}$ = 9.5 Hz, J_{56a} = 5.3 Hz, 1H, H-6a), 3.65 (dd, $^2J_{6a6b}$ = 9.5 Hz, J_{56b} = 4.3 Hz, 1H, H-6b). ^{13}C NMR (150 MHz, $CDCl_3$): δ 166.8 (*C*(O)CH$_2$Cl), 166.5 (Ph*C*O), 160.7 (*C*(NH)CCl$_3$), 137.1, 133.8–127.5 (Ph), 103.6 (C-1), 83.6 (C-4), 82.4 (C-3), 80.33 (C-2), 73.2 (Ph*C*H$_2$), 72.4 (Ph*C*H$_2$, C-5), 68.1 (C-6), 40.7 (C(O)*C*H$_2$Cl). HRMS (ESI): Calcd *m*/*z* for [M + Na]$^+$ $C_{31}H_{29}Cl_4NO_8$ 706.0539, found 706.0539. Calcd *m*/*z* for [M + K]$^+$ $C_{31}H_{29}Cl_4NO_8$ 722.0279, found 722.0273.

Allyl 2-*O*-benzoyl-3,6-di-*O*-benzyl-5-*O*-chloroacetyl-β-D-galactofuranosyl-(1→5)-2-*O*-benzoyl-3,6-di-*O*-benzyl-β-D-galactofuranoside (18). A carefully dried mixture of **13** (125 mg, 0.25 mmol) and **17** (219 mg, 0.32 mmol) was dissolved in CH_2Cl_2 (8 mL), powder MS 4 Å (130 mg) was added, and the mixture was stirred for 20 min. Then the temperature was decreased to −78 °C and TMSOTf (17 μL, 0.096 mmol) was added. The reaction mixture was kept at −40 to −30 °C for 1 h and then at −20 °C the reaction was stopped by the addition of 1 drop of Et_3N. Column chromatography (toluene–EtOAc 20 : 1) gave **18** (175 mg, 68%) as a colorless oil. R_f = 0.59 (toluene–ethyl acetate 10 : 1). $[\alpha]_D$ = −44° (*c* = 1, EtOAc). ^{1}H NMR (600 MHz, $CDCl_3$): δ 8.07–8.03, 7.65–7.08 (m, 30H, PhH), 5.97–5.90 (m, 1H, OCH$_2$C*H*CH$_2$), 5.59 (s, 1H, H-1^{II}), 5.53 (d, J_{23} = 1.5 Hz, 1H, H-2^{II}), 5.44 (d, J_{23} = 1.5 Hz, 1H, H-2^{I}), 5.33 (m, 1H, OCH$_2$CHC*H*$_2$), 5.30 (ddd, J_{45} = 4.9 Hz, J_{56a} = 7.3 Hz, J_{56b} = 4.2 Hz, 1H, H-5^{II}), 5.20 (m, 1H, OCH$_2$CHC*H*$_2$), 5.19 (s, 1H, H-1^{I}), 4.80 (d, J_{ab} = 11.7 Hz, 1H, 3-*O*-PhC*H*$_2^{I}$), 4.76 (d, J_{ab} = 12.0 Hz, 1H, 3-*O*-PhC*H*$_2^{II}$), 4.60 (d, J_{ab} = 11.7 Hz, 1H, 3-*O*-PhC*H*$_2^{I}$), 4.54 (d, J_{ab} = 12.0 Hz, 1H, 3-*O*-PhC*H*$_2^{II}$), 4.53 (d, J_{ab} = 11.9 Hz, 2H, 6-*O*-PhC*H*$_2^{I}$), 4.50 (d, J_{ab} = 11.9 Hz, 2H, 6-*O*-PhC*H*$_2^{I}$), 4.43 (dd, J_{43} = 5.8 Hz, J_{45} = 4.9 Hz, 1H, H-4^{II}), 4.38 (d, J_{ab} = 12.1 Hz, 1H, 6-*O*-PhC*H*$_2^{II}$), 4.34 (dd, J_{43} = 6.1 Hz, J_{45} = 4.2 Hz, 1H, H-4^{I}), 4.30 (d, J_{ab} = 12.1 Hz, 1H, 6-*O*-PhC*H*$_2^{II}$), 4.27 (br d, J_{34} = 6.1 Hz, 1H, H-3^{I}), 4.25–4.21 (m, 2H, H-5^{I}, OC*H*$_2$CHCH$_2$), 4.06 (m, 1H, OC*H*$_2$CHCH$_2$), 3.91 (br d, J_{34} = 5.8 Hz, 1H, H-3^{II}), 3.88 (d, J_{ab} = 14.2 Hz, 1H, C(O)C*H*$_2$Cl), 3.83 (d, J_{ab} = 14.2 Hz, 1H, C(O)C*H*$_2$Cl), 3.78 (dd, $^2J_{6a6b}$ = 10.2 Hz, J_{56a} = 7.4 Hz, 1H, H-6a^{I}), 3.74 (dd, $^2J_{6a6b}$ = 10.2 Hz, J_{56b} = 4.1 Hz, 1H, H-6b^{I}), 3.52 (dd, $^2J_{6a6b}$ = 10.9 Hz, J_{56a} = 7.3 Hz, 1H, H-6a^{II}), 3.47 (dd, $^2J_{6a6b}$ = 10.9 Hz, J_{56b} = 4.2 Hz, 1H, H-6b^{II}). ^{13}C NMR (150 MHz, $CDCl_3$): δ 166.7 (*C*(O)CH$_2$Cl), 165.4 (Ph*C*O), 165.2 (Ph*C*O), 138.0, 137.8, 137.6, 137.3 (quat. Ph), 135.0 (OCH$_2$*C*HCH$_2$), 134.5–127.4 (Ph), 117.4 (OCH$_2$CH*C*H$_2$), 106.2 (C-1^{II}), 105.0 (C-1^{I}), 83.8 (C-3^{I}), 83.0 (C-3^{II}), 82.1 (C-2^{I}), 82.0 (C-4^{I}), 81.6 (C-2^{II}), 82.1 (C-4^{II}), 74.6 (C-5^{I}), 73.4 (6-*O*-Ph*C*H$_2^{I}$), 72.9 (6-*O*-Ph*C*H$_2^{II}$), 72.8 (C-5^{II}), 72.5 (3-*O*-Ph*C*H$_2^{I}$), 72.3 (3-*O*-Ph*C*H$_2^{II}$), 80.0 (C-6^{I}), 68.6 (C-6^{II}), 67.8 (O*C*H$_2$CHCH$_2$), 40.6 (C(O)*C*H$_2$Cl). HRMS (ESI): Calcd *m*/*z* for [M + NH$_4$]$^+$ $C_{59}H_{59}ClO_{14}$ 1044.3932, found 1044.3923. Calcd *m*/*z* for [M + Na]$^+$ $C_{59}H_{59}ClO_{14}$ 1049.3486, found 1049.3487. Calcd *m*/*z* for [M + K]$^+$ $C_{59}H_{59}ClO_{14}$ 1065.3225, found 1065.3220.

Allyl 2-*O*-benzoyl-3,6-di-*O*-benzyl-5-*O*-chloroacetyl-β-D-galactofuranosyl-(1→5)-3,6-di-*O*-benzyl-β-D-galactofuranoside (19). A carefully dried mixture of **10** (25 mg, 0.062 mmol) and **17** (44 mg, 0.065 mmol) was dissolved in CH_2Cl_2 (2 mL), powder MS300 AW (30 mg) was added, and the mixture was stirred for 20 min. Then the temperature was decreased to −78 °C and TMSOTf (1 μL, cat.) was added. After 1 h at −15 °C the reaction was stopped by the addition of 1 drop of MeOH and Et_3N. Column chromatography (toluene–EtOAc 10 : 1) gave **19** (35 mg, 65%) as a colorless oil. R_f = 0.67 (toluene–ethyl acetate 5 : 1). $[\alpha]_D$ = −48° (*c* = 1, EtOAc). ^{1}H NMR (600 MHz, $CDCl_3$): δ 8.03 (d, *J* = 8.2 Hz, 2H, *o*-C(O)Ph), 7.64 (t, *J* = 7.5 Hz, 1H, *p*-C(O)Ph), 7.49 (dd, *J* = 8.2 Hz, *J* = 7.5 Hz, 2H, *m*-C(O)Ph), 7.37–7.18 (m, 20H, PhH), 5.97–5.90 (m, 1H, OCH$_2$C*H*CH$_2$), 5.64 (s, 1H, H-1^{II}), 5.42 (br s, 1H, H-2^{II}), 5.32 (m, 1H, OCH$_2$CHC*H*$_2$), 5.25 (m, 1H, H-5^{II}), 5.20 (m, 1H, OCH$_2$CHC*H*$_2$), 5.02 (s, 1H, H-1^{I}), 4.82 (d, J_{ab} = 12.1 Hz, 1H, 3-*O*-PhC*H*$_2^{II}$), 4.69 (d, J_{ab} = 12.0 Hz, 1H, 3-*O*-PhC*H*$_2^{I}$), 4.63 (d, J_{ab} = 12.1 Hz, 1H, 3-*O*-PhC*H*$_2^{II}$), 4.56 (d, J_{ab} = 12.2 Hz, 1H, 6-*O*-PhC*H*$_2^{I}$), 4.54 (d, J_{ab} = 12.0 Hz, 1H, 3-*O*-PhC*H*$_2^{II}$), 4.53 (d, J_{ab} = 12.2 Hz, 1H, 6-*O*-PhC*H*$_2^{I}$), 4.42 (d, J_{ab} = 12.1 Hz, 1H, 6-*O*-PhC*H*$_2^{II}$), 4.41 (dd, J_{43} = 4.0 Hz, J_{45} = 5.6 Hz, 1H, H-4^{II}), 4.35 (d, J_{ab} = 12.1 Hz, 1H, 6-*O*-PhC*H*$_2^{II}$), 4.26 (dd, J_{43} = 3.9 Hz, J_{45} = 2.1 Hz, 1H, H-4^{I}), 4.21 (m, 1H, OC*H*$_2$CHCH$_2$), 4.15 (d, J_{HOH} = 10.4 Hz, 1H, H-2^{I}), 4.09 (m, 1H, H-5^{I}), 4.03 (m, 1H, OC*H*$_2$CHCH$_2$), 3.98 (d, J_{34} = 3.9. Hz, 1H, H-3^{I}), 3.97 (d, J_{34} = 4.0 Hz, 1H, H-3^{II}), 3.90 (d, J_{ab} = 14.9 Hz, 1H, C(O)C*H*$_2$Cl), 3.85 (dd, $^2J_{6a6b}$ = 10.0 Hz, J_{56a} = 7.4 Hz, 1H, H-6a^{I}), 3.84 (d, J_{ab} = 14.9 Hz, 1H, C(O)C*H*$_2$Cl), 3.73 (dd, $^2J_{6a6b}$ = 10.2 Hz, J_{56b} = 4.3 Hz, 1H, H-6b^{I}), 3.51–3.44 (m, 2H, H-6a^{II}, H-6b^{II}), 2.99 (d, J_{HOH} = 10.4 Hz, 1H, OH). ^{13}C NMR (150 MHz): 166.7 (*C*(O)CH$_2$Cl), 165.2 (Ph*C*O), 138.0, 137.8, 137.5, 136.9 (quat. Ph), 134.3 (OCH$_2$*C*HCH$_2$), 133.6, 129.8–127.5 (Ph), 117.2 (OCH$_2$CH*C*H$_2$), 107.8 (C-1^{I}), 105.9 (C-1^{II}), 86.4 (C-3^{I}), 83.4 (C-4^{I}), 82.6 (C-4^{II}), 82.2 (C-3^{II}), 80.7 (C-2^{II}), 78.3 (C-2^{I}), 75.1 (C-5^{I}), 73.5 (6-*O*-Ph*C*H$_2^{I}$), 73.0 (C-5^{II}, 6-*O*-Ph*C*H$_2^{II}$), 72.3 (3-*O*-Ph*C*H$_2^{II}$), 72.1 (3-*O*-Ph*C*H$_2^{I}$), 71.0 (C-6^{I}), 68.3 (C-6^{II}), 68.0 (O*C*H$_2$CHCH$_2$), 40.7 (C(O)*C*H$_2$Cl). HRMS (ESI): Calcd *m*/*z* for [M + NH$_4$]$^+$ $C_{52}H_{55}ClO_{13}$ 940.3669, found 940.3669. Calcd *m*/*z* for [M + Na]$^+$ $C_{52}H_{55}ClO_{13}$ 945.3223, found 945.3229. Calcd *m*/*z* for [M + K]$^+$ $C_{52}H_{55}ClO_{13}$ 961.2963, found 961.2972.

Allyl 2-*O*-benzoyl-3,6-di-*O*-benzyl-5-*O*-chloroacetyl-β-D-galactofuranosyl-(1→5)-2-*O*-benzoyl-3,6-di-*O*-benzyl-β-D-galactofura-

noside (18) (alternative method *via* benzoylation of 19). To a solution of disaccharide **19** (35 mg, 0.038 mmol) and pyridine (30 μL, 0.38 mmol) in CH_2Cl_2 (2 mL) BzCl (26 μL, 0.22 mmol) was added. After completion of the reaction (overnight) the mixture was diluted using CH_2Cl_2, washed with sat. aq. $NaHCO_3$, and concentrated *in vacuo* with toluene. Column chromatography (toluene–EtOAc 15 : 1) gave **18** (34 mg, 87%) as a colorless oil.

2-*O*-Benzoyl-3,6-di-*O*-benzyl-5-*O*-chloroacetyl-β-D-galactofuranosyl-(1→5)-2-*O*-benzoyl-3,6-di-*O*-benzyl-β-D-galactofuranoside trichloroacetimidate (5). Allyl galactoside **18** (310 mg, 0.30 mmol) was deallylated according to GP II in MeOH (6 mL) using $PdCl_2$ (22 mg, 0.12 mmol). The resulting crude product was treated according to GP III in CH_2Cl_2 (2 mL) with CCl_3CN (150 μL, 1.50 mmol) and DBU (50 μL). Column chromatography (toluene–EtOAc 20 : 1 + 1 vol% of Et_3N) gave **5** (190 mg, 55%) as colorless syrup. ^{1}H NMR (600 MHz, $CDCl_3$): δ 8.62 (s, 1H, =NH), 8.07–8.01, 7.65–7.18 (m, 30H, PhH), 6.59 (s, 1H, H-1^{I}), 5.66 (br s, 1H, H-2^{I}), 5.51 (s, 1H, H-1^{I}), 5.47 (d, J_{23} = 1.4 Hz, 1H, H-2^{I}), 5.28 (m, 1H, H-5^{II}), 4.85 (d, J_{ab} = 11.5 Hz, 1H, 3-*O*-PhCH_2^{I}), 4.72 (d, J_{ab} = 11.9 Hz, 1H, 3-*O*-PhCH_2^{II}), 4.62 (d, J_{ab} = 11.5 Hz, 1H, 3-*O*-PhCH_2^{I}), 4.34 (t, J_{43} = J_{45} = 4.9 Hz, 1H, H-4^{I}), 4.50 (d, J_{ab} = 11.9 Hz, 1H, 3-*O*-PhCH_2^{II}), 4.48 (m, 2H, 6-*O*-PhCH_2^{I}), 4.40–4.35 (m, 3H, H-4^{II}, H-3^{I}, 6-*O*-PhCH_2^{II}), 4.27–4.23 (m, 2H, 6-*O*-PhCH_2^{II}, H-5^{I}), 3.89 (br d, J_{34} = 6.5 Hz, 1H, H-3^{II}), 3.88 (d, J_{ab} = 14.7 Hz, 1H, C(O)CH_2Cl), 3.84 (d, J_{ab} = 14.7 Hz, 1H, C(O)CH_2Cl), 3.78 (dd, $^2J_{6a6b}$ = 10.2 Hz, J_{56a} = 3.8 Hz, 1H, H-6a^{I}), 3.72 (dd, $^2J_{6a6b}$ = 10.2 Hz, J_{56b} = 7.5 Hz, 1H, H-6b^{I}), 3.51 (dd, $^2J_{6a6b}$ = 11.0 Hz, J_{56a} = 7.7 Hz, 1H, H-6a^{II}), 3.44 (dd, $^2J_{6a6b}$ = 11.0 Hz, J_{56b} = 3.9 Hz, 1H, H-6b^{II}). ^{13}C NMR (150 MHz, $CDCl_3$): δ 165.2 (*C*(O)CH_2Cl, 2Ph*C*O), 160.8 (*C*(NH)CCl_3), 137.7–137.2 (quat. Ph), 133.6–127.4 (Ph), 106.5 (C-1^{II}), 103.7 (C-1^{I}), 85.2 (C-4^{I}), 82.9 (C-3^{II}), 82.8 (C-4^{II}), 81.6 (C-2^{II}), 81.0 (C-3^{I}), 80.6 (C-2^{I}), 75.0 (C-5^{I}), 73.4 (6-*O*-Ph*C*H$_2^{I}$), 72.9 (6-*O*-Ph*C*H$_2^{II}$), 72.6 (C-5^{II}), 72.4 (3-*O*-Ph*C*H$_2^{I}$, 3-*O*-Ph*C*H$_2^{II}$), 70.3 (C-6^{I}), 68.8 (C-6^{II}), 40.6 (C(O)*C*H$_2$Cl). HRMS (ESI): Calcd *m*/*z* for Calcd *m*/*z* for $[M + Na]^+$ $C_{85}H_{55}Cl_4NO_{14}$ 1152.2269, found 1152.2241.

Allyl 2,3,5,6-tetra-*O*-benzoyl-β-D-galactofuranosyl-(1→5)-3,6-di-*O*-benzyl-β-D-galactofuranoside (21). A carefully dried mixture of **10** (37 mg, 0.092 mmol) and **20**[21] (74 mg, 0.10 mmol) was dissolved in CH_2Cl_2 (4 mL), powder MS300 AW (30 mg) was added, and the mixture was stirred for 20 min. Then the temperature was decreased to −78 °C and TMSOTf (1 μL, cat.) was added. After 1 h at −15 °C the reaction was stopped by the addition of 1 drop of MeOH and Et_3N. Column chromatography (toluene–EtOAc 8 : 1) gave **21** (56 mg, 62%) as a colorless oil. R_f = 0.57 (toluene–ethyl acetate 5 : 1). $[\alpha]_D$ = −24° (*c* = 1, EtOAc). ^{1}H NMR (400 MHz, $CDCl_3$): δ 8.11–7.85, 7.58–7.16 (m, 30H, PhH), 5.97 (m, 1H, H-5^{II}), 5.93–5.83 (m, 1H, OCH_2CHCH_2), 5.70 (s, 1H, H-1^{II}), 5.63 (d, J_{34} = 5.0 Hz, 1H, H-3^{II}), 5.53 (br s, 1H, H-2^{II}), 5.27 (m, 1H, OCH_2CHCH_2), 5.16 (m, 1H, OCH_2CHCH_2), 5.01 (s, 1H, H-1^{I}), 4.80 (dd, J_{43} = 5.0 Hz, J_{45} = 3.7 Hz, 1H, H-4^{II}), 4.68 (m, 2H, H-6a^{II}, H-6b^{II}), 4.63 (d, J_{ab} = 12.2 Hz, 1H, PhCH_2), 4.56 (d, J_{ab} = 11.9 Hz, 1H, PhCH_2), 4.49 (d, J_{ab} = 11.9 Hz, 1H, PhCH_2), 4.46 (d, J_{ab} = 12.2 Hz, 1H, PhCH_2), 4.26 (dd, J_{43} = 4.1 Hz, J_{45} = 3.0 Hz, 1H, H-4^{I}), 4.20–4.14 (m, 2H, OCH_2CHCH_2, H-2^{I}), 4.09 (m, 1H, H-5^{I}), 4.00–3.93 (m, 2H, H-3^{I}, OCH_2CHCH_2), 3.84 (dd, $^2J_{6a6b}$ = 10.0 Hz, J_{56a} = 7.0 Hz, 1H, H-6a^{I}), 3.71 (dd, $^2J_{6a6b}$ = 10.0 Hz, J_{56b} = 4.3 Hz, 1H, H-6b^{I}), 2.78 (d, J_{HOH} = 10.1 Hz, 1H, OH). ^{13}C NMR (100 MHz, $CDCl_3$): δ 166.1, 165.7, 165.3 (Ph*C*O), 137.9, 137.8, (quat. Ph), 134.2 (OCH_2CHCH_2), 133.5, 133.3, 133.2, 133.1 (quat. Ph), 130.1–127.6 (Ph), 117.1 (OCH_2CHCH_2), 107.6 (C-1^{I}), 105.0 (C-1^{II}), 85.8 (C-3^{I}), 83.1 (C-4^{I}), 82.3 (C-2^{II}), 82.0 (C-4^{II}), 78.7 (C-2^{I}), 77.7 (C-3^{II}), 75.8 (C-5^{I}), 73.5 (Ph*C*H$_2$), 72.1 (Ph*C*H$_2$), 70.8 (C-6^{I}), 70.5 (C-5^{II}), 68.0 (OCH_2CHCH_2), 63.6 (C-6^{II}). HRMS (ESI): Calcd *m*/*z* for $[M + NH_4]^+$ $C_{57}H_{54}O_{15}$ 996.3801, found 996.3793. Calcd *m*/*z* for $[M + Na]^+$ $C_{57}H_{54}O_{15}$ 1001.3355, found 1001.3348. Calcd *m*/*z* for $[M + K]^+$ $C_{57}H_{54}O_{15}$ 1017.3094, found 1017.3104.

Allyl 2,3,5,6-tetra-*O*-benzoyl-β-D-galactofuranosyl-(1→5)-2-*O*-benzoyl-3,6-di-*O*-benzyl-β-D-galactofuranoside (22). To a solution of **21** (56 mg, 0.057 mmol) and pyridine (50 μL, 0.6 mmol) in CH_2Cl_2 (2 mL) BzCl (50 μL, 0.6 mmol) was added and the reaction was left overnight. Then the mixture was diluted using CH_2Cl_2, washed with sat. aq. $NaHCO_3$, and concentrated *in vacuo* with toluene. Column chromatography (toluene–EtOAc 15 : 1) gave **22** (52 mg, 84%) as a colorless oil. R_f = 0.66 (toluene–ethyl acetate 10 : 1). $[\alpha]_D$ = −18° (*c* = 1, EtOAc). ^{1}H NMR (600 MHz, $CDCl_3$): δ 8.17–7.92, 7.55–7.17 (m, 35H, PhH), 6.01 (m, 1H, H-5^{II}), 5.88–5.80 (m, 1H, OCH_2CHCH_2), 5.69 (s, 1H, H-1^{II}), 5.65 (d, J_{34} = 5.1 Hz, 1H, H-3^{II}), 5.62 (br s, 1H, H-2^{II}), 5.42 (br s, 1H, H-2^{I}), 5.25 (m, 1H, OCH_2CHCH_2), 5.19 (s, 1H, H-1^{I}), 5.14 (m, 1H, OCH_2CHCH_2), 4.82–4.78 (m, 2H, H-4^{II}, PhCH_2), 4.69 (m, 2H, H-6a^{II}, H-6b^{II}), 4.56 (d, J_{ab} = 11.9 Hz, 1H, PhCH_2), 4.51 (d, J_{ab} = 12.0 Hz, 1H, PhCH_2), 4.46 (d, J_{ab} = 12.0 Hz, 1H, PhCH_2), 4.30 (t, J_{43} = J_{45} = 5.7 Hz, 1H, H-4^{I}), 4.24 (m, 1H, H-5^{I}), 4.18–4.13 (m, 2H, OCH_2CHCH_2, H-3^{I}), 3.98 (m, 1H, OCH_2CHCH_2), 3.73 (m, 1H, H-6a^{I}), 3.67 (m, 1H, H-6b^{I}). ^{13}C NMR (125 MHz): δ 166.0, 165.6, 165.5, 165.4, 165.2 (Ph*C*O), 137.9, 137.4, (quat. Ph), 134.5 (OCH_2CHCH_2), 133.8, 133.3, 133.2, 133.1, 132.9 (quat. Ph), 130.5–127.5 (Ph), 117.4 (OCH_2CHCH_2), 105.6 (C-1^{II}), 104.8 (C-1^{I}), 83.7 (C-3^{I}), 82.1, 82.0 (C-2^{I}, C-2^{II}), 81.9 (C-4^{I}), 81.5 (C-4^{II}), 82.0 (C-4^{II}), 77.5 (C-3^{II}), 75.4 (C-5^{I}), 73.4 (Ph*C*H$_2$), 72.4 (Ph*C*H$_2$), 70.8 (C-6^{I}), 70.4 (C-5^{II}), 67.7 (OCH_2CHCH_2), 63.8 (C-6^{II}). HRMS (ESI): Calcd *m*/*z* for $[M + NH_4]^+$ $C_{64}H_{58}O_{16}$ 1100.4063, found 1100.4054. Calcd *m*/*z* for $[M + Na]^+$ $C_{64}H_{58}O_{16}$ 1105.3617, found 1105.3612. Calcd *m*/*z* for $[M + K]^+$ $C_{64}H_{58}O_{16}$ 1121.3356, found 1121.3366.

2,3,5,6-Tetra-*O*-benzoyl-β-D-galactofuranosyl-(1→5)-2-*O*-benzoyl-3,6-di-*O*-benzyl-β-D-galactofuranoside trichloroacetimidate (6). Allyl galactoside **22** (47 mg, 0.043 mmol) was treated with $PdCl_2$ (4 mg, 0.022 mmol) according to GP II in 1 mL of MeOH. The resulting crude product was treated according to GP III in CH_2Cl_2 (2 mL) with CCl_3CN (22 μL, 0.22 mmol) and DBU (20 μL). Column chromatography (toluene–EtOAc 20 : 1 + 1 vol% of Et_3N) gave **6** (30 mg, 59%) as yellowish syrup. ^{1}H NMR (600 MHz, $CDCl_3$): δ 8.55 (s, 1H, =NH), 8.04–7.88, 7.54–7.15 (m, 30H, PhH), 6.49 (s, 1H, H-1^{I}), 6.00 (m, 1H, H-5^{II}), 5.65 (br s, 1H, H-2^{I}), 5.62 (s, 1H, H-1^{II}), 5.60 (d, J_{34} = 5.1 Hz, 1H, H-3^{II}), 5.57 (br s, 1H, H-2^{II}), 5.42 (br s, 1H, H-2^{I}), 4.84 (d, J_{ab} = 11.7 Hz, 1H, PhCH_2), 4.80 (dd, J_{43} = 5.1 Hz, J_{45} = 3.6 Hz,

1H, H-4^{II}), 4.67 (m, 2H, H-6a^{II}, H-6b^{II}), 4.56 (d, J_{ab} = 11.7 Hz, 1H, PhCH_2), 4.52 (t, J_{43} = J_{45} = 5.7 Hz, 1H, H-4^{I}), 4.49 (d, J_{ab} = 12.0 Hz, 1H, PhCH_2^{II}), 4.45 (d, J_{ab} = 12.0 Hz, 1H, PhCH_2), 4.31 (d, J_{34} = 5.5 Hz, 1H, H-3^{I}), 4.24 (m, 1H, H-5^{I}), 3.71 (m, 2H, H-6a^{I}, H-6b^{I}). ^{13}C NMR (125 MHz, $CDCl_3$): δ 166.0, 165.7, 165.6, 165.2, 165.2 (Ph*C*O), 160.7 (*C*(NH)CCl$_3$), 137.8, 137.3, (quat. Ph), 133.6, 133.4, 133.2, 133.0, 132.9 (quat. Ph), 129.9–127.5 (Ph), 105.8 (C-1^{II}), 103.4 (C-1^{I}), 84.9 (C-4^{I}), 83.0 (C-3^{I}), 81.8 (C-2^{II}), 81.6 (C-4^{II}), 80.8 (C-2^{I}), 77.4 (C-3^{II}), 75.8 (C-5^{I}), 73.4 (Ph*C*H$_2$), 72.3 (Ph*C*H$_2$), 70.5 (C-5^{II}), 70.3 (C-6^{I}), 64.0 (C-6^{II}). HRMS (ESI): Calcd *m*/*z* for $[M + Na]^+$ 1208.2400, found 1208.2390. Calcd *m*/*z* for $[M + K]^+$ 1224.2140, found 1224.2130.

3-Trifluoroacetamidopropyl 2,3,4-tri-*O*-benzoyl-α-D-mannopyranoside (3). A carefully dried suspension of **23** (375 mg, 0.58 mmol) in 3-trifluoroacetamidopropanol (200 mg, 1.16 mmol) was dissolved in CH_2Cl_2 (5 mL), 600 mg of MS 4 Å powder were added, and the mixture was stirred for 20 min. Then at −20 °C NIS (260 mg, 1.16 mmol) was added and after 20 min of stirring at −40 °C TfOH (10 μL, 0.12 mmol) was added. For 1 h the mixture was kept in the temperature range −20 to −15 °C, then at −15 °C the reaction mixture was quenched by the addition of 3 drops of pyridine. Column chromatography (toluene–EtOAc 15 : 1) gave the product of glycosylation, which was dissolved in 10 mL of TFA (90%, aq.) and stirred for 3 h. Then the mixture was diluted with toluene and concentrated *in vacuo*. Column chromatography (toluene–EtOAc 3 : 1) gave **3** (235 mg, 62%) as a colorless oil. R_f = 0.25 (toluene–ethyl acetate 3 : 1). $[\alpha]_D$ = −121° (*c* = 1, EtOAc). ^{1}H NMR (400 MHz, $CDCl_3$): δ 8.02–7.72 (m, 6H, *o*-C(O)Ph), 7.55–7.14 (m, 9H, PhH), 6.95 (br s, 1H, CH$_2$N*H*), 5.84 (dd, J_{34} = 10.0 Hz, J_{32} = 3.3 Hz, 1H, H-3), 5.76 (t, *J* = 10.0 Hz, 1H, H-4), 5.59 (dd, J_{23} = 3.3 Hz, J_{21} = 1.8 Hz, 1H, H-2), 5.02 (d, J_{12} = 1.8 Hz, 1H, H-1), 4.01 (m, 1H, H-5), 3.84 (ddd, $^2J_{ab}$ = 10.1 Hz, *J* = 6.9 Hz, *J* = 4.9 Hz, 1H, OCH_2CH$_2$CH$_2$N), 3.76 (dd, $^2J_{ab}$ = 12.7 Hz, J_{56a} = 2.6 Hz, 1H, H-6a), 3.72 (dd, $^2J_{ab}$ = 12.7 Hz, J_{56b} = 4.4 Hz, 1H, H-6b), 3.57 (ddd, $^2J_{ab}$ = 10.1 Hz, *J* = 6.9 Hz, *J* = 4.9 Hz, 1H, OCH_2CH$_2$CH$_2$N), 3.52 (m, 1H, OCH$_2$CH$_2$CH_2N), 3.49 (m, 1H, OCH$_2$CH$_2$CH_2N), 2.70 (br s, 1H, OH), 1.99–1.87 (m, 2H, OCH$_2$CH_2CH$_2$N). ^{13}C NMR (100 MHz, $CDCl_3$): δ 166.4, 165.6, 165.54 (Ph*C*O), 157.5 (q, $^2J_{CF}$ = 37.0 Hz, *C*(O)CF$_3$), 133.7, 133.6, 133.2 (quat. Ph), 130.0–128.3 (Ph), 115.9 (q, $^1J_{CF}$ = 287.7 Hz, C(O)*C*F$_3$), 97.9 (C-1), 71.4 (C-5), 70.5 (C-2), 69.7 (C-3), 67.1 (C-4), 66.1 (O*C*H$_2$CH$_2$CH$_2$N), 61.4 (C-6), 37.6 (OCH$_2$CH$_2$*C*H$_2$N), 28.6 (OCH$_2$*C*H$_2$CH$_2$N). HRMS (ESI): Calcd *m*/*z* for $[M + NH_4]^+$ $C_{32}H_{34}F_3NO_8$ 663.2160, found 663.2156. Calcd *m*/*z* for $[M + Na]^+$ $C_{32}H_{34}F_3NO_8$ 668.1714, found 668.1725. Calcd *m*/*z* for $[M + K]^+$ $C_{32}H_{34}F_3NO_8$ 684.1453, found 684.1452.

3-Trifluoroacetamidopropyl 2-*O*-benzoyl-4,5-di-*O*-benzyl-α-D-mannopyranoside (4). To a stirred solution of **24** (570 mg, 1.12 mmol) and pyridine (0.31 mL, 3.9 mmol) in CH_2Cl_2 (10 mL) chloroacetyl chloride (160 μL, 2.02 mmol) was slowly added. The reaction mixture was stirred for 40 min, diluted using CH_2Cl_2, washed with 1 M HCl and sat. aq. $NaHCO_3$, and concentrated *in vacuo*. To a crude product 3-trifluoroacetamidopropanol (380 mg, 2.24 mmol) was added and the mixture was carefully dried, dissolved in 5 mL of CH_2Cl_2, and stirred with MS300 AW for 20 min. Then the temperature was decreased to −20 °C, NIS (500 mg, 2.24 mmol) was added, and after 20 min of stirring at −40 °C TfOH (20 μL, 0.22 mmol) was added. The mixture was kept in the temperature range −20 to −15 °C for 1 h, then at −15 °C it was quenched by the addition of 3 drops of pyridine. Column chromatography (toluene–EtOAc 10 : 1) gave the product of glycosylation, which was treated according to GP I with thiourea (0.83 g, 11 mmol) and collidine (185 μL, 1.4 mmol) in MeOH (25 mL). Column chromatography of the residue (toluene–EtOAc 4 : 1) gave **4** (380 mg, 55%) as a colorless oil. R_f = 0.26 (toluene–ethyl acetate 5 : 1). $[\alpha]_D$ = −63° (*c* = 1, EtOAc). ^{1}H NMR (600 MHz, $CDCl_3$): δ 8.03 (d, *J* = 8.2 Hz, 2H, *o*-C(O)Ph), 7.58 (t, *J* = 7.5 Hz, 1H, *p*-C(O)Ph), 7.40 (dd, *J* = 8.2 Hz, *J* = 7.5 Hz, 2H, *m*-C(O)Ph), 7.39–7.25 (m, 10H, PhH), 6.89 (br s, 1H, CH$_2$N*H*), 5.33 (dd, J_{23} = 3.3 Hz, J_{21} = 1.8 Hz, 1H, H-2), 4.97 (d, J_{12} = 1.8 Hz, 1H, H-1), 4.81 (d, J_{ab} = 11.2 Hz, 1H, PhCH_2), 4.71 (d, J_{ab} = 12.0 Hz, 1H, PhCH_2), 4.64 (d, J_{ab} = 11.2 Hz, 1H, PhCH_2), 4.57 (d, J_{ab} = 12.0 Hz, 1H, PhCH_2), 4.21 (m, 1H, H-5), 3.95 (t, *J* = 9.5 Hz, 1H, H-4), 3.87–3.78 (m, 4H, H-6a, OCH_2CH$_2$CH$_2$N, H-6b, H-3), 3.57 (m, 1H, OCH_2CH$_2$CH$_2$N), 3.51 (m, 1H, OCH$_2$CH$_2$CH_2N), 3.43 (m, 1H, OCH$_2$CH$_2$CH_2N), 2.28 (d, J_{HOH} = 5.3 Hz, 1H, OH), 1.92–1.86 (m, 2H, OCH$_2$CH_2CH$_2$N). ^{13}C NMR (150 MHz, $CDCl_3$): δ 166.2 (Ph*C*O), 138.1, 138.0 (quat. Ph), 133.4 (*p*-C(O)-Ph), 129.8 (*o*-C(O)Ph), 129.5 (quat. Ph), 128.5–127.6 (Ph), 97.7 (C-1), 75.6 (C-4), 74.9 (Ph*C*H$_2$), 73.5 (Ph*C*H$_2$), 72.8 (C-2), 71.8 (C-3), 70.5 (C-5), 69.0 (C-6), 66.1 (O*C*H$_2$CH$_2$CH$_2$N), 38.0 (OCH$_2$CH$_2$*C*H$_2$N), 28.3 (OCH$_2$*C*H$_2$CH$_2$N). HRMS (ESI): Calcd *m*/*z* for $[M + NH_4]^+$ $C_{32}H_{34}F_3NO_8$ 635.2575, found 635.2576. Calcd *m*/*z* for $[M + Na]^+$ $C_{32}H_{34}F_3NO_8$ 640.2129, found 640.2130.

3-Trifluoroacetamidopropyl 2-*O*-benzoyl-3,6-di-*O*-benzyl-5-*O*-chloroacetyl-β-D-galactofuranosyl-(1→5)-2-*O*-benzoyl-3,6-di-*O*-benzyl-β-D-galactofuranosyl-(1→6)-2,3,4-tri-*O*-benzoyl-α-D-mannopyranoside (25). A carefully dried mixture of **3** (72 mg, 0.111 mmol) and **5** (105 mg, 0.093 mmol) was dissolved in CH_2Cl_2 (4 mL), powder MS 4 Å (100 mg) was added, and the mixture was stirred for 20 min. Then the temperature was decreased to −78 °C and TMSOTf (5 μL, 0.028 mmol) was added. The reaction mixture was kept at −20 to −40 °C for 1 h and then at −15 °C it was quenched by the addition of 1 drop of Et_3N. Column chromatography (toluene–EtOAc 12 : 1) gave **25** (130 mg, 85%) as a colorless oil. R_f = 0.70 (toluene–ethyl acetate 5 : 1). $[\alpha]_D$ = −75° (*c* = 1, EtOAc). ^{1}H NMR (600 MHz, $CDCl_3$): δ 8.15–7.83, 7.66–7.10 (m, 45H, PhH), 5.86 (dd, J_{23} = 3.4 Hz, J_{34} = 10.0 Hz, 1H, H-3^{I}), 5.77 (t, J_{34} = J_{45} = 10.0 Hz, 1H, H-4^{I}), 5.67 (dd, J_{12} = 1.6 Hz, J_{23} = 3.4 Hz, 1H, H-2^{I}), 5.59 (s, 1H, H-1^{III}), 5.51 (d, J_{23} = 1.6 Hz, 1H, H-2^{III}), 5.43 (d, J_{23} = 1.7 Hz, 1H, H-2^{II}), 5.34 (s, 1H, H-1^{II}), 5.25 (ddd, J_{45} = 5.4 Hz, J_{56a} = 6.8 Hz, J_{56b} = 5.2 Hz, 1H, H-5^{III}), 5.03 (d, J_{12} = 1.6 Hz, 1H, H-1^{I}), 4.74 (d, J_{ab} = 12.1 Hz, 1H, 3-*O*-PhCH_2^{III}), 4.68 (d, J_{ab} = 11.6 Hz, 1H, 3-*O*-PhCH_2^{II}), 4.55 (d, J_{ab} = 11.6 Hz, 1H, 3-*O*-PhCH_2^{II}), 4.53 (d, J_{ab} = 12.0 Hz, 1H, 3-*O*-PhCH_2^{III}), 4.45 (m, 2H, 6-*O*-PhCH_2^{II}), 4.39 (t, J_{43} = J_{45} = 5.4 Hz, 1H, H-4^{III}), 4.35–4.28 (m, 4H, H-3^{II}, H-5^{I}, H-4^{II}, 6-*O*-PhCH_2^{III}), 4.26 (d, J_{ab} = 12.1 Hz, 1H, 6-*O*-PhCH_2^{III}), 4.22 (m, 1H, H-5^{II}), 3.97 (m, 1H, OCH_2CHCH$_2$), 3.92

(m, 1H, H-3^{III}), 3.90 (m, 2H, H-6a^{I}, H-6b^{I}), 3.84 (d, J_{ab} = 14.8 Hz, 1H, C(O)CH_2Cl), 3.79 (d, J_{ab} = 14.8 Hz, 1H, C(O)CH_2Cl), 3.78 (m, 1H, H-6a^{II}), 3.64 (m, 1H, H-6a^{II}), 3.60–3.48 (m, 3H, OCH_2CHCH$_2$, 2OCH$_2$CH$_2$CH_2N), 3.46 (m, 2H, H-6a^{III}, H-6b^{III}), 2.00–1.90 (m, 2H, OCH$_2$CH_2CH$_2$N). ^{13}C NMR (150 MHz, $CDCl_3$): 166.7 (*C*(O)CH$_2$Cl), 165.7–165.4 (Ph*C*O), 138.0–137.4 (quat. Ph), 133.5–127.4 (Ph), 106.7 (C-1^{II}), 106.3 (C-1^{III}), 97.6 (C-1^{I}), 83.6 (C-3^{II}), 82.9 (C-3^{III}), 82.2 (2C, C-4^{II}, C-2^{II}), 81.6 (C-2^{II}), 81.3 (C-4^{III}), 74.1 (C-5^{II}), 73.4 (6-*O*-Ph*C*H$_2$^{II}), 72.9 (6-*O*-Ph*C*H$_2$^{III}), 72.8 (C-5^{III}), 72.7 (3-*O*-Ph*C*H$_2$^{II}), 72.3 (3-*O*-Ph*C*H$_2$^{III}), 71.2 (C-5^{I}), 71.1 (C-6^{II}), 70.4 (C-2^{I}), 69.9 (C-3^{I}), 68.4 (C-6^{III}), 67.4 (C-4^{I}), 66.4 (O*C*H$_2$CH$_2$CH$_2$N), 66.2 (C-6^{I}), 40.6 (C(O)*C*H$_2$Cl), 37.7 (OCH$_2$CH$_2$*C*H$_2$N), 28.5 (OCH$_2$*C*H$_2$CH$_2$N). HRMS (ESI): Calcd *m*/*z* for $[M + NH_4]^+$ $C_{88}H_{83}ClF_3NO_{23}$ 1631.5335, found 1631.5310. Calcd *m*/*z* for $[M + Na]^+$ $C_{88}H_{83}ClF_3NO_{23}$ 1636.4889, found 1636.4874. Calcd *m*/*z* for $[M + K]^+$ $C_{88}H_{83}ClF_3NO_{23}$ 1652.4628, found 1652.4607.

3-Trifluoroacetamidopropyl 2-*O*-benzoyl-3,6-di-*O*-benzyl-β-D-galactofuranosyl-(1→5)-2-*O*-benzoyl-3,6-di-*O*-benzyl-β-D-galactofuranosyl-(1→6)-2,3,4-tri-*O*-benzoyl-α-D-mannopyranoside (26). Trisaccharide **25** (130 mg, 0.080 mmol) was treated according to GP I with thiourea (61 mg, 0.8 mmol) and collidine (14 μL, 0.1 mmol) in MeOH (10 mL). Column chromatography (toluene–EtOAc 7 : 1) gave **26** (106 mg, 86%) as a colorless oil. R_f = 0.41 (toluene–ethyl acetate 5 : 1). $[\alpha]_D$ = −79° (*c* = 1, EtOAc). ^{1}H NMR (600 MHz, $CDCl_3$): δ 8.14–7.85, 7.64–7.16 (m, 45H, PhH), 5.89 (dd, J_{23} = 3.4 Hz, J_{34} = 10.0 Hz, 1H, H-3^{I}), 5.80 (t, J_{34} = J_{45} = 10.0 Hz, 1H, H-4^{I}), 5.69 (dd, J_{12} = 1.6 Hz, J_{23} = 3.4 Hz, 1H, H-2^{I}), 5.64 (s, 1H, H-1^{III}), 5.57 (d, J_{23} = 1.6 Hz, 1H, H-2^{III}), 5.46 (d, J_{23} = 1.7 Hz, 1H, H-2^{II}), 5.38 (s, 1H, H-1^{II}), (ddd, J_{45} = 5.4 Hz, J_{56a} = 6.8 Hz, J_{56b} = 5.2 Hz, 1H, H-5^{III}), 5.05 (d, J_{12} = 1.6 Hz, 1H, H-1^{I}), 4.76 (d, J_{ab} = 12.2 Hz, 1H, 3-*O*-PhCH_2^{III}), 4.70 (d, J_{ab} = 11.6 Hz, 1H, 3-*O*-PhCH_2^{II}), 4.59 (d, J_{ab} = 11.6 Hz, 1H, 3-*O*-PhCH_2^{II}), 4.57 (d, J_{ab} = 12.2 Hz, 1H, 3-*O*-PhCH_2^{III}), 4.48 (m, 2H, 6-*O*-PhCH_2^{II}), 4.41 (br d, J_{34} = 6.1 Hz, 1H, H-3^{II}), 4.38 (d, J_{ab} = 11.9 Hz, 1H, 6-*O*-PhCH_2^{III}), 4.36–4.32 (m, 3H, 6-*O*-PhCH_2^{III}, H-5^{I}, H-4^{II}), 4.29–4.26 (m, 2H, H-4^{III}, H-5^{II}), 4.15 (br d, J_{34} = 5.9 Hz, 1H, H-3^{III}), 3.97 (dt, $^2J_{ab}$ = 10.0 Hz, $^3J_{HCH2}$ = 6.2 Hz, 1H, OCH_2CHCH$_2$), 3.94–3.92 (m, 2H, H-6a^{I}, H-6b^{I}), 3.86–3.81 (m, 2H, H-5^{III}, H-6a^{II}), 3.74 (dd, $^2J_{6a6b}$ = 10.1 Hz, J_{56b} = 4.1 Hz, 1H, H-6b^{II}), 3.60–3.48 (m, 3H, OCH_2CHCH$_2$, OCH$_2$CH$_2$CH_2N), 3.44–3.38 (m, 2H, H-6a^{III}, H-6b^{III}), 2.37 (br s, 1H, 5-OH), 2.01–1.90 (m, 2H, OCH$_2$CH_2CH$_2$N). ^{13}C NMR (150 MHz, $CDCl_3$): 165.7–165.2 (Ph*C*O), 137.9–137.5 (quat. Ph), 133.5–127.4 (Ph), 106.6 (C-1^{II}), 106.4 (C-1^{III}), 97.5 (C-1^{I}), 83.5 (C-3^{II}), 83.4 (C-3^{III}), 83.2 (C-4^{III}), 82.2 (2C, C-4^{II}, C-2^{II}), 81.8 (C-2^{II}), 73.8 (C-5^{II}), 73.4 (6-*O*-Ph*C*H$_2$^{II}), 73.2 (6-*O*-Ph*C*H$_2$^{III}), 72.7 (3-*O*-Ph*C*H$_2$^{II}), 72.2 (3-*O*-Ph*C*H$_2$^{III}), 71.4 (C-6^{III}), 71.2 (C-5^{I}), 71.1 (C-6^{II}), 70.4 (C-2^{I}), 70.1 (C-5^{III}), 69.9 (C-3^{I}), 67.3 (C-4^{I}), 66.3 (O*C*H$_2$CH$_2$CH$_2$N), 66.1 (C-6^{I}), 37.6 (OCH$_2$CH$_2$*C*H$_2$N), 28.4 (OCH$_2$*C*H$_2$CH$_2$N). HRMS (ESI): Calcd *m*/*z* for $[M + NH_4]^+$ $C_{86}H_{82}F_3NO_{22}$ 1555.5619, found 1555.5596. Calcd *m*/*z* for $[M + Na]^+$ $C_{86}H_{82}F_3NO_{22}$ 1560.5173, found 1560.5162. Calcd *m*/*z* for $[M + K]^+$ $C_{86}H_{82}F_3NO_{22}$ 1576.4912, found 1576.4896.

3-Trifluoroacetamidopropyl 2-*O*-benzoyl-3,6-di-*O*-benzyl-5-*O*-chloroacetyl-β-D-galactofuranosyl-(1→5)-2-*O*-benzoyl-3,6-di-*O*-benzyl-β-D-galactofuranosyl-(1→5)-2-*O*-benzoyl-3,6-di-*O*-benzyl-β-D-galactofuranosyl-(1→5)-2-*O*-benzoyl-3,6-di-*O*-benzyl-β-D-galactofuranosyl-(1→6)-2,3,4-tri-*O*-benzoyl-α-D-mannopyranoside (27). A carefully dried mixture of **26** (77 mg, 0.050 mmol) and **5** (70 mg, 0.062 mmol) was dissolved in CH_2Cl_2 (3 mL), powder MS 4 Å (40 mg) was added, and the mixture was stirred for 20 min. Then the temperature was decreased to −78 °C and TMSOTf (3.5 μL, 0.019 mmol) was added. The reaction mixture was kept at −30 to −40 °C for 1 h and then at −15 °C it was stopped by the addition of 1 drop of Et_3N. Column chromatography (toluene–EtOAc 8 : 1) gave **27** (89 mg, 71%) as a colorless oil. R_f = 0.67 (toluene–ethyl acetate 5 : 1). $[\alpha]_D$ = −78° (*c* = 1, EtOAc). ^{1}H NMR (600 MHz, $CDCl_3$): δ 8.12–7.83, 7.64–7.10 (m, 75H, PhH), 5.86 (dd, J_{23} = 3.4 Hz, J_{34} = 10.0 Hz, 1H, H-3^{I}), 5.77 (t, J_{34} = J_{45} = 10.0 Hz, 1H, H-4^{I}), 5.67 (dd, J_{12} = 1.6 Hz, J_{23} = 3.3 Hz, 1H, H-2^{I}), 5.60 (s, 1H, H-1^{III}), 5.58(s, 1H, H-1^{IV}), 5.56 (m, 2H, H-1^{V}, H-2^{III}), 5.54 (br s, 1H, H-2^{IV}), 5.49 (d, J_{23} ≈ 1.3 Hz, 1H, H-2^{V}), 5.40 (d, J_{23} = 1.6 Hz, 1H, H-2^{II}), 5.19 (s, 1H, H-1^{II}), (ddd, J_{45} = 5.4 Hz, J_{56a} = 7.4 Hz, J_{56b} = 5.2 Hz, 1H, H-5^{III}), 5.02 (d, J_{12} = 1.6 Hz, 1H, H-1^{I}), 4.74–4.43 (m, 10H, PhCH_2), 4.37 (br d, J_{34} = 6.1 Hz, 1H, H-3^{II}), 4.35–4.20 (m, 13H, H-3^{III}, H-4^{III}, H-5^{I}, H-4^{II}, H-3^{IV}, H-4^{IV}, PhCH_2, H-4^{V}, H-5^{II}), 4.18 (d, J_{ab} = 12.1 Hz, 1H, PhCH_2), 4.10 (dt, *J* = 3.5 Hz, *J* = 7.2 Hz, 1H, H-5^{III}), 4.03 (br d, *J* = 7.9 Hz, 1H, H-5^{IV}), 3.95 (dt, *J* = 6.3 Hz, $^2J_{ab}$ = 10.2 Hz, 1H, OCH_2CHCH$_2$), 3.92–3.88 (m, 2H, H-6a^{I}, H-6b^{I}), 3.85 (br d, J_{34} = 5.8 Hz, 1H, H-3^{V}), 3.79–3.75 (m, 2H, H-6a^{II}, C(O)CH_2Cl), 3.74–3.67 (m, 4H, C(O)CH_2Cl, H-6a^{IV}, H-6a^{III}, H-6b^{II}), 3.58–3.48 (m, 5H, H-6b^{III}, OCH_2CHCH$_2$, OCH$_2$CH$_2$CH_2N, H-6b^{IV}), 3.39 (dd, $^2J_{6a6b}$ = 11.0 Hz, J_{56a} = 7.3 Hz, 1H, H-6a^{V}), 3.34 (dd, $^2J_{6a6b}$ = 11.0 Hz, J_{56b} = 3.9 Hz, 1H, H-6b^{V}), 2.00–1.89 (m, 2H, OCH$_2$CH_2CH$_2$N). ^{13}C NMR (150 MHz, $CDCl_3$): δ 166.6 (*C*(O)CH$_2$Cl), 165.7–165.0 (Ph*C*O), 138.0–137.2 (quat. Ph), 133.5–127.2 (Ph), 106.6 (C-1^{II}), 106.6 (C-1^{V}) 106.5 (C-1^{IV}), 106.2 (C-1^{III}), 97.5 (C-1^{I}), 84.0 (C-3^{IV}), 83.5 (C-3^{II}), 83.5 (C-3^{III}), 82.8 (C-3^{V}), 82.8 (C-4^{III}), 82.6 (C-4^{IV}), 82.2 (2C, C-2^{II}, C-4^{II}), 82.1 (C-2^{III}), 82.1 (C-2^{IV}), 81.4 (C-2^{V}), 81.4 (C-4^{V}), 74.3 (C-5^{IV}), 74.2 (C-5^{III}), 73.7 (C-5^{II}), 73.4 (Ph*C*H$_2$), 73.1 (Ph*C*H$_2$), 73.1 (Ph*C*H$_2$), 72.9 (C-5^{V}, Ph*C*H$_2$), 72.8 (Ph*C*H$_2$), 72.6 (Ph*C*H$_2$), 72.4 (Ph*C*H$_2$), 72.1 (Ph*C*H$_2$), 72.0 (C-6^{IV}), 71.3 (C-5^{I}), 71.2 (C-6^{III}), 70.7 (C-6^{IV}), 70.4 (C-2^{I}), 69.9 (C-3^{I}), 68.5 (C-6^{V}), 67.3 (C-4^{I}), 66.4 (O*C*H$_2$CH$_2$CH$_2$N), 66.0 (C-6^{I}), 40.5 (C(O)*C*H$_2$Cl), 37.6 (OCH$_2$CH$_2$*C*H$_2$N), 28.5 (OCH$_2$*C*H$_2$CH$_2$N). HRMS (ESI): Calcd *m*/*z* for $[M + NH_4]^+$ $C_{142}H_{135}ClF_3NO_{35}$ 2523.8794, found 2523.8749. Calcd *m*/*z* for $[M + Na]^+$ $C_{142}H_{135}ClF_3NO_{35}$ 2528.8347, found 2528.8378. Calcd *m*/*z* for $[M + 2NH_4]^{2+}$ $C_{142}H_{135}ClF_3NO_{35}$ 1270.9566, found 1270.9573.

3-Aminopropyl β-D-galactofuranosyl-(1→5)-β-D-galactofuranosyl-(1→5)-β-D-galactofuranosyl-(1→5)-β-D-galactofuranosyl-(1→6)-α-D-mannopyranoside (1). Compound **27** (35 mg, 0.014 mmol) was dissolved in EtOAc (1 mL), MeOH (1 mL) was added and 10% Pd/C (35 mg) powder was added. The reaction mixture was vigorously stirred in a H_2-atmosphere for 3 h and then filtered through the Celite layer. The filtrate was concentrated *in vacuo*, dissolved in 0.9 mL of 0.1 M MeONa in MeOH,

one drop of water was added, and the mixture was kept overnight, then 5 μL of AcOH were added, and the mixture was diluted with water and concentrated *in vacuo*. Gel-chromatography and subsequent lyophilization gave **1** (10 mg, 83%) as a white foam. ^{1}H NMR (600 MHz, D_2O): 5.22 (d, J_{12} = 2.0 Hz, 1H, H-1^V), 5.19 (m, 2H, H-1^{III}, H-1^{IV}), 5.03 (d, J_{12} = 1.5 Hz, 1H, H-1^{II}), 4.85 (d, J_{12} = 1.8 Hz, 1H, H-1^I), 4.17–4.14 (m, 5H, H-4^{III}, H-4^{IV}, H-2^{III}, H-2^{IV}, H-2^V), 4.13–4.08 (m, 5H, H-3^{II}, H-3^{III}, H-3^{IV}, H-2^{II}, H-4^{II}), 4.08–4.06 (m, 2H, H-3^V, H-4^V), 4.02 (m, 1H, H-6a^I), 3.98–3.92 (m, 4H, H-5^{II}, H-5^{III}, H-5^{IV}, H-2^I), 3.87–3.83 (m, 2H, OCH_2, H-5^V), 3.82–3.78 (m, 7H, H-6a^{III}, H-6b^{III}, H-6a^{IV}, H-6b^{IV}, H-6a^{II}, H-6b^{II}, H-3^I), 3.74–3.69 (m, 4H, H-6b^I, H-6a^V, H-5^I, H-4^I), 3.67 (dd, $^2J_{6a6b}$ = 11.7 Hz, J_{56b} = 7.3 Hz, 1H, H-6b^V), 3.61 (ddd, $^2J_{ab}$ = 10.2 Hz, J = 6.8 Hz, J = 5.4 Hz, 1H, OCH_2CHCH$_2$), 3.17–3.09 (m, 2H, $OCH_2CH_2CH_2N$), 2.02–1.96 (m, 2H, $OCH_2CH_2CH_2N$). ^{13}C NMR (150 MHz, D_2O): δ 108.7 (C-1^{II}), 108.0 (C-1^V) 107.9, 107.9 (C-1^{III}, C-1^{IV}), 100.8 (C-1^I), 83.6 (C-4^V), 82.8 (C-4^{II}), 82.5 (2C, C-4^{III}, C-4^{IV}), 82.3, 82.3, 82.2 (C-2^{III}, C-2^{IV}, C-2^V), 82.0 (C-2^{II}), 77.7 (C-3^{II}), 77.5 (2C, C-3^{III}, C-3^{IV}), 77.3 (C-3^V), 77.0 (C-5^{II}), 76.6, 76.5(C-5^{III}, C-5^{IV}), 72.7 (C-5^I), 71.5 (C-3^I), 71.5 (C-5^V), 70.9 (C-2^I), 67.8 (C-6^I), 67.6 (C-4^I), 66.0 (OCH_2), 63.8 (C-6^V), 62.1 (2C, C-6^{III}, C-6^{IV}), 61.9 (C-6^{II}), 38.5 ($OCH_2CH_2CH_2N$), 27.6 ($OCH_2CH_2CH_2N$). HRMS (ESI): Calcd m/z for $[M + H]^+$ $C_{33}H_{59}NO_{26}$ 886.3398, found 886.3396. Calcd m/z for $[M + Na]^+$ $C_{33}H_{59}NO_{26}$ 908.3218, found 908.3209.

3-Trifluoroacetamidopropyl 2-*O*-benzoyl-3,6-di-*O*-benzyl-5-*O*-chloroacetyl-β-D-galactofuranosyl-(1→5)-2-*O*-benzoyl-3,6-di-*O*-benzyl-β-D-galactofuranosyl-(1→3)-2-*O*-benzoyl-4,6-di-*O*-benzyl-α-D-mannopyranoside (28). A carefully dried mixture of **5** (15 mg, 0.013 mmol) and **4** (14 mg, 0.022 mmol) was dissolved in CH_2Cl_2 (1.5 mL), 30 mg of MS300 AW powder was added, and the mixture was stirred for 20 min. Then at −78 °C TMSOTf (1 μL, 0.015 mmol) was added and the mixture was kept in the temperature range −20 to −10 °C for 1 h, then at −15 °C the reaction mixture was quenched by the addition of 1 drop of Et_3N. Column chromatography (toluene–EtOAc 12 : 1) gave **27** (13 mg, 60%) as a colorless oil. R_f = 0.50 (toluene–ethyl acetate 5 : 1). $[\alpha]_D$ = −40° (c = 1, EtOAc). ^{1}H NMR (600 MHz, $CDCl_3$): δ 8.04–7.96, 7.66–7.10 (m, 45H, PhH), 5.53 (dd, J_{12} = 1.8 Hz, J_{23} = 3.1 Hz, 1H, H-2^I), 5.49 (s, 1H, H-1^{III}), 5.48 (s, 1H, H-1^{II}), 5.46 (d, J_{23} = 1.8 Hz, 1H, H-2^{III}), 5.43 (d, J_{23} = 1.3 Hz, 1H, H-2^{II}), 5.22 (m, 1H, H-5^{III}), 4.93 (d, J_{12} = 1.8 Hz, 1H, H-1^I), 4.90 (d, J_{ab} = 11.2 Hz, 1H, 4-*O*-PhCH_2^{I}), 4.74 (d, J_{ab} = 11.5 Hz, 1H, PhCH_2), 4.65 (d, J_{ab} = 12.0 Hz, 1H, PhCH_2), 4.64 (d, J_{ab} = 12.0 Hz, 1H, PhCH_2), 4.53 (d, J_{ab} = 12.0 Hz, 1H, PhCH_2), 4.49–4.42 (m, 3H, PhCH_2), 4.36 (dd, J_{23} = 3.1 Hz, J_{34} = 9.5 Hz, 1H, H-3^I), 4.34–4.30 (m, 3H, PhCH_2), 4.29–4.26 (m, 2H, H-4^{III}, H-4^{II}), 4.22 (d, J_{ab} = 12.1 Hz, 1H, PhCH_2), 4.31 (br d, J_{34} = 5.9 Hz, 1H, H-3^{II}), 4.07 (m, 1H, H-5^{II}), 3.94 (t, J_{34} = J_{45} = 9.5 Hz, 1H, H-4^I), 3.82 (d, J_{ab} = 14.6 Hz, 1H, C(O)CH_2Cl), 3.81 (m, 1H, H-3^{III}), 3.78 (d, J_{ab} = 14.6 Hz, 1H, C(O)CH_2Cl), 3.75 (m, 1H, OCH_2CH$_2$CH$_2$), 3.73 (m, 2H, H-6a^I, H-6b^I), 3.61 (dd, $^2J_{6a6b}$ = 10.2 Hz, J_{56a} = 8.0 Hz, 1H, H-6a^{II}), 3.52 (m, 1H, OCH_2CH$_2$CH$_2$), 3.45 (dd, $^2J_{6a6b}$ = 10.2 Hz, J_{56b} = 3.6 Hz, 1H, H-6b^{II}), 3.44–3.33 (m, 4H, $OCH_2CH_2CH_2N$, H-6a^{III}, H-6b^{III}, $OCH_2CH_2CH_2N$), 1.85 (m, 2H, $OCH_2CH_2CH_2N$). ^{13}C NMR (150 MHz, $CDCl_3$): δ 166.9 (*C*(O)CH_2Cl), 165.7–165.1 (Ph*C*O), 138.3–137.2 (quat. Ph), 133.4–127.3 (Ph), 106.3 (C-1^{III}), 102.7 (C-1^{II}), 98.0 (C-1^I), 84.3 (C-3^{II}), 82.9 (C-3^{III}), 82.8 (C-4^{II}), 81.8 (C-2^{II}), 81.6 (C-2^{III}), 80.9 (C-4^{III}), 75.0 (4-*O*-Ph*C*H$_2$^{I}), 74.9 (C-5^{II}), 73.5, 73.5 (2Ph*C*H$_2$), 73.3 (Ph*C*H$_2$), 73.1 (C-4^I), 72.8 (Ph*C*H$_2$), 72.6 (C-5^{III}), 72.3 (Ph*C*H$_2$), 72.1 (C-5^I), 71.5 (C-6^{II}), 69.1 (C-6^I), 68.8 (C-6^{III}), 68.1 (C-2^I), 65.6 (O*C*H$_2$CH$_2$CH$_2$N), 40.6 (C(O)*C*H$_2$Cl), 37.5 ($OCH_2CH_2CH_2N$), 28.4 ($OCH_2CH_2CH_2N$). HRMS (ESI): Calcd m/z for $[M + Na]^+$ $C_{88}H_{87}ClF_3NO_{21}$ 1608.5303, found 1608.5304. Calcd m/z for $[M + K]^+$ $C_{88}H_{87}ClF_3NO_{21}$ 1624.5043, found 1624.5027.

3-Trifluoroacetamidopropyl 2-*O*-benzoyl-3,6-di-*O*-benzyl-β-D-galactofuranosyl-(1→5)-2-*O*-benzoyl-3,6-di-*O*-benzyl-β-D-galactofuranosyl-(1→3)-2-*O*-benzoyl-4,6-di-*O*-benzyl-α-D-mannopyranoside (29). Trisaccharide **28** (8 mg, 0.005 mmol) was treated according to GP I with thiourea (10 mg, 0.14 mmol) and collidine (2.5 μL, 0.017 mmol) in MeOH (1.2 mL). Column chromatography (toluene–EtOAc 7 : 1) gave **29** (6 mg, 80%) as a colorless oil. R_f = 0.47 (toluene–ethyl acetate 5 : 1). $[\alpha]_D$ = −40° (c = 1, EtOAc). ^{1}H NMR (600 MHz, $CDCl_3$): δ 8.04–7.95, 7.59–7.10 (m, 45H, PhH), 5.54 (dd, J_{12} = 1.9 Hz, J_{23} = 3.1 Hz, 1H, H-2^I), 5.52 (s, 1H, H-1^{III}), 5.50 (s, 1H, H-1^{II}), 5.48 (d, J_{23} = 1.8 Hz, 1H, H-2^{III}), 5.36 (d, J_{23} = 1.4 Hz, 1H, H-2^{II}), 4.93 (d, J_{12} = 1.9 Hz, 1H, H-1^I), 4.90 (d, J_{ab} = 11.2 Hz, 1H, 4-*O*-PhCH_2^{I}), 4.74 (d, J_{ab} = 11.5 Hz, 1H, PhCH_2), 4.65 (d, J_{ab} = 12.0 Hz, 1H, PhCH_2), 4.63 (d, J_{ab} = 12.0 Hz, 1H, PhCH_2), 4.53 (d, J_{ab} = 12.0 Hz, 1H, PhCH_2), 4.50–4.44 (m, 3H, PhCH_2), 4.38 (dd, J_{23} = 3.1 Hz, J_{34} = 9.5 Hz, 1H, H-3^I), 4.34 (m, 2H, PhCH_2), 4.32–4.29 (m, 2H, H-4^{II}, PhCH_2), 4.27 (d, J_{ab} = 12.0 Hz, 1H, PhCH_2), 4.22 (br d, J_{34} = 5.9 Hz, 1H, H-3^{II}), 4.13–4.09 (m, 2H, H-4^{III}, H-5^{II}), 4.04 (dd, J_{32} = 1.8 Hz, J_{34} = 6.1 Hz, 1H, H-3^{III}), 3.94 (t, J_{34} = J_{45} = 9.5 Hz, 1H, H-4^I), 3.83 (m, 1H, H-5^I), 3.79–3.74 (m, 3H, OCH_2CH$_2$CH$_2$, H-6a^I, H-6b^I), 3.74–3.69 (m, 2H, H-5^{III}, H-6a^{III}), 3.67 (dd, $^2J_{6a6b}$ = 10.3 Hz, J_{56a} = 7.9 Hz, 1H, H-6a^{II}), 3.52 (m, 1H, OCH_2CH$_2$CH$_2$), 3.49 (dd, $^2J_{6a6b}$ = 10.3 Hz, J_{56b} = 3.6 Hz, 1H, H-6b^{II}), 3.44 (m, 1H, $OCH_2CH_2CH_2N$), 3.36 (m, 1H, $OCH_2CH_2CH_2N$), 3.29 (dd, $^2J_{6a6b}$ = 9.8 Hz, J_{56b} = 7.8 Hz, 1H, H-6a^{III}), 3.26 (dd, $^2J_{6a6b}$ = 9.8 Hz, J_{56b} = 4.1 Hz, 1H, H-6b^{III}), 2.25 (br s, 1H, OH), 1.85 (m, 2H, $OCH_2CH_2CH_2N$). ^{13}C NMR (150 MHz, $CDCl_3$): δ 165.7–165.2 (Ph*C*O), 138.3–137.2 (quat. Ph), 133.3–127.3 (Ph), 106.6 (C-1^{III}), 102.7 (C-1^{II}), 98.0 (C-1^I), 84.3 (C-3^{II}), 83.2 (C-3^{III}), 82.9 (C-4^{II}), 82.8(C-4^{III}), 81.9 (2C, C-2^{II}, C-2^{III}), 75.1 (4-*O*-Ph*C*H$_2$^{I}), 74.6 (C-5^{II}), 73.5, 73.5 (C-3^I, Ph*C*H$_2$), 73.3 (Ph*C*H$_2$), 73.2 (C-4^I), 72.6 (Ph*C*H$_2$), 72.1 (Ph*C*H$_2$), 72.1 (C-5^I), 71.6, 71.6 (C-6^{II}, C-6^{III}), 70.0 (C-5^I), 69.2 (C-6^I), 68.1 (C-2^I), 65.5 (O*C*H$_2$CH$_2$CH$_2$N), 37.5 ($OCH_2CH_2CH_2N$), 28.3 ($OCH_2CH_2CH_2N$). HRMS (ESI): Calcd m/z for $[M + NH_4]^+$ $C_{86}H_{86}F_3NO_{20}$ 1527.6034, found 1527.6025. Calcd m/z for $[M + Na]^+$ $C_{86}H_{86}F_3NO_{20}$ 1532.5587, found 1532.5586. Calcd m/z for $[M + K]^+$ $C_{86}H_{86}F_3NO_{20}$ 1548.5327, found 1548.5319.

3-Trifluoroacetamidopropyl 2,3,5,6-tetra-*O*-benzoyl-β-D-galactofuranosyl-(1→5)-2-*O*-benzoyl-3,6-di-*O*-benzyl-β-D-galactofuranosyl-(1→5)-2-*O*-benzoyl-3,6-di-*O*-benzyl-β-D-galactofuranosyl-(1→5)-2-*O*-benzoyl-3,6-di-*O*-benzyl-β-D-galactofuranosyl-(1→3)-2-*O*-benzoyl-4,6-di-*O*-benzyl-α-D-mannopyranoside (30). A carefully dried mixture of **29** (6 mg, 0.004 mmol) and **6** (7 mg,

0.006 mmol) was dissolved in CH_2Cl_2 (0.5 mL), powder MS300 AW (10 mg) was added, and the mixture was stirred for 20 min. Then the temperature was decreased to −78 °C and a solution of TMSOTf (0.3 μL, 0.002 mmol) in 0.1 mL CH_2Cl_2 was added. The reaction mixture was kept at −20 to −30 °C for 1 h and then at −15 °C was stopped by the addition of 1 drop of Et_3N. Column chromatography (toluene–EtOAc 8 : 1) gave **30** (8 mg, 80%) as a colorless oil. R_f = 0.48 (toluene–ethyl acetate 5 : 1). $[\alpha]_D$ = −38° (*c* = 1, EtOAc). ^{1}H NMR (600 MHz, $CDCl_3$): δ 8.03–7.84, 7.56–7.03 (m, 80H, PhH), 6.60 (br s, 1H, CH_2NH), 5.78 (m, 1H, H-5^V), 5.60 (s, 1H, H-1^{IV}), 5.59 (dd, J_{32} = 1.6 Hz, J_{34} = 5.1 Hz, 1H, H-3^V), 5.57 (s, 1H, H-1^V), 5.56 (d, J_{23} = 1.6 Hz, 1H, H-2^V), 5.55 (m, 1H, H-2^I), 5.54 (s, 1H, H-1^{III}), 5.52 (d, J_{23} = 2.3 Hz, 1H, H-2^{III}), 5.50 (d, J_{23} = 1.5 Hz, 1H, H-2^{IV}), 5.49 (s, 1H, H-1^{II}), 5.36 (d, J_{23} = 1.5 Hz, 1H, H-2^{II}), 4.93 (d, J_{12} = 1.9 Hz, 1H, H-1^I), 4.89 (d, J_{ab} = 11.2 Hz, 1H, 4-*O*-PhCH_2^{I}), 4.71 (d, J_{ab} = 11.4 Hz, 1H, PhCH_2), 4.66 (d, J_{ab} = 11.2 Hz, 1H, PhCH_2), 4.63 (d, J_{ab} = 11.9 Hz, 1H, PhCH_2), 4.52 (d, J_{ab} = 12.0 Hz, 1H, PhCH_2), 4.51–4.43 (m, 6H, 3PhCH_2, H-6a^V, H-4^V, H-6b^V), 4.38 (dd, J_{32} = 3.2 Hz, J_{34} = 9.5 Hz, 1H, H-3^I), 4.34–4.31 (m, 3H, 2PhCH_2, H-4^{II}), 4.30 (dd, J_{32} = 2.3 Hz, J_{34} = 3.4 Hz, 1H, H-3^{III}), 4.24–4.22 (m, 2H, H-3^{II}, PhCH_2), 4.21–4.16 (m, 6H, H-4^{III}, 3PhCH_2, H-3^{IV}, H-4^{IV}), 4.11 (m, 1H, H-5^{II}), 4.02 (m, 1H, H-5^{III}), 3.98 (m, 1H, H-5^{IV}), 3.94 (t, J_{34} = J_{45} = 9.5 Hz, 1H, H-4^I), 3.82 (m, 1H, H-5^I), 3.78–3.73 (m, 3H, OCH_2CH$_2$CH$_2$, H-6a^I, H-6b^I), 3.68–3.65 (m, 2H, H-6a^{II}, H-6a^{III}), 3.61 (m, 1H, H-6a^{IV}), 3.52 (m, 1H, OCH_2CH$_2$CH$_2$), 3.50 (dd, $^2J_{6a6b}$ = 11.0 Hz, J_{56b} = 4.7 Hz, 1H, H-6b^{II}), 3.46–3.33 (m, 4H, OCH$_2$CH$_2$CH_2N, H-6b^{IV}, H-6b^{III}, OCH$_2$CH$_2$CH_2N), 1.85 (m, 2H, OCH$_2$CH_2CH$_2$N). ^{13}C NMR (150 MHz, $CDCl_3$): δ 165.9–165.1 (Ph*C*O), 138.2–137.7 (quat. Ph), 133.4–127.2 (Ph), 106.4 (C-1^{III}), 106.3, 106.3 (C-1^{III}, C-1^{IV}), 102.9 (C-1^{II}), 98.0 (C-1^I), 84.3 (C-3^{II}), 83.8 (C-3^{III}), 83.5 (C-3^{IV}), 83.0 (C-4^{II}), 82.7 (C-4^{III}), 82.4 (C-4^{IV}), 82.2, 82.1 (C-2^{III}, C-2^{IV}), 81.8 (C-2^{II}), 81.8 (C-4^V), 81.6 (C-2^V), 77.2 (C-3^V), 75.0 (2C, 4-*O*-Ph*C*H$_2$^{I}, C-5^{IV}), 74.3 (C-5^{II}), 73.6 (C-3^I), 73.5 (C-5^{III}), 73.4 (Ph*C*H$_2$), 73.2 (Ph*C*H$_2$), 73.2 (C-4^I), 73.1 (Ph*C*H$_2$), 72.7 (Ph*C*H$_2$), 72.5 (Ph*C*H$_2$), 72.2 (Ph*C*H$_2$), 72.1 (C-5^I), 72.1 (C-6^{III}), 71.8 (C-6^{IV}), 71.2 (C-6^{II}), 70.4 (C-5^V), 69.2 (C-6^I), 68.2 (C-2^I), 65.5 (O*C*H$_2$CH$_2$CH$_2$N), 63.7 (C-6^{III}), 37.5 (OCH$_2$CH$_2$*C*H$_2$N), 28.3 (OCH$_2$*C*H$_2$CH$_2$N). HRMS (ESI): Calcd *m*/*z* for $[M + NH_4]^+$ $C_{147}H_{138}F_3NO_{35}$ 2551.9340, found 2551.9316. Calcd *m*/*z* for $[M + Na]^+$ $C_{147}H_{138}F_3NO_{35}$ 2556.8894, found 2556.8887. Calcd *m*/*z* for $[M + K]^+$ $C_{147}H_{138}F_3NO_{35}$ 2572.8633, found 2572.8616.

3-Aminopropyl β-D-galactofuranosyl-(1→5)-β-D-galactofuranosyl-(1→5)-β-D-galactofuranosyl-(1→5)-β-D-galactofuranosyl-(1→3)-α-D-mannopyranoside (2). Compound **30** (8 mg, 3.1 μmol) was dissolved in 1 mL of EtOAc–MeOH (1 : 1) and 10% Pd/C (11 mg) was added. The reaction mixture was vigorously stirred under a H_2 atmosphere for 3 h and then filtered through the Celite layer. The filtrate was concentrated *in vacuo*, dissolved in 0.5 mL of 0.1 M MeONa in MeOH, one drop of water was added, and the mixture was kept overnight, then 3 μL of AcOH were added, the mixture was diluted with water and concentrated *in vacuo*. Gel-chromatography and subsequent lyophilization gave **2** (2.0 mg, 72%) as a white foam. ^{1}H NMR (500 MHz, D_2O): δ 5.23 (br s, 1H, H-1^V), 5.20 (m, 2H, H-1^{III}, H-1^{IV}), 5.13 (br s, 1H, H-1^{II}), 4.92 (br s, 1H, H-1^I), 4.20–4.10 (m, 11H, H-4^{II}, H-4^{III}, H-4^{IV}, H-2^{II}, H-2^{III}, H-2^{IV}, H-2^V, H-3^{II}, H-3^{III}, H-3^{IV}, H-3^V), 4.10–4.07 (m, 2H, H-3^V, H-4^V), 4.00–3.91 (m, 4H, H-5^{II}, H-5^{III}, H-5^{IV}, H-6a), 3.91–3.60 (m, 17H), 3.19–3.12 (m, 2H, OCH$_2$CH$_2$CH_2N), 2.06–1.98 (m, 2H, OCH$_2$CH_2CH$_2$N). ^{13}C NMR (125 MHz, D_2O): δ 108.3 (3C, C-1^{III}, C-1^{IV}, C-1^V), 105.7 (C-1^{II}), 100.8 (C-1^I), 83.9 (C-4^V), 83.3 (C-4^{II}), 82.8, 82.7, 82.6, 82.5 (C-4^{III}, C-4^{IV}, C-2^{II}, C-2^{III}, C-2^{IV}, C-2^V), 78.2 (C-3^{II}), 77.7, 77.7, 77.6 (C-3^{III}, C-3^{IV}, C-3^V), 77.2 (C-5^{II}), 76.9, 76.9, 76.8 (C-5^{III}, C-5^{IV}, C-3^I), 74.0 (5-3^I), 71.8 (C-5^V), 67.9 (C-2^I), 66.3 (C-4^I), 66.2 (OCH$_2$), 64.0 (C-6^V), 62.4–62.2 (C-6^I, C-6^{II}, C-6^{III}, C-6^{IV}), 38.7 (OCH$_2$CH$_2$*C*H$_2$N), 27.9 (OCH$_2$*C*H$_2$CH$_2$N). HRMS (ESI): Calcd *m*/*z* for $[M + H]^+$ $C_{33}H_{59}NO_{26}$ 886.3398, found 886.3402. Calcd *m*/*z* for $[M + Na]^+$ $C_{33}H_{59}NO_{26}$ 908.3218, found 908.3218.

Acknowledgements

This work was supported by RSF grant 14-23-00199 (NEN). We thank Dr A.S. Dmitrenok for recording the NMR-spectra and Dr A.O. Chizhov for recording the high resolution mass spectra at the Department of Structural Studies of the Zelinsky Institute of Organic Chemistry, Moscow.

Notes and references

1 J. P. Latgé, *Clin. Microbiol. Rev.*, 1999, **12**, 310.
2 J. P. Latgé, H. Kobayashi, J. P. Debeaupuis, M. Diaquin, J. Sarfati, J. M. Wieruszeski, E. Parra, J. P. Bouchara and B. Fournet, *Infect. Immun.*, 1994, **62**, 5424.
3 L. Cattiaux, B. Sendid, M. Collot, E. Machez, D. Poulain and J. M. Mallet, *Bioorg. Med. Chem.*, 2011, **19**, 547.
4 H. M. Zuurmond, P. A. M. van der Klein, G. H. Veeneman and J. H. van Boom, *Recl. Trav. Chim. Pays-Bas*, 1990, **109**, 437.
5 G. H. Veeneman, S. Notermans, R. M. J. Liskamp, G. A. van der Marel and J. H. van Boom, *Tetrahedron Lett.*, 1987, **28**, 6695.
6 M. Fu, G. Zhang and J. Ning, *Carbohydr. Res.*, 2005, **340**, 25.
7 A. Imamura and T. Lowary, *Trends Glycosci. Glycotechnol.*, 2011, **23**, 134.
8 V. B. Krylov, D. A. Argunov, D. Z. Vinnitskiy, S. A. Verkhnyatskaya, A. G. Gerbst, N. E. Ustyuzhanina, A. S. Dmitrenok, J. Huebner, O. Holst, H.-C. Siebert and N. E. Nifantiev, *Chem. – Eur. J.*, 2014, **20**, 16516.
9 V. B. Krylov, A. G. Gerbst, D. A. Argunov, A. S. Dmitrenok, A. S. Shashkov, Z. Kaczynski, J. Huebner, O. Holst and N. E. Nifantiev, *Chem. – Eur. J.*, 2015, **21**, 1749.
10 T. Mandai, H. Okumoto, T. Oshitari, K. Nakanishi, K. Mikuni, K. J. Hara and K. Z. Hara, *Heterocycles*, 2000, **52**, 129.
11 K. Sato, H. Seki, A. Yoshitomo, H. Nanaumi, Y. Takai and Y. Ishido, *J. Carbohydr. Chem.*, 1998, **17**, 703.
12 V. B. Krylov, D. A. Argunov and N. E. Nifantiev, *Mendeleev Commun.*, 2014, **24**, 336.

13 A. H. Haines, *Adv. Carbohydr. Chem. Biochem.*, 1976, **33**, 11.
14 T. Ziegler, P. Kováč and C. P. Glaudemans, *Carbohydr. Res.*, 1989, **194**, 185.
15 M. Barbier, E. Grand and J. Kovensky, *Carbohydr. Res.*, 2007, **342**, 2635.
16 T. Ogawa, S. Nakabayashi and T. Kitajima, *Carbohydr. Res.*, 1983, **114**, 225.
17 J. Lüning, U. Möller, N. Debski and P. Welzel, *Tetrahedron Lett.*, 1993, **34**, 5871.
18 H. M. Zuurmond, P. A. M. van der Klein, G. A. van der Marel and J. H. van Boom, *Tetrahedron*, 1993, **49**, 6501.
19 A. A. Karelin, Y. E. Tsvetkov, G. Kogan, S. Bystricky and N. E. Nifantiev, *Russ. J. Bioorg. Chem.*, 2007, **33**, 110.
20 P. A. Belyakov, V. I. Kadentsev, A. O. Chizhov, N. G. Kolotyrkina, A. S. Shashkov and V. P. Ananikov, *Mendeleev Commun.*, 2010, **20**, 125.
21 C. Gallo-Rodriguez, L. Gandolfi and R. M. de Lederkremer, *Org. Lett.*, 1999, **1**, 245.

Organic LETTERS

Letter

pubs.acs.org/OrgLett

The Use of Pyranoside-into-Furanoside Rearrangement and Controlled O(5) → O(6) Benzoyl Migration as the Basis of a Synthetic Strategy To Assemble (1→5)- and (1→6)-Linked Galactofuranosyl Chains

Dmitry A. Argunov, Vadim B. Krylov, and Nikolay E. Nifantiev*

Laboratory of Glycoconjugate Chemistry, N.D. Zelinsky Institute of Organic Chemistry, Russian Academy of Sciences, Leninsky Prospect 47, 119991 Moscow, Russian Federation

Supporting Information

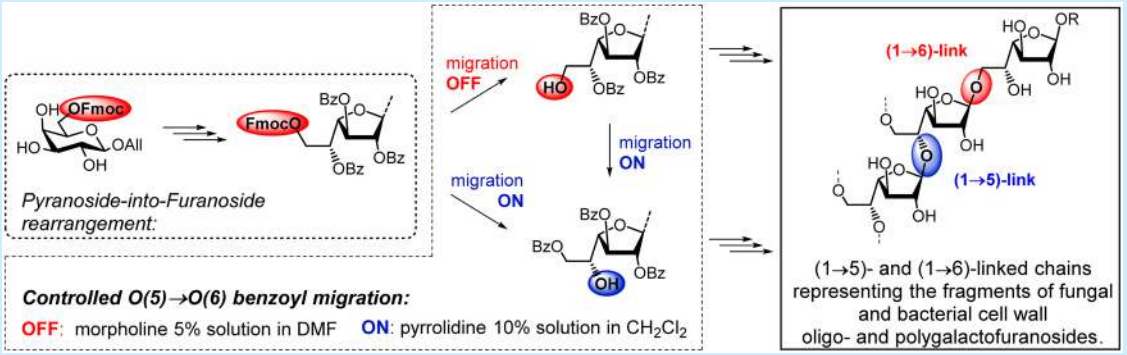

ABSTRACT: A new pyranoside-into-furanoside (PIF) rearrangement of selectively protected galactopyranosides, followed by controlled O(5) → O(6) benzoate migration, gives either 5-OH or 6-OH products. It has been applied for the synthesis of four oligosaccharides related to the galactomannan from *Aspergillus fumigatus*. The assembly of target oligosaccharides containing both (1→5) and (1→6) linkages between galactofuranosyl residues was performed by applying terminal mannoside and digalactofuranoside blocks, forming a versatile approach toward fungal and bacterial carbohydrate antigens containing both 5-O- and 6-O-substituted galactofuranoside residues.

Aspergillus fumigatus is a dangerous fungal pathogen that causes severe and often fatal invasive aspergillosis (IA) in immunocompromised patients.[1] At risk are patients with cancer and those undergoing intensive immunosuppressive therapy after receiving organ transplants.[2] Galactomannan is a specific carbohydrate antigen of *A. fumigatus*,[3] and therefore, its detection in the patient serum is used for diagnosis of IA.[1] Oligosaccharide ligands structurally related to galactomannan could potentially help with the development of vaccines against this dangerous pathogen.

Galactomannan represents a structurally diverse heteropolysaccharide build up from a poly-D-mannose backbone with oligogalactofuranoside side chains attached to some of the mannose units via (1→3) or (1→6) bonds.[3] The galactofuranoside residues in the side chains are mainly β-(1→5)-linked, although the presence of β-(1→6) linkages has also been reported (Figure 1A).[4] It is noteworthy that alternating (1→5)-/(1→6)-linked galactofuranoside chains are also produced by some other microorganisms, including the dangerous pathogen *Mycobacterium tuberculosis* as well as other *Mycobacterium* species (Figure 1B).[5] Polysaccharides of the bacteria *Actinobacillus pleuropneumoniae*[6] and *Bifidobacterium catenulatum*[7] also contain (1→5)-/(1→6)-linked galactofuranoside backbones bearing α-galactopyranoside branches (Figure 1C).

The need for oligosaccharide ligands related to galactomannan continues to challenge the development of synthetic approaches for their acquisition. Previously, the preparations of different oligosaccharide fragments of galactomannan corresponding to the homogalactofuranosyl or heterosaccharide chains were described.[8] In all synthesized oligosaccharides, the galactofuranoside units were interconnected with (1→5) linkages. However, for detailed immunological investigations, a more representative series of shorter and longer spacer armed oligosaccharide antigens with both (1→5) and (1→6) linkages between galactofuranosyl units was required. Herein we describe the synthesis of tri-, penta-, and heptasaccharides **1**–**3** related to the galactomannan of *A. fumigatus* as as well as pentasaccharide **4** containing one (1→6) linkage between galactofuranoside residues, which is isomeric to compound **2** (Figure 1).

Received: September 11, 2016
Published: October 19, 2016

DOI: 10.1021/acs.orglett.6b02735
Org. Lett. 2016, 18, 5504–5507

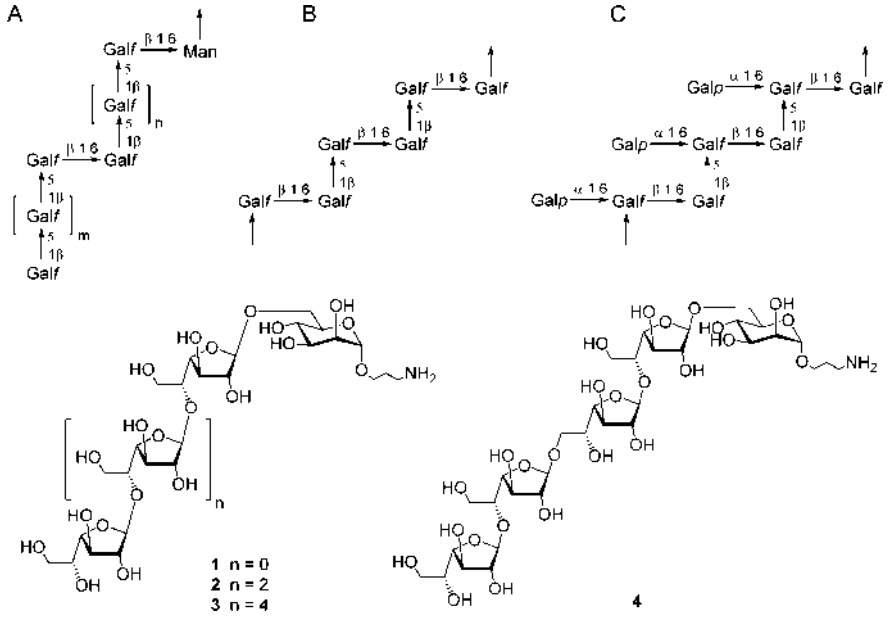

Figure 1. Structures of (A) galactomannan from *A. fumigatus*,[4] (B) arabinogalactan from *M. tuberculosis*,[5] (C) galactan from *A. pleuropneumoniae*[6] and *B. catenulatum*,[7] and target spacered oligosaccharides **1**–**4** related to galactomannan from *A. fumigatus*.

The synthesis of pentasaccharide **2** was previously performed by us with the use of a temporarily 5′-O-chloroacetylated galactofuranoside block suitable for homo-(1→5)-chain elongation.[8e] Herein we report syntheses based on the use of selectively protected allyl galactofuranoside **9** bearing a selectively removable 9-fluorenylmethoxycarbonate (Fmoc) group at O(6). Thus, O(6) deprotection permits subsequent chain elongation via (1→6) glycosylation. The choice of the Fmoc group as a temporary protection was argued by its stability under many reaction conditions, including ones in automated solid-phase synthesis.[9]

In order to prepare galactofuranoside **9**, regioselective introduction of the Fmoc group into allyl *β*-galactopyranoside **5**[10] in the presence of 2,6-lutidine was performed to give 6-O-acylated derivative **6** in 63% yield (Scheme 1).[11] Then **6** was transformed into isomeric furanoside **8** using the recently discovered pyranoside-into-furanoside (PIF) rearrangement[12] via totally sulfated intermediate **7**. Further per-O-benzoylation of **8** gave the desired bifunctional block **9**, which was transformed into glycosyl donor **10** via deallylation and imidation (**9** → **10**) or into 6-hydroxyglycosyl acceptor **11** by removal of the Fmoc group (Scheme 1).

Basic reaction conditions commonly used for Fmoc cleavage (e.g., treatment with piperidine in DMF[13]) could be accompanied by side benzoate migration. The O(5) → O(6) migration of the benzoyl group was also observed during acidic detritylation.[14] Thus, the search for a reliable Fmoc deprotection protocol was performed, first with the use of **9** as a model substrate. In particular, it was found that removal of the Fmoc group could be efficiently performed by treatment with more accessible pyrrolidine[15] (20% solution in DMF). The reaction was complete in less than 1 min. However, the formation of a mixture of the desired monosaccharide **11** (70%) and the benzoate migration product **12** (10%) was observed. The structure of product **12** was evident from proton chemical shifts (5.65 ppm for H(5) and 4.05–4.10 ppm for both H(6) in **11** vs 4.47 ppm for H(5) and 4.61 and 4.48 ppm for H(6) in **12**). To improve the reaction selectivity, we applied

Scheme 1. Synthesis of Galactofuranoside Products 8–12 Employing PIF Rearrangement and Controlled O(5) → O(6) Benzoyl Migration

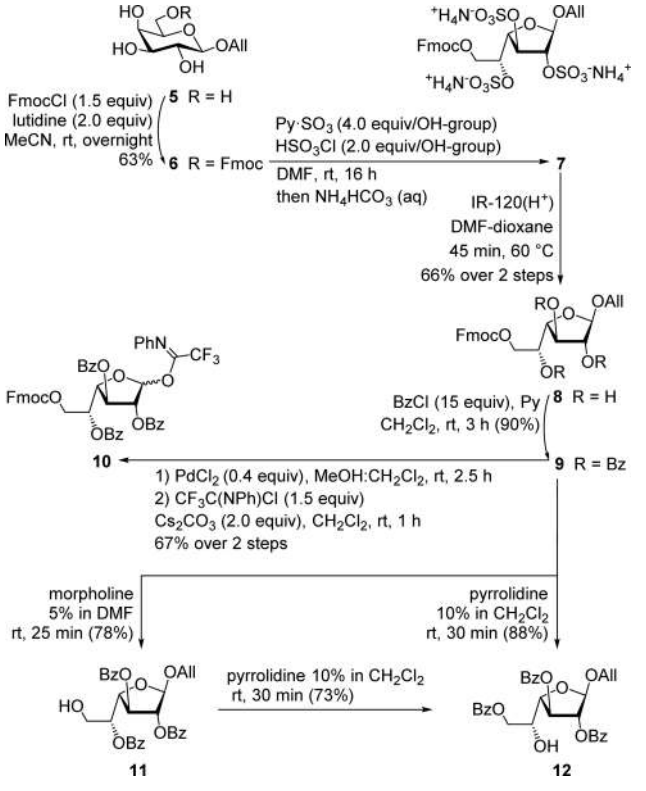

morpholine (5% solution in DMF) as a milder base. The reaction was complete in 25 min and gave furanoside **11** (78%) with only a trace (4%) of the migration product **12**, which was separated by SiO_2 column chromatography.

Product **12** with a free OH group at O(5) can be regarded as a convenient precursor for the synthesis of 5-O-substituted galactofuranoside derivatives, including the target (1→5)-linked

DOI: 10.1021/acs.orglett.6b02735
Org. Lett. 2016, 18, 5504–5507

Scheme 2. Assembly of Target Structures 1−4

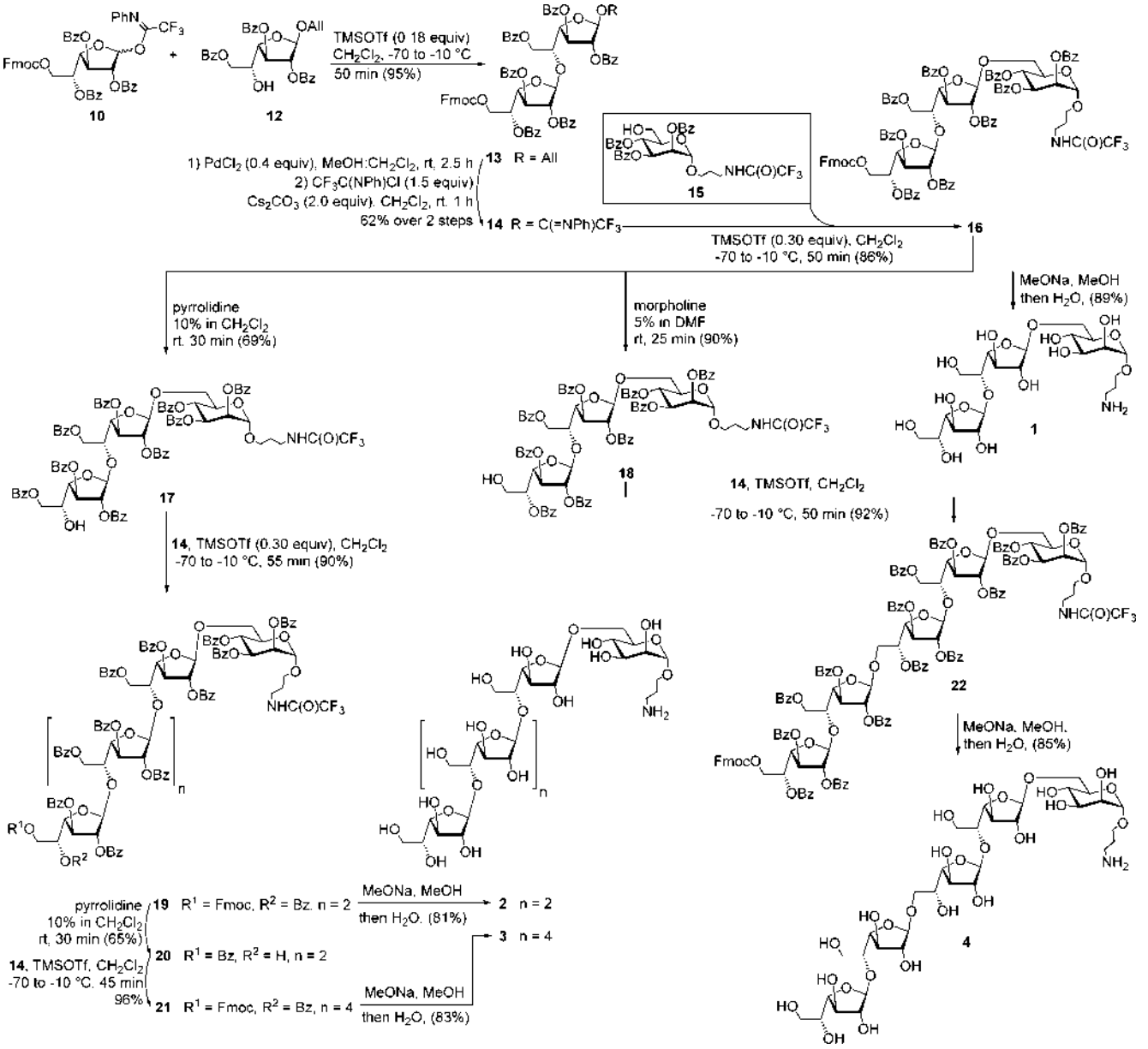

galactofuranoside chains related to *A. fumigatus* galactomannan. Thus, having encountered this side O(5) → O(6) benzoyl migration, we decided to perform this reaction in a preparative way in CH_2Cl_2 because it is known that the use of nonpolar solvents increases the migration rate.[16] Indeed, the O(5) → O(6) benzoyl migration rate under the treatment with pyrrolidine (10%) was significantly greater in CH_2Cl_2 than in DMF. Even initially the reaction migration product **12** was observed (TLC control), and after 20−30 min, only the product of benzoate migration, **12**, was detected in the reaction mixture. The 6-OH product **11** could be converted into the 5-OH derivative **12** in 73% yield by treatment with pyrrolidine in CH_2Cl_2, but the reverse reaction (**12** → **11**) in DMF does not take place.

For the synthesis of digalactoside building block **14**, TMSOTf-promoted coupling of donor **10** and acceptor **12** was performed to give the β-(1→5)-linked disaccharide precursor **13** (Scheme 2). Its structure, particularly the β configuration of the newly formed bond, was determined on the basis of the singlet shape of the H(1)′ signal ($J_{H(1)',H(2)'}$ < 1.0 Hz) and the characteristic low-field chemical shift of C(1)′ (105.5 ppm) in NMR spectra.[17] Removal of the allyl aglycon in **13** and the further introduction of the imidate group gave disaccharide donor **14**. Its coupling with known[8e] mannose acceptor **15** proceeded with stereoselective β-(1→6) bond formation to give the trisaccharide product **16**. The characteristic for β-galactofuranosides chemical shift of C(1)′ (106.4 ppm) and singlet shape of the H(1)′ signal as well as the low-field chemical shift of C(6) (66.1 ppm for **16** vs 61.4 ppm for **15**) confirmed the structure of the formed product. Deblocking of **16** by treatment with MeONa in MeOH afforded the desired trisaccharide **1**.

The conditions developed for the controlled Fmoc deprotection with or without Bz migration toward either 5-OH or 6-OH derivatives were applied for the transformation of trisaccharide **16**. Thus, its treatment with pyrrolidine in CH_2Cl_2 resulted in the formation of 5-hydroxy acceptor **17** in 69% yield. The structure of product **17** was confirmed by the low-

DOI: 10.1021/acs.orglett.6b02735
Org. Lett. 2016, 18, 5504−5507

field chemical shift of H(6)″ (4.48 ppm) and the high-field chemical shift of H(5)″ (4.35 ppm). On the other hand, removal of the Fmoc protection under "no migration" conditions by treatment with morpholine in DMF gave 6-OH acceptor **18** in 90% isolated yield. The structure of **18** was confirmed by the high-field shift of H(6)″ (3.95 ppm) and the low-field shift of H(5)″ (5.52 ppm).

Glycosylation of acceptors **17** and **18** by donor **14** gave protected oligosaccharides **19** and **22** containing β-(1→5)- and β-(1→6)-glycosyl bonds, respectively. Their deblocking afforded target pentasaccharides **2** and **4**. Removal of the Fmoc group in pentasaccharide **19** under "Bz migration" conditions (**19** → **20**) and subsequent glycosylation with donor **14** (**20** → **21**) afforded heptasaccharide **21**. Its deblocking gave the target heptasaccharide **3**.

In summary, a new approach for the synthesis of oligogalactofuranosyl chains built from β-(1→5)- and β-(1→6)-linked units was developed using PIF rearrangement in combination with controlled Bz migration under Fmoc removal conditions. The efficiency of the developed strategy was illustrated by the synthesis of tri-, penta-, and heptasaccharides related to the galactomannan of the *A. fumigatus* cell wall.

■ ASSOCIATED CONTENT

Supporting Information

The Supporting Information is available free of charge on the ACS Publications website at DOI: 10.1021/acs.orglett.6b02735.

Experimental procedures, complete characterization data, and copies of ^{1}H and ^{13}C NMR and mass spectra of all new compounds (PDF)

■ AUTHOR INFORMATION

Corresponding Author

*E-mail: nen@ioc.ac.ru.

Notes

The authors declare no competing financial interest.

■ ACKNOWLEDGMENTS

This work was supported by Russian Science Foundation Grant 14-23-00199 (N.E.N.). We thank Dr. A. S. Dmitrenok for recording the NMR spectra and Dr. A. O. Chizhov for recording the high-resolution mass spectra at the Department of Structural Studies of the Zelinsky Institute of Organic Chemistry, Moscow.

■ REFERENCES

(1) Latgé, J.-P. *Clin. Microbiol. Rev.* **1999**, *12*, 310−350.

(2) Herbrecht, R.; Denning, D. W.; Patterson, T. F.; Bennett, J. E.; Greene, R. E.; Oestmann, J. W.; Kern, W. V.; Marr, K. A.; Ribaud, P.; Lortholary, O.; Sylvester, R.; Rubin, R. H.; Wingard, J. R.; Stark, P.; Durand, C.; Caillot, D.; Thiel, E.; Chandrasekar, P. H.; Hodges, M. R.; Schlamm, H. T.; Troke, P. F.; de Pauw, B. *N. Engl. J. Med.* **2002**, *347*, 408−415.

(3) (a) Latgé, J. P.; Kobayashi, H.; Debeaupuis, J. P.; Diaquin, M.; Sarfati, J.; Wieruszeski, J. M.; Parra, E.; Bouchara, J. P.; Fournet, B. *Infect. Immun.* **1994**, *62*, 5424−5433. (b) Lee, M. J.; Sheppard, D. C. *J. Microbiol.* **2016**, *54*, 232−242.

(4) Kudoh, A.; Okawa, Y.; Shibata, N. *Glycobiology* **2015**, *25*, 74−87.

(5) (a) Richards, M. R.; Lowary, T. L. *ChemBioChem* **2009**, *10*, 1920−1938. (b) Daffe, M.; McNeil, M.; Brennan, P. J. *Carbohydr. Res.* **1993**, *249*, 383−398. (c) Lee, R. E. B.; Li, W.; Chatterjee, D.; Lee, R. E. *Glycobiology* **2005**, *15*, 139−151. (d) Tropis, M.; Lemassu, A.; Vincent, V.; Daffé, M. *Glycobiology* **2005**, *15*, 677−686.

(6) Beynon, L. M.; Perry, M. B.; Richards, J. C. *Can. J. Chem.* **1991**, *69*, 218−224.

(7) Nagaoka, M.; Hashimoto, S.; Shibata, H.; Kimura, I.; Kimura, K.; Sawada, H.; Yokokura, T. *Carbohydr. Res.* **1996**, *281*, 285−291.

(8) (a) Veeneman, G. H.; Notermans, S.; Liskamp, R. M. J.; van der Marel, G. A.; van Boom, J. H. *Tetrahedron Lett.* **1987**, *28*, 6695−6698. (b) Zuurmond, H. M.; van der Klein, P. A. M.; Veeneman, G. H.; van Boom, J. H. *Recl. Trav. Chim. Pays-Bas* **1990**, *109*, 437−441. (c) Cattiaux, L.; Sendid, B.; Collot, M.; Machez, E.; Poulain, D.; Mallet, J. M. *Bioorg. Med. Chem.* **2011**, *19*, 547−555. (d) Fu, M.; Zhang, G.; Ning, J. *Carbohydr. Res.* **2005**, *340*, 25−30. (e) Argunov, D. A.; Krylov, V. B.; Nifantiev, N. E. *Org. Biomol. Chem.* **2015**, *13*, 3255−3267.

(9) Seeberger, P. H. *Acc. Chem. Res.* **2015**, *48*, 1450−1463.

(10) Mandai, T.; Okumoto, H.; Oshitari, T.; Nakanishi, K.; Mikuni, K.; Hara, K. J.; Hara, K. Z. *Heterocycles* **2000**, *52*, 129.

(11) Ishihara, K.; Kurihara, H.; Yamamoto, H. *J. Org. Chem.* **1993**, *58*, 3791−3793.

(12) (a) Krylov, V. B.; Argunov, D. A.; Vinnitskiy, D. Z.; Verkhnyatskaya, S. A.; Gerbst, A. G.; Ustyuzhanina, N. E.; Dmitrenok, A. S.; Huebner, J.; Holst, O.; Siebert, H.-C.; Nifantiev, N. E. *Chem. - Eur. J.* **2014**, *20*, 16516−16522. (b) Krylov, V. B.; Gerbst, A. G.; Argunov, D. A.; Dmitrenok, A. S.; Shashkov, A. S.; Kaczynski, Z.; Huebner, J.; Holst, O.; Nifantiev, N. E. *Chem. - Eur. J.* **2015**, *21*, 1749−1754. (c) Vinnitskiy, D. Z.; Krylov, V. B.; Ustyuzhanina, N. E.; Dmitrenok, A. S.; Nifantiev, N. E. *Org. Biomol. Chem.* **2016**, *14*, 598−611. (d) Krylov, V. B.; Argunov, D. A.; Vinnitskiy, D. Z.; Gerbst, A. G.; Ustyuzhanina, N. E.; Dmitrenok, A. S.; Nifantiev, N. E. *Synlett* **2016**, *27*, 1659−1664.

(13) Vuljanic, T.; Bergquist, K.-E.; Clausen, H.; Roy, S.; Kihlberg, J. *Tetrahedron* **1996**, *52*, 7983−8000.

(14) (a) Pathak, A. K.; Pathak, V.; Seitz, L.; Maddry, J. A.; Gurcha, S. S.; Besra, G. S.; Suling, W. J.; Reynolds, R. C. *Bioorg. Med. Chem.* **2001**, *9*, 3129−3143. (b) Completo, G. C.; Lowary, T. L. *J. Org. Chem.* **2008**, *73*, 4513−4525.

(15) Chang, C.-D.; Waki, M.; Ahmad, M.; Meienhofer, J.; Lundell, E. O.; Haug, J. D. *Int. J. Pept. Protein Res.* **1980**, *15*, 59−66.

(16) Sjursnes, B. J.; Anthonsen, T. *Biocatal. Biotransform.* **1994**, *9*, 285−297.

(17) (a) Cyr, N.; Perlin, A. S. *Can. J. Chem.* **1979**, *57*, 2504−2511. (b) Gerbst, A. G.; Krylov, V. B.; Vinnitskiy, D. Z.; Dmitrenok, A. S.; Shashkov, A. S.; Nifantiev, N. E. *Carbohydr. Res.* **2015**, *417*, 1−10.

DOI: 10.1021/acs.orglett.6b02735
Org. Lett. 2016, 18, 5504−5507

Organic & Biomolecular Chemistry

PAPER

View Article Online
View Journal

Cite this: DOI: 10.1039/c7ob02734f

Synthesis of oligosaccharides related to galactomannans from *Aspergillus fumigatus* and their NMR spectral data†

V. B. Krylov,[a] D. A. Argunov,[a] A. S. Solovev,[a] M. I. Petruk,[a] A. G. Gerbst,[a] A. S. Dmitrenok,[a] A. S. Shashkov,[a] J.-P. Latgé[b] and N. E. Nifantiev *[a]

Received 7th November 2017,
Accepted 3rd January 2018

DOI: 10.1039/c7ob02734f

rsc.li/obc

The synthesis of model oligosaccharides related to antigenic galactomannans of the dangerous fungal pathogen *Aspergillus fumigatus* has been performed employing pyranoside-*into*-furanoside (PIF) rearrangement and controlled O(5) → O(6) benzoyl migration as key synthetic methods. The prepared compounds along with some previously synthesized oligosaccharides were studied by NMR spectroscopy with the full assignment of ^{1}H and ^{13}C signals and the determination of ^{13}C NMR glycosylation effects. The obtained NMR database on ^{13}C NMR chemical shifts for oligosaccharides representing galactomannan fragments forms the basis for further structural analysis of galactomannan related polysaccharides by a non-destructive approach based on the calculation of the ^{13}C NMR spectra of polysaccharides by additive schemes.

Introduction

Aspergillus fumigatus is an opportunistic fungal pathogen that can cause allergic bronchopulmonary aspergillosis, chronic aspergillosis and especially invasive aspergillosis (IA) – a life threatening disease with high morbidity and mortality rates among immunocompromised patients.[1–3] A major carbohydrate antigen produced by *A. fumigatus* is the polysaccharide galactomannan.[4] Its identification in a patient's serum employing a commercial sandwich enzyme immunoassay is used for the diagnosis of IA.[5]

Galactomannan is a complex heteropolysaccharide whose samples can be highly structurally diverse depending on the conditions of *A. fumigatus* cultivation. Despite numerous structural studies, some inconsistencies can be seen among the published data. Latgé *et al.* proposed a structure for two forms[4,6] of galactomannan representing in both cases an α-(1→2)- and α-(1→6)-linked poly-D-mannoside backbone bearing β-(1→5)-linked oligogalactofuranoside side chains attached to some of the mannose units *via* either β-(1→3)- or β-(1→6)-bonds (Fig. 1A). Recently, Shibata *et al.*[7] also revealed the presence of the β-(1→6)-linkage within the galactofuranoside chain[8] and the β-(1→2)- but not the β-(1→3)-attachment of the galactofuranoside side chain to the mannan backbone (Fig. 1B). Significant variations in the polysaccharide structure have been reported under different culture growth conditions.[7]

Polysaccharides structurally related to galactomannans from *A. fumigatus* have been reported in other fungal species in particular *Aspergillus ochraceus*,[9] *Malassezia furfur*,[10] *Malassezia pachydermatis*,[10] *Trichophyton rubrum*,[11] *Trichophyton mentagrophytes*,[11] *Paracoccidioides brasiliensis*[12] and others.[13] This stimulates the development of sensitive methods for the structural analysis of galactomannans. NMR spectroscopy is the most potent non-destructive method used to accomplish these tasks.

The chemical syntheses of galactofuranoside-containing oligosaccharides, related to mycobacterial arabinogalactan[14–16] or *Aspergillus* galactomannan[17–19] and others,[20] were previously reported. Surprisingly, there are well visible contradictions among the published ^{13}C NMR data for very similar Gal*f*-residues present in these oligosaccharides. For example, the ^{13}C NMR chemical shifts of Gal*f*-residues at the non-reducing end linked *via* (1→5)-bonds to the next Gal*f*-ring reported by Lowary *et al.*,[14] Reynolds *et al.*[15] and Gallo-Rodriguez *et al.*[17] (see compounds **A–C** in Table 1) are quite different. Similar deviations are found in data published for the terminal unit in Gal*f*-(1→6)-Gal*f*-fragments in oligosaccharides **D** and **E**. These examples of spectral discrepancy cannot be attributed to the differences of the used spectra recording conditions (temperature and concentration) or the remote influence of structural fragments along the oligosaccharide chains and probably are the results of the tentative assignment of NMR signals. Thus, a

[a]*Laboratory of Glycoconjugate Chemistry, N.D. Zelinsky Institute of Organic Chemistry, Russian Academy of Sciences, Leninsky Prospect 47, 119991 Moscow, Russia. E-mail: nen@ioc.ac.ru; Fax: (+)7-499-135-87-84; Tel: (+)7-499-135-87-84*
[b]*Unité des Aspergillus, Institut Pasteur, 25 rue du Docteur Roux, 75724 Paris Cedex 15, France*

† Electronic supplementary information (ESI) available: NMR data and copies of ^{1}H and ^{13}C spectra. See DOI: 10.1039/c7ob02734f

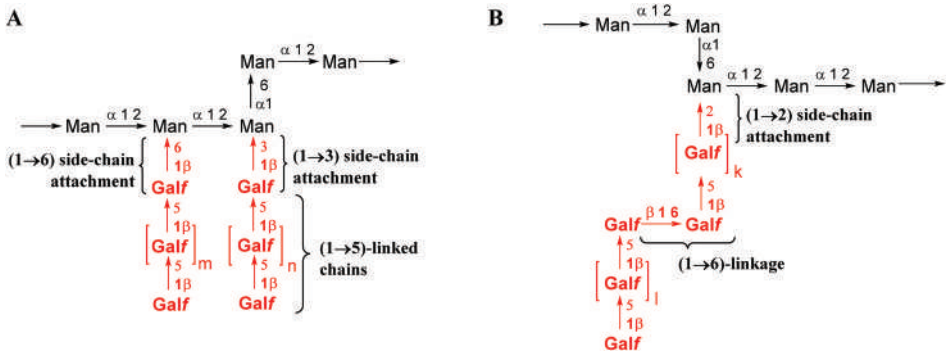

Fig. 1 Proposed structure of galactomannan (A) reported by Latgé *et al.* and[4] (B) additional structural elements reported by Shibata *et al.*[7]

Table 1 Assigned signals in the ^{13}C NMR spectra for the previously described oligosaccharides **A–E**. (δ, ppm; D_2O)

#	δ(C1)	δ(C2)	δ(C3)	δ(C4)	δ(C5)	δ(C6)
A[15]	107.71	81.58	76.74	82.81	70.77	62.07
B[14]	108.7	82.7	77.6	85.5	76.7	61.9
C[17]	109.0	83.6	78.7	84.6	n.d.[a]	64.2
D[15]	108.25	81.24	77.08	83.31	71.09	63.10
E[14]	107.9	81.2	77.6	83.9	70.4	61.9

[a] Not described. **A**[15] β-D-Gal*f*-(1→5)-β-D-Gal*f*-OC_8H_{17}. **B**[14] β-D-Gal*f*-(1→5)-β-D-Gal*f*-(1→6)-β-D-Gal*f*-(1→5)-β-D-Gal*f*-OC_8H_{17}. **C**[17] β-D-Gal*f*-(1→5)-β-D-Gal*f*-(1→5)-β-D-Gal*f*-STol. **D**[15] β-D-Gal*f*-(1→6)-β-D-Gal*f*-OC_8H_{17}. **E**[14] β-D-Gal*f*-(1→6)-β-D-Gal*f*-(1→5)-β-D-Gal*f*-OC_8H_{17}.

careful revision of the previous data is required for their further use in the NMR analysis of fungal galactomannans.

Herein, we report an NMR spectral study of a series of synthetic galactomannan related oligosaccharides **1–13** (Fig. 2). This work is aimed towards the development of NMR database suitable for further structural analysis of *Aspergillus* galactomannan and structurally related oligo- and polysaccharides. The synthesis of compounds **1–6**, **8** and **13** is also reported, while the preparation of oligosaccharides **7** and **9–12** was previously published.[21,22]

Results and discussion

Synthesis of oligosaccharides

The investigation of fine correlation between a galactomannan structure and NMR chemical shift values requires a representative series of model oligosaccharides with strictly defined composition containing different fragments of studied polysaccharide. Previously,[21] we reported the synthesis of two galactomannan related pentasaccharides **7** and **10** and oligosaccharides **9**, **11** and **12**.[22] In the present work, additionally required models such as homo-galactofuranosides **1–4** containing both β-(1→5)- and β-(1→6)-linked galactofuranosyl units and hetero-

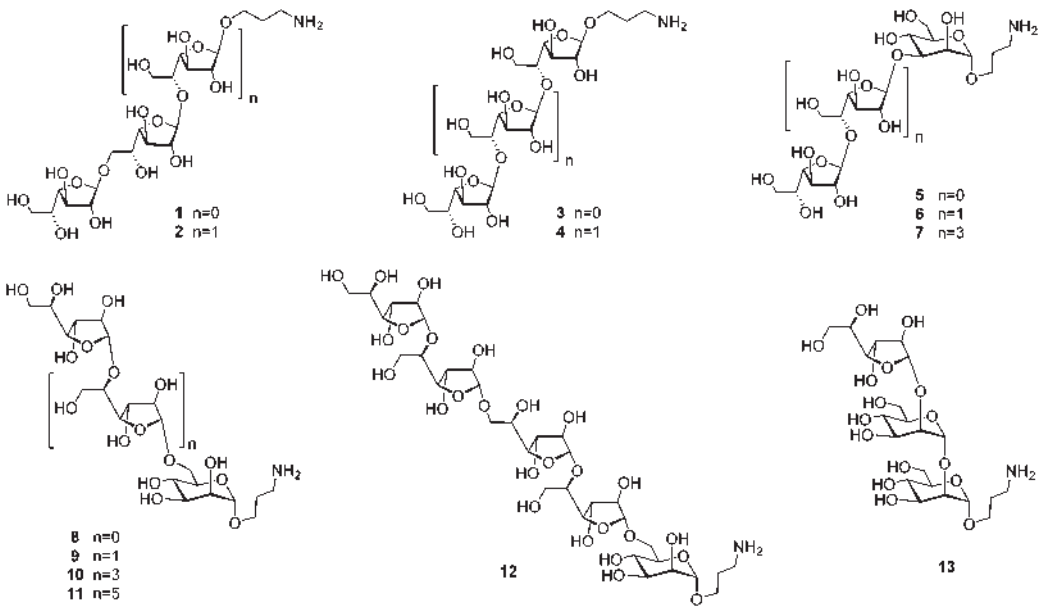

Fig. 2 Studied library of oligosaccharides related to galactomannans of *A. fumigatus*.

saccharides **5**, **6**, **8** and **13** have been obtained (Fig. 2). For their synthesis, glycosyl donor **16**[22] was chosen as a key galactofuranosyl building block. Its main feature was the presence of Fmoc-protection at O(6) which could be selectively removed by deblocking either a 6-OH or 5-OH group depending on the reaction conditions.[22] This made building block **16** suitable for assembling both types of linkages in the oligogalactofuranosyl chains.

The synthesis of glycosyl donor **16** was performed according to the procedure using pyranoside-*into*-furanoside (PIF) rearrangement,[23,24] first described in 2014. Starting pyranoside **14** was initially transformed into the corresponding furanoside **15** and then subjected to subsequent per-*O*-benzoylation, deallylation and imidation (**15** → **16**). The glycosylation of 3-trifluoroacetamidopropanol with donor **16** in the presence of TMSOTf gave **17**, a precursor to disaccharides **1** and **3** with β-(1→6)- and β-(1→5)-bonds, respectively (Scheme 1).

The removal of Fmoc-protection in monosaccharide **17** by treatment with morpholine in DMF gave product **18** with the free OH-group at C-6, which was further glycosylated with imidate **22**[25] yielding β-linked disaccharide **23**. The configuration of the newly formed bond was confirmed by the singlet shape of the H(1)′-signal ($J_{H1',H2'}$ < 1.0 Hz) and the characteristic low-field chemical shift of C(1)′ (105.86 ppm) in the NMR spectra. One-step deblocking of the obtained disaccharide **23** gave target compound **1**.

Alternatively, the removal of Fmoc-protection in **17** under conditions activating O(5) → O(6) benzoyl migration[22] (pyrrolidine in CH_2Cl_2) afforded 5-OH derivative **19** in 92% yield. The structure of product **19** was confirmed by ^{1}H NMR chemical shifts (4.43 ppm for H(5), and 4.51 and 4.62 ppm for H(6) in **19** *vs.* 5.61 ppm for H(5) and 4.05 ppm for both H(6) in **18**). The glycosylation of acceptor **19** with donors **16** and **20**[22] in the presence of TMSOTf gave β-linked di- **24** and trisaccharide **21**, respectively. Following the deblocking of the obtained oligosaccharides resulted in the formation of target compounds **3** and **4**.

Disaccharide **24** was also used for the preparation of trisaccharide **2** with alternating (1→6)- and (1→5)-linkages. For this purpose, Fmoc-protection in **24** was removed under conditions preventing benzoate migration (morpholine in DMF) to give acceptor **25** with the free hydroxyl group at O′(6) which was further glycosylated with imidate **22**. The deblocking of the obtained protected derivative **26** afforded target trisaccharide **2**.

Hetero-oligosaccharides **5**, **6**, **8** and **13** were prepared using mannoside acceptors **27**, **30** and **32** (Scheme 2). For the preparation of the oligosaccharides with the (1→3)-linkage between

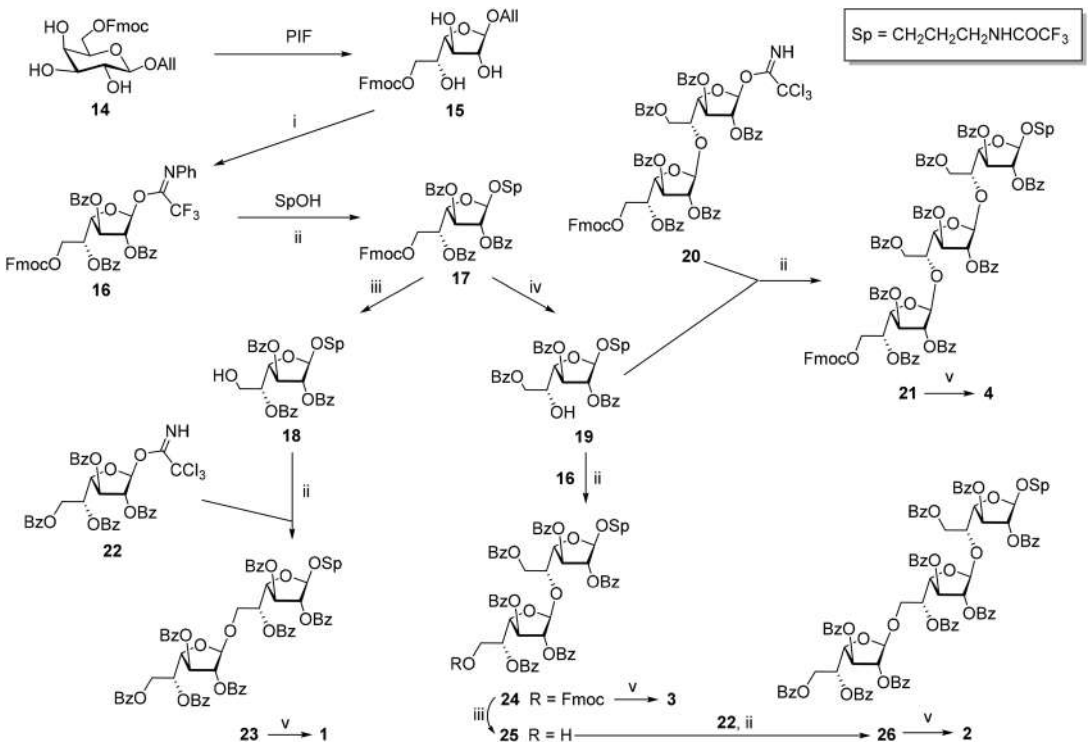

Scheme 1 Synthesis of the model oligosaccharides **1**–**4**. Reagents and conditions: PIF: (1) Py·SO_3, HSO_3Cl, DMF, 20 °C, 16 h, then an excess of NH_4HCO_3 aq.; (2) IR-120(H^+), dioxane–DMF, 60 °C, 45 min, 66% on 2 steps; (i) (1) BzCl, Py, CH_2Cl_2, 20 °C, 3 h; (2) $PdCl_2$, MeOH : CH_2Cl_2, 20 °C, 2.5 h; (3) $CF_3C(NPh)Cl$, Cs_2CO_3, CH_2Cl_2, 20 °C, 1 h, 60% on 3 steps; (ii) TMSOTf, MS300 AW, CH_2Cl_2, –80 → –10 °C, 50 min, 87% for **17**, 96% for **21**, 71% for **23**, 94% for **24**, 76% for **26**; (iii) morpholine, DMF, rt, 35 min, 86% for **18**, 78% for **25**; (iv) pyrrolidine, CH_2Cl_2, rt, 40 min, 92%; (v): MeONa, MeOH–H_2O, rt, overnight, 82% for **1**, 89% for **2**, 83% for **3**, 89% for **4**.

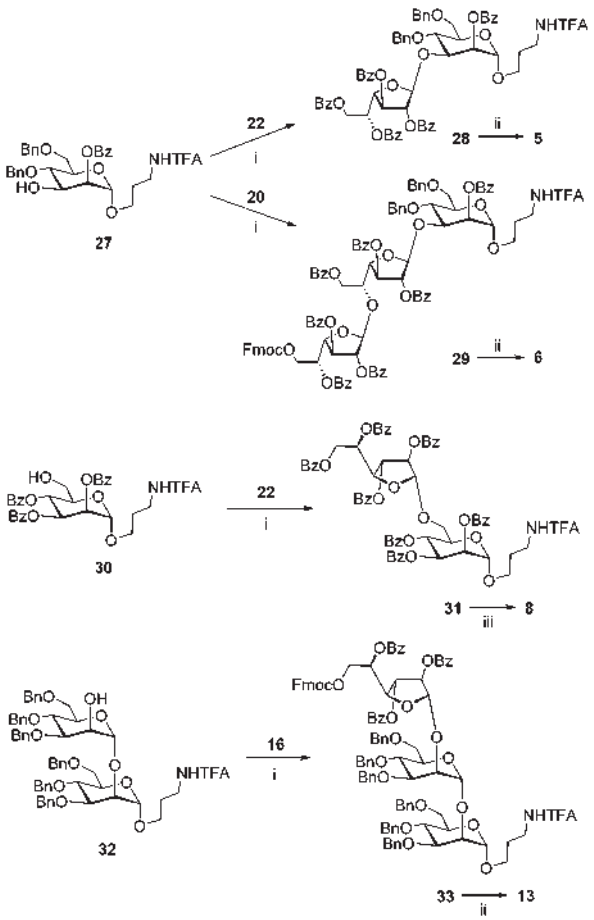

Scheme 2 Synthesis of the model oligosaccharides **5**, **6**, **8** and **13**. Reagents and conditions: (i) TMSOTf, MS300 AW, CH_2Cl_2, −80 → −10 °C, 50 min, 95% for **28**, 67% for **29**, 90% for **31**, 77% for **33**; (ii) (1) H_2, Pd/C, EtOAc, MeOH, rt, 1 h; (2) NaOH, MeOH−H_2O, rt, 1 h, 62% for **5** 80% for **6**, 80% for **13**; (iii) NaOMe, MeOH−H_2O, rt, overnight, 77%.

galactofuranose and mannose, the glycosylations of acceptor **27** [21] with either monosaccharide **22** [25] or disaccharide **20** [22] donors were performed. The disaccharide with the (1→6)-linkage was prepared by the glycosylation of acceptor **30** [21] with donor **22**.[22] The trisaccharide with the (1→2)-linkage was prepared by the glycosylation of acceptor **32** [26] with donor **16**. All the couplings proceeded with good yields and excellent β-stereoselectivity. The deblocking of the resulting protected precursors **28**, **29**, **31** and **33** gave target model oligosaccharides **5**, **6**, **8** and **13**, respectively.

NMR analysis of oligosaccharides

A complete signal assignment in the ^{1}H and ^{13}C NMR spectra of oligosaccharides **1–13** was successfully performed employing 2D NMR experiments: COSY, TOCSY, ROESY, HSQC, and HMBC. The chemical shifts were referenced to CH_3CN (δ ^{1}H – 2.06; ^{13}C – 1.47 ppm) used as an internal standard. The ^{13}C chemical shifts of the studied compounds are summarized in Table 2 (for ^{1}H chemical shifts see Table S1 in the ESI†). The ^{13}C chemical shifts were measured using ^{1}H-decoupled 1D ^{13}C NMR spectra, and the ^{1}H chemical shifts of overlapping signals were established from 2D ^{1}H–^{13}C HSQC spectra using the centres of the corresponding correlation signals.

It can be noted that the assignment of signals summarized in Table 2 has certain, often quite substantial deviations from the previously reported chemical shifts (see Introduction), in particular for the signals of C(1), C(6) and some other carbons. Typically, in the previous papers dedicated to the synthesis of Gal*f*-containing oligosaccharides, NMR signal assignment procedures were described only briefly and the resulting attribution was probably tentative or based on possibly erroneous data from older studies.

The studied series of oligosaccharides (**1–13**) contained 10 types of galactofuranosyl residues which differed in (1) the type of the glycoside linkage in them and (2) the type of the carbohydrate unit as the aglycon (Fig. 3). The variation in chemical shifts among different compounds for the same type of residue did not exceed ±0.1 ppm. The analysis of chemical shifts did not reveal any chain length influence or influence from distant residues which allowed the use of these data for the spectral investigation of different types of oligo- and polysaccharides.

An important feature for the analysis of the NMR spectra of large carbohydrate chains is the determination of ^{13}C NMR glycosylation effects.[27] They are the differences in chemical shifts for the corresponding carbon atoms within a residue taken as a part of an oligo- or polysaccharide and for the same residue in the parent mono- or oligosaccharide, non-glycosylated at the position under consideration. The differences in chemical shifts for atoms involved directly in the glycosidic linkage are called the α-effects of glycosylation.

The differences in chemical shifts for atoms bonded to the substituted carbon are the β-effects of glycosylation. To calculate the glycosylation effects, the ^{13}C NMR chemical shifts of β-galactofuranose (detected as minor signals in the spectrum of D-galactose solution in D_2O), α-D-Man-O$(CH_2)_3NH_2$ [28] and α-D-Man-(1→2)-α-D-Man-O$(CH_2)_3NH_2$ [26] were used. For example, Fig. 4 shows two monosaccharides used for the calculation of the glycosylation effects in the spectrum of disaccharide **5**.

The α-effects for anomeric carbon atoms are most informative for the elucidation of monosaccharide sequences in oligo- or polysaccharide chains. They are dependent on the direction of the linkage and the stereochemical configuration of the anomeric center involved, and are not influenced by the type of substitution in the glycosylating residue under consideration. The exceptions to this rule are 2-*O*-substituted residues due to the interference of the β-effects of the substitution with the α-effects of glycosylation.

The C(1) glycosylation effects for differently linked β-Gal*f* residues are shown in Table 3. It can be seen that their values are different for 2- (4.8 ppm, entry 1), 3- (3.4 ppm, entry 2), 5- (6.1 ppm, entry 4) and 6-linked (6.8 ppm, entries 3 and 5) glycosylating furanoses, but the two latter disacchar-

Table 2 ^{13}C NMR chemical shifts (δ, ppm; D_2O) of oligosaccharides **1–13**[a]

#	Unit	C(1)	C(2)	C(3)	C(4)	C(5)	C(6)
1	β-D-Gal*f*-OH	101.57	81.92	76.35	82.58	71.27	63.33
	β-D-Gal*f*-(1→	108.40	81.58	77.40	83.62	71.45	63.30
	→6)-β-D-Gal*f*-O$(CH_2)_3NH_2$	107.68	81.30	77.17	84.04	70.23	69.58
2	β-D-Gal*f*-(1→	108.49	81.59	77.37	83.56	71.45	63.34
	→6)-β-D-Gal*f*-(1→	107.51	81.83	77.28	83.67	70.16	69.89
	→5)-β-D-Gal*f*-O$(CH_2)_3NH_2$	107.69	81.44	77.08	82.83	76.48	61.35
3	β-D-Gal*f*-(1→	107.58	81.84	77.17	83.38	71.20	63.38
	→5)-β-D-Gal*f*-O$(CH_2)_3NH_2$	107.65	81.43	76.99	82.69	76.53	61.41
4	β-D-Gal*f*-(1→	107.69	81.96[d]	77.15	83.33	71.19	63.43
	→5)-β-D-Gal*f*-(1→	107.50	81.89[e]	77.08[d]	82.29	76.23	61.70
	→5)-β-D-Gal*f*-O$(CH_2)_3NH_2$	107.69	81.47	77.06[e]	82.75	76.66	61.39
5	β-D-Gal*f*-(1→	105.02	81.97	77.70	83.66	71.45	63.44
	→3)-α-D-Man*p*-O$(CH_2)_3NH_2$	100.20	67.28	76.10	65.66	73.43	61.45
6	β-D-Gal*f*-(1→	107.81	82.00	77.20	83.36	71.25	63.48
	→5)-β-D-Gal*f*-(1→	105.07	81.94	77.62	82.77	76.60	61.86
	→3)-α-D-Man*p*-O$(CH_2)_3NH_2$	100.25	67.34	76.26	65.68	73.45	61.69
7	β-D-Gal*f*-(1→	107.74	82.02[d]	77.06[d]	83.37	71.24	63.48
	→5)-β-D-Gal*f*-(1→[b]	107.74	82.05[e]	77.12[e]	82.19	76.22	61.69
				77.19	82.26	76.36	
	→5)-β-D-Gal*f*-(1→	105.12	81.94	77.65	82.73	76.63	61.79
	→3)-α-D-Man*p*-O$(CH_2)_3NH_2$	100.24	67.36	76.29	65.70	73.45	61.84
8	β-D-Gal*f*-(1→	108.41	81.50	77.31	83.56	71.44	63.28
	→6)-α-D-Man*p*-O$(CH_2)_3NH_2$	100.39	70.45	71.03	67.25	72.30	67.41
9	β-D-Gal*f*-(1→	107.63	81.87	77.17	83.33	71.18	63.43[d]
	→5)-β-D-Gal*f*-(1→	108.37	81.65	77.23	82.49	76.50	61.55[e]
	→6)-α-D-Man*p*-O$(CH_2)_3NH_2$	100.47	70.52	71.13	67.27	72.39	67.45
10	β-D-Gal*f*-(1→	107.67	81.86[d]	77.10	83.26	71.11	63.40
	→5)-β-D-Gal*f*-(1→[b]	107.53	81.95[e]	76.98	82.14	76.15	61.73
		107.57	81.97	77.10		76.27	
	→5)-β-D-Gal*f*-(1→	108.37	81.66	77.29	82.46	76.60	61.51
	→6)-α-D-Man*p*-O$(CH_2)_3NH_2$	100.46	70.51	71.15	67.26	72.37	67.43
11	β-D-Gal*f*-(1→	107.68	81.87[d]	77.10	83.27	71.16	63.41
	→5)-β-D-Gal*f*-(1→[c]	107.54	81.96[e]	76.98	82.15	76.25	61.70
		107.58	81.98	77.04		76.22	61.73
				77.11			
	→5)-β-D-Gal*f*-(1→	108.38	81.67	77.29	82.46	76.59	61.50
	→6)-α-D-Man*p*-O$(CH_2)_3NH_2$	100.47	70.51	71.13	67.25	72.38	67.44
12	β-D-Gal*f*-(1→	107.68	81.85	77.13	83.26	71.15	63.42
	→5)-β-D-Gal*f*-(1→	108.43	81.69[d]	77.32	82.54[d]	76.47	61.63
	→6)-β-D-Gal*f*-(1→	107.51	81.85	77.23	83.67	70.20	69.91
	→5)-β-D-Gal*f*-(1→	108.43	81.63[e]	77.32	82.49[e]	76.36	61.50
	→6)-α-D-Man*p*-O$(CH_2)_3NH_2$	100.47	70.51	71.13	67.26	72.37	67.44
13	β-D-Gal*f*-(1→	106.40	81.64	77.17	83.49	71.29	63.36
	→2)-α-D-Man*p*-(1→	100.25	75.42	70.13	67.80	74.03	61.64
	→2)-α-D-Man*p*-O$(CH_2)_3NH_2$	98.81	79.43	70.79	67.59	73.51	61.60

[a] Aglycon signals δ (ppm): Man*p*-O$\underline{C}H_2$-CH_2-CH_2-NH_2 – 65.68, Man*p*-OCH_2-$\underline{C}H_2$-CH_2-NH_2 – 27.21, Man*p*-OCH_2-CH_2-$\underline{C}H_2$-NH_2 – 38.13; Gal*f*-O$\underline{C}H_2$-CH_2-CH_2-NH_2 – 66.31, Gal*f*-OCH_2-$\underline{C}H_2$-CH_2-NH_2 – 27.19, Gal*f*-OCH_2-CH_2-$\underline{C}H_2$-NH_2 – 38.44, (internal standard $\underline{C}H_3CN$ – 1.47); [b] Two internal residues. [c] Four internal residues.[d,e] The assignment in this pair of chemical shifts may be reversed.

ides are not distinguishable on the basis of the glycosylation effects for C(1). Unfortunately, H(1) chemical shifts for the glycosylating Gal*f* residues in these two disaccharide fragments are also very close (5.02–5.04 ppm, Table S1†). In this case, more information can be given by the α-effects of substitution at C(6) of the glycosylated sugar residues, α-D-Man*p* (5.8 ppm) and β-D-Gal*f* (6.5 ppm). Additionally, the positions and integral intensities of H(6a,b)/C(6) correlation peaks in the HSQC spectra can also be used for the quantitative assessment of the relative content of the two disaccharide fragments in the polymer. However, this two-dimensional approach requires full analysis and certain assignment of NMR spectra.

NMR analysis of natural polysaccharides

All types of differently substituted Gal*f* residues were characterized by specific ^{13}C chemical shift patterns and ^{13}C NMR glycosylation effects which permitted their unambiguous identification in the ^{13}C-NMR spectra of natural polysaccharides. These signals could be regarded as "structure reporting" signals[29,30] suitable for the identification of the characteristic fragments of galactomannans and related polysaccharides which are usually available in very limited amounts and thus produce spectra with low signal intensities.

For example, the C(1) resonances of β-galactofuranoside residues represented the highest interest as structure report-

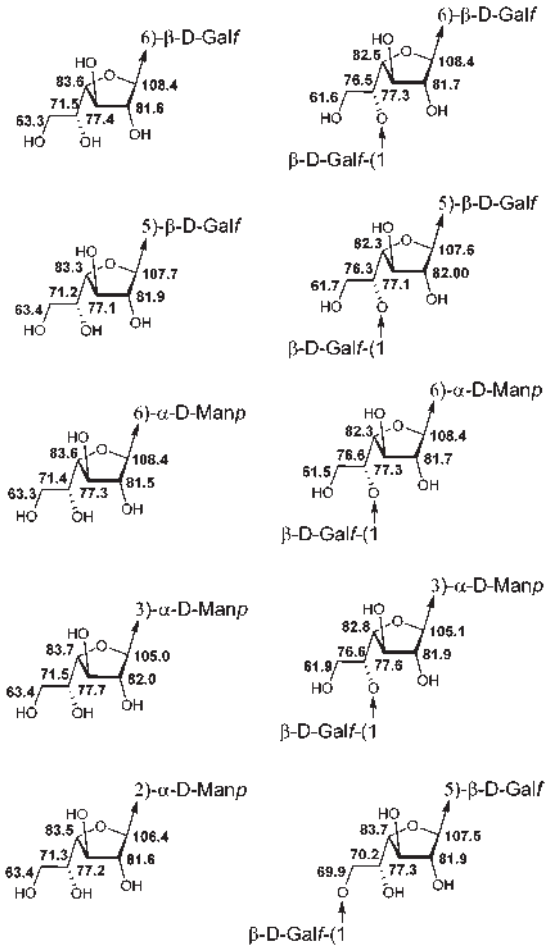

Fig. 3 Averaged ^{13}C NMR chemical shifts (δ, ppm; D_2O) of galactofuranosyl residues of different fragments of galactomannan chains.

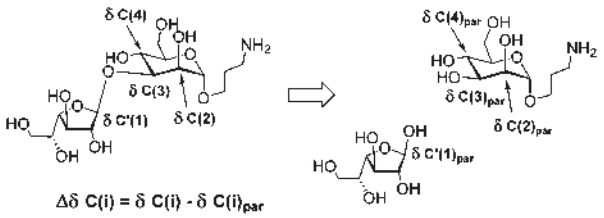

Fig. 4 Illustration of the calculation of ^{13}C NMR glycosylation effects ($\Delta\delta$) in disaccharide **5**.

Table 3 ^{13}C NMR glycosylation effects ($\Delta\delta$, ppm)

#	Linkage	α′-Effect, C(1)	α-Effect	β-Effects
1	β-D-Gal*f*-(1→2)-α-D-Man	4.8	(C2): 4.9	(C1): −2.7 (C3): −0.8
2	β-D-Gal*f*-(1→3)-α-D-Man	3.4	(C3): 4.9	(C2): −3.3 (C4): −1.7
3	β-D-Gal*f*-(1→6)-α-D-Man	6.8	(C6): 5.8	(C5): −1.1
4	β-D-Gal*f*-(1→5)-β-D-Gal*f*	6.1	(C5): 5.0	(C4): −1.0 (C6): −1.7
5	β-D-Gal*f*-(1→6)-β-D-Gal*f*	6.8	(C6): 6.5	(C5): −1.0

Table 4 ^{13}C NMR C(1)-shifts (δ, ppm; D_2O) of β-galactofuranoside residues in oligo- and polysaccharides with different aglycons

#	Terminal β-D-Gal*f*-units with different aglycon counterparts	C(1) in model oligo-saccharide	C(1) in polysaccharide (lit. data)
1	β-D-Gal*f*-(1→2)-D-Man	106.4	106.5[7 a]
2	β-D-Gal*f*-(1→3)-D-Man	105.0	105.4[11 b] 105.9[11 c]
3	β-D-Gal*f*-(1→5)-D-Gal*f*	107.6	107.7[7 a]
4	β-D-Gal*f*-(1→6)-D-Gal*f*/Man	108.4	108.5[7 a]

[a] Each chemical shift taken from ref. 7 has been decremented by 0.20 ppm for consistency with our chemical shift reference. [b] (1→6)-Mannosylated D-Man unit. [c] (1→2)-Mannosylated D-Man unit.

ing signals because they are located in a specific range (105–109 ppm) different from the anomeric signals of mannopyranoside units. The chemical shifts of β-galactofuranoside residues were strongly influenced by the nature of monosaccharide substituents at the anomeric site connected *via* β-(1→2)-, β-(1→3)-, β-(1→5)-, or β-(1→6)-linkages as illustrated by ^{13}C NMR data for model oligosaccharides (Table 4). They coincided well with the corresponding chemical shifts in the spectrum of galactomannan.[7,11] A small deviation (of 0.9 ppm) was observed only in the case of anomeric carbon in the β-galactofuranoside unit connected *via* the (1→3)-linkage to the (1→2)-mannosylated D-Man residue of the mannan backbone (see entry 2 in Table 4) and could be attributed to 2,3-vicinal branching.

To illustrate the applicability of the above mentioned structure reporting signals for the investigation of fungal galactomannans, we analysed the spectrum of galactomannan reported by Latgé *et al.*[4,6] Despite the fact that the presence of the β-D-Gal*f*-(1→3)-D-Man fragment was claimed by the authors, the signal of the anomeric carbon of the corresponding β-D-Gal*f*-unit was not observed in the spectrum (Fig. 1 in ref. 4). Hence, in the present study, the ^{13}C NMR spectrum was recorded for the galactomannan obtained under the reported conditions[4] and it contained the discussed signal. Due to its low intensity in the 1D ^{13}C NMR spectrum, the presence of the β-(1→3)-linked galactofuranoside unit was detected by a 2D HSQC spectral protocol (Fig. 5A).

The full assignment of the signals in the HSQC spectrum (Fig. 5A) revealed the presence of all the types of carbohydrate residues reported by Latgé *et al.*[4,6] However, the careful analysis of low intensity signals (Fig. 5B) suggested the presence of a very minor portion of structural elements reported by Shibata *et al.*:[7] the (1→2)-linkage between β-D-Gal*f* and α-D-Man residues and O(6)-glycosylated β-D-Gal*f* residues (see Fig. 1B). Their presence was confirmed by characteristic ^{1}H and ^{13}C chemical shifts that perfectly matched the data obtained for the corresponding model compounds **13** and **12**.

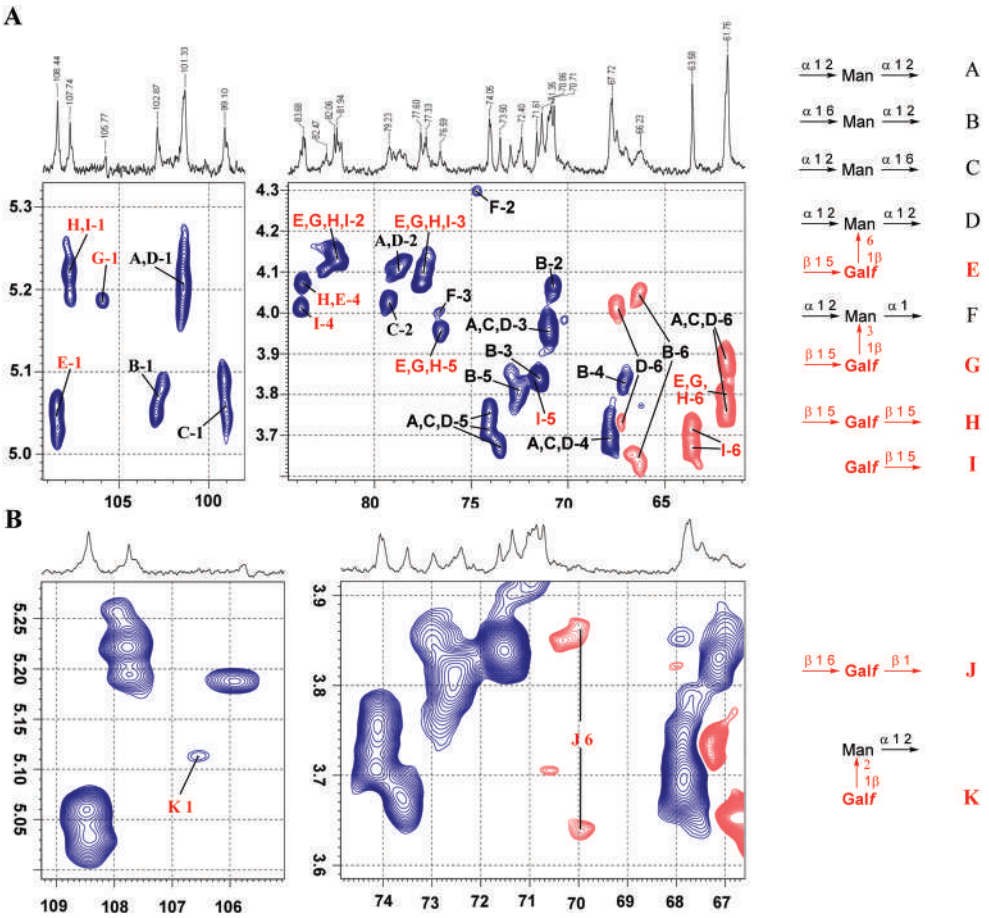

Fig. 5 Application of structure reporting signals for the analysis of natural galactomannan from *A. fumigatus*. (A) Overview of the HSQC spectrum with the assignment of major signals: anomeric (left) and polyol (right) region. (B) Analysis of low intensity signals reporting the structural elements as shown in Fig. 1B. The blue color indicates the positive phase signals referred to as CH or CH_3, whereas the red color indicates the negative phase signals referred to as CH_2 groups.

Conclusions

A series of model oligosaccharides representing key structural fragments of *Aspergillus* galactomannans was synthesised and studied by NMR spectroscopy. The obtained NMR database on ^{13}C NMR chemical shifts for different galactomannan fragments is shown to be useful for the verification of the previously established structures and further development of a non-destructive approach towards the structural analysis of galactomannan related polysaccharides based on the calculation of their ^{13}C NMR spectra by additive schemes.[31–35]

Experimental

General methods

All solvents were distilled and dried if necessary according to standard procedures (CH_2Cl_2, MeOH, toluene, and EtOAc) or purchased as dry (DMF and CH_3CN, Sigma-Aldrich). Commercial chemicals were used without purification unless noted. All glycosylation reactions were carried out using dry solvents under an Ar atmosphere. Molecular sieves for glycosylation reactions were activated prior to application at 180 °C under vacuum from an oil pump for 2 h. Analytical thin-layer chromatography (TLC) was performed on Silica Gel 60 F254 aluminium sheets (Merck), and visualization was accomplished using UV light or by charring at ~150 °C with 10% (v/v) H_3PO_4 in ethanol. Column chromatography was performed on Silica Gel 60, 40–63 μm (Merck). Gel-filtration was performed on a TSK-40 HW(S) column (400 × 17 mm) by elution with 0.1 M AcOH in water at a flow rate of 0.5 mL min^{-1}. ^1H and ^{13}C NMR spectra were recorded on Bruker AMX-400, Bruker DRX-500, and Bruker AV-600 spectrometers. The spectra of compounds **1–13** were recorded in a Shigemi NMR microtube in D_2O (0.25 mL). Chemical shifts were referenced to residual solvent signals. For samples in D_2O, acetonitrile was used as an internal standard. The average sample concentration was 30 μmol mL^{-1}. The signal assignment in the ^1H and ^{13}C NMR spectra was made using COSY, TOCSY, and ^1H–^{13}C HSQC and HMBC techniques. High-resolution mass spectra (HR MS) were recorded on a Bruker micrOTOF II instrument using electrospray ionization (ESI). The measure-

ments were performed in a positive ion mode (interface capillary voltage −4500 V); mass range from *m*/*z* 50 to *m*/*z* 3000 Da; external or internal calibration was made with Electrospray Calibrant Solution (Fluka). A syringe injection was used for solutions in a mixture of acetonitrile and water (50 : 50 v/v, flow rate 3 μL min^{-1}). Nitrogen was applied as a dry gas; the interface temperature was set at 180 °C.

Preparation of the galactomannan sample. *Aspergillus* galactomannan was obtained as described.[4,6] The NMR spectra of galactomannan (solution of 4 mg samples in 0.3 mL of D_2O) were recorded at 333 K.

Glycosylation with imidate donors (general procedure). A carefully dried mixture of imidate donor and glycosyl acceptor was dissolved in CH_2Cl_2 and molecular sieves MS300 AW (100 mg per 1 mL of the reaction mixture) were added. After 10 min of stirring, the temperature was decreased to −80 °C and TMSOTf (0.40 eq. to imidate donor) was added. The mixture was stirred for 50 min and the temperature was gradually raised to −10 °C and then the mixture was quenched with one drop of Et_3N. The reaction mixture was purified by column chromatography on silica gel (toluene–EtOAc, gradient 8 : 1 → 3 : 1) to give the glycosylation product.

3-Trifluoroacetamidopropyl 2,3,5-tri-*O*-benzoyl-6-*O*-(9-fluorenylmethoxycarbonyl)-β-D-galactofuranoside 17. The glycosylation of 3-trifluoroacetamidopropanol (22 mg, 0.13 mmol) with donor **16** (57 mg, 0.064 mmol) in 3 mL of CH_2Cl_2 as described in the general procedure gave monosaccharide **17** (49 mg, 87%) as a colourless syrup. R_f = 0.26 (toluene : EtOAc 10 : 1). ^{1}H NMR (400 MHz, $CDCl_3$) δ 8.10–7.13 (m, 23H, Fmoc, Bz), 5.98–5.92 (m, 1H, H-5), 5.65 (d, *J* = 5.5 Hz, 1H, H-3), 5.39 (s, 1H, H-2), 5.29 (s, 1H, H-1), 4.71–4.62 (m, 3H, H-4, 2 × H-6), 4.39 (dd, *J* = 10.3, 7.6 Hz, 1H, Fmoc-CH_2), 4.31 (dd, *J* = 10.3, 7.5 Hz, 1H, Fmoc-CH_2), 4.21 (t, *J* = 7.5 Hz, 1H, Fmoc-CH), 3.98–3.94 (m, 1H, OC*H*H′CH_2), 3.67–3.57 (m, 2H, OCH*H*′CH_2, CH_2C*H*H′NH), 3.54–3.48 (m, 1H, CH_2CH*H*′NH), 2.01–1.90 (m, 2H, $CH_2C\mathit{H}_2CH_2$). ^{13}C NMR (101 MHz, $CDCl_3$) δ 133.82 (Ar), 133.75 (Ar), 133.54 (Ar), 130.18 (Ar), 130.01 (Ar), 128.64 (Ar), 128.02 (Ar), 127.31 (Ar), 125.35 (Ar), 125.30 (Ar), 120.15 (Ar), 106.53 (C-1), 82.90 (C-2), 81.22 (C-4), 77.29 (C-3), 70.42 (Fmoc-$C\mathit{H}_2$), 70.10 (C-5), 66.61 (O$C\mathit{H}_2CH_2$), 66.23 (C-6), 46.75 (Fmoc-CH), 38.21 ($CH_2C\mathit{H}_2$NH), 28.29 ($CH_2C\mathit{H}_2CH_2$). HRMS (ESI): M = $C_{47}H_{40}F_3NO_{12}$. Calcd *m*/*z* for $[M + Na]^+$ 890.2395, found 890.2386.

Removal of Fmoc-protection without O(5) → O(6) Bz-migration (general procedure). To a solution of 6-*O*-Fmoc-protected saccharide (0.078 mmol) in dry DMF (0.4 mL), morpholine (20 μL) was added. After 35 min, the reaction mixture was poured into 1 M HCl (aq., 50 mL) and extracted with CH_2Cl_2 (50 mL × 2), and the combined organic phase was concentrated *in vacuo*. The residue was purified by column chromatography on silica gel (toluene–EtOAc, gradient 6 : 1 → 3 : 1) to afford the 6-OH product.

3-Trifluoroacetamidopropyl 2,3,5-tri-*O*-benzoyl-β-D-galactofuranoside 18. The removal of Fmoc-protection without Bz-migration in monosaccharide **17** (68 mg, 0.078 mmol) as described in the general procedure gave the product **18** (43 mg, 86%) as a colorless syrup. R_f = 0.44 (toluene : EtOAc 5 : 1). ^{1}H NMR (400 MHz, $CDCl_3$) δ 8.07 (d, *J* = 7.3 Hz, 2H, *o*-Ph), 8.03 (d, *J* = 7.3 Hz, 2H, *o*-Ph), 7.95 (d, *J* = 7.2 Hz, 2H, *o*-Ph), 7.61–7.28 (m, 9H, Ph), 5.66–5.58 (m, 2H, H-3, H-5), 5.41 (d, *J* = 1.5 Hz, 1H, H-2), 5.30 (s, 1H, H-1), 4.72 (dd, *J* = 5.5, 3.7 Hz, 1H, H-4), 4.10–3.99 (m, 2H, H-6_a, H-6_b), 3.95 (dt, *J* = 10.5, 5.2 Hz, 1H, OCH_2), 3.70–3.47 (m, 3H, OCH_2, CH_2N), 2.69 (br. s, 1H, OH), 2.02–1.86 (m, 2H, $OCH_2C\mathit{H}_2CH_2N$). ^{13}C NMR (100 MHz, $CDCl_3$) δ = 166.23 (Ph*C*(O)), 165.88 (Ph*C*(O)), 133.69, 133.64, 133.34, 129.91, 129.88, 129.85, 129.48, 128.82, 128.74, 128.53, 128.43 (Ar), 106.24 (C-1), 82.78 (C-2), 81.41 (C-4), 77.26 (C-3), 73.06 (C-5), 66.19 (OCH_2), 61.87 (C-6), 37.90 (CH_2N), 28.30 ($OCH_2C\mathit{H}_2CH_2N$). HRMS (ESI): M = $C_{32}H_{30}F_3NO_{10}$. Calcd *m*/*z* for $[M + Na]^+$ 668.1714, found 668.1707.

Removal of Fmoc-protection with O(5) → O(6) Bz-migration: preparation of 3-trifluoroacetamidopropyl 2,3,6-tri-*O*-benzoyl-β-D-galactofuranoside 19. To a solution of **17** (49 mg, 0.057 mmol) in dry CH_2Cl_2 (0.5 mL), pyrrolidine (24 μL) was added. After 40 min, the reaction mixture was diluted with CH_2Cl_2 and washed with 1 M HCl (aq.). The organic phase was concentrated *in vacuo*. The residue was purified by column chromatography (toluene : EtOAc 5 : 1) to afford the compound **19** (33 mg, 92%). R_f = 0.17 (toluene : EtOAc 5 : 1). ^{1}H NMR (600 MHz, $CDCl_3$) δ 8.12–8.00 (m, 6H, arom.), 7.63–7.39 (m, 9H, arom.), 7.30–7.20 (m, 2H, arom.), 5.72 (dd, *J* = 5.6, 2.2 Hz, 1H, H-3), 5.43 (d, *J* = 2.3 Hz, 1H, H-2), 5.22 (s, 1H, H-1), 4.62 (dd, *J* = 11.6, 6.3 Hz, 1H, H-6), 4.51 (dd, *J* = 11.6, 4.7 Hz, 1H, H-6′), 4.44–4.42 (m, 1H, H-5), 4.40 (dd, *J* = 5.6, 2.4 Hz, 1H, H-4), 3.89 (m, 1H, OC*H*H′CH_2), 3.63–3.53 (m, 2H, OC*H*H′CH_2, CH_2C*H*H′NH), 3.47–3.45 (m, 1H, CH_2CH*H*′NH), 2.82 (d, *J* = 8.4 Hz, 1H, 5-O*H*), 1.95–1.84 (m, 2H, $CH_2C\mathit{H}_2CH_2$). ^{13}C NMR (150 MHz, $CDCl_3$) δ 165.79 (arom.), 133.74 (arom.), 133.23 (arom.), 129.90 (arom.), 129.83 (arom.), 129.64 (arom.), 128.61 (arom.), 128.56 (arom.), 128.42 (arom.), 106.27 (C-1), 82.71 (C-4), 82.25 (C-2), 77.49 (C-3), 68.81 (C-5), 66.33 (O$C\mathit{H}_2CH_2$), 65.97 (C-6), 38.04 ($CH_2C\mathit{H}_2$NH), 28.19 ($CH_2C\mathit{H}_2CH_2$). HRMS (ESI): M = $C_{32}H_{30}F_3NO_{10}$. Calcd *m*/*z* for $[M + Na]^+$ 668.1714, found 668.1714.

3-Trifluoroacetamidopropyl 2,3,5-tri-*O*-benzoyl-6-*O*-(9-fluorenylmethoxycarbonyl)-β-D-galactofuranosyl-(1→5)-2,3,6-tri-*O*-benzoyl-β-D-galactofuranosyl-(1→5)-2,3,6-tri-*O*-benzoyl-β-D-galactofuranoside (21). The glycosylation of acceptor **19** (8 mg, 0.0125 mmol) with disaccharide donor **20** (19 mg, 0.014 mmol) in 1 mL of CH_2Cl_2 as described in the general procedure gave trisaccharide **21** (22 mg, 96%) as a colorless syrup. R_f = 0.55 (toluene : EtOAc 5 : 1). ^{1}H NMR (400 MHz, $CDCl_3$) δ 8.08–7.09 (m, 53H, Ph), 6.00–5.95 (m, 1H, H-5^{III}), 5.87 (dd, *J* = 5.5, 1.8 Hz, 1H, H-3^{I}), 5.84 (d, *J* = 5.0 Hz, 1H, H-3^{II}), 5.79 (s, 1H, H-1^{III}), 5.70 (s, 1H, H-1^{II}), 5.67–5.64 (m, 2H, H-2^{II}, H-2^{III}), 5.56 (d, *J* = 4.1 Hz, 1H, H-3^{III}), 5.35 (d, *J* = 1.7 Hz, 1H, H-2^{I}), 5.17 (s, 1H, H-1^{I}), 4.95 (dd, *J* = 5.1, 3.4 Hz, 1H, H-4^{III}), 4.82 (dd, *J* = 4.9, 3.2 Hz, 1H, H-4^{II}), 4.80–4.58 (m, 7H, H-6_a^{II}, H-6_a^{I}, H-6_a^{III}, H-6_b^{II}, H-6_b^{I}, H-5^{II}, H-5^{I}), 4.55–4.47 (m, 2H, H-4^{I}, H-6_b^{III}), 4.23 (dd, *J* = 10.0, 7.3 Hz, 1H, Fmoc-CH_2), 4.17–4.05 (m, 2H, Fmoc-CH_2, Fmoc-C*H*), 3.86 (dt, *J* = 10.3, 5.3 Hz, 1H, OCH_2), 3.61–3.49 (m, 2H, CH_2N, OCH_2), 3.47–3.38 (m, 1H,

CH_2N), 1.90–1.79 (m, 2H, $OCH_2CH_2CH_2N$). ^{13}C NMR (100 MHz, $CDCl_3$) δ = 166.19, 165.84, 165.68, 165.54, 165.29, 165.20, 154.76, 143.41, 143.25, 141.15 (quat. Ph), 133.63, 133.52, 133.44, 133.30, 133.25, 133.17, 133.11, 133.05, 132.99, 130.03, 129.81, 129.76, 129.70, 129.66, 129.61, 129.38, 128.85, 128.63, 128.54, 128.44, 128.30, 128.10, 127.74, 127.10, 126.35, 125.26, 125.20, 120.45, 119.88 (Ph), 106.00 (C-1^{I}), 105.53 (C-1^{II}), 105.47 (C-1^{III}), 83.42 (C-4^{II}), 82.48 (C-2^{I}), 82.26 (C-4^{I}), 82.02 (C-2^{III}), 81.90 (C-2^{II}), 81.74 (C-4^{III}), 77.66 (C-3^{III}), 77.22 (C-3^{II}), 76.57 (C-3^{I}), 73.69 (C-5^{I}), 73.17 (C-5^{II}), 70.17 (C-5^{III}), 70.10 (Fmoc-CH_2), 66.71 (C-6^{III}), 66.30 (OCH_2), 65.35 (C-6^{II}), 63.98 (C-6^{I}), 46.54 (Fmoc-*C*H), 38.15 (CH_2N), 28.14 ($OCH_2CH_2CH_2N$). HRMS (ESI): M = $C_{101}H_{88}F_3NO_{26}$. Calcd *m*/*z* for $[M + Na]^+$ 1810.5439, found 1810.5402.

Deblocking (general procedure). A solution of MeONa (0.1 M) in MeOH (1 mL) was added to the protected oligosaccharide (0.014 mmol) and the mixture was stirred for 1 h. Then, 1 drop of water was added and the reaction mixture was left overnight. Base was neutralized with AcOH (10 μL), and the reaction mixture was diluted with water and concentrated *in vacuo*. Gel chromatography on TSK-40 HW(S) followed by lyophilization afforded the unprotected compound as a white foam.

3-Aminopropyl β-D-galactofuranosyl-(1→5)-β-D-galactofuranosyl-(1→5)-β-D-galactofuranoside 4. The deblocking of compound **21** (22 mg, 0.012 mmol) as described in the general procedure afforded trisaccharide **4** (6 mg, 89%) as a white foam. HRMS (ESI): M = $C_{21}H_{39}NO_{16}$. Calcd *m*/*z* for $[M + H]^+$ 562.2342, found 562.2350.

3-Trifluoroacetamidopropyl 2,3,5,6-tetra-*O*-benzoyl-β-D-galactofuranosyl-(1→6)-2,3,5-tri-*O*-benzoyl-β-D-galactofuranoside 23. The glycosylation of acceptor **18** (13 mg, 0.020 mmol) with donor **22** (19 mg, 0.025 mmol) in 1 mL of CH_2Cl_2 as described in the general procedure gave disaccharide **23** (17 mg, 71%) as a colorless syrup. R_f = 0.45 (toluene : EtOAc 5 : 1). ^1H NMR (600 MHz, $CDCl_3$) δ 8.07–7.75 (m, 14H, *o*-Ph), 7.56–7.21 (m, 21H, Ph), 6.09 (dt, *J* = 7.4, 3.8 Hz, 1H, H-5), 5.87 (td, *J* = 6.3, 3.7 Hz, 1H, H-5), 5.66 (dd, *J* = 5.4, 1.5 Hz, 1H, H-3), 5.60 (d, *J* = 5.0 Hz, 1H, H-3), 5.44 (d, *J* = 0.9 Hz, 1H, H-2), 5.40 (s, 1H, H-1), 5.34 (d, *J* = 1.6 Hz, 1H, H-2), 5.24 (s, 1H, H-1), 4.81–4.70 (m, 4H, 2 × H-4, H-6_a^{II}, H-6_b^{II}), 4.18 (dd, *J* = 10.3, 6.7 Hz, 1H, H-6_a^{I}), 4.01 (dd, *J* = 10.3, 6.1 Hz, 1H, H-6_b^{I}), 3.90 (dt, *J* = 10.4, 5.2 Hz, 1H, OCH_2), 3.62–3.49 (m, 2H, OCH_2, CH_2N), 3.45–3.38 (m, 1H, CH_2N), 1.86–1.73 (m, 2H, $OCH_2CH_2CH_2N$). ^{13}C NMR (150 MHz, $CDCl_3$) δ = 166.22, 165.97, 165.72, 165.70, 165.67, 165.63, 165.34 (Ph*C*(O)), 133.58, 133.54, 133.48, 133.34, 133.24, 133.07, 129.96, 129.92, 129.85, 129.80, 129.73, 129.56, 129.51, 129.42, 128.87, 128.75, 128.70, 128.51, 128.46, 128.44, 128.41, 128.36, 128.32 (Ph), 106.56 (C-1), 105.86 (C-1), 83.06 (C-4), 81.96 (C-2), 81.78 (C-2), 81.34 (C-4), 77.51 (C-3), 77.12 (C-3), 70.78 (C-5), 70.18 (C-5), 66.64 (C-6), 65.28 (OCH_2), 63.67 (C-6×), 37.97 (CH_2N), 27.99 ($OCH_2CH_2CH_2N$). HRMS (ESI): M = $C_{66}H_{56}F_3NO_{19}$. Calcd *m*/*z* for $[M + Na]^+$ 1246.3291, found 1246.3265.

3-Aminopropyl β-D-galactofuranosyl-(1→6)-β-D-galactofuranoside 1. The deblocking of compound **23** (17 mg, 0.014 mmol) as described in the general procedure afforded disaccharide **1** (4.5 mg, 82%) as a white foam. HRMS (ESI): M = $C_{15}H_{29}NO_{11}$. Calcd *m*/*z* for $[M + H]^+$ 400.1813, found 400.1813.

3-Trifluoroacetamidopropyl 2,3,5-tri-*O*-benzoyl-6-*O*-(9-fluorenylmethoxycarbonyl)-β-D-galactofuranosyl-(1→5)-2,3,6-tri-*O*-benzoyl-β-D-galactofuranoside 24. The glycosylation of acceptor **19** (27 mg, 0.042 mmol) with donor **16** (45 mg, 0.051 mmol) in 1 mL of CH_2Cl_2 as described in the general procedure gave disaccharide **24** (52 mg, 94%) as a colorless syrup. R_f = 0.54 (toluene : EtOAc 5 : 1). ^1H NMR (500 MHz, $CDCl_3$) δ 8.07–7.68 (m, 12H, arom.), 7.56–7.14 (m, 26H, arom.), 6.07–6.00 (m, 1H, H-5^{II}), 5.88 (d, *J* = 5.7 Hz, 1H, H-3), 5.76 (s, 1H, H-1), 5.64 (s, 1H, H-2), 5.58 (d, *J* = 4.7 Hz, 1H, H-3), 5.37 (s, 1H, H-2), 5.20 (s, 1H. H-1), 4.98 (t, *J* = 3.9 Hz, 1H, H-4), 4.76 (dd, *J* = 11.7, 4.1 Hz, 1H, H-6_a), 4.71–4.52 (m, 5H, 3 × H-6, H-5^{I}, H-4), 4.28 (dd, *J* = 10.1, 7.9 Hz, 1H, Fmoc-CH_2), 4.23–4.17 (m, 1H, Fmoc-CH_2), 4.11 (t, *J* = 7.5 Hz, 1H, Fmoc-C*H*), 3.88 (dt, *J* = 10.0, 5.1 Hz, 1H, OCH_2), 3.60–3.42 (m, 3H, OCH_2, CH_2N), 1.91–1.77 (m, 2H, $OCH_2CH_2CH_2N$). ^{13}C NMR (125 MHz, $CDCl_3$) δ = 166.18, 165.96, 165.72, 165.59, 165.52, 165.25 (PhC(O)), 154.83, 143.34, 143.17, 141.17, 133.63, 133.34, 133.22, 133.13, 130.02, 129.82, 129.78, 129.66, 129.57, 129.39, 128.74, 128.61, 128.52, 128.39, 128.35, 128.22, 127.79, 127.77, 127.12, 127.06, 125.22, 125.16, 119.92 (Ph), 106.14 (C-1), 105.54 (C-1), 82.81 (C-4), 82.19 (C-2), 81.97 (C-2), 81.77 (C-4), 77.72 (C-3), 77.23 (C-3), 76.53 (C-5), 73.39 (C-5), 70.17 (Fmoc-CH_2), 66.58 (C-6), 66.47 (OCH_2), 64.23 (C-6), 46.53 (Fmoc-*C*H), 38.08 (CH_2N), 28.04 ($OCH_2CH_2CH_2N$). HRMS (ESI): M = $C_{74}H_{62}F_3NO_{20}$. Calcd *m*/*z* for $[M + Na]^+$ 1364.3709, found 1364.3705.

3-Aminopropyl β-D-galactofuranosyl-(1→5)-β-D-galactofuranoside 3. The deblocking of compound **24** (19 mg, 0.014 mmol) as described in the general procedure afforded disaccharide **3** (4.7 mg, 83%) as a white foam. HRMS (ESI): M = $C_{15}H_{29}NO_{11}$. Calcd *m*/*z* for $[M + H]^+$ 400.1813, found 400.1817.

3-Trifluoroacetamidopropyl 2,3,5-tri-*O*-benzoyl-β-D-galactofuranosyl-(1→5)-2,3,5-tri-*O*-benzoyl-β-D-galactofuranoside 25. The removal of Fmoc-protection without Bz-migration in disaccharide **24** (38 mg, 0.028 mmol) as described in the general procedure gave the product **25** (25 mg, 78%) as a colorless syrup. R_f = 0.58 (toluene : EtOAc 3 : 1). ^1H NMR (600 MHz, $CDCl_3$) δ 8.06–7.81 (m, 12H, *o*-Ph), 7.60–7.19 (m, 18H, Ph), 5.89 (dd, *J* = 5.7, 2.3 Hz, 1H, H-3), 5.76 (s, 1H, H-1), 5.66 (d, *J* = 1.4 Hz, 1H, H-2), 5.64–5.60 (m, 1H, H-5^{II}), 5.60–5.57 (m, 1H, H-3), 5.37 (d, *J* = 2.3 Hz, 1H, H-2), 5.21 (s, 1H, H-1), 5.05 (dd, *J* = 5.3, 2.8 Hz, 1H, H-4), 4.78 (dd, *J* = 11.8, 4.3 Hz, 1H, H-6_a^{I}), 4.71 (dd, *J* = 11.8, 6.8 Hz, 1H, H-6_b^{I}), 4.62–4.57 (m, 2H, H-4, H-5^{I}), 4.05–3.88 (m, 3H, H-6_a^{II}, H-6_b^{II}, OCH_2), 3.62–3.45 (m, 3H, OCH_2, CH_2N), 3.23 (br. s, 1H, OH), 1.97–1.81 (m, 2H, $OCH_2CH_2CH_2N$). ^{13}C NMR (150 MHz, $CDCl_3$) δ = 166.29, 166.23, 166.03, 165.63, 165.31 (Ph*C*(O)), 133.88, 133.67, 133.35, 133.17, 129.91, 129.89, 129.84, 129.79, 129.65, 128.85, 128.76, 128.61, 128.41, 128.38, 128.35, 128.22 (Ph), 106.24 (C-1), 105.86 (C-1), 82.74 (C-4), 82.35 (C-2), 82.02 (C-2), 81.63 (C-4), 77.69 (C-3), 73.66 (C-3), 72.97 (C-5), 66.42 (OCH_2), 64.43 (C-6),

61.34 (C-6), 38.08 (CH_2N), 28.11 ($OCH_2CH_2CH_2N$). HRMS (ESI): M = $C_{59}H_{52}F_3NO_{18}$. Calcd *m*/*z* for $[M + Na]^+$ 1142.3029, found 1142.3030.

3-Trifluoroacetamidopropyl 2,3,5,6-tetra-*O*-benzoyl-β-D-galactofuranosyl-(1→6)-2,3,5-tri-*O*-benzoyl-β-D-galactofuranosyl-(1→5)-2,3,6-tri-*O*-benzoyl-β-D-galactofuranoside 26. The glycosylation of acceptor **25** (25 mg, 0.022 mmol) with donor **22** (21 mg, 0.028 mmol) in 1 mL of CH_2Cl_2 as described in the general procedure gave trisaccharide **26** (28 mg, 76%) as a colorless syrup. R_f = 0.55 (toluene : EtOAc 5 : 1). ^{1}H NMR (400 MHz, $CDCl_3$) δ 8.04–7.72 (m, 20H, *o*-Ph), 7.53–7.13 (m, 30H, Ph), 6.10–6.02 (m, 1H, H-5), 5.99 (dt, *J* = 7.7, 4.0 Hz, 1H, H-5), 5.87 (dd, *J* = 5.8, 2.3 Hz, 1H, H-3), 5.75 (s, 1H, H-2), 5.64–5.61 (m, 2H, H-2, H-3), 5.54 (d, *J* = 5.0 Hz, 1H, H-3), 5.35–5.34 (m, 2H, 2 × H-2), 5.24 (s, 1H, H-1), 5.18 (s, 1H, H-1), 4.94 (t, *J* = 4.1 Hz, 1H, H-4), 4.79–4.56 (m, 6H, H-4, 4 × H-6, H-5^{I}), 4.53 (dd, *J* = 5.7, 3.9 Hz, 1H, H-4), 4.19–4.10 (m, 1H, H-6$_a^{II}$), 4.01 (dd, *J* = 11.2, 7.4 Hz, 1H, H-6$_b^{II}$), 3.87 (dt, *J* = 10.1, 5.0 Hz, 1H, OCH_2), 3.61–3.36 (m, 4H, OCH_2, CH_2N), 1.89–1.66 (m, 2H, $OCH_2CH_2CH_2N$). ^{13}C NMR (100 MHz, $CDCl_3$) δ = 166.17, 166.09, 165.88, 165.75, 165.62, 165.54, 165.25, 165.13 (Ph*C*(O)), 133.61, 133.54, 133.27, 133.22, 133.11, 132.96, 129.89, 129.78, 129.74, 129.69, 129.66, 129.60, 129.50, 128.88, 128.86, 128.84, 128.79, 128.77, 128.66, 128.57, 128.48, 128.37, 128.32, 128.28, 128.16 (Ph), 106.61 (C-1), 106.09 (C-1), 105.46 (C-1), 82.84 (C-4), 82.74 (C-2), 81.95 (2 × C-4), 81.88 (2 × C-2), 77.77 (C-3), 77.48 (C-3), 76.48 (C-3), 73.17 (C-4), 71.75 (C-5), 70.42 (C-5), 67.43 (C-6^{II}), 66.41 (OCH_2), 64.25 (C-6), 63.82 (C-6), 38.08 (CH_2N), 28.05 ($OCH_2CH_2CH_2N$). HRMS (ESI): M = $C_{93}H_{78}F_3NO_{27}$. Calcd *m*/*z* for $[M + Na]^+$ 1720.4606, found 1720.4585.

3-Aminopropyl β-D-galactofuranosyl-(1→6)-β-D-galactofuranosyl-(1→5)-β-D-galactofuranoside 2. The deblocking of compound **26** (28 mg, 0.016 mmol) as described in the general procedure afforded disaccharide **2** (8 mg, 89%) as a white foam. HRMS (ESI): M = $C_{15}H_{29}NO_{11}$. Calcd *m*/*z* for $[M + Na]^+$ 422.1633, found 422.1639.

3-Trifluoroacetamidopropyl 2,3,5,6-tetra-*O*-benzoyl-β-D-galactofuranosyl-(1→3)-2-*O*-benzoyl-4,6-di-*O*-benzyl-α-D-mannopyranoside 28. The glycosylation of acceptor **27** (19 mg, 0.031 mmol) with donor **22** (23 mg, 0.031 mmol) in 1 mL of CH_2Cl_2 as described in the general procedure gave disaccharide **28** (36 mg, 95%) as a colorless syrup. R_f = 0.38 (toluene : EtOAc 10 : 1). ^{1}H NMR (600 MHz, $CDCl_3$) δ 8.11–7.07 (m, 35H), 6.05 (ddd, 1H, H-5^{II}), 5.72 (s, 1H, H-1^{II}), 5.67 (dd, $J_{1,2}$ < 2 Hz, $J_{2,3}$ = 3.0 Hz, 1H, H-2^{I}), 5.58 (dd, $J_{2,3}$ = 1.4 Hz, $J_{3,4}$ = 5.8 Hz, 1H, H-3^{II}), 5.55 (d, 1H, H-2^{II}), 5.01 (d, 1H, H-1^{I}), 4.93 (d, *J* = 11.3 Hz, 1H, PhC*H*H′), 4.73 (dd, $J_{4,5}$ = 2.8 Hz, 1H, H-4^{II}), 4.72(dd, $J_{5,6}$ = 7.65 Hz, $J_{6,6'}$ = 11.5 Hz, 1H, H-6a^{II}), 4.69 (d, *J* = 11.9 Hz, 1H, PhCH*H*′), 4.66 (dd, $J_{5,6'}$ = 5.15 Hz, 1H, H-6b^{II}), 4.57 (d, 1H, PhC*H*H′), 4.53 (d, 1H, PhCH*H*′), 4.50 (dd, $J_{3,4}$ = 9.5 Hz, 1H, H-3^{I}), 4.11 (t, *J* = 9.3 Hz, 1H, H-4^{I}), 3.85 (m, 1H, OC*H*H′ CH_2), 3.78–3.77 (m, 2H, H-5^{I}, H-6a^{I}), 3.72 (d, *J* = 8.5 Hz, 1H, H-6b^{I}), 3.56 (m, 2H, OCH*H*′CH_2, C*H*H′N), 3.44 (m, 1H, CH*H*′N), 1.90 (m, 2H, $OCH_2CH_2CH_2N$). ^{13}C NMR (151 MHz, $CDCl_3$) δ 133.37, 133.28, 133.23, 133.16, 130.03, 129.93, 129.86, 129.80, 128.44, 128.37, 128.33, 128.27, 127.61, 127.57, 127.51, 127.47 (Ph), 102.28 (C-1^{II}), 97.76 (C-1^{I}), 82.36 (C-2^{II}), 81.52 (C-4^{II}), 78.04 (C-3^{II}), 75.22 (Ph*C*H_2), 73.60 (C-3^{I}), 73.45 (Ph*C*H_2), 73.36 (C-4^{I}), 72.08 (C-5^{I}), 69.69 (C-5^{II}), 68.96 (C-6^{I}), 67.99 (C-2^{I}), 65.51 (OCH_2), 63.55 (C-6^{II}), 37.85 (CH_2N), 28.45 ($CH_2CH_2CH_2$). HRMS (ESI): M = $C_{66}H_{60}F_3NO_{17}$. Calcd *m*/*z* for $[M + Na]^+$ 1218.3706, found 1218.370313.

3-Aminopropyl β-D-galactofuranosyl-(1→3)-α-D-mannopyranoside 5. To a solution of compound **28** (35 mg, 0.029 mmol) in EtOAc–MeOH 1 : 1 (1 mL), $Pd(OH)_2$ was added and the mixture was vigorously stirred overnight under a H_2 atmosphere. Then it was filtered through a Celite layer and concentrated *in vacuo*. To the residue, a solution of MeONa (0.1 M) in MeOH (0.6 mL) was added and the mixture was stirred for 1 h. Then, 1 drop of water was added and the reaction mixture was left overnight. Base was neutralized with AcOH (6 μL), and the reaction mixture was diluted with water and concentrated *in vacuo*. Gel chromatography on TSK-40 HW(S) followed by lyophilization afforded **5** (7.2 mg, 62%) as a white foam. HRMS (ESI): M = $C_{15}H_{29}NO_{11}$. Calcd *m*/*z* for $[M + H]^+$ 400.1813, found 400.1816.

3-Trifluoroacetamidopropyl 2,3,5-tri-*O*-benzoyl-6-*O*-(9-fluorenylmethoxycarbonyl)-β-D-galactofuranosyl-(1→5)-2,3,6-tri-*O*-benzoyl-β-D-galactofuranosyl-(1→3)-2-*O*-benzoyl-4,6-di-*O*-benzyl-α-D-mannopyranoside 29. The glycosylation of acceptor **27** (6 mg, 0.01 mmol) with donor **20** (14 mg, 0.01 mmol) in 0.5 mL of CH_2Cl_2 as described in the general procedure gave trisaccharide **29** (12 mg, 67%) as a colorless syrup. R_f = 0.54 (toluene : EtOAc 5 : 1). ^{1}H NMR (600 MHz, $CDCl_3$) δ 8.07–7.12 (m, 53H, arom.), 5.99–5.95 (m, 1H, H-5^{III}), 5.74 (s, 1H, H-1^{III}), 5.72 (dd, $J_{3,4}$ = 6.3 Hz, 1.9 Hz, 1H, H-3^{II}), 5.65 (d, *J* = 1.5 Hz, 1H, H-2^{III}), 5.64–5.61 (m, 2H, H-2^{I}, H-1^{II}), 5.57 (dd, *J* = 5.5, 1.2 Hz, 1H, H-3^{III}), 5.53 (d, *J* = 2.0 Hz, 1H, H-2^{II}), 4.97 (dd, *J* = 5.4, 3.4 Hz, 1H, H-4^{III}), 4.91–4.87 (m, 2H, H-1^{I}, PhCH_2), 4.67 (dd, *J* = 12.4, 4.1 Hz, 2H, H-6$_a^{III}$), 4.65–4.58 (m, 3H, PhCH_2, H-5^{II}, H-6$_a^{II}$), 4.56 (dd, *J* = 6.2, 3.9 Hz, 1H, H-4^{II}), 4.55–4.49 (m, 3H, H-6$_b^{II}$, H-6$_b^{III}$, PhCH_2), 4.45 (d, *J* = 11.9 Hz, 1H, PhCH_2), 4.37 (dd, *J* = 9.5, 3.1 Hz, 1H, H-3^{I}), 4.29 (dd, *J* = 10.5, 7.4 Hz, 1H, Fmoc-CH_2), 4.24 (dd, *J* = 10.5, 7.6 Hz, 1H, Fmoc-CH_2), 4.11 (t, *J* = 7.4 Hz, 1H, Fmoc-C*H*), 4.04 (t, *J* = 9.5 Hz, 1H, H-4^{I}), 3.73–3.68 (m, 1H, OCH_2), 3.59 (dd, *J* = 10.7, 3.9 Hz, 1H, H-6$_a^{I}$), 3.56–3.50 (m, 2H, H-6$_b^{I}$, H-5^{I}), 3.48–3.41 (m, 2H, OCH_2, NCH_2), 3.37–3.30 (m, 1H, CH_2N), 1.92–1.81 (m, 2H, $OCH_2CH_2CH_2N$). ^{13}C NMR (150 MHz, $CDCl_3$) δ = 166.40, 165.85, 165.67, 165.54, 165.53, 165.20, 165.04 (quat. Ph), 133.30, 133.14, 133.05, 130.03, 129.86, 129.82, 129.65, 128.43, 128.35, 128.33, 128.29, 128.25, 127.72, 127.52, 127.44, 127.08, 125.18, 119.89 (Ph), 105.36 (C-1^{III}), 102.11 (C-1^{II}), 97.78 (C-1^{I}), 82.43 (C-2^{II}), 82.27 (C-2^{III}), 82.10 (C-4^{II}), 81.75 (C-4^{III}), 77.73 (C-3^{II}), 77.56 (C-3^{III}), 75.11 (PhCH_2), 73.74 (C-3^{I}), 73.58 (C-5^{II}), 73.44 (PhCH_2), 73.18 (C-4^{I}), 71.84 (C-5^{I}), 70.25 (C-5^{III}), 70.05 (Fmoc-CH_2), 68.83 (C-6^{I}), 67.79 (C-2^{I}), 66.87 (C-6^{III}), 65.45 (OCH_2), 64.83 (C-6^{II}), 46.61 (Fmoc-C*H*), 37.75 (CH_2N), 28.45 ($OCH_2CH_2CH_2N$). HRMS (ESI): M = $C_{101}H_{88}NF_3NO_{26}$. Calcd *m*/*z* for $[M + Na]^+$ 1810.5439, found 1810.5402.

3-Aminopropyl β-D-galactofuranosyl-(1→5)-β-D-galactofuranosyl-(1→3)-α-D-mannopyranoside 6. The removal of all protec-

tive groups in compound **29** (12 mg, 0.0067 mmol) as described for the preparation of disaccharide **5** gave **6** (3 mg, 80%) as a white foam. HRMS (ESI): M = $C_{21}H_{39}NO_{16}$. Calcd *m*/*z* for $[M + Na]^+$ 584.2161, found 584.2158.

3-Trifluoroacetamidopropyl 2,3,5,6-tetra-*O*-benzoyl-β-D-galactofuranosyl-(1→6)-2,3,4-tri-*O*-benzoyl-α-D-mannopyranoside 31. The glycosylation of acceptor **30** (25 mg, 0.039 mmol) with donor **22** (32 mg, 0.043 mmol) in 1.5 mL of CH_2Cl_2 as described in the general procedure gave disaccharide **31** (43 mg, 90%) as a colorless syrup. R_f = 0.38 (toluene : EtOAc 10 : 1). ^{1}H NMR (600 MHz, $CDCl_3$) δ 8.14–7.15 (m, 35H), 6.06 (ddd, $J_{4,5}$ = 3.4 Hz, $J_{5,6}$ = 4.5 Hz, $J_{5,6'}$ = 7.8 Hz, 1H, H-5^{II}), 5.88 (dd, $J_{2,3}$ = 3.1 Hz, $J_{3,4}$ = 9.9 Hz, 1H, H-3^{I}), 5.84 (m, 1H, H-4^{I}), 5.68 (dd, $J_{1,2}$ = 1.7 Hz, 1H, H-2^{I}), 5.63 (dd, $J_{2,3}$ = 1.0 Hz, 1H, H-3^{II}), 5.56 (s, 1H, H-1^{II}), 5.53 (d, 1H, H-2^{II}), 5.08 (d, 1H, H-1^{I}), 4.77–4.74 (m, 2H, H-6^{II}, H-6′^{III}), 4.69 (dd, 1H, H-4^{II}), 4.35 (m, 1H, H-5^{I}), 4.12–3.91 (m, 3H, H-6a^{I}, H-6b′^{I}, OC*H*H′), 3.74–3.49 (m, 3H, OCH*H*′, CH_2N), 2.04 (m, 2H, $CH_2CH_2CH_2$). ^{13}C NMR (151 MHz, $CDCl_3$) δ 133.65, 133.58, 133.54, 133.52, 133.31, 133.24, 133.13, 130.00, 129.91, 129.89, 129.79, 129.74, 128.65, 128.49, 128.44, 128.38, 128.32 (*Ph*C(O)), 106.49 (C-1^{II}), 97.52 (C-1^{I}), 82.06 (C-2^{II}), 81.26 (C-4^{II}), 77.63 (C-3^{II}), 71.34 (C-5^{I}), 70.39 (C-2^{I}), 70.19 (C-5^{II}), 69.83 (C-3^{I}), 67.15 (C-4^{I}), 66.27 (O*C*H$_2$), 66.07 (C-6^{I}), 63.66 (C-6^{II}), 37.61 (*C*H$_2$N), 28.52 (CH$_2$*C*H$_2$CH$_2$). HRMS (ESI): M = $C_{66}H_{56}F_3NO_{19}$. Calcd *m*/*z* for $[M + Na]^+$ 1246.3291, found 1246.3255.

3-Aminopropyl β-D-galactofuranosyl-(1→6)-α-D-mannopyranoside 8. The deblocking of compound **31** (35 mg, 0.029 mmol) as described in the general procedure afforded disaccharide **8** (8.8 mg, 77%) as a white foam. HRMS (ESI): M = $C_{15}H_{29}NO_{11}$. Calcd *m*/*z* for $[M + H]^+$ 400.1813, found 400.1816.

3-Trifluoroacetamidopropyl 2,3,5-tri-*O*-benzoyl-6-*O*-(9-fluorenylmethoxycarbonyl)-β-D-galactofuranosyl-(1→2)-3,4,6-tri-*O*-benzyl-α-D-mannopyranosyl-(1→2)-3,4,6-tri-*O*-benzyl-α-D-mannopyranoside 33. The glycosylation of acceptor **32** (28 mg, 0.027 mmol) with donor **16** (20 mg, 0.023 mmol) in 2.0 mL of CH_2Cl_2 as described in the general procedure gave trisaccharide **33** (30 mg, 77%) as a colorless syrup. R_f = 0.38 (toluene : EtOAc 5 : 1). ^{1}H NMR (600 MHz, $CDCl_3$) δ 8.12 (d, J = 7.2 Hz, 2H, *o*-Ph), 8.02 (d, J = 7.3 Hz, 2H, *o*-Ph), 7.81 (d, J = 7.3 Hz, 2H, *o*-Ph), 7.71 (dd, J = 7.6, 3.0 Hz, 2H, Ph), 7.52–7.06 (m, 44H, arom.), 6.97 (t, J = 7.4 Hz, 1H, Ph), 6.89 (br s, 1H, NH), 5.97–5.93 (m, 1H, H-5^{III}), 5.50 (d, J = 4.1 Hz, 1H, H-3^{III}), 5.48 (s, 1H, H-2^{III}), 5.20 (s, 1H, H-1^{III}), 5.10 (d, J = 1.5 Hz, 1H, H-1^{II}), 4.88 (d, J = 1.6 Hz, 1H, H-1^{I}), 4.82 (d, J = 10.8 Hz, 1H, PhC*H*H′), 4.74–4.44 (m, 11H, 10 × PhC*H*H′, H-6a^{III}), 4.34 (d, J = 10.9 Hz, 1H, PhC*H*H′), 4.29–4.15 (m, 4H, H-2^{II}, Fmoc-CH_2, H-6b^{III}), 4.09 (t, J = 7.6 Hz, 1H, Fmoc-C*H*), 4.03–4.00 (m, 1H, H-2^{I}), 3.95–3.61 (m, 11H, H-3^{I}, H-4^{I}, H-5^{I}, H-6a^{I}, H-6b^{I}, H-3^{II}, H-4^{II}, H-5^{II}, H-6a^{II}, H-6b^{II}, OC*H*H′CH$_2$), 3.43–3.17 (m, 3H, OCH*H*′CH$_2$C*H*$_2$NH), 1.77–1.66 (m, 2H, CH$_2$C*H*$_2$CH$_2$). ^{13}C NMR (151 MHz, $CDCl_3$) δ 165.69, 165.29, 154.93, 143.43, 141.33, 138.44, 138.38, 133.54, 133.42, 133.26, 130.15, 129.98, 128.61–128.36, 128.09, 127.90, 127.71, 127.39, 127.27, 125.40, 125.36, 120.05 (arom.), 103.75 (C-1^{III}), 99.40 (C-1^{II}), 99.24 (C-1^{I}), 82.50 (C-4^{III}), 81.43 (C-2^{III}), 79.90 (C-3^{I}), 78.18 (C-3^{II}), 77.91 (C-3^{III}), 75.74, 75.34, 75.14, 75.06, 74.89, 73.70, 73.55, 72.69, 72.37 (6 × PhC*H*$_2$, C-2^{I}, C-4^{I}, C-5^{I}, C-2^{II}, C-4^{II}, C-5^{II}), 70.57 (C-5^{III}), 70.25 (Fmoc-C*H*$_2$), 69.99 (C-6^{II}), 69.59 (C-6^{I}), 66.88 (C-6^{III}), 66.02 (OC*H*$_2$CH$_2$), 46.72 (Fmoc-*C*H), 38.15 (*C*H$_2$NH), 28.26 (OCH$_2$*C*H$_2$CH$_2$NH). HRMS (ESI): M = $C_{101}H_{96}F_3NO_{22}$. Calcd *m*/*z* for $[M + Na]^+$ 1754.6268, found 1754.6258.

3-Aminopropyl β-D-galactofuranosyl-(1→2)-α-D-mannopyranosyl-(1→2)-α-D-mannopyranoside 13. The removal of all protective groups in compound **33** (25 mg, 0.014 mmol) as described for the preparation of disaccharide **5** gave **13** (6.5 mg, 80%) as a white foam. HRMS (ESI): M = $C_{21}H_{39}NO_{16}$. Calcd *m*/*z* for $[M + H]^+$ 562.2342, found 562.2342.

Conflicts of interest

There are no conflicts to declare.

Acknowledgements

This work was supported by RSF grant 14-23-00199 (NEN). We thank Dr Thierry Fontaine for providing the galactomannan sample. We thank Dr A. O. Chizhov for recording high resolution mass spectra in the Department of Structural Studies of the Zelinsky Institute of Organic Chemistry, Moscow.

References

1 J. R. Köhler, B. Hube, R. Puccia, A. Casadevall and J. R. Perfect, *Microbiol. Spectrum*, 2017, **5**, DOI: 10.1128/microbiolspec.FUNK-0014-2016.
2 R. R. Herbrecht, D. W. Denning, T. F. Patterson, J. E. Bennett, R. E. Greene, J.-W. Oestmann, W. V. Kern, K. A. Marr, P. Ribaud, O. Lortholary, R. Sylvester, R. H. Rubin, J. R. Wingard, P. Stark, C. Durand, D. Caillot, E. Thiel, P. H. Chandrasekar, M. R. Hodges, H. T. Schlamm, P. F. Troke and B. de Pauw, *N. Engl. J. Med.*, 2002, **347**, 408–415.
3 H. Kume, T. Yamazaki, T. Togano, M. Abe, H. Tanuma, S. Kawana and M. Okudaira, *Med. Mycol. J.*, 2011, **52**, 117–127.
4 J.-P. Latgé, H. Kobayashi, J.-P. Debeaupuis, M. Diaquin, J. Sarfati, J.-M. Wieruszeski, E. Parra, J.-P. Bouchara and B. Fournet, *Infect. Immun.*, 1994, **62**, 5424–5433.
5 D. Stynen, A. Goris, J. Sarfati and J. P. Latgé, *J. Clin. Microbiol.*, 1995, **33**, 497–500.
6 C. Costachel, B. Coddeville, J.-P. Latgé and T. Fontaine, *J. Biol. Chem.*, 2005, **280**, 39835–39842.
7 A. Kudoh, Y. Okawa and N. Shibata, *Glycobiology*, 2015, **25**, 74–87.
8 A. W. Van Bruggen-Van Der Lugt, H. J. Kamphuis, G. A. De Ruiter, P. Mischnick, J. H. Van Boom and F. M. Rombouts, *J. Bacteriol.*, 1992, **174**, 6096–6102.

9 S. Guo, W. Mao, M. Yan, C. Zhao, N. Li, J. Shan, C. Lin, X. Liu, T. Guo, T. Guo and S. Wang, *Carbohydr. Polym.*, 2014, **105**, 325–333.
10 N. Shibata, T. Saitoh, Y. Tadokoro and Y. Okawa, *Microbiology*, 2009, **155**, 3420–3429.
11 K. Ikuta, N. Shibata, J. S. Blake, M. V. Dahl, R. D. Nelson, K. Hisamichi, H. Kobayashi, S. Suzuki and Y. Okawa, *Biochem. J.*, 1997, **323**, 297–305.
12 R. P. Da Silva, C. Heiss, I. Black, P. Azadi, J. Q. Gerlach, L. R. Travassos, L. Joshi, M. Kilcoyne and R. Puccia, *Sci. Rep.*, 2015, **5**, 14213.
13 E. A. Leitão, V. C. Bittencourt, R. M. Haido, A. P. Valente, J. Peter-Katalinic, M. Letzel, L. M. de Souza and E. Barreto-Bergter, *Glycobiology*, 2003, **13**, 681–692.
14 G. C. Completo and T. L. Lowary, *J. Org. Chem.*, 2008, **73**, 4513–4525.
15 A. K. Pathak, V. Pathak, L. Seitz, J. A. Maddry, S. S. Gurcha, G. S. Besra, W. J. Suling and R. C. Reynolds, *Bioorg. Med. Chem.*, 2001, **9**, 3129–3143.
16 L. Gandolfi-Donadío, C. Gallo-Rodriguez and R. M. de Lederkremer, *J. Org. Chem.*, 2003, **68**, 6928–6934.
17 M. J. Tilve, C. R. Cori and C. Gallo-Rodriguez, *J. Org. Chem.*, 2016, **81**, 9585–9594.
18 L. Cattiaux, B. Sendid, M. Collot, E. Machez, D. Poulain and J.-M. Mallet, *Bioorg. Med. Chem.*, 2011, **19**, 547–555.
19 M. Fu, G. Zhang and J. Ning, *Carbohydr. Res.*, 2005, **340**, 25–30.
20 R. Euzen, V. Ferrières and D. Plusquellec, *Carbohydr. Res.*, 2006, **341**, 2759–2768.
21 D. A. Argunov, V. B. Krylov and N. E. Nifantiev, *Org. Biomol. Chem.*, 2015, **13**, 3255–3267.
22 D. A. Argunov, V. B. Krylov and N. E. Nifantiev, *Org. Lett.*, 2016, **18**, 5504–5507.
23 V. B. Krylov, D. A. Argunov, D. Z. Vinnitskiy, S. A. Verkhnyatskaya, A. G. Gerbst, N. E. Ustyuzhanina, A. S. Dmitrenok, J. Huebner, O. Holst, H.-C. Siebert and N. E. Nifantiev, *Chem. – Eur. J.*, 2014, **20**, 16516–16522.
24 V. B. Krylov, D. A. Argunov, D. Z. Vinnitskiy, A. G. Gerbst, N. E. Ustyuzhanina, A. S. Dmitrenok and N. E. Nifantiev, *Synlett*, 2016, 1659–1664.
25 C. Gallo-Rodriguez, L. Gandolfi and R. M. de Lederkremer, *Org. Lett.*, 1999, **1**, 245–248.
26 A. A. Karelin, Y. E. Tsvetkov, G. Kogan, S. Bystricky and N. E. Nifantiev, *Russ. J. Bioorg. Chem.*, 2007, **33**, 110–121.
27 A. S. Shashkov, G. M. Lipkind, Y. A. Knirel and N. K. Kochetkov, *Magn. Reson. Chem.*, 1988, **26**, 735–747.
28 B. Schumann, S. G. Parameswarappa, M. P. Lisboa, N. Kottari, F. Guidetti, C. L. Pereira and P. H. Seeberger, *Angew. Chem., Int. Ed.*, 2016, **55**, 14431–14434.
29 H. Van Halbeek, *Biochem. Soc. Trans.*, 1984, **12**, 601–605.
30 J. F. Vliegenthart, L. Dorland and H. van Halbeek, *Adv. Carbohydr. Chem. Biochem.*, 1983, **41**, 209–374.
31 G. M. Lipkind, A. S. Shashkov, Y. A. Knirel, E. V. Vinogradov and N. K. Kochetkov, *Carbohydr. Res.*, 1988, **175**, 59–75.
32 G. M. Lipkind, A. S. Shashkov, N. E. Nifant'ev and N. K. Kochetkov, *Carbohydr. Res.*, 1992, **237**, 11–22.
33 F. Lisacek, J. Mariethoz, D. Alocci, P. M. Rudd, J. L. Abrahams, M. P. Campbell, N. H. Packer, J. Ståhle, G. Widmalm, E. Mullen, B. Adamczyk, M. A. Rojas-Macias, C. Jin and N. G. Karlsson, *Methods Mol. Biol.*, 2017, **1503**, 235–264.
34 M. Lundborg and G. Widmalm, *Anal. Chem.*, 2011, **83**, 1514–1517.
35 A. G. Gerbst, V. B. Krylov, D. Z. Vinnitskiy, A. S. Dmitrenok, A. S. Shashkov and N. E. Nifantiev, *Carbohydr. Res.*, 2015, **417**, 1–10.

ChemPubSoc Europe

DOI: 10.1002/ejoc.201900389

EurJOC European Journal of Organic Chemistry

Full Paper

Oligosaccharide Synthesis

SPECIAL ISSUE

Convergent Synthesis of Oligosaccharides Structurally Related to Galactan I and Galactan II of *Klebsiella Pneumoniae* and their Use in Screening of Antibody Specificity

Dmitry A. Argunov,[a] Anastasiia S. Trostianetskaia,[a,b] Vadim B. Krylov,[a] Ekaterina A. Kurbatova,[c] and Nikolay E. Nifantiev*[a]

Abstract: *Klebsiella pneumoniae* Is a Gram-negative pathogenic bacterium that emerges a challenge for modern medicine due to intensively rising multi-drug resistance. Specific LPS O-chains represent promising targets for development of vaccines for immunoprophylaxis or immunotherapy of *K. pneumoniae*-caused diseases. Herein, the synthesis of di-, tetra-, and hexasaccharides which represent structural fragments of both galactan I and galactan II of *K. pneumoniae* LPS O-chains is described. The galactofuranoside building block used for assembling the galactan I chains was prepared by pyranoside-*into*-furanoside (PIF) rearrangement of the corresponding galactopyranoside precursor bearing an acid-labile temporary *p*-methoxybenzyl protecting group at O(3). The synthesized set of *K. pneumoniae* antigenic oligosaccharides in the form of their biotinylated derivatives was used to create a glycoarray which was applied for the screening of antibodies to galactan I and galactan II in anti-*K. pneumoniae* sera. The obtained results demonstrate the applicability of such a glycoarray-based assay for typing antibodies to *Klebsiella* strains belonging to most frequent O1 serogroup.

Introduction

Bacterial polysaccharides and corresponding synthetic oligosaccharides form the basis for the development of antibacterial glycoconjugate vaccines.[1–3] Among them the most challenging are the vaccines against multidrug-resistant bacteria of ESKAPE group causing nosocomial infections and epidemics.[4–6] The above abbreviation is acronymically formed from the first letters of six most dangerous pathogens where "K" goes from *Klebsiella pneumoniae*.

It is an emerging multi-drug resistant Gram-negative opportunistic bacterium, causing severe diseases in humans including pneumonia, urinary tract infections, intra-abdominal infections, meningitis, pyogenic liver abscesses, bacteremia and sepsis in immunocompromised patients.[7–9] More than 50 % of all clinical isolates of *K. pneumoniae* have multi-drug resistance[10] and represents a major public health problem worldwide.[11,12] Passive and active immunization is considered as a promising alternative to the antibiotic treatment.[13]

Capsular polysaccharides (K-antigens) and LPS O-chains (O-antigens) are critical for pathogenesis of *K. pneumoniae* infection and for development of antibacterial immune response and thus can be chosen as targets for development anti-*K. pneumoniae* vaccines for immunoprophylaxis or immunotherapy.[13–18] In particular, the application of protein-carrier conjugates of capsular polysaccharides[15,16,19] provided immune protection against carbapenem-resistant *K. pneumoniae*.

The polysaccharides linked to the core region of LPS represent the O-antigens of *K. pneumoniae*. The O-antigens of the most prevalent O1 serotype are built up from two polysaccharide types: galactan I and galactan II (Figure 1). Galactan I is located at the inner part of the O-chains. Galactan-I-like chains are also found in other *K. pneumoniae* serotypes (O2 and O2ac).[19,20] Branched form of galactan I, namely galactan III, was also reported for O2 serotype.[21,22] Galactans I–III are antigenic components of *K. pneumoniae* O1 and O2 serotypes which are the cause of 50–68 % of all *Klebsiella* infections and

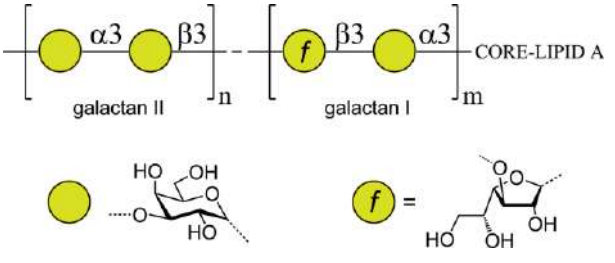

Figure 1. The structure of LPS O-chains of *K. pneumoniae* O1 serotype.[20] The carbohydrate sequences are represented according to symbol carbohydrate nomenclature.[23]

[a] *Laboratory of Glycoconjugate Chemistry, N.D. Zelinsky Institute of Organic Chemistry, Russian Academy of Sciences, Leninsky prospect 47, 119991 Moscow, Russian Federation*
E-mail: nen@ioc.ac.ru
http://zioc.ru/institute/laboratories/glycoconjugates
[b] *Higher Chemical College, D. I. Mendeleev University of Chemical Technology of Russia, Miusskaya sq. 9, 125047, Moscow, Russia*
[c] *Laboratory of Immunology, I. I. Mechnikov Research Institute for Vaccines and Sera, Moscow, Russia*

Supporting information and ORCID(s) from the author(s) for this article are available on the WWW under https://doi.org/10.1002/ejoc.201900389.

are the most prevailing serotypes among carbapenem-resistant clinical isolates.[13]

Herein we describe the synthesis of spacer-armed oligosaccharides **1a**–**6a** structurally related to galactan I and galactan II of *K. pneumoniae* LPS O-chains. To the best of our knowledge, the synthesis of galactan II related chains was not performed yet. The syntheses of Gal*f*-containing oligosaccharides related to galactan I described by Zhu and Yang[24] and Sweeney and

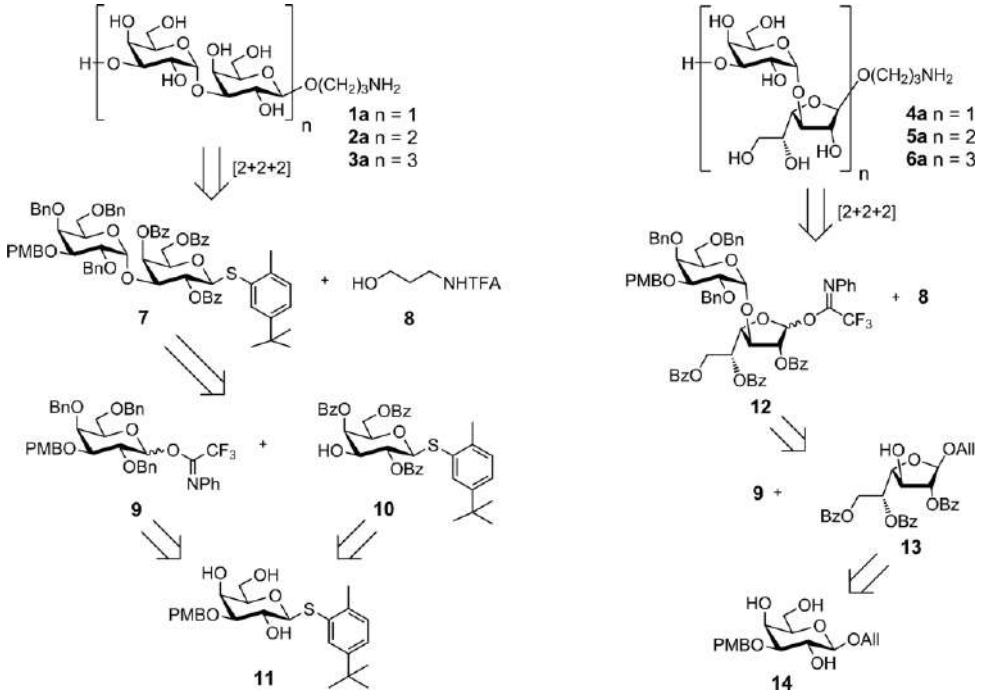

Scheme 1. The structure and retrosynthetic analysis of target compounds **1a**–**3a** (related to galactan II) and **4a**–**6a** (related to galactan I).

Dr. Dmitry A. Argunov graduated from Higher Chemical College of the Russian Academy of Sciences in 2013 and then joined the graduate school at ZIOC. He defended his PhD thesis in 2017 under the supervision of Dr. Vadim B. Krylov. His research interests are focused on preparative oligosaccharide synthesis, investigation of organic reaction, NMR-studies. The area of his research work covers the synthesis of furanoside-containing oligosaccharides related to fungal and bacterial pathogens. He is supervising master students and has 15 papers in peer-reviewed journals.

Anastasiia Trostianetskaia *is 4th-year student of Higher Chemical College of the Russian Academy of Sciences. She has been working in the Laboratory of glycoconjugate chemistry of ZIOC since 2016 under the supervision of Dr. Vadim B. Krylov. Her research areas are oligosaccharide synthesis, preparation of neoglycoconjugates and bioassaying.*

Dr. Vadim B. Krylov *is currently the senior scientific researcher in the Laboratory of glycoconjugate chemistry of ZIOC. He has got his chemical qualification within the original "ZIOC's system of continuous chemical education". It included primary education in Moscow Chemical Lyceum (2002), education in Higher Chemical College of RAS (2007) and post-graduate training at ZIOC (PhD theses in 2010 with Dr. Nadezhda E. Ustyuzhanina) in the Laboratory of glycoconjugate chemistry headed by Prof. Nikolay E. Nifantiev. He is a specialist in carbohydrate chemistry, glycoscience and biomedical investigations. He is actively involved in students' tutoring and is a co-author of more than 50 papers in peer-reviewed journals*

Prof. Ekaterina A. Kurbatova *is in the head of the Laboratory of therapeutic vaccines at the I. I. Mechnikov Research Institute for Vaccines and Sera. The fields of her research interests are opportunistic microorganisms, innate immunity, adaptive immunity, mucosal immunity, therapeutic and prophylactic vaccines.*

Prof. Nikolay E. Nifantiev *studied chemistry in M. V. Lomonosov Moscow State University and then received his Ph.D. in 1984 in Academician Nikolay K. Kochetkov's laboratory of ZIOC. In 1994 he established new research unit at ZIOC - the Laboratory of glycoconjugate chemistry. Prof. Nifantiev was elected to be the Corresponding Member of the Russian Academy of Sciences (from 2011). Prof. Nifantiev has published 350+ papers and 30+ national and international patents mainly within the area of the synthesis, NMR, and conformational studies of oligo- and polysaccharides. Recent interests have focused on development of glycoconjugate drugs, vaccines and diagnostic test-kits as well on the investigation of mechanisms of glycosylation reactions and 3D-structures of carbohydrate determinants.*

Lowary[25] were performed according to synthetic schemes which include the preparation of galactofuranose blocks in the first steps directly from unsubstituted galactose. The preparation of Gal*f*-containing di-, tetra- and hexasaccharides **4a**–**6a** described here includes first preparation of selectively substituted galactopyranoside block and its further pyranoside-*into*-furanoside (PIF) rearrangement into substituted galactofuranoside derivatate. Such approach was previously successfully applied by us to the synthesis of tetrasaccharide related to galactan I.[26] The previously employed synthetic strategy included PIF rearrangement of the disaccharide precursor and regioselective glycosylation of the 2,3-diol.[26] The synthetic scheme described below (see Scheme 1) is more efficient for preparation of longer oligosaccharides and included PIF rearrangement of galactopyranoside precursor **14** followed by glycosylation of monohydroxyl acceptors. In addition to the synthesis of compounds **1a**–**6a**, we describe also their transformation into biotinylated derivatives **1b**–**6b**, their arraying on a streptavidin-coated plate and the use of the formed glycoarray for screening of antibodies in sera against O1 serotype of *K. pneumoniae*.

Results and Discussion

Synthesis of oligosaccharides 1a–3a. The preparation of oligosaccharides **1a**–**3a** related to the galactan II was performed by [2+2+2] scheme chosen on the basis of retrosynthetic analysis (Scheme 1). It also suggested the use of α-(1→3)-linked disaccharide donor **7** with a temporary *p*-methoxybenzyl (PMB) protection at O(3) as the key building block to be prepared by the coupling of imidate **9** and acceptor **10**. Both were available from thiogalactoside **11** bearing PMB-group at O(3). According to this strategy, the synthesis of oligosaccharides **1a**–**3a** was started with the introduction of the PMB-protection at O(3) in thiogalactoside **15** (Scheme 2; for preparation of **15** see Supporting information) which was achieved by the subsequent treatment with Bu_2SnO and PMBCl in the presence of Bu_4NBr. The location of the PMB-group at O(3) in **11** was confirmed by the significant downfield chemical shift of C(3) in ^{13}C-NMR spectrum (81.5 ppm) and significant downfield shift of protons H(2), H(4), and H(6) in tribenzoate **17** obtained by per-O-benzoylation of triol **11** (see below).

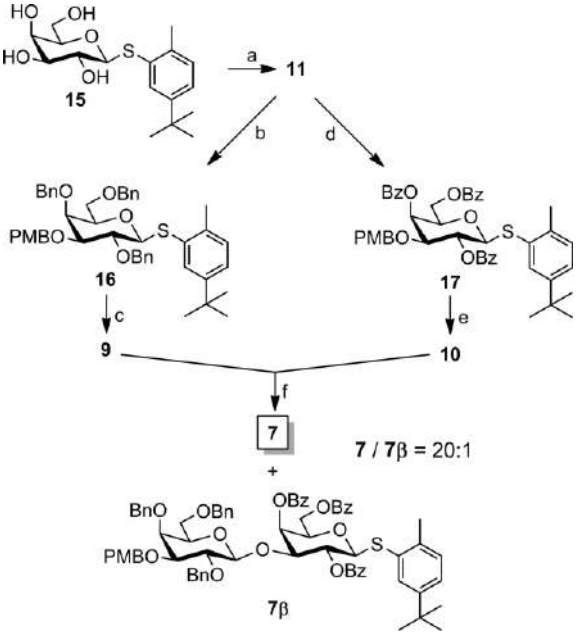

Scheme 2. Synthesis of disaccharide block **7**. (a) i: Bu_2SnO, toluene, Δ, 1.5 h; ii: PMBCl, Bu_4NBr, toluene, 60 °C, 42 %; (b) BnBr, NaH, DMF, 81 %; (c) i: NIS, acetone/H_2O, 10:1, 91 %; ii: ClC(NPh)CF_3, Cs_2CO_3, acetone, 98 %; (d) BzCl, Py, CH_2Cl_2, 91 %; (e) TFA 90 % (aq.), toluene, 92 %; (f) NIS, TfOH, AW-300 MS, Et_2O, 65 % for **7**, 3 % for **7β**.

Per-O-benzylation of triol **11** with BnBr and NaH gave tribenzyl ether **16** which was subsequently treated with NIS in aq. acetone (to cleave the thioglycoside bond and produce the

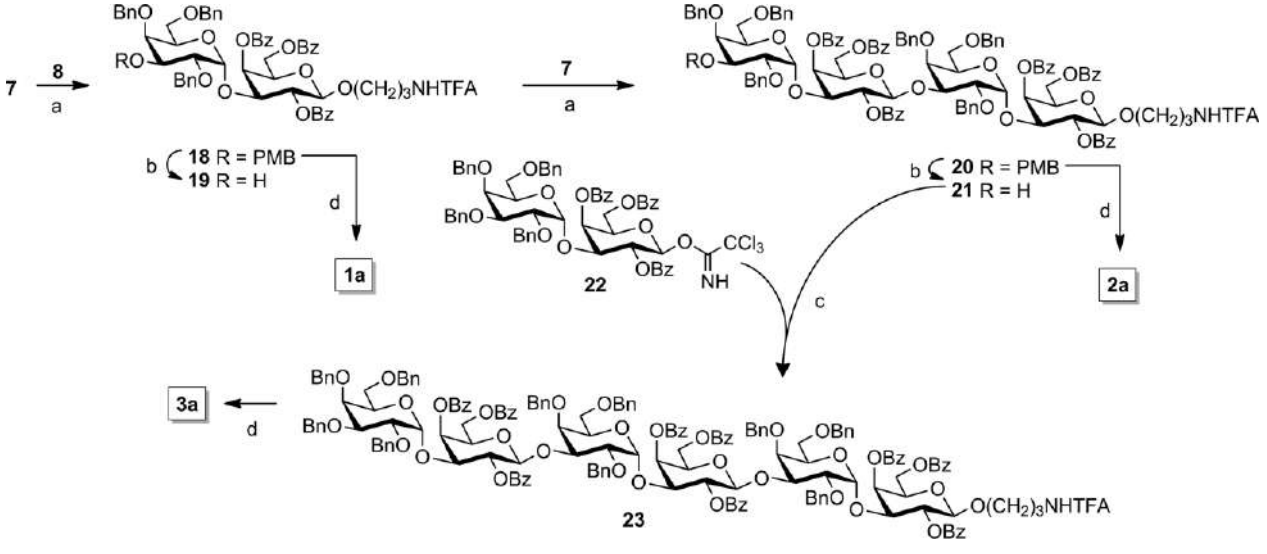

Scheme 3. Synthesis of oligosaccharides related to galactan II. (a) NIS, TfOH, AW-300 MS, CH_2Cl_2, 85 % for **18**, 90 % for **20**; (b) TFA 90 % (aq.), CH_2Cl_2, 90 % for **19**; 82 % for **21**; (c) TMSOTf, AW-300 MS, CH_2Cl_2, 85 %; (d) i: H_2, $Pd(OH)_2$/C (20 %), EtOAc/MeOH, 1:1; ii: MeONa, MeOH, then H_2O, 85 % for **1a**, 78 % for **2a**, 70 % for **3a**.

hemiacetal) and ClC(NPh)CF_3 in presence of Cs_2CO_3 to give the corresponding N-phenyl-trifluoroacetimidate **9**.

Per-O-benzoylation of triol **11** with BzCl and Py in CH_2Cl_2 and the subsequent hydrolysis of PMB-ether by aq. TFA in toluene gave glycosyl acceptor **10**. Its coupling with imidate **9** gave the mixture of isomeric (1→3)-linked disaccharides with strong predominance of desired α-linked **7** (α/β = 20:1, isolated yields). Anomeric configurations of α- (**7**) β-isomers (**7β**) were confirmed by the values of the corresponding coupling constant $^3J_{1,2}$ (3.3 and 9.8 Hz).

Coupling of 3-trifluoroacetamidopropanol **8** with disaccharide **7** gave spacer-armed disaccharide **18** (Scheme 3). It was treated with aq. TFA in CH_2Cl_2 to remove the PMB-protection and produce the glycosyl acceptor **19**. This product was then coupled with disaccharide donor **7** with the formation of tetrasaccharide **20**. The removal of the O-PMB group as described above and subsequent glycosylation with known imidate **22**[27] gave desired hexasaccharide **23**. All glycosylations by disaccharides **7** and **22** proceeded β-stereospecifically that was confirmed by the characteristic coupling constant $^3J_{1,2}$ (8.0 Hz) for the corresponding units in the formed products. O,N-Protected di-, tetra-, and hexa-saccharides (**18**, **20**, **23**) were deblocked by hydrogenolysis on $Pd(OH)_2/C$ and subsequent treatment with MeONa and NaOH in MeOH to give target oligosaccharides **1a**–**3a**.

Synthesis of oligosaccharides 4a–6a. The preparation of oligosaccharides **4a**–**6a** related to the galactan I was performed also by [2+2+2] scheme chosen on the basis of retrosynthetic analysis (Scheme 1). It also suggested the use of α-(1→3)-linked disaccharide donor **12** and its preparation by the coupling of furanoside **13** with donor **9**. Pyranoside-*into*-furanoside (PIF)[28–30] rearrangement of selectively O-substituted galactopyranoside **14** was suggested as the pathway towards furanoside block **13**.

According to this strategy, the synthesis of oligosaccharides **4a**–**6a** was started with the PIF-rearrangement of allyl galactoside **14**[31,32] bearing the PMB-group at O(3) (Scheme 4). Although in general this group can be easily removed under acidic conditions, it was retained under the conditions of PIF-rearrangement (step (a) on Scheme 4). Only the intermediate 2,4,6-trisulfated furanoside was produced, which after O- desulfation by IR-120 H^+ resin in MeCN-DMF gave furanoside **24**. The structure of furanoside **24** and in particular its β-anomeric configuration and location of the PMB-group at O(3) were confirmed by the characteristic signals in ^1H and ^{13}C NMR spectra (see Supporting information).

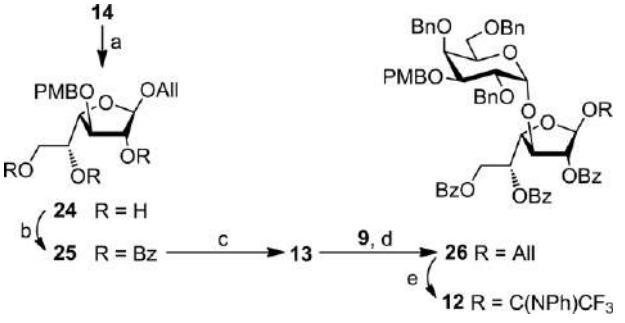

Scheme 4. Synthesis of disaccharide donor **12**. (a) i: Py•SO_3, HSO_3Cl, overnight, then excess of NH_4HCO_3 aq.; ii: IR-120(H^+), MeCN-DMF, 70 °C, 46 % over two steps; (b) BzCl, Py, CH_2Cl_2, 81 %; (c) TFA 90 % (aq.), CH_2Cl_2, 83 %; (d) **9**, TMSOTf, AW-300 MS, CH_2Cl_2, 74 %; (e) i: $PdCl_2$, MeOH/CH_2Cl_2, 5:1, 82 %; ii: ClC(NPh)CF_3, Cs_2CO_3, acetone, 95 %.

Per-O-benzoylation of triol **24** with BzCl and subsequent hydrolysis of PMB-ether by treatment with aq. TFA gave acceptor **13**, which was then coupled with donor **9** to give α-(1→3)-linked disaccharide **26** as the only product. α-Configuration of the newly formed glycosyl bond was confirmed by the characteristic coupling constant $^3J_{1,2}$ (3.7 Hz). Allyl aglycon was then removed by treatment with $PdCl_2$ in MeOH/CH_2Cl_2 followed by imidation of the formed hemiacetal to give N-phenyl-trifluoroacetimidate **12**.

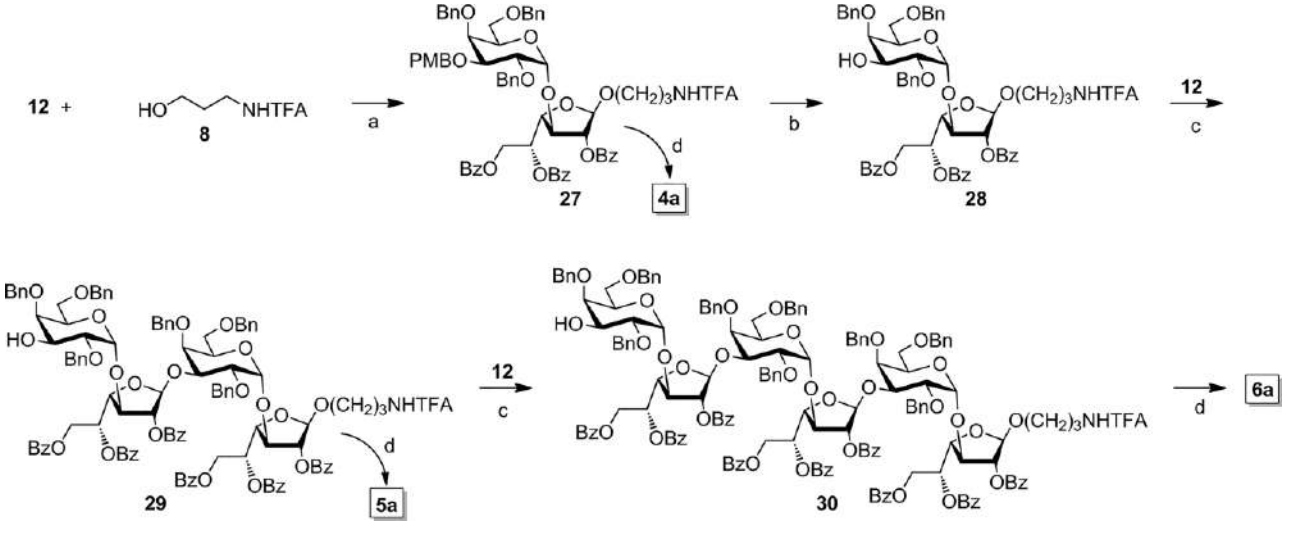

Scheme 5. Synthesis of oligosaccharides related to galactan I. (a) TMSOTf, AW-300 MS, CH_2Cl_2, 81 %; (b) TFA 90 % (aq.), CH_2Cl_2, 83 %; (c) TMSOTf, AW-300 MS, CH_2Cl_2, –50 → –15 °C, 76 % for **29**, 81 % for **30**; (d) i: H_2, $Pd(OH)_2/C$ (20 %), EtOAc/MeOH, 1:1; ii: MeONa, MeOH, then H_2O, 82 % for **4a**, 72 % for **5a**, 71 % for **6a**.

Coupling of donor **12** with 3-trifluoroacetamidopropanol **8** gave spacer-armed disaccharide **27**, which was then transformed into acceptor **28** by removal of the PMB-protection under acidic conditions (Scheme 5). Following glycosylation with donor **12** and removal of the PMB-group were performed in one operational step to give monohydroxy tetrasaccharide **29**. Its subsequent glycosylation-deprotection led to hexasaccharide **30**. Compounds **27**, **29**, and **30** were then O,N-deblocked as described above to give target oligosaccharides **4a**–**6a**.

Glycoarray formation and screening of anti-K. pneumoniae O1 sera. Oligosaccharides **1a**–**6a** were used as biotinylated derivatives **1b**–**6b** in the development of the glycoarray (Scheme 6). Compounds **1b**–**6b** were prepared by treatment of aminopropyl glycosides **1a**–**6a** with biotin derivative **31**[33] containing hexaethylene glycol spacer which is required for efficient spatial presentation of the carbohydrate ligands in the glycoarray for biological recognition. The structures of obtained biotinylated derivatives **1b**–**6b** were confirmed by HRMS-data and by presence of the characteristic signals of the biotin moiety in ^{1}H-NMR spectra of products **1b**–**6b** (see Supporting information).

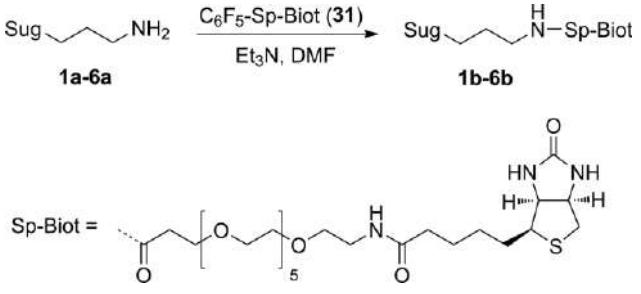

Scheme 6. Synthesis of biotinylated glycoconjugates **1b**–**6b**.

Biotinylated glycoconjugates **1b**–**6b** were immobilized on the surface of streptavidin-coated plates as described previously[34,35] to form glycoarray which was applied for screening of sera against *K. pneumoniae* O1 belonging to K-serotypes 1, 2 and 16.[36] Anti-sera were examined in 1:500 dilution (Figure 2) as well as 1:250 and 1:1000 (see Supporting Information). All three tested sera demonstrated significant concentration-dependent reactivity with hexasaccharide **3b** related to galactan II. The intensity of interaction decreased with shortening of the oligosaccharide ligand down to tetrasaccharide **2b**, while the disaccharide **1b** was poorly recognized by serum antibodies. The tetra- (**5b**) and hexasaccharide **6b** related to galactan I specifically recognized antibodies in sera against *K. pneumoniae* K-type 16 (but not K-types 1 and 2) while disaccharide **4b** was inactive. Antibodies in serum against *K. pneumoniae* O3:K11 interacted with neither galactan I nor galactan II related oligosaccharide ligands in the glycoarray; that is in agreement with the fact that these bacterial strains do not produce galactan I and galactan II polysaccharide chains.[20]

The obtained results correlate well with previously published data summarizing the screenings of blood sera from patients infected with *K. pneumoniae*.[13] These studies revealed remarkably higher titers of antibodies against *K. pneumoniae* O1 LPS

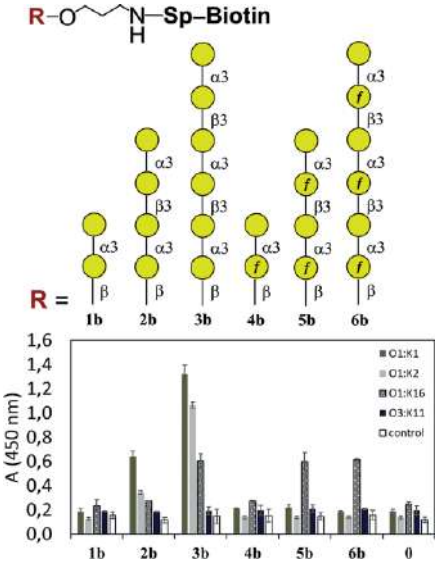

Figure 2. Screening of anti-*K. pneumoniae* antibodies in sera (1:500 dilution) on glycoarray build up from of biotinylated oligosaccharides **1b**–**6b.** Control – sera of intact animals, **0** – no coating antigen.

(containing both galactan I and galactan II) than against *K. pneumoniae* O2 LPS (containing galactan I but not galactan II). These data revealed domination of anti-galactan II antibodies over anti-galactan I antibodies in sera that was explained by higher immunogenicity of galactan II chains.[13,36]

Conclusions

The successful convergent synthesis of spacer-armed di-, tetra-, and hexasaccharides **1a**–**6a** structurally related to the galactan I and galactan II of *K. pneumoniae* O1 LPS O-chains was carried out using disaccharide donors **7** and **12** as the key building blocks. The preparation of galactofuranoside-containing block **12** was performed employing the PIF-rearrangement of a galactopyranoside precursor bearing the PMB-protecting group at O(3). Synthesized oligosaccharides **1a**–**6a** in the form of their biotinylated derivatives **1b**–**6b** were used as the components of a glycoarray built up on the surfaces of streptavidin-coated microtiter plates and applied for the screening of antibodies in anti-*K. pneumoniae* O1 sera. The obtained results demonstrated that hexasaccharide **3b** related to the galactan II was efficiently recognized by serum antibodies. It showed the potential of this oligosaccharide or its longer analogs for the use in vaccine and diagnostic kits development which are in the progress in this laboratory.

Experimental Section

General methods. All solvents for reactions were dried according to conventional procedures or purchased as dry. Dichloromethane (CH_2Cl_2) was distilled from CaH_2, and methanol (MeOH) was distilled from $Mg(OMe)_2$. Dimethylformamide (DMF) and acetonitrile (CH_3CN) was purchased as dry and used without further purification. Reagents for synthesis were commercial and used without further purification. All reactions involving air- or moisture-sensitive

reagents were carried out using dry solvents under dry argon. Molecular sieves AW-300 MS were crushed and activated prior to reaction for 5 minutes at 400–500 °C in vacuo. Amberlite IR-120 (Fluka) was washed with 1 M aq. HCl, H_2O, acetone and dried. Thin-layer chromatography (TLC) was carried out on aluminum plates coated with silica gel 60 F_{254} (Merck). Analysis TLC plates were inspected by UV light (λ = 254 nm) and developed by the treatment with a mixture of 15 % H_3PO_4 and orcinol (1.8 g/L) in EtOH/H_2O (95:5, v/v) followed by heating. Silica gel column chromatography was performed with Silica Gel 60 (40–63 μm, Merck). Flash chromatography was performed on Buchi Reveleris X2 system using Buchi FlashPure EcoFlex cartridges (irregular 40–63 μm silica). Gel-filtration was performed on a TSK-40 HW(S) column (420 × 25 mm) by elution with 0.1 M AcOH in water at a flow rate of 0.5 mL min^{-1}.

Spectroscopic methods. NMR spectra were recorded on Bruker Fourier 300HD (300 MHz), Bruker AV400 (400 MHz) or Bruker AV600 (600 MHz) spectrometers at temperatures denoted on the spectra. The resonance assignment in ^1H and ^{13}C NMR spectra was performed using 2D-experiments (COSY, HSQC and HMBC). Chemical shifts are reported in ppm referenced to tetramethylsilane as a standard for ^1H and solvent signal (δ = 77.16 for $CDCl_3$) for ^{13}C. High-resolution mass spectra (HRMS) were recorded on a Bruker micrOTOF II instrument using electrospray ionization (ESI). The measurements were performed in positive ion mode (interface capillary voltage –4500 V) or in negative ion mode (3200 V); mass range from m/z 50 to m/z 3000 Da; external or internal calibration was made with an electrospray calibrant solution (Fluka). A syringe injection was used for solutions in a mixture of acetonitrile and water (50:50 v/v, flow rate 3 μL min^{-1}). Nitrogen was applied as a dry gas; interface temperature was set at 180 °C.

Synthetic procedures. Full experimental details, characterization for all new compounds and copies of ^1H, ^{13}C, HSQC NMR, spectra are provided in the Supporting Information.

Assaying antibodies in sera against *K. pneumoniae* on glycoarray. The wells of 96-well Pierce™ streptavidin-coated plates were coated with synthetic biotinylated oligosaccharides **1b**–**6b** (100 μL of a 200 pmol/mL solution in wash buffer: PBS containing 0.05 % Tween-20 and 0.1 % BSA) and then incubated for 2 h at 37 °C. After washing three times with wash buffer, the plates were incubated with Klebsiella antisera (immune sera to *K. pneumoniae* obtained from the laboratory collection of Mechnikov Research Institute for Vaccine and Sera and Difco™ *Klebsiella* antisera set) in 1:250, 1:500, 1:1000 dilution for 1 h at 37 °C. After washing, horseradish peroxidase-labeled IgG anti-rabbit secondary antibodies (XEMA, Russia) was added and incubated for 1 h at 37 °C. After washing three times, color was developed using TMB mono-component substrate (100 μL) for 15 minutes and stopped with 50 μL of 1 M sulfuric acid. Absorbance was measured at 450 nm using MultiSkan GO plate reader (Thermo Fisher Scientific, USA). Sera of intact animals were used is a control. All measurements were independently repeated twice in triplicate. Results were represented as means ± SD.

Acknowledgments

The authors thank Drs. A. G. Gerbst and Y. E. Tsvetkov for reading this manuscript and ist critical discussion and also Drs. A. O. Chizhov and A. S. Dmitrenok for recording HRMS and NMR spectra in the Department of Structural Studies of the Zelinsky Institute of Organic Chemistry, Moscow, Russia. This work was supported by the Russian Scientific Foundation (grant 19–73–30017).

Keywords: Antibodies · Glycoarray · Furanosides · Oligosaccharides · Pyranosides

[1] F. Micoli, P. Costantino, R. Adamo, *FEMS Microbiol. Rev.* **2018**, *42*, 388–423.
[2] C. Anish, B. Schumann, C. L. Pereira, P. H. Seeberger, *Chem. Biol.* **2014**, *21*, 38–50.
[3] M. L. Gening, E. A. Kurbatova, Y. E. Tsvetkov, N. E. Nifantiev, *Russ. Chem. Rev.* **2015**, *84*, 1100.
[4] H. W. Boucher, G. H. Talbot, J. S. Bradley, J. E. Edwards, D. Gilbert, L. B. Rice, M. Scheld, B. Spellberg, J. Bartlett, *Clin. Infect. Dis. Off. Publ. Infect. Dis. Soc. Am.* **2009**, *48*, 1–12.
[5] L. B. Rice, *J. Infect. Dis.* **2008**, *197*, 1079–1081.
[6] J. N. Pendleton, S. P. Gorman, B. F. Gilmore, *Expert Rev. Anti-Infect. Ther.* **2013**, *11*, 297–308.
[7] R. Podschun, U. Ullmann, *Clin. Microbiol. Rev.* **1998**, *11*, 589–603.
[8] D. K. Pomakova, C.-B. Hsiao, J. M. Beanan, R. Olson, U. MacDonald, Y. Keynan, T. A. Russo, *Eur. J. Clin. Microbiol. Infect. Dis.***2012**, *31*, 981–989.
[9] G. Patel, S. Huprikar, S. H. Factor, S. G. Jenkins, D. P. Calfee, *Infect. Control Hosp. Epidemiol.* **2008**, *29*, 1099–1106.
[10] M. Edelstein, M. Pimkin, I. Palagin, I. Edelstein, L. Stratchounski, *Antimicrob. Agents Chemother.* **2003**, *47*, 3724–3732.
[11] J. H. Han, E. J. C. Goldstein, J. Wise, W. B. Bilker, P. Tolomeo, E. Lautenbach, *Clin. Infect. Dis.* **2017**, *64*, 839–844.
[12] L. Xu, X. Sun, X. Ma, *Ann. Clin. Microbiol. Antimicrob.* **2017**, *16*, 18.
[13] M. E. Pennini, A. De Marco, M. Pelletier, J. Bonnell, R. Cvitkovic, M. Beltramello, E. Cameroni, S. Bianchi, F. Zatta, W. Zhao, et al., *Nat. Commun.* **2017**, *8*, 1991.
[14] A. Gucchait, A. Ghosh, A. K. Misra, *Beilstein J. Org. Chem.* **2019**, *15*, 431–436.
[15] P. H. Seeberger, C. L. Pereira, N. Khan, G. Xiao, E. Diago-Navarro, K. Reppe, B. Opitz, B. C. Fries, M. Witzenrath, *Angew. Chem. Int. Ed.* **2017**, *56*, 13973–13978; *Angew. Chem.* **2017**, *129*, 14161.
[16] E. Diago-Navarro, M. P. Motley, G. Ruiz-Peréz, W. Yu, J. Austin, B. M. S. Seco, G. Xiao, A. Chikhalya, P. H. Seeberger, B. C. Fries, *mBio* **2018**, *9*, https://doi.org/10.1128/mBio.00091–18.
[17] S. D. Kobayashi, A. R. Porter, B. Freedman, R. Pandey, L. Chen, B. N. Kreiswirth, F. R. DeLeo, *mBio* **2018**, *9*, https://doi.org/10.1128/mBio.00297–18.
[18] T. Rollenske, V. Szijarto, J. Lukasiewicz, L. M. Guachalla, K. Stojkovic, K. Hartl, L. Stulik, S. Kocher, F. Lasitschka, M. Al-Saeedi, et al., *Nat. Immunol.* **2018**, *19*, 617–624.
[19] E. Vinogradov, E. Frirdich, L. L. MacLean, M. B. Perry, B. O. Petersen, J. Ø. Duus, C. Whitfield, *J. Biol. Chem.* **2002**, *277*, 25070–25081.
[20] B. R. Clarke, O. G. Ovchinnikova, S. D. Kelly, M. L. Williamson, J. E. Butler, B. Liu, L. Wang, X. Gou, R. Follador, T. L. Lowary, et al., *J. Biol. Chem.* **2018**, *293*, 4666–4679.
[21] K. Stojkovic, V. Szijártó, M. Kaszowska, T. Niedziela, K. Hartl, G. Nagy, J. Lukasiewicz, *Front. Microbiol.* **2017**, *8*, 684.
[22] V. Szijártó, L. M. Guachalla, K. Hartl, C. Varga, P. Banerjee, K. Stojkovic, M. Kaszowska, E. Nagy, J. Lukasiewicz, G. Nagy, *Int. J. Med. Microbiol.* **2016**, *306*, 89–98.
[23] A. Varki, R. Cummings, J. Esko, H. Freeze, G. Hart, J. Marth, *Essentials of Glycobiology*, Cold Spring Harbor, NY, **1999**.
[24] S.-Y. Zhu, J.-S. Yang, *Tetrahedron* **2012**, *68*, 3795–3802.
[25] R. P. Sweeney, T. L. Lowary, *Org. Lett.* **2019**, *21*, 1050–1053.
[26] S. A. Verkhnyatskaya, V. B. Krylov, N. E. Nifantiev, *Eur. J. Org. Chem.* **2017**, *2017*, 710–718.
[27] T. Li, T. Li, T. Cui, Y. Sun, F. Wang, H. Cao, R. R. Schmidt, P. Peng, *Org. Lett.* **2018**, *20*, 3862–3865.
[28] V. B. Krylov, D. A. Argunov, D. Z. Vinnitskiy, S. A. Verkhnyatskaya, A. G. Gerbst, N. E. Ustyuzhanina, A. S. Dmitrenok, J. Huebner, O. Holst, H.-C. Siebert, et al., *Chem. Eur. J.* **2014**, *20*, 16516–16522.
[29] V. B. Krylov, D. A. Argunov, D. Z. Vinnitskiy, A. G. Gerbst, N. E. Ustyuzhanina, A. S. Dmitrenok, N. E. Nifantiev, *Synlett* **2016**, *27*, 1659–1664.
[30] D. A. Argunov, V. B. Krylov, N. E. Nifantiev, *Org. Lett.* **2016**, *18*, 5504–5507.
[31] T. Yoshida, T. Chiba, T. Yokochi, K. Onozaki, T. Sugiyama, I. Nakashima, *Carbohydr. Res.* **2001**, *335*, 167–180.
[32] N. S. Schocker, S. Portillo, C. R. N. Brito, A. F. Marques, I. C. Almeida, K. Michael, *Glycobiology* **2016**, *26*, 39–50.

[33] Y. E. Tsvetkov, M. Burg-Roderfeld, G. Loers, A. Ardá, E. V. Sukhova, E. A. Khatuntseva, A. A. Grachev, A. O. Chizhov, H.-C. Siebert, M. Schachner, *J. Am. Chem. Soc.* **2012**, *134*, 426–435.
[34] A. L. Matveev, V. B. Krylov, L. A. Emelyanova, A. S. Solovev, Y. A. Khlusevich, I. K. Baykov, T. Fontaine, J.-P. Latgé, N. V. Tikunova, N. E. Nifantiev, *PloS One* **2018**, *13*, e0193938.
[35] V. B. Krylov, A. S. Solovev, D. A. Argunov, J.-P. Latgé, N. E. Nifantiev, *Heliyon* **2019**, *5*, e01173.
[36] D. S. Hansen, F. Mestre, S. Alberti, S. Hernández-Allés, D. Alvarez, A. Doménech-Sánchez, J. Gil, S. Merino, J. M. Tomás, V. J. Benedí, *J. Clin. Microbiol.* **1999**, *37*, 56–62.

Received: March 12, 2019

ChemPubSoc Europe

DOI: 10.1002/ejoc.201601413

EurJOC European Journal of Organic Chemistry

Full Paper

Oligosaccharide Synthesis

Pyranoside-into-Furanoside Rearrangement of 4-Pentenyl Glycosides in the Synthesis of a Tetrasaccharide-Related to Galactan I of *Klebsiella pneumoniae*

Stella A. Verkhnyatskaya,[a] Vadim B. Krylov,[a] and Nikolay E. Nifantiev*[a]

Abstract: An efficient strategy for synthesis of a spacer-armed tetrasaccharide related to galactan I of *Klebsiella pneumoniae* is described, which uses newly developed acid-free conditions for the pyranoside-into-furanoside (PIF) rearrangement of a digalactoside bearing a 4-pentenyl group at the anomeric position. The 4-pentenyl aglycon was successfully used both as a leaving group in the glycosylation of 3-(trifluoroacetamido)-propanol, and as a temporary anomeric protecting group, allowing conversion into an imidate donor. Regioselective coupling of the disaccharide blocks gave the desired tetrasaccharide sequence required for investigation of the interaction of galactan I with immune-system proteins.

Introduction

The Gram-negative bacterium *Klebsiella pneumoniae* is responsible for different diseases including pneumonia, bacteremia, urinary-tract infections, and pyogenic liver abscess with high incidence and mortality.[1,2] This bacterium is a frequent cause of nosocomial infections, and may be responsible for as much as 20 % of respiratory infections in neonatal intensive care units.[3]

The most common serotype of *K. pneumoniae* O1[4] has two O antigens: galactan I (repeating unit: [→3)-α-D-Gal*p*-(1→3)-β-D-Gal*f*-(1→]) and galactan II (repeating unit: [→3)-α-D-Gal*p*-(1→3)-β-D-Gal*p*-(1→]).[5] In other *K. pneumoniae* serotypes, the structure of galactan I is decorated with acetyl groups and monosaccharide branches [α-D-Gal*p*(1→2) or α-D-Gal*p*(1→4)]. The lipopolysaccharides (LPS) of *K. pneumoniae* are important virulence determinants,[6–9] and synthetic oligosaccharides[10–12] representing these carbohydrate sequences are required as model substrates for research into recognition of the LPS O chain by the immune system, and for vaccine design.

Recently, we reported a pyranoside-into-furanoside (PIF) rearrangement as an original and useful tool for the preparation of a variety of protected furanosides from the corresponding pyranosides.[12–15] In this paper, we describe the use of the PIF rearrangement for the efficient synthesis of a tetrasaccharide related to a galactan I motif.

Results and Discussion

Previously, a preparative protocol for the PIF rearrangement of different glycosides bearing an allyl group as a temporary protecting group at anomeric position was developed.[12–17] In this communication, we expand the scope of this process by using an aglycon that can act as a leaving group during glycosylation. Previous studies revealed that the PIF rearrangement proceeds efficiently for substrates bearing an electron-donating aglycon in an equatorial orientation.[13] Thus, we first studied the applicability in the PIF rearrangement of thioglycosides, which are widely used in glycosylation reactions.[18,19]

Treatment of thioethyl galactoside **1**[20] with the Py•SO_3 complex and HSO_3Cl, the standard conditions for the PIF rearrangement,[12] gave totally *O*-sulfated pyranoside derivative **2** within 30 min (Scheme 1). Unfortunately, extension of the reaction time resulted in the formation of a complex mixture of decomposition products with **3** as the dominant product. This could be connected with the instability of the thioethyl group under even mildly oxidative conditions. Direct sulfation of L-fucose with the Py•SO_3 complex in DMF gave an analogous mixture. The unsatisfactory results obtained with the thioethyl glycoside led us to study 4-*n*-pentenyl glycosides, which were proposed by Fraser-Reid et al.,[21,22] and which can be activated under similar conditions to those used for the activation of thioglycos-

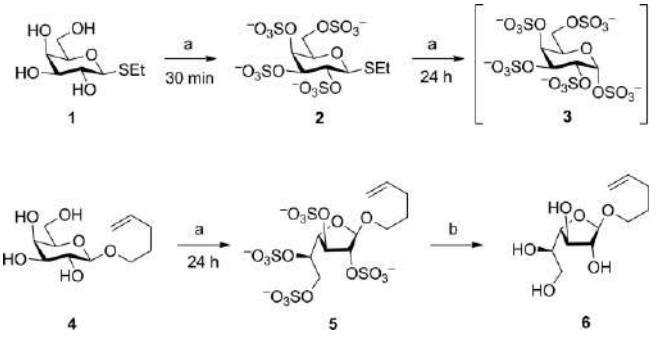

Scheme 1. Reagents and conditions: a) Py•SO_3, HSO_3Cl, DMF, 20 °C; b) DMF/dioxane = 1:5, IR-120 (H^+), 60 °C, 67 % for **6**.

[a] *Laboratory of Glycoconjugate Chemistry, N. D. Zelinsky Institute of Organic Chemistry, Russian Academy of Sciences,*
Leninsky prospect 47, 119991 Moscow, Russian Federation
E-mail: nen@ioc.ac.ru
http://zioc.ru/institute/laboratories/glycoconjugates

Supporting information and ORCID(s) from the author(s) for this article are available on the WWW under http://dx.doi.org/10.1002/ejoc.201601413.

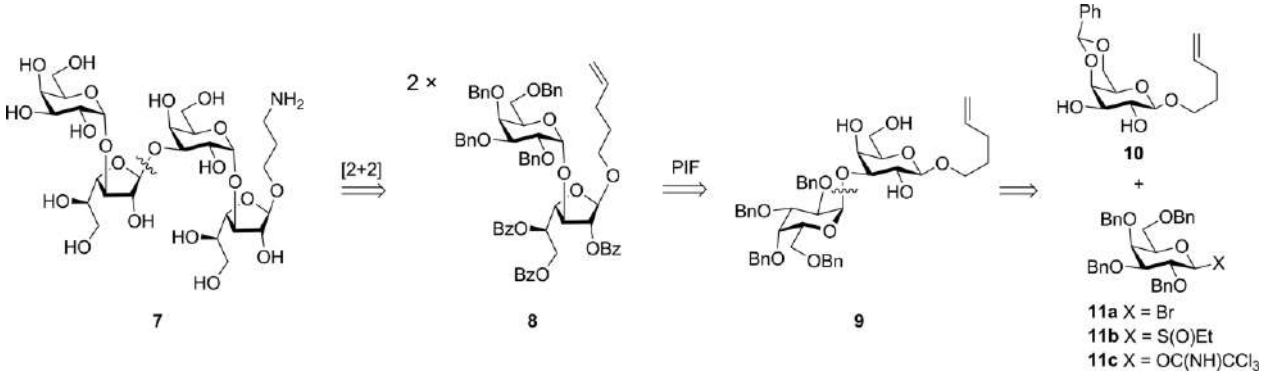

Scheme 2. Retrosynthetic analysis of target tetrasaccharide **7**.

ides. PIF rearrangement of pentenyl β-glycoside **4**[23] smoothly gave totally *O*-sulfated furanoside **5**, which was then subjected to solvolytic desulfation to give monosaccharide **6** in a good yield. Encouraged by this result, we developed a scheme for the synthesis of a spacer-armed tetrasaccharide related to galactan I of *K. pneumoniae* by using an anomeric 4-*n*-pentenyl group as a leaving group and a temporary protecting group.

The assembly of target tetrasaccharide **7** was planned according to a [2+2] synthetic scheme by using disaccharide precursor **8** for the preparation of both donor and acceptor building blocks (Scheme 2). The key step of the synthesis was the PIF-rearrangement of digalactoside **9** bearing a 4-*n*-pentenyl aglycon. The preparation of disaccharide **9** was planned to take place through the regio- and stereoselective coupling of readily available monosaccharide building blocks **10**[23] and **11**.[24–26]

The regioselective glycosylation of 4,6-*O*-benzylidene-protected acceptors with two free hydroxy groups at C-2 and C-3 is a well-known procedure for di- or oligosaccharide substrates,[27–29] but for monosaccharide acceptors it can be less regioselective.[30–32] Hence, our synthesis began with the optimization of glycosylation conditions for monosaccharide diol **10**[23] (Scheme 3). First, glycosylation of bromide **11a**[24] was studied under Lemieux conditions,[33] but this was not efficient; even after three days of treatment with Bu_4NBr, the conversion of bromide **11a** was low (TLC control). Size-exclusion column chromatography was successfully used to separate the disaccharide fraction from the monosaccharides; this could not be carried out efficiently by chromatography on silica gel due to the similar retention factors of the desired product **9** and the by-product resulting from hydrolysis of the donor. Thus, after filtration of the reaction mixture, the crude material was loaded onto Bio-Beads SX-3 to give a disaccharide fraction consisting mainly of three disaccharides **12**–**14** (Scheme 3) with a total yield of 39 % (Table 1, entry 1). From integration of the ^1H NMR spectrum (Figure 1), the ratio of disaccharides **12**/**13**/**14** was determined to be 6:3:1, with the desired α-(1→3)-linked product **12** being the major product.

The structures of disaccharides **12**–**14** were established on the basis of ^1H and ^{13}C NMR spectroscopic data. Thus, the stereochemistry of the newly formed bond in **12** was confirmed by the characteristic coupling constant $J_{1,2}$ = 3.7 Hz, typical for an α-galactopyranoside, and the chemical shift of the anomeric

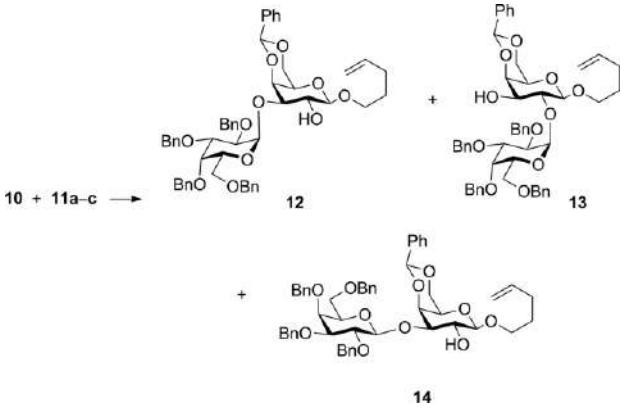

Scheme 3. Glycosylation of diol **10** with donors **11a**–**11c**.

Table 1. Reaction conditions in diol **10** glycosylations by donors **11a**–**11c**.

	Donor	Activation conditions	Ratio of **12**/**13**/**14**	Total yield of disaccharides (Yield of **12**)[a]
1	**11a**	Bu_4NBr, MS-4 Å DMF, room temp., 72 h	6:3:1	39 % (23 %)
2	**11a**	AgOTf, MS-4 Å CH_2Cl_2, –20 °C, 1 h	4.2:1.5:1	51 % (32 %)
3	**11b**	Tf_2O, DTBMP, MS-4 Å CH_2Cl_2, –50 °C, 2.5 h	7.3:1.8:1	61 % (44 %)
4	**11c**	TfOH, MS-4 Å THF/CH_2Cl_2 –80 → –50 °C, 1 h	25:1:5	79 % (64 %)

[a] Yield by NMR spectroscopy.

carbon (δ = 94.7 ppm). The site of glycosylation in disaccharide **12** was confirmed by the downfield shift of the C-3^I carbon (δ = 76.9 ppm); the chemical shift of C-2^I was found to be virtually unchanged (δ = 69.3 ppm). Disaccharide **13** was similarly proved to have an α-configuration of the glycosidic bond [$J_{1,2}$ = 3.9 Hz and δ(C-1^{II}) = 96.6 ppm]. However, the position of glycosylation (at O-2) was confirmed by the downfield chemical shift of the C-2^I carbon (δ = 79.4 ppm). The β-(1→3)-linkage in **14** was proved by the coupling constant $J_{1,2}$ = 7.7 Hz and chemical shift δ(C-1^{II}) = 103.0 ppm, which are typical for a β-galactopyranoside, and by the downfield shift of the C-3^I signal [δ(C-3^I) = 79.6 ppm and δ(C-2^I) = 67.0 ppm].

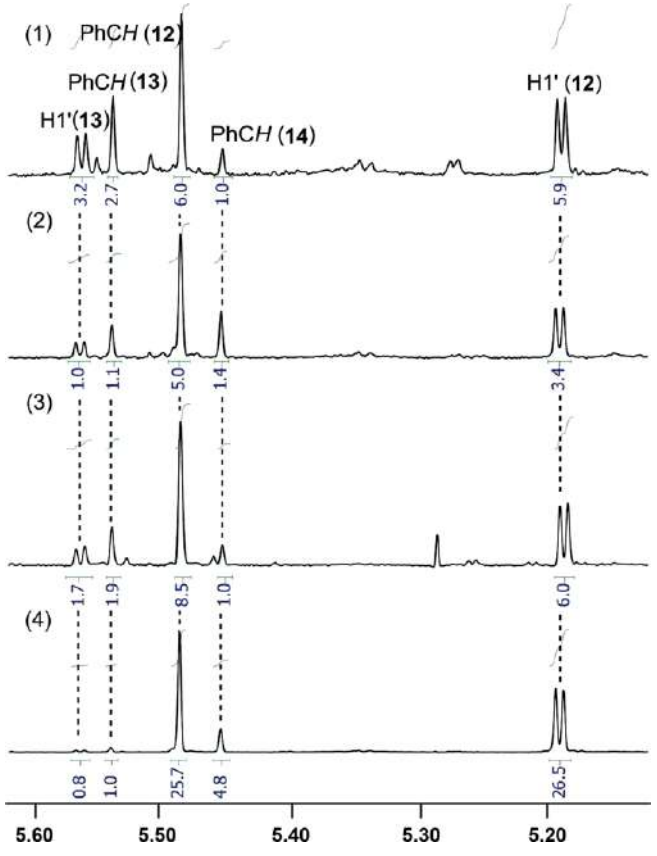

Figure 1. Parts of the ^{1}H NMR spectra of disaccharide fractions obtained in the glycosylations of diol **10** with donors **11a**–**11c** and subsequent separation of the disaccharide fractions by SX-3 gel filtration of the reaction mixtures. Numbers in parentheses correspond to entries in Table 1.

To improve the yield of the desired disaccharide **12**, different conditions for 1,2-*cis* glycosylation were studied. Coupling of diol **10** and bromide **11a** was carried out in the presence of AgOTf at –20 °C; this gave a mixture of disaccharides **12**–**14** in a total yield of 51 % with a ratio **12**/**13**/**14** of 4.2:1.5:1. (Table 1, entry 2, see also Figure 1). The use of sulfoxide donor[34] **11b** in the presence of triflic anhydride (Tf_2O) and 2,6-di-*tert*-butyl-4-methylpyridine (DTBMP) gave disaccharides **12**–**14** in 61 % yield with a component ratio of 7.3:1:1.8 (Table 1, entry 3). Schmidt's glycosylation[35] with glycosyl trichloroacetimidate **11c** activated by a catalytic amount of triflic acid (TfOH) in a mixed solvent of THF/CH_2Cl_2 (6:1)[36] at –80 °C produced a mixture of disaccharides in a good 79 % yield; the ratio of disaccharides **12**/**13**/**14** was 25:5:1 (Table 1, entry 4). After purification by column chromatography, target disaccharide **12** was isolated in 62 % yield. These conditions were chosen for the preparative synthesis of disaccharide **12**.

Next, the benzylidene group of disaccharide **12** was removed by treatment with TFA (trifluoroacetic acid; 90 % aq.) in CH_2Cl_2 (1:10 v/v). This produced disaccharide **9** in 96 % yield. This was then subjected to the PIF rearrangement (Scheme 4). The standard protocol for this rearrangement, which was successfully applied in the synthesis of oligosaccharides related to polysaccharides from *Aspergillus fumigatus*,[15,17] *Enterococcus feacalis*,[14] *Chordaria flagelliformis*,[16] involves treatment with a Py·SO_3/HSO_3Cl mixture, followed by neutralization with $NaHCO_3$, and solvolytic desulfation in the presence of acidic resin IR-120 (H^+). Unfortunately, under these conditions substrate **9** gave only 27 % of target disaccharide **16** (Scheme 4, Table 2, entry 1). To avoid the use of excess of $NaHCO_3$, which can interfere with the desulfation step, neutralization of the reaction mixture was achieved by the addition of ammonium hydrogen carbonate (NH_4HCO_3), which could then easily be evaporated. The new procedure led to an increase in the overall yield of compound **16** (Table 2, entry 2) to 38 %. We also carried out the reaction without the harsh chlorosulfonic acid, but with heating at 80 °C. This new high-temperature rearrangement protocol resulted in a further increase in the yield of **16** up to 53 % (Table 2, entry 3).

Table 2. Optimization of PIF-rearrangement conditions.

Entry	Conditions for *O* persulfation	Conditions for *O* desulfation	Isolated yield of **16**
1	1) Py·SO_3 (3.2 equiv./OH-group) HSO_3Cl (1.2 equiv./OH-group) DMF, r.t., 24 h 2) $NaHCO_3$	DMF/dioxane IR-120 (H^+) 60 °C, 3 h	27 %
2	1) Py·SO_3 (3.2 equiv./OH-group) HSO_3Cl (1.2 equiv./OH-group) DMF, r.t., 24 h 2) NH_4HCO_3	DMF/dioxane IR-120 (H^+) 60 °C, 3 h	38 %
3	1) Py·SO_3 (4.7 equiv./OH-group) DMF, 80 °C, 1.5 h 2) NH_4HCO_3	DMF/dioxane IR-120 (H^+) 90 °C, 10 min	53 %

ESI-HRMS analysis indicated that **9** and **16** were isomeric compounds, but their NMR spectra revealed considerable differences in the monosaccharide unit at the reducing end. The characteristic chemical shifts of C-1^I at δ = 107.9 ppm, and of the C-2^I, C-3^I, and C-4^I signals at δ = 80–90 ppm, confirmed the presence of a 3-*O*-substituted furanoside ring in disaccharide **16**, which agreed with the data in the literature.[37]

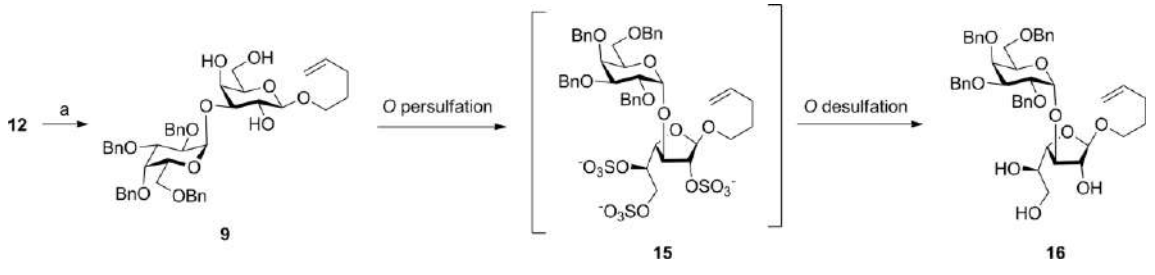

Scheme 4. Reagents and conditions: a) TFA (90 % aq.), CH_2Cl_2; for persulfation and *O*-desulfation conditions, see Table 2 below.

Disaccharide **16** was per-*O*-benzoylated with BzCl in the presence of pyridine to give compound **8**, which was then further converted into both glycosyl donor and acceptor building blocks (Scheme 5). To synthesize donor **19**, precursor **8** was transformed into hemiacetal **17** by treatment with NIS (*N*-iodosuccinimide) and an excess of TFA in CH_2Cl_2. Subsequent imidation by treatment with $ClC(NPh)CF_3$ and cesium carbonate gave **19**. For preparation of acceptor **20**, 3-(trifluoroacetamido)propan-1-ol was glycosylated with 4-pentenyl glycoside **8** in the presence of TMSOTf/NIS (TMS = trimethylsilyl) (**8**→**18**). The product was then subjected to catalytic hydrogenolysis, followed by 4,6-*O* benzylidenation (**18**→**20**). Unfortunately, glycosylation of acceptor **20** with 4-pentenyl donor **8** yielded a hardly separable mixture of products containing less than 10 % of the desired tetrasaccharide **21**. Coupling of acceptor **20** with imidate donor **19** at low temperature predominantly yielded β-(1→3)-linked tetrasaccharide **21** (42 %), though formation of the β-(1→2)-linked tetrasaccharide (19 %) and branched (1→2)- and (1→3)-linked hexasaccharides (18 %) was also observed. The structure of tetrasaccharide **21** was confirmed by analysis of its ^1H and ^{13}C NMR spectra together with ESI-HRMS data. The β-configuration of the newly formed bond was established by the characteristic chemical shift of C-1^{III} (δ = 107.9 ppm). The downfield shift of C-3^{II} (δ = 77.4 ppm) together with the spatial proximity of 1^{III}-H and 3^{II}-H observed in NOE experiments confirmed the formation of the (1→3) bond. Removal of the blocking groups in **21** gave the desired spacer-arm-equipped oligosaccharide **7**.

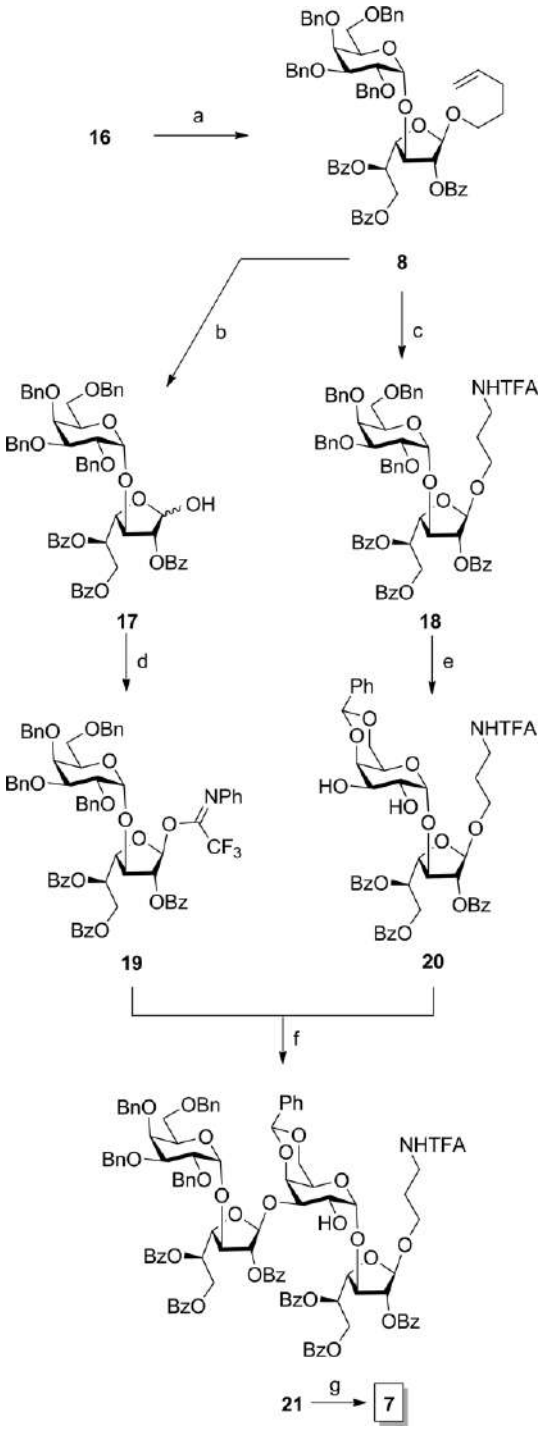

Scheme 5. Reagents and conditions: a) BzCl, Py, CH_2Cl_2, 93 %; b) NIS, TFA, CH_2Cl_2, 60 %; c) TMSOTf, NIS, CH_2Cl_2, $HO(CH_2)_3NHTFA$ (NHTFA = trifluoroacetamide), 79 %; d) $ClC(NPh)CF_3$, Cs_2CO_3, CH_2Cl_2, 95 %; e) 1) H_2, $Pd(OH)_2/C$, AcOH, EtOAc; 2) $PhCH(OMe)_2$, 58 %; f) TfOH, CH_2Cl_2, –60 °C, 42 %; g) 1) H_2, $Pd(OH)_2/C$, AcOH, EtOAc; 2) NaOMe, MeOH, H_2O, 40 °C, 63 %.

Conclusions

A convergent synthesis of spacer-arm-equipped tetrasaccharide **7** structurally related to galactan I from *K. pneumoniae* was carried out. High regioselectivity and stereoselectivity in the glycosylation of diol **10** were achieved through the use of trichloroacetimidate donor **11c** in a mixture of solvents THF/CH_2Cl_2, which gave α-(1→3)-linked digalactopyranoside **12**. A new, high-temperature, acid-free PIF rearrangement protocol was developed for the preparation of the disaccharide with a furanoside residue at the reducing end. Further biological investigations of the reported compounds are in progress, and the results will be published elsewhere.

Experimental Section

General Remarks: Solvents were distilled and dried if necessary according to standard procedures[38] (CH_2Cl_2, MeOH, toluene) or purchased as dry (DMF, pyridine, CH_3CN, from Sigma–Aldrich). Commercially sourced chemicals were used without purification unless otherwise noted. All reactions involving air- or moisture-sensitive reagents were carried out by using dry solvents under an argon atmosphere. All glycosylation reactions were carried out under dry argon. Molecular sieves (4 Å) for glycosylation reactions were activated before use at 180 °C under vacuum (oil pump) for 2 h. Analytical thin-layer chromatography (TLC) was carried out on Silica Gel 60 F254 aluminium sheets (Merck), and plates were visualized by using UV light or by charring at ca. 150 °C with H_3PO_4 (10 % v/v in ethanol). Column chromatography was carried out on Silica Gel 60, 40–63 μm (Merck). Preparative HPLC was carried out with a Supelcosil LC-Si column, 25 cm × 21.2 mm, 5 μm at a flow rate of 8 mL/min with a UV/Vis-155 detector (Gilson). Gel filtration was carried out on an SX-3 gel column (500 × 23 mm) eluting with toluene, or on a

TSK-40 HW(S) column (400 × 17 mm) eluting with AcOH (0.1 M in water) at a flow rate of 0.5 mL/min. Optical rotation values were measured with a JASCO P-2000 polarimeter at ambient temperature in the specified solvents. ^{1}H and ^{13}C NMR spectra were recorded with Bruker AMX-400, DRX-500, and Avance 600 spectrometers. Chemical shifts were referenced to residual solvent signals. Signals in ^{1}H and ^{13}C NMR spectra were assigned by using COSY, TOCSY, and ^{1}H,^{13}C HSQC spectra. Monosaccharide residues in oligosaccharides are numbered with Roman numerals starting from the reducing end. High-resolution mass spectra (HRMS) were recorded with a Bruker micrOTOF II instrument using electrospray ionization (ESI).[39] The measurements were carried out in positive-ion mode (interface capillary voltage –4500 V), with a mass range of m/z = 50–3000 Da; external or internal calibration was done by using Electrospray Calibrant Solution (Fluka). A syringe injection was used for solutions in a mixture of acetonitrile and water (50:50 v/v, flow rate 3 μL/min). Nitrogen was used as a dry gas; the interface temperature was set at 180 °C.

Acid-Promoted Sulfation of Ethyl 1-Thio-β-D-galactopyranoside (1): Py•SO_3 (81 mg, 0.51 mmol) and HSO_3Cl (13 μL, 0.20 mmol) were added to a stirred solution of pyranoside **1** (10 mg, 0.04 mmol) in DMF (0.5 mL). The resulting solution was kept for 30 min (or 24 h) at room temperature, and then the reaction mixture was neutralized by the addition of an aqueous solution of $NaHCO_3$ [$NaHCO_3$ (136 mg, 1.70 mmol) in H_2O (2 mL)]. The solvent was then evaporated in vacuo, and then coevaporated with H_2O and then with D_2O. The residue was then dissolved in D_2O, and NMR spectra were recorded.

Data for the sodium salt of ethyl 2,3,4,6-tetra-*O*-sulfonato-1-thio-β-D-galactopyranoside (**2**) (reaction time 30 min): ^{1}H NMR (400 MHz, D_2O): δ = 5.10 (d, J = 3.0 Hz, 1 H, 4-H), 4.79 (d, J = 9.7 Hz, 1 H, 1-H), 4.58 (dd, J = 9.6, 3.0 Hz, 1 H, 3-H), 4.42 (t, J = 9.6 Hz, 1 H, 2-H), 4.26 (dd, J = 9.8, 2.1 Hz, 1 H, 6a-H), 4.23–4.13 (m, 2 H, 5-H, 6b-H), 2.85–2.68 (m, 2 H, CH_2), 1.27 (t, J = 7.4 Hz, 1 H, CH_3) ppm. ^{13}C NMR (101 MHz, D_2O): δ = 88.1 (C-1), 81.1 (C-3), 80.1 (C-5), 79.8 (C-4), 78.7 (C-2), 72.1 (C-6), 29.2 (CH_2), 18.8 (CH_3) ppm.

Data for sodium salt of 1,2,3,4,6-penta-*O*-sulfonato-α-D-galactopyranoside (**3**) (reaction time 24 h): ^{1}H NMR (600 MHz, D_2O): δ = 6.11 (d, J = 3.7 Hz, 1 H, 1-H), 5.23 (d, J = 3.2 Hz, 1 H, 4-H), 4.80 (dd, J = 10.6, 3.1 Hz, 1 H, 3-H), 4.72 (dd, J = 10.5, 3.7 Hz, 1 H, 2-H), 4.61 (dd, J = 8.0, 4.0 Hz, 1 H, 5-H), 4.37 (dd, J = 11.3, 4.1 Hz, 1 H, 6a-H), 4.25 (dd, J = 11.2, 7.9 Hz, 1 H, 6b-H) ppm. ^{13}C NMR (101 MHz, D_2O): δ = 96.7 (C-1), 76.9 (C-4), 73.21 (C-3), 72.53 (C-2), 71.1 (C-5), 68.5 (C-6) ppm.

PIF Rearrangement of Pent-4-enyl β-D-Galactopyranoside (4): Py•SO_3 (81 mg, 0.51 mmol) and HSO_3Cl (13 μL, 0.20 mmol) were added to a stirred solution of pyranoside **4** (10 mg, 0.04 mmol) in DMF (0.5 mL). The resulting solution was kept for 24 h at room temperature, and then the mixture was neutralized by the addition of an aqueous solution of $NaHCO_3$ [$NaHCO_3$ (136 mg, 1.70 mmol) in H_2O (2 mL)]. The solvent was then evaporated in vacuo, and then coevaporated twice with water. The solid residue was dissolved in a minimal amount of water and then an excess of MeOH was added to precipitate the inorganic salts. The mixture was filtered, the solid was washed with MeOH, and the filtrate was concentrated to give per-*O*-sulfated furanoside **5**, which was used in the desulfation step without further purification.

Data for intermediate **5**: ^{1}H NMR (600 MHz, $CDCl_3$): δ = 5.95–5.87 (m, 1 H, C*H*=CH_2), 5.37 (s, 1 H, 1-H), 5.14–5.09 (m, 1 H, CH=CH_2), 5.04–5.01 (m, 2 H, 3-H, CH=CH_2), 4.90 (ddd, J = 7.6, 5.1, 2.4 Hz, 1 H, 5-H), 4.84 (s, 1 H, 2-H), 4.46 (dd, J = 4.6, 2.4 Hz, 1 H, 4-H), 4.35 (dd, J = 10.3, 5.2 Hz, 2 H, 6a-H), 4.25 (dd, J = 10.3, 7.7 Hz, 2 H, 6b-H), 3.77 (dt, J = 10.1, 6.7 Hz, 1 H, OCH_2-pent), 3.63 (dt, J = 10.1, 6.1 Hz, 1 H, OCH_2-pent), 2.15 (q, J = 7.1 Hz, 2 H, CH_2-pent), 1.75–1.68 (m, 2 H, CH_2-pent) ppm. ^{13}C NMR (151 MHz, D_2O): δ = 115.03 (CH=*C*H_2), 105.02 (C-1), 84.45 (C-2), 81.07 (C-3, C-4), 74.06 (C-5), 67.08 (OCH_2-pent), 65.78 (C-6), 29.58 (CH_2-pent), 27.81 (CH_2-pent) ppm.

The crude material was dissolved in DMF/dioxane (1:5; 6 mL), and IR-120 (H^+) was added until the pH was acidic. The reaction mixture was then stirred for 3 h at 60 °C, after which the resin was removed by filtration, and washed with EtOAc. The filtrate was concentrated in vacuo. The residue was purified by column chromatography (silica gel, $CHCl_3$/MeOH, 6:1, R_f = 0.33) to give furanoside **6** (6.7 mg, 67 %). ^{1}H NMR (400 MHz, CD_3OD): δ = 5.90–5.77 (m, 1 H, C*H*=CH_2), 5.02 (d, J = 17.0 Hz, 1 H, CH=CH_2), 4.95 (d, J = 10.1 Hz, 1 H, CH=CH_2), 4.85 (d, J = 1.5 Hz, 1 H, 1-H), 4.00 (dd, J = 6.5, 4.1 Hz, 1 H, 3-H), 3.96–3.89 (m, 2 H, 2-H, 4-H), 3.76–3.68 (m, 2 H, 5-H, OCH_2-pent), 3.64–3.59 (m, 2 H, 6-H), 3.43 (dt, J = 9.6, 6.6 Hz, 1 H, OCH_2-pent), 2.18–2.10 (m, 2 H, CH_2-pent), 1.73–1.63 (m, 2 H, CH_2-pent) ppm. ^{13}C NMR (101 MHz, CD_3OD): δ = 115.18 (CH=*C*H_2), 109.47 (C-1), 84.24 (C-4), 83.45 (C-2), 78.78 (C-3), 72.48 (C-5), 68.23 (OCH_2-pent), 64.61 (C-1), 31.39 (CH_2-pent), 30.07 (CH_2-pent) ppm. HRMS (ESI): calcd. for $C_{11}H_{20}O_6$ $[M + Na]^+$ 271.1152; found 271.1151.

Glycosylation of Diol 10

Procedure 1: Glycosylation with Bromide 11a under Lemieux Conditions: A solution of Br_2 in CH_2Cl_2 (50 μL,3 vol-%) was added to a solution of ethyl tetra-2,3,4,6-*O*-benzyl-1-thio-β-D-galactopyranoside (17 mg, 0.03 mmol) in CH_2Cl_2 (2 mL). After 10 min, the mixture was coevaporated twice with toluene, and the residue was dried in vacuo to give bromide **11a**, which was used for glycosylation without further purification.

A mixture of bromide **11a** (see above) and acceptor **10** (10 mg, 0.03 mmol) was dissolved in DMF (0.5 mL), and molecular sieves (4 Å, 100 mg) were added. The solution was stirred for 15 min. Then Bu_4NBr (66 mg, 0.21 mmol) was added, and the resulting solution was stirred for 3 d. The mixture was filtered through silica gel, and the solvent was removed under reduced pressure. The resulting syrup was loaded onto SX-3 gel to give a mixture of disaccharides **12**, **13**, and **14** (10 mg, 39 %, ratio **12**/**13**/**14** = 6:3:1).

Procedure 2: Glycosylation with Bromide 11a in the Presence of AgOTf: A solution of bromide **11a** [prepared from tetra-2,3,4,6-*O*-benzyl-1-thio-β-D-galactopyranoside (17 mg, 0.03 mmol) as described above] and acceptor **10** (10 mg, 0.03 mmol) in CH_2Cl_2 (1 mL) with molecular sieves (4 Å; 100 mg) was stirred for 15 min. The mixture was then cooled to –20 °C, and AgOTf (27 mg, 0.11 mmol) was added. When the TLC analysis indicated complete consumption of the donor, the reaction was quenched with a drop of pyridine. Then the mixture was diluted with CH_2Cl_2, and washed with $Na_2S_2O_3$ (5 % aq.) and water. The organic layer was dried with Na_2SO_4, and concentrated in vacuo. The mixture was loaded onto SX-3 gel to give a mixture of disaccharides **12**, **13**, and **14** (13 mg, 51 %, ratio **12**/**13**/**14** = 4.2:1.5:1).

Procedure 3: Glycosylation with Sulfoxide Donor 11b: A solution of sulfoxide donor **11b** (20 mg, 0.03 mmol) and 2,6-di-*tert*-butyl-4-methylpyridine (16 mg, 0.085 mmol) in CH_2Cl_2 (1 mL) with molecular sieves (100 mg) was stirred for 15 min, and then the mixture was cooled to –50 °C. Trifluoromethanesulfonic anhydride (7 μL, 0.04 mmol) was added, and the mixture was stirred for 10 min. Then a solution of acceptor **10** (11 mg, 0.03 mmol) in CH_2Cl_2 (0.5 mL) was added dropwise. The mixture was stirred for 2.5 h, then it was diluted with CH_2Cl_2 and washed with sat. aq. $NaHCO_3$. The organic layer was dried with Na_2SO_4, and concentrated in vacuo. The resi-

due was loaded onto SX-3 gel to give a mixture of disaccharides **12**, **13**, and **14** (17 mg, 61 %, ratio **12**/**13**/**14** = 7.3:1.8:1).

Procedure 4: Glycosylation with Trichloroacetimidate 11c: A mixture of donor **11c** (26 mg, 0.04 mmol), acceptor **10** (13 mg, 0.04 mmol), and molecular sieves (4 Å; 200 mg) in THF/CH_2Cl_2 (5:1; 2.8 mL) was stirred for 15 min at room temperature, and then it was cooled to –80 °C. Trifluoromethanesulfonic acid (10 µL, 0.1 mmol) was added, and the reaction mixture was stirred for 1 h. The mixture was then warmed to –50 °C, quenched with triethylamine, and filtered. The filtrate was concentrated in vacuo, and the residue was purified by gel filtration on SX-3 gel to give a mixture of disaccharides **12**, **13**, and **14** (26 mg, 79 %, ratio **12**/**13**/**14** = 25:1:5).

Pent-4-enyl 2,3,4,6-Tetra-*O*-benzyl-α-D-galactopyranosyl-(1→3)-4,6-*O*-benzylidene-β-D-galactopyranoside (12): ^{1}H NMR (600 MHz, $CDCl_3$): δ = 7.53–7.10 (m, 25 H, CH_{ar}, 5 Ph), 5.82 (m, 1 H, C*H*=CH_2-pent), 5.49 (s, 1 H, C*H*Ph), 5.19 (d, *J* = 3.7 Hz, 1 H, 1^{II}-H), 5.03 (dd, 1 H, CH=CH_2-pent), 4.93 (d, 1 H, CH_2Ph), 4.82 (d, 1 H, CH_2Ph), 4.71 (d, 1 H, CH_2Ph), 4.59 (m, 3 H, CH_2Ph), 4.46 (q, 2 H, CH_2Ph), 4.29 (m, 1 H, 6a^{I}-H), 4.25 (d, *J* = 3.7 Hz, 1 H, 4^{I}-H), 4.23 (m, 2 H, 5^{II}-H, CH_2-pent), 4.21 (d, *J* = 7.7 Hz, 1 H, 1^{I}-H), 4.09 (dd, *J* = 10.0, 3.6 Hz, 1 H, 2^{II}-H), 4.05–3.99 (m, 3 H, 3^{II}-H, 4^{II}-H, 6b^{I}-H), 3.98 (dd, *J* = 9.8, 7.7 Hz, 1 H, 2^{I}-H), 3.94 (m, 2 H, 6a^{II}-H), 3.66 (dd, *J* = 9.8, 3.5 Hz, 1 H, 3^{I}-H), 3.61–3.56 (m, 1 H, CH=CH_2-pent), 3.52 (m, 2 H, 6b^{II}-H), 3.46 (dd, *J* = 9.7, 5.9 Hz, 1 H, CH_2-pent), 3.28 (s, 1 H, 5^{I}-H), 2.14 (m, 2 H, CH_2-pent), 1.75 (m, 2 H, CH_2-pent) ppm. ^{13}C NMR (151 MHz, $CDCl_3$): δ = 129.0–126.5 (*C* 5 Ph), 114.93 (*C*H-pent), 103.2 (C-1^{I}), 101.3 (*C*HPh), 94.7 (C-1^{II}), 78.9 (C-3^{II}), 76.9 (C-3^{I}), 76.4 (C-2^{II}), 75.3 (C-4^{II}), 74.9 (CH_2Ph), 73.36 (CH_2Ph), 72.7 (C-4^{I}), 72.6 (CH_2Ph), 69.9 (C-5^{II}), 69.5 (C-6^{I}), 69.4 (*C*H_2-pent), 69.3 (C-2^{I}), 69.1 (C-6^{II}), 66.7 (C-5^{I}), 30.3, 28.9 (2 *C*H_2-pent) ppm.

Pent-4-enyl 2,3,4,6-Tetra-*O*-benzyl-α-D-galactopyranosyl-(1→2)-4,6-*O*-benzylidene-β-D-galactopyranoside (13): ^{1}H NMR (600 MHz, $CDCl_3$): δ = 7.53–7.10 (m, 25 H, CH_{ar}, 5 Ph), 5.77–5.71 (m, 1 H, C*H*=CH_2-pent), 5.56 (d, *J* = 3.9 Hz, 1 H, 1^{II}-H), 5.54 (s, 1 H, C*H*Ph), 5.00 (dd, 2 H, CH=CH_2-pent), 4.96 (d, 1 H, CH_2Ph), 4.92 (d, 1 H, CH_2Ph), 4.77 (d, 2 H, CH_2Ph), 4.71 (d, 2 H, CH_2Ph), 4.59 (d, 1 H, CH_2Ph), 4.58 (d, *J* = 7.3 Hz, 1 H, 1^{I}-H), 4.34–4.24 (m, 3 H, 6a^{I}-H, 5^{II}-H, 4^{II}-H), 4.22 (dd, *J* = 7.8, 4.7 Hz, 1 H, 3^{II}-H), 4.16 (d, *J* = 3.2 Hz, 1 H, 2^{II}-H), 4.11–3.87 (m, 3 H, 6^{II}-H, 2^{I}-H, 4^{I}-H), 3.85 (dd, *J* = 6.2, 2.7 Hz, 1 H, 3^{I}-H), 3.56–3.43 (m, 3 H, 6b^{I}-H, CH_2-pent), 3.42 (s, 1 H, 5^{I}-H), 2.33–2.28 (m, 2 H, CH_2-pent), 2.04–1.96 (m, 2 H, CH_2-pent) ppm. ^{13}C NMR (151 MHz, $CDCl_3$): δ = 138.0–126.6 (*C* 5 Ph), 138.2 (CH=CH_2-pent), 114.9, 138.2 (CH=CH_2-pent), 103.0 (C-1^{I}), 101.3 (*C*HPh), 96.6 (C-1^{II}), 79.4 (C-2^{I}), 76.4 (C-3^{II}), 76.2 (C-2^{II}), 75.2 (C-3^{I}), 74.8 (C-4^{I}), 74.3 (CH_2Ph), 73.6 (CH_2Ph), 73.5 (CH_2Ph), 72.6 (CH_2Ph), 71.7 (C-4^{II}), 69.9 (C-6^{II}), 69.2 (C-6^{I}), 68.90 (C-5^{II}), 66.7 (*C*H_2-pent), 66.4 (C-5^{I}), 29.0, 24.1 (2 *C*H_2-pent) ppm.

Pent-4-enyl 2,3,4,6-Tetra-*O*-benzyl-β-D-galactopyranosyl-(1→3)-4,6-*O*-benzylidene-β-D-galactopyranoside (14): ^{1}H NMR (600 MHz, $CDCl_3$): δ = 7.52–7.10 (m, 25 H, 5 Ph), 5.78–5.69 (m, 1 H, C*H*=CH_2-pent), 5.46 (s, 1 H, C*H*Ph), 5.03 (m, 1 H, CH=CH_2-pent), 4.96 (d, 1 H, CH_2Ph), 4.92 (d, 1 H, CH_2Ph), 4.85 (d, *J* = 7.8 Hz, 1 H, 1^{I}-H), 4.77 (d, 3 H, CH_2Ph), 4.71 (d, 2 H, CH_2Ph), 4.59 (d, 1 H, CH_2Ph), 4.30–4.21 (m, 4 H, 4^{I}-H, 6a^{I}-H, 5^{I}-H, 1^{II}-H), 4.06–3.84 (m, 5 H, 2^{II}-H, 3^{II}-H, 6b^{I}-H, 2^{I}-H, 4^{II}-H, CH_2-pent), 3.74 (dd, *J* = 9.9, 3.4 Hz, 1 H, 3^{I}-H), 3.58–3.42 (m, 2 H, 6^{II}-H, CH=CH_2-pent), 3.35 (s, 1 H, 5^{I}-H), 2.34–2.28 (m, 2 H, CH_2-pent), 2.09–1.96 (m, 2 H, CH_2-pent) ppm. ^{13}C NMR (151 MHz, $CDCl_3$): δ = 138.0–126.6 (*C* 5 Ph), 104.4 (C-1^{I}), 103.0 (C-1^{II}), 100.8 (PhC), 82.60, 79.6 (C-3^{I}), 76.8 (C-2^{II}), 76.8 (C-3^{II}), 76.2 (C-4^{I}), 74.8 (CH_2Ph), 74.0 (CH_2Ph), 73.9 (C-4^{II}), 73.7 (CH_2Ph), 73.6 (CH_2Ph), 70.6 (C-6^{II}), 69.2 (C-6^{I}), 67.0 (C-2^{I}), 66.8 (C-5^{I}), 66.7, 29.9, 24.1 (3 *C*H_2-pent) ppm.

Preparative Synthesis of Disaccharide 12: The glycosylation of acceptor **10** (1.17 g, 3.5 mmol) with donor **11c** (3.67 g, 5.4 mmol) as described in Procedure 4, above, followed by purification by column chromatography (toluene/EtOAc, 5:1, R_f = 0.38) gave disaccharide **12** (1.87 g, 62 %). $[\alpha]_D^{20}$ = +65.38 (*c* = 1.0, EtOAc). HRMS (ESI): calcd. for $C_{52}H_{58}O_{11}$ [M + Na]$^+$ 881.3871; found 881.3878.

Pent-4-enyl 2,3,4,6-Tetra-*O*-benzyl-α-D-galactopyranosyl-(1→3)-β-D-galactopyranoside (9): Disaccharide **12** (1.87 g, 2.18 mmol) (438 mg, 0.59 mmol) was dissolved in CH_2Cl_2 (4 mL), and TFA (90 % aq.; 4.4 mL) was added. The mixture was stirred at room temperature for 1 h. The mixture was then diluted with methanol (40 mL), and triethylamine was added until the pH was neutral. The mixture was then concentrated in vacuo. The residue was purified by column chromatography to give **9** (1.62 g, 96 %). R_f = 0.29 (toluene/EtOAc, 1:1). $[\alpha]_D^{20}$ = +14.59 (*c* = 1.0, $CHCl_3$). ^{1}H NMR (600 MHz, $CDCl_3$): δ = 7.41–7.22 (m, 20 H, CH_{ar}, 4 Ph), 5.80 (m, 1 H, C*H*=CH_2), 5.02 (m, 1 H, CH_2-pent), 4.97–4.94 (m, 1 H, CH_2-pent), 4.92 (d, 1 H, CH_2Ph), 4.89 4.85 (m, 2 H, CH_2Ph, 1^{II}-H), 4.75 (s, 2 H, CH_2Ph), 4.65 (d, 1 H, CH_2Ph), 4.56 (d, 1 H, CH_2Ph), 4.48 (d, 1 H, CH_2Ph), 4.42 (d, 1 H, CH_2Ph), 4.29 (t, *J* = 6.6 Hz, 1 H, 5^{II}-H), 4.18 (d, *J* = 7.8 Hz, 1 H, 1^{I}-H), 4.07 (dd, *J* = 10.2, 3.7 Hz, 1 H, 2^{II}-H), 4.01–3.98 (m, 2 H, 3^{II}-H, 4^{II}-H), 3.96–3.88 (m, 3 H, 6a^{II}-H, 6a^{I}-H, CH_2-pent), 3.80 (d, *J* = 3.5 Hz, 1 H, 4^{I}-H), 3.76 (dd, *J* = 11.7, 4.7 Hz, 1 H, 6b^{I}-H), 3.71 (dd, *J* = 9.3, 7.9 Hz, 1 H, 2^{I}-H), 3.57–3.49 (m, 3 H, 3^{I}-H, 6b^{II}-H, CH_2-pent), 3.44 (t, *J* = 5.6 Hz, 1 H, 5^{I}-H), 2.13 (q, *J* = 7.3 Hz, 2 H, CH_2-pent), 1.77–1.68 (m, 2 H, CH_2-pent) ppm. ^{13}C NMR (151 MHz, $CDCl_3$): δ = 138.6–137.9 (C_q, C_{ar}, 4 Ph), 138.2 (*C*H=CH_2-pent), 128.5–127.5 (C_{ar}, 4 Ph), 114.9 (CH=CH_2-pent), 103.2 (C-1^{I}), 95.9 (C-1^{II}), 79.4 (C-3^{II}), 79.3 (C-3^{I}), 76.1 (C-2^{II}), 74.8 (C-4^{II}), 74.7 (CH_2Ph), 74.6 (CH_2Ph), 74.1 (C-5^{I}), 73.3 (CH_2Ph), 72.7 (CH_2Ph), 69.9 (C-5^{II}), 69.8 (C-2^{I}), 69.2 (C-6^{II}), 68.8 (*C*H_2-pent), 66.4 (C-4^{I}), 62.6 (C-6^{I}), 30.1, 28.80 (2 *C*H_2-pent) ppm. HRMS (ESI): calcd. for $C_{45}H_{54}O_{11}$ [M + Na]$^+$ 793.3558; found 793.3552.

PIF Rearrangement: Pent-4-enyl 2,3,4,6-Tetra-*O*-benzyl-α-D-galactopyranosyl-(1→3)-β-D-galactofuranoside (16)

Procedure 1: The pyranoside-into-furanoside (PIF) rearrangement of disaccharide **9** (30 mg, 0.04 mmol) was carried out as described for monosaccharide **6** to give furanoside **16** (8 mg, 27 %).

Procedure 2: Py·SO_3 (60.4 mg, 0.38 mmol) and HSO_3Cl (10 µL, 0.15 mmol) were added to a stirred solution of **9** (30 mg, 0.04 mmol) in DMF (0.5 mL). The resulting solution was stirred for 24 h at room temperature, then the mixture was neutralized by the addition of an aqueous solution of NH_4HCO_3 (95 mg, 1.23 mmol), and the solvent was coevaporated twice with water. The residue was dissolved in a minimum amount of water, and then an excess of methanol was added, resulting the precipitation of the inorganic salts. This mixture was centrifuged at 3000 rpm, and the supernatant was concentrated. The crude material was dissolved in DMF/dioxane (1:5; 6 mL), and IR-120 (H^+) was added until the pH was acidic. The reaction mixture was stirred for 3 h at 60 °C, after which it was diluted with EtOAc and washed with H_2O and sat. aq. NaCl. The organic layer was dried with Na_2SO_4, and concentrated in vacuo. The product was purified by HPLC (Supelcosil LC-Si, 25 cm × 21.2, 5 µm, eluting with EtOAc) to give furanoside **16** (11 mg, 37 %).

Procedure 3: Py·SO_3 (950 mg, 6.0 mmol) was added to a stirred solution of disaccharide **9** (310 mg, 0.42 mg) in DMF (9 mL). The reaction mixture was stirred for 1.5 h at 80 °C, then it was neutralized by the addition of an aqueous solution of NH_4HCO_3 (0.95 g, 12 mmol), and the solvent coevaporated twice with water. The residue was dissolved in a minimum amount of water, and then an

excess of methanol was added, resulting the precipitation of the inorganic salts. The mixture was centrifuged at 3000 rpm, and the supernatant was concentrated. The resulting crude material was dissolved in DMF/dioxane (1:5; 9 mL), then IR-120 (H^+) was added until the pH was acidic. The resulting solution was heated to 90 °C. After 10 min, the mixture was filtered, and the filtrate was diluted with CH_2Cl_2 and washed with water and sat. aq. NaCl. The organic layer was dried with Na_2SO_4, and concentrated in vacuo. Purification by column chromatography on silica gel gave furanoside **16** (164 mg, 53 %). R_f = 0.18 (toluene/EtOAc, 1:1). $[\alpha]_D^{20}$ = +3.53 (*c* = 1.0, EtOAc). ^{1}H NMR (600 MHz, $CDCl_3$): δ = 7.40–7.19 (m, 20 H, C*H*$_{ar}$, 4 Ph), 5.81 (m, 1 H, C*H*=CH$_2$-pent), 5.02 (m, 1 H, CH=C*H*H), 4.96 (m, 1 H, CH=CH*H*), 4.91–4.88 (m, 3 H, C*H*$_2$Ph, 1^{II}-H, 1^{I}-H), 4.83–4.79 (m, 2 H, C*H*$_2$Ph), 4.72 (d, 1 H, C*H*$_2$Ph), 4.67 (d, 1 H, C*H*$_2$Ph), 4.51 (m, 2 H, C*H*$_2$Ph), 4.40 (d, 1 H, C*H*$_2$Ph), 4.11–4.05 (m, 2 H, 2^{II}-H, 2^{I}-H), 3.98 (dd, *J* = 9.0, 2.8 Hz, 1 H, 5^{I}-H), 3.87 (dd, *J* = 10.1, 2.8 Hz, 1 H, 4^{I}-H), 3.79 (dd, *J* = 8.8, 5.6 Hz, 2 H, 3^{II}-H, 3^{I}-H), 3.69 (m, 4 H, 4^{II}-H, 5^{II}-H, 6ab^{II}-H, C*H*H-pent), 3.59–3.54 (m, 1 H, 6a^{I}-H), 3.43 (dt, *J* = 9.6, 6.6 Hz, 1 H, CH*H*-pent), 3.14 (dd, *J* = 9.8, 3.1 Hz, 1 H, 6b^{I}-H), 2.12 (dd, *J* = 14.7, 6.9 Hz, 2 H, C*H*$_2$-pent), 1.68 (dt, *J* = 13.8, 6.8 Hz, 2 H, C*H*$_2$-pent) ppm. ^{13}C NMR (151 MHz, $CDCl_3$): δ = 138.5–137.1 (C$_q$, C$_{ar}$, 4 Ph), 131.2 (*C*H=CH$_2$), 128.6–127.6 (*C*H$_{ar}$, 4 Ph), 115.0 (CH=*C*H$_2$), 107.9 (C-1^{I}), 99.9 (C-1^{II}), 87.8 (C-3^{I}), 81.5 (C-2^{I}), 81.0 (C-4^{I}), 79.1 (C-3^{II}), 75.7 (C-2^{II}), 75.1 (C-5^{II}), 74.6, 74.1, 73.7, 73.3 (4 *C*H$_2$Ph), 72.3 (C-4^{II}), 71.0 (C-5^{I}), 70.0 (C-6^{I}), 67.9 (*C*H$_2$-pent), 64.0 (C-6^{II}), 30.34, 29.02 (2 *C*H$_2$-pent) ppm. HRMS (ESI): calcd. for $C_{45}H_{54}O_{11}$ [M + Na]$^+$ 793.3558; found 793.3552.

Pent-4-enyl 2,3,4,6-Tetra-*O*-benzyl-α-D-galactopyranosyl-(1→3)-2,5,6-tri-*O*-benzoyl-β-D-galactofuranoside (8): BzCl (2 mL, 17 mmol) and pyridine (1.37 mL, 17 mmol) were added to a solution of disaccharide **16** (1.46 g, 1.9 mmol) in CH_2Cl_2 (10 mL). The reaction mixture was stirred overnight, then it was diluted with CH_2Cl_2, and washed with sat. aq. $NaHCO_3$ and with HCl (1 M aq.). The organic layer was dried with Na_2SO_4, and concentrated in vacuo. Purification by column chromatography gave compound **8** (1.94 g, 93 %) as a white solid. R_f = 0.31 (petroleum ether/EtOAc, 5:1). $[\alpha]_D^{20}$ = +15.01 (*c* = 1.0, EtOAc). ^{1}H NMR (600 MHz, $CDCl_3$): δ = 8.17–8.14 (m, 2 H, *o*-H$_{ar}$-Bz^1), 8.02–8.00 (m, 2 H, *o*-H$_{ar}$-Bz^2), 7.93–7.89 (m, 2 H, *o*-H$_{ar}$-Bz^3), 7.66–7.18 (m, 29 H, C*H*$_{ar}$, 7 Ph), 5.93 (dt, *J* = 7.6, 3.8 Hz, 1 H, 5^{I}-H), 5.84 (m, 1 H, C*H*=CH$_2$), 5.47 (d, *J* = 2.1 Hz, 1 H, 2^{I}-H), 5.17 (s, 1 H, 1^{I}-H), 5.15 (d, *J* = 3.8 Hz, 1 H, 1^{II}-H), 5.07 (m, 1 H, CH=C*H*H), 5.00 (dd, *J* = 10.3, 1.4 Hz, 1 H, CH=CH*H*), 4.95 (d, 1 H, C*H*$_2$Ph), 4.85–4.80 (m, 3 H, C*H*$_2$Ph), 4.79–4.71 (m, 2 H, C*H*$_2$Ph), 4.71–4.66 (m, 2 H, 6ab^{I}-H), 4.58–4.54 (m, 1 H, 4^{I}-H, C*H*$_2$Ph), 4.34 (d, 1 H, C*H*$_2$Ph), 4.31 (dd, *J* = 6.7, 2.0 Hz, 1 H, 3^{I}-H), 4.24 (d, 1 H, C*H*$_2$Ph), 4.19–4.13 (m, 1 H, 5^{II}-H), 4.11 (dd, *J* = 10.1, 3.8 Hz, 1 H, 2^{II}-H), 4.06 (d, *J* = 2.2 Hz, 1 H, 4^{II}-H), 3.99 (dd, *J* = 10.1, 2.8 Hz, 1 H, 3^{II}-H), 3.76 (m, 1 H, C*H*$_2$-pent), 3.56–3.51 (m, 2 H, 6a^{II}-H, C*H*$_2$-pent), 3.38 (dd, *J* = 9.0, 5.4 Hz, 1 H, 6b^{II}-H), 2.22–2.15 (m, 2 H, C*H*$_2$-pent), 1.80–1.71 (m, 2 H, C*H*$_2$-pent) ppm. ^{13}C NMR (151 MHz, $CDCl_3$): δ = 166.0, 165.4, 162.3 [3 PhC(O)], 134.5 (*C*H=CH$_2$), 133.3–127.3 (*C*$_{ar}$, 7 Ph), 114.9 (CH=*C*H$_2$), 105.8 (C-1^{I}), 99.6 (C-1^{II}), 83.6 (C-3^{I}), 82.5 (C-2^{I}), 80.2 (C-4^{I}), 78.8 (C-3^{II}), 76.2 (C-2^{II}), 74.9 (C-4^{II}), 74.8, 73.3, 73.2, 72.9 (4 *C*H$_2$Ph), 70.2 (C-5^{I}), 69.8 (C-5^{II}), 68.1 (C-6^{II}), 66.9 (O*C*H$_2$-pent), 63.9 (C-6^{I}), 30.2, 28.7 (2 *C*H$_2$-pent) ppm. HRMS (ESI): calcd. for $C_{66}H_{66}O_{14}$ [M + Na]$^+$ 1105.4345; found 1105.4329.

2,3,4,6-Tetra-*O*-benzyl-α-D-galactopyranosyl-(1→3)-2,5,6-tri-*O*-benzoyl-β-D-galactofuranose (17): NIS (80 mg, 0.34 mmol) and an excess of TFA (205 μL, 2.68 mmol) were added to a solution of **8** (190 mg, 0.17 mmol) in CH_2Cl_2/H_2O (99:1; 20 mL). The mixture was stirred overnight, then it was diluted with CH_2Cl_2, and washed with aqueous solutions of $Na_2S_2O_3$ and $NaHCO_3$. The organic layer was dried with Na_2SO_4, and concentrated in vacuo. Purification by column chromatography gave **17** (107 mg, 60 %) as a yellowish syrup. R_f = 0.37 (toluene/EtOAc, 5:1). An anomeric mixture of hemiacetals was obtained, ratio β/α = 2:1. ^{1}H NMR (400 MHz, $CDCl_3$): δ = 8.16–7.91 (m, 12 H, *o*-H-Bz), 7.63–7.12 (m, 58 H, C*H*$_{ar}$-Ph), 5.87 (dt, *J* = 7.9, 4.0 Hz, 1 H, 5^{Iβ}-H), 5.84–5.78 (m, 1 H, 5^{Iα}-H), 5.73 (t, *J* = 4.4 Hz, 1 H, 1^{Iα}-H), 5.60 (s, 1 H, 2^{Iβ}-H), 5.39 (s, 1 H, 1^{Iβ}-H), 5.32 (dd, *J* 6.6, 4.4 Hz, 1 H, 2^{Iα}-H), 5.15 (d, *J* = 3.8 Hz, 1 H, 1^{IIβ}-H), 5.12 (d, *J* = 3.8 Hz, 1 H, 1^{IIα}-H), 4.95 (d, 1 H, C*H*$_2$Ph), 4.93–4.86 (m, 2 H, C*H*$_2$Ph), 4.83–4.80 (d, 1 H, C*H*$_2$Ph), 4.78–4.65 (m, 7 H, 6ab^{Iβ}-H, 4^{Iβ}-H, 3^{Iα}-H, C*H*$_2$Ph, 6^{Iα}-H), 4.65–4.49 (m, 4 H, C*H*$_2$Ph), 4.41 (d, 1 H, C*H*$_2$Ph), 4.38 (d, *J* = 5.5 Hz, 1 H, 3^{Iβ}-H), 4.32 (d, 1 H, C*H*$_2$Ph), 4.25–4.02 (m, 4 H, C*H*$_2$Ph, 5^{IIβ}-H, 2^{IIβ}-H), 4.02–3.88 (m, 6 H, 5^{IIα}-H, 4^{IIα}-H, 2^{IIα}-H, 4^{IIβ}-H 3^{IIβ}-H, 3^{Iα}-H), 3.78 (br. s, 1 H, OH^{β}), 3.53–3.40 (m, 3 H, 6b^{Iα}-H, OH^{α}, 6ab^{IIβ}-H), 3.28 (dd, *J* 8.9, 5.3 Hz, 1 H, 6b^{IIα}-H) ppm. ^{13}C NMR (101 MHz, $CDCl_3$): δ = 166.4–165.5 [PhC(O)], 138.7–138.4 (C$_q$, C$_{ar}$-Ph), 133.3–127.4 (C$_{ar}$-Ph), 100.8 (C-1^{Iβ}), 99.0 (C-1^{IIa}), 98.1 (C-1^{IIβ}), 95.4 (C-1^{Iα}), 82.6 (C-3^{Iβ}), 81.7 (C-2^{Iβ}), 81.6 (C-4^{Iβ}), 80.6 (C-3^{Ia}), 78.8 (C-3^{IIβ}, C-4^{Iα}), 78.4 (C-2^{Iα}), 76.3 (C-2^{Iβ}), 76.1 (C-2^{IIβ}), 74.9 (C-2^{IIα}), 74.6 (C-4^{IIβ}), 73.7, 73.6, 73.6, 73.3, 73.1, 72.8 (*C*H$_2$Ph), 72.5 (C-5^{Iα}), 70.6 (C-5^{Iβ}), 70.0 (C-5^{IIα}, C-5^{IIβ}), 69.3 (C-6^{IIβ}), 68.1 (C-6^{IIα}), 63.8 (C-6^{Iβ}), 63.3 (C-6^{Iα}) ppm. HRMS (ESI): calcd. for $C_{61}H_{58}O_{14}$ [M + Na]$^+$ 1037.3719; found 1037.3710.

3-(Trifluoroactamido)propyl 2,3,4,6-Tetra-*O*-benzyl-α-D-galactopyranosyl-(1→3)-2,5,6-tri-*O*-benzoyl-β-D-galactofuranoside (18): A mixture of donor **8** (400 mg, 0.37 mmol), 3-(trifluoroacetamido)propan-1-ol (316 mg, 1.85 mmol), and molecular sieves (AW300; 500 mg) in CH_2Cl_2 (5 mL) was stirred for 15 min at room temperature, and then it was cooled to –40 °C. NIS (203 mg, 0.90 mmol) and TfOH (35 μL, 0.19 mmol) were added. The reaction mixture was allowed to reach room temperature, then the mixture was diluted with CH_2Cl_2, quenched with aqueous $Na_2S_2O_3$, and washed with H_2O. The organic layer was dried with Na_2SO_4, and concentrated in vacuo. Purification by column chromatography gave spacer-arm-equipped disaccharide **18** (342 mg, 79 %) as a white solid. R_f = 0.21 (toluene/EtOAc, 10:1). $[\alpha]_D^{20}$ = +19.35 (*c* = 1.0, EtOAc). ^{1}H NMR (600 MHz, $CDCl_3$): δ = 8.15–8.11 (m, 2 H, *o*-H$_{ar}$-Bz^1), 8.01–7.95 (m, 2 H, *o*-H$_{ar}$-Bz^2), 7.95–7.89 (m, 2 H, *o*-H$_{ar}$-Bz^3), 7.62–7.11 (m, 29 H, C*H*$_{ar}$, 7 Ph), 5.89–5.84 (m, 1 H, 5^{I}-H), 5.31 (d, *J* = 2.5 Hz, 1 H, 2^{I}-H), 5.12–5.10 (m, 2 H, 1^{I}-H, 1^{II}-H), 4.91 (d, 1 H, C*H*$_2$Ph), 4.83–4.70 (m, 4 H, 2 C*H*$_2$Ph), 4.70–4.63 (m, 2 H, 6ab^{I}-H), 4.55–4.49 (m, 2 H, 4^{I}-H, C*H*$_2$Ph), 4.34 (dd, *J* = 7.1, 3.0 Hz, 1 H, 3^{I}-H), 4.21 (d, 1 H, C*H*$_2$Ph), 4.13 (d, 1 H, C*H*$_2$Ph), 4.09 (dd, *J* = 10.1, 3.8 Hz, 1 H, 2^{II}-H), 4.09 (dd, *J* = 10.1, 3.8 Hz, 1 H), 4.04–3.99 (m, 2 H, 5^{II}-H, 4^{II}-H), 3.93 (dd, *J* = 10.2, 2.7 Hz, 1 H, 3^{II}-H), 3.91–3.85 (m, 1 H, OC*H*HCH$_2$CH$_2$N), 3.55–3.42 (m, 4 H, 6a^{II}-H, OCH*H*CH$_2$CH$_2$N, OCH$_2$CH$_2$C*H*$_2$N), 3.30 (dd, *J* = 9.1, 5.5 Hz, 1 H, 6b^{II}-H), 1.91–1.83 (m, 2 H, OCH$_2$C*H*$_2$CH$_2$N) ppm. ^{13}C NMR (151 MHz, $CDCl_3$): δ = 166.1–165.9 [3 PhC(O)], 138.7–137.8 (C$_q$, C$_{ar}$-Ph), 133.5 (*o*-C$_{ar}$-Bz^1), 133.4 (*o*-C$_{ar}$-Bz^2), 133.1 (*o*-C$_{ar}$-Bz^3), 129.9–127.3 (C$_{ar}$-Ph), 106.4 (C-1^{I}), 99.5 (C-1^{II}), 83.5 (C-2^{I}), 82.6 (C-3^{I}), 80.0 (C-4^{I}), 78.8 (C-3^{II}), 76.1 (C-2^{II}), 74.8 (*C*H$_2$Ph), 74.7 (C-4^{II}), 73.5, 73.2, 72.8 (3 *C*H$_2$Ph), 70.1 (C-5^{II}, C-5^{I}), 68.3 (C-6^{II}), 66.0 (OCH$_2$CH$_2$CH$_2$N), 63.7 (C-6^{I}), 37.7 (OCH$_2$CH$_2$CH$_2$N), 27.8 (OCH$_2$CH$_2$CH$_2$N) ppm. HRMS (ESI): calcd. for $C_{66}H_{64}F_3NO_{15}$ [M + Na]$^+$ 1190.4120; found 1190.4094.

2,3,4,6-Tetra-*O*-benzyl-α-D-galactopyranosyl-(1→3)-2,5,6-tri-*O*-benzoyl-β-D-galactofuranosyl *N*-Phenyltrifluoroacetimidate (19): Hemiacetals **17** (107 mg, 0.11 mmol) were dissolved in CH_2Cl_2 (2 mL), and then *N*-phenyl-2,2,2-trifluoroacetimidoyl chloride (35 μL, 0.21 mmol) and Cs_2CO_3 were added. The mixture was stirred vigorously for 30 min at room temperature, then it was loaded on a column with silica gel (toluene, 1 % Et_3N). Purification by column chromatography (toluene/EtOAc, 25:1, 1 % Et_3N) gave **19** (125 mg, quantitative yield) as a yellowish oil. R_f = 0.61 (toluene/EtOAc, 10:1).

^{1}H NMR (600 MHz, $CDCl_3$): δ = 8.15–8.06 (m, 2 H, *o*-*H*-Bz^1), 8.03–7.95 (m, 2 H, *o*-*H*-Bz^2), 7.90 (d, *J* = 7.7 Hz, 2 H, *o*-*H*-Bz^3), 7.62–7.35 (m, 8 H, CH_{ar}-Ph), 7.33 (t, *J* = 7.8 Hz, 2 H, *m*-*H*-NPh), 7.31–7.12 (m, 10 H, CH_{ar}-Ph), 7.10 (t, *J* = 7.4 Hz, 1 H, *p*-*H*-NPh), 6.86 (d, *J* = 7.5 Hz, 1 H, *o*-*H*-NPh), 6.49 (br. s, 1 H, 1^I-H), 5.93–5.89 (m, 1 H, 5^I-H), 5.77 (s, 1 H, 2^I-H), 5.17 (d, *J* = 3.2 Hz, 1 H, 1^{II}-H), 4.95 (d, 1 H, CH_2Ph), 4.84 (dd, 2 H, CH_2Ph), 4.78–4.73 (m, 3 H, CH_2Ph, 4^I-H), 4.73–4.63 (m, 2 H, 6ab^I-H), 4.56 (d, 1 H, CH_2Ph), 4.45 (d, *J* = 3.9 Hz, 1 H, 1 H, 3^I-H), 4.37 (d, 1 H, CH_2Ph), 4.27 (d, 1 H, CH_2Ph), 4.21–4.08 (m, 2 H, 5^{II}-H, 2^{II}-H), 4.04 (s, 1 H, 4^{II}-H), 3.99 (dd, *J* = 3.2, 10.2 Hz, 1 H, 1 H, 3^{II}-H), 3.53 (t, *J* = 8.3 Hz, 1 H, 6a^{II}-H), 3.43 (dd, *J* = 9.0, 5.8 Hz, 1 H, 6b^{II}-H) ppm. ^{13}C NMR (151 MHz, $CDCl_3$): δ = 165.9–165.1 [Ph*C*(O)], 138.8–138.1 (C$_q$, *C*$_{ar}$-Ph), 133.4–127.4 (*CH*$_{ar}$-Ph), 124.3 (*p*-*C*-NPh), 119.6 (*o*-*C*-NPh), 102.4 (C-1^I), 99.8 (C-1^{II}), 83.14 (C-3^I), 83.12 (C-4^I), 81.4 (C-2^I), 78.8 (C-3^{II}), 76.2 (C-2^{II}), 75.0 (C-4^{II}), 74.8, 73.5, 73.3, 73.0 (*CH*$_2$Ph), 70.2 (C-5^{II}), 69.9 (C-5^I), 68.4 (C-6^{II}), 63.6 (C-6^I) ppm. HRMS (ESI): calcd. for $C_{69}H_{62}F_3O_{14}$ [M + Na]$^+$ 1208.4015; found 1208.3990.

3-(Trifluoroactamido)propyl 4,6-*O*-Benzylidene-α-D-galactopyranosyl-(1→3)-2,5,6-tri-*O*-benzoyl-β-D-galactofuranoside (20): Disaccharide **18** (342 mg, 0.29 mmol) was dissolved in EtOAc (5 mL), and Pd(OH)$_2$/C (10 %; 355 mg) and AcOH (40 μL) were added. The resulting mixture was stirred overnight under a hydrogen atmosphere at room temperature. Then the mixture was filtered through Celite, and the filtrate was concentrated in vacuo.

The debenzylated product was dissolved in CH_3CN (3 mL), and $PhCH(OMe)_2$ (70 μL, 0.46 mmol) and CSA (30 mg) were added. The mixture was stirred for 2 h, then the mixture was quenched by the addition of triethylamine (50 μL), and concentrated. Purification by column chromatography gave compound **20** (152 mg, 58 %). R_f = 0.15 (toluene/EtOAc, 2:1). $[\alpha]_D^{20}$ = +25.05 (*c* = 1.0, EtOAc). ^{1}H NMR (400 MHz, $CDCl_3$): δ = 8.13–8.08 (m, 2 H, *o*-*H*$_{ar}$-Bz^1), 8.00–7.95 (m, 2 H, *o*-*H*$_{ar}$-Bz^2), 7.95–7.87 (m, 2 H, *o*-*H*$_{ar}$-Bz^3), 7.63–7.29 (m, 14 H, CH_{ar}, 4 Ph), 5.89–5.83 (m, 1 H, 5^I-H), 5.51 (s, 1 H, C*H*Ph), 5.31 (d, *J* = 2.4 Hz, 1 H, 2^I-H), 5.15 (d, *J* = 2.4 Hz, 1 H, 1^{II}-H), 5.11 (s, 1 H, 1^I-H), 4.74 (m, 2 H, 6ab^I-H), 4.53 (dd, *J* = 7.0, 3.6 Hz, 1 H, 4^I-H), 4.33 (dd, *J* = 7.0, 3.2 Hz, 1 H, 3^I-H), 4.28 (s, 1 H, 3^{II}-H), 4.11–3.84 (m, 6 H, 2^{II}-H, 5^{II}-H, 4^{II}-H, 6ab^{II}-H, OC*H*HCH$_2$CH$_2$N), 3.66–3.39 (m, 3 H, OCH$_2$CH$_2$C*H*$_2$N, OCH*H*CH$_2$CH$_2$N), 1.98–1.84 (m, 2 H, OCH$_2$C*H*$_2$CH$_2$N) ppm. ^{13}C NMR (101 MHz, $CDCl_3$): δ = 166.4, 166.3, 166.1 [Ph*C*(O)], 137.6–133.5 (C$_q$, *C*$_{ar}$-Ph), 130.2–126.4 (*C*$_{ar}$-Ph), 106.4 (C-1^I), 101.3 (*C*HPh), 100.9 (C-1^{II}), 83.2 (C-2^I), 82.7 (C-3^I), 80.1 (C-4^I), 75.9 (C-3^{II}), 70.1 (C-5^I), 69.6 (C-2^{II}), 69.5 (C-4^{II}), 69.3 (C-5^{II}), 66.5 (OCH$_2$CH$_2$CH$_2$N), 64.1 (C-6^{II}), 63.5 (C-6^I), 38.2 (OCH$_2$*C*H$_2$CH$_2$N), 28.3 (OCH$_2$CH$_2$CH$_2$N) ppm. HRMS (ESI): calcd. for $C_{45}H_{44}F_3NO_{15}$ [M + Na]$^+$ 918.2555; found 918.2554.

3-(Trifluoroactamido)propyl 2,3,4,6-Tetra-*O*-benzyl-α-D-galactopyranosyl-(1→3)-2,5,6-tri-*O*-benzoyl-β-D-galactofuranosyl-(1→3)-4,6-*O*-benzylidene-α-D-galactopyranosyl-(1→3)-2,5,6-tri-*O*-benzoyl-β-D-galactofuranoside (21): A solution of donor **19** (78 mg, 0.07 mmol) and acceptor **20** (59 mg, 0.07 mmol) with molecular sieves (4 Å; 170 mg) in CH_2Cl_2 (0.8 mL) was stirred for 15 min, and then the mixture was cooled to –80 °C. TfOH (2 μL, 0.02 mmol) was added, and when TLC analysis indicated the complete consumption of the donor, the reaction mixture was loaded onto a column. Purification by column chromatography gave **21** (52 mg, 42 %) as a white solid. R_f = 0.21 (toluene/EtOAc, 5:1). ^{1}H NMR (600 MHz, $CDCl_3$): δ = 8.14–8.10 (m, 2 H, *o*-*H*-Bz^1), 8.06 (d, *J* = 7.2 Hz, 2 H, *o*-*H*-Bz^2), 7.98–7.91 (m, 8 H, *o*-*H*-Bz$^{3\text{-}6}$), 7.61–7.13 (m, 43 H, CH_{ar}-Ph), 5.92–5.88 (m, 1 H, 5^I-H), 5.86 (dt, *J* = 7.9, 4.0 Hz, 1 H, 5^{III}-H), 5.64 (d, *J* = 2.3 Hz, 1 H, 2^{III}-H), 5.43 (s, 1 H, C*H*Ph), 5.42 (s, 1 H, 1^{III}-H), 5.33 (d, *J* = 2.9 Hz, 1 H, 2^{III}-H), 5.19 (d, *J* = 3.8 Hz, 1 H, 1^{II}-H), 5.18 (d, *J* = 3.9 Hz, 1 H, 1^{IV}-H), 5.15 (s, 1 H, 1^I-H), 4.86 (d, 1 H, CH_2Ph), 4.81 (dd, *J* = 12.0, 3.9 Hz, 1 H, 6a^I-H), 4.76–4.65 (m, 5 H, 6b^I-H, 6a^{III}-H, 4^{III}-H, CH_2Ph), 4.61–4.56 (m, 3 H, 6b^{III}-H, 4^I-H, CH_2Ph), 4.50 (d, 1 H, CH_2Ph), 4.45–4.41 (m, 2 H, 3^I-H, CH_2Ph), 4.37 (d, *J* = 3.6 Hz, 1 H, 4^{II}-H), 4.35 (d, 1 H, CH_2Ph), 4.31 (dd, *J* = 6.2, 2.3 Hz, 1 H, 3^{III}-H), 4.27–4.22 (m, 2 H, 3^{II}-H, CH_2Ph), 4.14 (dd, *J* = 13.2, 6.7 Hz, 1 H, 5^{IV}-H), 4.05–4.00 (m, 2 H, 2^{IV}-H, 6a^{II}-H), 3.99 (dd, *J* = 10.1, 3.4 Hz, 1 H, 3^{II}-H), 3.92–3.88 (m, 1 H, OC*H*HCH$_2$CH$_2$N), 3.82–3.76 (m, 4 H, 3^{IV}-H, 6b^{II}-H, 5^{II}-H, 4^{IV}-H), 3.58 (m, *J* = 12.4, 6.1 Hz, 1 H, OCH$_2$CH$_2$C*H*HN), 3.55–3.49 (m, 1 H, OCH*H*CH$_2$CH$_2$N), 3.44–3.35 (m, 3 H, 6ab^{IV}-H, OCH$_2$CH$_2$CH*H*N), 1.98–1.86 (m, 2 H, OCH$_2$C*H*$_2$CH$_2$N) ppm. ^{13}C NMR (151 MHz, $CDCl_3$): δ = 166.1–165.8 [Ph*C*(O)], 138.8–137.7 (C$_q$, *C*$_{ar}$-Ph), 133.7–126.2 (*C*$_{ar}$-Ph), 107.9 (C-1^{III}), 106.1 (C-1^I), 100.6 (C-1^{II}), 99.3 (C-1^{IV}), 83.6 (C-3^{III}), 83.3 (C-2^I), 82.5 (C-3^I), 82.1 (C-2^{III}), 80.8 (C-4^{III}), 80.4 (C-4^I), 79.1 (C-3^{IV}), 77.4 (C-3^{II}), 76.2 (C-2^{IV}, C-4^{IV}), 74.9 (C-4^{II}), 74.7, 73.4, 73.3, 72.7 (*CH*$_2$Ph), 70.5 (C-5^{III}), 70.3 (C-5^I), 70.0 (C-5^{IV}), 69.0 (C-6^{II}), 68.9 (C-6^{IV}), 67.0 (C-2^{II}), 65.8 (OCH$_2$CH$_2$CH$_2$N), 63.7 (C-5^{II}), 63.6 (C-6^{III}), 63.4 (C-6^I), 37.9 (OCH$_2$CH$_2$*C*H$_2$N), 27.9 (OCH$_2$*C*H$_2$CH$_2$N) ppm. HRMS (ESI): calcd. for $C_{106}H_{100}F_3NO_{28}$ [M + Na]$^+$ 1914.6276; found 1914.6241.

3-Aminopropyl α-D-Galactopyranosyl-(1→3)-β-D-galactofuranosyl-(1→3)-α-D-galactopyranosyl-(1→3)-β-D-galactofuranoside (7): Tetrasaccharide **21** (26 mg, 0.01 mmol) was dissolved in EtOAc (1 mL), and Pd(OH$_2$)/C catalyst (10 %; 28 mg) and AcOH (15 μL) were added. The resulting mixture was stirred overnight under a hydrogen atmosphere, after which the mixture was filtered through Celite, and the filtrate was concentrated in vacuo.

The resulting product was suspended in MeOH (1 mL), and treated with NaOMe (1 M solution in MeOH; 100 μL). After 30 min, the solution was diluted with H_2O (200 μL) and an excess of NaOMe (1 M solution in MeOH; 300 μL) was added. The resulting mixture was stirred at 40 °C, and after 5 min it was neutralized by the addition of AcOH (0.1 M aq.; 4 mL). The solution was concentrated in vacuo, and the residue was purified by gel chromatography on TSK-40 HW to give compound **7** (6.2 mg, 63 %) as a white powder. ^{1}H NMR (600 MHz, D_2O): δ = 5.21 (d, *J* = 1.4 Hz, 1 H, 1^{III}-H), 5.07 (d, *J* = 3.9 Hz, 1 H, 1^{II}-H), 5.05 (d, *J* = 3.5 Hz, 1 H, 1^{IV}-H), 5.03 (d, *J* = 1.9 Hz, 1 H, 1^I-H), 4.41 (dd, *J* = 3.0, 1.4 Hz, 1 H, 2^{III}-H), 4.28 (dd, *J* = 3.0, 2.0 Hz, 1 H, 2^I-H), 4.24 (dd, *J* = 6.3, 4.2 Hz, 1 H, 4^{III}-H), 4.18 (dd, *J* = 6.2, 4.1 Hz, 1 H, 4^I-H), 4.13 (d, *J* = 2.8 Hz, 1 H, 4^{II}-H), 4.11 (t, *J* = 6.3 Hz, 1 H, 5^I-H), 4.09–4.03 (m, 2 H, 3^I-H, 5^{III}-H, 3^{III}-H), 3.99 (d, *J* = 2.4 Hz, 1 H, 4^{IV}-H), 3.95 (dd, *J* = 10.5, 3.9 Hz, 1 H, 2^{II}-H), 3.91–3.81 (m, 6 H, 3^{II}-H, 5^{II}-H, 3^{IV}-H, 5^{IV}-H, 2^{IV}-H, OC*H*HCH$_2$CH$_2$N), 3.78–3.73 (m, 4 H, 6ab^{III}-H, 6ab^I-H), 3.73–3.63 (m, 5 H, 6ab^{II}-H, 6ab^{IV}-H, OCH*H*CH$_2$CH$_2$CH$_2$N), 3.12 (t, *J* = 7.2 Hz, 2 H, OCH$_2$CH$_2$C*H*$_2$N), 2.02–1.95 (m, 2 H, OCH$_2$C*H*$_2$CH$_2$N) ppm. ^{13}C NMR (151 MHz, D_2O): δ = 109.3 (C-1^{III}), 107.5 (C-1^I), 99.7 (C-1^{IV}), 99.5 (C-1^{II}), 84.7 (C-3^{III}), 84.3 (C-3^I), 81.8 (C-4^{III}, C-4^I), 79.7 (C-2^{III}), 79.5 (C-2^I), 76.9 (C-3^{II}), 71.5 (C-5^{III}), 71.4 (C-5^I), 70.9 (C-5^{II}), 70.8 (C-3^{IV}), 69.3 (C-2^{IV}), 69.2 (C-4^{IV}, C-4^{II}), 68.2(C-5^{IV}),67.2(C-2^{II}),65.6(OCH$_2$CH$_2$CH$_2$N),62.8(C-6^{II}),62.7(C-6^{IV}),61.3 (C-6^{III}), 61.1 (C-6^I), 37.5 (OCH$_2$CH$_2$*C*H$_2$N), 26.8 (OCH$_2$CH$_2$CH$_2$N) ppm. HRMS (ESI): calcd. for $C_{27}H_{49}NO_{21}$ [M + Na]$^+$ 746.2689; found 746.2675.

Acknowledgments

This work was supported by the Russian Science Foundation (grant No.14-23-00199, to N. E. N.). We thank Dr. A. S. Dmitrenok for recording NMR spectra, and Dr. A. O. Chizhov for recording high-resolution mass spectra at the Department of Structural Studies of the Zelinsky Institute of Organic Chemistry, Moscow. We thank Dr. A. G. Gerbst for careful reading of manuscript, and for valuable comments.

Keywords: Carbohydrates · Glycosylation · Oligosaccharides · Rearrangement · Furanosides · Antigens

[1] G. Patel, S. Huprikar, S. H. Factor, S. G. Jenkins, D. P. Calfee, *Infect. Control Hosp. Epidemiol.* **2008**, *29*, 1099–1106.
[2] M. A. Enani, N. A. El-Khizzi, *Saudi Med. J.* **2012**, *33*, 782–786.
[3] A. Gupta, *Semin. Perinatol.* **2002**, *26*, 340–345.
[4] S. Alberti, S. Hernández-Allés, J. Gil, J. Reina, J. Martinez-Beltran, S. Camprubi, J. M. Tomás, V. J. Benedi, *J. Clin. Microbiol.* **1993**, *31*, 1379–1381.
[5] E. Vinogradov, E. Frirdich, L. L. MacLean, M. B. Perry, B. O. Petersen, J. Ø. Duus, C. Whitfield, *J. Biol. Chem.* **2002**, *277*, 25070–25081.
[6] V. Krishnapillai, *Infect. Immun.* **1971**, *4*, 177–188.
[7] P. F. Hsieh, M. C. Wu, F. L. Yang, C. T. Chen, T. C. Lou, Y. Y. Chen, S. H. Wu, J. C. Sheu, J. T. Wang, *Front. Microbiol.* **2014**, *5*, 608.
[8] P. F. Hsieh, T. L. Lin, F. L. Yang, M. C. Wu, Y. J. Pan, S. H. Wu, J. T. Wang, *PLoS One* **2012**, *7*, e33155.
[9] C. T. Fang, Y. P. Chuang, C. T. Shun, S. C. Chang, J. T. Wang, *J. Exp. Med.* **2004**, *199*, 697–705.
[10] S. Y. Zhu, J. S. Yang, *Tetrahedron* **2012**, *68*, 3795–3802.
[11] H. Wang, G. Zhang, J. Ning, *Carbohydr. Res.* **2003**, *338*, 1033–1037.
[12] V. B. Krylov, D. A. Argunov, D. Z. Vinnitskiy, S. A. Verkhnyatskaya, A. G. Gerbst, N. E. Ustyuzhanina, A. S. Dmitrenok, J. Huebner, O. Holst, H.-C. Siebert, N. E. Nifantiev, *Chem. Eur. J.* **2014**, *20*, 16516–16522.
[13] V. B. Krylov, D. A. Argunov, D. Z. Vinnitskiy, G. Gerbst, N. E. Ustyuzhanina, A. S. Dmitrenok, N. E. Nifantiev, *Synlett* **2016**, *27*, 1659–1664.
[14] V. B. Krylov, A. G. Gerbst, D. A. Argunov, A. S. Dmitrenok, A. S. Shashkov, Z. Kaczynski, J. Huebner, O. Holst, N. E. Nifantiev, *Chem. Eur. J.* **2015**, *21*, 1749–1754.
[15] D. A. Argunov, V. B. Krylov, N. E. Nifantiev, *Org. Lett.* **2016**, *18*, 5504–5507.
[16] D. Z. Vinnitskiy, V. B. Krylov, N. E. Ustyuzhanina, A. S. Dmitrenok, N. E. Nifantiev, *Org. Biomol. Chem.* **2016**, *14*, 598–611.
[17] D. A. Argunov, V. B. Krylov, N. E. Nifantiev, *Org. Biomol. Chem.* **2015**, *13*, 3255–3267.
[18] P. J. Garegg, *Adv. Carbohydr. Chem. Biochem.* **1997**, *52*, 179–205.
[19] J. D. Codée, R. E. Litjens, L. J. van den Bos, H. S. Overkleeft, G. A. van der Marel, *Chem. Soc. Rev.* **2005**, *34*, 769–782.
[20] R. U. Lemieux, *Can. J. Chem.* **1951**, *29*, 1070–1091.
[21] B. Fraser-Reid, P. Konradsson, D. R. Mootoo, U. E. Udodong, *J. Chem. Soc., Chem. Commun.* **1988**, 823–825.
[22] B. Fraser-Reid, U. E. Udodong, Z. Wu, H. Ottosson, J. R. Merritt, C. S. Rao, C. Roberts, R. Madsen, *Synlett* **1992**, 927–942.
[23] U. E. Udodong, C. S. Rao, B. Fraser-Reid, *Tetrahedron* **1992**, *48*, 4713–4724.
[24] H. Li, Q. Li, M. S. Cai, Z. J. Li, *Carbohydr. Res.* **2000**, *328*, 611–615.
[25] R. Dettmann, T. Ziegler, *Carbohydr. Res.* **2011**, *346*, 2348–2361.
[26] R. R. Schmidt, J. Michel, M. Roos, *Liebigs Ann. Chem.* **1984**, 1343–1357.
[27] G. Karki, V. N. Mishra, P. K. Mandal, *Glycoconjugate J.* **2016**, *33*, 63–78.
[28] M. R. Pratt, C. R. Bertozzi, *Org. Lett.* **2004**, *6*, 2345–2348.
[29] A. Toepfer, R. R. Schmidt, *Tetrahedron Lett.* **1992**, *33*, 5161–5164.
[30] R. T. Lee, Y. C. Lee, *Carbohydr. Res.* **1994**, *251*, 69–79.
[31] M. Kitajima, T. Fukatsu, *Carbohydr. Res.* **1983**, *112*, 158–164.
[32] P. G. Evans, H. M. Osborn, W. G. Suthers, *Tetrahedron Lett.* **2002**, *43*, 7855–7857.
[33] R. U. Lemieux, K. B. Hendriks, R. V. Stick, K. James, *J. Am. Chem. Soc.* **1975**, *97*, 4056–4062.
[34] D. Kahne, S. Walker, Y. Cheng, D. Van Engen, *J. Am. Chem. Soc.* **1989**, *111*, 6881–6882.
[35] R. R. Schmidt, *Angew. Chem. Int. Ed. Engl.* **1986**, *25*, 212–235; *Angew. Chem.* **1986**, *98*, 213–236.
[36] R. Eby, C. Schuerch, *Carbohydr. Res.* **1974**, *34*, 79–90.
[37] L. Baldoni, C. Marino, *J. Org. Chem.* **2009**, *74*, 1994–2003.
[38] W. L. F. Armarego, C. L. L. Chai (Eds.), *Purification of Laboratory Chemicals, 5th ed.*, Butterworth, Heinemann, **2003**.
[39] P. A. Belyakov, V. I. Kadentsev, A. O. Chizhov, N. G. Kolotyrkina, A. S. Shashkov, V. P. Ananikov, *Mendeleev Commun.* **2010**, *20*, 125–131.

Received: November 8, 2016

Glycochemistry

Definitive Structural Assessment of Enterococcal Diheteroglycan

Vadim B. Krylov,[a] Alexey G. Gerbst,[a] Dmitry A. Argunov,[a] Andrey S. Dmitrenok,[a] Alexander S. Shashkov,[a] Zbigniew Kaczynski,[b] Johannes Huebner,[c] Otto Holst,[d] and Nikolay E. Nifantiev*[a]

Abstract: *Enterococcus faecalis* is one of most important nosocomial and often multi-antibiotic resistant pathogens responsible for infections that are difficult to treat. Previously, a cell-wall polysaccharide termed diheteroglycan (DHG) was isolated and characterized as a promising vaccine candidate. However, the configuration of its lactic acid (LA) residue attached to the galactofuranoside unit was not assessed, although it influences conformation of DHG chain in terms of biological recognition and immune evasion. This study proves the *R* configuration of the LA residue by means of chemical analysis, investigation of intramolecular NMR nuclear Overhauser effects and molecular dynamics simulations of native DHG and corresponding *R* and *S* models, which were obtained by using pyranoside-*into*-furanoside rearrangement. As alternative treatment and prevention strategies for *E. faecalis* are desperately needed, this discovery may offer the prospect of a synthetic vaccine to actively immunize patients at risk.

Introduction

Enterococcus is currently the third most common Gram-positive pathogen to cause hospital-associated infections in the US, and the second most common pathogen isolated from ICU patients worldwide.[1,2] Although enterococci (i.e., *Enterococcus faecalis* as well as *Enterococcus faecium*) are intrinsically not as virulent as other Gram-positive cocci (e.g., *Staphylococcus aureus*), these infections often occur in immunocompromised patients[3] or as so-called "biofilm" infections, associated with implanted foreign bodies (such as artificial heart valves, catheters, stents, and shunts).[4] These infections are notoriously difficult to treat and often result in additional hospital stay and attributable mortality.[5] A polysaccharide termed diheteroglycan (DHG) comprising the repeating unit →6)-β-D-Gal*f*-(1→3)-β-D-Glc*p*-(1→ bearing one lactic acid substituent of unknown configuration at O-3 of Gal*f* was isolated from *E. faecalis* and structurally characterized.[6] Initial immunological studies revealed DHG to be a promising candidate for vaccine design[6] which encouraged deeper structural investigations of DHG. Particularly, the configuration of its lactic acid residue is an important antigenic structural component within the DHG chain, which influences its conformational behavior in terms of biological recognition and immune evasion.

Results and Discussion

NMR spectroscopy is one of the most informative methods for structural analysis of oligo- and polysaccharides but ^{1}H and ^{13}C NMR chemical shifts alone do not allow assessment of lactic acid configuration without comparison to data obtained on corresponding reference models. The straightforward way to determine an unknown configuration in a side chain is to reveal spectroscopically its spatial contacts with core polysaccharide fragments, and compare them to those of corresponding model compounds with predefined configuration of a studied asymmetric center. Particularly, the most informative spectroscopical characteristics for the elucidation of a particular molecular spatial organization are the values of *intra*molecular ^{1}H nuclear Overhauser effects (nOe). The ratio of two nOe values within a single molecule, also called the relative nOe, is in simple cases reciprocally proportional to the sixth order of the averaged proton–proton distance ratio.

Thus, nOe experiments were performed on DHG by applying standard 2D ROESY,[7] which revealed the spatial proximity of protons in the lactic acid residue and some of the Gal*f* ring protons (Figure 1), that is, the connectivities of H2 of lactic acid with H2, H3 and H4 of Gal*f* along with a weak interaction of CH_3 of lactic acid with H3 of Gal*f* were observed. The cross-peak $H2^{LA}$–$H2^{Galf}$ was much less intense than that of $H2^{LA}$–$H4^{Galf}$. Chemical shifts of $H2^{LA}$ and $H3^{Galf}$ protons were too

[a] *Dr. V. B. Krylov, Dr. A. G. Gerbst, D. A. Argunov, Dr. A. S. Dmitrenok, Prof. Dr. A. S. Shashkov, Prof. Dr. N. E. Nifantiev*
N.D. Zelinsky Institute of Organic Chemistry, Russian Academy of Sciences
Leninsky prospect 47, 119991 Moscow (Russian Federation)
E-mail: nen@ioc.ac.ru

[b] *Prof. Dr. Z. Kaczynski*
Faculty of Chemistry, University of Gdansk
Wita Stwosza 63, 80-308, Gdansk (Poland)

[c] *Prof. Dr. J. Huebner*
Division of Pediatric Infectious Diseases, Hauner Children's Hospital
Ludwigs-Maximilian University, Munich (Germany)

[d] *Prof. Dr. O. Holst*
Research Center Borstel, Leibniz-Center for Medicine and Biosciences
Borstel (Germany)

Supporting information for this article is available on the WWW under http://dx.doi.org/10.1002/chem.201405857.

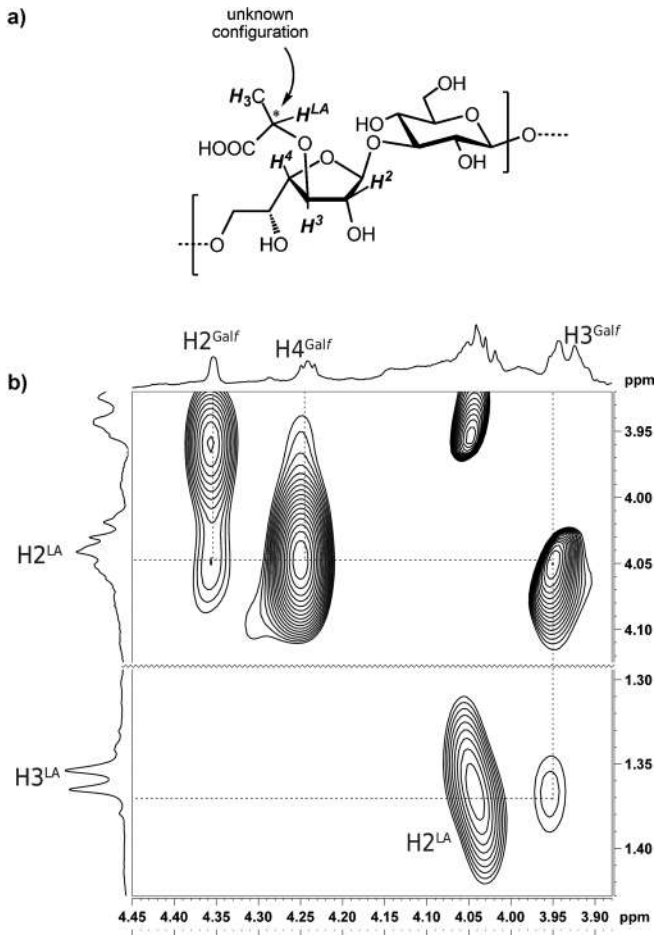

Figure 1. a) Structure of DHG from *E. faecalis*. b) Part of the ROESY spectrum illustrating correlation between protons of lactic acid and Gal*f*.

close and thus the corresponding cross-peak appeared nearly on the diagonal of the 2D spectrum and could not be used for quantitative measurements.

Galactofuranoside units[8] and the linkage through which lactic acid is attached are characterized by high flexibility, and the presence of several conformational minima is possible, while experimentally observed spectral parameters are ensemble-averaged. In this work the conformation of this linkage was described in terms of angles θ_1 ($H3^{Galf}$-$C3^{Galf}$-$O3^{Galf}$-$C2^{LA}$) and θ_2 ($H2^{LA}$-$C2^{LA}$-$O3^{Galf}$-$C3^{Galf}$; Figure 2). The analysis of the registered NMR data was conducted with the help of molecular modeling using molecular mechanics calculations.

We performed a molecular dynamics (MD) simulation for model monosaccharides **1** and **2** (Figure 2). MM3 force field[9] with solvent accessible surface area solvation model (SASA)[10] as implemented in TINKER v.5.0 software package[11] were used. First, local minima were located by scanning the torsions between Gal*f* and the lactic acid residue with the step of 10°. Then these minima were used as starting points for MD simulations. The length of each trajectory was 20 ns with snapshot structures being written every 2 ps, which yielded 10 000 structures for each compound. First 2000 structures in each trajectory were discarded and the rest 8000 were analyzed.

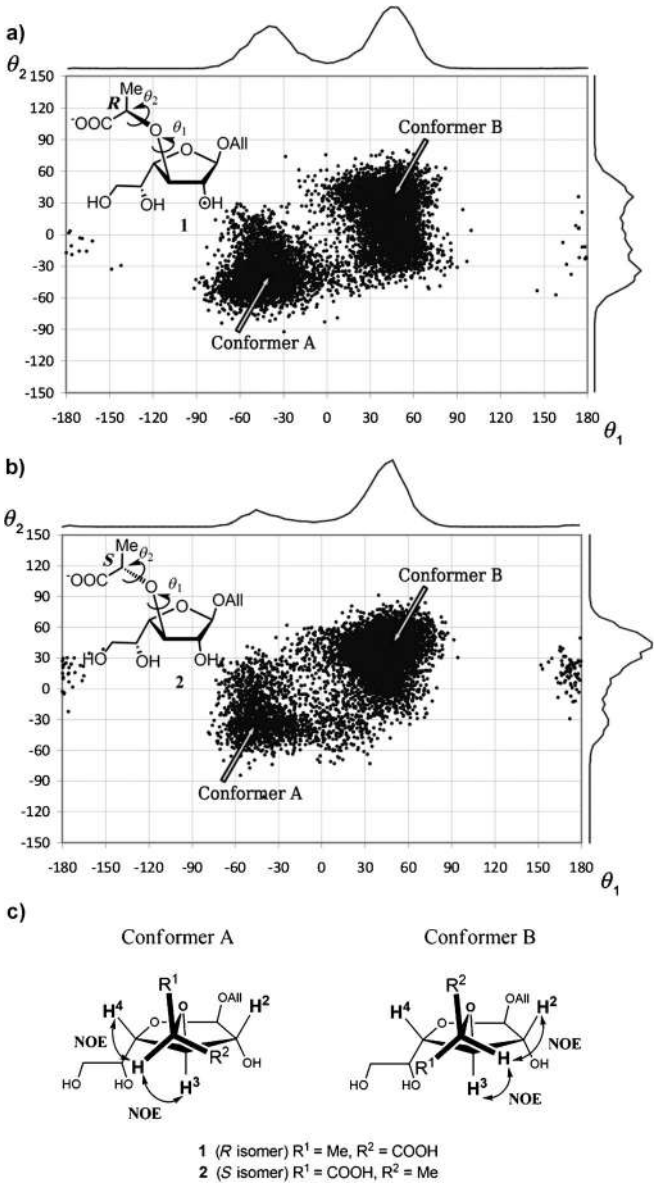

Figure 2. Conformational distributions of the lactic acid in compounds: a) **1**, and b) **2** as obtained from MD simulations, and c) schematic view of two major conformers presented in compounds **1** and **2**.

Conformational maps were plotted based on the obtained snapshots (Figure 2a and b) revealing the presence of two types of conformers. In the first one (conformer A in Figure 2c) H2 of lactic acid is in proximity to H4 and H3 of Gal*f* while in the second one (conformer B in Figure 2c) it is oriented towards H2 of Gal*f* retaining proximity to H3 (for detailed structural parameters of conformers A and B see the Supporting Information). It is remarkable that the ratio of these conformers is different for *R* and *S* models. Thus, for model compound **1** with *R* isomeric lactic acid ratio of conformers A and B is approximately 1:1.4 while for model compound **2** with *S* isomeric lactic acid ratio of conformers is about 1:4. This led us to the conclusion that nOe between $H2^{LA}$ and $H4^{Galf}$ should be significantly higher for *R* than for *S* isomer. This fact could be used as a criterion for the determination of lactic acid configuration by NMR methods.

To verify the data of molecular mechanics calculations the chemical synthesis of corresponding models **1** and **2** was performed. Since the methods of regioselective functionalization of furanoside residue were less developed than those for pyranosides, our strategy included the regioselective introduction of *S*- or *R*-configured lactic acid residue on the first steps followed by pyranoside-*into*-furanoside rearrangement[12] of selectively functionalized pyranoside precursors **5a** and **5b** (Scheme 1).

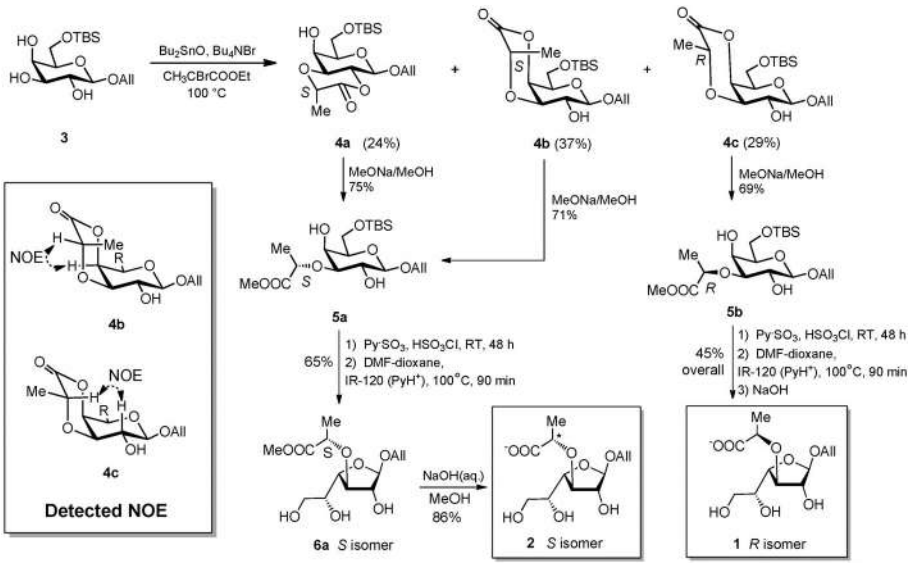

Scheme 1. Synthesis of model furanosides **1** and **2**.

According to this strategy 6-*O*-silylated β-D-galactopyranoside (**3**)[12] was alkylated with racemic ethyl 2-bromopropionate via an organotin intermediate.[13] Surprisingly, instead of an ethyl ester moiety this reaction gave a mixture of bicyclic lactones dominated by compounds **4a**–**4c**, which were isolated in their individual forms. Such formation of the rigid bicyclic structures gave us the opportunity to determine the configuration of the asymmetric center of lactic acid by NMR spectroscopy. Thus, the spatial proximity of the $H2^{LA}$ and $H4^{Galp}$ protons in **4b** but of $H2^{LA}$ and $H2^{Galp}$ in **4c** detected in nOe spectra (see Scheme 1 and the Supporting Information) enabled us to define the *S* and *R* configurations of lactic acid units in **4b** and **4c**, respectively.

The lactones **4b** and **4c** were transformed into esters **5a** and **5b** with *S* and *R* configured lactic acid by treatment with MeONa in anhydrous MeOH (Scheme 1). Configuration of lactic acid in lactone **4a** could not be clearly assessed from NMR data, however, its reaction with MeONa gave **5a** which identified *S*-configuration of lactic acid in lactone **4a**.

Pyranoside-*into*-furanoside rearrangement[12] of pyranosides **5a** under acidic sulfation conditions followed by solvolytic desulfation gave furanosides **6a**. This process included the removal of the TBS group. Further saponification of methyl esters in **6a** gave the desired model furanoside **2** (Scheme 1). In the same way furanoside **1** was prepared from pyranoside **5b**.

It should be noted that no racemization of lactic acid was observed during these steps.

The experimental 1D nOe data (Figure 3) for synthetic models **1** and **2** were in good agreement with those calculated theoretically (Table 1) using ensemble averaged internuclear distances obtained from the MD snapshots. As was expected from the conformational distributions, a significant difference in the nOe pattern was found between *R* and *S* isomers (Table 1). For the *R* isomer, considerable nOe's were predicted on both H2 and H4 protons of the furanoside ring, while for the *S* isomer nOe on H4 was predicted to be almost negligible as compared to nOe's on H3 and H2.

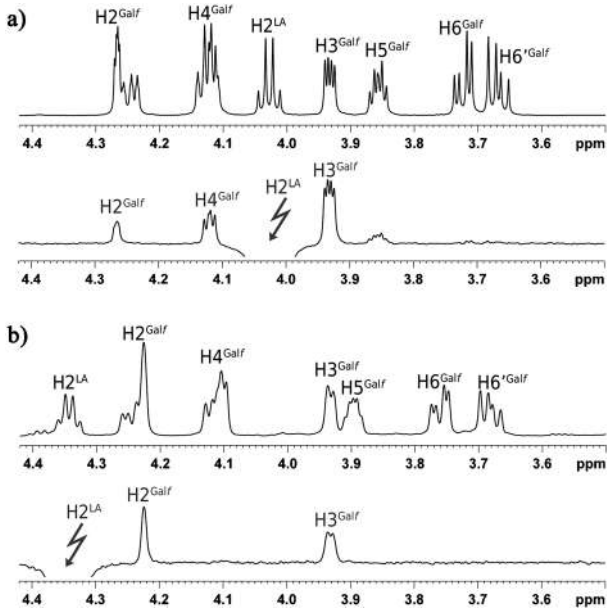

Figure 3. Excerpt of 1D nOe NMR spectra of model compounds: a) **1**, and b) **2**.

Table 1. Experimental and theoretical nOes for model isomers.

Method for nOe determination	*R* isomer **1**			*S* isomer **2**		
	H2	H3	H4	H2	H3	H4
theoretical	20	100	32	60	100	8
experimental	24	100	48	106	100	–

Indeed, the 1D nOe NMR spectrum of compound **1** indicated interactions $H2^{LA}$–$H3^{Galf}$ and $H2^{LA}$–$H4^{Galf}$, and less intensive with $H2^{Galf}$. On the contrary, for *S* isomer **2** only interactions between $H2^{LA}$ proton and $H2^{Galf}$ and $H3^{Galf}$ were observed, but no interaction with $H4^{Galf}$ could be identified (Figure 3). The

comparison of these results, especially the presence of the intensive cross-peak $H2^{LA}$–$H4^{Galf}$ in the enterococcal DHG suggested that its lactic acid residue had the *R* configuration.

Nevertheless, the conformational behavior of the lactic acid residue in model monosaccharides and in the polysaccharide may be different. To finally identify the lactic acid configuration, acid hydrolysis of DHG and of monosaccharides **1** and **2** was performed in aqueous TFA at 120 °C (Figure 4).[14] The resulting reaction mixtures were evaporated and subjected to further NMR analysis without purification.

The NMR analysis of products derived from acidic hydrolysis of polysaccharide DHG revealed the presence of two monosaccharide components: glucose and galactose with a lactyl substituent. It is known that chemical shifts can vary depending on pH of the medium. It especially concerns signals of C2 and H2 of the lactic acid unit. Therefore, the most reliable way to compare the products of DHG hydrolysis with reference compounds **7** and **8** was to use the latter ones as internal standards during NMR analysis. Thus, the addition of compound **7** [(*R*)-lactic acid residue] to the mixture of hydrolysis products did not add new signals, it only increased the intensity of the signals of **7** in the mixture (Figure 5). On the contrary, the addition of reference compound **8** [(*S*)-lactic acid residue] brought in a new set of signals corresponding to **8** since it had not been formed during the hydrolysis of DHQ. Similar conclusions were arrived at during the analysis of 2D HSQC NMR spectra (Figure 5 b) in which correlation peaks of $C2^{LA}$–$H2^{LA}$ for *R* and *S* isomers were well resolved. These data undoubtedly confirmed *R* configuration of the lactic acid residue in the DHG.

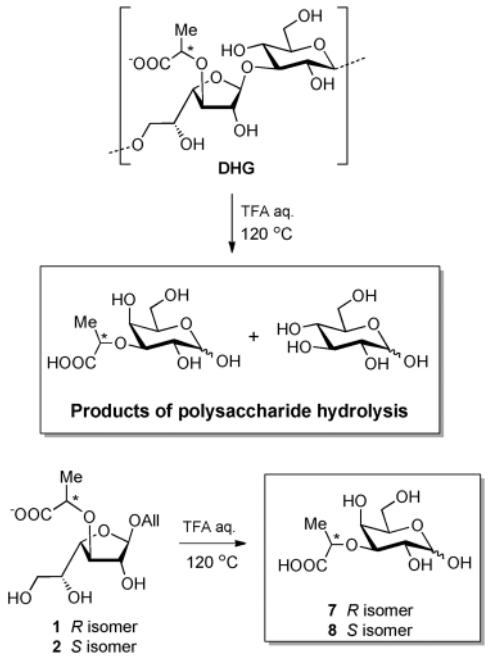

Figure 4. Acidic hydrolysis of DHG and model compounds **1** and **2**.

Conclusion

In conclusion, the *R* configuration of lactic acid in DHG from *E. faecalis* was determined by the combination of chemical analysis, nOe spectroscopy and molecular modeling of DHG

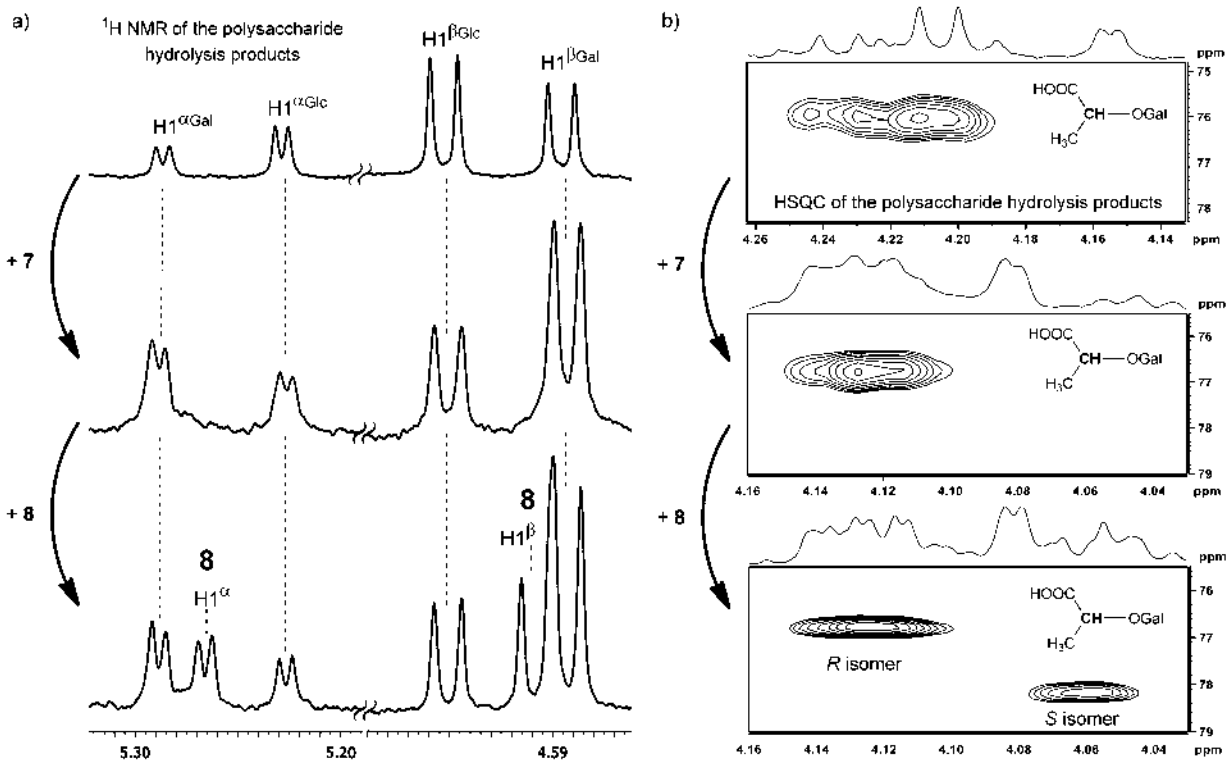

Figure 5. Part of: a) ^{1}H, and b) HSQC spectra of polysaccharide DHG hydrolysis products without and with addition of reference compounds **7** and **8**.

and corresponding model furanosides **1** and **2**. The knowledge of the precise structure of DHG permits the specification of the target synthetic structures for vaccine design and serological diagnostics. Observed tendencies for nOe of (*R*)- and (*S*)-lactic acid groups can be of use in the analyses of other oligo- and polysaccharides bearing these substituents.

Experimental Section

General information

All solvents for reactions were dried according to conventional procedures[15] or purchased as dry. Methanol (MeOH) was distilled over $Mg(OMe)_2$, toluene was distilled over Na/benzophenone, dioxane was purified by passing through alumogel columns then distilled over Na/benzophenone. Dimethylformamide (DMF) was purchased as dry and used without further purification. Reagents for synthesis were commercial and were used without further purification. All reactions involving air- or moisture-sensitive reagents were carried out using dry solvents under dry argon. Thin-layer chromatography (TLC) was carried out on aluminum plates coated with silica gel 60 F_{254} (Merck). Analysis TLC plates were inspected by the treatment with a mixture of 15% H_3PO_4 and orcinol (1.8 g L^{-1}) in EtOH/H_2O (95:5, v/v) followed by heating. Silica gel column chromatography was performed with silica gel 60 (40–63 μm, Merck). Reversed phase HPLC was performed on a C-18 column (10×250 mm, 5 μm) by elution with water/acetonitrile systems at a flow rate of 3 mL min^{-1}. Gel-filtration was performed on a Sephadex G-15 column (35×500 mm) by elution with water at a flow rate of 1 mL min^{-1}. Native diheteroglycan (DHG) was obtained as previously described.[6]

The NMR spectra were recorded on Bruker spectrometers Bruker AM 300 (300 MHz), DRX-500 (500 MHz) and AV-600 (600 MHz) equipped with 5 mm pulsed-field-gradient (PFG) probes. The spectra were acquired at the temperature of 303 K. Microtubes (Shigemi, Inc.) were sometimes used for sensitivity enhancement. The resonance assignment in ^1H and ^{13}C NMR spectra was performed by gradient enhanced 2D gCOSY, gNOESY, gHSQC, gHMBC, TOCSY and ROESY experiments. Mixing period for ROESY experiments were set at 300 ms. The 1D-gNOESY experiments were carried out at 303 K with mixing periods of 700 ms. NMR spectra were obtained using standard pulse sequence from the Bruker software. All spectra were transformed and analyzed with the Bruker Topspin 2.1 software. Chemical shifts are reported in ppm with the solvent residual peaks as standard. Chemical shifts are reported relative to chloroform (δ = 7.27 ppm) or methanol (δ = 3.31 ppm) for ^1H NMR and chloroform (δ = 77.0 ppm) or methanol (δ = 49.0 ppm) for ^{13}C NMR. The following abbreviations are used to explain the observed multiplicities: s (singlet), d (doublet), t (triplet), m (multiplet), q (quartet), and br (broad). Optical rotations were measured using a JASCO DIP-360 polarimeter at ambient temperature in solvents specified. High-resolution mass spectra (HR MS) were measured on a Bruker micrOTOF II instrument using electrospray ionization (ESI).[16] The measurements were performed in a positive ion mode (interface capillary voltage −4500 V) or in a negative ion mode (3200 V); mass range from *m/z* 50 to *m/z* 3000 Da; external or internal calibration was made with electrospray calibrant solution (Fluka). A syringe injection was used for solutions in a mixture of acetonitrile and water (50:50 v/v, flow rate 3 μL min^{-1}). Nitrogen was applied as a dry gas; interface temperature was set at 180 °C.

Selected synthetic procedures

Allyl 3-O-[(S)-1-carboxyethyl]-6-O-tert-butyldimethylsilyl-β-D-galactopyranoside 1′,2-lactone (4a), allyl 3-O-[(S)-1-carboxyethyl]-6-O-tert-butyldimethylsilyl-β-D-galactopyranoside 1′,4-lactone (4b), allyl 3-O-[(R)-1-carboxyethyl]-6-O-tert-butyldimethylsilyl-β-D-galactopyranoside 1′,4-lactone (4c)

A mixture of triol **3**[12] (210 mg, 0.628 mmol) and Bu_2SnO (178 mg, 0.715 mmol) in anhydrous toluene (13 mL) was refluxed with azeotropic removal of H_2O to a volume of 1.5 mL. Then ethyl 2-bromopropionate (0.48 mL, 3.71 mmol) and Bu_4NBr (274 mg, 0.85 mmol) were added, and the mixture was kept for 10 h at 100 °C and then cooled. The reaction mixture was diluted with anhydrous toluene (5 mL) and concentrated under normal pressure to a volume of 2 mL then cooled and loaded on a column. Column chromatography (silica gel, toluene/EtOAc = 3:1→2:1) afforded isomeric lactones **4a** (58.5 mg, 24%), **4b** (90.3 mg, 37%), **4c** (70.7 mg, 29%), and as a colorless oils.

4a: R_f = 0.67 (toluene/EtOAc = 1.5:1). $[\alpha]_D = -44°$ (*c* = 1, EtOAc). ^1H NMR (600 MHz, $CDCl_3$): δ = 5.99–5.91 (m, 1H, $OCH_2CH{=}CH_2$), 5.35 (d, *J* = 17.3 Hz, 1H, $OCH_2CH{=}CH_aH_b$), 5.23 (d, *J* = 10.5 Hz, 1H, $OCH_aH_bCH{=}CH_2$), 4.68 (q, *J* = 6.8 Hz, 1H, CH_3CH), 4.59 (dd, $J_{2,3}$ = 9.6, $J_{2,1}$ = 7.7 Hz, 1H, H-2), 4.55 (d, J_{12} = 7.7 Hz, 1H, H-1), 4.39 (dd, *J* = 12.7, *J* = 5.2 Hz, 1H, $OCH_aH_bCH{=}CH_2$), 4.21–4.15 (m, 2H, H-4, $OCH_aH_bCH{=}CH_2$), 3.97 (dd, $J_{6a,6b}$ = 10.5, $J_{6a,5}$ = 6.1 Hz, 1H, H-6_a), 3.90 (dd, $J_{6b,6a}$ = 10.5, $J_{6b,5}$ = 4.8 Hz, 1H, H-6_b), 3.68 (dd, $J_{3,2}$ = 9.6, $J_{3,4}$ = 3.0 Hz, 1H, H-3), 3.54 (t, $J_{5,6a} \approx J_{5,6b} \approx$ 5.4 Hz, 1H, H-5), 2.90 (d, J_{HOH} = 2.2 Hz, 1H, 4-OH), 1.54 (d, *J* = 6.8 Hz, 3H, CH_3CH), 0.91 (s, 9H, Si-*t*Bu), 0.11 (s, 3H, $SiMe_2$), 0.10 ppm (s, 3H, $SiMe_2$); ^{13}C NMR (150 MHz, $CDCl_3$): δ = 169.81 (CO), 133.43 ($OCH_2CH{=}CH_2$), 118.08 ($OCH_2CH{=}CH_2$), 99.11 (C-1), 75.33 (C-2), 74.28 (C-5), 73.32 (C-3), 70.86 (CH_3CH), 70.09 ($OCH_2CH{=}CH_2$), 67.55 (C-4), 62.41 (C-6), 25.78 (Si-*t*Bu), 18.23 (CMe_3), 17.61 (CH_3CH), −5.49 ppm ($2SiMe_2$); HRMS (ESI) calcd for $C_{18}H_{32}O_7Si$ $[M+Na]^+$ 411.1810; found 411.1803.

4b: R_f = 0.43 (toluene/EtOAc = 1.5:1). $[\alpha]_D = -63°$ (*c* = 1, EtOAc). ^1H NMR (600 MHz, $CDCl_3$): δ = 5.96–5.88 (m, 1H, $OCH_2CH{=}CH_2$), 5.31 (d, *J* = 17.2 Hz, 1H, $OCH_2CH{=}CH_aH_b$), 5.23 (d, *J* = 10.4 Hz, 1H, $OCH_2CH{=}CH_aH_b$), 4.73 (d, $J_{4,3}$ = 4.4 Hz, 1H, H-4), 4.44 (q, *J* = 6.5 Hz, 1H, CH_3CH), 4.36 (dd, *J* = 12.6, *J* = 5.3 Hz, 1H, $OCH_aH_bCH{=}CH_2$), 4.32 (d, $J_{1,2}$ = 7.8 Hz, 1H, H-1), 4.12 (dd, *J* = 12.6, *J* = 6.5 Hz, 1H, $OCH_aH_bCH{=}CH_2$), 4.06 (dd, $J_{3,2}$ = 9.2, $J_{3,4}$ = 4.3 Hz, 1H, H-3), 3.94 (dd, $J_{6a,6b}$ = 9.8, $J_{6a,5}$ = 8.0 Hz, 1H, H-6_a), 3.84 (dd, $J_{6b,6a}$ = 9.9, $J_{6b,5}$ = 5.8 Hz, 1H, H-6_b), 3.70 (dd, $J_{5,6a}$ = 8.1, $J_{5,6b}$ = 5.7 Hz, 1H, H-5), 3.62 (t, $J_{2,1} = J_{2,3}$ = 8.5 Hz, 1H, H-2), 2.58 (s, 1H, 2-OH), 1.50 (d, *J* = 6.5 Hz, 3H, CH_3CH), 0.88 (s, 9H, Si-*t*Bu), 0.08 ppm (2s, 6H, $SiMe_2$); ^{13}C NMR (150 MHz, $CDCl_3$): δ = 170.72 (CO), 133.51 ($OCH_2CH{=}CH_2$), 118.19 ($OCH_2CH{=}CH_2$), 101.23 (C-1), 73.88 (C-3), 73.04 (C-5), 71.58 (C-2), 71.06 (C-4), 70.12 ($OCH_2CH{=}CH_2$), 67.19 (CH_3CH), 60.26 (C-6), 25.78 (Si-*t*Bu), 18.16 (CMe_3), 16.68 (CH_3CH), −5.46 ($SiMe_2$), −5.53 ppm ($SiMe_2$); HRMS (ESI) calcd for $C_{18}H_{32}O_7Si$ $[M+Na]^+$ 411.1810; found 411.1804.

4c: R_f = 0.54 (toluene/EtOAc = 1.5:1). $[\alpha]_D = -71°$ (*c* = 1, EtOAc). ^1H NMR (500 MHz, $CDCl_3$): δ = 5.96–5.89 (m, 1H, $OCH_2CH{=}CH_2$), 5.32 (d, *J* = 17.2 Hz, 1H, $OCH_2CH{=}CH_aH_b$), 5.24 (d, *J* = 10.4 Hz, 1H, $OCH_2CH{=}CH_aH_b$), 4.77 (d, $J_{4,3}$ = 1.5 Hz, 1H, H-4), 4.51 (q, *J* = 6.9 Hz, 1H, CH_3CH), 4.39 (dd, *J* = 12.4, *J* = 5.5 Hz, 1H, $OCH_aH_bCH{=}CH_2$), 4.33 (d, *J* = 7.3 Hz, 1H, H-1), 4.13 (dd, *J* = 12.5, *J* = 6.6 Hz, 1H, $OCH_aH_bCH{=}CH_2$), 3.96–3.89 (m, 3H, H-2, H-3, H-6_a), 3.81 (dd, $J_{6b,6a}$ = 10.0, $J_{6b,5}$ = 6.0 Hz, 1H, H-6_b), 3.63 (t, $J_{5,6a} = J_{5,6b}$ = 6.6 Hz, 1H, H-5), 1.58 (d, *J* = 6.9 Hz, 3H, CH_3CH), 0.90 (s, 9H, Si-*t*Bu), 0.10 ppm (s, 6H, $SiMe_2$); ^{13}C NMR (150 MHz, $CDCl_3$): δ = 169.04 (CO), 133.38 ($OCH_2CH{=}CH_2$), 118.39 ($OCH_2CH{=}CH_2$), 101.92 (C-1), 74.29 (C-4),

74.03 (C-5), 72.33 (C-3), 70.24 ($OCH_2CH{=}CH_2$), 66.96 (CH_3CH), 66.65 (C-2), 60.09 (C-6), 25.79 (Si-*t*Bu), 18.80 (CH_3CH), −5.46 ppm ($SiMe_2$); HRMS (ESI) calcd for $C_{18}H_{32}O_7Si$ $[M+Na]^+$ 411.1810; found 411.1806.

Allyl 3-O-[(S)-1-(methoxycarbonyl)ethyl]-β-D-galactofuranoside (6a)

HSO_3Cl (39.9 μL, 0.605 mmol) was added dropwise to a stirred solution of monosaccharide **5a** (69.8 mg, 0.166 mmol) and $Py{\cdot}SO_3$ complex (794 mg, 4.98 mmol) in DMF (1.7 mL). The reaction mixture was kept for 48 h at 20 °C and then quenched with aqueous NH_4HCO_3 (931 mg in 20 mL H_2O, 11.79 mmol) and evaporated twice with water. The residue was dissolved in a minimal amount of water and then an excess of MeOH was added, which resulted in the precipitation of inorganic salts; the mixture was filtrated, the solid was washed with MeOH, and the filtrate was concentrated. The resulting crude sulfated furanoside, obtained as described above, was dissolved in DMF (3 mL), then dioxane (15 mL) and Amberlite (PyH^+-form; 700 mg) was added. The mixture was stirred at 100 °C for 90 min and then cooled to room temperature. The reaction mixture was filtered off, washed with EtOAc, the filtrate was concentrated under reduced pressure and diluted in $CHCl_3$ (30 mL) and washed with saturated aqueous NaCl (15 mL). The organic layer was concentrated, and the residue was purified by column chromatography on silica gel to give the furanoside derivative **6a** (33.1 mg, 65%) as a white solid. $R_f = 0.23$ (EtOAc). $[\alpha]_D = -61°$ ($c = 1$, MeOH). ^{1}H NMR (600 MHz, D_2O): $\delta = 6.00$–5.91 (m, 1H, $OCH_2CH{=}CH_2$), 5.35 (d, $J = 17.2$ Hz, 1H, $OCH_2CH{=}CH_aH_b$), 5.26 (d, $J = 10.4$ Hz, 1H, $OCH_2CH{=}CH_aH_b$), 5.06 (s, 1H, *H-1*), 4.41 (q, $J = 6.9$ Hz, 1H, CH_3CH), 4.24–4.18 (m, 2H, $OCH_aH_bCH{=}CH_2$, *H-2*), 4.11–4.05 (m, 2H $OCH_aH_bCH{=}CH_2$, *H-4*), 3.91 (dd, $J_{3,4} = 5.6$, $J_{3,2} = 2.0$ Hz, 1H, *H-3*), 3.87–3.83 (m, 1H, *H-5*), 3.79 (s, 3H), 3.73 (dd, $^2J_{6a,6b} = 11.8$, $J_{6a,5} = 4.4$ Hz, 1H, *H-6*$_a$), 3.66 (dd, $^2J_{6b,6a} = 11.8$, $J_{6b,5} = 7.4$ Hz, 1H, *H-6*$_b$), 1.42 ppm (d, $J = 6.9$ Hz, 3H, CH_3CH); ^{13}C NMR (125 MHz, D_2O): $\delta =$ 175.89 (*C*O), 133.95 ($OCH_2CH{=}CH_2$), 118.72 ($OCH_2CH{=}CH_2$), 107.38 (*C-1*), 85.47 (*C-3*), 82.53 (*C-4*), 79.33 (*C-2*), 74.68 (CH_3CH), 71.39 (*C-5*), 68.83 ($OCH_2CH{=}CH_2$), 63.22 (*C-6*), 53.16 (*Me*), 18.51 ppm (CH_3CH); HRMS (ESI) calcd for $C_{13}H_{32}O_8$ $[M+Na]^+$ 329.1207; found 329.1209.

General methods, spectroscopic and computational details, full experimental procedures, characterization for all new compounds and copies of ^{1}H, ^{13}C NMR and HRMS spectra are provided in the Supporting Information.

Acknowledgements

This work was supported by RSF grant 14-23-00199 (NEN). We thank Dr. A. O. Chizhov for recording the high resolution mass spectra at the Department of Structural Studies of the Zelinsky Institute of Organic Chemistry, Moscow.

Keywords: carbohydrates · conformation analysis · furanoside · lactic acid · rearrangement

[1] A. I. Hidron, J. R. Edwards, J. Patel, T. C. Horan, D. M. Sievert, D. A. Pollock, S. K. Fridkin, *Infect. Control Hosp. Epidemiol* **2008**, *29*, 996–1011.
[2] J. L. Vincent, M. Norrenberg, *Crit. Care Med.* **2009**, *37*, S296–S298.
[3] J. Huebner, C. R. Arciola, *Int. J. Artif. Organs* **2007**, *30*, 852–853.
[4] F. Fabretti, J. Huebner, *Int. J. Artif. Organs* **2005**, *28*, 1079.
[5] A. M. Butler, M. A. Olsen, L. R. Merz, R. M. Guth, K. F. Woeltje, B. C. Camins, V. J. Fraser, *Infect. Control Hosp. Epidemiol.* **2010**, *31*, 28.
[6] C. Theilacker, Z. Kaczyński, A. Kropec, I. Sava, L. Ye, A. Bychowska, O. Holst, J. Huebner, *PLoS One* **2011**, *6*, e17839.
[7] A. A. Bothner-By, R. L. Stephens, J. Lee, C. D. Warren, R. W. Jeanloz, *J. Am. Chem. Soc.* **1984**, *106*, 811–813.
[8] E. R. van Rijssel, P. van Delft, G. Lodder, H. S. Overkleeft, G. A. van der Marel, D. V. Filippov, J. D. Codée, *Angew. Chem. Int. Ed.* **2014**, *53*, 10381–10385; *Angew. Chem.* **2014**, *126*, 10549–10553.
[9] N. L. Allinger, Y. H. Yuh, J.-H. Lii, *J. Am. Chem. Soc.* **1989**, *111*, 8551–8566.
[10] T. Ooi, M. Oobatake, G. Némethy, H. A. Scheraga, *Proc. Natl. Acad. Sci. USA* **1987**, *84*, 3086–3090.
[11] P. Ren, J. W. Ponder, *J. Phys. Chem. B* **2003**, *107*, 5933–5947.
[12] V. B. Krylov, D. A. Argunov, D. Z. Vinnitskiy, S. A. Verkhnyatskaya, A. G. Gerbst, N. E. Ustyuzhanina, A. S. Dmitrenok, J. Huebner, O. Holst, H.-C. Siebert, N. E. Nifantiev, *Chem. Eur. J.* **2014**; DOI: 10.1002/chem.201405083.
[13] W. B. Severn, J. C. Richards, *J. Am. Chem. Soc.* **1993**, *115*, 1114–1120.
[14] P. Albersheim, D. J. Nevins, P. D. English, A. Karr, *Carbohydr. Res.* **1967**, *5*, 340–345.
[15] W. L. F. Armarego, C. L. L. Chai, *Purification of Laboratory Chemicals*, 5th ed., Butterworth, **2003**.
[16] P. A. Belyakov, V. I. Kadentsev, A. O. Chizhov, N. G. Kolotyrkina, A. S. Shashkov, V. P. Ananikov, *Mendeleev Commun.* **2010**, *20*, 125–131.

Received: October 28, 2014
Published online on November 24, 2014

ACS Infectious Diseases

pubs.acs.org/journal/aidcbc Article

Synthetic Oligomers Mimicking Capsular Polysaccharide Diheteroglycan are Potential Vaccine Candidates against Encapsulated *Enterococcal* Infections

D. Laverde,▲ F. Romero-Saavedra,▲ D. A. Argunov,▲ J. Enotarpi,▲ V. B. Krylov, E. Kalfopoulou, C. Martini, R. Torelli, G. A. van der Marel, M. Sanguinetti, J. D. C. Codée,* N. E. Nifantiev,* and J. Huebner*

Cite This: *ACS Infect. Dis.* 2020, 6, 1816−1826 Read Online

ACCESS | Metrics & More | Article Recommendations | Supporting Information

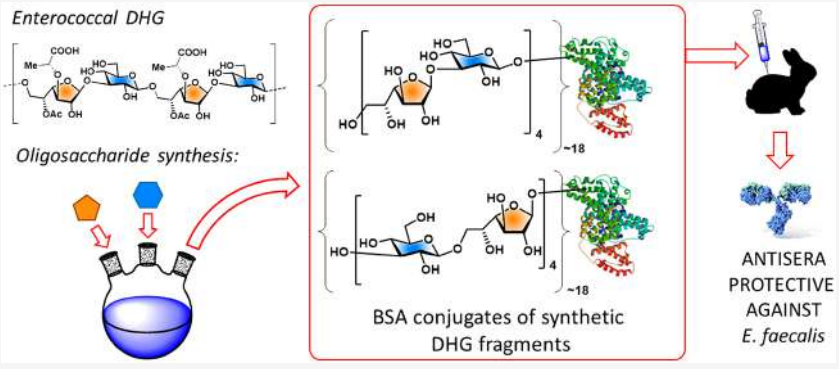

ABSTRACT: Infections caused by *Enterococcus* spp. are a major concern in the clinical setting. In *Enterococcus faecalis*, the capsular polysaccharide diheteroglycan (DHG), composed of ß-D-galactofuranose-(1 → 3)-ß-D-glucopyranose repeats, has been described as an important virulence factor and as a potential vaccine candidate against encapsulated strains. Synthetic structures emulating immunogenic polysaccharides present many advantages over native polysaccharides for vaccine development. In this work, we described the synthesis of a library of DHG oligomers, differing in length and order of the monosaccharide constituents. Using suitably protected thioglycoside building blocks, oligosaccharides up to 8-mer in length built up from either Gal*f*-Glc*p* or Glc*p*-Gal*f* dimers were generated, and we evaluated their immunoreactivity with antibodies raised against DHG. After the screening, we selected two octasaccharides, having either a galactofuranose or glucopyranose terminus, which were conjugated to a carrier protein for the production of polyclonal antibodies. The resulting antibodies were specific toward the synthetic structures and mediated *in vitro* opsonophagocytic killing of different encapsulated *E. feacalis* strains. The evaluated oligosaccharides are the first synthetic structures described to elicit antibodies that target encapsulated *E. faecalis* strains and are, therefore, promising candidates for the development of a well-defined enterococcal glycoconjugate vaccine.

KEYWORDS: *vaccine, capsular polysaccharide, diheteroglycan, synthetic carbohydrate, Enterococcus faecalis, opsonophagocytic assay*

Enterococci are one of the most common pathogens associated with nosocomial infections worldwide.[1] Their resistance to multiple antibiotics, including vancomycin and even new generation antibiotics like linezolid, tigecycline, and daptomycin, highlights the urgent need to develop alternative treatments to fight this remarkable opportunistic pathogen.[2,3] Bacterial polysaccharides, such as teichoic acids, capsular polysaccharides, and lipopolysaccharides are considered the most attractive targets for vaccine development, since they represent the bacterial first line of defense against complement and bacterial phagocytes.[4,5] For instance, in enterococci, cell-wall-associated polysaccharides and glycan structures implicated in colonization of epithelial surfaces, inflammation processes, and evasion of host immune system have been described as promising vaccine candidates.[6−10] Production of a polysaccharide-based vaccine for treatment and prevention of enterococcal infections is a realistic goal, since only a limited number of serotypes seem to exist.[11]

In *Enterococcus faecalis*, four different serotypes (CPS-A−CPS-D) have been described on the basis of analyses of

Received: February 11, 2020
Published: May 4, 2020

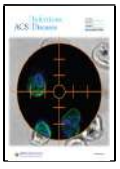

https://dx.doi.org/10.1021/acsinfecdis.0c00063
ACS Infect. Dis. 2020, 6, 1816−1826

different immunoreactivity of antisera raised against different prototype strains by ELISA and opsonophagocytic assay and by genetic analysis of the capsular polysaccharide *cps* locus.[10,12−14] Diheteroglycan (DHG) is a capsular polysaccharide produced by the *cps* locus in *Enterococcus faecalis*, is present in serotypes CPS-C and CPS-D strains, and has been demonstrated to mask lipoteichoic acid (LTA) in the bacteria preventing opsonization by anti-LTA antibodies.[10] The structure of this polysaccharide was first described in 1971 by Pazur et al. as a trisaccharide composed of glucose and galactose backbone with lactosyl and cellobiosyl substituents.[15] However, a more comprehensive structural elucidation of the DHG from *E. faecalis* Type 2 strain by Theilacker and coworkers showed that the polysaccharide repeating unit was → 6)-*β*-Gal*f*-(1 → 3)-*β*-D-Glc*p*-(1→ with *O*-acetylation in position 5 and lactic acid substitution at position 3 of the Gal*f* residue (see Figure 1A).[10] Finally, the definitive structure of the DHG was established when the R configuration of the lactic acid substituent in the DHG backbone was elucidated by Krylov et al.[16]

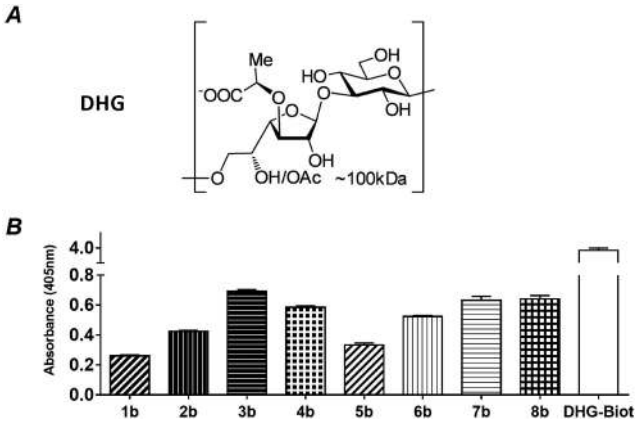

Figure 1. Structures of the synthetic DHG saccharides and their immunoreactivity with anti-DHG. (A) Structures of the repeating unit of the DHG from *E. faecalis* Type 2. (B) Antibodies raised against native DHG from *E. faecalis* Type 2 were evaluated for their ability to bind specifically the different synthetic DHG resembles of native DHG. Anti-DHG serum was used at final concentration of 41.2 *μ*g IgG/mL. Synthetic DHG saccharides, dimers **1b** and **5b**, tetramers **2b** and **6b**, hexamers **3b** and **7b**, and octamers **4b** and **8b** were used to coat the streptavidin coated plate with 0.1 *μ*g per well. Biotinylated DHG (DHG-Biot) was used as the control to assess the preferred ability of the anti-DHG serum for the antigenic structures tested. Absorbance was measured at 405 nm after 40 min of incubation with the substrate. Bars represent the mean of data, and the error bars represent the standard error of the mean.

Rabbit antiserum raised against DHG showed good protective efficacy in mice infected with *E. faecalis* strains of CPS-C and CPD-D serotype, making it a promising target for vaccine development to fight infections caused by encapsulated *E. faecalis* strains.[10] However, the development of a polysaccharide-based vaccine is challenging because of the disadvantages associated with antigen purity.[17] Naturally occurring polysaccharides, such as DHG, are microheterogeneous and their purification leads to complex mixtures varying in molecular weights with different end-groups and *O*-substitution patterns.[17] Synthetic glycoconjugates have emerged as an attractive alternative for the development of vaccines, since their well-defined structures have reproducible physical, chemical, biological, and immunogical properties.[4] In 2004, the large-scale synthesis of a glycoconjugate accomplished by the team of Verez-Bencomo culminated in the world's first synthetic carbohydrate vaccine against *Haemophilus influenzae* type b in humans.[18,19] Since then, other projects aiming for the synthesis of many bacterial capsular polysaccharide and lipopolysaccharides fragments from many pathogens have been reported with the ultimate goal to generate vaccine candidates.[20,21] So far, synthetic vaccines against Shigellosis, *Streptococcus pneumoniae*, and *Staphylococcus aureus* are in pre-clinical or early clinical evaluation.[22−26] Previously, we described a synthetic teichoic acid fragment that mimics lipoteichoic acid from *E. faecalis* and is able to induce opsonic and protective antibodies that is a potential vaccine against unencapsulated CPS-A and CPS-B *E. faecalis* strains.[27] In the present work, we systematically evaluate different synthetic fragments that mimic the native DHG from *E. faecalis* Type 2 to define the best candidates for vaccine development against encapsulated *E. faecalis* that cannot be targeted using a teichoic-acid-based vaccine.

RESULTS AND DISCUSSION

To discover a potent minimal DHG epitope, two series of DHG fragments were synthesized. The first was built up from [Gal*f*-Glc*p*]-dimer repeats,[28] while the second set was composed of the alternative frameshifted [Glc*p*-Gal*f*] dimers. Scheme 1 summarizes the syntheses of the glycan libraries. The first route of synthesis was based on the disaccharide building block **11**, containing temporary Fmoc-protection, obtained by coupling of furanoside donor **9**[29] and glycoside acceptor **10** (its synthesis described in the Supporting Information (SI)) with a 95% yield. Glycosylation of 3-trifluoroacetamidopropanol with donor **11** using a NIS/TfOH-system as a promotor resulted in spacer-containing disaccharide **12**. Temporary Fmoc-protection in **12** was removed by morpholine in DMF, which avoided benzoyl migration during deprotection[28] and obtained the desired acceptor in a 92% yield. The liberated hydroxyl group was subsequently glycosylated with donor **11**, resulting in tetrasaccharide **13** in a 85% yield. The removal of Fmoc-protection and glycosylation steps were repeated to form hexasaccharide **14** and octasaccharide **15** in good yields. The deprotection of oligosaccharides **12**−**15** was carried out by hydrolysis of benzylidene acetal in aqueous trifluoroacetic acid (TFA) in CH_2Cl_2, followed by the removal of acyl protections with MeONa in MeOH−H_2O to give the first series of DHG-fragments (**1a**−**4a**).

The second set of oligomers was obtained using key disaccharide **16**. This building block has the obvious advantage that no benzoyl migration can take place from the Gal*f* C(5) to the neighboring C(6) position during deprotection, as the *β*-D-Glc*p*-(1 → 6)-*β*-Gal*f* linkage is constructed at the building block level (see the SI for full experimental details). Key building block **16** was equipped with a levulinic (Lev) ester as a temporary protecting group for the elongation of the oligomers, a silylidene ketal masking the C4- and C6-hydoxyls of the glucosyl moiety. The other alcohol groups were masked as benzoyl esters. We have previously used[30] a very similar protecting group pattern for a glucosamine synthon in the automated solid phase assembly of hyaluronic acid oligosaccharides. These syntheses revealed that the silylidene group not only is very resistant to acidic glycosylation conditions but also it endows the neighboring C(3)−OH with excellent reactivity.[31] First, an azidopropanol spacer was introduced on

https://dx.doi.org/10.1021/acsinfecdis.0c00063
ACS Infect. Dis. 2020, 6, 1816−1826

Scheme 1. Synthesis of DHG Related Spacer-Armed Oligosaccharides and Their Conjugates with Biotin and BSA[a]

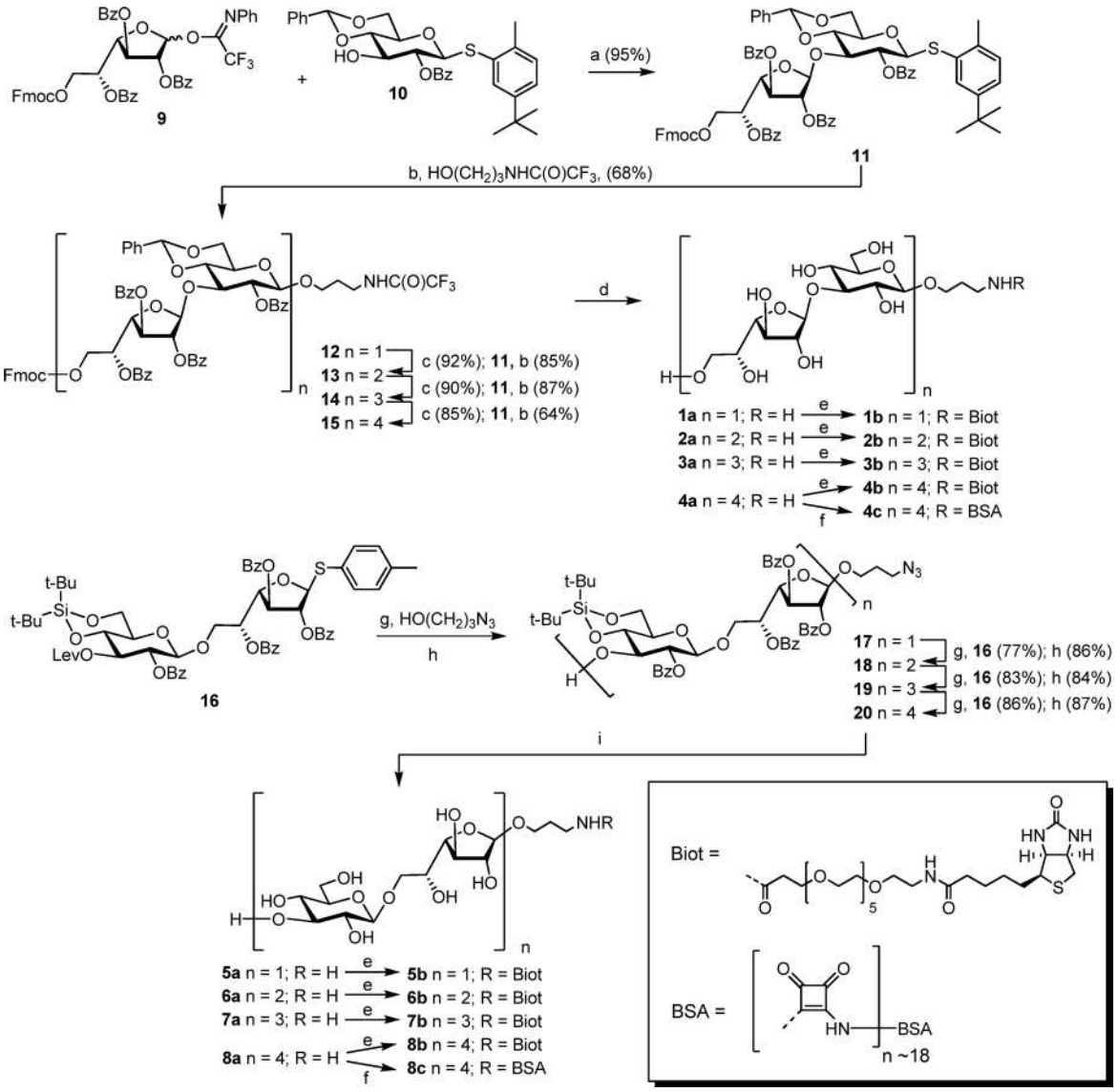

[a]Reagents and conditions: (a) TMSOTf, AW-300 MS, CH_2Cl_2, −70 → −10 °C; (b) NIS, TfOH, AW-300 MS, CH_2Cl_2, − 40 → − 5 °C; (c) morpholine (5 vol %), DMF; (d) first, TFA (90% aq), CH_2Cl_2; second, MeONa, MeOH, then H_2O, 76−65%; (e) C_6F_5O-Biot, Et_3N, DMF, room temperature (70−80%); (f) first, diethyl squarate, Et_3N, EtOH, H_2O; second, BSA, borate buffer (pH 9.0); (g) NIS, TMSOTf, CH_2Cl_2, − 40 → − 20 °C; (h) NH_2NH_2, PyH^+AcO^-/AcOH, 0 → +20 °C; (i) first, $Et_3N{\cdot}3HF$, THF, 80−85%; second, MeONa, MeOH; third, H_2, Pd cat, 80−90%.

the disaccharide, using NIS and catalytic amounts of trimethylsilyl trifluoromethanesulfonate (TMSOTf) to activate the thioglycoside, delivering **17** in 70% yield. The resulting dimer was treated with hydrazine acetate to selectively unmask the Lev group, giving an acceptor in 95% yield. In a [2 + 2] coupling tetrasaccharide, **18** was obtained in 77% yield. Subsequent levulinoyl removal and glycosylation cycles allowed for the generation of the hexa- and octasaccharide **19** and **20** oligosaccharides in good yields. The deprotection of the four fragments **17**−**20** was carried out by cleavage of the silyl groups using a solution of $Et_3N{\cdot}3HF$ in THF, followed by the removal of the benzoyl esters under Zemplén conditions, and finally, the reduction of the azide functionality through a hydrogenolysis reaction.

All synthesized DHG related oligosaccharides were equipped with a biotin group by treatment of aminopropyl glycosides **1a**−**8a** with biotin derivative C_6F_5O-Biot containing a hexaethylenglycol spacer, which is required for efficient spatial presentation of the oligosaccharide ligands in the glycoarray for biological recognition[32] after the immobilization on streptavidin coated plates (for examples, see refs 33−36). The structures of obtained biotinylated derivatives **1b**−**8b** were confirmed by HRMS data and by presence of the characteristic signals in ^1H NMR spectra (see Table S1 in the SI).

The conjugation of octasaccharides **4a** and **8a** with BSA was performed by the squarate method.[37] At the first step, the reaction of the parent oligosaccharides with diethyl squarate resulted in the monosubstituted adducts, which were then reacted with the free amino groups of BSA at pH 9, resulting in BSA-conjugates **4c** and **8c**. According to MALDI TOF mass spectrometry, the conjugates contained, on average, 18 octasaccharide antigenic ligands.

https://dx.doi.org/10.1021/acsinfecdis.0c00063
ACS Infect. Dis. 2020, 6, 1816−1826

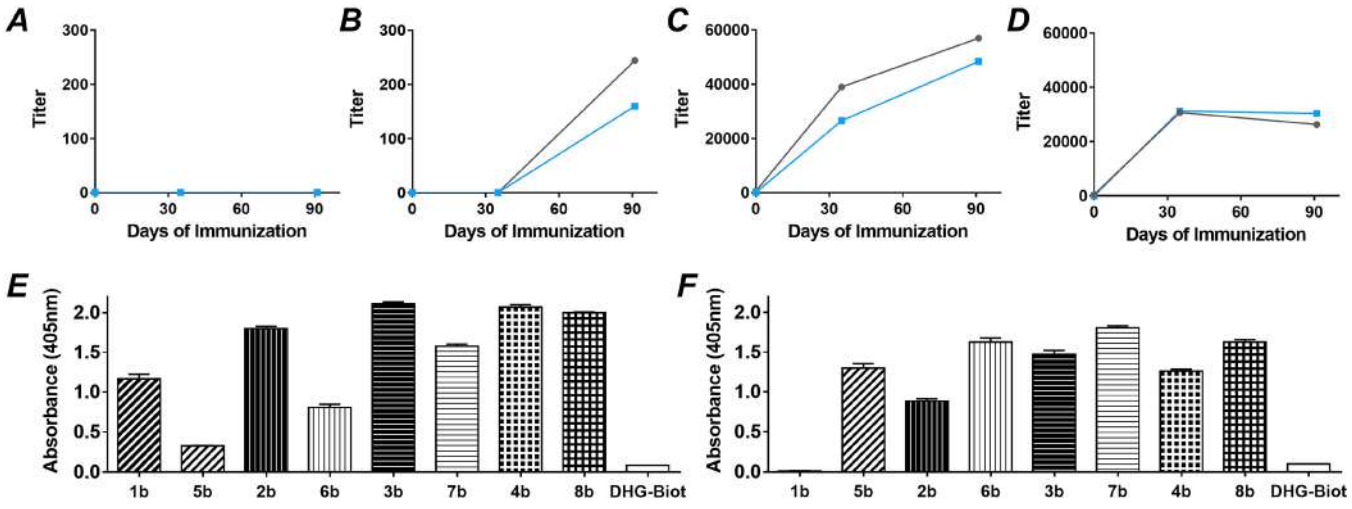

Figure 2. Specificity of sera raised against synthetic **4c** and **8c** conjugates. Rabbit sera obtained during immunization schedule were examined for specificity toward the different antigens. Streptavidin coated plates were coated with 1 μg per well of (A) carrier protein BSA, (B) the native DHG, and synthetic (C) **4c** and (D) **8c** conjugates. Rabbit sera anti-**4c** (black) and anti-**8c** (blue) were plated in 2-fold serial dilutions, starting with a dilution of 50 μg IgG/mL for each serum tested. (E) Anti-**4c** and (F) anti-**8c** at 1.25 and 2.4 μg/mL, respectively, were also examined for their immunoreactivity toward synthetic DHG saccharides, dimers **1b** and **5b**, tetramers **2b** and **6b**, hexamers **3b** and **7b**, and octamers **4b** and **8b**. Biotinylated DHG (DHG-Biot) was used as the control to assess the preferred ability of the anti-DHG serum for the antigenic structures tested.

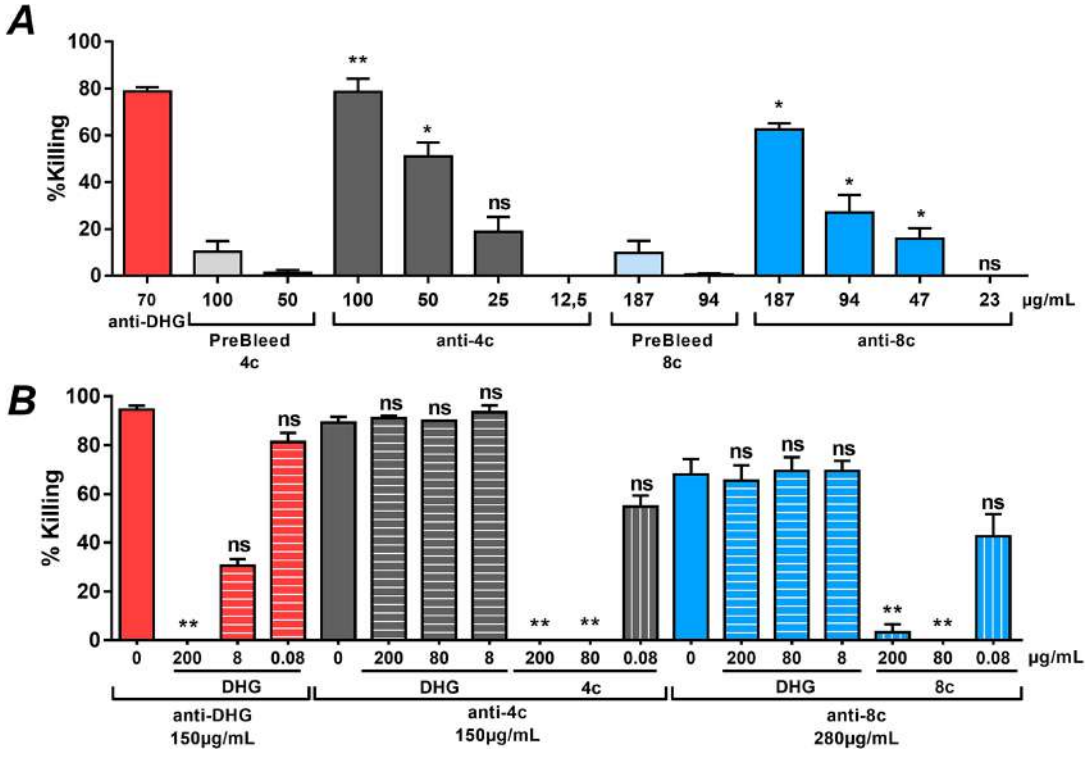

Figure 3. Analysis of opsonophagocytic killing activity of the antibodies. (A) Sera raised against **4c** and **8c** conjugates were evaluated in an opsonophagocytic assay to determine the opsonophagocytic killing activity of the sera against *E. faecalis* Type 2. Anti-**4c** (gray) and anti-**8c** (blue) sera were used at different concentrations, as shown in the *x*-axis. Serum raised against the native DHG polysaccharide was used as a positive control (red). (B) Specificity of the sera against the antigens was confirmed by inhibiting the opsonophagocytic killing activity with different amounts of the different antigens. Purified antibodies raised against synthetic **4c** (gray) and **8c** (blue) conjugates were used at a dilution yielding between 60 and 90% of killing and absorbed out with different amounts of native DHG (horizontal stripes) or synthetic DHG-conjugate (vertical stripes) as inhibitors. Serum raised against the native DHG polysaccharide was absorbed out with native DHG as a positive control. Sera without inhibitors were used as a positive control for opsonophagocytic killing. Effective opsonophagocytic (or inhibition of) killing in the anti-conjugate sera (anti-**4c** and anti-**8c**) was compared to pre-immune rabbit sera (PreBleed, in lighter color) by nonparametric Kruskal–Wallis test, followed by multiple comparisons using Dunn's post-test. Bars represent the mean of data, and the error bars represent the standard error of the mean (ns, nonsignificant, $^*P < 0.05$, and $^{**}P < 0.01$).

https://dx.doi.org/10.1021/acsinfecdis.0c00063
ACS Infect. Dis. 2020, 6, 1816–1826

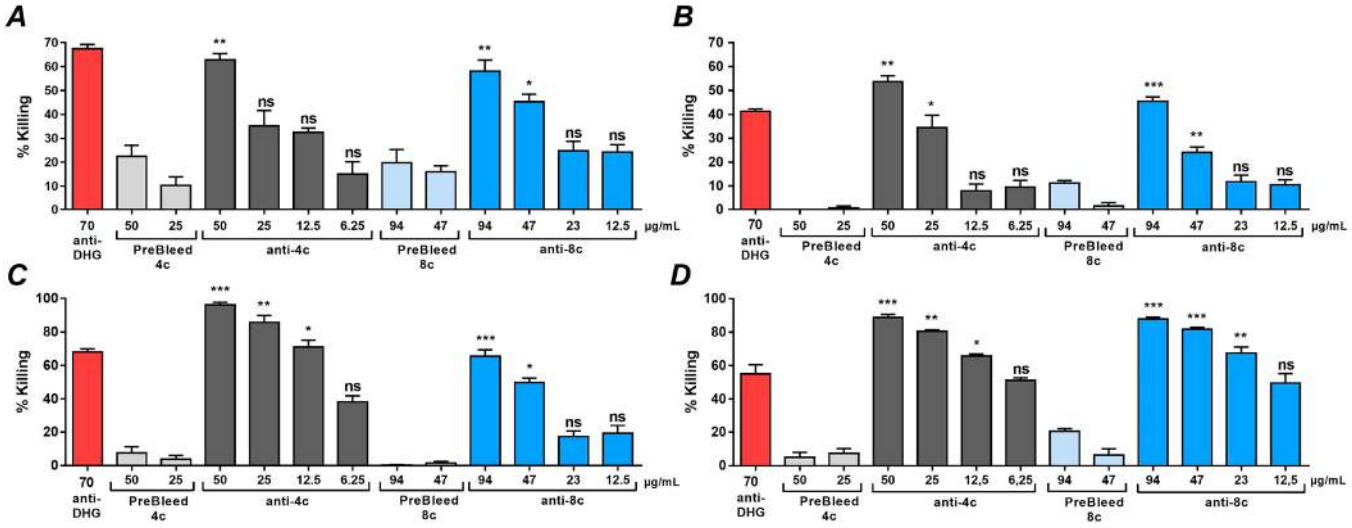

Figure 4. Opsonophagocytic killing activity of anti-**4c** and anti-**8c** sera against *E. faecalis* encapsulated bacterial strains. The antibodies raised against synthetic **4c** (gray) and **8c** (blue) conjugates were used at different concentrations. Evaluated *E. faecalis* CPS-C strains were (A) *E. faecalis* V583 and (B) *E. faecalis* FA2-2 and *E. faecalis* CPS-D strains were (C) *E. faecalis* Type 5 and (D) *E. faecalis* Type 18. Effective opsonophagocytic killing in the anti-conjugate sera (anti-**4c** and anti-**8c**) was compared to pre-immune rabbit sera (PreBleed, in lighter color) by a nonparametric Kruskal–Wallis test, followed by multiple comparisons using Dunn's post-test. Bars represent the mean of data, and the error bars represent the standard error of the mean (ns, nonsignificant, $*P < 0.05$, $**P < 0.01$, $***P < 0.001$).

After synthesis and characterization, the biotinylated compounds were evaluated for their ability to immunoreact with serum raised against native DHG in an ELISA using streptavidin coated plates (see Figure 1B). A clear length dependence was observed for the synthetic oligosaccharides, with the longer synthetic saccharides (i.e., octamers **4b** and **8b** and hexamers **3b** and **7b**) showing better immunoreactivity with anti-DHG serum than shorter ones (i.e., tetramers **2b** and **6b** and dimers **1b** and **5b**). This correlates with the previously described results, in which synthetic saccharides mimicking native polysaccharides conjugated to a carrier protein are good antigens that elicit opsonic and protective antibodies.[27,38,39] Here, we have shown that the synthesized hexa- and octa-oligosaccharides elicit the highest immunogenicity and may therefore partially mimic the immunogenic properties of the native DHG. Considering that the octasaccharides are not more difficult to synthesize than the hexasaccharides, and may better adopt the conformation of the native polysaccharide,[40] we decided to use the octasaccharides **4a** and **8a** for further immunological studies and evaluated their candidacy for vaccine development against enterococcal infections.

The conjugates **4c** and **8c** were used to immunize rabbits, and bleeds were taken at different time points during immunization. The resulting anti-**4c** and anti-**8c** sera were analyzed for specific IgG against native DHG, **4c**, **8c**, and BSA (see Figure 2A–D). No significant antibody levels were detected against the carrier protein BSA in the sera raised against conjugates **4c** and **8c** (see Figure 2A). Interestingly, low titers were raised against the native polysaccharide (see Figure 2B). This observation may be explained by the fact that the substitutions on the backbone structure of the native DHG polysaccharide mask the epitopes targeted by sera raised against the unsubstituted synthetic oligosaccharides **4c** and **8c**. Both sera exhibited very high titers against the conjugates (see Figure 2C,D), with the response against structure **4c** being higher than that against **8c**. These differences in immune responses may be explained by the monosaccharides at the terminus of the octasaccharides **4c** and **8c** being either a "non-self" galactofuranose, which is foreign residue for mammalian glycans, or a "self" glucose residue typical for host glycocalyx. Especially in the case of relatively short (with respect to native polysaccharides) synthetic oligosaccharides displaying less internal epitopes, the nature of the terminal sugar often plays an important role in recognition by antibodies.[24,41,42] To overcome the disparity in the immune response of the rabbits used for the immunization with the two conjugates, in subsequent experiments, the anti-**8c** serum was used 1.87 times more concentrated than the anti-**4c** serum.

The generated immune sera were further evaluated against the synthetic DHG saccharide library (see Figure 2E,F). As shown in Figure 2E, anti-**4c** immunoreacted preferentially with the structures with a terminal Gal*f*-β-(1 → 3)-unit at the left end of the chain. Both dimer fragments **1b** and **5b** were recognized by this serum with better immunoreactivity. However, the anti-**8c** serum only recognized the dimer fragment **5b** as being the smallest epitope capable of binding. Also for this serum, a slight preference in binding was observed for the Glc*p*-Gal*f*-repeating unit structures, although the preference was less pronounced in comparison to that of the anti-**4c** serum. Both sera showed no immunoreactivity toward biotinylated DHG at the concentration used, but at higher concentrations of sera (150 μg IgG/mL), an immunoreactivity similar to the saccharide library (2.0 U.A.) was observed toward Biotinylated DHG (see Figure S2).

Subsequently, opsonophagocytic killing activities of anti-**4c** and anti-**8c** were assessed against *E. faecalis* Type 2 strain, from where DHG was purified and structurally elucidated.[10,16] The pre-bleeds and terminal bleeds of the rabbits were evaluated at different concentrations to assess dose dependent killing activity of the target strain (Figure 3A). We observed that both terminal sera mediated opsonophagocytic killing of the bacterial strain at relatively low IgG concentrations (100 μg/mL for anti-**4c** and 187 μg/mL for anti-**8c**) that are comparable to previously reported antibodies raised against other Gram-positive bacterial capsular polysaccharides.[43–45] The lack of opsonophagocytic killing in samples with the pre-

https://dx.doi.org/10.1021/acsinfecdis.0c00063
ACS Infect. Dis. 2020, 6, 1816–1826

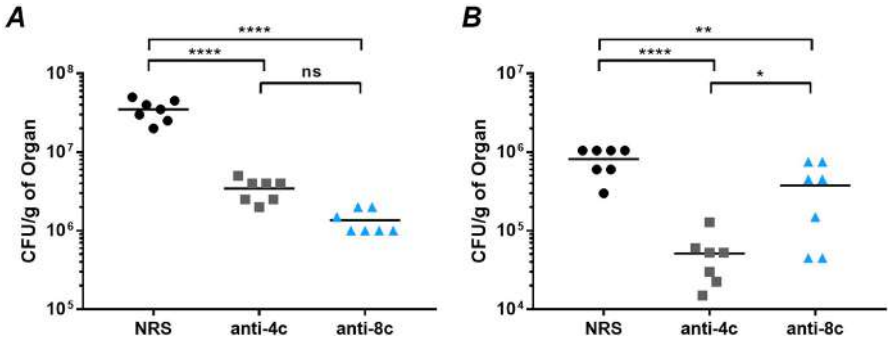

Figure 5. Mouse sepsis model. Mice were passively immunized with the sera raised against **4c** (gray squares) and **8c** (blue triangles) conjugates and challenged with *E. faecalis* Type 2. After 48 h of challenge, mice were sacrificed and their livers and kidneys were removed to assess viable counts. Panels (A) and (B) show the resulting viable counts in mice livers and kidneys challenged with *E. faecalis* Type 2, respectively. Each point represents the bacterial counts from a single mouse. Bars indicate the median CFU/g of organ for the group. Statistical analysis was done by one-way analysis of variance (ANOVA) with a Dunnett's correction post-test comparing between the animals immunized with the antibodies raised against the DHG-protein conjugates and control animals immunized with normal rabbit serum (NRS, black circles). Horizontal bars represent geometric means (ns, nonsignificant, $*P < 0.05$, $**P < 0.01$, $***P < 0.001$, $****P < 0.0001$).

immune sera demonstrates that the activities observed for the terminal bleeds are mainly due to antibodies raised by immunization with the conjugates. Moreover, control anti-DHG sera mediated opsonophagocytic killing at a slightly lower IgG concentration (i.e., 70 μg IgG/mL). This could be attributed to the fact that the native DHG possesses a more varied epitope repertoire because of its larger structure having different conformations and decorations, which may contribute to promote a better immune response. Also, the much higher antibody titers in anti-DHG sera against native polysaccharide (i.e., 6400 for anti-DHG (results not shown), 244 for anti-**4c** and 160 for anti-**8c** in Figure 2) could explain the observed differences in the opsonic activity.

Specificity of the opsonic antibodies toward the target antigens was confirmed by an opsonophagocytic inhibition assay OPIA (see Figure 3B). Purified antibodies were used to avoid interference of pre-existing antibodies or any other components in sera that may interact during the pre-absorption of the antibodies with the antigens for the OPIA.[46,47] The activity of control anti-DHG was completely abolished when pre-incubated with a high concentration of native DHG and was partly restored when the concentration of the DHG was lowered. Similarly, the **4c** and **8c** conjugates bound to the anti-**4c** and anti-**8c** antibodies, thereby inhibiting killing of the target strain. For both anti-conjugate sera, no inhibitory effect was observed when pre-incubation with native DHG was carried out. This could be explained by the microheterogeneities and substituents present in the native DHG that may have hindered the epitopes that anti-**4c** and anti-**8c** target since the conjugates mimic the structure of the native DHG backbone.[42,48]

After we demonstrated that the conjugates were able to elicit specific and opsonic antibodies against the target strain, we proceeded to investigate their cross-reactivity against different encapsulated *E. faecalis* strains. We selected different CPS-C (*E. faecalis* V583 and FA2-2) and CPS-D (*E. faecalis* Type 5 and Type 18) strains that are susceptible to antibodies raised against the native DHG isolated from *E. faecalis* Type 2.[10,12] Both anti-**4c** and anti-**8c** sera were able to mediate opsonic killing of all the strains tested (see Figure 4). Overall, both sera were more effective against CPS-D than CPS-C strains, exhibiting killing percentages ranging from 45 to 60 and 70 to 90%, respectively. Interestingly, *E. faecalis* CPS-D strains were more sensitive to anti-**4c** and anti-**8c** than to anti-DHG serum. These results could be explained due to the microheterogeneity in the DHG of the different evaluated serotype strains.[10,12,49] Possibly, DHG in CPS-D strains is less densely substituted (with acetyl and lactic acid groups) than the DHG from the CPS-C serogroup, making its DHG backbone more accessible to the raised antibodies. More structural data for the DHG of these *E. faecalis* serotypes is required to confirm this hypothesis.

Finally, the *in vivo* protective potential of the synthetic oligomer conjugates was evaluated in a mouse sepsis model (see Figure 5). Mice were passively immunized with normal rabbit serum (NRS), anti-**4c**, or anti-**8c** and were challenged with 1×10^8 CFU *E. faecalis* Type 2/mouse. Two days after bacterial challenge, animals were sacrificed, their organs were aseptically removed and homogenized, and the bacterial counts were enumerated by serial dilutions and plating. Both sera were able to significantly reduce the colony counts in livers and kidneys of the mice in comparison to NRS control. Differences in the protection conferred between the sera in mice livers were not statistically different. However, in mice kidneys, anti-**4c** sera significantly conferred a better protection than anti-**8c** sera. This correlates with the fact that the **4c** antigen is able to raise a better immune response, possibly because of the "non-self" galactofuranose residue at its terminus, as previously shown by the antibody titers and opsonophagocytic killing activities that are slightly superior to those exhibited by anti-**8c** sera. In addition, differences in the protection conferred by the two sera may be explained by variations in polysaccharide expression *in vivo*. It has been previously demonstrated in other Gram-positive pathogens, including *S. aureus*, that micro-environments (i.e., site of infection), bacterial strain, and/or stage of infection alter the polysaccharide composition in the pathogen.[50−53] Nevertheless, more comprehensive animal studies should be conducted to confirm this hypothesis.

In conclusion, we have generated a library of synthetic DHG fragments, ranging in length from dimers to octasaccharides, built up from either [Gal*f*-Glc*p*] or [Glc*p*-Gal*f*]-disaccharide repeats, which was used to identify synthetic DHG immunogens. The octasaccharides **4a** and **8a** were conjugated to BSA and used for immunization. The antibodies raised with the synthetic conjugates were able to mediate the opsonic killing of encapsulated *E. faecalis* CPS-C and CPS-D strains

https://dx.doi.org/10.1021/acsinfecdis.0c00063
ACS Infect. Dis. 2020, 6, 1816−1826

expressing DHG. Even though the native DHG capsule is decorated with acetyl and lactic acid substituents, the serum raised was capable of recognizing the native DHG, indicating that our glycoconjugates are appropriate immunogens to raise specific and opsonic antibodies. The role of lactic acid and *O*-acetyl substituents in *E. faecalis* DHG should be evaluated in future studies to determine whether these substituents constitute nonessential or protective epitopes, as has been described for other bacterial pathogens.[54−56] According to the antibody titers, for opsonophagocytic killing activity and protection *in vivo* conferred by sera against *E. faecalis* encapsulated strains, the **4c** antigen showed a slightly better immune response. This may be due to the fact that octasaccharide **4c** with the [Gal*f*-Glc*p*]-repeating unit presents a "non-self" sugar at its terminus, while **8c** has a "self" glucopyranose at this position, leading to inferior recognition by the immune system. Altogether, our results show that these synthetic structures mimicking DHG are promising vaccine candidates against the encapsulated *E. faecalis* strains that are a major concern in the clinical setting. These antigens could be used in combination with, for example, well-defined teichoic acid fragments and immunogenic proteins to generate broad coverage multivalent conjugate vaccines to fight these important nosocomial pathogens.

METHODS

Bacterial Strains and Culture Conditions. In this study, the Japanese prototype strain first described by Maekawa et al. *E. faecalis* Type 2 was used.[57] For the cross-reactivity tests, we used the vancomycin-resistant bloodstream isolate *E. faecalis* V583,[58] the derived strain from a patient isolate *E. faecalis* FA2-2,[59] and the Japanese prototype strains *E. faecalis* Type 5 and *E. faecalis* Type 18.[57] For the opsonophagocytic assays, strains were grown in Tryptic soy broth (Carl Roth) at 37 °C without agitation from an overnight grown plate of Tryptic soy agar, freshly prepared from the −80 °C bacterial stock. For polysaccharide purification, *E. faecalis* Type 2 was grown in Columbia broth (Becton Dickinson) supplemented with 2% glucose at 37 °C without agitation until an optical density of 0.8 at 600 nm was reached.

Native DHG Purification and biotinylation. DHG of *E. faecalis* was isolated as previously described.[60] Briefly, a bacterial strain was used to inoculate Columbia broth (Becton-Dickinson) supplemented with 2% glucose and incubated at 37°C without agitation until an optical density at 600 nm of 0.8 was reached. Bacterial cells were pelleted by centrifugation at 8000 rpm for 30 min at 4 °C and were resuspended with Tris-sucrose buffer (10 mM Tris-HCl, 25% sucrose, pH 8.0). After digestion of the bacterial cell wall using lysozyme and mutanolysin at 500 and 10 μg/mL, respectively, the cell debris and insoluble components were removed by centrifugation at 8000 rpm for 30 min at 4 °C. Then, the supernatant was treated with 100 μg/mL of nucleases and proteases and was dialyzed against deionized water prior to freeze-drying. Subsequently, the crude of polysaccharide was fractioned by size exclusion chromatography in a 1.6 cm × 90 cm sephacryl S-400 column (GE Healthcare) equilibrated in 50 mM Tris buffer (pH 7.2) buffer, using a flow rate of 0.5 mL/min. Eluted fractions were monitored by UV absorption at 214 and 254, with a differential refractometer (Gilson), and were analyzed for sugar, methylpentose, *O*-acetyl group, and phosphorus content by different colorimetric assays.[61−65] Fractions positive for sugar and *O*-acetyl and negative for phosphorus and methylpentose were combined, concentrated, and desalted with a 3 kDa Amicon Ultra-15 Centrifugal Filter Units (Merck Millipore) and were subjected to further purification with two in-series 5 mL HiTrap Q FF sepharose anion-exchange columns (GE Healthcare). For elution, a linear gradient from 0 to 1 M NaCl in 10 mM Tris buffer (pH 7.2) was used. Bound carbohydrate eluted from the column at 0.45 M NaCl, also positive for sugar and *O*-acetyl colorimetric assay and negative for phosphorus and methylpentose groups, were combined, concentrated, and desalted with a 3 kDa Amicon Ultra-15 Centrifugal Filter Units (Merck Millipore) prior to lyophilization. ^{1}H NMR of the purified DHG was recorded at 500 MHz in deuterated oxide D_2O to determine its purity for subsequent experiments (see the Supporting Information Figure S1).

The biotinylation of DHG was performed as described by Zhang et al.[45] Native DHG (1 mg) was dissolved in LPS-free water (cell culture grade; HyClone) at 5 mg/mL and mixed under vortexing with 1 mg of 1-cyano-4-dimethylaminopyridinium tetrafluoroborate at 100 mg/mL in acetonitrile (Sigma-Aldrich). After 30 s, the pH was increased to 8 by adding 7 μL of 0.2 M triethylamine (Sigma-Aldrich). Exactly after 2.5 min, 1 mg of Amine-PEG3-Biotin (Sigma-Aldrich) at 20 mg/mL in water was added. The mixture was incubated for 4 h at room temperature, and 25 mM of glycine was used to quench the reaction. Remaining biotin was removed by diafiltration using 3 kDa Amicon Ultra-15 Centrifugal Filter Units (Merck Millipore) against 10 mM Tris, pH 7.2. The concentrations of polysaccharide and biotin in the biotinylated DHG were quantified by anthrone assay and the biotin quantification kit (Pierce), respectively.

Synthesis of Saccharides Mimicking DHG and Conjugation. All synthetic procedures for the preparation of oligosaccharides **1a**−**8a**, their conjugates with biotin (**1b**−**8b**) and BSA (**4c**, **8c**), characterizations for new compounds, and copies of ^{1}H and ^{13}C NMR spectra are provided in the Supporting Information.

Rabbit Immunizations. A New Zealand white rabbit was immunized with purified DHG from *E. faecalis* Type 2 as described elsewhere (anti-DHG).[9] For **4c** and **8c** conjugates, a New Zealand white rabbit was immunized per antigen by two subcutaneous injections of 10 μg of conjugate given 1 week apart from each other. An intravenous (iv) injection of 5 μg of conjugate was given 7 days after, followed by two more iv injections of 5 μg of conjugate 2 days apart from each other. On day 35, the test bleed was taken, and 7, 14, 28, and 42 days later, iv boosts of 5 μg of antigen were performed. On day 91, a final bleed of each rabbit was taken. All sera were heated at 56 °C for 30 min to inactivate the complement components. Pre-immunization sera samples were taken twice from each rabbit 1 week apart from the first immunization as a control in the assays. Immune sera raised against conjugates were named anti-**4c** and anti-**8c**, respectively.

Quantification of Rabbit IgGs. Total rabbit IgG in both purified and unpurified anti-DHG, anti-**4c**, and anti-**8c** sera were quantified as previously described by Salauze et al.[66] Nunc-immuno Maxisorp MicroWell 96-well plates were coated with 0.1 μg per well of unlabeled antirabbit IgG (Sigma-Aldrich) in 0.2 M carbonate−bicarbonate coating buffer (15 mM sodium carbonate and 35 mM sodium bicarbonate, pH 9.6) and incubated overnight at 4 °C. Next day, wells were washed three times with 200 μL of washing buffer (WB: 0.9% sodium chloride supplemented with 0.1% Tween 20) and

https://dx.doi.org/10.1021/acsinfecdis.0c00063
ACS Infect. Dis. 2020, 6, 1816−1826

blocked with 200 μL of blocking buffer (BB: 3% BSA (Carl Roth)) in 1 × PBS at room temperature (RT) for 2 h. Meanwhile, dilutions of standard rabbit IgG (Sigma) ranging from 31.2 to 0.12 ng/mL as well as purified and unpurified antibodies in dilutions ranging from 1:10 000.000 to 1:50 000.000 were prepared in a blocking buffer. After incubation, wells were washed three times with 200 μL of WB and 100 μL in triplicate of samples, and standard dilutions were plated. Incubation was carried out for 2 h at RT, and the plates were then washed three times with 200 μL of WB. As the secondary antibody, 100 μL of alkaline-phosphatase-conjugated antirabbit IgG produced in goat (Sigma) diluted 1:1000 was used. Incubation was carried out for 2 h at RT. After, the plates were washed four times with 200 μL of WB. For detection, 100 μL of *p*-nitrophenyl phosphate (Sigma-Aldrich) at 1 mg/mL in glycine buffer (0.1 M glycine, 1 mM $MgCl_2$, and 1 mM $ZnCl_2$, pH 10.4) were used. After 30 min of incubation at RT, the reaction was stopped by adding 50 μL of 3 M sodium hydroxide and absorbance was measured at 405 nm. Antibody concentrations were calculated against the IgG calibration curve generated with standard rabbit IgG dilutions.

Screening of the Synthetic DHG Saccharides by ELISA. Anti-DHG serum specificity against different synthetic disaccharides mimicking the native DHG backbone was evaluated by ELISA. High capacity streptavidin coated plates (Thermo Fischer Scientific) were washed three times with tween-BSA buffer (TBB: 1×TBS, 0.1% BSA, and 0.05% Tween 20). Then, the wells were coated in triplicate with 1 μg of synthetic saccharides dissolved in TBB. Plates were incubated for 2 h at 4 °C, washed three times with 200 μL of TBB, and incubated with 100 μL of anti-DHG serum at the specified concentration for 2 h at RT with gentle shaking. Wells were washed three times with 200 μL of TBB and incubated for 30 min at RT with a 100 μL of alkaline-phosphatase-conjugated antirabbit IgG produced in goat at a 1:1000 dilution (Sigma). As a substrate, 100 μL of *p*-nitro phenyl phosphate (Sigma) was used at 1 mg/mL in glycine buffer. Plates were incubated at RT in the dark for 40 min; the reaction was stopped by adding 50 μL of 3 M sodium hydroxide, and the absorbance was measured at 405 nm.

Measurement of Antigen Specific Antibodies in Rabbit Sera by ELISA. Nunc-immuno Maxisorp 96-well plates were coated with 1 μg/well of either BSA, DHG, **4c**, or **8c** in 0.2 M sodium carbonate/bicarbonate buffer (60 mM Na_2CO_3, 140 mM $NaHCO_3$, pH 9.4) and incubated overnight at 4 °C. After incubation, wells were washed three times with 200 μL of PBS-Tween buffer (PTB: PBS, 0.05% Tween 20, pH 7.4) and blocked for 1 h with 100 μL of blocking buffer (PBS, 3% BSA, pH 7.4) at 37 °C. Meanwhile, 2-fold serial dilutions of rabbit sera were prepared, starting with a dilution of 100 μg IgG/mL for each serum tested. Later, wells were washed twice with 200 μL of PTB. After, 100 μL of the rabbit sera were plated in triplicates and incubated 1 h at 37 °C. Then, wells were washed three times with 200 μL of PTB prior to 1 h incubation with 100 μL of alkaline-phosphatase-conjugated antirabbit IgG produced in goat at a 1:1000 dilution (Sigma). After, wells were washed four times with 200 μL of PTB prior to 30 min incubation with 100 μL of the *p*-nitro phenyl phosphate substrate (Sigma) at 1 mg/mL in glycine buffer. The reaction was stopped by the addition of 50 μL of 3 M NaOH, and absorbance was measured at 405 nm. Serum IgG titers were calculated as follows: For each sample, a plot of the OD value against the reciprocal of the dilution (i.e., $\log_{10}$[dilution factor]) was used to calculate the intercept of an absorbance of 1 for each test; this was taken as the ELISA end point titer. The value extrapolated from the standard curve was then multiplied by the inverse of that dilution to generate the final inverse titer.

Purification of Rabbit Antibodies. Rabbit sera raised against DHG and synthetic conjugates were purified with a rProtein A GraviTrap column (GE Healthcare) according to manufacturers' instructions. In brief, 10 mL of binding buffer (20 mM sodium phosphate, pH 7.0) were used to equilibrate the column. Rabbit serum (2 mL) was supplemented with 100 μL of 20× binding buffer (0,4 M sodium phosphate, pH 7,0) before loading onto the column. The column was washed with 15 mL of 1× binding buffer, and seven fractions of 1 mL each were collected after eluting the antibodies by the addition of 10 mL of glycine buffer (0.1 M glycine-HCl, pH 2.7). Immediately after elution, fractions were mixed with 100 μL of 1 M Tris-HCl, pH 8.0, to preserve activity of acid-labile IgGs. Protein positive fractions containing the purified IgGs were collected and diafiltrated with PBS in a 30 kDa Amicon ultra-0.5 mL device (Merck Millipore).

Opsonophagocytic Assay (OPA) and Opsonophagocytic Inhibition Assay (OPIA). An *in vitro* opsonophagocytic assay was performed as described elsewhere.[60] For inhibition of opsonophagocytic activity, purified antibodies from the immune sera were inhibited by the corresponding synthetic conjugate or native DHG, accordingly. Concentrations ranging from 0.08 to 200 μg/mL of the sample were incubated overnight at 4 °C with an equal volume of a purified antibody (at 100 μg/mL of anti-DHG, 300 μg/mL of anti-**4c**, and 1.5 mg/mL of anti-**8c**). After incubation, the mixture of inhibitor/serum was used as a source of antibodies in an OPA as described above.

Mouse Sepsis Model: Passive immunization. The sepsis mouse infection experiment was performed as described previously with some modifications.[67−69] Briefly, BALB/c mice (weight, 20−25 g; Harlan) were split in three groups of seven mice and passively immunized as follows: intraperitoneally injected three times with 200 μL of either normal rabbit serum (NRS), anti-**4c**, or anti-**8c** at 48 and 24 h prior and 4 h after the bacterial challenge. Bacterial inoculum was prepared by growing *E. faecalis* Type 2 in brain heart infusion broth (Sigma) supplemented with 40% heat-inactivated horse serum (Sigma) until the stationary phase was reached. After, bacterial cells were harvested by centrifugation, and the resulting pellets were resuspended in sterile PBS to a concentration of 10^9 CFUs/mL. Prior to the bacterial challenge with 100 μL of the bacterial suspension, mice were anesthetized by intraperitoneal injection of 100 mg/g ketamine (Merial) and 12 mg/g xylazine (Bayer). The mice were monitored twice per day before they were sacrificed by cervical dislocation 48 h after the bacterial challenge. Kidneys and livers were aseptically removed, weighed, and homogenized in PBS for 120 s at a high speed in a stomacher (Pbi International). Serial dilutions were plated onto Enterococcus selective agar (Fluka Analytical) to determinate the colony-forming unit (CFU) numbers.

Statistics. For statistical analysis, a Prism version 7.00 (GraphPad) was used. The percentage of opsonophagocytic killing and absorbance in whole-cell ELISA was expressed as the geometrical mean with the standard errors of the mean. For OPA and OPIA, statistical significance was determined by nonparametric Kruskal−Wallis test followed by multiple comparisons using Dunn's post-test. *In vivo* experiments,

https://dx.doi.org/10.1021/acsinfecdis.0c00063
ACS Infect. Dis. 2020, 6, 1816−1826

results were subjected to statistical analysis by using one-way analysis of variance (ANOVA) with a Dunnett's multiple comparison test. P values <0.033 were considered statistically significant.

Ethics Statement. Rabbits were housed, immunized, and sampled by Biogenes (Berlin, Germany), in accordance with national and international animal welfare regulations. Rabbit immunizations at this facility were under approval from NIH/OLAW Animal Welfare Assurance (ID #A5755-01). Mouse experiments were conducted under a protocol approved by the Institutional Animal Use and Care Committee at Università Cattolica del Sacro Cuore, Fondazione Policlinico Universitario Agostino Gemelli IRCCS and authorized by Italian Ministry of Health (Protocol number: 1F295.37, 11/05/2017; Authorization number: 903/2017-PR, 11/05/2017) according to the Legislative Decree 116/92, which implemented the European Directive 86/609/EEC on laboratory animal protection in Italy.

■ ASSOCIATED CONTENT

Supporting Information

The Supporting Information is available free of charge at https://pubs.acs.org/doi/10.1021/acsinfecdis.0c00063.

Discussions of materials and methods used, synthetic procedures, and characterization data, schemes of synthetic pathways, table of synthesis yields and HRMS data, and figures of NMR spectra, specificity of sera, and MALDI-TOF spectra (PDF)

■ AUTHOR INFORMATION

Corresponding Authors

J. D. C. Codée − *Bio-Organic Synthesis, Leiden Institute of Chemistry, Leiden University, Leiden 2333 CC, Netherlands;* orcid.org/0000-0003-3531-2138; Email: jcodee@chem.leidenuniv.nl

N. E. Nifantiev − *N.D. Zelinsky Institute of Organic Chemistry, Russian Academy of Sciences, Moscow 119334, Russia;* orcid.org/0000-0002-0727-4050; Email: nen@ioc.ac.ru

J. Huebner − *Division of Paediatric Infectious Diseases, Dr. von Hauner Children's Hospital, Ludwig Maximilians University, Munich 80337, Germany;* orcid.org/0000-0003-1232-4646; Email: johannes.huebner@med.uni-muenchen.de

Authors

D. Laverde − *Division of Paediatric Infectious Diseases, Dr. von Hauner Children's Hospital, Ludwig Maximilians University, Munich 80337, Germany;* orcid.org/0000-0002-3925-269X

F. Romero-Saavedra − *Division of Paediatric Infectious Diseases, Dr. von Hauner Children's Hospital, Ludwig Maximilians University, Munich 80337, Germany*

D. A. Argunov − *N.D. Zelinsky Institute of Organic Chemistry, Russian Academy of Sciences, Moscow 119334, Russia*

J. Enotarpi − *Bio-Organic Synthesis, Leiden Institute of Chemistry, Leiden University, Leiden 2333 CC, Netherlands*

V. B. Krylov − *N.D. Zelinsky Institute of Organic Chemistry, Russian Academy of Sciences, Moscow 119334, Russia*

E. Kalfopoulou − *Division of Paediatric Infectious Diseases, Dr. von Hauner Children's Hospital, Ludwig Maximilians University, Munich 80337, Germany*

C. Martini − *Istituto di Microbiologia, Università Cattolica del Sacro Cuore, Rome 00168, Italy*

R. Torelli − *Dipartimento di Scienze di Laboratorio e Infettivologiche, Fondazione Policlinico Universitario "A. Gemelli" IRCCS, Rome 00168, Italy*

G. A. van der Marel − *Bio-Organic Synthesis, Leiden Institute of Chemistry, Leiden University, Leiden 2333 CC, Netherlands*

M. Sanguinetti − *Istituto di Microbiologia, Università Cattolica del Sacro Cuore, Rome 00168, Italy; Dipartimento di Scienze di Laboratorio e Infettivologiche, Fondazione Policlinico Universitario "A. Gemelli" IRCCS, Rome 00168, Italy*

Complete contact information is available at: https://pubs.acs.org/10.1021/acsinfecdis.0c00063

Author Contributions

▲D.L., F.R.-S., D.A.A., and J.E. contributed equally. D.L., F.R.-S., E.K., J.H., C.M., R.T., and M.S. conceived and designed the *in vitro* and *in vivo* experiments. J.E., J.D.C.C., V.B.K., D.A.A., and N.E.N. performed the synthetic experiments. D.L., F.R.-S., J.E., J.D.C.C., V.B,K., D.A.A., N.E.N., and J.H. cowrote the paper. D.L., F.R.-S., E.K., V.B.K., D.A.A., N.E.N., J.E., J.D.C.C., and J.H. participated in review and editing.

Notes

The authors declare no competing financial interest.

■ ACKNOWLEDGMENTS

The synthesis of oligosaccharide ligands **5a**−**8a** and glycoconjugates **1b**−**8b**, **4c**, and **8c** as well as the screening of sera on glycoarray was supported by the Russian Science Foundation (grant 19-73-30017). Other works were supported by the European Union's Horizon 2020 research and innovation program for funding work on this topic under the Marie Skłodowska-Curie grant agreement Glycovax No. 675671.

■ REFERENCES

(1) Agudelo Higuita, N., and Huycke, M. (2014) Enterococcal Disease, Epidemiology, and Implications for Treatment, *Enterococci: From Comensals to Leading Causes of Drug Resistant Inection*, pp 1−25, Massachusetts Eye and Ear Infirmary, Boston, MA.

(2) Arias, C. A., and Murray, B. E. (2012) The Rise of the Enterococcus: Beyond Vancomycin Resistance. *Nat. Rev. Microbiol. 10* (4), 266−278.

(3) Kristich, C. J., Rice, L. B., and Arias, C. A. (2014) Enterococcal Infection—Treatment and Antibiotic Resistance, *Enterococci: From Comensals to Leading Causes of Drug Resistant Inection*, pp 1−44, Massachusetts Eye and Ear Infirmary, Boston MA.

(4) Santana, V. F., Balbin, Y. V., Calderón, J. C., Icart, L. P., and Verez-Bencomo, V. (2008) Polysaccharide-Based Vaccines, in *Glycoscience* (Fraser-Reid, B. O., Tatsuta, K., and Thiem, J., Eds.) pp 2699−2723, Springer Berlin Heidelberg, Berlin, Germany.

(5) Nagy, E., Giefing, C., and von Gabain, A. (2008) Anti-Infective Antibodies: A Novel Tool to Prevent and Treat Nosocomial Diseases. *Expert Rev. Anti-Infect. Ther. 6* (1), 21−30.

(6) Sava, I. G., Zhang, F., Toma, I., Theilacker, C., Li, B., Baumert, T. F., Holst, O., Linhardt, R. J., and Huebner, J. (2009) Novel Interactions of Glycosaminoglycans and Bacterial Glycolipids Mediate Binding of Enterococci to Human Cells. *J. Biol. Chem. 284* (27), 18194−201.

(7) Fabretti, F., Theilacker, C., Baldassarri, L., Kaczynski, Z., Kropec, A., Holst, O., and Huebner, J. (2006) Alanine Esters of Enterococcal Lipoteichoic Acid Play a Role in Biofilm Formation and Resistance to Antimicrobial Peptides. *Infect. Immun. 74* (7), 4164−71.

(8) Huebner, J., Wang, Y., Krueger, W. A., Madoff, L. C., Martirosian, G., Boisot, S., Goldmann, D. A., Kasper, D. L., Tzianabos, A. O., and Pier, G. B. (1999) Isolation and Chemical Characterization of a Capsular Polysaccharide Antigen Shared by

Clinical Isolates of Enterococcus Faecalis and Vancomycin-Resistant Enterococcus Faecium. *Infect. Immun. 67* (3), 1213−9.
(9) Teng, F., Jacques-Palaz, K. D., Weinstock, G. M., and Murray, B. E. (2002) Evidence That the Enterococcal Polysaccharide Antigen Gene (Epa) Cluster Is Widespread in Enterococcus Faecalis and Influences Resistance to Phagocytic Killing of E. Faecalis. *Infect. Immun. 70* (4), 2010−2015.
(10) Theilacker, C., Kaczyński, Z., Kropec, A., Sava, I., Ye, L., Bychowska, A., Holst, O., and Huebner, J. (2011) Serodiversity of Opsonic Antibodies against *Enterococcus Faecalis* —Glycans of the Cell Wall Revisited. *PLoS One 6* (3), e17839.
(11) Koch, S., Hufnagel, M., Theilacker, C., and Huebner, J. (2004) Enterococcal Infections: Host Response, Therapeutic, and Prophylactic Possibilities. *Vaccine 22* (7), 822−30.
(12) Hufnagel, M., Hancock, L., Koch, S., Theilacker, C., Gilmore, M. S., and Huebner, J. (2004) Serological and Genetic Diversity of Capsular Polysaccharides in Enterococcus Faecalis. *J. Clin Microbiol 42*, 2548−2557.
(13) Hufnagel, M., Carey, V. J., Baldassarri, L., Reinert, R. R., and Huebner, J. (2006) Distribution of Four Capsular Serotypes of Enterococcus Faecalis among Clinical Isolates from Different Geographical Origins and Infection Sites. *Infection 34* (1), 22−25.
(14) Hancock, L., Shepard, B., and Gilmore, M. S. (2003) Molecular Analysis of the Enterococcus Faecalis Serotype 2 Polysaccharide Determinat. *J. Bacteriol. 185* (15), 4393−4401.
(15) Pazur, J. H., Anderson, J. S., and Karakawa, W. W. (1971) Glycans from Streptococcal Cell Walls. Immunological and Chemical Properties of a New Diheteroglycan from Streptococcus Faecalis. *J. Biol. Chem. 246* (6), 1793−1798.
(16) Krylov, V. B., Gerbst, A. G., Argunov, D. A., Dmitrenok, A. S., Shashkov, A. S., Kaczynski, Z., Huebner, J., Holst, O., and Nifantiev, N. E. (2015) Definitive Structural Assessment of Enterococcal Diheteroglycan. *Chem. - Eur. J. 21* (4), 1749−1754.
(17) Roy, R. (2004) New Trends in Carbohydrate-Based Vaccines. *Drug Discovery Today: Technol. 1* (3), 327−336.
(18) Fernández-Santana, V., González-Lio, R., Sarracent-Pérez, J., and Verez-Bencomo, V. (1998) Conjugation of 5-Azido-3-Oxapentyl Glycosides with Thiolated Proteins through the Use of Thiophilic Derivates. *Glycoconjugate J. 15* (6), 549−553.
(19) Verez-Bencomo, V. (2004) A Synthetic Conjugate Polysaccharide Vaccine Against Haemophilus Influenzae Type B. *Science (Washington, DC, U. S.) 305* (5683), 522−525.
(20) Colombo, C., Pitirollo, O., and Lay, L. (2018) Recent Advances in the Synthesis of Glycoconjugates for Vaccine Development. *Molecules 23* (7), 1712.
(21) Micoli, F., Costantino, P., and Adamo, R. (2018) Potential Targets for next Generation Antimicrobial Glycoconjugate Vaccines. *FEMS Microbiol. Rev. 42* (3), 388−423.
(22) Phalipon, A., Tanguy, M., Grandjean, C., Guerreiro, C., Belot, F., Cohen, D., Sansonetti, P. J., and Mulard, L. A. (2009) A Synthetic Carbohydrate-Protein Conjugate Vaccine Candidate against Shigella Flexneri 2a Infection. *J. Immunol. 182* (4), 2241−2247.
(23) Pozsgay, V. (1998) Synthesis of Glycoconjugate Vaccines against Shigella Dysenteriae Type 1. *J. Org. Chem. 63* (17), 5983−5999.
(24) Benaissa-Trouw, B., Lefeber, D. J., Kamerling, J. P., Vliegenthart, J. F. G., Kraaijeveld, K., and Snippe, H. (2001) Synthetic Polysaccharide Type 3-Related Di-, Tri-, and Tetrasaccharide−CRM197 Conjugates Induce Protection against Streptococcus Pneumoniae Type 3 in Mice. *Infect. Immun. 69* (7), 4698−4701.
(25) Bélot, F., Wright, K., Costachel, C., Phalipon, A., and Mulard, L. A. (2004) Blockwise Approach to Fragments of the O-Specific Polysaccharide of Shigella Flexneri Serotype 2a: Convergent Synthesis of A Decasaccharide Representative of a Dimer of the Branched Repeating Unit. *J. Org. Chem. 69* (4), 1060−1074.
(26) Gening, M. L., Maira-Litrán, T., Kropec, A., Skurnik, D., Grout, M., Tsvetkov, Y. E., Nifantiev, N. E., and Pier, G. B. (2010) Synthetic {beta}-(1->6)-Linked N-Acetylated and Nonacetylated Oligoglucosamines Used to Produce Conjugate Vaccines for Bacterial Pathogens. *Infect. Immun. 78* (2), 764−72.
(27) Laverde, D., Wobser, D., Romero-Saavedra, F., Hogendorf, W., van der Marel, G., Berthold, M., Kropec, A., Codee, J., and Huebner, J. (2014) Synthetic Teichoic Acid Conjugate Vaccine against Nosocomial Gram-Positive Bacteria. *PLoS One 9* (10), e110953.
(28) Krylov, V. B., Argunov, D. A., Vinnitskiy, D. Z., Verkhnyatskaya, S. A., Gerbst, A. G., Ustyuzhanina, N. E., Dmitrenok, A. S., Huebner, J., Holst, O., Siebert, H.-C., and Nifantiev, N. E. (2014) Pyranoside-into-Furanoside Rearrangement: New Reaction in Carbohydrate Chemistry and Its Application in Oligosaccharide Synthesis. *Chem. - Eur. J. 20* (50), 16516−16522.
(29) Argunov, D. A., Krylov, V. B., and Nifantiev, N. E. (2016) The Use of Pyranoside-into-Furanoside Rearrangement and Controlled O(5) → O(6) Benzoyl Migration as the Basis of a Synthetic Strategy To Assemble (1→5)- and (1→6)-Linked Galactofuranosyl Chains. *Org. Lett. 18* (21), 5504−5507.
(30) Walvoort, M. T. C., Volbeda, A. G., Reintjens, N. R. M., Van Den Elst, H., Plante, O. J., Overkleeft, H. S., Van Der Marel, G. A., and Codée, J. D. C. (2012) Automated Solid-Phase Synthesis of Hyaluronan Oligosaccharides. *Org. Lett. 14* (14), 3776−3779.
(31) Del Bino, L., Calloni, I., Oldrini, D., Raso, M. M., Cuffaro, R., Arda, A., Codée, J., Jiménez-Barbero, J., and Adamo, R. (2019) Regioselective Strategies for the Synthesis of Group Ia and Ib Streptococcus Related Glycans Enable Elucidating Unique Conformations of the Capsular Polysaccharides. *Chem. - Eur. J. 25*, 16169.
(32) Tsvetkov, Y. E., Burg-Roderfeld, M., Loers, G., Ardá, A., Sukhova, E. V., Khatuntseva, E. A., Grachev, A. A., Chizhov, A. O., Siebert, H.-C., Schachner, M., Jiménez-Barbero, J., and Nifantiev, N. E. (2012) Synthesis and Molecular Recognition Studies of the HNK-1 Trisaccharide and Related Oligosaccharides. The Specificity of Monoclonal Anti-HNK-1 Antibodies as Assessed by Surface Plasmon Resonance and STD NMR. *J. Am. Chem. Soc. 134* (1), 426−435.
(33) Komarova, B. S., Wong, S. S. W., Orekhova, M. V., Tsvetkov, Y. E., Krylov, V. B., Beauvais, A., Bouchara, J.-P., Kearney, J. F., Aimanianda, V., Latgé, J.-P., and Nifantiev, N. E. (2018) Chemical Synthesis and Application of Biotinylated Oligo-α-(1 → 3)- d -Glucosides To Study the Antibody and Cytokine Response against the Cell Wall α-(1 → 3)- d -Glucan of Aspergillus Fumigatus. *J. Org. Chem. 83* (21), 12965−12976.
(34) Komarova, B. S., Orekhova, M. V., Tsvetkov, Y. E., Beau, R., Aimanianda, V., Latgé, J.-P., and Nifantiev, N. E. (2015) Synthesis of a Pentasaccharide and Neoglycoconjugates Related to Fungal α-(1→3)-Glucan and Their Use in the Generation of Antibodies to Trace Aspergillus Fumigatus Cell Wall. *Chem. - Eur. J. 21* (3), 1029−1035.
(35) Krylov, V. B., Solovev, A. S., Argunov, D. A., Latgé, J.-P., and Nifantiev, N. E. (2019) Reinvestigation of Carbohydrate Specificity of EB-A2Monoclonal Antibody Used in the Immune Detection of Aspergillus Fumigatus Galactomannan. *Heliyon 5* (1), e01173.
(36) Argunov, D. A., Trostianetskaia, A. S., Krylov, V. B., Kurbatova, E. A., and Nifantiev, N. E. (2019) Convergent Synthesis of Oligosaccharides Structurally Related to Galactan I and Galactan II of Klebsiella Pneumoniae and Their Use in Screening of Antibody Specificity. *Eur. J. Org. Chem. 2019* (26), 4226−4232.
(37) Chernyak, A., Karavanov, A., Ogawa, Y., and Kováč, P. (2001) Conjugating Oligosaccharides to Proteins by Squaric Acid Diester Chemistry: Rapid Monitoring of the Progress of Conjugation, and Recovery of the Unused Ligand. *Carbohydr. Res. 330* (4), 479−486.
(38) Ferry, A., Malik, G., Guinchard, X., Větvička, V., and Crich, D. (2014) Synthesis and Evaluation of Di- and Trimeric Hydroxylamine-Based β-(1→3)-Glucan Mimetics. *J. Am. Chem. Soc. 136* (42), 14852−14857.
(39) Kaplonek, P., Khan, N., Reppe, K., Schumann, B., Emmadi, M., Lisboa, M. P., Xu, F.-F., Calow, A. D. J., Parameswarappa, S. G., Witzenrath, M., Pereira, C. L., and Seeberger, P. H. (2018) Improving Vaccines against Streptococcus Pneumoniae Using Synthetic Glycans. *Proc. Natl. Acad. Sci. U. S. A. 115* (52), 13353−13358.
(40) Theillet, F.-X., Frank, M., Vulliez-Le Normand, B., Simenel, C., Hoos, S., Chaffotte, A., Bélot, F., Guerreiro, C., Nato, F., Phalipon, A.,

https://dx.doi.org/10.1021/acsinfecdis.0c00063
ACS Infect. Dis. 2020, 6, 1816−1826

Mulard, L. A., and Delepierre, M. (2011) Dynamic Aspects of Antibody:Oligosaccharide Complexes Characterized by Molecular Dynamics Simulations and Saturation Transfer Difference Nuclear Magnetic Resonance. *Glycobiology 21* (12), 1570−1579.
(41) Schumann, B., Anish, C., Pereira, C. L., and Seeberger, P. H. (2013) Carbohydrate Vaccines, in *Biotherapeutics: Recent Developments Using Chemical and Molecular* (Jones, L. H., and McKnight, A. J., Eds.) pp 68−104, The Royal Society of Chemistry, Cambridge, UK.
(42) Astronomo, R. D., and Burton, D. R. (2010) Carbohydrate Vaccines: Developing Sweet Solutions to Sticky Situations? *Nat. Rev. Drug Discovery 9* (4), 308−324.
(43) Maira-Litrán, T., Kropec, A., Goldmann, D. A., and Pier, G. B. (2005) Comparative Opsonic and Protective Activities of Staphylococcus Aureus Conjugate Vaccines Containing Native Or. *Infect. Immun. 73* (10), 6752−6762.
(44) Park, S., Gerber, S., and Lee, J. C. (2014) Antibodies to Staphylococcus Aureus Serotype 8 Capsular Polysaccharide React with and Protect against Serotype 5 and 8 Isolates. *Infect. Immun. 82* (12), 5049−5055.
(45) Zhang, F., Lu, Y. J., and Malley, R. (2013) Multiple Antigen-Presenting System (MAPS) to Induce Comprehensive B-and T-Cell Immunity. *Proc. Natl. Acad. Sci. U. S. A. 110* (33), 13564−13569.
(46) Hufnagel, M., Kropec, A., Theilacker, C., and Huebner, J. (2005) Naturally Acquired Antibodies against Four Enterococcus Faecalis Capsular Polysaccharides in Healthy Human Sera. *Clin. Diagn. Lab. Immunol. 12*, 930−934.
(47) Goldenberg, H. B. B., McCool, T. L. L., and Weiser, J. N. N. (2004) Cross-Reactivity of Human Immunoglobulin G2 Recognizing Phosphorylcholine and Evidence for Protection against Major Bacterial Pathogens of the Human Respiratory Tract. *J. Infect. Dis. 190* (7), 1254−1263.
(48) Haji-Ghassemi, O., Blackler, R. J., Martin Young, N., and Evans, S. V. (2015) Antibody Recognition of Carbohydrate Epitopes. *Glycobiology 25* (9), 920−952.
(49) Cress, B. F., Englaender, J. A., He, W., Kasper, D., Linhardt, R. J., and Koffas, M. A. G. (2014) Masquerading Microbial Pathogens: Capsular Polysaccharides Mimic Host-Tissue Molecules. *FEMS Microbiol. Rev. 38* (4), 660−697.
(50) Mistretta, N., Brossaud, M., Telles, F., Sanchez, V., Talaga, P., and Rokbi, B. (2019) Glycosylation of Staphylococcus Aureus Cell Wall Teichoic Acid Is Influenced by Environmental Conditions. *Sci. Rep. 9* (1), 3212.
(51) Mohamed, N., Timofeyeva, Y., Jamrozy, D., Rojas, E., Hao, L., Silmon de Monerri, N. C., Hawkins, J., Singh, G., Cai, B., Liberator, P., Sebastian, S., Donald, R. G. K., Scully, I. L., Jones, C. H., Creech, C. B., Thomsen, I., Parkhill, J., Peacock, S. J., Jansen, K. U., Holden, M. T. G., and Anderson, A. S. (2019) Molecular Epidemiology and Expression of Capsular Polysaccharides in Staphylococcus Aureus Clinical Isolates in the United States. *PLoS One 14* (1), e0208356.
(52) Nanra, J. S., Timofeyeva, Y., Buitrago, S. M., Sellman, B. R., Dilts, D. A., Fink, P., Nunez, L., Hagen, M., Matsuka, Y. V., Mininni, T., Zhu, D., Pavliak, V., Green, B. A., Jansen, K. U., and Anderson, A. S. (2009) Heterogeneous in Vivo Expression of Clumping Factor A and Capsular Polysaccharide by Staphylococcus Aureus: Implications for Vaccine Design. *Vaccine 27* (25−26), 3276−3280.
(53) Mistretta, N., Brossaud, M., Telles, F., Sanchez, V., Talaga, P., and Rokbi, B. (2019) Glycosylation of Staphylococcus Aureus Cell Wall Teichoic Acid Is Influenced by Environmental Conditions. *Sci. Rep. 9* (1), 3212.
(54) Hitri, K., Kuttel, M. M., De Benedetto, G., Lockyer, K., Gao, F., Hansal, P., Rudd, T. R., Beamish, E., Rijpkema, S., Ravenscroft, N., and Bolgiano, B. (2019) O-Acetylation of Typhoid Capsular Polysaccharide Confers Polysaccharide Rigidity and Immunodominance by Masking Additional Epitopes. *Vaccine 37* (29), 3866−3875.
(55) Michon, F., Huang, C. H., Farley, E. K., Hronowski, L., Di, J., and Fusco, P. C. (2000) Structure Activity Studies on Group C Meningococcal Polysaccharide-Protein Conjugate Vaccines: Effect of O-Acetylation on the Nature of the Protective Epitope. *Dev. Biol. (Basel) 103*, 151−160.
(56) Berti, F., De Ricco, R., and Rappuoli, R. (2018) Role of O-Acetylation in the Immunogenicity of Bacterial Polysaccharide Vaccines. *Molecules 23* (6), 1340.
(57) Maekawa, S., Yoshioka, M., and Kumamoto, Y. (1992) Proposal of a New Shemefor the Serological Typing of Enterococcus Faecalis Strains. *Microbiol. Immunol. 36* (7), 671−681.
(58) Sahm, D. F., Kissinger, J., Gilmore, M. S., Murray, P. R., Mulder, R., Solliday, J., and Clarke, B. (1989) In Vitro Susceptibility Studies of Vancomycin-Resistant Enterococcus Faecalis. *Antimicrob. Agents Chemother. 33* (9), 1588−1591.
(59) Clewell, D. B., Tomich, P. K., Gawron-Burke, M. C., Franke, A. E., Yagi, Y., and An, F. Y. (1982) Mapping of Streptococcus Faecalis Plasmids PAD1 and PAD2 and Studies Relating to Transposition of Tn917. *J. Bacteriol. 152* (3), 1220−1230.
(60) Romero-Saavedra, F., Laverde, D., Kalfopoulou, E., Martini, C., Torelli, R., Martinez-Matamoros, D., Sanguinetti, M., and Huebner, J. (2019) Conjugation of Different Immunogenic Enterococcal Vaccine Target Antigens Leads to Extended Strain Coverage. *J. Infect. Dis. 220* (10), 1589−1598.
(61) Turula, V. E., Gore, T., Singh, S., and Arumugham, R. G. (2010) Automation of the Anthrone Assay for Carbohydrate Concentration Determinations. *Anal. Chem. 82* (5), 1786−1792.
(62) Dische, Z., and Shettles, L. B. (1948) A Specific Color Reaction of Methylpentoses and a Spectrophotometric Micromethod for Their Determination. *J. Biol. Chem. 175* (2), 595−603.
(63) Hébert, L., Courtin, P., Torelli, R., Sanguinetti, M., Chapot-Chartier, M.-P., Auffray, Y., and Benachour, A. (2007) Enterococcus Faecalis Constitutes an Unusual Bacterial Model in Lysozyme Resistance. *Infect. Immun. 75* (11), 5390−5398.
(64) Herstin, S. (1949) The Reaction of Acetylcholine and Other Carboxylic Acid Derivatives with Hydroxylamine, and Its Analytical Application. *J. Biol. Chem. 180* (1), 249−261.
(65) Lowry, O. H., Roberts, N. R., Wu, M.-L. L., Hixon, W. S., and Crawford, E. J. (1954) The Quantitative Histochemistry of Brain. II. Enzyme Measurements. *J. Biol. Chem. 207* (1), 19−37.
(66) Salauze, D., Serre, V., and Perrin, C. (1994) Quantification of Total IgM and IgG Levels in Rat Sera by a Sandwich ELISA Technique. *Comp. Haematol. Int. 4* (1), 30−33.
(67) Zhao, C., Hartke, A., La Sorda, M., Posteraro, B., Laplace, J.-M. M., Auffray, Y., and Sanguinetti, M. (2010) Role of Methionine Sulfoxide Reductases A and B of Enterococcus Faecalis in Oxidative Stress and Virulence. *Infect. Immun. 78* (9), 3889−97.
(68) Gentry-Weeks, C., Estay, M., Loui, C., and Baker, D. (2003) Intravenous Mouse Infection Model for Studying the Pathology of Enterococcus Faecalis Infections. *Infect. Immun. 71* (3), 1434−1441.
(69) Romero-Saavedra, F., Laverde, D., Budin-Verneuil, A., Muller, C., Bernay, B., Benachour, A., Hartke, A., and Huebner, J. (2015) Characterization of Two Metal Binding Lipoproteins as Vaccine Candidates for Enterococcal Infections. *PLoS One 10* (8), e0136625.

https://dx.doi.org/10.1021/acsinfecdis.0c00063
ACS Infect. Dis. 2020, 6, 1816−1826

Organic & Biomolecular Chemistry

ROYAL SOCIETY OF CHEMISTRY

PAPER

View Article Online
View Journal | View Issue

Cite this: *Org. Biomol. Chem.*, 2021, **19**, 2923

Synthesis and conformational analysis of vicinally branched trisaccharide β-D-Gal*f*-(1 → 2)-[β-D-Gal*f*-(1 → 3)-]-α-Gal*p* from *Cryptococcus neoformans* galactoxylomannan†

Vera S. Dorokhova,[a] Alexey G. Gerbst,[a] Bozhena S. Komarova,[a] José O. Previato,[b] Lúcia Mendonça Previato,[b] Andrey S. Dmitrenok,[a] Alexander S. Shashkov,[a] Vadim B. Krylov[a] and Nikolay E. Nifantiev *[a]

The synthesis of a vicinally branched trisaccharide composed of two D-galactofuranoside residues attached *via* β-(1 → 2)- and β-(1 → 3)-linkages to the α-D-galactopyranoside unit has been performed for the first time. The reported trisaccharide represents the galactoxylomannan moiety first described in 2017, which is the capsular polysaccharide of the opportunistic fungal pathogen *Cryptococcus neoformans* responsible for life-threatening infections in immunocompromised patients. The NMR-data reported here for the synthetic model trisaccharide are in good agreement with the previously assessed structure of galactoxylomannan and are useful for structural analysis of related polysaccharides. The target trisaccharide as well as the constituent disaccharides were analyzed by a combination of computational and NMR methods to demonstrate good convergence of the theoretical and experimental results. The results suggest that the furanoside ring conformation may strongly depend on the aglycon structure. The reported conformational tendencies are important for further analysis of carbohydrate–protein interaction, which is critical for the host response toward *C. neoformans* infection.

Received 11th October 2020,
Accepted 6th January 2021

DOI: 10.1039/d0ob02071k

rsc.li/obc

Introduction

Cryptococcus neoformans is an opportunistic fungal pathogen that causes life-threatening infections in immunocompromised patients. For example, cryptococcal meningitis is a severe nervous system infection associated with significant morbidity and mortality, especially among HIV/AIDS patients. The cells of *Cryptococcus neoformans* have large distinctive capsules that are composed mainly of two polysaccharides: glucuronoxylomannan (~90%) and galactoxylomannan (~10%).[1] Despite the predominance of glucuronoxylomannan in the polysaccharide capsule, galactoxylomannan has more pronounced immunomodulatory effects on host cellular immunity.[2] The investigation of immunological properties employing galactoxylomannan obtained from fungal capsules is complicated due to its structural heterogeneity. Galactoxylomannan consists of an α-(1 → 6)-linked α-galactan backbone, where every second α-Gal*p* residue is substituted at O-3 with α-Man*p*-(1 → 3)-α-Man*p*-(1 → 4)-β-Gal*p* side chains, which are in turn substituted with a variable number of β-(1 → 2)- and β-(1 → 3)-linked xylopyranose and β-(1 → 3)-GlcA residues (Fig. 1A). The α-galactan backbone is modified by galactofuranose residues. However, the position of their attachment differs from one published structure to another. Thus, Previato *et al.*[1] reported an alternative structure where two D-galactofuranoside residues attached *via* β-(1 → 2)- and β-(1 → 3)-linkages to an α-D-galactopyranoside of the backbone (shown on Fig. 1A). Previously, Heiss *et al.*[3] reported a structure where all Gal*f* units are placed on the O-2 of α-Gal*p* residues of the backbone chain branched at the O-3 position with β-Gal*p* units (shown in Fig. 1B).

The synthesis of a series of oligosaccharides, representing sheared fragments for glucuronoxylomannan and composed from xylose, mannose and glucuronic acid, has been performed by the groups of Oscarson[4,5] and Kong,[6,7] previously. However, to the best of our knowledge, the galactofuranoside-containing moiety of galactoxylomannan has not been investigated yet, despite the well-known significance of Gal*f* in microbial biology and pathogenesis.[8–11]

Herein, we report the synthesis of vicinally branched trisaccharide **1** as well as constituent disaccharides **2** and **3**

[a]*Laboratory of Glycoconjugate Chemistry, N.D. Zelinsky Institute of Organic Chemistry, Russian Academy of Sciences, Leninsky Prospect 47, 119991 Moscow, Russia. E-mail: nen@ioc.ac.ru; Fax: (+) 7-499-135-87-84; Tel: (+) 7-499-135-87-84*
[b]*Laboratório de Glicobiologia, Instituto de Biofísica Carlos Chagas Filho, Universidade Federal do Rio de Janeiro, 21941902 Rio de Janeiro, Brazil*

† Electronic supplementary information (ESI) available: Experimental procedures and copy of ^{1}H and ^{13}C spectra. See DOI: 10.1039/d0ob02071k

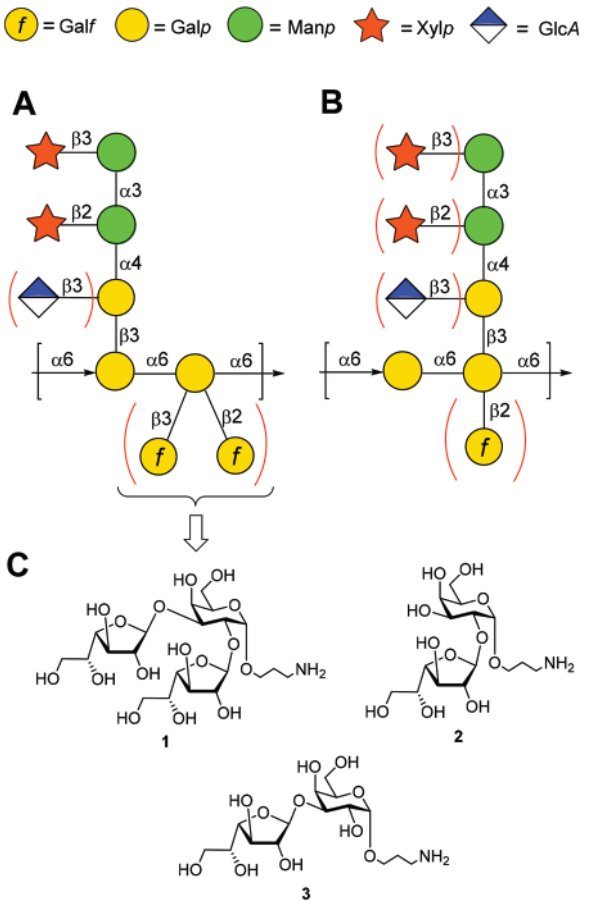

Fig. 1 Structures of galactoxylomannan proposed by Previato *et al.*[1] (A) and Heiss *et al.*[3] (B) With optional modification by Gal*f*, GlcA and Xyl*p* residues shown in red brackets; and synthesized model oligosaccharides **1–3** (C) studied in this work.

(Fig. 1C). These oligosaccharides were used for the confirmation of the native polysaccharide structure as well as for conformational analysis by means of theoretical and experimental NMR-methods. Reported conformational tendencies might be required for modelling of the interactions between galactoxylomannan and protein receptors.

Results and discussion

Synthesis of compounds 1–3

It can be supposed that the most rational approach towards the preparation of all three required compounds **1–3** can be based on galactofuranosylation of an appropriate 2,3-diol derivative of 3-fluoroacetamidopropyl α-D-galactopyranoside. Mostly, 4,6-*O*-benzylidene protected diols were used for the preparation of (1 → 3)-linked glycosides in typical yields of 50–95%.[12–15] In these cases, formation of the (1 → 2)-linked isomer was not documented, but products of bis glycosylation were observed. Sometimes, however, the regioselectivity of the couplings seems to be unpredictable. For instance, glycosylation of the same 4,6-*O*-benzylidene-protected diol with a glucosyl donor leads to the (1 → 3)-linked glycoside, while that with a xylosyl donor leads solely to the (1 → 2)-linked product.[16] Even the type of leaving group or reaction conditions influence the result of glycosylation of such a diol.[17] Also, directed preparation of both regioisomers, (1 → 2)-linked and (1 → 3)-linked, from 4,6-*O*-benzylidene[18] diol and also a 4,6-sililyden[19] diol was published.

Despite these exceptions, there is a general tendency for galactose 2,3-diols to predominantly form the (1 → 3)-linked product, which was confirmed in our experiments with galactofuranosylations (Scheme 1).

The published[17] glycosylation by imidate **5** of 4,6-*O*-benzylidene diol **4** at low temperature resulted in the predominant formation of (1 → 3)-linked tetrasaccharide **6** along with a smaller amount of its (1 → 2)-linked isomer and corresponding 2,3-di-glycosylated product. Our further attempt at glycosylation of 4,6-*O*-sililydene-diol **7** by a non-exhaustive amount of imidate **8** gave trisaccharide **9** as the main product but not the corresponding (1 → 2)- and (1 → 3)-linked disaccharides (data not published).

A galactose triol acceptor, protected at O-6, is an alternative to the 4,6-protected diols as in this type of diol, only OH-2 and OH-3 were shown to be active in different alkylation conditions.[20–27] More specifically, a 6-OTBDPS protected galactose acceptor, bearing 4-methylumbelliferyl aglycon, was demonstrated to produce under Lemieux conditions both fucosyl-(1 → 2)- and fucosyl-(1 → 3)-linked galactosides in one reaction with good yields.[28] Inspired by this example and taking into account all of the above mentioned considerations, we decided to study galactofuranosylation of the TBDPS-protected triol acceptor **12** (Scheme 2).

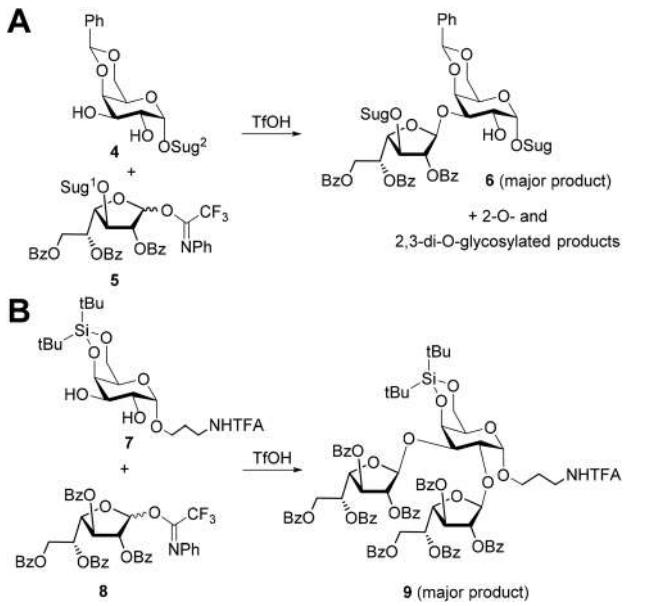

Scheme 1 Regioselectivity of 2,3-diol and 2,3,4-triol glycosylation: the example of 4,6-*O*-benzyliden (A) and 4,6-*O*-di-(*tert*-butyl)silylidene (B) protected acceptors (Sug^1, Sug^2 = protected galactoside residues); for details see ref. 17.

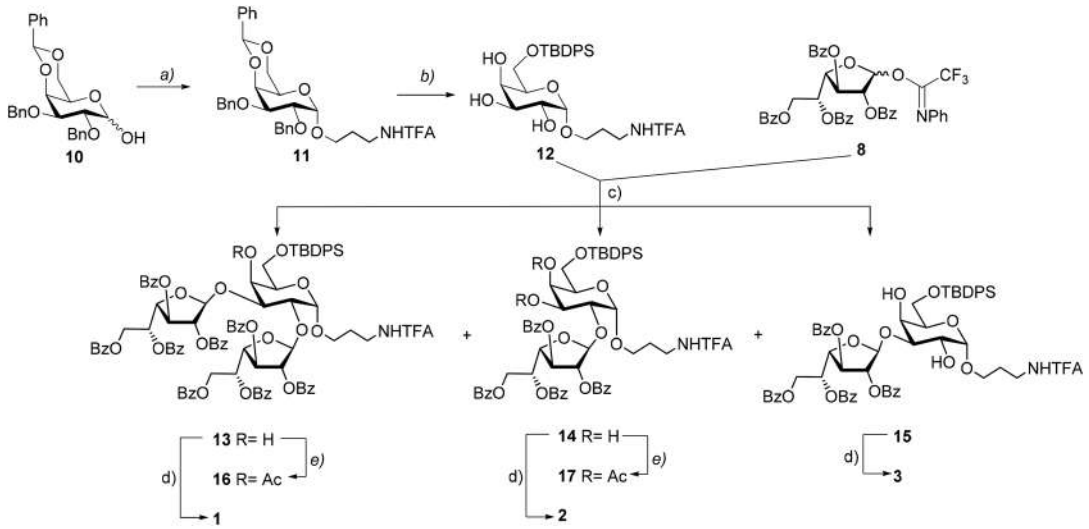

Scheme 2 Synthesis of trisaccharide **1** and disaccharides **2** and **3**. Reagents and conditions: (a) 1·CBr_4, PPh_3; 2·$NHTFA(CH_2)_3OH$, Bu_4NBr, MS 4A, CH_2Cl_2, 81% (α only); (b) 1·H_2, $Pd(OH)_2$/C, MeOH, EtOAc; 2·TBDPSCl, DMAP, Py, 98%; (c) see Table 1, entry 4; (d) 1·HF/H_2O, MeCN; 2·NaOMe, MeOH; 3·NaOH, H_2O, 43% for **1**, 59% for **2**, 61% for **3**; (e) Ac_2O, Py, 100% for **16**, 100% for **17**.

This product was prepared from the known hemiacetal **10**. Galactosyl bromide prepared *in situ* from monosaccharide **10** was treated with trifluoroacetamidopropanol in the presence of Bu_4NBr. 4,6-*O*-Benzyliden protection of the galactose was suggested to enhance the selectivity of the reaction to give the desired **11** in 83% yield selectively. Curiously, an attempt to prepare trifluoroacetamidopropyl α-galactoside with the use of tetrabenzylated galactoside instead of **10** lead to an anomeric mixture (see ESI†).

Following steps for the removal of benzyl and benzylidene groups with $Pd(OH)_2$/C from **11** and attachment of a TBDPS group to O-6 gave acceptor **12** in nearly quantitative yield. Its further glycosylation reactions were promoted with TBDMSOTf.

The first trial glycosylation of triol **12** by *N*-phenyltrifluoroacetimidoyl donor **8** (1.2 eq.) was performed in dichloromethane and led to the formation of 2-*O*-furanosyl-disaccaride **14** and 2,3-di-*O*-furanosyltrisaccaride **13** with yields of 9 and 37%, respectively (Table 1, entry 1; Scheme 2). To confirm that the galactofuranosyl residue was attached to O-2 of galactopyranoside, free hydroxyl groups of disaccharide **14** were acetylated to give **17**. As was expected, the chemical shifts of H-3 and H-4 of **17** in the ^{1}H-NMR spectrum moved from 3.95 to 5.03 ppm and from 4.55 to 5.56 ppm, respectively. In turn, change of the H-4 chemical shift of the acetylated trisaccharide **16** from 4.17 to 5.53 ppm proved the structure of **13**.

Assuming that the low yields in this glycosylation could be caused by poor solubility of the triol acceptor **12** in pure dichloromethane at low temperature, a mixture of dichloromethane and acetonitrile was used as a solvent for the next glycosylation (Table 1, entry 2). This time **13**, **14** and 3-*O*-furanosylated disaccharide **15** were formed in approximately equal quantities. In the third experiment, when a reduced amount of furanosyl donor **8** was added in two portions, only disaccharides **14** and **15** were formed (Table 1, entry 3). Replacement of the solvent mixture from $MeCN/CH_2Cl_2$ to $toluene/CH_2Cl_2$ led to an increase of the yields of both disaccharides and the trisaccharide (Table 1, entry 4). All three compounds, **13–15**, were isolated by silica gel column chromatography. Removal of a TBDPS group by HF in MeCN in **13–15** followed by catalytic debenzoylation afforded flawlessly targeted oligosaccharides **1–3**.

NMR analysis of compounds 1–3

Complete signal assignment of the NMR spectra of the target model oligosaccharides **1–3** was performed by applying 2D NMR experiments, namely ^{1}H–^{1}H-COSY and ^{1}H–^{13}C-HSQC experiments (for assignment details, see ESI†). Their ^{1}H and ^{13}C chemical shifts are summarized in Tables 2 and 3, respect-

Table 1 Experimental conditions and results of glycosylation of triol **12** by donor **8** (Scheme 2)

#	Donor (eq.)	Experimental conditions	Yield of **13** (%)	Yield of **14** (%)	Yield of **15** (%)	Unreacted **12**[a]
1	1.2	TBDMSOTf (0.3 eq.), CH_2Cl_2. −35 °C, 16 min	37	9	0	40–50%
2	1.2	TBDMSOTf (0.3 eq.), CH_2Cl_2/CH_3CN 1/2, −30 → 0 °C, 2 h	17	13	15	30–40%
3	0.4 + 0.2	TBDMSOTf (0.4 eq.), CH_2Cl_2/CH_3CN 1/2, −30 °C, 15 min	Not isolated	8	14	30–40%
4	0.4 + 0.2	TBDMSOTf (0.4 eq.), CH_2Cl_2/toluene 1/2, −30 °C, 25 min	47	16	16	15–20%

[a] According to TLC.

Table 2 ^{1}H-NMR chemical shifts (δ, ppm, D_2O) for trisaccharide **1** and disaccharides **2** and **3**

Compound	Unit	H-1	H-2	H-3	H-4	H-5	H-6A	H-6B
1	*α-D-Galp*	5.05	3.96	3.99	4.09	3.92	3.74	3.71
	(1 → 2)-β-D-Galf	5.15	4.12	4.07	3.96	3.83	3.70	3.63
	(1 → 3)-β-D-Galf	5.19	4.15	4.04	4.01	3.83	3.70	3.60
2	*α-D-Galp*	5.05	3.81	3.94	3.97	3.87	3.75	3.68
	(1 → 2)-β-D-Galf	5.12	4.12	4.06	3.91	3.80	3.68	3.63
3	*α-D-Galp*	4.98	3.96	3.91	4.12	3.96	3.74	3.74
	(1 → 3)-β-D-Galf	5.19	4.18	4.08	4.05	3.84	3.69	3.66

Table 3 ^{13}C-NMR chemical shifts (δ, ppm, D_2O) for trisaccharide **1** and disaccharides **2** and **3**

Compound	Unit	C-1	C-2	C-3	C-4	C-5	C-6
Model reference monosaccharides:							
α-D-Gal*p* [29]	*α-D-Galp*	99.12	68.71	70.09	69.85	71.69	61.88
β-D-Gal*f* [29]	*β-D-Galf*	102.60	82.9	77.4	83.70	72.30	64.40
1	*α-D-Galp*	98.64	75.38	76.09	69.87	71.22	61.59
	(1 → 2)-β-D-Galf	109.72	81.80	77.25	83.63	71.26	63.11
	(1 → 3)-β-D-Galf	109.43	81.88	77.51	83.42	71.13	62.92
2	*α-D-Galp*	98.56	76.58	68.76	69.57	71.23	61.53
	(1 → 2)-β-D-Galf	109.7	81.55	76.83	83.34	70.96	62.80
3	*α-D-Galp*	98.82	67.58	77.75	69.68	71.32	61.61
	(1 → 3)-β-D-Galf	109.53	81.83	77.21	83.21	71.09	63.08

ively. Corresponding glycosylation effects (Table 4) were calculated as the difference in chemical shift between the studied disaccharides and one of the used monosaccharide reference structures shown in the first part of Table 3. The glycosylation effects agreed with previously reported data.[29,30] The deviations from additivity in vicinally branched trisaccharide **1** were calculated as a difference between the experimental (δ_{exp}) and calculated (δ_{calc}) ^{13}C chemical shifts, where $\delta_{calc} = \delta_C(2) + \delta_C(3) - \delta_C(4)$ and is presented in Table 5. The obtained values are needed for calculating the NMR spectra according to additive schemes.[31,32]

The NMR data obtained for the synthetic oligosaccharides were compared with those reported for native galactoxylomannan isolated from *C. neoformans*. Each chemical shift taken from cited ref. 1 has been decremented by 0.8 ppm for consistency with our chemical shift reference (for details see the ESI†). Excellent convergence was observed for the galactofuranoside residue attached *via* a β-(1 → 3)-linkage; however, for the β-(1 → 2)-linked one, a significant discrepancy in the C(4) chemical shifts was detected (Fig. 2). Similar deviations were obtained when the NMR data of a polysaccharide published by Heiss *et al.*[3] were taken for comparison. This can be attributed to the influence of the polysaccharide backbone, which is absent in the oligosaccharide model. Indeed, in the polysaccharide, the β-(1 → 2)-linked galactofuranoside residue is in close spatial proximity to residue at the anomeric position of α-galactopyranoside, which can result in distortion of the flexible furanose ring. The NMR data for the α-galactopyranoside residue of the backbone in the polysaccharide and oligosaccharide were in good agreement. Detailed comparison of the NMR data for the oligo- and polysaccharide, including the ^{1}H NMR spectra, are presented in the ESI.†

Table 4 ^{13}C NMR α- and β-glycosylation effects ($\Delta\delta$, ppm) in the ^{13}C NMR spectra of trisaccharide **1** and disaccharides **2** and **3**

Compound	Unit	ΔδC-1	ΔδC-2	ΔδC-3	ΔδC-4	ΔδC-1′	ΔδC-1″
1	*2,3-di-(β-D-Galf)-α-D-Galp*	−0.48	6.67	6.0	0.02	7.12	6.83
2	*β-D-Galf-(1 → 2)-α-D-Galp*	−0.56	7.87	−1.33	—	7.1	—
3	*β-D-Galf-(1 → 3)-α-D-Galp*	—	−1.13	7.66	−0.17	—	6.93

Table 5 Deviations from additivity (ΔΔ, ppm) in the ^{13}C-NMR spectrum for the galactopyranoside unit of trisaccharide **1**

ΔΔδC-1	ΔΔδC-2	ΔΔδC-3	ΔΔδC-4	ΔΔδC-5	ΔΔδC-6	ΔΔδC-1′	ΔΔδC-1″
0.38	−0.07	−0.33	0.47	0.36	0.33	0.02	−0.1

Conformational analysis of compounds 1–3

Computational details. ORCA 4.2[33] software was used throughout the study. DFT calculations employed the B3LYP functional with the 6-31 g(d,p) basis set as an approach previously shown to perform satisfactorily during the modelling of propyl galactofuranoside.[34] RI-MP2 calculations were carried out using the def2-TZVPP basis set. NMR coupling constants were computed using DFT/B3LYP/pcJ-1 approximation.[35]

General considerations. Furanoside rings are generally more flexible than pyranosides,[36,37] and hence their extensive investigation was undertaken in this work. During our previous studies[34] of the conformational changes in furanoside rings induced by their complete sulfation and other conformational aspects of these structures,[38] we revealed the main conformers of the non-sulfated galactofuranoside. These results were supported by evidence from NMR spectroscopy, such as intra-ring H–H coupling constants and NOE. The main determined conformers for the non-sulfated rings were C3-*exo* or ones similar to them according to Cremer-Pople parameters (Fig. 3). The minor conformer in the case of the non-sulfated furanosides was O4-*exo* (Fig. 3), which, however, became dominant upon the introduction of sulfates.

The structures used for the calculations differed from experimental structures **1–3** by the absence of the amino group in the aglycon to avoid counter-ion complications. In the present work, we decided to use these conformers as starting structures for the modelling. Preliminary calculations using the B3LYP/6-31g(d,p) approach again tended to predict the dominance of the C3-*exo* conformer. However, according to the NMR data its amount in the equilibrium should have been minor. In particular, the studied disaccharides and the trisaccharide in this work were characterized with lower values of $J_{1,2}$ and $J_{2,3}$ ^{1}H–^{1}H coupling constants (Table 7) than those observed in the simple propyl-galactofuranoside.[34] Meanwhile, the C3-*exo* conformer (as well as the C4-*endo* conformer that is similar to it) provides rather large values of these couplings because of the corresponding protons being almost *pseudo*-axial and *trans*-oriented. Besides, when a glycosidic torsional scan was attempted, it occurred that sometimes the O4-*exo* conformer actually transformed into the C3-*exo*. After that, we decided to employ RI-MP2/def2-TZVPP approximation for the computational study as a method of the next level of theory above the DFT approach.

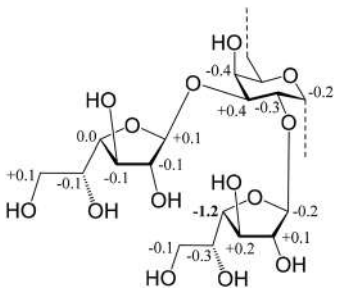

Fig. 2 The difference between the ^{13}C NMR chemical shifts ($\Delta\delta$) in the vicinally branched trisaccharide moiety of the galactoxylomannan reported by Previato *et al.*[1] and in trisaccharide **1** obtained in this work. For calculation details and data for ^{1}H NMR chemical shifts see the ESI.†

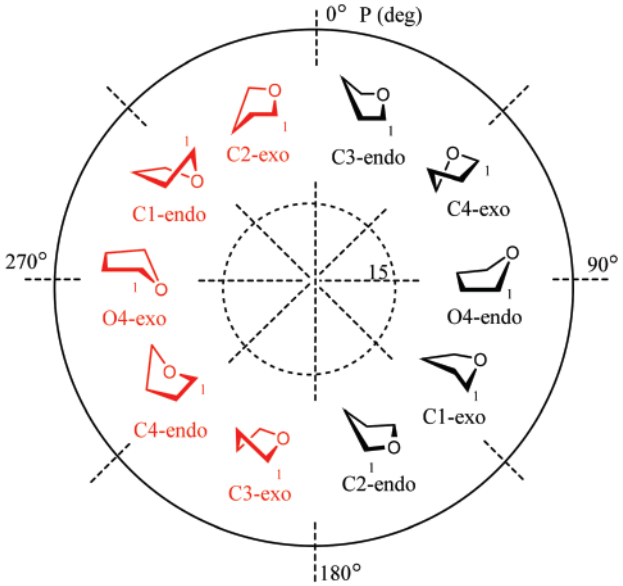

Fig. 3 Principal conformers of the galactofuranoside rings determined in this work.[34]

Conformational analysis of the disaccharide structures 2 and 3. The two disaccharide structures were used for additional examination of possible furanoside ring conformers employing the RI-MP2/def2-tzvp[39,40] method. That is, in addition to the above mentioned conformers, also C1-*endo* and C2-*exo* models were optimized at this level. This revealed that, contrary to what was observed for the propyl galactofuranoside,[34] they were identified as conformational minima, while previously, at the DFT and HF level, they tended to convert to one of the other furanoside conformers.

Using these newly found conformations, relaxed potential energy scans of ψ torsions of the glycosidic linkages were performed for both disaccharides at the RI-MP2/def2-tzvp level of theory. The scanned range was (−60°...+30°) with a 10° step. The φ angles were allowed to change during the constrained optimizations. This was done in order to save computational time. This approach is justified[41] since the behavior of the φ angles is mostly governed by the *exo*-anomeric effect and they have a more restricted range to change within.

Upon the analysis of the obtained results, it was found that still some conformers irreversibly changed to others lying near them on the *pseudo*-rotational ring (Fig. 3). Thus, in the case of the (1 → 2)-linked disaccharide, the O4-*exo* conformer underwent transformation into C1-*endo*, and in both disaccharides the C3-*exo* conformer changed to C4-*endo* during the dihedral scanning. In these cases the scan graph for just one conformer is given. The resulting scan graphs are shown in Fig. 4.

It can be seen that for the (1 → 2)-linked disaccharide all the found distinct conformers demonstrated a minimum of

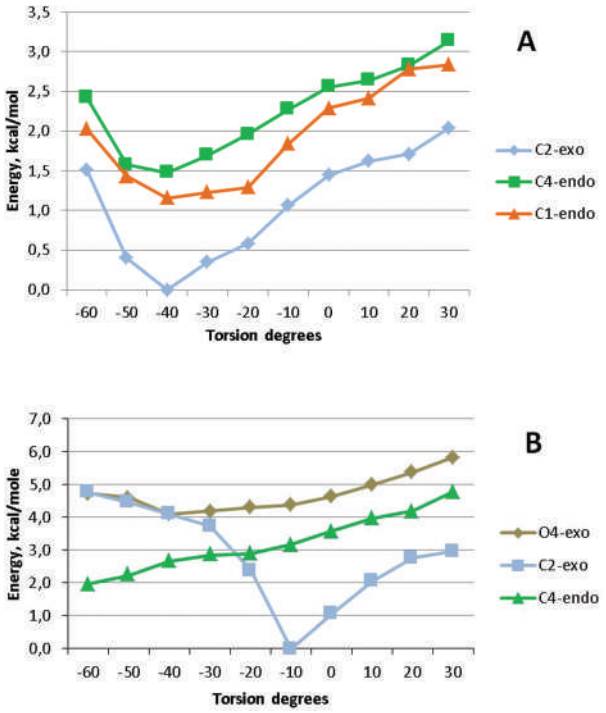

Fig. 4 Relaxed energy scan graphs for ψ torsions in (1 → 2)- (A) and (1 → 3)-linked (B) disaccharides.

the ψ torsion at around −40°. On the other hand, the C2-*exo* conformer appeared to be the most preferable, with the C1-*endo* being slightly over 1 kcal per mole higher, while C4-*exo* had the highest relative energy.

In the case of the (1 → 3)-linked disaccharide, the main preferable conformer seemed to be C2-*exo* with the minimum at around −10°. The O4-*exo* conformer exhibited the lowest energy at −40°, but this energy was more than 4 kcal per mole higher than that of the C2-*exo* minimum. Unlike the (1 → 2)-linkage, the C4-*endo* conformer did not show a minimum in the given range. Additional calculations beyond the −60° point demonstrated that its minimum was at the value of −70° (data not shown) and lay 1.9 kcal per mole higher than that of C2-*exo*.

The φ angles at the found minimum had the values of *ca.* 60°. All these results correlated qualitatively with the observed coupling constants (Table 7).

Conformational analysis of the trisaccharide 1. The newly found conformations along with those already known were used to construct starting trisaccharide structures for the relaxed torsional scans. The ψ torsion scans were also performed in the range of (−60°...+30°) with 10° step. In this case, the situation was more complex because two furanoside rings were supposed to change their conformations independently; therefore, several combinations of different conformers in the same trisaccharide molecule were used for scanning. In Table 6 the notations of these combinations are given.

The resulting scan graphs are shown in Fig. 5. It can be seen that for both linkages the lowest energy conformers are

Table 6 Combinations of the furanoside residue conformations used for relaxed torsion scans in trisaccharide **1**

Residue at O-2	Residue at O-3	Notation
C4-*endo*	C4-*endo*	**A**
O4-*exo*	C2-*exo*	**B**
C2-*exo*	C2-*exo*	**C**
C4-*endo*	C3-*exo*	**D**
C2-*exo*	C4-*endo*	**E**

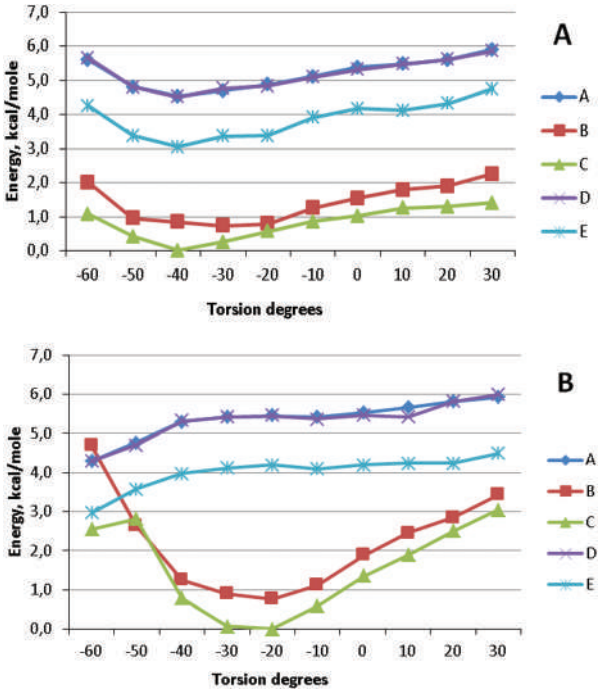

Fig. 5 Relaxed energy scan graphs for (1 → 2)- (A) and (1 → 3)- (B) ψ torsions in trisaccharide **1**.

those with the furanoside ring conformers initially set to either the C2-*exo* or O4-*exo* conformation (structures B and C). The minimal energy range for the (1 → 2)-linkage lies around −20°...−40°, that is, close enough to that of the (1 → 2)-linkage in the corresponding disaccharide. For the (1 → 3)-linkage, it is around the torsion values of −20°...−30°.

It can also be noted that in the structures found as having the lowest energy both in the trisaccharide and the disaccharides, the anomeric bond is generally *pseudo*-axially oriented, which is in correlation with the results recently obtained by Plazinski and Gaweda.[42] Also, these conformations, C2-*exo* and O4-*exo*, have their H-1, H-2 and H-3 protons in *pseudo*-equatorial orientations. This is illustrated in Fig. 6. Such mutual orientation of these protons is expected to account for the smaller $^{1}H–^{1}H$ couplings in the studied substances. This question was further studied in detail.

Calculation of the coupling constants. Their ψ torsion minima obtained from the constrained optimization during the scans were then re-optimized without constraints and used

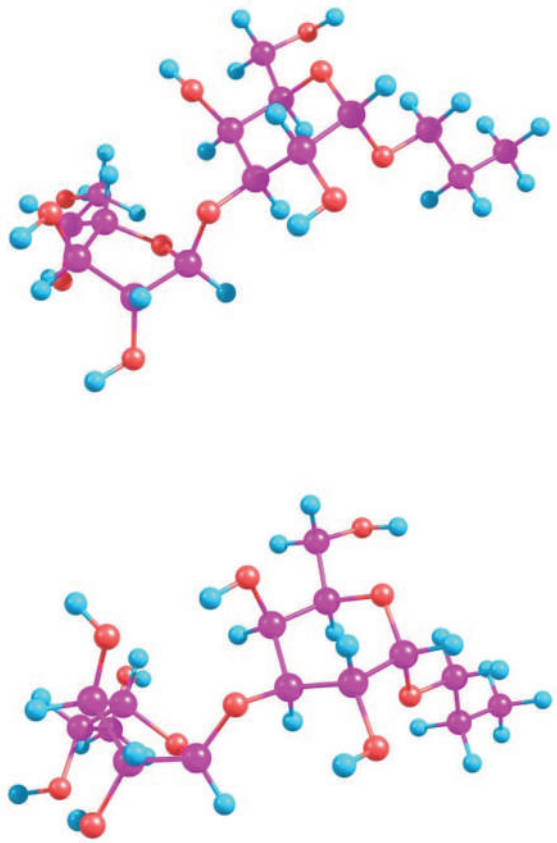

Fig. 6 O4-*exo* (top) and C2-*exo* (bottom) conformers of the (1 → 3)-linked galactobioside.

to calculate the *J*-coupling constants (both intra- and inter-ring) using the B3LYP/pcJ-1 approximation. The experimental coupling constants that are of primary interest for the conformational analysis are presented in Table 8. These are constants between protons H1, H2 and H3, that allow for the establishment of the monosaccharide ring conformations, and long-range C–H couplings that describe the conformation of the glycosidic linkage. This might suggest that the furanoside rings in these compounds are very flexible and other conformers having higher energies (such as C4-*endo*) also contribute to the equilibrium.

The couplings calculated for different conformers of the studied saccharide models are shown in Table 8. It can be seen that, although the C2-*exo*, O4-*exo* and C1-*endo* conformers seem to be of significantly lower energy, the coupling constants calculated using them alone are much smaller than those observed in the experiment (Table 7).

When the obtained minima were used for calculation of the long-range ^{13}C–^{1}H couplings around the glycosidic linkage, large deviations from the experimental values were observed. Therefore, several other optimized points found around the minima during torsional scanning were involved in the calculations. Their energies lay within 1.5 kcal per mole from the minima. Table 9 represents the found ranges for the ^{13}C–^{1}H constants.

Quite expectedly, the couplings corresponding to the φ angles fall within rather small ranges. This is explained by the fact that the behavior of these torsions is governed by the *exo*-anomeric effect and they were allowed to adopt only a limited range of values. On the contrary, the ψ-angle couplings demonstrate high variability depending on the torsion value. On one hand, this is because these torsions change in the range of *ca.* 40° in the mentioned energy limits. On the other hand, this corroborates with the fact that ^{13}C–^{1}H couplings involving atoms in the furanoside rings can have significantly larger values than those in pyranosides, even requiring proper re-parametrization of the corresponding empirical Karplus-type equation.[43]

Practically, these results suggest that the glycosidic linkages in these structures cannot be represented as a single conformation. Rather, they occupy a relatively wide basin with the "center" at around −20°...−40° of the ψ angle. Thus the studied compounds may be characterized, as a whole, as being conformationally flexible, and even the presence of the vicinal 2,3-branch does not affect this flexibility.

Table 7 Experimentally measured coupling constants in compounds **1–3** (Hz)

Compound	Unit	J_{H1-H2}	J_{H2-H3}	$J_{C1'-H1}$ (φ)	$J_{C1-H1'}$ (ψ)
1	β-D-Gal*f*-(1 → 2)	1.7	3.5	3.4 Hz	4.8 Hz
	β-D-Gal*f*-(1 → 3)	1.6	3.4	3.0 Hz	5.0 Hz
2	β-D-Gal*f*-(1 → 2)	1.5	3.8	3.4 Hz	4.8 Hz
3	β-D-Gal*f*-(1 → 3)	1.8	3.6	3.0 Hz	5.0 Hz
Gal*f*OPr[34]	β-D-Gal*f*	2.4	4.4		

Table 8 Calculated ^{1}H–^{1}H coupling constants for different conformers of the model oligosaccharides **1–3** (Hz)

Compound	Unit	J_{H1-H2}	J_{H2-H3}
1	(1 → 2)-β-D-Gal*f*	0.1 (C2-*exo*)	1.6 (C2-*exo*)
		0.8 (O4-*exo*)	1.2 (O4-*exo*)
		4.6 (C4-*endo*)	8.5 (C4-*endo*)
	(1 → 3)-β-D-Gal*f*	0.1 (C2-*exo*)	1.6 (C2-*exo*)
		0.9 (O4-*exo*)	1.4 (O4-*exo*)
		4.4 (C4-*endo*)	8.2 (C4-*endo*)
2	(1 → 2)-β-D-Gal*f*	0.1 (C2-*exo*)	1.6 (C2-*exo*)
		4.6 (C4-*endo*)	8.6 (C4-*endo*)
		0.7 (C1-*endo*)	1.5 (C1-*endo*)
3	(1 → 3)-β-D-Gal*f*	0.2 (C2-*exo*)	1.7 (C2-*exo*)
		4.4 (C4-*endo*)	8.4 (C4-*endo*)

Table 9 Ranges of the calculated ^{13}C–^{1}H coupling constants for the model oligosaccharides **1–3** (Hz)

Compound	Unit	$J_{C1'-H1}$ (φ)	$J_{C1-H1'}$ (ψ)
1	(1 → 2)-β-D-Gal*f*	3.0–3.5	3.9–6.0
	(1 → 3)-β-D-Gal*f*	2.8–3.5	4.0–5.8
2	(1 → 2)-β-D-Gal*f*	3.0–3.9	4.0–6.1
3	(1 → 3)-β-D-Gal*f*	3.1–3.8	4.2–5.9

Conclusion

Spacer armed trisaccharide **1** and constituting disaccharides **2** and **3** representing the vicinal branching point of *Cryptococcus neoformans* galactoxylomannan were synthesized starting from a triol glycosyl-acceptor. The prepared oligosaccharides are indispensable models for the investigation of the conformational behavior and glycobiological properties of fungal cell wall polysaccharides[44] by using approaches developed for galactomannan,[45–47] α-glucan[48,49] and galactosaminogalactan[50] polysaccharide antigens of *Aspergillus fumigatus*. Conformational analysis based on NMR and theoretical studies suggest that the furanoside ring conformations may depend also on the aglycon structure. The conformational tendencies in the furanoside rings observed in this study correlated well with the results recently obtained by Plazinski and Gaweda[42] in terms of the anomer substituent orientation. Our results are also in agreement with the knowledge that for furanosides, a different parametrization of the Karplus equation describing long-range C–H constants is required,[43] probably due to the deviations in the values of the C–O–C angle.

Conflicts of interest

There are no conflicts to declare.

Acknowledgements

This work was supported in part by the Russian Science Foundation (grant 19-73-30017). The authors wish to thank Dr Dmitry I. Sharapa (KIT IKFT) for fruitful discussions and technical assistance in the conduction of some of the RI-MP2 calculations.

Notes and references

1 J. O. Previato, E. Vinogradov, E. Maes, L. M. Fonseca, Y. Guerardel, P. A. V. Oliveira and L. Mendonça-Previato, *Glycobiology*, 2017, **27**, 582–592.
2 D. Decote-Ricardo, I. F. LaRocque-de-Freitas, J. D. B. Rocha, D. O. Nascimento, M. P. Nunes, A. Morrot, L. Freire-de-Lima, J. O. Previato, L. Mendonça-Previato and C. G. Freire-de-Lima, *Front. Med.*, 2019, **6**, 129.
3 C. Heiss, M. L. Skowyra, H. Liu, J. S. Klutts, Z. Wang, M. Williams, D. Srikanta, S. M. Beverley, P. Azadi and T. L. Doering, *J. Biol. Chem.*, 2013, **288**, 10994–11003.
4 L. Guazzelli, C. J. Crawford, R. Ulc, A. Bowen, O. McCabe, A. J. Jedlicka, M. P. Wear, A. Casadevall and S. Oscarson, *Chem. Sci.*, 2020, **11**, 9209–9217.
5 S. Oscarson, M. Alpe, P. Svahnberg, A. Nakouzi and A. Casadevall, *Vaccine*, 2005, **23**, 3961–3972.
6 W. Zhao and F. Kong, *Carbohydr. Res.*, 2005, **340**, 1673–1681.
7 J. Zhang and F. Kong, *Carbohydr. Res.*, 2003, **338**, 1719–1725.
8 B. Tefsen, A. F. J. Ram, I. van Die and F. H. Routier, *Glycobiology*, 2012, **22**, 456–469.
9 M. R. Richards and T. L. Lowary, *ChemBioChem*, 2009, **10**, 1920–1938.
10 P. Peltier, R. Euzen, R. Daniellou, C. Nugier-Chauvin and V. Ferrières, *Carbohydr. Res.*, 2008, **343**, 1897–1923.
11 M. Carla, A. Rinflerch and R. N. de Lederkremer, *Future Sci. OA*, 2017, **3**, FSO199.
12 R. Chevalier, B. Colsch, C. Afonso, N. Baumann, J.-C. Tabet and J.-M. Mallet, *Tetrahedron*, 2006, **62**, 563–577.
13 S. Ramadan, W. Yang, Z. Zhang and X. Huang, *Org. Lett.*, 2017, **19**, 4838–4841.
14 S. Canevari, D. Colombo, F. Compostella, L. Panza, F. Ronchetti, G. Russo and L. Toma, *Tetrahedron*, 1999, **55**, 1469–1478.
15 W. Yang, K. Yoshida, B. Yang and X. Huang, *Carbohydr. Res.*, 2016, **435**, 180–194.
16 G. Gu, Y. Du and R. J. Linhardt, *J. Org. Chem.*, 2004, **69**, 5497–5500.
17 S. A. Verkhnyatskaya, V. B. Krylov and N. E. Nifantiev, *Eur. J. Org. Chem.*, 2017, 710–718.
18 Q. Liu, H. Liu, L. Zhang, T. Guo, P. Wang, M. Geng and Y. Li, *Eur. J. Med. Chem.*, 2013, **64**, 1–15.
19 D. Kumagai, M. Miyazaki and S.-I. Nishimura, *Tetrahedron Lett.*, 2001, **42**, 1953–1956.
20 I. Matsuo, M. Isomura and K. Ajisaka, *J. Carbohydr. Chem.*, 1999, **18**, 841–850.
21 R.-Z. Li, H. Tang, L. Wan, X. Zhang, Z. Fu, J. Liu, S. Yang, D. Jia and D. Niu, *Chem*, 2017, **3**, 834–845.
22 H. Xu, Y. Lu, Y. Zhou, B. Ren, Y. Pei, H. Dong and Z. Pei, *Adv. Synth. Catal.*, 2014, **356**, 1735–1740.
23 M. Giordano and A. Iadonisi, *J. Org. Chem.*, 2014, **79**, 213–222.
24 L. Chan and M. S. Taylor, *Org. Lett.*, 2011, **13**, 3090–3093.
25 B. Ren, N. Yan and L. Gan, *RSC Adv.*, 2017, **7**, 46257–46262.
26 B. Ren, J. Lv, Y. Zhang, J. Tian and H. Dong, *ChemCatChem*, 2017, **9**, 950–953.
27 B. Ren, O. Ramström, Q. Zhang, J. Ge and H. Dong, *Chem. – Eur. J.*, 2016, **22**, 2481–2486.
28 H. Vankayalapati and G. Singh, *J. Chem. Soc., Perkin Trans. 1*, 2000, 2187–2193.
29 A. G. Gerbst, V. B. Krylov, D. Z. Vinnitskiy, A. S. Dmitrenok, A. S. Shashkov and N. E. Nifantiev, *Carbohydr. Res.*, 2015, **417**, 1–10.
30 V. B. Krylov, D. A. Argunov, A. S. Solovev, M. I. Petruk, A. G. Gerbst, A. S. Dmitrenok, A. S. Shashkov, J.-P. Latgé and N. E. Nifantiev, *Org. Biomol. Chem.*, 2018, **16**, 1188–1199.
31 G. M. Lipkind, A. S. Shashkov, N. E. Nifant'ev and N. K. Kochetkov, *Carbohydr. Res.*, 1992, **237**, 11–22.
32 N. K. Kochetkov, G. M. Lipkind, A. S. Shashkov and N. E. Nifant'ev, *Carbohydr. Res.*, 1990, **221**, 145–168.
33 F. Neese, *Wiley Interdiscip. Rev.: Comput. Mol. Sci.*, 2012, **2**, 73–78.

34 A. G. Gerbst, V. B. Krylov, D. A. Argunov, M. I. Petruk, A. S. Solovev, A. S. Dmitrenok and N. E. Nifantiev, *Beilstein J. Org. Chem.*, 2019, **15**, 685–694.
35 F. Jensen, *Theor. Chem. Acc.*, 2010, **126**, 371–382.
36 H. A. Taha, M. R. Richards and T. L. Lowary, *Chem. Rev.*, 2013, **113**, 1851–1876.
37 M. R. Richards, Y. Bai and T. L. Lowary, *Carbohydr. Res.*, 2013, **374**, 103–114.
38 A. G. Gerbst, V. B. Krylov and N. E. Nifantiev, *Carbohydr. Chem.*, 2021, **44**, 151–169.
39 F. Weigend and R. Ahlrichs, *Phys. Chem. Chem. Phys.*, 2005, **7**, 3297–3305.
40 A. Hellweg, C. Hättig, S. Höfener and W. Klopper, *Theor. Chem. Acc.*, 2007, **117**, 587–597.
41 C. A. Stortz and A. S. Cerezo, *Carbohydr. Res.*, 2002, **337**, 1861–1871.
42 K. Gaweda and W. Plazinski, *Eur. J. Org. Chem.*, 2020, 674–679.
43 B. Coxon, *Adv. Carbohydr. Chem. Biochem.*, 2009, **62**, 17–82.
44 V. B. Krylov and N. E. Nifantiev, *Curr. Top. Microbiol. Immunol.*, 2020, **425**, 1–16.
45 S. S. W. Wong, V. B. Krylov, D. A. Argunov, A. A. Karelin, J.-P. Bouchara, T. Fontaine, J.-P. Latgé and N. E. Nifantiev, *mSphere*, 2020, **5**, e00688-19.
46 V. B. Krylov, A. S. Solovev, D. A. Argunov, J.-P. Latgé and N. E. Nifantiev, *Heliyon*, 2019, **5**, e01173.
47 D. A. Argunov, V. B. Krylov and N. E. Nifantiev, *Org. Biomol. Chem.*, 2015, **13**, 3255–3267.
48 B. S. Komarova, M. V. Orekhova, Y. E. Tsvetkov, R. Beau, V. Aimanianda, J.-P. Latgé and N. E. Nifantiev, *Chem. – Eur. J.*, 2015, **21**, 1029–1035.
49 B. S. Komarova, S. S. W. Wong, M. V. Orekhova, Y. E. Tsvetkov, V. B. Krylov, A. Beauvais, J.-P. Bouchara, J. F. Kearney, V. Aimanianda, J.-P. Latgé and N. E. Nifantiev, *J. Org. Chem.*, 2018, **83**, 12965–12976.
50 E. D. Kazakova, D. V. Yashunsky, V. B. Krylov, J.-P. Bouchara, M. Cornet, I. Valsecchi, T. Fontaine, J.-P. Latge and N. E. Nifantiev, *J. Am. Chem. Soc.*, 2020, **142**, 1175–1179.

Organic & Biomolecular Chemistry

PAPER

View Article Online
View Journal

Cite this: DOI: 10.1039/c5ob02040a

The synthesis of heterosaccharides related to the fucoidan from *Chordaria flagelliformis* bearing an α-L-fucofuranosyl unit†

Dmitry Z. Vinnitskiy, Vadim B. Krylov, Nadezhda E. Ustyuzhanina, Andrey S. Dmitrenok and Nikolay E. Nifantiev*

Received 30th September 2015,
Accepted 26th October 2015

DOI: 10.1039/c5ob02040a

www.rsc.org/obc

Sulfated polysaccharides, fucoidans, from brown algae are built up mainly of α-L-fucopyranosyl units and form a group of natural biopolymers with a wide spectrum of biological activities. Systematic synthesis of oligosaccharides representing fucoidans' fragments gives molecular probes for detecting pharmacophores within fucoidan polysaccharide chains. Recently, it was discovered that the fucoidan from brown seaweed *Chordaria flagelliformis* contains not only α-L-fucopyranosyl units but also α-L-fucofuranosyl ones. To establish the influence of the unusual α-L-fucofuranose residue on the biological activity and conformational properties of fucoidans, the synthesis of selectively *O*-sulfated pentasaccharides, which represent the main repeating unit of the fucoidan from *C. flagelliformis*, was performed. The features of the synthesis were the use of the pyranoside-*into*-furanoside rearrangement to prepare the fucofuranoside precursor and remote stereocontrolling participation of *O*-acyl groups to manage stereoselective α-bond formation in glycosylation reactions.

Introduction

Sulfated polysaccharides, fucoidans, from brown seaweeds exhibit different types of biological activities including anticoagulant, antithrombotic, anti-inflammatory and antiangiogenic.[1–6] Fucoidan chains are built up mainly of sulfated α-L-fucopyranoside residues, but the fine structure of these biopolymers varies depending on the parent seaweed species.[2,4,5] The types of glycoside bonds between monosaccharide units, the degree and pattern of *O*-sulfation, and the presence of branches and non-fucose components were shown to influence the biological effects of fucoidans.[2,6,7]

To establish the structure–activity relationship within the fucoidans, we perform the systematic synthesis of oligosaccharides related to these biopolymers originated from different brown seaweed species. In addition to a variety of unsulfated[8] as well as selectively[9–11] per-*O*-sulfated[12] homofucooligosaccharides, di- and trisaccharides bearing an α-D-glucuronic acid residue[13] were also prepared.

Recently, it was discovered that the fucoidan from brown seaweed *Chordaria flagelliformis* contains not only α-L-fucopyranosyl units but also α-L-fucofuranosyl ones.[14] This fucoidan contains an α-(1→3)-linked polyfucopyranoside backbone where one third of the fucopyranosyl residues bear (1→2)-linked α-D-glucuronic acid substituents and a half of them hold a (1→4)-linked α-L-fucofuranosyl residue (Fig. 1A). The pattern of anti-inflammatory and anticoagulant activities[15] of this fucoidan dramatically differs from the activities of structurally related fucoidans (*e.g.* the fucoidans from the seaweed *Cladosiphon okamuranus*) but not containing a fucofuranosyl side unit. This difference may be attributed to the presence of the fucofuranosyl residue.

The biological role of specific fucoidan fragments cannot be established by using these biopolymers due to their structural irregularity, whereas the synthetic oligosaccharides with a strictly defined structure could be considered as appropriate tools for this purpose. Herewith we report the synthesis of tetra- (**1**, **2**) and pentasaccharides **3**, **4** related to the branch points of the fucoidan from the seaweed *C. flagelliformis*[14] as the models for further biological, NMR and conformational studies of the fucoidan from *C. flagelliformis*.

Laboratory of Glycoconjugate Chemistry, N.D. Zelinsky Institute of Organic Chemistry, Russian Academy of Sciences, Leninsky prospect 47, 119991 Moscow, Russian Federation. E-mail: nen@ioc.ac.ru; Fax: (+) 7-499-135-87-84

†Electronic supplementary information (ESI) available: Characterization data, NMR and HRMS spectra. See DOI: 10.1039/c5ob02040a

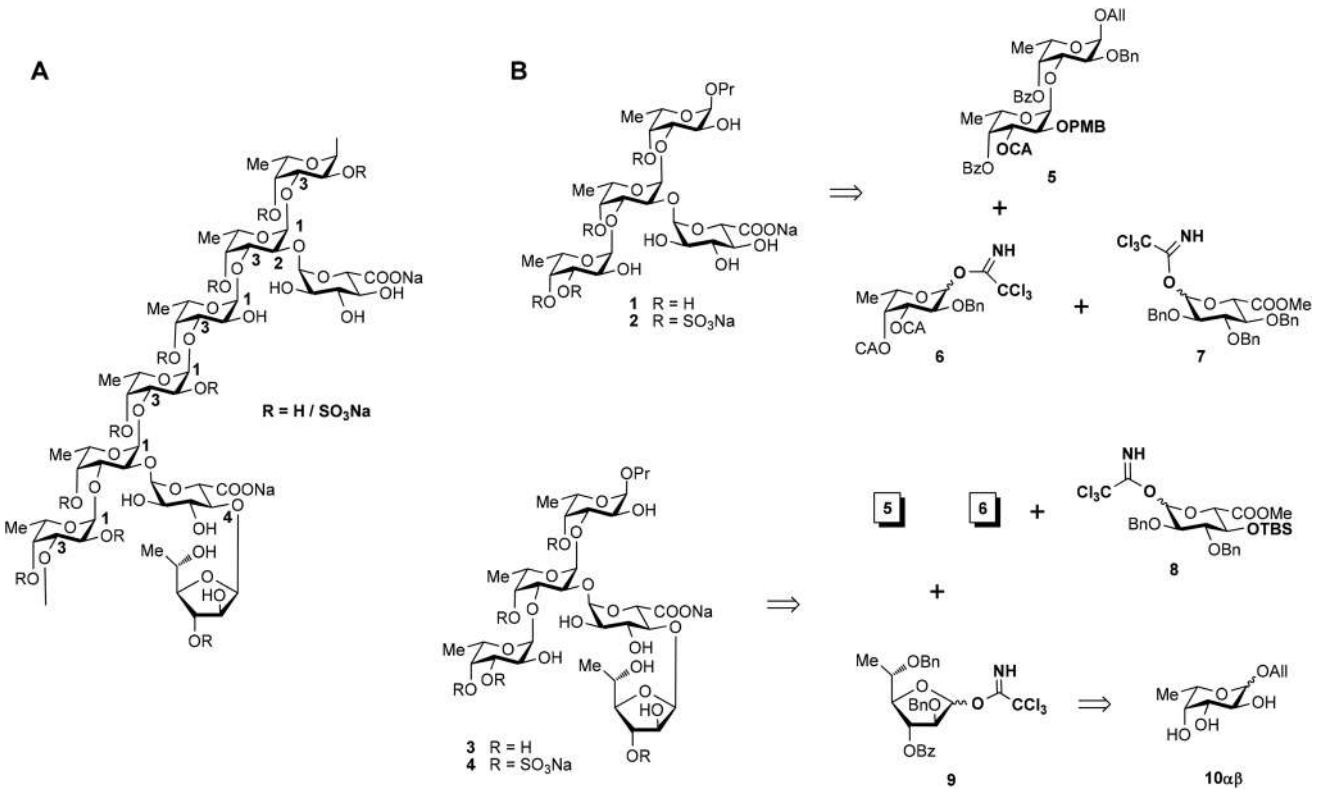

Fig. 1 (A) Tentative structure of fucoidan from the seaweed *C. flagelliformis*;[14] (B) target oligosaccharides **1–4** related to branched fragments of this fucoidan and retrosynthetic analysis of their structures which revealed synthetic blocks **5–9**.

Results and discussion

The starting blocks **5–9** for the preparation of target oligosaccharides **1–4** were selected based on the results of the retrosynthetic analyses shown in Fig. 1B. They suggest the use of the pyranoside-*into*-furanoside rearrangement[16–18] as a way to fucofuranosyl donor **9**. The blocks **6**[19] and **7**[20] were prepared according to the described synthetic protocols.

The synthesis of disaccharide glycosyl acceptor **5** was performed starting from allyl α-L-fucopyranoside **10α** which was first transformed into acceptor **11** using a one pot three-step process according to the published procedure.[10] A similar one pot reaction sequence followed by chloroacetylation was applied for the preparation of selectively protected allyl fucoside **12**. Its deallylation followed by imidate formation gave the donor **13**. TMSOTf-promoted coupling of **13** with acceptor **11** gave stereospecifically α-(1→3)-linked disaccharide **5** in an excellent yield of 95% (Scheme 1). The configuration of the formed bond was confirmed by the characteristic $J_{1,2}$ coupling constant value (3.5 Hz).

The synthesis of glucuronosyl donor **8** (Scheme 2) was performed starting from monosaccharide **14**[16] by its silylation (**14**→**15**), deallylation and imidate formation (**15**→**8**).

To assemble the target tetrasaccharides **1** and **2** the *p*-methoxybenzyl group in difucoside **5** was removed by acidic hydrolysis (transformation **5**→**16** shown in Scheme 3) and thus the

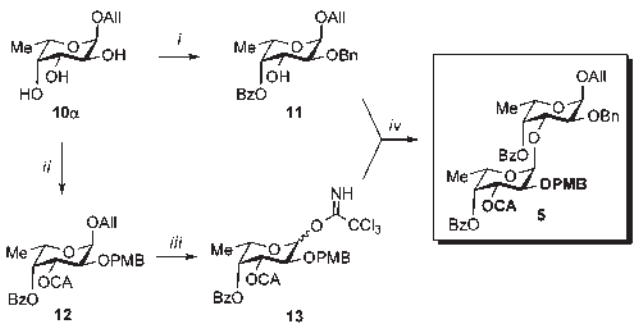

Scheme 1 Synthesis of disaccharide block **5**. Reagents and conditions: (i): (1) $PhC(OMe)_3$, CSA, DMF, rt, 2 h; (2) NaH (60%), BnBr, 0 °C, 2 h; (3) AcOH (80% aq.), rt, 20 min, 85%; (ii): (1) $PhC(OMe)_3$, CSA, DMF, rt, 2 h; (2) NaH (60%), PMBCl, Bu_4NI, 0 °C, 2 h; (3) AcOH (80% aq.), rt, 20 min; (4) CACl, Py, rt, 2 h; 79%; (iii): (1) $PdCl_2$, MeOH, rt, 1 h; (2) CCl_3CN, Cs_2CO_3, rt, 3 h, 76%; (iv): TMSOTf, CH_2Cl_2, −30 °C, 15 min, 95%.

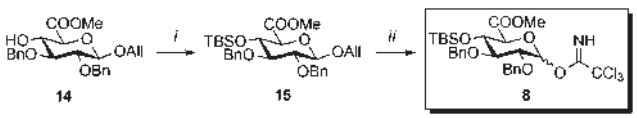

Scheme 2 Synthesis of synthetic block **8**. Reagents and conditions: (i): TBSCl, imidazole, rt, overnight, 94%; (ii): (1) $PdCl_2$, MeOH, rt, 1 h; (2) CCl_3CN, Cs_2CO_3, rt, 3 h, 72%.

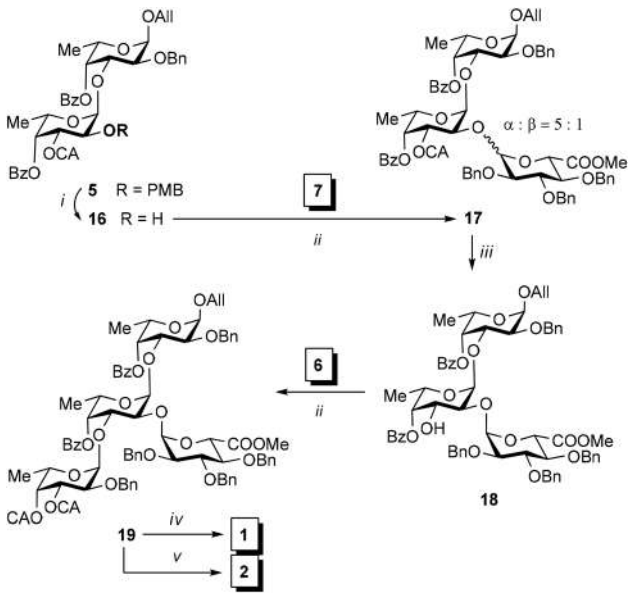

Scheme 3 Synthesis of the target tetrasaccharides **1** and **2**. Reagents and conditions: (i): TFA (90% aq.), CH_2Cl_2, rt, 10 min, 96%; (ii): TMSOTf, CH_2Cl_2, −30 °C, 15 min, 78% for **17**, 68% for **19**; (iii): $NH_2C(S)NH_2$, 2,4,6-collidine, MeOH, 65 °C, 24 h, 80%; (iv): (1) H_2, Pd/C, rt, 1 h; (2) NaOH 2N (aq.), MeOH, rt, 24 h, 91%; (v): (1) NaOH 2N(aq.), THF, MeOH, 65 °C, 10 h; (2) Py·SO_3, DMF, 40 °C, 3 h; (3) H_2, Pd/C, rt, 12 h, 81%.

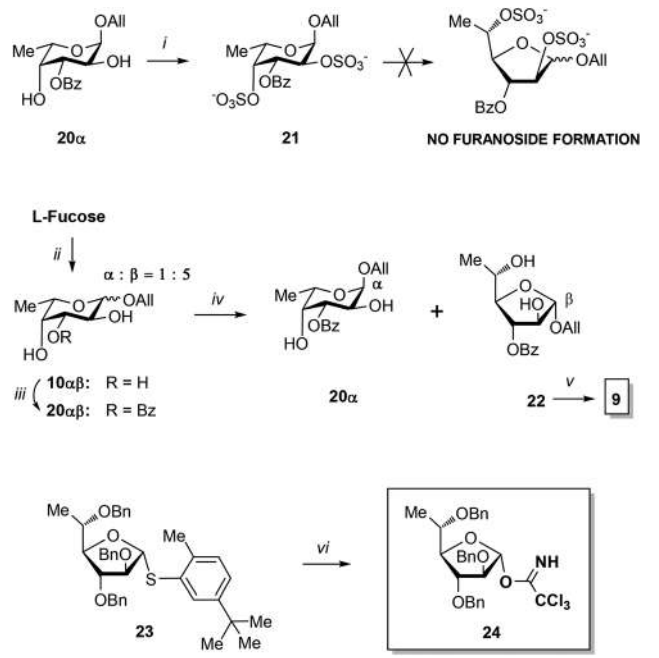

Scheme 4 Synthesis of block **9**. Reagents and conditions: (i): (1) Py·SO_3, HSO_3Cl, DMF, rt, 48 h; (2) $NaHCO_3$(aq), rt, 15 min; (ii): AlBr, NaOH, H_2O, rt, 24 h, 91%; (iii): BzCl, (i-Pr)$_2$NEt, 2-APB, rt, 1 h, 95% (iv): (1) Py·SO_3, HSO_3Cl, DMF, rt, 48 h; (2) $NaHCO_3$(aq), rt, 15 min; (3) IR-120(H^+), DMF–dioxane, 60 °C, 30 min, 66% for **22**, 13% for **20α**; (v): (1) BnBr, Ag_2O, rt, overnight; (2) $PdCl_2$, MeOH, rt, 1 h; (3) CCl_3CN, DBU, CH_2Cl_2, −30 °C, 2 h; (vi): (1) NBS, H_2O–acetone, 0 °C, 10 min; (2) CCl_3CN, DBU, CH_2Cl_2, −30 °C, 2 h, 72%.

liberated OH-group at C-2 was glycosylated by glucuronosyl donor **7** to give the trisaccharide product **17** as a 5 : 1 mixture of the corresponding α- and β-isomers this was assessed by integration of H-6′ signals in ^{1}H NMR spectra. Anomeric configurations of GlcA units were confirmed by the characteristic $J_{1,2}$ coupling constant values (3.9 Hz for α- and 7.6 Hz for the β-isomer). An individual α-isomer was obtained as compound **18** after dechloroacetylation of **17**.

Fucosylation of the acceptor **18** by the donor **6** in the presence of TMSOTf proceeded smoothly and gave the α-linked tetrasaccharide **19** as an only formed product. Configuration of the formed bond was confirmed by the characteristic $J_{1,2}$ coupling constant value (3.7 Hz). Its debenzylation by catalytic hydrogenolysis was accompanied by reduction of the allyl group into a propyl one; following saponification the target tetrasaccharide **1** was obtained. For the synthesis of selectively sulfated tetrasaccharide **2**, the acyl protections in precursor **19** were removed and thus the liberated OH-groups were sulfated by the complex Py·SO_3 in DMF. Following debenzylation and reduction of the allyl group into propyl one gave the target tetrasaccharide **2**.

The synthetic methods for preparation of selectively protected furanosides, in general, are more complicated than those for pyranosides. However, different innovative and facile approaches have intensively evolved nowadays.[21–25] Previously we developed a method for synthesis of furanoside **9** employing the novel pyranoside-into-furanoside rearrangement.[16] The reported[16] synthesis of donor **9** was started from the β-isomer of fucopyranoside **10**, however its preparation is multistep and laborious due to the necessity of difficult chromatographic separations. To optimize the synthesis of the block **9**, we tried to prepare it from easily available α-fucopyranoside **20α** (Scheme 4)[26] by its pyranoside-*into*-furanoside rearrangement.[16–18] But this reaction led only to per-*O*-sulfated pyranoside **21** but not to the desired furanoside product. Even elongation of the reaction time from 24 h up to 144 h did not allow us to detect any traces of furanoside. Thus, only the β-isomer **10β** is applicable for the preparation of fucofuranosyl donor **9**.

To synthesize the required **10β**, allylation of L-fucose with allyl bromide in the presence of NaOH was studied. It gave an anomeric mixture of allyl fucopyranosides **10αβ** (Scheme 4) with domination of the target β-isomer (α : β = 1 : 5). This mixture was subjected to regioselective 3-*O*-benzoylation,[27] pyranoside-*into*-furanoside rearrangement and solvolytic de-*O*-sulfation to give the non-rearranged α-pyranoside **20α** and β-furanoside **22**, which were easily separated by column chromatography. The formation of the furanoside ring was confirmed by ^{1}H and ^{13}C NMR spectra which corresponded to previously reported data for monosaccharide **22**.[16] Further dibenzylation of diol **22** followed by deallylation and imidate formation gave the fucofuranosyl donor **9**. Fucofuranosyl donor **24** was synthesized from thioglycoside **23**[28] by bromination

with NBS followed by hydrolysis and imidate formation (Scheme 4).

In spite of the recent progress in selective 1,2-*cis* furanosylation,[29–31] these methods are still insufficiently developed, while stereoselective α-L-fucofuranosylation has not been reported at all. To assess the possibility of the use of the stereodirecting effect of a remote *O*-acyl group to manage selective α-L-fucofuranosylation in the synthesis of target pentasaccharides **3** and **4**, we studied model fucofuranosylations of acceptor **14** by tri-*O*-benzylated donor **24** and selectively protected donor **9**[14] bearing an *O*-benzoyl group at O-3. Subsequent to the concept of stereodirecting participation of remote *O*-acyl groups in glycosylation reactions,[11,31–33] it was possible to expect the formation from donor **9** of the stabilized cation **A** (Scheme 5) that would be attacked by a nucleophile predominantly from the α-side and of the non-stabilized cation **B** from per-*O*-benzylated donor **21** whose nucleophile attack is possible from both α- and β-sides.

As expected, glycosylation of acceptor **14** by donor **9** with the stereodirecting 3-*O*-benzoyl group resulted in the formation of a mixture of disaccharides **25** with domination of the α-isomer (α : β = 4 : 1), while glycosylation with tri-*O*-benzylated donor **24** gave a mixture of α- and β-isomers **26** in a ratio of 1 : 2 as it was assessed by integration of H-6′ signals in their ^{1}H NMR spectra. Anomeric configurations were confirmed by characteristic chemical shifts of C-1′ in ^{13}C NMR spectra (*δ* 99.8 for α- and 107.1 for the β-isomer). This result proved the possibility of stereodirecting participation of the remote 3-*O*-benzoyl group and allows us to consider donor **9** as a promising building block for α-fucofuranosylation in the synthesis of target pentasaccharides **3** and **4**.

To prepare the pentasaccharides **3** and **4**, the coupling of the disaccharide **16** and the monosaccharide **8** was performed first and gave a mixture **27** of isomeric α- and β-linked trisaccharides in a ratio of 4 : 1 (Scheme 6) that was confirmed by integration of OMe signals in ^{1}H NMR spectra. An individual α-isomer was isolated in the form of monohydroxy derivative **28** after removal of the silyl group with aq. HF. The acceptor **28** was glycosylated by fucofuranosyl donor **9** to give a mixture of α- and β-linked tetrasaccharides in a ratio of 10 : 1. This result was even better than that of model glycosylation **9** + **14** (see Scheme 5). The individual α-isomer **29** was isolated in a yield of 79% and then subjected to de-*O*-chloroacetylation (**29**→**30**) followed by 3′-*O*-fucopyranosylation by donor **6** to give pentasaccharide **31**. Removal of all the protecting groups and reduction of the allyl group into a propyl one gave the pentasaccharide **3**. Alternatively, saponification of **31** by LiOH and Bu_4NOH in THF followed by *O*-sulfation and hydrogenolysis afforded the required selectively *O*-sulfated pentasaccharide **4**.

The structures of thus synthesized oligosaccharides **1–4** were assessed based on NMR spectroscopy and mass-spectrometry data. A complete assignment of ^{1}H and ^{13}C NMR spectra was performed using the combination of 2D experiments, including COSY, HSQC, HMBC, TOCSY, and ROESY (see Experimental and Table 1). The chemical shifts of central residues of non-sulfated oligosaccharides **1** and **3** were in good agreement with the published[14] data for the de-*O*-sulfated fucoidan from *C. flageliformis*.

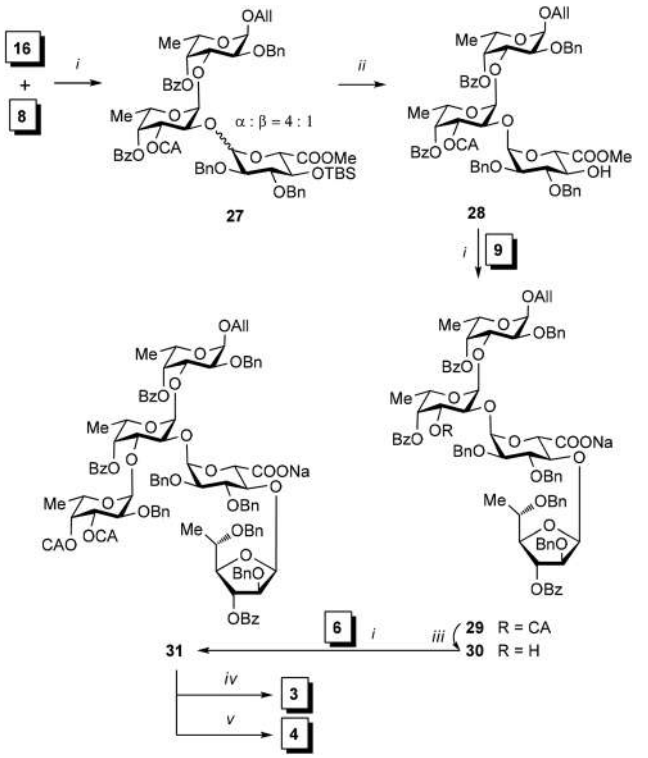

Scheme 6 Preparation of the target pentasaccharides **3–4**. Reagents and conditions: (i): TMSOTf, CH_2Cl_2, −30 °C, 15 min, 87% for **27**, 79% for **29**, 86% for **31**; (ii): HF (40% aq.), CH_3CN, 40 °C, 2 h, 77%; (iii): $NH_2C(S)NH_2$, 2,4,6-collidine, MeOH, 65 °C, 24 h, 80%; (iv): (1) H_2, Pd/C, rt, 1 h; (2) NaOH 2N(aq.), MeOH, rt, 24 h, 82%; (v): (1) LiOH 2N (aq.), THF, rt, 20 h; (2) Bu_4NOH, THF, rt, 48 h; (3) Py·SO_3, DMF, 40 °C, 3 h; (4) H_2, Pd/C, rt, 12 h, 76%.

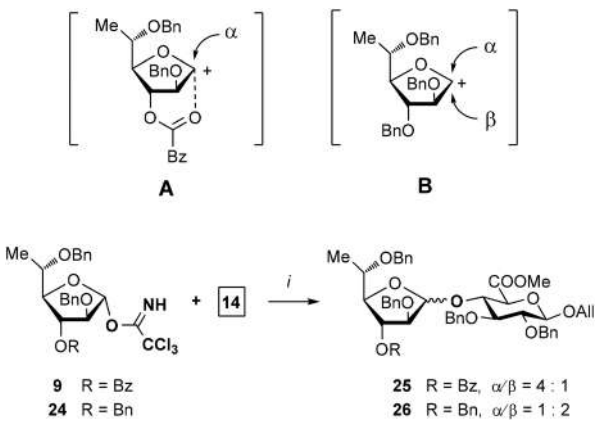

Scheme 5 Model glycosylations by fucofuranosyl donors **9** and **24**. Reagents and conditions: (i): TMSOTf, CH_2Cl_2, −30 °C, 15 min, 52% for 25, 60% for 26.

Table 1 ^{1}H and ^{13}C NMR chemical shifts for oligosaccharides **1**, **3** and desulfated fucoidan from *C. flagelliformis* (DSF)

		NMR chemical shift (δ)					
N	Residue	C-1/H-1	C-2/H-2	C-3/H-3	C-4/H-4	C-5/H-5	C-6/H-6
1	→2,3)-α-L-Fuc*p*-(1→3	95.32/5.15	71.61/4.19	74.10/4.29	68.28/4.12	67.62/4.29	16.52/1.24
3	→2,3)-α-L-Fuc*p*-(1→3	95.47/5.21	72.35/4.22	73.91/4.34	68.30/4.18	68.22/4.49	16.53/1.28
DSF	→2,3)-α-L-Fuc*p*-(1→3	95.9/5.15	71.8/4.19	73.9/4.29	68.2/4.14	67.8/4.34	16.7/1.20
1	α-D-GlcA*p*-(1→2	100.55/5.29	72.30/3.59	74.10/3.73	73.05/3.52	74.02/3.97	176.3/n/a
DSF	α-D-GlcA*p*-(1→2	100.8/5.31	72.2/3.62	74.1/3.71	72.7/3.54	73.5/4.00	176.0/—
3	→4)-α-D-GlcA*p*-(1→2	100.66/5.32	72.03/3.71	72.99/3.86	81.69/3.63	73.24/4.14	176.89/—
DSF	→4)-α-D-GlcA*p*-(1→2	100.8/5.29	72.7/3.70	73.1/3.80	81.4/3.60	72.9/4.10	176.0/—
3	α-L-Fuc*f*-(1→4	103.38/5.10	77.59/4.14	75.80/4.18	86.21/3.71	68.36/3.99	19.74/1.30
DSF	α-L-Fuc*f*-(1→4	103.5/5.02	77.7/4.08	75.9/4.08	86.2/3.63	68.2/3.91	19.8/1.22

Conclusions

The stereoselective synthesis of the oligosaccharides related to the branch points of the fucoidan from the seaweed *C. flagelliformis* has been performed by stepwise attachment of the corresponding monosaccharide residues to the starting disaccharide acceptor. The pyranoside-*into*-furanoside rearrangement was applied to the preparation of the fucofuranosyl donor. Stereodirecting participation of the remote *O*-acyl group was used to manage α-stereoselectivity of both fucopyranosylation and fucofuranosylation. Selectively *O*-sulfated oligosaccharides **2** and **4** represent useful models for investigation of the structure–activity relationship within fucoidan-related substances. The results of their biological and conformational studies will be published elsewhere.

Experimental

General methods

Commercial chemicals were used without purification unless mentioned. All solvents were distilled and dried if necessary according to standard procedures[34] or purchased dry (DMF, THF, CH_3CN, Acrus). All reactions involving air- or moisture-sensitive reagents were carried out using dry solvents under an Ar atmosphere. Thin-layer chromatography (TLC) was carried out on aluminum sheets coated with silica gel 60 F_{254} (Merck). TLC plates were inspected by UV light (λ = 254 nm) and developed by treatment with a mixture of 15% H_3PO_4 and orcinol (1.8 g l^{-1}) in EtOH/H_2O (95 : 5, v/v) followed by heating. Silica gel column chromatography was performed with Silica Gel 60 (40–63 μm, E. Merck). Solvents for column chromatography and thin layer chromatography (TLC) are listed in volume to volume ratios. Gel-filtration was performed on a Sephadex G-15 column (400 × 17 mm) by elution with water at a flow rate of 1.5 mL min^{-1}.

NMR spectra were recorded on Bruker AMX400 (400 MHz), Bruker DRX-500 (500 MHz), or Bruker AV600 (600 MHz) spectrometers equipped with 5 mm pulsed-field-gradient (PFG) probes at temperatures denoted in the spectra in the ESI.† Microtubes (Shigemi, Inc.) were used for sensitivity enhancement of small concentration probes. The resonance assignment in ^{1}H and ^{13}C NMR spectra was performed using various 2D–experiments (*e.g.*, COSY, NOESY, HSQC, HMBC, TOCSY, HSQC-TOCSY, and ROESY). Chemical shifts are reported in ppm referenced to the solvent residual peaks as a standard (δ 7.27 for chloroform or δ 3.31 methanol for ^{1}H NMR and δ 77.0 and δ 49.0 for ^{13}C NMR).

Optical rotations were measured using a JASCO P-2000 polarimeter at ambient temperature (22–25 °C).

High-resolution mass spectra (HRMS) were measured on a Bruker micrOTOF II instrument using electrospray ionization (ESI).[35] The measurements were performed in a positive ion mode (interface capillary voltage −4500 V) or in a negative ion mode (3200 V); mass range from *m*/*z* 50 to *m*/*z* 3000 Da; external or internal calibration was made with Electrospray Calibrant Solution (Fluka). A syringe injection was used for solutions in a mixture of acetonitrile and water (50 : 50 v/v, flow rate 3 μL min^{-1}). Nitrogen was applied as a dry gas; interface temperature was set at 180 °C.

Allyl 2-*O*-*p*-methoxybenzyl-3-*O*-chloroacetyl-4-*O*-benzoyl-α-L-fucopyranoside (12). Trimethyl orthobenzoate (1.3 mL, 7.35 mmol) and CSA (110 mg, 0.47 mmol) were added to a solution of allyl α-L-fucoside **10α** (1.00 g, 4.9 mmol) in DMF (10 mL). After 2 h the starting material disappeared (TLC control) and then the solution was cooled to 0 °C and 60% NaH (600 mg, 14.7 mmol) was added. The mixture was stirred at rt for 1 h, then cooled to 0 °C and *p*-methoxybenzyl chloride (2.00 mL, 14.7 mmol) and Bu_4NI (300 mg, 0.82 mmol) were added. After 1 h, ice-cold water (100 mL) was added to the reaction mixture and the suspension was extracted with CH_2Cl_2 (3 × 100 mL) and the combined organic layers were dried (Na_2SO_4) and concentrated. The resulting residue was dissolved in CH_2Cl_2 (5 mL) and 80% aq. AcOH (2 mL) was added. The mixture was kept at rt for 20 min, then H_2O (100 mL) was added and the mixture was extracted with CH_2Cl_2 (3 × 100 mL). The organic layers were concentrated and purified by flash column chromatography (silica gel, toluene–EtOAc, 2 : 1). The intermediate was dissolved in anhydrous CH_2Cl_2 (15 mL) and Py (1.2 mL, 14.7 mmol) and chloroacetyl chloride (0.6 mL, 7.35 mmol) were added. After 1 h, the mixture was diluted with $CHCl_3$ and washed successively with

1 M HCl, satd $NaHCO_3$, and water. The solvent was evaporated and the residue was chromatographed (silica gel, hexane–EtOAc, 6 : 1→3 : 1) to give the monosaccharide **12** (1.95 g, 79%) as a yellowish foam. R_f = 0.41 (hexane–EtOAc 3 : 1). $[\alpha]_D$ = −122° (*c* = 1, EtOAc). ^{1}H NMR (600 MHz, $CDCl_3$): δ 8.10–6.80 (m, 9H, 2 × Ar), 5.93–5.60 (m, 1H, CH_2CH═CH_2), 5.54–5.50 (m, 2H, H-3, H-4), 5.40–5.35 (m, 1H, CH_2CH═CHH'), 5.27–5.25 (m, 1H, CH_2CH═CHH'), 4.93 (d, $J_{1,2}$ = 3.6 Hz, 1H, H-1), 4.64 (d, 1H, *J* = 12.0 Hz, CHH'Ar), 4.56 (d, *J* = 12.0 Hz, 1H, CHH'Ar), 4.28 (q, *J* = 6.6 Hz, 1H, H-5), 4.22 (dd, *J* = 6.3 Hz, *J* = 13 Hz, 1H, $OCHH'CH$), 4.08 (dd, *J* = 6.3 Hz, *J* = 13 Hz, 1H, $OCHH'CH$), 3.98 (dd, $J_{1,2}$ = 3.7 Hz, $J_{2,3}$ = 10.3 Hz, 1H, H-2), 3.93 (m, 2H, $C(O)CH_2Cl$), 3.80 (s, 3H, OMe), 1.18 (d, $J_{5,6}$ = 6.6 Hz, 3H, H-6). ^{13}C NMR (150 MHz, $CDCl_3$): δ 166.5 (*C*(O)Ph), 166.2 ($C(O)CH_2Cl$), 133.7 (CH_2CH═CH_2), 133.3 (Ar), 129.8 (Ar), 129.6 (Ar), 128.5 (Ar), 118.0 (CH_2CH═CH_2), 113.8 (Ar), 96.4 (C-1), 72.6 (CH_2Ar), 72.5 (C-2), 72.3 (C-3), 71.9 (C-4), 68.7 (OCH_2CH), 64.3 (C-5), 55.2 (OMe), 40.6 ($C(O)CH_2Cl$), 15.9 (C-6). HRMS (ESI): Calcd *m*/*z* for $[M + Na]^+$ $C_{26}H_{29}ClO_8$ 527.1443, found 527.1444.

General procedure A, allyl cleavage and preparation of trichloroacetimidates

To a stirred solution of a starting allyl glycoside (1 mmol) in anhydrous MeOH (5 mL) $PdCl_2$ (71 mg, 0.4 mmol) was added and the mixture was vigorously stirred for 1 h. Then the mixture was filtered through a Celite layer, washed with MeOH. The filtrate was neutralized with Et_3N and evaporated *in vacuo*. The residue was purified by chromatography (silica gel, eluent: toluene/EtOAc = 5 : 1→2 : 1). The resulting hemiacetal was dissolved in CH_2Cl_2 (8 mL), trichloroacetonitrile (0.5 mL, 5 mmol) and Cs_2CO_3 (977 mg, 3 mmol) were added and the mixture was vigorously stirred at 20 °C for 3 h. Then the mixture was filtered through a Celite layer, washed with EtOAc and the filtrate was concentrated *in vacuo.* The residue was purified by chromatography on silica gel passivated by Et_3N (eluent: toluene/EtOAc = 20 : 1→10 : 1) to give a trichloroacetimidate as a white foam.

2-*O*-*p*-Methoxybenzyl-3-*O*-chloroacetyl-4-*O*-benzoyl-α,β-L-fucopyranoside trichloroacetimidates (13). Allyl fucoside **12** (1.44 g, 2.85 mmol) was treated according to the general procedure A to give trichloroacetimidates **13** (1.32 g, 76%, α : β = 1 : 2). For analytical purpose, the anomers were separated and characterized individually. For further glycosylation donor **13** was used as a mixture of α- and β-isomers.

For the α-isomer: R_f = 0.73 (hexane–EtOAc 2 : 1). ^{1}H NMR (600 MHz, $CDCl_3$): 8.57 (s, 1H, N*H*), 8.0–6.7 (9H, 2 × Ar), 6.47 (d, $J_{1,2}$ = 3.6 Hz, 1H, H-1), 5.55–5.51 (m, 1H, H-4), 5.44 (dd, $J_{2,3}$ = 10.5 Hz, $J_{3,4}$ = 3.3 Hz, 1H, H-3), 4.52 (m, 2H, CH_2Ar), 4.37 (q, *J* = 6.2 Hz, 1H, H-5), 4.08–4.04 (m, 1H, H-2), 3.85 (m, 2H, $C(O)CH_2Cl$), 3.69 (s, 3H, OMe), 1.14 (d, $J_{5,6}$ = 6.5 Hz, 3H, H-6). ^{13}C NMR (100 MHz, $CDCl_3$): δ 166.6 (*C*(O)Ph), 166.2 ($C(O)CH_2Cl$), 133.6 (Ar), 129.9 (Ar), 129.5 (Ar), 128.7 (Ar), 114.0 (Ar), 94.7 (C-1), 72.7 (CH_2Ar), 72.1 (C-3), 71.9 (C-2), 71.3 (C-4), 67.6 (C-5), 55.3 (OMe), 40.7 ($C(O)CH_2Cl$), 16.2 (C-6). Calcd *m*/*z* for $[M + Na]^+$ $C_{25}H_{25}Cl_4NO_8$ 630.0226, found 630.0233.

For the β-isomer: R_f = 0.55 (hexane–EtOAc 2 : 1). ^{1}H NMR (600 MHz, $CDCl_3$): δ 8.68 (s, 1H, N*H*), 8.0–6.7 (m, 9H, 2 × Ar), 5.80 (d, $J_{1,2}$ = 8.1 Hz, 1H, H-1), 5.40 (dd, $J_{3,4}$ = 3.5 Hz, $J_{4,5}$ = 0.9 Hz, 1H, H-4), 5.12 (dd, $J_{2,3}$ = 10.1 Hz, $J_{3,4}$ = 3.5 Hz, 1H, H-3), 4.74 (d, *J* = 10.9 Hz, 1H, CHH'Ar), 4.51 (1H, d, *J* = 10.9 Hz, CHH'Ar), 4.02–3.97 (m, 1H, H-5), 3.91 (dd, $J_{1,2}$ = 8.1 Hz, $J_{2,3}$ = 10.1 Hz, 1H, H-2), 3.76 (m, 2H, $C(O)CH_2Cl$), 3.67 (s, 3H, OMe), 1.27 (d, $J_{5,6}$ = 6.4 Hz, 3H, H-6). ^{13}C NMR (100 MHz, $CDCl_3$): δ 166.6 (*C*(O)Ph), 166.3 ($C(O)CH_2Cl$), 133.6 (Ar), 130.0 (Ar), 129.7 (Ar), 128.7 (Ar), 113.9 (Ar), 98.4 (C-1), 75.0 (C-2), 74.8 (C-3, CH_2Ar), 70.9 (C-4), 70.3 (C-5), 55.3 (OMe), 40.5 ($C(O)CH_2Cl$), 16.2 (C-6). Calcd *m*/*z* for $[M + Na]^+$ $C_{25}H_{25}Cl_4NO_8$ 630.0226, found 630.0230.

General procedure B, glycosylation

To a mixture of a glycosyl donor (1.1 mmol), a glycosyl acceptor (1.0 mmol) and molecular sieves 4 Å (1.00 g) in anhydrous CH_2Cl_2 (10 mL) 0.1 M TMSOTf in CH_2Cl_2 (50 μL) was added at −30 °C under argon protection. The mixture was stirred for 15 min, then neutralized with Et_3N and evaporated. The resulting material was purified by chromatography (silica gel, eluent: toluene/EtOAc = 15 : 1→5 : 1) to give a glycosylation product.

Allyl 2-*O*-*p*-methoxybenzyl-3-*O*-chloroacetyl-4-*O*-benzoyl-α-L-fucopyranosyl-(1→3)-2-*O*-benzyl-4-*O*-benzoyl-α-L-fucopyranoside (5). Glycosylation of acceptor **11** (250 mg, 0.628 mmol) with donor **13** (420 mg, 0.692 mmol) as described in the general procedure B gave disaccharide **5** (505 mg, 95%) as a colorless syrup. R_f = 0.50 (hexane–EtOAc 3 : 1). $[\alpha]_D$ = −229° (*c* = 1, EtOAc). ^{1}H NMR (600 MHz, $CDCl_3$): 8.04 (d, *J* = 7.1 Hz, 2H, *o*-Bz), 7.97 (d, *J* = 7.1 Hz, 2H, *o*-Bz), 7.62 (t, *J* = 7.5 Hz, 1H, *p*-Bz), 7.57 (t, *J* = 7.4 Hz, 1H, *p*-Bz), 7.50–7.32 (m, 9H, 2 × Bz, Bn), 7.04 (2H, d, *J* = 8.6 Hz, *o*-MBn), 6.71 (2H, d, *J* = 8.6 Hz, *m*-MBn), 5.97–6.05 (1H, m, CH_2CH═CH_2), 5.68 (d, $J_{3,4}$ = 3.3 Hz, 1H, H-4 (Fuc)), 5.50 (dd, $J_{2,3}$ = 10.5 Hz, $J_{3,4}$ = 3.3 Hz, 1H, H-3 (Fuc′)), 5.41 (dd, *J* = 1.6 Hz, *J* = 17.2 Hz, 1H, CH_2CH═CHH'), 5.34 (d, $J_{1,2}$ = 3.5 Hz, 1H, H-1 (Fuc′)), 5.32 (1H, d, $J_{3,4}$ = 3.3 Hz, H-4 (Fuc′)), 5.28 (1H, dd, *J* = 1.3 Hz, *J* = 10.4 Hz, CH_2CH═CHH'), 5.06 (d, $J_{1,2}$ = 3.7 Hz, 1H, H-1 (Fuc)), 4.78 (m, 2H, CH_2Ph), 4.48 (q, *J* = 6.5 Hz, 1H, H-5 (Fuc′)) 4.44–4.39 (m, 2H, H-3 (Fuc), CHH'PhOMe), 4.28–4.23 (m, 2H, $OCHH'CH$, CHH'PhOMe), 4.21 (q, *J* = 6.5 Hz, 1H, H-5 (Fuc)), 4.13 (dd, *J* = 6.3 Hz, *J* = 13.1 Hz, 1H, $OCHH'CH$), 4.08 (dd, $J_{1,2}$ = 3.7 Hz, $J_{2,3}$ = 10.2 Hz, 1H, H-2 (Fuc)), 3.93 (dd, $J_{1,2}$ = 3.5 Hz, $J_{2,3}$ = 10.5 Hz, 1H, H-2 (Fuc′)), 3.79 (m, 2H, CH_2Cl), 3.77 (s, 3H, OMe), 1.20 (d, $J_{5,6}$ = 6.6 Hz, 3H, H-6 (Fuc)), 1.01 (d, $J_{5,6}$ = 6.5 Hz, 3H, H-6 (Fuc′)). ^{13}C NMR (150 MHz, $CDCl_3$): δ 166.5 (*C*(O)Ph), 166.4 (*C*(O)Ph), 166.2 ($C(O)CH_2Cl$), 159.1 (*p*-MBn), 138.0 (Bn), 134.0 (CH_2CH═CH_2), 133.2 (*p*-Bz), 133.0 (*p*-Bz), 127.9–130.0 (Ar), 117.7 (CH_2CH═CH_2), 113.5 (*m*-MBn), 96.2 (C-1 (Fuc)), 93.0 (C-1 (Fuc′)), 74.6 (C-2 (Fuc)), 72.3 (C-3 (Fuc′)), 72.0 (C-4 (Fuc′)), 71.9 (CH_2PhOMe), 71.7 (C-2 (Fuc′)), 70.5 (C-3 (Fuc)), 69.7 (C-4 (Fuc)), 68.5 (OCH_2CH), 65.0 (C-5 (Fuc)), 64.6 (C-5 (Fuc′)), 55.2 (OMe), 40.6 (CH_2Cl), 16.3 (C-6 (Fuc)), 15.9 (C-6 (Fuc′)). HRMS(ESI): Calcd *m*/*z* for $[M + Na]^+$ $C_{46}H_{49}ClO_{13}$ 867.2754, found 867.2745.

Methyl(allyl 2,3-di-*O*-benzyl-4-*O*-*tert*-butyldimethylsilyl β-D-glucopyranoside)uronate (15). Imidazole (350 mg, 5.15 mmol) and TBSCl (680 mg, 4.48 mmol) were added to a solution of methyl (allyl 2,3-di-*O*-benzyl-β-D-glucopyranoside)uronate **14** (0.96 g, 2.24 mmol) in dry DMF (10 mL) and the resulting mixture was stirred overnight. Then the reaction mixture was diluted with EtOAc (100 mL) and washed with aqueous $NaHCO_3$ (5%, 100 mL). The organic layer was dried (Na_2SO_4) and concentrated *in vacuo*. The residue was purified by chromatography (silica gel, eluent: hexane/EtOAc = 20 : 1) to give product **15** (1.14 g, 94%) as a colorless oil. R_f = 0.90 (hexane–EtOAc 3 : 1). $[\alpha]_D$ = 12° (*c* = 1, EtOAc). ^{1}H NMR (600 MHz, $CDCl_3$): δ 7.34–7.20 (m, 10H, 2 × Ph), 5.89–5.96 (m, 1H, CH_2CH=CH_2), 5.33 (d, *J* = 17.2 Hz, 1H, CH_2CH=CHH'), 5.21 (d, *J* = 11.1 Hz, 1H, CH_2CH=CHH'), 5.02 (d, *J* = 11.4 Hz, 1H, CHH'Ph), 4.93 (d, *J* = 10.7 Hz, 1H, CHH'Ph), 4.71 (d, *J* = 11.5 Hz, 1H, CHH'Ph), 4.62 (d, *J* = 10.8 Hz, 1H, CHH'Ph), 4.53 (d, $J_{1,2}$ = 7.7 Hz, 1H, H-1), 4.42 (dd, *J* = 5.0 Hz, *J* = 12.7 Hz, 1H, $OCHH'$CH), 4.12 (dd, *J* = 6.2 Hz, *J* = 12.9 Hz, 1H, $OCHH'$CH), 3.94 (t, *J* = 9.0 Hz, 1H, H-4), 3.85 (d, *J* = 9.3 Hz, 1H, H-5), 3.79 (s, 3H, OMe), 3.54 (t, *J* = 8.7 Hz, 1H, H-2), 3.47 (t, *J* = 8.7 Hz, 1H, H-3), 0.86 (s, 9H, $Si(CH_3)_2C(CH_3)_3$), 0.01 (6H, s, $Si(CH_3)_2C(CH_3)_3$). ^{13}C NMR (150 MHz, $CDCl_3$): δ 169.0 (C-6), 138.8 (Bn), 138.3 (Bn), 133.8 (CH_2CH=CH_2), 127.0–129.8 (2 × Ar), 117.6 (CH_2CH=CH_2), 102.9 (C-1), 84.0 (C-3), 82.2 (C-2), 76.7 (C-5), 75.0 (CH_2Ph), 74.7 (CH_2Ph), 72.3 (C-4), 70.5 (OCH_2CH), 52.3 (OMe), 25.8 ($SiC(CH_3)_3$), 18.0 ($SiC(CH_3)_3$), −3.9 ($Si(CH_3)(CH_3)^tBu$), −5.2 ($Si(CH_3)(CH_3)^tBu$). HRMS(ESI): Calcd *m*/*z* for $[M + Na]^+$ $C_{30}H_{42}O_7Si$ 565.2592, found 565.2587.

Methyl(2,3-di-*O*-benzyl-4-*O*-*tert*-butyldimethylsilyl α,β-D-glucopyranosyl)uronate trichloroacetimidates (8). Allyl glycoside **15** (1.14 g, 2.1 mmol) was treated according to the general procedure A to give trichloroacetimidates **8** (977 mg, 72%, α : β = 2 : 1). R_f = 0.55 (hexane–EtOAc 5 : 1). ^{1}H NMR (600 MHz, $CDCl_3$): δ 8.65 (s, 1H, N*H*, β), 8.56 (s, 1H, N*H*, α), 7.09–7.28 (m, 20H, 2 × Ar α, 2 × Ar β), 6.43 (d, $J_{1,2}$ = 2.9 Hz, 1H, H-1 α), 5.87 (d, $J_{1,2}$ = 7.4 Hz, 1H, H-1 β), 4.79–5.00 (m, 3H, CHH'Ph α, CH_2Ph β), 4.46–4.71 (m, 5H, CH_2Ph α, CHH'Ph α, CH_2Ph β), 4.24 (d, 1H, $J_{4,5}$ = 9.5 Hz, H-5 α), 3.99–4.10 (m, 2H, H-4 β, H-5 β), 3.88 (t, *J* = 8.8 Hz, 1H, H-4 α), 3.63–3.80 (m, 9H, H-2 β, H-2 α, H-3 α, OMe α, OMe β), 3.81 (t, *J* = 8.1 Hz, 1H, H-3 β), 0.77 (s, 9H, $Si(CH_3)_2C(CH_3)_3$ α), 0.76 (s, 9H, $Si(CH_3)_2C(CH_3)_3$ β), −0.06 (s, 6H, $Si(CH_3)_2C(CH_3)_3$ β), −0.08 (s, 6H, $Si(CH_3)_2C(CH_3)_3$ α). ^{13}C NMR (100 MHz, $CDCl_3$): δ 169.2 (C-6 α), 168.7 (C-6 β), 138.7 (Bn α), 138.5 (Bn β), 137.7 (Bn β), 137.6 (Bn α), 128.5–127.0 (2 × Ar α, 2 × Ar β), 97.9 (C-1 β), 93.9 (C-1 α), 84.0 (C-3 β), 80.6 (C-3 α), 80.4 (C-2 β), 79.4 (C-2 α), 76.8 (C-5 β), 75.1 (CH_2Ph α), 74.6 (C-5 α, CH_2Ph β), 74.4 (CH_2Ph β), 73.0 (CH_2Ph α), 71.9 (C-4, α), 71.8 (C-4 β), 52.5 (OMe, α), 52.4 (OMe β), 25.8 ($SiC(CH_3)_3$ β), 25.8 ($SiC(CH_3)_3$ α), 18.0 ($SiC(CH_3)_3$ α), 18.0 ($SiC(CH_3)_3$ β), −3.9 ($Si(CH_3)(CH_3)^tBu$ α), −4.0 ($Si(CH_3)(CH_3)^tBu$ β), −5.2 ($Si(CH_3)(CH_3)^tBu$ β), −5.2 ($Si(CH_3)(CH_3)^tBu$ α). HRMS (ESI): Calcd *m*/*z* for $[M + Na]^+$ $C_{29}H_{38}Cl_3NO_7Si$ 668.1375, found 668.1371.

Allyl 3-*O*-chloroacetyl-4-*O*-benzoyl-α-L-fucopyranosyl-(1→3)-2-*O*-benzyl-4-*O*-benzoyl-α-L-fucopyranoside (16). Aqueous TFA (90%, 0.8 mL) was added dropwise to a solution of disaccharide **5** (580 mg, 0.69 mmol) in CH_2Cl_2 (8 mL). The reaction mixture was stirred for 10 min, then diluted with toluene (30 mL) and concentrated. The residue was purified by chromatography (silica gel, eluent: hexane/EtOAc = 7 : 1→4 : 1) to give product **16** (480 mg, 96%) as a colorless oil. R_f = 0.55 (toluene–EtOAc 6 : 1). $[\alpha]_D$ = −210° (*c* = 1, EtOAc). ^{1}H NMR (600 MHz, $CDCl_3$): δ 8.10 (d, *J* = 7.5 Hz, 2H, Bz), 8.05 (d, *J* = 7.5 Hz, 2H, Bz), 7.65–7.26 (m, 10H, 3 × Ar), 6.88 (d, *J* = 8.6 Hz, 1H, Bn), 6.02–5.94 (m, 1H, CH_2CH=CH_2), 5.54 (d, $J_{3,4}$ = 5.5 Hz, 1H, H-4 (Fuc)), 5.42–5.37 (m, 1H, CH_2CH=CHH'), 5.31–5.21 (m, 4H, H-1 (Fuc′), H-3 (Fuc′), H-4 (Fuc′), CH_2CH=CHH'), 5.08 (d, $J_{1,2}$ = 3.5 Hz, 1H, H-1 (Fuc)), 4.70–4.63 (m, 2H, CH_2Ph), 4.46–4.38 (m, 2H, H-3 (Fuc), H-5 (Fuc)), 4.27–4.18 (m, 2H, H-5 (Fuc′), $OCHH'$CH), 4.14–4.05 (m, 2H, H-2 (Fuc′), $OCHH'$CH), 4.02–3.93 (m, 3H, H-2 (Fuc), $C(O)CH_2Cl$), 2.56 (br s, 1H, 2-O*H*), 1.22 (d, 3H, $J_{5,6}$ = 6.5 Hz, H-6 (Fuc)), 0.91 (d, $J_{5,6}$ = 6.5 Hz, 3H, H-6 (Fuc′)). ^{13}C NMR (100 MHz, $CDCl_3$): δ 167.3 ($C(O)CH_2Cl$), 167.0 ($C(O)$Ph), 166.2 ($C(O)$Ph), 137.8 (Bn), 133.8 (CH_2CH=CH_2), 133.7 (*p*-Bz), 133.3 (*p*-Bz), 130.9–128.0 (3 × Ar), 117.8 (CH_2CH=CH_2), 96.6 (C-1 (Fuc′)), 96.0 (C-1 (Fuc)), 74.8 (C-2 (Fuc)), 73.2 (C-3 (Fuc′)), 73.1 (C-3 (Fuc)), 72.8 (CH_2Ph), 71.6 (C-4 (Fuc′)), 71.5 (C-4 (Fuc)), 68.6 (OCH_2CH), 66.8 (C-2 (Fuc′)), 65.3 (C-5 (Fuc)), 64.9 (C-5 (Fuc′)), 40.6 ($C(O)CH_2Cl$), 16.3 (C-6 (Fuc′)), 15.7 (C-6 (Fuc)). Calcd *m*/*z* for $[M + Na]^+$ $C_{38}H_{41}ClO_{12}$ 747.2184, found 747.2179.

Allyl methyl 2,3,4-tri-*O*-benzyl-α,β-D-glucopyranosyluronate-(1→2)-3-*O*-chloroacetyl-4-*O*-benzoyl-α-L-fucopyranosyl-(1→3)-2-*O*-benzyl-4-*O*-benzoyl-α-L-fucopyranosides (17). Glycosylation of acceptor **16** (133 mg, 0.185 mmol) with donor **7** (127 mg, 0.204 mmol) as described in the general procedure B gave trisaccharide **17** (171 mg, 78%, α : β = 5 : 1) as a colorless syrup. R_f = 0.40 (toluene–EtOAc 10 : 1). For the α-isomer: ^{1}H NMR (600 MHz, $CDCl_3$): δ 8.15 (d, *J* = 7.4 Hz, 2H, *p*-Bz), 8.08 (d, *J* = 7.4 Hz, 2H, *p*-Bz), 7.51–7.15 (m, 26H, 6 × Ar), 5.92–6.01 (m, 1H, CH_2CH=CH_2), 5.72 (d, $J_{3,4}$ = 3.0 Hz, 1H, H-4 (Fuc)), 5.68 (dd, $J_{2,3}$ = 10.5 Hz, $J_{3,4}$ = 3.3 Hz, 1H, H-3 (Fuc′)), 5.52 (d, $J_{1,2}$ = 3.2 Hz, 1H, H-1 (Fuc′)), 5.40–5.34 (m, 2H, H-4 (Fuc), OCH_2CH=CHH'), 5.30 (d, $J_{1,2}$ = 3.9 Hz, 1H, H-1 (GlcA)), 5.22 (d, *J* = 10.4 Hz, 1H, CH_2CH=CHH'), 5.02 (d, $J_{1,2}$ = 3.4 Hz, 1H, H-1 (Fuc)), 4.86 (d, *J* = 11.4 Hz, 1H, CHH'Ph), 4.80 (d, *J* = 11.1 Hz, 1H, CHH'Ph), 4.73 (d, *J* = 11.6 Hz, 1H, CHH'Ph), 4.66 (d, *J* = 10.9 Hz, 1H, CHH'Ph), 4.60–4.58 (m, 2H, CH_2Ph), 4.57–4.53 (m, 2H, H-5 (Fuc′), H-5 (GlcA)), 4.50–4.44 (m, 2H, H-3 (Fuc), CHH'Ph), 4.40 (dd, $J_{1,2}$ = 3.2 Hz, $J_{2,3}$ = 10.4 Hz, 1H, H-2 (Fuc′)), 4.25 (d, *J* = 10.9 Hz, 1H, CHH'Ph), 4.23–4.16 (m, 2H, H-5 (Fuc), $OCHH'$CH), 4.10 (dd, $J_{1,2}$ = 3.5 Hz, $J_{2,3}$ = 10.3 Hz, 1H, H-2 (Fuc)), 4.07–4.03 (m, 1H, $OCHH'$CH), 3.81 (s, 3H, OMe), 3.75–3.67 (m, 3H, H-3 (GlcA), H-4 (GlcA), $C(O)CHH'Cl$), 3.60–3.55 (m, 2H, H-2 (GlcA), $C(O)CHH'Cl$), 1.10 (d, $J_{5,6}$ = 6.5 Hz, 3H, H-6 (Fuc)), 1.06 (d, $J_{5,6}$ = 6.5 Hz, 3H, H-6 (Fuc′)). ^{13}C NMR (150 MHz, $CDCl_3$): δ 170.3 (C-6 (GlcA)), 166.4 ($C(O)CH_2Cl$), 166.1 ($C(O)$Ph), 166.0 ($C(O)$Ph), 138.6 (Bn), 138.2 (Bn), 138.1 (Bn), 137.9 (Bn), 133.9 (CH_2CH=CH_2), 133.4 (*p*-Bz), 132.9 (*p*-Bz), 130.5 (Bz), 129.8 (Bz), 129–127 (6 × Ar), 117.6 (CH_2CH=CH_2), 98.2 (C-1 (GlcA)), 96.2 (C-1 (Fuc)), 95.9

(C-1 (Fuc′)), 80.6 (GlcA)), 79.9 (C-4 (GlcA)), 79.3 (C-2 (GlcA)), 75.1 (*C*H_2Ph), 75.0 (*C*H_2Ph), 74.8 (C-2 (Fuc)), 73.0 (C-3 (Fuc′)), 72.9 (*C*H_2Ph), 72.8 (*C*H_2Ph), 72.1 (C-3 (Fuc)), 71.7 (C-4 (Fuc′)), 71.3 (C-2 (Fuc′)), 71.2 (C-4 (Fuc)), 70.7 (C-5 (GlcA)), 68.4 (O*C*H_2CH), 65.4 (C-5 (Fuc)), 64.8 (C-5 (Fuc′)), 52.7 (OMe), 40.5 (C(O)*C*H_2Cl), 16.2 (C-6 (Fuc)), 15.8 (C-6 (Fuc′)). Selected NMR signals for the minor β-isomer: ^{1}H NMR (400 MHz, $CDCl_3$): δ 4.44–4.47 (m, 3H, H-1 (GlcA), CH_2Ph), 3.85 (1H, d, $J_{4,5}$ = 9.8 Hz, H-5 (GlcA)), 3.52 (1H, t, J = 9.4 Hz, H-4 (GlcA)), 3.19 (1H, t, J = 9.1 Hz, H-3 (GlcA)), 3.01 (1H, dd, $J_{1,2}$ = 7.6 Hz, $J_{2,3}$ = 9.1 Hz, H-2 (GlcA)). ^{13}C NMR (100 MHz, $CDCl_3$): 100.0 (C-1 (GlcA)), 96.3 (C-1 (Fuc)), 91.9 (C-1 (Fuc′)), 83.6 (C-3 (GlcA)), 81.0 (C-2 (GlcA)), 78.8 (C-4 (GlcA)), 74.0 (C-5 (GlcA)). Calcd *m*/*z* for $[M + Na]^+$ $C_{66}H_{69}ClO_{18}$ 1207.4065, found 1207.4059.

Allyl methyl 2,3,4-tri-*O*-benzyl-α-D-glucopyranosyluronate-(1→2)-4-*O*-benzoyl-α-L-fucopyranosyl-(1→3)-2-*O*-benzyl-4-*O*-benzoyl-α-L-fucopyranoside (18). A mixture of trisaccharide **17** (150 mg, 0.114 mmol), 2,4,6-collidine (22.5 μL, 0.171 mmol), and thiourea (165 mg, 0.573 mmol) in MeOH (5 mL) and $CHCl_3$ (1 mL) was boiled under reflux for 24 h, cooled, and taken to dryness. A solution of the residue in $CHCl_3$ (50 mL) was washed with 1 M HCl (50 mL) and water (50 mL). The organic layer was dried (Na_2SO_4) and concentrated *in vacuo*. The residue was purified by column chromatography (silica gel, eluent: toluene/EtOAc = 20 : 1→10 : 1) to give **18** (101 mg, 80%) as a white foam. R_f = 0.30 (toluene–EtOAc 10 : 1), $[\alpha]_D$ = −104° (*c* = 1, EtOAc). ^{1}H NMR (600 MHz, $CDCl_3$): δ 8.13 (d, J = 7.0 Hz, 2H, Bz), 8.10 (J = 7.0 Hz, 2H, d, Bz), 7.62–7.07 (m, 26H, 6 × Ar), 5.98–5.90 (m, 1H, CH_2CH=CH_2), 5.69 (d, $J_{3,4}$ = 3.2 Hz, 1H, H-4 (Fuc)), 5.37–5.33 (m, 2H, H-1 (Fuc′), CH_2CH=CH*H*′), 5.22–5.19 (m, 2H, H-4 (Fuc′), CH_2–CH=C*H*H′), 5.07 (d, $J_{1,2}$ = 3.7 Hz, 1H, H-1 (GlcA)), 4.97 (d, $J_{1,2}$ = 3.7 Hz, 1H, H-1 (Fuc)), 4.79–4.62 (m, 7H, 3 × CH_2Ph, CH*H*′Ph), 4.57 (d, $J_{4,5}$ = 6.9 Hz, 1H, H-5 (GlcA)), 4.56 (d, J = 5.7 Hz, 1H, C*H*H′Ph), 4.42 (dd, $J_{2,3}$ = 10.1 Hz, $J_{3,4}$ = 3.2 Hz, 1H, H-3 (Fuc)), 4.38 (q, J = 6.4 Hz, 1H, H-5 (Fuc′)), 4.28 (dt, J_t = 2.9 Hz, $J_{2,3}$ = 10.1 Hz, 1H, H-3 (Fuc′)), 4.20–4.15 (m, 2H, H-5 (Fuc), OCH*H*′CH), 4.04–4.00 (m, 2H, H-2 (Fuc), OC*H*H′CH), 3.98 (dd, $J_{1,2}$ = 3.2 Hz, $J_{2,3}$ = 10.1 Hz, 1H, H-2 (Fuc′)), 3.91 (t, J = 9.4 Hz, 1H, H-3 (GlcA)), 3.79 (s, 3H, OMe), 3.68 (t, J = 9.6 Hz, 1H, H-4 (GlcA)), 3.51 (dd, $J_{1,2}$ = 3.9 Hz, $J_{2,3}$ = 9.9 Hz, 1H, H-2 (GlcA)), 3.48 (d, J = 2.5 Hz, 1H, 3-O*H*), 1.06 (d, $J_{5,6}$ = 6.5 Hz, 3H, H-6 (Fuc)), 1.04 (3H, d, $J_{5,6}$ = 6.4 Hz, H-6 (Fuc′)). ^{13}C NMR (150 MHz, $CDCl_3$): δ 170.3 (C-6 (GlcA)), 166.6 (Bz), 165.8 (Bz), 138.7 (Bn), 138.3 (Bn), 138.2 (Bn), 137.1 (Bn), 134.0 (CH_2CH=*C*H_2), 133.1 (Bz), 132.9 (Bz), 130.2 (Bz), 129.9 (Bz), 127.5–128.5 (6 × Ar), 117.4 (CH_2*C*H=CH_2), 100.8 (C-1 (GlcA)), 97.5 (C-1 (Fuc′)), 96.3 (C-1 (Fuc)), 81.3 (C-3 (GlcA)), 80.1 (C-4 (GlcA)), 79.3 (C-2 (Fuc′)), 78.5 (C-2 (GlcA)), 75.7 (C-2 (Fuc)), 75.4 (*C*H_2Ph), 75.2 (*C*H_2Ph), 74.1 (C-4 (Fuc′)), 73.9 (*C*H_2Ph), 73.4 (C-3 (Fuc)), 72.9 (*C*H_2Ph), 72.1 (C-4 (Fuc)), 70.9 (C-5 (GlcA)), 68.5 (O*C*H_2CH), 68.4 (C-3 (Fuc′)), 65.7 (C-5 (Fuc′)), 65.4 (C-5 (Fuc)), 52.6 (OMe), 16.1 (C-6 (Fuc)), 16.0 (C-6 (Fuc′)). Calcd *m*/*z* for $[M + Na]^+$ $C_{64}H_{68}O_{17}$ 1131.4349, found 1131.4344.

Allyl 2-*O*-benzyl-3,4-di-*O*-chloroacetyl-α-L-fucopyranosyl-(1→3)-{methyl 2,3,4-tri-*O*-benzyl-α-D-glucopyranosyluronate-(1→2)}-4-*O*-benzoyl-α-L-fucopyranosyl-(1→3)-2-*O*-benzyl-4-*O*-benzoyl-α-L-fucopyranoside (19). Glycosylation of acceptor **18** (122 mg, 0.11 mmol) with donor **6** (93 mg, 0.17 mmol) as described in the general procedure B gave tetrasaccharide **19** (112 mg, 68%) as a colorless syrup. R_f = 0.61 (toluene–EtOAc 10 : 1), $[\alpha]_D$ = −119° (*c* = 1, EtOAc). ^{1}H NMR (600 MHz, $CDCl_3$): δ 8.10 (d, J = 7.2 Hz, 2H, *o*-Bz), 8.00 (d, J = 7.2 Hz, 2H, *o*-Bz), 7.54 (t, J = 7.4 Hz, 1H, *p*-Bz), 7.49 (t, J = 7.4 Hz, 1H, *p*-Bz), 7.40–6.95 (m, 29H, 5 × Bn, 2 × Bz), 5.90–5.83 (m, 1H, CH_2CH=CH_2), 5.76 (d, $J_{3,4}$ = 3.1 Hz, 1H, H-4 (Fuc)), 5.50 (d, $J_{1,2}$ = 3.3 Hz, 1H, H-1 (Fuc′)), 5.36 (d, $J_{3,4}$ = 3.1 Hz, 1H, H-4 (Fuc′)), 5.32 (dd, $J_{2,3}$ = 10.4 Hz, $J_{3,4}$ = 3.3 Hz, 1H, H-3 (Fuc″)), 5.30–5.26 (m, 2H, H-1 (GlcA), CH_2CH=CH*H*′), 5.24 (d, $J_{1,2}$ = 3.7 Hz, 1H, H-1 (Fuc″)), 5.12 (dd, J = 1.2 Hz, J = 10.4 Hz, 1H, CH_2CH=C*H*H′), 5.05 (d, J = 12.5 Hz, 1H, CH*H*′Ph), 4.96 (d, $J_{3,4}$ = 3.3 Hz, 1H, H-4 (Fuc″)), 4.86 (d, $J_{1,2}$ = 3.6 Hz, 1H, H-1 (Fuc)), 4.80–4.74 (m, 3H, C*H*H′Ph, 2 × CH*H*′Ph), 4.69–4.57 (m, 4H, CH_2Ph, 2 × C*H*H′Ph), 4.44–4.39 (m, 3H, H-3 (Fuc), H-3 (Fuc′), H-5 (GlcA)), 4.34 (q, J = 6.5 Hz, 1H, H-5 (Fuc″)), 4.30–4.25 (m, 2H, H-2 (Fuc′), CH*H*′Ph), 4.18 (q, J = 6.6 Hz, 1H, H-5 (Fuc)), 4.14–4.06 (m, 3H, H-5 (Fuc′), OCH*H*′CH, C*H*H′Ph), 4.00–3.90 (m, 4H, H-2 (Fuc), OC*H*H′CH, C(O)CH_2Cl), 3.85 (t, J = 9.1 Hz, 1H, H-3 (GlcA)), 3.77 (t, J = 9.2 Hz, 1H, H-4 (GlcA)), 3.73 (s, 3H, OMe), 3.70–3.65 (m, 4H, H-2 (GlcA), H-2 (Fuc″), C(O)CH_2Cl), 1.10 (d, $J_{5,6}$ = 6.5 Hz, 3H, H-6 (Fuc)), 0.99 (d, $J_{5,6}$ = 6.5 Hz, 3H, H-6 (Fuc′)), 0.84 (d, $J_{5,6}$ = 6.5 Hz, 3H, H-6 (Fuc″)). ^{13}C NMR (150 MHz, $CDCl_3$): δ 170.2 (C-6 (GlcA)), 167.2 (*C*(O)CH_2Cl), 166.6 (*C*(O)CH_2Cl), 166.1 (*C*(O)Ph), 166.0 (*C*(O)Ph), 138.9 (Bn), 138.6 (Bn), 138.6 (Bn), 138.4 (Bn), 138.0 (Bn), 134.2 (CH_2*C*H=CH_2), 133.3 (*p*-Bz), 133.2 (*p*-Bz), 130.2 (*o*-Bz), 130.1 (*o*-Bz), 129.8–127.4 (5 × Bn, 2 × Bz), 117.7 (CH_2CH=*C*H_2), 99.3 (C-1 (GlcA)), 97.1 (C-1 (Fuc′)), 96.5 (C-1 (Fuc)), 92.4 (C-1 (Fuc″)), 81.8 (C-3 (GlcA)), 80.0 (C-4 (GlcA)), 79.2 (C-2 (GlcA)), 75.6 (C-2 (Fuc)), 75.3 (*C*H_2Ph), 75.0 (*C*H_2Ph), 74.5 (C-2 (Fuc′)), 74.0 (*C*H_2Ph), 73.9 (C-3 (Fuc)), 73.6 (C-4 (Fuc″)), 73.0 (*C*H_2Ph), 72.8 (C-4 (Fuc)), 72.4 (C-2 (Fuc″)), 72.2 (*C*H_2Ph), 72.0 (C-3 (Fuc″)), 71.3 (C-5 (GlcA)), 70.7 (C-3 (Fuc′)), 69.7 (C-4 (Fuc′)), 68.8 (O*C*H_2CH), 65.6 (C-5 (Fuc′)), 65.4 (C-5 (Fuc)), 64.5 (C-5 (Fuc″)), 52.7 (OMe), 40.6 (C(O)*C*H_2Cl), 40.6 (C(O)*C*H_2Cl), 16.3 (C-6 (Fuc′)), 16.2 (C-6 (Fuc)), 15.5 (C-6 (Fuc″)). Calcd *m*/*z* for $[M + Na]^+$ $C_{81}H_{86}Cl_2O_{23}$ 1519.4829, found 1519.4859.

Sodium salt propyl α-L-fucopyranosyl-(1→3)-{α-D-glucopyranosyluronate-(1→2)}-α-L-fucopyranosyl-(1→3)-α-L-fucopyranoside (1). A mixture of tetrasaccharide **19** (25 mg, 0.0177 mmol) and the catalyst 10% Pd/C (20 mg) in MeOH–EtOAc (1 : 1) (2 mL) was stirred under H_2 (1 atm) at rt for 1 h and then filtered through a Celite layer. The catalyst was carefully washed with MeOH and the combined filtrates were concentrated. The residue was dissolved in MeOH (1 mL) and treated with 2 M aq. NaOH (0.2 mL) for 24 h. The deprotected trisaccharide was isolated from the reaction mixture by gel-chromatography on a gel Sephadex G-15 with water elution followed by lyophilization to give **1** (11.3 mg, 91%) as a white amorphous powder; $[\alpha]_D$ = −140° (*c* = 1, H_2O). ^{1}H NMR (600 MHz, D_2O): δ 5.29 (d, $J_{1,2}$ = 4.8 Hz, 1H, H-1 (GlcA)), 5.17 (d, $J_{1,2}$ = 3.7 Hz, 1H, H-1 (Fuc″)), 5.15 (d, $J_{1,2}$ = 3.9 Hz, 1H, H-1 (Fuc′)), 4.93 (d, $J_{1,2}$ = 3.5 Hz,

1H, H-1 (Fuc)), 4.41 (q, J = 6.6 Hz, 1H, H-5 (Fuc″)), 4.32–4.26 (m, 2H, H-3 (Fuc′), H-5 (Fuc′)), 4.19 (dd, $J_{1,2}$ = 3.9 Hz, $J_{2,3}$ = 10.4 1H, Hz, H-2 (Fuc′)), 4.12 (d, $J_{3,4}$ = 2.9 Hz, 1H, H-4 (Fuc′)), 4.00–3.94 (m, 3H, H-5 (GlcA), H-2 (Fuc), H-3 (Fuc)), 4.10–4.05 (m, 2H, H-4 (Fuc), H-5 (Fuc)), 3.92 (dd, $J_{2,3}$ = 10.5 Hz, $J_{3,4}$ = 3.5 Hz, 1H, H-3 (Fuc″)), 3.84–3.80 (m, 2H, H-2 (Fuc″), H-4 (Fuc″)), 3.73 (t, J = 9.5 Hz, 1H, H-3 (GlcA)), 3.68 (q, J = 7.2 Hz, 1H, OCHH'CH$_2$), 3.59 (dd, $J_{1,2}$ = 4.8 Hz, $J_{2,3}$ = 9.9 Hz, 1H, H-2 (GlcA)), 3.54–3.49 (m, 2H, H-4 (GlcA), OCHH′CH$_2$), 1.68–1.61 (m, 2H, CH$_2$CH_2CH$_3$), 1.24 (m, 6H, H-6 (Fuc), H-6 (Fuc′)), 1.21 (d, $J_{5,6}$ = 6.6 Hz, 3H, H-6 (Fuc″)), 0.93 (t, J = 7.3 Hz, 3H, CH$_2$CH$_2$CH_3). ^{13}C NMR (150 MHz, D$_2$O): δ 100.6 (C-1 (GlcA)), 99.5 (C-1 (Fuc)), 95.3 (C-1 (Fuc′)), 94.5 (C-1 (Fuc″)), 75.0 (C-3 (Fuc)), 74.1 (C-3 (Fuc′), C-3 (GlcA)), 74.0 (C-5 (GlcA)), 73.1 (C-4 (Fuc″)), 73.1 (C-4 (GlcA)), 72.3 (C-2 (GlcA)), 71.6 (C-2 (Fuc′)), 71.3 (CH$_2$CH$_2$CH$_3$), 70.9 (C-3 (Fuc″)), 69.1 (C-2 (Fuc″)), 69.0 (C-4 (Fuc)), 68.4 (C-5 (Fuc″)), 68.3 (C-4 (Fuc′)), 67.8 (C-5 (Fuc)), 67.6 (C-5 (Fuc′)), 67.5 (C-2 (Fuc)), 23.3 (CH$_2$$CH_2CH_3$), C-6 (Fuc″)), C-6 (Fuc′), 16.5 (C-6 (Fuc), 11.1 (CH$_2$CH$_2$$CH_3$). Calcd m/z for [M + Na]$^+$ $C_{27}H_{45}NaO_{19}$ 719.2345, found 719.2335.

Sodium salt propyl 3,4-di-*O*-sulfonato-α-L-fucopyranosyl-(1→3)-{α-D-glucopyranosyluronate-(1→2)}-4-*O*-sulfonato-α-L-fucopyranosyl-(1→3)-4-*O*-sulfonato-α-L-fucopyranoside (2). To a solution of tetrasaccharide **19** (32 mg, 0.021 mmol) in THF–MeOH (3 : 1) (2.5 mL) 2 M aq. NaOH (0.4 mL) was added and the mixture was kept at 65 °C for 10 h. The solution was neutralized with Amberlite IR-120 (H$^+$), the resin was filtered off and the filtrate was concentrated. The residue was purified by chromatography (silica gel, eluent: CH$_2$Cl$_2$/MeOH = 25 : 1→10 : 1). The resulting tetraol was dissolved in DMF (2 mL) and Py·SO$_3$ (140 mg, 0.88 mmol) was added. The reaction mixture was kept at 40 °C for 3 h, then quenched with 1 M aq. NaHCO$_3$ up to pH 8–9 and concentrated *in vacuo*. The residue was dissolved in a minimal amount of water (0.4 mL) and then MeOH (5 mL) was added to precipitate inorganic salts. The solids were filtered off, washed with MeOH and the filtrate was concentrated. The residue was purified by chromatography (silica gel, eluent: CH$_2$Cl$_2$/MeOH = 10 : 1→1 : 1). A mixture of the resulting product and the catalyst 10% Pd/C (50 mg) in THF–EtOAc–EtOH (4 : 1 : 1) (3 mL) was stirred under H$_2$ (1 atm) at rt for 12 h and then filtered through a nylon membrane syringe filter (0.45 μm). The filtrate was concentrated and the residue was purified by gel-chromatography on a gel Sephadex G-15 with water elution followed by lyophilization to give **2** (19.5 mg, 81%) as a white amorphous powder; $[\alpha]_D$ = −103.00° (c = 1, H$_2$O). ^{1}H NMR (600 MHz, D$_2$O): δ 5.44 (d, $J_{1,2}$ = 3.9 Hz, 1H, H-1 (Fuc″)), 5.37 (d, $J_{1,2}$ = 4.1 Hz, 1H, H-1 (GlcA)), 5.30 (d, $J_{1,2}$ = 3.6 Hz, 1H, H-1 (Fuc′)), 4.92 (d, $J_{1,2}$ = 3.9 Hz, 1H, H-1 (Fuc)), 4.90 (d, $J_{3,4}$ = 2.8 Hz, 1H, H-4 (Fuc′)), 4.86 (d, $J_{3,4}$ = 3.0 Hz, 1H, H-4 (Fuc″)), 4.79 (d, $J_{3,4}$ = 2.8 Hz, 1H, H-4 (Fuc)), 4.73 (dd, $J_{2,3}$ = 10.5 Hz, $J_{3,4}$ = 3.0 Hz, 1H, H-3 (Fuc″)), 4.55–4.50 (2H, m, H-3 (Fuc′), H-5 (Fuc″)), 4.45 (q, J = 6.6 Hz, 1H, H-5 (Fuc′)), 4.24 (dd, $J_{1,2}$ = 3.6 Hz, $J_{2,3}$ = 10.4 Hz, 1H, H-2 (Fuc′)), 4.20 (q, J = 6.7 Hz, 1H, H-5 (Fuc)), 4.05–3.99 (m, 3H, H-2 (Fuc″), H-3 (Fuc), H-5 (GlcA)), 3.96 (dd, $J_{1,2}$ = 3.9 Hz, $J_{2,3}$ = 10.2 Hz, 1H, H-2 (Fuc)), 3.87 (t, J = 9.5 Hz, 1H, H-3 (GlcA)), 3.65–3.60 (m, 2H, H-2 (GlcA), OCHH'CH$_2$), 3.53–3.48 (m, 1H, OCHH′CH$_2$), 3.47 (t, J = 9.7 Hz, 1H, H-4 (GlcA)), 1.67–1.60 (m, 2H, CH$_2$CH_2CH$_3$), 1.32 (d, $J_{5,6}$ = 6.5 Hz, 3H, H-6 (Fuc″)), 1.31–1.29 (m, 6H, H-6 (Fuc), H-6 (Fuc′)), 0.92 (t, J = 7.4 Hz, 3H, CH$_2$CH$_2$CH_3). ^{13}C NMR (150 MHz, D$_2$O): δ 177.6 (C-6 (GlcA)), 100.4 (C-1 (GlcA)), 99.3 (C-1 (Fuc)), 98.5 (C-1 (Fuc′)), 94.4 (C-1 (Fuc″)), 80.6 (C-4 (Fuc″)), 80.2 (C-4 (Fuc)), 77.8 (C-4 (Fuc′)), 77.1 (C-3 (Fuc)), 76.8 (C-3 (Fuc″)), 74.2 (C-3 (GlcA)), 73.8 (C-5 (GlcA)), 73.3 (C-4 (GlcA)), 72.6 (C-2 (GlcA)), 72.5 (C-2 (Fuc′)), 71.9 (C-3 (Fuc′)), 71.4 (OCH$_2$CH$_2$), 68.6 (C-2 (Fuc)), 67.9 (C-5 (Fuc″)), 67.9 (C-5 (Fuc′)), 67.4 (C-5 (Fuc)), 67.4 (C-2 (Fuc″)), 23.3 (CH$_2$$CH_2CH_3$), C-6 (Fuc″)), 17.3–17.1 (C-6 (Fuc), C-6 (Fuc′), 11.2 (CH$_2$CH$_2$$CH_3$). Calcd m/z for [M + H]$^+$ $C_{27}H_{41}O_{31}S_4Na_5$ 1105.0076, found 1105.0060.

General procedure C, pyranoside-*into*-furanoside rearrangement

HSO$_3$Cl (26 μL, 0.39 mmol) was added dropwise to a stirred solution of a pyranoside derivative (0.10 mmol) and a Py·SO$_3$ complex (159 mg, 1.00 mmol) in DMF (1.2 mL). The reaction mixture was kept for 48 h at 20 °C and then quenched with aqueous NaHCO$_3$ (266 mg in 3 mL H$_2$O, 3.17 mmol) and evaporated twice with water. The residue was dissolved in a minimal amount of water and then MeOH was added to precipitate inorganic salts. The solids were filtered off, washed with MeOH, and the filtrate was concentrated and used for the *O*-desulfation and NMR analysis without additional purification.

Sodium salt allyl 2,4-di-*O*-sulfonato-3-*O*-benzyl-α-L-fucopyranoside (21). Treatment of allyl 3-*O*-benzyl-α-L-fucopyranoside (**20α**) as described in the general procedure C gave a totally *O*-sulfated derivative **21**. ^{1}H NMR (600 MHz, D$_2$O) δ 8.17 (d, J = 7.5 Hz, 2H, *o*-Bz), 7.75 (t, J = 7.5 Hz, 1H, *p*-Bz), 7.60 (t, J = 7.8 Hz, 2H, *m*-Bz), 6.09 (m, 1H, CH$_2$CH═CH$_2$), 5.50 (m, 2H, H-3, CH$_2$CH═CHH'), 5.39 (m, 2H, CH$_2$CH═CHH′, H-1), 4.98 (d, $J_{3,4}$ = 3.4 Hz, 1H, H-4), 4.90 (dd, $J_{2,3}$ = 10.7 Hz, $J_{2,1}$ = 3.8 Hz, 1H, H-2), 4.46 (q, $J_{5,6}$ = 6.6 Hz, 1H, H-5), 4.36 (m, 1H, OCHH′CH), 4.26 (m, 1H, OCHH'CH), 1.39 (d, $J_{6,5}$ = 6.6 Hz, 3H, H-6). ^{13}C NMR (150 MHz, D$_2$O) δ 168.1 (C(O)Ph), 134.0 (CH$_2$$C$H═CH$_2$), 129.9 (Ph), 128.8 (Ph), 118.8 (CH$_2$CH═CH$_2$), 95.8 (C-1), 77.5 (C-4), 72.3 (C-2), 69.5 (C-3), 69.1 (OCH$_2$CH), 65.8 (C-5), 15.8 (C-6).

Allyl α,β-L-fucopyranosides (10α,β). Allyl bromide (2.5 mL, 30 mmol) and NaOH (1.0 g, 25 mmol) was added to a stirred solution of L-fucose (2.0 g, 12 mmol) in water (20 mL). The mixture was vigorously stirred at 20 °C for 24 h and then diluted with water (100 mL), and washed with EtOAc (2 × 150 mL). The water layer was concentrated *in vacuo*. The residue was purified by column chromatography (silica gel, eluent: CH$_2$Cl$_2$/MeOH = 20 : 1→10 : 1) to give **10α,β** (2.22 g, 91%, α : β = 1 : 4) as an amorphous solid. R_f = 0.43 (EtOAc–MeOH 10 : 1). For the β-isomer: ^{1}H NMR (600 MHz, CDCl$_3$): δ 5.88 (m, 1H, CH$_2$CH═CH$_2$), 5.23 (d, J = 17.1 Hz, 1H, CH$_2$CH═CHH'), 5.09 (d, J = 10.6 Hz, 1H, CH$_2$CH═CHH′), 4.27 (m, 1H, OCHH'CH), 4.18 (d, $J_{1,2}$ = 7.7 Hz, 1H, H-1), 4.05

(m, 1H, OC*H*H′CH), 3.67–3.59 (m, 2H, H-2, H-4), 3.55–3.47 (m, 2H, H-3, H-5), 1.22 (d, $J_{5,6}$ = 6.7 Hz, 3H, H-6). ^{13}C NMR (100 MHz, $CDCl_3$): δ 134.14 ($CH_2CH{=}\mathit{C}H_2$), 117.32 ($CH_2\mathit{C}H{=}CH_2$), 101.83 (C-1), 73.82 (C-3), 71.39 (C-4), 70.66 (C-2), 70.35 (C-5), 69.84 (O$\mathit{C}H_2$CH), 16.10 (C-6). NMR signals of the minor α-isomer corresponded to previously reported data.[36]

Allyl 3-*O*-benzoyl-α,β-L-fucopyranosides (20α,β). Allyl α,β-L-fucopyranoside **10α,β** (2.0 g, 9.8 mmol) and 2-aminoethyl diphenylborinate (220 mg, 0.98 mmol) were dissolved in dry acetonitrile (20 mL). *N*,*N*-Diisopropylethylamine (2.56 mL, 14.7 mmol) and benzoyl chloride (1.7 mL, 14.8 mmol) were added, and the resulting mixture was stirred at room temperature for 1 h. Then the mixture was diluted with ethyl acetate, washed with water, and the aqueous layer was extracted back several times with ethyl acetate. The combined organic extracts were dried over Na_2SO_4, filtered, and concentrated *in vacuo*. The resulting crude material was purified by chromatography (silica gel, eluent: hexane/EtOAc = 1.5 : 1) to give monosaccharides **13** (2.87, 95%, α : β = 1 : 4) as a colorless oil. Spectral data of **20α,β** corresponded to previously reported data for the α-[26] and β-isomers.[16]

Allyl 3-*O*-benzoyl-β-L-fucofuranoside (22). Treatment of allyl 3-*O*-benzyl-α,β-L-fucopyranoside (**20α,β**) (1.0 g, 3.2 mmol) as described in the general procedure C (pyranoside-*into*-furanoside rearrangement) gave a crude mixture of totally *O*-sulfated monosaccharides. The products were dissolved in DMF–dioxane (2 : 5) (55 mL) and Amberlite IR-120(H^+) cation-exchange resin was added up to pH = 3. The reaction mixture was vigorously stirred at 60 °C for 30 min, cooled and neutralized with aqueous $NaHCO_3$. Saturated aqueous NaCl (200 mL) was added to the reaction mixture and desulfated products were extracted by EtOAc (2 × 150 mL). The combined organic layers were dried (Na_2SO_4) and concentrated. The resulting residue was purified by chromatography (silica gel, eluent: hexane/EtOA*c* = 4 : 1→2 : 1) to give monosaccharides **22** (655 mg, 66%) and **20α** (128 mg, 13%). Spectral data of **22** corresponded to previously reported data.[16]

2,3,5-Tri-*O*-benzyl-β-L-fucofuranoside trichloroacetoimidates (24). *N*-Bromosuccinimide (122 mg, 0.684 mmol) was added at 0 °C to a stirred solution of (2-methyl-5-*tert*-butylphenyl) 2,3,5-tri-*O*-benzyl-1-thio-β-L-fucofuranoside (**23**) (102 mg, 0.171 mmol) in aqueous acetone (1 : 9) (4 mL). The mixture was vigorously stirred for 10 min, then diluted with CH_2Cl_2 and washed with aq. $NaHCO_3$ (2 × 100 mL). The organic phase was dried over anhydrous Na_2SO_4 and concentrated under diminished pressure to give a white residue. To a solution of the above residue in anhydrous CH_2Cl_2 (2 mL) CCl_3CN (0.17 mL, 1.71 mmol) and DBU (15 μL, 0.10 mmol) were added at −30 °C under an argon atmosphere, and the mixture was then stirred for 2 h. The concentration of the reaction mixture followed by purification of the residue by chromatography on silica gel passivated by Et_3N (eluent: toluene/EtOAc = 20 : 1→10 : 1) gave trichloroacetimidate **24** (71 mg, 72%) as a white foam. R_f = 0.60 (hexane–EtOAc = 3 : 1). $[\alpha]_D$ = 22° (*c* = 1, EtOAc). ^{1}H NMR (400 MHz, $CDCl_3$): δ 8.43 (s, 1H, N*H*), 7.28–7.11 (m, 15H, 3 × Ar), 6.30 (s, 1H, H-1), 4.62 (d, 1H, *J* = 11.9 Hz, CH*H*′Ph), 4.49 (m, 3H, CH_2Ph, CH*H*′Ph), 4.36 (q, 2H, *J* = 11.8 Hz, CH_2Ph), 4.25 (t, *J* = 5.4 Hz, 1H, H-4), 4.15 (d, $J_{2,3}$ = 1.9 Hz, 1H, H-2), 3.96 (dd, $J_{2,3}$ = 1.8 Hz, $J_{3,4}$ = 5.9 Hz, 1H, H-3), 3.68 (dd, $J_{4,5}$ = 5.2 Hz, $J_{5,6}$ = 6.3 Hz, 1H, H-5), 1.14 (d, $J_{5,6}$ = 6.4 Hz, 3H, H-6). ^{13}C NMR (100 MHz, $CDCl_3$): δ 161.1 (C(NH)CCl_3), 138.6 (Ph), 137.8 (Ph), 137.5 (Ph), 128.7–127.5 (5 × Ar), 104.4 (C-1), 91.4 ($\mathit{C}Cl_3$), 87.1 (C-4), 86.7 (C-2), 83.3 (C-3), 73.6 (C-5), 72.0 (2 × $\mathit{C}H_2$Ph), 71.3 ($\mathit{C}H_2$Ph), 15.7 (C-6). Calcd *m*/*z* for $[M + Na]^+$ $C_{29}H_{30}Cl_3NO_5$ 600.1082, found 600.1092.

Allyl 2,5-di-*O*-benzyl-3-*O*-benzoyl-α,β-L-fucofuranosyl-(1→4)-methyl-2,3-di-*O*-benzyl-β-D-glucopyranozyl uronate (25). Glycosylation of acceptor **14** (184 mg, 0.43 mmol) with donor **9** (277 mg, 0.47 mmol) as described in the general procedure B gave disaccharides **26**: α-isomer (203 mg, 55%), β-isomer (48 mg, 13%). Spectral data of the **26** α-isomer corresponded to previously reported data.[16] Spectral data for the β-isomer: $[\alpha]_D$ = −27° (*c* = 1, EtOAc). ^{1}H NMR (600 MHz, $CDCl_3$): δ 8.14 (d, *J* = 7.2 Hz, 2H, Bz), 7.63 (t, *J* = 7.4 Hz, 1H, Bz), 7.51 (t, *J* = 7.8 Hz, 2H, Bz), 7.37–7.19 (m, 20H, 4 × Bn), 6.00–5.92 (m, 1H, $CH_2C\mathit{H}{=}CH_2$), 5.61 (s, 1H, H-1 (Fuc)), 5.42 (d, $J_{3,4}$ = 4.3 Hz, 1H, H-3 (Fuc)), 5.37 (d, *J* = 17.3 Hz, 1H, $CH_2CH{=}CH\mathit{H}'$), 5.25 (d, *J* = 10.5 Hz, 1H, $CH_2CH{=}C\mathit{H}H'$), 4.95 (d, *J* = 11.0 Hz, 1H, CH*H*′Ph), 4.87 (d, *J* = 11.0 Hz, 1H, CH*H*′Ph), 4.73–4.65 (m, 5H, CH_2Ph, CH*H*′Ph, 2 × C*H*H′Ph), 4.52 (d, $J_{1,2}$ = 7.4 Hz, 1H, H-1 (GlcA)), 4.49 (d, *J* = 11.8 Hz, 1H, C*H*H′Ph), 4.47–4.43 (m, 1H, OCH*H*′CH), 4.27 (dd, $J_{3,4}$ = 4.4 Hz, $J_{4,5}$ = 5.7 Hz, 1H, H-4 (Fuc)), 4.15 (dd, *J* = 13.5 Hz, *J* = 7.0 Hz, 1H, OC*H*H′CH), 4.11 (d, $J_{4,5}$ = 9.0 Hz, 1H, H-4 (GlcA)), 4.04 (s, 1H, H-2 (Fuc)), 3.94 (d, $J_{4,5}$ = 9.7 Hz, 1H, H-5 (GlcA)), 3.85–3.78 (m, 1H, H-5 (Fuc)), 3.77 (s, 3H, OMe), 3.63–3.55 (m, 2H, H-2 (GlcA), H-3 (GlcA)), 1.26 (3H, d, $J_{5,6}$ = 6.4 Hz, H-6 (Fuc)). ^{13}C NMR (150.9 MHz, $CDCl_3$): δ 168.5 (C-6 (GlcA)), 165.9 (C(O)Ph), 138.8 (Bn), 138.2 (Bn), 138.1 (Bn), 137.6 (Bn), 133.7 ($CH_2CH{=}\mathit{C}H_2$), 133.4 (Bz), 130–127 (Ar), 117.8 ($CH_2\mathit{C}H{=}CH_2$), 107.7 (C-1 (Fuc)), 102.7 (C-1 (GlcA)), 87.2 (C-2 (Fuc)), 85.6 (C-4 (Fuc)), 83.7 (C-3 (GlcA)), 81.6 (C-2 (GlcA)), 77.1 (C-3 (Fuc)), 76.4 (C-4 (GlcA)), 75.6 (C-5 (GlcA), $\mathit{C}H_2$Ph), 74.9 ($\mathit{C}H_2$Ph), 74.5 (C-5 (Fuc)), 71.7 ($\mathit{C}H_2$Ph), 71.5 ($\mathit{C}H_2$Ph), 70.6 (O$\mathit{C}H_2$CH), 52.8 (OMe), 16.0 (C-6 (Fuc)). Calcd *m*/*z* for $[M + Na]^+$ $C_{51}H_{54}O_{12}$ 881.3507, found 881.3516.

Allyl 2,3,5-tri-*O*-benzyl-α,β-L-fucofuranosyl-(1→4)-methyl-2,3-di-*O*-benzyl-β-D-glucopyranozyl uronate (26). Glycosylation of acceptor **14** (74 mg, 0.173 mmol) with donor **24** (110 mg, 0.190 mmol) as described in the general procedure B gave disaccharides **26** (88 mg, 60%, α : β = 1 : 2) as a colorless syrup. R_f = 0.50 (toluene–EtOAc = 3 : 1). ^{1}H NMR (400 MHz, $CDCl_3$): δ 7.41–7.20 (m, 75H, 5 × Ar α, 5 × Ar β). 5.99–5.88 (m, 3H, $CH_2C\mathit{H}{=}CH_2$ α, $CH_2C\mathit{H}{=}CH_2$ β), 5.49 (s, 2H, H-1 (Fuc β)), 5.38–5.30 (m, 3H, $CH_2CH{=}CH\mathit{H}'$ α, $CH_2CH{=}CH\mathit{H}'$ β), 5.22–5.19 (m, 4H, H-1 (Fuc α), $CH_2CH{=}C\mathit{H}H'$ α, $CH_2CH{=}C\mathit{H}H'$ β), 5.00–4.81 (m, 5H, CH*H*′Ph α, CH*H*′Ph β, CH_2Ph α), 4.78–4.59 (m, 6H, CH*H*′Ph α, CH*H*′Ph β, C*H*H′Ph α, C*H*H′Ph β), 4.59–4.46 (m, 11H, H-1 (GlcA α), H-1 (GlcA β), CH*H*′Ph α, CH*H*′Ph β, C*H*H′Ph α, C*H*H′Ph β, CH_2Ph α), 4.46–4.38 (m, 6H, OCH*H*′CH α, OCH*H*′CH β, C*H*H′Ph α, C*H*H′Ph β),

4.28 (m, 4H, CH_2Ph β), 4.17–4.07 (m, 6H, H-4 (GlcA α), H-4 (GlcA β), OCHH′CH α, OCHH′CH β), 4.04–3.95 (m, 8H, H-5 (GlcA β), H-2 (Fuc α), H-3 (Fuc α), H-2 (Fuc β), H-4 (Fuc β)), 3.94–3.89 (m, 3H, H-3 (Fuc β), H-5 (GlcA α)), 3.79 (t, 1H, J = 6.5 Hz, H-4 (Fuc α)), 3.71 (s, 6H, OMe β), 3.70 (s, 3H, OMe α), 3.74–3.63 (m, 6H, H-5 (Fuc α), H-5 (Fuc β), H-3 (GlcA α), H-3 (GlcA β)), 3.60–3.48 (m, 3H, H-2 (GlcA α), H-2 (GlcA β)), 1.20 (d, $J_{5,6}$ = 6.4 Hz, 6H, H-6 (Fuc β)), 1.03 (d, $J_{5,6}$ = 6.3 Hz, 3H, H-6 (Fuc α)). ^{13}C NMR (100.6 MHz, $CDCl_3$): δ 169.5 (C-6 (GlcA α)), 168.7 (C-6 (GlcA β)), 139.1–137.5 (m, 5 × Ar α, 5 × Bn β), 133.8 (CH_2CH═CH_2 α), 133.7 (CH_2CH═CH_2 β), 128.5–127.2 (5 × Ar α, 5 × Ar β), 117.7 (CH_2CH═CH_2 β), 117.6 (CH_2CH═CH_2 α), 107.1 (C-1 (Fuc β)), 102.7 (C-1 (GlcA β)), 102.6 (C-1 (GlcA α)), 99.8 (C-1 (Fuc α)), 88.2 (C-2 (Fuc β)), 85.3 (C-4 (Fuc β)), 84.1 (C-2 (Fuc α)), 83.6 (C-3 (GlcA β)), 83.3 (C-4 (Fuc α)), 83.1 (C-3 (Fuc β)), 82.7 (C-3 (GlcA α)), 81.8 (C-2 (GlcA α)), 81.6 (C-2 (GlcA β)), 80.8 (C-3 (Fuc α)), 76.5 (C-5 (Fuc α)), 76.1 (C-4 (GlcA α)), 76.0 (C-4 (GlcA β)), 75.2 (C-5 (GlcA β)), 75.1 (2 × CH_2Ph α,β), 74.8 (CH_2Ph β), 74.7 (CH_2Ph α), 74.7 (C-5 (GlcA α), 74.0 (C-5 (Fuc β)), 72.4 (CH_2Ph α), 72.1 (CH_2Ph α), 71.9 (CH_2Ph β), 71.4 (CH_2Ph β), 71.3 (CH_2Ph β), 71.1 (CH_2Ph α), 70.5 (OCH_2CH β), 70.4 (OCH_2CH α), 52.6 (OMe β), 52.5 (OMe α), 15.7 (C-6 (Fuc β), 15.6 (C-6 (Fuc α). Calcd m/z for [M + Na]$^+$ $C_{51}H_{56}O_{11}$ 867.3715, found 867.3726.

Allyl methyl 2,3-di-*O*-benzyl-4-*O*-*tert*-butyldimethylsilyl-α,β-D-glucopyranosyluronate-(1→2)-3-*O*-chloroacetyl-4-*O*-benzoyl-α-L-fucopyranosyl-(1→3)-2-*O*-benzyl-4-*O*-benzoyl-α-L-fucopyranoside (27). Glycosylation of acceptor **16** (290 mg, 0.4 mmol) with donor **8** (284 mg, 0.44 mmol) as described in the general procedure B gave trisaccharide **27** (420 mg, 87%, α : β = 4 : 1) as a colorless syrup. R_f = 0.55 (hexane–EtOAc = 3 : 1). For the α-isomer: ^{1}H NMR (600 MHz, $CDCl_3$): δ 8.17 (d, J = 7.4 Hz, 2H, Bz), 8.05 (d, J = 7.4 Hz, 2H, Bz), 7.50–7.05 (m, 21H, 5 × Ar), 6.00–5.92 (m, 1H, CH_2CH═CH_2), 5.77 (d, $J_{3,4}$ = 3.2 Hz, 1H, H-4 (Fuc)), 5.52 (dd, $J_{2,3}$ = 10.7 Hz, $J_{3,4}$ = 3.4 Hz, 1H, H-3 (Fuc′)), 5.40–5.35 (m, 2H, H-1 (Fuc′), CH_2CH═CHH′), 5.32 (d, $J_{3,4}$ = 3.4 Hz, 1H, H-4 (Fuc′)), 5.25 (d, J = 10 Hz, 1H, CH_2CH═CHH′), 5.19 (d, $J_{1,2}$ = 3.9 Hz, 1H, H-1 (GlcA)), 5.01 (d, $J_{1,2}$ = 3.7 Hz, 1H, H-1 (Fuc)), 4.84–4.75 (m, 2H, CH_2Ph), 4.70–4.50 (m, 4H, 2 × CH_2Ph), 4.49–4.39 (m, 2H, H-3 (Fuc), H-5 (Fuc′)), 4.35–4.31 (m, 1H, H-4 (GlcA)), 4.30–4.26 (m, 1H, H-2 (Fuc′)), 4.25–4.18 (m, 2H, H-5 (Fuc), OCHH′CH), 4.08–4.01 (m, 2H, H-2 (Fuc), OCHH′CH), 3.86–3.82 (m, 2H, H-3 (GlcA), H-5 (GlcA)), 3.78 (s, 3H, OMe), 3.60–3.54 (m, 2H, H-2 (GlcA), C(O)CHH′Cl), 3.44 (d, J = 15.4 Hz, 1H, C(O)CHH′Cl), 1.15 (d, $J_{5,6}$ = 6.5 Hz, 3H, H-6 (Fuc)), 0.92 (s, 9H, C(CH_3)$_3$), (d, $J_{5,6}$ = 6.5 Hz, 3H, H-6 (Fuc′)), 0.13 (s, 3H, Si(CH$_3$)(CH_3)), 0.11 (s, 3H, Si(CH_3)(CH$_3$)). ^{13}C NMR (150 MHz, $CDCl_3$): δ 169.9 (C-6 (GlcA)), 166.3 (C(O)Ph), 166.1 (C(O)Ph), 165.7 (C(O)CH_2Cl), 139.0 (Bn), 138.1 (Bn), 137.8 (Bn), 133.4 (CH_2CH═CH_2), 126.7–130.4 (5 × Ar), 117.9 (CH_2CH═CH_2), 98.1 (C-1 (Fuc), C-1 (GlcA)), 95.9 (C-1 (Fuc)), 80.2 (C-3 (GlcA)), 80.0 (C-2 (GlcA)), 75.8 (C-2 (Fuc)), 74.9 (C-3 (Fuc)), 74.6 (CH_2Ph), 72.8–72.3 (C-2 (Fuc′), C-3 (Fuc′), C-4 (Fuc′), C-4 (Fuc), C-4 (GlcA), C-5 (GlcA), 2 × CH_2Ph), 71.7 (C-4 (Fuc′)), 68.5 (OCH_2CH), 65.5 (C-5 (Fuc)), 65.0 (C-5 (Fuc′)), 52.4 (OMe), 40.4 (C(O)CH_2Cl), 25.8 (C(CH_3)$_3$), 16.2 (C-6 (Fuc)), 15.7 (C-6 (Fuc′)), −3.9 (Si(CH$_3$)(CH_3), −5.4 (Si(CH_3)(CH$_3$). Selected NMR signals for the minor β-isomer: ^{1}H NMR (600 MHz, $CDCl_3$): δ 4.50–4.42 (m, 3H, H-1 (GlcA), H-5 (Fuc′), CHH′Ph), 3.78 (d, $J_{4,5}$ = 9.5 Hz, 1H, H-5 (GlcA)), 3.61 (t, J = 8.7 Hz, 1H, H-4 (GlcA)), 3.00 (t, J = 8.7 Hz, 1H, H-2 (GlcA)), 2.91 (1H, t, J = 8.7 Hz, H-3 (GlcA)). ^{13}C NMR (150.9 MHz, $CDCl_3$): δ 99.8 (C-1 (GlcA)), 83.3 (C-3 (GlcA)), 81.4 (C-2 (GlcA)), 76.0 (C-5 (GlcA)), 71.7 (C-4 (GlcA)). Calcd m/z for [M + Na]$^+$ $C_{65}H_{77}ClO_{18}Si$ 1231.4460, found 1231.4455.

Allyl methyl 2,3-di-*O*-benzyl-α-D-glucopyranosyluronate-(1→2)-3-*O*-chloroacetyl-4-*O*-benzoyl-α-L-fucopyranosyl-(1→3)-2-*O*-benzyl-4-*O*-benzoyl-α-L-fucopyranoside (28). To a solution of protected trisaccharide **27** (388 mg, 0.32 mmol) in CH_3CN (7 mL) an aqueous solution of HF (40%, 1 mL) was added. The reaction mixture was stirred for 2 h at 40 °C and then diluted with $CHCl_3$ (30 mL) and washed twice with aqueous Na_2CO_3 (5%, 150 mL) and water (150 mL). The organic layer was concentrated and the residue was chromatographed (silica gel, eluent: toluene/acetone = 50 : 1→30 : 1) to give the desilylated derivative **27** (270 mg, 77%) as a colorless syrup. R_f = 0.51 (toluene–acetone = 10 : 1). $[\alpha]_D$ = −135.5° (c = 1, EtOAc). ^{1}H NMR (600 MHz, $CDCl_3$): δ 8.14 (d, J = 7.2 Hz, 2H, o-Ph (Bz)), 8.11 (d, J = 7.3 Hz, 2H, o-Ph (Bz)), 7.63 (t, J = 7.3 Hz, 1H, p-Ph (Bz)), 7.55–7.15 (m, 20H, 5 × Ph), 6.06–5.98 (m, 1H, CH_2CH═CH_2), 5.72 (d, $J_{3,4}$ = 2.7 Hz, 1H, H-4 (Fuc)), 5.65 (dd, $J_{2,3}$ = 10.7 Hz, $J_{3,4}$ = 3.3 Hz, 1H, H-3 (Fuc′)), 5.46–5.41 (m, 2H, H-1 (Fuc′), CH_2CH═CHH′), 5.35 (d, $J_{3,4}$ = 2.3 Hz, 1H, H-4 (Fuc′)), 5.29 (dd, J = 1.2 Hz, J = 10.5 Hz, 1H, CH_2CH═CHH′), 5.18 (d, $J_{1,2}$ = 3.0 Hz, 1H, H-1 (GlcA)), 5.13 (d, $J_{1,2}$ = 3.5 Hz, 1H, H-1 (Fuc)), 4.82–4.77 (m, 2H, CH_2Ph), 4.69 (q, J = 6.4 Hz, 1H, H-5 (Fuc)), 4.58 (dd, $J_{2,3}$ = 10.4 Hz, $J_{3,4}$ = 2.9 Hz, 1H, H-3 (Fuc)), 4.54–4.43 (m, 4H, H-5 (GlcA), CH_2Ph, CHH′Ph), 4.35 (dd, $J_{1,2}$ = 3.4 Hz, $J_{2,3}$ = 10.7 Hz, 1H, H-2 (Fuc′)), 4.32 (d, J = 11.4 Hz, 1H, CHH′Ph), 4.27 (dd, J = 5.0 Hz, J = 13.3 Hz, 1H, OCHH′CH), 4.23–4.17 (m, 2H, H-2 (Fuc), H-5 (Fuc)), 4.11 (dd, J = 6.0 Hz, J = 13.3 Hz, 1H, OCHH′CH), 3.94–3.88 (m, 1H, H-4 (GlcA)), 3.81 (s, 3H, OMe), 3.64 (dd, J = 15.4 Hz, J = 55.8 Hz, 2H, CH_2Cl), 3.54 (t, J = 7.6 Hz, 1H, H-3 (GlcA)), 3.48 (dd, $J_{1,2}$ = 3.1 Hz, $J_{2,3}$ = 8.1 Hz, 1H, H-2 (GlcA)), 1.16 (d, $J_{5,6}$ = 6.5 Hz, 3H, H-6 (Fuc)), 0.96 (d, $J_{5,6}$ = 6.5 Hz, 3H, H-6 (Fuc′)). ^{13}C NMR (150.9 MHz, $CDCl_3$): δ 170.0 (C-6 (GlcA)), 167.5 (C(O)CH_2Cl), 166.3 (C(O)Ph), 166.2 (C(O)Ph), 138.4 (Bn), 137.8 (Bn), 137.8 (Bn), 133.9 (CH_2CH═CH_2), 133.4 (Bz), 133.3 (Bz), 130–127 (Ar), 117.4 (CH_2CH═CH_2), 99.1 (C-1 (GlcA)), 91.1 (C-1 (Fuc)), 95.9 (C-1 (Fuc′)), 79.7 (C-3 (GlcA)), 77.0 (C-2 (GlcA)), 74.9 (C-2 (Fuc)), 73.9 (CH_2Ph), 73.3 (C-2 (Fuc′)), 73.1 (C-5 (GlcA)), 72.9 (CH_2Ph), 72.8 (CH_2Ph), 72.1 (C-4 (Fuc)), 72.0 (C-3 (Fuc′)), 71.8 (C-4 (Fuc′)), 71.4 (C-3 (Fuc)), 71.3 (C-4 (GlcA)), 68.5 (OCH_2CH), 65.9 (C-5 (Fuc)), 64.7 (C-5 (Fuc′)), 52.4 (OMe), 40.4 (CH_2Cl), 16.4 (C-6 (Fuc)), 15.5 (C-6 (Fuc′)). Calcd m/z for [M + Na]$^+$ $C_{59}H_{63}ClO_{18}$ 1117.3595, found 1117.3594.

Allyl methyl 2,5-di-*O*-benzyl-3-*O*-benzoyl-α-L-fucofuranosyl-(1→4)-2,3-di-*O*-benzyl-α-D-glucopyranosyluronate-(1→2)-3-*O*-chloroacetyl-4-*O*-benzoyl-α-L-fucopyranosyl-(1→3)-2-*O*-benzyl-4-*O*-benzoyl-α-L-fucopyranoside (29). Glycosylation of acceptor **28** (270 mg, 0.25 mmol) with donor **9** (165 mg, 0.28 mmol) as

described in the general procedure B gave tetrasaccharide **29** (297 mg, 79%) as a colorless syrup. R_f = 0.35 (hexane–EtOAc = 3 : 1). $[\alpha]_D$ = −107.8° (*c* = 1, EtOAc). ^{1}H NMR (600 MHz, $CDCl_3$): *δ* 8.25 (d, *J* = 7.3 Hz, 2H, *o*-Ph (Bz)), 8.09 (d, *J* = 8.0 Hz, 2H, *o*-Ph (Bz)), 8.01 (d, *J* = 8.0 Hz, 2H, Bz), 7.64–7.13 (m, 34H, 8 × Ar), 6.03–5.95 (m, 1H, CH_2CH=CH_2), 5.83 (t, *J* = 7.0 Hz, 1H, H-3 (Fucf)), 5.73 (d, $J_{3,4}$ = 3.0 Hz, 1H, H-4 (Fucp)), 5.61 (dd, $J_{2,3}$ = 10.7 Hz, $J_{3,4}$ = 3.3 Hz, 1H, H-3 (Fucp′)), 5.45 (d, $J_{1,2}$ = 3.2 Hz, 1H, H-1 (Fucp′)), 5.40–5.38 (m, 2H, H-1 (Fucf), CH_2CH=CHH'), 5.34 (d, $J_{3,4}$ = 3.3 Hz, 1H, H-4 (Fucp′)), 5.27 (dd, *J* = 1.3 Hz, *J* = 10.4 Hz, 1H, CH_2CH=CHH'), 5.24 (d, $J_{1,2}$ = 4.0 Hz, 1H, H-1 (GlcA)), 5.08 (d, $J_{1,2}$ = 3.6 Hz, 1H, H-1 (Fucp)), 4.83–4.77 (m, 3H, 3 × CHH'Ph), 4.74–4.70 (m, 2H, H-5 (GlcA), CHH'Ph), 4.64 (d, *J* = 11.9 Hz, 1H, CHH'Ph), 4.59–4.51 (m, 6H, H-5 (Fucp′), CH_2Ph, 3 × CHH'Ph), 4.47 (dd, $J_{2,3}$ = 10.2 Hz, $J_{3,4}$ = 3.1 Hz, 1H, H-3 (Fucp)), 4.36 (dd, $J_{1,2}$ = 3.2 Hz, $J_{2,3}$ = 10.6 Hz, 1H, H-2 (Fucp′)), 4.26–4.19 (m, 2H, H-5 (Fucp), OCHH'CH), 4.12 (dd, $J_{1,2}$ = 3.6 Hz, $J_{2,3}$ = 10.1 Hz, 1H, H-2 (Fucp)), 4.08–4.05 (m, 2H, H-2 (Fucf), OCHH'CH), 4.05–3.96 (m, 3H, H-3 (GlcA), H-4 (GlcA), H-4 (Fucf)), 3.90–3.86 (m, 4H, H-5 (Fucf), OMe), 3.68 (d, *J* = 15.4 Hz, 1H, CHH'Cl), 3.57–3.53 (m, 2H, H-2 (GlcA), CHH'Cl), 1.16 (d, $J_{5,6}$ = 6.5 Hz, 3H, H-6 (Fucp)), 1.04 (d, $J_{5,6}$ = 6.4 Hz, 3H, H-6 (Fucf)), 0.99 (d, $J_{5,6}$ = 6.5 Hz, 3H, H-6 (Fucp′)). ^{13}C NMR (150 MHz, $CDCl_3$): *δ* 170.3 (C-6 (GlcA)), 166.3 (*C*(O)CH_2Cl), 166.0 (*C*(O)Ph), 166.9 (*C*(O)Ph), 165.3 (*C*(O)Ph), 139.2 (Bn), 138.7 (Bn), 138.1 (Bn), 138.0 (Bn), 137.6 (Bn), 134.0 (CH_2CH=CH_2), 133.3 (Bz), 133.1 (Bz), 132.9 (Bz), 130–127 (Ar), 117.6 (CH_2CH=CH_2), 100.5 (C-1 (GlcA)), 98.5 (C-1 (Fucf)), 96.7 (C-1 (Fucp′)), 96.0 (C-1 (Fucp)), 82.5 (C-4 (Fucf)), 81.9 (C-2 (Fucf)), 80.0 (C-3 (GlcA)), 79.3 (C-2 (GlcA)), 77.0 (C-5 (Fucf)), 76.7 (C-4 (GlcA)), 75.5 (C-2 (Fucp)), 75.0 (C-3 (Fucf), CH_2Ph), 73.1 (C-3 (Fucp)), 72.8 (CH_2Ph), 72.7 (CH_2Ph), 72.5 (C-2 (Fucp′)), 72.3 (C-3 (Fucp′)), 71.9 (C-4 (Fucp′), CH_2Ph), 71.6 (C-4 (Fucp)), 71.5 (CH_2Ph), 70.6 (C-5 (GlcA)), 68.5 (OCH_2CH), 65.4 (C-5 (Fucp)), 64.8 (C-5 (Fucp′)), 52.7 (OMe), 40.5 (CH_2Cl), 16.2 (C-6 (Fucp)), 15.6 (C-6 (Fucp′)), 15.2 (C-6 (Fucf)). Calcd *m*/*z* for $[M + Na]^+$ $C_{86}H_{89}ClO_{23}$ 1547.5375, found 1547.5370.

Allyl 2,5-di-*O*-benzyl-3-*O*-benzoyl-α-L-fucofuranosyl-(1→4)-methyl 2,3-di-*O*-benzyl-α-D-glucopyranosyluronate-(1→2)-4-*O*-benzoyl-α-L-fucopyranosyl-(1→3)-2-*O*-benzyl-4-*O*-benzoyl-α-L-fucopyranoside (30). *O*-Dechloroacetylation of **29** (273 mg, 0.018 mmol) was performed as described for the preparation of **18** to give tetrasaccharide **30** (207 mg, 80%) as a colorless oil. R_f = 0.32 (Toluene–EtOAc = 10 : 1). $[\alpha]_D$ = −96.4° (*c* = 1, EtOAc). ^{1}H NMR (400 MHz, $CDCl_3$): *δ* 8.21 (d, *J* = 7.0 Hz, 2H, *o*-Ph (Bz)), 8.10 (d, *J* = 7.1 Hz, 2H, *o*-Ph (Bz)), 7.97 (d, *J* = 7.1 Hz, 2H, *o*-Ph (Bz)), 7.62–7.00 (m, 34H, 8 × Ar), 5.99–5.88 (m, 1H, CH_2CH=CH_2), 5.76 (t, *J* = 6.9 Hz, 1H, H-3 (Fucf)), 5.72 (d, $J_{3,4}$ = 2.9 Hz, 1H, H-4 (Fucp)), 5.39–5.33 (m, 2H, H-1 (Fucp), CH_2CH=CHH'), 5.31 (d, $J_{1,2}$ = 3.2 Hz, 1H, H-1 (Fucp′)), 5.25–5.19 (m, 2H, H-4 (Fucp′), CH_2CH=CHH'), 4.99–4.93 (m, 3H, H-1 (GlcA), H-1 (Fucf), CHH'Ph), 4.78–4.45 (m, 10H, H-5 (GlcA), 4 × CH_2Ph, CHH'Ph), 4.38–4.30 (m, 2H, H-3 (Fucp), H-5 (Fucp′)), 4.27–4.16 (m, 3H, H-3 (Fucp′), H-5 (Fucp), OCHH'CH), 4.08–3.96 (m, 5H, H-2 (Fucf), H-4 (Fucf), H-2 (Fucp), H-3 (GlcA), OCHH'CH), 3.94–3.87 (m, 2H, H-4 (GlcA), H-2 (Fucp′)), 3.86–3.80 (m, 4H, H-5 (Fucf), OMe), 3.49 (dd, $J_{1,2}$ = 3.8 Hz, $J_{2,3}$ = 9.6 Hz, 1H, H-2 (GlcA)), 1.23 (d, $J_{5,6}$ = 6.4 Hz, 3H, H-6 (Fucp)), 1.03 (d, $J_{5,6}$ = 6.4 Hz, 3H, H-6 (Fucp′)), 0.99 (d, $J_{5,6}$ = 6.3 Hz, 3H, H-6 (Fucf)). ^{13}C NMR (100 MHz, $CDCl_3$): *δ* 170.3 (C-6 (GlcA)), 166.6 (*C*(O)Ph), 165.8 (*C*(O)Ph), 165.4 (*C*(O)Ph), 139.2 (Bn), 138.6 (Bn), 138.4 (Bn), 137.8 (Bn), 137.2 (Bn), 134.0 (CH_2CH=CH_2), 133.3 (Bz), 132.1 (2 × Bz), 130–127 (8 × Ar), 117.8 (CH_2CH=CH_2), 101.0 (C-1 (GlcA)), 100.8 (C-1 (Fucp)), 98.0 (C-1 (Fucp′)), 95.2 (C-1 (Fucf)), 82.7 (C-2 (Fucf)), 82.0 (C-4 (Fucf)), 80.9 (C-3 (GlcA)), 80.1 (C-2 (Fucp′)), 78.8 (C-2 (GlcA)), 77.4 (C-5 (Fucf)), 77.1 (C-4 (GlcA)), 76.4 (C-2 (Fucp)), 75.7 (CH_2Ph), 75.1 (C-3 (Fucf)), 74.4 (C-3 (Fucp)), 74.0 (CH_2Ph), 74.0 (C-4 (Fucp′)), 73.0 (CH_2Ph), 72.4 (C-4 (Fucp)), 72.0 (CH_2Ph), 71.7 (CH_2Ph), 70.8 (C-5 (GlcA)), 68.7 (OCH_2CH), 68.1 (C-3 (Fucp′)), 65.6 (C-5 (Fucp′)), 65.3 (C-5 (Fucp)), 52.8 (OMe), 16.2 (C-6 (Fucp)), 16.1 (C-6 (Fucp′)), 15.2 (C-6 (Fucf)). Calcd *m*/*z* for $[M + Na]^+$ $C_{84}H_{88}O_{22}$ 1471.5659, found 1471.5650.

Allyl 2-*O*-benzyl-3,4-di-*O*-chloroacetyl-α-L-fucopyranosyl-(1→3)-{2,5-di-*O*-benzyl-3-*O*-benzoyl-α-L-fucofuranosyl-(1→4)-methyl-2,3-di-*O*-benzyl-α-D-glucopyranosyluronate-(1→2)}-4-*O*-benzoyl-α-L-fucopyranosyl-(1→3)-2-*O*-benzyl-4-*O*-benzoyl-α-L-fucopyranoside (31). Glycosylation of acceptor **30** (203 mg, 0.14 mmol) with donor **6** (115 mg, 0.21 mmol) as described in the general procedure B gave pentasaccharide **31** (297 mg, 79%) as a colorless syrup. R_f = 0.69 (toluene–EtOAc = 8 : 1). $[\alpha]_D$ = −96.75° (*c* = 1, EtOAc). ^{1}H NMR (400 MHz, $CDCl_3$): *δ* 8.16 (d, *J* = 7.1 Hz, 2H, *o*-Ph(Bz)), 7.98 (d, *J* = 7.1 Hz, 2H, *o*-Ph(Bz)), 7.96 (d, *J* = 7.1 Hz, 2H, *o*-Ph(Bz)), 7.58 (t, *J* = 7.3 Hz, 1H, *p*-Ph(Bz)), 7.50–7.00 (m, 38H, 9 × Ph), 5.91–5.80 (m, 1H, CH_2CH=CH_2), 5.78 (t, *J* = 6.8 Hz, 1H, H-3 (Fucf)), 5.70 (d, $J_{3,4}$ = 3.2 Hz, 1H, H-4 (Fucp)), 5.45 (d, $J_{1,2}$ = 3.9 Hz, 1H, H-1 (Fucp′)), 5.44 (d, $J_{1,2}$ = 4.2 Hz, 1H, H-1 (Fucf)), 5.37 (dd, $J_{2,3}$ = 10.4 Hz, $J_{3,4}$ = 3.4 Hz, 1H, H-3 (Fucp″)), 5.30 (dd, *J* = 1.6 Hz, *J* = 17.2 Hz, 1H, CH_2CH=CHH'), 5.22 (d, $J_{3,4}$ = 3.0 Hz, 1H, H-4 (Fucp′)), 5.20–5.15 (m, 2H, H-1 (Fucp″), CH_2CH=CHH'), 5.10 (d, $J_{3,4}$ = 3.3 Hz, 1H, H-4 (Fucp″)), 5.02 (d, $J_{1,2}$ = 3.9 Hz, 1H, H-1 (GlcA)), 5.00 (d, *J* = 14.2 Hz, 1H, CHH'Ph), 4.90 (d, $J_{1,2}$ = 3.7 Hz, 1H, H-1 (Fucp)), 4.88 (d, *J* = 10.2 Hz, 1H, CHH'Ph), 4.76–4.67 (m, 2 × CHH'Ph, 2 × CHH'Ph), 4.59–4.54 (m, 3H, H-5 (GlcA), CH_2Ph), 4.52–4.45 (m, 3H, H-5 (Fucp″), 2 × CHH'Ph), 4.33 (d, *J* = 12.5 Hz, 1H, CHH'Ph), 4.33 (m, 1H, H-3 (Fucp)), 4.30 (m, 1H, H-3 (Fucp′)), H-5 (Fucp), OCHH'CH, CHH'Ph), 4.17–4.08 (m, 5H, H-2 (Fucp′), H-5 (Fucp′), 4.07–3.95 (m, 6H, H-3 (GlcA), H-4 (GlcA), H-2 (Fucf), H-4 (Fucf), C(O)CH_2Cl), 3.92–3.86 (m, 2H, H-2 (Fucp), OCHH'CH), 3.81 (t, *J* = 6.5 Hz, 1H, H-5 (Fucf)), 3.79 (s, 3H, OMe), 3.72–3.60 (m, 4H, H-2 (GlcA), H-2 (Fucp″), C(O)CH_2Cl), 1.12–1.08 (m, 6H, H-6 (Fucp), H-6 (Fucf)), 0.98 (d, $J_{5,6}$ = 6.5 Hz, 3H, H-6 (Fucp″)), 0.93 (d, $J_{5,6}$ = 6.5 Hz, 3H, H-6 (Fucp′)). ^{13}C NMR (100 MHz, $CDCl_3$): *δ* 170.2 (C-6 (GlcA)), 167.1 (*C*(O)CH_2Cl), 166.5 (*C*(O)CH_2Cl), 165.8 (*C*(O)Ph), 165.3 (*C*(O)Ph), 139.0 (Bn), 138.7 (Bn), 138.5 (Bn), 138.4 (Bn), 138.0 (Bn), 137.8 (Bn), 133.9 (CH_2CH=CH_2), 133.1 (Bz), 133.1 (Bz), 133.0 (Bz), 130.3–127.0 (9 × Ar), 117.7 (CH_2CH=CH_2), 100.8 (C-1 (Fucf)), 99.5 (C-1 (GlcA)), 97.1 (C-1 (Fucp′)), 95.9 (C-1 (Fucp)), 92.3 (C-1 (Fucp″)), 82.5 (C-4 (Fucf)), 82.0 (C-2 (Fucf)), 80.9 (C-3 (GlcA)), 78.7 (C-2 (GlcA)), 76.7 (C-5 (Fucf)), 76.6

(C-4 (GlcA)), 76.4 (C-2 (Fucp)), 76.0 (C-2 (Fucp′)), 75.1 (*C*H_2Ph), 75.0 (C-3 (Fucf)), 74.0 (C-3 (Fucp)), 73.9 (*C*H_2Ph), 73.5 (C-4 (Fucp″)), 72.7 (C-4 (Fucp), *C*H_2Ph), 72.4 (C-2 (Fucp″)), 72.2 (*C*H_2Ph), 72.0 (C-3 (Fucp″), *C*H_2Ph), 71.7 (*C*H_2Ph), 71.0 (C-5 (GlcA)), 69.7 (C-3 (Fucp′)), 69.5 (C-4 (Fucp′)), 68.6 (O*C*H_2CH), 65.1 (C-5 (Fucp′)), 64.9 (C-5 (Fucp)), 64.0 (C-5 (Fucp″)), 52.8 (OMe), 40.5 (C(O)*C*H_2Cl), 40.4 (C(O)*C*H_2Cl), C-6 (Fucp′)), 16.0 (C-6 (Fucp), 15.3 (C-6 (Fucp″)), 15.3 (C-6 (Fucf)). Calcd *m*/*z* for $[M + Na]^+$ $C_{101}H_{106}Cl_2O_{28}$ 1859.6140, found 1859.6200.

Sodium salt propyl α-L-fucopyranosyl-(1→3)-{α-L-fucofuranosyl-(1→4)-α-D-glucopyranosyluronate-(1→2)}-α-L-fucopyranosyl-(1→3)-α-L-fucopyranoside (3). Deprotection of pentasaccharide **31** (27 mg, 0.014 mmol) as described for the preparation of compound **1** gave pentasaccharide **3** (9.7 mg, 82%) as a white amorphous powder. $[\alpha]_D$ = −77.3° (*c* = 1, H_2O). ^{1}H NMR (600 MHz, D_2O): δ 5.32 (d, $J_{1,2}$ = 4.0 Hz, 1H, H-1 (GlcA)), 5.23 (d, $J_{1,2}$ = 3.9 Hz, 1H, H-1 (Fucp″)), 5.21 (d, $J_{1,2}$ = 3.9 Hz, 1H, H-1 (Fucp′)), 5.10 (d, $J_{1,2}$ = 4.7 Hz, 1H, H-1 (Fucf)), 4.99 (br s, 1H, H-1 (Fucp)), 4.49 (q, *J* = 6.3 Hz, 1H, H-5 (Fucp′)), 4.36 (q, *J* = 6.5 Hz, 1H, H-5 (Fucp″)), 4.34 (dd, $J_{2,3}$ = 10.4 Hz, $J_{3,4}$ = 3.0 Hz, 1H, H-3 (Fucp′)), 4.22 (dd, $J_{1,2}$ = 3.8 Hz, $J_{2,3}$ = 10.4 Hz, 1H, H-2 (Fucp′)), 4.20–4.17 (m, 2H, H-3 (Fucf), H-4 (Fucp′)), 4.16–4.12 (m, 4H, H-4 (Fucp), H-5 (Fucp), H-2 (Fucf), H-5 (GlcA)), 4.03 (m, 2H, H-2 (Fucp), H-3 (Fucp)), 4.01–3.96 (m, 2H, H-3 (Fucp″), H-5 (Fucf)), 3.90–3.83 (m, 3H, H-3 (GlcA), H-2 (Fucp″), H-4 (Fucp″)), 3.74–3.68 (m, 3H, H-2 (GlcA), H-4 (Fucf), OCH*H*′CH_2), 3.63 (t, *J* = 9.5 Hz, 1H, H-4 (GlcA)), 3.61–3.56 (m, 1H, OC*H*H′CH_2), 1.75–1.67 (m, 2H, $CH_2CH_2CH_3$), 1.33 (d, $J_{5,6}$ = 6.6 Hz, 3H, H-6 (Fucp)), 1.31 (d, $J_{5,6}$ = 6.5 Hz, 3H, H-6 (Fucp″)), 1.30 (d, $J_{5,6}$ = 6.4 Hz, 3H, H-6 (Fucf)), 1.28 (d, $J_{5,6}$ = 6.6 Hz, 3H, H-6 (Fucp′)), 1.00 (t, *J* = 7.4 Hz, 3H, $CH_2CH_2CH_3$). ^{13}C NMR (150 MHz, D_2O): δ 176.9 (C-6 (GlcA)), 103.4 (C-1 (Fucf)), 100.7 (C-1 (GlcA)), 99.5 (C-1 (Fucp)), 95.5 (C-1 (Fucp′)), 94.5 (C-1 (Fucp″)), 86.2 (C-4 (Fucf)), 81.7 (C-4 (GlcA)), 77.6 (C-2 (Fucf)), 75.8 (C-3 (Fucf)), 75.3 (C-3 (Fucp)), 73.9 (C-3 (Fucp′)), 73.2 (C-5 (GlcA)), 73.1 (C-4 (Fucp″)), 73.0 (C-3 (GlcA)), 72.4 (C-2 (Fucp′)), 72.0 (C-2 (GlcA)), 71.3 (O*C*H_2CH$_2$), 70.8 (C-3 (Fucp″)), C-2 (Fucp″)), 69.1 (C-4 (Fucp), 68.4 (C-5 (Fucf)), 68.3 (C-4 (Fucp′)), 68.2 (C-5 (Fucp′)), 67.7 (C-5 (Fucp)), 67.6 (C-5 (Fucp″)), 67.5 (C-2 (Fucp)), 23.4 ($CH_2CH_2CH_3$), 19.7 (C-6 (Fucf)), 16.7 (C-6 (Fucp)), 16.5 (C-6 (Fucp′), C-6 (Fucp″)), 11.1 ($CH_2CH_2CH_3$). Calcd *m*/*z* for $[M + H]^+$ $C_{33}H_{55}NaO_{23}$ 843.3105, found 843.3108.

Sodium salt propyl 3,4-di-*O*-sulfonato-α-L-fucopyranosyl-(1→3)-{3-*O*-sulfonato-α-L-fucofuranosyl-(1→4)-α-D-glucopyranosyluronate-(1→2)}-4-*O*-sulfonato-α-L-fucopyranosyl-(1→3)-4-*O*-sulfonato-α-L-fucopyranoside (4). To a solution of pentasaccharide **31** (30 mg, 0.016 mmol) in THF (2 mL) 2 M aqueous NaOH (0.2 mL) was added and the mixture was kept at 20 °C for 20 h. Then 40% aqueous Bu_4NOH (0.1 mL) was added and the mixture was kept at 20 °C for another 48 h. The solution was neutralized with Amberlite IR-120 (H^+), cation-exchange resin was filtered off and the filtrate was concentrated. The residue was purified by chromatography (silica gel, eluent: CH_2Cl_2/MeOH = 25 : 1→6 : 1). The resulting pentaol was dissolved in DMF (2 mL) and Py·SO_3 (140 mg, 0.88 mmol) was added. The reaction mixture was kept at 40 °C for 3 h, then quenched with 1 M aq. $NaHCO_3$ up to pH 8–9 and concentrated *in vacuo*. The solid residue was dissolved in a minimal amount of water (~0.4 mL) and then MeOH (5 mL) was added to precipitate inorganic salts. The solids were filtered off, washed with MeOH and the filtrate was concentrated. The residue was purified by chromatography (silica gel, eluent: CH_2Cl_2/MeOH = 10 : 1→1 : 1). The mixture of the product and the catalyst 10% Pd/C (50 mg) in THF–EtOAc–EtOH (4 : 1 : 1) (3 mL) was stirred under H_2 (1 atm) at rt for 12 h and then filtered through a nylon membrane syringe filter (0.45 μm). The filtrate was concentrated and the residue was purified by column chromatography on a gel Sephadex G-15 with water elution followed by lyophilization to give **4** (16.8 mg, 76%) as a white amorphous powder. $[\alpha]_D$ = −87.7° (*c* = 1, H_2O). ^{1}H NMR (600 MHz, D_2O): δ 5.53 (d, $J_{1,2}$ = 3.8 Hz, 1H, H-1 (Fucp″)), 5.47 (br s, 1H, H-1 (GlcA)), 5.36 (d, $J_{1,2}$ = 3.0 Hz, 1H, H-1 (Fucp′)), 5.25 (d, $J_{1,2}$ = 4.9 Hz, 1H, H-1 (Fucf)), 5.03 (d, $J_{1,2}$ = 3.9 Hz, 1H, H-1 (Fucp)), 4.99 (d, $J_{3,4}$ = 2.5 Hz, 1H, H-4 (Fucp′)), 4.95 (d, $J_{3,4}$ = 2.7 Hz, 1H, H-4 (Fucp″)), 4.89 (d, $J_{3,4}$ = 2.7 Hz, 1H, H-4 (Fucp)), 4.85–4.81 (m, 2H, H-3 (Fucp″), H-3 (Fucf)), 4.66–4.60 (m, 2H, H-3 (Fucp′), H-5 (Fucp″)), 4.56 (q, $J_{5,6}$ = 6.6 Hz, 1H, H-5 (Fucp′)), 4.42 (t, *J* = 5.4 Hz, 1H, H-2 (Fucf)), 4.33–4.26 (m, 2H, H-2 (Fucp′), H-5 (Fucp)), 4.23 (d, $J_{4,5}$ = 9.2 Hz, 1H, H-5 (GlcA)), 4.18–4.15 (m, 1H, H-5 (Fucf)), 4.15–4.09 (m, 2H, H-2 (Fucp″), H-3 (Fucp)), 4.08–4.03 (m, 2H, H-2 (Fucp), H-3 (GlcA)), 4.00 (t, *J* = 5.2 Hz, 1H, H-4 (Fucf)), 3.80 (dd, $J_{1,2}$ = 2.9 Hz, $J_{2,3}$ = 9.7 Hz, 1H, H-2 (GlcA)), 3.77–3.72 (m, 1H, OCH*H*′CH_2), 3.70 (t, *J* = 9.6 Hz, 1H, H-4 (GlcA)), 3.63–3.58 (m, 1H, OC*H*H′CH_2), 1.78–1.71 (m, 2H, $CH_2CH_2CH_3$), 1.44–1.38 (m, 9H, H-6 (Fucp), H-6 (Fucp′), H-6 (Fucp″)), 1.34 (d, $J_{5,6}$ = 6.5 Hz, 3H, H-6 (Fucf)), 1.03 (t, *J* = 7.4 Hz, 3H, $CH_2CH_2CH_3$). ^{13}C NMR (150 MHz, D_2O): δ 177.0 (C-6 (GlcA)), 104.1 (C-1 (Fucf)), 100.3 (C-1 (GlcA)), 99.3 (C-1 (Fucp)), 99.1 (C-1 (Fucp′)), 94.5 (C-1 (Fucp″)), 86.2 (C-4 (Fucf)), 84.0 (C-3 (Fucf)), 82.3 (C-4 (GlcA)), 80.6 (C-4 (Fucp″)), 80.5 (C-4 (Fucp)), 77.9 (C-3 (Fucp)), 77.9 (C-4 (Fucp′)), 77.0 (C-2 (Fucf)), 76.8 (C-3 (Fucp″)), 73.0 (C-3 (GlcA), C-5 (GlcA)), 72.9 (C-2 (Fucp′)), 72.4 (C-2 (GlcA)), 71.9 (C-3 (Fucp′)), 71.4 (O*C*H_2CH$_2$), 68.7 (C-2 (Fucp)), 68.1 (C-5 (Fucp″)), 68.0 (C-5 (Fucf)), 67.9 (C-5 (Fucp′)), 67.5 (C-5 (Fucp)), 67.4 (C-2 (Fucp″)), 23.2 ($CH_2CH_2CH_3$), 19.7 (C-6 (Fucf)), 17.3 (C-6 (Fucp′)), 17.1 (C-6 (Fucp)), 17.1 (C-6 (Fucp″)), 11.1 ($CH_2CH_2CH_3$). Calcd *m*/*z* for $[M - 3Na + H]^{2-}$ $C_{33}H_{51}Na_3O_{38}S_5$ 642.0183, found 642.0159.

Acknowledgements

This work was supported by RSF grant 14-23-00199 (NEN). We thank Dr A. O. Chizhov for recording the high resolution mass spectra at the Department of Structural Studies of the Zelinsky Institute of Organic Chemistry, Moscow.

Notes and references

1 V. H. Pomin, *Biochim. Biophys. Acta*, 2012, **1820**, 1971.
2 A. Cumashi, N. A. Ushakova, M. E. Preobrazhenskaya, A. D'Incecco, A. Piccoli, L. Totani, N. Tinari, G. E. Morozevich,

A. E. Berman, M. I. Bilan, A. I. Usov, N. E. Ustyuzhanina, A. A. Grachev, C. J. Sanderson, M. Kelly, G. A. Rabinovich, S. Iacobelli and N. E. Nifantiev, *Glycobiology*, 2007, **17**, 541.
3 G. Jiao, G. Yu, J. Zhang and S. Ewart, *Mar. Drugs*, 2011, **9**, 196.
4 J. H. Fitton, *Mar. Drugs*, 2011, **9**, 1731.
5 A. I. Usov and M. I. Bilan, *Russ. Chem. Rev.*, 2009, **78**, 785.
6 N. E. Ustyuzhanina, N. A. Ushakova, K. A. Zyuzina, M. I. Bilan, A. L. Elizarova, O. V. Somonova, A. V. Madzhuga, V. B. Krylov, M. E. Preobrazhenskaya, A. I. Usov, M. V. Kiselevskiy and N. E. Nifantiev, *Mar. Drugs*, 2013, **11**, 2444.
7 D. O. Croci, A. Cumashi, N. A. Ushakova, M. E. Preobrazhenskaya, A. Piccoli, L. Totani, N. E. Ustyuzhanina, M. I. Bilan, A. I. Usov, A. A. Grachev, G. E. Morozevich, A. E. Berman, C. J. Sanderson, M. Kelly, P. Di Gregorio, C. Rossi, N. Tinari, S. Iacobelli, G. A. Rabinovich and N. E. Nifantiev, *PLoS One*, 2011, **6**, e17283.
8 E. A. Khatuntseva, N. E. Ustuzhanina, G. V. Zatonskii, A. S. Shashkov, A. I. Usov and N. E. Nifant'ev, *J. Carbohydr. Chem.*, 2000, **19**, 1151.
9 N. E. Ustyuzhanina, V. B. Krylov, A. I. Usov and N. E. Nifantiev, in *Progress in the synthesis of complex carbohydrate chains of plant and microbial polysaccharides*, ed. N. E. Nifantiev, Research Signpost, 2009, pp. 131–154.
10 N. E. Ustyuzhanina, V. B. Krylov, A. A. Grachev, A. G. Gerbst and N. E. Nifantiev, *Synthesis*, 2006, 4017.
11 A. G. Gerbst, N. E. Ustuzhanina, A. A. Grachev, E. A. Khatuntseva, D. E. Tsvetkov, D. M. Whitfield, A. Berces and N. E. Nifantiev, *J. Carbohydr. Chem.*, 2001, **20**, 821.
12 V. B. Krylov, Z. M. Kaskova, D. Z. Vinnitskiy, N. E. Ustyuzhanina, A. A. Grachev, A. O. Chizhov and N. E. Nifantiev, *Carbohydr. Res.*, 2011, **346**, 540.
13 N. S. Zlotina, N. E. Ustyuzhanina, A. A. Grachev, A. G. Gerbst and N. E. Nifantiev, *J. Carbohydr. Chem.*, 2008, **27**, 429.
14 M. I. Bilan, E. V. Vinogradova, E. A. Tsvetkova, A. A. Grachev, A. S. Shashkov, N. E. Nifantiev and A. I. Usov, *Carbohydr. Res.*, 2008, **343**, 2605.
15 N. E. Ustyuzhanina, N. A. Ushakova, M. E. Preobrazhenskaya, M. I. Bilan, E. A. Tsvetkova, V. B. Krylov, N. A. Anisimova, M. V. Kiselevskiy, N. V. Krukovskaya, C. Li, G. Yu, S. Saran, R. K. Saxena, A. I. Usov and N. E. Nifantiev, *Pure Appl. Chem.*, 2014, **86**, 1365.
16 V. B. Krylov, D. A. Argunov, D. Z. Vinnitskiy, S. A. Verkhnyatskaya, A. G. Gerbst, N. E. Ustyuzhanina, A. S. Dmitrenok, J. Huebner, O. Holst, H.-C. Siebert and N. E. Nifantiev, *Chem. – Eur. J.*, 2014, **20**, 16516.
17 V. B. Krylov, A. G. Gerbst, D. A. Argunov, A. S. Dmitrenok, A. S. Shashkov, Z. Kaczynski, J. Huebner, O. Holst and N. E. Nifantiev, *Chem. – Eur. J.*, 2015, **21**, 1749.
18 D. A. Argunov, V. B. Krylov and N. E. Nifantiev, *Org. Biomol. Chem.*, 2015, **13**, 3255.
19 N. E. Ustyuzhanina, P. A. Fomitskaya, A. G. Gerbst, A. S. Dmitrenok and N. E. Nifantiev, *Mar. Drugs*, 2015, **13**, 770.
20 A. Pews-Davtyan, A. Pirojan, I. Shaljyan, A. A. Awetissjan, H. Reinke and C. Vogel, *J. Carbohydr. Chem.*, 2003, **22**, 939.
21 P. Peltier, R. Euzen, R. Daniellou, C. Nugier-chauvin and V. Ferrières, *Carbohydr. Res.*, 2008, **343**, 1897.
22 A. Imamura and T. Lowary, *Trends Glycosci. Glycotechnol.*, 2011, **23**, 134.
23 C. Marino and L. Baldoni, *ChemBioChem*, 2014, **15**, 188.
24 R. Dureau, L. Legentil, R. Daniellou and V. Ferrières, *J. Org. Chem.*, 2012, **77**, 1301.
25 R. Dureau, M. Gicquel, I. Artur, J. P. Guégan, B. Carboni, V. Ferrières, F. Berrée and L. Legentil, *Org. Biomol. Chem.*, 2015, **13**, 4940.
26 A. Banaszek and V. Zaitsev, *Tetrahedron: Asymmetry*, 2004, **15**, 299.
27 D. Lee and M. S. Taylor, *J. Am. Chem. Soc.*, 2011, **133**, 3724.
28 A. G. Gerbst, V. B. Krylov, D. Z. Vinnitskiy, A. S. Dmitrenok, A. S. Shashkov and N. E. Nifantiev, *Carbohydr. Res.*, 2015, **417**, 1.
29 E. R. an Rijssel, P. van Delft, G. Lodder, H. S. Overkleeft, G. A. van der Marel, D. V. Filippov and J. D. Codée, *Angew. Chem., Int. Ed.*, 2014, **53**, 10381.
30 M. Gelin, V. Ferrieres and D. Plusquellec, *Eur. J. Org. Chem.*, 2000, 1423.
31 G. Gola and C. Gallo-Rodriguez, *RSC Adv.*, 2014, **4**, 3368.
32 B. S. Komarova, N. E. Ustyuzhanina, Y. E. Tsvetkov and N. E. Nifantiev, in *Modern Synthetic Methods in Carbohydrate Chemistry – From Monosaccharides to Complex Glycoconjugates*, ed. S. Vidal and D. Wertz, WILEY-VCH, Weinheim, 2013, pp. 125–159.
33 N. E. Ustyuzhanina, B. S. Komarova, N. S. Zlotina, V. B. Krylov, A. G. Gerbst, Y. E. Tsvetkov and N. E. Nifantiev, *Synlett*, 2006, 921.
34 W. L. F. Armarego and C. L. L. Chai, *Purification of Laboratory Chemicals*, Butterworth, Heinemann, 5th edn, 2003.
35 P. A. Belyakov, V. I. Kadentsev, A. O. Chizhov, N. G. Kolotyrkina, A. S. Shashkov and V. P. Ananikov, *Mendeleev Commun.*, 2010, **20**, 125.
36 H. J. Vermeer, C. M. van Dijk, J. P. Kamerling and J. F. Vliegenthart, *Eur. J. Org. Chem.*, 2001, 193.

Carbohydrate Research 417 (2015) 1–10

Contents lists available at ScienceDirect

Carbohydrate Research

journal homepage: www.elsevier.com/locate/carres

^{13}C-NMR glycosylation effects in (1→3)-linked furanosyl-pyranosides

Alexey G. Gerbst, Vadim B. Krylov, Dmitry Z. Vinnitskiy, Andrey S. Dmitrenok, Alexander S. Shashkov, Nikolay E. Nifantiev *

Laboratory of Glycoconjugate Chemistry, N.D. Zelinsky Institute of Organic Chemistry, Russian Academy of Sciences, Leninsky Prospect 47, 119991 Moscow, Russia

ARTICLE INFO

Article history:
Received 16 July 2015
Received in revised form 22 August 2015
Accepted 24 August 2015
Available online 28 August 2015

Keywords:
^{13}C NMR chemical shifts
^{13}C NMR glycosylation effects
Furanosides
Conformation analysis
ab initio calculations

ABSTRACT

Synthesis, theoretical conformational analysis (molecular mechanics and DFT calculations) and NMR spectral data including the ^{13}C-NMR glycosylation effects for six pairs of isomeric furanosyl-(1→3)-pyranosides with different anomeric and absolute configurations of furanosyl units as well as configurations of C2 and C4 in the pyranoside units are described. The determined ^{13}C-NMR glycosylation effects were shown to correlate with the pattern of intramolecular interactions around the inter-unit bonds.

1. Introduction

Determination of the configurations of constitutive monosaccharide units as well as the locations of inter-unit linkages represents the key step in structural analysis of oligo- and polysaccharides. NMR spectroscopy is the most potent non-destructive method used to accomplish these tasks. This technique can be applied today for a variety of very small samples (starting from 1 to 5 nmol for ^{1}H NMR spectra[1]) and can be performed within a reasonable time without degradation or chemical modification, allowing the types of monosaccharide units and the location of linkages between them to be established. ^{13}C-NMR glycosylation effects can be regarded as very informative characteristics that depend upon structural properties of the constitutive monosaccharides within larger carbohydrate chains. ^{13}C-NMR glycosylation effects, which represent the difference in chemical shifts between corresponding carbons (Ci) in the spectra of a constitutive monosaccharide and the same unit within an analysed larger molecule, have been intensively studied since the early 1980s for different linear and branched substances (for examples see refs. [2–6]) built up from pyranoside units. ^{13}C-NMR glycosylation effects are widely used now to calculate and predict ^{13}C-NMR data for unknown compounds.[7–13] On the other hand, for furanosyl-containing structures, ^{13}C-NMR glycosylation effects have been poorly investigated to date in spite of the frequent occurrence of furanosyl units in natural oligo- and polysaccharides. For example, furanosyl-pyranoside fragments are present in the structures of polysaccharides of many pathogens including *Mycobacterium tuberculosis*,[14] *Aspergillus fumigatus*,[15,16] *Enterococcus faecalis*,[17] *Klebsiella pneumonia*,[18,19] and others.

To address this deficiency mentioned above we initiated systematic synthesis, NMR and theoretical conformational analysis (molecular mechanics and DFT calculations) on a variety of furanosyl-pyranosides. The main focus of this study is on the determination of the corresponding ^{13}C-NMR glycosylation effects and their correlation with stereochemical and conformational characteristics of the studied compounds. In this communication we report on the preparation, conformational and NMR studies of six pairs of isomeric furanosyl-(1→3)-pyranosides **1α,β-6α,β**, where anomeric (α/β) and absolute (D-D/L-D) configurations of the furanosyl units as well as the spatial orientation of OH-groups (axial/equatorial) at C2 and C4 in the pyranoside residues are varied (Fig. 1). In our investigation D-galactofuranose and L-fucofuranose (6-deoxy-L-galactofuranose) were chosen as the glycosylating residues and D-gluco-, D-galacto- and D-mannopyranosides as the residues glycosylated at O-3. The glycosylation reaction was performed in a non-stereoselective way to give a mixture of α- and β-isomers that was analysed by NMR methods without separation.

2. Results and discussion

2.1. Synthesis of model disaccharide derivatives *1α,β-6α,β*

The synthesis of target disaccharide derivatives was performed employing galactofuranosyl and fucofuranosyl donors **9** and **11**,

* Corresponding author. Laboratory of Glycoconjugate Chemistry, N.D. Zelinsky Institute of Organic Chemistry, Russian Academy of Sciences, Leninsky Prospect 47, 119991 Moscow, Russia. Tel.: +7 499 135 8784; fax: +7 499 135 8784.
E-mail address: nen@ioc.ac.ru (N.E. Nifantiev).

http://dx.doi.org/10.1016/j.carres.2015.08.014
0008-6215/

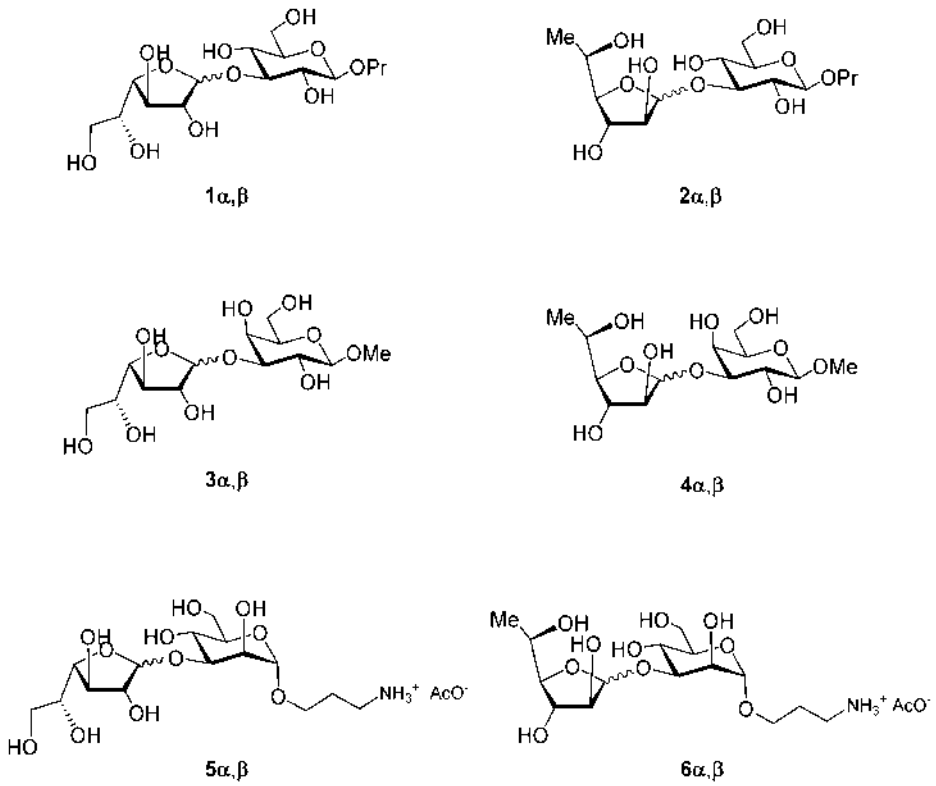

Fig. 1. Studied disaccharide derivatives **1α,β**-**6α,β**.

containing the 2-methyl-5-*tert*-butyl thiophenyl group.[20] Thiol **7**, used in the synthesis of these compounds, is a commercially available, less toxic and odourless alternative to thiophenol.[20] For the synthesis of donor **9**, D-galactose was first per-O-benzoylated and then treated with thiol **7** to give thioglycoside **8**.[20] It was further subjected to debenzoylation and exhaustive O-benzylation (Scheme 1) to produce galactosyl donor **9**. Unfortunately, the similar transformation of L-fucose was less efficient and gave a mixture of thiofuranoside **10** and its pyranoside analogue in the ratio 3/1. However, the desired furanoside **10** was isolated in individual form by reversed phase HPLC with a total yield of 21% starting from L-fucose. Its exhaustive O-benzylation gave fucofuranoside donor **11**.

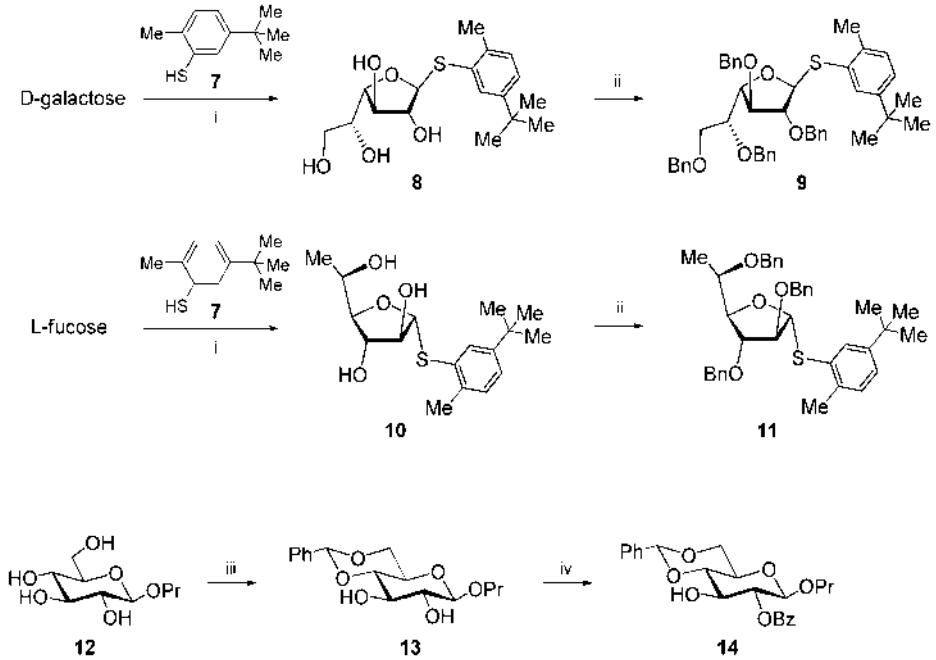

Scheme 1. Reagents and conditions: (i) (1) BzCl, Py, 60 °C; (2) **7**, $BF_3{\cdot}Et_2O$, CH_2Cl_2; (3) NaOH, MeOH, 73% for **8**,[18] 21% for **10** (from L-fucose); (ii) BnBr, NaH, DMF, 81% for **9**, 83% for **11**; (iii) $PhCH(OMe)_2$, CSA, CH_3CN; 84% (iv) (1) Bu_2SnO, PhMe, 110 °C; (2) BzCl, 62%.

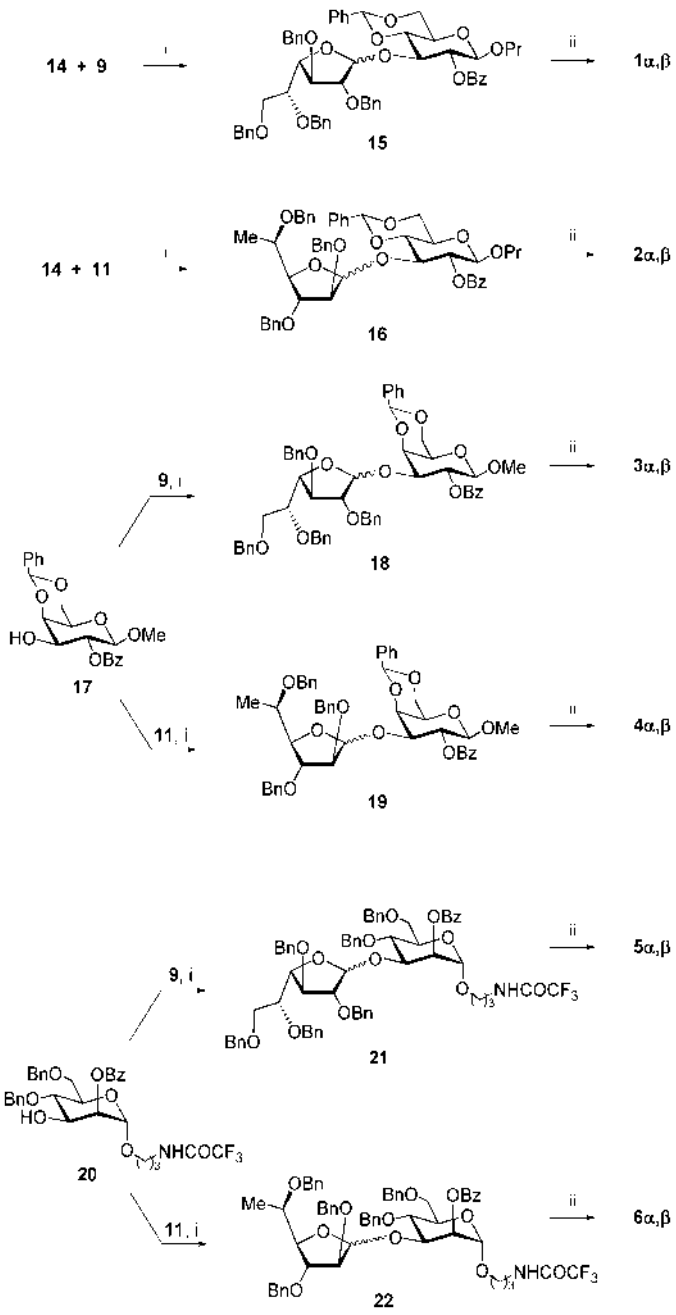

Scheme 2. Reagents and conditions: (i) NIS, TfOH, CH_2Cl_2, −15 °C, 79% for **14** (α/β = 1.2:1), 83% for **15**, (α/β = 2:1), 73% for **17** (α/β = 1.5:1), 77% for **18** (α/β = 7:3), 43% for **20** (α/β = 2:1), 40% for **21** (α/β = 2:3); (ii) (1) H_2, Pd/C, MeOH–EtOAc; (2) NaOH, MeOH–H_2O 80–70%.

The synthesis of acceptor **14** was performed from propyl glucoside **12** by its transformation into diol **13**, generating an organotin intermediate followed by regioselective 2-O-benzoylation to give the desired acceptor **14** (Scheme 1). The preparation of other glycosyl acceptors used in this work, namely galactoside **17**[21] and mannoside **20**[16] bearing free OH-groups at C-3, was described previously.

The coupling of both donors **9** and **11** with acceptors **14**, **17**[21] and **20**[16] gave the desired disaccharide mixtures **15**, **16**, **18**, **19**, **21**, and **22** of the corresponding α- and β-isomers (Scheme 2). Removal of protecting groups from these products by conventional procedures gave the series of disaccharide models **1α,β-6α,β**.

2.2. NMR analysis of model disaccharides **1α,β-6α,β**

In spite of the obtained disaccharides being mixtures of α- and β-isomers, complete signal assignment of their NMR spectra was successfully performed by applying 2D NMR experiments (see Experimental). The ^1H and ^{13}C chemical shifts of the studied compounds are summarized in Tables 1 and 2, respectively. Corresponding glycosylation effects (Table 3) were calculated as the difference in chemical shifts between the studied disaccharides and one of the used monosaccharide reference structures[22,23] shown in the first part of Table 2. It can be seen from Table 3 that α-effects of glycosylation strongly depend on the relative configurations of the glycon and aglycon. Thus for α-D-manno derivatives large effects are observed in case of α-D- and β-L-configurations of the glycosylating residue and small effects in case of their α-L- and β-D-configurations. This situation is reversed for β-D-galacto derivatives, and for β-D-gluco derivatives all α-effects are large. This reproduces the observations found previously.[2,3]

2.3. Computational studies

Oligosaccharides represent the case of biomolecular systems[24] whose conformational and spectral behaviour is influenced by structural characteristics of monosaccharide units linked through internal glycoside bonds. Upon the introduction of a glycosylating residue, the most pronounced spectral effect is observed on the glycosylated carbons, which usually undergo a down-field shift by 4–10 ppm (α-effect), while the resonances of the adjacent carbon atoms usually move up-field to a smaller extent (β-effect) (Fig. 2).[2] Other carbon resonances remain much less affected. These effects are thought to be correlated with spatial proton–proton interactions, which cause polarization of the C—H bond. The pioneering work in this field by Grant and Cheney dates back to 1960s.[25] In the cited article an equation was purposed, later named after Grant and Cheney, which allowed for quantitative calculations of these polarizations and thus the changes in chemical shifts. However, due to the still evolving state of computational chemistry in that decade, this equation was parametrized semi-empirically using very rough "typical" values of chemical bond lengths and angles, and nowadays it cannot be used for quantitative calculations. Meanwhile, the qualitative tendencies noted by Grant and Cheney are indeed true to a general extent.

In this work we performed computational studies for the structures containing the above mentioned disaccharide fragments in the form of methyl glycosides. Since the differences in chemical shifts occur due to interactions of C—H bonds in the neighbourhood of the glycosidic linkage, conformational analysis of the studied compounds was carried out to rationalize the observed glycosylation effect. Molecular dynamics (MD) using the MM3-1996 force field with TINKER v. 5.0 software[26] was employed to investigate the conformational state of the glycosidic linkages. The MD simulations were run in two approximations: *in vacuo* and using the continuum solvation model SASA (**S**olvent **A**ccessible **S**urface **A**rea[27]). After the analysis of MD trajectories, two types of dominating conformers were found for all the studied compounds (see Fig. 1) with the exception being those that contained a glucose residue (compounds **1α,β** and **2α,β**). For these compounds another conformer was found with ψ torsions of about 180° ("inverted" conformer). Fig. 3 shows the distributions of conformers as obtained from MD studies in SASA approximation and their 3D representations.

Although the conformer with large ψ torsions is unfavourable and its portion was expectedly low, it is not the first time that was encountered during the conformational analysis of carbohydrates. Previously, we reported the presence of such conformers in the MD simulations of β-(1→3)-linked glucosides related to a fungal cell wall glucan.[28] Interestingly, the portion of this conformer in the whole ensemble was significantly larger when the calculations were

Table 1
^{1}H NMR chemical shifts (δ, ppm; D_2O) for disaccharides **1α,β-6α,β**

#	Unit	H1	H2	H3	H4	H5	H6	H6′
1α	α-D-Gal*f*-(1→	5.23	4.09	4.22	3.8	3.72	3.59	
	→3)-β-D-Glc*p*-OPr	4.42	3.28	3.52	3.48	3.4	3.66	3.85
1β	β-D-Gal*f*-(1→	5.24	4.11	4.04	4.03	3.78	3.60	
	→3)-β-D-Glc*p*-OPr	4.42	3.34	3.58	3.39	3.4	3.66	3.85
2α	α-L-Fuc*f*-(1→	5.23	4.09	4.09	3.89	3.85	1.16[a]	
	→3)-β-D-Glc*p*-OPr	4.41	3.34	3.53	3.42	3.42	3.67	3.85
2β	β-L-Fuc*f*-(1→	5.26	4.11	3.89	3.89	3.85	1.17[a]	
	→3)-β-D-Glc*p*-OPr	4.43	3.26	3.61	3.48	3.4	3.67	3.85
3α	α-D-Gal*f*-(1→	5.18	4.18	4.33	3.90	3.81	3.67	
	→3)-β-D-Gal*p*-OMe	4.39	3.63	3.76	4.09	3.70	3.78	
3β	β-D-Gal*f*-(1→	5.22	4.22	4.09	4.07	3.85	3.69	
	→3)-β-D-Gal*p*-OMe	4.39	3.63	3.73	4.10	3.73	3.78	
4α	α-L-Fuc*f*-(1→	5.24	4.16	4.19	3.66	3.93	1.23[a]	
	→3)-β-D-Gal*p*-OMe	4.39	3.66	3.71	4.16	3.74	3.79	
4β	β-L-Fuc*f*-(1→	5.18	4.19	3.97	3.91	3.93	1.27[a]	
	→3)-β-D-Gal*p*-OMe	4.39	3.61	3.81	4.19	3.71	3.81	
5α	α-D-Gal*f*-(1→	5.22	4.17	4.33	3.87	3.83	3.65	
	→3)-α-D-Man*p*-O$(CH_2)_3NH_2$	4.91	4.19	3.84	3.82	3.69	3.80	3.91
5β	β-D-Gal*f*-(1→	5.16	4.18	4.11	4.09	3.87	3.71	
	→3)-α-D-Man*p*-O$(CH_2)_3NH_2$	4.93	4.18	3.91	3.75	3.67	3.80	3.91
6α	α-L-Fuc*f*-(1→	5.17	4.18	4.17	3.69	3.93	1.23[a]	
	→3)-α-D-Man*p*-O$(CH_2)_3NH_2$	4.92	4.11	3.89	3.79	3.68	3.79	3.92
6β	β-L-Fuc*f*-(1→	5.23	4.20	3.95	3.88	3.93	1.27[a]	
	→3)-α-D-Man*p*-O$(CH_2)_3NH_2$	4.87	4.11	3.89	3.79	3.68	3.79	3.92

[a] Signal of CH_3-group of fucofuranosyl unit.

performed *in vacuo*. The absence of this conformer in the MD trajectories of the other molecules is most probably explained by axial orientation of either 4-OH or 2-OH groups in galacto- and manno-residues, correspondingly, which may hinder rotation around the (1→3)-glycosidic linkage.

After preliminary molecular mechanics optimization, the obtained conformers **I**–**IV** were subjected to DFT (B3LYP functional with pcS-1 basis set) geometry optimization both in the gas phase. The same set of conformers was used for the geometry optimization employing the COSMO model to account for solvation. All optimizations were performed using the NWChem 6.3 program.[29] At this level of theory, again, a remarkable difference in the relative energies of conformers was found between the gas phase and their COSMO[30,31] approximation in the case of molecules **1α,β** and **2α,β**. In the gas

Table 2
^{13}C NMR chemical shifts of reference monosaccharides and disaccharides **1α,β-6α,β** (δ, ppm; D_2O)

#	Unit	C1	C2	C3	C4	C5	C6
Model reference monosaccharides							
β-D-Glc*p*-OPr[22]		103.1	74.1	76.8	70.6	76.8	61.7
β-D-Gal*p*-OMe[23]		103.9	70.8	72.9	68.8	75.2	61.1
α-D-Man*p*-OMe[23]		101.9	71.2	71.8	68.0	73.7	62.1
α-D-Gal*f*-OH[23]		96.6	77.9	75.9	82.4	73.3	64.2
β-D-Gal*f*-OH[23]		102.6	82.9	77.4	83.7	72.3	64.4
α-L-Fuc*f*-OH[23]		95.7	77.7	76.0	85.7	68.5	20.1
β-L-Fuc*f*-OH[23]		101.5	82.5	77.5	87.2	70.1	20.4
Disaccharides							
1α	α-D-Gal*f*-(1→	102.91	76.66	74.18	81.45	70.96	63.84
	→3)-β-D-Glc*p*-OPr	102.79	72.71	84.61	70.6	76.66	61.58
1β	β-D-Gal*f*-(1→	109.14	82.16	77.59	83.95	71.62	63.84
	→3)-β-D-Glc*p*-OPr	102.91	74.18	83.26	69.18	76.78	61.77
2α	α-L-Fuc*f*-(1→	102.78	74.89	77.26	85.44	67.71	19.36
	→3)-β-D-Glc*p*-OPr	102.87	74.02	84.88	69.14	76.39	61.44
2β	β-L-Fuc*f*-(1→	108.96	82.22	78.13	88.28	68.26	19.16
	→3)-β-D-Glc*p*-OPr	102.92	72.74	82.96	70.56	76.61	61.55
3α	α-D-Gal*f*-(1→	99.40	76.13	73.46	80.99	70.64	62.85
	→3)-β-D-Gal*p*-OMe	103.79	69.32	79.74	66.20	75.03	61.05
3β	β-D-Gal*f*-(1→	109.26	81.55	76.85	82.93	70.81	62.82
	→3)-β-D-Gal*p*-OMe	103.74	69.99	80.6	68.73	75.08	61.05
4α	α-L-Fuc*f*-(1→	102.20	76.69	74.17	84.8	67.29	18.54
	→3)-β-D-Gal*p*-OMe	103.64	69.81	81.99	68.56	74.9	61.16
4β	β-L-Fuc*f*-(1→	104.10	81.72	77.83	87.46	67.61	18.38
	→3)-β-D-Gal*p*-OMe	103.75	69.3	77.05	65.13	75.15	61.12
5α	α-D-Gal*f*-(1→	103.38	77.32	74.51	81.83	71.57	63.86
	→3)-α-D-Man*p*-O$(CH_2)_3NH_2$	100.44	70.81	81.64	66.56	73.87	62.18
5β	β-D-Gal*f*-(1→	105.59	84.23	78.27	82.54	72.01	64.02
	→3)-α-D-Man*p*-O$(CH_2)_3NH_2$	100.77	67.84	76.66	66.21	74.00	62.18
6α	α-L-Fuc*f*-(1→	100.22	75.40	77.69	86.08	68.69	19.46
	→3)-α-D-Man*p*-O$(CH_2)_3NH_2$	100.65	68.58	78.80	66.37	73.88	62.21
6β	β-L-Fuc*f*-(1→	110.35	82.85	78.80	88.47	68.69	19.44
	→3)-α-D-Man*p*-O$(CH_2)_3NH_2$	100.75	71.24	79.36	67.08	74.16	62.14

Table 3
^{13}C NMR α- and β-glycosylation effects (Δδ, ppm) in ^{13}C NMR spectra of disaccharides **1α,β-6α,β**

#	Linkage type	ΔδC1′ α-effect	Δδ C2 β-effect	Δδ C3 α-effect	Δδ C4 β-effect
1α	α-D-Gal*f*-(1→3)-β-D-Glc*p*	6.3	−1.4	7.8	0.0
1β	β-D-Gal*f*-(1→3)-β-D-Glc*p*	6.5	0.1	6.5	−1.4
2α	α-L-Fuc*f*-(1→3)-β-D-Glc*p*	7.1	−0.1	8.1	−1.5
2β	β-L-Fuc*f*-(1→3)-β-D-Glc*p*	7.5	−1.4	6.2	0.0
3α	α-D-Gal*f*-(1→3)-β-D-Gal*p*	2.8	−1.5	6.8	−2.6
3β	β-D-Gal*f*-(1→3)-β-D-Gal*p*	6.7	−0.8	7.7	−0.1
4α	α-L-Fuc*f*-(1→3)-β-D-Gal*p*	6.5	−1.0	9.1	−0.2
4β	β-L-Fuc*f*-(1→3)-β-D-Gal*p*	2.6	−1.5	4.1	−3.7
5α	α-D-Gal*f*-(1→3)-α-D-Man*p*	6.8	−0.4	9.8	−1.4
5β	β-D-Gal*f*-(1→3)-α-D-Man*p*	3.0	−3.4	4.9	−1.8
6α	α-L-Fuc*f*-(1→3)-α-D-Man*p*	4.5	−2.6	7.0	−1.6
6β	β-L-Fuc*f*-(1→3)-α-D-Man*p*	8.8	0.0	7.6	−0.9

phase the inverted conformer (type IV in Fig. 3) had an energy very close to that of the dominant conformers. When the COSMO approximation was applied its energy rose and became the highest among all the conformers, suggesting a population of just a few per cent.

A preliminary explanation for the observed glycosylation effects could be given based upon examination of the obtained conformers. For example, in the case of α-Gal*f*-Gal*p* disaccharide **3α** one of the two revealed types of conformers (type I) was characterized with regard to the spatial proximity of the H1′ and H4 protons. In both conformers (types I and II) a short distance between H1′ and H3 was also found. In β-Gal*f*-Gal molecule **3β** the average H1′–H4 distance was longer and the proximity between H1′ and H3 remained. The distance between H1′ and H2 was longer in both compounds (see Table 4). This explained why the glycosylation effect for this compound was stronger on the H4′ atom in the α-isomer, and was moderate on both the H2 and H4 atoms in the β-isomer. The result of this analysis was additionally confirmed by NOESY spectroscopy (Fig. 4, Table 5), where strong H1′–H3 and H1′–H4 interactions were observed while H1′–H2 contact was weak.

The same explanation could also be drawn for mannose containing disaccharides that possessed axial OH-substituents at C-2. However, the disaccharides containing a glucose residue at the "reducing end" represented a more difficult case. The spatial proximity between H1 and H2′ and H4′ was observed only in the "inverted" conformer (IV, Fig. 3) and the changes in chemical shifts were hard to explain. To get further insight into this result we undertook quantum chemical calculations of the chemical shifts. Calculation of the chemical shifts was done by means of DALTON 2013 software.[32] Again, DFT with B3LYP functional was employed, but a larger Ahlrichs TZVPP[33] basis set with 2 polarization functions (present in the DALTON basis set library as Turbomole-TZVPP) was used.

First, shielding constants for β-methyl glucoside were computed. Attention was primarily paid to the ^{13}C shielding constants of the intra-ring carbon atoms. Correlation between the calculated shielding constants and experimental chemical shifts of the mentioned compounds was evaluated. The squared correlation coefficient had a value of 0.990 with an average error of 1.5 ppm. The

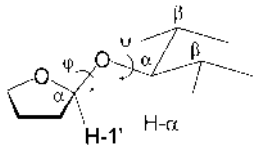

Fig. 2. Torsional angles determining the conformation of a glycosidic linkage and notations of α and β carbon atoms related to discussed spectral α- and β-glycosylation effects.

averaged shielding constant corresponding to the zero chemical shift was found to be 174.9. To calculate the glycosylation effects, the shielding constants calculated for the studied disaccharides were compared to those of the corresponding non-glycosylated monosaccharides. Table 6 demonstrates that for compounds of series **1α,β** and **2α,β** the only conformer that showed the correct pattern of changes in the computed β-effects of glycosylation for C4 and C2 atoms was that of the "inverted" type. The "Lemieux" type conformers seemed to be responsible only for the major α-glycosylation effect on the C3 atom.

2.4. Conclusions

In this work we employed methods of theoretical conformational analysis (molecular dynamics) to obtain structures of dominant conformers of six pairs of isomeric furanosyl-(1→3)-pyranosides with different anomeric and absolute configurations of furanosyl units as well as the configurations of C2 and C4 in pyranoside units. These data were used to qualitatively hypothesize about the possible values of glycosylation effects for each type of studied glycosidic linkage involving a furanoside moiety. Additionally, quantum mechanical calculations of nuclear shielding constants were used to elucidate the glycosylation effects semi-quantitatively. The obtained NMR characteristics enlarge currently available databases employed for computer assisted structural analysis of carbohydrates.

3. Experimental

3.1. General methods

All solvents were distilled and dried if necessary according to standard procedures[34] (CH_2Cl_2, MeOH, Toluene) or purchased as dry (DMF, Pyridine, CH_3CN; Sigma-Aldrich). Commercial chemicals were used without purification unless noted. All reactions involving air- or moisture-sensitive reagents were carried out using dry solvents under Ar atmosphere. All glycosylation reactions were carried out under dry Ar. Molecular sieves for glycosylation reactions were activated prior to application at 180 °C under vacuum from an oil pump during 2 h. Analytical thin-layer chromatography (TLC) was performed on Silica Gel 60 F254 aluminium sheets (Merck), and visualization was accomplished using UV light or by charring at ~150 °C with 10% (v/v) H_3PO_4 in ethanol. Column chromatography was performed on Silica Gel 60, 40–63 μm (Merck). Preparative RP HPLC was performed on a Supelcosil LC-18 column (5 μm, 250 × 10 mm) at a flow rate of 4 mL/min with a UV/VIS-155 detector (Gilson). Gel-filtration was performed on a TSK-40 HW(S) column (400 × 17 mm) by elution with 0.1 M AcOH in water at a flow rate of 0.5 mL/min. Optical rotation values were measured using a JASCO DIP-360 polarimeter at the ambient temperature in the solvents specified. ^{1}H and ^{13}C NMR spectra were recorded on Bruker AV-400, Bruker

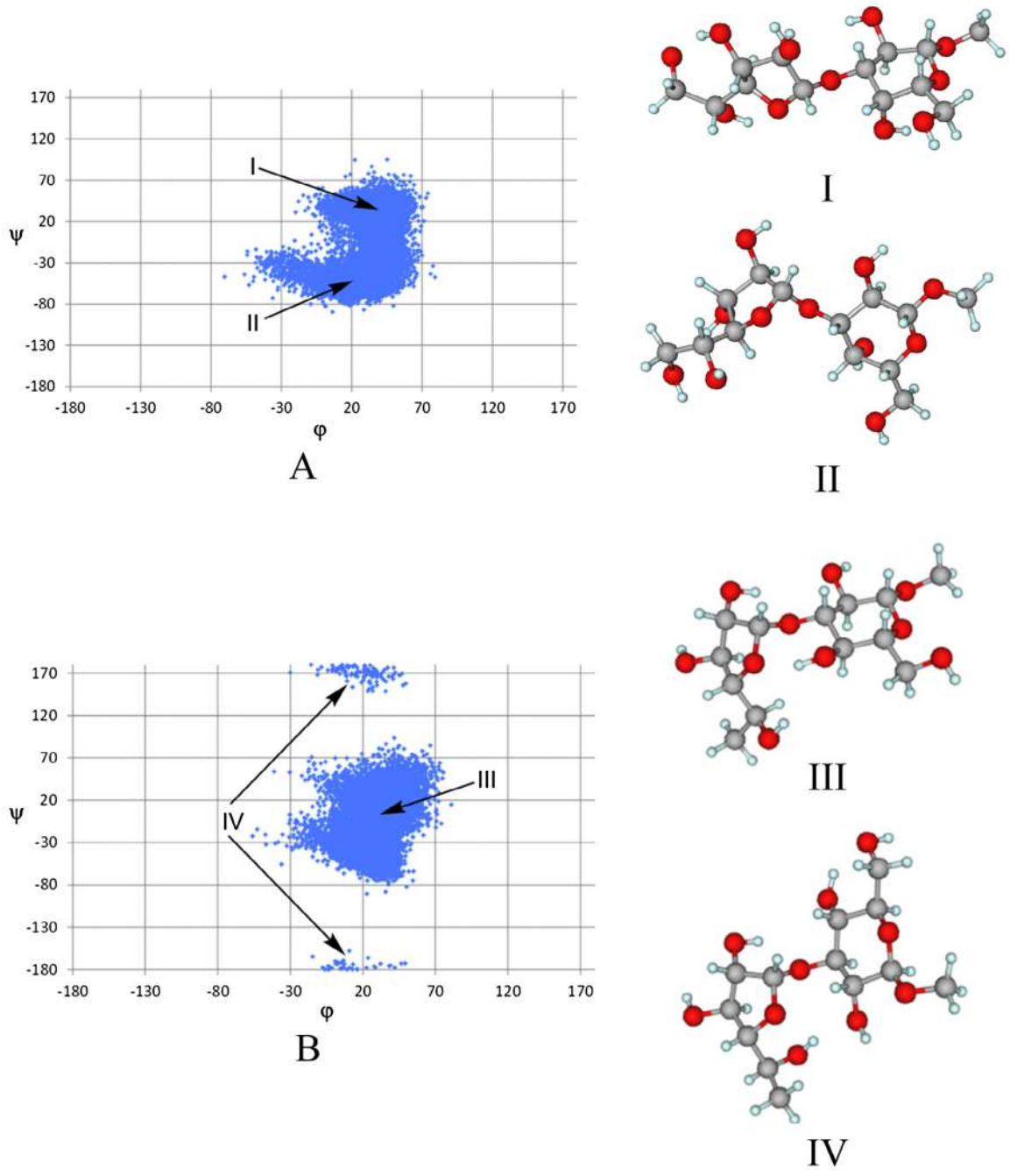

Fig. 3. Conformational maps and 3D representations of conformers for disaccharides without (A, compounds **3–6**) and with a glucoside residue (B, compounds **1** and **2**).

DRX-500, and Bruker AV-600 spectrometers. Chemical shifts were referenced to residual solvent signals. For samples in D_2O, acetone was used as internal standard. Average sample concentration was 30 μmol/mL. Signal assignment in ^{1}H and ^{13}C NMR spectra was made using COSY, TOCSY, and ^{1}H–^{13}C HSQC techniques. High-resolution mass spectra (HR MS) were measured on a Bruker micrOTOF II instrument using electrospray ionization (ESI).[35] The measurements were performed in a positive ion mode (interface capillary voltage –4500 V); mass range from m/z 50 to m/z 3000 Da; external or internal calibration was made with Electrospray Calibrant Solution (Fluka). A syringe injection was used for solutions in a mixture of acetonitrile and water (50:50 v/v, flow rate 3 μL/min). Nitrogen was applied as a dry gas; the interface temperature was set at 180 °C.

Table 4
Inter-proton distances in the dominant conformers of the compound series **2α,β** and **3α,β**

Disaccharide	Conformer type	Distances (Å)		
		H1′–H2	H1′–H3	H1′–H4
2α	III	3.56	2.75	4.48
	IV	2.35	3.63	2.21
2β	III	4.24	2.64	4.68
	IV	2.46	3.78	2.52
3α	I	4.54	2.73	2.22
	II	3.77	2.22	4.03
3β	I	4.48	2.28	2.04
	II	3.95	2.56	4.18

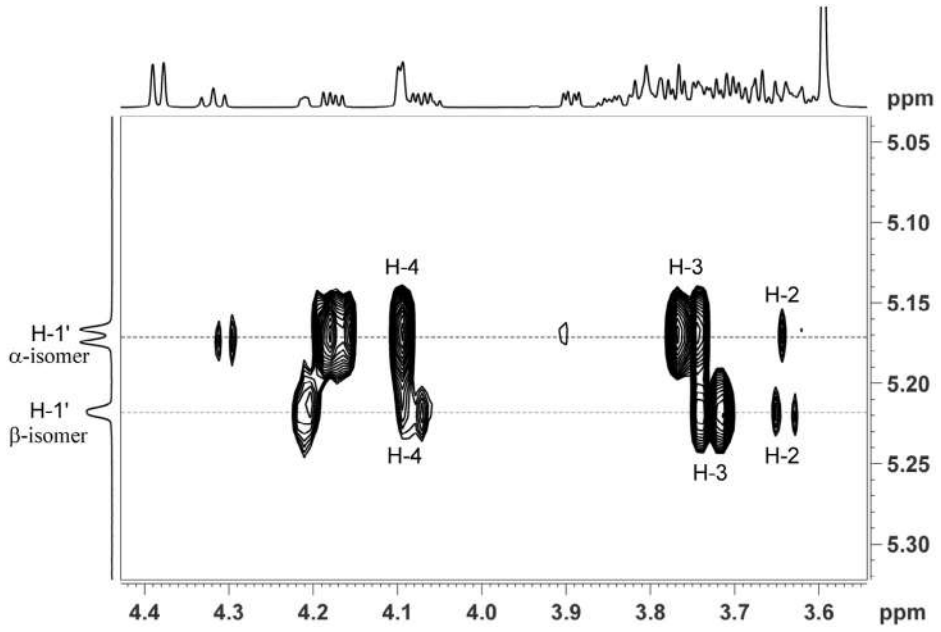

Fig. 4. Fragment of NOESY spectrum of the mixture of disaccharides **3α,β**.

TINKER MD simulations were performed in constant temperature mode at 300 K using the MM3-1996 force field. Simulation length was 20,000 ns for each structure with structural snapshots being written every 2 ns. The quantum mechanical optimizations were performed until the RMS gradient of 10^{-4}. In case of COSMO approximation, NWChem library parameters for water were used with the dielectric constant of 78.4.

*3.2. (2-Methyl-5-*tert*-butylphenyl) 2,3,5,6-tetra-O-benzyl-1-thio-β-D-galactofuranoside (**9**)*

Benzyl bromide (228 μL, 1.91 mmol) and NaH (77 mg of 60% dispersion, 1.93 mmol) were added to a solution of **8** (148 mg, 0.43 mmol) in dry DMF (3 mL). The mixture was stirred until TLC indicated disappearance of the starting material, diluted with EtOAc and washed with water (×2). The organic layer was dried with Na_2SO_4, the solvent was removed under reduced pressure and the residue was purified by column chromatography (petroleum ether–EtOAc, 25:1). Tetrabenzyl ether **9** (247 mg, 81%) was isolated as a colourless oil; R_f 0.65 (Petroleum ether–EtOAc, 4:1); $[\alpha]_D$ –93 (*c* 1, EtOAc); ^{1}H NMR (600 MHz, $CDCl_3$) δ 7.50–7.12 (m, 23H, SAr, Ph), 5.68 (d, 1H, $J_{1,2}$ 3.0 Hz, H-1), 4.80–4.74 (m, 2H, C*H*H'Ph), 4.63–4.52 (m, 5H, C*H*H'Ph), 4.45–4.39 (m, 2H, C*H*H'Ph, H-4), 4.24–4.17 (m, 2H, H-2, H-3), 3.92–3.88 (m, 1H, H-5), 3.85–3.80 (m, 1H, H-6), 3.80–3.74 (m, 1H, H-6′), 2.46 (s, 3H, CH_3Ar), 1.35 (s, 9H, ((CH_3)$_3$CAr)). ^{13}C NMR (150 MHz, $CDCl_3$) δ 149.56 ((CH_3)$_3$*C*Ar), 138.46–124.35 (*S*Ar, CH_2*Ph*), 89.89 (C-1), 88.83 (C-2), 83.05 (C-3), 81.11 (C-4), 76.47 (C-5), 73.49–72.07 (4 *C*H_2Ph), 71.30 (C-6), 31.42 ((*C*H_3)$_3$CAr), 20.32 (*C*H_3Ar). HRESIMS: found *m/z* 741.3000; calcd for $C_{45}H_{50}O_5S$ $[M+K]^+$ 741.3011.

Table 5
Relative inter-residue NOE measured by NOESY and calculated from MD trajectories (in parenthesis)

#	Linkage type	Relative NOE		
		H1′–H2	H1′–H3	H1′–H4
2α	α-L-Fuc*f*-(1→3)-β-D-Glc*p*	0.11 (0.04)	1.00	0.12 (0.04)
2β	β-L-Fuc*f*-(1→3)-β-D-Glc*p*	0.12 (0.07)	1.00	0.14 (0.07)
3α	α-D-Gal*f*-(1→3)-β-D-Gal*p*	0.12 (0.04)	1.00	0.64 (0.52)
3β	β-D-Gal*f*-(1→3)-β-D-Gal*p*	0.13 (0.03)	1.00	0.15 (0.10)

Table 6
Theoretical glycosylation effects in different conformers of glucose containing compounds **1α,β** and **2α,β**

Disaccharide	Conformer type	Glycosylation effect, ppm		
		H2	H3	H4
1α	III	0.2	10.3	–0.2
	IV	–4.1	0	–0.1
1β	III	0.1	8.9	–0.1
	IV	0.5	0	–3.4
2α	III	0.1	8.5	–0.2
	IV	–0.6	0	–2.4
2β	III	0	9.17	0
	IV	–3.2	0	–0.5

*3.3. (2-Methyl-5-*tert*-butylphenyl) 1-thio-β-L-fucofuranoside (**10**)*

A solution of L-fucose (1.00 g, 6.09 mmol) in anhydrous Py (10 mL) was refluxed for 2 h and then benzoyl chloride (3.0 mL, 25.8 mmol) was added in one portion through the condenser. The mixture was stirred at 60 °C for 1 h 30 and then cooled down to room temperature. Py was evaporated. The solution of the residue in CH_2Cl_2 was washed with aq. HCl (1 M), aq. $NaHCO_3$ and brine, dried over Na_2SO_4, filtered and concentrated to give an oil which was dissolved in anhydrous CH_2Cl_2 (10 mL). Thiol **7** (0.34 mL, 1.83 mmol) and boron trifluoride etherate (0.38 mL, 3.03 mmol) were added to the solution under argon. The mixture was stirred for 2 h at room temperature and then neutralized with a saturated aq $NaHCO_3$ solution at 0 °C. The product was extracted with CH_2Cl_2, and the organic layer was dried over Na_2SO_4, filtered and concentrated. The residue co-evaporated with anhydrous toluene and dissolved in anhydrous methanol (10 mL). Sodium methylate (1M in anhydrous methanol, 2 mL) was added and the mixture was stirred for 30 min and then neutralized (IR-120 (H^+) resin), filtered and concentrated. The residue was purified by column chromatography on silica gel (EtOAc, 100%) to give a mixture of furanoside **10** and (2-methyl-5-*tert*-butylphenyl)-1-thio-β-L-fucopyranoside which was then separated on preparative RP HPLC (gradient H_2O–MeOH) to give

416 mg (21%) of individual **10** as a colourless syrup and a mixture containing **10** and (2-methyl-5-*tert*-butylphenyl)-1-thio-β-L-fucopyranoside (~1:1 according to ^{1}H NMR data). Data for **10**: R_f 0.32 (EtOAc); $[\alpha]_D$ 172 (*c* 1, EtOAc); ^{1}H NMR (600 MHz, $CDCl_3$) δ 7.69–7.04 (m, 3H, SAr), 5.37 (d, 1H, $J_{1,2}$ 2.9 Hz, H-1), 4.28–4.12 (m, 2H, H-2, H-3), 4.03–3.95 (m, 2H, H-4, H-5), 2.41 (s, 3H, CH_3Ar), 1.41–1.19 (m, 12H, $(CH_3)_3$CAr, H-6). ^{13}C NMR (125 MHz, $CDCl_3$) δ 149.97 (($CH_3)_3$*C*Ar), 137.33–125.43 (SAr), 92.12 (C-1), 87.07 (C-4), 82.59 (C-2), 78.45 (C-3), 67.32 (C-5), 31.71 (($CH_3)_3$CAr), 20.74 (*C*H_3Ar), 20.23 (C-6). HRESIMS: found *m/z* 349.1435; calcd for $C_{17}H_{26}O_4S$ $[M + Na]^+$ 349.1444. Selected NMR data for (2-methyl-5-*tert*-butylphenyl)-1-thio-β-L-fucopyranoside: ^{1}H NMR (300 MHz, $CDCl_3$) δ 4.42 (d, 1H, $J_{1,2}$ 9.4 Hz, H-1), 3.71 (d, 1H, $J_{1,2}$ 3.1 Hz, H-4), 3.65 (t, 1H, $J_{2,1} = J_{2,3} = 9.3$ Hz, H-2), 3.60–3.54 (m, 2H, H-3, H-5), 1.29 (d, 3H, $J_{5,6}$ 6.5 Hz, H-6). ^{13}C NMR (75 MHz, $CDCl_3$) δ 88.55 (C-1), 75.03 (C-3, C-5), 71.70 (C-4), 70.08 (C-2), 16.68 (C-6).

3.4. (2-Methyl-5-tert-butylphenyl) 2,3,5-tri-O-benzyl-1-thio-β-L-fucofuranoside (**11**)

Exhaustive O-benzylation of **10** (225 mg, 0.69 mmol) as described for the preparation of **9** gave product **11** (342 mg, 83%) as a colourless syrup; R_f 0.52 (Petroleum ether–EtOAc, 5:1); $[\alpha]_D$ 98 (*c* 1, EtOAc); ^{1}H NMR (600 MHz, $CDCl_3$) δ 7.79–7.08 (m, 18H, SAr, Ph), 5.64 (d, 1H, $J_{1,2}$ 2.6 Hz, H-1), 4.72 (d, 1H, *J* 11.8 Hz, C*H*H'Ph), 4.63 (m, 1H, C*H*H'Ph), 4.56 (m, 2H, C*H*H'Ph), 4.50 (d, 1H, *J* 11.9 Hz, C*H*H'Ph), 4.45 (d, 1H, *J* 11.7 Hz, C*H*H'Ph), 4.27 (dd, 1H, $J_{3,4}$ 7.0, $J_{4,5}$ 3.9 Hz, H-4), 4.21 (t, 1H, *J* 3.0 Hz, H-2), 4.12 (dd, 1H, $J_{3,4}$ 7.1, $J_{2,3}$ 3.2 Hz, H-3), 3.79–3.74 (m, 1H, H-5), 2.45 (s, 3H, C*H*$_3$Ar), 1.33 (s, 9H, (C*H*$_3)_3$CAr), 1.31–1.28 (d, 3H, $J_{5,6}$ 6.4 Hz, H-6). ^{13}C NMR (150 MHz, $CDCl_3$) δ 149.55 (($CH_3)_3$*C*Ar), 137.52–124.49 (SAr, Ph), 89.87 (C-1), 88.95 (C-2), 83.83 (C-4), 83.48 (C-3), 73.17 (C-5), 72.25 (*C*H_2Ph), 72.07 (*C*H_2Ph), 71.23 (*C*H_2Ph), 31.36 (($CH_3)_3$Car), 20.34 (*C*H_3Ar), 16.08 (C-6). HRESIMS: found *m/z* 619.2844; calcd for $C_{38}H_{44}O_4S$ $[M + Na]^+$ 619.2853.

3.5. Propyl 4,6-O-benzylidene-β-D-glucopyranoside (**13**)

Benzaldehyde dimethyl acetal (154 µL, 1.03 mmol) and (+)-CSA (15 mg, 0.065 mmol) were added to a solution of propyl glucoside **12** (152 mg, 0.68 mmol) in dry CH_3CN (3 mL). The mixture was stirred for 3 h at 45 °C, then neutralized with Et_3N and the solvent was evaporated *in vacuo*. The residue was purified by column chromatography (silica gel, toluene–EtOAc, 2:1) to give diol **13** (181 mg, 84%) as a white solid. R_f 0.72 (EtOAc); $[\alpha]_D$ −70 (*c* 1, EtOAc); ^{1}H NMR (400 MHz, $CDCl_3$) δ 7.64–7.19 (m, 5H, Ph), 5.53 (s, 1H, C*H*Ph), 4.39 (d, 1H, $J_{1,2}$ 7.8 Hz, H-1), 4.34 (dd, 1H, $J_{5,6}$ 4.9, $J_{6,6'}$ 10.5, Hz, H-6), 3.90–3.74 (m, 3H, OC*H*H'CH_2CH_3, H-3, H-6′), 3.58–3.49 (m, 2H, OC*H*H'CH_2CH_3, H-4), 3.48–3.40 (m, 2H, H-5, H-2), 1.73–1.59 (m, 2H, $OCH_2CH_2CH_3$), 0.96 (t, 3H, *J* 7.4 Hz, $OCH_2CH_2CH_3$). ^{13}C NMR (100 MHz, $CDCl_3$) δ 137.00–126.30 (Ph), 103.15 (*C*HPh), 101.88 (C-1), 80.58 (C-4), 74.52 (C-2), 73.11 (C-3), 72.08 ($OCH_2CH_2CH_3$), 68.69 (C-6), 66.35 (C-5), 22.86 ($OCH_2CH_2CH_3$), 10.36 ($OCH_2CH_2CH_3$). HRESIMS: found m/z 333.1307; calcd for $C_{16}H_{22}O_6$ $[M + Na]^+$ 333.1309.

3.6. Propyl 2-O-benzoyl-4,6-O-benzylidene-β-D-glucopyranoside (**14**)

A mixture of diol **13** (169 mg, 0.54 mmol) and Bu_2SnO (162 mg, 0.65 mmol) in anhydrous toluene (10 mg) was refluxed with azeotropic removal of H_2O to a volume of 4 mL. The mixture was cooled to RT and treated with BzCl (75 µL, 0.65 mmol), kept for 1 h and then concentrated under reduced pressure. The residue was purified by column chromatography (silica gel, toluene–EtOAc, 5:1) to give monosaccharide **14** (140 mg, 62%) as a white solid. R_f 0.48 (toluene–EtOAc, 3:1); $[\alpha]_D$ −14 (*c* 1, EtOAc); ^{1}H NMR (400 MHz, $CDCl_3$) δ 8.30–7.15 (m, 10H, Ph), 5.60 (s, 1H, C*H*Ph), 5.23–5.18 (m, 1H, H-2), 4.70 (d, 1H, $J_{1,2}$ 7.9 Hz, H-1), 4.49–4.39 (m, 1H, H-6), 4.07 (m, 1H, H-3), 3.92–3.79 (m, 2H, OC*H*H'CH_2CH_3, H-6′), 3.74–3.63 (m, 1H, H-4), 3.59–3.45 (m, 2H, OH*H*'CH_2CH_3, H-5), 1.64–1.46 (m, 2H, $OCH_2CH_2CH_3$), 0.81 (t, 3H, *J* 7.9 Hz, $OCH_2CH_2CH_3$). ^{13}C NMR (100 MHz, $CDCl_3$) δ 133.27–126.30 (Ar), 101.92 (*C*HPh), 101.54 (C-1), 81.00 (C-4), 74.98 (C-2), 72.49 (C-3), 71.98 ($OCH_2CH_2CH_3$), 68.68 (C-6), 66.22 (C-5), 22.74 ($OCH_2CH_2CH_3$), 10.27 ($OCH_2CH_2CH_3$). HRESIMS: found m/z 437.1585; calcd for $C_{23}H_{26}O_7$ $[M + Na]^+$ 437.1571.

3.7. Glycosylation by furanosyl donors **9** and **11** (general procedure)

To a mixture of the glycosyl donor (0.06 mmol), glycosyl acceptor (0.05 mmol) and 4 Å (200 mg) molecular sieves in anhydrous CH_2Cl_2 (2 mL) were added at 0 °C under argon: NBS (27 mg, 0.15 mmol) and TfOH (1.8 µL, 0.02 mmol). After 30 min, the mixture was filtered, and successively washed with saturated aqueous $Na_2S_2O_3$, $NaHCO_3$, and brine. The organic layer was dried over Na_2SO_4 and concentrated. The residue was purified by column chromatography on silica gel (petroleum ether–EtOAc, gradient 8:1→3:1) to give disaccharides as a mixture of the α- and β-isomers as a colourless syrup.

3.8. Propyl 2,3,5,6-tetra-O-benzyl-(α,β)-D-galactofuranosyl-(1→3)-2-O-benzoyl-4,6-O-benzylidene-β-D-glucopyranosides (**15α,β**)

Glycosylation of glucoside **14** (21 mg, 0.05 mmol) with donor **9** (42 mg, 0.06 mmol) as described in the general procedure gave disaccharides **15α,β** (37 mg, 79%, α/β = 1.2:1) as a colourless syrup. R_f 0.23 (petroleum ether–EtOAc, 2:1); ^{1}H NMR (selected, 600 MHz, $CDCl_3$) δ 8.10 (d, 2.4H, *J* = 7.9 Hz, *o*-C(O)Ph), 8.01 (d, 2H, *J* = 7.9 Hz, *o*-C(O)Ph), 5.59 (s, 1H, PhC*H*), 5.56 (d, 1.2H, $J_{1,2}$ = 4.3 Hz, H-1$^{\alpha\text{-fur}}$), 5.44 (s, 1.2H, PhC*H*), 5.45–5.39 (m, 2.2H, 2 × H-2^{pyr}), 5.25 (s, 1H, H-1$^{\beta\text{-fur}}$), 1.63–1.46 (m, 4.4H, $OCH_2CH_2CH_3$), 0.84–0.72 (m, 6.6H, $OCH_2CH_2CH_3$). ^{13}C NMR (selected, 150 MHz, $CDCl_3$) δ 105.25 (C-1$^{\beta\text{-fur}}$), 101.80 (2 × C-1^{pyr}), 101.75 (PhCH), 101.59 (PhCH), 100.27 (C-1$^{\alpha\text{-fur}}$), 22.68 ($OCH_2CH_2CH_3$), 10.25 ($OCH_2CH_2CH_3$). HRESIMS: found m/z 959.3970; calcd for $C_{57}H_{60}O_{12}$ $[M + Na]^+$ 959.3977.

3.9. Propyl 2,3,5-tri-O-benzyl-(α,β)-L-fucofuranosyl-(1→3)-2-O-benzoyl-4,6-O-benzylidene-β-D-glucopyranosides (**16α,β**)

Glycosylation of glucoside **14** (21 mg, 0.05 mmol) with donor **11** (36 mg, 0.06 mmol) as described in the general procedure gave disaccharides **16α,β** (34 mg, 83%, α/β = 2:1) as a colourless syrup. R_f 0.25 (petroleum ether–EtOAc, 2:1); ^{1}H NMR (selected, 600 MHz, $CDCl_3$) δ 8.15 (d, 2H, *J* = 8.1 Hz, *o*-C(O)Ph), 8.10 (d, 1H, *J* = 8.0 Hz, *o*-C(O)Ph), 5.62 (s, 0.5H, PhC*H*), 5.57 (s, 1H, PhC*H*), 5.56 (s, 0.5H, H-1$^{\beta\text{-fur}}$), 5.50 (t, 1H, $J_{2,1} = J_{2,3}$ = 8.3 Hz, H-2^{pyr}), 5.39 (d, 1H, $J_{1,2}$ = 3.9 Hz, H-1$^{\alpha\text{-fur}}$), 5.33 (t, 0.5H, $J_{2,1} = J_{2,3}$ = 8.7 Hz, H-2^{pyr}), 1.60–1.48 (m, 3H, $OCH_2CH_2CH_3$), 0.85 (d, 1.5H, $J_{6,5}$ = 6.4 Hz, H-6^{fur}), 0.81–0.77 (m, 4.5H, $OCH_2CH_2CH_3$), 0.72 (d, 3H, $J_{6,5}$ = 6.2 Hz, H-6^{fur}). ^{13}C NMR (selected, 150 MHz, $CDCl_3$) δ 106.05 (C-1$^{\beta\text{-fur}}$), 101.99 (C-1^{pyr}), 101.85 (PhCH), 101.76 (PhCH), 101.59 (C-1^{pyr}), 97.98 (C-1$^{\alpha\text{-fur}}$), 22.67 ($OCH_2CH_2CH_3$), 15.37 (C-6^{fur}), 15.24 (C-6^{fur}), 10.19 ($OCH_2CH_2CH_3$). HRESIMS: found m/z 853.3556; calcd for $C_{50}H_{54}O_{11}$ $[M + Na]^+$ 853.3558.

3.10. Methyl 2,3,5,6-tetra-O-benzyl-(α,β)-D-galactofuranosyl-(1→3)-2-O-benzoyl-4,6-O-benzylidene-β-D-galactopyranosides (**18α,β**)

Glycosylation of galactoside **14** (19 mg, 0.05 mmol) with donor **9** (42 mg, 0.06 mmol) as described in the general procedure gave disaccharides **18α,β** (33 mg, 73%, α/β = 1.5:1) as a colourless syrup. R_f 0.61 (toluene–EtOAc, 4:1); ^{1}H NMR (selected, 600 MHz, $CDCl_3$) δ 8.11 (d, 2H, *J* = 7.2 Hz, *o*-C(O)Ph), 8.02 (d, 3H, *J* = 7.2 Hz, *o*-C(O)Ph), 5.70 (dd, 1.5H, $J_{2,3}$ = 9.8 Hz, $J_{2,1}$ = 8.4 Hz, H-2^{pyr}), 5.63 (dd, 1H,

$J_{2,3}$ = 9.9 Hz, $J_{2,1}$ = 8.3 Hz, H-2^{pyr}), 5.60 (s, 1.5H, PhC*H*), 5.39 (br. s, 2.5H, H-1$^{\alpha\text{-fur}}$, PhC*H*), 5.25 (s, 1H, H-1$^{\beta\text{-fur}}$), 4.58 (d, 1H, $J_{1,2}$ = 8.3 Hz, H-1^{pyr}), 4.41 (d, 1.5H, $J_{1,2}$ = 8.4 Hz, H-1^{pyr}), 3.53 (s, 4.5H, O*Me*). ^{13}C NMR (150 MHz, $CDCl_3$) δ 108.05 (C-1$^{\beta\text{-fur}}$), 101.86 (C-1^{pyr}), 101.75 (C-1^{pyr}), 101.21 (PhCH), 100.70 (PhCH), 95.44 (C-1$^{\alpha\text{-fur}}$), 56.12 (O*Me*). HRESIMS: found m/z 926.4099; calcd for $C_{55}H_{56}O_{12}$ $[M + NH_4]^+$ 926.4110.

3.11. Methyl 2,3,5-tri-O-benzyl-(α,β)-L-fucofuranosyl-(1→3)-2-O-benzoyl-4,6-O-benzylidene-β-D-galactopyranosides (**19α,β**)

Glycosylation of galactoside **14** (19 mg, 0.05 mmol) with donor **9** (42 mg, 0.06 mmol) as described in the general procedure gave disaccharides **19α,β** (31 mg, 77%, α/β = 2.3:1) as a colourless syrup. R_f 0.46 (petroleum ether–EtOAc, 3:1); R_f 0.20 (petroleum ether–EtOAc, 2:1); ^{1}H NMR (selected, 600 MHz, $CDCl_3$) δ 8.08 (d, J = 7.2 Hz, 3.3H, *o*-C(O)Ph), 5.71 (dd, 2.3H, $J_{2,3}$ = 9.8 Hz, $J_{2,1}$ = 8.2 Hz, H-2^{pyr}), 5.63 (dd, 1H, $J_{2,3}$ = 9.8 Hz, $J_{2,1}$ = 8.2 Hz, H-2^{pyr}), 5.59 (s, 1H, PhC*H*), 5.39 (s, 2.3H, PhC*H*), 5.33 (s, 1H, H-1$^{\beta\text{-fur}}$), 5.28 (d, 2.3H, J = 4.2 Hz, H-1$^{\alpha\text{-fur}}$), 4.61 (d, 1H, $J_{1,2}$ = 8.2 Hz, H-1^{pyr}), 4.57 (d, 2.3H, $J_{1,2}$ = 8.2 Hz, H-1^{pyr}), 3.56 (s, 3H, OMe), 3.53 (s, 7H, OMe), 1.19 (d, 7H, J = 6.3 Hz, H-6^{fur}), 1.12 (d, 3H, J = 6.4 Hz, H-6^{fur}). ^{13}C NMR (selected, 150 MHz, $CDCl_3$) δ 101.98 (2 × C-1^{pyr}), 101.90 (C-1$^{\beta\text{-fur}}$), 101.58 (C-1$^{\alpha\text{-fur}}$), 101.31 (PhCH), 100.82 (PhCH), 56.21 (O*Me*), 55.90 (O*Me*), 15.87 (C-6^{fur}), 15.39 (C-6^{fur}). HRESIMS: found m/z 825.3246; calcd for $C_{49}H_{50}O_{11}$ $[M + Na]^+$ 825.3245.

3.12. 3-Trifluoroacetamidopropyl 2,3,5,6-tetra-O-benzyl-(α,β)-D-galactofuranosyl-(1→3)-2-O-benzoyl-4,6-di-O-benzyl-α-D-mannopyranoside (**21α,β**)

Glycosylation of mannoside **20** (31 mg, 0.05 mmol) with donor **11** (36 mg, 0.06 mmol) as described in the general procedure gave disaccharides **22α,β** (25 mg, 43%, α/β = 2:1) as a colourless syrup. R_f 0.31 (petroleum ether–EtOAc, 3:1); ^{1}H NMR (selected, 600 MHz, $CDCl_3$) δ 5.64 (m, 1H, H-2^{pyr}), 5.61 (m, 2H, H-2^{pyr}), 5.46 (s, 1H, H-1$^{\beta\text{-fur}}$), 5.37 (d, 2H, J = 4.3 Hz, H-1$^{\alpha\text{-fur}}$), 5.01 (br. s, 2H, H-1^{pyr}), 4.96 (br. s, 1H, H-1^{pyr}). ^{13}C NMR (selected, 150 MHz, $CDCl_3$) δ 101.60 (C-1$^{\beta\text{-fur}}$), 101.27 (C-1$^{\alpha\text{-fur}}$), 98.09 (C-1^{pyr}), 97.79 (C-1^{pyr}), 72.69 (C-2^{pyr}), 69.09 (C-2^{pyr}). HRESIMS: found m/z 1162.4521; calcd for $C_{66}H_{68}F_3NO_{13}$ $[M + Na]^+$ 1162.4535.

3.13. 3-Trifluoroacetamidopropyl 2,3,5-tri-O-benzyl-(α,β)-L-fucofuranosyl-(1→3)-2-O-benzoyl-4,6-di-O-benzyl-α-D-mannopyranoside (**22α,β**)

Glycosylation of mannoside **20** (31 mg, 0.05 mmol) with donor **11** (36 mg, 0.06 mmol) as described in the general procedure gave disaccharides **22α,β** (21 mg, 40%, α/β = 2:3) as a colourless syrup. R_f 0.37 (petroleum ether–EtOAc, 3:1); ^{1}H NMR (selected, 600 MHz, $CDCl_3$) δ 8.07 (d, 3H, J = 7.4 Hz, *o*-C(O)Ph), 8.03 (d, 2H, J = 7.5 Hz, *o*-C(O)Ph), 7.42–7.10 (m, arom.), 5.72 (m, 1H, H-2^{pyr}), 5.56 (m, 1.5H, H-2^{pyr}), 5.49 (d, 1H, J = 4.1 Hz, H-1$^{\alpha\text{-fur}}$), 5.39 (s, 1.5H, H-1$^{\beta\text{-fur}}$), 4.98 (br. s, 1.5H, H-1^{pyr}), 4.96 (br. s, 1H, H-1^{pyr}), 3.56–3.44 (m, 3.5H, CH_2N), 1.98–1.88 (m, 3.5H, OCH$_2$CH_2CH$_2$N), 1.22 (d, 4.5H, J = 6.5 Hz, H-6^{fur}), 0.76 (d, 3H, J = 6.3 Hz, H-6^{fur}). ^{13}C NMR (selected, 150 MHz, $CDCl_3$) δ 108.14 (C-1$^{\beta\text{-fur}}$), 97.89 (C-1^{pyr}), 97.58 (C-1^{pyr}), 95.02 (C-1$^{\alpha\text{-fur}}$), 72.67 (C-2^{pyr}), 67.45 (C-2^{pyr}), 37.29 (*C*H$_2$N), 28.21 (OCH$_2$CH$_2$CH$_2$N), 15.45 (C-6^{fur}). HRESIMS: found m/z 1056.4116; calcd for $C_{59}H_{62}F_3NO_{12}$ $[M + Na]^+$ 1056.4116.

3.14. Removal of protecting groups (general procedure)

The protected disaccharide (20 μmol) was dissolved in 2 mL of EtOAc–MeOH (1:1) and 10% Pd/C (20 mg) was added. The reaction mixture was vigorously stirred in H_2 atmosphere for 24 h and then filtered through the celite layer. The filtrate was concentrated *in vacuo*, dissolved in 1 mL of 0.1 M MeONa in MeOH, one drop of water was added, and the mixture was kept overnight; then 6 μL of AcOH were added, the mixture was diluted with water and concentrated *in vacuo*. Gel-chromatography and subsequent lyophilization gave the unprotected disaccharides as a white foam.

3.15. Propyl (α,β)-D-galactofuranosyl-(1→3)-β-D-glucopyranosides (**1α,β**)

Deprotection of **15α,β** (35 mg, 37 μmol) as described in the general procedure gave disaccharides **1α,β** (11 mg, 78%, α/β = 1.2:1) as a white foam. For NMR data see Tables 1 and 2 in the Results and discussion section. HRESIMS: found m/z 407.1522; calcd for $C_{15}H_{28}O_{11}$ $[M + Na]^+$ 407.1524.

3.16. Propyl (α,β)-D-fucofuranosyl-(1→3)-β-D-glucopyranosides (**2α,β**)

Deprotection of **16α,β** (31 mg, 37 μmol) as described in the general procedure gave disaccharides **2α,β** (11 mg, 77%, α/β = 2:1) as a white foam. For NMR data see Tables 1 and 2 in the Results and discussion section. HRESIMS: found m/z 391.1567; calcd for $C_{15}H_{28}O_{10}$ $[M + Na]^+$ 391.1575.

3.17. Methyl (α,β)-D-galactofuranosyl-(1→3)-β-D-galactopyranosides (**3α,β**)

Deprotection of **18α,β** (30 mg, 37 μmol) as described in the general procedure gave disaccharides **3α,β** (9.3 mg, 70%, α/β = 1.5:1) as a white foam. For NMR data see Tables 1 and 2 in the Results and discussion section. HRESIMS: found m/z 379.1200; calcd for $C_{13}H_{24}O_{11}$ $[M + Na]^+$ 379.1211.

3.18. Methyl (α,β)-D-fucofuranosyl-(1→3)-β-D-galactopyranosides (**4α,β**)

Deprotection of **19α,β** (30 mg, 37 μmol) as described in the general procedure gave disaccharides **4α,β** (9.7 mg, 76%, α/β = 7:3) as a white foam. For NMR data see Tables 1 and 2 in the Results and discussion section. HRESIMS: found m/z 363.1259; calcd for $C_{13}H_{24}O_{10}$ $[M + Na]^+$ 363.1262.

3.19. 3-Aminopropyl (α,β)-D-galactofuranosyl-(1→3)-α-D-mannopyranosides (**5α,β**)

Deprotection of **21α,β** (23 mg, 20 μmol) as described in the general procedure gave disaccharides **5α,β** (7.1 mg, 77%, α/β = 2:1) as a white foam. For NMR data see Tables 1 and 2 in the Results and discussion section. HRESIMS: found m/z 400.1805; calcd for $C_{15}H_{30}NO_{11}$ $[M]^+$ 400.1813.

3.20. 3.19 3-Aminopropyl (α,β)-D-fucofuranosyl-(1→3)-α-D-mannopyranosides (**6α,β**)

Deprotection of **22α,β** (20 mg, 19 μmol) as described in the general procedure gave disaccharides **6α,β** (7.0 mg, 83%, α/β = 2:3) as a white foam. For NMR data see Tables 1 and 2 in the Results and discussion section. HRESIMS: found m/z 384.1861; calcd for $C_{15}H_{30}NO_{10}$ $[M]^+$ 384.1864.

Acknowledgments

This work was supported by RSF grant 14-23-00199 (N.E.N.). We thank Dr. A. O. Chizhov for recording the high resolution mass spectra

in the Department of Structural Studies of the Zelinsky Institute of Organic Chemistry, Moscow.

References

1. Duus JØ, Gotfredsen CH, Bock K. *Chem Rev* 2000;**100**:4589–614.
2. Shashkov AS, Lipkind GM, Knirel YA, Kochetkov NK. *Magn Res Chem* 1988;**26**:735–47.
3. Lipkind GM, Shashkov AS, Knirel YA, Vinogradov EV, Kochetkov NK. *Carbohydr Res* 1988;**175**:59–75.
4. Nifant'ev NE, Backinowsky LV, Lipkind GM, Shashkov AS, Kochetkov NK. *Bioorg Khim* 1991;**17**:517–30.
5. Kochetkov NK, Lipkind GM, Shashkov AS, Nifant'ev NE. *Carbohydr Res* 1991;**221**:145–68.
6. Lipkind GM, Shashkov AS, Nifant'ev NE, Kochetkov NK. *Carbohydr Res* 1992;**237**:11–22.
7. Bock K, Brignole A, Sigurskjold BW. *J Chem Soc Perkin Trans 2* 1986;1711–3.
8. Jansson PE, Kenne L, Widmalm G. *Carbohydr Res* 1989;**188**:169–91.
9. Stortz CA, Cerezo AS. *J Carbohydr Chem* 1998;**17**:1405–19.
10. Lundborg M, Widmalm G. *Anal Chem* 2011;**83**:1514–7.
11. Lundborg M, Fontana C, Widmalm G. *Biomacromolecules* 2011;**12**:3851–5.
12. Fontana C, Weintraub A, Widmalm G. *ChemPlusChem* 2013;**78**:1327–9.
13. Toukach FV, Ananikov VP. *Chem Soc Rev* 2013;**42**:8376–415.
14. Gurjar MK, Reddy LK, Hotha S. *Org Lett* 2001;**3**:321–3.
15. Latgé JP, Kobayashi H, Debeaupuis JP, Diaquin M, Sarfati J, Wieruszeski JM, et al. *Infect Immun* 1994;**62**:5424–33.
16. Argunov DA, Krylov VB, Nifantiev NE. *Org Biomol Chem* 2015;**13**:3255–67.
17. Krylov VB, Gerbst AG, Argunov DA, Dmitrenok AS, Shashkov AS, Kaczynski Z, et al. *Chem Eur J* 2015;**21**:1749–54.
18. Kol O, Wieruszeski J, Strecker G, Fournet B, Zalisz R, Smets P. *Carbohydr Res* 1992;**236**:339–44.
19. Krylov VB, Argunov DA, Vinnitskiy DZ, Verkhnyatskaya SA, Gerbst AG, Ustyuzhanina NE, et al. *Chem Eur J* 2014;**20**:16516–22.
20. Cattiaux L, Sendid B, Collot M, Machez E, Poulain D, Mallet JM. *Bioorg Med Chem* 2011;**19**:547–55.
21. Busse H, Hakoda M, Stanley M, Streicher H. *J Carbohydr Chem* 2007;**26**(3):159–94.
22. Sigurskjold BW, Haunstrup IB, Bock K. *Acta Chem Scand* 1992;**46**:451–8.
23. Breitmaier E, Voelter W, editors. *Carbon-13 NMR spectroscopy*. 3rd ed. Weinheim: VCH; 1989. p. 384.
24. Ananikov VP, Khokhlova EA, Egorov MP, Sakharov AM, Zlotin SG, Kucherov AV, et al. *Mendel Commun* 2015;**25**:75–82.
25. Cheney BV, Grant DM. *J Am Chem Soc* 1967;**89**:5319–27.
26. Ponder JW. *TINKER: Software Tools for Molecular Design, 5.0*. Saint Louis, MO: Washington University School of Medicine; 2009 <http://dasher.wustl.edu/tinker>.
27. Ooi T, Oobatake M, Némethy G, Scheraga HA. *Proc Natl Acad Sci U S A* 1987;**84**:3086–90.
28. Gerbst AG, Grachev AA, Yashunsky DV, Tsvetkov YE, Shashkov AS, Nifantiev NE. *J Carbohydr Chem* 2013;**32**:205–21.
29. Valiev M, Bylaska EJ, Govind N, Kowalski K, Straatsma TP, van Dam HJJ, et al. *Comput Phys Commun* 2010;**181**:1477–89.
30. Klamt A, Schuurmann G. *J Chem Soc Perkin Trans 2* 1993;**5**:799–805.
31. York DM, Karplus M. *J Phys Chem A* 1999;**103**:11060–79.
32. Aidas K, Angeli C, Bak KL, Bakken V, Bast R, Boman L, et al. *WIREs Comput Mol Sci* 2014;**4**:269–84.
33. Schafer A, Huber C, Ahlrichs R. *J Chem Phys* 1994;**100**:5829–35.
34. Armarego WLF, Chai CLL, editors. *Purification of laboratory chemicals*. 5th ed. Butterworth: Heinemann; 2003.
35. Belyakov PA, Kadentsev VI, Chizhov AO, Kolotyrkina NG, Shashkov AS, Ananikov VP. *Mendel Commun* 2010;**20**:125–31.

Carbohydrate Research 436 (2016) 20–24

Contents lists available at ScienceDirect

Carbohydrate Research

journal homepage: www.elsevier.com/locate/carres

Ring distortion in pyranosides caused by per-O-sulfation

Alexey G. Gerbst, Vadim B. Krylov, Dmitry A. Argunov, Arsenii S. Solovev, Andrey S. Dmitrenok, Alexander S. Shashkov, Nikolay E. Nifantiev*

Laboratory of Glycoconjugate Chemistry, N.D. Zelinsky Institute of Organic Chemistry, Russian Academy of Sciences, Leninsky Prospect 47, 119991 Moscow, Russian Federation

ARTICLE INFO

Article history:
Received 2 August 2016
Received in revised form
26 October 2016
Accepted 26 October 2016
Available online 29 October 2016

Keywords:
Pyranoside
O-sulfation
Conformation analysis
ab initio calculations

ABSTRACT

Distortion of the ring conformation in β-gluco- and β-xylopyranosides upon their per-O-sulfation was observed. In the case of glucose, a conformation intermediate between $^{3,O}B$ and $^{3}S_1$ was found, while complete $^{4}C_1 \rightarrow {}^{1}C_4$ inversion was detected in xylopyranoside. The conformational changes were evidenced experimentally by measuring intra-ring $^{1}H-{}^{1}H$ coupling constants and nuclear Overhauser effect (NOE) and were additionally confirmed by *ab initio* calculations.

1. Introduction

Polysulfated carbohydrate derivatives are biologically interesting compounds because of their ability to bind to various protein receptors in human. For example, heparan sulfate and heparin are able to interact with different growth factors and blood coagulation factors which determine their role in developmental processes, angiogenesis and blood coagulation [1]. Other sulfated polysaccharides, such as fucoidans from brown seaweeds [2–4] or fucosylated chondroitin sulfate from marine invertebrates [5,6] can mimic the shape of natural ligands and demonstrate a wide variety of biological activities in mammalian.

Theoretical studies of carbohydrate-protein binding require accurate knowledge of spatial and conformational behaviour of highly sulfated carbohydrates. It is well known that bulky substituents can significantly change the geometry of pyranoside ring. The inversion of "normal" $^{4}C_1$ conformation of β-glucopyranose into axial-rich $^{1}C_4$ form is induced by introduction of bulky silyl protective groups at O2 and O3 [7,8]. The conformational changes strongly modify the chemical behaviour of the pyranoside substrate by influencing on the spatial environment of the reaction center and change stereoelectronic effects [9].

The O-sulfation of a carbohydrate derivative can also strongly modify conformational behaviour of the pyranoside ring [10–12]. In particular, "unusual" *J*-coupling constants were reported for highly sulfated β-glucopyranoside [10] and β-xylopyranoside [11] derivatives which were attributed to $^{1}C_4$ chair - $^{4}C_1$ chair equilibrium [11]. In the present work an alternative interpretation of conformational changes for O-sulfated β-glucopyranoside is suggested and justified by molecular modeling and NOE experiments.

The interest to the conformation of totally sulfated pyranosides rise from the recently discovered pyranoside-*into*-furanoside (PIF) rearrangement which opens the way to the synthesis of different furanoside building blocks [13–15]. During the investigation of scope and limitations of the PIF rearrangement [16] we found that exhaustive sulfation of β-glucopyranoside derivative led to significant distortion of the pyranoside ring which was revealed by the pattern of *J*-coupling constants in ^{1}H NMR spectrum [16]. Moreover, theoretical modeling of the PIF reaction pathway showed plausible presence of intermediate and transition state in unusual non-chair conformation [16]. Conformational behaviour of sulfated carbohydrates is critical for deeper understanding of the PIF rearrangement mechanism and explanation of exceptional reactivity of some substrates. Thus, in the present communication the conformational changes of pyranoside ring occurring under exhaustive sulfation are studied in more details.

* Corresponding author.
E-mail address: nen@ioc.ac.ru (N.E. Nifantiev).

http://dx.doi.org/10.1016/j.carres.2016.10.011
0008-6215/

2. Results and discussion

In our recent work on the PIF rearrangement [16] we performed the exhaustive per-O-sulfation of the wide series of monosaccharides including *gluco*- (**1,2**), *galacto*- (**3,4**) and *manno*-pyranosides (**5,6**) with both α- and β-anomeric configuration resulting in formation of per-O-sulfated pyranosides **1s**-**6s**. The comparison of intra-ring *J*-coupling constants for compounds **1s**-**6s** [16] and parent monosaccharides **1**–**4,** [17] **5**–**6** [16] is presented in Table 1. For galactose and mannose derivatives in both anomeric forms (**3**–**6**) and α-isomeric glucose derivative (**2**) the difference in *J*-coupling constants is insignificant which indicates no conformational changes of pyranoside ring upon the per-O-sulfation. However, in case of β-glucoside **1** we observed drastic changes of *J*-coupling constant pattern.

To confirm this result, rather unexpected for such common sugar as glucose, we additionally investigated the pentapyranosides which are more flexible due to absence of hydroxymethyl group at C-5. The O-sulfation of available α- and β-methyl xylopyranosides (**8** and **7**) and α- and β-methyl arabinopyranosides (**9** and **10**) was performed by treating with Py·SO_3 complex in DMF and after neutralization with NH_4HCO_3 corresponding totally sulfated pyranosides **7s**-**10s** were isolated on TSK gel. The comparison of NMR data for non-sulfated (**7**–**10**) and per-O-sulfated pentapyranosides (**7s**-**10s**) is presented in Table 2.

The observed tendency for pentapyranosides in general repeats the data for hexapyranosides. The sulfation of monosaccharides with axial orientation of anomeric substituent **8** and **10** did not effect on the pattern of *J*-coupling constants while the dramatic changes were observed for β-xylopyranoside. As opposed to β-galactose derivatives **3** pronounced changes in *J*-coupling constants were observed for α-arabinoside **9**.

Analysis of the pattern of *J*-coupling constants suggested (Tables 1 and 2) that in case of β-*gluco*- and β-*xylo*-pyranosides the saccharides existed supposedly in a distorted conformation instead of the normal $^4C_1$. Thus for xylose all $^1H-^1H$ vicinal coupling constants, except $^3J_{5,5'}$, when compared to the corresponding values of the parent non-sulfated saccharide (Table 2), had almost negligibly small values, which could be attributed to equatorial orientation of all the ring protons, meaning that it existed in the completely inverted $^1C_4$ conformation. In the case of glucose, however, spin-spin couplings were measurable, although they were also considerably lower than those for the non-sulfated glucose. Investigation of glucoside **1s** in the temperature range of 0–40 °C did not reveal any measurable changes in *J*-coupling constants and in line shapes (see Supplementary data). These data did not allow for conclusion about the conformational preference of the glucoside, thus theoretical modeling was undertaken.

Ab initio calculations were carried out at HF level to get further insight into this problem. Since it was suspected that pentapyranosides could undergo complete $^4C_1 \rightarrow {}^1C_4$ ring inversion, geometries of all the studied structures, both penta- and, for comparison, hexapyranosides were optimized in order to obtain their energies in $^4C_1$ and $^1C_4$ conformations. Rather predictably, for all the non-sulfated compounds the calculations revealed preference for $^4C_1$ over $^1C_4$ conformation, although in case of the pentoses the energy difference was somewhat smaller. When the computational results for sulfated derivatives were analyzed, the lower energies of $^1C_4$ conformations in comparison with $^4C_1$ were found for the pentoses, thus giving support for the assumption that they could invert completely, at least in the case of xylose.

Surprisingly, when completely sulfated glucopyranoside was subjected to the geometry optimization, the resulting low-energy conformation was intermediate between $^{3,O}B$ and $^3S_1$ with Cremer-Pople parameters $\varphi = 17.7°$, $\theta = 83.1°$, $Q = 0.67$ (Fig. 1). $^1H-^1H$ intra-ring *J*-coupling constants estimated according to Karplus rule did not get exact match with those observed experimentally, but qualitative decrease of *J*-coupling constants as

Table 1
Intra-ring $^1H-^1H$ coupling constants measured for parent non-sulfated and sulfated gluco- (**1**, **2**), galacto- (**3**, **4**) and mannopyranosides (**5**, **6**).

	Compound		Solvent	$J_{1,2}$	$J_{2,3}$	$J_{3,4}$	$J_{4,5}$	$J_{5,6}$	$J_{5,6'}$	$\lvert J_{6,6'}\rvert$
1[a]	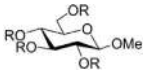	R=H	D_2O	8.0	9.4	9.2	9.7	2.3	6.0	12.3
1[b]		R=H	CD_3OD	7.9	9.3	n.d.[c]	n.d.[c]	1.9	5.3	12.0
1s[b]		R=SO_3NH_4	D_2O	5.0	5.0	5.9	5.9	3.3	7.9	10.9
1s[b]		R=SO_3NH_4	CD_3OD	3.1	2.6	3.3	3.6	4.3	8.0	10.6
2[a]	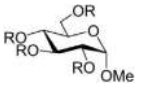	R=H	D_2O	3.8	9.8	9.1	10.0	2.3	5.4	12.3
2s[d]		R=SO_3Na	D_2O	3.6 (3.6)[e]	9.9 (9.8)	9.9 (8.8)	9.9	2.1	6.7	11.4
3[a]	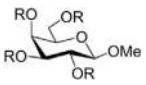	R=H	D_2O	7.9	9.9	3.5	1.1	4.4	7.9	11.8
3s[d]		R=SO_3Na	D_2O	7.7 (7.5)[g]	9.9 (9.6)	3.1 (3.0)	–[f] (0)	3.6 (3.3)	8.3 (8.0)	11.3 (11.5)
4[a]	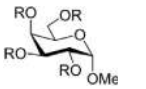	R=H	D_2O	3.9	10.3	3.5	1.2	4.2	8.2	11.7
4s[d]		R=SO_3Na	D_2O	3.7	10.6	3.1	–[f]	3.3	8.7	11.3
5[d]	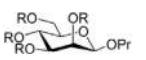	R=H	D_2O	–[f]	3.2	9.5	9.5	2.5	5.6	11.8
5s[d]		R=SO_3Na	D_2O	1.6	3.1	8.4	8.4	2.6	7.7	11.1
6[d]	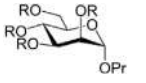	R=H	D_2O	1.7	3.2	9.5	9.5	2.4	5.5	11.8
6s[d]		R=SO_3Na	D_2O	–[f]	–[f]	9.6	9.6	–[f]	n.d.[c]	11.0

[a] Data were taken from Tafazzoli et al. [17].
[b] The values of proton-proton couplings were measured on the base of first-order analysis of obtained proton spectra.
[c] *J*-coupling constant cannot be measured due to the overlap of signals.
[d] Data were taken from our previous work [16].
[e] Data in parentheses were taken from Wessel et al. [10].
[f] *J*-coupling constant was not resolved due to very small value.
[g] Data in parentheses were taken from Probst et al. [11].

Table 2
Intra-ring ^{1}H-^{1}H coupling constants measured for parent non-sulfated and sulfated xylo- (**7**, **8**) and arabinopyranosides (**9**, **10**).

Compound	Structure		Solvent	$J_{1,2}$	$J_{2,3}$	$J_{3,4}$	$J_{4,5}$	$J_{4,5'}$	$\lvert J_{5,5'}\rvert$
7[a]	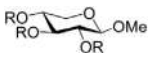	R=H	D_2O	7.9	9.3	9.1	10.6	5.5	11.7
7s[b]		R=SO_3NH_4	D_2O	–[c]	–[c]	–[c]	1.8	1.8	13.3
8[d]	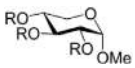	R=H	D_2O	3.7	9.6	9.6	4.8	10.9	11.1
8s[b]		R=SO_3NH_4	D_2O	3.1	8.3	8.1	5.1	8.8	11.9
9[b]	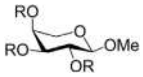	R=H	D_2O	7.6	9.6	n.d.[e]	n.d.[e]	n.d.[e]	n.d.[e]
9s[b]		R=SO_3NH_4	D_2O	4.4	6.7	3.4	6.7	3.1	12.2
10[b]	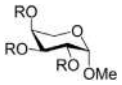	R=H	D_2O	2.9	n.d.[e]	n.d.[e]	2.5	1.0	12.8
10s[b]		R=SO_3NH_4	D_2O	3.6	10.2	3.4	2.5	–[c]	13.2

[a] Data were taken from Hricovini et al. [18].
[b] The values of proton-proton couplings were measured on the base of first-order analysis of obtained proton spectra.
[c] *J*-coupling constant was not resolved due to very small value.
[d] Data were taken from Malkina et al. [19].
[e] *J*-coupling constant cannot be measured due to the overlap of signals.

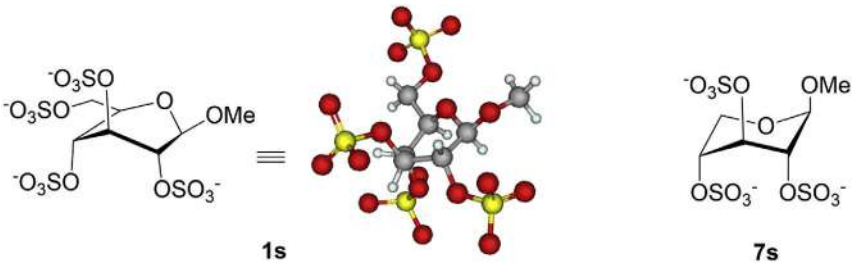

Fig. 1. Energy optimized structure of the per-O-sulfated methyl-β-D-glucopyranoside **1s** and schematic representation of methyl-β-D-xylopyranoside **7s**.

compared to the non-sulfated derivative was reproduced.

To confirm the complicated conformation of glucoside **1s**, nuclear Overhauser effects (NOE) were measured in 1D-NOESY experiments (Fig. 2, Table 3). In CD_3OD, where conformational changes were most pronounced (see *J*-coupling constants in Table 1), measured NOE perfectly matched the interatomic distances in the optimized structure of **1s**. In particular, strong H5-H1 and negligibly weak H5-H3 NOE confirmed the skew boat like conformation of the ring rather than the normal $^4C_1$ conformation where these NOE should be approximately equal. In D_2O the H5-H3

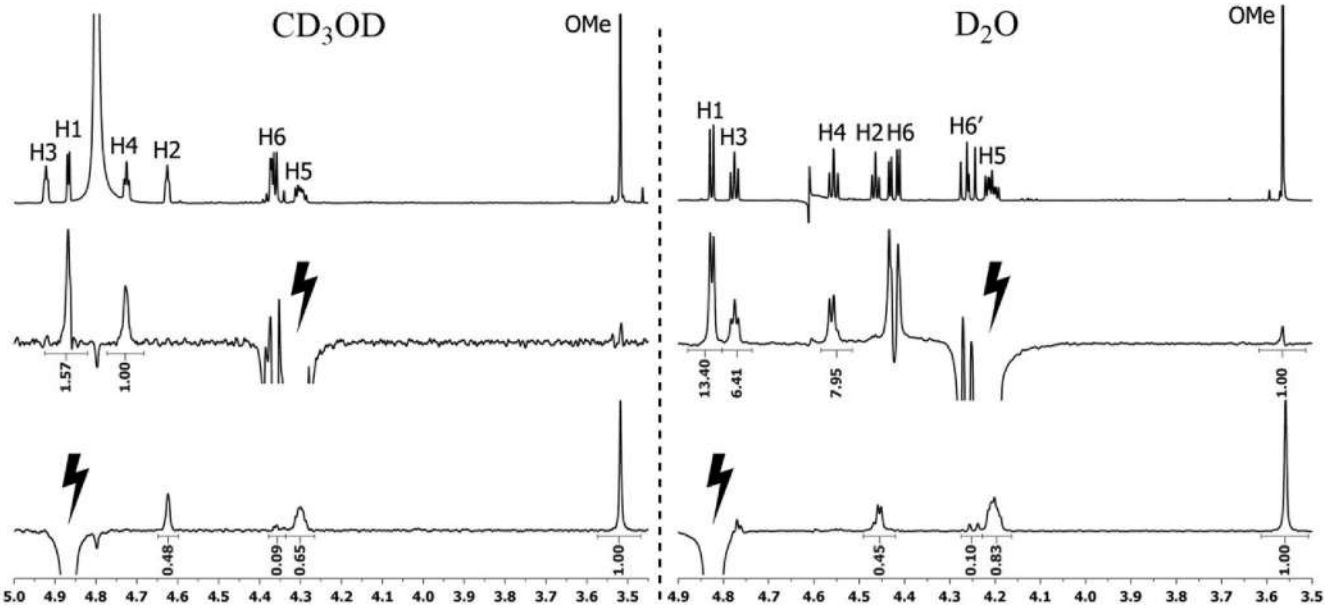

Fig. 2. 1D-NOESY experiments for per-O-sulfated β-methyl-glucoside **1s** in CD_3OD (left) and D_2O (right) upon pre-irradiation H5 or H1.

Table 3
NOE measured for the sulfated glucopyranose **1s**. Interatomic distances (Å) in the optimized structure are given in parentheses.

Solvent	Observed relative NOE upon the pre-irradiation of H1			Observed relative NOE upon the pre-irradiation of H5		
	H1-Me	H1-H2	H1-H5	H5-H4	H5-H3	H5-H1
CD_3OD	1	0.48 (2.98)	0.65 (2.36)	1 (2.86)	<0.1 (4.07)	1.57 (2.36)
D_2O	1	0.45	0.83	1	0.81	1.69

NOE was measurable, however it was significantly weaker than H5-H1 which could be explained by equilibrium between $^4C_1$ and skew boat conformation.

3. Conclusions

In the course of this work ring distortion in simple monosaccharides upon exhaustive sulfation was observed. Particularly, the most pronounced effect was found in the case of compounds bearing all equatorial substituents – β-xylose and β-glucose. The pattern of spin-spin coupling constants and *ab initio* calculations suggested inverted chair conformations for β-xylose instead of the usual $^4C_1$ conformation. In case of β-glucose a complex distorted conformation of the sugar ring was assumed which was confirmed by NOE experiments and quantum chemistry calculations. Our results proposed the alternative interpretation of conformational changes in β-glucose as compared to previously suggested equilibrium between $^1C_4$ and $^4C_1$ conformers. Precise information about spatial organization of sulfated derivatives is highly interesting for understanding of mechanism of newly discovered pyranoside-*into*-furanoside rearrangement.

4. Experimental

4.1. Computational studies

Ab initio calculations were performed using DALTON2013 program. HF approximation with 6-31 + G* basis set was employed. All the studied structures were treated as anions. Geometry optimization was performed until the RMS gradient reached the value of 10^{-4}.

4.2. NMR studies

^1H and ^{13}C NMR spectra were recorded on Bruker AV-600 spectrometer. Chemical shifts were referenced to signal of acetone used as internal standard. Average sample concentration was 30 μmol/mL. Signal assignment in ^1H and ^{13}C NMR spectra was made using COSY and $^1H-^{13}C$ HSQC techniques. The 1D-gNOESY experiments were carried out at 313 K with mixing periods of 700 ms. NMR spectra were obtained using standard pulse sequence from the Bruker software. All spectra were transformed and analyzed with the Bruker Topspin 2.1 software.

4.3. Synthesis of per-O-sulfated monosaccharide derivatives (general procedure)

The solution of pyranoside (0.1 mmol) and Py·SO_3 (3 equiv./OH-group) in DMF (1 mL) were stirred at 25 °C for 30 min. Then the solution was neutralized with aqueous solution of NH_4HCO_3, concentrated in vacuo and then co-evaporated with H_2O. Gel-chromatography was performed on TSK-40 HW(S) column (400 × 17 mm) by elution with 0.1 M AcOH in water at a flow rate of 0.5 mL/min and subsequent lyophilization gave the sulfated monosaccharide as a white foam.

4.4. Methyl 2,3,4,6-terta-O-sulfonato-β-D-glucopyranoside ammonium salt (1s)

Per-O-sulfation of methyl β-D-glucopyranoside **1** (20 mg, 0.10 mmol) as described in general procedure gave monosaccharide **1s** (52 mg, 84%). ^1H NMR (600 MHz, D_2O) δ 4.81 (d, $J_{1,2}$ 5.0 Hz, 1H, H-1), 4.76 (dd, $J_{2,3}$ 5.0 Hz, $J_{3,4}$ 5.9 Hz, 1H, H-3), 4.54 (t, *J* 5.9 Hz, 1H, H-4), 4.46 (t, 1H, H-2), 4.43 (dd, $J_{5,6}$ 3.3 Hz, $J_{6,6'}$ 10.9 Hz, 1H, H-6), 4.25 (dd, $J_{5,6'}$ 7.9 Hz, 1H, H-6′), 4.20–4.15 (m, 1H, H-5), 3.57 (s, 3H, $-CH_3$). ^1H NMR (600 MHz, CD_3OD) δ 4.94 (dd, $J_{2,3}$ 2.6 Hz, $J_{3,4}$ 3.3 Hz, 1H, H-3), 4.88 (d, $J_{1,2}$ 3.1 Hz, 1H, H-1), 4.73 (dd, $J_{4,5}$ 3.6 Hz, 1H, H-4), 4.63 (dd, 1H, H-2), 4.40 (dd, $J_{5,6}$ 4.3 Hz, $J_{6,6'}$ 10.6 Hz, 1H, H-6) 4.36 (dd, $J_{5,6'}$ 8.0, 1H, H-6′), 4.32–4.28 (m, 1H, H-5), 3.54 (s, 3H, $-CH_3$). ^{13}C NMR (150 MHz, D_2O) δ 101.22 (C-1), 75.88 (C-2), 75.37 (C-3), 73.58 (C-5), 72.44 (C-4), 68.05 (C-6), 57.11 ($-CH_3$). ^{13}C NMR (150 MHz, MeOD) δ = 102.87 (C-1), 76.17 (C-2), 75.91 (C-5), 75.46 (C-3), 72.93 (C-4), 69.59 (C-6), 57.15 ($-CH_3$).

4.5. Methyl 2,3,4-tri-O-sulfonato-β-D-xylopyranoside ammonium salt (7s)

Per-O-sulfation of methyl β-D-xylopyranoside **7** (16 mg, 0.10 mmol) as described in general procedure gave monosaccharide **7s** (29 mg, 64%). ^1H NMR (600 MHz, D_2O) δ 4.91 (s, 1H, H-1), 4.85–4.81 (m, 1H, H-3), 4.56–4.53 (m, 1H, H-4), 4.45–4.43 (m, 1H, H-2), 4.17 (dd, $J_{4,5}$ 1.8 Hz, $J_{5,5'}$ 13.3 Hz, 1H, H-5), 3.88 (dd, $J_{4,5'}$ 1.8 Hz, 1H, H-5′), 3.46 (s, 3H, $-CH_3$). ^{13}C NMR (150 MHz, D_2O) δ 98.42 (C-1), 71.34 (C-2), 70.94 (C-4), 70.84 (C-3), 57.31 (C-5), 55.57 ($-CH_3$).

4.6. Methyl 2,3,4-tri-O-sulfonato-α-D-xylopyranoside ammonium salt (8s)

Per-O-sulfation of methyl α-D-xylopyranoside **8** (16 mg, 0.10 mmol) as described in general procedure gave monosaccharide **8s** (31 mg, 67%). ^1H NMR (600 MHz, D_2O) δ 5.07 (d, $J_{1,2}$ 3.1 Hz, 1H, H-1), 4.69 (dd, $J_{2,3}$ 8.3 Hz, $J_{3,4}$ 8.1 Hz, 1H, H-3), 4.46–4.41 (m, 1H, H-4), 4.40 (dd, 1H, H-2), 4.09 (dd, $J_{4,5}$ 5.1 Hz, $J_{5,5'}$ 11.9 Hz, 1H, H-5), 3.83 (dd, $J_{4,5'}$ 8.8 Hz, 1H, H-5′), 3.48 (s, 3H, $-CH_3$). ^{13}C NMR (150 MHz, D_2O) δ = 98.25 (C-1), 75.65 (C-3), 75.04 (C-2), 73.95 (C-4), 61.08 (C-5), 56.36 ($-CH_3$).

4.7. Methyl 2,3,4-tri-O-sulfonato-α-D-arabinopyranoside ammonium salt (9s)

Per-O-sulfation of methyl α-D-arabinopyranoside **9** (16 mg, 0.10 mmol) as described in general procedure gave monosaccharide **9s** (27 mg, 59%). ^1H NMR (600 MHz, D_2O) δ 4.90–4.86 (m, 1H, H-4), 4.78 (dd, $J_{2,3}$ 6.7 Hz, $J_{3,4}$ 3.4 Hz, 1H, H-3), 4.75 (d, $J_{1,2}$ 4.4, 1H, H-1), 4.63 (dd, 1H, H-2), 4.18 (dd, $J_{4,5}$ 6.7 Hz, $J_{5,5'}$ 12.2 Hz, 1H, H-5), 3.83 (dd, $J_{4,5'}$ 3.1 Hz, 1H, H-5′), 3.55 (s, 3H, $-CH_3$). ^{13}C NMR (150 MHz, D_2O) δ 100.49 (C-1), 74.40 (C-2), 73.98 (C-3), 71.64 (C-4), 59.63 (C-5), 56.55 ($-CH_3$).

4.8. Methyl 2,3,4-tri-O-sulfonato-β-D-arabinopyranoside ammonium salt (10s)

Per-O-sulfation of methyl β-D-arabinopyranoside **10** (16 mg, 0.10 mmol) as described in general procedure gave monosaccharide **10s** (27 mg, 59%). ^1H NMR (600 MHz, D_2O) δ 5.29 (d, $J_{1,2}$ 3.6 Hz, 1H, H-1), 5.09 (m, 1H, H-4), 4.82 (dd, $J_{2,3}$ 10.2 Hz, $J_{3,4}$ 3.4 Hz, 1H, H-3), 4.67 (dd, 1H, H-2), 4.17 (dd, $J_{4,5}$ 2.5 Hz, $J_{5,5'}$ 13.2 Hz, 1H, H-5), 4.05 (d, 1H, H-5′), 3.57 (s, 3H, $-CH_3$). ^{13}C NMR (150 MHz, D_2O) δ 98.15 (C-1), 75.53 (C-4), 72.65 (C-2), 72.08 (C-3), 60.10 (C-5), 55.73 ($-CH_3$).

Acknowledgments

This work was supported by RSF grant 14-23-00199 (NEN).

Appendix A. Supplementary data

Supplementary data related to this article can be found at http://dx.doi.org/10.1016/j.carres.2016.10.011.

References

[1] M.C.Z. Meneghetti, A.J. Hughes, T.R. Rudd, H.B. Nader, A.K. Powell, E.A. Yates, M.A. Lima, J. R. Soc. Interface 12 (2015) 20150589.
[2] N.E. Ustyuzhanina, M.I. Bilan, A.G. Gerbst, N.A. Ushakova, E.A. Tsvetkova, A.S. Dmitrenok, A.I. Usov, N.E. Nifantiev, Carbohydr. Polym. 136 (2016) 826–833.
[3] N.E. Ustyuzhanina, N.A. Ushakova, K.A. Zyuzina, M.I. Bilan, A.L. Elizarova, O.V. Somonova, A.V. Madzhuga, V.B. Krylov, M.E. Preobrazhenskaya, A.I. Usov, M.V. Kiselevskiy, Mar. Drugs 11 (2013) 2444–2458.
[4] A. Cumashi, N.A. Ushakova, M.E. Preobrazhenskaya, A. D'Incecco, A. Piccoli, L. Totani, N. Tinari, G.E. Morozevich, A.E. Berman, M.I. Bilan, A.I. Usov, N.E. Ustyuzhanina, A.A. Grachev, C.J. Sanderson, M. Kelly, G.A. Rabinovich, S. Iacobelli, N.E. Nifantiev, Glycobiology 17 (2007) 541–552.
[5] A.G. Gerbst, N.E. Ustyuzhanina, N.E. Nifantiev, Mendeleev Commun. 25 (2015) 420–421.
[6] N.E. Ustyuzhanina, M.I. Bilan, A.S. Dmitrenok, A.S. Shashkov, M.I. Kusaykin, V.A. Stonik, N.E. Nifantiev, A.I. Usov, Glycobiology 26 (2016) 449–459.
[7] H. Yamada, K. Tanigakiuchi, K. Nagao, K. Okajima, T. Mukae, Tetrahedron Lett. 45 (2004) 9207–9209.
[8] C.H. Marzabadi, J.E. Anderson, J. Gonzalez-Outeirino, P.R. Gaffney, C.G. White, D.A. Tocher, L.J. Todaro, J. Am. Chem. Soc. 125 (2003) 15163–15173.
[9] C.M. Pedersen, L.U. Nordstrøm, M. Bols, J. Am. Chem. Soc. 129 (2007) 9222–9235.
[10] H.P. Wessel, S. Bartsch, Carbohydr. Res. 274 (1995) 1–9.
[11] K.C. Probst, H.P. Wessel, J. Carbohydr. Chem. 20 (2001) 549–560.
[12] T. Nagatsuka, H. Uzawa, Y. Nishida, Chem. Comm. 27 (2009) 4109–4111.
[13] V.B. Krylov, D.A. Argunov, D.Z. Vinnitskiy, S.A. Verkhnyatskaya, A.G. Gerbst, N.E. Ustyuzhanina, A.S. Dmitrenok, J. Huebner, O. Holst, H.-Ch. Siebert, N.E. Nifantiev, Chem. Eur. J. 20 (2014) 16516–16522.
[14] V.B. Krylov, A.G. Gerbst, D.A. Argunov, A.S. Dmitrenok, A.S. Shashkov, Z. Kaczynski, J. Huebner, O. Holst, N.E. Nifantiev, Chem. Eur. J. 21 (2015) 1749–1754.
[15] D.A. Argunov, V.B. Krylov, N.E. Nifantiev, Org. Biomol. Chem. 13 (2015) 3255–3267.
[16] V.B. Krylov, D.A. Argunov, D.Z. Vinnitskiy, A.G. Gerbst, N.E. Ustyuzhanina, A.S. Dmitrenok, N.E. Nifantiev, Synlett 27 (2016) 1659–1664.
[17] M. Tafazzoli, M. Ghiasi, Carbohydr. Res. 342 (2007) 2086–2096.
[18] M. Hricovini, O.L. Malkina, F. Bizik, L.T. Nagy, V.G. Malkin, J. Phys. Chem. A 101 (1997) 9756–9762.
[19] O.L. Malkina, M. Hricovini, F. Bizik, V.G. Malkin, J. Phys. Chem. A 105 (2001) 9188–9195.

Conference paper

Alexey G. Gerbst, Vadim B. Krylov and Nikolay E. Nifantiev*

Conformational changes in common monosaccharides caused by per-O-sulfation

https://doi.org/10.1515/pac-2018-1212

Abstract: Polysulfated carbohydrates play an important role in many biological processes because of their ability to bind to various protein receptors such as different growth factors, blood coagulation factors, adhesion lectins etc. Precise information about spatial organization of sulfated derivatives is of high demand for molecular modelling of such interactions as well as for understanding of the mechanism of pyranoside-*into*-furanoside rearrangement. In this review we summarize the changes recently revealed for the conformations of common pyranosides and furanosides upon total O-sulfation which were studied by means of NMR spectroscopy as well as molecular modelling. It was found that pentoses, being more flexible, undergo complete conformational chair inversion. Meanwhile, for hexoses the situation strongly depends on the monosaccharide configuration. Conformational changes are most pronounced in *gluco*-compounds though quantum chemical calculations helped to establish that no complete chair inversion occurred. In furanosides distortions of two types were observed: either the ring conformation or the conformation of the side chain changed. The presented data may be used for the analysis of chemical, physical and biological properties of sulfated carbohydrates.

Keywords: *ab initio* calculations; conformation analysis; ICS-29; monosaccharides; NMR; O-sulfation.

Introduction

Sulfated derivatives of carbohydrates represent significant biological interest due to their ability to exhibit different types of physiological activity including anticoagulant, anti-inflammatory, antiangiogenic [1–4]. The mechanism of these actions is based on specific interactions with certain protein receptors [5, 6]. For example, heparan sulfate interacts with fibroblast growth factors [7], chemokines [8], antithrombin-III [9], etc. Remarkably, conformational flexibility of a certain residue within the polysaccharide chain (iduronic acid) plays a key role in binding and biological properties of the whole polysaccharide [10]. Moreover, it was shown that conformational behaviour of iduronic acid, and thus the profile of biological activity of heparan sulfate fragments, is regulated by the sulfation pattern [11, 12].

Additionally, recently discovered pyranoside-*into*-furanoside rearrangement [13, 14] and the method for preparation of highly sulfated oligosaccharides [15, 16] open new ways for utilization of exhaustively sulfated derivatives as precursors of valuable synthetic blocks for oligosaccharide synthesis [17–21]. Investigation

Article note: A collection of invited papers based on presentations at the 29th International Carbohydrate Symposium (ICS-29), held in the University of Lisbon, Portugal, 14–19 July 2018.

***Corresponding author: Nikolay E. Nifantiev,** Laboratory of Glycoconjugate Chemistry, N. D. Zelinsky Institute of Organic Chemistry, Russian Academy of Sciences, Leninsky Prospect 47, 119991 Moscow, Russia, e-mail: nen@ioc.ac.ru.
https://orcid.org/0000-0002-0727-4050
Alexey G. Gerbst and Vadim B. Krylov: Laboratory of Glycoconjugate Chemistry, N. D. Zelinsky Institute of Organic Chemistry, Russian Academy of Sciences, Leninsky Prospect 47, 119991 Moscow, Russia

of mechanism of pyranoside-*into*-furanoside rearrangement [13, 14, 22] and understanding of its driving force [23] required precise data about spatial organization of highly sulfated derivatives.

Conformations of common hexoses are thought, as a rule, to be $^4C_1$ or $^1C_4$ depending on the monosaccharide configuration (D or L). However, modification of carbohydrates with bulky and negatively charged sulfate groups is expected to lead to changes of their conformations, which should be taken into account within *in silico* modelling of carbohydrate-protein interactions or mechanistic investigations of rearrangements of sulfated derivatives. Such changes were not studied in detail until recently. In this review we summarise the recent works devoted to changes in the conformation behaviour of common pyranosides and furanosides upon their total O-sulfation.

Conformational behaviour of totally O-sulfated pyranosides

During our studies of the newly discovered pyranoside-*into*-furanoside (PIF) rearrangement that proceeds *via* totally sulfated monosaccharides we came across pronounced changes in NMR spectra of these compounds as compared to the parent non-sulfated structures. Thus, sometimes ^1H-^1H coupling constants in the sulfated derivatives differed drastically from those in the free sugars.

In our work [24] several hexoses and pentoses were investigated. Particularly these were α- and β-isomers of *arabino*-, *xylo*-, *gluco*-, *galacto*- and *manno*-monosaccharides taken as methyl glycosides (Fig. 1). The analysis of their NMR spectra allowed for the following conclusions. First, monosaccharides with α-configuration of the anomeric center as well as β-galactose and β-mannose did not undergo significant conformation changes caused by introduction of sulfates. On the other hand β-xylose completely inverted from $^4C_1$ into $^1C_4$ upon the O-sulfation. This was clear both from changes in inter-proton coupling constants and quantum chemical calculations. Pronounced changes occurred in the β-glucoside. Although the latter fact had been already mentioned in 1995 by Wessel [25, 26], he did not provide sufficient data to come to a certain conclusion

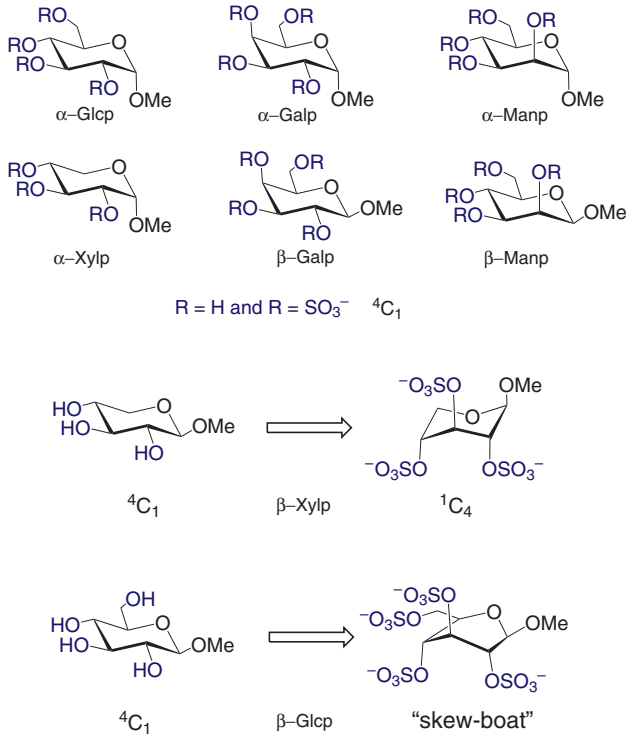

Fig. 1: Dominant conformations of common monosaccharides in totally O-sulfated and non-sulfated form.

about what transformations took place and just postulated that they probably resulted from $^4C_1$ to $^1C_4$ chair inversion. However, in work [24] with the use of nuclear Overhauser effect it was shown that dominant conformations of β-glucoside were skew-boats.

To gain further insight into this problem we conducted a detailed study [27] of the β-glucuronic acid propyl glycoside that contained an additional charged group. This monosaccharide is widely present in natural biopolymers, namely, chondroitin sulfates (Fig. 2).

Using quantum chemistry methods (HF/6-311++G** level of theory) and NMR experiments it was found that the distortion in the pyranoside ring of the glucuronic acid upon exhaustive sulfation is primarily explained by presence of two skew-boat conformers, $^0S_2$ and $^3S_1$ (Fig. 3) [27]. Appearance of the fully inverted conformer $^1C_4$ (suggested by several investigators before) is unlikely due to its higher relative energy and is not confirmed by NOE experiments. This also explains the unusual downfield shift of the anomeric proton upon sulfation. In methanol the proportion of the skewed conformers additionally increases due to its lower polarity. Considering that glucuronic acid is of important constituting blocks in such biologically significant polysaccharides as chondroitin sulfates, this knowledge may be very useful for correct modelling of interactions between CS or their fragments and protein targets.

Two sets of NMR characteristics had to be evaluated during this work [27]: ^1H-^1H coupling constants and ^1H chemical shifts (Tables 1 and 2, respectively). Chemical shifts for the two skewed conformers ($^0S_2$ and $^3S_1$) and for the both chair conformations ($^4C_1$ and $^1C_4$) of sulfated monosaccharides **2a**,**b** were calculated and

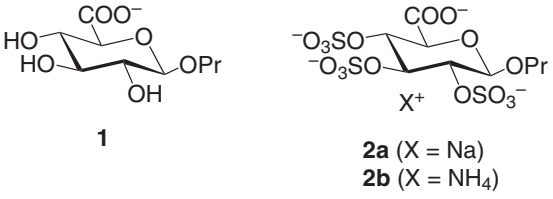

Fig. 2: Studied β-glucuronic acid propyl glycosides.

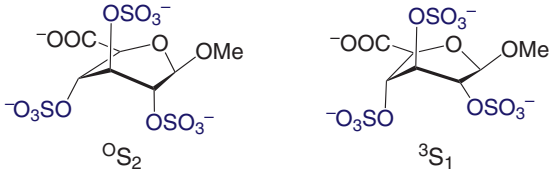

Fig. 3: Schematic view of skew-boat conformers $^0S_2$ and $^3S_1$ in per-O-sulfated β-glucuronic acid propyl glycosides. In $^0S_2$ conformer sulfates at C-2 and C-3 are located in trans orientation, however in $^3S_1$ conformer sulfates at C-3 and C-4 are trans orientated.

Table 1: Experimental and calculated chemical shifts for the conformers of structures **2a**,**b**.

Compound	Conformer	H-1	H-2	H-3	H-4	H-5
2a	Experimental	4.86	4.46	4.90	5.05	4.33
	$^0S_2$	4.82	4.43	4.87	4.57	4.08
	$^3S_1$	4.46	4.41	5.41	5.64	4.24
	$^4C_1$	4.34	3.79	4.74	4.53	3.83
	$^1C_4$	4.83	4.26	5.77	5.22	4.50
2b	Experimental	4.91	4.61	5.02	5.29	4.52
	$^0S_2$	4.75	3.84	4.52	5.69	3.72
	$^3S_1$	4.73	4.13	4.71	5.97	4.28
	$^4C_1$	4.31	3.29	4.24	4.25	3.67

Table 2: Experimental and calculated coupling constants for the conformers of structures **2a**.

Conformer	$J_{1,2}$	$J_{2,3}$	$J_{3,4}$	$J_{4,5}$
Experimental	6.3	2.9	4.7	3.6
$^{0}S_{2}$	0.2	3.7	0.6	8.9
$^{3}S_{1}$	6.2	0.6	4.2	0.8
$^{4}C_{1}$	7.5	10.4	9.7	9.5

For the calculated values no counter-ions were considered.

compared to the experimental data (Table 1). These data shows, that the computed chemical shifts exhibit sufficiently good correlation with the experimental ones. It was found that, $^{0}S_{2}$ and $^{1}C_{4}$ conformers showed significant downfield shift of the anomeric proton. Although the $^{1}C_{4}$ conformer energy of was considerably higher than for the skew conformers. Additional NOE experiments were undertaken to finally establish if the inverted $^{1}C_{4}$ conformer played any role. These results strongly support the idea that the skew-boat conformers make large contribution to the conformational equilibrium of the persulfated glucuronide.

Calculated ^{1}H-^{1}H coupling constants are presented in Table 2. As expected, they do not change very much for the same conformer upon the solvent change as they primarily depend on the values of torsional angles. $^{0}S_{2}$ and $^{3}S_{1}$ conformers are complimentary to each other in the sense that their $J_{H1\text{-}H2}$, $J_{H2\text{-}H3}$ and $J_{H3\text{-}H4}$ constant values alternate between them. Thus a combination of these two conformers should be sufficient to describe the whole experimental picture where $J_{H2\text{-}H3}$ and $J_{H3\text{-}H4}$ are almost equally small and $J_{H1\text{-}H2}$ is a bit larger though significantly smaller than in the non-sulfated compound **1**.

Conformational behaviour of totally O-sulfated furanosides

The furanosides naturally have greater conformational flexibility than pyranosides and thus the effect of O-sulfation in them should be more pronounced. Indeed, the pattern of *J*-coupling constants significantly differed for non-sulfated and per-*O*-sulfated furanosides which allowed for a conclusion that their conformations changed after the sulfation [28]. To rationalize these changes, we undertook theoretical conformational analysis of monosaccharides **3–5** and **3s–5s** (Fig. 4). This analysis included both studies of the conformation of the furanoside ring and conformation of the side chain at C(4). The conformation of the furanoside ring can be one of ten envelopes (E) or ten twist (T) forms while the conformation of the exocyclic chain (i.e. rotation of C4 – C5 and C5 – C6 bonds) is described by corresponding torsion angles.

Geometry optimization of all possible furanoside *pseudo*-rotamers for all the studied monosaccharides, both in non-sulfated (**3–5**) and sulfated (**3s–5s**) forms, tended to produce one or two low-energy conformers which differed from each other by less than 2 kcal/mol, while the other found conformations had considerably higher energies. For all the structures examined changes in the ring conformation upon the introduction of sulfates are observed. Particularly, in the mannoside, preference for ring conformers changes: while in the free form the calculations predict it to exist preferably in C3-endo conformation (Fig. 5), in the sulfated

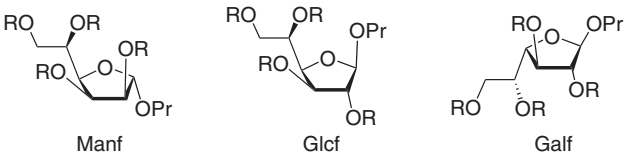

3 (R = H) **3s** (R = SO_3^-)
4 (R = H) **4s** (R = SO_3^-)
5 (R = H) **5s** (R = SO_3^-)

Fig. 4: Studied propyl furanosides **3–5** and **3s-5s**.

form C1-exo conformer becomes dominant. In the glucoside, the conformation of the furanoside ring in the conformer with minimal energy remains approximately the same C2-exo. In case of the galactosides the low energy C3-exo conformers which should dominate in the non-sulfated form disappear after introduction of O-sulfates and conformational shift towards C1-endo occurs [28].

In case of the mannoside **3** and glucoside **4**, in the absence of sulfates, the preferable conformation of the C4-C5 bond is characterized with trans-orientation of H4 and H5 protons. However, for their sulfated derivatives **3s**, **4s** gauche-rotamer is dominant (Fig. 6). This observation is obviously connected with introduction of sulfate at O-5. Thus, in non-sulfated form the most bulky group at C-5 is CH_2OH which prefers to take the trans-orientation to C3-atom of the ring. However, in sulfated derivatives SO_3-group at O-5, due to its size, is tended it locate in trans- orientation to C(3) (see Fig. 6). In the case of galactose **5**, however, the situation is more complex. This saccharide in its furanoside form supposedly has increased conformational flexibility, because for its lowest energy conformer all three rotamers around C4-C5 bond do not have great energy difference between each other [28].

All the mentioned changes certainly affect the values of the ^1H-^1H coupling constants. To study this influence in detail, DFT/B3LYP/pcJ-1 calculation of the constants for low-energy conformers was performed (Table 3). The first thing to note is that for non-sulfated α-propyl mannofuranoside **3** in the lowest-energy conformer (HF/6-311++G** level of theory) all the computed intra-ring constants, and, to some extent, $^3J_{4,5}$ reproduce the experimental values. According to the calculations the drastic decrease of the experimentally measured H1-H2 coupling constant in the mannofuranoside upon sulfation arises from the change of the

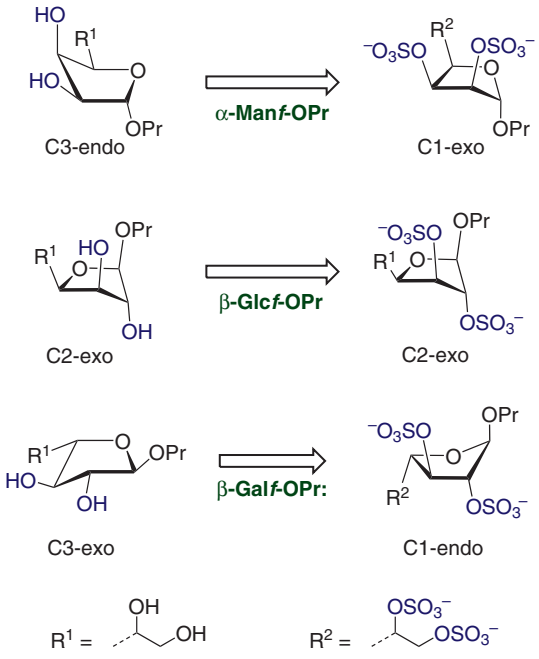

Fig. 5: Conformation of furanoside ring in low-energy conformers for non-sulfated and per-O-sulfated propyl furanosides.

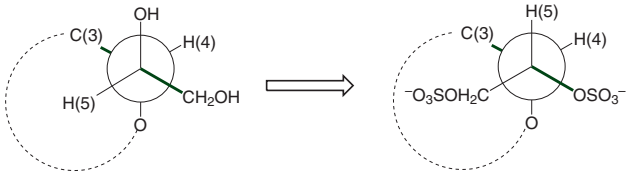

Fig. 6: Changes in preferable conformation of the C(4)-C(5) bond caused by per-O-sulfation propyl furanosides.

Table 3: Experimental ^1H-^1H coupling constants (Hz) and those calculated for different conformers (Hz) for furanosides **3–5** and **3s–5s**.

Entry	Compound	Furanoside ring conformation (H4-C4-C5-H5 dihedral)	Relative energy, kcal/mol	$J_{1,2}$	$J_{2,3}$	$J_{3,4}$	$J_{4,5}$
1	**3**	Experimental	–	4.6	4.6	2.9	8.8
2		C3-endo (+179°)	0.0	4.9	4.4	2.6	9.6
3		C1-exo (+178°)	1.6	0.3	5.5	8.3	9.8
4	**3s**	Experimental	–	1.2	5.6	7.0	2.8
5		C1-exo (+70°)	0.0	0.3	6.9	9.9	1.8
6		C3-endo (+84°)	1.2	5.6	5.0	2.7	0.5
7	**4**	Experimental	-	<1	1.2	4.5	9.0
8		C2-exo (+174°)	0.0	0.1	0.5	5.4	10.0
10	**4s**	Experimental	–	<1	0.7	4.8	4.9
11		C2-exo (+84°)	0.0	0.1	0.8	5.9	0.5
12	**5**	Experimental	–	2.4	4.4	6.8	4.0
13		C3-exo (−57°)	0.0	4.8	8.5	9.4	1.6
14		C3-exo (+53°)	1.0	5.2	8.1	9.5	6.3
15		C3-exo (+173°)	1.5	4.8	7.2	9.6	8.4
16		O4-exo (−59°)	1.2	0.3	1.4	6.9	6.4
17		O4-exo (+52°)	1.8	0.3	1.3	6.5	1.7
18	**5s**	Experimental	–	<1	<1	4.6	2.4
19		C1-endo (−63°)	0.0	0.1	0.4	3.9	1.4

conformational preference towards C1-exo in the sulfated saccharide. Good agreement between the theoretical and experimental data was obtained also in the case of the sulfated compounds **4s** and **5s** [28].

Conclusions

Thus, we can conclude that introduction of sulfate groups into different monosaccharide residues results in serious changes of their conformational behavior. The origin of such effects lies in the repulsive interactions between the bulky and charged sulfate groups. In case of pyranosides, the most pronounced effect was found in the case of compounds bearing all equatorial substituents – β-xylose, β-glucose and β-glucuronic acid glycosides. The experimental pattern of spin-spin coupling constants and *ab initio* calculations suggest inverted chair conformations for β-xylose instead of the usual $^4C_1$ conformation. In case of β-glucose and glucuronic acid a complex distorted conformation of the sugar ring was assumed which was confirmed by NOE experiments and quantum chemistry calculations. In furanosides distortions of two types were observed: either the ring conformation or the conformation of the side chain changed. The presented data may be used for the analysis of chemical, physical and biological properties of sulfated carbohydrate, as well as for mechanistic investigation of pyranoside-*into*-furanoside rearrangement and for understanding of its driving force.

Acknowledgments: This work was supported by the Russian Science Foundation, Funder Id: http://dx.doi.org/10.13039/501100006769, (grant 14-23-00199).

References

[1] T. N. Laremore, F. Zhang, J. S. Dordick, J. Liu, R. J. Linhardt. *Curr. Opin. Chem. Biol.* **13**, 633 (2009).
[2] N. E. Ustyuzhanina, M. I. Bilan, A. S. Dmitrenok, A. S. Shashkov, M. I. Kusaykin, V. A. Stonik, N. E. Nifantiev, A. I. Usov. *Glycobiology* **26**, 449 (2015).

[3] N. E. Ustyuzhanina, M. I. Bilan, A. G. Gerbst, N. A. Ushakova, E. A. Tsvetkova, A. S. Dmitrenok, A. I. Usov, N. E. Nifantiev. *Carbohydr. Polym.* **136**, 826 (2016).
[4] N. E. Ustyuzhanina, N. A. Ushakova, K. A. Zyuzina, M. I. Bilan, A. L. Elizarova, O. V. Somonova, A. V. Madzhuga, V. B. Krylov, M. E. Preobrazhenskaya, A. I. Usov, M. V. Kiselevskiy, N. E. Nifantiev. *Mar. Drugs* **11**, 2444 (2013).
[5] M. C. Z. Meneghetti, A. J. Hughes, T. R. Rudd, H. B. Nader, A. K. Powell, E. A. Yates, M. A. Lima. *J. R. Soc. Interface* **12**, 0589 (2015).
[6] A. G. Gerbst, N. E. Ustyuzhanina, N. E. Nifantiev. *Mendeleev Commun.* **6**, 420 (2015).
[7] A. Canales, J. Angulo, R. Ojeda, M. Bruix, R. Fayos, R. Lozano, G. Giménez-Gallego, M. Martín-Lomas, P. M. Nieto, J. Jiménez-Barbero. *J. Am. Chem. Soc.* **127**, 5778 (2005).
[8] Z. Johnson, A. E. Proudfoot, T. M. Handel. *Cytokine Growth Factor Rev.* **16**, 625 (2005).
[9] M. Petitou, C. A. A. van Boeckel. *Angew. Chem. Int. Ed Engl.* **43**, 3118 (2004).
[10] B. Casu, M. Petitou, M. Provasoli, P. Sinaÿ. *Trends Biochem. Sci.* **13**, 221 (1988).
[11] P.-H. Hsieh, D. F. Thieker, M. Guerrini, R. J. Woods, J. Liu. *Sci. Rep.* **6**, 29602 (2016).
[12] B. M. Sattelle, S. U. Hansen, J. Gardiner, A. Almond. *J. Am. Chem. Soc.* **132**, 13132 (2010).
[13] V. B. Krylov, D. A. Argunov, D. Z. Vinnitskiy, S. A. Verkhnyatskaya, A. G. Gerbst, N. E. Ustyuzhanina, A. S. Dmitrenok, J. Huebner, O. Holst, H.-C. Siebert, N. E. Nifantiev. *Chem.- Eur. J.* **20**, 16516 (2014).
[14] V. B. Krylov, D. A. Argunov, D. Z. Vinnitskiy, A. G. Gerbst, N. E. Ustyuzhanina, A. S. Dmitrenok, N. E. Nifantiev. *Synlett* **27**, 1659 (2016).
[15] V. B. Krylov, N. E. Ustyuzhanina, A. A. Grachev, N. E. Nifantiev. *Tetrahedron Lett.* **49**, 5877 (2008).
[16] V. B. Krylov, Z. M. Kaskova, D. Z. Vinnitskiy, N. E. Ustyuzhanina, A. A. Grachev, A. O. Chizhov, N. E. Nifantiev. *Carbohydr. Res.* **346**, 540 (2011).
[17] V. B. Krylov, A. G. Gerbst, D. A. Argunov, A. S. Dmitrenok, A. S. Shashkov, Z. Kaczynski, J. Huebner, O. Holst, N. E. Nifantiev, *Chem.- Eur. J.* **21**, 1749 (2015).
[18] V. B. Krylov, D. A. Argunov, A. S. Solovev, M. I. Petruk, A. G. Gerbst, A. S. Dmitrenok, A. S. Shashkov, J.-P. Latgé, N. E. Nifantiev. *Org. Biomol. Chem.* **16**, 1188 (2018).
[19] S. A. Verkhnyatskaya, V. B. Krylov, N. E. Nifantiev. *Eur. J. Org. Chem.* **2017**, 710 (2017).
[20] D. A. Argunov, V. B. Krylov, N. E. Nifantiev. *Org. Lett.* **18**, 5504 (2016).
[21] D. A. Argunov, V. B. Krylov, N. E. Nifantiev. *Org. Biomol. Chem.* **13**, 3255 (2015).
[22] A. G. Gerbst, V. B. Krylov, N. E. Nifantiev. *Russ. Chem. Bull.* **64**, 558 (2015).
[23] A. G. Gerbst, V. B. Krylov, D. A. Argunov, A. S. Dmitrenok, N. E. Nifantiev. *ACS Omega* **4**, 1139 (2019).
[24] A. G. Gerbst, V. B. Krylov, D. A. Argunov, A. S. Solovev, A. S. Dmitrenok, A. S. Shashkov, N. E. Nifantiev. *Carbohydr. Res.* **436**, 20 (2016).
[25] H. P. Wessel, S. Bartsch. *Carbohydr. Res.* **274**, 1 (1995).
[26] K. C. Probst, H. P. Wessel. *J. Carbohydr. Chem.* **20**, 549 (2001).
[27] A. G. Gerbst, D. Z. Vinnitsky, A. S. Dmitrenok, N. E. Ustyuzhanina, N. E. Nifantiev. *Carbohydr. Res.* **455**, 81 (2018).
[28] A. G. Gerbst, V. B. Krylov, D. A. Argunov, M. I. Petruk, A. S. Solovev, A. S. Dmitrenok, N. E. Nifantiev. *Beilstein J. Org. Chem.* **15**, 685 (2019).

BEILSTEIN JOURNAL OF ORGANIC CHEMISTRY

Influence of per-O-sulfation upon the conformational behaviour of common furanosides

Alexey G. Gerbst[1], Vadim B. Krylov[1], Dmitry A. Argunov[1], Maksim I. Petruk[1,2], Arsenii S. Solovev[1,2], Andrey S. Dmitrenok[1] and Nikolay E. Nifantiev[*1]

Full Research Paper

Open Access

Address:
[1]Laboratory of Glycoconjugate Chemistry, N.D. Zelinsky Institute of Organic Chemistry, Russian Academy of Sciences, Leninsky prospect 47, 119991 Moscow, Russia and [2]M.V. Lomonosov Moscow State University, Moscow, 119991, Russia

Email:
Nikolay E. Nifantiev[*] - nen@ioc.ac.ru

* Corresponding author

Keywords:
ab initio calculations; conformational analysis; furanosides; NMR; sulfation

Beilstein J. Org. Chem. **2019,** *15,* 685–694.
doi:10.3762/bjoc.15.63

Received: 12 November 2018
Accepted: 27 February 2019
Published: 15 March 2019

Associate Editor: S. Flitsch

Abstract

The studies on the recently discovered pyranoside-*into*-furanoside rearrangement have led us to conformational investigations of furanosides upon their total sulfation. Experimental NMR data showed that in some cases drastic changes of the ring conformation occurred while sometimes only the conformation of the exocyclic C4–C5 linkage changed. Herein we describe a combined quantum chemical and NMR conformational investigation of three common monosaccharide furanosides as their propyl glycosides: α-mannose, β-glucose and β-galactose. Full exploration of the furanoside ring by means of ab initio calculations was performed and coupling constants were calculated for each of the low-energy conformers. The results demonstrated preferred *trans*-orientation of H4–H5 protons in the non-sulfated molecules which changed to *gauche*-orientation upon sulfation. The effect is less pronounced in the galactosides. For all the studied structures changes in the conformational distribution were revealed by quantum mechanical calculations, that explained the observed changes in intraring coupling constants occurring upon introduction of sulfates.

Introduction

Changes in the conformations of monosaccharides expectedly accompany their modification with different functional groups. Thus, spatial repulsion of silyl groups results in inversion or distortion of the pyranoside ring [1,2], which strongly modifies the chemical behaviour of the pyranoside substrate by influencing the spatial environment of the reaction center and changing stereoelectronic effects [3-5]. A rather complex case is observed for sulfate groups; in addition to van der Waals interactions their negative charges contribute to the electrostatic forces. The per-O-sulfation results in drastic conforma-

tional changes of pyranosides: β-glucopyranosides, β-xylopyranosides and β-glucuronides [6-9].

The furanosides are generally more conformationally flexible than pyranosides [10,11] and thus the effects of substitution in them are more complex. The conformational effects underlay the striking stereoselectivity in the glycosylation reaction by furanosyl donors [12]. Conformational analysis of furanosides includes both conformation of the furanoside ring and conformation of the side chain at C(4). The conformation of the furanoside ring can be one of ten envelope (E) or ten twist (T) forms and it is convenient to describe it using the *pseudo*-rotation diagram [13]. The conformation of the exocyclic chain (i.e., rotation of C4−C5 and C5−C6 bonds) is described by two torsion angles [10].

The knowledge of conformational changes occurring in sulfated furanosides may be important for better understanding of the driving force of the pyranoside-*into*-furanoside rearrangement [14-16], which is widely used for preparative synthesis of different oligosaccharides, including fragments of a galactomannan from *Aspergillus* fumigatus [17-19], diheteroglycan from *Enterococcus faecalis* [20], galactan I from *Klebsiella pneumoniae* [21] and fucoidan from brown seaweed *Chordaria flagelliformis* [22].

In this communication the conformational analysis of three common per-O-sulfated furanosides is reported.

Results and Discussion

Synthesis of per-O-sulfated furanosides

Propyl α-D-mannofuranoside (**1**) was prepared from D-mannose and *n*-propanol via Fischer reaction using ion-exchange resin IR-120(H^+) as acidic catalyst. The reaction was performed under kinetic control and was stopped at low conversion of the starting mannose to avoid formation of the pyranoside product [23]. The desired furanoside **1** was isolated from the reaction mixture by column chromatography with a yield of 12%. Parent propyl β-D-glucofuranoside (**2**) and propyl β-D-galactofuranoside (**3**) were prepared using analogous reactions (Scheme 1). The use of the *n*-propyl group as an aglycon allowed for efficient purification of the desired glycosides utilizing C18 reversed-phase chromatography. Galactofuranoside **3** was previously synthesized using pyranoside-*into*-furanoside rearrangement [14].

The per-O-sulfation [24,25] of parent furanosides **1**–**3** was performed by their treatment with an excess of Py·SO_3 complex in DMF. After the reaction was finished, the reaction mixture was neutralized with aqueous NH_4HCO_3, concentrated in vacuo, dried and used for further NMR analysis without additional purification (Scheme 1).

NMR data of furanosides **1**–**3** and **1s**–**3s**

^1H and ^{13}C NMR spectra of parent monosaccharides **1**–**3** and their per-O-sulfated derivatives **1s**–**3s** were recorded in D_2O. The signal assignment was performed using 2D COSY and

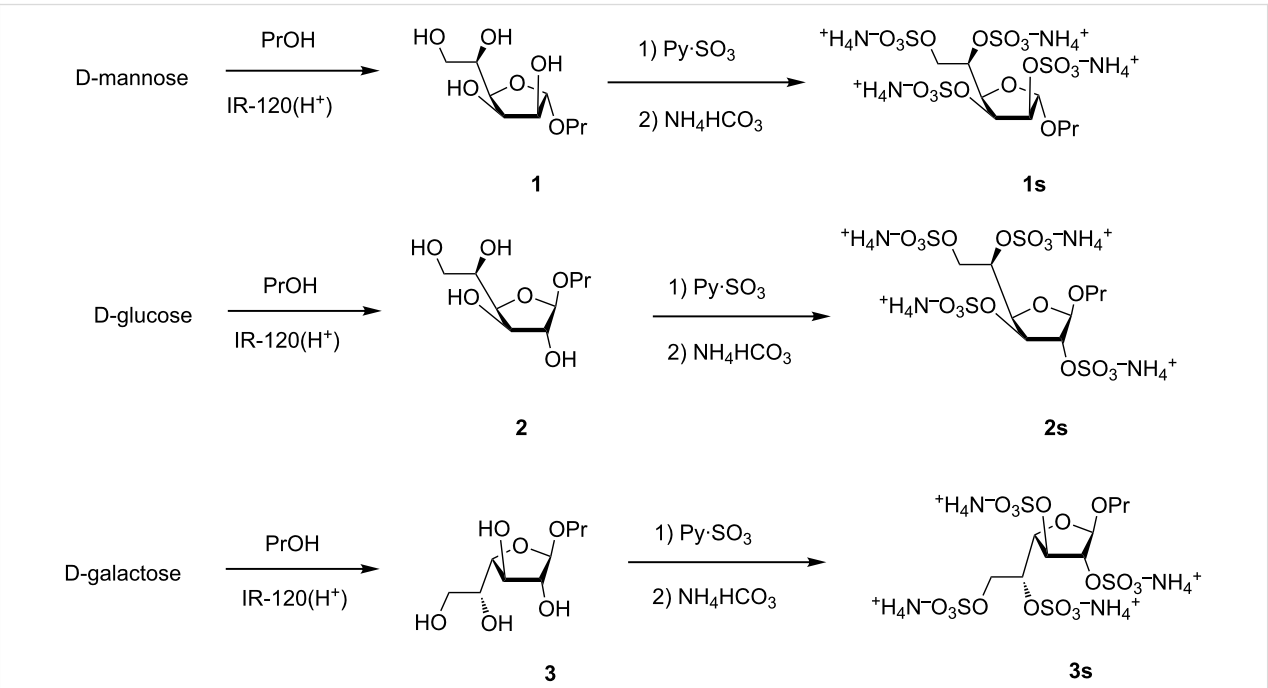

Scheme 1: Studied monosaccharides **1**–**3** and **1s**–**3s** and their preparation.

HSQC. *J* coupling constants were measured directly from 1D ^{1}H NMR spectra. In case of overlapping signals *J* coupling constants were extracted from 2nd order spectra simulations using Bruker TopSpin software (DAISY). The obtained results (see Tables 1–3) showed good coincidence with previously published data for related monosaccharides [15,26,27].

Table 1: ^{1}H NMR chemical shifts of non-sulfated (**1**–**3**[a]) and per-O-sulfated (**1s**–**3s**[b]) propyl furanosides.

compound	^{1}H (δ, ppm)						
	H(1)	H(2)	H(3)	H(4)	H(5)	H(6a)	H(6b)
1	4.96	4.07	4.24	3.98	3.84	3.72	3.54
1s	5.33	4.77	5.29	4.79	4.89	4.47	4.17
2	4.89	4.05	4.15	4.06	3.89	3.76	3.59
2s	5.29	5.05	5.03	4.74	4.88	4.55	4.24
3	4.92	3.97	4.00	3.88	3.74	3.63	3.58
3s	5.36	4.83	5.05	4.44	4.90	4.35	4.25

[a] ^{1}H chemical shifts for the propyl aglycon in non-sulfated compounds: H(1a) = 3.63; H(1b) = 3.47; H(2) = 1.51; H(3) = 0.82 ppm; [b] ^{1}H chemical shifts for the propyl aglycon in per-O-sulfated compounds: H(1a) = 3.69; H(1b) = 3.59; H(2) = 1.61; H(3) = 0.91 ppm.

Table 2: ^{13}C NMR chemical shifts of non-sulfated (**1**–**3**[a]) and per-O-sulfated (**1s**–**3s**[b]) propyl furanosides.

compound	^{13}C (δ, ppm)					
	C(1)	C(2)	C(3)	C(4)	C(5)	C(6)
1	107.4	76.7	71.1	79.1	69.0	63.0
1s	104.0	78.3	75.0	77.1	76.2	66.9
2	108.0	79.6	74.7	80.9	69.5	63.4
2s	106.9	83.0	78.9	80.8	75.8	67.8
3	107.0	80.9	76.4	82.3	70.8	62.8
3s	105.5	84.9	81.4	81.4	74.6	66.3

[a] ^{13}C chemical shifts for the propyl aglycon in non-sulfated compounds: C(1) = 71.4; C(2) = 22.2; C(3) = 9.7 ppm; [b] ^{13}C chemical shifts for the propyl aglycon in per-O-sulfated compounds: C(1) = 70.4; C(2) = 22.1; C(3) = 9.9 ppm.

Table 3: ^{1}H–^{1}H NMR *J* coupling constants of non-sulfated (**1**–**3**) and per-O-sulfated (**1s**–**3s**) propyl furanosides.

compound	*J* constants (Hz)						
	$J_{1,2}$	$J_{2,3}$	$J_{3,4}$	$J_{4,5}$	$J_{5,6a}$	$J_{5,6b}$	$J_{6a,6b}$
1	4.6	4.6	2.9	8.8	2.8	6.2	−12.1
1s	1.2	5.6	7.0	2.8	2.4	7.9	−11.4
2	<1	1.2	4.5	9.0	2.8	6.1	−12.0
2s	<1	<1 (≈0.7)	4.8	4.9	2.3	5.8	−11.2
3	2.4	4.4	6.8	4.0	4.3	7.5	−11.7
3s	<1	<1	4.6	2.4	5.3	7.5	−10.4

As can be seen from Table 3, *J* coupling constants significantly differ for non-sulfated and per-*O*-sulfated furanosides which allows for a conclusion that their conformations are changed after the sulfation. To rationalize these changes, we undertook theoretical conformational analysis of monosaccharides **1**–**3** and **1s**–**3s**.

Conformational analysis of the furanoside ring

For the theoretical exploration of the conformational properties of the furanoside rings several starting structures were generated for each compound. They represented all possible furanoside *pseudo*-rotamers. Additionally, for each of these structures the torsional angle H4–C4–C5–H5 defining the conformation of the exocyclic C4–C5 bond was set either to +60°, −60° or 180°. The only exception was the sulfated mannoside **1s**, where $^3J_{H4\text{-}H5}$ was very small suggesting low contribution of the 180° conformer. The starting conformation of the propyl aglycon was always chosen as follows: O4–C1–O1–CH_2 torsion was set to +60° or −60° depending on α- or β-configuration of the sugar in accordance with the *exo*-anomeric effect. Other starting torsions in the propyl group had *trans*-orientation. Geometry optimizations of all the thus obtained structures were carried out at ab initio HF/6-311++G** level using the COSMO continual solvation model with parameters for water. For complete computational details see the Experimental part.

For all the three studied monosaccharides, both in non-sulfated (**1**–**3**) and sulfated (**1s**–**3s**) forms, the geometry optimizations tended to produce one or two low-energy conformers which differed from each other by less than 2 kcal/mol. The other conformations found had considerably higher energies. For non-sulfated structures **1**–**3** sometimes high-energy conformations were obtained with the same puckering state of the furanoside ring (see Tables in Supporting Information File 1). Examination of these conformations revealed that these deviations were due to unfavorable orientation of the 2-OH and 3-OH hydroxy groups. In these cases re-optimization of the high-energy conformer was performed to ensure that energy would converge to the minimum.

Table 4 shows the descriptions of all the low-energy conformations obtained. The whole list of the resulting conformers can be found in Supporting Information File 1. All the obtained conformers are plotted on the *pseudo*-rotation wheel diagrams, where low-energy conformers are shown in red dots (Figure 1). Schematic views of the obtained low-energy conformers are shown in Figure 2.

From Table 4 it can be seen that in case of the mannoside **1** and glucoside **2**, in the absence of sulfates, the preferable conforma-

Table 4: Low-energy conformers obtained after ab initio geometry optimizations of compounds **1**–**3** and **1s**–**3s**.

compound		main low-energy conformers	value of H4–C4–C5–H5 dihedral	relative energy, kcal/mol[a]	conformer notation	P	v
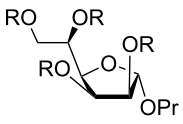	R = H	C3-*endo*	+179°	0.0	**A**	23	39
	R = H	C1-*exo*	+178°	0.7	**B**	130	38
	R = SO_3^-	C3-*endo*	+84°	1.2	**C**	22	40
	R = SO_3^-	C1-*exo*	+70°	0.0	**D**	131	39
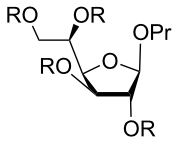	R = H	C2-*exo*	+174°	0.0	**E**	−20	32
	R = H	O4-*endo*	+173°	0.2	**F**	88	41
	R = SO_3^-	C2-*exo*	+84°	0.0[b]	**G**	−8	33
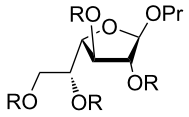	R = H	C3-*exo*	−57°	0.0	**H**	−148	39
	R = H	C3-*exo*	+53°	1.0	**I**	−151	38
	R = H	C3-*exo*	+173°	1.5	**J**	−147	37
	R = H	O4-*exo*	−59°	1.2	**K**	−91	38
	R = H	O4-*exo*	+52°	1.8	**L**	−88	39
	R = SO_3^-	C1-*endo*	−63°	0.0[b]	**M**	−65	37

[a]Values relative to the lowest energy conformer for each structure are given. [b]The conformer with minimal relative energy is presented. The other conformers can be found in Supporting Information.

tion of the C4–C5 bond is characterized with *trans*-orientation of H4 and H5 protons. However, for their sulfated derivatives **1s**, **2s** the *gauche*-rotamer was dominant. This observation is obviously connected with the introduction of sulfate at O5. Thus, in the non-sulfated form the most bulky group at C(5) is CH_2OH which prefers to adopt the *trans*-orientation to the C3 atom of the ring. However, in sulfated derivatives the SO_3^- group at O5, due to its size, tends to have *trans*-orientation to C(3) (see Figure 2). In the case of galactose **3**, however, the situation is more complex. This saccharide in its furanoside form has increased conformational flexibility around the C4–C5 bond, because for its lowest energy conformer (C3-*exo*) all three rotamers (**H**, **I**, **J**) do not have great energy difference between each other. For its other ring conformer, O4-*exo*, two C4–C5 rotamers (**K**, **L**) are possible according to the calculation results.

For all the examined structures changes in the ring conformation upon the introduction of sulfates are observed. Particularly, in the mannoside prevalence of the conformers changes: while in the free form of **1** the calculations predict it to exist preferably in C3-*endo* conformation (Table 4, conformer **A**), in the sulfated form the C1-*exo* conformer becomes dominant (conformer **D**). In the glucoside, the conformation of the furanoside ring in the conformer with minimal energy stays approximately the same (C2-*exo* for both **E** and **G** conformers), however, O4-*endo* conformer (conformer **F**) which is present in non-sulfated form **2** disappears in the sulfated one (**2s**). In case of the galactosides the low energy C3-*exo* conformers (**H**, **I**, **J**) which should dominate in non-sulfated form **3** disappear after introduction of O-sulfates and conformational shift to C1-*endo* (conformer **M**) occurs.

Additionally, pseudorotational analysis of compounds **1**–**3** and **1s**–**3s** was performed using the MatLab program developed by P. M. S. Hendrickx and J. C. Martins [28]. The results are shown in Table 5. Comparison of the ring puckering parameters obtained from this analysis with those for the lowest energy conformers in Table 4 shows that they are of the same range and demonstrate the same tendencies as found from quantum mechanical calculations.

All the mentioned changes certainly affect the values of the intraring ^1H–^1H coupling constants. To study this influence in detail, DFT/B3LYP/pcJ-1 calculation of the constants for low-energy conformers (**A**–**M**) denoted in Table 4 was performed (Table 6). The first thing to note is that for non-sulfated α-propyl mannofuranoside **1** in the lowest-energy conformer **A** all the computed intraring constants, and, to some extent, $^3J_{4,5}$ reproduce the experimental values (Table 6, entries 1 and 2). According to the calculations the drastic decrease of the experimentally measured H1–H2 coupling constant in the mannofura-

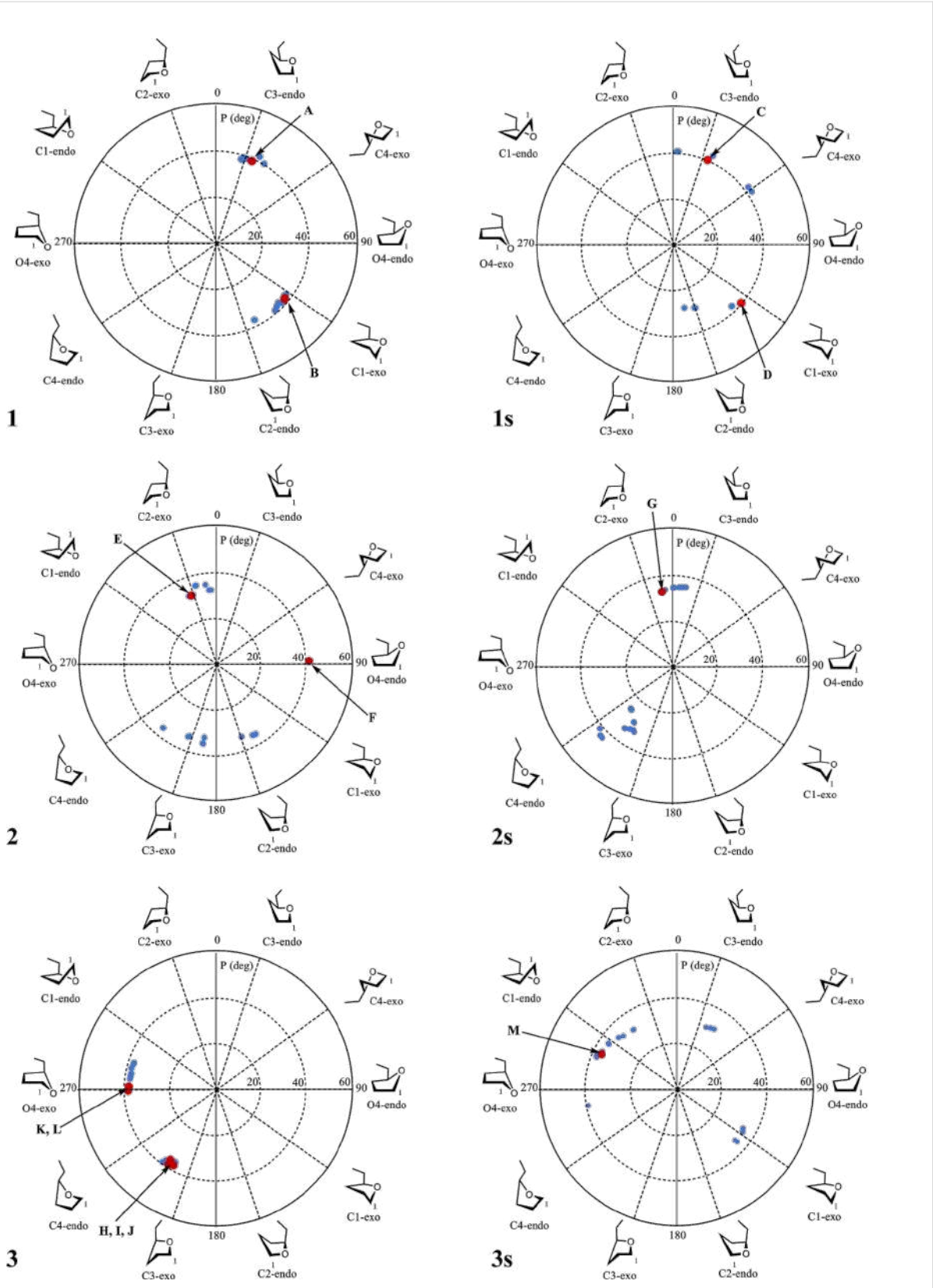

Figure 1: The *pseudo*-rotation wheels showing different optimized structures of furanosides **1**–**3** and **1s**–**3s**. The lower energy conformations (denoted as in Table 4) are colored in red.

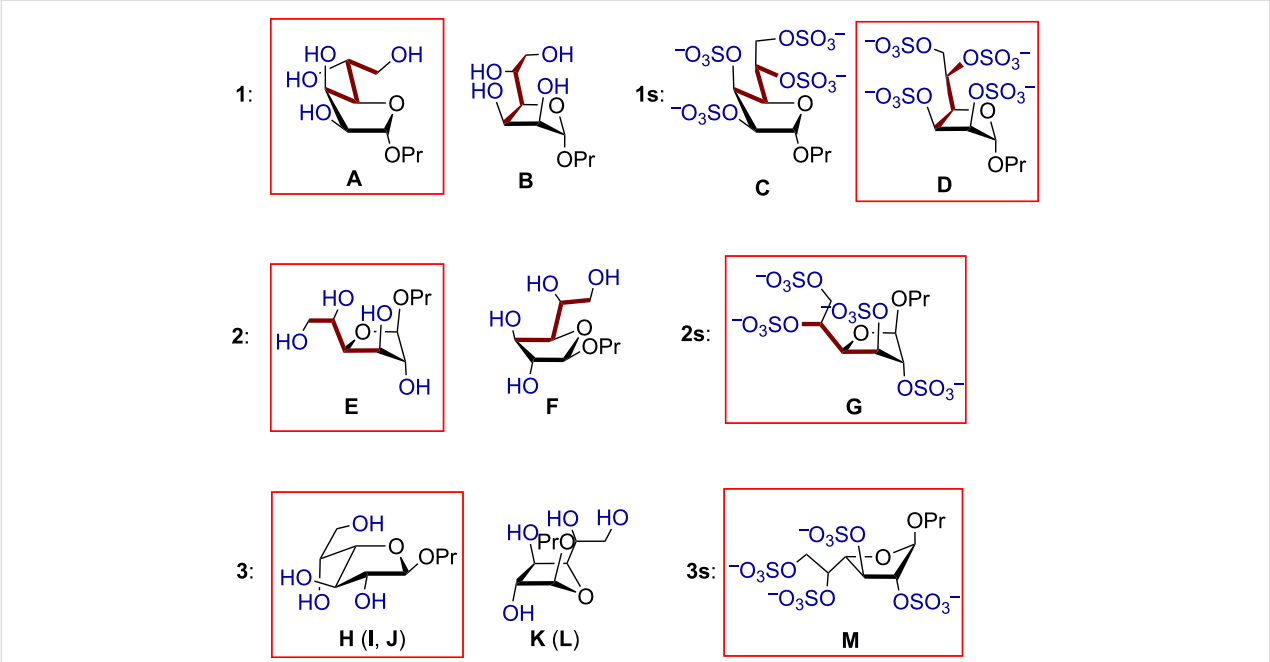

Figure 2: Schematic views of low energy conformers **A**–**M**. The minimal energy conformers are embedded in red frames. The substituents at C4–C5 bond located in *trans*-position are shown in brown. The conformers H–J and K, L only differ in the H4–C4–C5–H5 dihedral angle (see Table 4).

Table 5: Best-fit conformers obtained after pseudorotaional analysis of compounds **1**–**3** and **1s**–**3s**.

compound	best-fit conformer parameters (found by MatLab [28])		RMSD (Hz)
	P	v	
1	20.4	45.3	0.61
1s	184.5	44.2	0.32
2	6.2	33.3	0.36
2s	29.9	35.0	0.01
3	−155.2	20.4	0.21
3s	−64.1	35.5	0.05

noside upon sulfation arises from the change of the conformational preference towards C1-*exo* (conformer **D**) in the sulfated saccharide.

The changes in conformation of side chain from *trans* into *gauche* rotamers (H4–C4–C5–H5 dihedral angle) upon the sulfation were clearly seen from the $^3J_{4,5}$ coupling constants. Additionally to justify that the correct conformers for C4–C5 bond were obtained, two J-HMBC experiments were performed to measure the the H4–C6 $^3J_{C\text{-}H}$ coupling whose value could distinguish between the three possible rotamers. Reasonable coincidence with the calculations was obtained: for the non-sulfated mannoside **1** the measured constant was 3 Hz (calcd. 3.6 Hz) and for the sulfated compound **1s** it was 5 Hz (calcd. 5.7 Hz).

The same calculations of coupling constants were performed for the glucosides and galactosides. In the case of the non-sulfated compounds **2** and **3** (Table 6) combination of the coupling constants calculated for the found conformers generally reproduced the experimental values of the intraring couplings. The only exception was conformer **F** of the glucoside **2** (Table 6, entry 9), whose $^3J_{H1\text{-}H2}$ coupling is quite large while its relative energy is comparable (although still higher) than that of the main conformer **E** (Table 6, entry 8).

Good agreement between the theoretical and experimental data was obtained also in the case of the sulfated compounds **2s** and **3s** (Table 6, entries 10, 11, 18 and 19). However, it needs to be mentioned, that among other constants calculated for conformer **G** of **2s** (Table 6, entry 10), $^3J_{H4\text{-}H5}$ deviates strongly from that measured experimentally (Table 6, entry 10). We attribute it to the fact that no counter-ions were considered in the calculations and thus the energies of the other rotamers around C4–C5 linkage could have been overestimated.

The rotation around the C5–C6 bond in furanosides obviously results in additional conformers. The investigation of conformational behavior of acyclic polyols was not the primary goal of this study, but to make sure that the rotation around C5–C6 is free and does not influence the conformation of the furanoside ring and thus the intraring couplings, the additional conformations were considered for mannosides **1** and **1s** (Table 7). The previously found conformers (**A** and **B** for the free mannoside **1**

Table 6: Experimental ^{1}H–^{1}H coupling constants (Hz) and those calculated for different conformers (Hz) for furanosides **1**–**3** and **1s**–**3s**.

entry	compound	conformer notation	relative energy, kcal/mol	$J_{1,2}$	$J_{2,3}$	$J_{3,4}$	$J_{4,5}$
1	**1**	experimental	–	4.6	4.6	2.9	8.8
2		conformer **A**	0.0	4.9	4.4	2.6	9.6
3		conformer **B**	1.6	0.3	5.5	8.3	9.8
4	**1s**	experimental	–	1.2	5.6	7.0	2.8
5		conformer **D**	0.0	0.3	6.9	9.9	1.8
6		conformer **C**	1.2	5.6	5.0	2.7	0.5
7	**2**	experimental	–	<1	1.2	4.5	9.0
8		conformer **E**	0.0	0.1	0.5	5.4	10.0
9		conformer **F**	0.2	5.4	1.4	5.0	9.5
10	**2s**	experimental	–	<1	0.7	4.8	4.9
11		conformer **G**	0.0	0.1	0.8	5.9	0.5
12	**3**	experimental	–	2.4[a]	4.4[a]	6.8[a]	4.0[a]
13		conformer **H**	0.0	4.8	8.5	9.4	1.6
14		conformer **I**	1.0	5.2	8.1	9.5	6.3
15		conformer **J**	1.5	4.8	7.2	9.6	8.4
16		conformer **K**	1.2	0.3	1.4	6.9	6.4
17		conformer **L**	1.8	0.3	1.3	6.5	1.7
18	**3s**	experimental	–	<1	<1	4.6	2.4
19		conformer **M**	0.0	0.1	0.4	3.9	1.4

[a]The constant was obtained by second order spectrum simulation in Topspin DAISY.

and **C** and **D** for its sulfated counter-part **1s**) had the C5–C6 bond in *gauche-trans* orientation (denotation of conformers see on Figure 3). The geometry optimizations showed that *gauche-gauche* conformers are also possible (Table 7, entries 3, 5, 9 and 11) and for the non-sulfated mannoside **1** *trans-gauche* rotamer was also found (Table 7, entry 6). It can be seen that, indeed, the rotation around this bond quite expectedly changes the values of the H5–H6 coupling constants, but additionally it significantly influences the vicinal $H6_{proR}$-$H6_{proS}$ coupling. The values of the intra-ring constants as well as $J_{4,5}$ during the rotation change very slightly or do not change at all.

Conclusion

Conformational analysis of several common monosaccharides in the furanoside form was performed in order to study molecular geometry changes occurring upon total sulfation. It was found that these changes generally affected either the furanoside ring conformation or the conformation of C4–C5 side bond. Particularly, all the studied structures exhibited preference for *trans*-placement of H4 and H5 protons in the non-sulfated form which changed to *gauche*-orientation upon the introduction of sulfates. This tendency was less pronounced in the galactosides where in the free form all three C4–C5 rotamers were found to have rather low energies. The mannoside in the free form was theoretically predicted to exist preferably in C3-*endo* conformation while in the sulfated form C1-*exo* conformer became dominant. In the glucoside, O4-*endo* conformer disappeared in the sulfated form and in the galactoside conformational shift to C1-*endo* occurred.

Experimental

General procedures

Commercial chemicals were used without purification unless noted. All solvents for reactions were purchased as dry (DMF,

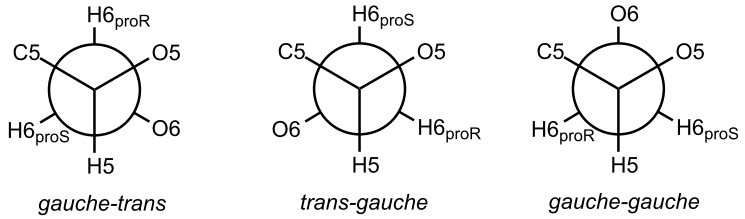

Figure 3: Denotation of conformers obtained during rotation around C5–C6 bond.

Table 7: Experimental ^{1}H–^{1}H coupling constants (Hz) for α-propyl mannofuranosides (**1**, **1s**) and those calculated for its different conformers (Hz).

entry	conformer notation and orientation of C5–C6 bond	relative energy, kcal/mol	$J_{1,2}$	$J_{2,3}$	$J_{3,4}$	$J_{4,5}$	$J_{5,6a}$	$J_{5,6b}$	$J_{6a,6b}$[a]
1	experimental for **1**	–	4.6	4.6	2.9	8.8	2.8	6.2	12.1
2	conformer **A**, *gauche-trans*	0.0	4.9	4.4	2.6	9.6	2.5	10.3	−8.9
3	conformer **A**, *gauche-gauche*	1.3	4.8	4.5	2.7	9.8	2.7	1.4	−10.6
4	conformer **B**, *gauche-trans*	0.7	0.3	5.7	8.1	10.1	2.5	10.2	−9.4
5	conformer **B**, *gauche-gauche*	2.0	0.3	5.6	8.4	10.3	2.7	1.5	−11.2
6	conformer **B**, *trans-gauche*	1.6	0.3	5.5	8.3	9.8	10.1	3.1	−12.2
7	experimental for **1s**	–	1.2	5.6	7.0	2.8	2.4	7.9	11.4
8	conformer **D**, *gauche-trans*	0.0	0.3	6.9	9.9	1.8	1.7	10.2	−11.8
9	conformer **D**, *gauche-gauche*	3.6	0.3	7.0	10.0	1.9	5.8	0.5	−12.1
10	conformer **C**, *gauche-trans*	1.2	5.6	5.0	2.7	0.5	1.9	10.0	−11.2
11	conformer **C**, *gauche-gauche*	3.6	6.2	4.9	2.7	0.6	5.6	0.5	−11.5

[a]The sign of the constant was not determined experimentally.

n-propanol) solvents for chromatography (EtOAc, MeOH, H_2O) were HPLC grade. Thin-layer chromatography (TLC) was carried out on aluminum sheets coated with silica gel 60 F_{254} (Merck). Analysis TLC plates were developed by treatment with a mixture of 15% H_3PO_4 and orcinol (1.8 g/L) in EtOH/H_2O (95:5, v/v) followed by heating.

NMR and computational studies

^{1}H and ^{13}C NMR spectra were recorded on Bruker AV-400 or Bruker Fourier 300HD spectrometers equipped with 5 mm pulsed-field-gradient (PFG) probes at temperatures denoted in the spectra in Supporting Information File 1. The resonance assignment in ^{1}H and ^{13}C NMR spectra was performed using 2D experiments COSY and HSQC. Chemical shifts are reported in ppm. NMR spectra were obtained using a standard pulse sequence from the Bruker software. In *J*-HMBC experiments the delay for the long-range couplings was optimized for 1.5 Hz. All spectra were transformed and analyzed with the Bruker Topspin 3.6 software.

Geometry optimization were performed using the ORCA 2.9.1 program [29,30]. RHF approximation with 6-311++G** basis set was employed [31]. Sulfates in the studied structures were treated as anions without presence counterions. COSMO [32] model was applied with built-in parameters for water. Geometry optimizations were performed until the RMS gradient reached a value less than 10^{-4}. Coupling constants were computed using DFT/B3LYP/pcJ-1 [33] approximation and DALTON-2015 software [34]. Only Fermi-contact terms were evaluated.

Synthesis of propyl α-D-mannofuranoside (**1**)

To a suspension of D-mannose (400 mg, 2.22 mmol) in *n*-propanol (4 mL) was added resin IR-120(H^+) (475 mg). The mixture was heated to 80 °C and stirred for 4 h. Then the resin was filtered off. The residue was purified by column chromatography (EtOAc/MeOH 20:1) to afford compound **1** (59 mg, 12%) as a colorless syrup. R_f = 0.32 (EtOAc/MeOH 10:1).

Synthesis of propyl β-D-glucofuranoside (**2**) and β-D-galactofuranoside (**3**)

The preparations of furanosides **2** and **3** were performed as described above for mannofuranoside **1**, however, the HPLC (C-18, eluted with MeOH/H_2O) was additionally applied to separate α- and β-furanosides. The resulted yields of furanosides **2** and **3** were 10% and 24%, respectively.

General protocol for per-O-sulfation

A solution of furanoside (0.02 mmol) and Py·SO_3 (0.4 mmol) in DMF (500 μL) was stirred at 25 °C for 30 min. Then the reaction mixture was neutralized with an aqueous solution of NH_4HCO_3, concentrated in vacuo and then co-evaporated with H_2O. The residue was dissolved in D_2O (550 μL) and used for recording of NMR spectra.

Supporting Information

Supporting Information File 1

Copies of ^{1}H and ^{13}C NMR spectra of compounds **1**–**3** and **1s**–**3s** and computational details for all found conformers.
[https://www.beilstein-journals.org/bjoc/content/supplementary/1860-5397-15-63-S1.pdf]

Acknowledgements

This work was supported by the Russian Scientific Foundation 19-73-30017 (NEN).

ORCID® iDs

Nikolay E. Nifantiev - https://orcid.org/0000-0002-0727-4050

References

1. Marzabadi, C. H.; Anderson, J. E.; Gonzalez-Outeirino, J.; Gaffney, P. R. J.; White, C. G. H.; Tocher, D. A.; Todaro, L. J. *J. Am. Chem. Soc.* **2003,** *125,* 15163–15173. doi:10.1021/ja035936x
2. Yamada, H.; Tanigakiuchi, K.; Nagao, K.; Okajima, K.; Mukae, T. *Tetrahedron Lett.* **2004,** *45,* 9207–9209. doi:10.1016/j.tetlet.2004.10.078
3. Komarova, B. S.; Gerbst, A. G.; Finogenova, A. M.; Dmitrenok, A. S.; Tsvetkov, Y. E.; Nifantiev, N. E. *J. Org. Chem.* **2017,** *82,* 8897–8908. doi:10.1021/acs.joc.7b01167
4. Pedersen, C. M.; Nordstrøm, L. U.; Bols, M. *J. Am. Chem. Soc.* **2007,** *129,* 9222–9235. doi:10.1021/ja071955l
5. Abronina, P. I.; Malysheva, N. N.; Litvinenko, V. V.; Zinin, A. I.; Kolotyrkina, N. G.; Kononov, L. O. *Org. Lett.* **2018,** *20,* 6051–6054. doi:10.1021/acs.orglett.8b02424
6. Gerbst, A. G.; Krylov, V. B.; Argunov, D. A.; Solovev, A. S.; Dmitrenok, A. S.; Shashkov, A. S.; Nifantiev, N. E. *Carbohydr. Res.* **2016,** *436,* 20–24. doi:10.1016/j.carres.2016.10.011
7. Gerbst, A. G.; Vinnitsky, D. Z.; Dmitrenok, A. S.; Ustyuzhanina, N. E.; Nifantiev, N. E. *Carbohydr. Res.* **2018,** *455,* 81–85. doi:10.1016/j.carres.2017.11.009
8. Wessel, H. P.; Bartsch, S. *Carbohydr. Res.* **1995,** *274,* 1–9. doi:10.1016/0008-6215(95)00131-c
9. Probst, K. C.; Wessel, H. P. *J. Carbohydr. Chem.* **2001,** *20,* 549–560. doi:10.1081/car-100108273
10. Taha, H. A.; Richards, M. R.; Lowary, T. L. *Chem. Rev.* **2013,** *113,* 1851–1876. doi:10.1021/cr300249c
11. Richards, M. R.; Bai, Y.; Lowary, T. L. *Carbohydr. Res.* **2013,** *374,* 103–114. doi:10.1016/j.carres.2013.03.030
12. van Rijssel, E. R.; van Delft, P.; Lodder, G.; Overkleeft, H. S.; van der Marel, G. A.; Filippov, D. V.; Codée, J. D. C. *Angew. Chem., Int. Ed.* **2014,** *53,* 10381–10385. doi:10.1002/anie.201405477
13. Altona, C.; Geise, H. J.; Romers, C. *Tetrahedron* **1968,** *24,* 13–32. doi:10.1016/0040-4020(68)89003-9
14. Krylov, V. B.; Argunov, D. A.; Vinnitskiy, D. Z.; Verkhnyatskaya, S. A.; Gerbst, A. G.; Ustyuzhanina, N. E.; Dmitrenok, A. S.; Huebner, J.; Holst, O.; Siebert, H.-C.; Nifantiev, N. E. *Chem. – Eur. J.* **2014,** *20,* 16516–16522. doi:10.1002/chem.201405083
15. Krylov, V. B.; Argunov, D. A.; Vinnitskiy, D. Z.; Gerbst, A. G.; Ustyuzhanina, N. E.; Dmitrenok, A. S.; Nifantiev, N. E. *Synlett* **2016,** *27,* 1659–1664. doi:10.1055/s-0035-1561595
16. Gerbst, A. G.; Krylov, V. B.; Argunov, D. A.; Dmitrenok, A. S.; Nifantiev, N. E. *ACS Omega* **2019,** *4,* 1139–1143. doi:10.1021/acsomega.8b03274
17. Argunov, D. A.; Krylov, V. B.; Nifantiev, N. E. *Org. Biomol. Chem.* **2015,** *13,* 3255–3267. doi:10.1039/c4ob02634a
18. Argunov, D. A.; Krylov, V. B.; Nifantiev, N. E. *Org. Lett.* **2016,** *18,* 5504–5507. doi:10.1021/acs.orglett.6b02735
19. Krylov, V. B.; Argunov, D. A.; Solovev, A. S.; Petruk, M. I.; Gerbst, A. G.; Dmitrenok, A. S.; Shashkov, A. S.; Latgé, J.-P.; Nifantiev, N. E. *Org. Biomol. Chem.* **2018,** *16,* 1188–1199. doi:10.1039/c7ob02734f
20. Krylov, V. B.; Gerbst, A. G.; Argunov, D. A.; Dmitrenok, A. S.; Shashkov, A. S.; Kaczynski, Z.; Huebner, J.; Holst, O.; Nifantiev, N. E. *Chem. – Eur. J.* **2015,** *21,* 1749–1754. doi:10.1002/chem.201405857
21. Verkhnyatskaya, S. A.; Krylov, V. B.; Nifantiev, N. E. *Eur. J. Org. Chem.* **2017,** 710–718. doi:10.1002/ejoc.201601413
22. Vinnitskiy, D. Z.; Krylov, V. B.; Ustyuzhanina, N. E.; Dmitrenok, A. S.; Nifantiev, N. E. *Org. Biomol. Chem.* **2016,** *14,* 598–611. doi:10.1039/c5ob02040a
23. Bishop, C. T.; Cooper, F. P. *Can. J. Chem.* **1962,** *40,* 224–232. doi:10.1139/v62-038
24. Krylov, V. B.; Ustyuzhanina, N. E.; Grachev, A. A.; Nifantiev, N. E. *Tetrahedron Lett.* **2008,** *49,* 5877–5879. doi:10.1016/j.tetlet.2008.07.135
25. Krylov, V. B.; Kaskova, Z. M.; Vinnitskiy, D. Z.; Ustyuzhanina, N. E.; Grachev, A. A.; Chizhov, A. O.; Nifantiev, N. E. *Carbohydr. Res.* **2011,** *346,* 540–550. doi:10.1016/j.carres.2011.01.005
26. Ferrières, V.; Bertho, J.-N.; Plusquellec, D. *Carbohydr. Res.* **1998,** *311,* 25–35. doi:10.1016/s0008-6215(98)00197-9
27. Angyal, S. J. *Carbohydr. Res.* **1979,** *77,* 37–50. doi:10.1016/s0008-6215(00)83791-x
28. Hendrickx, P. M. S.; Martins, J. C. *Chem. Cent. J.* **2008,** *2,* No. 20. doi:10.1186/1752-153x-2-20
29. Neese, F. *Wiley Interdiscip. Rev.: Comput. Mol. Sci.* **2012,** *2,* 73–78. doi:10.1002/wcms.81
30. *Libint: A library for the evaluation of molecular integrals of many-body operators over Gaussian functions,* 2.3.1; , http://libint.valeyev.net.
31. Krishnan, R.; Binkley, J. S.; Seeger, R.; Pople, J. A. *J. Chem. Phys.* **1980,** *72,* 650–654. doi:10.1063/1.438955
32. Klamt, A.; Schüürmann, G. *J. Chem. Soc., Perkin Trans. 2* **1993,** 799–805. doi:10.1039/p29930000799
33. Jensen, F. *Theor. Chem. Acc.* **2010,** *126,* 371–382. doi:10.1007/s00214-009-0699-5
34. Aidas, K.; Angeli, C.; Bak, K. L.; Bakken, V.; Bast, R.; Boman, L.; Christiansen, O.; Cimiraglia, R.; Coriani, S.; Dahle, P.; Dalskov, E. K.; Ekström, U.; Enevoldsen, T.; Eriksen, J. J.; Ettenhuber, P.; Fernández, B.; Ferrighi, L.; Fliegl, H.; Frediani, L.; Hald, K.; Halkier, A.; Hättig, C.; Heiberg, H.; Helgaker, T.; Hennum, A. C.; Hettema, H.; Hjertenæs, E.; Høst, S.; Høyvik, I.-M.; Iozzi, M. F.; Jansík, B.; Jensen, H. J. A.; Jonsson, D.; Jørgensen, P.; Kauczor, J.; Kirpekar, S.; Kjærgaard, T.; Klopper, W.; Knecht, S.; Kobayashi, R.; Koch, H.; Kongsted, J.; Krapp, A.; Kristensen, K.; Ligabue, A.; Lutnæs, O. B.; Melo, J. I.; Mikkelsen, K. V.; Myhre, R. H.; Neiss, C.; Nielsen, C. B.; Norman, P.; Olsen, J.; Olsen, J. M. H.; Osted, A.; Packer, M. J.; Pawlowski, F.; Pedersen, T. B.; Provasi, P. F.; Reine, S.; Rinkevicius, Z.; Ruden, T. A.; Ruud, K.; Rybkin, V. V.; Sałek, P.; Samson, C. C. M.; Sánchez de Merás, A.; Saue, T.; Sauer, S. P. A.; Schimmelpfennig, B.; Sneskov, K.; Steindal, A. H.; Sylvester-Hvid, K. O.; Taylor, P. R.; Teale, A. M.; Tellgren, E. I.; Tew, D. P.; Thorvaldsen, A. J.; Thøgersen, L.; Vahtras, O.; Watson, M. A.; Wilson, D. J. D.; Ziolkowski, M.; Ågren, H. *Wiley Interdiscip. Rev.: Comput. Mol. Sci.* **2014,** *4,* 269–284. doi:10.1002/wcms.1172

frontiers in Molecular Biosciences

ORIGINAL RESEARCH
published: 25 August 2021
doi: 10.3389/fmolb.2021.719396

Computational and NMR Conformational Analysis of Galactofuranoside Cycles Presented in Bacterial and Fungal Polysaccharide Antigens

Alexey G. Gerbst, Vadim B. Krylov and Nikolay E. Nifantiev**

Laboratory of Glycoconjugate Chemistry, N.D. Zelinsky Institute of Organic Chemistry RAS, Moscow, Russia

Unlike pyranoside cycles which are generally characterized by strictly defined conformational preferences, furanosides are flexible and may adopt a wide range of available conformations. During our previous studies, conformational changes of galactofuranoside cycles upon total sulfation were described computationally, using a simple Hartree–Fock (HF) method, and principal conformers of the 5-membered galactose ring were revealed. However, in the case of more complex disaccharide structures, it was found that this method and the widely applied DFT-B3LYP produced results that deviated from experimental evidence. In this study, other DFT functionals (PBE0 and double hybrid B2PLYP) along with RI-MP2 are employed to study the conformational behavior of the galactofuranoside ring. Reinvestigation of galactofuranosides with a lactic acid substituent at O-3 revealed that changes in the orientation of lactic acid residue at O-3 might induce conformational changes of the furanoside cycle. Such findings are important for further modeling of carbohydrate–protein interaction.

Keywords: substituted galactofuranosides, conformations, DFT, MP2, shielding constants

OPEN ACCESS

Edited by:
Hans-Christian Siebert, RI-B-NT, Germany

Reviewed by:
Anirban Bhunia, Bose Institute, India
Joon-Hwa Lee, Gyeongsang National University, South Korea
Thomas Eckert, Justus Liebig Universität, Germany

****Correspondence:***
Alexey G. Gerbst
alger@ioc.ac.ru
Nikolay E. Nifantiev
nen@ioc.ac.ru

Specialty section:
This article was submitted to Structural Biology, a section of the journal Frontiers in Molecular Biosciences

Received: *02 June 2021*
Accepted: *27 July 2021*
Published: *25 August 2021*

Citation:
Gerbst AG, Krylov VB and Nifantiev NE (2021) Computational and NMR Conformational Analysis of Galactofuranoside Cycles Presented in Bacterial and Fungal Polysaccharide Antigens. Front. Mol. Biosci. 8:719396. doi: 10.3389/fmolb.2021.719396

INTRODUCTION

The understanding of the 3D structure of biologically important oligosaccharide sequences and of their conformational mobility is required for the assessment of their immunodeterminant fragments and prediction of the topology of oligosaccharide binding to cellular receptors and lectins (Zhang et al., 2017). In this context, galactofuranoside containing oligosaccharide determinants which are often presented in the antigenic polysaccharide chains of pathogenic bacteria and fungi represents a special interest because of its biological importance (Richards and Lowary, 2009; Krylov and Nifantiev, 2020). In particular, galactofuranoside units were discovered as structural components of polysaccharides of *Klebsiella* (Rollenske et al., 2018; Argunov et al., 2019; Whitfield et al., 2020), *Enterococcus* (Krylov et al., 2015; Laverde et al., 2020), *Mycobacteria* (Bhamidi et al., 2011; Lowary, 2016), *Aspergillus* (Costachel et al., 2005; Kudoh et al., 2015; Krylov et al., 2018), *Cryptococcus* (Previato et al., 2017), and other pathogens.

Furanoside rings are generally considered to be more flexible than pyranosides. In our previous studies of the conformational changes in furanoside rings upon their complete sulfation, we revealed the main conformers of the non-sulfated galactofuranoside. These

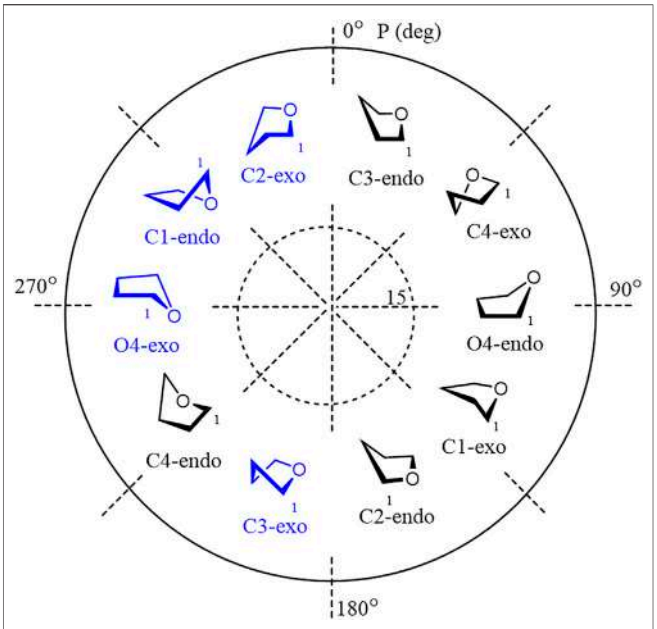

FIGURE 1 | Main investigated conformers of the galactofuranoside ring (in blue).

results were supported by evidence from NMR spectroscopy, such as intra-ring H–H coupling constants and NOE (Gerbst et al., 2019a). The main determined conformers for the non-sulfated rings were C3-*exo* or the ones similar to them according to Cremer–Pople parameters (**Figure 1**). The minor conformer in the case of the non-sulfated furanosides was O4-*exo* (**Figure 1**) which, however, became dominant upon the introduction of sulfates. The computational method employed in the referenced study was the HF/6-311++G** level of theory. Also, we employed the same method to study the driving force of the pyranoside-into-furanoside rearrangement (Gerbst et al., 2019b).

However, in a further study (Dorokhova et al., 2021), we found that this approximation may not always produce correct results when computing the relative energies of the furanoside ring conformation. In the mentioned work, the conformations of furanoside rings in di- and trisaccharides were studied, and the results on their dependence upon the conformation of the glycosidic linkage were summarized. Herein, we attempted a detailed analysis of the application of various approximations to the energy analysis of furanoside conformers. The objects of the study are shown in **Figure 2**. Disaccharides 1 and 2 (that relate to the fragments of *Cryptococcus neoformans* galactoxylomannan) are model structures lacking an amino group in the propyl aglycon; synthesis of the full structures is described in the study by (Dorokhova et al., 2021), monosaccharide 3 is from the study by (Gerbst et al., 2019a), and synthesis of 3-O-(R)-lactic acid derivative 4 (that relates to the fragment of *Enterococcus faecalis* diheteroglycan) and its (S)-isomer 5 is described in the study by (Krylov et al., 2015).

MATERIALS AND METHODS

ORCA (Neese, 2012) (version 4.2) software was used throughout the study. DFT calculations employed either the 6-31G (d,p) (Hehre et al., 1972), 6-311++G**, or def2-TZVP (Weigend and Ahlrichs, 2005) basis sets with the B3LYP or PBE0 functional (see details in the text). Grimme dispersion correction was employed

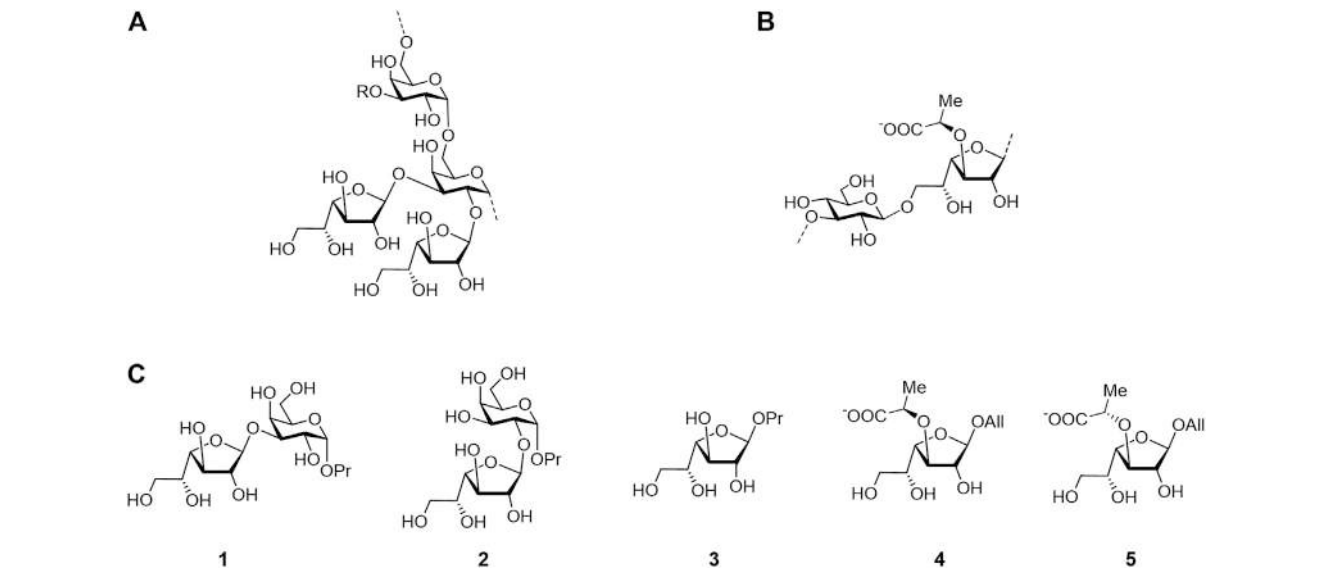

FIGURE 2 | Structure of the *Cryptococcus neoformans* galactoxylomannan backbone **(A)**, *Enterococcus faecalis* diheteroglycan **(B)**, and related mono- and disaccharides studied in this work **(C)**.

TABLE 1 | Conversion of different conformers during geometry optimizations of disaccharide **1**.

Method	Starting conformer	Resulting conformer
HF/6-311++G**	O4-*exo*	O4-*exo*
B3LYP/6-311++G**	O4-*exo*	C3-*exo*
B3LYP/6-31G (d,p)	O4-*exo*	C3-*exo*
HF/6-31G (d,p)	O4-*exo*	C1-*endo*
RI-MP2/def2-TZVP	O4-*exo*	O4-*exo*
B2PLYP/def2-TZVP	O4-*exo*	O4-*exo*
HF/6-311++G**	C3-*exo*	C3-*exo*
B3LYP/6-311++G**	C3-*exo*	C3-*exo*
RI-MP2/def2-TZVP	C3-*exo*	C3-*exo*
B2PLYP/def2-TZVP	C3-*exo*	C3-*exo*

where noted in the text. All RI-B2PLYP and RI-MP2 calculations were carried out using the def2-TZVP basis set. NMR shielding constants were computed using DFT/B3LYP/def2-TZVPP (Weigend and Ahlrichs, 2005) approximation with the GIAO option and the automatic auxiliary JK basis set (Stoychev et al., 2017). The conductor-like polarizable continuum model (CPCM) of solvation (Barone and Cossi, 1998) with parameters for water was used to account for bulk solvent effects. No counter-ions were considered in the calculations.

RESULTS

The problem that inspired this investigation first occurred in the study by (Dorokhova et al., 2021) when we started the conformational analysis of model disaccharides 1 and 2. When the use of the previously approbated method, HF/6-311++G**, was attempted, it was found that the C3-*exo* conformer was predicted to be more preferable than O4-*exo* by the order of 2 kcal/mole. This contradicted the experimentally observed intra-ring $^{1}H–^{1}H$ couplings. Additionally, when the computational methods varied, sometimes during torsional scans on the glycosidic linkages in these disaccharides, we encountered a situation that could be determined to be "a conformational hell": the desired O4-*exo* conformer often irreversibly transformed into C3-*exo* and never *vice versa* (**Table 1**).

Finally, it was found that the RI-MP2/def2-TZVP approach provided satisfactory results. This method was chosen as being of the higher level of theory since it takes into account the electronic correlation. The main conformers found for these disaccharides finally turned out to be O4-*exo* and C2-*exo* (**Figure 3**). This suggested re-investigation of the furanoside ring conformations in the simple propyl-galactofuranoside 3. A variety of methods (including hybrid B3LYP and PBE0 and double hybrid B2PLYP DFT functionals along with the RI-MP2 approach) was applied to conduct geometry optimization of its C3-*exo* and O4-*exo* conformers. The results are presented in **Table 2**.

Additionally, we compared the lengths of endocyclic C–C and C–O bonds for the C3-*exo* conformer of this compound computed using different methods with those obtained using the X-ray method for a galactofuranoside containing disaccharide (PDB entry 4XAD). The results are presented in **Table 3**. It can be seen that all the carbon–carbon bonds are by several hundredths of an angstrom (but not more than 0.05 Å). Meanwhile, all the C–O bonds are slightly underestimated. We attribute this discrepancy to the fact that the experimental values were obtained in the crystal, while the calculations were carried out in bulk water using the CPCM model.

The electronic energies obtained for both conformers are the same for B3LYP and both PBE0 approaches. This occurs because both these methods indeed transform the O4-*exo* conformer into the C3-*exo*, like it was the case for structures 1 and 2. When the dispersion correction (D3) is applied, the starting conformation does not change during the geometry optimization, and the C3-*exo* conformer is predicted to be 0.4 kcal/mole more preferable.

For the double-hybrid B2PLYP DFT and pure MP2, however, the final energy values differ, which reflects the fact that the initial ring conformation is retained. These differences in the table values correspond to 0.9 kcal/mole for B2PLYP and 0.2 kcal/mole for MP2, while the C3-*exo* conformer is still more preferable. The resulting conformers obtained at the MP2 level are shown in **Figure 4**.

Next, we performed a re-investigation of monosaccharides 4 and 5, which are allyl galactofuranosides substituted at O-3 with a lactic acid residue having an R- or S-configuration. Such units are present in a capsule polysaccharide (diheteroglycan) of

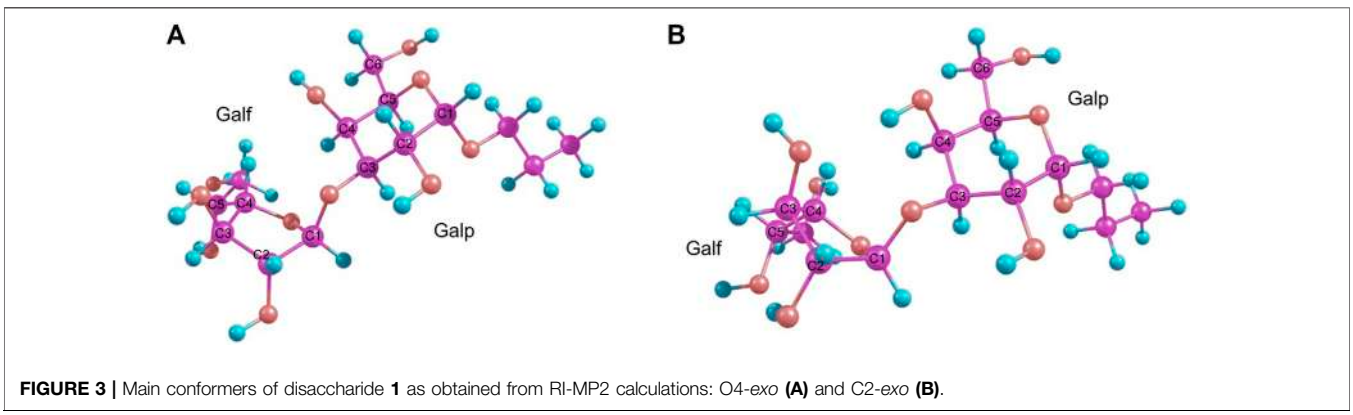

FIGURE 3 | Main conformers of disaccharide **1** as obtained from RI-MP2 calculations: O4-*exo* **(A)** and C2-*exo* **(B)**.

TABLE 2 | Electronic energies (a.u.) obtained for conformers of monosaccharide **3** using different methods.

Method	Electronic energies of conformers (a.u.)		ΔE (kcal/mole)
	C3-*exo*	O4-*exo*	
B3LYP/6-31G (d,p)	–804.6851292	-[a]	n.a
PBE0/6-31G (d,p)	–804.2509974	-[a]	n.a
PBE0/def2-TZVP	–804.5633591	-[a]	n.a
B3LYP/6-31G (d,p)/D3	–804.7357417	–804.7351638	0.4
B2PLYP/def2-TZVP	–804.8280619	–804.8266101	0.9
RI-MP2/def2-TZVP	–803.6819645	–803.6816517	0.2

[a]*Conversion into the C3-exo conformer during optimization occurred.*

TABLE 3 | Comparison of experimental (PDB entry 4XAD) and computed bond lengths for the C3-*exo* conformation of monosaccharide **3** (Å).

Method	C1-C2	C2-C3	C3-C4	C4-O4	O4-C1
Experimental	1.50642	1.49672	1.51769	1.44631	1.44390
B3LYP/6-31G (d,p)	1.53746	1.52996	1.53765	1.43834	1.42992
PBE0/6-31G (d,p)	1.53055	1.52182	1.52912	1.42569	1.41786
PBE0/def2-TZVP	1.52493	1.51683	1.52533	1.42365	1.41698
B3LYP/6-31G (d,p)/D3	1.53790	1.52939	1.53460	1.43574	1.42562
B2PLYP/def2-TZVP	1.52828	1.52182	1.52907	1.43494	1.42670
RI-MP2/def2-TZVP	1.52645	1.51571	1.52326	1.43259	1.42558

Enterococcus faecalis. The same scope of methods was applied for these molecules (**Table 4** and **Table 5**). The resulting energies for each isomer are presented in **Table 4** and **Table 5**. One of the most important features of these two structures is the orientation of the lactic acid substituent whose tertiary proton (H-Lact) can be spatially closer either to the H-2, H-4, or H-3 proton of the furanoside ring. The difference in its orientation helps to establish absolute configuration of the lactic acid (Krylov et al., 2015).

It can be seen that the C2-*exo* conformer with the spatial proximity of the lactic acid proton to H-4 has the lowest energy for structure 4 (R-lactic acid derivative), while for structure 5, it is O4-*exo* with the lactic acid proton oriented toward H-2. Generally, its orientation toward H-2 is more pronounced in the latter molecule, while in structure 4, both orientations seem possible. Graphical representations of the lowest energy conformers with the inter-proton distances are given in **Figure 5**.

As for the conformers with the spatial proximity of H-Lact to the H-3 ring, proton conformational changes were detected that depended upon the computational method and the structure involved. In the case of molecule 4, all DFT methods (except double-hybrid B2PLYP) transformed the starting conformations, C1-*endo*, C2-*exo*, and O4-*exo*, to C3-*exo*. The other two methods rendered the O4-*exo* conformation as the result, except for the starting C3-*exo*, which was retained. In both cases, H-Lact and H-3 remained close to each other with the distances of ca. 2.20–2.24 Å. For S-isomer 5, C1-*endo* changed to O4-*exo*, keeping H-Lact and H-3-close, while O4-*exo* itself did not change. C2-*exo* did not change either, but the lactic acid residue slightly rotated toward H-2, distances from H-Lact

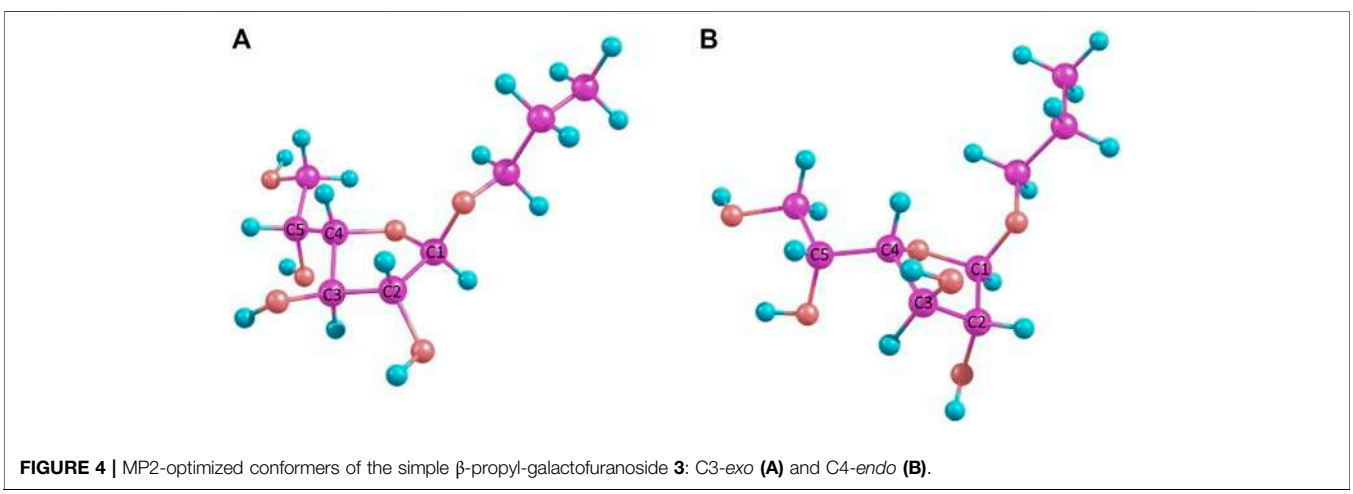

FIGURE 4 | MP2-optimized conformers of the simple β-propyl-galactofuranoside **3**: C3-*exo* **(A)** and C4-*endo* **(B)**.

TABLE 4 | Relative energies (kcal/mole, against the lowest energy conformer marked in bold) for principal conformers of the D-lactic acid derivative **4**) of the furanoside ring calculated at different levels of theory.

Conformer	Levels of theory					
	B3LYP/6-31G (d,p)	PBE0/6-31G (d,p)	PBE0/def2-TZVP	B3LYP/6-31G (d,p)/D3	B2PLYP/def2-TZVP	RI-MP2/def2-TZVP
				**H-4—H-Lact** proximity		
C3-*exo*	4.5	4.6	2.2	5.2	2.8	3.5
C2-*exo*	**0.0**	**0.0**	**0.0**	**0.0**	**0.0**	**0.0**
O4-*exo*	3.1	2.7	1.8	2.9	2.0	1.8
C1-*endo*	3.2	2.8	1.8	2.6	2.2	1.9
			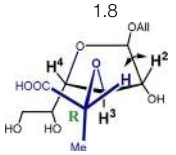	**H-2—H-Lact** proximity		
C3-*exo*	3.8	4.0	1.3	5.2	2.2	3.0
C2-*exo*	3.1	3.3	1.9	2.7	2.2	3.1
O4-*exo*	4.6	4.5	2.0	5.1	2.5	3.0
C1-*endo*	4.6	4.4	2.1	5.1	2.5	3.1
			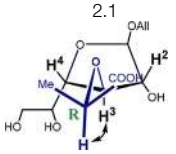	**H-3—H-Lact** proximity		
C3-*exo*	−4.8	−5.0	1.1	−4.7	0.9	0.3
O4-*exo*	-[a]	-[a]	-[a]	-[a]	1.5	1.4

[a]*Conversion into the C3-exo conformer during optimization.*

to H-3 and H-2 being 2.36 Å and 3.26 Å, respectively. The C3-*exo* conformation did not change but had the largest energy. Meanwhile, for the listed conformers, the energies were sometimes below the lowest ones mentioned in **Table 4** and **Table 5**.

After that, ^{1}H NMR shielding constants were calculated for the obtained conformers except for the C3-*exo*/H-3 conformer of molecule 5, since it had significantly higher energy. The DFT B3LYP approach with a triple zeta basis with two polarization functions (def2-TZVPP) was applied because smaller basis sets can produce unreliable results for this task. As input structures for these calculations, RI-MP2–optimized conformations were used. These were chosen because the RI-MP2 approach is supposed to provide more accurate results. It was found that shielding constants for the anomeric proton, as a rule, did not change significantly. Knowing its experimentally measured chemical shift of 5.06 ppm (Krylov et al., 2015), a value of 31.65 was chosen as a shielding constant corresponding to a chemical shift of 0 ppm. The resulting chemical shifts along with the experimental ones for both compounds are given in **Table 6** and **Table 7**, and the discussion on them can be found in the next section.

DISCUSSION

While conformations of pyranoside rings have been extensively studied and their conformational preferences are well known in general cases, furanosides represent a more complex subject due to their ring flexibility. A number of investigations are present that employ different quantum mechanical methods with various basis sets, but they are all focused primarily on the conformations of pentafuranosides [for a review, see (Taha et al., 2013)]. More often, conformations of furanoside rings were studied using methods of molecular mechanics. In the work by (Richards et al., 2013), the conformation of methyl galactofuranosides was studied, but the study was limited to the B3LYP functional with 6-31G* or 6-31+G**, and the investigated structures did not contain ring substituents. A recent work (Gaweda et al., 2020) was dedicated to the computational study of the exo- and endo-anomeric effect in furanoside rings. However, these authors employed a rather small basis set [6-31G(d)] but an advanced functional, M062X. This choice was justified because they use only simple model molecules for their study. Our results reported above demonstrate that when dealing with more complicated structures, much more strongly resembling those occurring in real biologically important molecules, conventionally used HF and DFT methods may not always work. For example, even in a simple propyl galactofuranoside 3, DFT methods without dispersion correction failed to reproduce the O4-*exo* conformation as a stationary point, converting it to C3-*exo*. Expectedly, usage of methods with more precise accounting for electronic correlation (the double-hybrid B2PLYP

TABLE 5 | Relative energies (kcal/mole, against the lowest energy conformer marked in bold) for principal conformers of the L-lactic acid derivative **5**) of the furanoside ring calculated at different levels of theory.

Conformer	Levels of theory					
	B3LYP/6-31G (d,p)	PBE0/6-31G (d,p)	PBE0/def2-TZVP	B3LYP/6-31G (d,p)/D3	B2PLYP/def2-TZVP	RI-MP2/def2-TZVP
			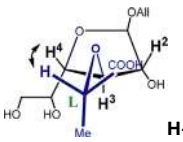			
			H-4—H-Lact proximity			
C3-*exo*	7.4	9.3	4.1	10.1	4.2	5.3
C2-*exo*	7.0	6.9	4.6	6.3	4.7	5.1
O4-*exo*	8.8	9.4	6.3	9.2	6.1	7.0
O4-*exo*	8.8	9.4	6.3	9.2	6.1	7.0
			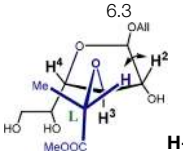			
			H-2—H-Lact proximity			
C3-*exo*	4.6	4.8	2.6	5.2	2.3	2.5
C2-*exo*	3.8	3.4	1.6	3.7	2.2	1.6
O4-*exo*	**0.0**	**0.0**	**0.0**	**0.0**	**0.0**	**0.0**
C1-*endo*	3.0	3.2	1.2	3.5	0.9	0.4
			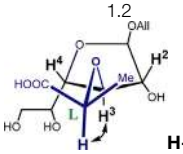			
			H-3—H-Lact proximity			
O4-*exo*	5.8	5.0	3.9	7.2	2.3	2.0
C2-*exo*[a]	6.4	5.3	2.9	–0.6	3.1	2.5
C3-*exo*	9.5	10.2	10.0	7.3	6.7	5.9

[a]*The lactic acid residue slightly rotated toward H-2.*

functional and RI-MP2) gives results similar to those obtained with D3 correction, although the energy values differ slightly (**Table 2**). Meanwhile, as was previously shown in the study by (Krylov et al., 2015), the presence of the O4-*exo* conformer is necessary to explain the observed intra-ring ^{1}H–^{1}H couplings. A similar effect was observed for structures 1 and 2, where more-or-less sensible conformational analysis was not possible without the use of MP2-based approaches. Of course, B3LYP/6-31G (d,p)/D3 outperforms MP2 methods in terms of time on the same computing resources. Probably, further

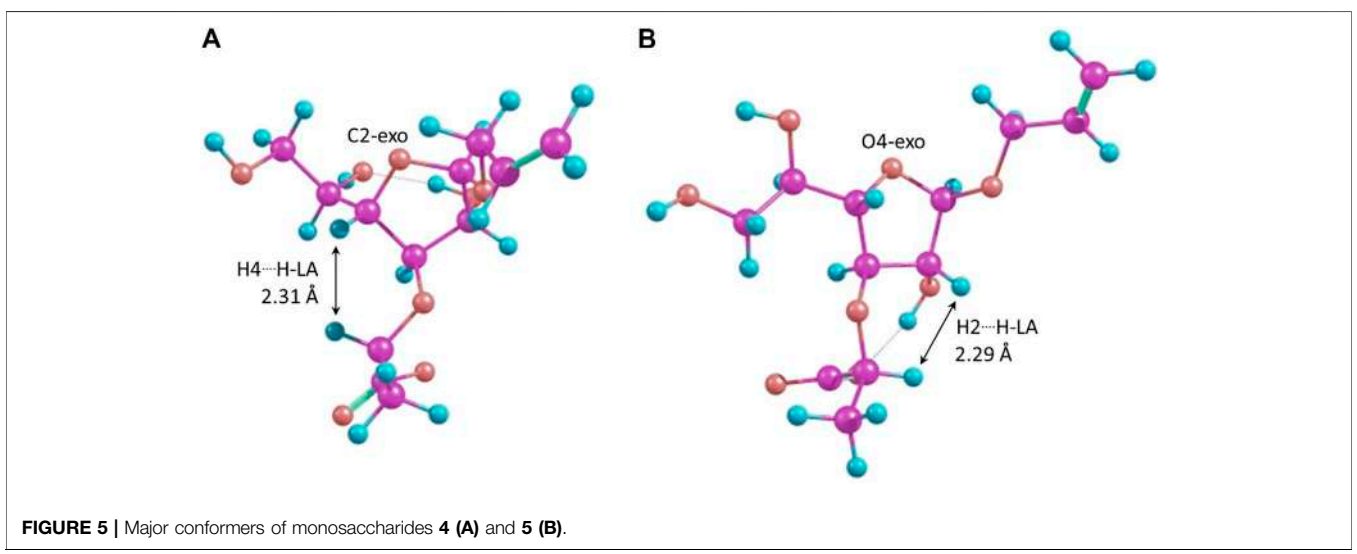

FIGURE 5 | Major conformers of monosaccharides **4 (A)** and **5 (B)**.

TABLE 6 | ^{1}H chemical shifts (ppm) obtained from the computed shielding constants for conformer structure **4** and the experimental ones marked in bold (Krylov et al., 2015).

Conformer/ring proton spatially close to the lactic acid proton	H-1	H-2	H-3	H-4	H-5	H-6	H-6′
C3-*exo*/H-2	5.02	4.16	4.33	3.94	4.11	3.96	3.99
C3-*exo*/H-4	5.38	4.50	3.80	4.16	4.19	4.69	3.87
C2-*exo*/H-2	5.06	3.97	4.14	4.48	4.12	3.94	3.95
C2-*exo*/H-4	5.05	3.92	4.16	4.71	4.00	3.95	3.94
C1-*endo*/H-2	5.16	4.19	3.66	3.80	3.93	4.05	3.63
C1-*endo*/H-4	5.15	4.32	3.82	3.96	3.66	4.08	3.61
O4-*exo*/H-2	5.15	4.20	3.67	3.81	3.93	4.02	3.59
O4-*exo*/H-4	5.17	4.33	3.91	3.99	3.62	4.05	3.56
C3-*exo*/H-3	5.09	4.34	3.44	3.88	3.96	3.96	3.76
O4-*exo*/H-3	5.00	5.14	3.36	3.76	3.85	3.92	3.69
Experimental	**5.06**	**4.25**	**3.9**	**4.07**	**3.86**	**3.72**	**3.67**

TABLE 7 | ^{1}H chemical shifts (ppm) obtained from the computed shielding constants for conformer structure **5** and the experimental ones marked in bold (Krylov et al., 2015).

Conformer/ring proton spatially close to the lactic acid proton	H-1	H-2	H-3	H-4	H-5	H-6	H-6′
C3-*exo*/H-2	5.00	4.36	3.81	3.79	3.91	5.57	3.49
C3-*exo*/H-4	4.93	4.13	4.13	3.87	3.99	3.95	4.01
C2-*exo*/H-2	5.06	4.09	4.18	4.49	4.17	3.90	3.93
C2-*exo*/H-4	5.06	3.93	4.28	4.63	4.20	3.95	3.99
C1-*endo*/H-2	5.04	4.37	3.79	3.70	3.87	5.04	3.52
C1-*endo*/H-4	5.16	4.27	3.73	3.89	3.81	3.82	3.75
O4-*exo*/H-2	5.09	4.28	3.62	3.86	3.88	4.16	3.48
O4-*exo*/H-4	5.17	4.24	3.74	3.92	3.83	4.16	3.76
O4-*exo*/H-3	5.07	3.92	3.88	4.94	4.76	4.02	4.02
O4-*exo*[a]/H-3	5.12	4.30	3.79	3.88	4.02	5.83	3.49
Experimental	**5.06**	**4.25**	**3.91**	**4.08**	**3.85**	**3.73**	**3.66**

[a]*The lactic acid residue slightly rotated toward H-2.*

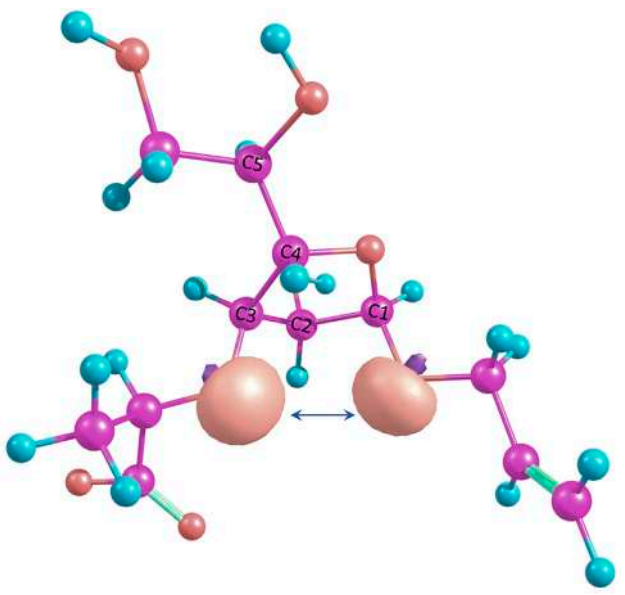

FIGURE 6 | Suggested 1-3-*syn*-diaxial repulsion between O-3 and O-1 in the O4-*exo* conformation illustrated by NBO lone pairs.

investigations are needed to establish whether the use of the former approximation is always sufficient to model furanoside ring conformations.

Changes in furanoside ring puckering occurring during modeling of conformers with the spatial proximity of H-Lact and H-3 ring protons in structures 4 and 5 can be explained by the so-called 1-3-*syn*-diaxial repulsion. In these conformers, when O-3 and O-1 substituents are initially pseudo-axially oriented, lone pairs on the oxygen atoms become oriented in a way causing them to move away from each other. This is illustrated in **Figure 6**, showing these lone-pair orbitals as calculated using NBO6 software (Glendening et al., 2013). This results either in a ring conformation change or in rotation of the O-3 substituent. O-1 is less prone to rotation due to the anomeric effect. This is confirmed by the fact that the C3-*exo* conformation is always retained.

This effect is also encountered in pyranosides. For example, in the work by (Komarova et al., 2017), we observed that this effect can cause conformational interchanges in idopyranosides. Presumably, in furanosides, it may influence to a larger extent since these molecules are not as conformationally rigid as pyranosides.

For structures 4 and 5, the calculations demonstrate that the furanoside ring conformation does not affect the preferable orientation of the 3-O-lactic acid substituent. For the R-isomer contacts between H-Lact and H2 and H4, protons are observed for each of the considered conformers. For the S-isomer, a strong preference for H-Lact/H2 contact is demonstrated. Energy values allow the suggestion that R-isomer 4 might exist preferably with H-Lact in proximity to H-3 with the possibility to rotate either

toward H-2 or toward H-4, which is accompanied by the ring conformation change. For S-isomer 5, conformations in which H-Lact is in proximity to H-4 are not likely to give a significant contribution. This explains the previously observed NOE (Krylov et al., 2015) and confirms that the absolute configuration of the lactic acid substituent was determined correctly.

NMR techniques are a powerful tool for conformation analysis of carbohydrates (Lipkind et al., 1992; Grachev et al., 2009). In the described case, we performed analysis of the computed chemical shifts. The computed values presented in **Table 6** and **Table 7** do not allow us to determine definite trends in them upon the conformational changes. The anomeric H-1 chemical shift is probably the most conserved one. The wide range of computed chemical shifts for H-6 protons is most likely due to their dependence upon the side chain conformation. Some values for H-2, H-3, and H-4 computed chemical shifts (e.g., C3-*exo*, C1-*endo*, and O4-*exo* in **Table 7**; C3-*exo* and C2-*exo* in **Table 7**) have shown that these shifts rather depend upon the lactic acid residue orientation. This situation cannot be called unexpected, as the same can be found in pyranosides, too, but the absence of any pronounced changes upon the change in ring puckering makes these structures different from six-membered sugar rings, in which even a slight distortion can cause considerable shift changes (Gerbst et al., 2018).

CONCLUSION

Several DFT and MP2-based methods were compared in modeling of furanoside ring conformations, including ones with a lactic acid substituent. It was found that at least dispersion correction should be applied to achieve sensible results. MP2 methods also perform well, although they are certainly more time-demanding. It is demonstrated that changes in the orientation of the lactic acid residue at O-3 induce conformational changes of the furanoside cycle. Meanwhile, the unsubstituted propyl galactofuranoside exhibits just two primary conformers. These ring conformational changes occur upon the substituent rotation, most likely through the 1-3-*syn*-diaxial repulsion. This should be kept in mind since in pyranosides, this repulsion can also occur but is not considered to affect the conformation in general cases. This might also mean that the range of adoptable conformations for the furanoside rings may depend upon the substation pattern. It is shown that while in pyranosides, ^{1}H NMR chemical shifts considerably depend on the conformational distortion, this is not the case for furanosides, where these shifts rather depend on a ring substituent orientation.

Considering the ongoing progress of computational methods, particularly in the structural analysis of carbohydrates (Gerbst et al., 2021), these results may present interest for further investigation of the biologically important furanoside-containing compounds.

DATA AVAILABILITY STATEMENT

The original contributions presented in the study are included in the article/Supplementary Material; further inquiries can be directed to the corresponding authors.

AUTHOR CONTRIBUTIONS

AG, VK, and NN conceived the project, designed the experiments, and interpreted the data. AG performed calculations. AG, VK, and NN wrote the manuscript. All authors have read and agreed to the published version of the manuscript.

FUNDING

This research was funded by the RSF, grant number 19-73-30017.

REFERENCES

Argunov, D. A., Trostianetskaia, A. S., Krylov, V. B., Kurbatova, E. A., and Nifantiev, N. E. (2019). Convergent Synthesis of Oligosaccharides Structurally Related to Galactan I and Galactan II ofKlebsiella Pneumoniaeand Their Use in Screening of Antibody Specificity. *Eur. J. Org. Chem.* 2019, 4226–4232. doi:10.1002/ejoc.201900389

Barone, V., and Cossi, M. (1998). Quantum Calculation of Molecular Energies and Energy Gradients in Solution by a Conductor Solvent Model. *J. Phys. Chem. A.* 102, 1995–2001. doi:10.1021/jp9716997

Bhamidi, S., Scherman, M. S., Jones, V., Crick, D. C., Belisle, J. T., Brennan, P. J., et al. (2011). Detailed Structural and Quantitative Analysis Reveals the Spatial Organization of the Cell Walls of *In Vivo* Grown Mycobacterium leprae and *In Vitro* Grown Mycobacterium tuberculosis. *J. Biol. Chem.* 286, 23168–23177. doi:10.1074/jbc.m110.210534

Costachel, C., Coddeville, B., Latgé, J.-P., and Fontaine, T. (2005) Glycosylphosphatidylinositol-anchored Fungal Polysaccharide in Aspergillus fumigatus. *J. Biol. Chem.* 280, 39835–39842. doi:10.1074/jbc.M510163200

Dorokhova, V. S., Gerbst, A. G., Komarova, B. S., Previato, J. O., Previato, L. M., Dmitrenok, A. S., et al. (2021). Synthesis and Conformational Analysis of Vicinally Branched Trisaccharide β-d-Galf-(1 → 2)-[β-D-Galf-(1 → 3)-]-α-Galp from Cryptococcus Neoformans Galactoxylomannan. *Org. Biomol. Chem.* 19, 2923–2931. doi:10.1039/D0OB02071K

Gaweda, K., Plazinski, W., and Plazinski, W. (2020). The Endo - and Exo -Anomeric Effects in Furanosides. A Computational Study. *Eur. J. Org. Chem.* 2020, 674–679. doi:10.1002/ejoc.201901473

Gerbst, A. G., Krylov, V. B., Argunov, D. A., Dmitrenok, A. S., and Nifantiev, N. E. (2019b). Driving Force of the Pyranoside-*Into*-Furanoside Rearrangement. *ACS Omega* 4, 1139–1143. doi:10.1021/acsomega.8b03274

Gerbst, A. G., Krylov, V. B., Argunov, D. A., Petruk, M. I., Solovev, A. S., Dmitrenok, A. S., et al. (2019a). Influence of Per-O-Sulfation upon the Conformational Behaviour of Common Furanosides. *Beilstein J. Org. Chem.* 15, 685–694. doi:10.3762/bjoc.15.63

Gerbst, A. G., Krylov, V. B., and Nifantiev, N. E. (2020). Application of Computational Methods for the Studies of Carbohydrate Reactivity. *Carbohydr. Chem.* 44, 151–169. doi:10.1039/9781788013864-00151

Gerbst, A. G., Vinnitsky, D. Z., Dmitrenok, A. S., Ustyuzhanina, N. E., and Nifantiev, N. E. (2018). Conformational Study of Persulfated Propyl Glucuronide. *Carbohydr. Res.* 455, 81–85. doi:10.1016/j.carres.2017.11.009

Glendening, E. D., Badenhoop, J. K., Reed, A. E., Carpenter, J. E., Bohmann, J. A., Morales, C. M., et al. (2013). *Theoretical Chemistry Institute*. Madison, WI: University of Wisconsin. Available at: http://nbo6.chem.wisc.edu.

Grachev, A. A., Gerbst, A. G., Shashkov, A. S., and Nifantiev, N. E. (2009). Application of Modern NMR Techniques for Conformational Analysis of Oligo- and Polysaccharides. *Russ. Chem. Rev.* 78, 717–736. doi:10.1070/RC2009v078n08ABEH004061

Hehre, W. J., Ditchfield, R., and Pople, J. A. (1972). Self-Consistent Molecular Orbital Methods. XII. Further Extensions of Gaussian-type Basis Sets for Use in Molecular Orbital Studies of Organic Molecules. *J. Chem. Phys.* 56, 2257–2261. doi:10.1063/1.1677527

Komarova, B. S., Gerbst, A. G., Finogenova, A. M., Dmitrenok, A. S., Tsvetkov, Y. E., and Nifantiev, N. E. (2017). 1,3-*syn*-Diaxial Repulsion of Typical Protecting Groups Used in Carbohydrate Chemistry in 3-O-Substituted Derivatives of Isopropyl D-Idopyranosides. *J. Org. Chem.* 82, 8897–8908. doi:10.1021/acs.joc.7b01167

Krylov, V. B., Argunov, D. A., Solovev, A. S., Petruk, M. I., Gerbst, A. G., Dmitrenok, A. S., et al. (2018). Synthesis of Oligosaccharides Related to Galactomannans fromAspergillus Fumigatusand Their NMR Spectral Data. *Org. Biomol. Chem.* 16, 1188–1199. doi:10.1039/c7ob02734f

Krylov, V. B., Gerbst, A. G., Argunov, D. A., Dmitrenok, A. S., Shashkov, A. S., Kaczynski, Z., et al. (2015). Definitive Structural Assessment of Enterococcal Diheteroglycan. *Chem. Eur. J.* 21, 1749–1754. doi:10.1002/chem.201405857

Krylov, V. B., and Nifantiev, N. E. (2020). Synthetic Carbohydrate Based Anti-fungal Vaccines. *Drug Discov. Today Tech.* 35-36, 35–43. doi:10.1016/j.ddtec.2020.11.002

Kudoh, A., Okawa, Y., and Shibata, N. (2015). Significant Structural Change in Both O- and N-Linked Carbohydrate Moieties of the Antigenic Galactomannan from *Aspergillus fumigatus* Grown under Different Culture Conditions. *Glycobiology* 25, 74–87. doi:10.1093/glycob/cwu091

Laverde, D., Romero-Saavedra, F., Argunov, D. A., Enotarpi, J., Krylov, V. B., Kalfopoulou, E., et al. (2020). Synthetic Oligomers Mimicking Capsular Polysaccharide Diheteroglycan Are Potential Vaccine Candidates against EncapsulatedEnterococcalInfections. *ACS Infect. Dis.* 6, 1816–1826. doi:10.1021/acsinfecdis.0c00063

Lipkind, G. M., Shashkov, A. S., Nifant'ev, N. E., and Kochetkov, N. K. (1992). Computer-assisted Analysis of the Structure of Regular Branched Polysaccharides Containing 2,3-disubstituted Rhamnopyranose and Mannopyranose Residues on the Basis of 13C NMR Data. *Carbohydr. Res.* 237, 11–22. doi:10.1016/s0008-6215(92)84229-l

Lowary, T. L. (2016) Twenty Years of Mycobacterial Glycans: Furanosides and beyond. *Acc. Chem. Res.* 49, 1379–1388. doi:10.1021/acs.accounts.6b00164

Neese, F. (2012). The ORCA Program System. *Wires Comput. Mol. Sci.* 2, 73–78. doi:10.1002/wcms.81

Previato, J. O., Vinogradov, E., Maes, E., Fonseca, L. M., Guerardel, Y., Oliveira, P. A. V., et al. (2017). Distribution of theO-Acetyl Groups and β-galactofuranose Units in Galactoxylomannans of the Opportunistic fungusCryptococcus Neoformans. *Glycobiology* 27, 582–592. doi:10.1093/glycob/cww127

Richards, M. R., Bai, Y., and Lowary, T. L. (2013). Comparison between DFT- and NMR-Based Conformational Analysis of Methyl Galactofuranosides. *Carbohydr. Res.* 374, 103–114. doi:10.1016/j.carres.2013.03.030

Richards, M. R., and Lowary, T. L. (2009). Chemistry and Biology of Galactofuranose-Containing Polysaccharides. *ChemBioChem* 10, 1920–1938. doi:10.1002/cbic.200900208

Rollenske, T., Szijarto, V., Lukasiewicz, J., Guachalla, L. M., Stojkovic, K., Hartl, K., et al. (2018). Cross-specificity of Protective Human Antibodies against *Klebsiella pneumoniae* LPS O-Antigen. *Nat. Immunol.* 19, 617–624. doi:10.1038/s41590-018-0106-2

Stoychev, G. L., Auer, A. A., and Neese, F. (2017). Automatic Generation of Auxiliary Basis Sets. *J. Chem. Theor. Comput.* 13, 554–562. doi:10.1021/acs.jctc.6b01041

Taha, H. A., Richards, M. R., and Lowary, T. L. (2013). Conformational Analysis of Furanoside-Containing Mono- and Oligosaccharides. *Chem. Rev.* 113, 1851–1876. doi:10.1021/cr300249c

Weigend, F., and Ahlrichs, R. (2005). Balanced Basis Sets of Split Valence, Triple Zeta Valence and Quadruple Zeta Valence Quality for H to Rn: Design and Assessment of Accuracy. *Phys. Chem. Chem. Phys.* 7, 3297–3305. doi:10.1039/B508541A

Whitfield, C., Williams, D. M., and Kelly, S. D. (2020). Lipopolysaccharide O-Antigens-Bacterial Glycans Made to Measure. *J. Biol. Chem.* 295, 10593–10609. doi:10.1074/jbc.REV120.009402

Zhang, R., Wu, L., Eckert, T., Burg-Roderfeld, M., Rojas-Macias, M. A., Lütteke, T., et al. (2017). Lysozyme's Lectin-like Characteristics Facilitates its Immune Defense Function. *Quart. Rev. Biophys.* 50, e09. doi:10.1017/S0033583517000075

Conflict of Interest: The authors declare that the research was conducted in the absence of any commercial or financial relationships that could be construed as a potential conflict of interest.

Publisher's Note: All claims expressed in this article are solely those of the authors and do not necessarily represent those of their affiliated organizations, or those of the publisher, the editors, and the reviewers. Any product that may be evaluated in this article, or claim that may be made by its manufacturer, is not guaranteed or endorsed by the publisher.

QRB DISCOVERY
journals.cambridge.org/qrb

REPORT

Lysozyme's lectin-like characteristics facilitates its immune defense function

Ruiyan Zhang[1,2], Lisha Wu[3], Thomas Eckert[4,5], Monika Burg-Roderfeld[5], Miguel A. Rojas-Macias[5], Thomas Lütteke[5], Vadim B. Krylov[6], Dmitry A. Argunov[6], Aritreyee Datta[7], Philipp Markart[8,9], Andreas Guenther[10], Bengt Norden[3], Roland Schauer[9], Anirban Bhunia[7], Mushira Abdelaziz Enani[11], Martin Billeter[12]*, Axel J. Scheidig[2]*, Nikolay E. Nifantiev[6]* and Hans-Christian Siebert[1]*

[1] *RI-B-NT Research Institute of Bioinformatics and Nanotechnology, Franziusallee 177, 24148 Kiel, Germany*
[2] *Department of Structural Biology, Institute of Zoology, Christian-Albrechts-University, Am Botanischen Garten 1-9, 24118 Kiel, Germany*
[3] *Department of Chemical and Biological Engineering, Chalmers University of Technology, 41296 Gothenburg, Sweden*
[4] *Clinic of Obstetrics, Gynecology and Andrology for Small and Large Animals, Justus-Liebig-University, Justus-Liebig-University Giessen, Frankfurter Str. 106, 35392 Giessen, Germany*
[5] *Institute for Veterinary Physiology and Biochemistry, Justus-Liebig-University, Frankfurter Str.100, 35392 Giessen, Germany*
[6] *Laboratory of Glycoconjugate Chemistry, N.D. Zelinsky Institute of Organic Chemistry, Russian Academy of Sciences, Leninsky prospect 47, 119991 Moscow, Russian Federation*
[7] *Department of Biophysics, Bose Institute, P-1/12 CIT Scheme VII (M), Kolkata 700054, India*
[8] *Pneumology, Heart-Thorax-Center Fulda, Pacelliallee 4 – 36043 Fulda, Germany*
[9] *Institute of Biochemistry, Christian-Albrechts-University, Olshausenstrasse 40, 24098 Kiel, Germany*
[10] *Medical Clinic II, Justus-Liebig-University, Klinikstraße 33, 35392 Giessen, Germany; Member of the German Center for Lung Research (DZL)*
[11] *Infectious Diseases Division, Department of Medicine, King Fahad Medical City, PO Box 59046, Riyadh 11525, Kingdom of Saudi Arabia*
[12] *Department of Chemistry and Molecular Biology, University of Gothenburg, 40530 Gothenburg, Sweden*

Quarterly Reviews of Biophysics (2017), **50**, e9, page 1 of 12 doi:10.1017/S0033583517000075

Abstract. Interactions between human lysozyme (HL) and the lipopolysaccharide (LPS) of *Klebsiella pneumoniae* O1, a causative agent of lung infection, were identified by surface plasmon resonance. To characterize the molecular mechanism of this interaction, HL binding to synthetic disaccharides and tetrasaccharides representing one and two repeating units, respectively, of the O-chain of this LPS were studied. pH-dependent structural rearrangements of HL after interaction with the disaccharide were observed through nuclear magnetic resonance. The crystal structure of the HL-tetrasaccharide complex revealed carbohydrate chain packing into the A, B, C, and D binding sites of HL, which primarily occurred through residue-specific, direct or water-mediated hydrogen bonds and hydrophobic contacts. Overall, these results support a crucial role of the Glu35/Asp53/Trp63/Asp102 residues in HL binding to the tetrasaccharide. These observations suggest an unknown glycan-guided mechanism that underlies recognition of the bacterial cell wall by lysozyme and may complement the HL immune defense function.

* Authors for correspondence: M. Billeter, Department of Chemistry and Molecular Biology, University of Gothenburg, Box 462, 40530 Gothenburg, Sweden. Tel: +46 31 7863925; Fax: +46 31 7862599; Email: martin.billeter@chem.gu.se
A. J. Scheidig, Department of Structural Biology, Institute of Zoology, Christian-Albrechts-University, Am Botanischen Garten 1-9, 24118 Kiel, Germany. Tel: +49 431 8804286; Fax: +49 431 8804929; Email: axel.scheidig@strubio.uni-kiel.de.
N. E. Nifantiev, N.D. Zelinsky Institute of Organic Chemistry, Russian Academy of Sciences, Leninsky prospect 47, 119991 Moscow, Russian Federation. Tel: +7 499 1358784; Fax: +7 499 1358784; Email: nen@ioc.ac.ru
H-C. Siebert, RI-B-NT Research Institute of Bioinformatics and Nanotechnology, Franziusallee 177, 24148 Kiel, Germany. Tel.: +49 431 66878443; Fax: +49 431 56 06 295; Email: hcsiebert@aol.com

1. Introduction

Lower respiratory tract infections are among the top 10 causes of death worldwide and are of particular relevance in chronic lung diseases. Lysozyme is one of the most abundant antimicrobial proteins in the airways and alveoli. The concentration of this enzyme in the surface liquid of the human airway is estimated to be 20–100 μg ml^{-1}, which is sufficient to kill important pulmonary pathogens such as Gram-positive *Staphylococcus aureus* and Gram-negative *Pseudomonas aeruginosa* (Travis *et al.* 1999). *Klebsiella pneumoniae*, which is a frequent cause of nosocomial

infection and may be responsible for up to 20% of the respiratory infections in neonatal intensive care units (Gupta, 2002), is also specifically attacked by lysozyme (Markart *et al.* 2004).

Human lysozyme (HL, also known as muramidase, *N*-acetyl muramide glycanohydrolase, or EC 3.2.1.17; Fig. 1*a*) is a 130-amino acid cationic protein that cleaves the glycosidic bonds of *N*-acetyl-muramic acid (Fig. 1*c*), thereby damaging the bacterial cell wall (Fig. 1*b*) and ultimately killing bacteria by lysis in cooperation with defensins. An inter-domain cleft in HL contains six binding pockets (labeled A–F in Fig. 1*a*), and a strictly conserved catalytic residue Glu35 is located between the D and E sites (Chipman & Sharon, 1969). Co-crystallization of HL with N-acetyl-chitohexaose $(GlcNAc)_6$ (Fig. 1*c*) has revealed a crystal structure with non-covalently linked $(GlcNAc)_4$ and $(GlcNAc)_2$ in subsites A–D and E–F, respectively (Song *et al.* 1994).

In addition to the well-known muramidase activity of HL, increasing evidence suggests the existence of non-enzymatic and/or nonlytic modes of action against Gram-negative and Gram-positive bacteria (Lee-Huang *et al.* 2005; Masschalck & Michiels, 2003). Furthermore, lysozyme has antitumor (Osserman *et al.* 1973) and antiviral activities (Lee-Huang *et al.* 2005), and it enhances the immune system (Siwicki *et al.* 1998). The mechanisms of these activities remain unclear, and the dominant questions involve how HL recognizes pathogenic microbes.

Bacterial LPSs represent the group of important virulence factors, which are recognized by antibodies and pattern recognition receptors in the initial steps of innate immune response to Gram-negative bacteria. These processes and their physico-chemical characteristics were previously studied using surface plasmon resonance (SPR)-method (Shin *et al.* 2007; Young *et al.* 1999). The ability of lysozyme to interact with lipopolysaccharides (LPSs) was demonstrated in the late 1980s (Ohno & Morrison, 1989a, b). However, the details of this interaction (i.e. how binding specificity is established between specific parts of the lysozyme protein and the LPS carbohydrate units) have not been examined. The attraction between lysozyme and LPS has been largely attributed to non-specific hydrophobic interactions of lysozyme with lipid A, which is the innermost hydrophobic component of LPS and is primarily responsible for its toxicity. To examine whether lysozyme specifically interacts with bacterial LPS and particularly with the O-chains that form the outer layer of the bacterial cell wall, we performed SPR-based experiments as previously described (Tsvetkov *et al.* 2012). By SPR experiments we detected the interaction between HL and LPS from *K. pneumoniae* O1, which is associated with the development of severe hospital-acquired infections and is clinically relevant to infections beyond those of the airways (Enani, 2015; Enani & El-Khizzi, 2012). SPR permitted to measure corresponding dissociation constant (K_d) of 0·41 mM and association and dissociation rate constants (k_a and k_d) of 216 M^{-1} s^{-1} and 0·0886 s^{-1}, respectively (online Fig. S1 in Supplementary Information). To assess whether the O-chains of these LPSs were involved in the observed interactions, we combined nuclear magnetic resonance (NMR), molecular modeling, data mining and X-ray crystallography techniques to investigate HL binding to synthetic disaccharide **1** (Krylov *et al.* 2014) and tetrasaccharide **2** (Fig. 1*d*), which represented one and two repeating units of the O-chain of *K. pneumoniae* O1, respectively, at the sub-molecular level.

2. Materials and methods

2.1 Lysozyme

Recombinant HL was provided by T. E. Weaver (Cincinnati Children's Hospital Medical Center, Cincinnati, USA). The HL was purified as previously described for other lysozymes (Akinbi *et al.* 2000; Markart *et al.* 2004).

2.2 Oligosaccharides

The synthesis of disaccharide **1** was performed using the recently discovered pyranoside-*into*-furanoside rearrangement (Krylov *et al.* 2014, 2016). The synthesis of tetrasaccharide **2** (Verkhnyatskaya *et al.* 2017) was based on similar approaches and is described in the online supplementary information (Scheme S1).

2.3 SPR analysis

SPR was performed on a protein interaction array system (ProteOn XPR36, Bio-Rad, Munich, Germany). Vertical channels of a GLM sensor chip were activated with undiluted EDAC-sNHS 1:1 mixtures according to the amine coupling kit (Biorad). HL was immobilized from 100 μg ml^{-1} solutions in 10 mM acetate buffer pH 4·5 on the activated sides of channel. Remaining active sides of the channels were blocked by treatment with 1 M ethanolamine. All steps were performed in phosphate buffered saline pH 7·4 containing 0·005% Tween 20 (PBS-T) running buffer using a flow rate of 30 μl min^{-1} and 150 μl total reaction volume, respectively. A regeneration of the sensor surface was performed before each testing by injecting 0.85% phosphoric acid solution at 100 μl min^{-1} for 18 s.

LPS of *Klebsiella* was diluted in running buffer and different concentrations (10, 20, 40, 80 μM) were injected for 60 s association time corresponding to a total reaction volume of 100 μl at 100 μl min^{-1} followed by 600 s dissociation step using an equal flow rate via channels A1–A4 (horizontal channels). Interaction binding signal (RU) raw data of channels were referenced by subtraction of the unspecific binding signals on uncovered channel. Double reference was carried out by subsequent subtraction of unspecific binding signals measured in a reference channel with

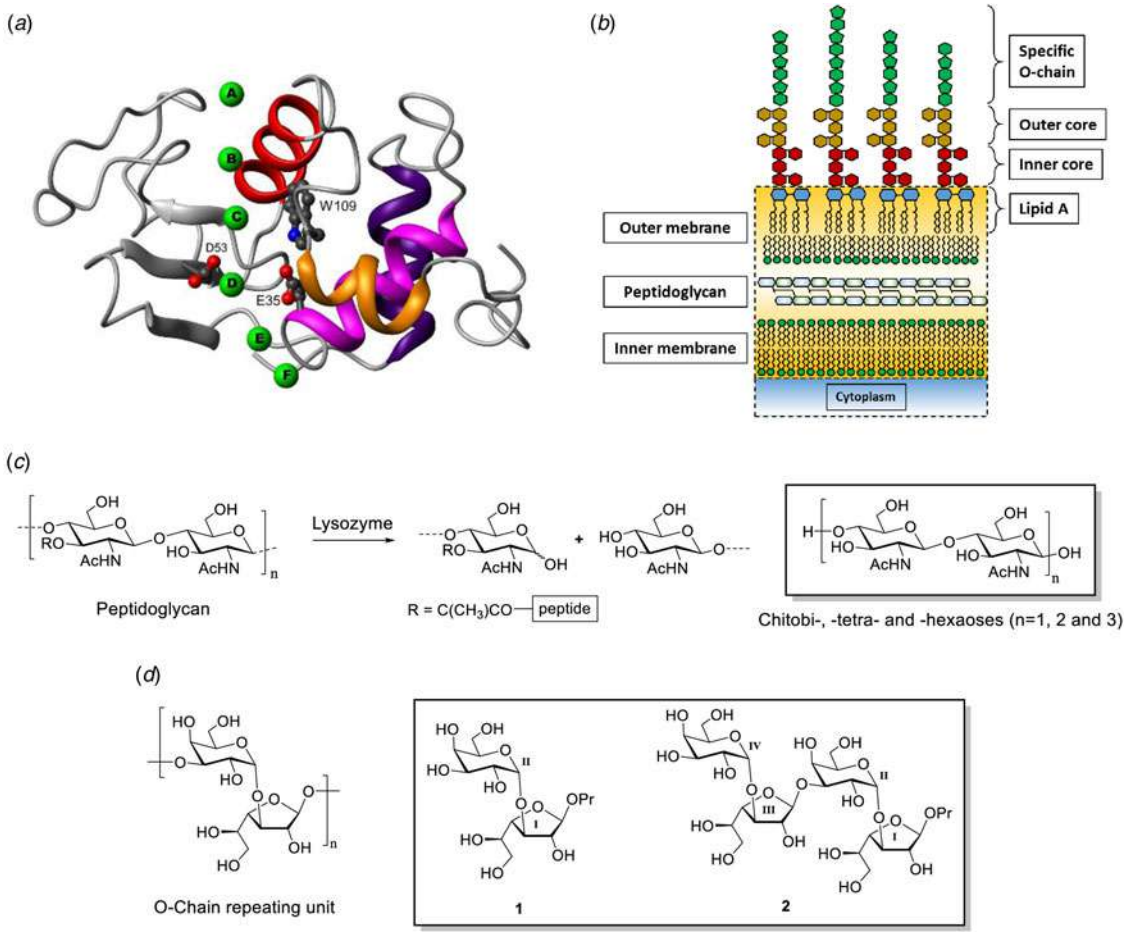

Fig. 1. Lysozyme and its carbohydrate ligands (*a*) Structure of HL (PDB code 1LZS) with selected residues (Glu35, Asp53, and Trp109). Binding sites A–F are indicated by letters in green circles. Helices are colored as follows: a, violet; b, magenta; c, red; d, orange. In the orientation shown, the α-domain is to the right of the binding cleft and the β-domain is to the left. (*b*) Schematic drawing of the LPS molecule and its position in the outer layer of the outer membrane of Gram-negative bacteria; for clarity, membrane associated proteins and integral membrane proteins are not shown. (*c*) Hydrolysis of the (1→4)-glycosidic bond between N-acetyl muramic acid and N-acetyl glucosamine in the peptidoglycan. (*d*) Structures of the repeating unit of the O-chain of the *K. pneumoniae* O1 lipopolysaccharide and the structurally related synthetic disaccharide **1** and tetrasaccharide **2**. Monosaccharide units are numbered with Roman numerals.

PBS-T. Data were analyzed with the computer software (ProteOn manager software, Bio-Rad). Kinetic constants were calculated using Langmuir model kinetic analysis of the ProteOn manager software (Bio-Rad).

2.4 NMR sample preparation

All samples were prepared by dissolving lyophilized HL in 0·3 ml H_2O containing 20 mM sodium phosphate buffer and 10% D_2O. Final concentrations of all samples were 0·5 mM protein as determined by measurement of the molar extinction coefficient, using E1% = 25·5 for HL. For mixtures of lysozyme with disaccharide **1**, a 40 mM stock solution was prepared. The following samples were prepared: pure HL as well as 1:1 mixtures of these proteins with disaccharide**1** at pH 3·8 and 5·5. Additional samples for HL were prepared in a similar manner for the pH titrations described below.

2.5 NMR measurements

All NMR spectra were recorded on a Varian Unity INOVA 800 MHz spectrometer at 35 °C using 3 mm Shigemi tubes. The ^{1}H chemical shifts were referenced to DSS. For disaccharide–lysozyme interaction measurements, equivalent amounts of disaccharide**1** were added to the enzymes. Homonuclear 2D NOESY (mixing time 150 ms) and TOCSY (mixing time 50 ms) with spectral width 11 204 Hz for both dimensions were acquired with 512 increments in the indirect dimension and 4096 data points in the direct dimension, using Watergate solvent suppression and a pulse sequence repetition delay of 1·5 s. All data were processed with the NMRPipe software package (Delaglio *et al.* 1995) by zero-filling to 1024 points in the indirect dimension and ending with either a Gaussian or a shifted sine-bell function. After zero-filling the digital resolution was 0·0015 ppm for the direct dimension and 0·014 ppm for

the indirect dimension. For pKa determinations of HL, 10 NOESY spectra were recorded in the pH range 3·8–8·1 (3·8, 4·2, 4·6, 5·0, 5·5, 6·2, 6·8, 7·4, 7·7 and 8·1). A separate sample of HL was prepared for recording of 22 1D spectra covering the pH range of 3·17–8·13 in steps of ∼0·2 units. All 1D datasets were defined by 4096 complex points and consisted of 256 transients. The digital resolution of the 1D spectra was 0·0024 ppm after zero-filling. Xeasy (Bartels *et al.* 1995), Mnova (Claridge, 2009), and CCPNmr (Vranken *et al.* 2005) were used for analysis and resonance assignment. Line widths are defined as half-width at half-height of a peak; for most peaks the line width was estimated to be 0·01 ppm.

All pH adjustments were made by addition of small aliquots of either H_3PO_4 or NaOH. The pH meter was calibrated with standard solutions (from Sigma) at pH 4 and 7. The temperature dependence of the pH reading for HL was checked by recalibrating the pH meter at 35 °C: the difference between an incubated lysozyme sample at 35 °C and at room temperature was less than 0·1 pH unit. The pH for each sample was measured before and after each experiment to warrant constant conditions.

2.6 Signal assignments

^{1}H resonance assignments at pH 3·8 and pH 5·5, both at 35 °C, were obtained for HL by transferring chemical shifts from the Biological Magnetic Resonance Bank (BMRB, http://www.bmrb.wisc.edu/) (Ulrich *et al.* 2008) entries 5130 and 1093, respectively, to the NOESY and TOCSY spectra. Based on chemical shift changes, conclusions about interactions between lysozymes and disaccharide **1** could be made in several cases as described in the main text. However, no intermolecular NOEs were detectable, suggesting dynamic binding modes only.

2.7 Molecular modeling and data mining

Docking studies were performed with the AutoDock 4·2 software, which uses the Lamarckian Genetic Algorithm (LGA) implemented therein. For the docking of the LPS disaccharide fragment **1** with human or chicken lysozyme, the required file for the ligand was created by combining the Gaussian and AutoDock 4·2 software packages. The grid size was set to 126, 126, and 126 Å along the *X*-, *Y*-, and *Z*-axis; in order to recognize the LPS glycan binding site of HL, the blind docking simulation was adopted. The docking parameters used were the following: LGA population size = 150; maximum number of energy evaluations = 250 000. The lowest binding energy conformer was taken from 10 different conformations for each docking simulation and the resultant minimum energy conformation was applied for further analysis. The MOLMOL (Koradi *et al.* 1996) and PyMOL (DeLano, 2002) software packages were applied for visualization and analysis of the docked complex. Data mining of protein–carbohydrate interactions in the Protein Data Bank (PDB) was performed with GlyVicinity at a redundancy level of 70% (www.glycosciences.de/tools/glyvicinity/). Only non-covalently bound ligands in structures with a resolution of at least 3 Å have been considered. The analysed dataset comprised 498 amino acids that have been found within a 4 Å radius of 73 alpha-galactose residues in 73 different PDB entries.

2.8 X-ray

For crystallization, the hanging-drop vapor-diffusion method was performed in 24-well plates. Single crystals of the HL were obtained by mixture of 2 µl of the reservoir solution (0·8 M NaCl, 25 mM NaOAc, pH 4·4–5·6) with 2 µl of the protein solution (50 mg ml^{-1} in 100 mM NaCl, 10 mM phosphate buffer, pH 6·0). These drops were equilibrated against 1 ml of the reservoir solution at 291 K. For co-crystallization, the protein solution was mixed with a 10-fold excess of tetrasaccharide 2 and incubated for 30 min at room temperature prior to setting up the crystallization drop. Data collection for X-ray diffraction was performed at 100 K. The crystals were transferred into liquid nitrogen for flash-cooling without the prior addition of cryoprotectants. All data processing was performed using the XDS/XSCALE (Kabsch, 2010) program package. Molecular replacement was carried out using the MOLREP (Vagin & Teplyakov, 1997) program with the HL structure (PDB id: 1REX) (Muraki *et al.* 1996) as the search model. Model building and refinement were performed with the Refmac5 program as implemented in the CCP4 suite (Murshudov *et al.* 2011; Winn *et al.* 2011) and PHENIX (Adams *et al.* 2010). The COOT (Emsley *et al.* 2010) graphics program was used to interpret the electron density maps and to rebuild the structure.

3. Results

3.1 NMR observations of structural rearrangements of the binding site of HL

The lysozyme enzymatic reaction requires an initial protonated form of the highly conserved Glu35, which exhibits a high pKa of 6·8 (Kuramitsu *et al.* 1974). Two pH-based NMR titrations of lysozyme without (see below and Fig. 2) and with (see below and Fig. 3) the weakly binding disaccharide **1** were used to provide atomistic insights into the relationship between the (de)protonation of Glu35 and its associated structural rearrangements in the surrounding helices, which were suspected to control the continuation of the catalysis reaction and hence influence specificity.

The pH dependence of the lysozyme binding site modulations was analyzed for free lysozyme and lysozyme in the presence of the weakly binding disaccharide **1** (Fig. 1*d*), and conclusions regarding the interactions between lysozyme and disaccharide **1** were made on the basis of chemical

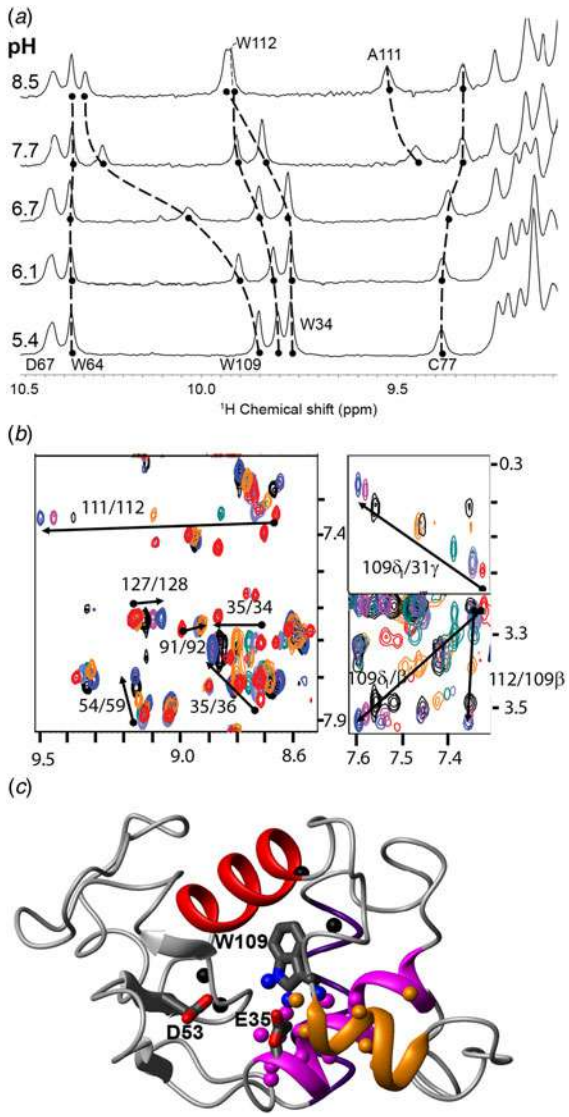

Fig. 2. NMR-based investigation of free human lysozyme (*a*) 1D spectra of pure HL at various pH values (indicated on the left border). For clarity, we show the residues, indole ring proton of Trp (Trp109, Trp112, and Trp34) and the HN of Cys77 and Ala111 (shown in top two traces), which show strong chemical shift perturbation. (*b*) Selected 2D NOESY regions for HL at various pH values. Spectra for the different pH values are colored as follows: 3·8, red; 5·0, light blue; 5·5, green; 6·8, orange; 7·4, black; 7·7, purple; 8·1, dark blue. Chemical shifts that varied with pH are indicated by arrows on or beside the corresponding peaks with different colors. Peak contours are calibrated such that the intensities of the HN–HN cross-peaks for helix c are constant across all pH values. (*c*) Epitope mapping of HL from the pH titration, based on all resonances listed in the first part of online Table S1. Side chains are shown and labeled for Glu35, Asp53 and Trp109. Spheres are color-coded as follows: atoms on helix b are magenta, atoms on helix d are orange, and Trp109 side-chain atoms are blue (Hβ2, Hδ1 and Hϵ1). Additionally, black spheres mark the HN positions from the following residues: 58 and 59 (near D53), 100 (at the end of the red helix c), and HN 108 (before Trp109). The structure is rotated by 30° around a vertical axis with respect to Fig. 1*a*; the helix coloring is the same, and helix a is presented as a thin violet curve for clarity.

shift changes. However, intermolecular NOEs between these two molecules were undetectable, thus suggesting the existence of only dynamic binding modes for which no stable structure could be determined. The results were therefore compared with the stable complex of lysozyme with tetrasaccharide **2** (Fig. 1*d*), which occupies four binding sites (A, B, C, and D) (Fig. 1*a*).

3.2 NMR-based investigation of free human lysozyme

Titrations in the 3·8–8·5 pH range were observed for free HL by 1D and 2D NMR (online Table S1, Supplementary Information). Figure 2*a* shows 1D spectra for different pH values, illustrating that the indole ring proton (Hϵ1) of residues Trp34, Trp109, Trp112, and the amide protons of Cys77 and Ala111 are strongly affected by pH. The most pronounced change was observed for Trp109, with a shift to lower field by 0·43 ppm, whereas Trp64 and the overlapping Trp28 (at 9·13 ppm, not shown) did not titrate in the 3·8–8·5 pH range. 2D NOESY spectra complemented the 1D titrations and provided a comprehensive picture of the chemical and structural changes in the enzyme (Fig. 2*b*). Again, large changes were observed for the HN of Ala111 (around pH 6·8) and for various side-chain atoms of Trp109. Additional chemical shift perturbations were also observed in large portions of helices b and d (Fig. 1*a*). The observed effects outside of these two helices included Gln58, Ile59, Val100 and Ala108 (online Table S1, Supplementary Information).

The strongest shift changes in the spatial neighborhood of the catalytic residue Glu35 were revealed by mapping of these shift changes onto the 3D structure of HL; they affect most of the b and d helices, and the loop between the second and third β-strands from the β-domain (Fig. 2*c*). Changes involving the HNs of residues Gln58, Ile59, Val100 and Ala108, were located in the plane of the Trp109 ring, thus indicating rotation of this ring. The common pKa value (within the measurement error) of all these resonances, about pH 6·8, coincided with the reported (and unusually high) pKa value of the catalytic Glu35 protonation site (Kuramitsu *et al.* 1974); this strongly indicated that all of these events are coupled (online Table S1 and Fig. S2 and S3 Supplementary Information). The common pKa value (within the measurement error) of all these resonances, about pH 6·8, coincided with the reported (and unusually high) pKa value of the catalytic Glu35 protonation site (Kuramitsu *et al.* 1974), and furthermore identical pKa strongly indicated that all of these events are coupled (online Table S1, Supplementary Information). The large shift variation of ~0·84 ppm for the HN of Ala111 is probably the result of an adjacent charge change, and the obvious cause of this shift variation is the Glu35 side chain, whose carboxyl group is nearby at 3·4 Å (Harata *et al.* 1998). The remarkable behavior of the HN of Ala111 was an important observation that demonstrated a direct coupling between helices b and

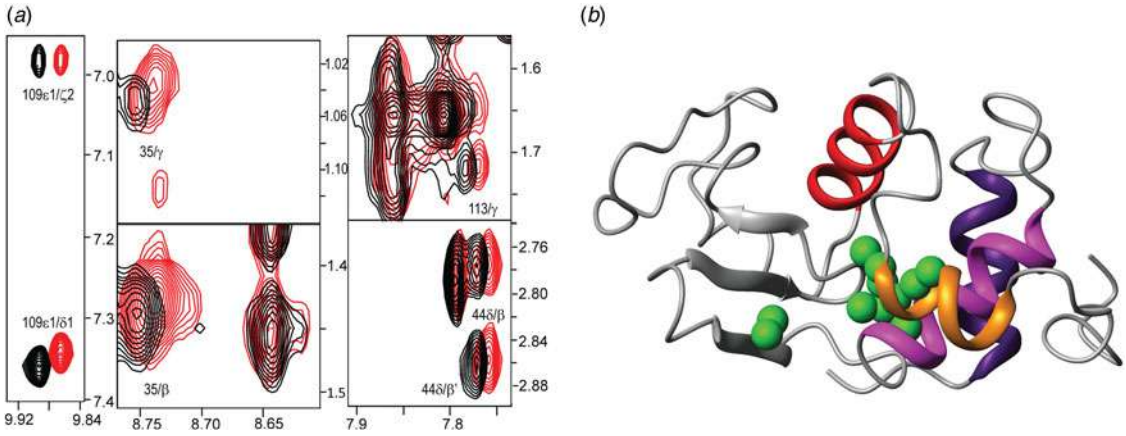

Fig. 3. Interaction between human lysozyme and disaccharide **1**, observed by NMR. (*a*) Selected regions from the 2D NOESY spectra of pure human lysozyme (red) and a 1:1 mixture with disaccharide **1** (black) demonstrate some of the shift changes observed after the addition of disaccharide **1**. Peak labeling is as described in Fig. 2*b*. (*b*) Mapping of resonances with chemical shift changes exceeding 0·07 ppm (online Table S1) after the addition of disaccharide **1** onto the 3D structure of lysozyme; the atoms are indicated as green spheres. The structure has an identical orientation and helix coloring to that described in Fig. 1*a*.

d. The next largest shift changes concerned the Trp109 side chain, which is an important component of the binding site surface and exhibited direct interactions with Glu35; the shortest distance between these side chains is 2·2 Å.

In addition to the well-known relative motions of the two domains required for ligand binding, HL undergoes a series of specific processes, both chemical and structural, when the pH is varied near 6·8. These processes include large parts of the α-domain with the catalytic Glu35, the side chain of Trp109, most of the b and d helices, and the loop between the second and third β-strands from the β-domain (Fig. 2*c*). The identical pKa (within the measurement error) of all relevant resonances strongly indicated that all of these events are coupled (online Table S1, Supplementary Information). Although some strong interactions with Glu35 have been previously reported (Kuramitsu *et al.* 1974) (e.g. with Trp109) or can be assumed on the basis of their proximities (e.g. to the amide of Ala 111), other titrating residues appeared to be too far away from Glu35 to show direct effects due to the charge change upon (de)protonation; reports have instead focused on a higher flexibility of the α-domain that involves mutual rearrangements between helices b and d, which mirrors similar observations regarding factors such as ligand binding, temperature or pressure variations (Refaee *et al.* 2003; Young *et al.* 1994). The relative position of helices b and d within the α-domain modulated by the hydrogen bonding network with Glu35, Trp109 and Ala111 is further defined by the previously described interaction between Arg115 and Trp34, and the Arg115Glu mutation has been reported to modify both the position of helix d and the enzyme activity (Harata *et al.* 1998). Thus, (de)protonation of Glu35 appears to trigger processes that spread over most of the α-domain.

3.3 Interaction between HL and disaccharide 1, observed by NMR

The binding sites of the c-type lysozyme include six individual subsites (labeled A–F, Fig. 1*a*) for specific interactions with multiple saccharide rings (Chipman & Sharon, 1969). Mixtures of HL and disaccharide **1** (Fig. 1*d*) yield observable chemical shift value changes at only pH 5·5; effects caused by intermolecular interactions were undetectable at pH 3·8. At pH 5·5, the nuclei in the residues surrounding the D-F sub-sites that show changes were Glu35 HN and Hγ, Asn44 H, Trp109 Hδ1 and Hϵ1, and Arg113 HN (Fig. 3*a*).

The affected residues were mapped onto the 3D structure of HL in Fig. 3*b* and demonstrated transient binding at subsites D and E (Fig. 1*a*). Helices b and d and the catalytic Glu35 in particular responded to the addition of disaccharide **1**. Furthermore, a chemical shift change was observed on the β-domain in the center of the first strand (Asn44). Since Trp109 is part of the binding cleft (Fig. 1*a*), it is unsurprising that the aforementioned structural changes mediated by this tryptophan were affected by ligand binding. The observations of chemical shift changes for Arg113, whose location was distal to all binding sites and buried behind the preceding helix loop (residues 110–111), were in agreement with a coupling between the ligand-binding and conformational effects.

3.4 Molecular modeling of the interaction between HL and disaccharide 1

Molecular modeling (Kar *et al.* 2016; Zhang *et al.* 2016) and data mining (Lütteke *et al.* 2005; Rojas-Macias & Lütteke, 2015) tools are necessary for general discussions of the principles of carbohydrate–protein interactions. In order to gain insight into the binding mode for disaccharide **1**, molecular

modeling is a rational tool to use. During the docking, each simulation includes 100 runs, which generate 100 conformers for the ligand. The top 10 conformers with low energy were selected for further analysis. For this step, both energy and ligand binding were considered. In fact, in the end, only the conformer with the lowest energy was selected for interaction description, which also shows a rational binding conformation. Figure 4*a* displays the most favorable energetic structure of HL and disaccharide **1**. A close-up view of the basic pocket with the LPS-interacting side chains is presented in Fig. 4*b*. Red dashed lines indicate the hydrogen bonds. The simulation of the binding for disaccharide **1** indicated its interaction with HL at the substrate binding sites C and D. This observation is in agreement with the analysis based on the crystal structure of HL with the tetrasaccharide **2** since the binding sites C and especially D provided most of the interactions between sugar and protein. Comparisons of this specific result with similar cases in the PDB uncovered numerous meaningful agreements. The protein–carbohydrate interaction analysis in the PDB revealed that Trp, Tyr, Asp, Asn and His were the most overrepresented amino acids in the vicinity of α-D-Gal*p* residues (Fig. 4*c*). The previously described data mining approach (Bhunia *et al.* 2010; Lütteke *et al.* 2005) provided important information regarding the amino acid residues that typically occur in the vicinity of α-D-Gal*p*. Using our data mining protocols, we performed an overview of the molecular interactions between α-D-Gal*p* and the functional groups of certain amino acid residues (Fig. 4*c*) in relation to the general structural aspects of lysozyme–carbohydrate interactions.

Molecular modeling calculations with respect to the electrostatic surface potentials and hydrophobic patches were also performed (online Fig. S4). The differences in the patterns of the electrostatic surface potentials suggest variations in ligand binding and deviations in the aggregation/fibrillation behavior between human and avian lysozyme.

3.5 X-ray crystallography-based study of the interaction between HL and tetrasaccharide 2

To provide data that are independent of the results of the NMR measurements and molecular modeling calculations, X-ray crystallographic experiments were performed for human lysozyme. Extensive experiments to co-crystallize HL with bound disaccharide **1** (Fig. 1*d*) at different pH values failed. We did not observe a convincing electron density for bound disaccharide, even after the crystals were soaked with high disaccharide concentrations. We assume that the disaccharide was too short to provide sufficient interaction opportunities with the protein to form a stable complex. Therefore, the study of a longer oligosaccharide ligand representing a larger polysaccharide fragment was initiated.

The crystal complex of HL with tetrasaccharide **2** was successfully obtained by co-crystallization of 1·9 mM HL in the presence of 20 mM tetrasaccharide **2**. The X-ray diffraction resolution of the crystals was approximately 1·0 Å. A summary of the data collection and structure refinement is presented in Table 1. For details regarding the definitions of the individual parameters, see online Table S2 in the Supplementary Information.

The refined structure of HL in complex with tetrasaccharide **2** reveals the binding of tetrasaccharide **2** near the A, B, C, and D substrate-binding sites of the enzyme (Fig. 5). The Gal*f*–I furanoside unit of tetrasaccharide **2** is located near site A, and the Gal*p*-II pyranoside unit is located near site B. The second repeating unit (Gal*f*-III)-(Gal*p*-IV) is in proximity to sites C and D. Both Gal*p* units of tetrasaccharide **2** adopt a chair conformation. Overall, there are eight direct hydrogen bonds between tetrasaccharide **2** and the amino acid residues of HL. Seven residues (Ile59, Asn60, Tyr63, Trp64, Ala76, Asp102, and Trp109) form hydrophobic interactions. Through comparison with tetra N-acetyl-D-glucosamine, it is clear that the sugar ring systems of tetrasaccharide **2** are not identically positioned. However, a similar number of direct hydrogen bonds, hydrophobic interactions and water-mediated bridged hydrogen bonds jointly contribute to the overall binding affinity.

Based on number and ratio, an important contribution to the overall binding affinity for tetrasaccharide **2** seems to be provided by bridged hydrogen bonds that are mediated by approximately 20 water molecules within the binding pocket toward the following lysozyme residues: Glu35, Asp49, Asp53, Asn60, Tyr63, Val99, Arg98, Gly105, Ala108, Val110, and Ala111 (Fig. 6 and online Table S3, Supplementary Information). This ratio and mix of interactions is similar to those observed for $(GlcNAc)_4$ (PDB entry 1LZR) and $(GlcNAc)_4/(GlcNAc)_2$ (PDB entry 1LZS) (Song *et al.* 1994) bound to HL. The superposition of HL-**2** with HL-$(GlcNAc)_4$ and with HL-$(GlcNAc)_4/(GlcNAc)_2$ resulted in RMSD values of 0·23 and 0·46 Å, respectively (based on 130 C-alpha positions), thus indicating that the 3D structures of the protein-ligand complexes are similar in all three complexes.

The binding modes of tetrasaccharides **2** and $(GlcNAc)_4$ in the A, B, C, and D sites display small but significant differences. Specifically, Arg98 forms a direct hydrogen bond between its side-chain atom, Nε2, and the O1 atom of the Gal*f*-I unit in site A of the HL-**2** complex. Additionally, water molecules mediate a bridged hydrogen bond between the NH group of Arg98 and the OH group of Gal*f*-I. Arg98 is not involved in the binding of $(GlcNAc)_4$ or $(GlcNAc)_2$ to HL.

The major interactions of the Gal*p*-II unit in site B of HL are managed by direct hydrogen bonds with the surrounding amino acid residues Tyr63, Asp102, and Gln104. In addition to the hydrogen bond between atom O7 and the OH group

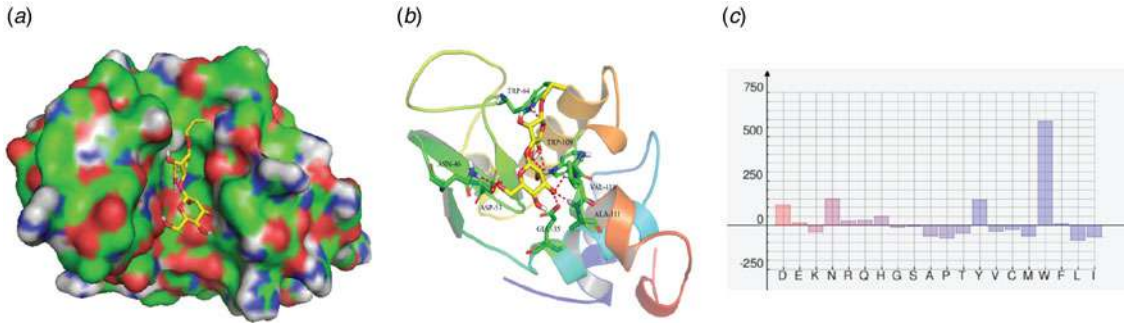

Fig. 4. Molecular modeling of the interaction between human lysozyme and disaccharide **1**. (*a*) Molecular surface of lysozyme with carbons (green), oxygens (red), nitrogens (blue) and polar hydrogens (gray). (*b*) Close-up view of the basic pocket with disaccharide **1** shown in stick rendering and with hydrogen bonds indicated by red dashed lines. (*c*) Amino acid residues in the vicinity of α-Gal in the protein-carbohydrate complexes deposited in the PDB, which indicates the deviation from natural abundance. Trp, Tyr, Asp, and His are overrepresented by greater than 100% (i.e. they are observed twice as often or more in a 4 Å radius of α-Gal compared with an average protein).

Table 1. *Data collection and refinement statistics*

PDB entry	5LSH
Data collection	
Temperature (K)	100
Resolution range (Å)[a]	29·05–1·061 (1·099–1·061)
Space group	*P* 2(1)2(1)2(1)
Unit cell a, b, c (Å)	33·1, 56·0, 60·5
Multiplicity[a]	11·9 (9·8)
Completeness (%)[a]	92 (69)
Mean (I)/σ(I)[a]	17·06 (1·52)
$R_{p.i.m.}$ (%)[a,b]	7·6 (108·8)
CC(1/2) (%)[a,b]	100 (63·3)
Refinement	
R-work (%)[a,b]	18·1 (32·4)
R-free (%)[a,b]	20·4 (33·6)
B-factors (Å^2) (No. of non-hydrogen atoms)	
All	11·4 (1414)
Ligand KTS	16·6 (90)
Water molecules	20·9 (160)
rmsd (bonds) (Å)	0·013
rmsd (angle) (°)	1·58
Rotamer outliers (%)	1·7
Ramachandran plot statistics (%)	
Favored	97·0
Allowed	2·8
Outliers	0·0

[a] Values in parentheses are for the high-resolution shell.
[b] For details regarding the definitions of the individual parameters, see online Table S2 in the Supplementary Information.

of Tyr63, the aromatic plane of Tyr63 provides a strong hydrophobic interaction with the Gal*p*-II moiety. A similar interaction of Tyr63 with the second GlcNAc residue is present within the HL-$(GlcNAc)_4$ complex. Notably, the orientation of the Tyr63 side chain in the HL-**2** complex is rotated by ca. 10° for an optimal interaction with the shifted sugar position in comparison with the GlcNAc unit. The Oδ2 side-chain atom of the Asp102 residue contributes two hydrogen bonds to the binding of the first two sugar units of **2**, but only one direct hydrogen bond to the first GlcNAc unit is observed in $(GlcNAc)_4$. In the HL-$(GlcNAc)_4$/$(GlcNAc)_2$ complex, atom Oδ1 forms two hydrogen bonds with atoms N and O6 of the first GlcNAc moiety of $(GlcNAc)_4$/$(GlcNAc)_2$. As a consequence of these differences, tetrasaccharide **2** adopts a closer binding orientation toward the 'bottom' of the binding pocket, as compared with $(GlcNAc)_4$ and $(GlcNAc)_4$/$(GlcNAc)_2$.

The Gal*f*-III unit is located near the C substrate-binding site. Only one direct hydrogen bond is formed between the Trp64 atom Nε1 and atom O19. Similar hydrogen bonds are contributed by these two residues for sugar binding in the HL complex to produce HL-$(GlcNAc)_4$ and HL-$(GlcNAc)_4$/$(GlcNAc)_2$. The unit Gal*p*-IV is located between the two substrate-binding sites, C and D. The only two direct hydrogen bonds are formed between atom O16 and the main-chain atom O of Gln58 and between atom O15 and the main-chain atom N of Asn60. Within the HL-$(GlcNAc)_4$ complex, a similar hydrogen bond is contributed by Gln58 to the fourth GlcNAc moiety. Additionally, two residues, Asn46 and Asp53, form direct hydrogen bonds with GlcNAc atom O1 in the HL-$(GlcNAc)_4$ complex. Interestingly, in the HL-$(GlcNAc)_4$/$(GlcNAc)_2$ complex, Gln58 is not involved in the interaction with the fourth GlcNAc moiety; instead, it is involved in the interaction with the Asn46 side chain and the main-chain atoms of Ala108 and Val110. Notably, approximately 10 water molecules play an important role in mediating interactions between unit Gal*p*-IV of tetrasaccharide **2** and the Glu35, Asp49, Ser51, Asp53, Gln58, Gln104, Ala108, and Ala111 residues near the D and E substrate-binding sites. It is possible that a fifth sugar moiety may be adopted within this interaction network, which would contribute to a further gain in binding affinity.

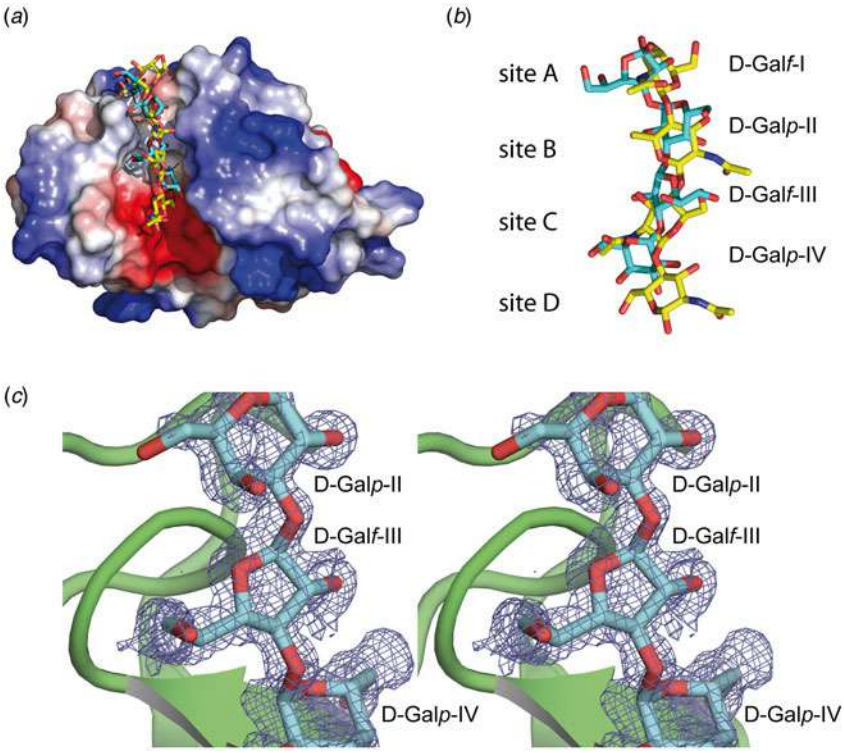

Fig. 5. Molecular surface of HL in the complex with tetrasaccharide **2**. (*a*) Representation of the molecular surface of HL is colored according to the electrostatic potential. Tetrasaccharide **2** is represented by sticks for one conformation (carbon atoms in cyan and oxygen atoms in red) and by black lines for an alternative conformation. The HL (PDB-entry 1LZR)-bound chitotetraose $(GlcNAc)_4$ ligand is superimposed and represented by sticks (carbon atoms in yellow). (*b*) Close-up view of the superimposed ligands, tetrasaccharide **2** (carbon atoms in cyan) and $(GlcNAc)_4$ (carbon atoms in yellow, oxygen atoms in red and nitrogen atoms in blue. (*c*) Representation in stereo of the electron density $2F_{obs}$-$1F_{calc}$ omit map defining bound tetrasaccharide **2**. The Gal*p*-II, Gal*f*-III and Gal*p*-IV units are represented by sticks (carbon atoms in cyan and oxygen atoms in red). The protein backbone is indicated by a ribbon representation in green. The representation was generated using PyMOL v.1.6 (DeLano, 2002).

4. Discussion

This study is the first to indicate that tetrasaccharide **2**, which represents part of the O-chain of the *K. pneumoniae* O1 LPS, binds to HL at its conserved sites (A, B, C, and D) within the substrate binding pocket; this binding occurs mainly through direct hydrogen bonds and indirect hydrogen bonds that are mediated by water molecules. Our SPR experiments indicated a specific binding of LPS fragments to lysozyme, however with a rather low on-rate. A couple of synchronously occurring processes have to be considered for the evaluation of this slow on-rate: closing/opening of the binding cleft, rearrangement of side chains, water molecules have to be squeezed out of the binding cleft before the sugar molecule can bind and finally the sugar has to adopt an optimal conformation. In the case of dihydrofolate reductase the dynamic events during catalysis were deciphered e.g. by NMR experiments and helped to model the energy landscape (Boehr *et al.* 2006). We have performed a combination of molecular dynamic simulation, NMR-spectroscopy, and X-ray crystallography to thoroughly characterize the ligand binding. Our NMR titrations provide a detailed picture of how the active site and the overall structure are related to each other. At pH 6·8, deprotonation of Glu35 occurs, which inactivates the enzyme at this unusually high pKa value, and helices b (with Glu35) and d undergo a substantial repositioning as indicated by the mapping of pH titration effects in Fig. 2*c*. Because one of the first catalysis steps also involves the deprotonation of Glu35, these domain-wide structural changes are likely to modulate the continuation of the catalysis reaction. Together with earlier studies (Refaee *et al.* 2003; Young *et al.* 1994), our data indicate a general flexibility and lower stability of helix d, which can be affected by numerous factors, including sugar binding and temperature changes. The ability of lysozyme to exhibit complex responses to environmental changes is evidenced by the following observations: the titration effects observed for the proton probes on Glu35, Trp109 and Ala111; the line broadening of local motions that involve Trp109 and Ala111; the spatial neighborhood of these three residues, which allows for direct interactions; and the wide range of titrating resonances on helices b and d. These structural rearrangements appear to be strongly coupled to enzyme activation by the (de)protonation of Glu35.

The carbohydrate binding site of HL displays a strong structural plasticity. This fact agrees with earlier observations by NMR relaxation studies, that the binding of carbohydrates

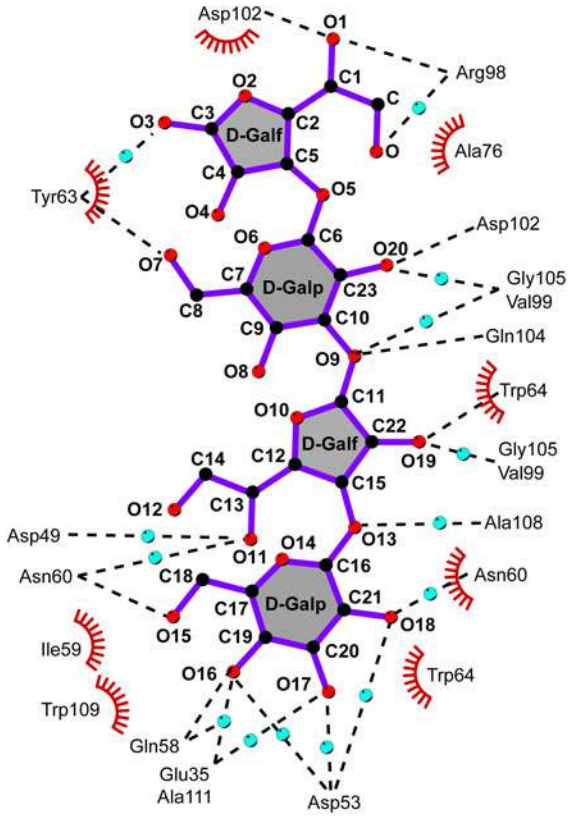

Fig. 6. Binding site of human lysozyme with bound tetrasaccharide **2**. The ligand is shown as a ball-and-stick representation; the bonds are indicated in purple. The protein residues are represented without side chains. Hydrogen bonds are shown as black dashed lines, and the spoked arcs represent protein residues that form hydrophobic interactions with the ligand. The cyan spheres indicate water molecules, which provide bridged hydrogen bonds between the ligand atoms and amino acid residues. The individual interactions are provided in online Table S3 of the Supplementary Information. The representation was derived from an analysis with LigPlot+ (Laskowski & Swindells, 2011).

to proteins is significantly determined by changes in conformational entropy (see for example Diehl *et al.* 2010). This may take various forms, for example of transient interactions such as water-bridged hydrogen bonds, or of changes in protein dynamics without observation of structural changes in crystal structures. Only a few amino acid residues are in direct hydrogen-bonding contact with the oligosaccharide chain. Most interactions are formed by hydrophobic contacts and particularly by water-mediated bridged hydrogen bonds. These latter two modes of interaction are less constraining and can be used to adopt binding environments for various ligands. The lectin-like ability of HL to interact with the O-chain of bacterial LPS highlights the strong possibility of a new role of HL in immune defense functions. This study may enable future developments of new and important therapeutic approaches to prevent and treat bacterial infections.

4.1 Speculation

The investigated lectin-like ability of HL to interact with the O-polysaccharide chain of bacterial LPS shows the possibility of an unknown glycan-guided mechanism of lysozyme's biological role. It underlies recognition of the bacterial cell wall by lysozyme and may complement its known immune defense functions. Further investigation of carbohydrate specificity of lysozyme with the use of larger linear and branched oligosaccharide ligands related to the O-chain of *K. pneumoniae* O1 as well as of antigenic polysaccharides of others bacterial pathogens may show the scope and limitations of the studied phenomenon.

Supplementary material

The supplementary material for this article can be found at https://doi.org/10.1017/S0033583517000075.

Acknowledgements

The Swedish NMR Centre is acknowledged for supplying instrument time and support. Diffraction data were collected on a P14 operated by EMBL at the PETRAIII storage ring (Hamburg, Germany). We are grateful to the beamline staff for providing assistance in using the beamline. We thank Dr Timothy Weaver (Cincinnati Children's Hospital Medical Center, Cincinnati, USA) for the provision of human recombinant lysozyme.

Financial support

This work was supported by the King Abdullah University of Science and Technology (grant KUK-11-008-23 awarded to B.N. with a Ph.D. position for L.W.) and the European Research Council (ERC-2008-AdG 227700 to B.N.). Beamtime on the P14 at the EMBL outstation in Hamburg was funded by a BioStruct-X grant. We thank the Sialic Acids Society for financial support. The synthetic portion of the work was supported by the RSF (grant 14-23-00199 to N.E.N.). A.D. would like to thank CSIR, Govt. of India for senior research fellowship.

Conflict of interest

None

References

Adams, P. D., Afonine, P. V., Bunkóczi, G., Chen, V. B., Davis, I. W., Echols, N., Headd, J. J., Hung, L.-W., Kapral, G. J., Grosse-Kunstleve, R. W., McCoy, A. J., Moriarty, N. W., Oeffner, R., Read, R. J., Richardson, D. C., Richardson, J. S., Terwilliger, T. C. & Zwart, P. H. (2010). PHENIX: a comprehensive Python-based system for macromolecular structure solution. *Acta*

Crystallographica Section D: Biological Crystallography **66**(2), 213–221.

Akinbi, H. T., Epaud, R., Bhatt, H. & Weaver, T. E. (2000). Bacterial killing is enhanced by expression of lysozyme in the lungs of transgenic mice. *Journal of Immunology* **165**, 5760–5766.

Bartels, C., Xia, T. H., Billeter, M., Güntert, P. & Wüthrich, K. (1995). The program XEASY for computer-supported NMR spectral analysis of biological macromolecules. *Journal of Biomolecular NMR* **6**, 1–10.

Bhunia, A., Vivekanandan, S., Eckert, T., Burg-Roderfeld, M., Wechselberger, R., Romanuka, J., Bächle, D., Kornilov, A. V., von der Lieth, C.-W., Jiménez-Barbero, J., Nifantiev, N. E., Schachner, M., Sewald, N., Lütteke, T., Gabius, H.-J. & Siebert, H.-Ch. (2010). Why structurally different cyclic peptides can be glycomimetics of the HNK-1 carbohydrate antigen. *Journal of the American Chemical Society* **132**, 96–105.

Boehr, D. D., McElheny, D., Dyson, H. J. & Wright, P. E. (2006) The dynamic energy landscape of dihydrofolate reductase catalysis. *Science* **313**, 1638–1642.

Chipman, D. M. & Sharon, N. (1969). Mechanism of lysozyme action. *Science* **165**, 454–465.

Claridge, T. (2009). Software review of MNova: NMR data processing, analysis, and prediction software. *Journal of Chemical Information and Modeling* **49**, 1136–1137.

Delaglio, F., Grzesiek, S., Vuister, G. W., Zhu, G., Pfeifer, J. & Bax, A. D. (1995). NMRPipe: a multidimensional spectral processing system based on UNIX pipes. *Journal of Biomolecular NMR* **6**, 277–293.

DeLano, W. L. (2002). The PyMOL molecular graphics system. (DeLano Scientific, San Carlos, California, USA, 2002). http://www.pymol.org.

Diehl, C., Engström, O., Delaine, T., Håkansson, M., Genheden, S., Modig, K., Leffler, H., Ryde, U., Nilsson, U. J. & Akke, M. (2010). Protein flexibility and conformational entropy in ligand design targeting the carbohydrate recognition domain of galectin-3. *Journal of the American Chemical Society* **132**, 14577–14589.

Emsley, P., Lohkamp, B., Scott, W. G. & Cowtan, K. (2010). Features and development of Coot. *Acta Crystallographica Section D: Biological Crystallography* **66**, 486–501.

Enani, M. A. (2015). Antimicrobial resistance. Insights from the declaration of world alliance against antibiotic resistance. *Saudi medical Journal* **36**, 11–12.

Enani, M. A. & El-Khizzi, N. A. (2012). Community acquired *Klebsiella pneumoniae*, K1 serotype. Invasive liver abscess with bacteremia and endophthalmitis. *Saudi medical Journal* **33**, 782–786.

Gupta, A. (2002). Hospital-acquired infections in the neonatal intensive care unit-*Klebsiella pneumoniae*. *Seminars in Perinatology* **26**, 340–345.

Harata, K., Abe, Y. & Muraki, M. (1998). Full-matrix least-squares refinement of lysozymes and analysis of anisotropic thermal motion. *Proteins: Structure, Function, and Bioinformatics* **30**, 232–243.

Kabsch, W. (2010). Integration, scaling, space-group assignment and post-refinement. *Acta Crystallographica Section D: Biological Crystallography* **66**(2), 133–144.

Kar, R. K., Gazova, Z., Bednarikova, Z., Mroue, K. H., Ghosh, A., Zhang, R., Ulicna, K., Sieber, H.-Ch., Nifantiev, N. E. & Bhunia, A. (2016). Evidence for Inhibition of lysozyme amyloid fibrillization by peptide fragments from human lysozyme: a combined spectroscopy, microscopy, and docking study. *Biomacromolecules* **17**, 1998–2009.

Koradi, R., Billeter, M. & Wüthrich, K. (1996). MOLMOL: a program for display and analysis of macromolecular structures. *Journal of Molecular Graphics* **14**, 51–55.

Krylov, V. B., Argunov, D. A., Vinnitskiy, D. Z., Gerbst, A. G., Ustyuzhanina, N. E., Dmitrenok, A. S. & Nifantiev, N. E. (2016). The pyranoside-into-furanoside rearrangement of alkyl glycosides: scope and limitations. *Synlett* **27**, 1659–1664.

Krylov, V. B., Argunov, D. A., Vinnitskiy, D. Z., Verkhnyatskaya, S. A., Gerbst, A. G., Ustyuzhanina, N. E., Dmitrenok, A. S., Huebner, J., Holst, O., Siebert, H.-Ch & Nifantiev, N. E. (2014). Pyranoside-into-furanoside rearrangement: new reaction in carbohydrate chemistry and its application in oligosaccharide synthesis. *Chemistry–A European Journal* **20**, 16516–16522.

Kuramitsu, S., Ikeda, K., Hamaguchi, K., Fujio, H., Amano, T., Shiro, M. I. W. A. & Nishina, T. (1974). Ionization constants of Glu 35 and Asp 52 in hen, turkey, and human lysozymes. *Journal of Biochemistry* **76**, 671–683.

Laskowski, R. A. & Swindells, M. B. (2011). LigPlot+: multiple ligand–protein interaction diagrams for drug discovery. *Journal of Chemical Information and Modeling* **51**, 2778–2786.

Lee-Huang, S., Maiorov, V., Huang, P. L., Ng, A., Lee, H. C., Chang, Y. T., Kallenbach, N., Huang, P. L. & Chen, H. C. (2005). Structural and functional modeling of human lysozyme reveals a unique nonapeptide, HL9, with anti-HIV activity. *Biochemistry* **44**, 4648–4655.

Lütteke, T., Frank, M. & von der Lieth, C. W. (2005). Carbohydrate structure suite (CSS): analysis of carbohydrate 3D structures derived from the PDB. *Nucleic Acids Research* **33**, D242–D246.

Markart, P., Korfhagen, T. R., Weaver, T. E. & Akinbi, H. T. (2004). Mouse lysozyme M is important in pulmonary host defense against *Klebsiella pneumoniae* infection. *American Journal of Respiratory and Critical Care Medicine* **169**, 454–458.

Masschalck, B. & Michiels, C. W. (2003). Antimicrobial properties of lysozyme in relation to foodborne vegetative bacteria. *Critical Reviews in Microbiology* **29**, 191–214.

Muraki, M., Harata, K., Sugita, N. & Sato, K. I. (1996). Origin of carbohydrate recognition specificity of human lysozyme revealed by affinity labeling. *Biochemistry* **35**, 13562–13567.

Murshudov, G. N., Skubák, P., Lebedev, A. A., Pannu, N. S., Steiner, R. A., Nicholls, R. A., Winn, M. D., Long, F. & Vagin, A. A. (2011). REFMAC5 for the refinement of macromolecular crystal structures. *Acta Crystallographica Section D: Biological Crystallography* **67**, 355–367.

Ohno, N. & Morrison, D. C. (1989*a*). Lipopolysaccharide interactions with lysozyme differentially affect lipopolysaccharide immunostimulatory activity. *European Journal of Biochemistry* **186**, 629–636.

Ohno, N. & Morrison, D. C. (1989*b*). Lipopolysaccharide interaction with lysozyme. Binding of lipopolysaccharide to lysozyme and inhibition of lysozyme enzymatic activity. *Journal of Biological Chemistry* **264**, 4434–4441.

Osserman, E. F., Klockars, M. A. T. T. I., Halper, J. A. M. E. S. & Fischel, R. E. (1973). Effects of lysozyme on normal and transformed mammalian cells. *Nature* **243**, 331–335.

Refaee, M., Tezuka, T., Akasaka, K. & Williamson, M. P. (2003). Pressure-dependent changes in the solution structure of hen egg-white lysozyme. *Journal of Molecular Biology* **327**, 857–865.

Rojas-Macias, M. A. & Lütteke, T. (2015). Statistical analysis of amino acids in the vicinity of carbohydrate residues performed by GlyVicinity. *Methods in Molecular Biology* **1273**, 215–226.

Shin, H. J., Lee, H., Park, J. D., Hyun, H. C., Sohn, H. O., Lee, D. W. & Kim, Y. S. (2007). Kinetics of binding of LPS to recombinant CD14, TLR4, and MD-2 proteins. *Molecules and Cells* **24**, 119–124.

Siwicki, A. K., Klein, P., Morand, M., Kiczka, W. & Studnicka, M. (1998). Immunostimulatory effects of dimerized lysozyme (KLP-602) on the nonspecific defense mechanisms and protection against furunculosis in salmonids. *Veterinary Immunology and Immunopathology* **61**, 369–378.

Song, H., Inaka, K., Maenaka, K. & Matsushima, M. (1994). Structural changes of active site cleft and different saccharide binding modes in human lysozyme co-crystallized with hexa-N-acetyl-chitohexaose at pH 4·0. *Journal of Molecular Biology* **244**, 522–540.

Travis, S. M., Conway, B. A. D., Zabner, J., Smith, J. J., Anderson, N. N., Singh, P. K., Greenberg, E. P. & Welsh, M. J. (1999). Activity of abundant antimicrobials of the human airway. *American Journal of Respiratory Cell and Molecular Biology* **20**, 872–879.

Tsvetkov, Y. E., Burg-Roderfeld, M., Loers, G., Ardá, A., Sukhova, E. V., Khatuntseva, E. A., Grachev, A. A., Chizhov, A. O., Siebert, H.-Ch., Schachner, M., Jiménez-Barbero, J. & Nifantiev, N. E. (2012). Synthesis and molecular recognition studies of the HNK-1 trisaccharide and related oligosaccharides. The specificity of monoclonal anti-HNK-1 antibodies as assessed by surface plasmon resonance and STD NMR. *Journal of the American Chemical Society* **134**, 426–435.

Ulrich, E. L., Akutsu, H., Doreleijers, J. F., Harano, Y., Ioannidis, Y. E., Lin, J., Livny, M., Mading, S., Maziuk, D., Miller, Z., Nakatani, E., Schulte, C. F., Tolmie, D. E., Wenger, R. K., Yao, H. & Markley, J. L. (2008). BioMagResBank. *Nucleic Acids Research* **36**, D402–D408.

Vagin, A. & Teplyakov, A. (1997). MOLREP: an automated program for molecular replacement. *Journal of Applied Crystallography* **30**, 1022–1025.

Verkhnyatskaya, S. A., Krylov, V. B. & Nifantiev, N. E. (2017). Pyranoside-into-furanoside rearrangement of 4-pentenyl glycoside in the synthesis of tetrasaccharide related to galactan I of *Klebsiella pneumoniae*. *European Journal of Organic Chemistry* **2017**, 710–718.

Vranken, W. F., Boucher, W., Stevens, T. J., Fogh, R. H., Pajon, A., Llinas, M., Ulrich, E. L., Markley, J. L., Ionides, J. & Laue, E. D. (2005). The CCPN data model for NMR spectroscopy: development of a software pipeline. *Proteins: Structure, Function, and Bioinformatics* **59**, 687–696.

Winn, M. D., Ballard, C. C., Cowtan, K. D., Dodson, E. J., Emsley, P., Evans, P. R., Keegan, R. M., Krissinel, E. B., Leslie, A. G. W., McCoy, A., McNicholas, S. J., Murshudov, G. N., Pannu, N. S., Potterton, E. A., Powell, H. R., Read, R. J., Vagin, A. & Wilson, K. S. (2011). Overview of the CCP4 suite and current developments. *Acta Crystallographica Section D: Biological Crystallography*, **67**, 235–242.

Young, A. C., Tilton, R. F. & Dewan, J. C. (1994). Thermal expansion of hen egg-white lysozyme: comparison of the 1·9 Å resolution structures of the tetragonal form of the enzyme at 100 K and 298 K. *Journal of Molecular Biology*, **235**, 302–317.

Young, N. M., Gidney, M. A. J., Gudmundsson, B. E., MacKenzie, C. R., To, R., Watson, D. C. & Bundle, D. R. (1999). Molecular basis for the lack of mimicry of Brucella polysaccharide antigens by Ab2γ antibodies. *Molecular Immunology* **36**, 339–347.

Zhang, R., Eckert, T., Lutteke, T., Hanstein, S., Scheidig, A. J., Bonvin, A., Nifantiev, N. E., Kozar, T., Schauer, R., Enani, M. A. & Siebert, H. C. (2016). Structure-function relationships of antimicrobial peptides and proteins with respect to contact molecules on pathogen surfaces. *Current Topics in Medicinal Chemistry* **16**, 89–98.

ACS OMEGA

Article

Cite This: ACS Omega 2019, 4, 4206−4220

http://pubs.acs.org/journal/acsodf

Nanomedical Relevance of the Intermolecular Interaction Dynamics—Examples from Lysozymes and Insulins

Ruiyan Zhang,[†,‡,§] Ning Zhang,[†] Marzieh Mohri,[‡] Lisha Wu,[∥] Thomas Eckert,[⊥,#] Vadim B. Krylov,[▽] Andrea Antosova,[○] Slavomira Ponikova,[○] Zuzana Bednarikova,[○] Philipp Markart,[◆,¶] Andreas Günther,[◆] Bengt Norden,[∥] Martin Billeter,[⋈] Roland Schauer,[⋈] Axel J. Scheidig,[§] Bhisma N. Ratha,[⧖] Anirban Bhunia,[⧖] Karsten Hesse,[●] Mushira Abdelaziz Enani,[¤] Jürgen Steinmeyer,[☼] Athanasios K. Petridis,[◎] Tibor Kozar,[◑] Zuzana Gazova,[○] Nikolay E. Nifantiev,[▽] and Hans-Christian Siebert*[,‡]

[†]Institute of Biopharmaceutical Research, Liaocheng University, Liaocheng 252059, P. R. China

[‡]RI-B-NT Research Institute of Bioinformatics and Nanotechnology, Franziusallee 177, 24148 Kiel, Germany

[§]Institute of Zoology, Department of Structural Biology, Christian-Albrechts-University, Am Botanischen Garten 1-9, 24118 Kiel, Germany

[∥]Department of Chemical and Biological Engineering, Chalmers University of Technology, 41296 Gothenburg, Sweden

[⊥]Department of Chemistry and Biology, University of Applied Sciences Fresenius, Limburger Str. 2, 65510 Idstein, Germany

[#]Institut für Veterinärphysiolgie und Biochemie, Fachbereich Veterinärmedizin, Justus-Liebig-Universität Gießen, Frankfurter Str. 100, 35392 Gießen, Germany

[▽]Laboratory of Glycoconjugate Chemistry, N.D. Zelinsky Institute of Organic Chemistry, Russian Academy of Sciences, Leninsky prospect 47, 119991 Moscow, Russian Federation

[○]Department of Biophysics Institute of Experimental Physics, Slovak Academy of Sciences, Watsonova 47, 04001 Kosice, Slovakia

[◆]Medical Clinic II, Justus-Liebig-University, Klinikstraße 33, 35392 Giessen, Germany

[¶]Pneumology, Heart-Thorax-Center Fulda, Pacelliallee 4, 36043 Fulda, Germany

[⋈]Department of Chemistry and Molecular Biology, University of Gothenburg, 40530 Gothenburg, Sweden

[⋈]Institute of Biochemistry, Christian-Albrechts-University, Olshausenstrasse 40, 24098 Kiel, Germany

[⧖]Biomolecular NMR and Drug Design Laboratory, Department of Biophysics, Bose Institute, P-1/12 CIT Scheme VII (M), 700054 Kolkata, India

[●]Tierarztpraxis Dr. Karsten Hesse, Rathausstraße 16, 35460 Stauffenberg, Germany

[¤]Infectious Diseases Division, Department of Medicine, King Fahad Medical City, P.O. Box 59046, 11525 Riyadh, Kingdom of Saudi Arabia

[☼]Laboratory for Experimental Orthopaedics, Department of Orthopaedics, Justus-Liebig-University, Paul-Meimberg-Str. 3, D-35392 Giessen, Germany

[◎]Neurochirurgische Klinik, Universität Düsseldorf, Geb. 11.54, Moorenstraße 5, 40255 Düsseldorf, Germany

[◑]Center for Interdisciplinary Biosciences, TIP-UPJS, Jesenna 5, 04001 Kosice, Slovakia

Supporting Information

ABSTRACT: Insulin and lysozyme share the common features of being prone to aggregate and having biomedical importance. Encapsulating lysozyme and insulin in micellar nanoparticles probably would prevent aggregation and facilitate oral drug delivery. Despite the vivid structural knowledge of lysozyme and insulin, the environment-dependent oligomerization (dimer, trimer, and multimer) and associated structural dynamics remain elusive. The knowledge of the intra- and intermolecular interaction profiles has cardinal importance for the design of encapsulation protocols. We

continued...

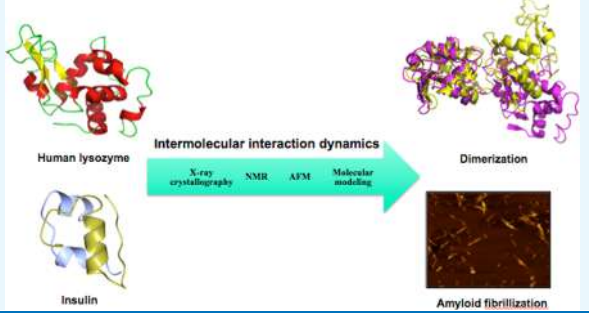

Received: September 21, 2018
Accepted: November 28, 2018
Published: February 27, 2019

DOI: 10.1021/acsomega.8b02471
ACS Omega 2019, 4, 4206−4220

have employed various biophysical methods such as NMR spectroscopy, X-ray crystallography, Thioflavin T fluorescence, and atomic force microscopy in conjugation with molecular modeling to improve the understanding of interaction dynamics during homo-oligomerization of lysozyme (human and hen egg) and insulin (porcine, human, and glargine). The results obtained depict the atomistic intra- and intermolecular interaction details of the homo-oligomerization and confirm the propensity to form fibrils. Taken together, the data accumulated and knowledge gained will further facilitate nanoparticle design and production with insulin or lysozyme-related protein encapsulation.

INTRODUCTION

Several natural and synthetic proteins of pharmacological importance (including, but not limited to, lysozyme and insulin) are prone to aggregation into insoluble polymeric fibrils, a biologically and industrially unwanted feature. To extend the long-term usability of pharmacologically significant proteins, their inactivation caused by unfolding and/or aggregation needs to be minimized. As lysozyme and insulin are well-established protein drugs, these can serve as model components to study conditions that could help stabilize proteins and prevent them from aggregation. Formation of lysozyme (muramidase)[1−3] or insulin complexes[4−6] into higher aggregates or fibrils, but also their occurrence in native states, needs to be studied by a combination of biochemical and biophysical techniques to shed light into the mechanism of amyloid formation. Protein misfolding and consequent aggregation are associated with more than 20 diseases.[7] Although a significant amount of work has been conducted to study the amyloid-related problems of living organisms, neither the mechanisms of fibril creation nor some ways of their disruption are fully understood yet. What is assumed nowadays is that inter- and intramolecular interactions could play the decisive role for amyloidogenic processes. Both insulin and lysozyme belong to the group of amyloidogenic proteins. There are currently several commercial variations of insulin available: synthetic human insulin (e.g., Actrapid, Lispro), porcine insulin (Caninsulin), and glargine insulins (Lantus, Abasaglar, Glaritus, and Basalog) in which one amino acid is replaced and two Arg residues are added. Beside these variations, in the case of the glargine insulins, different expression vectors (*Escherichia coli* for Lantus and Abasaglar, and yeast for Glaritus and Basalog) are used and lead to minor conformational differences. This fact has to be carefully considered when insulin structural data sets are compared. Variations in the production and formulation processes can be correlated with alterations in structure and dynamics of the proteins under study. Glycosylation impurities have been described for the glargine insulins (Glaritus and Basalog) that are expressed in yeasts.[4−6,8] Such kind of glycosylation that does not occur in standard insulins may influence their structural properties, for example, the aggregation behavior of these glargine biosimilars, but could also enhance their lifetime as it is in the case of naturally occurring glycosylated hormones such as erythropoietin.[9] However, this kind of insulin glycosylation has to be considered as impurity since it does not occur at all in glargine insulin (Glaritus and Basalog) molecules in a homogenous way. Glargine insulin is a human insulin analog, with three amino acid difference. In the A-chain of glargine insulin, Asn at position 21 is mutated to Gly. In the B-chain of glargine insulin, two Arg residues at positions 31 and 32 are added. Recently, Hermanns et al.[10] discussed the clinical impact of such modifications on diabetes therapies. In the synthetic insulin Lispro (marketed by Eli Lilly as Humalog), the penultimate lysine and proline residues on the C-terminal end of the B-chain are reversed in comparison to human insulin. This small modification in the primary sequence does not influence the receptor binding but blocks the formation of dimers and hexamers.[11,12] This has a significant impact on bioavailability since Lispro is active immediately. In comparison to our biophysical studies on insulin variants (human or porcine insulin vs the long-acting synthetic glargine insulin Lantus, Abasaglar, Glaritus, or Basalog), the corresponding physical parameters for larger proteins with similar clinical relevance, that is, lysozyme (here human lysozyme (HL) and hen egg white lysozyme (HEWL)), could be obtained.

Lysozyme has been used for years as a model for amyloid aggregation.[13] Recently, we have reported the ability of lysozymes to specifically bind certain sections from the carbohydrate part of lipopolysaccharide (LPS) from *Klebsiella pneumoniae*.[14] Nonionic detergents can also easily interact with amino acids of the amyloidogenic region of HEWL of the lysozyme,[15] affecting thus the amyloid fibrillization that can also be inhibited by phospholipids.[16] Furthermore, the effects of detergents[17] and natural products[18,19] on insulin and lysozyme aggregation and lysozyme and insulin antiamyloid structure−function screening of small libraries[20] have been reported recently.

Analysis of the corresponding intermolecular interactions is of importance also for the design of target-directed nanoparticles because the carbohydrate recognition part of the protein can be regarded as an intrinsic anchor unit for cell-surface-exposed contact structures. The surface properties (e.g., the electrostatic surface potentials) of the two lysozymes under study (HL and HEWL) due to several variances in the amino acid sequences differ from each other. These differences can be correlated with the aggregation/fibrillization behavior of the two lysozyme species—HL and HEWL. It has to be emphasized that for both classes of biomolecules (insulins and lysozymes), new data with respect to the aggregation dynamics can be achieved when the arsenal of biophysical techniques is applied in a way that all processes on the submolecular and in the case of ion involvement are considered. Similar to the aggregation behavior of glargine insulins also in the case of the lysozymes under study Arg residues and the corresponding charges play a crucial role in both dimer and multimer formations. Knowledge about all crucial details in relation to the structural stability under different physical and chemical conditions is essential for the optimal clinical application of encapsulated protein drugs. In the case of the encapsulation of small organic compounds that are used, for example, as antipsychotic drugs, it is of relevance to analyze their structural behavior at a high precision level using ab initio calculations.[21−23] The requirements to utilize quantum chemical approaches relate to hindered rotations in partial double bonds that are often occurring in medications that are used as therapeutics against schizophrenia and other psychotic diseases.[24] Also in the case of larger drugs, one has to proceed in a similar way when these compounds have to be encapsulated in target-directed nanoparticles.[25−27] Accordingly, we centered our attention on studies of the structure, aggregation, and intermolecular interaction profiles of these proteins and on

DOI: 10.1021/acsomega.8b02471
ACS Omega 2019, 4, 4206−4220

Table 1. Different Crystal Forms of Human Lysozyme under Different Crystallization Conditions

	crystallization condition			unit cell dimension				
				a	*b*	*c* (Å)		
crystal ID	pH	buffer	temperature (K)	*α*	*β*	*γ*	space group	subunit number/asymmeric unit
Hlys #1	4.4	25 mM NaOAc	291	33.22	56.12	60.95	*P*212121	1
		0.8 M NaCl		90.00	90.00	90.00		
Hlys #2	5.8	50 mM Na citrate	291	42.84	63.93	109.81	*P*212121	2
		0.8 M NaCl		90.00	90.00	90.00		
ref #1 (PBD:1LZS)	4.0	30 mM sodium phosphate	277	32.53	46.99	162.25	*P*212121	2
		1.8 M NaCl		90.00	90.00	90.00		
ref #2 (PBD:1LZR)	6.0	30 mM sodium phosphate	286	34.01	56.51	60.91	*P*212121	1
		2.5 M NaCl		90.00	90.00	90.00		

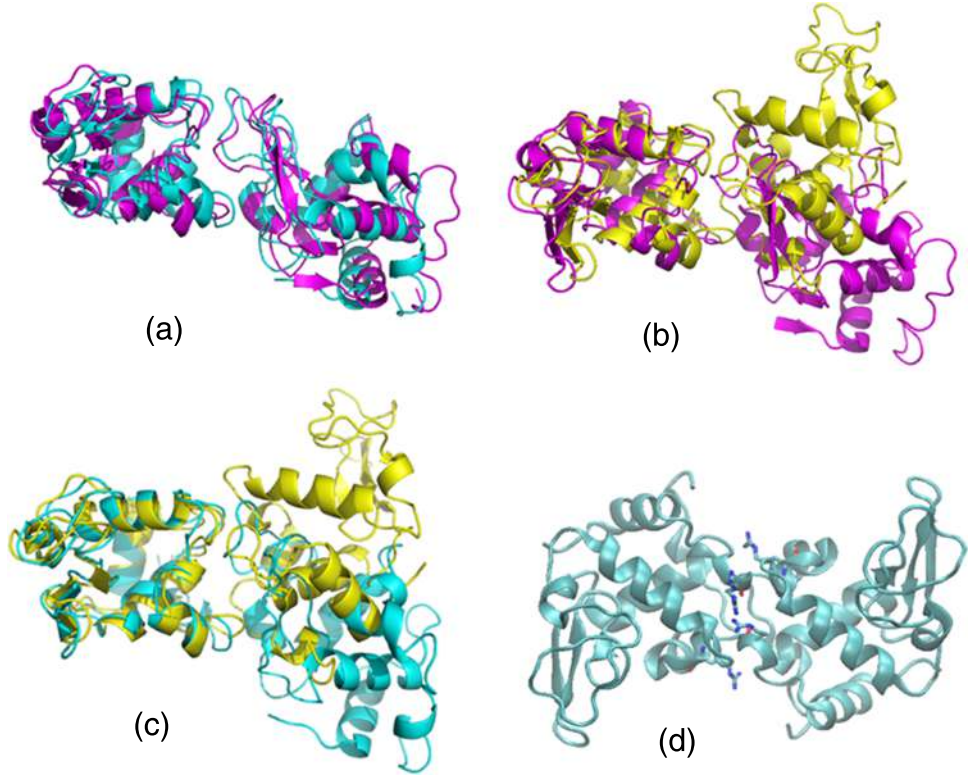

Figure 1. Superposition of (a) HL structure from molecular modeling (modeled dimeric arrangement, cyan) and crystal structure of HL, crystallized at pH 4 (obtained from PDB—1lzs.pdb;[32] purple). (b) Homodimeric model structure of HL, crystallized at a pH value of 5.8 (yellow) and the 1lzs.pdb—crystal structure (purple). (c) Homodimeric model structure of HL (yellow) and modeled dimeric arrangement of HL (cyan). (d) Crucial arginine residues at the interfaces of both monomers (Arg21, Arg107) are highlighted by a licorice presentation.

possibilities to encapsulate them into lipid nanoparticle carriers. In the case of an effective oral peptide/protein drug delivery, it is essential that so-called absorption enhancers enable an efficient transfer from the gastrointestinal tract to the bloodstream. Therefore, the drug-containing nanoparticles and the target cell in the intestine have to interact in a specific way. As the target molecules of these nanoparticles, cell-surface-exposed carbohydrate structures such as sialic acids[14,27−31] will be our main focus. We selected insulin and lysozyme as two well-characterized proteins in combination with a set of biophysical techniques to perform an exemplary study for protein stability and optional forms of drug delivery.

RESULTS AND DISCUSSION

X-ray Crystallography Assay and Molecular Modeling Analysis. By variation of crystallization conditions for the structure determination of HL in complex with a tetrasaccharide,[14] we have obtained crystals of HL with one lysozyme molecule per asymmetric unit (monomeric form) and crystals with two lysozyme molecules per asymmetric unit (dimeric form), as shown in Table 1 (Hlys #1 and Hlys #2, respectively). The arrangement of the two lysozyme molecules within this dimeric form differs significantly from the dimeric arrangement as predicted based on monomeric lysozyme by molecular modeling approaches as described before (Figure 1a−c). In addition, we have not found further evidence for these in silico results when human lysozyme has been analyzed with NMR methods at different pH values since monomers seem to be the preferred state.

Ten different insulin clusters resulted from Haddock 2.2 dimer simulation. Energy optimization was carried out on all of these dimers using the Hyperchem 8.0 program to assess the energetically most favorable structure. Table 2 summarizes the results from this minimization.

DOI: 10.1021/acsomega.8b02471
ACS Omega 2019, 4, 4206−4220

Table 2. Hyperchem Energy Evaluation of the Insulin Dimeric Clusters

cluster	energy in kcal/mol
1	1467.3
2	1478.6
3	1481.0
4	1481.7
5	1488.1
6	1491.7
7	1493.0
8	1500.2
9	1502.9
10	1506.7

Protein dimer 1 corresponds to the crystal structure 1lzs.pdb. The other dimeric structures exhibit only a few kcal/mol higher energy. Molecular dynamics (MD) simulations were performed to evaluate the possible existence of the dimeric forms under physiological conditions. Protein dimer 1 as well as the protein dimer from the crystal structure 1lzs.pdb were stable at pH = 7.4 at 298 K in physiological saline solution for 10 ns and showed only little fluctuations during the simulation. Accordingly, we can assume that the human lysozyme may exist in dimeric form under physiological conditions.

In the case of the insulins under study (human insulin, Actrapid/Lispro; porcine insulin, Caninsulin; and the synthetic long-acting glargine insulins), higher aggregates were not detected by NMR under the chosen measurement conditions. However, structural data sets based on X-ray or neutron diffraction experiments are available in the protein data bank: 3w7y.pdb, 1mso.pdb, and 3fhp.pdb.

Thioflavin T (ThT) Fluorescence Assay and Atomic Force Microscopy (AFM) Analysis. Comparing fibril formations of HL and HEWL using ThT assay, significant differences were observed in kinetics of fibrillization and amount of amyloid fibril aggregates (Figure 2). The time dependences of amyloid fibril formation determined for hen (red circles, HEWL) and human (blue triangles, HL) lysozymes (10 μM) differ in the lag phase, slope of the elongation phase, and value of plateau phase corresponding to the fibril mass. The formation of non-native states of lysozyme required for amyloid fibrillization that is occurring during lag phase was significantly prolonged in the case of human lysozyme with lag phase about 28 min. Hen egg white lysozyme form these species under 10 min. The overall time for formation of mature fibrils was also different—about 50 min for HL and 20 min for HEWL to achieve plateau for the fluorescence intensities. The observed kinetic characteristics of HL and HEWL fibrillization are summarized in Table 3. The lower fluorescence intensities of the plateau phase (10 000 au) for HL compare to HEWL (70 000 au), suggesting formation of a lower amount of fibrillar structure or their association to bigger clusters.

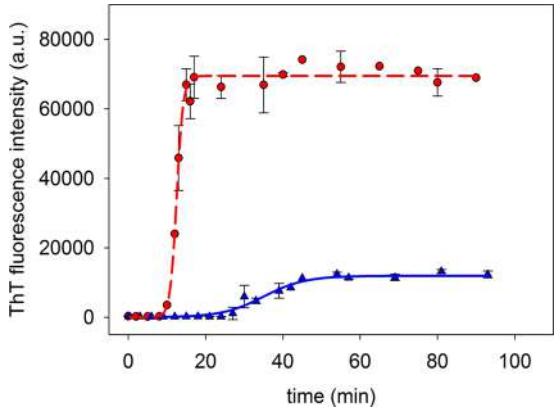

Figure 2. Time dependences of amyloid fibril formation determined for hen egg white (red circles) and human (blue triangles) lysozyme (10 μM). The aliquots were selected at given time intervals, and the extent of lysozyme fibrillization was monitored by Thioflavin T (ThT) fluorescence assay (20 μM, ThT). The error bars represent the average deviation for repeated measurements of three separate samples. The curves were obtained by fitting of the average values by a nonlinear least-square method using Sigmoidal curve-parameter 4 in SigmaPlot software. The times of about 50 min (HL) and 20 min (HEWL) correspond to the plateau for the fluorescence intensities.

Atomic Force Microscopy (AFM) is an important technique for visualization of amyloid aggregates. The obtained AFM images of lysozyme aggregates (Figure 3 a,b) confirmed the ThT results.

These two complementary methods were also used for a detailed analysis of insulin fibril formation. Differences between fibril formation of human insulin and glargine insulin using ThT assay are still detectable (Figure 4) but not so obvious as in the case of lysozymes (Figure 2). Fibril formation of both types of insulin follows the nucleation polymerization model. The modified amino acid chain of the glargine insulin does not lead to stronger alterations when comparing glargine with human insulin during the fibril-formation process; however, insulin Basalog (blue triangles) has a longer lag phase (4.5 min) when compared to human insulin t_{lag} equal to 1.5 min (green triangles). The differences in other kinetic parameters ($t_{1/2}$, $t_{plateau}$, and I_{fluo}max) are not so significant and are presented in Table 3.

After 2 h, the morphologies of human insulin and glargine insulin fibrils visualized using the AFM technique show small but characteristic differences (Figure 5a,b). Glargine insulin (Figure 5b) forms unbranched fibrils that are thinner than fibrils of human insulin (Figure 5a).

Next, we tested with NMR methods whether critical parameters of the insulins and lysozyme for further structural comparison can be obtained under physiological conditions.

NMR Results—Analyses of Human, Porcine, and Glargine Insulins as well as Human Lysozyme from Transgenic Cow. We have found that it is possible to record NMR spectra of insulin drugs taken directly from the injection pen (Figure 6a,b). Large excipient signals were detected, but they do not disturb our structural analysis of the compounds itself in a significant way. The two one-dimensional (1D) NMR spectra Figure 6a (top, bottom) show Abasaglar glargine probes from two different charges, which were stored in a slightly different way. One probe was stored permanently in the refrigerator; the other one was stored for one night outside the refrigerator at room temperature. The 1D spectra of the two probes are completely identical and can therefore not be discriminated although the injection pens have been treated under different cooling conditions. Also in the corresponding nuclear Overhauser enhancement (NOESY) spectra (Figure 6b), no differences were detected. It turned out that especially the NOESY spectra of Abasaglar glargine insulin can be evaluated despite the strong excipient signals in a sufficient way.

Contrary to the Abasaglar insulin probes that were taken directly from the injection pen, all signals of the human lysozyme extracted from the milk of transgenic cow belong to the protein

DOI: 10.1021/acsomega.8b02471
ACS Omega 2019, 4, 4206−4220

Table 3. Kinetic Parameters of Insulin and Lysozyme Amyloid Fibrillization

kinetic parameters	HL	HEWL	human insulin	glargine insulin
lag-time (t_{lag}) (min)	28 ± 0.4	10 ± 0.3	1.5 ± 0.1	4.5 ± 0.2
half-time ($t_{1/2}$) (min)	29 ± 0.6	13 ± 0.2	6.2 ± 0.3	8.2 ± 0.2
I_{fluo}max (au)	10 000 ± 100	70 000 ± 200	47 000 ± 150	55 000 ± 200
$t_{plateau}$ (min)	50 ± 0.2	20 ± 0.1	6.8 ± 0.2	11.4 ± 0.6

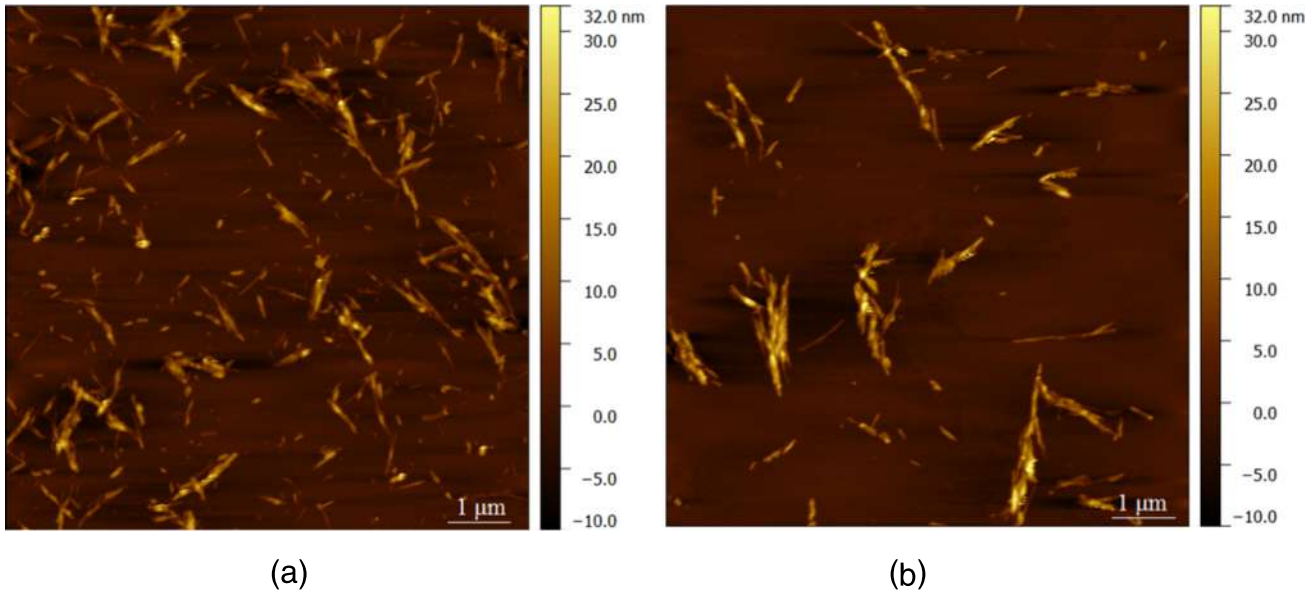

Figure 3. AFM images of (a) human lysozyme (HL) and (b) hen egg white lysozyme (HEWL) amyloid fibrils confirm the (ThT) fluorescence assay results by another biophysical technique in an independent way.

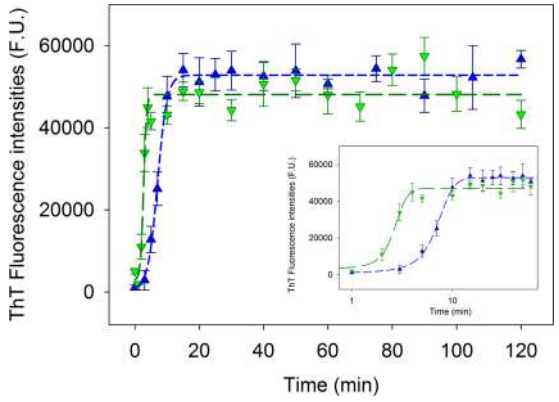

Figure 4. Time dependences of amyloid fibril formation determined for glargine insulin Basalog (blue triangles) and human insulin (green triangles) (10 μM). Left side, complete time period. Inset, time period of fibril formation between 1 and 15 min. The data were fitted with sigmoidal curve-parameter 4 with the equation: $y_0 + a/(1 + \exp(-(x - x_0)/b))$.

(Figure 7a). The NOESY (Figure 7b) and total correlation spectroscopy (TOCSY) (Figure 7c) were used to confirm that the human lysozyme analyzed from another source in a former study[14] and the human lysozyme extracted from the milk of transgenic cow do not differ from each other. With these data, it is now possible to discuss the intermolecular interaction dynamics for various insulins and lysozymes in detail.

An overlay of the 1D NMR spectrum glargine insulin Lantus (blue) with that of Glaritus (red) confirms the detected differences over the whole spectral range (Figure S1). An overlay of the two-dimensional (2D) NMR spectra of the glargine insulin Lantus (blue) with the glargine insulin Glaritus (red) shows differences, which concern the Asn18 residue in a certain spectral region (Figure S2). Furthermore, an extra peak has been detected in the case of the glargine insulin Glaritus (red) (Figure S2). It has to be emphasized here that the corresponding ligand−receptor complex does not show any involvement of Asn18 in receptor binding (Figure S3). Therefore, any potential modification at this position (e.g., glycosylation) will not have a significant impact on receptor binding.

The 1D NMR spectrum of the porcine insulin Caninsulin (MSD), which is presented in Figure S4, is a medication used for diabetes treatment in dogs. The amino acid sequence of Caninsulin is identical to pig (porcine) insulin. The Thr residue at position 30 in the B-chain is replaced by Ala in porcine insulin in comparison to human insulin. The sharp signals point to monomeric states of this insulin in the NMR tube.

Molecular Modeling Supported NMR Analyses of HL and HEWL Lysozymes in Comparison to Insulins. Owing to the complexity and robustness of nanoparticle delivery systems of protein drugs, it is essential to consider the complementarity of experimental and modeling data in the development of optimal encapsulation strategies. We combined at first the experimental and molecular modeling data that were obtained for lysozyme (HL and HEWL) (Figure 8a−f) and then compared them with the corresponding experimental and theoretical data gained for insulins (Figure 9a−e). The relation between pH values and lysozyme (HL and HEWL) structures is indicated by the overlay presentations shown in Figure 8c,d. When human lysozyme is encapsulated in nanoparticles for a therapeutic use, precise knowledge of the submolecular details

DOI: 10.1021/acsomega.8b02471
ACS Omega 2019, 4, 4206−4220

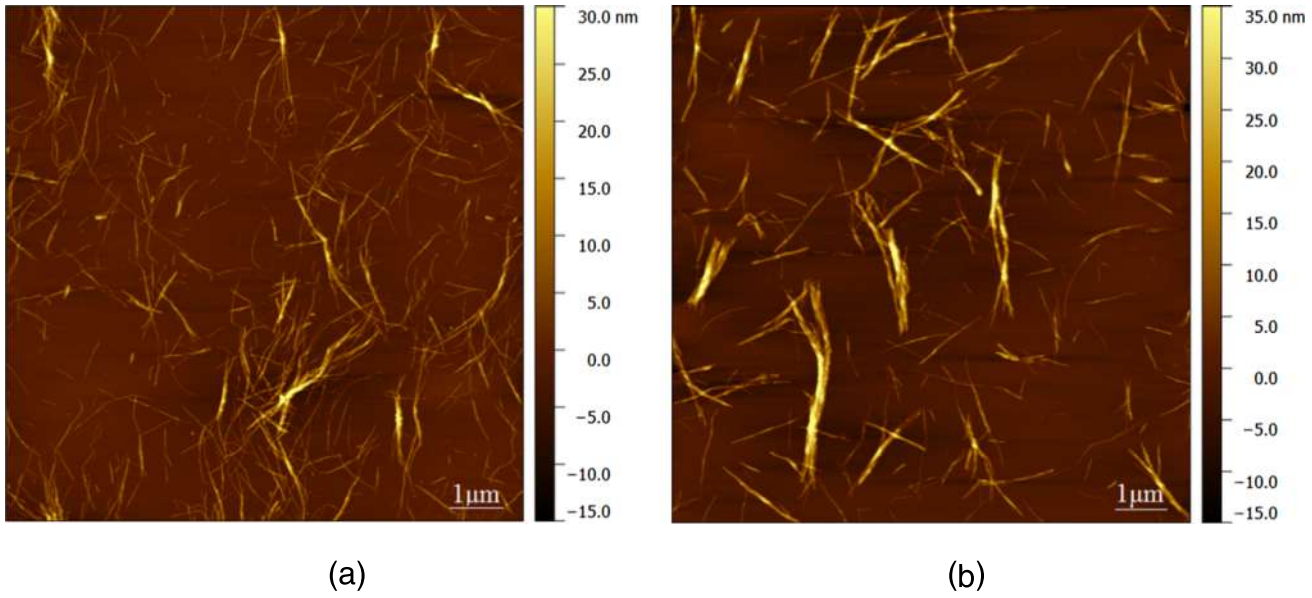

Figure 5. AFM images of 10 μM glargine insulin Basalog (a) and human insulin (b) after 2 h incubation at 65 °C with constant stirring (1200 rpm).

about its carbohydrate affinity[14] is of importance because this part of the molecule can be considered as a vital target unit. Three essential amino acids—Tyr63 (yellow), Arg98 (red), and Trp109 (blue)—are stabilizing the complex (5lsh.pdb), highlighted in Figure 8e. The surface presentation of the same complex shown in Figure 8f visualizes the shape of the carbohydrate recognition part of human lysozyme. The human lysozyme (Figure 8a–f) and insulin (Figure 9a–e) data are valuable references when MD simulations in micelles are considered and were performed for nanoparticles as indicated in Figure 10. The surface presentations of the glargine insulin Lantus (Figure 9a, monomer) and the porcine insulin Caninsulin (Figure 9b, monomer) including their electrostatic surface potentials can be compared with each other and taken as starting structures in our MD simulations. It is necessary to correlate the data sets describing dimeric forms of human insulin (3w7y.pdb, 1mso.pdb) and porcine insulin (3fhp.pdb) as presented in Figure 9c–e illustrating structural data of lysozymes.

Encapsulation of insulin into adequately sized liposome nanoparticles could facilitate optimal oral delivery of insulin while eliminating possible fibrillation processes in tissue around the injection areas. In silico methodologies were utilized to assess the nanoparticle size–insulin saturation relationships. Several differently sized liposome nanoparticles with diameters from around 35 nm up to approaching 120 nm were constructed using the PACKMOL[37] program. The number of non-hydrogen atoms of insulin needed for molecular dynamics (MD) simulations can be decreased by three quarters when employing the coarse-grained (CG) approach/representation of atoms. Several observations employing different-level CG modeling (both Monte Carlo and MD simulations) for insulins and lysozymes[38−47] were published recently. The total number of CG atoms in our case of glargine insulin is reduced to 95. Consequently, hundreds of insulin molecules can be easily modeled and encapsulated into differently sized liposomal nanoparticles. Figure 10 represents nine such models sized from 35 to 120 nm.

The structure of the 65 nm liposomal nanoparticle with embedded glargine insulins, as shown in Figure 11, was generated using the PACKMOL[37] program. All-atom approach for insulins was used in original building step, as seen in Figure 11c,d. In the geometry-optimized spherical model, as seen from the highlighted insulin–insulin intermolecular distance, the molecules are far away from each other to allow aggregation. The lipid molecules (CG models of dipalmitoylphosphatidylcholine (DPPC) and dilauroylphosphatidylcholine (DLPC) used in this particular model; Figure 11e and 11f), restrict the motion of the insulins reducing thus their possibility to aggregate. As expected, specific intermolecular interaction processes are also dependent on certain ions in the protein environment. Figure 11a shows the ribbon presentation of porcine insulin in the presence of a trimethylamine *N*-oxide molecule (similar to the Abasaglar formulation of glargine insulin) based on the X-ray structure 3t2a.pdb. Figure 11b displays the same presentation of an X-ray structure of porcine insulin without the trimethylamine *N*-oxide (4a7e.pdb).

The combined molecular analysis methodologies, presented and applied here as the inaugural part for drug encapsulation strategy, have wide application options in addition to our tests on lysozyme and insulin. The strategy could also be applied for example to antimicrobial defensins and neuraminidases in cancer therapy. In any case, it is essential that the nanoparticles have a target function with respect to contact structures on the corresponding cell surfaces. The MARCKS-ED peptide with its polysialic acid affinity[28] is a good candidate to become a suitable targeting peptide on the nanoparticle surface. The data presented in this publication have to be considered as essential information for better understanding of the submolecular interactions in relation to the aggregation dynamics of protein drugs. Encapsulation into liposome nanoparticles could improve the delivery strategies for these therapeutics. The molecular surface properties of the protein drugs were studied with a combination of biophysical and biochemical methods including sophisticated analytical techniques and newly developed concepts.[49−54] Large-scale production of insulin[53] and the status quo of opportunities of insulin treatment[53] as described in the corresponding articles might initialize the distinct need for better understanding of the aggregation behavior of insulins (human, porcine, and synthetic glargine variants). This is valid

DOI: 10.1021/acsomega.8b02471
ACS Omega 2019, 4, 4206−4220

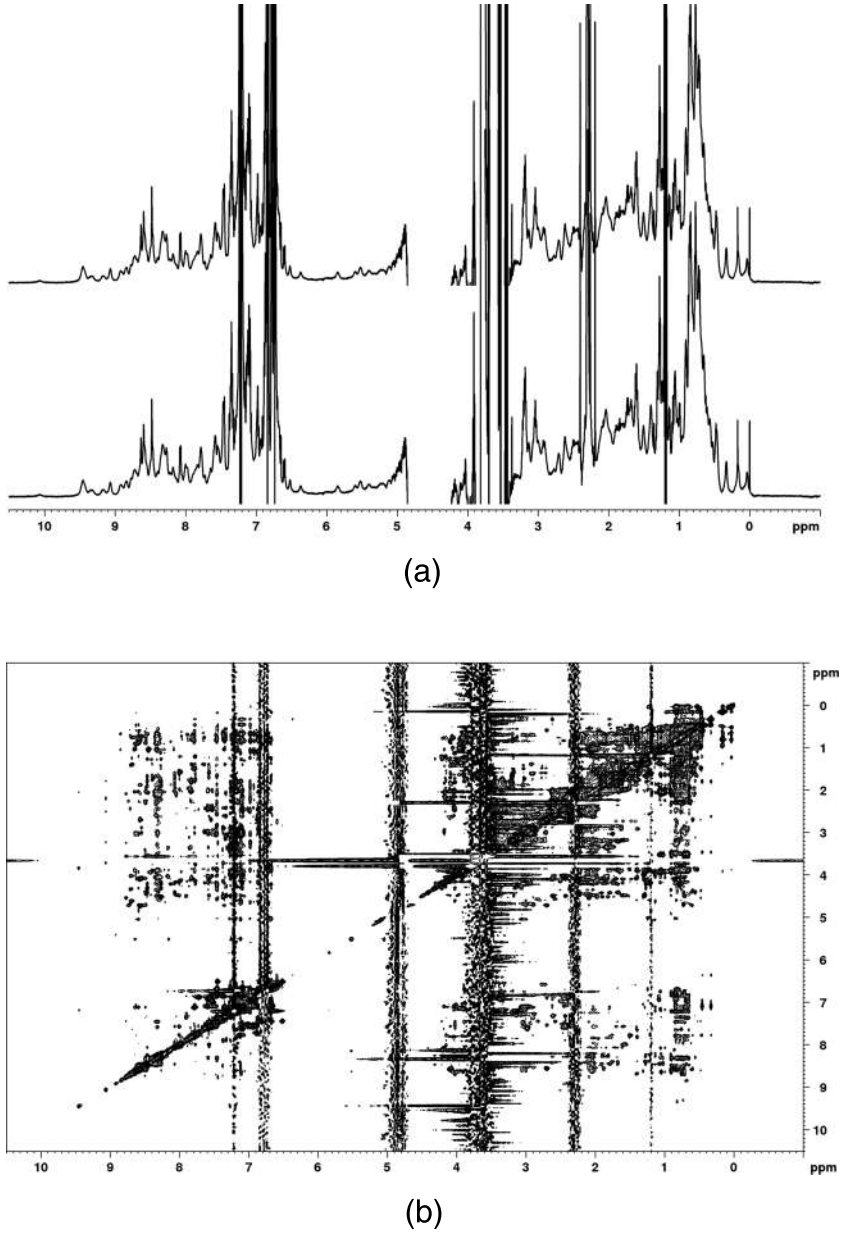

Figure 6. (a) Abasaglar glargine insulin spectra taken from different charges of insulin pens, which were stored under slightly different cooling conditions. The 1D NMR spectra of the two charges in top and bottom show identical signals. (b) NOESY NMR spectrum of the Abasaglar glargine insulin sample. Although the excipients produce strong disturbing signals, it is possible to structurally analyze the protein drug in its solution taken directly from the injection pen.

also in a similar way for lysozymes (HL and HEWL), especially specific intermolecular interactions in order to proceed toward potential applications in the framework of innovative nanomedical therapies. In the case of lysozymes, the results on specific interactions with the carbohydrate part of the LPS chains on pathogen surfaces have just been published.[14] The findings with respect to an intrinsic molecular target function can be combined with the concept of targeting peptides on the surfaces of nanoparticles. When protein drugs are delivered by nanoparticles with target-directed absorption enhancers (e.g., certain collagen fragments) on their surfaces, the molecular fine-tuning of all components of the delivery system is the crucial step for a therapeutic success. Therefore, it is of highest importance to carefully evaluate the data concerning the structure−function relationship of the aggregation dynamics of lysozymes and insulins as described here. Certain parameters such as pH values, temperature, and electrostatic potentials have to be correlated with excipient and specific receptor interactions as obtained by a combination of biophysical techniques and molecular modeling methods. Consequently, the structural and physiological properties (adjusted or personalized) of insulin or lysozyme embedded into a delivery nanoparticle could be directly correlated with the functional effects in the patient's organism after their release.

CONCLUSIONS

Liposomal encapsulation for drug delivery is a significant technique as it provides an alternative to injections, and currently many research groups around the world are carrying out research[55−57] to develop needle-free drug delivery

DOI: 10.1021/acsomega.8b02471
ACS Omega 2019, 4, 4206−4220

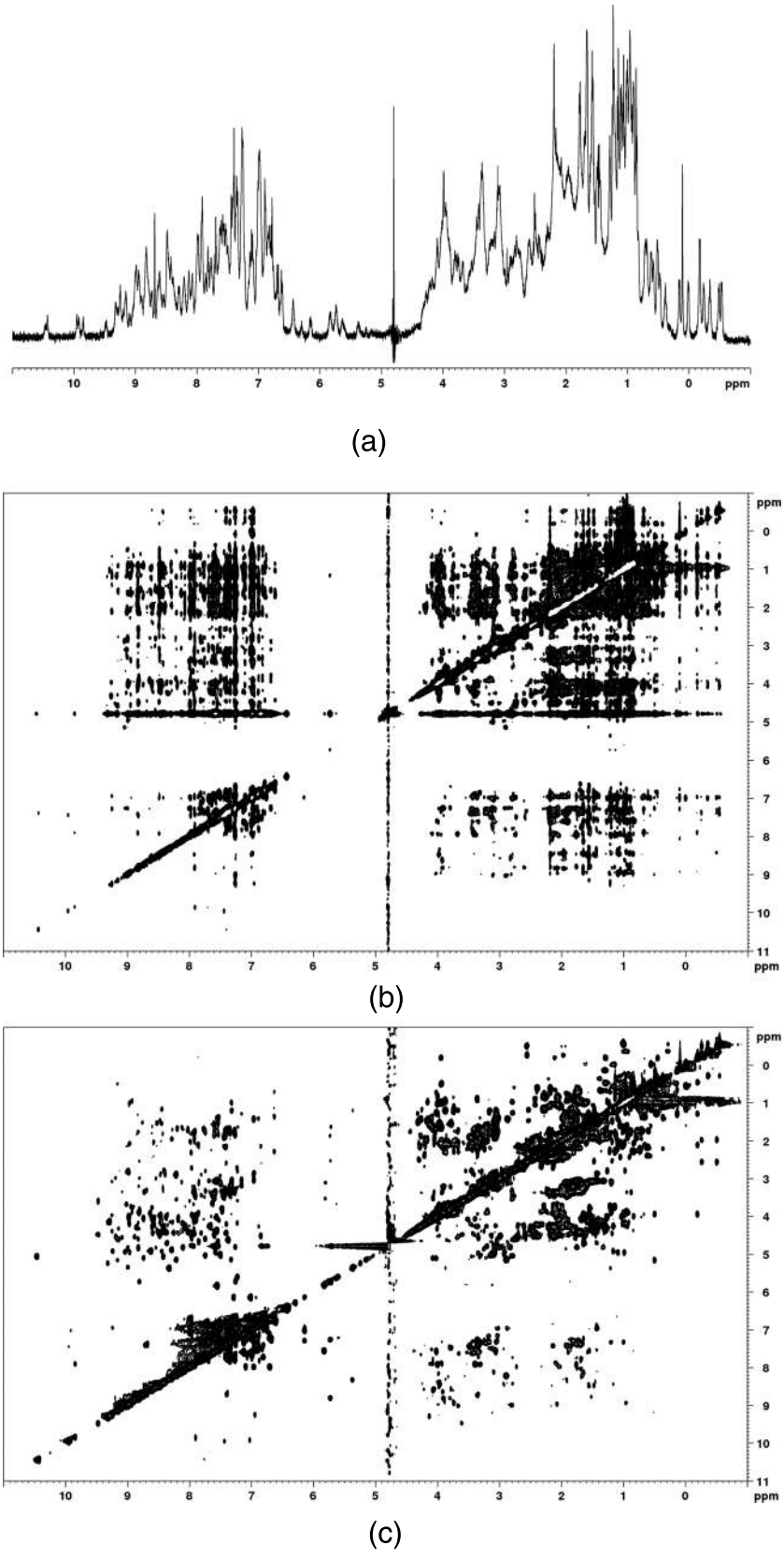

Figure 7. a) One-dimensional proton NMR spectrum of human lysozyme extracted from the milk of clone cows. The corresponding NOESY (b) and TOCSY (c) spectra are also shown. The evaluation of these spectra have led to the conclusion that no significant differences exist between the structures of the human lysozyme analyzed in a former study[14] and human lysozyme extracted from the milk of clone cows.

techniques, which will improve patient compliance. The current study is focused on understanding the homo-oligomerization of the important amyloidogenic proteins lysozyme and insulin. Both are well-established amyloidogenic proteins, and both are

DOI: 10.1021/acsomega.8b02471
ACS Omega 2019, 4, 4206−4220

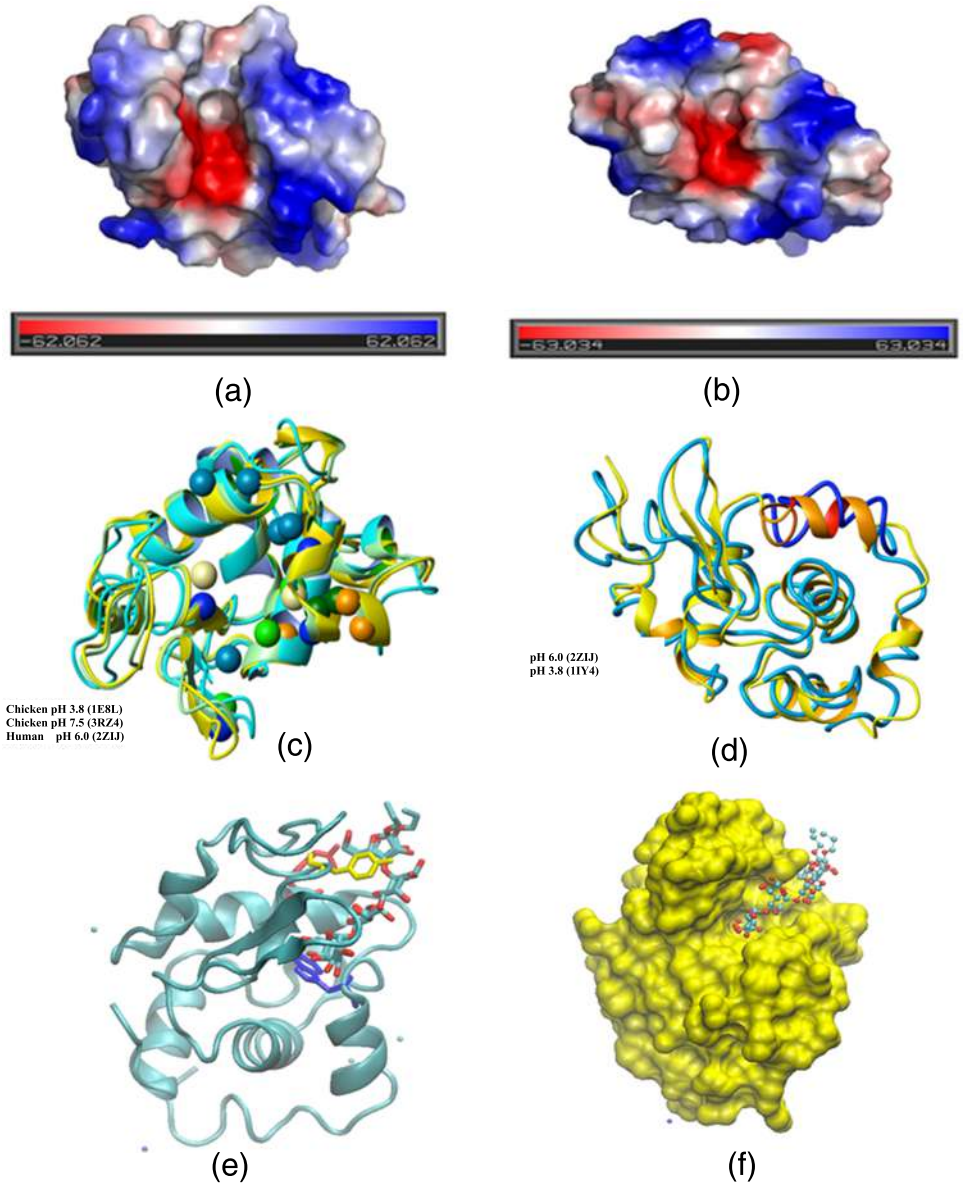

Figure 8. Surface representations of (a) HL and (b) HEWL with electrostatic surface potential. Electrostatic potentials were calculated with PyMOL.[33] Red and blue colors represent the negative and positive electrostatic potentials, respectively. (c) Overlay of structures for a comparison of pH-dependent effects in human (HL) and chicken (HEWL) lysozymes. (d) Overlay of two human lysozyme (HL) structures for a comparison of pH-dependent effects. (e) Backbone and (f) surface representation of human lysozyme in complex with the tetrasaccharide O-antigen LPS fragment from *K. pneumoniae* (5lsh.pdb[14]). Crucial amino acids that are stabilizing the complex are highlighted on the left side by the following color code: Tyr63 (yellow), Arg98 (red), and Trp109 (blue).

therapeutic agents. Clinical cases show that insulin can form amyloid particles at the site of injection known as insulin balls.[58−61] To prevent such undesired amyloidosis, it is necessary to develop advanced drug delivery systems,[62] in conjunction with insulin manufacture and treatment.[63−65] Liposomal encapsulation of insulin can be a convenient alternative drug delivery strategy. The association state of the proteins is an important determinant factor of protein encapsulation into lipid-based colloidal carriers[66] along with lipid−protein interaction.[67] Furthermore, one needs to consider the interaction of the protein with the chosen lipid model as it is another important determinant factor, which can be studied in silico prior to wet lab experiments.

Our results show that under the different molecular environmental conditions, the association state of lysozyme and insulin varies. The variability in the molecular association governs the amyloid kinetics and the final aggregation state, as conferred from the amyloid kinetic studies of lysozyme and insulin variants. These results can help device encapsulation strategies for different lysozymes and insulins. Several other peptide-based therapeutics can be further studied as discussed in an earlier section for designing the liposomal protein encapsulation.

EXPERIMENTAL SECTION

NMR Sample Preparation. All samples were prepared by dissolving lyophilized human lysozyme (HL) or hen egg white lysozyme (HEWL) in 0.3 mL of H_2O containing 20 mM sodium phosphate buffer and 10% D_2O. Final concentrations of all samples were 0.5 mM protein as determined by measurement of

DOI: 10.1021/acsomega.8b02471
ACS Omega 2019, 4, 4206−4220

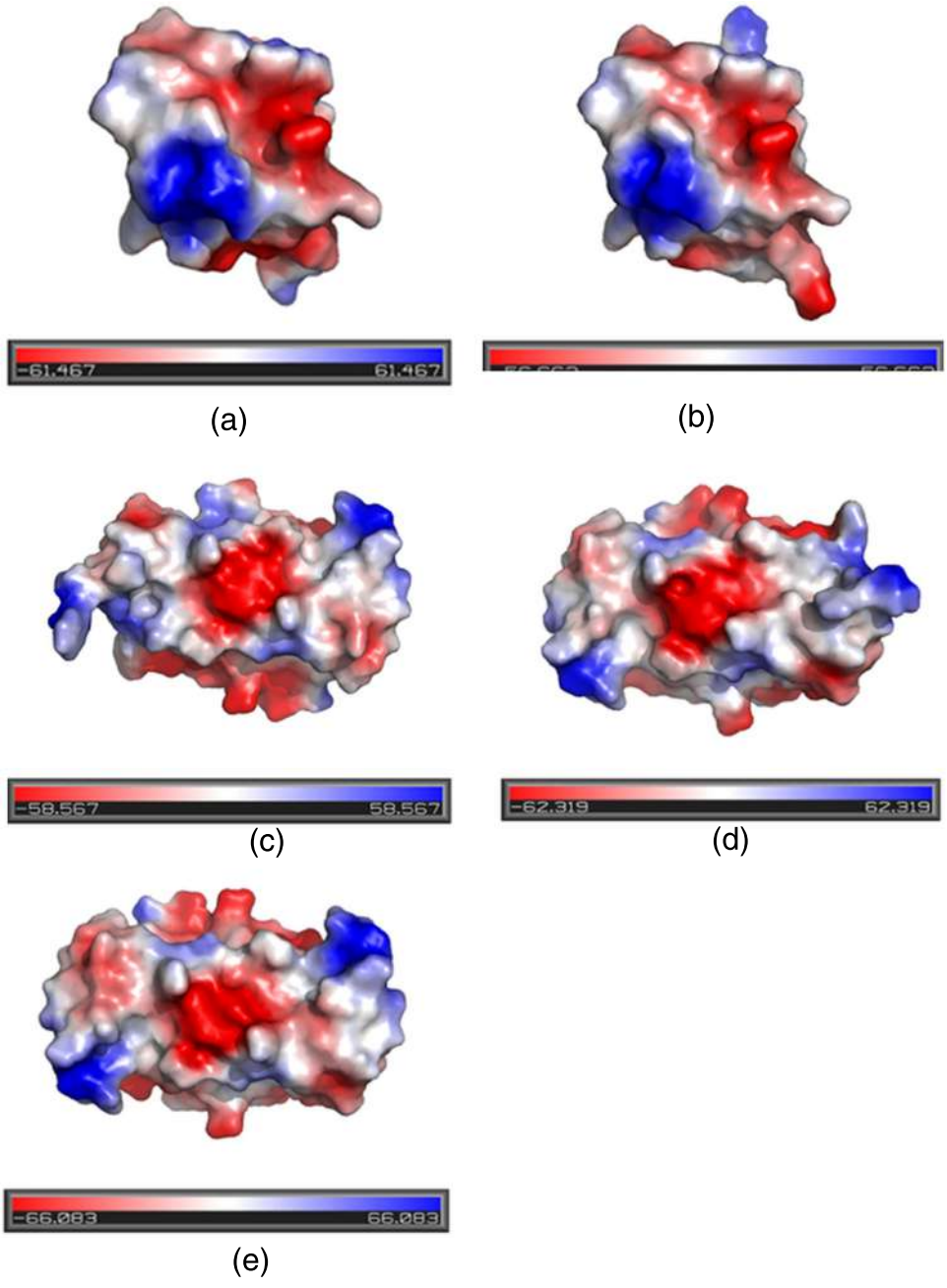

Figure 9. (a) Electrostatic surface potential of the glargine insulin monomer (4iyd.pdb). (b) Electrostatic surface presentation of the porcine insulin Caninsulin monomer (3t2a.pdb).[34] Surface representations of human insulin— dimeric form (c) 3w7y.pdb and (d) 1mso.pdb[35] in comparison to (e) dimeric porcine insulin 3fhp.pdb.[36] The electrostatic potentials were calculated with PyMOL.[33] Red and blue colors represent negative and positive electrostatic potentials, respectively.

the molar extinction coefficient, using E1% (w/v) = 25.5 for HL and 26.4 for HEWL. The following samples were prepared: pure HL and HEWL at pH 3.8 and 5.5, respectively. Additional samples for HL were prepared in a similar manner for the pH titrations described below.

NMR spectroscopy including pH adjustments and pK_a measurements of HL: All NMR spectra were obtained using a Varian Unity INOVA 800 MHz spectrometer at 35 °C. The 1H chemical shifts were referenced to 4,4-dimethyl-4-silapentane-1-sulfonic acid. All experiments were run with 3 mm Shigemi tubes. Homonuclear two-dimensional (2D) NOESY and TOCSY (64 transients for each) with spectral width 11204 Hz for both dimensions were acquired with 512 increments in the indirect dimension and 4096 data points in the direct dimension using Watergate solvent suppression and a pulse sequence repetition delay of 1.5 s. The NMRPipe[68] software package was used to process all NMR data by zero-filling to 1024 points in the indirect dimension and ending with either a Gaussian or a shifted sine-bell function. The digital resolution was 0.0015 and 0.014 ppm for the direct and indirect dimensions, respectively, after zero-filling. The following mixing times were used: 150 ms for the NOESYs and 50 ms for the TOCSYs. Ten NOESY spectra were recorded at different pH values between the range 3.8 and 8.1 (3.8, 4.2, 4.6, 5.0, 5.5, 6.2, 6.8, 7.4, 7.7, and 8.1) for pK_a determination of HL. A separate set of HL samples was used to record 1D spectra at 22 different pH conditions in between

DOI: 10.1021/acsomega.8b02471
ACS Omega 2019, 4, 4206−4220

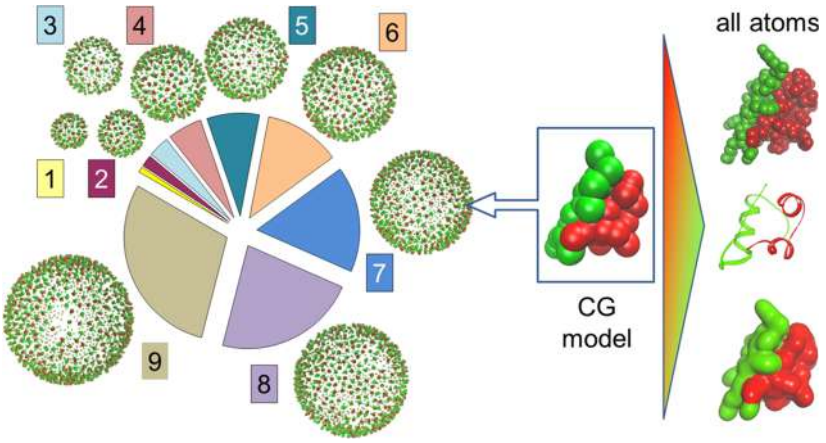

Figure 10. Structure−volume correlations of glargine insulin in "coarse-grained" (CG) presentation encapsulated into nine differently sized nanoparticles. The central pie chart illustrates the increase of the particle volumes. The insulin color coding (chain A red, chain B green) and the CG to all-atoms reverse engineering are shown in the right part of the figure (in CPK, ribbon and surface presentation). Particle sizes (radius): (1) 18 nm; (2) 23 nm; (3) 28 nm; (4) 33 nm; (5) 38 nm; (6) 43 nm; (7) 48 nm; (8) 53 nm; and (9) 58 nm.

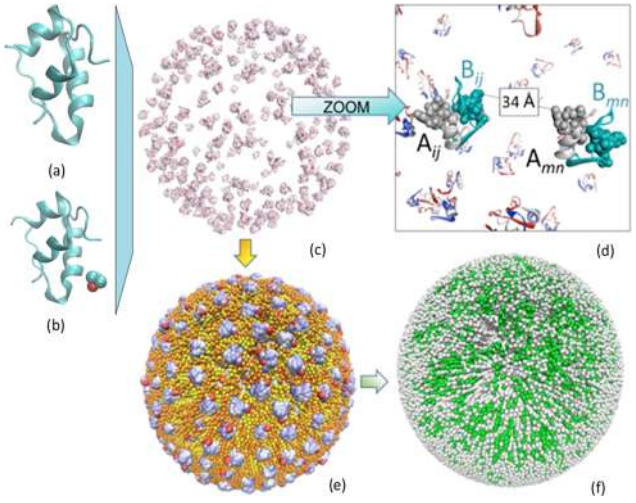

Figure 11. (a) 4a7e.pdb, porcine insulin without trimethylamine *N*-oxide;[48] (b) 3t2a.pdb, porcine insulin with trimethylamine *N*-oxide;[34] (c) all-atom molecular surface representation of glargine insulins embedded into the globular (~65 nm) nanoparticle; (d) zoomed ribbon representation of insulin with CPK highlighting of the amyloidogenic segment; (e) and (f) insulin structures (shown in all-atom CPK representation) embedded into the lipid bilayer (coarse-grained modeling of DPPC and DLPC with different coloring schemes for the inner (orange and yellow) and outer (green and white) layers). The insulin molecules loaded into the liposome are protected from solvent and other environmental effects.

3.17 and 8.13 in step increment of ~0.2 units. All 1D data sets were defined by 4096 complex points and consisted of 256 transients. The digital resolution of the 1D spectra was 0.0024 ppm after zero-filling. XEASY,[69] MNova,[70] and CCPNmr[71] were used for analysis and resonance assignment. Line widths are defined as half-width at half-height of a peak; for most peaks, the line width was estimated to be 0.01 ppm. NMR-derived models are displayed with the MOLMOL program.[72]

For adjusting pH values, either H_3PO_4 or NaOH was used by addition of small aliquots. The standard solutions (from Sigma) at pH 4 and 7 were used to calibrate the pH meter. The temperature dependence of the pH reading for HL was checked by recalibrating the pH meter at 35 °C: the difference between an incubated lysozyme sample at 35 °C and at room temperature was less than 0.1 pH unit. Before and after each experiment, the pH for each sample was measured to warrant constant conditions.

The list of excipients in Abasaglar insulin is as follows: zinc oxide, metacresol, glycerol, hydrochloric acid (for pH adjustment), sodium hydroxide (for pH adjustment), and water for injections. Therefore, strong signals from metacresol and glycerol occur in the spectra beside the protein signals.

In the case of human lysozyme, which was isolated from the milk of cloned transgenic cows, only the pure protein was extracted and therefore no disturbing signals were occurring in the corresponding spectra.[53]

Molecular Modeling. The structure of human lysozyme was investigated for its dimerization potential with the web server Haddock 2.2.[73] For this purpose, the respective monomer proteins from 1lzs.pdb[32] were used. The different protein−protein docking results were subjected to an energy minimization with the program Hyperchem 8.0[74] using the CHARMM27 force field[75] in an aqueous environment. To test the stability of the dimeric proteins, an MD simulation over 10 ns at 298 K was carried out with the dimer from 1lzs.pdb, as well as with the most energetically favorable dimer from the Haddock 2.2 experiment at pH = 7.4 in physiological saline. For this, the program YASARA v.12.11.25[76] with the NOVA force field was used. The PyMOL[33] software package was applied for visualization of the monomers and dimers.

The PACKMOL[37] program was used to build the liposome structures containing the embedded insulin molecules. The combination of NAMD/VMD[77,78] programs was used for further structural modeling and visualization. Coarse-grained models of modeling dilauroylphosphatidylcholine (DLPC) and modeling dipalmitoylphosphatidylcholine (DPPC) were used in liposome generation, whereas both all-atom and CG models of insulin were applied for the protein embedment. The PACKMOL[37]-created structures were then transformed into formats suitable for MD programs for CG simulations (GROMACS[79−84] and LAMMPS[85]) with the help of TopoTools (https://sites.google.com/site/akohlmey/software/topotools), VMD plugin, and Moltemplate (https://www.moltemplate.org/). The Martini force field[86−88] was used for CG simulations. Finally, the OVITO[89] program was used for structure control and trajectory analysis.

DOI: 10.1021/acsomega.8b02471
ACS Omega 2019, 4, 4206−4220

X-ray Crystallography. The crystallization and structure determination of human lysozyme were performed as described previously.[14] In brief, human lysozyme crystals were obtained at 18 °C using the hanging drop vapor diffusion method. Crystals were grown in 0.8 M NaCl, 25 mM NaOAc buffer (pH 4.4), 0.8 M NaCl, and 50 mM NaCitrate buffer (pH 5.8). All data collections were performed at 100 K and were processed with the XDS/XSCALE[90] program package. The human lysozyme structure (PDB id: 1rex)[91] was used as the search model for molecular replacement with the MOLREP program.[92] The Refmac5 program as implemented in the CCP4 suite[93,94] and PHENIX[95] was used for model building and refinement.

Amyloid Fibrillization of Hen and Human Lysozymes, Glargine, and Human Insulin. Hen egg white (HEWL) and human (HL) lysozyme amyloid fibrils were prepared through the incubation of 10 μM lysozyme at 65 °C with constant stirring (1200 rpm) in 70 mM glycine buffer containing 80 mM NaCl, pH 2.7. Human and glargine insulin solutions at 10 μM final concentration prepared in 100 mM NaCl−HCl buffer, pH1.6, were incubated at 65 °C, 1200 rpm for 2 h. To study kinetics of fibrillization processes, aliquots of lysozymes/insulins were withdrawn at varying times. Formation of amyloid aggregates was observed using the ThT assay. All experiments were performed in triplicate, and the presented data represent average values with standard deviations. The data were fitted with sigmoidal curve-parameter 4 with the equation: $y_0 + a/(1 + \exp(-(x - x_0)/b))$ using SigmaPlot software. The presence of lysozyme/insulin amyloid fibrils was confirmed by atomic force microscopy.

Thioflavin T Fluorescence Assay. The amyloid aggregation of lysozymes and insulins was assayed by a significant enhancement of Thioflavin T (ThT) fluorescence in the presence of amyloid fibrils. Thioflavin T was added to lysozyme/insulin samples (10 μM) to a final concentration of 20 μM. Measurements were performed in a 96-well plate using a Synergy MX (BioTek) spectrofluorimeter. The excitation wavelength was set at 440 nm and the emission recorded at 485 nm. The excitation and emission slits were adjusted to 9.0/9.0 nm, and the top probe vertical offset was 6 mm.[96−100]

Atomic Force Microscopy. Samples were deposited by drop casting on the freshly cleaved mica surface. After 5 min adsorption, the samples were washed with ultrapure water and left to dry. The protein concentration of 10 μM was used. AFM images were taken by a Scanning Probe Microscope (Veeco di Innova, Bruker AXS Inc., Madison) in a tapping mode using uncoated silicon cantilevers TESPA, unmounted with force constant 42 N/m and nominal resonance frequency ν = 320 kHz, with Al reflective coating (Bruker AFM Probes, Camarillo). The resolution of the image was 512 pixels per line (512 × 512 pixels/image) with a scan rate of 0.5 kHz. All the images are unfiltered.[96−100]

■ ASSOCIATED CONTENT

Supporting Information

The Supporting Information is available free of charge on the ACS Publications website at DOI: 10.1021/acsomega.8b02471.

Overlay of one-dimensional NMR spectra of the glargine insulin Lantus and glargine insulin Glaritus (Figure S1); overlay of crucial parts of glargine insulin 2D NMR-spectra (Figure S2); complex of human insulin with its receptor (Figure S3); 1D NMR-spectrum of Caninsulin (Figure S4) (PDF)

■ AUTHOR INFORMATION

Corresponding Author

*E-mail: hcsiebert@aol.com.

ORCID

Anirban Bhunia: 0000-0002-8752-2842
Zuzana Gazova: 0000-0002-0670-3431
Nikolay E. Nifantiev: 0000-0002-0727-4050

Notes

The authors declare no competing financial interest.

■ ACKNOWLEDGMENTS

This work was supported by the Open Project of Shandong Collaborative Innovation Center for Antibody Drugs (No. CIC-AD1834) and Tai-Shan Scholar Research Fund of Shandong Province of China. This work was also technically supported by Engineering Research Center for Nanomedicine and Drug Delivery Systems. The Swedish NMR Centre is acknowledged for supplying instrument time and support. This work was supported by the King Abdullah University of Science and Technology (grant KUK-11-008-23 awarded to B.N. with Ph.D. position for L.W.) and the European Research Council (ERC-2008-AdG 227700 to B.N.). We thank the Sialic Acids Society for financial support. Parts of the work were supported by RSF grant 14-23-00199 (NEN). On the Slovak side, the work was supported by project VEGA 2/0145/17, 2/0030/18, and SAS-MOST JRP 2015/5. This work was partly supported by Council of Scientific and Industrial Research (CSIR), Govt. of India (02(0292)/17/EMR-II) (to AB). Supports from EU projects 26220120033, 26210120002, 26110230097, and 26210120012 (IEP SAS Kosice, Slovakia) are gratefully acknowledged. We also thank Prof. Dr Frank D Sönnichsen (Otto Diels Institute for Organic Chemistry, Christian Albrechts University, Kiel, Germany) for his helpful support with respect to some of our NMR experiments. Last but not least, Dr Anna Kozarova (University of Windsor, Windsor, Ontario, Canada) is highly acknowledged for critical reading and helpful comments on the manuscript.

■ REFERENCES

(1) Teneback, C. C.; Scanlon, T. C.; Wargo, M. J.; Bement, J. L.; Griswold, K. E.; Leclair, L. W. Bioengineered lysozyme reduces bacterial burden and inflammation in a murine model of mucoid *Pseudomonas aeruginosa* lung infection. *Antimicrob. Agents Chemother.* **2013**, *57*, 5559−5564.

(2) Markart, P.; Korfhagen, T. R.; Weaver, T. E.; Akinbi, H. T. Mouse lysozyme M is important in pulmonary host defense against *Klebsiella pneumoniae* infection. *Am. J. Respir. Crit. Care Med.* **2004**, *169*, 454−458.

(3) Akinbi, H. T.; Epaud, R.; Bhatt, H.; Weaver, T. E. Bacterial killing is enhanced by expression of lysozyme in the lungs of transgenic mice. *J. Immunol.* **2000**, *165*, 5760−5766.

(4) Heinemann, L.; Hompesch, M. Biosimilar insulins: how similar is similar? *J. Diabetes Sci. Technol.* **2011**, *5*, 741−754.

(5) DeVries, J. H.; Gough, S. C.; Kiljanski, J.; Heinemann, L. Biosimilar insulins: a European perspective. *Diabetes, Obes. Metab.* **2015**, *17*, 445−451.

(6) Beran, D.; Ewen, M.; Laing, R. Constraints and challenges in access to insulin: a global perspective. *Lancet Diabetes Endocrinol.* **2016**, *4*, 275−285.

(7) Gong, H.; He, Z.; Peng, A.; Zhang, X.; Cheng, B.; Sun, Y.; Zheng, L.; Huang, K. Effects of several quinones on insulin aggregation. *Sci. Rep.* **2015**, *4*, No. 5648.

DOI: 10.1021/acsomega.8b02471
ACS Omega 2019, 4, 4206−4220

(8) Owens, D. R.; Landgraf, W.; Schmidt, A.; Bretzel, R. G.; Kuhlmann, M. K. The emergence of biosimilar insulin preparations–a cause for concern? *Diabetes Technol. Ther.* **2012**, *14*, 989−996.
(9) Jelkmann, W. Molecular biology of erythropoietin. *Intern. Med.* **2004**, *43*, 649−659.
(10) Hermanns, N.; Kulzer, B.; Kohlmann, T.; Jacob, S.; Landgraf, W.; Theobald, K.; Haak, T. Treatment satisfaction and quality-of-life between type 2 diabetes patients initiating long- vs intermediate-acting basal insulin therapy in combination with oral hypoglycemic agents–a randomized, prospective, crossover, open clinical trial. *Health Qual. Life Outcomes* **2015**, *13*, No. 77.
(11) Brems, D. N.; Alter, L. A.; Beckage, M. J.; Chance, R. E.; DiMarchi, R. D.; Green, L. K.; Long, H. B.; Pekar, A. H.; Shields, J. E.; Frank, B. H. Altering the association properties of insulin by amino acid replacement. *Protein Eng., Des. Sel.* **1992**, *5*, 527−533.
(12) Weiss, M. A.; Hua, Q. X.; Lynch, C. S.; Frank, B. H.; Shoelson, S. E. Heteronuclear 2D NMR studies of an engineered insulin monomer: assignment and characterization of the receptor-binding surface by selective deuterium and carbon-13 labeling with application to protein design. *Biochemistry* **1991**, *30*, 7373−7389.
(13) Swaminathan, R.; Ravi, V. K.; Kumar, S.; Kumar, M. V.; Chandra, N. Lysozyme: a model protein for amyloid research. *Adv. Protein Chem. Struct. Biol.* **2011**, *84*, 63−111.
(14) Zhang, R. Y.; Wu, L. S.; Eckert, T.; Burg-Roderfeld, M.; Rojas-Macias, M. A.; Lutteke, T.; Krylov, V. B.; Argunov, D. A.; Datta, A.; Markart, P.; Guenther, A.; Norden, B.; Schauer, R.; Bhunia, A.; Enani, M. A.; Billeter, M.; Scheidig, A. J.; Nifantiev, N. E.; Siebert, H. C. Lysozyme's lectin-like characteristics facilitates its immune defense function. *Q. Rev. Biophys.* **2017**, *50*, 1−12.
(15) Siposova, K.; Kozar, T.; Musatov, A. Interaction of nonionic detergents with the specific sites of lysozyme amyloidogenic region - inhibition of amyloid fibrillization. *Colloids Surf., B* **2017**, *150*, 445−455.
(16) Ponikova, S.; Kubackova, J.; Bednarikova, Z.; Marek, J.; Demjen, E.; Antosova, A.; Musatov, A.; Gazova, Z. Inhibition of lysozyme amyloidogenesis by phospholipids. Focus on long-chain dimyristoyl-phosphocholine. *Biochim. Biophys. Acta, Gen. Subj.* **2017**, *1861*, 2934−2943.
(17) Siposova, K.; Sedlak, E.; Kozar, T.; Nemergut, M.; Musatov, A. Dual Effect of Non-ionic Detergent Triton X-100 on Insulin Amyloid Formation. *Colloids Surf., B* **2019**, *173*, 709−718.
(18) Siposova, K.; Kozar, T.; Huntosova, V.; Tomkova, S.; Musatov, A. Inhibition of amyloid fibril formation and disassembly of pre-formed fibrils by natural polyphenol rottlerin. *Biochim. Biophys. Acta, Proteins Proteomics* **2018**, DOI: 10.1016/j.bbapap.2018.10.002.
(19) Zheng, Q.; Lazo, N. D. Mechanistic Studies of the Inhibition of Insulin Fibril Formation by Rosmarinic Acid. *J. Phys. Chem. B* **2018**, *122*, 2323−2331.
(20) Donabedian, P. L.; Evanoff, M.; Monge, F. A.; Whitten, D. G.; Chi, E. Y. Substituent, Charge, and Size Effects on the Fluorogenic Performance of Amyloid Ligands: A Small-Library Screening Study. *ACS Omega* **2017**, *2*, 3192−3200.
(21) Siebert, H. C.; Tajkhorshid, E.; Dabrowski, J. Barrier to rotation around the C-sp(2)-C-sp(2) bond of the ketoaldehyde enol ether MeC(O)CH═CH-OEt as determined by C-13 NMR and ab initio calculations. *J. Phys. Chem. A* **2001**, *105*, 8488−8494.
(22) Ogawa, N.; Kaga, M.; Endo, T.; Nagase, H.; Furuishi, T.; Yamamoto, H.; Kawashima, Y.; Ueda, H. Quetiapine free base complexed with cyclodextrins to improve solubility for parenteral use. *Chem. Pharm. Bull.* **2013**, *61*, 809−815.
(23) Mofarrah, E.; Habibi-Khorassani, S. M.; Maghsoodlou, M. T.; Shahraki, M. The hindered internal rotations in isomerism forms of a particular phosphorane involving 2-chloro-phenothiazine: Dynamic 1H NMR study. *Indian J. Chem.* **2015**, *54*, 1528−1534.
(24) Jafari, S.; Fernandez-Enright, F.; Huang, X. F. Structural contributions of antipsychotic drugs to their therapeutic profiles and metabolic side effects. *J. Neurochem.* **2012**, *120*, 371−384.
(25) Duong, A. D.; Ruan, G.; Mahajan, K.; Winter, J. O.; Wyslouzil, B. E. Scalable, semicontinuous production of micelles encapsulating nanoparticles via electrospray. *Langmuir* **2014**, *30*, 3939−3948.
(26) Prabhu, R. H.; Patravale, V. B.; Joshi, M. D. Polymeric nanoparticles for targeted treatment in oncology: current insights. *Int. J. Nanomed.* **2015**, *10*, 1001−1018.
(27) Chen, X.; Ramstrom, O.; Yan, M. Glyconanomaterials: Emerging applications in biomedical research. *Nano Res.* **2014**, *7*, 1381−1403.
(28) Zhang, R.; Loers, G.; Schachner, M.; Boelens, R.; Wienk, H.; Siebert, S.; Eckert, T.; Kraan, S.; Rojas-Macias, M. A.; Lutteke, T.; Galuska, S. P.; Scheidig, A.; Petridis, A. K.; Liang, S.; Billeter, M.; Schauer, R.; Steinmeyer, J.; Schroder, J. M.; Siebert, H. C. Molecular Basis of the Receptor Interactions of Polysialic Acid (polySia), polySia Mimetics, and Sulfated Polysaccharides. *ChemMedChem* **2016**, *11*, 990−1002.
(29) Zhang, R.; Eckert, T.; Lutteke, T.; Hanstein, S.; Scheidig, A.; Bonvin, A. M.; Nifantiev, N. E.; Kozar, T.; Schauer, R.; Enani, M. A.; Siebert, H. C. Structure-Function Relationships of Antimicrobial Peptides and Proteins with Respect to Contact Molecules on Pathogen Surfaces. *Curr. Top. Med. Chem.* **2015**, *16*, 89−98.
(30) Eckert, T.; Stötzel, S.; Burg-Roderfeld, M.; Sewing, J.; Lütteke, T.; Nifantiev, N. E.; Vliegenthart, J. F. G.; Siebert, H. C. In Silico Study on Sulfated and Non-Sulfated Carbohydrate Chains from Proteoglycans in Cnidaria and Interaction with Collagen. *Open J. Phys. Chem.* **2012**, *2*, 123−133.
(31) Bhunia, A.; Vivekanandan, S.; Eckert, T.; Burg-Roderfeld, M.; Wechselberger, R.; Romanuka, J.; Bachle, D.; Kornilov, A. V.; von der Lieth, C. W.; Jimenez-Barbero, J.; Nifantiev, N. E.; Schachner, M.; Sewald, N.; Lutteke, T.; Siebert, H. C. Why Structurally Different Cyclic Peptides Can Be Glycomimetics of the HNK-1 Carbohydrate Antigen. *J. Am. Chem. Soc.* **2010**, *132*, 96−105.
(32) Song, H.; Inaka, K.; Maenaka, K.; Matsushima, M. Structural changes of active site cleft and different saccharide binding modes in human lysozyme co-crystallized with hexa-N-acetyl-chitohexaose at pH 4.0. *J. Mol. Biol.* **1994**, *244*, 522−540.
(33) DeLano, W. L. *The PyMOL Molecular Graphics System*, 2002.
(34) Marshall, H.; Venkat, M.; Seng, N. S.; Cahn, J.; Juers, D. H. The use of trimethylamine N-oxide as a primary precipitating agent and related methylamine osmolytes as cryoprotective agents for macromolecular crystallography. *Acta Crystallogr., Sect. D: Biol. Crystallogr.* **2012**, *68*, 69−81.
(35) Smith, G. D.; Pangborn, W. A.; Blessing, R. H. The structure of T6human insulin at 1.0 Å resolution. *Acta Crystallogr., Sect. D: Biol. Crystallogr.* **2003**, *59*, 474−482.
(36) Iwai, W.; Yamada, T.; Kurihara, K.; Ohnishi, Y.; Kobayashi, Y.; Tanaka, I.; Takahashi, H.; Kuroki, R.; Tamada, T.; Niimura, N. A neutron crystallographic analysis of T6 porcine insulin at 2.1 A resolution. *Acta Crystallogr., Sect. D: Biol. Crystallogr.* **2009**, *65*, 1042−1050.
(37) Martínez, L.; Andrade, R.; Birgin, E. G.; Martinez, J. M. PACKMOL: a package for building initial configurations for molecular dynamics simulations. *J. Comput. Chem.* **2009**, *30*, 2157−2164.
(38) Li, J.; Chu, M. K.; Lu, B.; Mirzaie, S.; Chen, K.; Gordijo, C. R.; Plettenburg, O.; Giacca, A.; Wu, X. Y. Enhancing thermal stability of a highly concentrated insulin formulation with Pluronic F-127 for long-term use in microfabricated implantable devices. *Drug Delivery Transl. Res.* **2017**, *7*, 529−543.
(39) Carlsson, F.; Malmsten, M.; Linse, P. Monte Carlo Simulations of Lysozyme Self-Association in Aqueous Solution. *J. Phys. Chem. B* **2001**, *105*, 12189−12195.
(40) Abramo, M. C.; Caccamo, C.; Costa, D.; Pellicane, G.; Ruberto, R. Molecular dynamics of an embedded-charge model of lysozyme aqueous solutions. *J. Phys. Chem. B* **2010**, *114*, 9109−9118.
(41) Abramo, M. C.; Caccamo, C.; Calvo, M.; Conti Nibali, V.; Costa, D.; Giordano, R.; Pellicane, G.; Ruberto, R.; Wanderlingh, U. Molecular dynamics and small-angle neutron scattering of lysozyme aqueous solutions. *Philos. Mag.* **2011**, *91*, 2066−2076.
(42) Zhang, L.; Bai, S.; Sun, Y. Modification of Martini force field for molecular dynamics simulation of hydrophobic charge induction

DOI: 10.1021/acsomega.8b02471
ACS Omega 2019, 4, 4206−4220

chromatography of lysozyme. *J. Mol. Graphics Modell.* **2011**, *29*, 906−914.
(43) Abramo, M. C.; Caccamo, C.; Costa, D.; Pellicane, G.; Ruberto, R.; Wanderlingh, U. Effective interactions in lysozyme aqueous solutions: a small-angle neutron scattering and computer simulation study. *J. Chem. Phys.* **2012**, *136*, No. 035103.
(44) Zheng, W.; Glenn, P. Probing the folded state and mechanical unfolding pathways of T4 lysozyme using all-atom and coarse-grained molecular simulation. *J. Chem. Phys.* **2015**, *142*, No. 035101.
(45) Yu, G.; Zhou, J. Understanding the curvature effect of silica nanoparticles on lysozyme adsorption orientation and conformation: a mesoscopic coarse-grained simulation study. *Phys. Chem. Chem. Phys.* **2016**, *18*, 23500−23507.
(46) Wizert, A.; Iskander, D. R.; Cwiklik, L. Interaction of lysozyme with a tear film lipid layer model: A molecular dynamics simulation study. *Biochim. Biophys. Acta, Biomembr.* **2017**, *1859*, 2289−2296.
(47) Singh, A. K.; Burada, P. S.; Bhattacharya, S.; Bag, S.; Bhattacharya, A.; Dasgupta, S.; Roy, A. Microwave-radiation-induced molecular structural rearrangement of hen egg-white lysozyme. *Phys. Rev. E* **2018**, *97*, No. 052416.
(48) Burkhardt, A.; Warmer, M.; Panneerselvam, S.; Wagner, A.; Zouni, A.; Glockner, C.; Reimer, R.; Hohenberg, H.; Meents, A. Fast high-pressure freezing of protein crystals in their mother liquor. *Acta Crystallogr., Sect. F: Struct. Biol. Cryst. Commun.* **2012**, *68*, 495−500.
(49) Siebert, H. C.; Burg-Roderfeld, M.; Eckert, T.; Stotzel, S.; Kirch, U.; Diercks, T.; Humphries, M. J.; Frank, M.; Wechselberger, R.; Tajkhorshid, E.; Oesser, S. Interaction of the alpha2A domain of integrin with small collagen fragments. *Protein Cell* **2010**, *1*, 393−405.
(50) Stötzel, S.; Schurink, M.; Wienk, H.; Siebler, U.; Burg-Roderfeld, M.; Eckert, T.; Kulik, B.; Wechselberger, R.; Sewing, J.; Steinmeyer, J.; Oesser, S.; Boelens, R.; Siebert, H. C. Molecular organization of various collagen fragments as revealed by atomic force microscopy and diffusion-ordered NMR spectroscopy. *ChemPhysChem* **2012**, *13*, 3117−3125.
(51) Schadow, S.; Siebert, H. C.; Lochnit, G.; Kordelle, J.; Rickert, M.; Steinmeyer, J. Collagen Metabolism of Human Osteoarthritic Articular Cartilage as Modulated by Bovine Collagen Hydrolysates. *PLoS One* **2013**, *8*, No. e53955.
(52) Schadow, S.; Simons, V. S.; Lochnit, G.; Kordelle, J.; Gazova, Z.; Siebert, H. C.; Steinmeyer, J. Metabolic Response of Human Osteoarthritic Cartilage to Biochemically Characterized Collagen Hydrolysates. *Int. J. Mol. Sci.* **2017**, *18*, No. 207.
(53) Lu, D.; Liu, S.; Ding, F.; Wang, H.; Li, J.; Li, L.; Dai, Y.; Li, N. Large-scale production of functional human lysozyme from marker-free transgenic cloned cows. *Sci. Rep.* **2016**, *6*, No. 22947.
(54) Wong, C. Y.; Martinez, J.; Dass, C. R. Oral delivery of insulin for treatment of diabetes: status quo, challenges and opportunities. *J. Pharm. Pharmacol.* **2016**, *68*, 1093−1108.
(55) Dimov, N.; Kastner, E.; Hussain, M.; Perrie, Y.; Szita, N. Formation and purification of tailored liposomes for drug delivery using a module-based micro continuous-flow system. *Sci. Rep.* **2017**, *7*, No. 12045.
(56) Colletier, J.-P.; Chaize, B.; Winterhalter, M.; Fournier, D. Protein encapsulation in liposomes: efficiency depends on interactions between protein and phospholipid bilayer. *BMC Biotechnol.* **2002**, No. 9.
(57) Hirai, M.; Sato, S.; Kimura, R.; Hagiwara, Y.; Kawai-Hirai, R.; Ohta, N.; Igarashi, N.; Shimizu, N. Effect of protein-encapsulation on thermal structural stability of liposome composed of glycosphingolipid/cholesterol/phospholipid. *J. Phys. Chem. B* **2015**, *119*, 3398−3406.
(58) Nagase, T.; Katsura, Y.; Iwaki, Y.; Nemoto, K.; Sekine, H.; Miwa, K.; Oh-i, T.; Kou, K.; Iwaya, K.; Noritake, M.; Matsuoka, T. The insulin ball. *Lancet* **2009**, *373*, 184.
(59) Yumlu, S.; Barany, R.; Eriksson, M.; Rocken, C. Localized insulin-derived amyloidosis in patients with diabetes mellitus: a case report. *Hum. Pathol.* **2009**, *40*, 1655−1660.
(60) Kudo-Watanuki, S.; Kurihara, E.; Yamamoto, K.; Mukai, K.; Chen, K. R. Coexistence of insulin-derived amyloidosis and an overlying acanthosis nigricans-like lesion at the site of insulin injection. *Clin. Exp. Dermatol.* **2013**, *38*, 25−29.
(61) Lonsdale-Eccles, A. A.; Gonda, P.; Gilbertson, J. A.; Haworth, A. E. Localized cutaneous amyloid at an insulin injection site. *Clin. Exp. Dermatol.* **2009**, *34*, e1027−e1028.
(62) Banerjee, A.; Ibsen, K.; Brown, T.; Chen, R.; Agatemor, C.; Mitragotri, S. Ionic liquids for oral insulin delivery. *Proc. Natl. Acad. Sci. U. S. A.* **2018**, *115*, 7296−7301.
(63) Walsh, G. Therapeutic insulins and their large-scale manufacture. *Appl. Microbiol. Biotechnol.* **2004**, *67*, 151−159.
(64) Davis, A.; Kuriakose, J.; Clements, J. N. Faster Insulin Aspart: A New Bolus Option for Diabetes Mellitus. *Clin. Pharmacokinet.* **2018**, DOI: 10.1007/s40262-018-0696-8.
(65) Sandow, J.; Landgraf, W.; Becker, R.; Seipke, G. Equivalent Recombinant Human Insulin Preparations and their Place in Therapy. *Eur. Endocrinol.* **2015**, *11*, No. 10.
(66) Martins, S.; Sarmento, B.; Ferreira, D. C.; Souto, E. B. Lipid-based colloidal carriers for peptide and protein delivery − liposomes versus lipid nanoparticles. *J. Nanomed.* **2007**, *2*, 595−607.
(67) Ratha, B. N.; Kim, M.; Sahoo, B.; Garai, K.; Lee, D.; Bhunia, A. Insulin-eukaryotic model membrane interaction: Mechanistic insight of insulin fibrillation and membrane disruption. *Biochim. Biophys. Acta* **2018**, *1860*, 1917−1926.
(68) Delaglio, F.; Grzesiek, S.; Vuister, G. W.; Zhu, G.; Pfeifer, J.; Bax, A. NMRPipe: a multidimensional spectral processing system based on UNIX pipes. *J. Biomol. NMR* **1995**, *6*, 277−93.
(69) Bartels, C.; Xia, T. H.; Billeter, M.; Guntert, P.; Wuthrich, K. The program XEASY for computer-supported NMR spectral analysis of biological macromolecules. *J. Biomol. NMR* **1995**, *6*, 1−10.
(70) Claridge, T. *Software Review of MNova: NMR Data Processing, Analysis, and Prediction Software*; ACS Publications, 2009.
(71) Vranken, W. F.; Boucher, W.; Stevens, T. J.; Fogh, R. H.; Pajon, A.; Llinas, M.; Ulrich, E. L.; Markley, J. L.; Ionides, J.; Laue, E. D. The CCPN data model for NMR spectroscopy: development of a software pipeline. *Proteins* **2005**, *59*, 687−96.
(72) Koradi, R.; Billeter, M.; Wuthrich, K. MOLMOL: a program for display and analysis of macromolecular structures. *J. Mol. Graph.* **1996**, *14*, 51−5 29-32 .
(73) van Zundert, G. C. P.; Rodrigues, J.; Trellet, M.; Schmitz, C.; Kastritis, P. L.; Karaca, E.; Melquiond, A. S. J.; van Dijk, M.; de Vries, S. J.; Bonvin, A. The HADDOCK2.2 Web Server: User-Friendly Integrative Modeling of Biomolecular Complexes. *J. Mol. Biol.* **2016**, *428*, 720−725.
(74) *Hyperchem*, version 8.0; Hypercube, Inc.: Gainesville, FL, 2007.
(75) MacKerell, A. D.; Bashford, D.; Bellott, M.; Dunbrack, R. L.; Evanseck, J. D.; Field, M. J.; Fischer, S.; Gao, J.; Guo, H.; Ha, S.; Joseph-McCarthy, D.; Kuchnir, L.; Kuczera, K.; Lau, F. T. K.; Mattos, C.; Michnick, S.; Ngo, T.; Nguyen, D. T.; Prodhom, B.; Reiher, W. E.; Roux, B.; Schlenkrich, M.; Smith, J. C.; Stote, R.; Straub, J.; Watanabe, M.; Wiorkiewicz-Kuczera, J.; Yin, D.; Karplus, M. All-atom empirical potential for molecular modeling and dynamics studies of proteins. *J. Phys. Chem. B* **1998**, *102*, 3586−3616.
(76) Krieger, E.; Koraimann, G.; Vriend, G. Increasing the precision of comparative models with YASARA NOVA–a self-parameterizing force field. *Proteins* **2002**, *47*, 393−402.
(77) Phillips, J. C.; Braun, R.; Wang, W.; Gumbart, J.; Tajkhorshid, E.; Villa, E.; Chipot, C.; Skeel, R. D.; Kale, L.; Schulten, K. Scalable molecular dynamics with NAMD. *J. Comput. Chem.* **2005**, *26*, 1781−802.
(78) Humphrey, W.; Dalke, A.; Schulten, K. VMD: visual molecular dynamics. *J. Mol. Graphics* **1996**, *14*, 33−8 27-8 .
(79) Berendsen, H. J. C.; Vanderspoel, D.; Vandrunen, R. Gromacs - A Message-Passing Parallel Molecular-Dynamics Implementation. *Comput. Phys. Commun.* **1995**, *91*, 43−56.
(80) Lindahl, E.; Hess, B.; van der Spoel, D. GROMACS 3.0: a package for molecular simulation and trajectory analysis. *J. Mol. Model.* **2001**, *7*, 306−317.
(81) Van Der Spoel, D.; Lindahl, E.; Hess, B.; Groenhof, G.; Mark, A. E.; Berendsen, H. J. GROMACS: fast, flexible, and free. *J. Comput. Chem.* **2005**, *26*, 1701−18.

DOI: 10.1021/acsomega.8b02471
ACS Omega 2019, 4, 4206−4220

(82) Hess, B.; Kutzner, C.; van der Spoel, D.; Lindahl, E. GROMACS 4: Algorithms for Highly Efficient, Load-Balanced, and Scalable Molecular Simulation. *J. Chem. Theory Comput.* **2008**, *4*, 435−47.
(83) Pronk, S.; Pall, S.; Schulz, R.; Larsson, P.; Bjelkmar, P.; Apostolov, R.; Shirts, M. R.; Smith, J. C.; Kasson, P. M.; van der Spoel, D.; Hess, B.; Lindahl, E. GROMACS 4.5: a high-throughput and highly parallel open source molecular simulation toolkit. *Bioinformatics* **2013**, *29*, 845−54.
(84) Abraham, M. J.; Murtola, T.; Schulz, R.; Páll, S.; Smith, J. C.; Hess, B.; Lindahl, E. GROMACS: High performance molecular simulations through multi-level parallelism from laptops to supercomputers. *SoftwareX* **2015**, *1−2*, 19−25.
(85) Plimpton, S. Fast Parallel Algorithms for Short-Range Molecular Dynamics. *J. Comput. Phys.* **1995**, *117*, 1−19.
(86) Marrink, S. J.; de Vries, A. H.; Mark, A. E. Coarse grained model for semiquantitative lipid simulations. *J. Phys. Chem. B* **2004**, *108*, 750−760.
(87) Marrink, S. J.; Risselada, H. J.; Yefimov, S.; Tieleman, D. P.; de Vries, A. H. The MARTINI force field: Coarse grained model for biomolecular simulations. *J. Phys. Chem. B* **2007**, *111*, 7812−7824.
(88) Monticelli, L.; Kandasamy, S. K.; Periole, X.; Larson, R. G.; Tieleman, D. P.; Marrink, S. J. The MARTINI coarse-grained force field: Extension to proteins. *J. Chem. Theory Comput.* **2008**, *4*, 819−834.
(89) Stukowski, A. Visualization and analysis of atomistic simulation data with OVITO - the Open Visualization Tool. *Modell. Simul. Mater. Sci. Eng.* **2010**, *18*, No. 015012.
(90) Kabsch, W. Integration, scaling, space-group assignment and post-refinement. *Acta Crystallogr., Sect. D: Biol. Crystallogr.* **2010**, *66*, 133−144.
(91) Muraki, M.; Harata, K.; Sugita, N.; Sato, K.-i. Origin of Carbohydrate Recognition Specificity of Human Lysozyme Revealed by Affinity Labeling. *Biochemistry* **1996**, *35*, 13562−13567.
(92) Vagin, A.; Teplyakov, A. MOLREP: an Automated Program for Molecular Replacement. *J. Appl. Crystallogr.* **1997**, *30*, 1022−1025.
(93) Winn, M.; Ballard, C.; Keegan, R.; Pelios, G.; Zhao, N.; Krissinel, E. The CCP4 software suite - current status and future developments. *Acta Crystallogr., Sect. A: Found. Crystallogr.* **2010**, *66*, s127.
(94) Murshudov, G. N.; Skubák, P.; Lebedev, A. A.; Pannu, N. S.; Steiner, R. A.; Nicholls, R. A.; Winn, M. D.; Long, F.; Vagin, A. A. REFMAC5 for the refinement of macromolecular crystal structures. *Acta Crystallogr., Sect. D: Biol. Crystallogr.* **2011**, *67*, 355−367.
(95) Adams, P. D.; Afonine, P. V.; Bunkóczi, G.; Chen, V. B.; Davis, I. W.; Echols, N.; Headd, J. J.; Hung, L.-W.; Kapral, G. J.; Grosse-Kunstleve, R. W.; McCoy, A. J.; Moriarty, N. W.; Oeffner, R.; Read, R. J.; Richardson, D. C.; Richardson, J. S.; Terwilliger, T. C.; Zwart, P. H. PHENIX: a comprehensive Python-based system for macromolecular structure solution. *Acta Crystallogr., Sect. D: Biol. Crystallogr.* **2010**, *66*, 213−221.
(96) Antosova, A.; Chelli, B.; Bystrenova, E.; Siposova, K.; Valle, F.; Imrich, J.; Vilkova, M.; Kristian, P.; Biscarini, F.; Gazova, Z. Structure-activity relationship of acridine derivatives to amyloid aggregation of lysozyme. *Biochim. Biophys. Acta, Gen. Subj.* **2011**, *1810*, 465−74.
(97) Siposova, K.; Bystrenova, E.; Antosova, A.; Koneracka, M.; Zavisova, V.; Kopcansky, P.; Gazova, Z. Attenuation of the insulin amyloid aggregation in presence of Fe3O4-based magnetic fluids. *Gen. Physiol. Biophys.* **2013**, *32*, 209−14.
(98) Gazova, Z.; Siposova, K.; Kurin, E.; Mucaji, P.; Nagy, M. Amyloid aggregation of lysozyme: the synergy study of red wine polyphenols. *Proteins* **2013**, *81*, 994−1004.
(99) Vuong, Q. V.; Siposova, K.; Nguyen, T. T.; Antosova, A.; Balogova, L.; Drajna, L.; Imrich, J.; Li, M. S.; Gazova, Z. Binding of glyco-acridine derivatives to lysozyme leads to inhibition of amyloid fibrillization. *Biomacromolecules* **2013**, *14*, 1035−43.
(100) Viet, M. H.; Siposova, K.; Bednarikova, Z.; Antosova, A.; Nguyen, T. T.; Gazova, Z.; Li, M. S. In Silico and in Vitro Study of Binding Affinity of Tripeptides to Amyloid beta Fibrils: Implications for Alzheimer's Disease. *J. Phys. Chem. B* **2015**, *119*, 5145−55.

DOI: 10.1021/acsomega.8b02471
ACS Omega 2019, 4, 4206−4220

Conference paper

Vadim B. Krylov, Lucia Paulovičová, Ema Paulovičová, Yury E. Tsvetkov and Nikolay E. Nifantiev*

Recent advances in the synthesis of fungal antigenic oligosaccharides

DOI 10.1515/pac-2016-1011

Abstract: The driving force for the constant improvement and development of new synthetic methodologies in carbohydrate chemistry is a growing demand for biologically important oligosaccharide ligands and neoglycoconjugates thereof for numerous biochemical investigations such as cell-*to*-pathogen interactions, immune response, cell adhesion, etc. Here we report our syntheses of the spacer-armed antigenic oligosaccharides related to three groups of the polysaccharides of the fungal cell-wall including α- and β-mannan, α- and β-glucan and galactomannan chains, which include new rationally designed synthetic blocks, efficient solutions for the stereoselective construction of glycoside bonds, and novel strategy for preparation of furanoside-containing oligosaccharides based on recently discovered pyranoside-*into*-furanoside (PIF) rearrangement.

Keywords: fungal antigens; fungal cell wall; ICS-28; oligosaccharide; pyranoside-*into*-furanoside rearrangement.

Introduction

Natural oligosaccharides and glycoconjugates play a crucial role acting as lectin receptors in different processes determining cell life cycle, cell-*to*-pathogen interactions and infection, cell adhesion and others. This makes spacer-armed oligosaccharide ligands and neoglycoconjugates thereof (i.e. molecular probes in which an oligosaccharide is attached via a spacer to a label or carrier) indispensable tools for the research of the processes which are determined by carbohydrate-lectin interactions to investigate and assess the structural features responsible for specific recognition of carbohydrate ligands in such processes, define ligand-receptor binding topology, and understand the biological functions and mechanisms of action of the corresponding natural glycoconjugates [1, 2].

Recent studies of the mechanisms of cell recognition have revealed a key role of various natural glycoconjugates. Among them, the carbohydrate antigens of fungal and bacterial pathogens are remained to be investigated. Their study is often complicated or even impossible because of very low availability of oligosaccharide of these groups from natural objects that additionally stimulates the development of efficient

Article note: A collection of invited papers based on presentations at the XXVIII International Carbohydrate Symposium (ICS-28), New Orleans, July 17–21 2016.

***Corresponding author: Nikolay E. Nifantiev,** Laboratory of Glycoconjugate Chemistry, N. D. Zelinsky Institute of Organic Chemistry, Russian Academy of Sciences, Leninsky Prospect 47, 119991 Moscow, Russia, e-mail: nen@ioc.ac.ru; nifantiev@gmail.com

Vadim B. Krylov and Yury E. Tsvetkov: Laboratory of Glycoconjugate Chemistry, N. D. Zelinsky Institute of Organic Chemistry, Russian Academy of Sciences, Leninsky Prospect 47, 119991 Moscow, Russia

Lucia Paulovičová and Ema Paulovičová: Department of Immunochemistry of Glycoconjugates, Center for Glycomics, Institute of Chemistry, Slovakia Slovak Academy of Sciences, Dubravská cesta 9, 84538 Bratislava, Slovakia

chemical schemes for their preparation in practical amounts. In this communication, we provide an overview of the schemes which were recently developed by us for the syntheses of linear and branched oligosaccharides related to the polysaccharides of fungal cell wall including α- and β-mannans, α- and β-glucans and galactomannan. These developments include new rationally designed synthetic blocks, efficient solutions for the stereoselective construction of glycoside bonds, and novel strategy for preparation of furanoside containing oligosaccharides based on recently discovered pyranoside-*into*-furanoside (PIF) rearrangement.

Synthesis of linear and branched oligosaccharides structurally related to the mannan of the *Candida* cell-wall

The yeast *Candida albicans* is an opportunistic pathogenic microorganism. It is a component of the normal microflora of the majority of healthy individuals, but is able to cause severe infections in immunocompromised patients such as HIV patients and those undergoing immunosuppressive therapy or prolonged treatment with antibiotics [3, 4]. The cell surface of *C. albicans* first comes into contact with host cells, plays the main role in the adhesion of the pathogen, intercellular communication, and carries important antigenic determinants of the fungus [5, 6]. The main surface antigen of *C. albicans* is mannan which represents the carbohydrate part of the cell wall mannoprotein. This polysaccharide has a comb-like structure with an α-(1→6)-linked main chain, to which relatively short oligomannoside side chains built of α-(1→2)-, α-(1→3)-, α-(1→6)- and β-(1→2)-linked mannose units are attached via α-(1→2)-linkages. These side chains are responsible for the antigenic specificity of *Candida* species. The generalized structure of the mannan and structures of epitopes corresponding to the various antigenic factors [7] of *Candida* are shown in Fig. 1.

We synthesized in the past decade a wide range of oligosaccharides corresponding to the antigenic factors 1, 4, 6, 9 and 34. The synthesis of the linear α-(1→2)-tetramannoside **7** related to the antigenic factor 1 is depicted in Fig. 2 [8]. It was based on the stepwise chain elongation by one monosaccharide unit. Thiomannoside **1** [9] was used as the glycosyl donor. On the one hand, the presence of a 2-*O*-acetyl group in **1** was sought to ensure α-stereoselectivity of mannosylation due to the anchimeric participation. On the other hand, this group could be easily removed to produce a glycosyl acceptor for the next glycosylation. Two initial cycles of mannosylation and deacetylation proceeded smoothly and provided corresponding glycosyl acceptors **2** and **3** in good yields. However, when thioglycoside **1** was coupled with **3**, the predominant formation of the product of β-mannosylation (42 % vs. 28 % of the α-product) was unexpectedly observed. Application of 2-*O*-benzoylated donor **4** instead of **1** strongly enhanced α-stereoselectivity of mannosylation and provided the α-linked trisaccharide in 64 % yield. Final glycosylation of trisaccharide acceptor **5** with

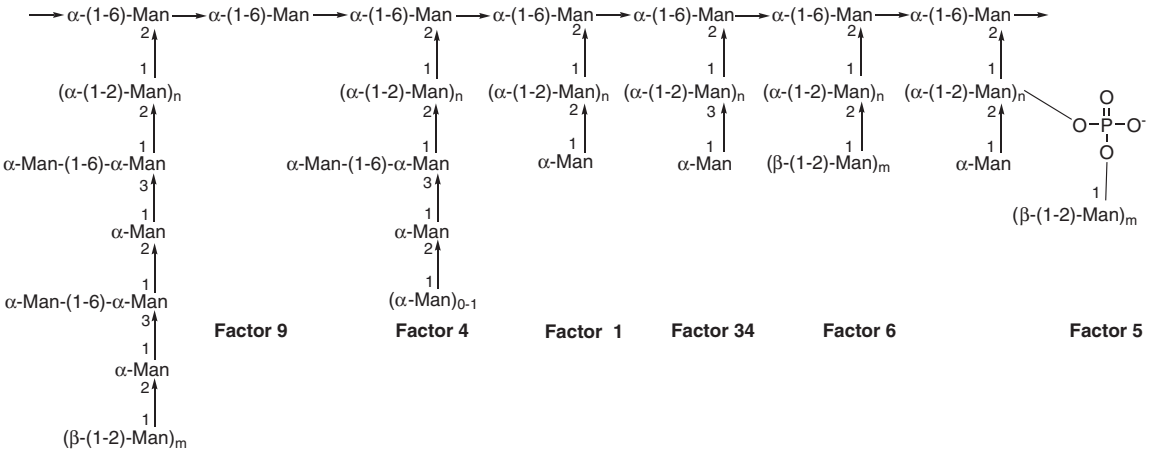

Fig. 1: Structure of the mannan of the *Candida* cell wall.

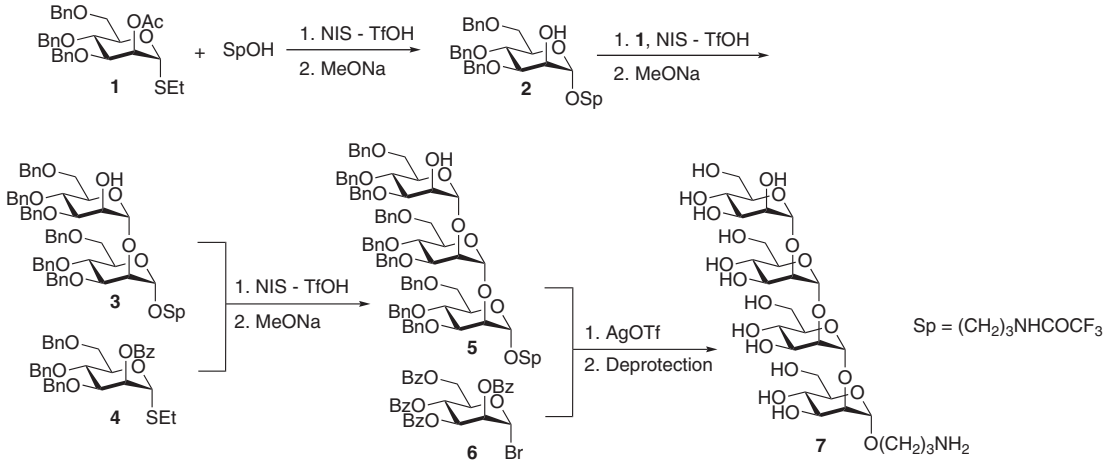

Fig. 2: Synthesis of the linear α-(1→2)-tetramannoside related to the antigenic factor 1.

mannosyl bromide **6** gave the expected tetrasaccharide that was subjected to deprotection to afford free tetrasaccaride **7**.

Unlike the synthesis of **7**, other oligomannosides described in this section were prepared using a convergent blockwise approach. Thus, [2+2] glycosylation was applied for the assembly of a tetrasaccharide **10** with the terminal α-(1→3)-linked mannose unit corresponding to the antigenic factor 34 (Fig. 3) [8]. Used α-(1→3)-linked disaccharide donor block **9** was obtained by AgOTf-promoted glycosylation of thiomannoside **8** with mannosyl bromide **6**. Subsequent coupling of **9** with dimannoside **3** and removal of the protecting groups from the resulting tetrasaccharide provided the target product **10**.

Linear heptasaccharide **21** built of alternating α-(1→2)- and α-(1→3)-mannose residues with a terminal β-(1→2)-mannose unit represented the antigenic factor 9 devoid of α-(1→6)-linked side mannose residues. The latter was synthesized using [3+4] glycosylation in the final step of the oligosaccharide chain assembly (Fig. 4) [10].

At first, the donor and acceptor blocks **15** and **19** were prepared. β-Mannosylation of allyl glycoside **12** [11] with thioglycoside **11** [12] under Crich's conditions [13] afforded β-disaccharide **13** in 69 % yield. Replacement of the 4,6-*O*-benzylidene group by benzoates and transformation of the allyl glycoside into trichloroacetimidate provided glycosyl donor **14** that was coupled with acceptor **8** to furnish trisaccharide donor block **15**. To prepare acceptor block **19**, acceptor **8** was glycosylated with mannosyl chloride **16** [14] with the formation of disaccharide **17**. The acetyl group in **17** was replaced by a chloroacetyl one to give donor **18** as the removal of the acetyl group by acidic methanolysis from the corresponding tetrasaccharide obtained by glycosylation of **3** with **17** was sluggish and produced acceptor **19** in a low yield. Condensation of **18** with **3** followed by removal of the chloroacetyl group from the glycosylation product with thiourea provided necessary acceptor **19**. Final glycosylation of **19** with **15** afforded heptasaccharide **20**; subsequent deprotection of **20** gave free oligomannoside **21**.

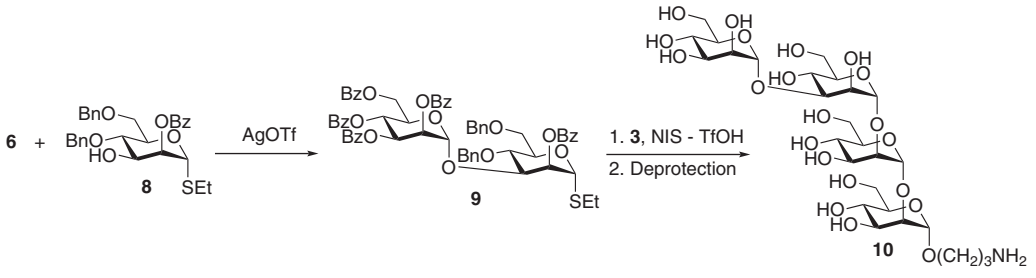

Fig. 3: Synthesis of the linear tetramannoside related to the antigenic factor 34.

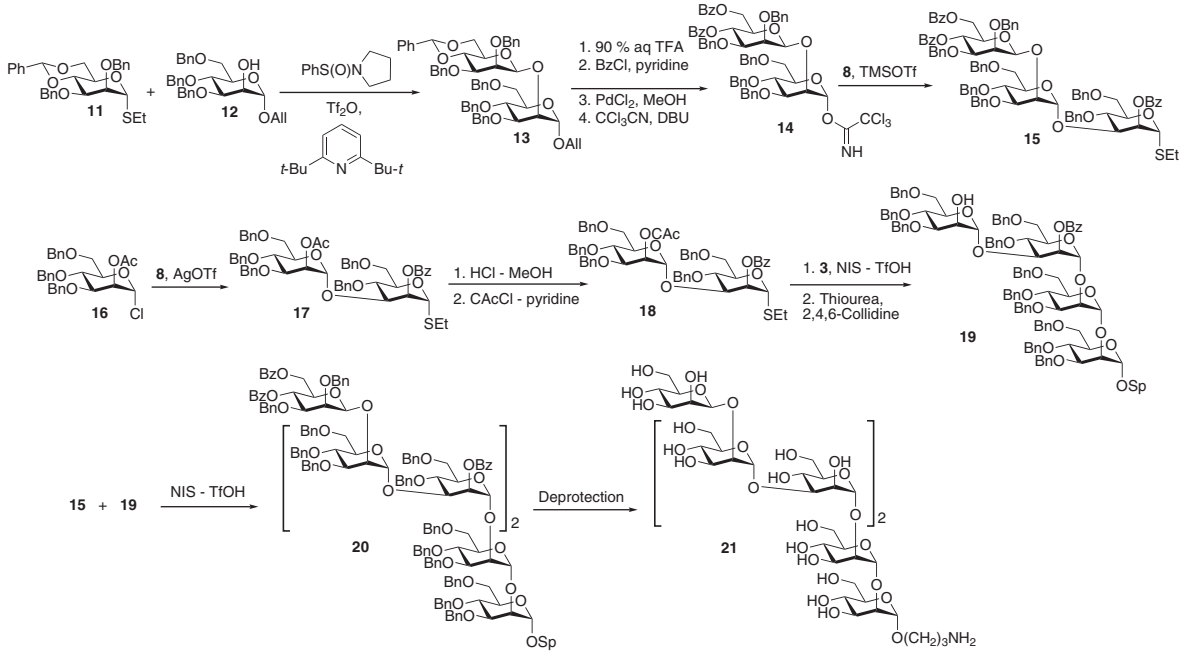

Fig. 4: Synthesis of the linear heptamannoside related to the antigenic factor 9.

3,6-Branched oligomannosides related to the antigenic factor 4 were also synthesized with the use of the blockwise approach. Pentasaccharide **25** was obtained by [3+2] glycosylation (Fig. 5) [15]. Branched trisaccharide glycosyl donor **23** was prepared by the Bredereck glycosylation [16] of 3,6-dityryl ether **22** with mannosyl bromide **6** in the presence of AgOTf. Further coupling of **23** with disaccharide acceptor **3** afforded pentasaccharide **24** that was subjected to deprotection with the formation of free product **25.**

Branched hexasaccharide **32** was assembled from disaccharide blocks **3**, **27** and **31** (Fig. 6) [15]. Monosaccharide precursor **26** of the mannose residue in the branching point contained different protecting groups at O-3 and O-6, thus providing an opportunity to attach different glycosyl substituents to these positions. The Bredereck glycosylation of **26** with mannosyl bromide **6** afforded disaccharide donor **27**. Its coupling with acceptor **3** followed by acidic removal of the silyl protection produced tetrasaccharide acceptor **28**. The third disaccharide block **31** was obtained in 60 % yield by glycosylation of thiomannoside **30** [17] with trichloroacetimidate **29** [18]. It is noteworthy that AgOTf-promoted glycosylation of **30** with bromide **6** provided disaccharide **31** in a much lower yield (~20 %) due to the predominant transfer of the EtS group from acceptor **30** to donor **6**. Since donor **31** contained a nonparticipating glycosyl substituent at O-2 of the glycosylating mannose residue, its reaction with **28** was not stereospecific and afforded the necessary α-hexasaccharide in a moderate yield (44 %) along with the corresponding β-anomer (14 %). Removal of protecting groups from the α-product gave hexasaccharide **32.**

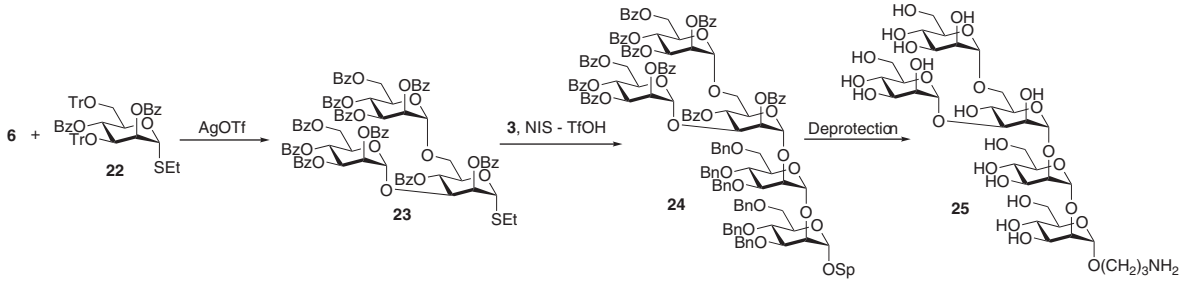

Fig. 5: Synthesis of the branched pentamannoside related to the antigenic factor 4.

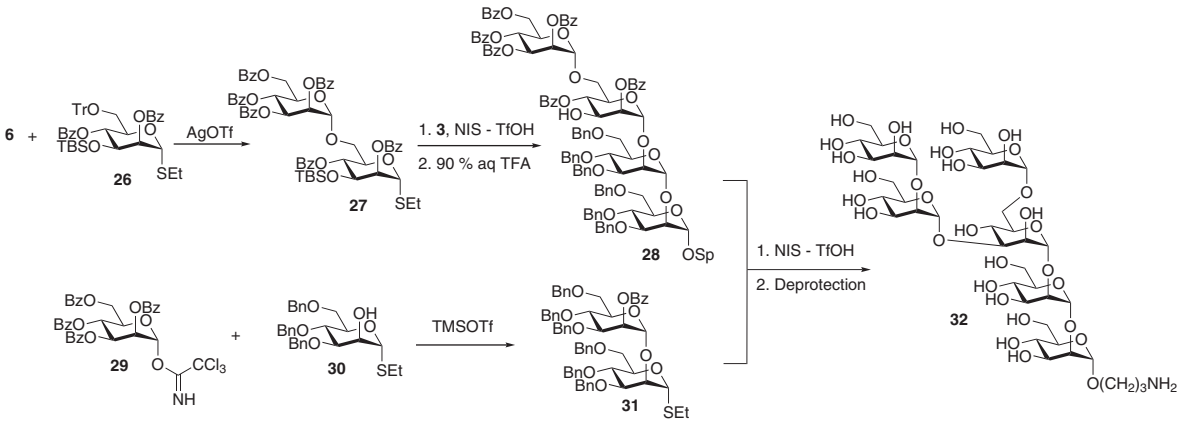

Fig. 6: Synthesis of the branched hexamannoside related to the antigenic factor 4.

We have also synthesized a series of oligosaccharides, in which β-(1 → 2)-mannoside blocks comprising 1–4 monosaccharide residues are attached via a glycoside bond to O-2 of the terminal unit of an α-(1 → 2)-oligomannoside chain. This type of β-(1 → 2)-oligomannosides is referred to as acid-stable mannan and corresponds to the antigenic factor 6. β-Mannosylation is one of the most difficult cases of glycosylation reactions [19]. Two general approaches to β-mannosylation are known to date. The first one is indirect and based on initial β-glucosylation followed by inversion of the configuration at C-2 in the glucose residue [20]. The second one is based on direct β-mannosylation with conformationally rigid 4,6-*O*-benzylidene-protected mannosyl donors [21]. In contrast to the first approach that allows the chain elongation to be performed by only one monosaccharide unit, more efficient blockwise assembly of (1 → 2)-oligomannoside chains [22, 23] is possible in the case of direct β-mannosylation. There is also a single example [24] of the preparation of β-(1 → 2)-oligomannosides using the intramolecular aglycon delivery (for a review see [25]).

Our synthesis was based on direct β-mannosylation with donor blocks containing up to four mannose residues for the assembly of the target oligosaccharides. One of our aims was to ascertain, whether the donor blocks larger than the reported dimannosides [22, 23] can successfully be applied to the introduction of long β-(1 → 2)-oligomannoside sequences into an oligosaccharide chain. The synthesis of the oligomannoside donors is outlined in Fig. 7 [26, 27]. Disaccharide thioglycoside **33** was used as the starting material. Its oxidation with *m*CPBA led to sulfoxide **34**, and removal of the PMP group provided disaccharide acceptor **35**.

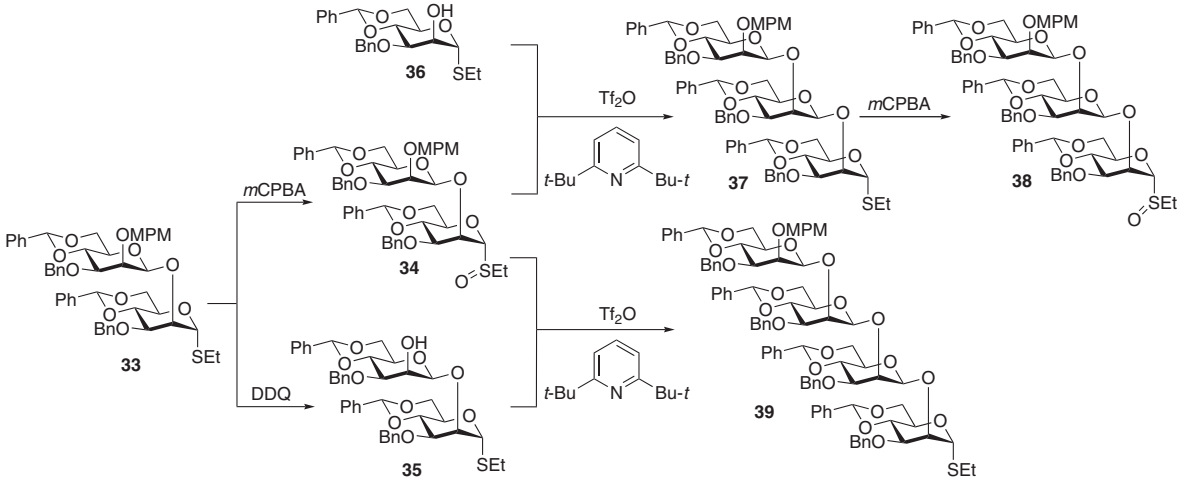

Fig. 7: Synthesis of oligomannosyl donors for the assembly of β-(1 → 2)-oligomannosides.

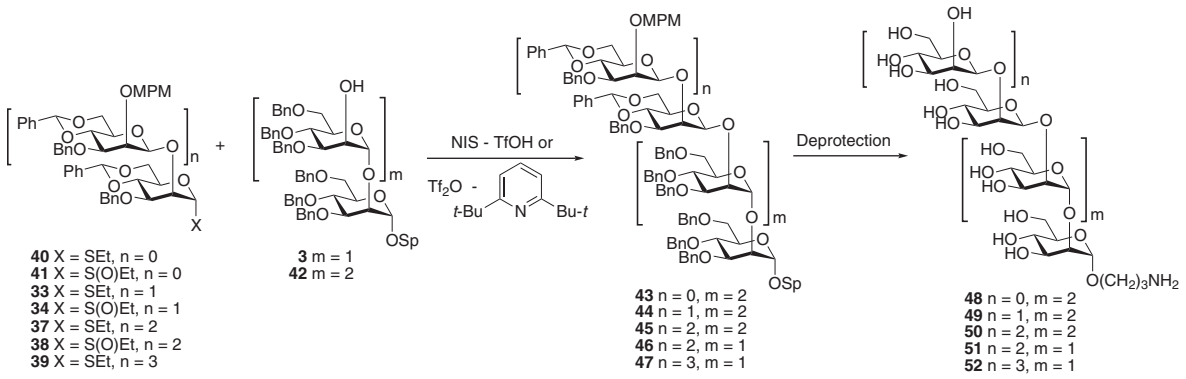

Fig. 8: Synthesis of oligomannosides related to the antigenic factor 6.

β-Mannosylation of acceptors **36** [28] and **35** with sulfoxide **34** under preactivation conditions [21] produced tri- and tetramannoside donors **37** and **39**, respectively. Oxidation of **37** gave sulfoxide **38**.

The set of available β-(1→2)-oligomannoside donors **33**, **34**, and **37–39** together with known monosaccharide donors **40** and **41** [29] allowed the synthesis of oligomannosides comprising from one to four β-mannosyl units (Fig. 8). Besides, having three pairs of thioglycoside and sulfoxide donors, we could study the influence of the donor type and activation conditions on the efficiency of β-mannosylation. Published data concerning these issues are contradictory [19, 21]. Within the pair of the monosaccharide donors, NIS–TfOH-promoted mannosylation of acceptor **42** with thioglycoside **40** without preactivation [21] provided a higher yield (37 %) of tetrasaccharide **43** than that with sulfoxide **41** under preactivation conditions (17 %). A similar result was obtained in the case of dimannoside donors: glycosylation of **42** with thioglycoside **33** without preactivation gave 65 % of pentasaccharide **44**, while sulfoxide **34** with preactivation provided a lower yield of **44** (37 %). On the contrary, only glycosylation of **42** with trisaccharide sulfoxide **38** under preactivation conditions gave hexasacchride **45** in a modest yield (27 %), while no formation of **45** was observed upon glycosylation with thioglycoside **37**. Finally, NIS–TfOH-promoted glycosylation of acceptor **3** with tri- and tetrasacchride thioglycosides **37** and **39** afforded oligosaccharides **46** and **47** in yields of 41 and 53 %, respectively.

Two conclusions may be drawn from these results: first, the donor blocks larger than dimannosides can be applied for the blockwise synthesis of oligosaccharides comprising long β-(1→2)-oligomannoside sequences; second, the efficiency of β-mannosylation with mono- and oligomannoside donors seems to depend more on the structure of the reaction partners than on the applied activation protocol (i.e. with or without preactivation of the donor). Removal of the protecting groups from compounds **43–47** furnished free oligomannosides **48–52**.

Some of the oligomannosides described in this section were conjugated to BSA [8, 10, 15] using a squarate procedure [30]. Immunomodulatory properties of these glycoconjugates have extensively been studied [31–35] as well.

Synthesis of linear and branched oligosaccharides structurally related to fungal β-glucan

β-(1→3)-Glucan is the major structural polysaccharide of the fungal cell wall, constituting approximately 50–60 % of the wall by dry weight [36]. The presence of this highly conserved glycopolymer in different pathogenic fungal species makes it a rational target for vaccine development. Conjugates of either natural β-(1→3)-glucan, laminarin [37], or linear synthetic β-(1→3)-oligoglucosides [38, 39] with carrier proteins were shown to be immunogenic and protective in mice against infections induced by *Candida albicans* and

Aspergillus fumigatus. This opens a very good prospect to develop an efficient vaccine against both these dangerous pathogens because of the presence of β-(1 → 3)-glucan as the component of their cell wall. Important biological properties of β-(1 → 3)-glucans stimulated considerable activity in the chemical synthesis of β-(1 → 3)-oligoglucosides that was summarized by us in a recent review [40]. The most of published syntheses of β-(1 → 3)-oligoglucosides were based on application of glycosyl acceptors protected with 4,6-*O*-benzylidene and 2-*O*-acyl groups. However, the use of regioselective 3-*O*-glycosylation of 4,6-*O*-benzylidene-protected glycosyl acceptors with a free 2-OH group [41] seems to be more convenient. In our synthesis, we employed regioselective 3-*O*-glycosylation of 4,6-*O*-benzylidene-protected 2,3-diol glycosyl acceptors by a disaccharide donor block for the chain elongation. The synthesis of the donor block and a trisaccharide acceptor is presented in Fig. 9.

Glycosylation of 2,3-diol **54** [42] with trichloroacetimidate **53** [43] displayed good regioselectivity providing the corresponding β-(1 → 3)-disaccharide in 55 % yield along with its β-(1 → 2)-linked isomer (8 %), which were easily separated by silica gel column chromatography. Subsequent conventional benzoylation of free 2-OH gave disaccharide thioglycoside **55**. Similar regioselective glycosylation of spacer-armed 2,3-diol **56** [44] with **55** followed by benzoylation of the remaining 2-OH group resulted in the formation of trisaccharide **57**. Selective removal of the acetyl groups in the presence of benzoates was achieved by brief treatment of **57** with a large excess (50 equiv.) of hydrazine hydrate; as a result, acceptor **58** was obtained in 79 % yield. However, for the further chain elongation, we decided to use a glycosyl donor containing chloroacetyl groups as temporary protections of 2,3-diol to ensure its more reliable and efficient liberation for the next glycosylation step. To this aim, the acetyl groups in **55** were removed with hydrazine hydrate and the diol formed was chloroacetylated to furnish donor **59**. The assembly of a series of β-(1 → 3)-oligoglucosides comprising the odd number of monosaccharide units from donor **59** and acceptor **58** is presented in Fig. 10.

NIS–TfOH-promoted glycosylation of **58** with **59** was completely regioselective and produced β-(1 → 3)-linked pentasaccharide **60** in 91 % yield. The hydroxyl group in the former acceptor glucose residue was acetylated, and then the chloroacetyl groups were selectively removed to provide a new acceptor. Its glycosylation with **59** afforded heptasaccharide **61**. Iteration of acetylation, dechloroacetylation and glycosylation afforded in sequence nonasaccharide **62**, undecasaccharide **63** and tridecasaccharide **64**. Transformation of the protected oligomers into free 3-aminopropyl glycosides **65**–**70** included successive acidic removal of the benzylidene groups, basic deacylation and hydrogenolysis of the *N*-benzyloxycarbonyl group.

We have also synthesized two branched hexaglucosides in which a single β-(1 → 6)-glucose residue is attached either to the first or to the central glucose unit of a linear β-(1 → 3)-pentaglucoside core. The synthesis was based on the initial assembly of a linear β-(1 → 3)-pentaglucoside that bore a selectively removable 4,6-*O*-(*p*-methoxybenzylidene) group in the glucose residue subsequently forming the branching point (Figs. 11 and 12) [45]. Many of the mono- and oligosaccharide synthetic block used in the above synthesis of linear oligoglucosides were also employed for the preparation of the branched oligosaccharides.

Selective TMSOTf-promoted glycosylation of diol **56** with trichloroacetimidate **53** afforded disaccharide **71** that was subjected to benzoylation and selective deacetylation to give disaccharide diol **72**. The glucose block with the 4,6-*O*-(*p*-methoxybenzylidene) group was introduced by glycosylation of diol **72** with imidate

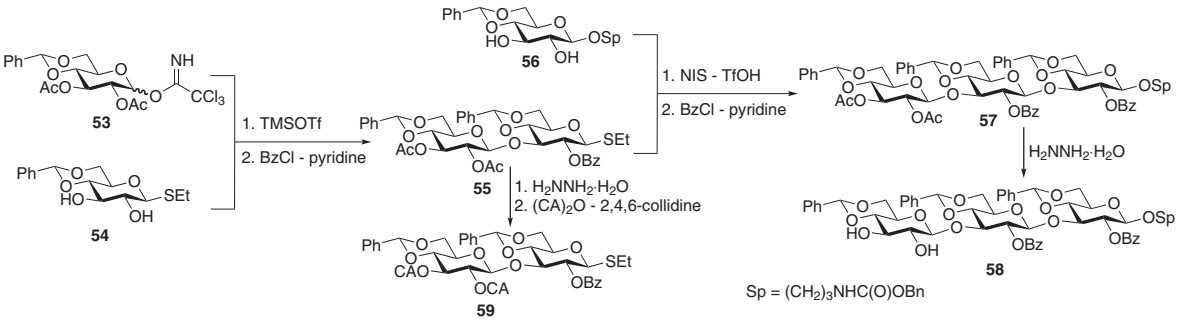

Fig. 9: Synthesis of the disaccharide glycosyl donor and the trisaccharide glycosyl acceptor.

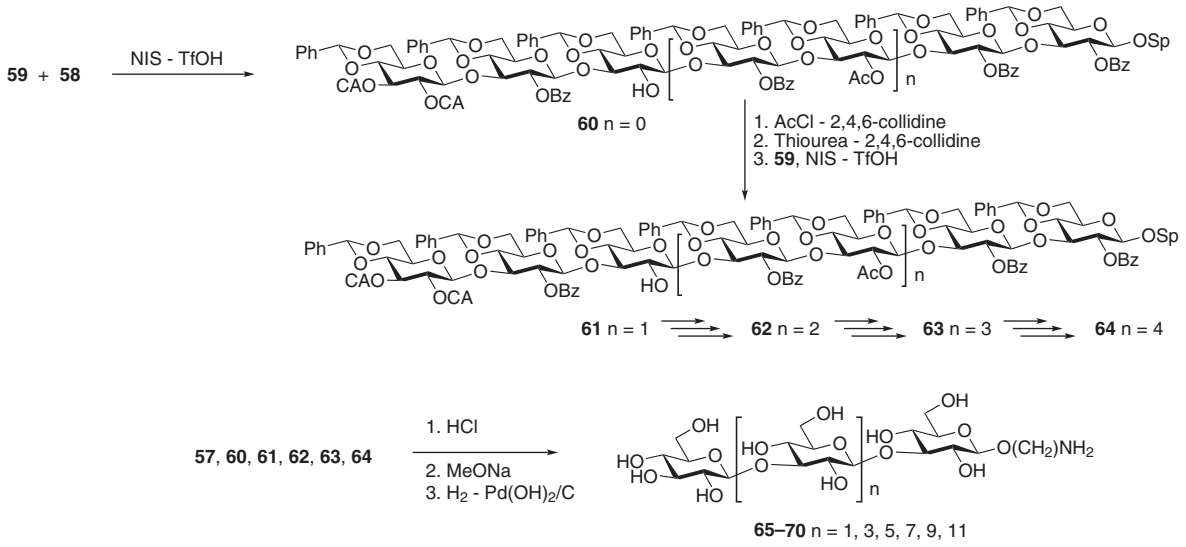

Fig. 10: Assembly of linear β-(1 → 3)-oligoglucosides.

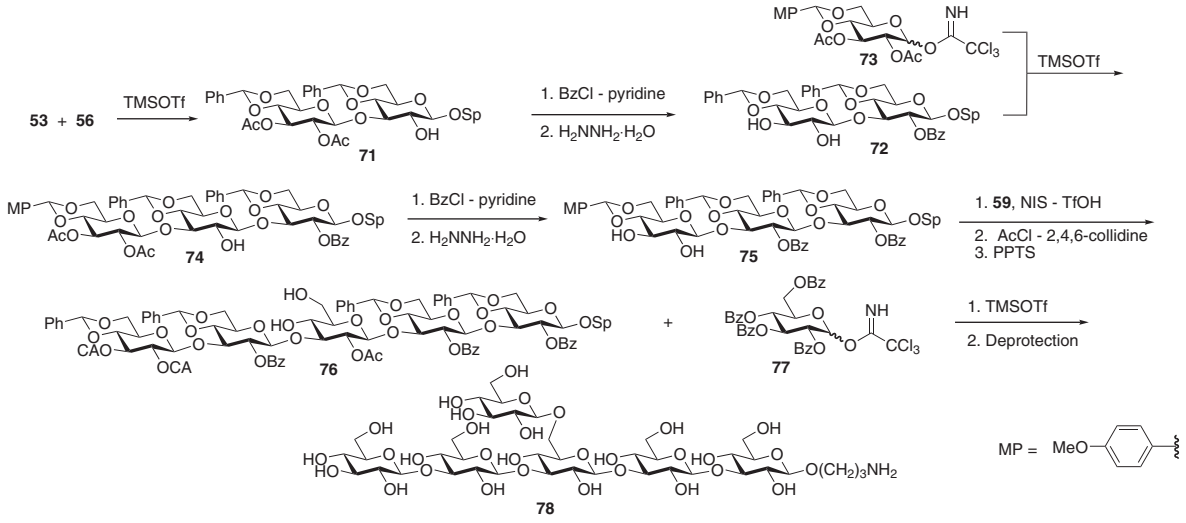

Fig. 11: Synthesis of the hexaglucoside with branching in the central glucose unit of the linear core.

73 resulting in the formation of trisaccharide **74.** Subsequent benzoylation and deacetylation of **74** provided trisaccharide diol **75.** Its glycosylation with thioglycoside **59**, acetylation of free 2-OH in the pentasaccharide formed and selective hydrolysis of *p*-methoxybenzylidene acetal produced pentasaccharide acceptor **76** for the final attachment of the side glucose unite. Selective glycosylation of the primary hydroxyl group in **76** with imidate **77** afforded a hexasaccharide (65 %) that was deprotected as described above for the linear analogs to provide target free oligosaccharide **78.**

The second branched hexasaccharide was prepared in a similar way (Fig. 12) [45]. 4,6-*O*-(*p*-Methoxybenzylidene)-protected acceptor **79** representing the glucose unit at the reducing end of the chain was twice elongated using disaccharide thioglycosides **59** and **55**. First glycosylation with **59** afforded trisaccharide **80** that was converted into acceptor **81**, and the second glycosylation with **55** produced pentasaccharide **82**. Selective removal of the *p*-methoxybenzylidene protection from **82** gave triol **83**. Glycosylation of **83** with trichloroacetimidate **84** proceeded regioselectively at the primary OH group and provided a hexasacchride in 70 % yield; its subsequent deprotection resulted in the formation of target product **85.**

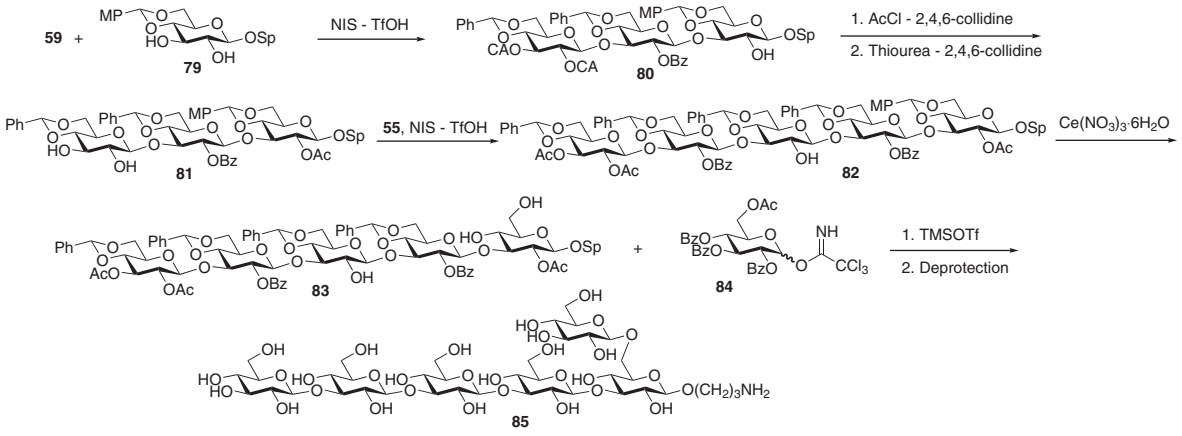

Fig. 12: Synthesis of the hexaglucoside with branching in the first glucose unit of the linear core.

Linear nonaglucoside **68** and branched hexaglucoside **78** were conjugated to BSA via a squarate linker. The conjugates were studied in respect to the development of an antifungal vaccine [34, 46]. Protective effect of active immunization with the conjugate of linear nonaglucoside **78** has been revealed in vivo in the experimental hematogenously disseminated *C. albicans* infection [46].

Synthesis of linear oligosaccharides structurally related to α-glucan of *Aspergillus fumigatus* cell wall

Aspergillus fumigatus is a very common air-borne mold causing severe and usually fatal invasive aspergillosis infection in immunosuppressed hospital patients. At risk are mainly patients in onco-hematology units and those undergoing intensive immunosuppressive therapy after receiving organ transplants. α-(1→3)-Glucan is the major polysaccharide of *A. fumigatus* cell wall and constitutes 19 and 40 % of the conidial and mycelial cell wall polysaccharides, respectively. It contributes to the virulence of diverse fungal pathogens and is involved in the aggregation of germinating conidia and biofilm formation. Moreover, it has been shown in experimental murine aspergillosis models that α-(1→3)-glucan has a prominent immunological role conferring a long-term survival [47]. The study of functions of this polysaccharide is complicated by its insolubility in water, therefore, synthetic soluble α-(1→3)-glucooligosaccharides of strictly defined structure and their conjugates with protein carriers and labels would provide tools for better control of antibody production with better definition of the epitope recognized and help in the identification of the human receptor for this polysaccharide.

The prerequisite for efficient preparation of sufficiently long α-(1→3)-oligoglucosides (Fig. 13) is high α-stereoselectivity at each glycosylation step. We planned to achieve it using the remote anchimeric assistance of acyl groups [48, 49]. Model investigations showed that glucosyl *N*-phenyltrifluoroacetimidates bearing two participating acyl groups at O-3 and O-6 or a single acyl group at O-6 only provided high efficiency and α-stereoselectivity of glucosylation [50]. The ability of the 6-*O*-acylated glucosyl donors to highly stereoselective α-glucosylation was of particular importance, since it enabled application of α-(1→3)-linked disaccharide and potentially higher oligosaccharide donor blocks, containing a 6-*O*-acyl group in the glycosylating glucose unit, for the chain elongation without loss of α-stereoselectivity.

The successful use of this finding for the synthesis of the α-(1→3)-pentaglucoside is presented in Fig. 13 [51]. Selectively removable *p*-methoxyphenyl and levulinoyl groups serving for temporary protection of 3-OH and the anomeric position, respectively provided the simple and efficient interconversion of donor and acceptor blocks. Glycosyl acceptor **89** representing the reducing end of the chain was synthesized from 4,6-*O*-benzylidene derivative **86** by successive removal of the anomeric MP group, conversion of the

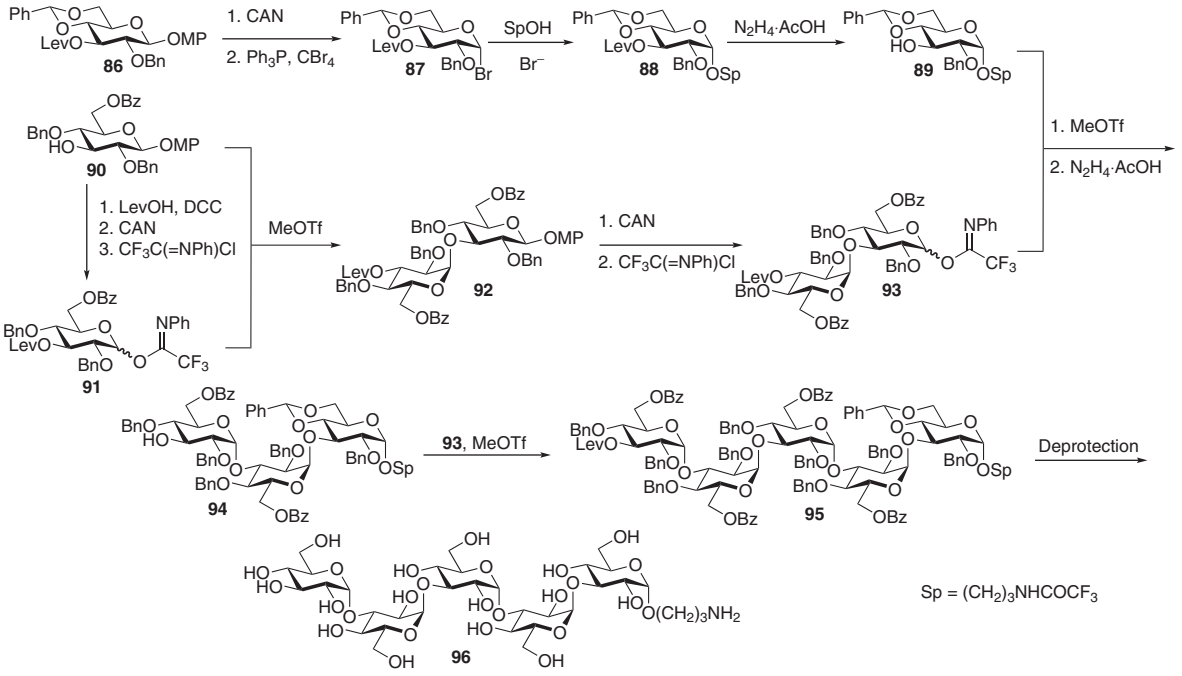

Fig. 13: Synthesis of α-(1→3)-pentaglucoside.

hemiacetal formed into glycosyl bromide **87**, halide-catalyzed α-glucosylation of 3-trifluoroacetamidopropanol and removal of the levulinoyl group from glycoside **88**. The donor and acceptor blocks for the chain elongation were prepared from the single precursor **90**. Acylation of 3-OH, removal of the anomeric MP group and acylation of the anomeric hydroxyl with $CF_3C(=NPh)Cl$ afforded monosaccharide glucosyl donor **91**. Its MeOTf-promoted coupling with acceptor **90** smoothly gave α-disaccharide **92** (90 %) that was converted in two steps into disaccharide donor **93** in total yield of 70 %. Glycosylation of acceptor **89** with **93** followed by removal of the levulinoyl group afforded trisaccharide acceptor **94**. In the final step, **94** was coupled with imidate **93** to provide α-pentasaccharide in 68 % yield. Deprotection of **95** included successive removal of the Lev group with hydrazine acetate, removal of the benzyl and benzylidene groups by catalytic hydrogenolysis and basic splitting of O- and N-acyl groups and gave free α-(1→3)-pentaglucoside **96**. This compound was conjugated to BSA via a squarate linker, and the conjugate obtained was used for induction of antibodies in mice. These polyclonal antibodies were shown to be efficient for immunolabeling α-(1→3)-glucan-positive morphotypes of *A. fumigatus* [51].

Synthesis of linear oligosaccharides structurally related to *Aspergillus* galactomannan

Galactomannan is a specific carbohydrate antigen of *A. fumigatus* [52]. Diagnosis of invasive aspergillosis infections commonly employs detection of this polysaccharide antigen circulating in the patient serum [52]. Moreover, galactomannan is considered as a promising base for development of approaches to the aspergillosis treatment using vaccines or therapeutic antibodies. With regard to the importance of *A. fumigatus* galactomannan, we initiated the synthesis of related antigenic oligosaccharides. Galactomannan represents a structurally diverse heteropolysaccharide build up from poly-D-mannose backbone with β-(1→5)-linked oligogalactofuranoside side chains attached to some of the mannose units via (1→6)- and/or (1→3)-bonds [53]. We performed (Fig. 14) the synthesis of two galactomannan-related heterosaccharides **109** and **112** containing both (1→6)- and (1→3)-linkages between galactose and mannose moieties [54].

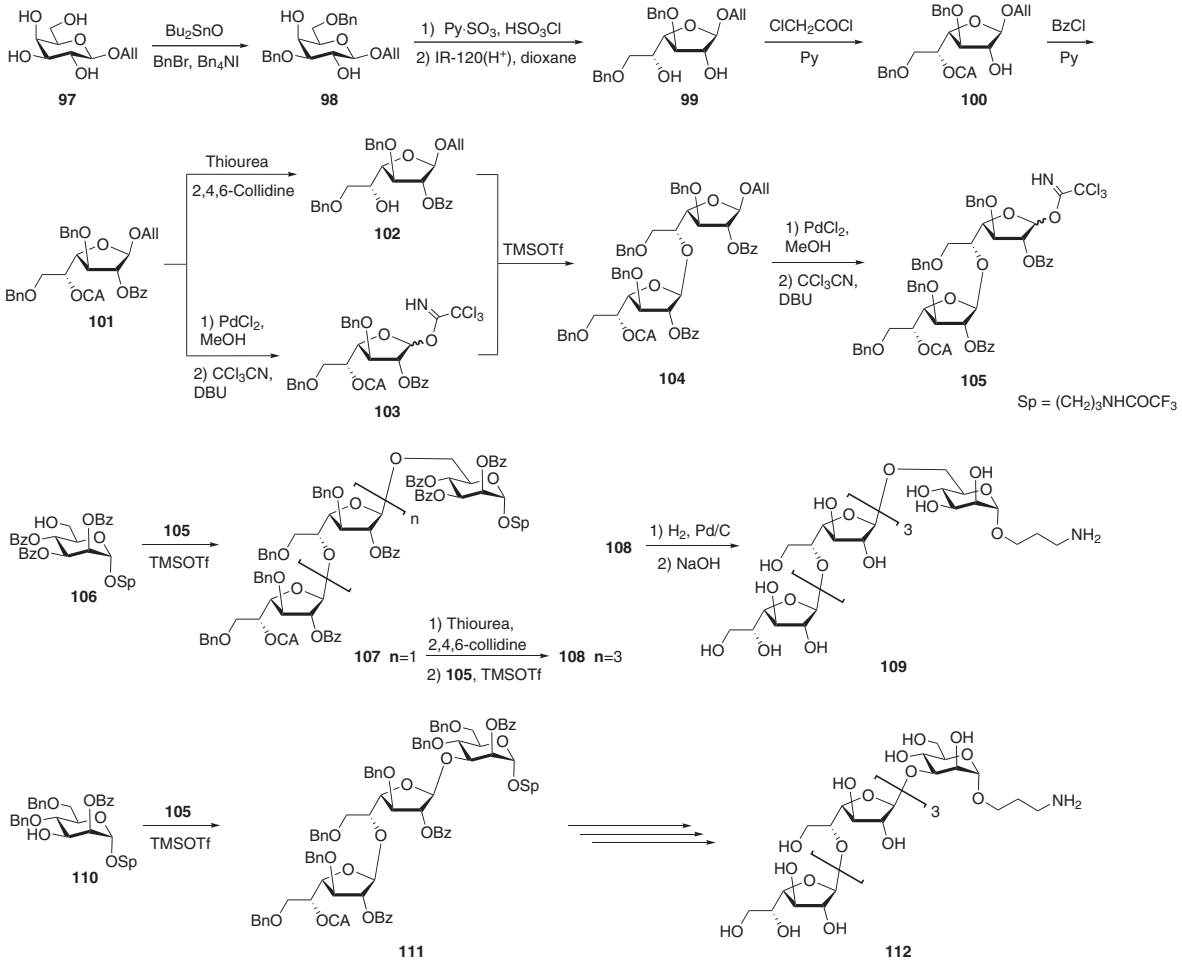

Fig. 14: Synthesis of pentasaccharides **109** and **112** related to the galactomannan from *A. fumigatus*.

The synthesis was carried out with the use of the recently discovered PIF-rearrangement [55–58] of selectively O-substituted galactopyranoside **98** which was prepared by regioselective 3,6-di-O-benzylation of allyl galactoside **97** via the organotin intermediate. PIF-rearrangement of pyranoside **98** into sulfated furanoside occurred upon treatment with the Py·SO_3 complex and chlorosulfonic acid; subsequent solvolytic *O*-desulfation in dioxane in the presence of Amberlite IR-120 (H^+) afforded furanoside **99**. The reactivity of the 5-OH and 2-OH groups in diol **99** was rather different. Thus, chloroacetylation of **99** in the presence of pyridine in DCM at low temperatures smoothly produced 5-O-acylated product **100**, which was then benzoylated to give orthogonally protected precursor **101**. A part of compound **101** was transformed into glycosyl-acceptor **102** by dechloroacetylation with thiourea and another part of **101** was deallylated and converted into trichloroacetimidate to give glycosyl donor **103**. The coupling of **102** and **103** in the presence of TMSOTf gave exclusively β-linked disaccharide **104**. Anomeric O-deallylation and subsequent trichloroacetimidoylation of disaccharide **104** gave desired disaccharide donors **105**.

Spacer-armed mannoside **106** was glycosylated with disaccharide donor **105** to give trisaccharide **107** with newly formed β-(1→6)-bond. O-Dechloroacetylation and subsequent glycosylation by trichloroacetimidate **105** gave pentasaccharide **108**. Its full deprotection yielded target spacer-armed pentasaccharide **109**. For the synthesis of isomeric pentasaccharide **112** comprising the β-(1→3)-bond between galactoside and mannoside residues, spacer-armed mannoside acceptor **110** was glycosylated with disaccharide donor **105**. Further chain elongation followed by complete O-deblocking gave desired pentasaccharide **112**.

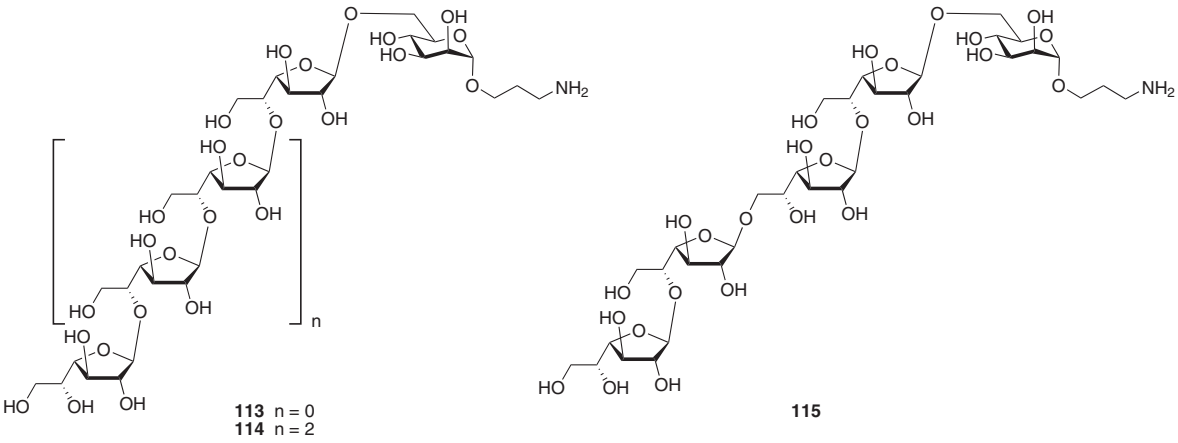

Fig. 15: Synthesized oligosaccharides **113–115** related to the galactomannan from *A. fumigatus*.

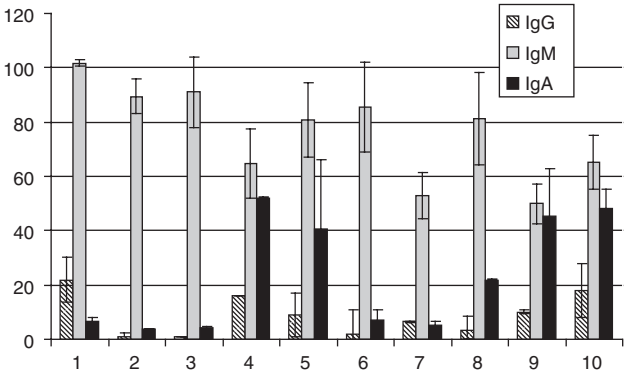

Fig. 16: An overview of sera anti-oligosaccharide specific Ig class antibody responses. Biotinylated derivatives of oligosaccharide ligands [***1*** – Galf(1→5)-[Galf(1→5)]$_3$-(1→6)-αMan; ***2*** – Galf(1→5)-[Galf(1→5)]$_3$-(1→3)-αMan; ***3*** – βGlc-(1→3)-βGlc-(1→3)-[βGlc-(1→6)]-βGlc-(1→3)-βGlc-(1→3)-βGlc; ***4*** – βGlc-(1→3)-[βGlc(1→3)]$_7$-βGlc; ***5*** – βMan-(1→2)-αMan-(1→3)-αMan-(1→2)-αMan-(1→3)-αMan-(1→2)-αMan-(1→2); ***6*** – αMan-(1→2)-αMan-(1→3)-[αMan-(1→6)]-αMan-(1→2)-αMan-(1→2)-αMan; ***7*** – αMan-(1→2)-[αMan-(1→3)]-αMan-(1→2)-αMan-(1→2)-αMan; ***8*** – αMan-(1→3)-αMan-(1→2)-αMan-(1→2)-αMan; ***9*** – αMan-(1→2)-αMan-(1→2)-αMan; ***10*** – βMan-(1→2)-αMan-(1→2)-αMan] were used as antigens. Study cohort comprised 32 patients with RVC (Dept. Clin. Immunol. Allergol., OISE, Bratislava, Slovakia). Sera levels were determined by modified ELISA anti-*Candida* (Biogema, Košice, Slovakia).

Prepared oligosaccharides **109** and **112** were conjugated to BSA using squarate procedure [30] and labeled with biotin. These glycoconjugates were used for generation of monoclonal antibodies and also as model ligands for determination of their ligand specificity.

The above synthetic approaches together with controlled O(5)→O(6) benzoyl migration were also applied [59] for the synthesis of tri- (**113**) and heptasaccharide **114** and to the synthesis of pentasaccharide **115** (Fig. 15) whose oligo-galactofuranosyl sequence contains not only β-(1→5)-bonds but also one β-(1→6)-bond which was detected in minor components of galactomannan [60].

Conclusion and prospects

Described syntheses considerably extend the repertoire of chemical approaches towards stereo- and regioselective assembling of homo- and heterosaccharide chains which are structurally related to polysaccharide components of fungal cell wall. The carbohydrate derivatives of this group are required for a variety of

glycobiologic and pharmaceutical investigations including the screening of specificity of anti-carbohydrate Abs [46, 51, 61], design of immunogens and preparation MAbs for in vitro diagnostics for detecting sera Ig-isotypic antibodies (for example see Fig. 16 and [34]) or monitoring of the efficacy of anti-fungal treatment and disease progression. Synthetic spacered oligosaccharide ligands are also required in the development of therapeutic MAbs and vaccines (see also [62]), search for inhibitors of the polysaccharide biosynthesis and blockers of fungal adhesion to host cells. Synthetic oligosaccharides of defined structure representing different fragments of fungal polysaccharides are also indispensable models for different spectral investigations [63], including computer-assisted ones [64, 65] and conformational analysis to assess the details of 3D spatial organization of fungal carbohydrate antigens and their interaction with related receptors. β-(1→3)-Glucan related oligosaccharide ligands represent also an interest as potential vector components which may enhance vaccine efficiency by its targeting to dendritic cells carrying Dectin-1 [66, 67].

Acknowledgments: This work was supported by the Russian Science Foundation (grant 14-23-00199).

References

[1] *Synthetic Oligosaccharides*: *Indispensable Probes for the Life Sciences*, P. Kovac (Ed.), ACS Symposium Series 560; American Chemical Society: Washington, DC (1994).
[2] *Essentials of Glycobiology*, A. Varki, R. Cummings, J. Esko, H. Freeze, G. Hart, J. Marth (Eds.). Cold Spring Harbor Laboratory Press, Cold Spring Harbor, New York (2009).
[3] M. A. Pfaller, R. N. Jones, S. A. Messer, M. B. Edmond, R. P. Wenzel. *Diagn. Microbiol. Infect. Dis.* **31**, 327 (1998).
[4] P. G. Pappas, J. H. Rex, J. Lee, R. J. Hamill, R. A. Larsen, W. Powderly, C. A. Kauffman, N. Hyslop, J. E. Mangino, S. Chapman, H. W. Horowitz, J. E. Edwards, W. E. Dismukes. *Clin. Infect. Dis.* **37**, 634 (2003).
[5] L. A. Perez-Garcia, D. F. Diaz-Jimenez, A. Lopez-Esparza, H. M. Mora-Montes. *J. Glycobiol.* **1**, 102 (2011).
[6] J. Masuoka. *Clin. Micribiol. Rev.* **17**, 281 (2004).
[7] S. Suzuki. *Curr. Top. Med. Mycol.* **8**, 57 (1997).
[8] A. A. Karelin, Y. E. Tsvetkov, G. Kogan, S. Bystricky, N. E. Nifantiev. *Russ. J. Bioorg. Chem.* **33**, 110 (2007).
[9] T. Peters. *Liebigs Ann. Chem.* **1991**, 135 (1991).
[10] A. A. Karelin, Y. E. Tsvetkov, L. Paulovičová, S. Bystrický, E. Paulovičová, N. E. Nifantiev. *Carbohydr. Res.* **344**, 29 (2009).
[11] T. Ogawa, T. Nukada. *Carbohydr. Res.* **136**, 135 (1985).
[12] P. J. Garreg, I. Kvarnstroem, G. Niklasson, S. C. T. Svensson, *J. Carbohydr. Chem.* **12**, 933 (1993).
[13] D. Crich, A. Banerjee, W. Li, Q. Yao. *J. Carbohydr. Chem.* **24**, 415 (2005).
[14] T. Ogawa, K. Katano, K. Sasajima, M. Matsui. *Tetrahedron* **37**, 2779 (1981).
[15] A. A. Karelin, Y. E. Tsvetkov, L. Paulovičová, S. Bystrický, E. Paulovičová, N. E. Nifantiev. *Carbohydr. Res.* **345**, 1283 (2010).
[16] H. Bredereck, A. Wagner, G. Faber, H. Ott, J. Rauther. *Chem. Ber.* **92**, 1135 (1959).
[17] H. Paulsen, M. Heume, H. Neurnberger. *Carbohydr. Res.* **200**, 127 (1990).
[18] F. Bien, T. Ziegler. *Tetrahedron: Asymmetry* **9**, 781 (1998).
[19] X. Zhu, R. R. Schmidt. *Angew. Chem. Int. Ed.* **48**, 1900 (2009).
[20] F. Mathew, M. Mach, K. C. Hazen, B. Fraser-Reid. *Synlett* 1319 (2003).
[21] D. Crich, S. Sun, *Tetrahedron* **54**, 8321 (1998).
[22] J. Rahkila, F. S. Ekholm, R. Panchadhayee, A. Ardá, F J. Cañada, J. Jiménez-Barbero, R. Leino. *Carbohydr. Res.* **383**, 58 (2014).
[23] F. Dromer, R. Chevalier, B. Sendid, L. Improvisi, T. Jouault, R. Robert, J. M. Mallet, D. Poulain. *Antimicrob. Agents Chemother.* **46**, 3869 (2002).
[24] V. Gannedi, A. Ali, P. P. Singh, R. A. Vishwakarma. *Tetrahedron Lett.* **55**, 2945 (2014).
[25] A. Ishiwata, Y. J. Lee, Y. Ito. *Org. Biomol. Chem.* **8**, 3596 (2010).
[26] A. A. Karelin, Y. E. Tsvetkov, E. Paulovičová, L. Paulovičová, N. E. Nifantiev. *Russ. Chem. Bull. Int. Ed.* **64**, 2942 (2015).
[27] A. A. Karelin, Y. E. Tsvetkov, E. Paulovičová, L. Paulovičová, N. E. Nifantiev. *Eur. J. Org. Chem.* **2016**, 1173 (2016).
[28] D. Crich, S. Sun, J. Brunckova. *J. Org. Chem.* **61**, 605 (1996).
[29] D. Crich, A. Banerjee, Q. Yao. *J. Am. Chem. Soc.* **126**, 14930 (2004).
[30] L. F. Tietze, M. Arlt, M. Beller, K.-H. Glusenkamp, E. Jahde, M. Rajewsky. *Chem. Ber.* **124**, 1215 (1991).
[31] L. Paulovičová, S. Bystricky, E. Paulovičová, A. A. Karelin, Y. E. Tsvetkov, N. E. Nifantiev. *FEMS Immunol. Med. Microbiol.* **58**, 307 (2010).
[32] L. Paulovičová, E. Paulovičová, A. A. Karelin, Y. E. Tsvetkov, N. E. Nifantiev, S. Bystrický. *Int. Immunopharmacol.* **14**, 179 (2012).
[33] L. Paulovičová, E. Paulovičová, A. A. Karelin, Y. E. Tsvetkov, N. E. Nifantiev, S. Bystrický. *Scand. J. Immunol.* **77**, 431 (2013).

[34] E. Paulovičová, L. Paulovičová, R. Pilišiová, S. Bystrický, D. V. Yashunsky, A. A. Karelin, Y. E. Tsvetkov, N. E. Nifantiev. *FEMS Yeast Res*. **13**, 659 (2013).
[35] L. Paulovičová, E. Paulovičová, A. A. Karelin, Y. E. Tsvetkov, N. E. Nifantiev, S. Bystrický. *J. Microbiol. Immunol. Infec.* **48**, 9 (2015).
[36] S. M. Bowman, S. J. Free. *Bioessays* **28**, 799 (2006).
[37] A. Torosantucci, C. Bromuro, P. Chiani, F. De Bernardis, F. Berti, C. Galli, F. Norelli, C. Bellucci, L. Polonelli, P. Costantino, R. Rappuoli, A. Cassone. *J. Exp. Med.* **202**, 597 (2005).
[38] C. Bromuro, M. Romano, P. Chiani, F. Berti, M. Tontini, D. Proietti, E. Mori, A. Torosantucci, P. Costantino, R. Rappuoli, A. Cassone. *Vaccine* **28**, 2615 (2010).
[39] G. Liao, Z. Zhou, S. Burgula, J. Liao, C. Yuan, Q. Wu, Z. Guo. *Bioconjugate Chem.* **26**, 466 (2015).
[40] Y. E. Tsvetkov, E. A. Khatuntseva, D. V. Yashunsky, N. E. Nifantiev. *Russ. Chem. Bull. Int. Ed.* **64**, 990 (2015).
[41] H. Tanaka, T. Kawai, Y. Adachi, S. Hanashima, Y. Yamaguchi, N. Ohno, T. Takahashi. *Bioorg. Med. Chem.* **20**, 3898 (2012).
[42] R. Verduyn, M. Douwes, P. A. M. van der Klein, E. M. Moesinger, G. A. van der Marel, J. H. van Boom. *Tetrahedron* **49**, 7301 (1993).
[43] S. Weiler, R. R. Schmidt. *Tetrahedron Lett.* **39**, 2299 (1998).
[44] Y. Wang, Q. Yan, J. Wu, L.-H. Zhang, X.-S. Ye. *Tetrahedron* **61**, 4313 (2005).
[45] D. V. Yashynsky, Y. E. Tsvetkov, N. E. Nifantiev. *Russ. Chem. Bull. Int. Ed.* **64**, 2922 (2015).
[46] E. Paulovičová, L. Paulovičová, R. Pilišiová, V. Jančinová, D. V. Yashunsky, A. A. Karelin, Y. E. Tsvetkov, N. E. Nifantiev. *Cell. Microbiol.* **18**, 1294 (2016).
[47] A. Beauvais, S. Bozza, O. Kniemeyer, C. Formosa, V. Balloy, C. Henry, R. W. Roberson, E. Dague, M. Chignard, A. A. Brakhage, L. Romani, J. P. Latgé. *PLoS Pathog.* **9**, e10037162013 (2013); and references cited therein.
[48] B. S. Komarova, N. E. Ustyuzhanina, Y. E. Tsvetkov, N. E. Nifantiev. "Stereocontrol of 1,2-cis-glycosylation by remote o-acyl protecting groups," in *Modern Synthetic Methods in Carbohydrate Chemistry: From Monosaccharides to Complex Glycoconjugates*, S. Vidal, D. Werz (Eds.), pp. 125–159, Wiley, Weinheim (2013).
[49] B. S. Komarova, M. V. Orekhova, Y. E. Tsvetkov, N. E. Nifantiev. "Contribution of carbohydrate chemistry to assessment of the biological role of natural α-glucosides," in *Specialists Periodical Reports: Carbohydrate Chemistry – Chemical and Biological Approaches*, A. P. Rauter, T. Lindhorst, Y. Queneau (Eds.), Vol. 41, pp. 187–237, RSC, Cambridge (2015).
[50] B. S. Komarova, M. V. Orekhova, Y. E. Tsvetkov, N. E. Nifantiev. *Carbohydr. Res.* **384**, 70 (2014).
[51] B. S. Komarova, M. V. Orekhova, Y. E. Tsvetkov, R. Beau, V. Aimanianda, J.-P. Latgé, N. E. Nifantiev. *Chem. Eur. J.* **21**, 1029 (2015).
[52] J. P. Latgé. *Clin. Microbiol. Rev*. **12**, 310 (1999).
[53] J. P. Latgé, H. Kobayashi, J. P. Debeaupuis, M. Diaquin, J. Sarfati, J. M. Wieruszeski, E. Parra, J. P. Bouchara, B. Fournet. *Infect. Immun*. **62**, 5424 (1994).
[54] D. A. Argunov, V. B. Krylov, N. E. Nifantiev. *Org. Biomol. Chem.* **13**, 3255 (2015).
[55] V. B. Krylov, D. A. Argunov, D. Z. Vinnitskiy, S. A. Verkhnyatskaya, A. G. Gerbst, N. E. Ustyuzhanina, A. S. Dmitrenok, J. Huebner, O. Holst, H.-C. Siebert, N. E. Nifantiev. *Chem. Eur. J.* **20**, 16516 (2014).
[56] V. B. Krylov, A. G. Gerbst, D. A. Argunov, A. S. Dmitrenok, A. S. Shashkov, Z. Kaczynski, J. Huebner, O. Holst, N. E. Nifantiev. *Chem. Eur. J.* **21**, 1749 (2015).
[57] D. Z. Vinnitskiy, V. B. Krylov, N. E. Ustyuzhanina, A. S. Dmitrenok, N.E. Nifantiev. *Org. Biomol. Chem.* **14**, 598 (2016).
[58] V. B. Krylov, D. A. Argunov, D. Z. Vinnitskiy, A. G. Gerbst, N. E. Ustyuzhanina, A. S. Dmitrenok, N. E. Nifantiev. *Synlett* **27**, 1659 (2016).
[59] D. A. Argunov, V. B. Krylov, N. E. Nifantiev. *Org. Lett.* **18**, 5504 (2016).
[60] A. Kudoh, Y. Okawa, N. Shibata. *Glycobiology* **25**, 74 (2015).
[61] Y. E. Tsvetkov, M. Burg-Roderfeld, G. Loers, A. Arda, E. V. Sukhova, E. A. Khatuntseva, A. A. Grachev, A. O. Chizhov, H.-C. Siebert, M. Schachner, J. Jimenez-Barbero, N. E. Nifantiev. *J. Am. Chem. Soc*. **134**, 426 (2012).
[62] A. Cassone. *Nature Rev. Microbiol.* **11**, 884 (2013).
[63] A. G. Gerbst, V. B. Krylov, D. Z. Vinnitskiy, A. S. Dmitrenok, A. S. Shashkov, N. E. Nifantiev. *Carbohydr. Res*. **417**, 1 (2015).
[64] G. M. Lipkind, A. S. Shashkov, N. E. Nifant'ev, N. K. Kochetkov. *Carbohydr. Res.* **237**, 11 (1992).
[65] N. K. Kochetkov, G. M. Lipkind, A. S. Shashkov, N. E. Nifant'ev. *Carbohydr. Res.* **221**, 145 (1991).
[66] T. Lipinski, A. Fitieh, J. St. Pierre, H. L. Ostergaard, D. R. Bundle, N. Touret. *J. Immunol.* **190**, 4116 (2013).
[67] A. Donadei, S. Gallorini, F. Berti, D. T. O'Hagan, R. Adamo, B. C. Baudner. *Mol. Pharmaceutics*, **12**, 1662 (2015).

Synthetic Oligosaccharides Mimicking Fungal Cell Wall Polysaccharides

Vadim B. Krylov and Nikolay E. Nifantiev

Contents

Abstract The cell wall of pathogenic fungi is highly important for the development of fungal infections and is the first cellular component to interact with the host immune system. The fungal cell wall is mainly built up of different polysaccharides representing ligands for pattern recognition receptors (PRRs) on immune cells and antibodies. Purified fungal polysaccharides are not easily available; in addition, they are structurally heterogenic and have wide molecular weight distribution that limits the possibility to use natural polysaccharides to assess the structure of their active determinants. The synthetic oligosaccharides of definite structure representing distinct polysaccharide fragments are indispensable tools for a variety of biological investigations and represent an advantageous alternative to natural polysaccharides. The attachment of a spacer group to these oligosaccharides permits their efficient transformation into immunogenic glycoconjugates as well as their immobilization on plates or microbeads. Herein, we summarize current information on synthetic availability of the variety of oligosaccharides related to main types of fungal cell wall components: galactomannan, α- and β-mannan, α- and β-(1 → 3)-glucan, chitin, chitosan, and others. These data are supplemented with published results of biochemical and immunological applications of synthetic oligosaccharides as

V. B. Krylov · N. E. Nifantiev (✉)
Laboratory of Glycoconjugate Chemistry, N.D. Zelinsky Institute of Organic Chemistry, Russian Academy of Sciences, Leninsky Prospect 47, 119991 Moscow, Russia
e-mail: nen@ioc.ac.ru

Current Topics in Microbiology and Immunology
https://doi.org/10.1007/82_2019_187

molecular probes especially as the components of thematic glycoarrays suitable for characterization of anti-polysaccharide antibodies and cellular lectins or PRRs.

1 Introduction

Nowadays, the prevalence of fungal infections, especially severe invasive mycoses, is increasing all over the world and emerges as a challenge for modern medicine (Brown et al. 2012). The mortality rate associated with invasive fungal infections often exceeds 50%, which is connected both with delays in diagnostic and limited number of available anti-fungal drugs. Difficulties in disease management also arise from the poorly understood mechanism of interaction between the host immune system and fungal pathogens and especially the mechanism of fungal adaptation to host conditions allowing escape from the host defense reactions.

The fungal cell wall is the first component of a pathogen in contact with the immune system. The cell wall of most fungi contains a structural skeleton composed of chitin and branched β-(1 → 3)-glucan. This rigid central core is decorated with amorphous polysaccharides in which composition varies with the fungal species. Figure 1 is a schematic representation of the cell wall of different fungal species although the cellular localization of the different components of the cell wall is not clearly demonstrated for most polysaccharides. Moreover, the covalent and noncovalent forces holding together the different components remain often hypothetical.

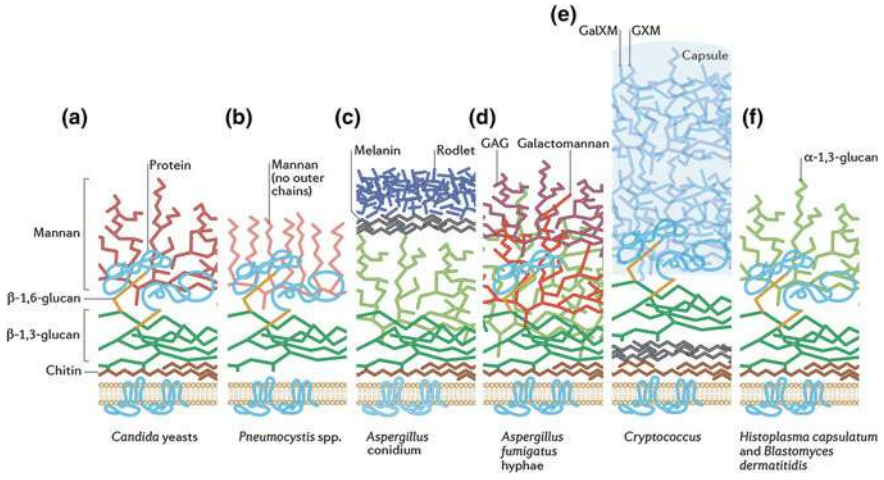

Fig. 1 Schematic view of cell wall composition of main human fungal pathogens. Reprinted by permission from Springer Nature: Nature Reviews Microbiology, vol. 14, Interactions of fungal pathogens with phagocytes, Erwig L.P., Gow N.A.R., pp. 163–176, Copyright, 2016

It is more and more obvious that polysaccharides play a major role in the immune interaction of the host with the pathogen (Hall and Gow 2013; Erwig and Gow 2016; Snarr et al. 2017). Moreover, cell wall polysaccharide antigenic markers of invasive fungal infections used in their diagnosis (Nelson et al. 1990; Tamura and Finkelman 2005; Cuenca-Estrella et al. 2012; Ullmann et al. 2018). In spite of the obvious importance of fungal cell wall polysaccharides for immune response modulation and for fungal infections diagnostic, little is known about the exact structure of their antigenic or immunogenic epitopes. This knowledge is essential for the understanding of the cellular immune response against the cell wall and for the development of diagnostic tests based on the use of circulating antigens antibodies.

To date, only the role of β-(1 → 3)-glucan and its associated receptor (Dectin 1) has been precisely analyzed (Brown 2006).

Precise quantitative analysis of carbohydrate-binding properties of anti-fungal lectins and antibodies could be performed using arrays composed of structurally defined glycans representing all the major carbohydrate structures present in the cell wall of fungal pathogens. The idea of using a comprehensive carbohydrate array for a wide range of glycobiology purposes has been proposed early by the Consortium for Functional Glycomics (CFG, http://www.functionalglycomics.org) since 2001 (Blixt et al. 2004; Raman et al. 2006). A number of thematic glycoarrays were designed and successfully applied to analyze viral and bacterial infections, cancer process, autoimmune disorders, etc. For example, microarrays composed of human glycans were used to survey the host specificity of different strains of influenza viruses (Stevens et al. 2006). Arrays were used for the analysis of glycan-specific antibodies against tumors in patient sera (Wang et al. 2008). An array composed of synthetic glycans related to cell wall polysaccharides from the human pathogen *Mycobacterium tuberculosis* and other mycobacteria was developed and applied for screening of specificity of immune system receptors (Zheng et al. 2017).

Various formats of arrays in which carbohydrate ligands are attached to microbeads, microtiter plate, chip, or glass slide have been used to study glycan–protein interactions. The immobilization techniques, though widely varying, can be divided into two main categories—noncovalent and covalent binding (Park et al. 2013) (Fig. 2). An example of noncovalent binding is attachment of lipid-conjugated oligosaccharides (neoglycolipids, NGLs) to nitrocellulose surface via hydrophobic interactions which is widely used to prepare glycan microarrays (Li and Feizi 2018) (Fig. 2a). Covalent and site-specific immobilization requires both introduction of a reactive functional group into the glycan and chemical derivatization of the surface (*e.g.* attachment of amine-linked sugars to the N-hydroxysuccinimide ester-coated surface, Fig. 2b) (Blixt et al. 2004).

Another immobilization strategy is based on a very strong biotin–streptavidin interaction ($K_d \sim 10^{-15}$ M) which, being formally noncovalent, is energetically closer to covalent binding. The attachment of biotin-linked sugars to the streptavidin-coated surface (Fig. 2c) has strong advantages. First of all, the amount of ligand is defined by the binding capacity of the surface which is well

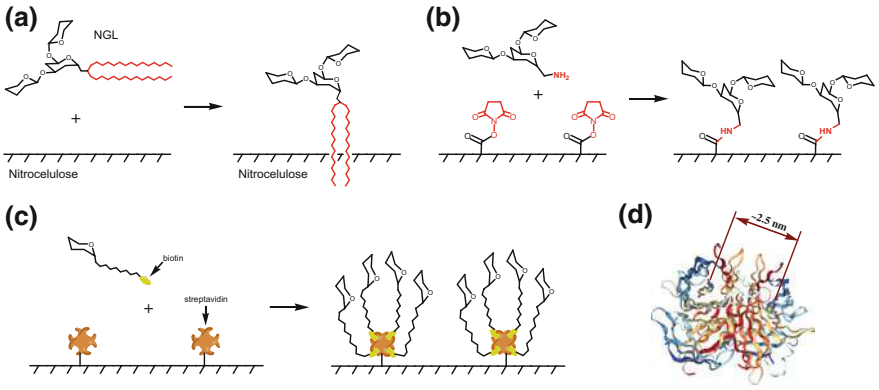

Fig. 2 Strategies of glycan immobilization on a surface. **a** noncovalent attachment of lipid-conjugated glycans to nitrocellulose; **b** covalent attachment of amine-linked sugars to the NHS ester-coated surface; **c** attachment via biotin–streptavidin interaction; and **d** structure of biotin–streptavidin complex (PDB: 6j6j), the distance between biotin-binding sites is shown

documented. Thus, the molar density of the coating glycan is constant and does not depend on its molecular weight, charge, and hydrophilic/hydrophobic properties. Another advantage is the standardized distance between binding sites. The streptavidin molecule is composed of four biotin-binding subunits with the average distance between biotin molecules of about 2.5 nm. For a standard commercial microtiter plate with the biotin-binding capacity of 5 pmol per well, the calculated average distance between biotin-binding streptavidin subunits is 6.1 nm assuming their uniform distribution. This exceeds the size of the immobilized oligosaccharide molecules allowing the study of the interaction properties of individual carbohydrate ligands (Galanina et al. 2003).

The value of carbohydrate arrays as a powerful and easy tool for investigation of protein–carbohydrate interactions is well recognized. However, there are no publications reporting a comprehensive glycoarray covering all the polysaccharide types of the fungal cell wall. In this review, we summarize the currently available information on synthetic availability of the variety of oligosaccharides related to major fungal cell wall polysaccharides.

2 Thematic Glycoarrays

Due to their insolubility and their complex heterogenic structure, pure fungal polysaccharides are not easy to obtain. This complicates the possibility to use them as probes to investigate their immune role. An alternative to natural polysaccharides is to use synthetic oligosaccharides of definite structure representing distinct polysaccharide fragments. For over 15 years, our laboratory has been performing

systematic synthesis of oligosaccharides related to the main types of fungal cell wall polysaccharides: galactomannan, α- and β-mannans, α- and β-(1 → 3)-glucans, chitin, galactosaminogalactan, galactoxylomannan, and others. The use of such oligosaccharides is illustrated with examples of biochemical and immunological applications of the use of synthetic oligosaccharides as molecular probes suitable for the characterization of anti-polysaccharide antibodies and cellular lectins.

2.1 Galactomannan

A specific carbohydrate antigen produced by *Aspergillus* and *Penicillium* species is a galactomannan (Latgé et al. 1994). It is a complex heteropolysaccharide built up of mannopyranose and galactofuranose monosaccharide residues. Latgé et al. (1994) proposed its structure representing α-(1 → 2)-/α-(1 → 6)-linked poly-D-mannoside backbone bearing β-(1 → 5)-linked oligogalactofuranoside side chains attached to some of the mannose units via either β-(1 → 3)- or β-(1 → 6)-bonds. Shibata et al. (Kudoh et al. 2015; Krylov et al. 2018a) revealed the presence of additional structural elements: β-(1 → 6)-linkage within the oligogalactofuranoside side chain and in addition to β-(1 → 3)- or β-(1 → 6)-bonds, β-(1 → 2)-attachment of the galactofuranoside side chain to the mannan backbone (Fig. 3a).

The first synthesized oligosaccharide fragments of the galactomannan corresponding to the homo-galactofuranosyl chains of variable length were either naïve or biotinylated (Veeneman et al. 1987; Zuurmond et al. 1990; Cattiaux et al. 2011). The first synthesis of a heterosaccharide fragment containing both galactofuranosyl and mannopyranosyl residues was then undertaken (Fu et al. 2005). Recently, galactomannan-related oligosaccharides (Argunov et al. 2015, 2016; Krylov et al. 2018a) have been synthesized employing an alternative synthetic strategy based on a new reaction in carbohydrate chemistry, namely pyranoside-*into*-furanoside rearrangement (Krylov et al. 2014, 2016; Gerbst et al. 2019), and controlled O(5) → O(6) benzoyl migration (Argunov et al. 2016). A library of 13 synthetic oligosaccharides (shown in Fig. 3B) was prepared in the form of aminopropyl glycosides allowing their further modification, conjugation, and application in different fields of glycoscience.

The synthetic galactomannan fragments (**10** on Fig. 3b) and immunogens prepared thereof were used for generation of monoclonal antibodies (mAb) and characterization of their specificity (Matveev et al. 2018). Thus, 7B8 and 8G4 mAbs, obtained by immunization of mice with BSA-conjugate of the synthetic pentasaccharide, efficiently recognized natural galactomannan of *A. fumigatus.*

The glycoarray formed from biotinylated oligosaccharides related to galactomannan (Fig. 3b) was used to establish fine carbohydrate specificity of anti-galactomannan poly- and monoclonal antibodies.

The galactomannan glycoarray was employed to reinvestigate the carbohydrate specificity of the EB-A2 monoclonal antibody used in the commercial Aspergillus sandwich immune assay. It was shown that EB-A2 could recognize

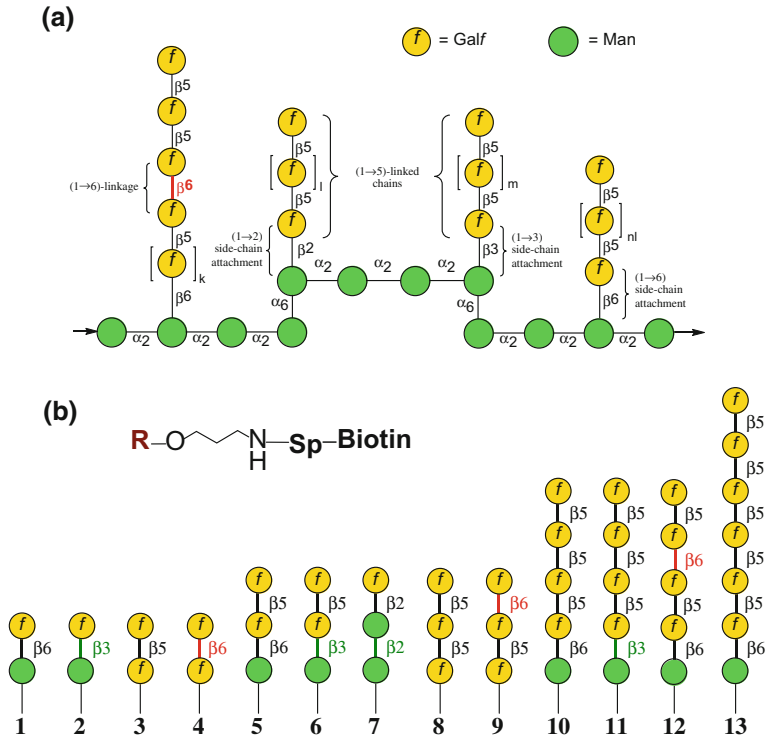

Fig. 3 **a** Tentative structure of galactomannan summarizing the structural features reported by Latgé (Latgé et al. 1994) and Shibata (Kudoh et al. 2015); **b** synthetic oligosaccharides prepared as aminopropyl glycosides. The carbohydrate sequences are represented according to symbol carbohydrate nomenclature (Neelamegham et al. 2019)

oligosaccharides sequences containing only disaccharide Galf-β-(1 → 5)-Galf fragment (Krylov et al. 2019), but not the tetrasaccharide one as had been reported previously (Stynen et al. 1992). This result could explain the occurrence of false-positive signals due to the presence of such epitope not only in *A. fumigatus* galactomannan but also in other bacteria and non-Aspergillus fungi. Monoclonal antibodies 7B8 and 8G4 recognize longer oligosaccharides sequences (Matveev et al. 2018) containing β-(1 → 5)-linked trigalactofuranoside (**8** on Fig. 3b) and pentasaccharide β-D-Galf-[(1 → 5)-β-D-Galf]$_3$-(1 → 6)-α-D-Manp (**10** on Fig. 3b) respectively.

Assaying of polyclonal rabbit antibodies obtained using different preparations of *Aspergillus* species as immunogens and purified on affine sorbent revealed different specificity profiles of anti-galactomannan antibodies. In all the cases, the smallest carbohydrate fragment recognized by the pAb consisted of two β-(1 → 5)-linked galactofuranosyl residues (Krylov et al. 2018c, b).

Synthetic oligosaccharides were also used to investigate the immunobiological activity of the galactomannan. Its action was studied using RAW 264.7 cell line murine macrophages and human PBMCs. Significant immunomodulating efficacy of the galactomannan-related oligosaccharides was established by a proliferation/cytotoxicity assay, phagocytosis and inductive cytokines, and growth factors release (Paulovičová et al. 2017). Oligosaccharides with Galf(1 → 5)Galf blocks was shown to induce the secretion of cytokines and chemokines by immune cells (Wong et al. 2020).

2.2 α- and β-Mannan

The outer layer of the cell wall of *Candida* species consists of mannoproteins. Their mannan moieties are important for host–fungal interactions and virulence. The mannan has a comb-like structure with an α-(1 → 6)-linked backbone bearing different types of oligomannoside side chains depending on the fungal species (Shibata et al. 2012) (Fig. 4a). Some oligosaccharides have a phosphodiester linkage which can be selectively cleaved by treatment with a weak acid solution, releasing the "acid-labile" fraction of the mannan. Early studies have shown that these mannoside fragments are responsible for the serotyping of *Candida* species and are so-called antigenic factors (Fig. 4a) (Suzuki 1997). Numerous studies have also shown the essential immunological role of these mannans (Netea et al. 2008).

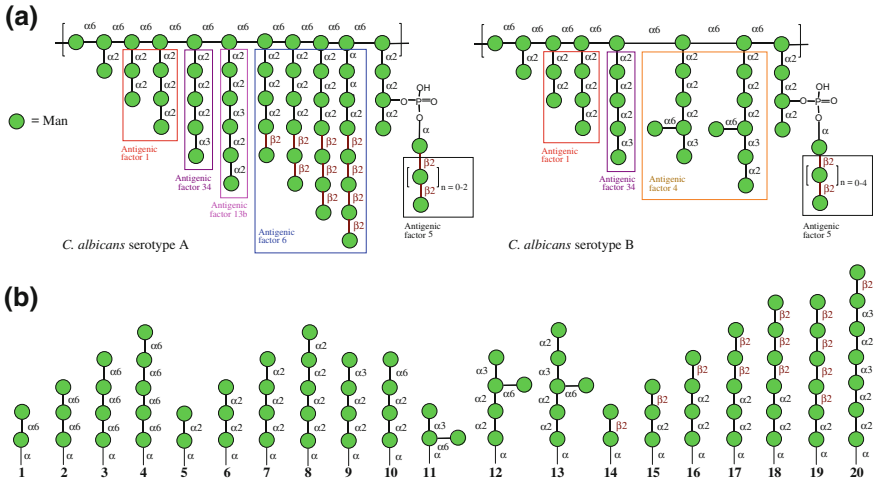

Fig. 4 **a** Structure of the cell wall mannan of *C. albicans* serotypes A and B with marked structures of main antigenic factors; **b** synthesized oligosaccharides related to mannan fragments. All synthetic ligands were prepared as aminopropyl glycosides. The carbohydrate sequences are represented according to symbol carbohydrate nomenclature (Neelamegham et al. 2019)

The synthesis of oligosaccharides related to fragments of yeast cell wall mannans was described in a monograph published in 2009 (Collot et al. 2009). The synthetic works published afterward were considered in a review by Karelin et al. in 2017 (Karelin et al. 2017). The systematic syntheses of oligosaccharides related to *Candida* mannan have been performed in our laboratory since 2007 and allow construction of a representative library of aminopropyl glycosides corresponding to main antigenic factors of yeast pathogens (Fig. 4b). For example, linear α-(1 → 6)-linked oligosaccharides **1**–**4** represent the mannan backbone, α-(1 → 2)-linked oligosaccharides **5**–**8** correspond to antigenic factor 1 (Karelin et al. 2007), and branched oligosaccharides **11**–**13** are related to antigenic factor 4 (Karelin et al. 2010; Argunov et al. 2011).

Preparation of β-linked oligomannosides is a special problem due to the lack of efficient and reliable corresponding synthetic methods. This task commonly requires application of original approaches. Chemo-enzymatic synthesis was developed for preparation of disaccharide ligand **14** with a β-mannoside linkage. It included chemical cleavage and enzymatic dephosphorylation of biotechnologically available phosphomannan followed by its chemical derivatization (Karelin et al. 2019). The strategy based on direct β-mannosylation with conformationally rigid 4,6-O-benzylidene protected mannosyl donors was applied for the synthesis of ligands **15**–**20** related to antigenic factors 5 and 6 (Karelin et al. 2015, 2016).

Synthetic oligosaccharides and corresponding conjugates mimicking *C. albicans* mannan were employed to study the interactions of immune cells with *Candida*. BSA-based conjugates of synthetic oligomannosides effectively induced humoral and cell-mediated immunity. The immunomodulating activity of the conjugates was evaluated based on the induction of pro-inflammatory cytokines. Mice immunization with BSA-conjugates resulted in the production of polyclonal antibodies against synthetic oligosaccharides that were capable of recognizing branched α-oligomannoside structures on the cell wall of *C. albicans* yeast and hyphae (Paulovičová et al. 2013a). Additionally, the anti-sera obtained after mice immunization with BSA-mannooligosaccharides conjugates were able to enhance phagocytosis of *C. albicans* cells by polymorphonuclear leukocytes (Paulovicová et al. 2010; Paulovičová et al. 2013b). It is also worth to mention that the collected databases of NMR-spectral characteristics for synthesized oligosaccharides can be used for the development of computer-assisted method for structural analysis of fungal mannans as it was applied for bacterial polysaccharides including vicinally branched ones (Lipkind et al. 1992).

2.3 α- and β-(1 → 3)-Glucans

Although the glucans (and especially β-(1 → 3)-D-glucan with their associated Dectin1 receptor) have been shown to be essential in the pathogenic life of different fungi, their immunological role has been insufficiently analyzed. The main restriction for the use of glucans from natural sources arises from their limited

solubility. Accordingly, the soluble oligosaccharides related to specified glucan fragments and conjugates thereof are highly demanded mimetics of such polysaccharides.

The synthetic approaches to β-(1 → 3)-D-glucan-related oligosaccharides are relatively well elaborated (Tsvetkov et al. 2015). Syntheses of linear (Yashunsky et al. 2016a) and branched (Yashunsky et al. 2016b) 3-aminopropyl glycosides of β-(1 → 3)-D-glucooligosaccharides were performed. β-(1 → 6)-D-Glucotetraoside and the corresponding biotinylated derivative was synthesized from monosaccharide building blocks via successive glycosylation with a monosaccharide donor (Yashunsky et al. 2018).

The synthesis of α-(1 → 3)-glucooligosaccharides with a predefined structure required special methods of 1,2-*cis*-glycosylation. Strategies based on remote participation of acyl protecting groups were developed (Komarova et al. 2014, 2016) and successfully applied (Komarova et al. 2015, 2018) to obtain oligo-α-(1 → 3)-D-glucosides containing from three to eleven glucose units (Fig. 5). An alternative synthetic approach to the assembly of oligosaccharides related to α-(1 → 3)-glucans (Wang et al. 2019) and α-(1 → 4)-glucans (Wang et al. 2018) was suggested in Codée's group. However, to the best of our knowledge, the results of their biochemical and immunological application studies have not been published yet.

Synthetically prepared oligosaccharides were used to generate mono- and polyclonal antibodies. For example, mouse monoclonal antibodies 3G11 and 5H5 were generated using synthetic nona-β-(1 → 3)-D-glucoside conjugated with the bovine serum albumin (G9-BSA) (Matveev et al. 2019). The glycoarray which included linear and branched synthetic oligosaccharide demonstrated that 5H5 mAbs recognized the linear triglucoside fragment, while 3G11 mAbs could bind the pentasaccharide. In addition, anti-*C. albicans* activity of 3G11 and 5H5 mAbs was demonstrated in vivo and in vitro experiments. Active immunization by synthetically prepared G9-BSA also had revealed effective induction of specific humoral responses against *C. albicans* infection (Paulovičová et al. 2016).

Immunization of mice with the BSA-conjugate of penta-α-(1 → 3)-D-glucoside led to generation of antibodies that recognized α-glucan on *A. fumigatus* cell surface

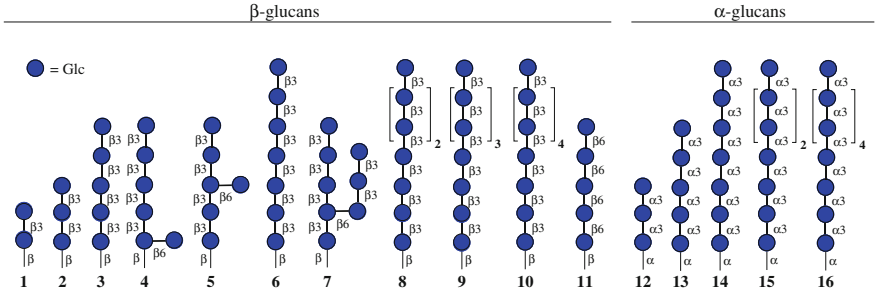

Fig. 5 Oligosaccharides related to α- and β-glucans

(Komarova et al. 2015). Additionally, synthetic biotinylated oligo-α-glucosides loaded on a streptavidin-coated plate were able to recognize human anti-α-glucan antibodies in sera of patients with aspergillosis and induced cytokine responses upon stimulation of human peripheral blood mononuclear cells (Komarova et al. 2018).

2.4 Polysaccharides Composed of 2-Deoxy-2-Aminosugars

In this section, a group of cell wall polysaccharides and corresponding oligosaccharide fragments composed of amino sugars is considered. The most common among them is chitin, an insoluble linear polymer, built up of β-(1 → 4)-linked *N*-acetylglucosamine units. This polysaccharide forms the inner layer of the fungal cell wall and is responsible for its rigidity (Erwig and Gow 2016). Deacetylated chitin, termed chitosan, is produced by many fungal species during their life cycle and plays regulatory and signaling roles. Chitin blocks the recognition of *C. albicans* by human PBMCs and murine macrophages, leading to significant reductions in cytokine production (Mora-Montes et al. 2011). Galactosaminogalactan (GAG) is the polysaccharide exposed on the outer surface of *A. fumigatus* cells. It acts as an immunosuppressor helping the fungal pathogen to survive in the host medium (Fontaine et al. 2011). Structurally, GAG represents a linear heterogeneous polysaccharide composed of α-(1 → 4)-linked galactose and N-acetylgalactosamine units. Both monosacharides are randomly distributed along the chain with the percentage of galactose ranging from 15 to 60%. GAG inhibits pro-inflammatory Th17 and Th1 responses in human peripheral blood mononuclear cells by inducing the expression of the anti-inflammatory interleukin-1 receptor antagonist (IL-1Ra), which blocks IL-1β signaling (Gresnigt et al. 2014). Additionally, immunosuppressive GAG activity associated with diminishing neutrophil infiltrates was observed in in vivo experiments (Fontaine et al. 2011).

The matter of a special interest is β-(1 → 6)–linked poly-*N*-acetyl-D-glucosamine (PNAG). Originally, it was isolated from the polysaccharide capsule of *Staphylococcus aureus* and developed as a promising target for antibacterial therapy and prophylaxis (Gening et al. 2007, 2010). To the best of our knowledge, this polysaccharide was not isolated from fungal species, though immunofluorescence labeling with specific monoclonal antibodies detected PNAG in such fungal species as *C. albicans*, *A. flavus*, *Fusarium solani*, and *C. neoformans*, additionally anti-PNAG antibodies have protective effect against these fungi (Cywes-Bentley et al. 2013).

Due to its poor solubility, using natural chitin for immunobiological studies is difficult. Synthetic chitooligosaccharides do not have these disadvantages. Thus, spacer-armed chitotriose, chitopentaose, and chitoheptaose and their biotinylated derivatives were prepared using a properly protected monosaccharide acceptor and a disaccharide donor (Yudina et al. 2015, 2016). The synthetic scheme developed for synthesis of GAG-related oligosaccharides involved the use of phenyl

2-azido-2-deoxy-1-seleno-α-D-galactosides (Mironov et al. 2004) allowing highly α-stereoselective formation of the glycoside bond (Khatuntseva et al. 2016). The synthesis of the GAG-related biotinylated oligo-α-(1 → 4)-D-galactosamines comprising from 2 to 6 monosaccharide units and of N-acetylated derivatives of above glycoconjugates was performed. Obtained series of GAG mimetics was used to investigate the epitopes recognized by anti-GAG monoclonal antibodies and of antibodies in blood sera of patients with allergic bronchopulmonary and chronic pulmonary aspergilloses (Kazakova et al. 2020) (Fig. 6).

3 Conclusions

The elucidation of the immune response modulation by fungal cell wall components is a highly important but a very complex task. The purification of standardized individual cell wall polysaccharides is almost impossible due to high variability and sensitivity of their structure to minor changes in cultivation conditions. Moreover, natural polysaccharides are highly heterogenic which can result in a high variability between the immune response against different strains.

The approach based on the use of synthetically prepared fragments related to fungal cell wall glycans is the most appropriate to elucidate the complex immune response against the fungal cell wall. In this review, we summarized recent works on synthesis of oligosaccharides related to polysaccharides of the fungal cell wall and a few examples of their potential to investigate their interactions with the host. All synthetic molecules were prepared in spacer-armed form which made possible their biotinylation and controlled site-specific immobilization on streptavidin-coated microtiter plates. The oligosaccharide ligands were combined to thematic glycoarrays used to determine fine specificity of antibodies and innate immune

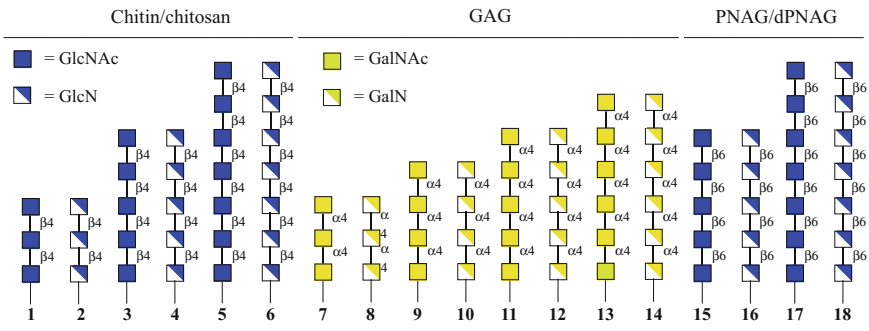

Fig. 6 Synthetic oligosaccharides related to polysaccharides composed of N-acetylated and non-acetylated aminosugars: chitin/chitosan; galactosaminogalactan (GAG); and β-(1 → 6)–linked poly-*N*-acetyl-D-glucosamine (PNAG) and its deacetylated derivative (dPNAG). The carbohydrate sequences are represented according to symbol carbohydrate nomenclature (Neelamegham et al. 2019)

system receptors. The data obtained with such glycoarrays have obvious practical importance for development of new diagnostic kits and vaccines for treatment and prophylaxis of fungal infections.

Acknowledgements This work was supported by the Russian Science Foundation (grant 19-73-30017). We thank Professor J.-P. Latgé and Dr. A. G. Gerbst for critical reading this manuscript and valuable comments.

References

Argunov DA, Karelin AA, Grachev AA et al (2011) A new synthesis of the 3, 6-branched hexasaccharide fragment of the cell wall mannan in *Candida albicans*, corresponding to the antigenic factor 4. Russ Chem Bull 60:1004–1011

Argunov DA, Krylov VB, Nifantiev NE (2015) Convergent synthesis of isomeric heterosaccharides related to the fragments of galactomannan from *Aspergillus fumigatus*. Org Biomol Chem 13:3255–3267. https://doi.org/10.1039/C4OB02634A

Argunov DA, Krylov VB, Nifantiev NE (2016) The use of pyranoside-*into*-furanoside rearrangement and controlled O(5) → O(6) benzoyl migration as the basis of a synthetic strategy to assemble (1 → 5)-and (1 → 6)-linked galactofuranosyl chains. Org Lett 18:5504–5507. https://doi.org/10.1021/acs.orglett.6b02735

Blixt O, Head S, Mondala T et al (2004) Printed covalent glycan array for ligand profiling of diverse glycan binding proteins. Proc Nat Acad Sci USA 101:17033–17038. https://doi.org/10.1073/pnas.0407902101

Brown GD (2006) Dectin-1: a signalling non-TLR pattern-recognition receptor. Nat Rev Immunol 6:33–43. https://doi.org/10.1038/nri1745

Brown GD, Denning DW, Gow NAR et al (2012) Hidden killers: human fungal infections. Sci Transl Med 4:165rv13. https://doi.org/10.1126/scitranslmed.3004404

Cattiaux L, Sendid B, Collot M et al (2011) Synthetic biotinylated tetra β (1 → 5) galactofuranoside for in vitro aspergillosis diagnosis. Bioorg Med Chem 19:547–555

Collot M, Loukou C, Mallet J-M (2009) Chemical synthesis of the oligosaccharidic fragments of yeast mannans. In: Nifantiev NE (ed) Progress in the synthesis of complex carbohydrate chains of plant and microbial polysaccharides. Transworld Research Network, Kerala, pp 371–398

Cuenca-Estrella M, Verweij PE, Arendrup MC et al (2012) ESCMID* guideline for the diagnosis and management of *Candida* diseases 2012: diagnostic procedures. Clin Microbiol Infect 18 (Suppl 7):9–18. https://doi.org/10.1111/1469-0691.12038

Cywes-Bentley C, Skurnik D, Zaidi T et al (2013) Antibody to a conserved antigenic target is protective against diverse prokaryotic and eukaryotic pathogens. Proc Nat Acad Sci USA 110: E2209–E2218. https://doi.org/10.1073/pnas.1303573110

Erwig LP, Gow NA (2016) Interactions of fungal pathogens with phagocytes. Nat Rev Microbiol 14:163. https://doi.org/10.1038/nrmicro.2015.21

Fontaine T, Delangle A, Simenel C et al (2011) Galactosaminogalactan, a new immunosuppressive polysaccharide of *Aspergillus fumigatus*. PLoS Pathog 7:e1002372

Fu M, Zhang G, Ning J (2005) First synthesis of the immunodominant β-galactofuranose-containing tetrasaccharide present in the cell wall of *Aspergillus fumigatus*. Carbohyd Res 340:25–30

Galanina OE, Mecklenburg M, Nifantiev NE et al (2003) GlycoChip: multiarray for the study of carbohydrate-binding proteins. Lab Chip 3:260–265. https://doi.org/10.1039/B305963D

Gening ML, Maira-Litrán T, Kropec A et al (2010) Synthetic β-(1 → 6)-linked *N*-acetylated and nonacetylated oligoglucosamines used to produce conjugate vaccines for bacterial pathogens. Infect Immun 78:764–772. https://doi.org/10.1128/IAI.01093-09

Gening ML, Tsvetkov YE, Pier GB, Nifantiev NE (2007) Synthesis of β-(1 → 6)-linked glucosamine oligosaccharides corresponding to fragments of the bacterial surface polysaccharide poly-*N*-acetylglucosamine. Carbohyd Res 342:567–575

Gerbst AG, Krylov VB, Argunov DA et al (2019) Driving force of the pyranoside-*into*-furanoside rearrangement. ACS Omega 4:1139–1143. https://doi.org/10.1021/acsomega.8b03274

Gresnigt MS, Bozza S, Becker KL et al (2014) A polysaccharide virulence factor from *Aspergillus fumigatus* elicits anti-inflammatory effects through induction of Interleukin-1 receptor antagonist. PLoS Pathog 10:e1003936. https://doi.org/10.1371/journal.ppat.1003936

Hall RA, Gow NAR (2013) Mannosylation in *Candida albicans*: role in cell wall function and immune recognition. Mol Microbiol 90:1147–1161. https://doi.org/10.1111/mmi.12426

Karelin AA, Tsvetkov YE, Kogan G et al (2007) Synthesis of oligosaccharide fragments of mannan from *Candida albicans* cell wall and their BSA conjugates. Russ J Bioorg Chem 33:110–121

Karelin AA, Tsvetkov YE, Nifantiev NE (2017) Synthesis of oligosaccharides related to polysaccharides of the cell wall of the fungi *Candida* and *Aspergillus*. Russ Chem Rev 86:1073–1126. https://doi.org/10.1070/RCR4750

Karelin AA, Tsvetkov YE, Paulovičová E et al (2015) Blockwise synthesis of a pentasaccharide structurally related to the mannan fragment from the *Candida albicans* cell wall corresponding to the antigenic factor 6. Russ Chem Bull 64:2942–2948

Karelin AA, Tsvetkov YE, Paulovičová E et al (2016) A blockwise approach to the synthesis of (1 → 2)-linked Oligosaccharides corresponding to fragments of the acid-stable β-mannan from the *Candida albicans* cell wall. Eur J Org Chem 2016:1173–1181

Karelin AA, Tsvetkov YE, Paulovičová L et al (2010) Synthesis of 3,6-branched oligomannoside fragments of the mannan from *Candida albicans* cell wall corresponding to the antigenic factor 4. Carbohyd Res 345:1283–1290

Karelin AA, Ustyuzhanina NE, Tsvetkov YE, Nifantiev NE (2019) Synthesis of a biotinylated probe from biotechnologically derived β-D-mannopyranosyl-(1 → 2)-D-mannopyranose for assessment of carbohydrate specificity of antibodies. Carbohyd Res 471:39–42

Kazakova ED, Yashunsky DV, Krylov VB et al (2020) Biotinylated oligo-α-(1 → 4)-D-galactosamines and their *N*-acetylated derivatives: α-stereoselective synthesis and immunology application. Submitted

Khatuntseva EA, Sherman AA, Tsvetkov YE, Nifantiev NE (2016) Phenyl 2-azido-2-deoxy-1-selenogalactosides: a single type of glycosyl donor for the highly stereoselective synthesis of α-and β-2-azido-2-deoxy-D-galactopyranosides. Tetrahedron Lett 57:708–711. https://doi.org/10.1016/j.tetlet.2016.01.013

Komarova BS, Orekhova MV, Tsvetkov YE, Nifantiev NE (2014) Is an acyl group at O-3 in glucosyl donors able to control α-stereoselectivity of glycosylation? The role of conformational mobility and the protecting group at O-6. Carbohyd Res 384:70–86. https://doi.org/10.1016/j.carres.2013.11.016

Komarova BS, Orekhova MV, Tsvetkov YE et al (2015) Synthesis of a pentasaccharide and neoglycoconjugates related to fungal α-(1 → 3)-glucan and their use in the generation of antibodies to trace *Aspergillus fumigatus* cell wall. Chem Eur J 21:1029–1035. https://doi.org/10.1002/chem.201404770

Komarova BS, Tsvetkov YE, Nifantiev NE (2016) Design of α-selective Glycopyranosyl donors relying on remote Anchimeric assistance. Chem Rec 16:488–506. https://doi.org/10.1002/tcr.201500245

Komarova BS, Wong SSW, Orekhova MV et al (2018) Chemical synthesis and application of biotinylated oligo-α-(1 → 3)-D-glucosides to study the antibody and cytokine response against the cell wall α-(1 → 3)-D-glucan of *Aspergillus fumigatus*. J Org Chem 83:12965–12976. https://doi.org/10.1021/acs.joc.8b01142

Krylov VB, Argunov DA, Solovev AS et al (2018a) Synthesis of oligosaccharides related to galactomannans from *Aspergillus fumigatus* and their NMR spectral data. Org Biomol Chem 16:1188–1199. https://doi.org/10.1039/C7OB02734F

Krylov VB, Argunov DA, Vinnitskiy DZ et al (2014) Pyranoside-*into*-furanoside rearrangement: new reaction in carbohydrate chemistry and its application in Oligosaccharide synthesis. Chem Eur J 20:16516–16522. https://doi.org/10.1002/chem.201405083

Krylov VB, Argunov DA, Vinnitskiy DZ et al (2016) The pyranoside-*into*-furanoside rearrangement of alkyl glycosides: scope and limitations. Synlett 27:1659–1664. https://doi.org/10.1055/s-0035-1561595

Krylov VB, Petruk MI, Glushko NI et al (2018b) Carbohydrate specificity of antibodies against phytopathogenic fungi of the *Aspergillus* genus. Appl Biochem Microbiol 54:522–527

Krylov VB, Petruk MI, Grigoryev IV et al (2018c) Study of the carbohydrate specificity of antibodies against *Aspergillus fumigatus* using the library of synthetic mycoantigens. Russ J Bioorg Chem 44:80–89

Krylov VB, Solovev AS, Argunov DA et al (2019) Reinvestigation of carbohydrate specificity of EB-A2 monoclonal antibody used in the immune detection of *Aspergillus fumigatus* galactomannan. Heliyon 5:e01173. https://doi.org/10.1016/j.heliyon.2019.e01173

Kudoh A, Okawa Y, Shibata N (2015) Significant structural change in both O-and N-linked carbohydrate moieties of the antigenic galactomannan from *Aspergillus fumigatus* grown under different culture conditions. Glycobiology 25:74–87. https://doi.org/10.1093/glycob/cwu091

Latgé J-P, Kobayashi H, Debeaupuis J-P et al (1994) Chemical and immunological characterization of the extracellular galactomannan of *Aspergillus fumigatus*. Infect Immun 62:5424–5433

Li Z, Feizi T (2018) The neoglycolipid (NGL) technology-based microarrays and future prospects. FEBS Lett 592:3976–3991. https://doi.org/10.1002/1873-3468.13217

Lipkind GM, Shashkov AS, Nifant'ev NE, Kochetkov NK (1992) Computer-assisted analysis of the structure of regular branched polysaccharides containing 2,3-disubstituted rhamnose and mannose residues on the basis of ^{13}C-NMR data. Carbohyd Res 237:11–22

Matveev AL, Krylov VB, Emelyanova LA et al (2018) Novel mouse monoclonal antibodies specifically recognize *Aspergillus fumigatus* galactomannan. PLoS ONE 13:e0193938. https://doi.org/10.1371/journal.pone.0193938

Matveev AL, Krylov VB, Khlusevich YA et al (2019) Novel mouse monoclonal antibodies specifically recognizing β-(1 → 3)-D-glucan antigen. PLoS ONE 14:e0215535. https://doi.org/10.1371/journal.pone.0215535

Mironov Y, Sherman A, Nifantiev N (2004) Homogeneous azidophenylselenation of glycals using of $TMSN_3$-Ph_2Se_2-$PhI(OAc)_2$. Tetrahedron Lett 45:9107–9110

Mora-Montes HM, Netea MG, Ferwerda G et al (2011) Recognition and blocking of innate immunity cells by *Candida albicans* chitin. Infect Immun 79:1961–1970. https://doi.org/10.1128/IAI.01282-10

Neelamegham S, Aoki-Kinoshita K, Bolton E et al (2019) Updates to the symbol nomenclature for glycans (SNFG) guidelines. Glycobiology. https://doi.org/10.1093/glycob/cwz045

Nelson MR, Bower M, Smith D et al (1990) The value of serum cryptococcal antigen in the diagnosis of cryptococcal infection in patients infected with the human immunodeficiency virus. J Infect 21:175–181

Netea MG, Brown GD, Kullberg BJ, Gow NAR (2008) An integrated model of the recognition of *Candida albicans* by the innate immune system. Nature Rev Microbiol 6:67–78. https://doi.org/10.1038/nrmicro1815

Park S, Gildersleeve JC, Blixt O, Shin I (2013) Carbohydrate microarrays. Chem Soc Rev 42:4310–4326. https://doi.org/10.1039/c2cs35401b

Paulovičová E, Paulovičová L, Hrubiško M et al (2017) Immunobiological activity of synthetically prepared immunodominant galactomannosides structurally mimicking *Aspergillus* galactomannan. Front Immunol 8:1273

Paulovičová E, Paulovičová L, Pilišiová R et al (2013a) Synthetically prepared glycooligosaccharides mimicking *Candida albicans* cell wall glycan antigens—novel tools to study host-pathogen interactions. FEMS Yeast Res 13:659–673. https://doi.org/10.1111/1567-1364.12065

Paulovičová E, Paulovičová L, Pilišiová R et al (2016) The evaluation of β-(1 → 3)-nonaglucoside as an anti-*Candida albicans* immune response inducer. Cell Microbiol 18:1294–1307. https://doi.org/10.1111/cmi.12631

Paulovicová L, Bystrický S, Paulovicová E et al (2010) Model α-mannoside conjugates: immunogenicity and induction of candidacidal activity. FEMS Immunol Med Microbiol 58:307–313. https://doi.org/10.1111/j.1574-695X.2009.00642.x

Paulovičová L, Paulovičová E, Karelin AA et al (2013b) Effect of branched α-oligomannoside structures on induction of anti-*Candida* humoral immune response. Scand J Immunol 77:431–441. https://doi.org/10.1111/sji.12044

Raman R, Venkataraman M, Ramakrishnan S et al (2006) Advancing glycomics: implementation strategies at the consortium for functional glycomics. Glycobiology 16:82R–90R. https://doi.org/10.1093/glycob/cwj080

Shibata N, Kobayashi H, Suzuki S (2012) Immunochemistry of pathogenic yeast, *Candida* species, focusing on mannan. Proc Japan Acad Ser B 88:250–265

Snarr BD, Qureshi ST, Sheppard DC (2017) Immune recognition of fungal polysaccharides. J Fungi (Basel) 3. https://doi.org/10.3390/jof3030047

Stevens J, Blixt O, Paulson JC, Wilson IA (2006) Glycan microarray technologies: tools to survey host specificity of influenza viruses. Nat Rev Microbiol 4:857–864. https://doi.org/10.1038/nrmicro1530

Stynen D, Sarfati J, Goris A et al (1992) Rat monoclonal antibodies against *Aspergillus galactomannan*. Infect Immun 60:2237–2245

Suzuki S (1997) Immunochemical study on mannans of genus *Candida*. I. Structural investigation of antigenic factors 1, 4, 5, 6, 8, 9, 11, 13, 13b and 34. Curr Top Med Mycol 8:57–70

Tamura H, Finkelman MA (2005) Detection and Measurement of (1 → 3)-β-D-Glucan with *Limulus amebocyte* lysate-based reagents. In: Toxicology of 1-3-beta-glucans. CRC Press, pp 191–210

Tsvetkov YE, Khatuntseva EA, Yashunsky DV, Nifantiev NE (2015) Synthetic β-(1 → 3)-D-glucooligosaccharides: model compounds for the mechanistic study of β-(1 → 3)-D-glucan bioactivities and design of antifungal vaccines. Russ Chem Bull 64:990–1013. https://doi.org/10.1007/s11172-015-0969-4

Ullmann AJ, Aguado JM, Arikan-Akdagli S et al (2018) Diagnosis and management of *Aspergillus* diseases: executive summary of the 2017 ESCMID-ECMM-ERS guideline. Clin Microbiol Infect 24:e1–e38. https://doi.org/10.1016/j.cmi.2018.01.002

Veeneman GH, Notermans S, Liskamp RMJ et al (1987) Solid-phase synthesis of a naturally occurring β-(1 → 5)-linked D-galactofuranosyl heptamer containing the artificial linkage arm L-homoserine. Tetrahedron Lett 28:6695–6698

Wang C-C, Huang Y-L, Ren C-T et al (2008) Glycan microarray of Globo H and related structures for quantitative analysis of breast cancer. Proc Nat Acad Sci USA 105:11661–11666. https://doi.org/10.1073/pnas.0804923105

Wang L, Overkleeft HS, van der Marel GA, Codée JD (2019) Reagent controlled stereoselective assembly of α-(1,3)-glucans. Eur J Org Chem 2019:1994–2003. https://doi.org/10.1002/ejoc.201800894

Wang L, Overkleeft HS, van der Marel GA, Codée JD (2018) Reagent controlled stereoselective synthesis of α-glucans. J Am Chem Soc 140:4632–4638. https://doi.org/10.1021/jacs.8b00669

Wong S, Krylov VB, Argunov DA et al (2020) Potential of chemically synthesized oligosaccharides to define th carbohydrate moieties of the fungal cell wall responsible for the human immune response. The example of the *Aspergillus fumigatus* galactomannan. mSphere, in press

Yashunsky DV, Karelin AA, Tsvetkov YE, Nifantiev NE (2018) Synthesis of 3-aminopropyl β-(1 → 6)-D-glucotetraoside and its biotinylated derivative. Carbohyd Res 455:18–22. https://doi.org/10.1016/j.carres.2017.11.001

Yashunsky DV, Tsvetkov YE, Grachev AA et al (2016a) Synthesis of 3-aminopropyl glycosides of linear β-(1 → 3)-D-glucooligosaccharides. Carbohyd Res 419:8–17. https://doi.org/10.1016/j.carres.2015.10.012

Yashunsky DV, Tsvetkov YE, Nifantiev NE (2016b) Synthesis of 3-aminopropyl glycoside of branched β-(1 → 3)-D-glucooctaoside. Carbohyd Res 436:25–30. https://doi.org/10.1016/j.carres.2016.11.005

Yudina ON, Tsvetkov YE, Nifantiev NE (2015) Synthesis of 2-aminoethyl glycosides of chitooligosaccharides. Russ Chem Bull 64:2932–2941

Yudina ON, Tsvetkov YE, Nifantiev NE (2016) Conditions of catalytic hydrogenolysis for the simultaneous reduction of azido group and debenzylation of chitooligosaccharides. Synthesis of biotinylated derivatives of chitooligosaccharides. Russ Chem Bull 65:2937–2942

Zheng RB, Jégouzo SAF, Joe M et al (2017) Insights into interactions of mycobacteria with the host innate immune system from a novel array of synthetic Mycobacterial Glycans. ACS Chem Biol 12:2990–3002. https://doi.org/10.1021/acschembio.7b00797

Zuurmond HM, Van der Klein PAM, Veeneman GH, Van Boom JH (1990) A convenient iodonium-ion-assisted synthesis of an immunologically active tetrameric β (1 → 5)-linked D-galactofuranoside from the extracellular polysaccharide of *Aspergillus* and *Penicillium* species. Recl Trav Chim Pays-Bas 109:437–441

Drug Discovery Today: Technologies
Vol. 35, 2020

Translating basic research into novel vaccine

Synthetic carbohydrate based anti-fungal vaccines

Vadim B. Krylov, Nikolay E. Nifantiev*

Laboratory of Glycoconjugate Chemistry, N.D. Zelinsky Institute of Organic Chemistry, Russian Academy of Sciences, Leninsky Prospect 47, 119991 Moscow, Russia

Emerging growth of antimycotic resistance among fungal pathogens stimulates the development of corresponding vaccines and therapeutic monoclonal antibodies for active and passive immunization. The polysaccharide components of the fungal cell wall which are not present in humans and mammalians are regarded as promising targets for development of antifungal immunotherapy. Unfortunately, purified fungal antigens related to cell wall polysaccharides are not easily available from natural sources. Moreover, most of these polysaccharides are extremely heterogenic, comprised of different antigenic factors exhibiting different immunogenic properties. Today, the design of efficient antifungal vaccines requires a reliable alternative for such polymers, challenging the synthesis of complex oligosaccharide structures related to polysaccharide antigens. Special attention should be paid to the selection of the target epitope to ensure the protective properties of the vaccine. This review discusses the potential of fungal cell-wall polysaccharides as the basis for development glycoconjugate vaccines on the basis of synthetic oligosaccharides and summarizing contemporary challenges in this field.

Section editor: Dr. J.D.C Codee – Leiden Institute of Chemistry, Leiden University, Einsteinweg 55, 2333 CC Leiden, The Netherlands.
Dr. Robert Adamo – GSK, Via Fiorentina 1, 53100 Siena, Italy.

Introduction

The prevalence of acute or chronic fungal diseases significantly increased over the past decade leading to death, long term illness and reduced life quality of infected patients [1]. Meanwhile, drug resistance increase among clinical isolates of fungal pathogens challenges the development of new strategies for treatment and prevention of the illness [2]. Many studies have provided evidence for protection from fungal infections by means of active and passive immunization [3]. The impact of monoclonal antibodies as tools to combat acute fungal infection was recently summarized in review [4]. Anti-fungal vaccines are conceived as media for prevention or help to cure fungal diseases in patients who need to be treated with transplants, immunosuppressive or anticancer therapy [5]. As active immunization can be efficient against chronic fungal diseases, several vaccine formulations are currently undergoing clinical trials on patients suffering from recurrent vulvovaginal candidiasis [6].

The cell wall is the outer component of the fungal pathogen responsible for initial recognition by the host immune system. The causative agents of the most significant and fatal invasive fungal infections belong to genera *Aspergillus*, *Candida*, *Cryptococcus*, have different structural organization and composition of their cell walls, which is schematically represented in Fig. 1. In all these pathogens the fungal cell wall is mainly composed of different polysaccharides which are

*Corresponding author.: N.E. Nifantiev (nen@ioc.ac.ru)

 https://doi.org/10.1016/j.ddtec.2020.11.002

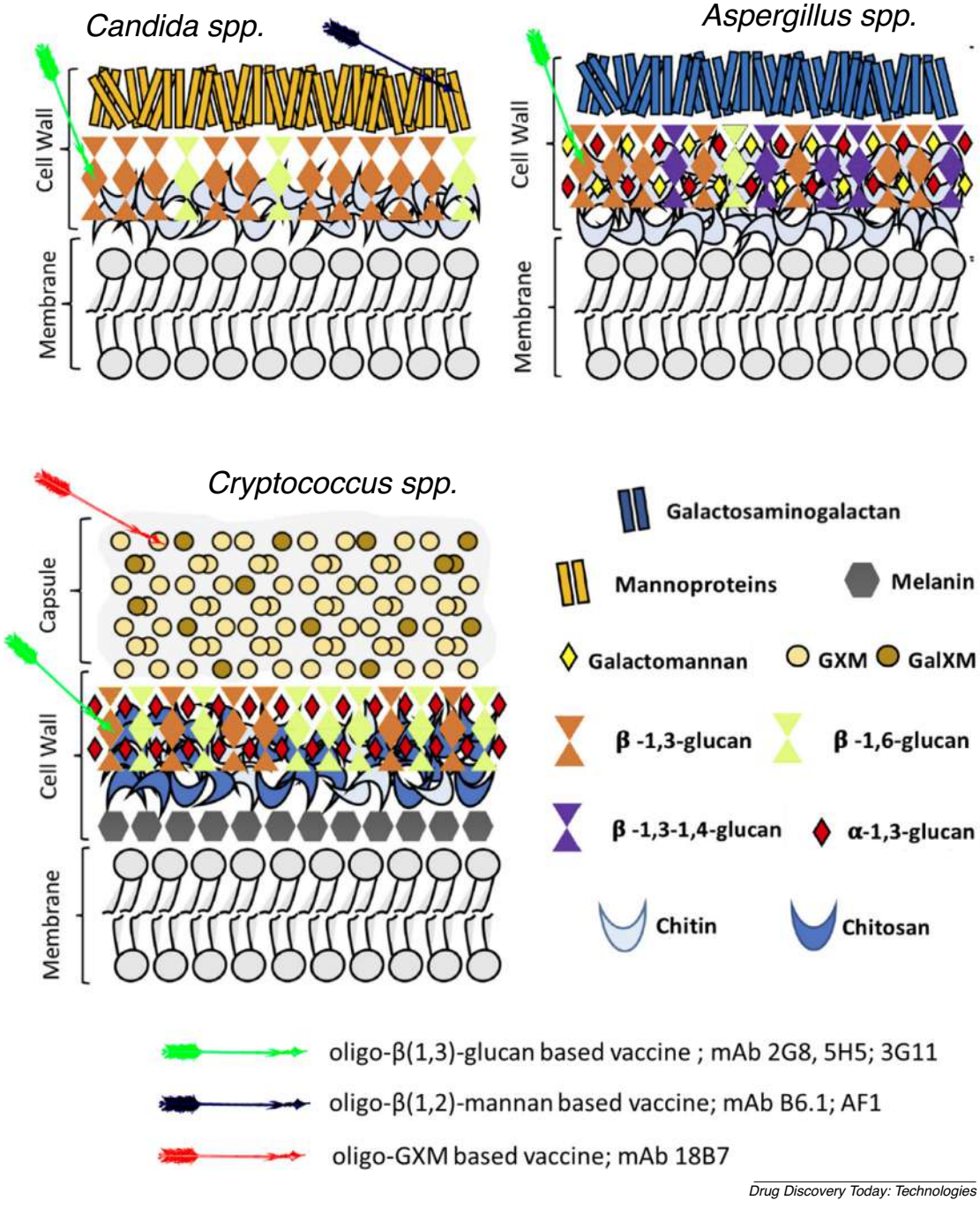

Fig. 1. Structural organization and polysaccharide components of cell walls of *Candida albicans*, *Cryptococcus neoformans* and *Aspergillus fumigatus*. Adapted with permission from [10].

bound by covalent and non-covalent interactions forming the complex multi-layer architecture. The inner layer of the fungal cell wall is composed mainly of chitin, chitosan and glucan polysaccharides (Fig. 1), while its outer layer presents an array of highly variable specific polysaccharides and glycoproteins. Most of the above-mentioned polysaccharides are not present in humans and thus can be considered as excellent targets for antifungal immunotherapy. Below the evolution of anti-fungal vaccines is described based on synthetically accessible oligosaccharides and targeting (1) *Candida* mannan, (2) pan-fungal β-D-glucan, (3) *Cryptococcus* glucuronoxylomannan as well as other promising types of antigenic polysaccharides of fungal cell-wall.

Anti-fungal vaccines based on oligosaccharides related to *Candida* -mannan fragments

The outer layer of *Candida* spp. cell wall consists of proteins highly glycosylated by mannoside carbohydrate chains. This

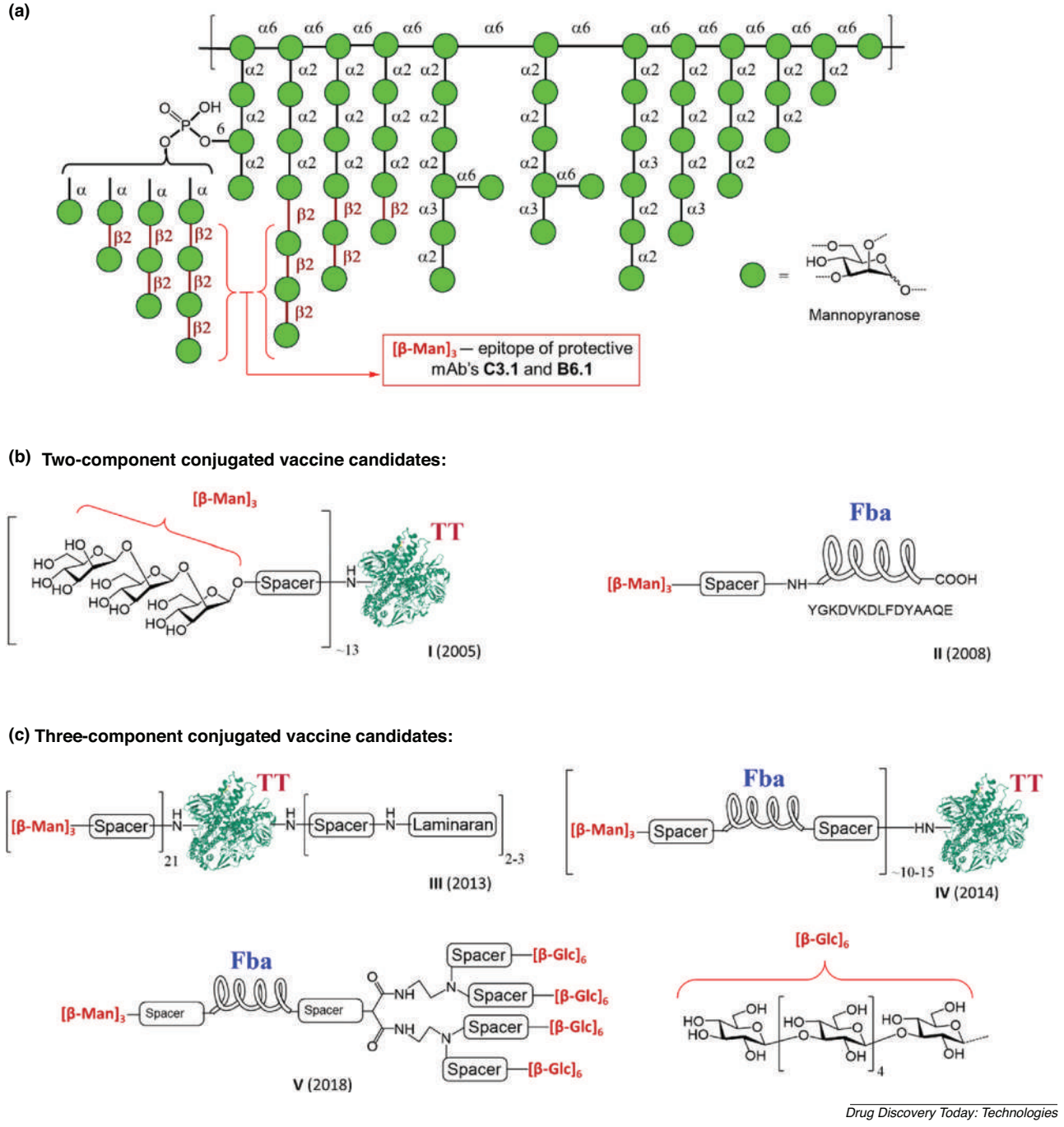

Fig. 2. Anti-fungal vaccine candidates based on β-mannan trisaccharide developed by Bundle and coworker. Tentative structure of the cell wall mannan of *C. albicans* (A) with marked structures of protective [β-Man]$_3$ epitope used for design two-component (B) and three-component (C) vaccine constructions.

mannan polysaccharide is characterized by a set of different structural motifs, namely antigenic factors, distinguished by size, type of the glycoside bond, presence of phosphodiester linkages, branching points *etc.* (Fig. 2,A) [7]. The composition of the mannan varies depending on species and strain of *Candida* microorganism. Due to complex and irregular structure *Candida* mannan exhibits unreproducible immunogenic properties which make its use problematic for the vaccine design. Thus, the primary task to solve this limitation is to select a well-defined epitope to ensure the efficiency and safety of the vaccine.

Anti-*C. albicans* monoclonal antibodies (mAb) C3.1 and B6.1, generated through hybridoma techniques from mice vaccinated with a natural mannan-liposome preparation, efficiently protect against disseminated candidiasis and vaginal infection in animal model [8]. The fine carbohydrate specificity of these antibodies was mapped using a library of synthetic oligosaccharide ligands, related to mannan anti-

gen revealing recognition of the same β-(1→2)-linked trimannoside epitope [9].

The observations described above suggest that β-D-Man-(1→2)-β-D-Man-(1→2)-β-D-Man- ([β-Man]$_3$ on Fig. 2) is the optimal oligosaccharide for a conjugated vaccine. To prove this conclusion, the target trisaccharide was synthesized and conjugated with tetanus toxoid (TT) vaccine carrier to form a semi-synthetic vaccine prototype **I** (Fig. 2,B) able to stimulate the generation of protective antibodies against candidiasis [11]. In 2008, the first fully synthetic glycopeptide vaccine **II** (Fig. 2,B) based on target β-mannan trisaccharide was designed and used to combat disseminated candidiasis in mice [12]. Specific Th-peptide carrier (Fba) was selected from *Candida albicans* cell wall proteins by algorithm peptide epitope searches and prepared using automated peptide synthesizer [12].

The efficiency of the above mentioned two-component conjugated prototype vaccine can be improved by using the three component ones. Laminarin, a β-(1→3)-glucan of seaweed origin, was incorporated into the original [β-Man]$_3$-TT conjugate to enhance immunogenicity of obtained conjugate **III** (Fig. 2,C) to target dendric cells Dectin-1 receptor [13]. The alternative way to construct three component glycoconjugate vaccines containing β-mannan related trisaccharide ([β-Man]$_3$) and polypeptide *C. albicans* epitope Fba conjugated to a tetanus toxoid carrier **IV** (Fig. 2,C) was developed in the same group in 2014 [14]. Similar three component glycopeptide vaccine, but based on the keyhole limpet hemocyanin (KLH), was prepared by another research group in 2019 [15] demonstrating the great potential of these types of conjugates as antifungal vaccines.

In 2018, a fully synthetic dendritic three component vaccine candidate **V** (Fig. 2,C) containing (1) β-(1→2)-mannotrisaccharide ([β-Man]$_3$), (2) *C. albicans* T-cell oligopeptide (Fba) and (3) β-(1→3)-glucohexasaccharide ([β-Glc]$_6$, as Dectin-1 ligand) was also reported [16]. However, the designed immunogen induced antibody response but lower then the above mentioned glycopeptide conjugate based on tetanus toxoid [16]. Nevertheless the example of totally synthetic low molecular weight glycoconjugate **V** demonstrated principle possibility of the development of protein-carrier free carbohydrate vaccine.

Anti-fungal vaccines based on oligosaccharides related to -glucan fragments

Conjugates of natural β-(1→3)-D-glucans and synthetic β-(1→3)-D-glucooligosaccharides are being intensively investigated as key components of potential antifungal vaccines. The immunological potencies studied of conjugates depend on the structure of the carbohydrate ligand (length, presence of branching points), nature of the protein carrier, conjugation degree (''carbohydrate loading''), and methods of attachment. For the first time, a glycoconjugate vaccine composed of β-glucan polysaccharide laminarin conjugated with the diphtheria toxoid CRM197 was prepared and showed promising results on protection against major fungal pathogens in different animal models [17].

The following vaccine evolution included switching from natural polysaccharides to well-defined synthetic spacered oligosaccharides in combination with site-controlled conjugation methods. Thus, to have insights on β-glucan epitope that mediates antifungal protection, the synthetic linear 15-mer and branched 17-mer bearing the β-(1→6)-glucose residue on each fifth unit of the backbone were conjugated with CRM197 (see conjugates **VIb** and **VIII**, respectively in Fig. 3, A) [18]. The linear synthetic 15-mer induced high titers of anti-β-(1→3)-glucan IgG which protected mice in lethal challenge with *C. albicans* [18]. On the other hand using the branched 17-mer resulted in loss of protection against the fungal infection [18]. Interestingly, even the relatively short linear glucosyl 6-mer based vaccine candidate **VIa** (Fig. 3,A), which was studied next, elicited a level of protective IgG antibodies comparable to that induced by conjugates of longer β-glucooligosaccharide chains [19].

Additionally, the influence of the conjugation site in protein carrier was studied by using linear hexaglucoside ligand [20,21] attached selectively *via* tyrosine or lysine units of CRM-197. In spite of lower degree of conjugation in first preparation it induced higher levels of anti-glucan IgG. Remarkably, introduction of two hexasaccharide chains through one tyrosine residue did not increase the immunological potency of the conjugate [20,21]. Despite the above noted evidence that the protective antifungal epitope is a linear β-(1→3)-glucan sequence, glycoconjugates of β-(1→6)-branched oligosaccharides with KLH **VII** (Fig. 3,A) described in Ref. [22] was shown to elicit high level of IgG antibodies which were able to bind to natural β-glucans and fungal cells and provide effective protection against systemic *C. albicans* infection in mice.

The synthetic nona-β-(1→3)-D-glucoside conjugated with bovine serum albumin (BSA) was used to generate monoclonal antibodies 5H5 and 3G11 which demonstrated protective activity in *in vivo* experiments with mice [23]. This study which can be regarded as the investigation of the mechanism of vaccine action demonstrated once again that oligosaccharides related to β-(1→3)-D-glucan fragments are promising vaccine components with proven antifungal properties against different fungal pathogens. This conclusion stimulates further development of anti-fungal vaccine product.

Anti-fungal vaccines based on oligosaccharides related to *Cryptococcus* glucuronoxylomannan fragments

Glucuronoxylomannan (GXM) is the major component of the *Cryptococcus neoformans* capsule and has an extremely complex chemical structure. The first evidence that GXM can be regarded as a target for immunotherapy was obtained

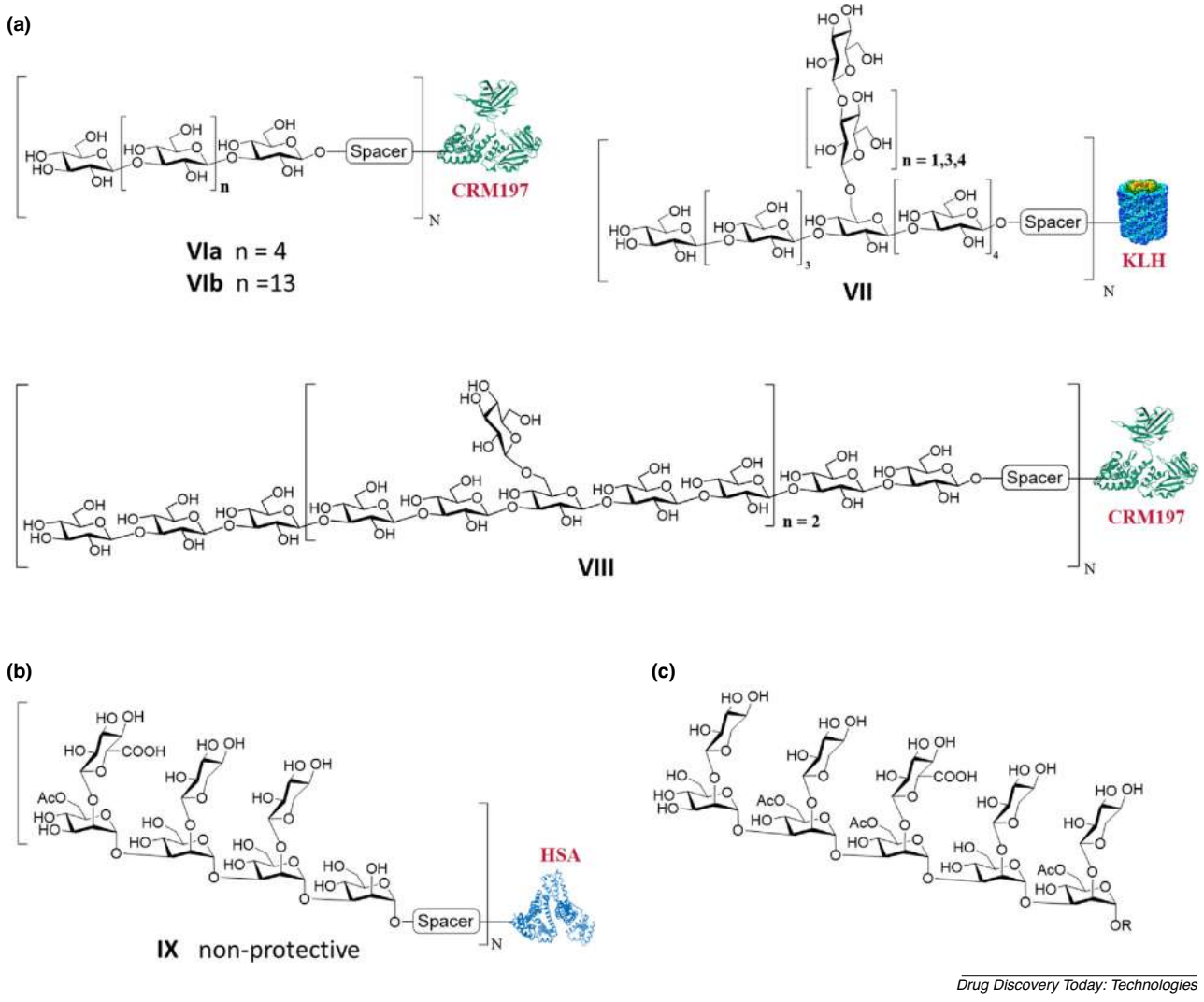

Fig. 3. Anti-fungal vaccine candidates **VI-VIII** based on synthetic oligosaccharides related to β-(1→3)-D-glucan fragments (A). The conjugate **IX** (B) of synthetic heptasaccharide representing repeating motif of glucuronoxylomannan of *C. neoformans* serotype A and human serum albumin (HSA) eliciting non-protective antibodies (see main text for details). The structure of serotype A decasaccharide recognized by protective mAbs and regarded as an attractive candidate for further vaccine development (C).

using natural polysaccharide conjugated with tetanus toxoid [24]. A set of mAbs prepared from mice infected with *C. neoformans* and mice immunized with GXM-TT recognized the identical carbohydrate epitopes in the GXM [25]. Further studies showed that immunization with GXM-TT protected mice against *C. neoformans* infection [26], whereas the analysis of obtained monoclonal antibodies demonstrated the generation of both protective and non-protective ones. Thus, further studies were directed towards determination of the protective epitope structure for its application as a well-characterized synthetic ligand in the conjugated vaccine.

First, the conjugate of synthetic heptasaccharide **IX** representing putative repeating motif of serotype A of *C. neoformans* (Fig. 3,B) and human serum albumin (HSA) was prepared and tested in mice [27]. The conjugate elicited high-titer IgG response when given with complete Freund's adjuvant, but not without it, as opposed to GXM-TT. Surprisingly, anti-serum was most reactive with serotype D and B cells, but not with serotype A, however the strong interaction with serotype A GXM was shown by ELISA. Further detailed studies demonstrated that, unfortunately, the generated antibodies could not protect mice against challenge with *C. neoformans* [28].

To elucidate the oligosaccharide structure which could be regarded as a efficient ligand for vaccine development, the fine carbohydrate specificity of protective and non-protective monoclonal antibodies was studied in detail using the synthetic glycan array containing immobilized oligosaccharides related to GXM fragments, ranging from di- to octadecasaccharides. The serotype A decasaccharide (shown in Fig. 3,C) interacted well with most of the anti-GXM mAbs including two mAbs that had been shown to be protective in mice, 2H1

(IgG1) and 18B7 (IgG1) [29]. These results revealed a serotype A decasaccharide (Fig. 3,C) as an attractive candidate for further vaccine development.

Prospects

In addition to the above discussed main types of fungal cell wall polysaccharides, alternative carbohydrate antigens attract attention as promising targets for vaccine development. Of special interest is β-(1→6)–linked poly-*N*-acetyl-D-glucosamine (PNAG), originally isolated from the polysaccharide capsule of *Staphylococcus aureus* [30]. Further studies demonstrated that this polysaccharide spreads among a wide range of pathogens, including fungal species, such as *C. albicans*, *Aspergillus flavus*, *Fusarium solani*, and *C. neoformans*. PNAG-specific monoclonal antibodies were able to protect mice from *C. albicans*, *A. flavus*, *A. fumigatus* and *F. solani* in the keratitis model [31]. Polyclonal antibodies obtained after immunization of mice with a conjugate of a synthetic oligosaccharide fragment of PNAG and tetanus toxoid also demonstrated antifungal activity in opsonophagocytosis assay [30,31].

Polysaccharide chitin is also regarded as a target for the development of pan-fungal therapeutics. Chitin-specific recombinant chimera was constructed from the chitin recognizing domain of the WGA lectin and the Fc fragment of murine IgG_{2a}. Obtained WGA-Fc chimera were able to protect mice in challenge with a lethal dose of *H. capsulatum* and additionally increased killing of the fungal pathogens by murine macrophages *in vitro* [32].

Increasing attention is paid to the investigation of oligosaccharides related to galactosaminogalactan [33], α-(1→3)-glucan [34], and galactomannan [35] found in *A. fumigatus*. All these polysaccharides play an important role in modulation of host immune response, which was elucidated using related oligosaccharide fragments [36,37]. Antigen-specific antibodies generated using semi-synthetic immunogens (conjugates of synthetic oligosaccharide with BSA) were able to recognize fungal cell wall. The evaluation of their protective properties *in vivo* is currently ongoing and will be published elsewhere.

Ex vivo T-cell technologies against invasive fungal diseases are currently regarded as a new promising branch of immunotherapeutic approach particularly valuable for hematopoietic stem cell transplant patients. T-helper cells specific to fungal antigens could be adoptively transferred to immunocompromised individuals inducing protective response. The manufacturing methods for fungus-specific T-cell isolation and expansion *ex vivo* are discussed in detail in reviews [38,39]. It should be noted that only natural fungal extracts and individual recombinant proteins were used as fungal associated antigens for the election of T-cells. To the best of our knowledge there was only one published example where T-cells were adopted to recognize fungal carbohydrate antigen. Bioengineering CAR (chimeric antigen receptor) T-cells were prepared by expression of the Dectin-1 carbohydrate-recognition domain that binds fungal β-(1→3)-glucan which led to inhibition of *A. fumigatus* hyphal growth *in vitro* and protection against *Aspergillus* infection *in vivo* [40].

Interestingly, synthetic oligosaccharides related to mannan [41] and galactomannan [42] fungal antigens demonstrated immunomodulatory activities on the RAW 264.7 cell line murine macrophages as *in vitro* innate immunity cell model. Exposure of macrophage with structurally diverse oligosaccharides resulted in different manner on proliferation, cytokine profile release and phagocytic activity which allowed identifying oligosaccharide structure with the most potent immunobiological activity. Such oligosaccharides can be considered as potential *in vitro* immunomodulating agents for prospective design of cellular therapeutic technologies against fungal pathogens. More detailed description of immunological aspects of fungal vaccines development is described in the review by M.R. Romano et al. [43] which is the part of present special issue of this journal.

Chemical synthesis of oligosaccharide vaccine ligands related to antigenic polysaccharides of fungal cell-wall

The synthesis of oligosaccharide ligands related to immunodeterminant fragments of fungal polysaccharides requires efficient chemical methods for carbohydrate chain assembling. The main problem that has to be solved is the performance of highly stereoselective 1,2-*cis*-glycosylations. Especially problematic is β-mannosylation which is essential, for example in the preparation of the β-trimannoside *Candida* vaccine ligand (see Fig. 2). Two general approaches to the β-mannoside bond formation have been applied. The first one is indirect and based on the initial β-glucosylation followed by epimerization of C-2 atom in glucose unit. Particularly, the inversion of C-2 configuration *via* an oxidation-reduction sequence was applied by Bundle and cowokers [11] (see Table). The alternative approach is based on the direct mannosylation with conformationally rigid 4,6-*O*-benzylidene-protected mannosyl donors *via* intermediate formation of anomeric triflates [44]. Particularly, this strategy was applied by Karelin at al. for the preparation of β-mannosides related to antigenic factor 6 of *Candida albicans* [45].

The problem of 1,2-*cis*-stereoselectivity of glycosylation arises within the synthesis of *Aspergillus* α-glucan related oligosaccharides. This task can be accomplished using α-stereodirecting protective groups in the structure of glucosyl donors. Thus, a participating protecting group at O-3 and O-6 allows reaching excellent α-stereoselectivity due to its remote anchimeric assistance [46] to give a series of homo-α-(1→3)-glucooligosaccharides up to 11-mer [34,37]. Reagent controlled α-(1→3)-glycosylation was also efficiently used by Codee et al. in the assembling of large homo-α-(1→3)-glucoside chains [47].

Table 1. Synthetic methods applied for preparation of oligosaccharides related to fungal polysaccharides.

Fungal polysaccharide	Synthetic challenge	Proposed synthetic approach
Mannan	Stereodirected formation of β-mannopyranosides	Epimerization at C-2 *via* an oxidation-reduction sequence [111]. 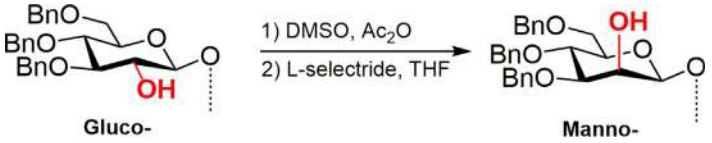 β-Selective mannosylation [44]. 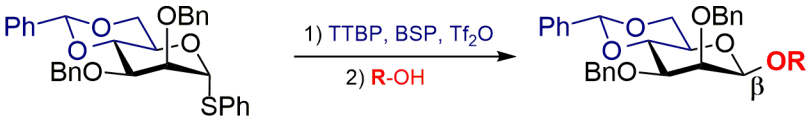 **Fixed conformation of cycle in mannosyl donor** **Intermediate formation of anomeric triflate** ⇒ **β-mannosylation**
α-Glucan	Stereodirected α-glucosylation	Stereoselective α-glucosylation with remote participation of O-acyl groups [34,37,46] 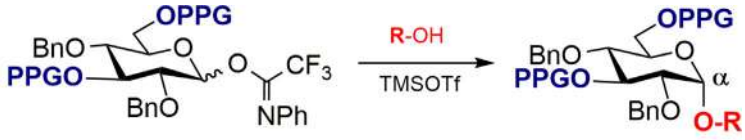 **PPG** - participating protecting group at O-3 and O-6 ⇒ **α-glucosylation**
β-Glucan	Regiodirected formation of (1→3)-linkage	Regioselective glucosylation of 2,3-diols [48]. 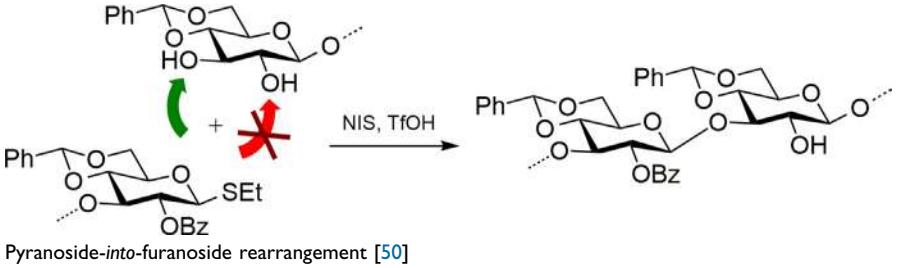
Galactomannan	Efficient synthesis of furanoside building blocks	Pyranoside-*into*-furanoside rearrangement [50] 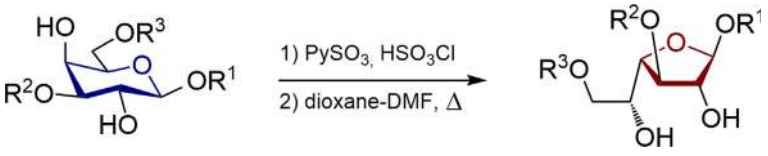
Galactosaminogalactan	Efficient synthesis of α-glycosylating galactosamine building blocks	Azidophenylselenylation of galactals [55] 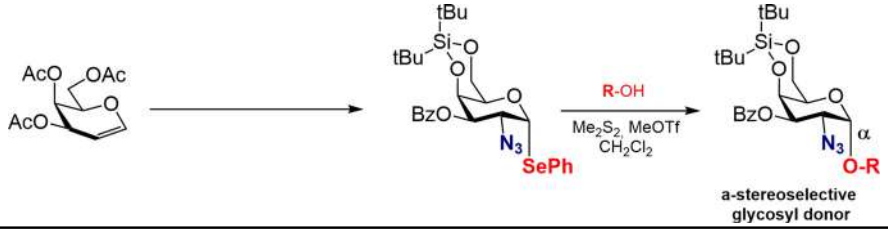

The efficient synthetic strategy developed by Yashunsky at al. [48] provides high regio- and stereoselectivity of β-(1→3)-glucan chain assembling. The key point of the synthesis is the use of a thioglucoside donor and 2,3-diolic glucosyl acceptors with 4,6-O-benzylidene protection [48]. This scheme allows preparation of a large series of linear and branched oligoglucosides for further immunological studies [23,49].

For the preparation of oligosaccharides related to the fragments of *Aspergillus* galactomannan, efficient protocols for the synthesis of furanoside building blocks are highly demanded. Pyranoside-*into*-furanoside rearrangement discovered in 2014 [50] allows transformation of selectively protected pyranosides into corresponding furanosides *via* acid-promoted O-sulfation followed by solvolytic desulfation. This method was successfully applied for the preparation of a representative series of galactomannan related oligosaccharides [51–53].

Aspergillus produces also another one antigenic polysaccharide, namely galactosaminogalactan, which attracted very

big research interest and can be also regarded as the basis for vaccine and therapeutic antibody developments. Effective syntheses of galactosaminogalactan related oligosaccharides which were performed very recently [33,54] were based on the use of specially developed azidophenylselenylation of galactals [55] producing 2-azido-2deoxy-1-selenoglycosides which can be used as efficient α- and β-glycosyl donors [56]. The preparation of such derivatives under flow-condition was also recently reported [57].

Described in this section results show how the complexity of fungal polysaccharide structures and their practical significance stimulate continuous development of new synthetic methodologies expanding the availability of fungal carbohydrate epitopes. Outlined synthetic approaches are summarized in the Table 1.

Conclusion

Immuno-enhancing strategies for the prevention and treatment of fungal infections attract interest due to the constantly rising prevalence of fungal diseases and emerging antimicrobial resistance of fungal pathogens. Passive and active immunization is regarded as efficient approach for prevention of both recurrent mucosal and blood stream systemic life-threatening infections. Current vaccine development strategy tends to reject the use of natural antigenic polysaccharides in favor for structurally defined synthetic oligosaccharide ligands [58]. Such compounds are used in preparation of conjugated vaccines and as screening antigens in selection of protective monoclonal antibodies. Precise information about the structure of the recognizing epitope [23,35,59,60], available through the screening on thematic glyco-arrays [58,61], is important for understanding specificity and cross-reactivity of immune response. Modern development of safe and effective vaccine candidate should include structure-based rational design of the target fungal epitope and must be based on optimal conjugation strategy and formulation technology in order to manage efficient immune response with required specificity.

Conflict of interest

The authors declare that the research was conducted in the absence of any commercial or financial relationships that could be construed as a potential conflict of interest.

Acknowledgments

This work was supported in part by the Russian Science Foundation (grant 19-73-30017). The authors thank Dr. A. G. Gerbst for critical reading of manuscript and its fruitful discussion.

References

[1] Brown GD, Denning DW, Gow NAR, Levitz SM, Netea MG, White TC. Hidden killers: human fungal infections. Sci Transl Med 2012;4165rv13.
[2] Srinivasan A, Lopez-Ribot JL, Ramasubramanian AK. Overcoming antifungal resistance. Drug Discov Today Technol 2014;11:65–71.
[3] Boniche C, Rossi SA, Kischkel B, Barbalho FV, Moura ÁND, Nosanchuk JD, et al. Immunotherapy against systemic fungal infections based on monoclonal antibodies. J Fungi 2020;6.
[4] Ulrich S, Ebel F. Monoclonal antibodies as tools to combat fungal infections. J Fungi 2020;6.
[5] Cassone A, Casadevall A. Recent progress in vaccines against fungal diseases. Curr Opin Microbiol 2012;15:427–33.
[6] Cassone A. Development of vaccines for Candida albicans: fighting a skilled transformer. Nat Rev Microbiol 2013;11:884–91.
[7] Shibata N, Kobayashi H, Suzuki S. Immunochemistry of pathogenic yeast, Candida species, focusing on mannan. Proc Jpn Acad Ser B Phys Biol Sci 2012;88:250–65.
[8] Han Y, Riesselman MH, Cutler JE. Protection against candidiasis by an immunoglobulin G3 (IgG3) monoclonal antibody specific for the same mannotriose as an IgM protective antibody. Infect Immun 2000;68:1649–54.
[9] Johnson MA, Cartmell J, Weisser NE, Woods RJ, Bundle DR. Molecular recognition of Candida albicans (1-&2)-β-mannan oligosaccharides by a protective monoclonal antibody reveals the immunodominance of internal saccharide residues. J Biol Chem 2012;287:18078–90.
[10] Garcia-Rubio R, de Oliveira HC, Rivera J, Trevijano-Contador N. The fungal cell wall: candida, Cryptococcus, and Aspergillus species. Front Microbiol 2019;10:2993.
[11] Wu X, Bundle DR. Synthesis of glycoconjugate vaccines for Candida albicans using novel linker methodology. J Org Chem 2005;70:7381–8.
[12] Xin H, Dziadek S, Bundle DR, Cutler JE. Synthetic glycopeptide vaccines combining beta-mannan and peptide epitopes induce protection against candidiasis. Proc Natl Acad Sci U S A 2008;105:13526–31.
[13] Lipinski T, Fitieh A, St Pierre J, Ostergaard HL, Bundle DR, Touret N. Enhanced immunogenicity of a tricomponent mannan tetanus toxoid conjugate vaccine targeted to dendritic cells via Dectin-1 by incorporating β-glucan. J Immunol Baltim Md 1950 2013;190:4116–28.
[14] Cartmell J, Paszkiewicz E, Dziadek S, Tam P-H, Luu T, Sarkar S, et al. Synthesis of antifungal vaccines by conjugation of β-1,2 trimannosides with T-cell peptides and covalent anchoring of neoglycopeptide to tetanus toxoid. Carbohydr Res 2015;403:123–34.
[15] Liao J, Pan B, Liao G, Zhao Q, Gao Y, Chai X, et al. Synthesis and immunological studies of β-1,2-mannan-peptide conjugates as antifungal vaccines. Eur J Med Chem 2019;173:250–60.
[16] Bundle DR, Paszkiewicz E, Elsaidi HRH, Mandal SS, Sarkar SA. Three Component Synthetic Vaccine Containing a β-Mannan T-Cell Peptide Epitope and a β-Glucan Dendritic Cell Ligand. Molecules 2018;23.
[17] Torosantucci A, Bromuro C, Chiani P, De Bernardis F, Berti F, Galli C, et al. A novel glyco-conjugate vaccine against fungal pathogens. J Exp Med 2005;202:597–606.
[18] Bromuro C, Romano M, Chiani P, Berti F, Tontini M, Proietti D, et al. Beta-glucan-CRM197 conjugates as candidates antifungal vaccines. Vaccine 2010;28:2615–23.
[19] Adamo R, Tontini M, Brogioni G, Romano MR, Costantini G, Danieli E, et al. Synthesis of laminarin fragments and evaluation of a β-(1, 3) glucan hexasaccaride-CRM197 conjugate as vaccine candidate against Candida albicans. J Carbohydr Chem 2011;30:249–80.
[20] Adamo R, Hu Q-Y, Torosantucci A, Crotti S, Brogioni G, Allan M, et al. Deciphering the structure–immunogenicity relationship of anti-Candida glycoconjugate vaccines. Chem Sci 2014;5:4302–11.
[21] Hu Q-Y, Allan M, Adamo R, Quinn D, Zhai H, Wu G, et al. Synthesis of a well-defined glycoconjugate vaccine by a tyrosine-selective conjugation strategy. Chem Sci 2013;4:3827–32.
[22] Liao G, Zhou Z, Liao J, Zu L, Wu Q, Guo Z. 6-O-Branched Oligo-β-glucan-Based antifungal glycoconjugate vaccines. ACS Infect Dis 2016;2:123–31.
[23] Matveev AL, Krylov VB, Khlusevich YA, Baykov IK, Yashunsky DV, Emelyanova LA, et al. Novel mouse monoclonal antibodies specifically recognizing β-(1→3)-D-glucan antigen. PLoS One 2019;14e0215535.
[24] Devi SJ, Schneerson R, Egan W, Ulrich TJ, Bryla D, Robbins JB, et al. Cryptococcus neoformans serotype A glucuronoxylomannan-protein conjugate vaccines: synthesis, characterization, and immunogenicity. Infect Immun 1991;59:3700–7.

[25] Casadevall A, Mukherjee J, Devi SJ, Schneerson R, Robbins JB, Scharff MD. Antibodies elicited by a Cryptococcus neoformans-tetanus toxoid conjugate vaccine have the same specificity as those elicited in infection. J Infect Dis 1992;165:1086–93.
[26] Devi SJ. Preclinical efficacy of a glucuronoxylomannan-tetanus toxoid conjugate vaccine of Cryptococcus neoformans in a murine model. Vaccine 1996;14:841–4.
[27] Oscarson S, Alpe M, Svahnberg P, Nakouzi A, Casadevall A. Synthesis and immunological studies of glycoconjugates of Cryptococcus neoformans capsular glucuronoxylomannan oligosaccharide structures. Vaccine 2005;23:3961–72.
[28] Nakouzi A, Zhang T, Oscarson S, Casadevall A. The common Cryptococcus neoformans glucuronoxylomannan M2 motif elicits non-protective antibodies. Vaccine 2009;27:3513–8.
[29] Guazzelli L, Ulc R, Bowen A, Crawford C, McCabe O, Jedlicka AJ, et al. A synthetic glycan array containing Cryptococcus neoformans glucuronoxylomannan capsular polysaccharide fragments allows the mapping of protective epitopes. Chem Sci 2020;11:9209–17.
[30] Cywes-Bentley C, Skurnik D, Zaidi T, Roux D, Deoliveira RB, Garrett WS, et al. Antibody to a conserved antigenic target is protective against diverse prokaryotic and eukaryotic pathogens. Proc Natl Acad Sci U S A 2013;110: E2209–2218.
[31] Zhao G, Zaidi TS, Bozkurt-Guzel C, Zaidi SH, Lederer JA, Priebe GP, et al. Efficacy of antibody to PNAG against keratitis caused by fungal pathogens. Invest Ophthalmol Vis Sci 2016;57:6797–804.
[32] Liedke SC, Miranda DZ, Gomes KX, Gonçalves JLS, Frases S, Nosanchuk JD, et al. Characterization of the antifungal functions of a WGA-Fc (IgG2a) fusion protein binding to cell wall chitin oligomers. Sci Rep 2017;7:12187.
[33] Kazakova ED, Yashunsky DV, Krylov VB, Bouchara J-P, Cornet M, Valsecchi I, et al. Biotinylated oligo-α-(1→ 4)-D-galactosamines and their N-acetylated derivatives: α-stereoselective synthesis and immunology application. J Am Chem Soc 2020;142:1175–9.
[34] Komarova BS, Orekhova MV, Tsvetkov YE, Beau R, Aimanianda V, Latgé J-P, et al. Synthesis of a pentasaccharide and neoglycoconjugates related to fungal α-(1→3)-glucan and their use in the generation of antibodies to trace Aspergillus fumigatus cell wall. Chem Eur J 2015;21:1029–35.
[35] Matveev AL, Krylov VB, Emelyanova LA, Solovev AS, Khlusevich YA, Baykov IK, et al. Novel mouse monoclonal antibodies specifically recognize Aspergillus fumigatus galactomannan. PLoS One 2018;13e0193938.
[36] Wong SSW, Krylov VB, Argunov DA, Karelin AA, Bouchara J-P, Fontaine T, et al. Potential of chemically synthesized oligosaccharides to define the carbohydrate moieties of the fungal cell wall responsible for the human immune response, using Aspergillus fumigatus galactomannan as a model. MSphere 2020;5e5:e00688-19.
[37] Komarova BS, Wong SSW, Orekhova MV, Tsvetkov YE, Krylov VB, Beauvais A, et al. Chemical synthesis and application of biotinylated oligo-α-(1→3)-D-glucosides to study the antibody and cytokine response against the cell wall α-(1→3)-D-glucan of Aspergillus fumigatus. J Org Chem 2018;83:12965–76.
[38] Papadopoulou A, Kaloyannidis P, Yannaki E, Cruz CR. Adoptive transfer of Aspergillus-specific T cells as a novel anti-fungal therapy for hematopoietic stem cell transplant recipients: progress and challenges. Crit Rev Oncol Hematol 2016;98:62–72.
[39] Castellano-Gonzalez G, Clancy LE, Gottlieb D. Prospects for adoptive T-cell therapy for invasive fungal disease. Curr Opin Infect Dis 2017;30:518–27.
[40] Kumaresan PR, Manuri PR, Albert ND, Maiti S, Singh H, Mi T, et al. Bioengineering T cells to target carbohydrate to treat opportunistic fungal infection. Proc Natl Acad Sci U S A 2014;111:10660–65.
[41] Paulovičová E, Paulovičová L, Farka P, Karelin AA, Tsvetkov YE, Krylov VB, et al. Importance of Candida Antigenic factors: structure-driven immunomodulation properties of synthetically prepared mannooligosaccharides in RAW264.7 macrophages. Front Cell Infect Microbiol 2019;9:378.
[42] Paulovičová E, Paulovičová L, Hrubiko M, Krylov VB, Argunov DA, Nifantiev NE. Immunobiological activity of synthetically prepared immunodominant galactomannosides structurally mimicking Aspergillus galactomannan. Front Immunol 2017;8:1273.
[43] Romano M, Del Bino L. Role of carbohydrate antigens in antifungal glycoconjugate vaccine and immunotherapy. Drug Discov Today Technol 2020. accepted.
[44] Crich D, Sun S. Direct formation of β-mannopyranosides and other hindered glycosides from thioglycosides. J Am Chem Soc 1998;120:435–6.
[45] Karelin AA, Tsvetkov YE, Paulovičová E, Paulovičová L, Nifantiev NE. A blockwise approach to the synthesis of (1→2)-Linked oligosaccharides corresponding to fragments of the acid-stable β-Mannan from the Candida albicans cell wall. Eur J Org Chem 2016;2016:1173–81.
[46] Komarova BS, Tsvetkov YE, Nifantiev NE. Design of α-Selective glycopyranosyl donors relying on remote anchimeric assistance. Chem Rec 2016;16:488–506.
[47] Wang L, Overkleeft HS, van der Marel GA, Codée JD. Reagent controlled stereoselective assembly of α-(1, 3)-Glucans. Eur J Org Chem 2019;2019:1994–2003.
[48] Yashunsky DV, Tsvetkov YE, Grachev AA, Chizhov AO, Nifantiev NE. Synthesis of 3-aminopropyl glycosides of linear β-(1→3)-D-glucooligosaccharides. Carbohydr Res 2016;419:8–17.
[49] Yashunsky DV, Tsvetkov YE, Nifantiev NE. Synthesis of 3-aminopropyl glycoside of branched β-(1→3)-D-glucooctaoside. Carbohydr Res 2016;436:25–30.
[50] Krylov VB, Argunov DA, Vinnitskiy DZ, Verkhnyatskaya SA, Gerbst AG, Ustyuzhanina NE, et al. Pyranoside-into-Furanoside rearrangement: new reaction in carbohydrate chemistry and its application in oligosaccharide synthesis. Chem Eur J 2014;20:16516–22.
[51] Argunov DA, Krylov VB, Nifantiev NE. Convergent synthesis of isomeric heterosaccharides related to the fragments of galactomannan from Aspergillus fumigatus. Org Biomol Chem 2015;13:3255–67.
[52] Argunov DA, Krylov VB, Nifantiev NE. The use of pyranoside-into-Furanoside rearrangement and controlled O(5)→O(6) benzoyl migration as the basis of a synthetic strategy to assemble (1→5)-and (1→6)-Linked galactofuranosyl chains. Org Lett 2016;18:5504–7.
[53] Krylov VB, Argunov DA, Solovev AS, Petruk MI, Gerbst AG, Dmitrenok AS, et al. Synthesis of oligosaccharides related to galactomannans from Aspergillus fumigatus and their NMR spectral data. Org Biomol Chem 2018;16:1188–99.
[54] Zhang Y, Gómez-Redondo M, Jiménez-Osés G, Arda A, Overkleeft HS, van Der Marel GA, et al. Synthesis and Structural Analysis of Aspergillus fumigatus Galactosaminogalactans featuring α-galactose, α-galactosamine and α-N-acetyl galactosamine linkages. Angew Chem 2020;31:12746–50.
[55] Mironov YV, Sherman AA, Nifantiev NE. Homogeneous azidophenylselenylation of glycals using TMSN3–Ph2Se2–PhI (OAc) 2. Tetrahedron Lett 2004;45:9107–10.
[56] Khatuntseva EA, Sherman AA, Tsvetkov YE, Nifantiev NE. Phenyl 2-azido-2-deoxy-1-selenogalactosides: a single type of glycosyl donor for the highly stereoselective synthesis of α-and β-2-azido-2-deoxy-d-galactopyranosides. Tetrahedron Lett 2016;57:708–11.
[57] Guberman M, Pieber B, Seeberger PH. Safe and scalable continuous flow azidophenylselenylation of Galactal to prepare galactosamine building blocks. Org Process Res Dev 2019;23:2764–70.
[58] Krylov VB, Nifantiev NE. Synthetic oligosaccharides mimicking fungal cell Wall polysaccharides. In: Latgé J-P, editor. The fungal cell Wall an Armour and a weapon for human fungal pathogens. Springer Nature Switzerland AG; 2020. p. 1–16.
[59] Krylov VB, Solovev AS, Argunov DA, Latgé J-P, Nifantiev NE. Reinvestigation of carbohydrate specificity of EB-A2 monoclonal antibody used in the immune detection of Aspergillus fumigatus galactomannan. Heliyon 2019;5e01173.
[60] Schubert M, Xue S, Ebel F, Vaggelas A, Krylov V, Nifantiev N, et al. Monoclonal antibody AP3 binds galactomannan antigens displayed by the pathogens Aspergillus flavus, A. Fumigatus and A. Parasiticus. Front Cell Infect Microbiol 2019;9:234.
[61] Krylov VB, Petruk MI, Grigoryev IV, Lebedin YS, Glushko NI, Khaldeeva EV, et al. Study of the carbohydrate specificity of antibodies against Aspergillus fumigatus using a library of synthetic mycoantigens. Russ J Bioorganic Chem 2018;44:1–12.

AMERICAN SOCIETY FOR MICROBIOLOGY | mSphere®

OPINION/HYPOTHESIS
Host-Microbe Biology

Potential of Chemically Synthesized Oligosaccharides To Define the Carbohydrate Moieties of the Fungal Cell Wall Responsible for the Human Immune Response, Using *Aspergillus fumigatus* Galactomannan as a Model

Sarah Sze Wah Wong,[a]* Vadim B. Krylov,[b] Dmitry A. Argunov,[b] Alexander A. Karelin,[b] Jean-Phillipe Bouchara,[c] Thierry Fontaine,[a] Jean-Paul Latgé,[a]* Nikolay E. Nifantiev[b]

[a]Unité des Aspergillus, Institut Pasteur, Paris, France
[b]Laboratory of Glycoconjugate Chemistry, N. D. Zelinsky Institute of Organic Chemistry, Russian Academy of Sciences, Moscow, Russia
[c]Groupe d'Etude des Interactions Hôte-Pathogène (EA 3142), UNIV Brest, Angers, France

ABSTRACT Methodologies to identify epitopes or ligands of the fungal cell wall polysaccharides influencing the immune response of human pathogens have to date been imperfect. Using the galactomannan (GM) of *Aspergillus fumigatus* as a model, we have shown that synthetic oligosaccharides of distinct structures representing key fragments of cell wall polysaccharides are the most precise tools to study the serological and immunomodulatory properties of a fungal polysaccharide.

KEYWORDS *Aspergillus fumigatus*, aspergillosis, antibodies, cytokines, chemokines, immunology, *Aspergillus*, galactomannan, glycoarray

Fungi are the only eukaryotes protected by a polysaccharide shell with an ambivalent function among pathogens, having a protective role against environmental stress and a negative role in the induction of an antifungal immune response (1). The carbohydrate fragments of the cell wall polysaccharide responsible for the induction of the immune response have often been poorly defined due to a lack of efficient tools. Currently, mutants lacking one polysaccharide due to the deletion of genes regulating its biosynthesis or polysaccharides purified from the cell wall are used. The first approach is indirect and does not take into account the putative compensatory reactions resulting from the gene deletion. The second approach results from purification of the cell wall polysaccharides. However, if it is possible to identify the target oligosaccharides in the case of long homogenous polysaccharides [and has been very appropriate in the identification of dectin-1, a receptor recognizing specifically the β-(1→3)-glucan chains (2)], this approach is more difficult when the composition of the repeating units of the polysaccharide is complex. This is the case for the galactomannan of *Aspergillus fumigatus*, which is composed of tetraose repeats with mannose units with α-(1→2) and α-(1→6) linkages bound to short side chains comprising β-(1→5)- and β-(1→6)-linked galactofuranose units of various lengths (3–5). It is even more difficult in the case of long polysaccharides without repeating units, such as the galactosaminogalactan of this species (6). The isolation of absolutely pure water-insoluble polysaccharide from the cell wall and the solubilization of immunoreactive oligosaccharides are difficult without structural modifications resulting from the harsh chemical extraction procedure required to solubilize the cell wall oligosaccharides.

In this report, we present an analysis of the oligosaccharides responsible for the immune response of the human host against the galactomannan (GM) of *A. fumigatus*. Even though galactofuran has been recognized as a potent *Aspergillus* immunogen (1, 7), the GM fragments modulating the host immune response have not been fully

Citation Wong SSW, Krylov VB, Argunov DA, Karelin AA, Bouchara J-P, Fontaine T, Latgé J-P, Nifantiev NE. 2020. Potential of chemically synthesized oligosaccharides to define the carbohydrate moieties of the fungal cell wall responsible for the human immune response, using *Aspergillus fumigatus* galactomannan as a model. mSphere 5:e00688-19. https://doi.org/10.1128/mSphere.00688-19.

Editor Aaron P. Mitchell, Carnegie Mellon University

Address correspondence to Jean-Paul Latgé, jean-paul.latge@pasteur.fr, or Nikolay E. Nifantiev, nen@ioc.ac.ru.

* Present address: Sarah Sze Wah Wong, Molecular Mycology Unit, UMR2000, CNRS, Institut Pasteur, Paris, France; Jean-Paul Latgé, School of Medicine, University of Crete, Heraklion, Greece.

Cell wall glycoarray
Published 8 January 2020

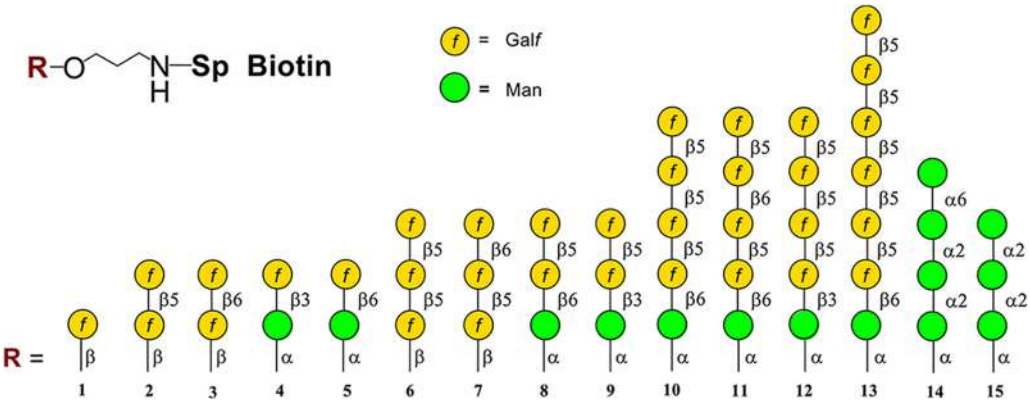

FIG 1 The structure of oligosaccharide ligands representing key structural elements of the galactofuranosylated side chains (ligands 1 to 13) and mannan backbone (ligands 14 and 15) of *A. fumigatus* galactomannan.

characterized. This study presents a new approach based on the use of synthetic oligosaccharides which allows a precise and unbiased identification of the carbohydrates responsible for the immune response.

Glycoarray of oligosaccharides encompassing the complete structure of the galactomannan of *Aspergillus fumigatus*. All fragments of the galactomannan molecule used in this study were chemically synthesized (Fig. 1). Oligosaccharides 1 to 13 related to galactofuranosylated side chains of galactomannan were obtained as previously described (4, 8, 9). Manno-oligosaccharides 14 and 15 (for preparation, see Text S1 in the supplemental material) represented a repeating unit of the mannan backbone of galactomannan. All oligosaccharides were biotinylated (10) and adsorbed to a streptavidin-coated plate to quantify the immune response.

The glycoarray with Gal*f*(1→5)Gal*f* blocks can be used to trace specific antibodies in sera from ABPA and CPA patients. No antibodies recognizing oligomannosides 14 and 15 were detected in the chronic pulmonary aspergillosis (CPA) or allergic bronchopulmonary aspergillosis (ABPA) patient sera (Fig. 2 and Text S2). Similarly, no antibodies recognizing ligands 1, 4, and 5 containing only one galactofuranose (Gal*f*) unit were detected in sera from controls and patients (Fig. 2). In contrast, the ligands with two Gal*f* units linked through a (1→5) linkage (ligands 2, 8, and 9), but not through a (1→6) linkage (ligand 3), gave antibody titers which were significantly higher in patients with ABPA or CPA than in the controls ($P < 0.0001$) (Fig. 2). Ligand 13 had the highest area under curve (AUC) value for both ABPA and CPA patient sera (Tables S1 to S4). However, the differences with oligosaccharides 6 to 13 were not statistically significant for patient discrimination (Tables S1 to S4). Interestingly, the presence of one to two Gal*f*(1→6)Gal*f* blocks in oligonucleotide-Gal*f* sequences with Gal*f*(1→5)Gal*f* blocks (ligands 7 and 11) did not affect their ability to distinguish between control and patient sera (Tables S1 to S4). The nature of the linkage between the oligonucleotide-Gal*f* chain and mannan (Man) unit [either a β-(1→3) linkage for ligands 9 and 12 or a β-(1→6) linkage for ligands 8 and 10] did not affect the level of antibody recognition (Fig. 2 and Tables S1 to S4).

Early studies with immunocompetent patients with CPA or ABPA have shown that high antibody titers against GM were detected in the sera of these patients (7). Even though the immunodominance of the oligonucleotide-Gal*f* sequences in GM has been repeatedly shown in the past, the chemical nature of the epitope recognized in GM was not precisely identified (1). The use of a set of chemically synthesized oligosaccharides representing different parts of side oligonucleotide-Gal*f* sequences in GM has permitted the identification of the epitope recognized by the anti-*A. fumigatus* antibodies. Interestingly, no antibodies bound to the oligomannosides which are fragments of the repeating units of the mannan backbone of *Aspergillus* cell wall GM. This situation is entirely different from the mannan of *Candida* species. The *Candida* cell wall mannans

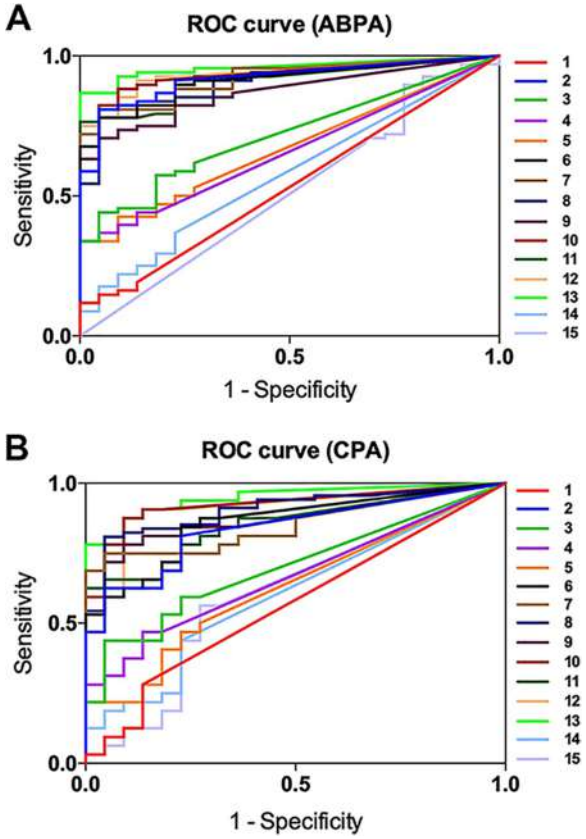

FIG 2 Results of enzyme-linked immunosorbent assay (ELISA) data with different oligosaccharide ligands related to *A. fumigatus* galactomannan and sera of aspergillosis patients. (A and B) The results are expressed as receiver operating characteristic (ROC) curves plotted for ABPA patient sera (A) and CPA patient sera (B) with regard to the control sera. Sensitivity represents the fraction of patient sera ranking as positive (true positive), and specificity represents the fraction of control sera ranking as negative (true negative). See Tables S1 and S2 for the statistical significance of the results.

are well-known antigens recognized in patient sera and have been used in the past for serotyping this species (11). The antibody response against *Candida* mannan is mainly associated with the linear α-(1→2)-linked side chains of the mannan core and the β-(1→2)-mannan oligosaccharides. Accordingly, the linkages between the mannose residues are essential for determining an immune response (11). Similarly, in *A. fumigatus*, the linkages between the galactofuranose residues and the size of the oligosaccharides are important since β-(1→6) linkages are not recognized unless they are intercalated with β-(1→5) linkages. These results showed that the recognition of the GM by the human antibodies is not dependent on a strict three-dimensional structure of the oligonucleotides. In addition, it is interesting to note that a Gal*f* disaccharide is a recognized antigenic epitope, while earlier studies have specified that the best oligosaccharide sequences usually recognized by antibodies have a degree of polymerization of 4 or 5.

Oligosaccharides with Gal*f*(1→5)Gal*f* blocks can be used to understand the secretion of cytokines and chemokines by immune cells. The production of the specific cytokines interleukin 1 beta (IL-1β), IL-1Ra, IL-6, and tumor necrosis factor alpha (TNF-α) and chemokines CCL2, CCL3, CCL4, CCL5, and CXCL1 (known to be associated with aspergillosis [12, 13]) produced by peripheral blood mononuclear cells (PBMCs) in the presence of the oligosaccharides was quantified (Fig. 3 and 4 and Text S3). The findings and conclusions based on the analysis were basically similar for the chemokines and cytokines. Like for the antibody study, the ligands with only one Gal*f* unit (ligands 1 and 3 to 5) and oligomannosides (ligands 14 and 15) did not induce the

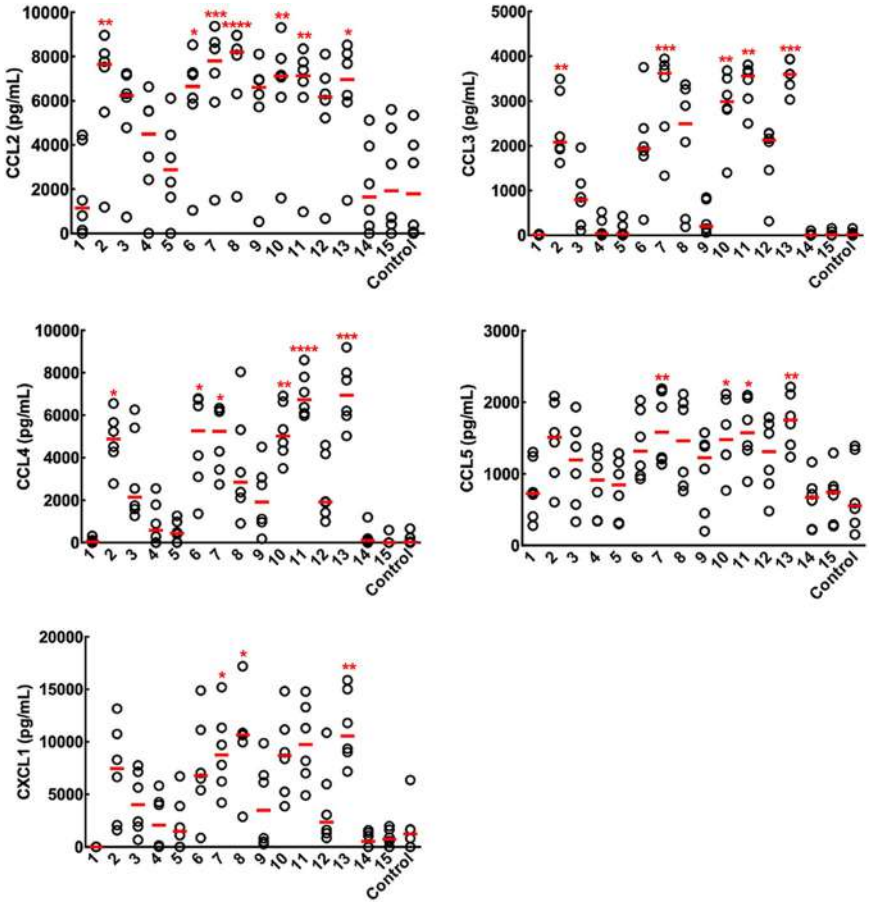

FIG 3 Chemokine induction by the oligosaccharides. The biotinylated oligosaccharides 1 to 15 were coated onto streptavidin microtiter plates, and PBMCs (six donors) were added to the microtiter plates in RPMI medium supplemented with 10% normal human serum. Controls are unstimulated PBMCs on streptavidin or nonstreptavidin microtiter plates. The chemokine concentrations obtained from each donor are plotted as dots, where the center red line indicates the median. The median chemokine concentrations were compared with those of the unstimulated PBMCs (control) by a Kruskal-Wallis test and Dunn's multiple-comparison test (****, $P < 0.0001$; ***, $P < 0.001$; **, $P < 0.01$; *, $P < 0.05$).

production of cytokines and chemokines (Fig. 3). Similar amounts of cytokines and chemokines are produced in the presence of heat-inactivated serum or normal serum, indicating that the production of cytokines and chemokines is independent of the complement (data not shown). The analysis of the response of the trisaccharide and pentasaccharide 8 and 10, respectively, and their isomers, 9 and 12, respectively, showed that the nature of the chemical linkage of the galactofuran to the mannan chain significantly influenced the production of cytokines and chemokines (in contrast to the antibody data); the β-(1→3) linkage between tetra-Gal*f*- and Man was found to be detrimental to the production of cytokines. In contrast, the occurrence of a β-(1→6) linkage inside the galactofuran composed of (1→5) linkages did not influence cytokine and chemokine production (compare ligands 10 and 11). Like for the antibody epitope, galactofuranosides of two units with one β-(1→5) linkage between Gal*f* residues induced the production of cytokines and chemokines, although at a very limited amount, especially for the cytokines. Heptasaccharide 13 significantly induced the highest expression of all the chemokines and cytokines tested (Fig. 4).

The chemokines (CCL3, CCL2, and CCL5) followed in this study have been previously shown to be associated with aspergillosis since they are involved in the recruitment of neutrophils, platelets, and monocytes, but the molecules responsible for the chemokine production have not been identified (12, 13). GM has been previously recognized to induce the production of cytokines, but the conclusions on the pro- or anti-

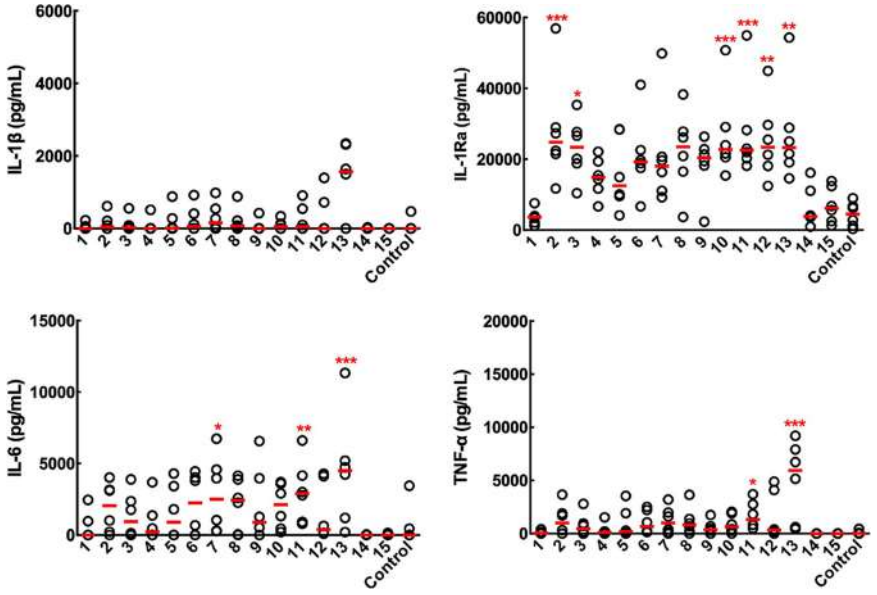

FIG 4 Cytokine induction by the oligosaccharides. The amounts of cytokines in the culture medium were examined by ELISA. The median chemokine concentrations were compared with those of the unstimulated PBMCs (control) by a Kruskal-Wallis test and Dunn's multiple-comparison test (****, $P < 0.0001$; ***, $P < 0.001$; **, $P < 0.01$; *, $P < 0.05$).

inflammatory function of GM have been controversial (14–16). The results indicated that in contrast to antibodies, the production of cytokines and chemokines was facilitated by longer chains of β-(1→5)-linked Gal*f* units. It will be now possible to analyze the presentation of the carbohydrate antigen on the major histocompatibility complexes. Similarly to patient antibodies, the production of cytokine and chemokines from PBMCs was not induced by GM-related oligomannosides. Again, this situation is opposite from the immune response against *Candida* spp. *Candida* mannan induces a strong immune cellular response. However, these studies were mostly based on the use of mannosyltransferase mutants rather than on the use of pure oligosaccharides, and conclusions were indirectly based on the lack of or modified response seen with the mutants rather than on a direct positive response of the cell toward pure oligosaccharides (17). Compensatory reactions resulting from the gene deletion often modify the composition of the cell wall; consequently, the immune response against the mutant may not result from the lack of the target polysaccharides but may be hidden by the modifications of the cell wall resulting from these compensatory reactions (1). Moreover, the discrepancy between immunological studies run with polysaccharides might be due to the insufficient purification of the polysaccharide used, since the precise characterization of the immunostimulatory activities of polysaccharides requires the use of pure polysaccharides (1, 18).

The purity of chemically synthesized oligosaccharides can be easily controlled and will make synthetic oligosaccharides a perfect tool to understand the immune role of carbohydrate moieties. In addition, the biotinylation of the oligosaccharides allows their quantitative immobilization onto streptavidin-coated devices, which can allow amplification of the response between the oligosaccharides and the immune cell surface. Even though many receptors (mannose-binding lectin, mannose receptor, dectin-2, dendritic cell-specific intercellular adhesion molecule-3 grabbing nonintegrin [DC-SIGN], intelectin-1, and even dectin-1) have been claimed to bind to GM (1, 14, 15, 19, 20), the binding has not been demonstrated biochemically. Such chemical tools will be the best use for such a demonstration.

Conclusion. Even though glycoarrays have been developed in the past (21, 22), they have not been focused specifically on fungal polysaccharides. Recent studies demonstrated that glycoarrays cannot be universal and that the carbohydrate molecules

blotted on the array have to be specifically designed for the specific research project considered since not all oligosaccharides present in nature can be deposited on a single array. This study demonstrated that chemically synthesized oligosaccharides specifically designed to represent fragments of the fungal cell wall are appropriate tools to investigate precisely the immune response against this insoluble polysaccharide shell. We have in our hands oligosaccharides from all essential cell wall polysaccharides of *A. fumigatus* cell wall [α- and β-(1→3)-glucans, chitin, galactomannan, and galactosaminogalactan]. These oligosaccharides have now been bound to streptavidin beads to follow their internalization and their recognition at the phagosome level using a strategy previously developed by others to analyze the interactions between β-(1→3)-glucan and dectin-1 at the phagosomal level (23). Such approach will allow a precise definition of the mediators other than immunoglobulins, which can play a role in inducing an immune response against the cell wall components. In addition, such a strategy can also be applied to all cell wall polysaccharides from various human fungal pathogens.

SUPPLEMENTAL MATERIAL

Supplemental material is available online only.

TEXT S1, DOCX file, 0.1 MB.

TEXT S2, DOCX file, 0.1 MB.

TEXT S3, DOCX file, 0.1 MB.

TABLE S1, DOCX file, 0.1 MB.

TABLE S2, DOCX file, 0.1 MB.

TABLE S3, DOCX file, 0.1 MB.

TABLE S4, DOCX file, 0.1 MB.

ACKNOWLEDGMENTS

This work was supported by the Russian Science Foundation (grant 19-73-30017), the Agence Nationale pour la Recherche (grant AfuInf ANR-16-CE92-0039), and la Fondation pour la Recherche Médicale (grant DEQ20150331722 LATGE Equipe FRM 2015) to J.-P.L.

We declare no competing interests.

REFERENCES

1. Latgé JP, Beauvais A, Chamilos G. 2017. The cell wall of the human fungal pathogen *Aspergillus fumigatus*: biosynthesis, organization, immune response, and virulence. Annu Rev Microbiol 71:99–116. https://doi.org/10.1146/annurev-micro-030117-020406.
2. Brown GD, Gordon S. 2001. Immune recognition. A new receptor for beta-glucans. Nature 413:36–37. https://doi.org/10.1038/35092620.
3. Latgé JP, Kobayashi H, Debeaupuis JP, Diaquin M, Sarfati J, Wieruszeski JM, Parra E, Bouchara JP, Fournet B. 1994. Chemical and immunological characterization of the extracellular galactomannan of *Aspergillus fumigatus*. Infect Immun 62:5424–5433.
4. Krylov V, Argunov D, Solovev A, Petruk M, Gerbst A, Dmitrenok A, Shashkov A, Latgé J-P, Nifantiev N. 2018. Synthesis of oligosaccharides related to galactomannans from *Aspergillus fumigatus* and their NMR spectral data. Org Biomol Chem 16:1188–1199. https://doi.org/10.1039/c7ob02734f.
5. Kudoh A, Okawa Y, Shibata N. 2015. Significant structural change in both O- and N-linked carbohydrate moieties of the antigenic galactomannan from *Aspergillus fumigatus* grown under different culture conditions. Glycobiology 25:74–87. https://doi.org/10.1093/glycob/cwu091.
6. Fontaine T, Delangle A, Simenel C, Coddeville B, van Vliet SJ, van Kooyk Y, Bozza S, Moretti S, Schwarz F, Trichot C, Aebi M, Delepierre M, Elbim C, Romani L, Latgé J-P. 2011. Galactosaminogalactan, a new immunosuppressive polysaccharide of *Aspergillus fumigatus*. PLoS Pathog 7:e1002372. https://doi.org/10.1371/journal.ppat.1002372.
7. Sarfati J, Monod M, Recco P, Sulahian A, Pinel C, Candolfi E, Fontaine T, Debeaupuis J-P, Tabouret M, Latgé J-P. 2006. Recombinant antigens as diagnostic markers for aspergillosis. Diagn Microbiol Infect Dis 55:279–291. https://doi.org/10.1016/j.diagmicrobio.2006.02.002.
8. Argunov DA, Krylov VB, Nifantiev NE. 2015. Convergent synthesis of isomeric heterosaccharides related to the fragments of galactomannan from *Aspergillus fumigatus*. Org Biomol Chem 13:3255–3267. https://doi.org/10.1039/c4ob02634a.
9. Argunov DA, Krylov VB, Nifantiev NE. 2016. The use of pyranoside-into-furanoside rearrangement and controlled O(5)→O(6) benzoyl migration as the basis of a synthetic strategy to assemble (1→5)- and (1→6)-linked galactofuranosyl chains. Org Lett 18:5504–5507. https://doi.org/10.1021/acs.orglett.6b02735.
10. Komarova BS, Wong SSW, Orekhova MV, Tsvetkov YE, Krylov VB, Beauvais A, Bouchara JP, Kearney JF, Aimanianda V, Latge JP, Nifantiev NE. 2018. Chemical synthesis and application of biotinylated oligo-alpha-(1→3)-D-glucosides to study the antibody and cytokine response against the cell wall alpha-(1→3)-D-glucan of *Aspergillus fumigatus*. J Org Chem 83:12965–12976. https://doi.org/10.1021/acs.joc.8b01142.
11. Shibata N, Kobayashi H, Suzuki S. 2012. Immunochemistry of pathogenic yeast, *Candida* species, focusing on mannan. Proc Jpn Acad Ser B Phys Biol Sci 88:250–265. https://doi.org/10.2183/pjab.88.250.
12. Phadke AP, Mehrad B. 2005. Cytokines in host defense against *Aspergillus*: recent advances. Med Mycol 43(Suppl 1):S173–S176. https://doi.org/10.1080/13693780500052099.
13. Loeffler J, Ok M, Morton OC, Mezger M, Einsele H. 2010. Genetic polymorphisms in the cytokine and chemokine system: their possible importance in allogeneic stem cell transplantation. Curr Top Microbiol Immunol 341:83–96. https://doi.org/10.1007/82_2010_22.
14. Serrano-Gómez D, Domínguez-Soto A, Ancochea J, Jimenez-Heffernan JA, Leal JA, Corbí AL. 2004. Dendritic cell-specific intercellular adhesion molecule 3-grabbing nonintegrin mediates binding and internalization

of *Aspergillus fumigatus* conidia by dendritic cells and macrophages. J Immunol 173:5635–5643. https://doi.org/10.4049/jimmunol.173.9.5635.
15. Toledano V, Hernández-Jiménez E, Cubillos-Zapata C, Flandez M, Álvarez E, Varela-Serrano A, Cantero R, Valles G, García-Rio F, López-Collazo E. 2015. Galactomannan downregulates the inflammation responses in human macrophages via NFkappaB2/p100. Mediators Inflamm 2015:942517. https://doi.org/10.1155/2015/942517.
16. Chiodo F, Marradi M, Park J, Ram AF, Penades S, van Die I, Tefsen B. 2014. Galactofuranose-coated gold nanoparticles elicit a pro-inflammatory response in human monocyte-derived dendritic cells and are recognized by DC-SIGN. ACS Chem Biol 9:383–389. https://doi.org/10.1021/cb4008265.
17. Hall RA, Gow NA. 2013. Mannosylation in *Candida albicans*: role in cell wall function and immune recognition. Mol Microbiol 90:1147–1161. https://doi.org/10.1111/mmi.12426.
18. Ferreira SS, Passos CP, Madureira P, Vilanova M, Coimbra MA. 2015. Structure-function relationships of immunostimulatory polysaccharides: a review. Carbohydr Polym 132:378–396. https://doi.org/10.1016/j.carbpol.2015.05.079.
19. Garred P, Genster N, Pilely K, Bayarri-Olmos R, Rosbjerg A, Ma YJ, Skjoedt MO. 2016. A journey through the lectin pathway of complement-MBL and beyond. Immunol Rev 274:74–97. https://doi.org/10.1111/imr.12468.
20. Wesener DA, Wangkanont K, McBride R, Song X, Kraft MB, Hodges HL, Zarling LC, Splain RA, Smith DF, Cummings RD, Paulson JC, Forest KT, Kiessling LL. 2015. Recognition of microbial glycans by human intelectin-1. Nat Struct Mol Biol 22:603–610. https://doi.org/10.1038/nsmb.3053.
21. Geissner A, Reinhardt A, Rademacher C, Johannssen T, Monteiro J, Lepenies B, Thépaut M, Fieschi F, Mrázková J, Wimmerova M, Schuhmacher F, Götze S, Grünstein D, Guo X, Hahm HS, Kandasamy J, Leonori D, Martin CE, Sharavathi G, Parameswarappa S, Pasari S, Schlegel MK, Tanaka H, Guozhi X, Yang Y, Pereira CL, Anish C, Seeberger PH. 2019. Microbe-focused glycan array screening platform. Proc Natl Acad Sci U S A 116:1958–1967. https://doi.org/10.1073/pnas.1800853116.
22. Rillahan CD, Paulson JC. 2011. Glycan microarrays for decoding the glycome. Annu Rev Biochem 80:797–823. https://doi.org/10.1146/annurev-biochem-061809-152236.
23. Mansour MK, Tam JM, Khan NS, Seward M, Davids PJ, Puranam S, Sokolovska A, Sykes DB, Dagher Z, Becker C, Tanne A, Reedy JL, Stuart LM, Vyas JM. 2013. Dectin-1 activation controls maturation of β-1,3-glucan-containing phagosomes. J Biol Chem 288:16043–16054. https://doi.org/10.1074/jbc.M113.473223.

frontiers in Immunology

ORIGINAL RESEARCH
published: 13 October 2017
doi: 10.3389/fimmu.2017.01273

Immunobiological Activity of Synthetically Prepared Immunodominant Galactomannosides Structurally Mimicking *Aspergillus* Galactomannan

Ema Paulovičová[1], Lucia Paulovičová[1], Martin Hrubiško[2], Vadim B. Krylov[3], Dmitry A. Argunov[3] and Nikolay E. Nifantiev[3]**

[1] Cell Culture Laboratory, Department of Immunochemistry of Glycoconjugates, Center for Glycomics, Institute of Chemistry, Slovak Academy of Sciences, Bratislava, Slovakia, [2] Department of Clinical Immunology and Allergy, Oncology Institute of St. Elisabeth, Bratislava, Slovakia, [3] Laboratory of Glycoconjugate Chemistry, N.D. Zelinsky Institute of Organic Chemistry, Russian Academy of Sciences, Moscow, Russia

OPEN ACCESS

Edited by:
Uday Kishore, Brunel University London, United Kingdom

Reviewed by:
Lalit Kumar Dubey, University of Lausanne, Switzerland
Taruna Madan, National Institute for Research in Reproductive Health, India

***Correspondence:**
Ema Paulovičová
ema.paulovicova@savba.sk;
Nikolay E. Nifantiev
nen@ioc.ac.ru

Specialty section:
This article was submitted to Molecular Innate Immunity, a section of the journal Frontiers in Immunology

Received: *16 June 2017*
Accepted: *25 September 2017*
Published: *13 October 2017*

Citation:
Paulovičová E, Paulovičová L, Hrubiško M, Krylov VB, Argunov DA and Nifantiev NE (2017) Immunobiological Activity of Synthetically Prepared Immunodominant Galactomannosides Structurally Mimicking Aspergillus Galactomannan. Front. Immunol. 8:1273. doi: 10.3389/fimmu.2017.01273

The study is oriented at the *in vitro* evaluation of the immunobiological activity and efficacy of synthetically prepared isomeric pentasaccharides representing fragments of *Aspergillus fumigatus* cell-wall galactomannan and containing β-(1→5)-linked tetragalactofuranoside chain attached to O-6 (**GM-1**) or O-3 (**GM-2**) of a spacer-armed mannopyranoside residue. These compounds were studied as biotinylated conjugates which both demonstrated immunomodulatory activities on the RAW 264.7 cell line murine macrophages as *in vitro* innate immunity cell model. Immunobiological studies revealed time- and concentration-dependent efficient immunomodulation. The proliferation of RAW 264.7 macrophages was induced at higher concentration (100 μg/mL) of studied glycoconjugates and longer exposure (48 h), with more pronounced efficacy for **GM-1**. The increase of proliferation followed the previous increase of IL-2 production. The cytokine profile of the macrophages treated with the glycoconjugates was predominantly pro-inflammatory Th1 type with significant increase of TNFα, IL-6, and IL-12 release for both glycoconjugates. The RAW 264.7 macrophages production of free radicals was not significantly affected by glycoconjugates stimulation. The phagocytic activity of RAW 264.7 cells was reduced following **GM-1** treatment and was significantly increased after 24 h stimulation with **GM-2**, contrary to 48 h stimulation. Moreover, the synthetically prepared galactomannoside derivatives have been evaluated as efficient serodiagnostic antigens recognized by specific Ig isotypes, and significant presence of specific IgM antibodies in serum of patients suffering from vulvovaginitis was observed.

Keywords: *Aspergillus*, *Candida*, galactomannan, mannan, RAW 264.7, cytokines

INTRODUCTION

Throughout the past decades, the incidence of opportunistic systemic fungal infections has a significant rise due to increased numbers of immunocompromised adult and pediatric individuals. *Candida* species are the most common ubiquitous medically important opportunistic fungi followed by *Aspergillus* species (1–3). Invasive aspergillosis is the second most frequent systemic fungal

infection with increasing incidence over the last 20 years (4). *Aspergillus* spp. principally affect the lungs causing the four main *Aspergillus*-related syndromes: (i) allergic bronchopulmonary aspergillosis, (ii) chronic necrotizing *Aspergillus* pneumonia (also termed chronic necrotizing pulmonary aspergillosis), (iii) aspergilloma, and (iv) invasive aspergillosis. Hematogenous dissemination of *Aspergillus* beyond the lungs has been documented in patients who are severely immunocompromised (5). Within an 1 year period (from 2016 until present), the 1.47-fold increase in *Aspergillus* spp. in clinical isolates from upper airways and 1.8-fold increase in *Aspergillus* spp. clinical isolates from the lower respiratory tract have been documented. Moreover, the cutaneous aspergilli isolates increased 2.15 times within this period (raw data were obtained and analyzed with permission of MEDIREX Inc., HPL Mycology Labs., Slovakia).

Invasive aspergillosis has become the major cause of morbidity and mortality in immunocompromised patients with mortality rates as high as 90%. Almost 61% of patients with invasive aspergillosis have an underlying hematologic disease or have undergone bone marrow transplantation (6). Risk factors for the development of invasive aspergillosis include prolonged or repeated episodes of severe neutropenia, transplantation of solid organs or receipt of an allogenic stem cell transplant, grade III or IV graft-vs.-host disease, prolonged use of corticosteroid therapy, treatment with T-cell immunosuppressants, and inherited severe immunodeficiency (7–12). Etiological agent of more than 90% of invasive mycoses caused by *Aspergilli* is an *Aspergillus fumigatus* (*A. fumigatus*) (13). The treatment of invasive fungal infections failed in nearly 50% cases of invasive aspergillosis (14). Furthermore, resistant *Aspergillus* infections are frequently encountered in the antifungal drug-naïve patient as a result of increasing incidence of environmental *A. fumigatus* isolates harboring azole resistance mechanisms. *In vivo* selection of acquired resistance during medical treatment is increasingly more accounted in the patients with chronic forms of aspergillosis on the long-term azole treatment (15).

The anti-*Aspergillus* host immune defense is mediated by a complex of responses of the innate immune system phagocytic cells, resident alveolar macrophages, which ingest and kill *Aspergillus* conidia. Next, polymorphonuclear leukocytes destroy germinating *Aspergillus* hyphae, which escaped from macrophages. Neutrophils participate in the adaptive T helper cell response that in turn modulates antifungal activity, enhancing the phagocyte effector cell function (16). There are intensive efforts to design the effective model of subcellular fungal vaccines for either active or passive immunization in humans based on the dominant fungal cell-wall derived moieties (17–21).

In the vaccine model, different preparations of *A. fumigatus* antigens accelerated expansion of various CD4 T-cell subsets (22). The vaccinating potential of different *Aspergillus* antigens against invasive pulmonary aspergillosis, using antigen with the immunoadjuvant murine CpG oligodeoxynucleotide (CpG/Ag model) and dendritic cells model has been also studied (22).

Generally, the *A. fumigatus* cell wall is composed of a fibrillar skeleton made of β-(1→3)-glucan chains with 3,6-branches bound to chitin, galactomannan, and β-(1→3)/(1→4)-glucan, embedded in an amorphous alkali-soluble cement mainly composed of α-(1→3)-glucan and galactose polymers: galactomannan and galactosaminogalactan (23, 24).

Galactomannan is a hetero-polysaccharide composed of a mannan core and galactofuransyl side-chain found in the cell wall primarily of mold-like fungi especially in *Aspergillus* spp. and *Penicillium* spp. but is also found in other species of fungi. The backbone chain of *Aspergillus* galactomannan comprises the (1→2)/(1→6)-linked α-D-mannopyranosyl residues substituted at O-3 or O-6 by oligo-β-D-galactofuranosyl-containing side-chains connected mainly *via* (1→5)-links. Such β-D-Gal*f*-bearing chains are regarded as immunodominant epitopes, especially when they are (1→5)-linked (25, 26). The immunodominant epitopes are located in tetra- and hexasaccharides containing β-D-Gal*f*-(1→5)-β-Gal terminal groups (27). Kudoh et al. reported the presence of β-1,6-linked Gal*f* residues in addition to the β-1,5-linked Gal*f* residues in the O-linked and N-linked carbohydrate moieties of the galactomannan from *A. fumigatus* (28). As concerned content, the differences between conidia and hyphae alkali-soluble and insoluble fractions thereof have been reported. The exposition of galactomannan in an alkali-insoluble fraction of conidia has been higher, i.e., 26 vs. 5% present in hyphae (29).

Herewith, we report for the first time a comparative study of the immunobiological activity and immunomodulating efficacy of synthetically prepared pentasaccharide derivatives **GM-1** and **GM-2** (**Figure 1**), whose structure mimics the corresponding fragments of *A. fumigatus* galactomannan bearing β-(1→5)-linked tetragalactofuranoside chain attached to O-3 or O-6 of the mannopyranoside residue. This study is focused on the assessment of proliferative activities, stimulated release of Th1and Th17 interleukins and growth factors, phagocytosis, free radicals release, expression of CD11b and F4/80 following RAW 264.7 macrophages GM-1 and GM-2 exposure. The evaluation of synthetically prepared oligosaccharide conjugates structurally related to *A. fumigatus* galactomannan as serodiagnostic immunogens for *in vitro* diagnostics of mycosis has been studied.

MATERIALS AND METHODS

Synthesis of Biotinylated Glycoconjugates GM-1 and GM-2

Glycoconjugates **GM-1** and **GM-2** were prepared by the biotinylation of parent ligands (30–32) according to the previously described (33) biotinylation protocol.

Cell Culture and Exposition

Stock solution and individual glycoconjugate doses were prepared aseptically using pre-sterilized disposable plasticwares and apyrogenic, sterile aqua pro injectione (Fresenius, Kabi Italia S.r.l., Verona). The solutions were filtered using a syringe with a 0.2-μm filter (Q-Max®Syringe filter) under sterile laminar flow conditions (Biohazard II, Esco). The safety cabinet was wiped down with 70% ethanol p.a. and sterilized with a germicidal UV lamp for 30 min before each experiment. The

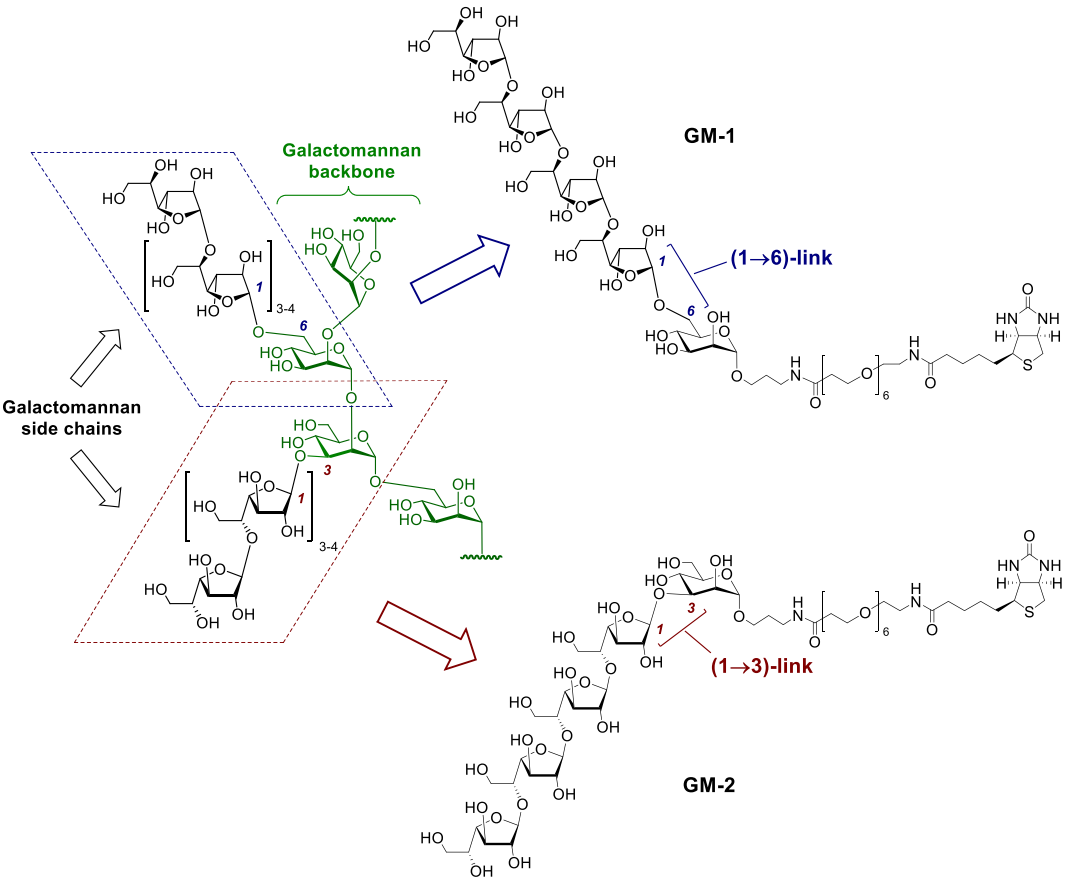

FIGURE 1 | Hypothetical structure of the galactomannan secreted by *A. fumigatus* (**GM-native**) (25) and synthetic biotinylated probes **GM-1** and **GM-2** representing its (1→6)- and (1→3)-linked epitopes.

stock solution has been assayed with an EndoLISA® enzyme-linked immunosorbent assay (ELISA)-based Endotoxin Detection Assay (Hyglos) and measured with a Cytation 5 Imager Multi-Mode Reader (BioTek, USA) to ascertain endotoxin-free conditions.

Cell line murine macrophages RAW 264.7 (ATCC®TIB-71™, ATCC, UK) were cultured in complete Dulbecco's Modified Eagle Medium for 24 h at 37°C in a 5% CO_2 atmosphere and 90–100% relative humidity until approx 80% confluency. Cell viability was assayed with the Trypan blue dye exclusion method using a TC20™ automated cell counter (Bio-Rad Laboratories, Inc., USA). The starting inocula of 1×10^5 cells/mL/well (93.6% viable cells) were seeded in a 24-well cell culture plate (Sigma-Aldrich, USA) and exposed to 10 and 100 µg per well of **GM-1** and **GM-2** conjugates, respectively, to include two different concentrations with diverse stimulatory capabilities. Concanavalin A (Con A, 10 µg/mL, Sigma-Aldrich, St Louis, MO, USA), phytohemagglutinin (PHA, 10 µg/mL, Sigma-Aldrich, St Louis, MO, USA) and pokeweed mitogen (1 µg/mL, Sigma-Aldrich, St Louis, MO, USA) were used as positive controls.

In vitro exposition was performed for 3, 24, and 48 h, respectively. Morphological characteristics and viability were controlled ahead of flowcytometric evaluation. The exposed cells were subjected to immunocytometric determination of phagocytic activity and phenotyping immediately following cell separation by centrifugation. The cell culture media were stored at −20°C until further use.

Proliferation and Cytotoxicity

The impact of **GM-1** and **GM-2** conjugates on RAW 264.7 cells' proliferation and glycoconjugates' potential cytotoxicity was evaluated by the bioluminescent measurement of adenosine triphosphate (ATP), marker of metabolically active cells levels, using the ViaLight™ plus kit (Lonza, USA) according to the manufacturer's instructions. The intensity of emitted light was measured with a Cytation 5 Cell Imaging Multi-Mode Reader (BioTek Instruments, Inc., USA). Light emission expressed as relative light units was recorded continuously for 1 s and evaluated on the basis of peak values. The proliferation of unstimulated cells was considered to be the baseline. The proliferation index was calculated by the ratio between the induced proliferation (stimulated cells) and the baseline (unstimulated cells) proliferation. Hence, the proliferation index of negative control, i.e., unstimulated cells, is equal to one.

Determination of Interleukins and Growth Factors

The levels of interleukins and growth factors in cell culture supernates mediated by the exposure with glycoconjugates **GM-1** and **GM-2**, respectively, were assayed with Quantikine ELISA® Mouse M-CSF [Cat#MMC00, R&D, USA, minimum detectable dose (MDD) <5 pg/mL], Platinum ELISAs®: Mouse IL-12 (p70) (Cat#BMS616, MDD 4 pg/mL), Mouse GM-CSF (Cat#BMS612, MDD 2 pg/mL), Mouse IL-17(Cat#BMS6001, MDD 1.6 pg/mL), Mouse IL-2(Cat#BMS601, MDD 5.3 pg/mL), and Mouse IL-6 (Cat#BMS603/2, MDD 6.5 pg/mL); Instant ELISAs®: Mouse IL-1β (Cat#BMS600/2INST, MDD 3 pg/mL), Mouse tumor necrosis factor (TNF)-α (Cat#BMS607/2INST, MDD 4 pg/mL), Mouse IL-10 (Cat#BMS614INST, MDD 5.28 pg/mL), all from Affymetrix e-Bioscience, USA, according to the instructions of the manufacturer.

Determination of Free Radicals

The cell culture supernates obtained after the treatment of RAW 264.7 cells by glycoconjugates **GM-1** and **GM-2** were assayed for total content of free radicals (Free radicals kit; SediumR&D, Czech Republic). The assay is based on the ability of chlorophyllin to transfer electrons due to its electron-rich double-bonds structure. The free radicals media levels were assayed *via* calibration based on a Fe^{2+}/Fe^{3+} reactive shift and were expressed as millimoles Fe^{2+}/L. The unstimulated cells free radical production was used to determine the baseline value.

Immunocytometry

The **GM-1** and **GM-2** conjugates' exposed RAW 264.7 cells were subjected to immunoflow cytometry using a Beckman Coulter FC 500 flow cytometer equipped with a 488-nm argon laser and a 637 nm HeNe collinear laser and controlled by the CXP software (Beckman Coulter, Fullerton, CA, USA). Gates were set to exclude the debris and damaged cells using forward scatter vs. side scatter dot plot discrimination. The settings were optimized either using proper isotype control (in immunophenotyping assay) or *Candida albicans* fluorescein isothiocyanate (FITC)-untreated cell culture (in phagocytosis). For each sample fluorescence histograms of 10,000 cells (immunophenotyping) or 5,000 cells (phagocytosis) were generated and analyzed (green fluorescence, 525-nm band-pass filter, FL1 channel). All samples were analyzed in duplicates. The data are expressed as percentage or as a mean of fluorescence intensity.

For immunocytometric assays, **GM-1** and **GM-2** conjugates exposed RAW 264.7 cells were stained directly with FITC-conjugated rat anti-mouse monoclonal antibodies: F4/80 and CD11b (both from eBioscience, Inc., CA, USA). The appropriate antibody isotype-negative controls were used separately to achieve correct gating. The FITC-conjugated monoclonal antibodies (5 μL) and **GM-1** and **GM-2** conjugates treated RAW 264.7 cells (50 μL) were added to 5-mL sterile tubes (Beckman Coulter, Fullerton, CA, USA) and incubated for 30 min in the dark at 4°C. After this, the samples were evaluated by immunoflowcytometry.

Phagocytosis

Measurement of phagocytosis, i.e., the ingestion of labeled *Candida albicans* (*C. albicans*) cells, took place under controlled conditions, using incubation with (FITC)-labeled *C. albicans* for 30 min at 37°C. Following treatment, the reaction was stopped by placing the samples on ice. Based on the difference between the resulting total amount of phagocyting cells and the amount of phagocyting cells following fluorescence quenching using Trypan Blue, the amounts of adherent extracellular and ingested intracellular *Candida* cells were determined.

Fluorescence Quenching Cytofluorometric Assay

The extracellular FITC-fluorescence has been quenched by 0.4% trypan blue dye (Sigma-Aldrich, USA). Immunocytometric analysis of trypan blue treated RAW 264.7 cells was performed following 30-min cell incubation in dark. Differentiation between attached and ingested *C. albicans*–FITC labeled cells was performed using the same protocol as previously described.

Study Population

The serological assays were performed in a patient cohort comprising forty female participans (38.2 ± 8.4 years) with atopy and a history of recurrent vaginal mycosis (Dept. Clin. Immunol. and Allergy). Inhalant allergy was present in 63% of patients. The exclusion criteria were recent or ongoing antibiotic or immunosuppressive therapy. *Candida* spp., *Aspergillus* spp., and *Saccharomyces* spp. isolated from vaginal (94.42%) or cervical (5.58%) swabs undergone typing and identification (MEDIREX Inc., HPL Mycology Labs., Slovakia). Alyostal® Stallergenes Skin prick test (SPT), including *C. albicans* allergen (Alyostal R Stallergenes), was performed on the patients' forearm according to the international and national guidelines. SPT was evaluated after 15–20 min and rated as positive if the wheal diameter was ≥3 mm and the negative control was negative.

Control Group

Sixty-five female blood donors (National Blood Service, Slovak Republic) aged 18–56 years (average 35.9 ± 18.6) were enrolled as healthy control subjects.

Sera Samples

All sera samples have been taken before the onset of antifungal and/or immunomodulative therapy, respectively. The sera samples for the determination of anti-oligogalactomannan and anti-mannan antibodies were collected and immediately stored at −70°C until the further use. The specimens were analyzed retrospectively and the results had no influence on therapeutic decisions.

Determination of Anti-GM-1 and -GM-2 IgG, IgA, and IgM Isotypes

The ELISA for the determination of IgG, IgA, and IgM sera antibodies specific to studied galactomannosides has been developed by the modification of ELISA anti-*Candida* II based on *C. albicans* cell glycan antigens (Biogema, Slovakia). Synthetically prepared biotinylated oligogalactomannans (in 0.2 M TRIS-HCl

buffer pH 7.0) were applied onto streptavidin coated microplates (Bioamat, SNC, Italy) (2 μg/mL, 200 μL/well) for 24 h at room temperature. After that, the plates were overcoated with 0.05 M carbonate–bicarbonate buffer (pH 9.5) with 0.025% Tween 20 and washed out. The plates were blocked with 1% BSA in 0.05 M carbonate–bicarbonate buffer. Sera samples have been examined for the **GM-1**- and **GM-2**-specific IgG, IgA, and IgM antibodies with peroxidase-labeled anti-human IgA, IgG, and IgM antibodies (KPL, USA). The plates were developed with 3,3′,5,5′-tetramethylbenzidine chromogenic substrate (Kem-En-Tec Diagnostics) and scanned at 450/630 nm (Microplate reader MRXII, Dynex, USA). According to the absence of appropriate international standards, the concentrations of different Ig isotypic antibodies were evaluated based on the calibration curve using internal standard, i.e., positive sera pool with an established value of 100 arbitrary units (U). The cut-off values were calculated according to blood donors' IgG/IgM/IgA anti-**GM-1** and **GM-2** sera values (average + 3 SD). The patients' results were expressed as calculated mean ± SEMs of two independent measurements. Anti-mannan IgG, IgA, and IgM antibodies were assayed as previously described (34).

Ethics

The research protocol and the study have been approved by the Local Ethical Committee of the Oncology Institute of St. Elisabeth, Bratislava, Slovakia (15.12.2010). Written informed consent to participate in the experimental research study and for blood collection and subsequent laboratory examinations, in accordance with the principles in the Helsinki Declaration, was obtained from each patient prior to study enrollment. All patients were recruited from the outpatient department of the Department of Clinical Immunology and Allergy. Patient's age, disease process, drug history, family history, and clinical signs and symptoms were documented at the first visit of Clinical Immunology and Allergy ambulance as a standard procedure.

Statistical Analysis

The results of *in vitro* experiments with patient sera and RAW 264.7 cells were evaluated as mean values ± SD. Normality of data distribution was evaluated according to Shapiro–Wilk's test at the 0.05 level of significance. Statistical comparison was performed using one-way ANOVA and *post hoc* Bonferroni's tests. The results were significant if the differences equaled or exceeded the 95% confidence level ($P < 0.05$). Statistics was performed using the ORIGIN 7.5 PRO software (OriginLab Corporation, Northampton, MA, USA). Pearson's correlation coefficient was used to compare the strength of the relationship between immunobiological variables.

RESULTS

GM-1 and GM-2 Glycoconjugates Possess the Capability to Increase the Proliferation of Murine Macrophages RAW 264.7

The effect of pentasaccharide-biotin conjugates **GM-1** and **GM-2** on the macrophage cell line RAW 264.7 proliferation was monitored by ATP bioluminescence as a marker of cell viability using the ViaLight™ plus kit. As shown in **Figure 2**, shorter stimulation periods (3 and 24 h) of RAW 264.7 cells did not alter the proliferation of macrophages. The 48-h stimulation resulted in a dose-dependent increase in RAW 264.7 proliferation for both tested biotinylated pentasaccharides. Thus, the stimulation with higher concentration of glycoconjugates (100 μg/mL) induced significantly more pronounced increase of RAW 264.7 proliferation (**GM-1:** 2.97-fold, and **GM-2:** 2.31-fold) compared

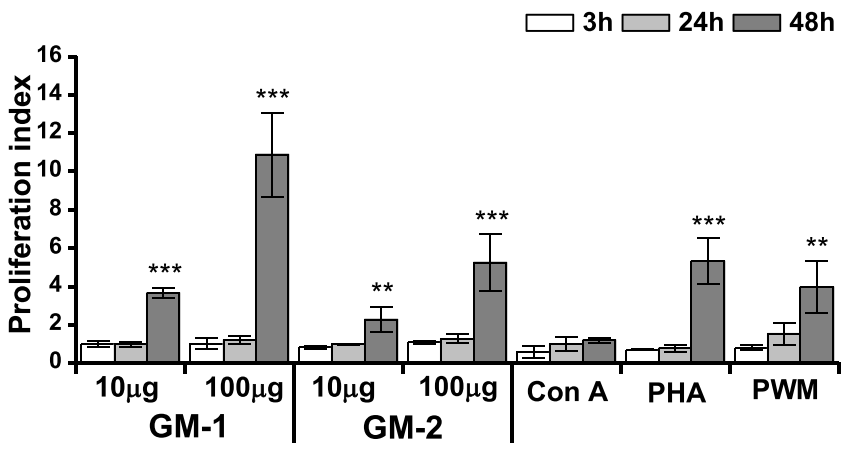

FIGURE 2 | Effect of glycoconjugates GM-1 and GM-2 on proliferation of RAW264.7 macrophages. Cell proliferation was determined by ViaLight™ plus kit. RAW264.7 cells were treated with glycoconjugates **GM-1** or **GM-2** at concentrations of 10 and 100 μg/mL and with concanavalin A (Con A, 10 μg/mL), phytohemagglutinin (PHA, 10 μg/mL) and pokeweed mitogen (PWM, 1 μg/mL) as positive controls for 3, 24, and 48 h. Each value presents the mean ± SD of proliferation index (ratio of average relative light units (RLU) in the presence of stimulant to average relative light units obtained without stimulation). According to calculation formula of proliferation index, the proliferation index of negative control-untreated cells is equal to one. The statistical significance of differences between stimulated cells and untreated cells using one-way ANOVA and *post hoc* Bonferroni's tests is expressed: **—$0.001 < P < 0.01$, ***—$P < 0.001$.

to the 10 μg/mL concentration with even higher efficacy for glycoconjugate **GM-1** than **GM-2**.

Cytokine and Free Radical Responses of RAW 264.7 Macrophages *In Vitro* to GM-1 and GM-2 Glycoconjugates

Generally, macrophages are tissue-resident professional phagocytes and antigen-presenting cells which differentiate from circulating peripheral blood monocytes. The diversity and plasticity is typical for the cells of the monocyte-macrophage lineage. The initial cross-talk and interaction of macrophages with specific cytokines following antigenic trigger determines their functional phenotype, thus influencing their engagement in processes of the antigen-presentation, phagocytosis, and regulatory functions. Microenvironment in which macrophages are situated provides diverse signals that could influenced the cell proliferation and differentiation, secretion of free radicals and is able to divergently bias the macrophage's phenotype toward highly microbicidal or immunosuppressive macrophages.

The *in vitro* effect of glycoconjugates **GM-1** and **GM-2** on RAW 264.7 macrophages cytokines production was analyzed by the determination of pro-inflammatory cytokines TNFα, IL-1β, IL-6, IL-17, IL-12, IL-2, anti-inflammatory cytokine IL-10 and hemopoietic growth factors M-CSF, GM-CSF in supernatants obtained from cultures of RAW264.7 macrophages after the 24 or 48 h treatment (**Figure 3**). Stimulation of RAW 264.7 cells with glycoconjugate **GM-1** for 24 h resulted in a significant increase of TNFα (1.8-fold), IL-17 (1.8-fold), and GM-CSF (1.4-fold) production using a concentration of 10 μg/mL. Higher **GM-1** conjugate concentration (100 μg/mL) induced a more intense statistically significant increase of TNFα (2.9-fold), IL-17 (3.1-fold), and GM-CSF (1.8-fold) production and in addition increase of IL-6 (2.5-fold), IL-12 (1.9-fold), and IL-2 (2.1-fold), production during the 24-h treatment. Stimulation of RAW 264.7 cells with glycoconjugate **GM-1** for 48 h increased the M-CSF (1.9-fold) and IL-12 (1.9-fold) production by using concentration 10 μg/mL. The higher **GM-1** concentration (100 μg/mL) during 48-h stimulation induced a statistically significantly higher production, compared to the control, of mainly all analyzed cytokines except for pro-inflammatory cytokine TNFα (0.7-fold lower than control).

After the 24-h treatment at higher **GM-1** concentration (100 μg/mL) the production of pro-inflammatory cytokines TNFα, IL-6, IL-17, IL-12, IL-2, and hemopoietic growth factor GM-CSF were more efficiently induced compared to the lower **GM-1** concentration (10 μg/mL). The 48-h simulation period of RAW 264.7 cells determined the 100 μg/mL concentration of glycoconjugate **GM-1** as a preferable inducer of IL-6, IL-17, IL-12, IL-2, and both hemopoietic growth factors (M-CSF and GM-CSF) production (**Figure 3**). The stimulation of RAW 264.7 cells with glycoconjugate **GM-1** did not significantly influence the IL-1β and IL-10 production (**Figure 3**).

The 24-h stimulation period of RAW 264.7 cells with 10 μg/mL concentration of glycoconjugate **GM-2**, likewise GM-1 conjugate, significantly increased the production of pro-inflammatory cytokines TNFα (2.8-fold), and IL-17 (1.6-fold), but without effect on GM-CSF production. The higher **GM-2** concentration (100 μg/mL) possess similarly as GM-1 higher ability of cytokines induction and evoked an increase in the production of mainly all cytokines, with the highest effect on TNFα (6.3-fold), IL-6 (17.4-fold), IL-17 (9.3-fold), IL-12 (12.5-fold), and IL-2 (3.6-fold) production. After the longer 48-h stimulation period, the 10 μg/mL concentration of glycoconjugate **GM-2** increased the production of IL-6 (1.4-fold), M-CSF (1.4-fold), IL-17 (1.3-fold), and IL-12 (1.9-fold). Contrary to (1→6)-linked glycoconjugate **GM-1**, the 48-h stimulation of RAW 264.7 cells with (1→3)-linked isomer **GM-2** at 100 μg/mL concentration did not significantly increase the production of GM-CSF and IL-2, and induced a statistically significant increase of IL-6 (7.7-fold), M-CSF (1.4-fold), IL-17 (1.8-fold), and IL-12 (13.9-fold) production. Similarly as with glycoconjugate **GM-1**, the stimulation of RAW 264.7 cells with **GM-2** did not significantly influence the IL-1β and IL-10 production (**Figure 3**).

At higher concentration of 100 μg/mL, glycoconjugate **GM-2** more efficiently induced an increase in analyzed cytokines for both monitored time periods (24 and 48 h). The 10 μg/mL concentration of glycoconjugate **GM-2** evoked a time-dependent increase in cytokines production, favoring 48-h stimulation period. The 100 μg/mL concentration of **GM-2** more efficiently induced the production of cytokines during the 24-h stimulation time period (**Figure 3**).

Cell culture media following 24- and 48-h RAW 264.7 exposure with glycoconjugates **GM-1** and **GM-2** were assayed for free radicals release. The resulting values were compared with control (untreated cells) and with ConA or PHA treated cells (**Figure 4**).

Evidently, free radicals had been triggered only with a 100 μg/mL concentration of glycoconjugate **GM-1** following 24-h exposure; media release has been higher by 7% compared to untreated control. The concentration-dependent increasing trend has been observed for **GM-1** conjugate: 100 μg/mL concentration induces 10 and 4% increases in free radicals media levels following 24 and 48 h over the 10 μg/mL concentration induction, although the induced free radicals production did not significantly exceed the basal free radicals production of untreated RAW 264.7 cells. This tendency was not manifested with glycoconjugate **GM-2**. The overall inductive free radicals release caused by glycoconjugates **GM-1** and **GM-2** was apparently lower in comparison with ConA induction, except for 24-h treatment with glycoconjugate **GM-1** (100 μg/mL) resulting in 4% increase over the ConA induced level, and significantly lower than PHA induction of free radicals release (**Figure 4**).

GM-1 and GM-2 Glycoconjugates Effect on the Phagocytic Activity of RAW264.7 Cells

The influence of glycoconjugates **GM-1** and **GM-2** on RAW 264.7 functionality has been evaluated on the basis of phagocytic capability. The phagocytic activity of exposed RAW264.7 cells and ingestion of *C. albicans*–FITC complex have been determined following 24- and 48-h exposure, respectively, with 10 and 100 μg/mL of both pentasaccharides **GM-1** and **GM-2**.

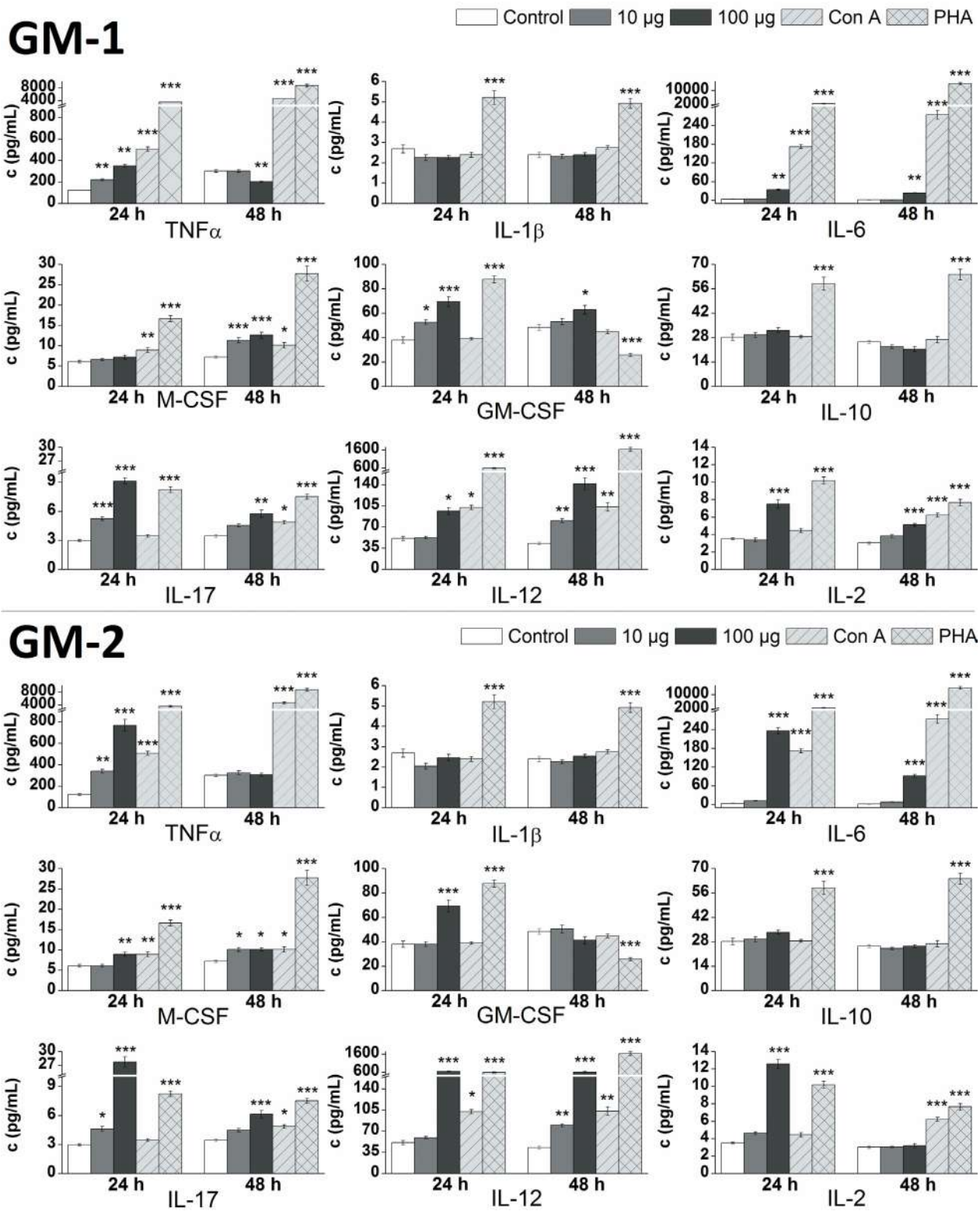

FIGURE 3 | Effect of glycoconjugates GM-1 and GM-2 on RAW 264.7 macrophages cytokines production. Concentrations of cytokines in media after 24- or 48-h stimulation of RAW 264.7 macrophages in response to stimulation with 10 or 100 μg/mL concentration of glycoconjugates **GM-1** or **GM-2**, to positive controls concanavalin A (Con A, 10 μg/mL) and phytohemagglutinin (PHA, 10 μg/mL). Negative control represents untreated RAW 264.7 cells (Control). All data are presented as Mean ± SD. Tests were carried out in triplicate. The statistical significance of differences between stimulated cells and untreated cells using one-way ANOVA and *post hoc* Bonferroni's tests is expressed: ***—$P < 0.001$, **—$0.001 < P < 0.01$, *—$0.01 < P < 0.05$.

To discriminate internalized FITC-labeled *Candida* cells from those attached to the cell membrane trypan blue, the quenching method has been applied as the cells attached to the cell membrane can be quenched (**Table 1**).

The immunocytometric assay of RAW 264.7 cells exposed to glycoconjugates **GM-1** and **GM-2** revealed the influence on effective phagocytosis of *C. albicans*–FITC complex. Evidently, both oligosaccharides exerted rather different effects especially on the process of cellular ingestion and internalization (**Table 1**). The amount of internalized *C. albicans*–FITC cells following the 48-h exposure of glycoconjugates **GM-1** at a concentration of 10 μg/mL resulted in a 16.1-fold decrease ($P < 0.001$) and following exposure with a concentration of 100 μg/mL the similar 17.2-fold decrease ($P < 0.001$) vs. untreated control has been determined. Compared to the results reached with glycoconjugate **GM-2**, the 17.4-fold decrease (at 10 μg/mL) and 16.6-fold (at 100 μg/mL) decrease have been detected after 48-h exposure. RAW 264.7 cells exposure to glycoconjugate **GM-2** did not regulate the ability of macrophage cells to phagocyte the *C. albicans*–FITC complex, and correlation analysis vs. control reveled $r = 0.938$ (10 μg/mL concentration) and $r = 0.981$ (100 μg/mL).

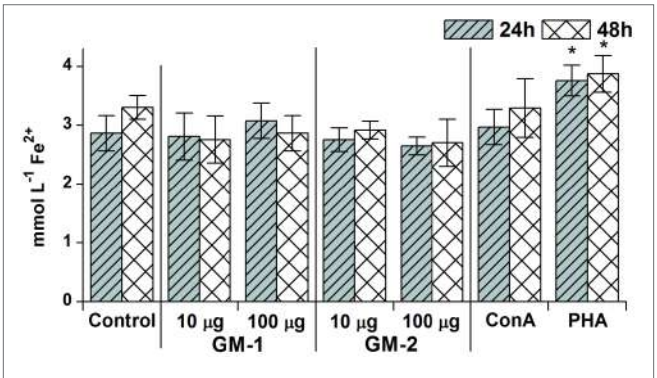

FIGURE 4 | Concentration- and time-dependent pattern of free radicals' release. The release after 24 or 48 h stimulation of RAW264.7 macrophages in response to stimulation with 10 or 100 μg/mL concentration of glycoconjugates **GM-1** or **GM-2** and to concanavalin A (Con A, 10 μg/mL) and phytohemagglutinin (PHA, 10 μg/mL) as a positive controls; control represents untreated cells (Control). All data are presented as mean ± SD. Tests were carried out in triplicate. The statistical significance of differences between stimulated cells and untreated cells using one-way ANOVA and *post hoc* Bonferroni's tests is expressed: *—$0.01 < P < 0.05$.

The Influence of Conjugates GM-1 and GM-2 on RAW264.7 Macrophages Cell Surface Antigens F4/80 and CD11b Expression

To establish the influence of conjugates **GM-1** and **GM-2** 24- and 48-h exposure on RAW264.7 macrophage cell-line, the macrophages major cell surface antigens F4/80 and CD11b (Mac-1 α; integrin αM chain part of the CD11b/CD18 heterodimer) expression has been followed (**Figure 5**). The treatment of RAW264.7 macrophage cells with glycoconjugates **GM-1** or **GM-2** at 10 or 100 μg/mL concentrations resulted in almost unchanged (24-h treatment) or a statistically insignificantly decreased (48-h treatment) CD11b expression, compared to non-treated control cells, except for significant decrease after 48-h treatment with glycoconjugate **GM-2** at 10 μg/mL concentration (33% decrease vs. control, $P < 0.05$). Comparing the individual conjugates in the context of the behavior of exposed RAW264.7 cells an increasing tendency of both surface antigens has been observed in the concentration- and time-dependent manner following the treatment with compounds **GM-1** or **GM-2** (**Figure 5**). The overall increase vs. control, i.e., untreated cells, has not been observed.

The kinetics of membrane protein F4/80 expression exerts the same trend; the expression of F4/80 is time- and concentration-dependent (**Figure 5**). The 24- and 48-h stimulation period of RAW 264.7 with 100 μg/mL concentration of glycoconjugate **GM-2** significantly increased the F4/80 expression over the expression triggered with 10 μg/mL (1.52-fold increase, $P < 0.05$). The decreasing trend of kinetics of F4/80 and CD11b following exposure with both structures, compared to control, i.e., untreated cells, has been more evident for isomer **GM-1** vs. control (2.96-fold for 10 μg/mL and 24 h, 2.2-fold for 100 μg/mL and 24 h vs. 1.39-fold and 1.17-fold for **GM-2** conjugate at the same time and concentration conditions).

The correlation between the time- and concentration-dependent CD11b and F4/80 expression on RAW264.7 macrophage cells following the exposure to (1→6)-linked isomer **GM-1** was $r = 0.96$

TABLE 1 | RAW264.7 macrophage phagocytosis of *C. albicans*–FITC (%) following 24- and 48-h cell treatment with glycoconjugates GM-1 and GM-2 analyzed by flow cytometry.

Sample	Dose, μg/mL	Cell bound and internalized *C. albicans*–FITC		Internalized *C. albicans*–FITC		Membrane attached *C. albicans*–FITC	
		24 h	48 h	24 h	48 h	24 h	48 h
Control		39.3 ± 3.2	56.7 ± 4.2	12.1 ± 1.2	25.8 ± 2.1	27.2 ± 2.5	30.9 ± 1.8
GM-1	10	24.4 ± 2.3	27.4 ± 2.1**	4.8 ± 1.2**	1.6 ± 0.2***	19.6 ± 0.5*	25.8 ± 1.6
	100	21.7 ± 1.9	28.9 ± 1.7**	2.1 ± 0.9**	1.5 ± 0.3***	18.9 ± 0.9*	27.4 ± 0.9
GM-2	10	51.3 ± 3.4**	63 ± 2.9	7.7 ± 0.8	27.8 ± 2.5	43.6 ± 2.2**	35.2 ± 1.7
	100	46.4 ± 2.8*	56.7 ± 3.7	15.7 ± 1.8	24.9 ± 1.8	30.7 ± 1.9	31.8 ± 1.5

*Control represents untreated cells (Control). The amount of membrane attached C. albicans–FITC is expressed as a difference between the population of cell membrane attached and cell internalized C. albicans–FITC and Trypan blue unquenched population, i.e., internalized cells. All data are presented as Mean ± SD. Tests were carried out in triplicate. The statistical significance of differences between untreated cells and stimulated cells using one-way ANOVA and post hoc Bonferroni's tests is expressed as: ***—$P < 0.001$, **—$0.001 < P < 0.01$, *—$0.01 < P < 0.05$.*

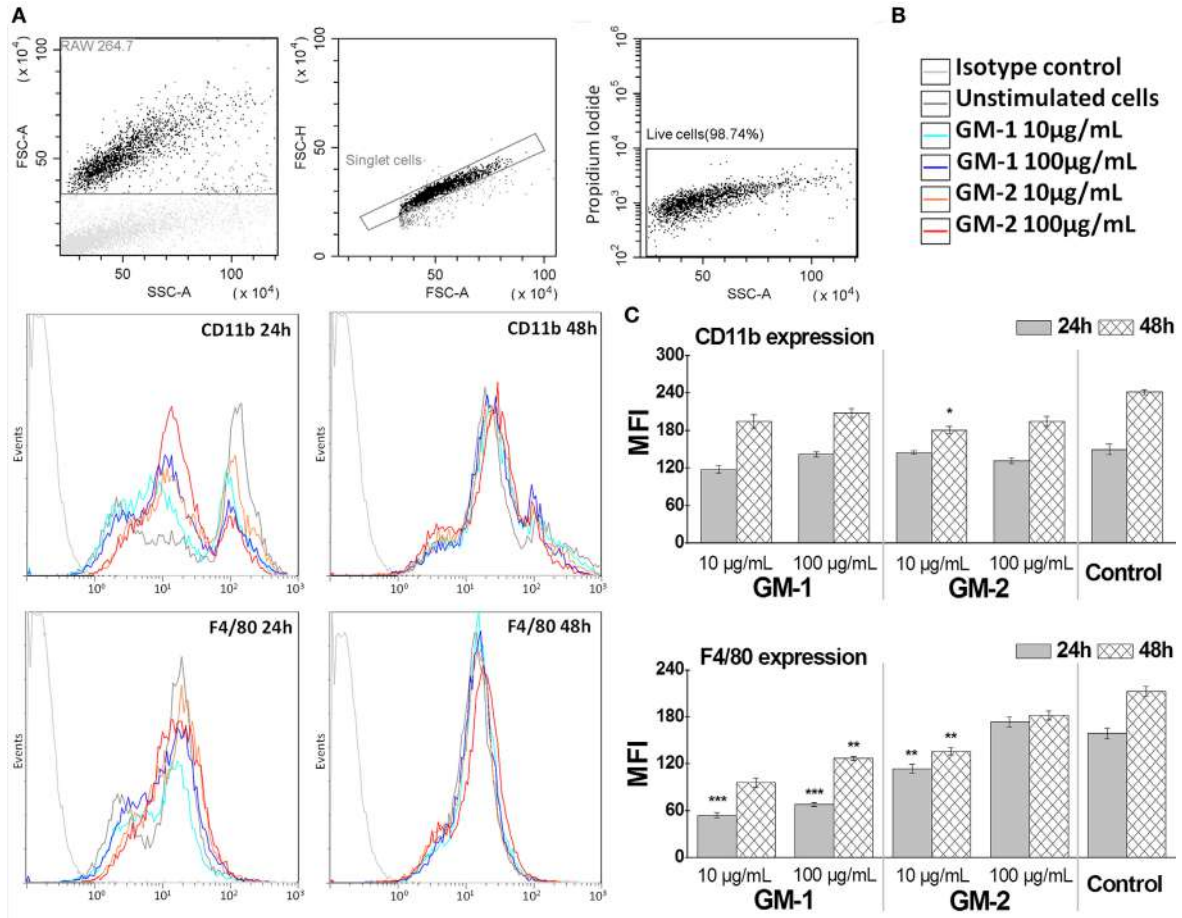

FIGURE 5 | Immunocytometric measurement of RAW264.7 macrophage cell-line expression of major cell surface antigens F4/80 and CD11b following of the treatment by glycoconjugates GM-1 or GM-2 at 10 or 100 µg/mL concentrations. Gates were set to exclude the cellular debris using forward scatter vs. side scatter dot plot discrimination, doublets and dead cells **(A)**. The settings were optimized using proper isotype control. Fluorescence histograms **(B)** of 10,000 cells were generated and analyzed (green fluorescence, 525-nm band-pass filter). The data **(C)** are expressed as a mean of fluorescence intensity. The statistical significance of differences between untreated cells (Control) and stimulated cells using one-way ANOVA and *post hoc* Bonferroni's tests is expressed as follows: ***—$P < 0.001$, **—$0.001 < P < 0.01$, *—$0.01 < P < 0.05$.

and while following the exposure to (1→3)-linked **GM-2** it was $r = 0.46$.

Sera Levels of Anti-GM-1 and -GM-2 IgG, IgA, and IgM Isotypes

Sera levels of anti-**GM-1** and anti-**GM-2** antibodies were assayed in *Candida* vulvovaginitis patients and healthy controls (blood donors) (**Figure 6**). Evidently, the class distribution of anti-**GM-1** and anti-**GM-2** antibodies has revealed IgM as the highest abundant isotype, followed by IgA and IgG. Statistically, the most significant have been the sera levels of IgM anti-**GM-1** ($P < 0.01$) and IgM anti-**GM-2** ($P < 0.01$). The correlation between these two anti-pentasacchride specific IgMs is 0.99. The sera values of antigen specific IgM anti-**GM-1** were 3.92-fold increased vs. blood donors' values; and for specific IgM anti-**GM-2** the 5.33-fold increase has been observed. Both pentasaccharide IgM isotypic antibodies were significantly lower in comparison with anti-*C. albicans* mannan antibodies, i.e., for IgM anti-**GM-2** (declined by 31.9%, $P < 0.001$, $r = 0.96$) and for IgM anti-**GM-1** the reduction was 35.22% ($P < 0.01$, $r = 0.95$).

The next most profound reactive isotype in the vulvovaginitis group has been IgA anti-**GM-1** demonstrated a 2.02-fold increase compared to healthy controls ($P < 0.05$). The 1.7-fold increase in specific IgA anti-**GM-2** over the healthy blood donors values has been statistically insignificant. The comparison with *Candida* mannan IgA response revealed a high correlation with anti-**GM-1** ($r = 0.97$) and a lower one for anti-**GM-2** ($r = 0.81$). Both pentasaccharides revealed similar IgA response compared to *C. albicans* mannan (**Figure 6**). The IgG antigen-specific response has been 1.81-fold increased with pentasaccharide **GM-1** over blood donors values and almost comparable with anti-mannan IgG ($r = 0.98$). The IgG anti-**GM-2** level was 1.09 times higher in the vulvovaginitis group than that in the control group. The vulvovaginitis group exerted a 2.52-fold decrease in anti-**GM-2** pentasaccharide IgG compared to anti-mannan IgG ($r = 0.76$).

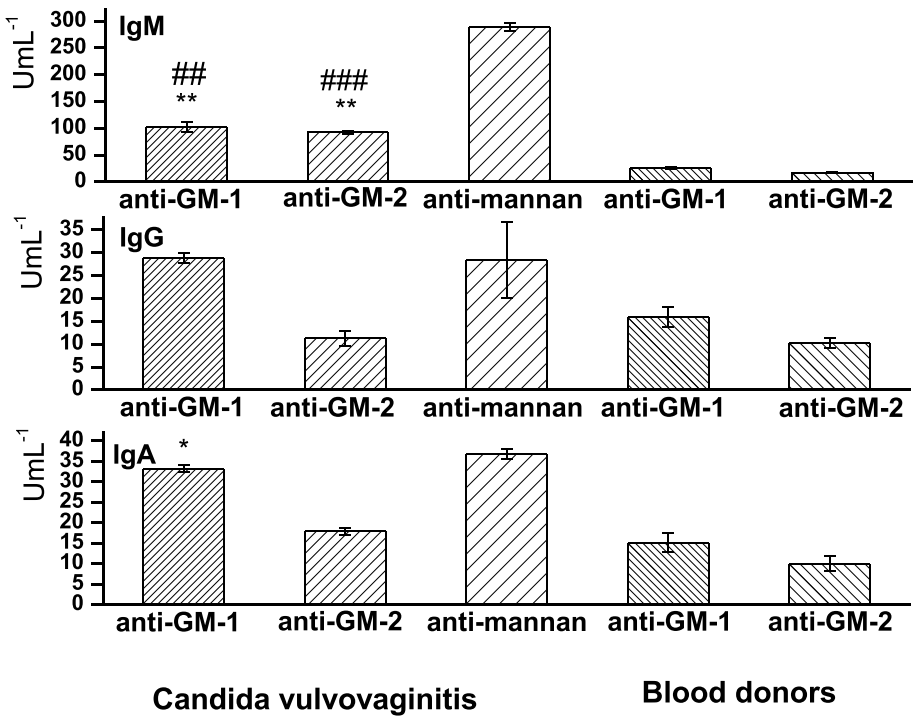

FIGURE 6 | Distribution of sera levels of anti-GM-1, anti-GM-2, and anti-mannan isotype class antibodies in vulvovaginitis patients and healthy controls (blood donors). Data are presented as mean ± SD. Analyses were carried out in triplicate. The statistical significance of differences between controls (blood donors) and vulvovaginitis patients using one-way ANOVA and *post hoc* Bonferroni's tests is expressed as: **—$0.001 < P < 0.01$, *—$0.01 < P < 0.05$. The statistical significance of differences between anti-mannan Abs and anti-**GM-1** and anti-**GM-2** Abs using one-way ANOVA and *post hoc* Bonferroni's tests is expressed as follows: ###—$P < 0.001$, ##—$0.001 < P < 0.01$.

DISCUSSION

The mold *A. fumigatus* is characterized by three morphotypes: (i) resting conidia, (ii) swollen conidia, and (iii) hyphae. The cell-walls of the mycelium and conidium are different especially at the level of the surface layer, which plays a significant role in the specific recognition of invading *A. fumigatus* by phagocytic cells of the immune system (24). The recognition of *A. fumigatus* conidia and hyphae is mediated by pattern recognition receptors (PRRs) either soluble and/or cell-bound receptors. The cell wall and its constituents symbolize the remarkable host–invader communication interface. Conidial germination starts with hydrophobic layer degradation and exposure of inner cell wall components, mainly polysaccharides such as chitin, β-glucan, mannan, and galactomannan. These represent pathogen-associated molecular patterns (PAMPs) recognized by PRRs (35, 36). Rizetto et al. (37) showed that the immune response induced by *Aspergillus* spp. may be dependent on variations of the fungus strain that could present diverse virulence factors and therefore increased or reduced infectivity. Generally, toll-like receptors and C-type lectin receptors as TLR2, TL4, and TLR9, Dectin-1, Dectin-2, DC-SIGN, mannose receptor, etc. on phagocytes directly recognize surface ligands on *A. fumigatus* and participate in pro-inflammatory and anti-inflammatory signaling responses resulting in cytokine and reactive oxygen species (ROS) release, thus supporting the antifungal activity (38–41). Of note, several polymorphisms of human TLRs, e.g., TLR1, TLR2, TLR4, TLR6, or TLR9, have been associated with increased risk of invassive aspergillosis in susceptible hosts (42–44).

Various interleukins and growth factors are engaged in host inter-reactivity with *A. fumigatus*. Bozza et al. (22) revealed that different preparations of *A. fumigatus* antigens induced the expansion of various CD4 T-cell subsets with secreted antigens promoting the differentiation of Th2 cells, membrane components Th1 cells, and glycolipids Th17 cells. In murine models of aspergillosis, α-(1→3)-glucan and β-(1→3)-glucan chains induce a protective response through the activation of Th1 and Th17 or Treg responses, whereas galactomannan favors the disease through the activation of the Th2/Th17 response (22).

In invasive aspergillosis, Th1-cell responses are associated with the resistance and onset of protective immunity, whereas Th2 responses are associated with progressive disease, more tissue damage, and poor survival. Th1-produced cytokines, including interferon-γ, interleukins IL-6, IL-12, TNF-α, and IL-1 activate neutrophils and pulmonary macrophages, the key effector cells in invasive aspergillosis, whereas Th2 cytokines, particularly IL-4 and IL-10, are associated with reduced IL-12 and TNF-α and worse outcome (45). Interestingly, the profile of the cytokine pattern depends on various aspects, such as the route of infection, immunological status of the host, type of *Aspergillus* antigens, etc. (2, 46, 47).

RAW 264.7 exposure to glycoconjugates **GM-1** and **GM-2** resulted in the accelerated cell-release of Th1 pro-inflammatory cytokines (**Figure 3**), TNF-α, IL-6, IL-12, IL-2, and hemopoietic growth factors GM-CSF and M-CSF associated with anti-*A. fumigatus* responses, this cytokine pattern is consistent with the results of Roilides et al. (48). Moreover, the G-CSF, GM-CSF, and M-CSF are cytokines with promising therapeutic efficacy and play critical roles in the host defense response during infection (49, 50). *In vitro* M-CSF has been shown to augment the antifungal activity of monocytes/macrophages against both conidia and hyphae of *A. fumigatus*, partly *via* enhancement of oxidation-dependent mechanisms (49).

Next, in a response to isomers **GM-1** and **GM-2** stimuli, the enhancement of media-release of IL-17 has been revealed. IL-17, signature cytokine of Th17 cells, is engaged in antimicrobial protection and induction of inflammation (51). Chai et al. has pointed out the role of this unique cytokine in Th17 anti-*A. fumigatus* immune responses (46). The Th1/Th17 polarized increased reactivity of the relevant signature cytokines TNF-a, IL-12, IL-17, IL-6, and IL-2 has been evidently structure-dependent, more apparent with (1→3)-linked **GM-2,** especially with 100 μg/mL concentration.

Resistance to *A. fumigatus* infection is associated with high levels of Th1 cytokines including IL-2, IL-12, and TNF-α (4). The statistically significant high media levels ($P < 0.001$) of these cytokines have been detected following the exposure with glycoconjugates **GM-1** and **GM-2** (**Figure 3**). On the contrary, disease progression is associated with Th2 cytokines IL-4 and IL-10 (4). Evidently, both galactomannosides **GM-1** and **GM-2** did not induce the significant IL-10 release over basal levels of untreated RAW2 64.7 cells (1.14-fold increase with 100 μg/mL of **GM-1** and 1.19-fold increase with 100 μg/mL of **GM-2**) (**Figure 3**).

Concerning concentration- and time-dependent cytokines' release following cell exposure to glycoconjugate **GM-1**, the statistically significant tight correlations have been revealed between TNF-α and IL-1β ($r = 0.96562$, $P = 0.03438$); IL-6 ($r = 0.99394$, $P = 0.00606$); M-CSF ($r = 0.99869$, $P = 0.00131$), IL-12 ($r = 0.99885$, $P = 0.00115$); IL-2 ($r = 0.92829$, $P = 0.04171$); IL-17 ($r = 0.94871$, $P = 0.04129$); and IL-10 ($r = –0.91585$, $P = 0.0325$). Correlation analysis confirmed the similar trends of kinetics of these cytokines release also with isomer **GM-2**. The cell exposure to this compound (10 μg/mL) resulted in a tight correlation exerted by TNF-α and IL-1β ($r = 0.87965$, $P = 0.012035$); IL-6 ($r = 0.99453$, $P = 0.00547$); M-CSF ($r = 0.99938$, $P = 0.000623$); GM-CSF ($r = 0.99291$, $P = 0.00709$); IL-12 ($r = 0.99968$, $P = 0.000315$); IL-2 ($r = 0.9579$, $P = 0.04205$), IL-17 ($r = 0.97497$, $P = 0.02503$); and IL-10 ($r = –0.90181$, $P = 0.0411$).

Obviously, the Th1/Th17 prospectively antifungal protective immunobiological efficiency could be assumed. Conjugates **GM-1** and **GM-2** induced IL-10 tight negative correlation with TNF-α, associated with anti-inflammatory signaling are of interest. According to the observed time-dependent down-regulation of several cytokines (from 24 to 48 h treatment), we can hypothesized engagement of relevant cytokine receptors and their interactions with media-produced cytokines subsequently resulting into the binding and uptake of released cytokine and regulatory feedback loop between cytokines and immune cells.

Thus, both synthetically prepared compounds **GM-1** and **GM-2** partially mimicking the *Aspergillus* galactomannan represented the appropriate model structures for *in vivo and in vitro* immunobiological studies. Their immunocompatibility has been confirmed based on the tests on functionality of RAW 264.7 macrophages treated with **GM-1** and **GM-2**, i.e., the trend of cell-line expression of major cell surface antigens F4/80 and CD11b following cell-exposure (**Figure 5**). Both markers represent pan macrophage antigens involved in cell adhesion and presumably in cell–cell interactions (F4/80) and, chemotaxis, phagocytosis, and apoptosis (CD11b) (**Figure 5**).

The induced changes of F4/80 expression demonstrated the association with concentration of glycoconjugates and exposition time as detected by cell-proliferation and phagocytosis. The free radical release did not exert this tendency (**Figure 4**).

The physiological concentration of ROS is essential to prevent immunometabolic disturbances. Oxidative stress induced by free radicals has been associated with the development of various diseases (52).

Obviously, phagocytosis plays the central role in anti-*Aspergillus* immunity. Innate effector phagocyting cells comprise alveolar macrophages, dendritic cells, neutrophils, and monocytes engaged in processes of hyphae and conidia engulfment, internalization, and killing *via* oxidative or non-oxidative mechanisms. *In vitro* studies documented the delay of conidial killing by alveolar macrophages after phagocytosis corresponding to the time when conidia become swollen (44). Interestingly, conidial phagocytosis involved DC-SIGN and complement recepor 3 and resulted in a protective Th1 response, while hyphal phagocytosis *via* Fc receptor and complement receptor 3 generates an unfavorable Th2 response (44). The experiments on RAW 264.7 phagocytosis and *Candida* internalization triggered by glycoconjugates **GM-1** and **GM-2** revealed a more efficient cell attachment and internalization with (1→3)-linked **GM-2** over (1→6)-linked **GM-1** (**Table 1**). Presumably, the structural epitopes of this formula resembled those of natural galactomannan more tightly compared to glycoconjugate **GM-1**. Evidently, both conjugates are able to initiate the process of phagocytosis, accompanied especially by the release of TNF-α, IL-6, IL-12, IL-2, Il-17 cytokines, and hemopoietic growth factors GM-CSF and M-CSF contributing to the regulation of inflammation (**Figure 3**). The significant increase of cell bound and internalized *C. albicans* cells by RAW 264.7 macrophages has been detected following 24 h cell pre-exposition with **GM-2** at 10 μg/mL ($P < 0.01$) and 100 μg/mL ($P < 0.05$).

Although the exposition of RAW 264.7 to **GM-1** upregulated the secretion of these cytokines and growth factors (**Figure 3**) to lesser degree than **GM-2**, the sequential process of phagocytosis has been inhibited (**Table 1**). Yet, we are not able fully to explain the decrease in phagocytosis despite the increase in Th1 type of cytokines. According to the known antigenic cross-reactivity between *Aspergillus* spp. and *Candida* spp. (53), one can suppose the interactions between *C. albicans* cellular PAMPs (e.g., mannan), **GM-1** and relevant RAW 264.7 PRRs. Evidently, **GM-1** comprised more cross-reactive

epitopes reflecting the structure of candidal ones. This item needs further investigation.

Thus, the engagement of isomer (1→3)-linked **GM-2** in processes of recognition (recognition receptors DC-SIGN, Dectin-1, or TLRs) and subsequent attachment, engulfment and internalization is obviously over (1→6)-linked isomer **GM-1**. The DC-SIGN receptor binds dormant *Aspergillus* conidia in a galactomannan-dependent manner leading to the internalization of spores (54).

The commercial diagnostics of aspergillosis is based on EB-A2 monoclonal antibody reacting with the specific epitope of galactomannan. It is an IgM antibody with an avidity constant of 2×10^9–5×10^9 M binding to an epitope located on the β-(1→5) galactofuranosyl-containing side chain of the galactomannan molecule. The epitope recognized by the EB-A2 MAb is a common oligosaccharide moiety of a wide range of intracellular and extracellular glycoproteins of *Aspergillus* species EB-A2, and similar epitope seems to be present in other fungi (55, 56). Galactomannan is not unique to *Aspergillus* sp., apart from *Aspergillus* sp. galactomannan is found in different amounts also in *Penicillium*, *Fusarium*, *Alternaria*, and *Histoplasma* (57, 58). Moreover, Swanink et al. (53) suggested the reactivity of *Candida* sp. in galactomannnan assay due to cross-reacting antigens. In *Aspergillus*, histochemistry false positive staining of *Candida* was observed with both polyclonal and monoclonal *Aspergillus* antibodies (59). The serapositivity of anti-**GM-1** and -**GM-2** isotypic antibodies in *Candida*-colpitis cohort demonstrated the cross-reactivity of *Asperillus* related structures **GM-1** and **GM-2** (**Figure 6**). Evidently, these structures comprised the main cross-reactive epitopes.

For comparison, sera from vulvovaginitis patients have been subjected to seradiagnostics based on glycoconjugates **GM-1** and **GM-2**, in parallel with *Candida* mannan assay. The pattern of antigenspecific IgM > IgA > IgG immune responses reactive with structures **GM-1** and **GM-2** (**Figure 6**) reflected the previously observed kinetics of anti-*C. albicans* mannan and anti-*C. albicans* glucan antibodies in atopic patients suffering from vulvovaginitis (34), thus suggesting the immunobiological importance of such fungal oligoglycosidic structures. Our recent findings demonstrate the IgM as dominant isotype also in serological studies of Candida vulvovaginitis patients using different synthetically prepared glycosides (60). Generally, specific anti-glycoside IgM is elevated in active fungal infection along with IgA, while elevated antigen-specific IgG are characteristic for reccurent attacks (61). Nowadays, the specific role of natural IgM antibodies has been stressed (62, 63).

The *Aspergillus* gynecological infections are rare, according to MEDIREX Inc., HPL Mycology Labs., Slovakia, *Aspergillus* sp. represent 1/5,500 of all positive mycological isolates from uterus and cervix. Gupta et al. (64) reported simultaneous infection with *Aspergillus* sp. and cervical squamous cell carcinoma in the female genital tract attributed to the opportunistic nature of infection in the immunocompromised state due to the underlying malignancy. Genitourinary aspergillosis is rare in non-immunocompromised patients, only few reports have been documented (65–67).

CONCLUSION

The ability of synthetically prepared isomeric galactomannoside derivatives **GM-1** and **GM-2** related to *Aspergillus* galactomannan antigen to interact with murine macrophages RAW 264.7 was studied. Significant immunomodulative effectivity of glycoconjugates **GM-1** and **GM-2** has been established *via* proliferation/cytotoxicity assay, phagocytosis and inductive interleukins and growth factors release. The protective Th1 and Th17 polarization has been revealed, especially with (1→3)-linked **GM-2**, which is more efficient trigger of the internalization and of *Candida* engulfment by RAW 264.7 cells.

The sera-crossreactivity with glycoconjugates **GM-1** and **GM-2** observed in vulvovaginitis patients revealed the clinical relevance of studied pentasccharide chains especially one with βGalf-(1→6)-αMan fragment present in the pentasaccharide **GM-1**.

In conclusion, it can be stated that synthetically prepared glycoconjugates **GM-1** and **GM-2** partially mimicking the structure of *Aspergillus* galactomannan represent the suitable *in vitro* and prospectively *in vivo* models for further immunobiological and immunotoxicological studies, potential antigens for *in vitro* diagnostics of aspergillosis and antifungal therapy monitoring.

ETHICS STATEMENT

The research protocol and the study have been approved by the Local Ethical Committee of the Oncology Institute of St. Elisabeth, Bratislava, Slovakia. Written informed consent to participate in the research study and for blood collection and subsequent laboratory examinations, in accordance with the principles in the Helsinki Declaration, was obtained from each patient prior to study enrollment. Patient's age, disease process, drug history, family history, and clinical signs and symptoms were documented at the first visit.

AUTHOR CONTRIBUTIONS

EP—executed the experimental design and performance of immunobiological studies, performed the human serodiagnostics, analyzed and interpreted the data. LP—performed immunobiological experiments and graphic data evaluation. MH—identified patient cohort, determined patient feasibility, and managed patient recruitment for the trial. VK and DA—performed the chemical syntheses of the oligosaccharide derivatives and analyzed the results. NN—planned the synthetic study, analyzed the results of synthetic part, and compared the data with contemporary literature.

FUNDING

This work was supported by the Scientific Grant Agency of the Slovak Republic VEGA (project 2/0098/17) and by the Slovak Research and Development Agency under the contract No. APVV-15-0161. The synthetic part of the work was supported by the RSF (grant 14-23-00199 to NN).

REFERENCES

1. Lehrnbecher T, Groll AH. Invasive fungal infections in the pediatric population. *Expert Rev Anti Infect Ther* (2011) 9(3):275–8. doi:10.1586/eri.11.1
2. Romani L. Cell mediated immunity to fungi: a reassessment. *Med Mycol* (2008) 46(6):515–29. doi:10.1080/13693780801971450
3. Weaver CT, Hatton RD, Mangan PR, Harrington LE. IL-17 family cytokines and the expanding diversity of effector T cell lineages. *Annu Rev Immunol* (2007) 25:821–52. doi:10.1146/annurev.immunol.25.022106.141557
4. Chotirmall SH, Al-Alawi M, Mirkovic B, Lavelle G, Logan PM, Greene CM, et al. *Aspergillus*-associated airway disease, inflammation, and the innate immune response. *Biomed Res Int* (2013) 2013:723129. doi:10.1155/2013/723129
5. Pagano L, Caira M, Valentini CG, Posteraro B, Fianchi L. Current therapeutic approaches to fungal infections in immunocompromised hematological patients. *Blood Rev* (2010) 24(2):51–61. doi:10.1016/j.blre.2009.11.003
6. Gregg KS, Kauffman CA. Invasive aspergillosis: epidemiology, clinical aspects, and treatment. *Semin Respir Crit Care Med* (2015) 36(5):662–72. doi:10.1055/s-0035-1562893
7. Baddley JW, Andes DR, Marr KA, Kontoyiannis DP, Alexander BD, Kauffman CA, et al. Factors associated with mortality in transplant patients with invasive aspergillosis. *Clin Infect Dis* (2010) 50(12):1559–67. doi:10.1086/652768
8. Barchiesi F, Mazzocato S, Mazzanti S, Gesuita R, Skrami E, Fiorentini A, et al. Invasive aspergillosis in liver transplant recipients: epidemiology, clinical characteristics, treatment, and outcomes in 116 cases. *Liver Transpl* (2015) 21(2):204–12. doi:10.1002/lt.24032
9. Brown GD, Denning DW, Gow NA, Levitz SM, Netea MG, White TC. Hidden killers: human fungal infections. *Sci Transl Med* (2012) 4(165):165rv13. doi:10.1126/scitranslmed.3004404
10. Munoz P, Ceron I, Valerio M, Palomo J, Villa A, Eworo A, et al. Invasive aspergillosis among heart transplant recipients: a 24-year perspective. *J Heart Lung Transplant* (2014) 33(3):278–88. doi:10.1016/j.healun.2013.11.003
11. Saghrouni F, Ben Youssef Y, Gheith S, Bouabid Z, Ben Abdeljelil J, Khammari I, et al. Twenty-nine cases of invasive aspergillosis in neutropenic patients. *Med Mal Infect* (2011) 41(12):657–62. doi:10.1016/j.medmal.2011.09.011
12. Singh N, Suarez JF, Avery R, Lass-Florl C, Geltner C, Pasqualotto AC, et al. Risk factors and outcomes in lung transplant recipients with nodular invasive pulmonary aspergillosis. *J Infect* (2013) 67(1):72–8. doi:10.1016/j.jinf.2013.03.013
13. Kauffman CA. Fungal infections. *Proc Am Thorac Soc* (2006) 3(1):35–40. doi:10.1513/pats.200510-110JH
14. Herbrecht R, Fluckiger U, Gachot B, Ribaud P, Thiebaut A, Cordonnier C. Treatment of invasive *Candida* and invasive *Aspergillus* infections in adult haematological patients. *Eur J Cancer Suppl* (2007) 5(2):49–59. doi:10.1016/j.ejcsup.2007.06.007
15. Arendrup MC. Update on antifungal resistance in *Aspergillus* and *Candida*. *Clin Microbiol Infect* (2014) 20(Suppl 6):42–8. doi:10.1111/1469-0691.12513
16. Nedel WL, Kontoyiannis DR, Pasqualotto AC. Aspergillosis in patients treated with monoclonal antibodies. *Rev Iberoam Micol* (2009) 26(3):175–83. doi:10.1016/j.riam.2009.04.001
17. Carvalho A, Cunha C, Iannitti RG, Casagrande A, Bistoni F, Aversa F, et al. Host defense pathways against fungi: the basis for vaccines and immunotherapy. *Front Microbiol* (2012) 3:176. doi:10.3389/fmicb.2012.00176
18. Cutler JE, Deepe GS Jr, Klein BS. Advances in combating fungal diseases: vaccines on the threshold. *Nat Rev Microbiol* (2007) 5(1):13–28. doi:10.1038/nrmicro1537
19. Edwards JE Jr. Fungal cell wall vaccines: an update. *J Med Microbiol* (2012) 61(Pt 7):895–903. doi:10.1099/jmm.0.041665-0
20. Pikman R, Ben-Ami R. Immune modulators as adjuncts for the prevention and treatment of invasive fungal infections. *Immunotherapy* (2012) 4(12):1869–82. doi:10.2217/imt.12.127
21. Vecchiarelli A, Pericolini E, Gabrielli E, Pietrella D. New approaches in the development of a vaccine for mucosal candidiasis: progress and challenges. *Front Microbiol* (2012) 3:294. doi:10.3389/fmicb.2012.00294
22. Bozza S, Clavaud C, Giovannini G, Fontaine T, Beauvais A, Sarfati J, et al. Immune sensing of *Aspergillus fumigatus* proteins, glycolipids, and polysaccharides and the impact on Th immunity and vaccination. *J Immunol* (2009) 183(4):2407–14. doi:10.4049/jimmunol.0900961
23. Komarova BS, Orekhova MV, Tsvetkov YE, Beau R, Aimanianda V, Latge JP, et al. Synthesis of a pentasaccharide and neoglycoconjugates related to fungal alpha-(1 – >3)-glucan and their use in the generation of antibodies to trace *Aspergillus fumigatus* cell wall. *Chemistry* (2015) 21(3):1029–35. doi:10.1002/chem.201404770
24. Latge JP. 30 years of battling the cell wall. *Med Mycol* (2017) 55(1):4–9. doi:10.1093/mmy/myw076
25. Latge JP, Kobayashi H, Debeaupuis JP, Diaquin M, Sarfati J, Wieruszeski JM, et al. Chemical and immunological characterization of the extracellular galactomannan of *Aspergillus fumigatus*. *Infect Immun* (1994) 62(12):5424–33.
26. Latge JP, Mouyna I, Tekaia F, Beauvais A, Debeaupuis JP, Nierman W. Specific molecular features in the organization and biosynthesis of the cell wall of *Aspergillus fumigatus*. *Med Mycol* (2005) 43(Suppl 1):S15–22. doi:10.1080/13693780400029155
27. Leitao EA, Bittencourt VC, Haido RM, Valente AP, Peter-Katalinic J, Letzel M, et al. Beta-galactofuranose-containing O-linked oligosaccharides present in the cell wall peptidogalactomannan of *Aspergillus fumigatus* contain immunodominant epitopes. *Glycobiology* (2003) 13(10):681–92. doi:10.1093/glycob/cwg089
28. Kudoh A, Okawa Y, Shibata N. Significant structural change in both O- and N-linked carbohydrate moieties of the antigenic galactomannan from *Aspergillus fumigatus* grown under different culture conditions. *Glycobiology* (2015) 25(1):74–87. doi:10.1093/glycob/cwu091
29. Mouyna I, Fontaine T. Cell wall of aspergillus fumigatus: a dynamic structure. In: Latgé J-P, Steinbach WJ, editors. *Aspergillus fumigatus and Aspergillosis*. American Society of Microbiology (2009). p. 169–83.
30. Argunov DA, Krylov VB, Nifantiev NE. Convergent synthesis of isomeric heterosaccharides related to the fragments of galactomannan from *Aspergillus fumigatus*. *Org Biomol Chem* (2015) 13(11):3255–67. doi:10.1039/c4ob02634a
31. Argunov DA, Krylov VB, Nifantiev NE. The use of pyranoside-into-furanoside rearrangement and controlled O(5) – > O(6) benzoyl migration as the basis of a synthetic strategy to assemble (1 – >5)- and (1 – >6)-linked galactofuranosyl chains. *Org Lett* (2016) 18(21):5504–7. doi:10.1021/acs.orglett.6b02735
32. Krylov VB, Argunov DA, Vinnitskiy DZ, Verkhnyatskaya SA, Gerbst AG, Ustyuzhanina NE, et al. Pyranoside-into-furanoside rearrangement: new reaction in carbohydrate chemistry and its application in oligosaccharide synthesis. *Chemistry* (2014) 20(50):16516–22. doi:10.1002/chem.201405083
33. Tsvetkov YE, Burg-Roderfeld M, Loers G, Arda A, Sukhova EV, Khatuntseva EA, et al. Synthesis and molecular recognition studies of the HNK-1 trisaccharide and related oligosaccharides. The specificity of monoclonal anti-HNK-1 antibodies as assessed by surface plasmon resonance and STD NMR. *J Am Chem Soc* (2012) 134(1):426–35. doi:10.1021/ja2083015
34. Paulovicova E, Bujdakova H, Chupacova J, Paulovicova L, Kertys P, Hrubisko M. Humoral immune responses to *Candida albicans* complement receptor 3-related protein in the atopic subjects with vulvovaginal candidiasis. Novel sensitive marker for *Candida* infection. *FEMS Yeast Res* (2015) 15(2):fou001. doi:10.1093/femsyr/fou001
35. Inoue M, Shinohara ML. Clustering of pattern recognition receptors for fungal detection. *PLoS Pathog* (2014) 10(2):e1003873. doi:10.1371/journal.ppat.1003873
36. Netea MG, Ferwerda G, van der Graaf CA, Van der Meer JW, Kullberg BJ. Recognition of fungal pathogens by toll-like receptors. *Curr Pharm Des* (2006) 12(32):4195–201. doi:10.2174/138161206778743538
37. Rizzetto L, Giovannini G, Bromley M, Bowyer P, Romani L, Cavalieri D. Strain dependent variation of immune responses to *A. fumigatus*: definition of pathogenic species. *PLoS One* (2013) 8(2):e56651. doi:10.1371/journal.pone.0056651
38. Loures FV, Rohm M, Lee CK, Santos E, Wang JP, Specht CA, et al. Recognition of *Aspergillus fumigatus* hyphae by human plasmacytoid dendritic cells is mediated by dectin-2 and results in formation of extracellular traps. *PLoS Pathog* (2015) 11(2):e1004643. doi:10.1371/journal.ppat.1004643

39. Mambula SS, Sau K, Henneke P, Golenbock DT, Levitz SM. Toll-like receptor (TLR) signaling in response to *Aspergillus fumigatus*. *J Biol Chem* (2002) 277(42):39320–6. doi:10.1074/jbc.M201683200
40. Roeder A, Kirschning CJ, Rupec RA, Schaller M, Korting HC. Toll-like receptors and innate antifungal responses. *Trends Microbiol* (2004) 12(1): 44–9. doi:10.1016/j.tim.2003.11.003
41. Taylor PR, Martinez-Pomares L, Stacey M, Lin HH, Brown GD, Gordon S. Macrophage receptors and immune recognition. *Annu Rev Immunol* (2005) 23:901–44. doi:10.1146/annurev.immunol.23.021704.115816
42. Carvalho A, Cunha C, Carotti A, Aloisi T, Guarrera O, Di Ianni M, et al. Polymorphisms in toll-like receptor genes and susceptibility to infections in allogeneic stem cell transplantation. *Exp Hematol* (2009) 37(9):1022–9. doi:10.1016/j.exphem.2009.06.004
43. Chai LY, Vonk AG, Kullberg BJ, Netea MG. Immune response to *Aspergillus fumigatus* in compromised hosts: from bedside to bench. *Future Microbiol* (2011) 6(1):73–83. doi:10.2217/fmb.10.158
44. Park SJ, Mehrad B. Innate immunity to *Aspergillus* species. *Clin Microbiol Rev* (2009) 22(4):535–51. doi:10.1128/CMR.00014-09
45. Sambatakou H, Pravica V, Hutchinson IV, Denning DW. Cytokine profiling of pulmonary aspergillosis. *Int J Immunogenet* (2006) 33(4):297–302. doi:10.1111/j.1744-313X.2006.00616.x
46. Chai LY, van de Veerdonk F, Marijnissen RJ, Cheng SC, Khoo AL, Hectors M, et al. Anti-*Aspergillus* human host defence relies on type 1 T helper (Th1), rather than type 17 T helper (Th17), cellular immunity. *Immunology* (2010) 130(1):46–54. doi:10.1111/j.1365-2567.2009.03211.x
47. Sales-Campos H, Tonani L, Cardoso CR, Kress MR. The immune interplay between the host and the pathogen in *Aspergillus fumigatus* lung infection. *Biomed Res Int* (2013) 2013:693023. doi:10.1155/2013/693023
48. Roilides E, Filioti J, Gil-Lamaignere C. Cytokines and the host defense against *Aspergillus fumigatus*. In: Kotb M, Calandra T, editors. *Cytokines and Chemokines in Infectious Diseases Handbook*. Totowa, NJ: Humana Press (2003). p. 215–26.
49. Kandalla PK, Sarrazin S, Molawi K, Berruyer C, Redelberger D, Favel A, et al. M-CSF improves protection against bacterial and fungal infections after hematopoietic stem/progenitor cell transplantation. *J Exp Med* (2016) 213(11):2269–79. doi:10.1084/jem.20151975
50. Kasahara S, Jhingran A, Dhingra S, Salem A, Cramer RA, Hohl TM. Role of granulocyte-macrophage colony-stimulating factor signaling in regulating neutrophil antifungal activity and the oxidative burst during respiratory fungal challenge. *J Infect Dis* (2016) 213(8):1289–98. doi:10.1093/infdis/jiw054
51. Veldhoen M. Interleukin 17 is a chief orchestrator of immunity. *Nat Immunol* (2017) 18(6):612–21. doi:10.1038/ni.3742
52. Hybertson BM, Gao B, Bose SK, McCord JM. Oxidative stress in health and disease: the therapeutic potential of Nrf2 activation. *Mol Aspects Med* (2011) 32(4–6):234–46. doi:10.1016/j.mam.2011.10.006
53. Swanink CM, Meis JF, Rijs AJ, Donnelly JP, Verweij PE. Specificity of a sandwich enzyme-linked immunosorbent assay for detecting *Aspergillus* galactomannan. *J Clin Microbiol* (1997) 35(1):257–60.
54. Serrano-Gomez D, Dominguez-Soto A, Ancochea J, Jimenez-Heffernan JA, Leal JA, Corbi AL. Dendritic cell-specific intercellular adhesion molecule 3-grabbing nonintegrin mediates binding and internalization of *Aspergillus fumigatus* conidia by dendritic cells and macrophages. *J Immunol* (2004) 173(9):5635–43. doi:10.4049/jimmunol.173.9.5635
55. Barton RC. Laboratory diagnosis of invasive aspergillosis: from diagnosis to prediction of outcome. *Scientifica (Cairo)* (2013) 2013:459405. doi:10.1155/2013/459405
56. Stynen D, Sarfati J, Goris A, Prevost MC, Lesourd M, Kamphuis H, et al. Rat monoclonal antibodies against *Aspergillus* galactomannan. *Infect Immun* (1992) 60(6):2237–45.
57. Huang YT, Hung CC, Hsueh PR. *Aspergillus* galactomannan antigenemia in *Penicilliosis marneffei*. *AIDS* (2007) 21(14):1990–1. doi:10.1097/QAD.0b013e3282eeb413
58. Mikulska M, Furfaro E, Del Bono V, Gualandi F, Raiola AM, Molinari MP, et al. Galactomannan testing might be useful for early diagnosis of fusariosis. *Diagn Microbiol Infect Dis* (2012) 72(4):367–9. doi:10.1016/j.diagmicrobio.2011.12.009
59. Schuetz AN, Cohen C. *Aspergillus* immunohistochemistry of culture-proven fungal tissue isolates shows high cross-reactivity. *Appl Immunohistochem Mol Morphol* (2009) 17(6):524–9. doi:10.1097/PAI.0b013e3181a38e05
60. Krylov Vadim B, Paulovičová L, Paulovičová E, Tsvetkov Yury E, Nifantiev Nikolay E. Recent advances in the synthesis of fungal antigenic oligosaccharides. *Pure Appl Chem* (2017) 89(7):885–98. doi:10.1515/pac-2016-1011
61. Casadevall A. Antibody immunity and invasive fungal infections. *Infect Immun* (1995) 63(11):4211–8.
62. Gronwall C, Vas J, Silverman GJ. Protective roles of natural IgM antibodies. *Front Immunol* (2012) 3:66. doi:10.3389/fimmu.2012.00066
63. Ehrenstein MR, Notley CA. The importance of natural IgM: scavenger, protector and regulator. *Nat Rev Immunol* (2010) 10(11):778–86. doi:10.1038/nri2849
64. Gupta P, Goyal S, Kaushal M. Concomitant *Aspergillus* species infection and squamous cell carcinoma diagnosed on Pap Smear. *Turk Patoloji Derg* (2016) 32(1):54–6. doi:10.5146/tjpath.2013.01198
65. Baggish MS, Ventolini G. Vulvovaginal colonization by *Aspergillus* species in nonimmunocompromised women. *J Gynecol Surg* (2008) 24(2):55–60. doi:10.1089/gyn.2008.B-00242-1
66. Agarwal N, Seth A, Kulshrestha V, Kochar S, Kriplani A. Spontaneous vesicovaginal fistula caused by genitourinary aspergillosis. *Int J Gynaecol Obstet* (2009) 105(1):63–4. doi:10.1016/j.ijgo.2008.11.005
67. Ventolini G. *Aspergillus* and vaginal colonization. *J Anc Dis Prev Rem* (2014) 2:e115. doi:10.4172/2329-8731.1000e115

Conflict of Interest Statement: The authors declare that the research was conducted in the absence of any commercial or financial relationships that could be construed as a potential conflict of interest.

JACS
JOURNAL OF THE AMERICAN CHEMICAL SOCIETY
pubs.acs.org/JACS
Communication

Biotinylated Oligo-α-(1 → 4)-D-galactosamines and Their N-Acetylated Derivatives: α-Stereoselective Synthesis and Immunology Application

Ekaterina D. Kazakova, Dmitry V. Yashunsky, Vadim B. Krylov, Jean-Philippe Bouchara, Murielle Cornet, Isabel Valsecchi, Thierry Fontaine, Jean-Paul Latgé, and Nikolay E. Nifantiev*

Cite This: J. Am. Chem. Soc. 2020, 142, 1175−1179
Read Online

ABSTRACT: Using 3-*O*-benzoyl-4,6-*O*-di-*tert*-butylsilylidene-2-azido-2-deoxy-selenogalactoside, biotinylated oligo-α-(1 → 4)-D-galactosamines comprising from two to six GalN units were prepared for the first time together with their N-acetylated derivatives. The combination of blocking groups used herein provided stereocontrol for the α-stereospecific glycosylation, to show also high efficiency of phenyl 2-azido-2-deoxy-selenogalactosides as glycosyl donors. The obtained glycoconjugates are related to fragments of exopolysaccharide galactosaminogalactan (GG) found in *Aspergillus fumigatus*, which is the most important airborne human fungal pathogen in industrialized countries. The synthesized glycoconjugates were arrayed on streptavidin-coated plates and used to investigate the GG epitopes recognized by mouse monoclonal antibodies against GG and by human antibodies in the sera of patients with aspergillosis. The obtained data showed that the oligo-α-(1 → 4)-D-galactosamines and their N-acetylated derivatives allowed the first precise analysis of the specificity of the antibody responses to this extremely complex fungal polysaccharide.

Aspergillus fumigatus is one of the most important invasive human fungal pathogens in industrialized countries. It causes invasive fungal infections with high mortality rates that remain over 50%, even when using known antifungal agents.[1] The cell wall exopolysaccharide galactosaminogalactan (GG) of *Aspergillus fumigatus* is a major virulence factor of this human fungal pathogen.[2] GG is a high-molecular-weight biopolymer with a very complex structure consisting of α-(1 → 4)-linked galactose, galactosamine, and N-acetylgalactosamine units.[3] It plays a major role in the adhesion of the mycelium to abiotic and biotic substrates and in biofilm formation.[2−4] Most importantly, it has immunosuppressive properties that favor fungal infection. Moreover, anti-GG antibodies have been detected in human sera, and antibodies can easily be induced in mice hyperimmunized with purified GG.[3,4] The carbohydrate epitopes responsible for the immune function of GG are currently unknown. Due to the structural heterogeneity of GG and especially the lack of repeating units,[2,5,6] the only way to answer this question is to use a series of labeled oligosaccharides representing different GG-related fragments as molecular probes.

Herein, we describe the first synthesis of oligo-α-(1 → 4)-D-galactosamines (**35**−**39**, Scheme 2) comprising from two to six monosaccharide units and containing a biotinylated aglycon spacer as well as their N-acetylated derivatives (**41**−**45**). Galactosaminides **34** and **40** were also synthesized.

The assembly of the target oligosaccharides is a complex task because the α-(1,2-*cis*)-stereoselectivity of the glycosylation must be controlled and the axial 4-OH groups of the galactopyranose units have relatively low reactivity. In this context, the use of a 2-azido-2-deoxygalactosyl donor with a "nonparticipating" N_3 group should both facilitate α-stereoselective galactosylation[7] and offer a free NH_2 group during GalN-unit generation when required.

Based on the above considerations, the target oligosaccharides were synthesized using selectively O-substituted phenyl 2-azido-2-deoxy-selenogalactoside **5** (Scheme 1), which belongs to a new type of 2-azido-2-deoxygalactosyl donor.[8−10] Selenoglycoside **5** was prepared via azidophenylselenylation of the galactal,[11] which is a shorter process than typically used protocols for the preparation of 2-azido-2-deoxygalactosyl donors via azidonitration of glycals.[12]

The di-(*tert*-butyl)silylidene (DTBS) group was selected to protect O-4 and O-6 because of its steric hindrance, which disfavors the formation of undesirable β-glycosylation products.[13] Despite the previous observation[10,14] of the good efficiency of 3-O-benzylated 2-azido-2-deoxygalactosyl donors, a 3-O-benzoyl group was applied in this work as a temporary protecting group on O-3 of the glycosyl donor **5** because 3-benzoates offer α-stereocontrol through remote anchimeric participation.[9,15−18] The synthesis of the designed donor **5** is shown in Scheme 1 and is described in the Supporting Information.

Several preliminary α-galactosylation experiments with donor **5** and aliphatic and monosaccharide acceptors showed that the optimal promoter system is Me_2S_2−MeOTf, which is more convenient than the previously used NIS−TMSOTf[8] or Ph_2SO−Tf_2O systems,[10] which require the use of low

Received: October 30, 2019
Published: January 8, 2020

https://dx.doi.org/10.1021/jacs.9b11703
J. Am. Chem. Soc. 2020, 142, 1175−1179

Scheme 1. Synthesis of Monosaccharide Donor 5, Acceptors 11 and 12, and Carbohydrate Blocks 13−19[a]

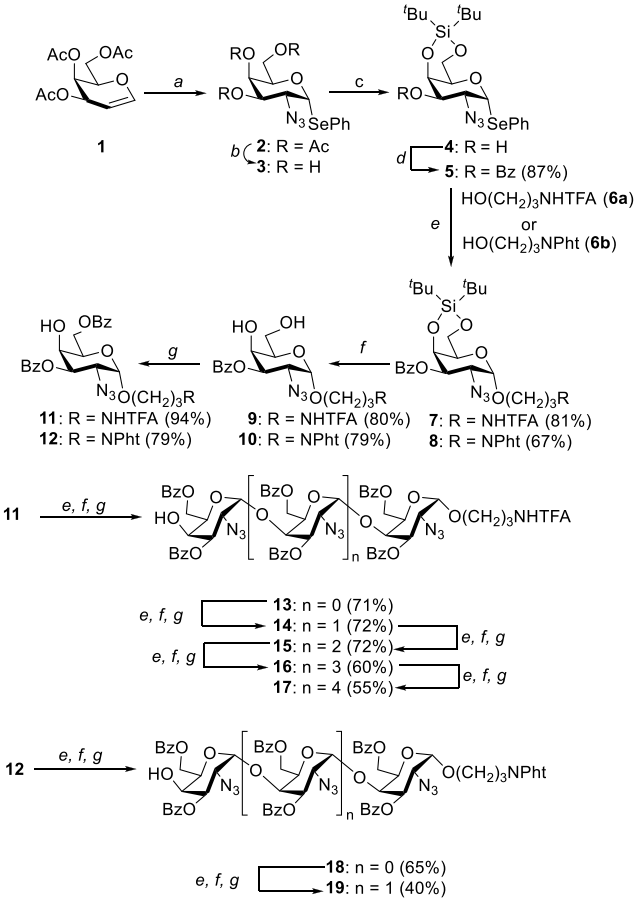

[a]Reagents and conditions: (a)[11] Se_2Ph_2, $TMSN_3$, $PhI(OAc)_2$, CH_2Cl_2, −30 → −18 °C; (b) 1 M MeONa, MeOH, CH_2Cl_2; (c) $DTBSCl_2$, AgOTf, Py; (d) BzCl, Py; (e) **5**, Me_2S_2, MeOTf, MS 4 Å, CH_2Cl_2 (f) 40% aq HF, Py; (g) BzCl, Py, 0 °C.

temperatures and produce a substantial amount of byproducts. The glycosylation of *N*-(3-trifluoroacetyl)-propanol (**6a**) with **5** proceeded smoothly, leading to the expected α-linked product 7. Removal of the DTBS group (→ **9**), followed by regioselective 6-O-benzoylation, gave the desired glycosyl acceptor **11** with a free OH group at C-4. Its structure was confirmed by a combination of 1D and 2D NMR spectral data. In particular, the α-configuration of the anomeric center was assessed based on the $J_{H1,H2}$ constant (3.6 Hz). The location of the Bz groups at O-3 and O-6 and the presence of a free OH group at C-4 were confirmed by the characteristic low-field signals of H-3 and H-6a,b (δ_{H3} 5.43 ppm; δ_{H6a} 4.49 ppm, δ_{H6b} 4.51 ppm) and the high-field signal of H-4 (δ_{H4} 4.37 ppm).

The glycosylation of acceptor **11** with donor **5**, removal of the DTBS group, and 6′-O-benzoylation gave disaccharide glycosyl acceptor **13**. Subjecting this compound to multiple cycles of these reactions under similar conditions afforded the tri- (**14**), tetra- (**15**), penta- (**16**), and hexasaccharide (**17**) glycosyl acceptors. Their structures, particularly the location of the Bz groups and free OH groups as well as the α-configuration of the anomeric centers, were confirmed by a combination of 1D and 2D NMR spectra, and these data are summarized in the Supporting Information.

The N_3 groups in products **11** and **13**−**17** were effectively reduced by catalytic hydrogenation over $Pd(OH)_2/C$ in the presence of Boc_2O and Et_3N to produce N-Boc-protected aminogalactosides **21**−**26** (Scheme 2). Their saponification by

Scheme 2. Synthesis of Biotinylated Glycoconjugates 34−45[b]

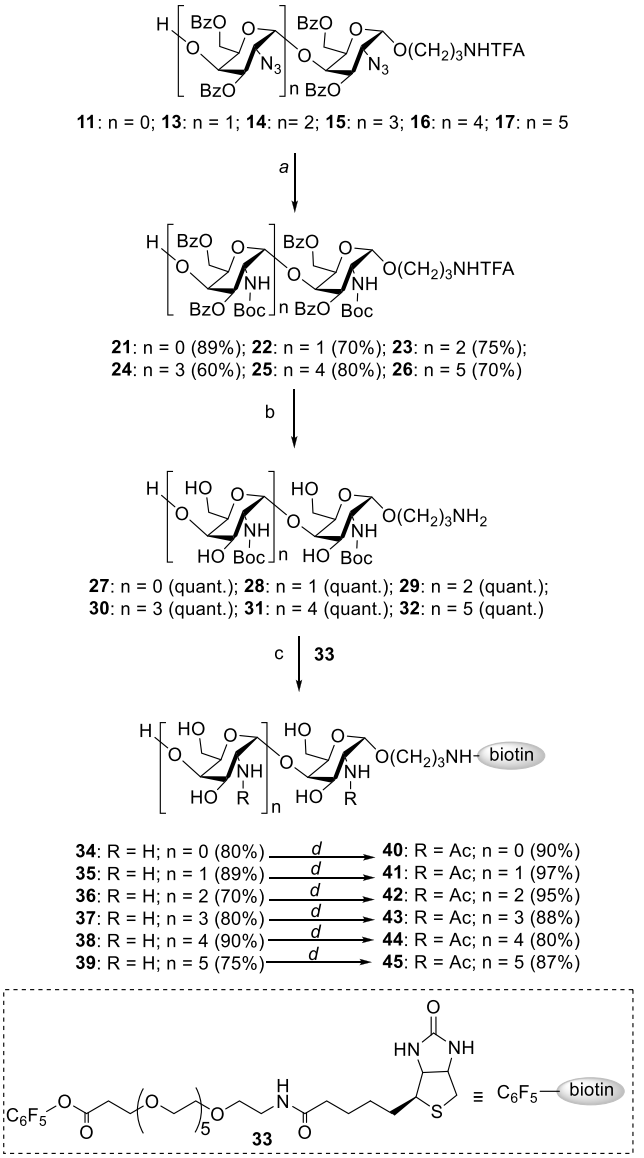

[b]Reagents and conditions: (a) $Pd(OH)_2/C$, Et_3N, Boc_2O, EtOAc, atm. H_2; (b) 1 M MeONa, CH_2Cl_2−MeOH (1:3), then 1 M NaOH; (c) **33**, Et_3N, DMF, then CF_3COOH; (d) Ac_2O, Et_3N, MeOH.

treatment with MeONa and aq NaOH afforded compounds **27**−**32**, which were then biotinylated with reagent **33**[19] via an unprotected spacer aminopropyl group. Acid hydrolysis with trifluoroacetic acid (TFA) cleaved the N-Boc protecting groups, affording target galactosamine-containing glycoconjugates **34**−**39**. Parts of these products were N-acetylated to give *N*-acetylgalactosamine-containing conjugates **40**−**45**. The structures of products **34**−**45** were established by a combination of 1D and 2D NMR spectroscopy, and these data are summarized in the Supporting Information.

https://dx.doi.org/10.1021/jacs.9b11703
J. Am. Chem. Soc. 2020, 142, 1175−1179

In parallel with the above syntheses, the application of 3-phtalimidopropanol (**6b**) instead of the N-TFA analogue **6a** was studied as well. The above-described chemical protocols were used to effectively synthesize mono-, di-, and trisaccharide derivatives **12**, **18**, and **19** (Scheme 1). The latter were successfully converted to unprotected products **27**–**29**, identical to those obtained previously using *N*-(3-trifluoroacetyl)-propanol as a spacer. The elongation of the oligosaccharide chain with compound **19** was not continued because the standard procedures for the removal of the O-benzoyl and N-phthaloyl protecting groups with hydrazine hydrate were not quantitative and were accompanied by the formation of acylhydrazides, resulting in the presence of contaminants in the target oligosaccharides.

Biotinylated oligosaccharides **34**–**45**, together with their analogues possessing N-acetylated and nonacetylated GlcN units (**46**–**49**)[20,21] (Figure 1), were immobilized on

β-D-GlcN-[(1→4)-β-D-GlcN]$_4$-O(CH$_2$)$_3$-NH-biotin **46**

β-D-GlcN-[(1→6)-β-D-GlcN]$_4$-O(CH$_2$)$_3$-NH-biotin **47**

β-D-GlcNAc-[(1→4)-β-D-GlcNAc]$_4$-O(CH$_2$)$_3$-NH-biotin **48**

β-D-GlcNAc-[(1→6)-β-D-GlcNAc]$_4$-O(CH$_2$)$_3$-NH-biotin **49**

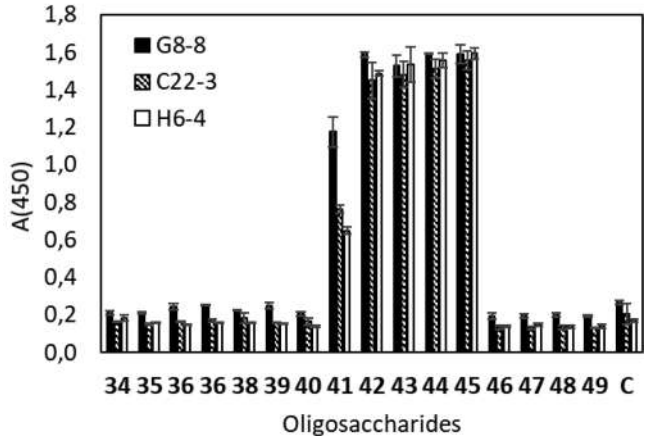

Figure 1. Assay of carbohydrate specificity of anti-GG monoclonal antibodies by ELISA on a glycoarray of biotinylated glycoconjugates **34**–**47**. C: control without carbohydrate ligand.

streptavidin-coated microtiter plates to form a glycoarray, which was used to analyze the specificity of anti-GG mouse mAbs[1] G8-8, C22-3, and H6-4, as described for the analysis of other monoclonal antibodies directed toward *Aspergillus* polysaccharide antigens, namely, α-(1 → 3)-glucan[22,23] and galactomannan.[24] It was revealed that the minimal epitope recognized with mAbs is a disaccharide consisting of two GalNAc units with an α-(1 → 4)-linkage. All three MAbs inoculated with GG recognized the same epitope, indicating that it was immunodominant in hyperimmunized mice (Figure 1).

The preliminary assays with the glycoarray composed of biotinylated oligosaccharides **35**–**39** and **41**–**45** showed that anti-GG antibodies in the sera of patients with allergic bronchopulmonary and chronic pulmonary aspergillosis (ABPA and CPA) recognized both N-acetylated and non-acetylated oligogalactosamines with a degree of polymerization (dp) of at least 3 (Figure 1S). Further elongation of the oligosaccharide ligand favors its better recognition by the serum anti-GG antibodies. Accordingly, hexasaccharides **39** and **45** were used to further analyze the levels of anti-GG antibodies in the sera of cohorts of patients with ABPA and CPA. The level of antibodies that recognized these hexasaccharides was significantly higher in the sera of aspergillosis patients than that in the control sera (Figure 2). The difference was more pronounced with antibodies directed against N-acetylated ligand **45** than nonacetylated **39**.

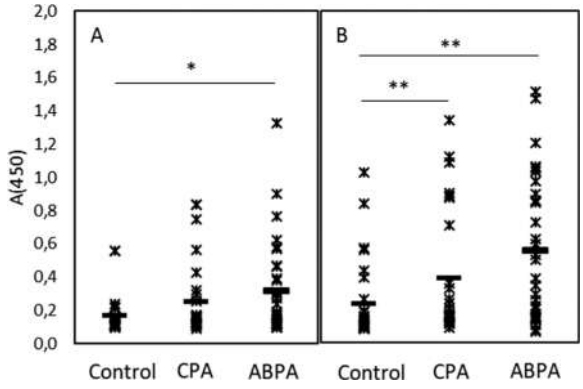

Figure 2. Testing the carbohydrate specificities of sera from patients with CPA (N = 25) or ABPA (N = 30) or healthy controls (N = 26) using nonacetylated conjugate **39** (A) and its N-acetylated analogue **45** (B). Mann–Whitney test: * - significant, 0.01 < p < 0.05; ** - very significant, p < 0.01.

In conclusion, the syntheses demonstrated good synthetic potential of phenyl 2-azido-2-deoxy-selenogalactoside glycosyl donors in combination with the Me_2S_2/MeOTf activation system, which is applicable to the glycosylation of low reactive glycosyl acceptors derived from 4-hydroxylated GalN. Our data showed that the oligo-α-(1 → 4)-galactosamine conjugates are an important set of molecular probes to better elucidate an innate and cellular immune response in aspergillosis patients.

■ ASSOCIATED CONTENT

Supporting Information

The Supporting Information is available free of charge at https://pubs.acs.org/doi/10.1021/jacs.9b11703.

General methods, full experimental procedures, characterization data for all new compounds, copies of ^{1}H and ^{13}C NMR, and ELISA experiments (PDF)

■ AUTHOR INFORMATION

Corresponding Author

Nikolay E. Nifantiev – *Russian Academy of Sciences, Moscow, Russian Federation;* orcid.org/0000-0002-0727-4050; Email: nen@ioc.ac.ru

Other Authors

Ekaterina D. Kazakova – *Russian Academy of Sciences, Moscow, Russian Federation*

Dmitry V. Yashunsky – *Russian Academy of Sciences, Moscow, Russian Federation*

Vadim B. Krylov – *Russian Academy of Sciences, Moscow, Russian Federation*

Jean-Philippe Bouchara – *CHU Angers, Angers, France*

Murielle Cornet − *University of Grenoble Alpes, Grenoble, France*
Isabel Valsecchi − *Institut Pasteur, Paris, France*
Thierry Fontaine − *Institut Pasteur, Paris, France*
Jean-Paul Latgé − *Institut Pasteur, Paris, France, and University of Crete, Heraklion, Greece*

Complete contact information is available at: https://pubs.acs.org/10.1021/jacs.9b11703

Notes

The authors declare no competing financial interest.

■ ACKNOWLEDGMENTS

The synthesis of biotinylated glycoconjugates and the screening of monoclonal antibodies by glycoarray was supported by Russian Science Foundation Grant 19-73-30017 (N.E.N.); the analysis of the patients' sera was supported by the French Government's Investissement d'Avenir program, Laboratoire d'Excellence "Integrative Biology of Emerging Infectious Diseases" (Grant No. ANR-10-LABX-62-IBEID) (J.P.L.) and Agence Nationale de la Recherche (ANR 16 CE92 0039-01 AFUINF) (J.P.L.).

■ REFERENCES

(1) Brown, G. D.; Denning, D. W.; Gow, N. A. R.; Levitz, S. M.; Netea, M. G.; White, T. C. Hidden Killers: Human Fungal Infections. *Sci. Transl. Med.* **2012**, *4*, 165rv13−165rv13.

(2) Briard, B.; Muszkieta, L.; Latgé, J.-P.; Fontaine, T. Galactosaminogalactan of *Aspergillus fumigatus*, a Bioactive Fungal Polymer. *Mycologia* **2016**, *108*, 572−580.

(3) Fontaine, T.; Delangle, A.; Simenel, C.; Coddeville, B.; van Vliet, S. J.; van Kooyk, Y.; Bozza, S.; Moretti, S.; Schwarz, F.; Trichot, C.; Aebi, M.; Delepierre, M.; Elbim, C.; Romani, L.; Latge, J.-P. Galactosaminogalactan, a New Immunosuppressive Polysaccharide of *Aspergillus fumigatus*. *PLoS Pathog.* **2011**, *7*, No. e1002372.

(4) Loussert, C.; Schmitt, C.; Prevost, M.-C.; Balloy, V.; Fadel, E.; Philippe, B.; Kauffmann-Lacroix, C.; Latgé, J. P.; Beauvais, A. *In Vivo* Biofilm Composition of *Aspergillus fumigatus*. *Cell. Microbiol.* **2010**, *12*, 405−410.

(5) Lee, M. J.; Gravelat, F. N.; Cerone, R. P.; Baptista, S. D.; Campoli, P. V.; Choe, S.-I.; Kravtsov, I.; Vinogradov, E.; Creuzenet, C.; Liu, H.; Berghuis, A. M.; Latgé, J.-P.; Filler, S. G.; Fontaine, T.; Sheppard, D. C. Overlapping and Distinct Roles of Aspergillus Fumigatus UDP-Glucose 4-Epimerases in Galactose Metabolism and the Synthesis of Galactose-Containing Cell Wall Polysaccharides. *J. Biol. Chem.* **2014**, *289*, 1243−1256.

(6) Gravelat, F. N.; Beauvais, A.; Liu, H.; Lee, M. J.; Snarr, B. D.; Chen, D.; Xu, W.; Kravtsov, I.; Hoareau, C. M. Q.; Vanier, G.; Urb, M.; Campoli, P.; Al Abdallah, Q.; Lehoux, M.; Chabot, J. C.; Ouimet, M. C.; Baptista, S. D.; Fritz, J. H.; Nierman, W. C.; Latgé, J.-P.; Mitchell, A. P.; Filler, S. G.; Fontaine, T.; Sheppard, D. C. *Aspergillus* Galactosaminogalactan Mediates Adherence to Host Constituents and Conceals Hyphal β-Glucan from the Immune System. *PLoS Pathog.* **2013**, *9*, No. e1003575.

(7) Nigudkar, S. S.; Demchenko, A. V. Stereocontrolled 1,2- *cis* Glycosylation as the Driving Force of Progress in Synthetic Carbohydrate Chemistry. *Chem. Sci.* **2015**, *6*, 2687−2704.

(8) Khatuntseva, E. A.; Sherman, A. A.; Tsvetkov, Y. E.; Nifantiev, N. E. Phenyl 2-Azido-2-Deoxy-1-Selenogalactosides: A Single Type of Glycosyl Donor for the Highly Stereoselective Synthesis of α- and β-2-Azido-2-Deoxy-D-Galactopyranosides. *Tetrahedron Lett.* **2016**, *57*, 708−711.

(9) Hagen, B.; Ali, S.; Overkleeft, H. S.; van der Marel, G. A.; Codée, J. D. C. Mapping the Reactivity and Selectivity of 2-Azidofucosyl Donors for the Assembly of N-Acetylfucosamine-Containing Bacterial Oligosaccharides. *J. Org. Chem.* **2017**, *82*, 848−868.

(10) Hagen, B.; van Dijk, J. H. M.; Zhang, Q.; Overkleeft, H. S.; van der Marel, G. A.; Codée, J. D. C. Synthesis of the Staphylococcus Aureus Strain M Capsular Polysaccharide Repeating Unit. *Org. Lett.* **2017**, *19*, 2514−2517.

(11) Mironov, Y. V.; Sherman, A. A.; Nifantiev, N. E. Homogeneous Azidophenylselenylation of Glycals Using $TMSN_3$−Ph_2Se_2−$PhI(OAc)_2$. *Tetrahedron Lett.* **2004**, *45* (49), 9107−9110.

(12) Lemieux, R. U.; Ratcliffe, R. M. The Azidonitration of Tri-O-Acetyl-D-Galactal. *Can. J. Chem.* **1979**, *57*, 1244−1251.

(13) Imamura, A.; Matsuzawa, N.; Sakai, S.; Udagawa, T.; Nakashima, S.; Ando, H.; Ishida, H.; Kiso, M. The Origin of High Stereoselectivity in Di-Tert-Butylsilylene-Directed α-Galactosylation. *J. Org. Chem.* **2016**, *81*, 9086−9104.

(14) Fusari, M.; Fallarini, S.; Lombardi, G.; Lay, L. Synthesis of Di- and Tri-Saccharide Fragments of Salmonella Typhi Vi Capsular Polysaccharide and Their Zwitterionic Analogues. *Bioorg. Med. Chem.* **2015**, *23*, 7439−7447.

(15) Komarova, B. S.; Orekhova, M. V.; Tsvetkov, Y. E.; Nifantiev, N. E. Contribution of Carbohydrate Chemistry to Assessment of the Biological Role of Natural Alpha-Glucosides. In *Specialist Periodical Reports: Carbohydrate Chemistry − Chemical and Biological Approaches*; Rauter, A. P., Lindhorst, T. K., Queneau, Y., Eds.; Royal Society of Chemistry: Cambridge, U.K., 2016; Vol. *41*, pp 187−237.

(16) Komarova, B. S.; Tsvetkov, Y. E.; Nifantiev, N. E. Design of α-Selective Glycopyranosyl Donors Relying on Remote Anchimeric Assistance. *Chem. Rec.* **2016**, *16*, 488−506.

(17) Gerbst, A. G.; Ustuzhanina, N. E.; Grachev, A. A.; Khatuntseva, E. A.; Tsvetkov, D. E.; Whitfield, D. M.; Berces, A.; Nifantiev, N. E. Synthesis, NMR, and Conformational Studies of Fucoidan Fragments. III. Effect of Benzoyl Group at O-3 on Stereoselectivity of Glycosylation by 3-O- and 3,4-Di-O-Benzoylated 2-O-Benzylfucosyl Bromides. *J. Carbohydr. Chem.* **2001**, *20*, 821−831.

(18) Khatuntseva, E. A.; Ustuzhanina, N. E.; Zatonskii, G. V.; Shashkov, A. S.; Usov, A. I.; Nifant'ev, N. E. Synthesis, NMR and Conformational Studies of Fucoidan Fragments. I. Desulfated 2,3- and 3,4-Branched Trisaccharide Fragments and Constituting Disaccharides. *J. Carbohydr. Chem.* **2000**, *19*, 1151−1173.

(19) Tsvetkov, Y. E.; Burg-Roderfeld, M.; Loers, G.; Ardá, A.; Sukhova, E. V.; Khatuntseva, E. A.; Grachev, A. A.; Chizhov, A. O.; Siebert, H.-C.; Schachner, M. Synthesis and Molecular Recognition Studies of the HNK-1 Trisaccharide and Related Oligosaccharides. The Specificity of Monoclonal Anti-HNK-1 Antibodies as Assessed by Surface Plasmon Resonance and STD NMR. *J. Am. Chem. Soc.* **2012**, *134*, 426−435.

(20) Gening, M. L.; Tsvetkov, Y. E.; Pier, G. B.; Nifantiev, N. E. Synthesis of Beta-(1→6)-Linked Glucosamine Oligosaccharides Corresponding to Fragments of the Bacterial Surface Polysaccharide Poly-N-Acetylglucosamine. *Carbohydr. Res.* **2007**, *342*, 567−575.

(21) Krylov, V. B.; Petruk, M. I.; Argunov, D. A.; Khatuntseva, E. A.; Toplishek, M. V.; Komarova, B. S.; Karelin, A. A.; Yudina, O. N.; Menshov, V. M.; Yashunskii, D. V.; Tsvetkov, Y. E.; Nifantiev, N. E. Study of the Carbohydrate Specificity of Antibodies Against Aspergillus Fumigatus Using the Library of Synthetic Mycoantigens. *Russ. J. Bioorg. Chem.* **2018**, *44*, 80−89.

(22) Komarova, B. S.; Orekhova, M. V.; Tsvetkov, Y. E.; Beau, R.; Aimanianda, V.; Latge, J.-P.; Nifantiev, N. E. Synthesis of a pentasaccharide and neoglycoconjugates related to fungal α-(1→3)-glucan and their use in antibodies generation to trace *Aspergillus fumigatus* cell wall. *Chem. - Eur. J.* **2015**, *21*, 1029−1035.

(23) Komarova, B. S.; Wong, S. S. W.; Orekhova, M. V.; Tsvetkov, Y. E.; Krylov, V. B.; Beauvais, A.; Bouchara, J.-P.; Kearney, J. F.; Aimanianda, V.; Latgé, J.-P.; Nifantiev, N. E. Chemical Synthesis and Application of Biotinylated Oligo-α-(1→3)-D-Glucosides To Study the Antibody and Cytokine Response against the Cell Wall α-(1→3)-D-Glucan of *Aspergillus fumigatus*. *J. Org. Chem.* **2018**, *83*, 12965−12976.

(24) Krylov, V. B.; Solovev, A. S.; Argunov, D. A.; Latgé, J.-P.; Nifantiev, N. E. Reinvestigation of Carbohydrate Specificity of EB-A2Monoclonal Antibody Used in the Immune Detection of *Aspergillus fumigatus* Galactomannan. *Heliyon* **2019**, *5*, No. e01173.

https://dx.doi.org/10.1021/jacs.9b11703
J. Am. Chem. Soc. 2020, 142, 1175−1179

JOC The Journal of Organic Chemistry
Article
Cite This: J. Org. Chem. 2018, 83, 12965−12976
pubs.acs.org/joc

Chemical Synthesis and Application of Biotinylated Oligo-α-(1 → 3)-D-Glucosides To Study the Antibody and Cytokine Response against the Cell Wall α-(1 → 3)-D-Glucan of *Aspergillus fumigatus*

Bozhena S. Komarova,[†,⊥] Sarah S. W. Wong,[‡,⊥] Maria V. Orekhova,[†] Yury E. Tsvetkov,[†] Vadim B. Krylov,[†] Anne Beauvais,[‡] Jean-Philippe Bouchara,[§] John F. Kearney,[∥] Vishukumar Aimanianda,[‡] Jean-Paul Latgé,[*,‡,#] and Nikolay E. Nifantiev[*,†]

[†]Laboratory of Glycoconjugate Chemistry, N.D. Zelinsky Institute of Organic Chemistry, Russian Academy of Sciences, Leninsky prospect 47, 119991 Moscow, Russia

[‡]Unité des *Aspergillus*, Institut Pasteur, 25 rue du Docteur Roux, 75724 Paris Cedex 15, France

[§]Groupe d'Etude des Interactions Hôte-Pathogène (EA 3142), UNIV Brest, 74521-49045 Angers, France

[∥]University of Alabama, Birmingham, Alabama 35294-2182, United States

Supporting Information

ABSTRACT: Biotinylated hepta-, nona- and undeca-α-(1 → 3)-D-glucosides representing long oligosaccharides of α-(1 → 3)-D-glucan, one of the major components of the cell walls of the fungal pathogen *Aspergillus fumigatus*, were synthesized for the first time via a blockwise strategy. Convergent assembly of the α-(1 → 3)-D-glucan chains was achieved by glycosylation with oligoglucoside derivatives bearing 6-*O*-benzoyl groups. Those groups are capable of remote α-stereocontrolling participation, making them efficient α-directing tools even in the case of large glycosyl donors. Synthetic biotinylated oligoglucosides (and biotinylated derivatives of previously synthesized tri- and penta-α-(1 → 3)-D-glucosides) loaded on streptavidin microtiter plates were shown to be better recognized by anti-α-(1 → 3)-glucan human polyclonal antibodies and to induce higher cytokine responses upon stimulation of human peripheral blood mononuclear cells than their natural counterpart, α-(1 → 3)-D-glucan, immobilized on a conventional microtiter plate. Attachment of the synthetic oligosaccharides equipped with a hydrophilic spacer via the streptavidin−biotin pair allows better spatial presentation and control of the loading compared to the random sorption of natural α-(1 → 3)-glucan. Increase of oligoglucoside length results in their better recognition and enhancement of cytokine production. Thus, using synthetic α-(1 → 3)-glucan oligosaccharides, we developed an assay for the host immune response that is more sensitive than the assay based on native α-(1 → 3)-glucan.

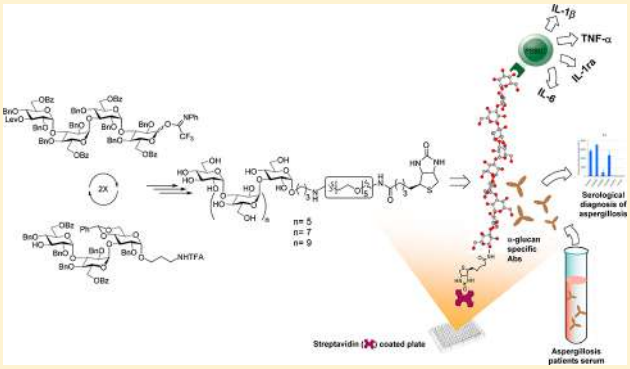

INTRODUCTION

Aspergillus fumigatus is the most ubiquitous airborne human fungal pathogen.[1] The fungal cell wall is at the forefront of interactions between the host and pathogen and thus requires extensive investigation. The cell wall of *A. fumigatus* is a complex and dynamic structure, and it is mainly composed of polysaccharides such as β-(1 → 3)-D-glucan, α-(1 → 3)-D-glucan, chitin, galactomannan and galactosaminogalactan.[2] α-(1 → 3)-Glucan is the major amorphous component of the *A. fumigatus* cell wall (accounting for approximately 20 and 40% of the conidium and mycelium cell walls, respectively).[3] It was shown in murine models of aspergillosis that α-(1 → 3)-glucan plays a role in innate and adaptive immunity.[4,5] However, the high molecular weight and water insolubility of α-(1 → 3)-glucan restrict its potential applications. Thus, synthetic α-(1 → 3)-glucooligosaccharides with different degrees of polymerization (dp values) will be invaluable tools for analyzing the host immune response against α-(1 → 3)-glucan,[6] especially since the size of the α-(1 → 3)-glucan molecule can be used to tune the immune response.[7]

We describe here the preparation of spacered hepta-, nona- and undeca-α-(1 → 3)-D-glucosides. During their synthesis, we also studied the applicability of methods used for controlling α-stereoselectivity in case of small glycosyl donors for glucosylations with much larger donors. The corresponding biotinylated derivatives of these oligosaccharides and previously synthesized[6] tri- and pentaglucoside derivatives were also prepared. These oligosaccharides of different chain lengths were used to analyze the immune response in comparison to

Received: May 4, 2018
Published: October 2, 2018

DOI: 10.1021/acs.joc.8b01142
J. Org. Chem. 2018, 83, 12965−12976

Scheme 1. Assembly of Hepta-, Nona- and Undecaglucosides 8, 10 and 11 Related to Fragments of *A. fumigatus* α-(1 → 3)-Glucan[a]

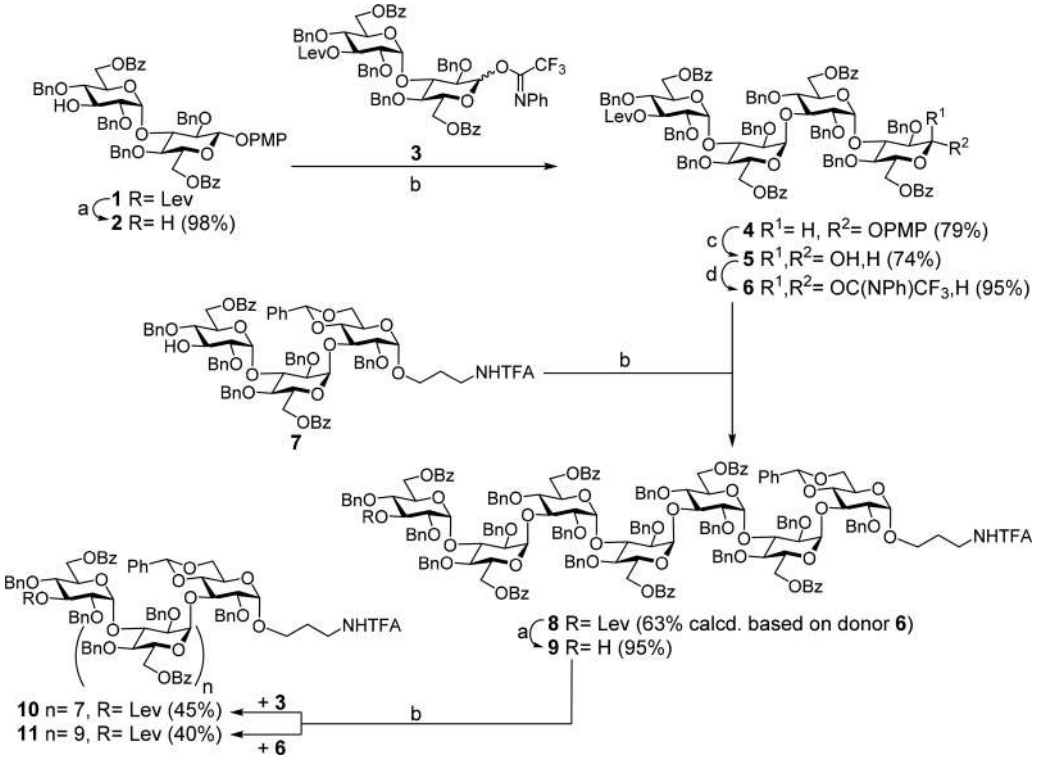

[a]Reagents and conditions: (a) $N_2H_4{\cdot}H_2O$, AcOH, (b) MeOTf, CH_2Cl_2, −35 °C → 0 °C, (c) CAN, H_2O, benzene, CH_3CN, (d) $CF_3C(NPh)Cl$, K_2CO_3, acetone.

that of the native α-(1 → 3)-glucan extracted from the *A. fumigatus* cell wall.

RESULTS AND DISCUSSION

Synthesis of Hepta-, Nona- and Undecasaccharides Related to α-(1 → 3)-Glucan of *A. fumigatus* and Their Biotinylated Conjugates. The synthesis of the target compounds, representing large oligosaccharides, was achieved by a convergent scheme based on the use of a tetrasaccharide glycosyl donor block (Scheme 1). The main problem in the assembly of oligoglucoside chains of this type is the 1,2-*cis* stereoselectivity in the synthesis of α-glucosides, which is known to be a nontrivial task.[8] To develop new methods for 1,2-*cis*-selective glycosylations, we have been constantly investigating the effect of stereoelectronic properties and other electronic interactions of protecting groups on the stereochemistry of the glycosylation,[9−14] and in particular, we have studied the possibility of remote anchimeric assistance. To achieve this goal, the use of the corresponding 6-*O*-benzoylated glycosylating agents was explored. The benzoyl group at O-6 is thought to possess an α-stereodirecting effect because of its ability to shield the β-face of the reaction intermediate, an oxocarbenium ion, the structure of which controls the stereochemistry of the glycosylation.[6,10,11,14]

We successfully employed a stereoselective α-glucosylation for the assembly of short α-glucooligosaccharide chains using mono- and disaccharide glucosyl donors.[6,10,14,15] Thus, we investigated the applicability of the discussed methods for achieving stereocontrolled α-glucosylations with large oligosaccharide glycosyl donors.

The synthesis of the tetrasaccharide donor bearing a stereodirecting benzoyl group at O-6 started from the transformation of disaccharide block **1** into disaccharide acceptor **2** by treatment with hydrazine acetate. The tetrasaccharide chain was built by the α-selective coupling of disaccharide donor **3** and acceptor **2** assisted by the α-directing benzoyl group at O-6 of the donor. After a routine purification, α-linked tetrasaccharide product **4** was isolated in 79% yield along with a minor amount of the β-linked byproduct (Scheme 1).

On the way to tetrasaccharide donor **6**, glycoside **4** was converted into hemiacetal **5** in 74% yield by removing the *p*-methoxyphenyl group with CAN in a heterogeneous mixture of CH_3CN, benzene and water.[6] Then, hemiacetal **5** was converted to trifluoroacetimidate donor **6** by treatment with *N*-phenyltrifluoroacetimidoyl chloride in the presence of K_2CO_3. The reaction of tetrasaccharide donor **6** with previously synthesized[6] acceptor **7** afforded stereochemically pure heptasaccharide **8** in 63% yield (based on donor **6**) after HPLC purification. The optimum order for mixing the reagents was found to be the simultaneous addition of donor **6** and the promoter to acceptor **7**, which was used in a two-fold excess and had been pretreated with activated molecular sieves. At the end of the reaction, the excess acceptor **7** was fully recovered.

Compound **8** was transformed into heptasaccharide acceptor **9** by removal of the levulinoyl group with hydrazine acetate. Glycosylation of the acceptor with 2 equiv of 6-*O*-benzoylated disaccharide donor **3** produced nonasaccharide **10** in 45% yield. Considering that the reversed order of addition of the reagents increased the yield of heptasaccharide **8**, the

DOI: 10.1021/acs.joc.8b01142
J. Org. Chem. 2018, 83, 12965−12976

Scheme 2. Deprotection of Hepta-, Nona- and Undecasaccharides 9, 10, and 11 and Preparation of Biotinylated Conjugates 20−22[a]

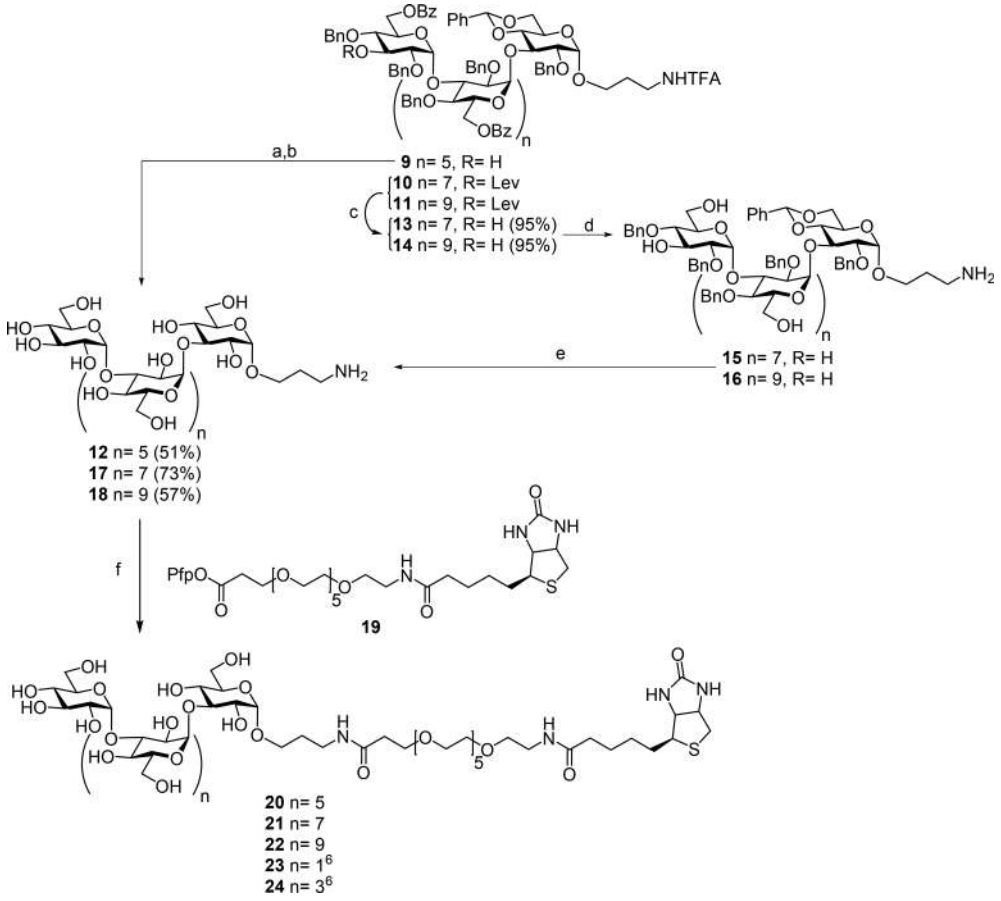

[a]Reagents and conditions: (a) $Pd(OH)_2/C$, H_2, MeOH, EtOAc, (b) NaOH, MeOH, (c) $N_2H_4{\cdot}H_2O$, AcOH, (d) NaOH, H_2O, CH_2Cl_2, MeOH, (e) Na, NH_3, THF, −78 °C, (f) **19**, Et_3N, DMF.

applicability of this trick was explored to increase the yield of nonasaccharide **10**. However, in this case, the reversed order of addition did not change the yield. In addition, the use of 2 equiv of costly acceptor **9** is not practical. Undecasaccharide **11** was prepared by glycosylation of acceptor **9** with 2 equiv of tetrasaccharide donor **6** in 40% yield.

The stereochemistry of the newly formed bonds in hepta-, nona- and undecasaccharides **8**, **10** and **11** and in tetrasaccharide **4** was confirmed by ^{1}H NMR spectroscopy. The $J_{1,2}$ coupling constants were in the range of 3.5−3.7 Hz, confirming the 1,2-*cis*-orientation of all glucosidic bonds and, in particular, the newly formed bonds. In addition, the chemical shifts of C-1 of each glucose residue (except that at the reducing end) were found to be in the range of δ 96−98 ppm, which is characteristic of carbons in α-glucosidic bonds. Whenever it was not possible to measure the $J_{1,2}$ constants, the HSQC correlations of H-1 and their C-1 counterpart indicated that all C-1 resonances were within δ 96−98 ppm. The full assignment of every ring signal was made for heptasaccharide **8** with the help of its HMBC spectrum, which additionally confirmed the α-configuration of every glycosidic bond in compound **8**.

To prepare free heptasaccharide **12**, compound **9** was initially subjected to hydrogenolysis over $Pd(OH)_2/C$ in a mixture of ethyl acetate and methanol. Then, the debenzylated product was treated with NaOH in MeOH to remove the *O*- and *N*-acyl protecting groups. Product **12** was isolated from the reaction mixture in 51% yield by size-exclusion chromatography (Scheme 2).

Due to the poor solubility of partially debenzylated intermediates of **14** and their adhesion to the Pd catalyst, we had to use sodium in liquid ammonia for the removal of the benzyl groups. Protected undecasaccharide **14** was treated with 1 M NaOH to remove the benzoyl groups. Then, a THF solution of **16** was treated with a solution of sodium in liquid ammonia. Compound **18** was obtained in 57% yield after purification by successive size-exclusion and C18 reversed-phase chromatography steps.

Applying the same procedure to nonasaccharide **13** (prepared from **10** by removal of the Lev group) led to free **17** in a high yield (73%). Notably, this yield exceeds that of the hydrogenolysis-debenzoylation sequence used for the synthesis of heptasaccharide **12**.

The structures of compounds **12**, **17** and **18** were confirmed by NMR and HRMS data. The absence of signals corresponding to aryl protons in the ^{1}H NMR spectra corroborated the removal of benzyl and benzoyl groups, and the integrals of the signals belonging to the anomeric protons at δ 5.41−5.35 and 4.96 confirmed that products **12**, **17** and **18** contained 7, 9 and 11 α-linked monosaccharides, respectively. The signals corresponding to the spacer methylene fragment

DOI: 10.1021/acs.joc.8b01142
J. Org. Chem. 2018, 83, 12965−12976

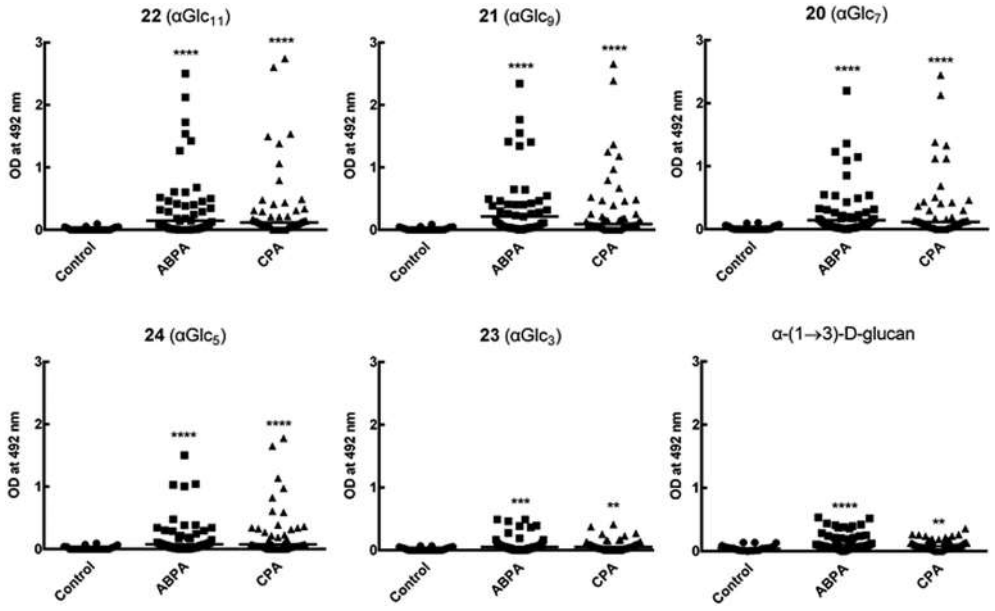

Figure 1. Detection of anti-α-(1 → 3)-glucan antibodies in the sera of patients with *Aspergillus* infections by enzyme-linked immunosorbent assay (ELISA) with oligosaccharide ligands **20**–**24** and α-(1 → 3)-glucan. The mean OD values of triplicate evaluations of each serum in the two patient groups with allergic bronchopulmonary aspergillosis (ABPA) or chronic pulmonary aspergillosis (CPA) were plotted in the graphs. The bars are the median of the mean OD values of the sera. The median OD values of both the ABPA and CPA serum groups obtained with the biotinylated oligosaccharides and the native α-(1 → 3)-glucan were all significantly higher than those of the control serum group (without *Aspergillus* infection) when compared by Kruskal–Wallis test and Dunn's multiple comparison test (****p < 0.0001, ***p < 0.001, **p < 0.01).

linked to the nitrogen shifted from δ >3.40 to <3.24, indicating deprotection of the amino group.

Hepta- (**12**), nona- (**17**) and undecasaccharide **18** were conjugated with biotinylated linker **19**[16] to give corresponding biotinylated derivatives **20**–**22**. The presence of biotin in the products was confirmed by MS and ^{1}H NMR analyses.

Detection of Anti-α-(1 → 3)-Glucan Antibodies in Sera of Patients with Aspergillus Infections Using α-(1 → 3)-Glucan-Related Oligosaccharides. Synthetic α-(1 → 3)-oligo glucosides **20**–**22** together with previously synthesized[6] tri- and pentaglucoside derivatives **23** and **24** were used to investigate the presence of anti-α-(1 → 3)-glucan-specific antibodies in sera from patients with allergic bronchopulmonary aspergillosis (ABPA) or chronic pulmonary aspergillosis (CPA). Biotinylated α-(1 → 3)-oligosaccharides were loaded on streptavidin microtiter plates, and the antibody titers against them, as well as against the natural α-(1 → 3)-glucan loaded on a microtiter plate, were evaluated. All biotinylated α-(1 → 3)-oligoglucosides **20**–**24** and the natural α-(1 → 3)-glucan were able to detect anti-α-(1 → 3)-glucan-specific antibodies in the serum samples (Figure 1).

The levels of α-(1 → 3)-glucan-specific antibodies in the sera of the immunocompetent aspergillosis patients (ABPA and CPA) were significantly higher than those in the sera of the control individuals. Moreover, the antibody titer values for the sera of ABPA and CPA patients were similar to those of the penta- to undecaoligosaccharides, while those obtained with the trisaccharide and the natural α-(1 → 3)-glucan were lower. Furthermore, the patients with invasive pulmonary aspergillosis (IPA) did not have antibodies against α-(1 → 3)-glucan due to suppression of their immune systems (data not shown).

The oligo-α-(1 → 3)-glucosides were also used to investigate the epitope recognized by two monoclonal antibodies (MAbs) against α-(1 → 3)-glucan, A16 and J558.[17] MAbs A16 and J558 were positively labeled on the surface of the *A. fumigatus* germ tubes (see Figure S1 in the Supporting Information). In contrast, the germ tubes of the triple α-(1 → 3)-glucan synthase mutant (Δ*ags1/ags2/ags3*), which does not produce α-(1 → 3)-glucan,[4] were not labeled with these two monoclonal antibodies (Figure S1). By ELISA, we showed that A16 and J558 were also able to recognize the oligo-α-(1 → 3)-glucosides from 5 to 11 dp (Figure 2). The slightly lower OD observed with the trisaccharide suggested that the epitope that is recognized by these monoclonal antibodies is linear and at least a tetra- or pentasaccharide. However, none of the monoclonal antibodies could recognize the natural α-(1 → 3)-glucan when it was loaded on the

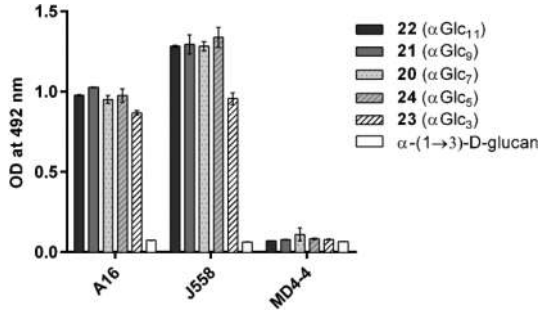

Figure 2. Identification of the oligo-α-(1 → 3)-glucan epitope recognized by monoclonal anti-α-(1 → 3)-glucan antibodies. Biotinylated α-(1 → 3)-glucan oligosaccharides were bound to streptavidin-coated plates, and natural α-(1 → 3)-glucan was loaded onto usual (streptavidin-uncoated) plates. The optical density (OD) value indicated the level of binding between the two monoclonal anti-α-(1 → 3)-glucan antibodies (A16 and J558) and the oligo-α-(1 → 3)-glucan. An antihen egg lysozyme IgM antibody (MD4–4) was used as a control. All the oligo-α-(1 → 3)-glucans were recognized by both monoclonal anti-α-(1 → 3)-glucan antibodies (A16 and J558), whereas the natural α-(1 → 3)-glucan was not recognized.

DOI: 10.1021/acs.joc.8b01142
J. Org. Chem. 2018, 83, 12965–12976

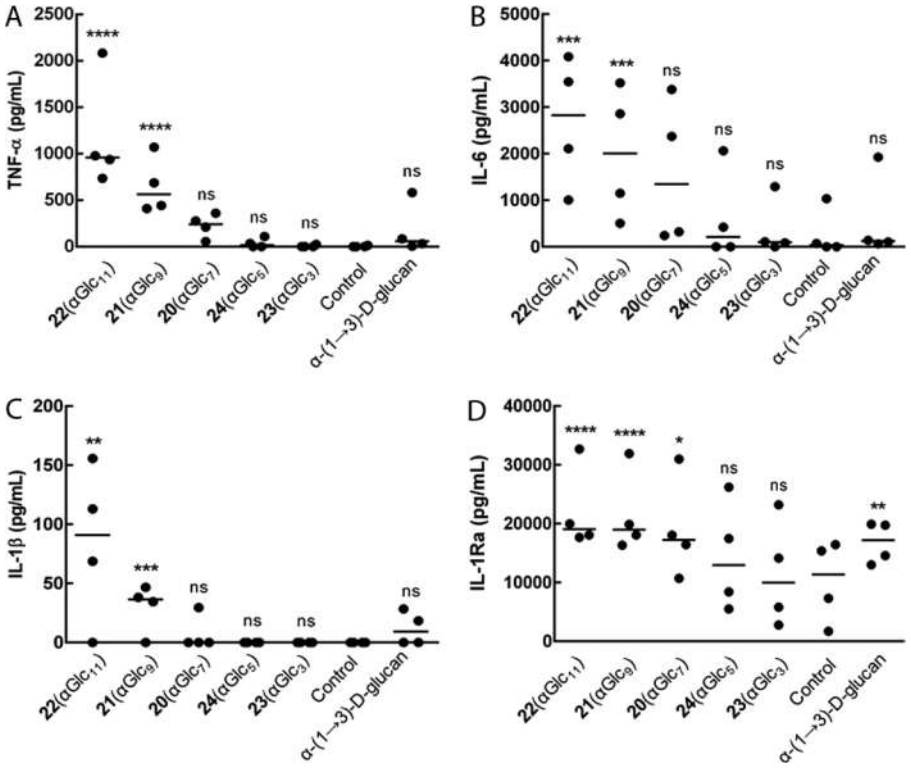

Figure 3. Levels of cytokine formation induced by the different biotinylated α-(1 → 3)-glucan oligosaccharides. PBMCs of four donors were coincubated with biotinylated α-(1 → 3)-glucan oligosaccharides immobilized on streptavidin microtiter plates or with free natural high-molecular-weight water-insoluble α-(1 → 3)-glucan (10 μg/mL) in suspension on nonstreptavidin plates. The coincubation was performed in RPMI supplemented with 10% normal human serum at 37 °C for 24 h. Thereafter, the supernatant was collected for quantification of the cytokines (A) TNF-α, (B) IL-6, (C) IL-1β and (D) IL-1Ra by ELISA. The dots represent the mean cytokine concentration of triplicate evaluations of samples from each donor, and the lines represent the median of the four mean values. The cytokine concentrations induced by the oligosaccharides and the native α-(1 → 3)-glucan were compared to that of the control by nonparametric one-way ANOVA (Kruskal–Wallis test) with Dunn's multiple comparison (****p < 0.0001, ***p < 0.001, **p < 0.01, *p < 0.05, ns = not significant). The length of the oligosaccharides is directly proportional to the level of cytokine induction. Undecasaccharide **22** and nonasaccharide **21** significantly induced the production of all tested cytokines, while the shorter oligosaccharides, **20**, **23**, and **24**, did not (A–D). Although some cytokine induction is observed with the natural α-(1 → 3)-glucan, the induction was only statistically significant for IL-1Ra (D).

microtiter plate, but they were able to react with the mycelial surface and recognize α-(1 → 3)-glucan in solution (data not shown). This difference could be explained by an unfavorable spatial presentation of this polymer when loaded on the plastic surface of the microtiter plate. The major conclusion of these experiments is that α-(1 → 3)-oligoglucosides can be used to diagnose *Aspergillus* infection (ABPA and CPA) in immunocompetent patients.

Ability of Synthetic α-(1 → 3)-Glucan-Related Oligosaccharides To Induce Cytokines. Peripheral blood mononuclear cells (PBMCs) isolated from human blood samples were stimulated by oligo-α-(1 → 3)-glucosides **20**–**24** that were preimmobilized on streptavidin plates or free in solution. The immunogenic effects of the preimmobilized oligosaccharides were compared to that of the natural α-(1 → 3)-glucan in suspension. The production of pro-inflammatory (TNF-α, IL-6 and IL-1β) and anti-inflammatory cytokines (IL-1Ra) by the PBMCs was then examined and compared with the control (unstimulated PBMCs). Under these experimental conditions, it was found that only the immobilized nona- and undecasaccharides, **21** and **22**, were able to stimulate cytokine production in PBMCs (Figure 3A–D). In addition, the cytokine induction level was directly proportional to the length of the oligo-α-(1 → 3)-glucosides (Figure 3A–D).

Upon immobilization and incubation with PBMCs, the biotinylated nona- and undecasaccharides, **21** and **22**, induced significantly higher cytokine production compared to that in the unstimulated control, while no significant induction was observed with shorter oligo-α-(1 → 3)-glucosides **20**, **24** and **23** (although there was a trend in stimulating the production of cytokines by heptasaccharide **20**). Under these experimental conditions, the free natural cell wall α-(1 → 3)-glucan was capable of inducing only low levels of pro-inflammatory cytokines (the levels were not significantly different from those in the controls), but a significant induction of the anti-inflammatory cytokine IL-1Ra was observed (Figure 3D). In contrast, microtiter-plate-loaded natural α-(1 → 3)-glucan and free oligosaccharides failed to stimulate cytokine secretion in PBMCs (data not shown).

However, the ELISA and cytokine data obtained with biotinylated oligosaccharides **20**–**24** and natural cell wall α-(1 → 3)-glucan cannot be directly compared since very different protocols for immobilization on the microtiter plates were used for these compounds (the biotinylated and natural oligosaccharides). Despite these discrepancies, our results indicated that the spatial presentation of the oligosaccharides on the streptavidin plates is favorable for analysis of the immune response to cell wall polysaccharides.

DOI: 10.1021/acs.joc.8b01142
J. Org. Chem. 2018, 83, 12965–12976

Similar observations also apply to other immunological studies on cell wall polysaccharides, which demonstrated that shorter soluble oligosaccharides in their free form were not able to elicit significant immune responses despite associating with their respective pattern recognition receptors (PRRs).[7,18−21]

All these examples are consistent with the "fibril hypothesis", which proposes that short soluble oligosaccharides can bind to a single pattern-recognition receptor without inducing an immune response, whereas fibrillar polysaccharides can be sensed by several PRR molecules, leading to increased triggering of signaling events and activation of the immune response.[22,23] Another explanation is that the water-insoluble polysaccharide is phagocytosed and degraded to small fragments in the phagolysosome by reactive oxidants. This random degradation will lead to the production of oligosaccharides of different sizes (as shown for bacterial polysaccharides),[24] which can then stimulate an immune response. However, plate-loaded natural α-(1 → 3)-glucan failed to induce cytokine secretion in PBMCs, which could be explained by the loss of epitopic signature upon loading.

■ SUMMARY AND OUTLOOK

In conclusion, hepta-, nona- and undecasaccharides representing larger fragments of α-(1 → 3)-glucan were prepared for the first time. Highly α-selective oligosaccharide chain assembly was achieved using a tetrasaccharide glycosyl donor bearing a benzoyl group at O-6, which controls α-bond formation due to remote stereodirecting assistance. The corresponding biotinylated derivatives of the oligo-α-(1 → 3)-D-glucosides represent a set of oligosaccharides that could be used to investigate glycan−protein interactions and cytokine induction associated with the immune response to *A. fumigatus*.

The obtained immunological results showed that synthetic oligo-α-(1 → 3)-glucosides are specifically recognized by aspergillosis patient antibodies and are able to induce the production of pro- and anti-inflammatory cytokines. The length of the synthetic oligo-α-(1 → 3)-glucoside influences the immune response. The immune response against synthesized oligoglucosides was studied with the help of their biotinylated derivatives immobilized on streptavidin-coated plate. Oligosaccharide recognition using such a protocol is more efficient than using a natural cell wall α-(1 → 3)-glucan, whose drawbacks are high molecular weight and water insolubility. Oligoglucosides attached to the microtiter well surface via a streptavidin−biotin pair revealed the critical importance of controlled immobilization and spatial presentation of these ligands for efficient immune response.

Finally, these biotinylated reagents will be invaluable in (1) the development of diagnostic tools for aspergillosis, in distinguishing immunocompetent and immunocompromised patients with aspergillosis and in (2) improving our understanding of the interactions of α-(1 → 3)-glucan with host immune systems, especially the spatial epitope structure of α-(1 → 3)-glucan in eliciting an immune response, and these results should present new perspectives for the identification and structural assessment of host immune cell receptor(s) for α-(1 → 3)-glucan.

■ EXPERIMENTAL SECTION

Chemical Synthesis of Biotinylated Oligosaccharides 20−22: General Methods. All glycosylation reactions were carried out under dry Ar. Molecular sieves MS AW-300 for glycosylation reactions were activated prior to use at 180 °C under a vacuum generated by an oil pump for 1 h. Dichloromethane was successively distilled from diethanolamine, P_2O_5, and CaH_2 under Ar. For the glycosylation reactions, dichloromethane was freshly redistilled from CaH_2. Pyridine was dried by distillation from P_2O_5. Analytical thin-layer chromatography (TLC) was performed on silica gel 60 F254 aluminum sheets (Merck), and visualization was accomplished using UV light or by charring at 150 °C with 10% (v/v) H_3PO_4 in ethanol. Column chromatography was performed on silica gel 60, 40−63 μm (Merck). Preparative HPLC separations were performed on a Supelcosil LC-SI column (5 μm, 250 × 21.2 mm) at a flow rate of 8 mL/min with a K-2401 refractive index detector (Knauer). Data processing was performed using MultiChrom Software. Optical rotation values were measured using a JASCO DIP-360 polarimeter at ambient temperature in the specified solvent. ^{1}H and ^{13}C NMR spectra were recorded on Bruker AV-400, Bruker AV-600, and Bruker Avance spectrometers. Chemical shifts were referenced to residual solvent signals. Signals in the ^{1}H and ^{13}C NMR spectra were assigned using COSY, TOCSY, and ^{1}H−^{13}C HSQC techniques. High-resolution mass spectra were acquired by electrospray ionization on a Micro-TOF II (Bruker Daltonics) instrument.

*p-Methoxyphenyl 6-O-benzoyl-2,4-di-O-benzyl-α-D-glucopyranosyl-(1 → 3)-6-O-benzoyl-2,4-di-O-benzyl-β-D-glucopyranoside (**2**).* Disaccharide **1** (150 mg, 0.135 mmol) was dissolved in 1.2 mL of a 1 M solution of hydrazine hydrate in pyridine−acetic acid (3:2). The mixture was stirred for 2 h, then acetylacetone (240 μL, 2.4 mmol) was added, and then the solvents were removed under reduced pressure. Product **2** (134 mg, 98%) was purified by column chromatography (toluene−acetonitrile 20:1). Foam, R_f 0.44 (light petroleum/EtOAc 2:1); $[\alpha]_D^{22}$ +45.2 (c = 1 in $CHCl_3$); ^{1}H NMR (600 MHz, $CDCl_3$) δ_H 8.11 (d, 2H, α-Bz), 8.06 (d, 2H, α-Bz), 7.67 (t, 1H, Ar), 7.60−7.50 (m, 3H, Ar), 7.46−7.18 (m, 22H, Ar), 7.04 (d, J 9.1 Hz, 2H, C_6H_4OMe), 6.78 (d, J 9.1 Hz, 2H, C_6H_4OMe), 5.67 (d, $J_{1^b,2^b}$ 3.7 Hz, 1H, H-1^b), 5.13 (d, J_{gem} 10.1 Hz, 1H, PhCH_2), 5.06 (d, J_{gem} 11.3 Hz, 1H, PhCH_2), 4.97 (d, $J_{1^a,2^a}$ 7.5 Hz, 1H, H-1^a), 4.94 (d, J_{gem} 11.1 Hz, 1H, PhCH_2), 4.81 (d, J_{gem} 10.1, 1H, PhCH_2), 4.74 (d, J_{gem} 11.8 Hz, 1H, PhCH_2), 4.72−4.69 (m, 2H, H-6A^a, PhCH_2), 4.66−4.59 (m, 2H, PhCH_2), 4.56 (m, 1H, H-5^b), 4.45−4.38 (m, 2H, H-6B^a, H-6A^b), 4.30 (t, $J_{3^b,2^b} = J_{3^b,4^b}$ 9.7 Hz, 1H, H-3^b), 4.22 (dd, $J_{6Bb,5b}$ 4.6 Hz, $J_{6B^b,6B^a}$ 12.1 Hz, 1H, H-6B^b), 4.14 (t, $J_{3^a,2^a} = J_{3^a,4^a}$ 8.6 Hz, H-3^a), 3.89−3.83 (m, 3H, H-5^a, H-2^a, H-4^a), 3.82 (s, 3H, OCH_3), 3.56 (t, $J_{4^b,3^b} = J_{4^b,5^b}$ 9.8 Hz, 1H, H-4^b), 3.49 (dd, $J_{2^b,1^b}$ 3.6 Hz, $J_{2^b,3^b}$ 9.8 Hz, 1H, H-2^b); ^{13}C NMR (150.9 MHz, $CDCl_3$) δ_C 166.1 (PhC(O)), 155.4 ($C_6H_4OCH_3$), 151.3 ($C_6H_4OCH_3$), 137.5, 133.1, 132.9, 130.1, 129.7, 128.7, 128.6, 128.5, 128.4, 128.3, 128.1, 128.0, 127.9, 127.8, 127.3 (Ar), 118.3, 114.5 ($C_6H_4OCH_3$), 102.9 (C-1^a), 96.6 (C-1^b), 79.9 (C-2^a), 79.6, 79.5 (C-3^a, C-2^b), 78.9 (C-4^a), 78.1 (C-4^b), 74.9, 74.7, 74.0 (PhCH_2), 73.9 (C- 3^b), 73.5 (PhCH_2), 72.9 (C-5^a), 68.8 (C-5^b), 63.5 (C-6^a, C-6^b), 55.6 (OCH_3). Anal. calcd for $C_{61}H_{60}O_{14}$: C, 72.03; H, 5.95. Found: C, 71.81; H, 5.80.

*p-Methoxyphenyl 6-O-benzoyl-2,4-di-O-benzyl-3-O-levulinoyl-α-D-glucopyranosyl-(1 → 3)-6-O-benzoyl-2,4-di-O-benzyl-α-D-glucopyranosyl-(1 → 3)-6-O-benzoyl-2,4-di-O-benzyl-α-D-glucopyranosyl-(1 → 3)-6-O-benzoyl-2,4-di-O-benzyl-β-D-glucopyranoside (**4**).* A solution of donor **3** (318 mg, 0.270 mmol) and acceptor **2** (229 mg, 0.225 mmol) in dry CH_2Cl_2 (5.5 mL) was stirred with MS AW 300 (550 mg) for 1 h. Then, the mixture was cooled to −35 °C, and MeOTf (30.5 μL, 0.270 mmol) was added. The solution was allowed to warm slowly to −10 °C. After 2 h, methanol (30 μL) and triethylamine (60 μL) were added. The solids were removed by filtration and washed with CH_2Cl_2, and the filtrate was washed with saturated aqueous $NaHCO_3$ and water. The organic layer was separated, and the solvent was evaporated under reduced pressure. The residue was purified by column chromatography (light petroleum/EtOAc 2:1) and by HPLC (toluene/acetonitrile 15:1) to afford foam **4** (355 mg, 0.178 mmol, 79%) and **4*β*** (13 mg, 0.0065 mmol, 3%).

4: Foam, R_f 0.17 (light petroleum/EtOAc 2:1); $[\alpha]_D^{26}$ +103.0 (c = 1 in $CHCl_3$); ^{1}H NMR (600 MHz, $CDCl_3$) δ_H 8.13−8.05 (m, 8H, α-Bz), 7.66−6.98 (m, 54H, Ar), 6.76 (d, J 9.1 Hz, 2H, C_6H_4OMe), 5.78

DOI: 10.1021/acs.joc.8b01142
J. Org. Chem. 2018, 83, 12965−12976

(d, $J_{1^c,2^c}$ 3.6 Hz, 1H, H-1^c), 5.71 (t, $J_{3^d,2^d} = J_{3^d,4^d}$ 9.6 Hz, 1H, H- 3^d), 5.66 (d, $J_{1^d,2^d}$ 3.5 Hz, 1H, H-1^d), 5.64 (d, $J_{1^b,2^b}$ 3.7 Hz, 1H, H-1^b), 5.08 (d, J_{gem} 10.5 Hz 1H, PhCH_2), 4.92 (d, $J_{1^a,2^a}$ 7.4 Hz, 1H, H-1^a), 4.90–4.82 (m, 4H, 4PhCH_2), 4.71–4.67 (m, 3H, 2PhCH_2, H-6A^a), 4.63 (m, 1H, H-5^b), 4.57–4.47 (m, 10H, H-5^c, H-5^d, H-3^b, H-6A^b, 7PhCH_2), 4.46–4.35 (m, 6H, H-6A^c, H-6A^d, H-6B^a, H-3^c, 2PhCH_2), 4.19–4.14 (m, 2H, H-3^a, H-6B^b), 4.10–4.04 (m, 7H, H-6B^c, H-6B^d), 3.88–3.81 (m, 4H, H-4^a, H-2^a, H-5^a, H-4^c), 3.80 (s, 1H, OCH_3), 3.76 (t, $J_{4^b,3^b} = J_{4^b,5^b}$ 9.7 Hz, 1H, H-4^b), 3.63- 3.54 (m, 3H, H-2^b, H-2^c, H-4^d), 3.50 (dd, $J_{2^d,1^d}$ 3.5 Hz, $J_{2^d,3^d}$ 10.1 Hz, 1H, H-2^c), 2.66–2.63 (m, 2H, CH_2CH$_2$C(O)CH$_3$), 2.47–2.43 (m, 2H, CH$_2$CH_2C(O)CH$_3$), 2.17 (s, 3H, CH_3); ^{13}C NMR (150.9 MHz, CDCl$_3$) δ_C 206.1 (CH$_3$C(O)CH$_2$), 171.8 (CH$_2$C(O)O), 166.1 (PhC(O)), 155.3 (C_6H$_4$OCH$_3$), 151.3 (C_6H$_4$OCH$_3$), 137.7, 137.6, 137.5, 137.4, 133.0, 130.2, 130.1, 129.7, 128.5, 128.4, 128.3, 128.2, 128.1, 127.7, 127.6, 127.5, 127.3, 127.1, 126.7, 126.6 (Ar), 118.3, 114.5 (C_6H$_4$OCH$_3$), 102.8 (C-1^a), 96.9 (C-1^d), 95.9, 95.8 (C-1^b, C-1^c), 79.72, 79.66 (C-2^a, C-4^b), 79.2 (C-3^a, C-4^c), 78.83, 78.75, 78.61 (C-4^a, C-2^c, C-2^b), 77.7 (C-2^d), 76.5 (C-4^d), 76.1 (C-3^c), 75.4 (C-3^b), 74.3 (PhCH$_2$), 74.1 (C-3^b, PhCH$_2$), 73.4, 73.3, 73.2, 73.1 (PhCH$_2$), 72.8 (C-5^a), 68.5 (C-5^b, C-5^c, C-5^d), 63.7 (C-6^a), 63.5 (C-6^b), 63.3 (C-6^c), 63.2 (C-6^d), 55.6 (OCH$_3$), 37.8 (CH$_2$CH$_2$C(O)CH$_3$), 29.8 (CH$_3$), 28.1 (CH$_2$CH$_2$C(O)CH$_3$). Anal. calcd for $C_{120}H_{118}O_{28}$: C, 71.77; H, 5.92. Found: C, 71.73; H, 5.77.

4*β*: Foam, R_f 0.17 (light petroleum/EtOAc 2:1); $[\alpha]_D^{26}$ +56.8 (*c* = 1 in CHCl$_3$); ^{1}H NMR (600 MHz, CDCl$_3$) δ_H 8.12–8.03 (m, 8H, *o*-Bz), 7.65–7.10 (m, 52H, Ar), 6.98 (d, *J* 9.1 Hz, 2H, C_6H_4OMe), 6.75 (d, *J* 9.1 Hz, 2H, C_6H_4OMe), 5.78 (t, $J_{3^d,2^d} = J_{3^d,4^d}$ 9.8 Hz, 1H, H-3^d), 5.63 (d, $J_{1^d,2^d}$ 3.5 Hz, 1H, H-1^d), 5.58 (d, $J_{1^b,2^b}$ 3.4 Hz, 1H, H-1^b), 5.19 (d, $J_{1^c,2^c}$ 7.9 Hz, 1H, H-1^c), 5.12 (d, J_{gem} 10.5 Hz, 1H, PhCH_2), 5.05 (d, J_{gem} 11.0 Hz, 1H, PhCH_2), 4.99 (d, J_{gem} 11.0 Hz, 1H, PhCH_2), 4.94 (d, J_{gem} 12.3 Hz, 1H, PhCH_2), 4.92 (d, J_{gem} 13.0 Hz, 1H, PhCH_2), 4.89 (d, $J_{1^a,2^a}$ 7.6 Hz, 1H, H-1^a), 4.86 (d, J_{gem} 11.6 Hz, 1H, PhCH_2), 4.76 (d, J_{gem} 9.9 Hz, 1H, PhCH_2), 4.68–4.56 (m, 6H, 4PhCH_2, H-5^d, H-6A^a, H-3^b), 4.55–4.41 (m, 8H, H-5^b, H-6A^b, H-6A^c, 5PhCH_2), 4.40–4.31 (m, 4H, H-A^c, H-6B^a, H-6A^d, H-6B^b), 4.19–4.12 (m, 2H, H-6B^c, H-6B^d), 4.05 (t, $J_{3^a,2^a} = J_{3^a,4^a}$ 9.6 Hz, 1H, H-3^a), 3.95 (t, $J_{3^c,3^c} = J_{3^c,4^c}$ 9.0 Hz, 1H, H-3^c), 3.86–3.77 (m, 6H, H-4^c, H-5^a, H-2^a, OCH_3), 3.73–3.68 (m, 1H, H-4^a, H-4^d), 3.62–3.53 (m, 4H, H-2^b, H-2^c, H-4^b, H-2^d), 3.24 (m, 1H, H-5^c), 2.68–2.65 (m, 2H, CH_2CH$_2$C(O)CH$_3$), 2.52–2.47 (m, 2H, CH$_2$CH_2C(O)CH$_3$), 2.17 (s, 3H, CH_3); ^{13}C NMR (150.9 MHz, CDCl$_3$) δ_C 206.1 (CH$_3$C(O)CH$_2$), 171.8 (CH$_2$C(O)O), 166.1 (PhC(O)), 155.3 (C_6H$_4$OCH$_3$), 151.3 (C_6H$_4$OCH$_3$), 137.8, 137.6, 137.5, 137.3, 133.0, 130.1, 129.7, 129.6, 128.6, 128.5, 128.4, 128.3, 128.2, 128.1, 128.0, 127.9, 127.7, 127.6, 127.5, 127.4, 126.9 (Ar), 118.2, 114.5 (C_6H$_4$OCH$_3$), 102.8 (C-1^a), 102.5 (C-1^c), 96.8 (C-1^d), 96.3 (C-1^b), 81.6, 81.5 (C-2^b, C-2^c), 81.1 (C-3^a), 80.6 (C-2^a), 79.2 (C-4^c), 78.7 (C-3^c), 78.3 (C-4^a), 77.8 (C-2^d), 77.2 (C-3^b), 76.3 (C-4^d), 75.9 (C-4^b, PhCH$_2$), 75.6, 74.5, 74.2, 73.5, 73.4, 73.1 (C-3^d, PhCH$_2$), 72.7 (C-5^a), 72.3 (C-5^c), 69.3 (C-5^b), 68.8 (C-5^d), 63.9 (C-6^b), 63.8 (C-6^a), 63.2 (C-6^c), 62.8 (C-6^d), 55.6 (OCH$_3$), 37.7 (CH$_2$CH$_2$C(O)CH$_3$), 29.7 (CH$_3$), 28.1 (CH$_2$CH$_2$C(O)CH$_3$). Anal. calcd for $C_{120}H_{118}O_{28}$: C, 71.77; H, 5.92. Found: C, 71.65; H, 5.83.

6-O-Benzoyl-2,4-di-O-benzyl-3-O-levulinoyl-α-D-glucopyranosyl-(1 → 3)-6-O-benzoyl-2,4-di-O-benzyl-α-D-glucopyranosyl-(1 → 3)-6-O-benzoyl-2,4-di-O-benzyl-α-D-glucopyranosyl-(1 → 3)-6-O-benzoyl-2,4-di-O-benzyl-β-D-glucopyranose (***5***). CAN (482 mg, 0.879 mmol) was added to a suspension of tetrasaccharide **4** (353 mg, 0.176 mmol) in a mixture of acetonitrile/water/benzene (13.6:3.3:1, 14 mL) at 0 °C. The resulting mixture was stirred at this temperature until TLC showed disappearance of the starting material (20 min). The mixture was diluted with EtOAc and washed with saturated aqueous NaHCO$_3$ and water. The organic layer was separated, and the solvent was evaporated under reduced pressure. Purification of the residue by column chromatography (toluene/EtOAc 7:1) afforded title compound **5** (249 mg, 74%) as a syrupy mixture of *α*- and *β*-anomers. Syrup, R_f (toluene/EtOAc 5:1) 0.25; ^{1}H NMR (600 MHz, CDCl$_3$) δ_H 8.16–8.06 (m, Ar), 7.68–6.96 (m, Ar), 5.78–5.75 (m, H-1$^{c\alpha}$, H-1$^{c\beta}$), 5.70 (t, *J* 9.6 Hz, H-3$^{d\alpha}$, H-3$^{d\beta}$), 5.67 (d, *J* 3.8 Hz, H-1$^{d\alpha}$, H-1$^{d\beta}$), 5.66–5.64 (m, H-1$^{b\beta}$, H-1$^{b\alpha}$), 5.29 (m, $J_{1^{a\alpha},2^{a\alpha}}$ 3.7 Hz, H-1$^{a\alpha}$), 4.99 (d, J_{gem} 10.6 Hz, PhCH_2), 4.87 (d, J_{gem} 12.1 Hz, PhCH_2), 4.85–4.79 (m, H-1$^{a\beta}$, PhCH_2), 4.79–4.72 (m, PhCH_2), 4.71–4.36 (m, PhCH_2, H-5$^{b\alpha}$, H-5$^{c\alpha}$, H-5$^{d\alpha}$, H-5$^{b\beta}$, H-5$^{c\beta}$, H-5$^{d\beta}$, H-6A$^{a\alpha}$, H-6A$^{a\beta}$, H-6B$^{a\alpha}$, H-6B$^{a\beta}$, H-6A$^{b\alpha}$, H-6A$^{c\alpha}$, H-6A$^{d\alpha}$, H-6A$^{b\beta}$, H-6A$^{c\beta}$, H-6A$^{d\beta}$, H-3$^{a\alpha}$, H-3$^{b\alpha}$, H-3$^{c\alpha}$, H-3$^{b\beta}$, H-3$^{c\beta}$), 4.33 (m, H-5$^{a\alpha}$), 4.24–4.04 (m, H-3$^{a\beta}$, H-6B$^{b\alpha}$, H-6B$^{c\alpha}$, H-6B$^{d\alpha}$, H-6B$^{b\beta}$, H-6B$^{c\beta}$, H-6B$^{d\beta}$), 3.88–3.75 (m, H-4$^{a\alpha}$, H-4$^{a\beta}$, H-4$^{b\alpha}$, H-4$^{b\beta}$, H-4$^{c\alpha}$, H-4$^{c\beta}$, H-5$^{a\beta}$), 3.68 (dd, $J_{2^{a\alpha},1^{a\alpha}}$ 3.6 Hz, $J_{2a^{\alpha},3a^{\alpha}}$ 9.2 Hz, H-2$^{a\alpha}$), 3.61–3.53 (m, H-4$^{d\alpha}$, H-4$^{d\beta}$, H-2$^{a\beta}$, H-2$^{b\alpha}$, H-2$^{b\beta}$, H-2$^{c\alpha}$, H-2$^{c\beta}$), 3.47–3.43 (dd, H-2$^{d\alpha}$, H-2$^{d\beta}$), 2.66–2.60 (m, CH_2CH$_2$C(O)CH$_3$), 2.46–2.43 (m, CH$_2$CH_2C(O)CH$_3$), 2.17 (s, CH_3); ^{13}C NMR (150.9 MHz, CDCl$_3$) δ_C 206.1 (CH$_3$C(O)CH$_2$), 171.8 (CH$_2$C(O)O), 166.2, 166.1 (PhC(O)), 138.0, 137.8, 137.6, 137.5, 137.4, 136.9, 133.1, 133.0, 130.2, 130.1, 130.0, 129.7, 128.6, 128.5, 128.4, 128.3, 128.2, 128.1, 127.7, 127.5, 127.4, 127.3, 127.1, 127.0, 126.7, 126.6 126.5 (Ar), 97.9 (C-1^{ab}), 96.9, 95.8, 95.7 (C-1), 90.4 (C-1$^{a\alpha}$), 81.1, 79.9, 79.7, 79.2, 78.8, 78.7, 78.6, 78.5, 78.4, 77.7, 76.5, 76.1 (C-2, C-4, C-3), 75.3, 74.9, 74.6, 74.2, 74.0, 73.3, 73.0, 72.9, 72.7 (C-3, C-5, PhCH$_2$), 68.5, 68.3, 68.2 (C-5), 63.8, 63.5, 63.4, 63.3 (C-6), 55.6 (OCH$_3$), 37.8 (CH$_2$CH$_2$C(O)CH$_3$), 29.8 (CH$_3$), 28.1 (CH$_2$CH$_2$C(O)CH$_3$). Anal. calcd for $C_{113}H_{112}O_{27}$: C, 71.35; H, 5.94. Found: C, 71.22; H, 5.83.

O-(6-O-Benzoyl-2,4-di-O-benzyl-3-O-levulinoyl-α-D-glucopyranosyl-(1 → 3)-6-O-benzoyl-2,4-di-O-benzyl-α-D-glucopyranosyl-(1 → 3)-6-O-benzoyl-2,4-di-O-benzyl-α-D-glucopyranosyl-(1 → 3)-6-O-benzoyl-2,4-di-O-benzyl-β-D-glucopyranosyl) N-phenyltrifluoroacetimidate (***6***). *N*-Phenyltrifluoroacetimidoyl chloride (16.2 *μ*L, 0.10 mmol) and K$_2$CO$_3$ (22 mg, 0.15 mmol) were added to a solution of hemiacetal **6** (128 mg, 0.067 mmol) in acetone (1.3 mL). The reaction mixture was vigorously stirred until consumption of the starting material (monitored by TLC). The mixture was filtered through a Celite pad, and the filtrate was concentrated under reduced pressure. The residue was subjected to column chromatography (toluene/EtOAc 12:1) to provide **6** (132 mg, 95%) as a syrupy mixture of *α*- and *β*-anomers. Syrup, R_f 0.41 (light petroleum/EtOAc 1.5:1); ^{1}H NMR (600 MHz, CDCl$_3$) δ_H 8.14–8.06 (m, *α*-Bz), 7.66–7.01 (m, Ar), 6.80 (d, NPh), 6.71 (d, NPh), 6.49 (bs, 1H, H-1$^{a\alpha}$), 5.83 (bs, 1H, H-1$^{a\beta}$), 5.79–5.76 (mix. H-1), 5.76–5.70 (mix. H-3^d), 5.68–5.63 (mix. H-1), 5.57 (d, *J* 3.6 Hz, H-1$^{\beta}$), 4.93–4.61 (PhCH_2, H-5, H-6), 4.60–4.35 (PhCH_2, H-3, H-5, H-6), 4.30–4.10 (H-5$^{a\alpha}$, H-3$^{a\beta}$, H-6), 3.90–3.74 (H-2, H-4), 3.64–3.49 (H-2, H-4), 2.68–2.63 (CH_2CH$_2$C(O)CH$_3$), 2.48–2.44 (CH$_2$CH_2C(O)CH$_3$), 2.17 (s, CH_3); ^{13}C NMR (150.9 MHz, CDCl$_3$) δ_C 206.0 (CH$_3$C(O)CH$_2$), 171.8 (CH$_2$C(O)O), 166.1 (PhC(O)O), 137.9, 137.8, 137.6, 133.1, 133.0, 130.3, 129.7, 128.7, 128.5, 128.4, 128.3, 128.2, 128.1, 128.0, 127.8, 127.6, 127.5, 127.3, 127.2, 127.1, 126.9, 126.8, 124.3, 119.5, 119.3 (Ar), 97.0, 96.2, 95.9, 95.7 (C-1), 92.5 (C-1$^{a\alpha}$), 79.8, 79.6, 79.4, 79.3, 79.1, 79.0, 78.9, 78.8, 78.4, 78.2, 78.0, 77.8, 76.8 (C-2, C-4), 76.4, 75.7, 75.4, 75.2, 74.5, 74.2, 74.1, 73.5, 73.4, 73.3, 73.2, 73.1, 72.8 (PhCH$_2$, C-3), 71.0 (C-5$^{a\alpha}$), 68.7, 68.6, 68.4 (C-5), 63.6, 63.4, 63.3, 63.2 (C-6), 37.8 (CH$_2$CH$_2$C(O)CH$_3$), 29.7 (CH$_3$), 28.2 (CH$_2$CH$_2$C(O)CH$_3$). Anal. calcd for $C_{121}H_{116}F_3NO_{27}$: C, 70.10; H, 5.64. Found: C, 70.22; H, 5.73.

3-Trifluoroacetamidopropyl 6-O-benzoyl-2,4-di-O-benzyl-3-O-levulinoyl-α-D-glucopyranosyl-(1 → 3)-6-O-benzoyl-2,4-di-O-benzyl-α-D-glucopyranosyl-(1 → 3)-6-O-benzoyl-2,4-di-O-benzyl-α-D-glucopyranosyl-(1 → 3)-6-O-benzoyl-2,4-di-O-benzyl-α-D-glucopyranosyl-(1 → 3)-6-O-benzoyl-2,4-di-O-benzyl-α-D-glucopyranosyl-(1 → 3)-2-O-benzyl-4,6-O-benzylidene-α-D-glucopyranoside (***8***). A solution of acceptor 7[6] (414 mg, 0.295 mmol) in dry CH$_2$Cl$_2$ (5 mL) was stirred with MS AW 300 (660 mg) for 1 h. Then, the mixture was cooled to −35 °C, and a solution of **6** (245 mg, 0.118 mmol) in CH$_2$Cl$_2$ (1.1 mL) and a solution of MeOTf (13 *μ*L, 0.116 mmol) in CH$_2$Cl$_2$ (0.275 mL) were slowly added over 1 h. The solution was allowed to warm slowly to −10 °C, and then methanol (50 *μ*L) and triethylamine (50 *μ*L) were added. The solids were removed by filtration and washed with CH$_2$Cl$_2$. The filtrate was washed with saturated aqueous NaHCO$_3$ and water, the organic layer was separated, and the solvent was evaporated under reduced pressure. The residue was purified by column chromatography (light

DOI: 10.1021/acs.joc.8b01142
J. Org. Chem. 2018, 83, 12965–12976

petroleum/EtOAc 3:1→ 1:1) and by HPLC (hexane/EtOAc 1.3:1) to afford **8** (245 mg, 0.0745 mmol, 63%) and recover **7** (256 mg, 0.182 mmol). Compound **8**, foam, R_f 0.16 (hexane/EtOAc 1.5:1); $[\alpha]_D^{23}$ +175.3 (c = 1, $CHCl_3$); ^{1}H NMR (600 MHz, $CDCl_3$) δ_H 8.16−8.05 (m, 12H, α-Bz), 7.67−7.02 (m, 81H, Ar, NH), 6.94−6.89 (m, 4H, Ar), 6.86 (d, 2H, Ar), 6.25 (d, 2H, Ar), 5.73 (d, 1H, $J_{1^d,2^d}$ 3.7 Hz, H-1^d), 5.70 (d, 1H, $J_{1^c,2^c}$ 3.7 Hz, H-1^c), 5.66 (t, 1H, $J_{3^g,4^g} = J_{3^g,2^g}$ 9.6 Hz, H-3^g), 5.63 (d, 1H, $J_{1^f,2^f}$ 3.7 Hz, H-1^f), 5.61 (d, 1H, $J_{1^b,2^b}$ 3.7 Hz, H-1^b), 5.60 (d, 1H, $J_{1^e,2^e}$ 3.7 Hz, H-1^e), 5.58 (d, 1H, $J_{1^g,2^g}$ 3.6 Hz, H-1^g), 5.28 (s, 1H, PhCH), 4.87 (d, 1H, $J_{1^a,2^a}$ 3.7 Hz, H-1^a), 4.81−4.25 (m, 45H, 26PhCH$_2$, H-5^{b-g}, H-6A^{a-g}, H-3^{a-f}), 4.07−3.93 (m, 7H, H-6B^{b-g}, OCH$_2$CH$_2$CH$_2$NA), 3.89−3.80 (m, 3H, H-4^b, H-4^c, H-5^a), 3.81−3.69 (m, 7H, H-4^a, H-4^d, H-4^e, H-4^f, H-6B^a, H-2^a, OCH$_2$CH$_2$CH$_2$NA), 3.59−3.40 (m, 9H, H-4^g, 6H-2, OCH$_2$CH$_2$CH$_2$NB, OCH$_2$CH$_2$CH$_2$NB), 2.62 (m, 2H, CH$_2$CH$_2$C(O)CH$_3$), 2.41 (m, 2H, CH$_2$CHC(O)CH$_{32}$), 2.17 (s, 1H, CH$_3$), 1.99 (m, 2H, OCH$_2$CH$_2$CH$_2$N); ^{13}C NMR (100.6 MHz, $CDCl_3$) δ_C 206.1 (CH$_2$C(O)CH$_3$), 171.8 (CH$_2$C(O)O), 166.3, 166.2 (PhOC(O)), 137.7, 133.0, 130.2, 129.7, 129.6, 128.6, 128.5, 128.4, 128.3, 128.2, 128.1, 128.0, 127.6, 127.5, 127.3, 127.2, 127.1, 127.0, 126.9, 126.7, 126.5, 126.4, 126.3 (Ar), 102.3 (PhCH), 97.9 (C-1^a), 96.8 (C-1^g), 96.1 (C-1^c), 95.6 (C-1^e), 95.5 (C-1^d, C-1^f), 95.3 (C-1^b), 82.8 (C-4^a), 79.5, 79.4, 79.2 (C-4^{b-f}), 78.4 (C-2^b, C-2^c), 78.2, (C-2^d, C-2^e), 78.1 (C-2^a), 77.6 (C-2^g), 76.8 (C-2^f), 76.5 (C-4^g), 75.9 (C-3^f), 75.2 (C-3^b), 74.5, 74.4 (C-3^c, C-3^d, C-3^e), 74.0 (PhCH$_2$, C-3^g), 73.6, 73.2, 73.1, 72.9, 72.8, 72.7, 72.6, 72.5, 72.0, 71.9, 71.6, 70.6 (PhCH$_2$, C-3^a), 69.0 (C-6^a), 68.4, 68.1, 68.0, 67.5 (C-5^{b-g}), 67.2 (OCH$_2$CH$_2$CH$_2$N), 63.6, 63.3, 63.2, 63.0 (C-6^{b-g}), 62.3 (C-5^a), 38.5 (OCH$_2$CH$_2$CH$_2$N), 37.7 (CH$_2$CH$_2$C(O)CH$_3$), 29.8 (CH$_3$), 28.4 (OCH$_2$CH$_2$CH$_2$N), 28.1 (CH$_2$CH$_2$C(O)CH$_3$). Anal. calcd for $C_{192}H_{190}F_3NO_{45}$: C, 70.12; H, 5.82; N, 0.43. Found: C, 70.24; H, 5.96; N, 0.40.

*3-Trifluoroacetamidopropyl 6-O-benzoyl-2,4-di-O-benzyl-α-D-glucopyranosyl-(1 → 3)-6-O-benzoyl-2,4-di-O-benzyl-α-D-glucopyranosyl-(1 → 3)-6-O-benzoyl-2,4-di-O-benzyl-α-D-glucopyranosyl-(1 → 3)-6-O-benzoyl-2,4-di-O-benzyl-α-D-glucopyranosyl-(1 → 3)-6-O-benzoyl-2,4-di-O-benzyl-α-D-glucopyranosyl-(1 → 3)-2-O-benzyl-4,6-O-benzylidene-α-D-glucopyranoside (**9**).* Heptasaccharide **8** (29 mg, 0.0069 mmol) was dissolved in 0.5 mL of a 1 M solution of hydrazine hydrate in pyridine−acetic acid (3:2). After 2 h, acetylacetone (102 μL, 1 mmol) was added, and the solvents were removed under reduced pressure. The residue was purified by column chromatography (toluene−EtOAc, 15:1 → 5:1) to give compound **9** (25 mg, 89%) as a foam. R_f 0.40 (hexane/EtOAc 1.2:1); $[\alpha]_D^{23}$ +174.2 (c = 1, $CHCl_3$); ^{1}H NMR (600 MHz, $CDCl_3$) δ_H 8.15−8.03 (m, 12H, α-Bz), 7.65−7.00 (m, 77H, Ar, NH), 6.93−6.87 (m, 4H, Ar), 6.84 (d, 2H, Ar), 6.68−6.64 (m, 4H, Ar), 6.22 (d, 2H, Ar), 5.71 (d, 1H, $J_{1^d,2^d}$ 3.8 Hz, H-1^d), 5.69 (d, 1H, $J_{1^c,2^c}$ 3.7 Hz, H-1^c), 5.60 (d, 2H, H-1^b, H-1^f), 5.58 (d, 1H, $J_{1^e,2^e}$ 3.8 Hz, H-1^e), 5.56 (d, 1H, $J_{1^g,2^g}$ 3.6 Hz, H-1^g), 5.26 (s, 1H, PhCH), 4.87 (d, 1H, $J_{1^a,2^a}$ 3.8 Hz, H-1^a), 4.79−4.23 (m, 45H, 26PhCH$_2$, H-5^{b-g}, H-6A^{a-g}, H-3^{a-f}), 4.12 (t, $J_{3^g,2^g} = J_{3^g,4^g}$ 9.3 Hz, 1H, H-3^g), 4.08 (m, 1H, H-6B^g), 4.05−3.91 (m, 6H, H-6B^{b-f}, OCH$_2$CH$_2$CH$_2$NA), 3.90−3.81 (m, 3H, H-4^b, H-4^c, H-5^a), 3.79−3.69 (m, 7H, H-4^a, H-4^d, H-4^e, H-4^f, H-6B^a, H-2^a, OCH$_2$CH$_2$CH$_2$NA), 3.54 (dd, $J_{2^c,1^c}$ 3.2 Hz, $J_{2^c,3^c}$ 10.3 Hz, 1H, H-2^c), 3.52−3.38 (m, 8H, H-4^g, 5H-2, OCH$_2$CH$_2$CH$_2$NB, OCH$_2$CH$_2$CH$_2$NB), 3.35 (dd, $J_{2^g,1^g}$ 3.5 Hz, $J_{2^g,3^g}$ 9.8 Hz, H-2^g), 1.98 (m, 2H, OCH$_2$CH$_2$CH$_2$N); ^{13}C NMR (150.9 MHz, $CDCl_3$) δ_C 171.8 (CH$_2$C(O)O), 166.2 (PhOC(O)), 137.7, 137.6, 137.5, 133.1, 130.1, 129.9, 129.6, 129.3, 128.6, 128.5, 128.3, 128.2, 128.1, 128.0, 127.9, 127.8, 127.6, 127.5, 127.4, 127.3, 127.2, 127.1, 127.0, 126.8, 126.7, 126.6, 126.5, 126.3, 126.2, 126.1 (Ar), 102.3 (PhCH), 97.8 (C-1^a), 96.6 (C-1^g), 96.0 (C-1^c), 95.5 (C-1^d, C-1^e, C-1^f), 95.2 (C-1^b), 82.7 (C-4^a), 79.4, 79.3, 79.2 (C-4^{b-f}), 79.1 (C-2^g), 78.3, 78.0, 77.8 (C-2^{a-f}), 76.8 (C-4^g), 75.5 (C-3^f), 75.1 (C-3^b), 74.3, 74.2 (C-3^c, C-3^d, C-3^e, PhCH$_2$), 73.6, 73.4 (PhCH$_2$, C-3^g), 73.0, 72.8, 72.7, 72.6, 72.5, 72.4, 71.9, 71.8, 71.6 (PhCH$_2$, C-3^a), 70.5 (PhCH$_2$), 69.0 (C-6^a), 68.1, 67.9, 67.6, 67.3 (C-5^{b-g}), 67.2 (OCH$_2$CH$_2$CH$_2$N), 63.5, 63.2, 62.9 (C-6^{b-g}), 62.2 (C-5^a), 38.5 (OCH$_2$CH$_2$CH$_2$N), 28.4 (OCH$_2$CH$_2$CH$_2$N). Anal. calcd for $C_{187}H_{184}F_3NO_{43}$: C, 70.40; H, 5.81; N, 0.44. Found: C, 70.14; H, 5.94; N, 0.54.

*3-Trifluoroacetamidopropyl 6-O-benzoyl-α-D-glucopyranosyl-(1 → 3)-6-O-benzoyl-α-D-glucopyranosyl-(1 → 3)-6-O-benzoyl-α-D-glucopyranosyl-(1 → 3)-6-O-benzoyl-α-D-glucopyranosyl-(1 → 3)-6-O-benzoyl-α-D-glucopyranosyl-(1 → 3)-α-D-glucopyranoside (**12**).* To a solution of **9** (45 mg, 0.0137 mmol) in methanol (2.8 mL) and EtOAc (0.85 mL) was added Pd(OH)$_2$/C (45 mg), and the resulting mixture was vigorously stirred under hydrogen overnight. The catalyst was removed by filtration through a Celite pad, and the filtrate was concentrated under reduced pressure. The residue was dissolved in MeOH (6 mL), and aqueous 1 M NaOH (0.6 mL) was added. The solution was allowed to react for 12 h and then neutralized with 1 M AcOH (0.6 mL) and concentrated. The residue was subjected to gel-permeation chromatography on a TSK HW-40(S) column in 0.1 M AcOH. The appropriate fractions were pooled and freeze-dried to give **12** (8.5 mg, 51%) as a fluffy solid. R_f 0.14 (*n*-butanol/ethanol/water/15% NH$_4$OH 0.5:1:0.8:0.4); $[\alpha]_D^{24}$ +205.2 (c = 1 in H$_2$O); ^{1}H NMR (600 MHz, D$_2$O) δ_H 5.41−5.35 (m, 6H, H-1^{b-g}), 4.96 (d, $J_{1^a,2^a}$ 3.8 Hz, 1H, H-1^a), 4.08−4.01 (m, 6H, H-5^{b-g}), 3.95−3.61 (m, 28H, OCH$_2$CH$_2$CH$_2$N, H-3^{a-g}, H-6^{a-g}, H-4^{a-f}, H-2^{a-f}, H-5^a), 3.58 (dd, $J_{2^g,1^g}$ 3.9 Hz, $J_{2^g,3^g}$ 9.9 Hz, 1H, H-2^g), 3.45 (t, $J_{4^g,3^g} = J_{4^g,2^g}$ 9.6 Hz, 1H, H-4^g), 3.24−3.12 (m, 2H, 2OCH$_2$CH$_2$CH$_2$N), 2.08−2.00 (m, 2H, 2OCH$_2$CH$_2$CH$_2$N); ^{13}C NMR (150.9 MHz, D$_2$O) δ_C 100.6, 100.5 (C-1^{b-g}), 99.8 (C-1^a), 81.5, 81.3, 81.1 (C-3^{a-f}), 74.2 (C-3^g), 73.1, 73.0, 72.9 (C-5^{a-f}, C-2^g), 71.7, 71.0, 70.8 (C-2^{a-f}, C-4^{a-g}), 67.1 (OCH$_2$CH$_2$CH$_2$N), 61.8, 61.5 (C-6^{a-g}), 39.1 (OCH$_2$CH$_2$CH$_2$N), 27.8 (OCH$_2$CH$_2$CH$_2$N); HRMS (ESI-TOF) m/z [M + H]$^+$ calcd for $C_{45}H_{80}NO_{36}$ 1210.4455, found 1210.4431.

*3-Trifluoroacetamidopropyl 6-O-benzoyl-2,4-di-O-benzyl-3-O-levulinoyl-α-D-glucopyranosyl-(1 → 3)-6-O-benzoyl-2,4-di-O-benzyl-α-D-glucopyranosyl-(1 → 3)-6-O-benzoyl-2,4-di-O-benzyl-α-D-glucopyranosyl-(1 → 3)-6-O-benzoyl-2,4-di-O-benzyl-α-D-glucopyranosyl-(1 → 3)-6-O-benzoyl-2,4-di-O-benzyl-α-D-glucopyranosyl-(1 → 3)-6-O-benzoyl-2,4-di-O-benzyl-α-D-glucopyranosyl-(1 → 3)-6-O-benzoyl-2,4-di-O-benzyl-α-D-glucopyranosyl-(1 → 3)-2-O-benzyl-4,6-O-benzylidene-α-D-glucopyranoside (**10**).* A solution of donor **3** (54 mg, 0.046 mmol) and heptasaccharide acceptor **9** (80 mg, 0.025 mmol) in dry CH_2Cl_2 (1.3 mL) was stirred with MS AW 300 (130 mg) for 1 h. Then, the mixture was cooled to −35 °C and MeOTf (5.2 μL, 0.046 mmol) was added. The solution was allowed to warm slowly to −10 °C. After 2 h, methanol (10 μL) and triethylamine (15 μL) were added. The solids were removed by filtration and washed with CH_2Cl_2. The filtrate was washed with saturated aqueous $NaHCO_3$ and water, the organic layer was separated, and the solvent was evaporated under reduced pressure. The residue was purified by column chromatography (light petroleum/EtOAc 2:1 → 1.5:1) and by HPLC (hexane/EtOAc 1.1:1) to afford **10** (47 mg, 0.011 mmol, 45%) as a foam. R_f 0.26 (hexane/EtOAc 1.2:1); $[\alpha]_D^{24}$ +180.0 (c = 1, $CHCl_3$); ^{1}H NMR (600 MHz, $CDCl_3$) δ_H 8.18−8.06 (m, 16H, α-Bz), 7.68−7.03 (m, 101H, Ar, NH), 6.95−6.85 (m, 6H, Ar), 6.78−6.71 (m, 8H, Ar), 5.75 (d, 1H, $J_{1,2}$ 3.7 Hz, H-1), 5.73 (d, 1H, $J_{1,2}$ 3.7 Hz, H-1), 5.66 (t, 1H, $J_{3^i,4^i} = J_{3^i,2^i}$ 9.6 Hz, H-3^i), 5.65−5.60 (m, 5H, H-1), 5.59 (d, 1H, $J_{1,2}$ 3.5 Hz, H-1), 5.30 (s, 1H, PhCH), 4.90 (d, 1H, $J_{1^a,2^a}$ 3.7 Hz, H-1^a), 4.84−4.27 (m, 58H, 34PhCH$_2$, 8H-5, 9H-6A, 8H-3), 4.07−3.94 (m, 9H, 8H-6B, OCH$_2$CH$_2$CH$_2$NA), 3.91−3.85 (m, 3H, 2H-4, H-5^a), 3.82−3.73 (m, 9H, 6H-4, H-6B^a, H-2^a, OCH$_2$CH$_2$CH$_2$NA), 3.60−3.41 (m, 11H, H-4^e, 8H-2, OCH$_2$CH$_2$CH$_2$NB, OCH$_2$CH$_2$CH$_2$NB), 2.64 (m, 2H, CH$_2$CH$_2$C(O)CH$_3$), 2.44 (m, 2H, CH$_2$CH$_2$C(O)CH$_3$), 2.17 (s, 1H, CH$_3$), 2.00 (m, 2H, OCH$_2$CH$_2$CH$_2$N); ^{13}C NMR (150.9 MHz, $CDCl_3$) δ_C 206.2 (CH$_2$C(O)CH$_3$), 171.8 (CH$_2$C(O)O), 166.4, 166.2 (PhOC(O)), 137.7, 133.1, 130.2, 129.7, 129.6, 128.7, 128.5, 128.4, 128.3, 128.2, 128.1, 128.0, 127.7, 127.6, 127.5, 127.2, 127.0, 126.9, 126.8, 126.7, 126.4, 126.3, 126.2 (Ar), 102.4 (PhCH), 97.9 (C-1^a), 96.8 (C-1), 96.1 (C-1), 95.6 (C-1), 95.5 (C-1), 95.3 (C-1), 82.8 (C-4^a), 79.5, 79.4, 79.3, 79.2 (C-4), 78.4, 78.1, 77.6, 77.3, 77.1, 76.9 (C-2), 76.5 (C-4), 75.9, 75.2, 74.4, 74.0 (C-3), 73.6, 73.2, 73.1, 72.8, 72.7 (PhCH$_2$, C-3), 72.6, 72.5, 72.0, 71.9, 71.6, 70.6 (PhCH$_2$), 69.0 (C-6^a), 68.3, 68.1,

DOI: 10.1021/acs.joc.8b01142
J. Org. Chem. 2018, 83, 12965−12976

68.0, 67.7, 67.4 (C-5), 67.3 ($OCH_2CH_2CH_2N$), 63.6, 63.3, 63.0 (C-6), 62.3 (C-5^a), 38.5 ($OCH_2CH_2CH_2N$), 37.7 ($CH_2CH_2C(O)CH_3$), 29.8 (CH_3), 28.4 ($OCH_2CH_2CH_2N$), 28.0 ($CH_2CH_2C(O)CH_3$). Anal. calcd for $C_{246}H_{242}F_3NO_{57}$: C, 70.66; H, 5.83; N, 0.33. Found: C, 70.61; H, 5.77; N, 0.39.

*3-Trifluoroacetamidopropyl 6-O-benzoyl-2,4-di-O-benzyl-3-O-levulinoyl-α-D-glucopyranosyl-(1 → 3)-6-O-benzoyl-2,4-di-O-benzyl-α-D-glucopyranosyl-(1 → 3)-6-O-benzoyl-2,4-di-O-benzyl-α-D-glucopyranosyl-(1 → 3)-6-O-benzoyl-2,4-di-O-benzyl-α-D-glucopyranosyl-(1 → 3)-6-O-benzoyl-2,4-di-O-benzyl-α-D-glucopyranosyl-(1 → 3)-6-O-benzoyl-2,4-di-O-benzyl-α-D-glucopyranosyl-(1 → 3)-6-O-benzoyl-2,4-di-O-benzyl-α-D-glucopyranosyl-(1 → 3)-6-O-benzoyl-2,4-di-O-benzyl-α-D-glucopyranosyl-(1 → 3)-6-O-benzoyl-2,4-di-O-benzyl-α-D-glucopyranosyl-(1 → 3)-6-O-benzoyl-2,4-di-O-benzyl-α-D-glucopyranosyl-(1 → 3)-2-O-benzyl-4,6-O-benzylidene-α-D-glucopyranoside (**11**).* A solution of tetrasaccharide donor **6** (119 mg, 0.057 mmol) and heptasaccharide acceptor **9** (86 mg, 0.027 mmol) in dry CH_2Cl_2 (2 mL) was stirred with MS AW 300 (200 mg) for 1 h. Then, the mixture was cooled to −35 °C and MeOTf (6.5 μL, 0.057 mmol) was added. The solution was allowed to warm slowly to −10 °C. After 2 h, methanol (10 μL) and triethylamine (15 μL) were added. The solids were removed by filtration and washed with CH_2Cl_2. The filtrate was washed with saturated aqueous $NaHCO_3$ and water, the organic layer was separated, and the solvent was evaporated under reduced pressure. The residue was purified by column chromatography (light petroleum/EtOAc 2:1→ 1.5:1) and by HPLC (hexane/EtOAc 1.2:1) to afford **11** (56 mg, 0.011 mmol, 40%) as a foam. R_f 0.26 (hexane/EtOAc 1.2:1); $[\alpha]_D^{24}$ +183.8 (*c* = 1, $CHCl_3$); ^{1}H NMR (600 MHz, $CDCl_3$) δ_H 8.18−8.06 (m, 20H, α-Bz), 7.68−6.93 (m, 123H, Ar, N*H*), 6.98−6.86 (m, 6H, Ar), 6.78−6.71 (m, 12H, Ar), 5.74 (d, 1H, $J_{1,2}$ 3.6 Hz, H-1), 5.71 (d, 1H, $J_{1,2}$ 3.5 Hz, H-1), 5.67 (t, 1H, $J_{3^k,4^k}$=$J_{3^k,2^k}$ 9.7 Hz, H-3^k), 5.65−5.57 (m, 8H, H-1), 5.28 (s, 1H, PhC*H*), 4.88 (d, 1H, $J_{1^a,2^a}$ 3.6 Hz, H-1^a), 4.83−4.26 (m, 73H, 42PhCH_2, 10H-5, 11H-6A, 10H-3), 4.09−3.96 (m, 11H, 10H-6B, $OCH_2CH_2CH_2NA$), 3.92−3.83 (m, 3H, 2H-4, H-5^a), 3.82−3.72 (m, 11H, 8H-4, H-6B^a, H-2^a, $OCH_2CH_2CH_2NA$), 3.58−3.40 (m, 13H, H-4^k, 10H-2, $OCH_2CH_2CH_2NB$, $OCH_2CH_2CH_2NB$), 2.64 (m, 2H, $CH_2CH_2C(O)CH_3$), 2.44 (m, 2H, $CH_2CH_2C(O)CH_3$), 2.17 (s, 1H, CH_3), 2.00 (m, 2H, $OCH_2CH_2CH_2N$); ^{13}C NMR (125.8 MHz, $CDCl_3$) δ_C 206.2 ($CH_2C(O)CH_3$), 171.8 ($CH_2C(O)O$), 166.2 (PhOC(O)), 137.7, 133.0, 130.1, 129.6, 128.6, 128.5, 128.3, 128.2, 128.2, 128.0, 127.6, 127.5, 127.2, 127.1, 127.0, 126.9, 126.7, 126.4, 126.3, 126.2 (Ar), 102.3 (PhCH), 97.9 (C-1^a), 96.8 (C-1), 96.1 (C-1), 95.5 (C-1), 95.3 (C-1), 82.7 (C-4^a), 79.5, 79.3, 79.12, 79.06 (C-4), 78.4, 78.3, 78.0, 77.6, 77.5, 76.8 (C-2), 76.4 (C-4), 75.9, 75.2, 74.3, 73.9 (C-3), 73.6, 73.2, 73.1, 72.8, 72.7 ($PhCH_2$, C-3), 72.6, 72.5, 71.9, 71.6, 70.5 ($PhCH_2$), 69.0 (C-6^a), 68.3, 68.0, 67.7, 67.4 (C-5), 67.2 ($OCH_2CH_2CH_2N$), 63.5, 63.3, 62.9 (C-6), 62.3 (C-5^a), 38.5 ($OCH_2CH_2CH_2N$), 37.7 ($CH_2CH_2C(O)CH_3$), 29.8 (CH_3), 28.4 ($OCH_2CH_2CH_2N$), 28.0 ($CH_2CH_2C(O)CH_3$). Anal. calcd for $C_{300}H_{294}F_3NO_{69}$: C, 71.01; H, 5.84. Found: C, 70.93; H, 5.98.

*3-Trifluoroacetamidopropyl 6-O-benzoyl-2,4-di-O-benzyl-α-D-glucopyranosyl-(1 → 3)-6-O-benzoyl-2,4-di-O-benzyl-α-D-glucopyranosyl-(1 → 3)-6-O-benzoyl-2,4-di-O-benzyl-α-D-glucopyranosyl-(1 → 3)-6-O-benzoyl-2,4-di-O-benzyl-α-D-glucopyranosyl-(1 → 3)-6-O-benzoyl-2,4-di-O-benzyl-α-D-glucopyranosyl-(1 → 3)-6-O-benzoyl-2,4-di-O-benzyl-α-D-glucopyranosyl-(1 → 3)-6-O-benzoyl-2,4-di-O-benzyl-α-D-glucopyranosyl-(1 → 3)-6-O-benzoyl-2,4-di-O-benzyl-α-D-glucopyranosyl-(1 → 3)-2-O-benzyl-4,6-O-benzylidene-α-D-glucopyranoside (**13**).* Nonasaccharide **10** (29 mg, 0.0069 mmol) was dissolved in 0.5 mL of a 1 M solution of hydrazine hydrate in pyridine−acetic acid (3:2). After 2 h, acetylacetone (102 μL, 1 mmol) was added, and the solvents were removed under reduced pressure. The residue was purified by column chromatography (toluene−EtOAc, 15:1 → 5:1) to afford product **13** (25 mg, 89%). R_f 0.32 (toluene/EtOAc 5:1); $[\alpha]_D^{23}$ +194.6 (*c* = 1, $CHCl_3$); ^{1}H NMR (600 MHz, $CDCl_3$) δ_H 8.08−7.96 (m, 16H, α-Bz), 7.59−6.93 (m, 101H, Ar, N*H*), 6.88−6.84 (m, 4H, Ar), 6.81−6.77 (m, 2H, Ar), 6.68−6.61 (m, 8H, Ar), 5.65 (d, 1H, $J_{1,2}$ 3.8 Hz, H-1), 5.62 (d, 1H, $J_{1,2}$ 3.8 Hz, H-1), 5.56−5.50 (m, 5H, H-1), 5.49 (d, $J_{1,2}$ 3.6 Hz, 1H, H-1), 5.19 (s, 1H, PhC*H*), 4.80 (d, 1H, $J_{1^a,2^a}$ 3.6 Hz, H-1^a), 4.76−4.18 (m, 59H, 34PhCH_2, 8H-5, 9H-6A, 8H-3), 3.99−3.84 (m, 9H, 8H-6B, $OCH_2CH_2CH_2NA$), 3.83−3.72 (m, 3H, 2H-4, H-5^a), 3.72−3.60 (m, 9H, 6H-4, H-6B^a, H-2^a, $OCH_2CH_2CH_2NA$), 3.48−3.26 (m, 11H, H-4^i, 8H-2, $OCH_2CH_2CH_2NB$, $OCH_2CH_2CH_2NB$), 1.90 (m, 2H, $OCH_2CH_2CH_2N$); ^{13}C NMR (150.9 MHz, $CDCl_3$) δ_C 166.3, 166.2, 166.1 (PhOC(O)), 137.9, 137.7, 137.5, 137.2, 136.8, 133.0, 130.2, 130.1, 129.7, 129.6, 129.3, 128.6, 128.5, 128.4, 128.3, 128.2, 128.1, 128.0, 127.8, 127.6, 127.5, 127.3, 127.2, 127.1, 127.0, 126.9, 126.8, 126.7, 126.6, 126.5, 126.3 (Ar), 102.3 (PhCH), 97.9 (C-1^a), 96.6 (C-1), 96.1 (C-1), 95.5 (C-1), 95.3 (C-1), 82.8 (C-4^a), 79.5, 79.4, 79.2 (C-4), 78.5, 78.1, 77.9 (C-2), 75.6, 75.2 (C-3), 74.4, 74.3, 73.6, 73.5, 73.4, 73.1, 72.9, 72.8, 72.7, 72.6, 72.5, 71.9, 71.6, 70.6 ($PhCH_2$, C-3), 69.0 (C-6^a), 68.2, 68.0, 67.7, 67.5 (C-5), 67.2 ($OCH_2CH_2CH_2N$), 63.6, 63.3, 63.0 (C-6), 62.3 (C-5^a), 38.5 ($OCH_2CH_2CH_2N$), 28.0 ($OCH_2CH_2CH_2N$). Anal. calcd for $C_{241}H_{236}F_3NO_{55}$: C, 70.89; H, 5.83. Found: C, 71.05; H, 5.99.

*3-Trifluoroacetamidopropyl 6-O-benzoyl-2,4-di-O-benzyl-α-D-glucopyranosyl-(1 → 3)-6-O-benzoyl-2,4-di-O-benzyl-α-D-glucopyranosyl-(1 → 3)-6-O-benzoyl-2,4-di-O-benzyl-α-D-glucopyranosyl-(1 → 3)-6-O-benzoyl-2,4-di-O-benzyl-α-D-glucopyranosyl-(1 → 3)-6-O-benzoyl-2,4-di-O-benzyl-α-D-glucopyranosyl-(1 → 3)-6-O-benzoyl-2,4-di-O-benzyl-α-D-glucopyranosyl-(1 → 3)-6-O-benzoyl-2,4-di-O-benzyl-α-D-glucopyranosyl-(1 → 3)-6-O-benzoyl-2,4-di-O-benzyl-α-D-glucopyranosyl-(1 → 3)-6-O-benzoyl-2,4-di-O-benzyl-α-D-glucopyranosyl-(1 → 3)-6-O-benzoyl-2,4-di-O-benzyl-α-D-glucopyranosyl-(1 → 3)-2-O-benzyl-4,6-O-benzylidene-α-D-glucopyranoside (**14**).* Undecasaccharide **11** (40 mg, 0.0079 mmol) was dissolved in 0.5 mL of a 1 M solution of hydrazine hydrate in pyridine−acetic acid (3:2), and the mixture was allowed to react for 2 h. Acetylacetone (102 μL, 1 mmol) was added, and the solvents were removed under reduced pressure. The residue was purified by column chromatography (toluene−EtOAc, 15:1 → 5:1) to provide **14** (38 mg, 97%) as a foam. R_f 0.40 (toluene/EtOAc 5:1); $[\alpha]_D^{24}$ +197.5 (*c* = 1, $CHCl_3$); ^{1}H NMR (600 MHz, $CDCl_3$) δ_H 8.19−8.07 (m, 20H, α-Bz), 7.69−7.04 (m, 123H, Ar, N*H*), 6.97−6.92 (d, 4H, Ar), 6.89−6.87 (d, 2H, Ar), 6.74−6.67 (m, 12H, Ar), 5.75 (d, 1H, $J_{1,2}$ 3.7 Hz, H-1), 5.73 (d, 1H, $J_{1,2}$ 3.7 Hz, H-1), 5.66−5.60 (m, 7H, H-1), 5.59 (d, *J* 3.5 Hz, H-1), 5.31 (s, 1H, PhC*H*), 4.91 (d, 1H, $J_{1^a,2^a}$ 3.8 Hz, H-1^a), 4.86−4.27 (m, 73H, 42PhCH_2, 10H-5, 11H-6A, 10H-3), 4.17 (t, $J_{3^k,2^k}$ = $J_{3^k,4^k}$ 9.2 Hz, 1H, H-3^k), 4.11 (m, 1H, H-6B), 4.07−3.94 (m, 10H, 9H-6B, $OCH_2CH_2CH_2NA$), 3.94−3.87 (m, 3H, 2H-4, H-5^a), 3.83−3.73 (m, 11H, 8H-4, H-6B^a, H-2^a, $OCH_2CH_2CH_2NA$), 3.59 (dd, *J* 3.8 Hz, *J* 9.7 Hz, H-2), 3.54 (dd, *J* 3.7 Hz, *J* 9.6 Hz, H-2), 3.53−3.42 (m, 10H, H-4^k, 7H-2, $OCH_2CH_2CH_2NB$, $OCH_2CH_2CH_2NB$), 3.39 (m, *J* 3.4 Hz, *J* 9.8 Hz, 1H, H-2), 1.96 (m, 2H, $OCH_2CH_2CH_2N$); ^{13}C NMR (150.9 MHz, $CDCl_3$) δ_C 166.2 (PhOC(O)), 137.6, 137.5, 133.0, 130.1, 129.6, 129.3, 128.6, 128.5, 128.4, 128.2, 128.1, 128.0, 127.9, 127.8, 127.6, 127.4, 127.2, 127.0, 126.8, 126.7, 126.5, 126.3, 126.1 (Ar), 102.3 (PhCH), 97.8 (C-1^a), 96.6 (C-1), 96.1 (C-1), 95.5 (C-1), 95.3 (C-1), 82.7 (C-4^a), 79.5, 79.2, 78.3, 77.9, 77.8, 76.8 (C-2, C-4),75.5, 75.1 (C-3), 74.3, 74.2, 73.6, 73.5, 73.4, 73.0, 72.8, 72.7 ($PhCH_2$, C-3), 72.4, 71.8, 71.6, 70.5 ($PhCH_2$), 69.0 (C-6^a), 68.1, 67.9, 67.6 (C-5), 67.2 ($OCH_2CH_2CH_2N$), 63.5, 63.2, 62.9 (C-6), 62.3 (C-5^a), 38.5 ($OCH_2CH_2CH_2N$), 28.4 ($OCH_2CH_2CH_2N$). Anal. calcd for $C_{295}H_{288}F_3NO_{67}$: C, 71.20; H, 5.83; N, 0.28. Found: C, 71.31; H, 5.75; N, 0.31.

*3-Aminopropyl α-D-glucopyranosyl-(1 → 3)-α-D-glucopyranosyl-(1 → 3)-α-D-glucopyranosyl-(1 → 3)-α-D-glucopyranosyl-(1 → 3)-α-D-glucopyranosyl-(1 → 3)-α-D-glucopyranosyl-(1 → 3)-α-D-glucopyranosyl-(1 → 3)-α-D-glucopyranosyl-(1 → 3)-α-D-glucopyranoside (**17**).* Nonasaccharide **13** (27 mg, 6.1 μmol) was dissolved in 3 mL of CH_2Cl_2/MeOH (1:1), and 3 M NaOH (0.3 mL) was added. The mixture was stirred overnight and then quenched with AcOH. The solvents were evaporated, and the residue was passed through silica gel (CH_2Cl_2/MeOH 15:1 → 5:1). The product was dissolved in 2.0 mL of anhydrous THF and added dropwise to 10 mL of a dark blue solution of Na in liquid ammonia at −78 °C. After 45 min, the mixture was quenched with MeOH, and the ammonia was removed with the stream of argon. The mixture was diluted with water, AcOH was added until pH = 7, and the resulting solution was filtered through a nylon filter. The solvents were evaporated, and the residue was subjected to gel-permeation chromatography on a TSK HW-

DOI: 10.1021/acs.joc.8b01142
J. Org. Chem. 2018, 83, 12965−12976

40(S) column in 0.1 M AcOH and then reversed-phase C_{18} column chromatography and freeze-dried to give **17** (6.9 mg, 57.5%) as a fluffy solid. R_f 0.13 (*n*-butanol/ethanol/water/15% NH_4OH 0.5:1:0.8:0.4); $[\alpha]_D^{23}$ +254.0 (*c* = 1 in H_2O); ^1H NMR (600 MHz, D_2O) δ_H 5.40−5.35 (m, 8H, H-1^{b-i}), 4.96 (d, $J_{1^a,2^a}$ 3.8 Hz, 1H, H-1^a), 4.08−4.02 (m, 8H, H-5^{b-i}), 3.95−3.63 (m, 43H, $OCH_2CH_2CH_2N$, H-3^{a-i}, H-6^{a-i}, H-4^{a-h}, H-2^{a-h}, H-5^a), 3.58 (dd, $J_{2^i,1^i}$ 3.9 Hz, $J_{2^i,3^i}$ 9.9 Hz, 1H, H-2^i), 3.45 (t, $J_{4^i,3^i} = J_{4^i,2^i}$ 10.0 Hz, 1H, H-4^i), 3.24−3.12 (m, 2H, $2OCH_2CH_2CH_2N$), 2.08−2.00 (m, 2H, $2OCH_2CH_2CH_2N$); ^{13}C NMR (150.9 MHz, D_2O) δ_C 100.6, 100.5 (C-1^{b-i}), 99.8 (C-1^a), 81.3, 81.1 (C-3^{a-h}), 74.2 (C-3^i), 73.1, 73.0, 72.9 (C-5^{a-i}, C-2^i), 71.6, 71.1, 70.9 (C-2^{a-h}, C-4^{a-i}), 67.1 ($OCH_2CH_2CH_2N$), 61.8, 61.6 (C-6^{a-i}), 39.1 ($OCH_2CH_2CH_2N$), 27.8 ($OCH_2CH_2CH_2N$); HRMS (ESI-TOF) *m*/*z* $[M + 2H]^{2+}$ calcd for $C_{57}H_{101}NO_{46}$ 767.7792, found 767.7781.

*3-Aminopropyl α-D-glucopyranosyl-(1 → 3)-α-D-glucopyranosyl-(1 → 3)-α-D-glucopyranosyl-(1 → 3)-α-D-glucopyranosyl-(1 → 3)-α-D-glucopyranosyl-(1 → 3)-α-D-glucopyranosyl-(1 → 3)-α-D-glucopyranosyl-(1 → 3)-α-D-glucopyranosyl-(1 → 3)-α-D-glucopyranosyl-(1 → 3)-α-D-glucopyranoside (**18**).* Undecasaccharide **14** (32 mg, 6.5 μmol) was dissolved in 3.5 mL of CH_2Cl_2/MeOH (1:1), and 3 M NaOH (0.35 mL) was added. The mixture was stirred overnight and then quenched with AcOH. The solvents were evaporated, and the residue was passed through silica gel (CH_2Cl_2/MeOH 15:1→ 5:1). The residue was dissolved in 2.5 mL of anhydrous THF and added dropwise to 15 mL of a dark blue solution of Na in liquid ammonia at −78 °C. After 45 min, the mixture was quenched with MeOH, and the ammonia was removed with the stream of argon. The mixture was diluted with water, AcOH was added until pH = 7, and the solution was filtered through a nylon filter. The solvents were evaporated, and the residue was subjected to gel-permeation chromatography on a TSK HW-40(S) column in 0.1 M AcOH and then reversed-phase C_{18} column chromatography and freeze-dried to give **18** (6.9 mg, 57.5%) as a fluffy solid. R_f 0.13 (*n*-butanol/ethanol/water/15% NH_4OH 0.5:1:0.8:0.4); $[\alpha]_D^{24}$ +223.1 (*c* = 1 in H_2O); ^1H NMR (600 MHz, D_2O) δ_H 5.40−5.35 (m, 10H, H-1^{b-k}), 4.96 (d, $J_{1^a,2^a}$ 3.8 Hz, 1H, H-1^a), 4.08−4.00 (m, 10H, H-5^{b-k}), 3.95−3.65 (m, 43H, $OCH_2CH_2CH_2NA$, H-3^{a-k}, H-6^{a-k}, H-4^{a-j}, H-2^{a-j}, H-5^a), 3.63 (m, 1H, $OCH_2CH_2CH_2NB$), 3.58 (dd, $J_{2^k,1^k}$ 3.9 Hz, $J_{2^k,3^k}$ 9.9 Hz, 1H, H-2^k), 3.45 (t, $J_{4^k,3^k} = J_{4^k,2^k}$ 10.0 Hz, 1H, H-4^k), 3.24−3.10 (m, 2H, $2OCH_2CH_2CH_2N$), 2.06−1.97 (m, 2H, $2OCH_2CH_2CH_2N$); ^{13}C NMR (125.8 MHz, D_2O) δ_C 100.5, 100.4 (C-1^{b-k}), 99.6 (C-1^a), 81.1, 80.9 (C-3^{a-j}), 74.0 (C-3^k), 73.0, 72.9, 72.8 (C-5^{a-k}, C-2^k), 71.5, 71.0, 70.8 (C-2^{a-j}, C-4^{a-j}), 70.6 (C-4^k), 67.0 ($OCH_2CH_2CH_2N$), 61.6, 61.4 (C-6^{a-k}), 39.0 ($OCH_2CH_2CH_2N$), 27.8 ($OCH_2CH_2CH_2N$); HRMS (ESI-TOF) *m*/*z* $[M + H]^+$ calcd for $C_{69}H_{120}NO_{56}$ 1858.6567, found 1858.6555.

*Conjugate of the Pentasaccharide with Biotin (**20**).* A 0.062 M solution of biotin-activated ester **19** in DMF (100 μL) and dry triethylamine (8 μL) were added to a solution of **12** (1.8 mg, 0.0015 mmol) in DMF (100 μL) + H_2O (100 μL). After 19 h, the solvent was removed under reduced pressure, and the product was purified by gel-permeation chromatography (TSK HW-40(S), 0.1 M AcOH). The appropriate fractions were freeze-dried to give **20** (1.3 mg, 50%) as a fluffy solid. R_f 0.65 (*n*-butanol/ethanol/water/15% NH_4OH 0.5:1:0.8:0.4); ^1H NMR (600 MHz, D_2O) δ_H 5.40−5.36 (m, 6H, H-1^{b-g}), 4.92 (d, 1H, $J_{1^a,2^a}$ 3.8 Hz, H-1^a), 4.63 (dd, *J* 4.9 Hz, *J* 8.0 Hz, 1H, $SCH(CH_2)CHCH$), 4.43 (dd, *J* 4.5 Hz, *J* 8.0 Hz, 1H, $SCH(CH_2)CHCH$), 4.08−4.01 (m, 7H, H-5^{a-h}), 3.94−3.88 (m, 5H, H-3^{b-f}), 3.88−3.82 (m, 8H, H-3^a, H-6A^{a-g}), 3.81−3.73 (m, 12H, H-6B^{a-g}, H-3^g, $NC(O)CH_2CH_2O$, $OCH_2CH_2CH_2N^A$), 3.72−3.61 (m, 35H, H-4^{a-f}, H-2^{a-f}, H-5^a, 5 OCH_2CH_2O, OCH_2CH_2N), 3.60−3.53 (m, 2H, H-2^g, $OCH_2CH_2CH_2N^B$), 3.44 (t, $J_{4^g,3^g} = J_{4^g,2^g}$ 9.6 Hz, 1H, H-4^g), 3.40 (t, *J* 5.4 Hz, 2H, OCH_2CH_2N), 3.37−3.30 (m, 3H, $OCH_2CH_2CH_2N$, $SCH(CH_2)CHNH$), 3.00 (dd, *J* 5.0 Hz, *J* 13.0 Hz, 1H, $SCH(CH_2)CHCHCH_2^A$), 2.80 (d, *J* 13.0 Hz, 1H, $SCH(CH_2)CHCHCH_2^B$), 2.53 (t, *J* 6.2 Hz, 2H, $NC(O)CH_2CH_2O$), 2.29 (t, *J* 7.3 Hz, 2H, $C(O)CH_2CH_2CH_2CH_2$), 1.87 (m, 2H, $OCH_2CH_2CH_2N$), 1.75 (m, 1H, $C(O)CH_2CH_2CH_2CH_2CH_2^A$), 1.70−1.55 (m, 3H, $C(O)CH_2CH_2CH_2CH_2$, $C(O)CH_2CH_2CH_2CH_2^A$), 1.46−1.39 (m, 2H, $C(O)CH_2CH_2CH_2CH_2$); ^{13}C NMR (150.9 MHz, D_2O) δ_C 177.7, 174.7 (C(O)), 100.6, 100.4 (C-1^{b-g}), 99.5 (C-1^a), 81.4, 81.3 (C-3^{a-f}), 74.1 (C-3^g), 73.1, 73.0, 72.9 (C-5^{a-g}, C-2^g), 71.6, 71.2, 71.1, 70.9, 70.8, 70.7 (C-2^{a-f}, C-4^{a-g}), 70.1 ($NC(O)CH_2CH_2O$), 68.1 ($C(O)CH_2CH_2O$), 66.7 ($OCH_2CH_2CH_2N$), 63.3 ($SCH(CH_2)CHCH$), 61.8, 61.6 (C-6^{a-i}, $SCH(CH_2)CHCH$), 56.6 ($SCH(CH_2)CHNH$), 40.9 ($SCH(CH_2)CHCHCH_2$), 40.2 ($NC(O)CH_2CH_2O$), 37.8 ($OCH_2CH_2CH_2N$), 37.4 ($NC(O)CH_2CH_2O$), 36.7 ($C(O)CH_2CH_2CH_2CH_2$), 29.5 ($OCH_2CH_2CH_2N$), 29.4, 29.1, 28.9 ($C(O)CH_2CH_2CH_2CH_2$, $C(O)CH_2CH_2CH_2CH_2$, $OCH_2CH_2CH_2N$), 26.4 ($C(O)CH_2CH_2CH_2CH_2$); HRMS (ESI-TOF) *m*/*z* $[M - 2H]^{2-}$ calcd for $C_{82}H_{142}N_4O_{55}S$ 1046.4006, found 1046.3994.

*Conjugate of the Undecasaccharide with Biotin (**22**).* A 0.062 M solution of biotin-activated ester **19** in DMF (26 μL) and dry triethylamine (6.4 μL) was added to a solution of **18** (3 mg, 0.0016 mmol) in DMF (100 μL) + H_2O (100 μL). After 12 h, the solvent was removed under reduced pressure, and the product was purified by gel-permeation chromatography (TSK HW-40(S), 0.1 M AcOH). The appropriate fractions were freeze-dried to give **22** (1.9 mg, 49%) as a fluffy solid. R_f 0.60 (*n*-butanol/ethanol/water/15% NH_4OH 0.5:1:0.8:0.4); ^1H NMR (600 MHz, D_2O) δ_H 5.40−5.36 (m, 8H, H-1^{b-k}), 4.93 (d, 1H, $J_{1^a,2^a}$ 3.8 Hz, H-1^a), 4.62 (dd, *J* 4.9 Hz, *J* 8.0 Hz, 1H, $SCH(CH_2)CHCH$), 4.44 (dd, *J* 4.5 Hz, *J* 8.0 Hz, 1H, $SCH(CH_2)CHCH$), 4.08−4.01 (m, 10H, H-5^{b-k}), 3.95−3.89 (m, 9H, H-3^{b-j}), 3.89−3.82 (m, 12H, H-3^a, H-6A^{a-k}), 3.83−3.74 (m, 14H, H-6B^{a-k}, H-3^k, $NC(O)CH_2CH_2O$, $OCH_2CH_2CH_2N^A$), 3.73−3.63 (m, 43H, H-4^{a-j}, H-2^{a-j}, H-5^a, 5 OCH_2CH_2O, OCH_2CH_2N), 3.60−3.54 (m, 2H, H-2^k, $OCH_2CH_2CH_2N^B$), 3.45 (t, $J_{4^k,3^k} = J_{4^k,2^k}$ 9.6 Hz, 1H, H-4^k), 3.41 (t, *J* 5.4 Hz, 2H, OCH_2CH_2N), 3.38−3.31 (m, 3H, $OCH_2CH_2CH_2N$, $SCH(CH_2)CHNH$), 3.02 (dd, *J* 5.0 Hz, *J* 13.0 Hz, 1H, $SCH(CH_2)CHCHCH_2^A$), 2.80 (d, *J* 13.0 Hz, 1H, $SCH(CH_2)CHCHCH_2^B$), 2.54 (t, *J* 6.2 Hz, 2H, $NC(O)CH_2CH_2O$), 2.29 (t, *J* 7.3 Hz, 2H, $C(O)CH_2CH_2CH_2CH_2$), 1.89 (m, 2H,

DOI: 10.1021/acs.joc.8b01142
J. Org. Chem. 2018, 83, 12965−12976

$OCH_2CH_2CH_2N$), 1.75 (m, 1H, $C(O)CH_2CH_2CH_2CH_2^A$), 1.71−1.58 (m, 3H,$C(O)CH_2CH_2CH_2CH_2$, $C(O)CH_2CH_2CH_2CH_2^A$), 1.47−1.41 (m, 2H, $C(O)CH_2CH_2CH_2CH_2CH_2$); ^{13}C NMR (150.9 MHz, D_2O) δ_C 177.7, 174.7 (C(O)), 100.6, 100.5, 100.44 (C-1^{b-k}), 99.5 (C-1^a), 81.4, 81.3 (C-3^{a-j}), 74.1 (C-3^k), 73.1, 73.0, 72.9 (C-5^{a-k}, C-2^k), 71.6, 71.2, 71.1, 70.9, 70.7 (C-2^{a-j}, C-4^{a-k}), 70.1 ($NC(O)CH_2CH_2O$), 68.1 ($C(O)CH_2CH_2O$), 66.7 ($OCH_2CH_2CH_2N$), 63.3 ($SCH(CH_2)CHCH$), 61.8, 61.5 (C-6^{a-k}, $SCH(CH_2)CHCH$), 56.6 ($SCH(CH_2)CHNH$), 40.9 ($SCH(CH_2)CHCHCH_2$), 40.2 ($NC(O)CH_2CH_2O$), 37.8 ($OCH_2CH_2CH_2N$), 37.4 ($NC(O)CH_2CH_2O$), 36.7 ($C(O)CH_2CH_2CH_2CH_2$), 29.5 ($OCH_2CH_2CH_2N$), 29.1, 29.1, 28.9 ($C(O)CH_2CH_2CH_2CH_2$, $C(O)CH_2CH_2CH_2CH_2$, $OCH_2CH_2CH_2N$), 26.4 ($C(O)CH_2CH_2CH_2CH_2$); HRMS (ESI-TOF) m/z $[M + 2H]^{2+}$ calcd for $C_{94}H_{164}N_4O_{65}S$ 1210.9697, Found 1210.9697.

Biological Assays. *Coating of Streptavidin Microtiter Plates with Biotinylated α-(1 → 3)-Glucan Oligosaccharides.* Biotinylated α-(1 → 3)-glucan oligosaccharides **20**−**24** were loaded on streptavidin-coated 96-well microtiter plates (R&D Systems or Pierce/ThermoFisher) as described.[25] The streptavidin-coated plates were washed once with PBS supplemented with 1% bovine serum albumin (PBS-BSA). The oligosaccharides were diluted at 100 ng/mL in PBS-BSA, and 100 μL of solution was added to each well. After incubation for 1 h at room temperature, the plates were extensively washed with PBS-BSA.

Use of Streptavidin Plates Coated with Oligosaccharides for the Characterization and Detection of Specific Anti-α-(1 → 3)-Glucan Antibodies and Epitope Identification. The oligosaccharide-coated plates were incubated with the monoclonal antibodies (diluted 1:250 in PBS-BSA) or human sera (diluted 1:500 in PBS-BSA in triplicates) at room temperature for 1 h.

A secondary antibody (goat antimouse IgG (whole molecule) conjugated with HRP or antihuman IgG-Fc antibody conjugated with HRP (Sigma-Aldrich) (both 1:1000 in PBS-BSA) was added to each well, and the plates were incubated for 1 h at room temperature. After washing, the recognition was quantified by *O*-phenylenediamine (OPD) with OD readings at 492 nm. A total of 122 serum samples from 49 aspergillosis patients and 21 healthy individuals were collected with written consent from Angers Hospital (Angers, France). The aspergillosis patients included those with allergic bronchopulmonary aspergillosis (ABPA) (26 patients, 47 serum samples) and chronic pulmonary aspergillosis (CPA) (23 patients, 53 serum samples).

The immunogenicity of the α-(1 → 3)-glucan biotinylated oligosaccharides was compared to that of native α-(1 → 3)-glucan. Cell wall α-(1 → 3)-glucan was extracted from *A. fumigatus* mycelium as described previously.[26] Microtiter plates (96-wells, Greiner) were coated with 25 μg/mL native cell wall α-(1 → 3)-glucan in carbonate buffer (50 mM, pH 9.6) overnight. The wells were extensively watched with PBS supplemented with 0.05% Tween 20 and blocked for 1 h with PBS-BSA as described above for the streptavidin plates.

Immunolabeling of Germ Tubes of A. fumigatus by Anti-α-(1 → 3)-Glucan Monoclonal Antibodies. The *A. fumigatus* strain CEA17_Δ*akuB*^{KU80} (Ku80) and a triple α-(1 → 3)-glucan synthase mutant (Δ*ags1*/*ags2*/*ags3*) with a cell wall devoid of α-(1 → 3)-glucan were used.[4] Conidia (5×10^5 conidia/mL) was inoculated on eight-well glass-bottom α-slides (Ibidi, Martinsried, Germany) in 250 μL of Brian medium[27] at 30 °C for 18 h. Germinated conidia were permeabilized as described previously.[28] Briefly, germinated conidia were fixed with 2.5% *p*-formaldehyde overnight at 4 °C and washed with phosphate-buffered saline pH 7.0 (PBS) containing 0.1 M NH_4Cl and then with PBS. Fixed germinated conidia were permeabilized by successive incubation in Glucanex (Novozymes) for cell wall removal in the extraction solution containing Nonidet P-40 detergent and then in methanol. Immunolabeling was performed as previously described.[4] Permeabilized germinated conidia were incubated with the anti-α-(1 → 3)-glucan monoclonal antibodies A-16 (IgA) or J558 (IgM) (8 μg/mL)[17] followed by an antimouse IgG conjugated to Alexa488 (antimouse IgG-A488, 1:500 diluted; Sigma). Samples were observed under a fluorescence microscope. MD4−4 (antihen egg lysosome IgM) was used as the negative control.

Use of Streptavidin Plates Coated with Oligosaccharides To Monitor the Induction of Cytokines. PBMCs were isolated from whole-blood samples obtained from Hôpital Saint-Louis (Paris, France), through the Etablissement Français du Sang (Paris, France), from four healthy donors with written consent. The use of this material was approved by the ethics committees of Institut Pasteur and the Etablissement Français du Sang (convention 12/EFS/023). PBMCs were isolated by a Ficoll-Hypaque density gradient. First, the whole-blood samples were diluted in PBS (ratio 1:1). The diluted blood was then layered on top of 15 mL of Ficoll-Hypaque in 50 mL sterile polystyrene conical bottom tubes and centrifuged at 1800 rpm for 20 min at 22 °C. The buffy coat interface was collected and washed once with sterile PBS by centrifugation at 1500 rpm for 10 min at 22 °C. To remove the platelets, the PBMCs were washed again with sterile PBS by centrifugation at 1200 rpm for 10 min at 22 °C. Finally, the PBMCs were resuspended in 20 mL of RPMI-1690 medium supplemented with 10% normal human serum (ZenBio Inc., USA). The number of viable PBMCs per milliliter was counted by a Luna-FLTM dual fluorescence cell counter with acridine orange/propidium iodide cell viability kit (Logos Biosystems, South Korea). PBMCs (2.5×10^5 cells/well in RPMI supplemented with 10% normal human serum) were added to the wells of the streptavidin-coated plates that had been precoated with the oligosaccharides. The supernatant was collected after 24 h of incubation at 37 °C in a humid chamber with a 5% CO_2/95% air atmosphere. The supernatant was stored at −20 °C until further quantification of the TNF-α, IL-6, IL-1β and IL-1Ra levels by DuoSet ELISA kits following the manufacturer's instructions (R&D Systems). The induction of cytokines by free oligosaccharides was examined in nonstreptavidin plates. In addition, the induction of cytokines by high-molecular-weight water-insoluble α-(1 → 3)-glucan (10 μg/mL) in suspension or loaded on nonstreptavidin plates was examined with the same procedures.

Statistical Analysis. Data analyses were performed by one-way ANOVA nonparametric tests (Kruskal−Wallis or Friedman tests) with Dunn's multiple comparison test in GraphPad software Prism. A *p*-value <0.05 was considered significant.

■ ASSOCIATED CONTENT

Supporting Information

The Supporting Information is available free of charge on the ACS Publications website at DOI: 10.1021/acs.joc.8b01142.

^1H NMR and ^{13}C NMR spectra of compounds **2**, **4**−**6**, **8**−**18**, **20**, **21**, and **22** and immunolabeling of germ tubes of *A. fumigatus* (PDF)

■ AUTHOR INFORMATION

Corresponding Authors

*E-mail: jean-paul.latge@pasteur.fr.

*Tel/Fax: +7-499-135-87-84. E-mail: nen@ioc.ac.ru.

ORCID

Nikolay E. Nifantiev: 0000-0002-0727-4050

Present Address

#State Key Laboratory of Mycology, Chinese Academy of Science, Beijing, China.

Author Contributions

⊥BSK and SSWW contributed equally.

Notes

The authors declare no competing financial interest.

■ ACKNOWLEDGMENTS

This work was supported in part by the Russian Science Foundation (grant 14-50-00126) and by the French ANR

agency and Fondation de la Recherche Medicale (DEQ20150331722 LATGE Equipe FRM 2015).

REFERENCES

(1) Latgé, J.-P.; Steinbach, W. J. *Aspergillus fumigatus and Aspergillosis*; ASM Press: Washington, D.C., 2009.
(2) Latgé, J.-P.; Beauvais, A.; Chamilos, G. The Cell Call of the Human Fungal Pathogen *Aspergillus Fumigatus*: Biosynthesis, Organization, Immune Response, and Virulence. *Annu. Rev. Microbiol.* **2017**, *71*, 99−116.
(3) Henry, C.; Latgé, J. P.; Beauvais, A. α-1,3 Glucans are Dispensable in *Aspergillus Fumigatus*. *Eukaryotic Cell* **2012**, *11*, 26−29.
(4) Beauvais, A.; Bozza, S.; Kniemeyer, O.; Formosa, C.; Balloy, V.; Henry, C.; Roberson, R. W.; Dague, E.; Chignard, M.; Brakhage, A. A.; Romani, L.; Latgé, J.-P. Deletion of the α-(1,3)-Glucan Synthase Genes Induces a Restructuring of the Conidial Cell Wall Responsible for the Avirulence of *Aspergillus Fumigatus*. *PLoS Pathog.* **2013**, *9*, e1003716.
(5) Bozza, S.; Clavaud, C.; Giovannini, G.; Fontaine, T.; Beauvais, A.; Sarfati, J.; D'Angelo, C.; Perruccio, K.; Bonifazi, P.; Zagarella, S.; Moretti, S.; Bistoni, F.; Latgé, J.-P.; Romani, L. Immune Sensing of *Aspergillus Fumigatus* Proteins, Glycolipids, and Polysaccharides and the Impact on Th Immunity and Vaccination. *J. Immunol.* **2009**, *183*, 2407−2414.
(6) Komarova, B. S.; Orekhova, M. V.; Tsvetkov, Y. E.; Beau, R.; Aimanianda, V.; Latgé, J.-P.; Nifantiev, N. E. Synthesis of a Pentasaccharide and Neoglycoconjugates Related to Fungal α-(1→3)-Glucan and Their Use in the Generation of Antibodies to Trace *Aspergillus Fumigatus* Cell Wall. *Chem. - Eur. J.* **2015**, *21*, 1029−1035.
(7) Stephen-Victor, E.; Karnam, A.; Fontaine, T.; Beauvais, A.; Das, M.; Hegde, P.; Prakhar, P.; Holla, S.; Balaji, K. N.; Kaveri, S. V.; Latgé, J.-P.; Aimanianda, V.; Bayry, J. *Aspergillus Fumigatus* Cell Wall α-(1,3)-Glucan Stimulates Regulatory T Cell Polarization by Inducing PD-L1 Expression on Human Dendritic Cells. *J. Infect. Dis.* **2017**, *216*, 1281−1294.
(8) Nigudkara, S. S.; Demchenko, A. V. Stereocontrolled 1,2-*cis* Glycosylation as the Driving Force of Progress in Synthetic Carbohydrate Chemistry. *Chem. Sci.* **2015**, *6*, 2687−2704.
(9) Komarova, B. S.; Gerbst, A. G.; Finogenova, A. M.; Dmitrenok, A. S.; Tsvetkov, Y. E.; Nifantiev, N. E. 1,3-*syn*-Diaxial Repulsion of Typical Protecting Groups Used in Carbohydrate Chemistry in 3-*O*-Substituted Derivatives of Isopropyl d-Idopyranosides. *J. Org. Chem.* **2017**, *82*, 8897−8908.
(10) Komarova, B. S.; Dorokhova, V. S.; Tsvetkov, Y. E.; Nifantiev, N. E. Synthesis of a Biotinylated Penta-α-(1→6)-d-glucoside Based on the Rational Design of an α-Stereoselective Glucosyl Donor. *Org. Chem. Front.* **2018**, *5*, 909−928.
(11) Komarova, B. S.; Tsvetkov, Y. E.; Nifantiev, N. E. Design of α-Selective Glycopyranosyl Donors Relying on Remote Anchimeric Assistance. *Chem. Rec.* **2016**, *16*, 488−506.
(12) Komarova, B. S.; Orekhova, M. V.; Tsvetkov, Y. E.; Nifantiev, N. E. Is an Acyl Group at O-3 in Glucosyl Donors Able to Control α-Stereoselectivity of glycosylation? The role of Conformational Mobility and the Protecting Group at O-6. *Carbohydr. Res.* **2014**, *384*, 70−86.
(13) Ustyuzhanina, N.; Komarova, B.; Zlotina, N.; Krylov, V.; Gerbst, A.; Tsvetkov, Y.; Nifantiev, N. Stereoselective α-Glycosylation with 3-*O*-Acetylated d-Gluco Donors. *Synlett* **2006**, *6*, 921−923.
(14) Komarova, B. S.; Tsvetkov, Y. E.; Knirel, Y. A.; Zähringer, U.; Pier, G. B.; Nifantiev, N. E. Synthesis of a Common Trisaccharide Fragment of Glycoforms of the Outer Core Region of the *Pseudomonas Aeruginosa* Lipopolysaccharide. *Tetrahedron Lett.* **2006**, *47*, 3583−3587.
(15) Komarova, B. S.; Tsvetkov, Y. E.; Pier, G. B.; Nifantiev, N. E. First Synthesis of Pentasaccharide Glycoform I of the Outer Core Region of the *Pseudomonas Aeruginosa* Lipopolysaccharide. *J. Org. Chem.* **2008**, *73*, 8411−8421.
(16) Tsvetkov, Y. E.; Burg-Roderfeld, M.; Loers, G.; Ardá, A.; Sukhova, E. V.; Khatuntseva, E. A.; Grachev, A. A.; Chizhov, A. O.; Siebert, H.-C.; Schachner, M.; Jiménez-Barbero, J.; Nifantiev, N. E. Synthesis and Molecular Recognition Studies of the HNK-1 Trisaccharide and Related Oligosaccharides. The Specificity of Monoclonal Anti-HNK-1 Antibodies as Assessed by Surface Plasmon Resonance and STD NMR. *J. Am. Chem. Soc.* **2012**, *134*, 426−435.
(17) Kearney, J. F.; McCarthy, M. T.; Stohrer, R.; Benjamin, W. H.; Briles, D. E. Induction of Germ-line Anti-alpha 1−3 Dextran Antibody Responses in Mice by Members of the Enterobacteriaceae Family. *J. Immunol.* **1985**, *135*, 3468−3472.
(18) Beauvais, A.; Perlin, D. S.; Latgé, J. P. Role of α(1−3) Glucan in *Aspergillus Fumigatus* and Other Human Fungal Pathogens. In *Fungi in the Environment*; Gadd, G. M., Watkinson, S. C., Dyer, P., Eds.; Cambridge University Press, 2007; pp 269−288.
(19) Elder, M. J.; Webster, S. J.; Chee, R.; Williams, D. L.; Hill Gaston, J. S.; Goodall, J. C. β-Glucan Size Controls Dectin-1-Mediated Immune Responses in Human Dendritic Cells by Regulating IL-1 Production. *Front. Immunol.* **2017**, *8*, 14−16.
(20) Brown, G. D.; Herre, J.; Williams, D. L.; Willment, J. A.; Marshall, A. S. J.; Gordon, S. Dectin-1 Mediates the Biological Effects of β-Glucans. *J. Exp. Med.* **2003**, *197*, 1119−1124.
(21) Gantner, B. N.; Simmons, R. M.; Canavera, S. J.; Akira, S.; Underhill, D. M. Collaborative Induction of Inflammatory Responses by Dectin-1 and Toll-like Receptor 2. *J. Exp. Med.* **2003**, *197*, 1107−1117.
(22) Latgé, J. Tasting the Fungal Cell Wall. *Cell. Microbiol.* **2010**, *12*, 863−872.
(23) Becker, K. L.; Aimanianda, V.; Wang, X.; Gresnigt, M. S.; Ammerdorffer, A.; Jacobs, C. W.; Gazendam, R. P.; Joosten, L. A. B.; Netea, M. G.; Latgé, J. P.; van de Veerdonk, F. L. *Aspergillus* Cell Wall Chitin Induces Anti- and Proinflammatory Cytokines in Human PBMCs via the Fc-γ Receptor/Syk/PI3K Pathway. *mBio* **2016**, *7*, e01823−15.
(24) Cobb, B. A.; Wang, Q.; Tzianabos, A. O.; Kasper, D. L. Polysaccharide Processing and Presentation by the MHCII Pathway. *Cell* **2004**, *117*, 677−87.
(25) Matveev, A. L.; Krylov, V. B.; Emelyanova, L. A.; Solovev, A. S.; Khlusevich, Y. A.; Baykov, I. K.; Fontaine, T.; Latgé, J.-P.; Tikunova, N. V.; Nifantiev, N. E. Novel Mouse Monoclonal Antibodies Specifically Recognize *Aspergillus fumigatus* Galactomannan. *PLoS One* **2018**, *13*, e0193938.
(26) Beauvais, A.; Maubon, D.; Park, S.; Morelle, W.; Tanguy, M.; Huerre, M.; Perlin, D. S.; Latge, J. P. Two α(1−3) Glucan Synthases with Different Functions in *Aspergillus fumigatus*. *Appl. Environ. Microbiol.* **2005**, *71*, 1531−1538.
(27) Brian, P. W.; Dawkins, A. W.; Grove, J. F.; Hemming, H. G.; Lowe, D.; Norris, G. L. F. Phytotoxic Compounds Produced by *Fusarium equiseti*. *J. Exp. Bot.* **1961**, *12*, 1−12.
(28) Harris, S. D.; Morrell, J. L.; Hamer, J. E. Identification and Characterization of *Aspergillus Nidulans* Mutants Defective in Cytokinesis. *Genetics* **1994**, *136*, 517−532.

DOI: 10.1021/acs.joc.8b01142
J. Org. Chem. 2018, 83, 12965−12976

frontiers in Cellular and Infection Microbiology

ORIGINAL RESEARCH
published: 08 November 2019
doi: 10.3389/fcimb.2019.00378

Importance of *Candida* Antigenic Factors: Structure-Driven Immunomodulation Properties of Synthetically Prepared Mannooligosaccharides in RAW264.7 Macrophages

Ema Paulovičová[1], Lucia Paulovičová[1], Pavol Farkaš[1], Alexander A. Karelin[2], Yury E. Tsvetkov[2], Vadim B. Krylov[2] and Nikolay E. Nifantiev[2]**

[1] Cell Culture & Immunology Laboratory, Department of Immunochemistry of Glycoconjugates, Center for Glycomics, Institute of Chemistry, Slovak Academy of Sciences, Bratislava, Slovakia, [2] Laboratory of Glycoconjugate Chemistry, N.D. Zelinsky Institute of Organic Chemistry, Russian Academy of Sciences, Moscow, Russia

The incidence and prevalence of serious fungal infections is rising, especially in immunosuppressed individuals. Moreover, co-administration of antibiotics and immunosuppressants has driven the emergence of new multidrug-resistant pathogens. The significant increase of multidrug-resistant pathogens, together with their ability to form biofilms, is associated with morbidity and mortality. Research on novel synthetically prepared immunomodulators as potential antifungal immunotherapeutics is of serious interest. Our study demonstrated the immunobiological activity of synthetically prepared biotinylated mannooligosaccharides mimicking *Candida* antigenic factors using RAW264.7 macrophages. Macrophage exposure to the set of eight structurally different mannooligosaccharides induced a release of Th1, Th2, Th17, and Treg cytokine signature patterns. The observed immune responses were tightly associated with structure, dose, exposure time, and selected signature cytokines. The viability/cytotoxicity of the mannooligosaccharide formulas was assessed based on cell proliferation. The structure-based immunomodulatory activity of the formulas was evaluated with respect to the length, branching and conformation of the various formulas. Glycoconjugate formulas with terminal β-mannosyl-units tended to be more potent in terms of *Candida* relevant cytokines IL-12 p70, IL-17, GM-CSF, IL-6, and TNFα induction and cell proliferation, and this tendency was associated with structural differences between the studied glycoconjugate formulas. The eight tested mannooligosaccharide conjugates can be considered potential *in vitro* immunomodulative agents suitable for *in vitro Candida* diagnostics or prospectively for subcellular anti-*Candida* vaccine design.

Keywords: *Candida*, oligomannosides, RAW 264.7, cytokines, proliferation

OPEN ACCESS

Edited by:
Laura Alcazar-Fuoli, Carlos III Health Institute, Spain

Reviewed by:
Jill R. Blankenship, University of Nebraska Omaha, United States
Ian A. Cleary, Grand Valley State University, United States

****Correspondence:***
Ema Paulovičová
ema.paulovicova@savba.sk
Nikolay E. Nifantiev
nen@ioc.ac.ru

Specialty section:
This article was submitted to Fungal Pathogenesis, a section of the journal Frontiers in Cellular and Infection Microbiology

Received: *04 July 2019*
Accepted: *21 October 2019*
Published: *08 November 2019*

Citation:
Paulovičová E, Paulovičová L, Farkaš P, Karelin AA, Tsvetkov YE, Krylov VB and Nifantiev NE (2019) Importance of Candida Antigenic Factors: Structure-Driven Immunomodulation Properties of Synthetically Prepared Mannooligosaccharides in RAW264.7 Macrophages. Front. Cell. Infect. Microbiol. 9:378. doi: 10.3389/fcimb.2019.00378

INTRODUCTION

Most *Candida* species, including the facultative pathogenic strains, belong to the normal commensal mycobiota of immunocompetent individuals. The factors affecting the candidosis are diverse, including the prolonged antifungal treatment in long-term care, immunosuppression associated with anticancer therapy and transplantation of solid organ or bone marrow, immunosuppressive states as diabetes mellitus and HIV, use of vascular devices and hospitalization at intensive care units (Richter et al., 2005; Angiolella et al., 2008; Adiguzel et al., 2010; Cortés and Corrales, 2018). Next, immunocompromised persons with genetic immune system defects are at high risk for mucocutaneous and invasive fungal infections (Vinh, 2011; Cunha and Carvalho, 2012; Pichard et al., 2015; Beenhouwer, 2018). Approximately 17 different *Candida* species are known etiological agents of human infections; more than 90% of systemic infections are caused by *Candida albicans (C. albicans)*, *Candida glabrata (C. glabrata), Candida parapsilosis (C. parapsilosis), Candida tropicalis (C. tropicalis)*, and *Candida krusei (C. krusei)* (Pfaller et al., 2002). The new multidrug-resistant species *Candida auris (C. auris)* was recently isolated (Sears and Schwartz, 2017; Forsberg et al., 2019). $CD4^+$-derived T-cell subpopulations Th1, Th2, and Th17 contribute to anti-*Candida* cellular immune protection. The protective anticandidal Th1 response requires the activity of various cytokines, such as interferon gamma (IFN-γ), transforming growth factor beta (TGF-β), interleukin 6 (IL-6), tumor necrosis factor alpha (TNFα), and IL-12. The induction of the protective antifungal Th1 immune response is inhibited by Th2 cytokines, such as IL-4 and IL-10 (Ito, 2011; Netea et al., 2015; Richardson and Moyes, 2015; Gow et al., 2017). In early infection, neutralization of Th1 cytokines, mainly IFN-γ and IL-12, leads predominately to the onset of Th2 rather than Th1 responses. Th2-type responses are frequently associated with susceptibility to recurrent or persistent infection and fungal allergy. TNFα, IL-1β, IL-6, IL-8, and colony-stimulating factors (CSFs) are among the major proinflammatory cytokines associated with the interaction of immune-competent cells with *Candida* cells. TNFα is thought to be essential in the primary control of disseminated infection caused by *C. albicans.* Although IL-1 shares common properties with TNFα, both IL-1β and IL-6, acting mainly through recruitment of polymorphonuclear neutrophils (PMNs), presumably are not as essential as TNFα in the innate antifungal response. IL-12 is recognized as essential to induce the protective Th1 response to the fungus, simultaneously blocking the Th2 response. The crucial role of the Th17 subset has been associated with anti-*Candida* effectiveness, especially the mucosal immune response (Romani, 2003; Rizzetto et al., 2010; van de Veerdonk and Netea, 2010). Proinflammatory cytokines, such as IL-12, IL-15, and TNFα, have been studied as candidate adjuvants in preclinical trials based on their ability to upregulate the antifungal Th1 response (Ashman and Papadimitriou, 1995; Romani, 2011; Pikman and Ben-Ami, 2012; Naglik, 2014).

Fungal cell wall antigenically active polysaccharides, such as N-linked and O-linked α- and β-mannans, chitin, α- and β-glucans, galactomannan, galactosaminogalactan, glucuronoxylomannan, and some others, are essential immunogens that play crucial roles during host-fungus interactive communication. Cell-wall components act as pathogen-associated molecular patterns (PAMPs), recognized by the immune system through pattern recognition receptors (PRRs) such as TLR2, TLR4, dectin-2, dectin-1, Mincle, DC-SIGN, or galectin-3, on the surfaces of epithelia and myeloid cells (Netea et al., 2006, 2008, 2015; Moyes and Naglik, 2011; Perez-Garcia et al., 2011; Romani, 2011; Cunha and Carvalho, 2012; Salek-Ardakani et al., 2012; Hall and Gow, 2013; Moyes et al., 2015; Zheng et al., 2015; Gow et al., 2017; Snarr et al., 2017).

Generally, specific PAMP–PRR interactions activate the inflammatory response by triggering interleukins and growth factors cell release and phagocytosis. *O*-linked mannans are recognized via TL4 receptor (Netea et al., 2006), α- linked *N*-mannans are sensed through mannose receptor, dectin-2, Mincle, and DC-SIGN (Harris et al., 2009; McKenzie et al., 2010), and the specific receptor for β-mannan is galectin-3 (Jouault et al., 2006; Linden et al., 2013). Chitin cooperates with the mannose receptor and induces TLR9 and NOD-2dependentIL-10 release (Wagener et al., 2014; Erwig and Gow, 2016). Recently, it has been demonstrated that chitin particles of small size stimulated IL-17, IL-12, IL-23, IL-10, and TNF-α in macrophages via a MyD88- and TLR2-dependent pathway (Da Silva et al., 2008, 2009). Additionally, Dectin-1 receptor on macrophages and TLR-2 recognizes β-1,3-glucan (Brown and Gordon, 2001; Brown et al., 2002, 2003; Brown, 2006). Dectin-1 uses Syk kinase and the CARD9 to stimulate IL-10, TLR2 via the MyD88 is required for the production of IL-12p40 (Dennehy et al., 2008; Netea et al., 2008), and both pathways collaborate in TNF- stimulation. Moreover, dectin-1 and galectin-3 interact synergistically to improve the outcome of host immune response to *C. albicans* (Gantner et al., 2003; Taylor et al., 2007; Esteban et al., 2011).

The antigenic factors of mannan from medically relevant *Candida* species have been characterized and their chemical structures determined in several studies (Nishikawa et al., 1982; Suzuki and Fukazawa, 1982; Shibata et al., 1995; Fukazawa et al., 1997; Suzuki, 1997). The antigenic determinants of cell wall polysaccharides and oligosaccharides from medically important yeasts have been studied for their serological specificity and biological activity (Fukazawa et al., 1997). The investigation of species-specific antigenic factor variations of *Candida* mannan and oligomannosyl structures is essential to evaluate the structure-activity relationship, since mannan structure and epitope availability intensely affect its immunobiological behavior (Trinel et al., 1992; Fukazawa et al., 1997; Suzuki, 1997; Shibata et al., 2007). The particular structure of mannan, comprising an α-1,6-mannoside backbone and side chains with α/β-1,2-mannoside or α/β-1,3-mannoside moieties of variable lengths, varies for different *Candida* species and is dependent on the expression of a complex network of mannan biosynthesis, trafficking, and cell wall remodeling genes (Shibata et al., 2012). Different growth conditions are likely to modulate the activation of cell wall signaling cascades, expression of cell wall biosynthesis genes, and alterations in mannan composition (Ernst and Pla, 2011; Lowman et al., 2011). The role of

mannosylation in fungal biology and virulence has been studied using *C. albicans* mutants; the suitability of these mutants for exploring the significance of specific mannan epitopes on cell function, pathogenesis and immune recognition has been proposed (Hall and Gow, 2013; Hall et al., 2013; West et al., 2013). Several studies have attempted to design and develop an anti-*Candida* vaccine based on cell wall-derived structures (Ito, 2011; Richardson and Moyes, 2015; Tso et al., 2018; Piccione et al., 2019). The immunogenic polysaccharide cell wall structures applied in experimental vaccine models include 65 kDa mannoproteins (Sandini et al., 2007), β-1,3-glucan (Torosantucci et al., 2005), and β-1,2- mannosides (Han et al., 1999; Cutler, 2005). These model structures were effective in humoral antibody-mediated antifungal protection. Several monoclonal antibodies were protective in preclinical studies: anti- β-1,3-glucan mAb2G8 (Torosantucci et al., 2005), anti-mannoprotein mAb C7 (Moragues et al., 2003), anti-idiotypic antibodies (Magliani et al., 2004), anti-mannan mAb (Han et al., 1999; Cutler, 2005), and anti-glycosyl mAb (Kavishwar and Shukla, 2006). These antibodies efficiently appeared as candidacidal (Moragues et al., 2003; Magliani et al., 2004; Kavishwar and Shukla, 2006), growth inhibitory, or they neutralized heat shock protein 90 (Hsp90) (Torosantucci et al., 2005). Moreover, mannan conjugated in certain vaccine formulas has already been included in clinical trials (Apostolopoulos et al., 2006; Pashov et al., 2011).

Mannan has also been studied as a promising bioactive material for drug nanocarrier systems and vaccine adjuvant formulations (Tang et al., 2009). Moreover, nanoliposomes with orthogonally bound mannan represent a platform for the development of targeted drug delivery systems and self-adjuvanted carriers for construction of recombinant vaccines (Bartheldyova et al., 2019). Concerning the design of anti-fungal vaccination therapy, apart from *Candida* cell wall moieties, potential new anti-*Candida* drugs have targeted the growth and virulence factors of *C. albicans*, including core signaling components of the high-osmolarity glycerol (HOG) and target of rapamycin (TOR) signaling pathways (Li et al., 2015), as well as various immunomodulators, e.g., colony-stimulating factors and proinflammatory cytokines (Pikman and Ben-Ami, 2012).

Natural *Candida* mannan is a complex polysaccharide structure containing linear and branched fragments composed of α- and β-mannose units, as seen in **Figure 1** (Klis et al., 2001), with the carbohydrate sequences represented according to symbol carbohydrate nomenclature (Varki et al., 1999). Thus, the use of such a heterogenic structure is problematic for the assessment of the biological role of its distinct fragments. However, the application of synthetic mannooligosaccharide derivatives, related to the structures of selected antigenic factors of *Candida* mannan, creates the opportunity to assess the biological roles of each antigenic factor.

Our work investigated the immunomodulation properties of antigenically active distinct parts of *C. albicans* mannan by using a series of structurally related synthetic mannooligosaccharides.

MATERIALS AND METHODS

Synthesis of Biotinylated Oligomannosides 1–8

Mannooligosaccharide conjugate formulas **1** (Krylov et al., 2018a), **2** (Krylov et al., 2018a,b), **3** (Karelin et al., 2007),

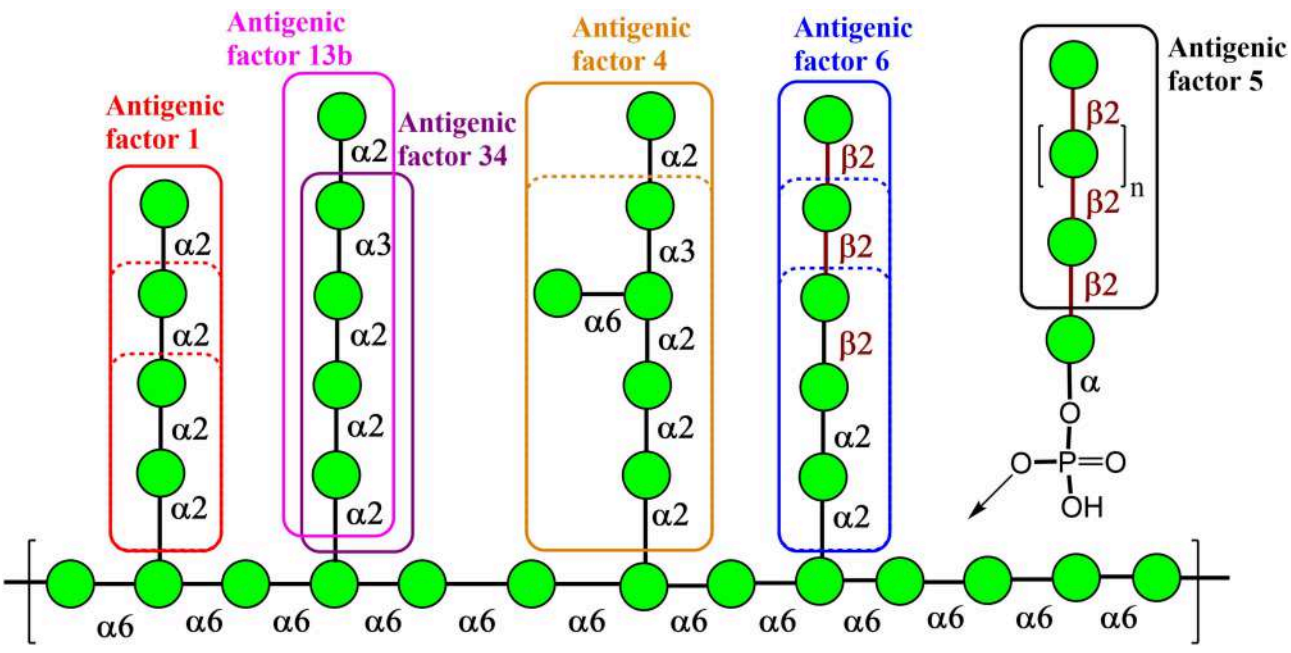

FIGURE 1 | Key structural elements of the cell wall mannan from the fungus *Candida albicans* representing its antigenic factors. The carbohydrate sequences are represented according to symbol carbohydrate nomenclature (Varki et al., 1999).

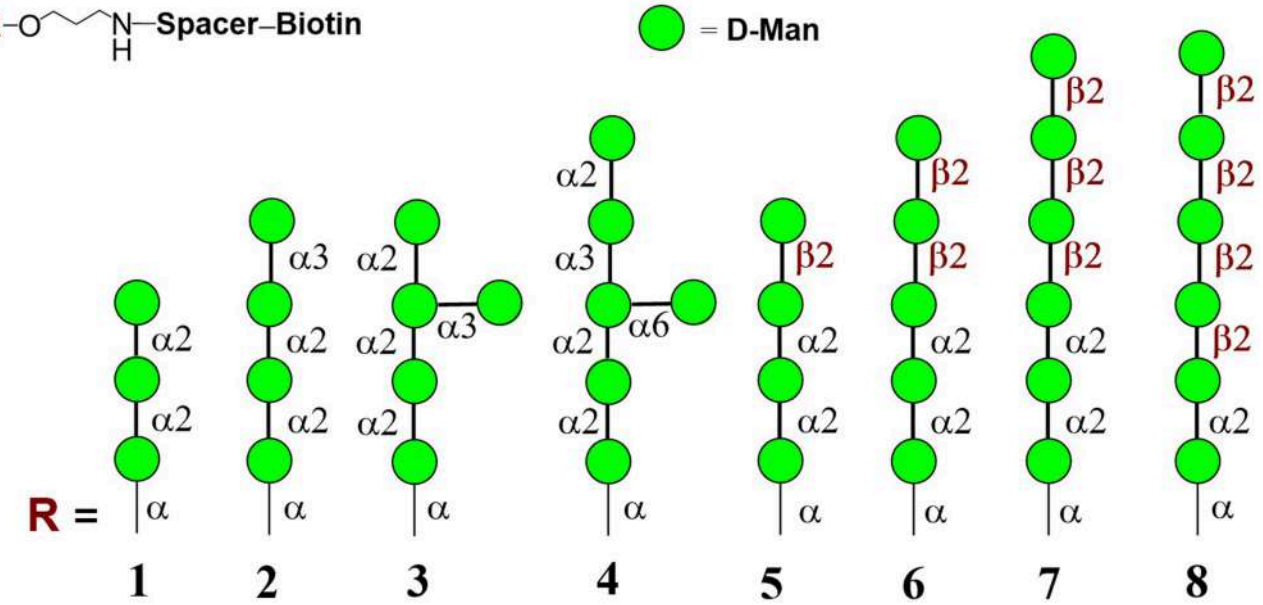

FIGURE 2 | Structures of studied biotinylated mannooligosaccharides **1**–**8** (Argunov et al., 2019).

4 (Karelin et al., 2010), and **5**–**8** (Karelin et al., 2016) were prepared by the biotinylation of parent ligands according to previously described biotinylation protocols (**Figure 2**) (Tsvetkov et al., 2012).

Isolation of Natural Cellular Mannan and Preparation of FITC-Labeled Mannan

The yeast strain *Candida albicans* CCY 29-3-100 (serotype A) (CCY Culture Collection of Yeasts, Institute of Chemistry, Center for Glycomics, Slovak Academy of Sciences, Bratislava, Slovakia) was used to isolate and purify cellular mannan from fresh biomass. Mannan was extracted by autoclaving in 0.2 mol/l NaCl (120°C, 700 kPa) for 10 min and purified using precipitation with Fehling reagent according to a previously described method (Peat et al., 1961).

For the preparation of FITC-labeled mannan, *C. albicans* CCY 29-3-100 mannan (54 mg) was suspended in 1.00 mL of dimethyl sulfoxide and 2.0 μL of pyridine was added. The suspension was heated in a thermoblock at 95°C until the mannan dissolved (3 h). Then, 20 mg of isothiocyanatofluorescein (FITC) was added and heated for another 2 h at 95°C. The reaction was quenched by addition of 10 mL of water, and the result was dialyzed using cellulose membrane tube (cut-off = 14,000, Sigma) against 0.05 % NaHCO3 (1 × 0.9 L, 4 h stirred) and deionized water [8 × 0.9 L, 4 h on stirrer or 12 h in the refrigerator (5°C)] and then lyophilized (FreeZone 18 Liter Console Freeze Dry System, Labconco Corporation, Kansas City, USA).

Preparation of Stock Solutions of Natural Cellular Mannan and Synthetically Prepared Mannooligosaccharides

Stock solutions and different dilutions of natural cellular mannan and glycoconjugate formulas **1**–**8** were prepared aseptically using pre-sterilized disposable plastic wares and sterile, apyrogenic aqua pro injectione (Fresenius Kabi Italia S.r.l., Verona, Italy). All solutions were prepared in a laminar flow hood and sterilized using a 0.2-μm filter (Q-Max® Syringe filter, Frisenette ApS, Knebel, Denmark) before exposure. The laminar flow cabinet was sterilized with 70% ethanol p.a. and UV for 30 min prior to each experiment. The stock solutions were assayed with EndoLISA® ELISA-based Endotoxin Detection Assay (Hyglos, Bernried am Starnberger See, Germany) and evaluated using the Cytation 5 Imager Multi-Mode Reader (BioTek, Winooski, USA) to ascertain endotoxin-free exposure conditions.

Cell Maintenance and Culture, Cell Exposure

The murine macrophage-like RAW 264.7 cell line was selected in the present study because this cell model has been frequently used in *in vitro* studies on phagocytosis, cytokine production, and to evaluate potential bioactive substances to predict their effect *in vivo*.

RAW 264.7 (ATCC® TIB-71™, ATCC, Manassas, USA) cells were cultured in complete Dulbecco's Modified Eagle Medium for 24 h and 48 h, at 37°C under 5% CO_2 atmosphere and 90–100% relative humidity until ∼80% confluence. Viability of cells was determined by Trypan Blue dye exclusion method using a TC20™ automated cell counter (Bio-Rad Laboratories, Inc., Hercules, USA). The starting inoculum of 1×10^5 cells/mL/well (98.3% of viable cells) was seeded in a 24-well cell culture plate (Sigma-Aldrich, St. Louis USA) and exposed to 10 and 100 μg per well of glycoconjugates for 24 and 48 h. Cell mitogens Concanavalin A (Con A; 10 μg/mL, Sigma-Aldrich), phytohemagglutinin (PHA; 10 μg/mL, Sigma-Aldrich), pokeweed mitogen (PWM, 1 μg/mL, Sigma-Aldrich), and lipopolysaccharide (LPS; 1 μg/mL, Sigma-Aldrich) were used

as positive controls. The cell culture media were separated and stored at −20°C until further use. Cell morphology and viability were assayed before ELISA and evaluation of cytotoxicity. The interaction of FITC-labeled *Candida* mannan (100 μg/mL) and RAW 264.7 macrophage cells (1×10^5 cells/mL) was evaluated using either light and fluorescence microscopy (AxioVision Imager A.1, magnification 630x; Zeiss, Wetzlar, Germany) or confocal imaging (Axio Observer LSM 880 employing an Airyscan Plan-Apochromat 63x/1.4 oil DIC M27 optical lens and Zen 2 software) with application of 3D Z-stack imaging (Zeiss).

Cell Proliferation and Cytotoxicity

The influence of glycoconjugates on RAW 264.7 cell proliferation and cytotoxicity was evaluated using the cell proliferation assay ViaLight™ plus kit (Lonza, Rockland, ME, USA) according to the manufacturer's recommendations. Cellular ATP was determined with luciferase-based luminescence quantification. The intensity of emitted light was measured using the Cytation 5 Cell Imaging Multi-Mode Reader (BioTek Instruments, Inc.). Light emission was recorded continuously for 1 s and peak values were evaluated and expressed as relative light units (RLU). The values of unexposed cells were considered the baseline. The proliferation index was calculated as the ratio between the stimulated cells (glycoconjugate formula-treated cells) and the baseline proliferation of unexposed cells. Thus, the proliferation index of the negative control, i.e., unexposed cells, was equal to one.

Determination of Interleukins and Growth Factors

The levels of interleukins and growth factors in cell culture supernates induced by exposure with glycoconjugate formulas **1**–**8** were assayed according to the manufacturer's instructions with Platinum ELISAs® (eBioscience, Thermo Fisher Scientific, Waltham, USA): Mouse IL-12 p70 (MDD 4 pg/mL), Mouse granulocyte-macrophage colony-stimulating factor (GM-CSF;MDD 2 pg/mL), Mouse IL-17 (MDD 1.6 pg/mL), and Mouse IL-6 (MDD 6.5 pg/mL), and Instant ELISAs® (eBioscience): Mouse tumor necrosis factor (TNF)-α (MDD 4 pg/mL), and Mouse IL-10 (MDD 5.28 pg/mL).

To compare the effect of different glycoconjugates on RAW 264.7 macrophage interleukins and growth factors, analyses were performed on raw cytokine concentration data and cytokine concentration data normalized to viable cell counts of untreated control RAW 264.7 cells. The raw concentrations of cytokines determined by ELISA were divided by the RLU [ATP detection systems to quantify viable cells, ViaLightTM plus kit (Lonza, USA)] of living cells in a corresponding sample and multiplied by the RLU of untreated control RAW 264.7 cells.

Statistical Analysis

The experimental results were expressed as mean values ± SD. Normality of data distribution was established according to the Shapiro–Wilk test at the 0.05 level of significance. Statistical comparisons were performed by one-way ANOVA and *post-hoc* Bonferroni tests. Pearson's correlation coefficient was used to compare the strength of the relationship between immunobiological variables. Results were significant when the differences equaled or exceeded the 95% confidence level ($P < 0.05$). Statistics were performed using ORIGIN 7.5 PRO software (OriginLab Corporation, Northampton, USA).

RESULTS

Modern chemical methods enable regio- and stereoselective assembling of linear and branched structures similar to *C. albicans* mannan (Collot et al., 2009; Karelin et al., 2017; Krylov et al., 2017). Here we report the results of our investigation into the structure-driven immunomodulating properties of synthetically prepared mannooligosaccharides in RAW264.7 macrophages using a synthetically prepared panel of biotinylated mannooligosaccharides, formulas **1**–**8** (**Figure 2**). These oligomannosides represented antigenic factor 1 (formula **1**), factor 34 (formula **2**), factor 4 (formula **4**), and factor 6 (formulas **5**–**8**) of *C. albicans* mannan. Side chains related to formula **3** were also found in *C. albicans* mannan (Kogan et al., 1988), but their antigenic specificity is not yet clear.

As natural *Candida* mannan (section Isolation of natural cellular mannan and preparation of FITC-labeled mannan) was utilized in all experiments as a comparative substance, evaluation of its interaction with RAW 264.7 cells was essential. Fluorescently labeled natural mannan was used to visualize the cell interaction and endocytotosis of *Candida* mannan by the murine macrophage RAW 264.7 cells. Evaluation of the interaction was performed with light and fluorescence microscopy (**Figure 3A**) and 3D Z-stack imaging (**Figure 3B**). The patterns documented the ingestion of mannan and its inclusion into subcellular compartments.

Interactions of Natural Mannan and Glycoconjugate Formulas 1–8 With Murine Macrophage Cell Line RAW 264.7, and Influence on Cell Proliferation

The effect of glycoconjugate formulas **1**–**8** on macrophage cell line RAW 264.7 proliferation was monitored by adenosine triphosphate (ATP) bioluminescence as a marker of cell viability (**Figure 4**). The lower concentration of glycoconjugate formulas **1**–**4** (10 μg/mL, **Figure 4A**) slightly decreased the proliferation of RAW 264.7 macrophages. Improved proliferation was observed for formula **1**, which is comprised of three α-1,2-Man units (24 h treatment). The higher concentration of formulas **1**–**4** (100 μg/mL, **Figure 4A**), which are comprised exclusively of α-linkages between Man residues, significantly decreased the proliferation of RAW 264.7 macrophages (between 94 and 98% reduction). As opposed to the α-mannooligosaccharides, treatment of RAW 264.7 macrophages with formulas **5**–**8**, which also contain β-1,2-linked Man units, slightly increased proliferation after 24 h, and the increase was more significant after 48 h stimulation (**Figure 4B**). The highest proliferations were observed for the 10 μg/mL concentration of tetramer formula **5**, which contains one terminal β-1,2-linked Man unit (2.1 times higher than control), and hexamer formula **8**, which contains a tetrameric block of β-1,2-linked Man units (2.2

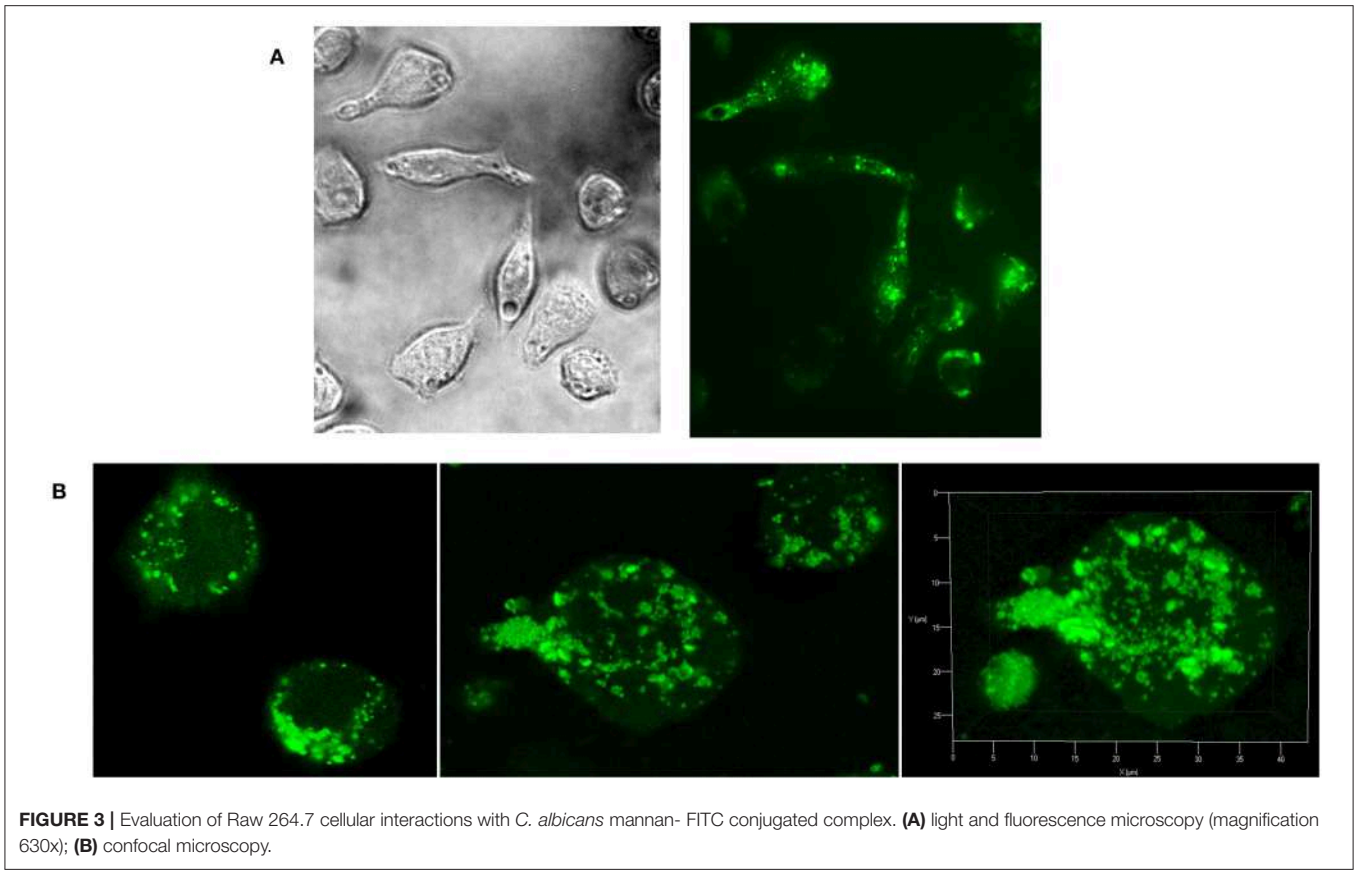

FIGURE 3 | Evaluation of Raw 264.7 cellular interactions with *C. albicans* mannan- FITC conjugated complex. **(A)** light and fluorescence microscopy (magnification 630x); **(B)** confocal microscopy.

times higher than control). The proliferation of RAW 264.7 macrophages treated by glycoconjugates for 48 h was significantly lower (formulas **1**–**4**: $p < 0.01$, formulas **5**–**8**: $p < 0.01$) compared with natural *C. albicans* mannan (M, **Figure 4C**).

Cytokine Responses of RAW 264.7 Macrophages *in vitro* to Glycoconjugate Formulas 1–8

The *in vitro* stimulatory effect of glycoconjugate formulas **1**–**8** on RAW 264.7 macrophage cytokine production was determined by the levels of pro-inflammatory cytokines TNFα, IL-6, IL-17, IL-12, anti-inflammatory cytokine IL-10, and haemopoietic growth factor GM-CSF in supernatants obtained from cultures of RAW264.7 macrophages after 24 or 48 h treatments [not normalized raw cytokine concentrations (**Supplementary Figures 1**, **2**) and cytokine concentrations normalized to viable cell counts of untreated control RAW 264.7 cells (**Figures 5**, **6**)].

Non-normalized raw cytokine concentrations data showed that stimulation of RAW 264.7 cells with the lower concentration of glycoconjugate formulas **1**–**4** (10 μg/mL), which contain linked Man residues, resulted in a slight increase of TNFα production; maximal effect was observed for formula **1** (24 h treatment: 1.37-fold increase and 48 h treatment: 1.48-fold increase, **Supplementary Figure 1**). The stimulation of RAW 264.7 macrophages with the higher concentration of glycoconjugate formulas (100 μg/mL) significantly decreased TNFα production (more than 70% decrease compared to the control). However, IL-6 and GM-CSF production showed different concentration dependencies. The higher concentration of glycoconjugate formulas **1**–**4** (100 μg/mL) induced comparable or higher IL-6 and GM-CSF secretion than the lower concentration (10 μg/mL) (**Supplementary Figure 1**). The highest IL-6 and GM-CSF release was observed for glycoconjugate formula **3** (IL-6: 3.2-fold increase, GM-CSF: 1.9-fold increase).

Glycoconjugate formulas **1**–**4** induced increased IL-17 production (**Supplementary Figure 1**). The higher concentration of glycoconjugate formulas **1**–**4** (100 μg/mL) induced higher IL-17 secretion, except for glycoconjugate formula **3**, for which IL-17 production declined with increasing glycoconjugate concentration (**Supplementary Figure 1**). Production of IL-12 showed a structure related dependency (**Supplementary Figure 1**). The most effective IL-12 inducer was glycoconjugate formula **1**, and induction efficacy declined slightly with increasing number of mannose units in glycoconjugate formulas **1**–**4** (**Supplementary Figure 1**). Glycoconjugate formulas **1**–**4** did not significantly influence IL-10 production (non-normalized data, **Supplementary Figure 1**). The results indicated a higher proinflammatory response associated with glycoconjugate formulas **1**–**4,** containing linked Man residues, with significant reduction of RAW 264.7 macrophage proliferation.

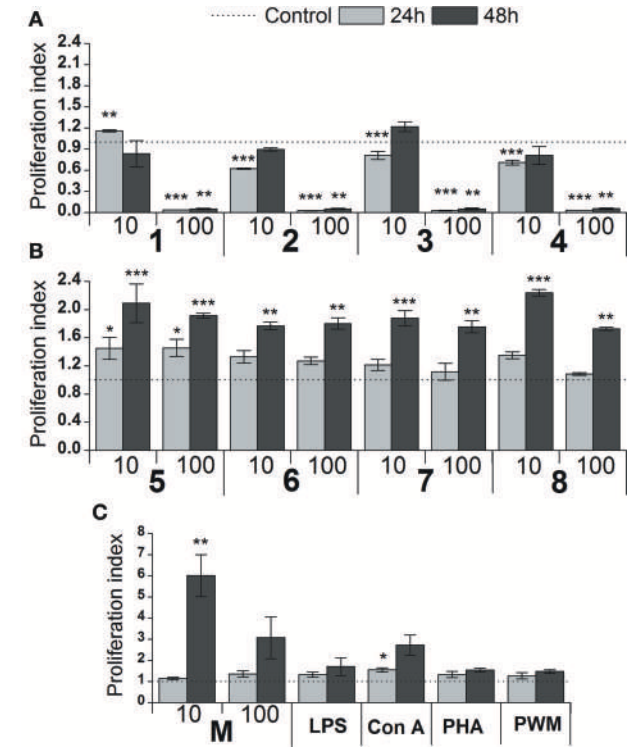

FIGURE 4 | Effect of glycoconjugate formulas **1–8** on proliferation of RAW264.7 macrophages. **(A)**: glycoconjugate formulas **1**, **2**, **3**, and **4**; **(B)**: glycoconjugate formulas **5**, **6**, **7**, and **8**; 10 and 100 μg/mL); **(C)**: *C. albicans* mannan (M, 10 and 100 μg/mL), lipopolysaccharide (LPS, 1 μg/mL), Concanavalin A (Con A, 10 μg/mL), phytohemagglutinin (PHA, 10 μg/mL) and pokeweed mitogen (PWM, 1 μg/mL) for 24 and 48 h. Each value represents the mean ± SD of the proliferation index. The statistical significance of differences between stimulated cells and untreated cells are expressed: *$0.01 < P < 0.05$, **$0.001 < P < 0.01$, ***$P < 0.001$.

The stimulation of RAW 264.7 macrophages with glycoconjugate formulas **5–8** showed a different impact on TNFα production compared to glycoconjugate formulas **1–4** (**Supplementary Figure 2**). Higher TNFα production was observed during the shorter exposure period (24 h). The higher tested concentration (100 μg/mL) significantly increased TNFα production, with maximal efficacy for glycoconjugate formula **6** (24 h: 29.4-fold increase, 48 h: 13.4-fold increase compared to the control). Production of IL-6, GM-CSF, IL-17, and IL-12 also showed a concentration dependency, with higher efficacy for the higher concentrations of glycoconjugate formulas **5–8** (100 μg/mL). The highest IL-6 secretion was induced by glycoconjugate formula **6** (**Supplementary Figure 2**, 24 h: 48.8-fold increase, 48 h: 40.0-fold increase, compared to the control). Additionally, glycoconjugate formula **6** induced a strong increase in IL-17, IL-12, and IL-10 production (**Supplementary Figure 2**). Stimulation with β-mannooligosaccharides **6** and **8** for 24 h markedly increased the production of TNFα (100 μg/mL, $p < 0.001$), IL-6 (100 μg/mL, $p < 0.001$), IL-12 (100 μg/mL, $p < 0.001$), and IL10 (100 μg/mL, $p < 0.001$) compared with natural *C. albicans* mannan.

Due to the tested glycoconjugates having a significant effect on RAW 264.7 macrophage proliferation, especially for glycoconjugate formulas **1–4** that contain α-linked Man residues, the raw data of cytokine concentrations in the culture supernatants were normalized to the viable cell counts of untreated control RAW 264.7 cells for each experiment. We observed that the normalization of cytokine concentration data showed no significant trend change for stimulation of RAW 264.7 macrophages with the β-mannooligosaccharide glycoconjugates (formulas **5–8**) (**Figure 6**). Out of all tested β-mannooligosaccharide glycoconjugates, the most effective cytokine inducers were glycoconjugate formulas **6** and **8**. The highest TNFα (24 h: 23.2-fold increase), IL-6 (24 h, 38.5-fold increase), IL-12 (24 h: 15.6-fold increase), and IL-10 (24 h: 15.3-fold increase) secretion was induced by glycoconjugate formula **6**. The GM-CSF (24 h: 14.5-fold increase) and IL-17 (24 h: 3.1-fold increase) was most effectively induced by β-mannooligosaccharide glycoconjugate formula **8**. Normalization of the cytokine concentration data after stimulation with α-mannooligosaccharide glycoconjugates (formulas **1–4**) (**Figure 5**) accentuated the release of cytokines induced by the higher concentration of glycoconjugates (100 μg/mL). We observed significant capability to induce TNFα, IL-6, GM-CSF, IL-17, and IL-12 production accompanied by an increase of IL-10 after stimulation with all α-mannooligosaccharide glycoconjugates, induced especially with higher 100 μg/mL concentration, that strongly reduced the proliferation of RAW 264.7 cells. The highest production of TNFα, IL-6, GM-CSF, and IL-10 was observed after the shorter exposure time (24 h) with glycoconjugate formula **3**.

The influence of glycoconjugate formulas **1–8** on Th1 and Th2 polarization was revealed based on the TNFα (Th1) to IL-10 (Th2) and IL-6 (Th2) to IL-10 (Th2) ratios (**Figure 7**). Th1 dominance was represented by a higher ratio, while a lower ratio expressed a Th2 dominated environment. Concerning the ratios following 24 and 48 h exposures with 100 and 10 μg/mL of glycoconjugate formulas **1–4**, Th1 dominance based on the TNFα/IL-10 ratio was revealed for conjugate formulas **1** and **4**, while conjugate formulas **2** and **3** exerted Th1 dominance with higher TNFα/IL-10 ratios over IL-6/IL-10 ratios only at the lower concentration (10 μg/mL) after 48 h exposure. For conjugate formulas **5–8**, the values of the TNFα/IL-10 ratios overcame the values of the IL-6/IL-10 ratios following 24 and 48 h exposures with both concentrations for all conjugates, reflecting Th1 dominance.

The resulting *in vitro* proinflammatory effect of glycoconjugate formulas **5-8**, containing terminal β-mannosyls, overcame that of the α-mannooligosaccharides. This was supported by statistically insignificant correlations between the release of proinflammatory cytokines following 24 and 48 h exposures with α-mannooligosaccharides. Significant overall correlations were determined between the release of proinflammatory cytokines induced by individual β-mannooligosaccharides glycoconjugate formulas following 24 h exposure: TNFα and IL-6 ($R = 0.994$ $p = 5.38 \times 10^{-7}$), TNFα and IL-12 ($R = 0.969$ $p = 6.71 \times 10^{-5}$), and IL-12 and IL-6 (R

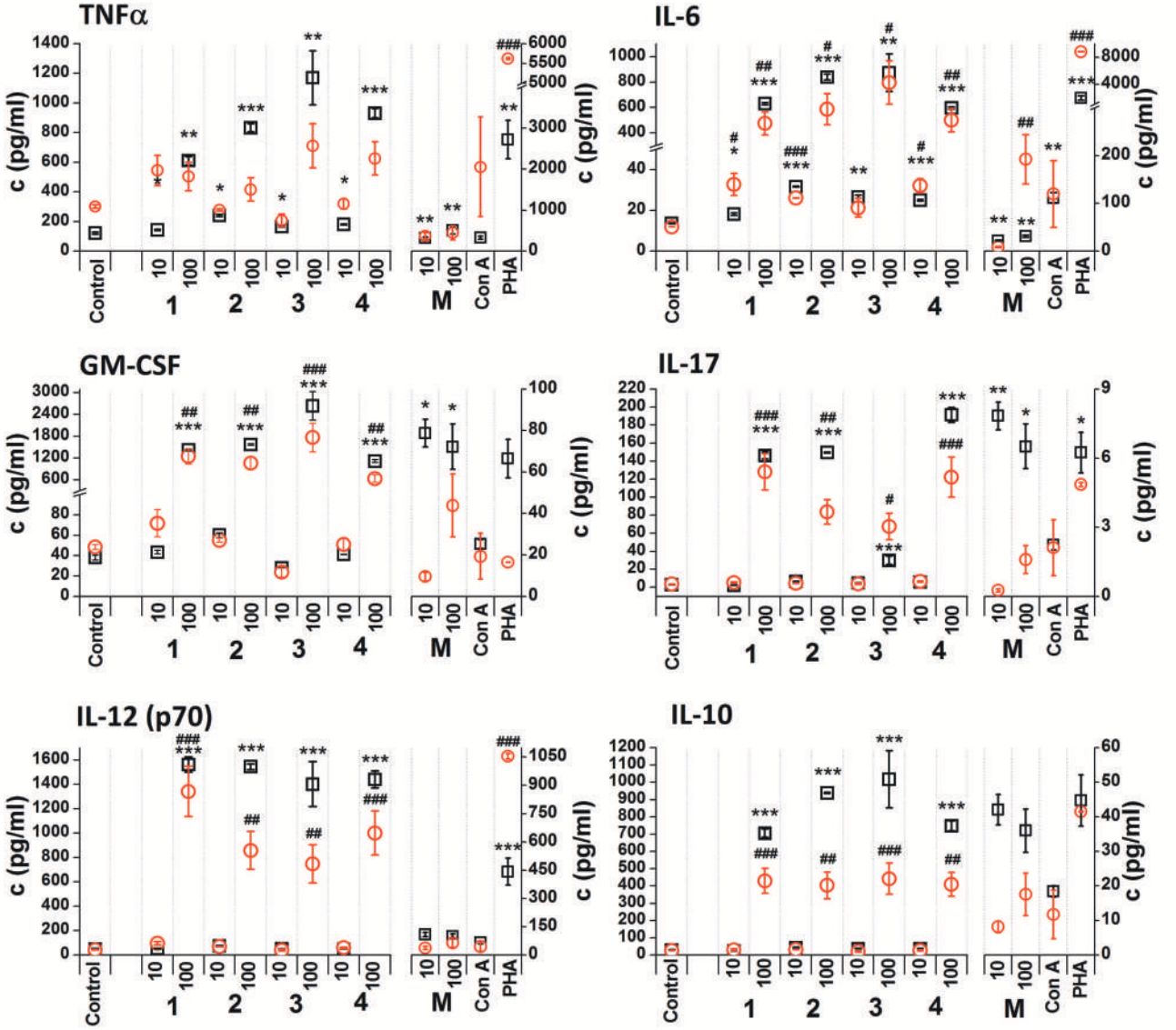

FIGURE 5 | Effect of glycoconjugate formulas **1**–**4** on RAW 264.7 macrophage cytokine production. Negative control represents untreated cells (Control); positive controls: *C. albicans* mannan (M, 10 or 100 μg/mL), Concanavaline A (Con A, 10 μg/mL) and phytohemagglutinin (PHA, 10 μg/mL). All data were normalized to the viable cells' count of untreated control cells of each experiment and are presented as Mean ± SD. Tests were carried out in triplicate. The statistical significance of differences between untreated cells and stimulated cells are expressed: 24 h treatment: $^{***}P < 0.001$, $^{**}0.001 < P < 0.01$, $^{*}0.01 < P < 0.05$; 48 h treatment: $^{\#\#\#}P < 0.001$, $^{\#\#}0.001 < P < 0.01$, $^{\#}0.01 < P < 0.05$.

$= 0.989$ $p = 2.61 \times 10^{-6}$). After 48 h, a significant correlation was also revealed between IL-17 and IL-12 ($R = 0.877$ $p = 0.0042$).

DISCUSSION

Several attempts have been made to synthesize relevant mannan epitopes with immunobiological effectiveness. Synthetically prepared mannooligosaccharides mimicking *Candida* antigenic factors (Karelin et al., 2010, 2015, 2016, 2017) represent promising study models to establish the immunomodulating activity of such formulas on humoral and cellular immunity for subcellular anti-*Candida* vaccine construction (Paulovicova et al., 2010, 2012, 2014; Paulovicova L. et al., 2013).

The immunobiological importance and vaccination potency of synthetically prepared β-1,2-mannopyranosyl trisaccharide mimicking the structure of the *C. albicans* cell surface epitope has previously been studied (Xin et al., 2008, 2012; Costello and Bundle, 2012; Cartmell et al., 2015; Bundle et al.,

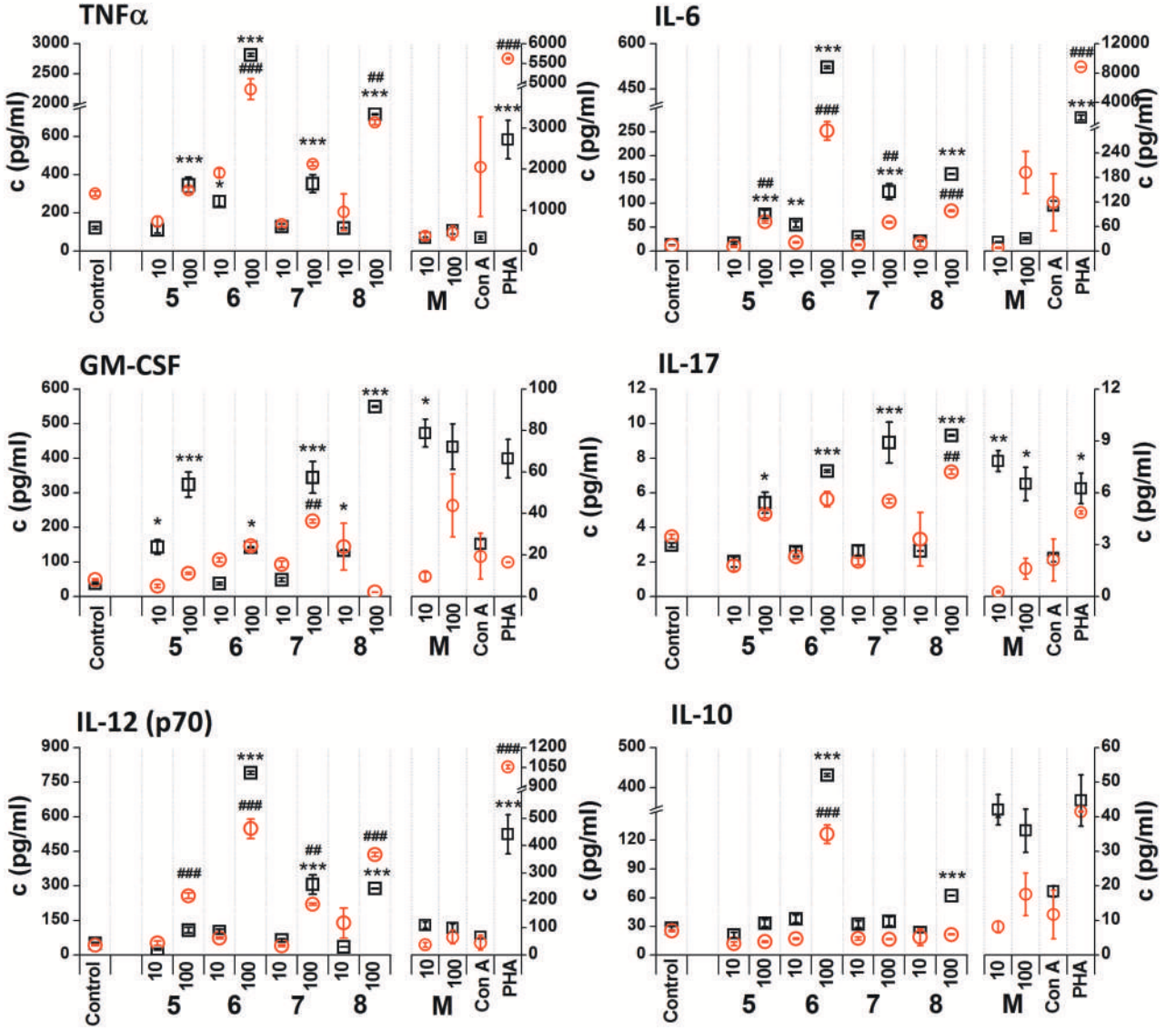

FIGURE 6 | Effect of glycoconjugate formulas **5**–**8** on RAW 264.7 macrophage cytokine production. Negative control represents untreated cells (Control); positive controls: *C. albicans* mannan (M, or 100 μg/mL), Concanavaline A (Con A, 10 μg/mL) and phytohemagglutinin (PHA, 10 μg/mL). All data were normalized to the viable cells' count of untreated control cells of each experiment and are presented as mean ± SD. Tests were carried out in triplicate. The statistical significance of differences between untreated cells and stimulated cells are expressed as follows: 24 h treatment: $^{***}P < 0.001$, $^{**}0.001 < P < 0.01$, $^{*}0.01 < P < 0.05$; 48 h treatment: $^{\#\#\#}P < 0.001$, $^{\#\#}0.001 < P < 0.01$, $^{\#}0.01 < P < 0.05$.

2018). Next, a novel tetrasaccharide construct consisting of β-1,2-mannopyranosyl trisaccharide and α-mannopyranoside was designed and suggested as a model of the *C. albicans* phosphodiester epitope (Dang et al., 2012). Glycoarrays formed by biotinylated oligosaccharides loaded on streptavidin-coated surfaces were previously shown to be indispensable instruments for the investigation of carbohydrate antigen recognition by immune cells (Komarova et al., 2015, 2018; Akhmatova et al., 2016; Paulovicova et al., 2016, 2017; Kurbatova et al., 2017; Argunov et al., 2019; Schubert et al., 2019).

Moreover, the sera reactivity and determination of antigen-specific isotypic antibodies against synthetically prepared mannooligosaccharides were evaluated in a cohort of patients with vulvovaginal candidosis (Karelin et al., 2016; Paulovicova et al., 2016, 2017). Postvaccination antisynthetic heptamannoside polyclonal sera inhibited growth of the azole-resistant clinical strain *C. albicans* CCY 29-3-164 and reduced the number of colony-forming units throughout an experimental mucosal infection (Paulovicova E. et al., 2013). Next, sera cytokine patterns of Th1/Th2/Th17 polarization of immune responses

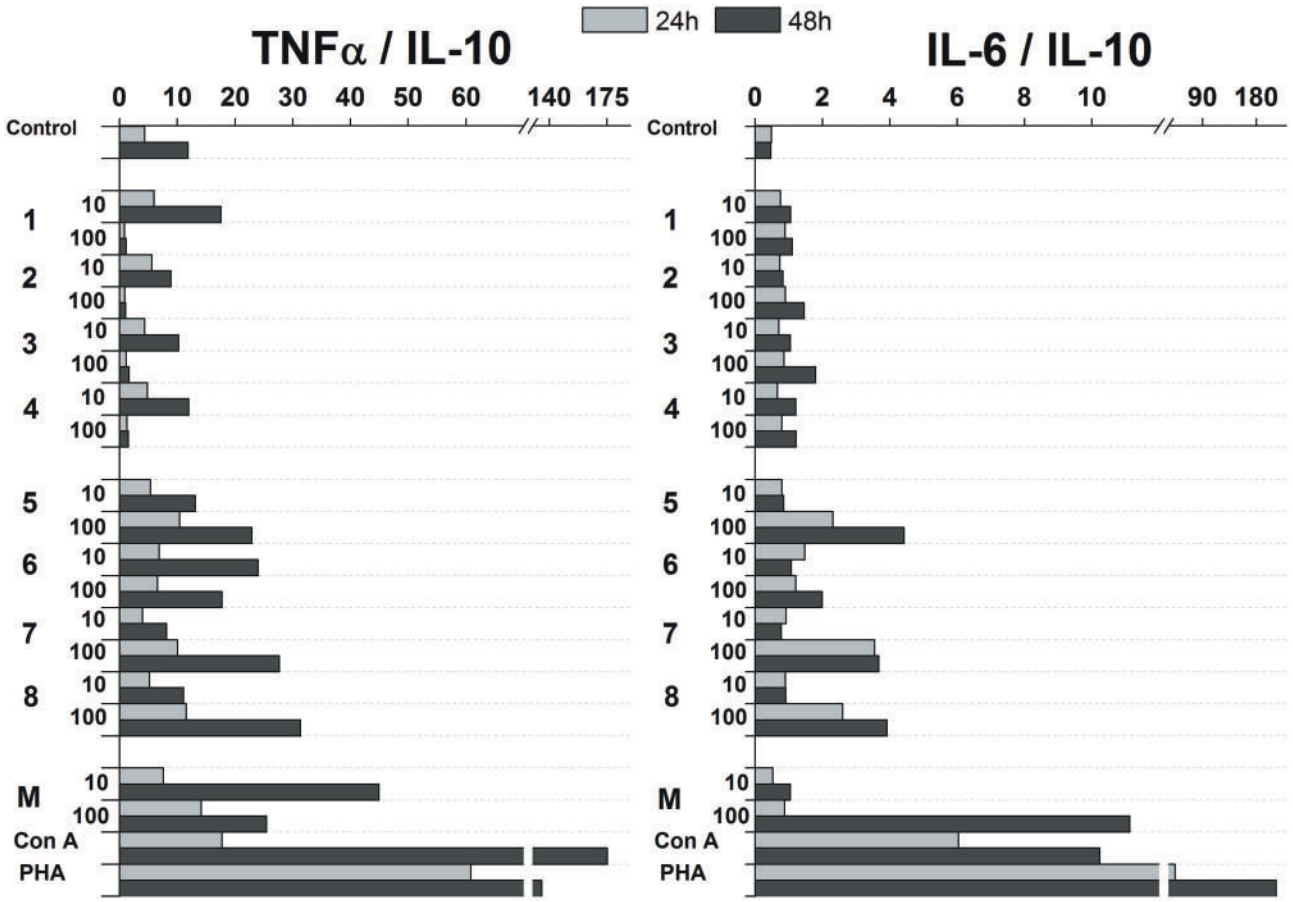

FIGURE 7 | Influence of glycoconjugate formulas **1–8** on Th1 and Th2 polarization based on TNFα to IL-10 and IL-6 to IL-10 ratios.

by synthetic oligosaccharide–BSA conjugates revealed a tight structure-activity relationship (Paulovicova E. et al., 2013; Paulovicova et al., 2017).

Here, the proliferating and cytokine-inducing activities of a series of synthetically prepared nanopolymers mimicking native *C. albicans* cell wall immunogenic moieties were studied using RAW264.7 cell exposure (**Figure 4**). The cell proliferation results revealed almost immunoinhibitory activity of α- mannoside formulas **1–4** (trisaccharide through hexasaccharide), with more pronounced activity with increasing concentration ($p < 0.001$), in contrast with native *C. albicans* cell wall mannan (**Figure 4**). These findings concur with previously published studies (Podzorski et al., 1989, 1990) that reported the immunoinhibitory influence of members of a family of mannose oligosaccharides (disaccharide through hexasaccharide) derived from cetyltrimethylammonium bromide (CTAB) mannan (native *C. albicans* mannan prepared by complexation with CTAB). CTAB mannan was a potent stimulator of lymphoproliferative when added to human peripheral blood mononuclear cells (PMBCs) from donors responsive to *Candida*; it had no inhibitory influence on lymphoproliferation induced by *Candida* or other antigens. Two major oligomannosyl components, mannobiose and mannotriose, of CTAB mannan with an inhibitory effect on cell proliferation were demonstrated to be bound mainly through α(1,2) linkages (Hayette et al., 1992). In contrast, synthetically prepared mannooligosaccharide formulas **5–8** with terminal β-mannosyl units (**Figure 3**) exerted a stimulatory effect on RAW264.7 cell proliferation ($p < 0.001$). Thus, the immunobiological properties of the studied mannooligosaccharides are dose- and structure-dependent. Cell release of interleukins and growth factors associated with inflammation and proliferation was induced by mannooligomers to different extents depending on the oligomer structures (normalized data: **Figures 5**, **6**, not normalized data: **Supplementary Figures 1**, **2**).

Upregulation of cytokines such as TNFα, IL-6, IL-12, GM-CSF was more evident with mannooligosaccharides with terminal β-mannosyl units. Acceleration of secretion of anti-inflammatory cytokine IL-10 with Th1-inhibiting properties was also revealed with β-mannooligosaccharides (**Supplementary Figure 2**). Association between pro- and anti-inflammatory cytokines, in addition to Th1, Th2 and Th17 polarization, is an important prerequisite for the assessment of immunogenic substance behavior. The influence of glycoconjugate formulas **1–8** on

Th1 and Th2 polarization, based on TNFα to IL-10 and IL-6 to IL-10 ratios (**Figure 7**), resulted in a predominant Th1 immune response. Th1 dominance, represented by higher TNFα/IL-10 and IL-6/IL-10 ratios with higher dose and following prolonged treatment, was revealed with tested **1**–**8** formulas, and was more evident for formulas **5**–**8** with β-terminal mannosyls; the Th2 dominated environment was not determined. The observed immune response was tightly associated with dose, exposure time, and selected signature cytokines. The TNFα/IL-10 ratio was more descriptive than the IL-6/IL-10 ratio, presumably due to dual IL-6 roles, i.e., anti-inflammatory activities of IL-6 are mediated by classic signaling, whereas proinflammatory responses of IL-6 are mediated by trans-signaling (Scheller et al., 2011). Saijo et al. reported induced release of cytokines, such as IL-12p40, IL-6, TNFα, and IL-10, from wild-type bone marrow-derived dendritic cells (BMDCs) by treatment with *C. albicans* water soluble fraction (CAWs) and *C. albicans* mannans (Saijo et al., 2010). Moreover, they also observed the secretion of yeast- and hyphae-specific cytokines following cell exposure with both *C. albicans* morphoforms. *C. albicans* mannan, glucomannoprotein and phospholipomannan, containing β-1,2 oligomannosides, induced TNFα in association with degree of polymerization (DP). Jouault et al. noted that TNFα-release occurred most in the presence of relatively long chains of β-oligomannosides (i.e., an oligomannoside comprised of eight mannose units was superior to shorter chains, and oligomannosides of less than four mannose units were not active) (Jouault et al., 1995). Evidently a minimal DP of 4 was necessary to induce production of cytokine (Poulain et al., 1997). With synthetically prepared α- and β- oligomannosides, effective TNFα release was triggered by trimannosides. The ability of β-oligomannosides to induce release of TNFα was also demonstrated by Cutler (2001).

Additionally, cell exposure to conjugate formula **6**, which comprises 2 β and 3α mannosyls, exerted the highest media release of IL-12p70, IL-6, TNFα, and IL-10 (**Figure 6**). Interestingly, conjugate formula **8**, with 4β and 2α-linked mannosyls, induced higher IL-17 and regulatory GM-CSF cell release than the other β-oligomannosides (**Figure 6**).

CONCLUSIONS

Our data suggest an immunobiological role for synthesized mannooligosaccharides that closely resemble *Candida* cell wall mannooligomers. The observed Th1/Th2/Th17 immune responses were tightly associated with structure, dose, exposure time, and selected signature cytokines. Glycoconjugate formulas **5**–**8**, with terminal β-mannosyl-units, tended to be more potent than glycoconjugate formulas **1**–**4** in terms of *Candida* relevant cytokines IL-12 p70, IL-17, GM-CSF, IL-6, and TNFα induction and cell proliferation, and this tendency was associated with structural differences between the studied glycoconjugate formulas. Obtained results warrant further systematic investigation of the immunological properties of carbohydrate antigens of the *Candida* cell wall toward the selection of efficient structures suitable for application as immunomodulative agents either for *in vitro Candida* diagnostics or prospectively for subcellular anti-*Candida* vaccine design.

DATA AVAILABILITY STATEMENT

All datasets generated for this study are included in the article/**Supplementary Material**.

AUTHOR CONTRIBUTIONS

EP, LP, and NN contributed to the conception and design of the study, performed the immunobiological research and analyzed data, acquired funding, and prepared the original draft. PF performed the modification and characterization of mannan. AK, YT, and VK performed the chemical syntheses and analyzed data. All authors contributed to manuscript revision, read, and approved the submitted version.

FUNDING

The synthetic part of this work was supported by the Russian Science Foundation (grant 19-73-30017), while the immunological part of the work was supported by the Scientific Grant Agency of the Slovak Republic VEGA (project 2/0098/17) and the Slovak Research and Development Agency (contract N° APVV-15-0161).

SUPPLEMENTARY MATERIAL

The Supplementary Material for this article can be found online at: https://www.frontiersin.org/articles/10.3389/fcimb.2019.00378/full#supplementary-material

REFERENCES

Adiguzel, N., Karakurt, Z., Gungor, G., Yazicioglu Mocin, O., Acarturk, E., Sogukpinar, O., et al. (2010). Mortality rates and risk factors associated with nosocomial Candida infection in a respiratory intensive care unit. *Tuberkuloz ve toraks* 58, 35–43.

Akhmatova, N. K., Kurbatova, E. A., Akhmatov, E. A., Egorova, N. B., Logunov, D. Y., Gening, M. L., et al. (2016). The effect of a BSA conjugate of a synthetic hexasaccharide related to the fragment of capsular polysaccharide of *Streptococcus pneumoniae* type 14 on the activation of innate and adaptive immune responses. *Front. Immunol.* 7:248. doi: 10.3389/fimmu.2016.00248

Angiolella, L., Stringaro, A. R., De Bernardis, F., Posteraro, B., Bonito, M., Toccacieli, L., et al. (2008). Increase of virulence and its phenotypic traits in drug-resistant strains of *Candida albicans*. *Antimicrob. Agents Chemother.* 52, 927–936. doi: 10.1128/AAC.01223-07

Apostolopoulos, V., Pietersz, G. A., Tsibanis, A., Tsikkinis, A., Drakaki, H., Loveland, B. E., et al. (2006). Pilot phase III immunotherapy study in early-stage breast cancer patients using oxidized mannan-MUC1 [ISRCTN71711835]. *Breast Cancer Res.* 8:R27. doi: 10.1186/bcr1505

Argunov, D. A., Trostianetskaia, A. S., Krylov, V. B., Kurbatova, E. A., and Nifantiev, N. E. (2019). Convergent synthesis of oligosaccharides structurally related to galactan I and galactan II of *Klebsiella pneumoniae* and their use

in screening of antibody specificity. *Eur. J. Org. Chem.* 2019, 4226–4232 doi: 10.1002/ejoc.201900389

Ashman, R. B., and Papadimitriou, J. M. (1995). Production and function of cytokines in natural and acquired immunity to *Candida albicans* infection. *Microbiol. Rev.* 59, 646–672.

Bartheldyova, E., Turanek Knotigova, P., Zachova, K., Masek, J., Kulich, P., Effenberg, R., et al. (2019). N-Oxy lipid-based click chemistry for orthogonal coupling of mannan onto nanoliposomes prepared by microfluidic mixing: synthesis of lipids, characterisation of mannan-coated nanoliposomes and in vitro stimulation of dendritic cells. *Carbohydr. Polym.* 207, 521–532. doi: 10.1016/j.carbpol.2018.10.121

Beenhouwer, D. O. (2018). "Chapter 17 - Molecular basis of diseases of immunity," in *Molecular Pathology, 2nd Edn.* eds W. B. Coleman and G. J. Tsongalis (London: Academic Press), 329–345. doi: 10.1016/B978-0-12-802761-5.00017-1

Brown, G. D. (2006). Dectin-1: a signalling non-TLR pattern-recognition receptor. *Nat. Rev. Immunol.* 6, 33–43. doi: 10.1038/nri1745

Brown, G. D., and Gordon, S. (2001). Immune recognition. A new receptor for beta-glucans. *Nature* 413, 36–37. doi: 10.1038/35092620

Brown, G. D., Herre, J., Williams, D. L., Willment, J. A., Marshall, A. S., and Gordon, S. (2003). Dectin-1 mediates the biological effects of beta-glucans. *J. Exp. Med.* 197, 1119–1124. doi: 10.1084/jem.20021890

Brown, G. D., Taylor, P. R., Reid, D. M., Willment, J. A., Williams, D. L., Martinez-Pomares, L., et al. (2002). Dectin-1 is a major beta-glucan receptor on macrophages. *J. Exp. Med.* 196, 407–412. doi: 10.1084/jem.20020470

Bundle, D. R., Paszkiewicz, E., Elsaidi, H. R. H., Mandal, S. S., and Sarkar, S. (2018). A three component synthetic vaccine containing a beta-Mannan T-cell peptide epitope and a beta-Glucan dendritic cell ligand. *Molecules* 23:E1961. doi: 10.3390/molecules23081961

Cartmell, J., Paszkiewicz, E., Dziadek, S., Tam, P. H., Luu, T., Sarkar, S., et al. (2015). Synthesis of antifungal vaccines by conjugation of beta-1,2 trimannosides with T-cell peptides and covalent anchoring of neoglycopeptide to tetanus toxoid. *Carbohydr. Res.* 403, 123–134. doi: 10.1016/j.carres.2014.06.024

Collot, M., Loukou, C., Mallet, J.-M., and N.E., N. (2009). "Chemical synthesis of the oligosaccharidic fragments of yeast mannans," in *Progress in the Synthesis of Complex Carbohydrate Chains of Plant and Microbial Polysaccharides*, ed N. E. Nifantiev (Trivandrum: Transworld Research Network), 371–398.

Cortés, J. A., and Corrales, F. I. (2018). "Invasive candidiasis: epidemiology and risk factors," in Fungal *Infection*, eds É. S. d. Loreto and J. S. M. Tondolo (London: IntechOpe).

Costello, C., and Bundle, D. R. (2012). Synthesis of three trisaccharide congeners to investigate frame shifting of beta1,2-mannan homo-oligomers in an antibody binding site. *Carbohydr. Res.* 357, 7–15. doi: 10.1016/j.carres.2012.03.019

Cunha, C., and Carvalho, A. (2012). Host genetics and invasive fungal diseases: towards improved diagnosis and therapy? *Expert Rev. Anti Infect. Ther.* 10, 257–259. doi: 10.1586/eri.12.3

Cutler, J. E. (2001). N-glycosylation of yeast, with emphasis on *Candida albicans*. *Med. Mycol.* 39 (Suppl. 1), 75–86. doi: 10.1080/mmy.39.1.75.86

Cutler, J. E. (2005). Defining criteria for anti-mannan antibodies to protect against candidiasis. *Curr. Mol. Med.* 5, 383–392. doi: 10.2174/1566524054022576

Da Silva, C. A., Chalouni, C., Williams, A., Hartl, D., Lee, C. G., and Elias, J. A. (2009). Chitin is a size-dependent regulator of macrophage TNF and IL-10 production. *J. Immunol.* 182, 3573–3582. doi: 10.4049/jimmunol.0802113

Da Silva, C. A., Hartl, D., Liu, W., Lee, C. G., and Elias, J. A. (2008). TLR-2 and IL-17A in chitin-induced macrophage activation and acute inflammation. *J. Immunol.* 181, 4279–4286. doi: 10.4049/jimmunol.181.6.4279

Dang, A. T., Johnson, M. A., and Bundle, D. R. (2012). Synthesis of a *Candida albicans* tetrasaccharide spanning the beta1,2-mannan phosphodiester alpha-mannan junction. *Org. Biomol. Chem.* 10, 8348–8360. doi: 10.1039/c2ob26355f

Dennehy, K. M., Ferwerda, G., Faro-Trindade, I., Pyz, E., Willment, J. A., Taylor, P. R., et al. (2008). Syk kinase is required for collaborative cytokine production induced through Dectin-1 and Toll-like receptors. *Eur. J. Immunol.* 38, 500–506. doi: 10.1002/eji.200737741

Ernst, J. F., and Pla, J. (2011). Signaling the glycoshield: maintenance of the *Candida albicans* cell wall. *Int. J. Med. Microbiol.* 301, 378–383. doi: 10.1016/j.ijmm.2011.04.003

Erwig, L. P., and Gow, N. A. (2016). Interactions of fungal pathogens with phagocytes. *Nat. Rev. Microbiol.* 14, 163–176. doi: 10.1038/nrmicro.2015.21

Esteban, A., Popp, M. W., Vyas, V. K., Strijbis, K., Ploegh, H. L., and Fink, G. R. (2011). Fungal recognition is mediated by the association of dectin-1 and galectin-3 in macrophages. *Proc. Natl. Acad. Sci. U.S.A.* 108, 14270–14275. doi: 10.1073/pnas.1111415108

Forsberg, K., Woodworth, K., Walters, M., Berkow, E. L., Jackson, B., Chiller, T., et al. (2019). Candida auris: the recent emergence of a multidrug-resistant fungal pathogen. *Med. Mycol.* 57, 1–12. doi: 10.1093/mmy/myy054

Fukazawa, Y., Kagaya, K., Suzuki, M., and Shinoda, T. (1997). "Serological specificity and biological activity of cell wall polysaccharides of medically important yeasts," in *Fungal Cells in Biodefense Mechanism,* eds S. Suzuki and M. Suzuki (Tokyo: Saigon Publishing), 17–24.

Gantner, B. N., Simmons, R. M., Canavera, S. J., Akira, S., and Underhill, D. M. (2003). Collaborative induction of inflammatory responses by dectin-1 and Toll-like receptor 2. *J. Exp. Med.* 197, 1107–1117. doi: 10.1084/jem.20021787

Gow, N. A. R., Latge, J. P., and Munro, C. A. (2017). The fungal cell wall: structure, biosynthesis, and function. *Microbiol. Spectr.* 5, 1–25. doi: 10.1128/microbiolspec.FUNK-0035-2016

Hall, R. A., Bates, S., Lenardon, M. D., Maccallum, D. M., Wagener, J., Lowman, D. W., et al. (2013). The Mnn2 mannosyltransferase family modulates mannoprotein fibril length, immune recognition and virulence of *Candida albicans*. *PLoS Pathog.* 9:e1003276. doi: 10.1371/journal.ppat.1003276

Hall, R. A., and Gow, N. A. (2013). Mannosylation in *Candida albicans*: role in cell wall function and immune recognition. *Mol. Microbiol.* 90, 1147–1161. doi: 10.1111/mmi.12426

Han, Y., Ulrich, M. A., and Cutler, J. E. (1999). *Candida albicans* mannan extract-protein conjugates induce a protective immune response against experimental candidiasis. *J. Infect. Dis.* 179, 1477–1484. doi: 10.1086/314779

Harris, M., Mora-Montes, H. M., Gow, N. A., and Coote, P. J. (2009). Loss of mannosylphosphate from *Candida albicans* cell wall proteins results in enhanced resistance to the inhibitory effect of a cationic antimicrobial peptide via reduced peptide binding to the cell surface. *Microbiology* 155, 1058–1070. doi: 10.1099/mic.0.026120-0

Hayette, M. P., Strecker, G., Faille, C., Dive, D., Camus, D., Mackenzie, D. W., et al. (1992). Presence of human antibodies reacting with *Candida albicans* O-linked oligomannosides revealed by using an enzyme-linked immunosorbent assay and neoglycolipids. *J. Clin. Microbiol.* 30, 411–417.

Ito, J. I. (2011). T cell immunity and vaccines against invasive fungal diseases. *Immunol. Invest.* 40, 825–838. doi: 10.3109/08820139.2011.595472

Jouault, T., El Abed-El Behi, M., Martinez-Esparza, M., Breuilh, L., Trinel, P. A., Chamaillard, M., et al. (2006). Specific recognition of *Candida albicans* by macrophages requires galectin-3 to discriminate *Saccharomyces cerevisiae* and needs association with TLR2 for signaling. *J. Immunol.* 177, 4679–4687. doi: 10.4049/jimmunol.177.7.4679

Jouault, T., Lepage, G., Bernigaud, A., Trinel, P. A., Fradin, C., Wieruszeski, J. M., et al. (1995). Beta-1,2-linked oligomannosides from *Candida albicans* act as signals for tumor necrosis factor alpha production. *Infect. Immun.* 63, 2378–2381.

Karelin, A. A., Tsvetkov, Y. E., Kogan, G., Bystricky, S., and Nifantiev, N. E. (2007). Synthesis of oligosaccharide fragments of mannan from *Candida albicans* cell wall and their BSA conjugates. *Russ. J. Bioorg. Chem.* 33, 110–121. doi: 10.1134/S106816200701013X

Karelin, A. A., Tsvetkov, Y. E., and Nifantiev, N. E. (2017). Synthesis of oligosaccharides related to cell wall polysaccharides of the fungi *Candida* and *Aspergillus*. *Russ. Chem. Rev.* 86, 1073–1126. doi: 10.1070/RCR4750

Karelin, A. A., Tsvetkov, Y. E., Paulovičová, E., Paulovičová, L., and Nifantiev, N. E. (2015). Blockwise synthesis of a pentasaccharide structurally related to the mannan fragment from the *Candida albicans* cell wall corresponding to the antigenic factor 6. *Russ. Chem. Bull.* 64, 2942–2948. doi: 10.1007/s11172-015-1251-5

Karelin, A. A., Tsvetkov, Y. E., Paulovicova, E., Paulovicova, L., and Nifantiev, N. E. (2016). A blockwise approach to the synthesis of (1 -> 2)-linked oligosaccharides corresponding to fragments of the acid-stable beta-mannan from the *Candida albicans* cell wall. *Eur. J. Org. Chem.* 2016, 1173–1181. doi: 10.1002/ejoc.201501464

Karelin, A. A., Tsvetkov, Y. E., Paulovicova, L., Bystricky, S., Paulovicova, E., and Nifantiev, N. E. (2010). Synthesis of 3,6-branched oligomannoside fragments of the mannan from *Candida albicans* cell wall corresponding to the antigenic factor 4. *Carbohydr. Res.* 345, 1283–1290. doi: 10.1016/j.carres.2009.11.012

Kavishwar, A., and Shukla, P. K. (2006). Candidacidal activity of a monoclonal antibody that binds with glycosyl moieties of proteins of *Candida albicans*. *Med. Mycol.* 44, 159–167. doi: 10.1080/13693780500266038

Klis, F. M., de Groot, P., and Hellingwerf, K. (2001). Molecular organization of the cell wall of *Candida albicans*. *Med. Mycol.* 39 (Suppl. 1), 1–8. doi: 10.1080/744118876

Kogan, G., Pavliak, V., and Masler, L. (1988). Structural studies of mannans from the cell-walls of the pathogenic yeasts *Candida albicans* Serotype-A and serotype-B and *Candidia parapsilosis*. *Carbohydr. Res.* 172, 243–253. doi: 10.1016/S0008-6215(00)90858-9

Komarova, B. S., Orekhova, M. V., Tsvetkov, Y. E., Beau, R., Aimanianda, V., Latge, J. P., et al. (2015). Synthesis of a pentasaccharide and neoglycoconjugates related to fungal alpha-(1 -> 3)-glucan and their use in the generation of antibodies to trace *Aspergillus fumigatus* cell wall. *Chem. A Eur. J.* 21, 1029–1035. doi: 10.1002/chem.201404770

Komarova, B. S., Wong, S. S. W., Orekhova, M. V., Tsvetkov, Y. E., Krylov, V. B., Beauvais, A., et al. (2018). Chemical synthesis and application of biotinylated oligo-alpha-(1 –> 3)-d-glucosides to study the antibody and cytokine response against the cell wall alpha-(1 –> 3)-d-glucan of *Aspergillus fumigatus*. *J. Org. Chem.* 83, 12965–12976. doi: 10.1021/acs.joc.8b01142

Krylov, V. B., Paulovicova, L., Paulovicova, E., Tsvetkov, Y. E., and Nifantiev, N. E. (2017). Recent advances in the synthesis of fungal antigenic oligosaccharides. *Pure Appl. Chem.* 89, 885–898. doi: 10.1515/pac-2016-1011

Krylov, V. B., Petruk, M. I., Grigoryev, I. V., Lebedin, Y. S., Glushko, N. I., Khaldeeva, E. V., et al. (2018a). Study of the carbohydrate specificity of antibodies against *Aspergillus fumigatus* using the library of synthetic mycoantigens. *Russ. J. Bioorg. Chem.* 44, 80–89. doi: 10.1134/S1068162017060073

Krylov, V. B., Petruk, M. I., Karelin, A. A., Yashunuskii, D. V., Tsvetkov, Y. E., Glushko, N. I., et al. (2018b). Carbohydrate specificity of antibodies against yeast preparations of *Saccharomyces cerevisiae* and *Candida krusei*. *Appl. Biochem. Microbiol.* 54, 665–669. doi: 10.1134/S0003683818060108

Kurbatova, E. A., Akhmatova, N. K., Akhmatova, E. A., Egorova, N. B., Yastrebova, N. E., Sukhova, E. V., et al. (2017). Neoglycoconjugate of tetrasaccharide representing one repeating unit of the *Streptococcus pneumoniae* type 14 capsular polysaccharide induces the production of opsonizing IgG1 antibodies and possesses the highest protective activity as compared to hexa- and octasaccharide conjugates. *Front. Immunol.* 8:659. doi: 10.3389/fimmu.2017.00659

Li, X., Hou, Y., Yue, L., Liu, S., Du, J., and Sun, S. (2015). Potential targets for antifungal drug discovery based on growth and virulence in *Candida albicans*. *Antimicrob. Agents Chemother.* 59, 5885–5891. doi: 10.1128/AAC.00726-15

Linden, J. R., De Paepe, M. E., Laforce-Nesbitt, S. S., and Bliss, J. M. (2013). Galectin-3 plays an important role in protection against disseminated candidiasis. *Med. Mycol.* 51, 641–651. doi: 10.3109/13693786.2013.770607

Lowman, D. W., Ensley, H. E., Greene, R. R., Knagge, K. J., Williams, D. L., and Kruppa, M. D. (2011). Mannan structural complexity is decreased when *Candida albicans* is cultivated in blood or serum at physiological temperature. *Carbohydr. Res.* 346, 2752–2759. doi: 10.1016/j.carres.2011.09.029

Magliani, W., Conti, S., Salati, A., Vaccari, S., Ravanetti, L., Maffei, D. L., et al. (2004). Therapeutic potential of yeast killer toxin-like antibodies and mimotopes. *FEMS Yeast Res.* 5, 11–18. doi: 10.1016/j.femsyr.2004.06.010

McKenzie, C. G., Koser, U., Lewis, L. E., Bain, J. M., Mora-Montes, H. M., Barker, R. N., et al. (2010). Contribution of *Candida albicans* cell wall components to recognition by and escape from murine macrophages. *Infect. Immun.* 78, 1650–1658. doi: 10.1128/IAI.00001-10

Moragues, M. D., Omaetxebarria, M. J., Elguezabal, N., Sevilla, M. J., Conti, S., Polonelli, L., et al. (2003). A monoclonal antibody directed against a *Candida albicans* cell wall mannoprotein exerts three anti-C. albicans activities. *Infect. Immun.* 71, 5273–5279. doi: 10.1128/IAI.71.9.5273-5279.2003

Moyes, D. L., and Naglik, J. R. (2011). Mucosal immunity and *Candida albicans* infection. *Clin. Dev. Immunol.* 2011:346307. doi: 10.1155/2011/346307

Moyes, D. L., Richardson, J. P., and Naglik, J. R. (2015). *Candida albicans*-epithelial interactions and pathogenicity mechanisms: scratching the surface. *Virulence* 6, 338–346. doi: 10.1080/21505594.2015.1012981

Naglik, J. R. (2014). Candida immunity. *N. J. Sci.* 2014:27. doi: 10.1155/2014/390241

Netea, M. G., Brown, G. D., Kullberg, B. J., and Gow, N. A. (2008). An integrated model of the recognition of *Candida albicans* by the innate immune system. *Nat. Rev. Microbiol.* 6, 67–78. doi: 10.1038/nrmicro1815

Netea, M. G., Gow, N. A., Munro, C. A., Bates, S., Collins, C., Ferwerda, G., et al. (2006). Immune sensing of *Candida albicans* requires cooperative recognition of mannans and glucans by lectin and Toll-like receptors. *J. Clin. Invest.* 116, 1642–1650. doi: 10.1172/JCI27114

Netea, M. G., Joosten, L. A., van der Meer, J. W., Kullberg, B. J., and van de Veerdonk, F. L. (2015). Immune defence against *Candida* fungal infections. *Nat. Rev. Immunol.* 15, 630–642. doi: 10.1038/nri3897

Nishikawa, A., Shinoda, T., and Fukazawa, Y. (1982). Immunochemical determinant and serological specificity of *Candida krusei*. *Mol. Immunol.* 19, 367–373. doi: 10.1016/0161-5890(82)90202-4

Pashov, A., Monzavi-Karbassi, B., and Kieber-Emmons, T. (2011). Glycan mediated immune responses to tumor cells. *Hum. Vaccin.* 7, 156–165. doi: 10.4161/hv.7.0.14578

Paulovicova, E., Paulovicova, L., Hrubisko, M., Krylov, V. B., Argunov, D. A., and Nifantiev, N. E. (2017). Immunobiological activity of synthetically prepared immunodominant galactomannosides structurally mimicking *Aspergillus* galactomannan. *Front. Immunol.* 8:1273. doi: 10.3389/fimmu.2017.01273

Paulovicova, E., Paulovicova, L., Pilisiova, R., Bystricky, S., Yashunsky, D. V., Karelin, A. A., et al. (2013). Synthetically prepared glycooligosaccharides mimicking *Candida albicans* cell wall glycan antigens–novel tools to study host-pathogen interactions. *FEMS Yeast Res.* 13, 659–673. doi: 10.1111/1567-1364.12065

Paulovicova, E., Paulovicova, L., Pilisiova, R., Jancinova, V., Yashunsky, D. V., Karelin, A. A., et al. (2016). The evaluation of beta-(1 –> 3)-nonaglucoside as an anti-*Candida albicans* immune response inducer. *Cell. Microbiol.* 18, 1294–1307. doi: 10.1111/cmi.12631

Paulovicova, L., Bystricky, S., Paulovicova, E., Karelin, A. A., Tsvetkov, Y. E., and Nifantiev, N. E. (2010). Model alpha-mannoside conjugates: immunogenicity and induction of candidacidal activity. *FEMS Immunol. Med. Microbiol.* 58, 307–313. doi: 10.1111/j.1574-695X.2009.00642.x

Paulovicova, L., Paulovicova, E., and Bystricky, S. (2014). Immunological basis of anti-Candida vaccines focused on synthetically prepared cell wall mannan-derived manno-oligomers. *Microbiol. Immunol.* 58, 545–551. doi: 10.1111/1348-0421.12195

Paulovicova, L., Paulovicova, E., Karelin, A. A., Tsvetkov, Y. E., Nifantiev, N. E., and Bystricky, S. (2012). Humoral and cell-mediated immunity following vaccination with synthetic *Candida* cell wall mannan derived heptamannoside-protein conjugate Immunomodulatory properties of heptamannoside-BSA conjugate. *Int. Immunopharmacol.* 14, 179–187. doi: 10.1016/j.intimp.2012.07.004

Paulovicova, L., Paulovicova, E., Karelin, A. A., Tsvetkov, Y. E., Nifantiev, N. E., and Bystricky, S. (2013). Effect of branched -oligomannoside structures on induction of anti-Candida humoral immune response. *Scand. J. Immunol.* 77, 431–441. doi: 10.1111/sji.12044

Peat, S., Whelan, W. J., and Edwards, T. E. (1961). 6. Polysaccharides of baker's yeast. Part IV. Mannan. *J. Chem. Soc.* 29–34. doi: 10.1039/jr9610000029

Perez-Garcia, L. A., Diaz-Jimenez, D. F., Lopez-Esparza, A., and Mora-Montes, H. M. (2011). Role of cell wall polysaccharides during recognition of *Candida albicans* by the innate immune system. *J. Glycobiol.* 1, 1–7. doi: 10.4172/jgb.1000102

Pfaller, M. A., Messer, S. A., Hollis, R. J., and Jones, R. N. (2002). Antifungal activities of posaconazole, ravuconazole, and voriconazole compared to those of itraconazole and amphotericin B against 239 clinical isolates of *Aspergillus* spp. and other filamentous fungi: report from SENTRY Antimicrobial Surveillance Program, 2000. *Antimicrob. Agents Chemother.* 46, 1032–1037. doi: 10.1128/AAC.46.4.1032-1037.2002

Piccione, D., Mirabelli, S., Minto, N., and Bouklas, T. (2019). Difficult but not impossible: in search of an anti-Candida vaccine. *Curr. Trop. Med. Rep.* 6, 42–49. doi: 10.1007/s40475-019-00173-2

Pichard, D. C., Freeman, A. F., and Cowen, E. W. (2015). Primary immunodeficiency update: part II. Syndromes associated with mucocutaneous candidiasis and noninfectious cutaneous manifestations. *J. Am. Acad. Dermatol.* 73, 367–381; quiz 381–362. doi: 10.1016/j.jaad.2015.01.055

Pikman, R., and Ben-Ami, R. (2012). Immune modulators as adjuncts for the prevention and treatment of invasive fungal infections. *Immunotherapy* 4, 1869–1882. doi: 10.2217/imt.12.127

Podzorski, R. P., Gray, G. R., and Nelson, R. D. (1990). Different effects of native *Candida albicans* mannan and mannan-derived oligosaccharides on antigen-stimulated lymphoproliferation in vitro. *J. Immunol.* 144, 707–716.

Podzorski, R. P., Herron, M. J., Fast, D. J., and Nelson, R. D. (1989). Pathogenesis of candidiasis. Immunosuppression by cell wall mannan catabolites. *Arch. Surg.* 124, 1290–1294. doi: 10.1001/archsurg.1989.01410110044009

Poulain, D., Jouault, T., and Trinel, P. A. (1997). "Immunoreactivity of *Candida albicans* β-1,2 linked oligomannosides and phospholipomannan," in *Fungal Cells in Biodefense Mechanism*, eds. S. Suzuki and M. Suzuki (Tokyo: Saigon Publishing), 175–181.

Richardson, J. P., and Moyes, D. L. (2015). Adaptive immune responses to *Candida albicans* infection. *Virulence* 6, 327–337. doi: 10.1080/21505594.2015.1004977

Richter, S. S., Galask, R. P., Messer, S. A., Hollis, R. J., Diekema, D. J., and Pfaller, M. A. (2005). Antifungal susceptibilities of Candida species causing vulvovaginitis and epidemiology of recurrent cases. *J. Clin. Microbiol.* 43, 2155–2162. doi: 10.1128/JCM.43.5.2155-2162.2005

Rizzetto, L., Kuka, M., De Filippo, C., Cambi, A., Netea, M. G., Beltrame, L., et al. (2010). Differential IL-17 production and mannan recognition contribute to fungal pathogenicity and commensalism. *J. Immunol.* 184, 4258–4268. doi: 10.4049/jimmunol.0902972

Romani, L. (2003). "Cytokines of innate and adaptive immunity to *Candida albicans*," in *Cytokines and Chemokines in Infectious Diseases Handbook*, eds. M. Kotb and T. Calandra (Totowa, NJ: Humana Press), 227–241. doi: 10.1385/1-59259-309-7:227

Romani, L. (2011). Immunity to fungal infections. *Nat. Rev. Immunol.* 11, 275–288. doi: 10.1038/nri2939

Saijo, S., Ikeda, S., Yamabe, K., Kakuta, S., Ishigame, H., Akitsu, A., et al. (2010). Dectin-2 recognition of alpha-mannans and induction of Th17 cell differentiation is essential for host defense against *Candida albicans*. *Immunity* 32, 681–691. doi: 10.1016/j.immuni.2010.05.001

Salek-Ardakani, S., Cota, E., and Bignell, E. (2012). Host-fungal interactions: key players of antifungal immunity. *Expert Rev. Anti Infect. Ther.* 10, 149–151. doi: 10.1586/eri.11.169

Sandini, S., La Valle, R., De Bernardis, F., Macrì, C., and Cassone, A. (2007). The 65 kDa mannoprotein gene of *Candida albicans* encodes a putative β-glucanase adhesin required for hyphal morphogenesis and experimental pathogenicity. *Cell. Microbiol.* 9, 1223–1238. doi: 10.1111/j.1462-5822.2006.00862.x

Scheller, J., Chalaris, A., Schmidt-Arras, D., and Rose-John, S. (2011). The pro- and anti-inflammatory properties of the cytokine interleukin-6. *Biochim. Biophys. Acta* 1813, 878–888. doi: 10.1016/j.bbamcr.2011.01.034

Schubert, M., Xue, S., Ebel, F., Vaggelas, A., Krylov, V. B., Nifantiev, N. E., et al. (2019). Monoclonal antibody AP3 binds galactomannan antigens displayed by the pathogens *Aspergillus flavus*, *A. fumigatus*, and A. parasiticus. *Front. Cell. Infect. Microbiol.* 9:234. doi: 10.3389/fcimb.2019.00234

Sears, D., and Schwartz, B. S. (2017). *Candida auris*: an emerging multidrug-resistant pathogen. *Int. J. Infect. Dis.* 63, 95–98. doi: 10.1016/j.ijid.2017.08.017

Shibata, N., Ikuta, K., Imai, T., Satoh, Y., Satoh, R., Suzuki, A., et al. (1995). Existence of branched side chains in the cell wall mannan of pathogenic yeast, *Candida albicans*. Structure-antigenicity relationship between the cell wall mannans of *Candida albicans* and Candida parapsilosis. *J. Biol. Chem.* 270, 1113–1122. doi: 10.1074/jbc.270.3.1113

Shibata, N., Kobayashi, H., and Suzuki, S. (2012). Immunochemistry of pathogenic yeast, Candida species, focusing on mannan. *Proc. Jpn. Acad. Ser. B Phys. Biol. Sci.* 88, 250–265. doi: 10.2183/pjab.88.250

Shibata, N., Suzuki, A., Kobayashi, H., and Okawa, Y. (2007). Chemical structure of the cell-wall mannan of *Candida albicans* serotype A and its difference in yeast and hyphal forms. *Biochem. J.* 404, 365–372. doi: 10.1042/BJ20070081

Snarr, B. D., Qureshi, S. T., and Sheppard, D. C. (2017). Immune recognition of fungal polysaccharides. *J. Fungi* 3:47. doi: 10.3390/jof3030047

Suzuki, M., and Fukazawa, Y. (1982). Immunochemical characterization of *Candida albicans* cell wall antigens: specific determinant of *Candida albicans* serotype A mannan. *Microbiol. Immunol.* 26, 387–402. doi: 10.1111/j.1348-0421.1982.tb00189.x

Suzuki, S. (1997). "Structural investigation of mannans of medicinally relevant Candida species; Determination of chemical structures of antigenic factors, 1, 4, 5, 6, 9 and 13b," in *Fungal Cells in Biodefense Mechanism*, eds S. Suzuki and M. Suzuki (Tokyo: Saigon Publishing), 1–16.

Tang, C. K., Sheng, K. C., Esparon, S. E., Proudfoot, O., Apostolopoulos, V., and Pietersz, G. A. (2009). Molecular basis of improved immunogenicity in DNA vaccination mediated by a mannan based carrier. *Biomaterials* 30, 1389–1400. doi: 10.1016/j.biomaterials.2008.11.010

Taylor, P. R., Tsoni, S. V., Willment, J. A., Dennehy, K. M., Rosas, M., Findon, H., et al. (2007). Dectin-1 is required for beta-glucan recognition and control of fungal infection. *Nat. Immunol.* 8, 31–38. doi: 10.1038/ni1408

Torosantucci, A., Bromuro, C., Chiani, P., De Bernardis, F., Berti, F., Galli, C., et al. (2005). A novel glyco-conjugate vaccine against fungal pathogens. *J. Exp. Med.* 202, 597–606. doi: 10.1084/jem.20050749

Trinel, P. A., Faille, C., Jacquinot, P. M., Cailliez, J. C., and Poulain, D. (1992). Mapping of *Candida albicans* oligomannosidic epitopes by using monoclonal antibodies. *Infect. Immun.* 60, 3845–3851.

Tso, G. H. W., Reales-Calderon, J. A., and Pavelka, N. (2018). The elusive anti-Candida vaccine: lessons from the past and opportunities for the future. *Front. Immunol.* 9:897. doi: 10.3389/fimmu.2018.00897

Tsvetkov, Y. E., Burg-Roderfeld, M., Loers, G., Arda, A., Sukhova, E. V., Khatuntseva, E. A., et al. (2012). Synthesis and molecular recognition studies of the HNK-1 trisaccharide and related oligosaccharides. The specificity of monoclonal anti-HNK-1 antibodies as assessed by surface plasmon resonance and STD NMR. *J. Am. Chem. Soc.* 134, 426–435. doi: 10.1021/ja2083015

van de Veerdonk, F. L., and Netea, M. G. (2010). T-cell subsets and antifungal host defenses. *Curr. Fungal Infect. Rep.* 4, 238–243. doi: 10.1007/s12281-010-0034-6

Varki, A., Cummings, R., Esko, J., Freeze, H., Hart, G., and Marth, J. (1999). *Essentials of Glycobiology*. New York, NY: Cold Spring Harbor.

Vinh, D. C. (2011). Insights into human antifungal immunity from primary immunodeficiencies. *Lancet Infect. Dis.* 11, 780–792. doi: 10.1016/S1473-3099(11)70217-1

Wagener, J., Malireddi, R. K., Lenardon, M. D., Koberle, M., Vautier, S., MacCallum, D. M., et al. (2014). Fungal chitin dampens inflammation through IL-10 induction mediated by NOD2 and TLR9 activation. *PLoS Pathog.* 10:e1004050. doi: 10.1371/journal.ppat.1004050

West, L., Lowman, D. W., Mora-Montes, H. M., Grubb, S., Murdoch, C., Thornhill, M. H., et al. (2013). Differential virulence of *Candida glabrata* glycosylation mutants. *J. Biol. Chem.* 288, 22006–22018. doi: 10.1074/jbc.M113.478743

Xin, H., Cartmell, J., Bailey, J. J., Dziadek, S., Bundle, D. R., and Cutler, J. E. (2012). Self-adjuvanting glycopeptide conjugate vaccine against disseminated candidiasis. *PLoS ONE* 7:e35106. doi: 10.1371/journal.pone.0035106

Xin, H., Dziadek, S., Bundle, D. R., and Cutler, J. E. (2008). Synthetic glycopeptide vaccines combining beta-mannan and peptide epitopes induce protection against candidiasis. *Proc. Natl. Acad. Sci. U.S.A.* 105, 13526–13531. doi: 10.1073/pnas.0803195105

Zheng, N. X., Wang, Y., Hu, D. D., Yan, L., and Jiang, Y. Y. (2015). The role of pattern recognition receptors in the innate recognition of *Candida albicans*. *Virulence* 6, 347–361. doi: 10.1080/21505594.2015.1014270

Conflict of Interest: The authors declare that the research was conducted in the absence of any commercial or financial relationships that could be construed as a potential conflict of interest.

Heliyon

Received:
20 September 2018
Revised:
20 December 2018
Accepted:
23 January 2019

Cite as: Vadim B. Krylov, Arsenii S. Solovev, Dmitry A. Argunov, Jean-Paul Latgé, Nikolay E. Nifantiev. Reinvestigation of carbohydrate specificity of EB-A2 monoclonal antibody used in the immune detection of *Aspergillus fumigatus* galactomannan. Heliyon 5 (2019) e01173. doi: 10.1016/j.heliyon.2019.e01173

Reinvestigation of carbohydrate specificity of EB-A2 monoclonal antibody used in the immune detection of *Aspergillus fumigatus* galactomannan

Vadim B. Krylov [a], **Arsenii S. Solovev** [a], **Dmitry A. Argunov** [a], **Jean-Paul Latgé** [b,**], **Nikolay E. Nifantiev** [a,*]

[a] *N.D. Zelinsky Institute of Organic Chemistry, Russian Academy of Sciences, Leninsky Prospect 47, 119991 Moscow, Russia*

[b] *Unité des Aspergillus, Institut Pasteur, 25 Rue du Docteur Roux, 75724 Paris Cedex 15, France*

[*] Corresponding author.

[**] Corresponding author.

E-mail addresses: jplatge@pasteur.fr (J.-P. Latgé), nen@ioc.ac.ru (N.E. Nifantiev).

Abstract

Great progresses have been made in the recent years in the detection of circulating galactofuranose-bearing molecules for the diagnosis of aspergillosis. However, the test used in the clinical practice is hampered by the occurrence of false positives. A glycoarray with dozens of oligosaccharides structurally related to the *Aspergillus fumigatus* galactomannan has allowed us to reinvestigate the carbohydrate specificity of the EB-A2 monoclonal antibody used in the Platelia™ Aspergillus sandwich immune assay. We have now demonstrated that the mAb can recognize shorter oligosaccharides than the previously reported tetrasaccharide Gal*f*-β-(1→5)-Gal*f*-β-(1→5)-Gal*f*-β-(1→5)-Gal*f*-β and oligosaccharides which contains alternating β-(1→5)/β-(1→6)-linkages. This result could explain the occurrence of false-positive signals due to the presence of the abovementioned

https://doi.org/10.1016/j.heliyon.2019.e01173

epitopes not only in *A. fumigatus* galactomannan but also in other bacteria and fungi.

Keywords: Health sciences, Biochemistry, Immunology, Microbiology, Infectious disease

1. Introduction

The detection of circulating galactomannan (GM) is a recognized criterion for the diagnosis of invasive aspergillosis [1, 2, 3]. The commercial kit Platelia™ Aspergillus enzyme immunoassay used in the clinics is based on an immunoassay with the rat IgM EB-A2 which has been shown to recognize oligosaccharides composed of at least four β-(1→5)-galactofuranosyl units [4, 5]. This epitope is present on the galactomannan, which is a major component of the Aspergillus cell wall and occurs as side chains of the linear mannan core. Despite a good sensitivity and specificity, the performance of the Platelia™ Aspergillus GM immunoassay has been shown to be far from perfect, particularly among patients receiving mold-active prophylaxis or treatment or pediatric patients [6, 7]. This is mainly due to the occurrence of false positives encountered for this test.

Many reasons have been proposed to be responsible for false positive results with the commercial GM test. First, some of the false positive results come from an erroneous operational use of the test [8]. Some other false positive data result from the presence of GM in the circulating fluid of the patient which was not linked to an *Aspergillus* infection: the major example is connected with the use of Tazocin™ (Piperacilin-Tazobacam) whose raw material utilized for the production of the antibiotics was contaminated by filamentous ascomycetes such as *Penicillium* or *Aspergillus* which both are source of GM. The use of Tazocin™ which is not contaminated by GM solved this problem [9].

False positive data have been also associated with intake of contaminated food and enteral nutrition [10]. Similarly to Tazocin™, a better purification of solutions containing low-molecular-weight organic acids which are produced by a fermentation process involving *Aspergillus* resolved these problems like in cases of false positivity due to the intravenous injection of sodium gluconate [11]. Other invasive fungal infections are suspected to be associated with the release of GM: (i) it has been demonstrated chemically that *Penicillium* secretes a polysaccharide with a β-(1→5)-galactofuranoside epitope similar to the one present in *Aspergilli* species [12] and that the GM test can be used to detect *Penicillium marneffei* infections (Huang et al, 2007) [13]; (ii) a positivity of the ELISA test has been noticed with the yeasts *Cryptococcus* and *Histoplasma* while the presence of β-(1→5)-galactofuranoside units has not been reported in these yeast species. Some of the false

https://doi.org/10.1016/j.heliyon.2019.e01173

positives still remain unexplained such as the positivity of multiple myeloma patients exempt of aspergillosis infections [14].

The false positivity can also result from cross reactions knotted with the presence of different bacteria of the human microbiota including *Escherichia coli* [15], *Rhodococcus equi* [16], *Corynebacterium jeikeium* [15] and *Bifidobacterium* spp [17]. They produce a galctofuranoside epitope also recognized by the EB-A2 mAb and may be responsible for false positivity in patients in the late phase of allogeneic hematopoietic stem cell transplantation with heavy gastrointestinal Graft vs Host disease [18]. Moreover, (i) N-glycans and glycolipids which do not bear the tetragalactofuranosyl moiety are recognized by this monoclonal antibody [19] and (ii) recent studies have shown that side chains of GM are not exclusively composed of linear β-(1→5)-galactofuranosyl units [20] but contain a certain amount of β-(1→6)-linked galactofuranosyl units attached to the mannan backbone [21, 22]. All these data have raised some questions on the exact nature of the epitope recognized by the EB-A2 mAb and suggested that the mAb used in the commercial kit may recognize multiple carbohydrate epitopes, a classical fact with anti-carbohydrate antibodies. The multiplicity of the epitopes recognized may be also a reason for the occurrence of some of the false positives reported in the literature which affects the performance of the test for the diagnosis of invasive aspergillosis.

2. Results & discussion

To reinvestigate the nature of the carbohydrate epitope recognized by the mAb EB-A2 a glycoarray composed of synthetic oligosaccharides with definite structures representing key fragments of the galactomannan of *A. fumigatus* was used. The selection of synthetic oligosaccharide derivatives **1**−**13** (Fig. 1A) for this study was based on the most recent definition of the galactofuranyl-containing structures of *Aspergillus* galactomannan. Oligosaccharides **1**−**13** were prepared [22, 23, 24] using pyranoside-*into*-furanoside rearrangement [25, 26] and biotynilation using an activated biotin derivative [27] containing a hydrophilic hexaethylene glycol linker. The wells of 96-well streptavidin-coated plates (Thermo Scientific, Rockford, U.S.A.) were coated with biotin-tagged oligosaccharides at a concentration of 15 pmol/well. After two hours incubation with EB-A2 conjugated with peroxidase (working solution from the Platelia *Aspergillus* Ag Kit) and revealed following the instructions of the manufacturer.

The use of the glycoarray has expanded the number of oligosaccharide ligands recognized by mAb EB-A2. The minimal recognized galactomannan fragment is a disaccharide Gal*f*-β-(1→5)-Gal*f*. Moreover, this disaccharide fragment is recognized as the terminal part of the polysaccharide chain (as in compounds **2**, **6**, **8**, **9**, **10**, **11**−**13**) or within the internal part of the chain (see compound **7**). In addition,

https://doi.org/10.1016/j.heliyon.2019.e01173

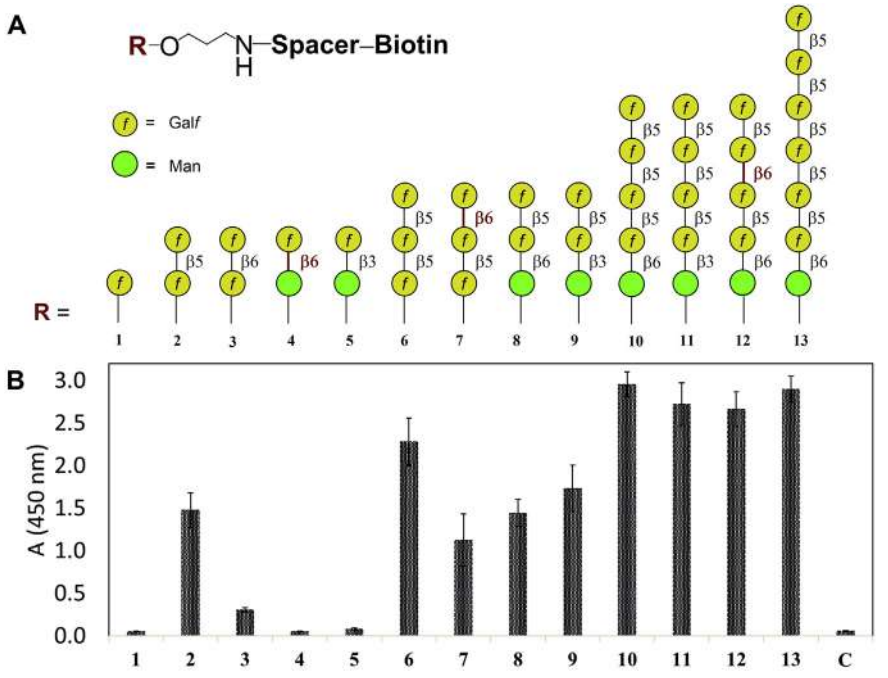

Fig. 1. Investigation of the oligosaccharide specificity of EB-A2 mAb. (A) The thematic glycoarray composed of oligosaccharide ligands representing key structural elements of the *A. fumigatus* galactomannan chain, and (B) the results of assaying the carbohydrate specificity of EB-A2 mAb on the glycoarray.

the data shown in Fig. 1B confirmed the results of earlier studies [5], demonstrating that the oligosaccharide ligand with four Gal*f*-β-(1→5) units belongs to the best recognized sequences. However, no difference was observed between the isomeric pentasaccharides **10** and **12,** which contained only β-(1→5) linkages or alternating β-(1→5) and β-(1→6) linkages in their tetragalactofuranosyl fragments. This observation may explain why the structurally different polysaccharides of *B. bifidum* and *B. catenulatum* are recognized by EB-A2 mAb [28, 29], since *B. bifidum* produces lipoteichoic acid polysaccharide containing an oligo-β-(1→5)-galactofuranosyl backbone [30], while *B. catenulatum* produces a polysaccharide with alternating β-(1→5)- and β-(1→6)-galactofuranosyl units [31].

3. Conclusion

This study indicates that the mAb EB-A2 used in the kit for the detection of the circulating GM for the diagnosis of aspergillosis, recognizes multiple epitopes that are all present in the native GM molecule. The multiplicity of the epitopes recognized by the mAb can be a major cause for the occurrence of false positive results which impacts the performance of the existing test. Substitution of EB-A2 mAb in the immune assay with an antibody capable of recognizing a larger epitope should increase the specificity of the assay and will facilitate the decision for the initiation of

https://doi.org/10.1016/j.heliyon.2019.e01173

an antifungal therapy. Synthetic immunogens which contain the oligosaccharide ligands of necessary length and structure can be regarded as promising instruments for obtaining of monoclonal antibodies with required epitope specificity and affinity to GM [32, 33] which may be better adapted for the conception of a more specific test in the serological diagnosis of invasive aspergillosis.

Declarations

Author contribution statement

Vadim B. Krylov, Arsenii S. Solovev, Dmitry A. Argunov: Conceived and designed the experiments; Performed the experiments; Analyzed and interpreted the data.

Jean-Paul Latgé, Nikolay E. Nifantiev: Analyzed and interpreted the data; Contributed reagents, materials, analysis tools or data; Wrote the paper.

Funding statement

This work was supported by Russian Science Foundation grant 14-23-00199.

Competing interest statement

The authors declare no conflict of interest.

Additional information

No additional information is available for this paper.

References

[1] T.F. Patterson, G.R. Thompson III, D.W. Denning, J.A. Fishman, S. Hadley, R. Herbrecht, D.P. Kontoyiannis, K.A. Marr, V.A. Morrison, M.H. Nguyen, Practice guidelines for the diagnosis and management of aspergillosis: 2016 update by the Infectious Diseases Society of America, Clin. Infect. Dis. 63 (2016) e1−e60.

[2] A.J. Ullmann, J.M. Aguado, S. Arikan-Akdagli, D.W. Denning, A.H. Groll, K. Lagrou, C. Lass-Flörl, R.E. Lewis, P. Munoz, P.E. Verweij, Diagnosis and management of Aspergillus diseases: executive summary of the 2017 ESCMID-ECMM-ERS guideline, Clin. Microbiol. Infect. 24 (2018) e1−e38.

[3] B. De Pauw, T.J. Walsh, J.P. Donnelly, D.A. Stevens, J.E. Edwards, T. Calandra, P.G. Pappas, J. Maertens, O. Lortholary, C.A. Kauffman, Revised definitions of invasive fungal disease from the European organization for research and treatment of cancer/invasive fungal infections cooperative group

https://doi.org/10.1016/j.heliyon.2019.e01173

and the national institute of allergy and infectious diseases mycoses study group (EORTC/MSG) consensus group, Clin. Infect. Dis. 46 (2008) 1813−1821.

[4] D. Stynen, A. Goris, J. Sarfati, J.P. Latge, A new sensitive sandwich enzyme-linked immunosorbent assay to detect galactofuran in patients with invasive aspergillosis, J. Clin. Microbiol. 33 (1995) 497−500.

[5] D. Stynen, J. Sarfati, A. Goris, M.C. Prevost, M. Lesourd, H. Kamphuis, V. Darras, J.P. Latge, Rat monoclonal antibodies against Aspergillus galactomannan, Infect. Immun. 60 (1992) 2237−2245.

[6] T. Lehrnbecher, A. Hassler, A.H. Groll, K. Bochennek, Diagnostic approaches for invasive aspergillosis-specific considerations in the pediatric population, Front. Microbiol. 9 (2018) 518.

[7] A. Vena, E. Bouza, A. Álvarez-Uría, J. Gayoso, P. Martín-Rabadán, F. Cajuste, J. Guinea, J. Gómez Castellá, R. Alonso, P. Munoz, The misleading effect of serum galactomannan testing in high-risk haematology patients receiving prophylaxis with micafungin, Clin. Microbiol. Infect. Off. Publ. Eur. Soc. Clin. Microbiol. Infect. Dis. 23 (2017) 1000.e1−1000.e4.

[8] N. Guigue, S. Lardeux, A. Alanio, S. Hamane, M. Tabouret, S. Bretagne, Importance of operational factors in the reproducibility of Aspergillus galactomannan enzyme immune assay, PLoS One 10 (2015) e0124044.

[9] M. Mikulska, E. Furfaro, V. Del Bono, A.M. Raiola, S. Ratto, A. Bacigalupo, C. Viscoli, Piperacillin/tazobactam (Tazocin™) seems to be no longer responsible for false-positive results of the galactomannan assay, J. Antimicrob. Chemother. 67 (2012) 1746−1748.

[10] S.-I. Kimura, Y. Akahoshi, H. Nakano, N. Harada, K. Kameda, T. Ugai, H. Wada, R. Yamasaki, Y. Ishihara, K. Kawamura, K. Sakamoto, M. Ashizawa, M. Sato, K. Terasako-Saito, H. Nakasone, M. Kikuchi, R. Yamazaki, J. Kanda, S. Kako, A. Tanihara, J. Nishida, Y. Kanda, False-positive Aspergillus galactomannan and its kinetics in allogeneic hematopoietic stem cell transplantation, J. Infect. 70 (2015) 520−540.

[11] I. Spriet, K. Lagrou, J. Maertens, L. Willems, A. Wilmer, J. Wauters, Plasmalyte: No longer a culprit in causing false-positive galactomannan test results, J. Clin. Microbiol. 54 (2016) 795−797.

[12] C.J. Unkefer, J.E. Gander, The 5-O-beta-D-galactofuranosyl-containing glycopeptide from Penicillium charlesii. Carbon 13 nuclear magnetic resonance studies, J. Biol. Chem. 254 (1979) 12131−12135.

https://doi.org/10.1016/j.heliyon.2019.e01173

[13] Y.-T. Huang, C.-C. Hung, C.-H. Liao, H.-Y. Sun, S.-C. Chang, Y.-C. Chen, Detection of circulating galactomannan in serum samples for diagnosis of Penicillium marneffei infection and cryptococcosis among patients infected with human immunodeficiency virus, J. Clin. Microbiol. 45 (2007) 2858–2862.

[14] J.-H. Ko, K.R. Peck, J.Y. Lee, S.Y. Cho, Y.E. Ha, C.-I. Kang, D.R. Chung, K. Kim, E.-S. Kang, J.-H. Song, Multiple myeloma as a major cause of false-positive galactomannan tests in adult patients with cancer, J. Infect. 72 (2016) 233–239.

[15] C.M. Swanink, J.F. Meis, A.J. Rijs, J.P. Donnelly, P.E. Verweij, Specificity of a sandwich enzyme-linked immunosorbent assay for detecting Aspergillus galactomannan, J. Clin. Microbiol. 35 (1997) 257–260.

[16] C.J. Clancy, R.A. Jaber, H.L. Leather, J.R. Wingard, B. Staley, L.J. Wheat, C.L. Cline, K.H. Rand, D. Schain, M. Baz, M.H. Nguyen, Bronchoalveolar lavage galactomannan in diagnosis of invasive pulmonary aspergillosis among solid-organ transplant recipients, J. Clin. Microbiol. 45 (2007) 1759–1765.

[17] M.A. Mennink-Kersten, D. Ruegebrink, R.R. Klont, A. Warris, F. Gavini, H.J.O. den Camp, P.E. Verweij, Bifidobacterial lipoglycan as a new cause for false-positive platelia Aspergillus enzyme-linked immunosorbent assay reactivity, J. Clin. Microbiol. 43 (2005) 3925–3931.

[18] Y. Asano-Mori, Y. Kanda, K. Oshima, S. Kako, A. Shinohara, H. Nakasone, M. Kaneko, H. Sato, T. Watanabe, N. Hosoya, K. Izutsu, T. Asai, A. Hangaishi, T. Motokura, S. Chiba, M. Kurokawa, False-positive Aspergillus galactomannan antigenaemia after haematopoietic stem cell transplantation, J. Antimicrob. Chemother. 61 (2008) 411–416.

[19] W. Morelle, M. Bernard, J.-P. Debeaupuis, M. Buitrago, M. Tabouret, J.-P. Latgé, Galactomannoproteins of Aspergillus fumigatus, Eukaryot. Cell 4 (2005) 1308–1316.

[20] J.-P. Latgé, H. Kobayashi, J.-P. Debeaupuis, M. Diaquin, J. Sarfati, J.-M. Wieruszeski, E. Parra, J.-P. Bouchara, B. Fournet, Chemical and immunological characterization of the extracellular galactomannan of Aspergillus fumigatus, Infect. Immun. 62 (1994) 5424–5433.

[21] A. Kudoh, Y. Okawa, N. Shibata, Significant structural change in both O-and N-linked carbohydrate moieties of the antigenic galactomannan from Aspergillus fumigatus grown under different culture conditions, Glycobiology 25 (2015) 74–87.

https://doi.org/10.1016/j.heliyon.2019.e01173

[22] V.B. Krylov, D.A. Argunov, A.S. Solovev, M.I. Petruk, A.G. Gerbst, A.S. Dmitrenok, A.S. Shashkov, J.-P. Latgé, N.E. Nifantiev, Synthesis of oligosaccharides related to galactomannans from Aspergillus fumigatus and their NMR spectral data, Org. Biomol. Chem. 16 (2018) 1188−1199.

[23] D.A. Argunov, V.B. Krylov, N.E. Nifantiev, Convergent synthesis of isomeric heterosaccharides related to the fragments of galactomannan from Aspergillus fumigatus, Org. Biomol. Chem. 13 (2015) 3255−3267.

[24] D.A. Argunov, V.B. Krylov, N.E. Nifantiev, The use of pyranoside-into-furanoside rearrangement and controlled O(5)→O(6) benzoyl migration as the basis of a synthetic strategy to assemble (1→5)-and (1→6)-linked galactofuranosyl chains, Org. Lett. 18 (2016) 5504−5507.

[25] V.B. Krylov, D.A. Argunov, D.Z. Vinnitskiy, S.A. Verkhnyatskaya, A.G. Gerbst, N.E. Ustyuzhanina, A.S. Dmitrenok, J. Huebner, O. Holst, H.-C. Siebert, Others, pyranoside-into-furanoside rearrangement: new reaction in carbohydrate chemistry and its application in oligosaccharide synthesis, Chem. Eur J. 20 (2014) 16516−16522.

[26] V.B. Krylov, D.A. Argunov, D.Z. Vinnitskiy, A.G. Gerbst, N.E. Ustyuzhanina, A.S. Dmitrenok, N.E. Nifantiev, The pyranoside-into-furanoside rearrangement of alkyl glycosides: scope and limitations, Synlett 27 (2016) 1659−1664.

[27] Y.E. Tsvetkov, M. Burg-Roderfeld, G. Loers, A. Ardá, E.V. Sukhova, E.A. Khatuntseva, A.A. Grachev, A.O. Chizhov, H.-C. Siebert, M. Schachner, Synthesis and molecular recognition studies of the HNK-1 trisaccharide and related oligosaccharides. The specificity of monoclonal anti-HNK-1 antibodies as assessed by surface plasmon resonance and STD NMR, J. Am. Chem. Soc. 134 (2011) 426−435.

[28] M.A. Mennink-Kersten, R.R. Klont, A. Warris, H.J.O. den Camp, P.E. Verweij, Bifidobacterium lipoteichoic acid and false ELISA reactivity in aspergillus antigen detection, Lancet 363 (2004) 325−327.

[29] M.A. Mennink-Kersten, J.P. Donnelly, P.E. Verweij, Detection of circulating galactomannan for the diagnosis and management of invasive aspergillosis, Lancet Infect. Dis. 4 (2004) 349−357.

[30] W. Fisher, 'Lipoteichoic acid'of Bifidobacterium bifidum subspecies pennsylvanicum DSM 20239, FEBS J. 165 (1987) 639−646.

[31] M. Nagaoka, S. Hashimoto, H. Shibata, I. Kimura, K. Kimura, H. Sawada, T. Yokokura, Structure of a galactan from cell walls of Bifidobacterium catenulatum YIT4016, Carbohydr. Res. 281 (1996) 285−291.

https://doi.org/10.1016/j.heliyon.2019.e01173

[32] M. Schubert, H. Spiegel, S. Schillberg, G. Nölke, Aspergillus-specific antibodies – targets and applications, Biotechnol. Adv. 36 (2018) 1167–1184.

[33] A.L. Matveev, V.B. Krylov, L.A. Emelyanova, A.S. Solovev, Y.A. Khlusevich, I.K. Baykov, T. Fontaine, J.-P. Latgé, N.V. Tikunova, N.E. Nifantiev, Novel mouse monoclonal antibodies specifically recognize Aspergillus fumigatus galactomannan, PLoS One 13 (2018) e0193938.

https://doi.org/10.1016/j.heliyon.2019.e01173

БИООРГАНИЧЕСКАЯ ХИМИЯ, 2018, том 44, № 6, с. 78–86

УДК 577.114.5:616-097

УГЛЕВОДНАЯ СПЕЦИФИЧНОСТЬ АНТИТЕЛ ПРОТИВ *Aspergillus fumigatus*. ИССЛЕДОВАНИЕ С ИСПОЛЬЗОВАНИЕМ БИБЛИОТЕКИ СИНТЕТИЧЕСКИХ МИКОАНТИГЕНОВ

© 2017 г. В. Б. Крылов[1], М. И. Петрук[1], И. В. Григорьев[2], Ю. С. Лебедин[2], Н. И. Глушко[3], Е. В. Халдеева[3], Д. А. Аргунов[1], Е. А. Хатунцева[1], М. В. Топлишек[1], Б. С. Комарова[1], А. А. Карелин[1], О. Н. Юдина[1], В. М. Меньшов[1], Д. В. Яшунский, Ю. Е. Цветков[1], Н. Э. Нифантьев[1,*]

[1]ФГБУН Институт органической химии им. Н.Д. Зелинского РАН, 119991, Москва, Ленинский просп., 47

[2]ООО "ХЕМА", 105264 Москва, 9-я Парковая ул., 48

[3]ФБУН Казанский научно-исследовательский институт эпидемиологии и микробиологии 420015, Казань, ул. Большая Красная, 67

Поступила в редакцию 28.06.2017 г.
Принята к печати 04.07.2017 г.

Анализ углеводной специфичности антител, полученных при иммунизации лабораторных животных с помощью иммуногенов, приготовленных из мицелия или культуральной жидкости *Aspergillus fumigatus*, проведен с использованием библиотеки синтетических олигосахаридных биотинилированных производных. Показано, что основная часть анти-полисахаридных антител распознает в использованных иммуногенах галактоманнан, причем предпочтительно его фрагменты, содержащие больше двух β-(1→5)-связанных галактофуранозильных звеньев. Полученные данные могут составить основу для разработки иммуноферментных тест-систем для обнаружения данного опасного грибкового патогена.

Ключевые слова: Aspergillus fumigatus, аспергилез, антиген, антитело, галактоманнан, диагностикум.

DOI: 10.7868/S0132342318010086

ВВЕДЕНИЕ

Патогенный гриб *Aspergillus fumigatus* относится к высшим плесневым грибам, способным вызывать у больных с ослабленным иммунитетом тяжелейшие и практически неизлечимые инвазивные микозы [1, 2]. Данный гриб повсеместно распространен в природе (воздух, почва, растения, кожа человека и животных), в связи с чем крайне востребованы методы контроля зараженности помещений, продуктов питания, а также *in vitro*-диагностика пациентов, находящихся в группе риска [3]: онкологические больные, больные с ВИЧ-инфекцией, а также пациенты, получающие иммуносупрессивную терапию. Количество выявляемых случаев инвазивного аспергиллеза растет с каждым годом, и критическим фактором для его лечения является своевременное диагностирование. Известно, что при запоздалом лечении смертность достигает 90–100%, в то время как обнаружение заболевания до первых клинических проявлений позволяет существенно снизить этот показатель [4, 5].

Существующие диагностические тесты на наличие инвазивных микозов характеризуются недостаточной чувствительностью и специфичностью [6, 7]. Культуральное исследование выявляет рост грибов в крови только в 50–60% случаев и требует существенных затрат времени. Кроме того, результаты лабораторных тестов являются неспецифичными, и, таким образом, клиницисты обязаны принимать решения, основываясь, прежде всего на высоком индексе риска развития заболевания [8].

Другим подходом к диагностике аспергиллеза являются серологические тесты, позволяющие обнаруживать определенные антигены клеточной стенки гриба и соответствующие антитела в биологических жидкостях пациента [8]. К настоящему времени за рубежом зарегистрированы

Сокращения: EDAC – 1-этил-3-(3-диметиламинопропил) карбодиимид.

* Автор для связи (тел.: +7(499)135-87-84; эл. почта: nen@ioc.ac.ru).

экспресс-диагностикумы аспергиллеза, основанные на детектировании галактоманнана клеточной стенки *A. fumigatus* [2], а также тест на инвазивные микозы у людей, позволяющий измерять концентрацию β-(1→3)-*D*-глюкана, который содержится в клеточной стенке большинства грибов [9]. Однако такие диагностические наборы дорогостоящие, кроме того возможны ошибки при определении микозов [6–8]. На настоящий момент данные диагностические наборы не зарегистрированы в России.

Создание высокоспецифичных серологических диагностикумов требует выявления подходящих антигенов, в качестве которых могут выступать компоненты клеточной стенки гриба. Клеточная стенка гриба *A. fumigatus* представляет собой сложную биологическую структуру, включающую такие полисахариды как α- и β-глюканы, хитин, маннан, галактоманнан и другие [10]. Эти полисахариды являются потенциальными антигенными маркерами для обнаружения данного патогена. Однако чрезвычайно сложное строение и высокая гетерогенность, а также трудности их воспроизводимого выделения и очистки не позволяют детально охарактеризовать распознаваемые иммунной системой углеводные структуры.

Целью данной работы являлась эпитопная характеристика поликлональных антител против *A. fumigatus*, которая стала возможна только благодаря библиотеке синтетических углеводных микоантигенов, отвечающих основным типам природных грибковых полисахаридов.

РЕЗУЛЬТАТЫ И ОБСУЖДЕНИЯ

Для генерации антител против *A. fumigatus* были использованы иммуногены двух типов: приготовленные из мицелия либо из культуральной жидкости. Для приготовления препарата первого типа биомассу мицелия отмывали от питательной среды раствором хлористого натрия с последующим центрифугированием. Полученную субстанцию инактивировали ацетоном, а затем высушивали, гомогенизировали и экстрагировали раствором хлористого натрия. Концентрирование ультрафильтрацией с порогом исключения 10 кДа позволило получить необходимый антигенный препарат. Жидкость, в которой проводили культивирование плесневых грибов, была также использована для приготовления иммуногена, для этого ее концентрировали на мембране с порогом исключения 10 кДа.

Полученные таким образом препараты были использованы для иммунизации лабораторных животных, которую выполняли с интервалом 2 недели свежеприготовленной эмульсией препарата с полным адъювантом Фрейнда для первой иммунизации и с неполным адъювантом Фрейнда для последующих иммунизаций. Забор крови проводили с помощью вакуумных пробирок с разделяющим гелем и активатором свертывания (SiO_2). Полученную сыворотку стабилизировали 0.1% азидом натрия и хранили при +4 °C.

Очистку сывороток и выделение высокоспецифичных поликлональных антител осуществляли с использованием аффинной хроматографии. Для изготовления аффинных сорбентов, антигены диализовали на мембранах с порогом исключения 10 кДа, до общей концентрации по белку 10 мг/мл (определение по методу Лоури), а затем наносили на активированную матрицу в присутствии карбодиимидного сшивающего реагента 1-этил-3-(3-диметиламинопропил)карбодиимида (EDAC). Полученный сорбент использовали в хроматографических колонках, на которые наносили кроличьи сыворотки. После нанесения сыворотки колонку промывали фосфатно-солевым буфером, а затем сорбировавшиеся антитела смывали 0.1 М раствором уксусной кислоты. Полученную фракцию очищенных антител нейтрализовали добавлением 1М Трис-буфера (pH 7.4) и стабилизировали 0.1% азидом натрия.

Углеводную специфичность исследовали с использованием библиотеки синтезированных нами ранее олигосахаридов, родственных основным типам полисахаридов клеточной стенки грибов (табл. 1). Ди- и пентасахариды **(I)** и **(II)** [11–13] отвечают различным участкам сложного гетеросахарида – галактоманнана [2], выделенного ранее из *A. fumigatus*. Нонаглюкогид **(III)** [14, 15] соответствует α-глюкану, содержащемуся в клеточной стенке *A. fumigatus*. Нона- и октаглюкозиды **(IV)**, **(V)** [16, 17] соответствуют линейному и разветвленному участкам β-глюкана, общего антигена для разнообразных представителей царства грибов. Три- **(VI)** и тетрасахариды **(VII)** [18] родственны маннанам грибов, и кроме того, отвечают главной цепи галактоманнана из *A. fumigatus*. Пентасахарид **(VIII)** [19, 20] является фрагментом хитина, основного компонента клеточной стенки грибов.

Иммобилизацию данных олигосахаридов на поверхности планшета осуществляли за счет сверхпрочного нековалентного взаимодействия стрептавидина и биотина. Для этого все изученные соединения биотинилировали под действием активированного эфира биотина **(IX)** в DMF и присутствии триэтиламина (схема 1). Образование производных **(Ib), (IIb), (IVb)–(VIIIb)** подтверждалось характерными сигналами биотинового фрагмента в ^{1}H-ЯМР-спектрах (4.62 м.д. – H(6a); 4.42 м.д. – H(3a); 3.02 м.д. – H(6) и др.),

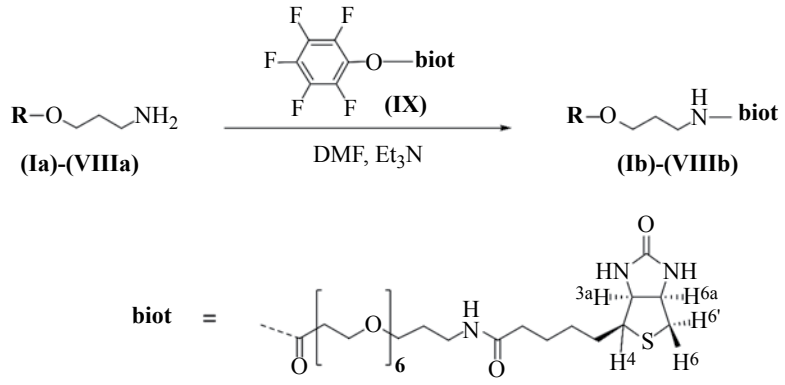

Схема. Получение биотинилированных производных олигосахаридов **(Ib)** – **(VIIIb)**, отвечающих основным типам фрагментов грибковых полисахаридов.

а также данными масс-спектров высокого разрешения.

Биотинилированные олигосахариды количественно абсорбировали на дне лунок стрептавидиновых планшетов с образованием гибридных молекулярных систем [21], в которых иммобилизованные на пластике через стрептавидин-биотиновую пару олигосахаридные лиганды эффективно экспонированы для связывания с антителами. Образование углевод-белкового комплекса детектировали обработкой поверхности лунки проявляющим конъюгатом вторичных антител с ферментной меткой и последующим добавлением хромогенного субстрата [22]. Исследованные антитела использовали в различных разбавлениях для более точного определения антигенной специфичности. Каждое измерение проводили не менее 3 раз, использовали антитела из независимо полученных пулов сыворотки (см. рис. 1)

Исследование углеводной специфичности поликлональных антител, полученых против мицелиального антигена выявило существенное связывание с олигосахаридами **(Ib)** и **(IIb)**, родственными галактоманнану, причем более крупный пентасахарид распознавался лучше. Значительно слабее изученное антитело связывалось с олигосахаридами **(IVb)** и **(Vb)** родственными β-глюкану. В одном из пулов антител наблюдалась активность к тетраманнозиду, содержащему концевую α-(1→6)-гликозидную связь, однако данное наблюдение не воспроизводилось для антител из других пулов и скорее всего не связано с исследуемым антигеном.

Углеводная специфичность поликлональных антител, полученных при иммунизации

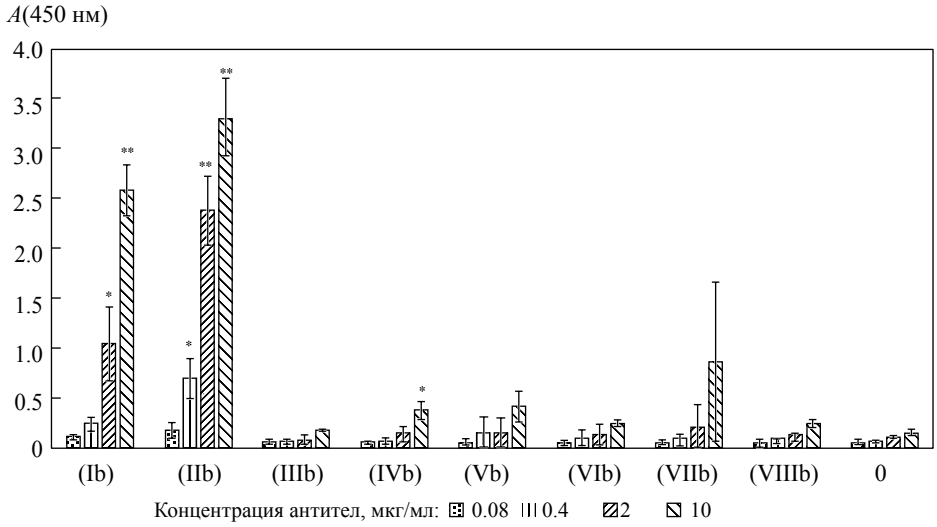

Рис. 1. Углеводная специфичность поликлональных антител, полученных при иммунизации экстрактом мицелия (знаками * и ** отмечены статистически значимые результаты по отношению к контролю; $P < 0.05$ и $P < 0.01$ соответственно).

Таблица 1. Олигосахаридные лиганды R–O–$(CH_2)_3$–NH_2 (Ia)–(VIIIa), и их конъюгаты с биотином R–O–$(CH_2)_3$–NHbiotin (Ib)–(VIIIb) (см. схему 1)

Соединение	**R**
(Ia,b)	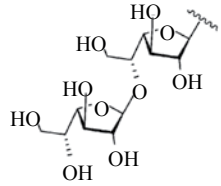
(IIa,b)	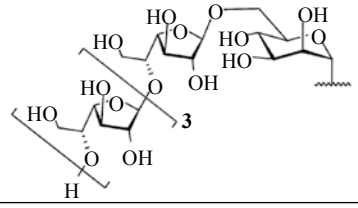
(IIIa,b)	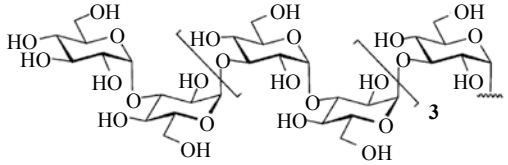
(IVa,b)	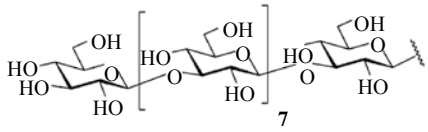
(Va,b)	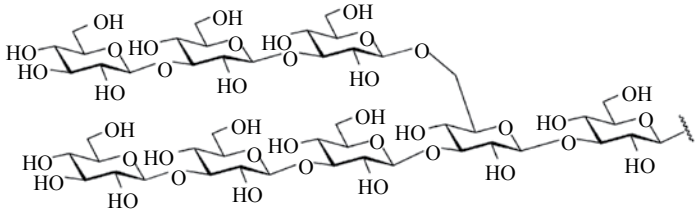
(VIa,b)	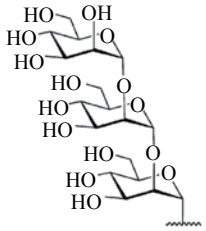
(VIIa,b)	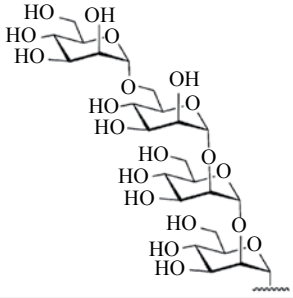
(VIIIa,b)	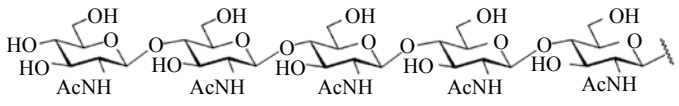

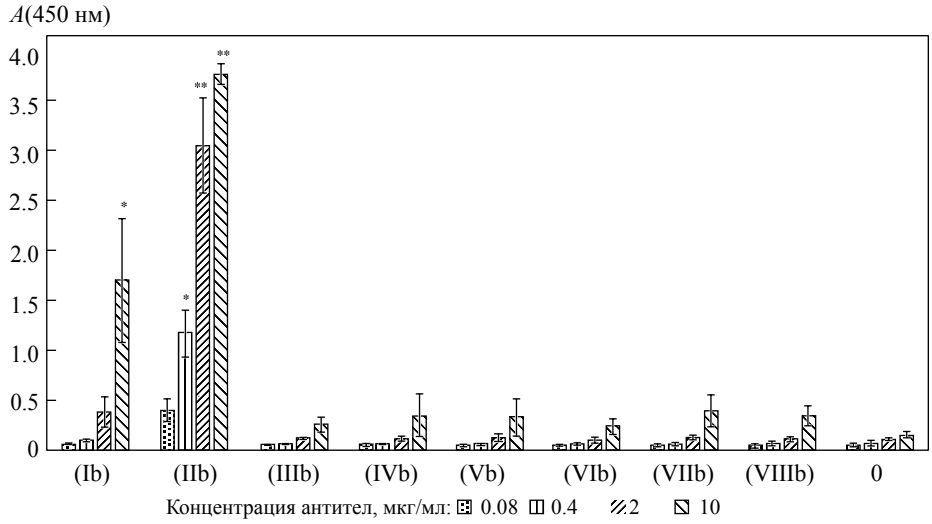

Рис. 2. Углеводная специфичность поликлональных антител, полученных при иммунизации препаратом культуральной жидкости (знаками * и ** отмечены статистически значимые результаты по отношению к контролю; $P < 0.05$ и $P < 0.01$ соответственно).

антигеном из культуральной жидкости, была похожа на описанные выше результаты для антител против мицелиального антигена. Наиболее хорошо эти антитела связывают олигосахариды **(Ib)** и **(IIb)**, родственные галактоманнану. Однако, антитела против мицелиального иммуногена несколько лучше распознают дисахарид **(Ib)**, чем антитела, полученные с использованием культуральной жидкости. Это может быть связано с разной презентацией углеводных эпитопов в иммуногенах из разных источников.

Взаимодействие поликлональных антител с углеводными эпитопами, отвечающими галактоманнану, было детально исследовано с помощью расширенной библиотеки синтетических лигандов. Для этого полученные нами ранее спейсерированные олигосахариды **(Xa)–(XVIIa)** [11, 12] биотинилировали по описанной выше методике с образованием производных **(Xb)–(XVIIb)** (Табл. 2).

Исследование взаимодействия олигосахаридов **(Ib), (IIb), (Xb)–(XVIIb)** с поликлональными антителами, полученными с помощью мицелиального иммуногена, осуществлялось методом иммуноферментного анализа по описанной выше методике. В результате было показано, что соединения **(Xb)–(XIIb)**, содержащие только один галактофуранозный остаток распознаются слабо.

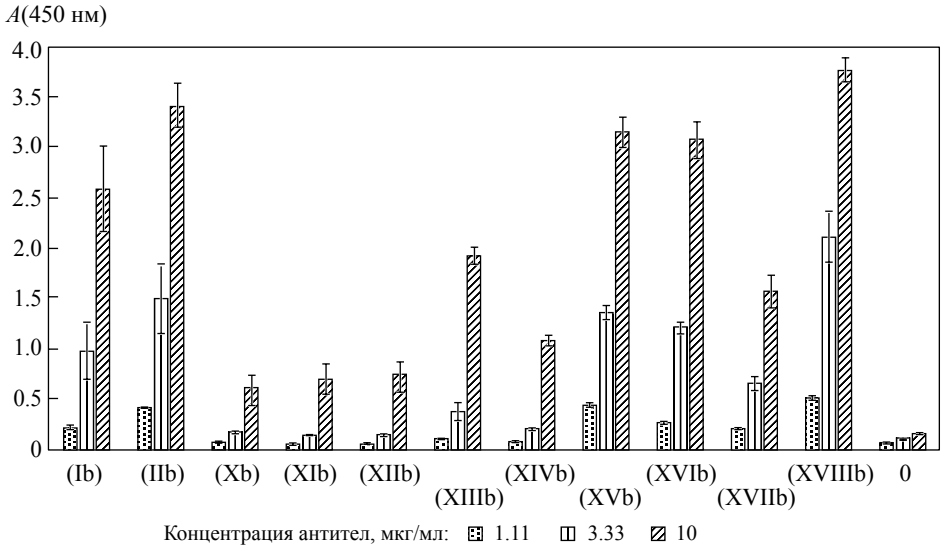

Рис. 3. Взаимодействие поликлональных антител, полученных при иммунизации экстрактом мицелия, с использованием биотинилированных олигосахаридных производных, родственных галактоманнану *A. fumigatus*.

Таблица 2. Олигосахаридные лиганды **(Xa)–(XVIIIa)**, и их конъюгаты с биотином **(Xb)–(XVIIIb)**, отвечающих фрагментам галактоманнана *A. fumigatus*.

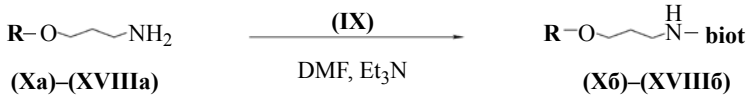

(Xa)–(XVIIIa) **(Xб)–(XVIIIб)**

Соединение	R	Соединение	R
(Xa, b)	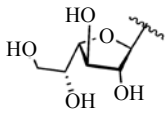	**(XVa, b)**	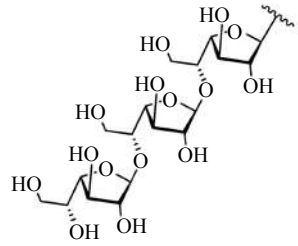
(XIa, b)	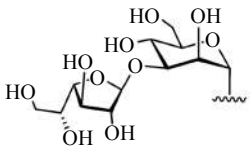	**(XVIa, b)**	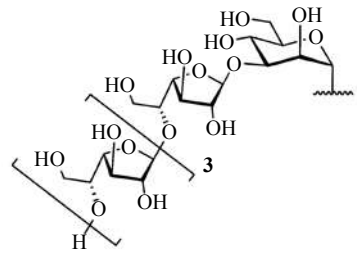
(XIIa, b)	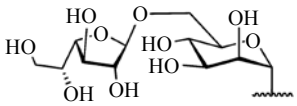	**(XVIIa, b)**	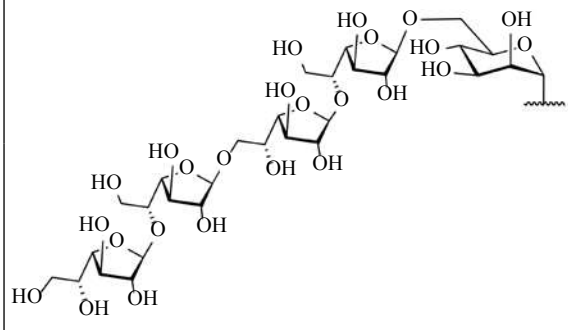
(XIIIa, b)	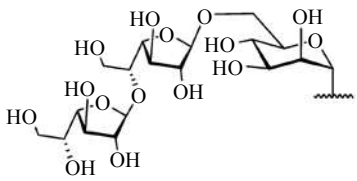		
(XIVa, b)	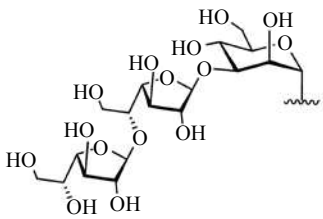	**(XVIIIa, b)**	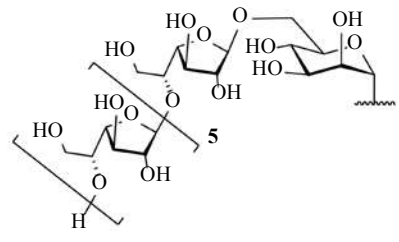

Более интенсивное связывание наблюдалось для олигосахаридов **(Ib), (XIIIb)**, **(XIVb)** и **(XVIIb)**, содержащих β-(1→5)-связанный дигалактозидный фрагмент. Цепи, содержащие 3 и более β-(1→5)-связанных галактофуранозидных остатков, взаимодействовали с антителами наиболее интенсивно.

Таким образом, установлено, что основным полисахаридным антигенным компонентом в использованных иммуногенах из гриба *A. fumigatus* является галактоманнан. Кроме этого показано, что использованные поликлональные антитела распознают преимущественно эпитопы, содержащие больше двух β-(1→5)-связанных галактофуранозильных звеньев. Полученная информация востребована для создания диагностических наборов, позволяющих выявлять опасные заболевания, вызываемые грибами рода *A. fumigatus*, а также при экологическом контроле грибковой контаминации продуктов питания и помещений.

ЭКСПЕРИМЕНТАЛЬНАЯ ЧАСТЬ

Получение иммуногенов. Культивирование плесневого гриба *A. fumigatus* проводили в течение 10–14 сут при 26 °C на среде Чапека до полного развития вегетативного или полового спороношения, отдельно собирали мицелий и культуральную жидкость. Биомассу мицелия дважды отмывали от питательной среды 10-кратным объемом 0.85% раствора хлористого натрия (pH 7.0) и центрифугировали при 2000 *g* в течение 10 мин при 4 °C, после чего обрабатывали ацетоном в течение 16–18 ч для инактивации, высушивали и размалывали в тонкий однородный порошок. Мицелий экстрагировали пятикратным объемом 1M раствора хлористого натрия. Экстракт мицелия и культуральную жидкость концентрировали на мембране Biomax PBGC09005 с порогом исключения 10кДа и хранили при –20 °C.

Иммунизация

Антисыворотки против иммуногенов получали на 5 самцах кроликов породы "Калифорнийский кролик" в возрасте 4–6 месяцев. Животных иммунизировали с интервалом 2 недели свежеприготовленной эмульсией конъюгата (0.2 мг препарата антигена по белку в 0.5 мл дистиллированной воды на кролика) с полным адъювантом Фрейнда для первой иммунизации и с неполным адъювантом Фрейнда для последующих иммунизаций. Эмульсию готовили в соотношении раствор конъюгата / адъювант – 1:1. В ходе иммунизации эмульсию вводили в 3–6 мест подкожно вдоль позвоночника. Забор крови проводили из краевой вены уха с помощью вакуумных пробирок Green Vac-Tube 0238 с разделяющим гелем и активатором свертывания (SiO_2). Полученную сыворотку консервировали 0.1% азида натрия и хранили при +4 °C.

Выделение антител

Экстракты антигенов диализовали против 0.15M раствора хлористого натрия на мембранах с порогом исключения 10 кДа, определяли общий белок по методу Лоури и доводили концентрацию до 10 мг/мл. Активированную матрицу CH-sepharose 4B (Sigma) промывали 0.15M раствором хлорида натрия, смешивали с раствором антигена в соотношении 1:1, добавляли EDAC (Sigma) из расчета 20 мг на 1 мл финального объема. Инкубировали смесь при комнатной температуре 18–24 ч при постоянном перемешивании.

Для выделения кроличьих антител осветленные сыворотки наносили на 20-мл колонку с сорбентом со скоростью 1 мл/мин. После нанесения колонку отмывали фосфатно-солевым буфером. Связанные антитела элюировали 0.1M уксусной кислотой (pH 2.8) и нейтрализовали добавлением 1M Трис-буфера. Выделенные антитела консервировали 0.1% азида натрия и хранили при +4 °C.

Получение биотинилированных гликоконъюгатов

Синтез биотинилированных конъюгатов **(IIIb)** [14–15] и **(VIIIb)** [20] был описан ранее.

Биотинилированные конъюгаты **(Ib), (IIb)**, **(IVb)–(VIIb)**, **(Xb)–(XVIIIb)** получали согласно схеме по ранее опубликованному нами методу [23].

К растворам олигосахаридов **(Ia), (IIa)**, **(IVa)–(VIIa)**, **(Xa)–(XVIIIa)** (2.15 мкмоль) в 100 мкл абс. DMF прибавляли 38.3 мкл 0.068 M раствора пентафторфенилового эфира производного биотина **(IX)** [23] в DMF и 10 мкл сухого Et_3N. Реакционную смесь перемешивали 12 ч при комнатной температуре, растворитель удаляли в вакууме масляного насоса. Остаток подвергали гель-хроматографии на колонке с гелем Toyo Pearl TSK HW-40(S) (16 × 350 мм) в 0.1 M AcOH и получали биотинилированные производные **(Ib), (IIb)**, **(IVb)–(VIIb)**, **(Xb)–(XVIIIb)** с выходами (65%–75%). В спектрах ЯМР полученных продуктов присутствовали соответствующие сигналы их углеводных частей, практически не отличающиеся от соответствующих данных спектров исходных (3-аминопропил) гликозидов [11–18], а также характеристичные сигналы биотинилированного фрагмента. Спектр ЯМР ^1H (600 МГц, D_2O, характеристичные сигналы, δ, м.д., J, Гц): биотиновый фрагмент: 4.62 (1 H, д.д, $J^{6a,3a}$ 8.0, $J^{6a,6}$4.9, H6a,); 4.42 (1 H, д.д, $J^{6a,3a}$ 8.0, $J^{3a,4}$4.5, H3a); 3.02 (1 H, д.д, $J^{6.6'}$ 13.1, $J^{6.6a}$ 5.0, H6); 2.81 (1 H, д, $J^{6.6'}$ 13.0, H6′); 2.27 (2 H, т, *J* 7.3, $NHCOCH_2C\underline{H}_2CH_2$).

Таблица 3. Данные масс-спектров соединений **(Ib), (IIb)**, **(IVb)–(VIIb)**, **(Xb)–(XVIIIb)**.

Соединение	Ион	Брутто-формула	Найдено (*m/z*)	Вычислено (*m/z*)
(Ib)	$[M + Na]^+$	$C_{40}H_{72}N_4O_{20}S$	978.3777	983.4353
(IIb)	$[M + Na]^+$	$C_{58}H_{102}N_4O_{35}S$	1469.5924	1469.5938
(IVb)	$[M + Na + H]^{2+}$	$C_{82}H_{142}N_4O_{55}S$	1059.4049	1059.4062
(Vb)	$[M + Na + H]^{2+}$	$C_{76}H_{132}N_4O_{50}S$	978.3777	978.3797
(VIb)	$[M + Na]^+$	$C_{46}H_{82}N_4O_{25}S$	1145.4845	1145.4881
(VIIb)	$[M + Na]^+$	$C_{52}H_{92}N_4O_{30}S$	1307.5427	1307.5409
(Xb)	$[M + Na]^+$	$C_{34}H_{62}N_4O_{15}S$	821.3820	821.3825
(XIb)	$[M + Na]^+$	$C_{40}H_{72}N_4O_{20}S$	983.4343	983.4353
(XIIb)	$[M + Na]^+$	$C_{40}H_{72}N_4O_{20}S$	983.4347	983.4353
(XIIIb)	$[M - H]^-$	$C_{46}H_{82}N_4O_{25}S$	1121.4919	1121.4916
(XIVb)	$[M + Na]^+$	$C_{46}H_{82}N_4O_{25}S$	1145.4893	1145.4881
(XVb)	$[M + Na]^+$	$C_{46}H_{82}N_4O_{25}S$	1145.4859	1145.4881
(XVIb)	$[M - 2H]^{2-}$	$C_{58}H_{102}N_4O_{35}S$	722.2950	722.2962
(XVIIb)	$[M + Na]^+$	$C_{58}H_{102}N_4O_{35}S$	1469.5924	1469.5938
(XVIIIb)	$[M + Na]^+$	$C_{70}H_{122}N_4O_{45}S$	1793.6979	1793.6994

Данные масс-спектров соединений **(Ib), (IIb)**, **(IVb)–(VIIb)**, **(Xb)–(XVIIIb)** представлены в табл. 3.

Иммуноферментный анализ

Иммуноферментный анализ на стрептавидиновых планшетах Pierce® Streptavidin Coated 96 Well Plates (Thermo Scientific, США) проводили в соответствии с инструкцией производителя (фирма "Thermo Scientific Inc.", США, www.thermoscintific.com/pierce) при использовании фосфатно-солевого буфера (ФСБ), содержащего 0.05% Tween 20 и 0.1% бычьего сывороточного альбумина в качестве разводящего и отмывающего растворов. Биотинилированные олигосахариды **(Ib)–(VIIIb)**, **(Xb)–(XVIIIb)** абсорбировали на дне лунок (15 пмоль олигосахарида в 100 мкл разводящего раствора на одну лунку) в течение 2 ч при 22°C, затем содержимое планшета вытряхивали, промывали 3 раза и наносили исследуемые антитела (100 мкл) указанной концентрации. Планшет инкубировали 30 мин при 22°C, после чего содержимое планшета вытряхивали, промывали 3 раза. Сорбированные антитела проявляли с использованием меченных пероксидазой хрена IgG против иммуноглобулинов кролика (ХЕМА, Россия) и однокомпонентного хромогенного субстрата TMB. Оптическое поглощение продуктов ферментативной реакции измеряли на приборе "Multiskan GO" при длине волны 450 нм. Измерения для каждой концентрации антител проводили не менее 3 раз.

Методы статистической обработки данных

Проверку на статистическую достоверности различий осуществляли с помощью t-критерия Стьюдента (различия считались статистически значимыми при $p < 0.05$). Расчеты выполнялись в программе Excel.

БЛАГОДАРНОСТИ

Авторы выражают благодарность А.О. Чижову и А.С. Дмитренку за спектральную характеристику соединений в Отделе структурных исследований ИОХ РАН. Работа выполнена при поддержке Российского научного фонда (грант 14-23-00199).

СПИСОК ЛИТЕРАТУРЫ

1. *Latgé J.P., Steinbach W.J.* Aspergillus fumigatus and aspergillosis. Washington: ASM Press, 2009.
2. *Latgé J.P.* // Clin. Microbiol. Rev. 1999. V. 12. P. 310–350.
3. *Walsh T.J., Anaissie E.J., Denning D.W., Herbrecht R., Kontoyiannis D.P., Marr K.A., Patterson T.F.* // Clin. Infect. Dis. 2008. V. 46. P. 327–360.

4. *Groll A.H., Shah P.M., Mentzel C., Schneider M., Just-Nuebling G., Huebner K.* // J. Infect. 1996. V. 33. P. 23–32.
5. *Kohno S.* // Clin. Infect. Dis. 2008. V. 47. P. 1185–1187.
6. *Mennink-Kersten M.A., Klont R.R., Warris A., den Camp H.J.O., Verweij P.E.* // The Lancet 2004. V. 363. P. 325–327.
7. *Mennink-Kersten M.A., Ruegebrink D., Klont R.R., Warris A., Gavini F., den Camp H.J.O., Verweij P.E.* // J. Clin. Microbiol 2005. V. 43. P. 3925–3931.
8. *Arvanitis M., Anagnostou T., Fuchs B.B., Caliendo A.M., Mylonakis E.* // Clin. Microbiol. Rev. 2014. V. 27. P. 490–526.
9. *Pickering J.W., Sant H.W., Bowles C.A., Roberts W.L., Woods G.L.* // J. Clin. Microbiol. 2005. V. 43. P. 5957–5962.
10. *Latgé J.P.* // Mol. Microbiol. 2007. V. 66. P. 279–290.
11. *Argunov D.A., Krylov V.B., Nifantiev N.E.* // Org. Biomol. Chem. 2015. V. 13. P. 3255–3267.
12. *Argunov D.A., Krylov V.B., Nifantiev N.E.* // Org. Lett. 2016. V. 18. P. 5504–5507.
13. *Krylov V.B., Argunov D.A., Vinnitskiy D.Z., Verkhnyatskaya S.A., Gerbst A.G., Ustyuzhanina N.E., Dmitrenok A.S., Huebner J., Holst O., Siebert H.-C., Nifantiev N.E.* // Chem. Eur. J. 2014. V. 20. P. 16516–16522.
14. *Komarova B.S., Orekhova M.V., Tsvetkov Y.E., Beau R., Aimanianda V., Latgé J.P., Nifantiev N.E.* // Chem. Eur. J. 2015. V. 21. P. 1029–1035.
15. *Орехова М.В.* Синтез олигосахаридов, отвечающих α-(1–3)-глюкану *Aspergillus fumigatus* (синтез). Дис. канд. хим. наук. М.: Институт органической химии им. Н.Д. Зелинского РАН. 2016. С. 205. [*Orekhova M.V.* Synthesis of oligosaccharides related α-(1–3)-glucan of *Aspergillus fumigatus* (synthesis), PhD thesis, N.D. Zelinsky Institute of Organic Chemistry RAS, 2016. P. 205.]
16. *Yashunsky D.V., Tsvetkov Y.E., Grachev A.A., Chizhov A.O., Nifantiev N.E.* // Carbohydr. Res. 2016. V. 419. P. 8–17.
17. *Yashunsky D.V., Tsvetkov Y.E., Nifantiev N.E.* // Carbohydr. Res. 2016. V. 436. P. 25–30.
18. *Karelin A.A., Tsvetkov Y.E., Paulovičová E., Paulovičová L., Nifantiev N.E.* // Eur. J. Org. Chem. 2016. V. 2016. P. 1173–1181.
19. *Юдина О.Н., Цветков Ю.Е., Нифантьев Н.Э.* // Изв. АН. Сер. хим. 2015. Т. 12. С. 2932–2941. [*Yudina O.N., Tsvetkov Y.E., Nifantiev N.E.* // Russ. Chem. Bull. (Int. Ed.) 2015. V. 64. P. 2932–2941.]
20. *Юдина О.Н., Цветков Ю.Е., Нифантьев Н.Э.* // Изв. АН. Сер. хим. 2016. Т. 12. С. 2937–2942. [*Yudina O.N., Tsvetkov Y.E., Nifantiev N.E.* // Russ. Chem. Bull. (Int. Ed.). 2016. V. 65. P. 2937–2942.]
21. *Ananikov V.P., Galkin K.I., Egorov M.P., Sakharov A.M., Zlotin S.G., Redina E.A., Isaeva V.I., Kustov L.M., Gening M.L., Nifantiev N.E.* // Mendeleev Commun. 2016. V. 26. P. 365–374.
22. *Курбатова Е.А., Ахматова Э.А., Ахматова Н.К., Егорова Н.Б., Ястребова Н.Е., Романенко Э.Е., Леонова А.Ю., Поддубиков А.В., Цветков Ю.Е., Сухова Е.В., Генинг М.Л., Яшунский Д.В., Нифантьев Н.Э.* // Изв. АН. Сер. хим. 2016. Т. 6. С. 1608–1616. [*Kurbatova E.A., Akhmatova E.A., Akhmatova N.K., Egorova N.B., Yastrebova N.E., Romanenko E.E., Leonova A.Y., Poddubikov A.V., Tsvetkov Y.E., Sukhova E.V., Gening M.L., Yashunsky D.V., Nifantiev N.E.* // Russ. Chem. Bull. (Int. Ed.). 2016. V. 65. P. 1608–1616.]
23. *Tsvetkov Y.E., Burg-Roderfeld M., Loers G., Arda A., Sukhova E.V., Khatuntseva E.A., Grachev A.A., Chizhov A.O., Siebert H.-C., Schachner M., Jimenez-Barbero J., Nifantiev N.E.* // J. Am. Chem. Soc. 2012. V. 134. P. 426–435.

Study of the carbohydrate specificity of antibodies against *Aspergillus fumigatus* using a library of synthetic mycoantigens

V. B. Krylov[1], M. I. Petruk[1], I. V. Grigoryev[2], Y. S. Lebedin[2], N. I. Glushko[3], E. V. Khaldeeva[3], D. A. Argunov[1], E. A. Khatuntseva[1], M. V. Toplishek[1], B. S. Komarova[1], A. A. Karelin[1], O. N. Yudina[1], V. M. Menshov[1], D. V. Yasunskii[1], Y. E. Tsvetkov[1], N. E. Nifantiev[1,*]

**Phone: +7(499)-135-87-84; e-mail: nen@ioc.ac.ru*
[1]Laboratory of Glycoconjugate Chemistry, N.D. Zelinsky Institute of Organic Chemistry, Russian Academy of Sciences, 119991 Moscow, Leninsky prospect 47
[2]XEMA Company Limited, 105264 Moscow, 9 Parkovaya str., 48
[3]Kazan Scientific Research Institute of Epidemiology and Microbiology, 420015, Kazan, Bolshaya Krasnaya str., 67

Using the library of biotinylated synthetic oligosaccharides, the carbohydrate specificity of antibodies obtained by immunizing laboratory animals with immunogens prepared from the *Aspergillus fumigatus* cell wall was analyzed. It has been shown that the main part of anti-polysaccharide antibodies recognizes galactomannan in the used immunogens, and preferably its fragments containing more than two β-(1→5)-linked galactofuranosyl units. The data obtained can form the basis for the development of enzyme immunoassay for the detection of this dangerous fungal pathogen.

Keywords: Aspergillus fumigatus, aspergillosis, antigen, antibody, galactomannan, diagnosticum

ПРИКЛАДНАЯ БИОХИМИЯ И МИКРОБИОЛОГИЯ, 2018, том 54, № 5, с. 1–7

УДК 577.114.5:616-097

ИССЛЕДОВАНИЕ УГЛЕВОДНОЙ СПЕЦИФИЧНОСТИ АНТИТЕЛ ПРОТИВ ПРЕПАРАТОВ УСЛОВНО ПАТОГЕННЫХ ГРИБОВ РОДА *Aspergillus*

© 2018 г. В. Б. Крылов[1], М. И. Петрук[1], Н. И. Глушко[2], Е. В. Халдеева[2], В.Л. Мокеева[3], Е.Н. Биланенко[3], Ю. С. Лебедин[4], С.А. Еремин[3], Н. Э. Нифантьев[1, *]

[1]*Институт органической химии им. Н.Д. Зелинского РАН, Москва, 119991, Россия*

[2]*Казанский научно-исследовательский институт эпидемиологии и микробиологии, Казань, 420015, Россия*

[3]*Московский государственный университет им. М.В. Ломоносова, Москва,119991, Россия*

[4]*ООО "ХЕМА", Москва, 105264, Россия*

**e-mail: nen@ioc.ac.ru*

Поступила в редакцию 27.12.2017 г.

Проведена иммунизация лабораторных животных (калифорнийских кроликов) препаратами, приготовленными из биомассы грибов *Aspergillus fumigatus, Aspergillus niger* и *Aspergillus repens*. Для анализа углеводной специфичности использовали библиотеку синтетических биотинилированных олигосахаридов, содержащих ключевые фрагменты антигенных полисахаридов клеточной стенки этих грибов – галактоманнана, α- и β-глюканов, маннана и хитина. Показано, что анти-углеводные антитела, полученные после иммунизации животных препаратами, приготовленными из биомассы *A. fumigatus* и *A. repens,* преимущественно распознавали эпитопы, содержащие галактофуранозидные остатки, в то время как основная часть антител против *A. niger* связывалась с хитоолигосахаридным лигандом. Полученные данные позволили создать основу для обнаружения специфических видовых маркеров, необходимых для разработки иммуноферментных тест-систем.

Ключевые слова: Aspergillus fumigatus, *Aspergillus niger*, *Aspergillus repens*, аспергиллез, антиген, антитело

DOI: 10.1134/S0555109918050094

Род *Aspergillus* представляет крупный анаморфный род аскомицетов (*Trichocomaceae*, *Eurotiales*, *Eurotiomycetes* и *Ascomycota*), который среди грибов занимает одно из ведущих мест по числу таксонов, распространению, биологической активности и значимости для человека. В настоящее время он включает более 300 видов, которые распространены повсеместно и занимают разные экологические ниши. Аспергиллы часто выделяют из почвы, с мертвых органических субстратов, но они могут колонизировать и живые организмы. Эти грибы чрезвычайно важны для человека, поскольку используются в биотехнологических процессах и производстве продуктов питания, а также присутствуют в окружающей человека среде и влияют на его здоровье [1–3]. Интерес к аспергиллам обусловлен, с одной стороны, присутствием у них комплекса ферментов, антимикробных веществ и органических кислот, используемых в биотехнологии, пищевой промышленности и медицине. С другой стороны, эти грибы образуют токсичные метаболиты, участвуя в гниении продуктов питания, а также проявляют патогенные для животных и человека свойства. К наиболее распространенным их микотоксинам относят афлатоксины, охратоксины и стеригматоцистин [4], которые могут вызывать тяжелые отравления. Эти грибы провоцируют у человека аллергические реакции, а при пониженном иммунитете могут стать причиной микозов [5].

Наибольшую опасность для человека представляют инвазивные заболевания, вызываемые грибами и значительно распространившиеся в последнее время [5–9]. Так, грибы рода *Aspergillus* (прежде всего *A. fumigatus*) способны поражать легкие пациентов с ослабленным иммунитетом, вызывая тяжелейшее и практически неизлечимое заболевание – инвазивный аспергиллез легких (**ИАЛ**) [5–8]. Смертность от ИАЛ составляет 50% даже при своевременной диагностике и начале лечения, а в случае ее задержки на 10 сут смертность приближается к 100% [9, 10]. К группе риска относятся пациенты, находящиеся в отделениях интенсивной терапии, получающие иммуноподавляющую терапию после операций по трансплантации органов, онкобольные, проходящие курс химиотерапии, и больные с ВИЧ-инфекцией [11].

В отличие от поражения организма млекопитающих и человека *A. fumigatus* случаи поражения грибом *A. niger* более редки. Однако вследствие повсеместного распространения *A. niger* люди часто подвергаются воздействию его спор, присутствующих в воздухе, помещениях и на пищевых продуктах, что вызывает у них аллергические реакции. *A. niger* также продуцирует микотоксины, проявляющие гепатоканцерогенные свойства [12]. Этот гриб может быть патогеном многих сельскохозяйственных культур [12].

Чрезвычайно важно выявлять и адекватно идентифицировать аспергиллы. В течение длительного времени классификация и идентификация таксонов (подродов, секций и видов) рода *Aspergillus* базировалась на фенотипических признаках [13], позднее получили широкое внедрение их молекулярные, хемотаксономические и филогенетические исследования [1, 14]. Во многом данные филогенетического анализа совпадают с результатами, полученными по морфолого-культуральным признакам, однако, в ряде случаев морфологически близкие виды оказываются различны генетически [14]. В настоящее время признана необходимость комплексного анализа с привлечением максимально возможных методов и подходов.

Альтернативными подходами к выявлению заражения грибами являются методы, основанные на ПЦР и MALDI-TOF-спектрометрии [15, 16]. Отдельное место занимают такие иммунологические методы, как иммуноферментный, иммунохроматографический, иммунофлуоресцентный и иммуно-ПЦР анализы [17–20]. Этот подход является наиболее универсальным, однако требует получения и характеристики высокоспецифичных антител.

Клеточная стенка грибов представляет собой сложную биологическую структуру, состоящую из разнообразных полисахаридов: хитина, линейных и разветвленных α- и β-глюканов, α- и β-маннанов, галактоманнана и других [6, 21]. Углеводы широко представлены в составе растворимых полисахаридов и гликопротеинов у экзоантигенов, продуцируемых клеткой во внешнее пространство [6, 21]. Эти полисахариды относятся к потенциальным антигенным маркерам при обнаружении патогенного гриба. Однако их чрезвычайно сложное строение и структурная гетерогенность, а также трудности их выделения и очистки не позволяют детально охарактеризовать распознаваемые иммунной системой углеводы.

Цель работы – охарактеризовать углеводную специфичность поликлональных антител против *A. fumigatus*, *A. repens* и *A. niger* с использованием тематического гликоряда синтетических олигосахаридов, отвечающих основным типам полисахаридов их клеточной стенки.

МЕТОДИКА

Получение иммуногенов. Для получения иммуногенов использовали биомассу трех видов грибов из рода *Aspergillus: A. fumigatus* Fresen., *A. niger* Tiegh., *A. repens* (Corda) Sacc. Штаммы грибов были получены из коллекции кафедры микологии и альгологии Биологического факультета МГУ им. М.В. Ломоносова.

Для получения биомассы *A. fumigatus* и *A. niger* выращивали в поверхностной культуре на жидкой среде Чапека (г/л): $NaNO_3$ – 2, KH_2PO_4 – 1, $MgSO_4$ – 0.5, KCl – 0.5, $FeSO_4$ – 0.01, сахароза – 20. *A. repens* проявлял ксерофильные свойства на ксерофильной среде, следующего состава: NaCl – 100 г, солодовый экстракт (15%Б) – 300 мл, H_2O – 700 мл. В качестве инокулята использовали водный смыв с 2-недельной культуры гриба, выращенной в пробирках на скошенной агаризованной среде. В качалочные колбы со 150 мл среды вносили по 10^7 КОЕ спор грибов и инкубировали в течение 14–23 сут при 26°C. За этот период времени на поверхности жидкой среды образовывалась пленка, состоящая из плотного сплетения гиф, а сверху на мицелии развивалось спороношение. Грибную массу извлекали стерильным шпателем (или пинцетом) из колбы, ополаскивали сначала стерильной дистиллированной водой, а потом дважды промывали 10-кратным объемом 0.85%-ного раствора хлористого натрия (pH 7.0), освобождая от питательной среды. Центрифугировали при 2000 *g* в течение 10 мин при 4°C, после чего обрабатывали ацетоном в течение 16–18 ч, высушивали и размалывали в тонкий однородный порошок.

Для экстракции иммуногенов порошок мицелия обрабатывали пятикратным объемом 1 М раствора хлористого натрия. Экстракт концентрировали на мембране Biomax PBGC09005 с порогом исключения 10 кДа (“Sigma”, США) и хранили при –20°C.

Иммунизация. Антисыворотки против иммуногенов получали на 5 самцах кроликов породы “Калифорнийский кролик” в возрасте 4–6 мес. Животных иммунизировали с интервалом 2 нед свежеприготовленной эмульсией иммуногенов (0.2 мг по белку антигена в 0.5 мл дистиллированной воды на кролика) с полным адъювантом Фрейнда для первой иммунизации и с неполным адъювантом Фрейнда для последующих. Эмульсию готовили в соотношении раствор конъюгата/адъювант – 1 : 1. В ходе иммунизации эмульсию вводили подкожно в 3–6 мест вдоль позвоночника. Кровь забирали из краевой вены уха с помощью вакуумных пробирок Green Vac-Tube 0238 (“GC Pharma”, Республика Корея) с разделяющим гелем и активатором свертывания (SiO_2). Полученную сыворотку консервировали 0.1%-ным раствором азида натрия и хранили при 4°C.

Выделение антител. Экстракты антигенов диализовали против 0.15 М раствора хлористого натрия на мембранах с порогом исключения 10 кДа, определяли общий белок методом Лоури и доводили их концентрацию до 10 мг/мл. Активированную матрицу CH-sepharose 4B ("Sigma", США) промывали 0.15 М раствором хлорида натрия, смешивали с раствором антигена в соотношении 1 : 1, добавляли (1-этил-3-(3-диметиламинопропил)карбодиимид (**ЕДАК**, "Sigma", США) из расчета 20 мг на 1 мл финального объема. Инкубировали смесь в течение 18–24 ч при постоянном перемешивании и комнатной температуре.

Полученный сорбент использовали для выделения специфичных антител из сывороток кроликов аффинной хроматографией. Для этого осветленные сыворотки наносили со скоростью 1 мл/мин на колонку с сорбентом объемом 20 мл. После нанесения колонку промывали фосфатно-солевым буфером (**ФСБ**). Связавшиеся антитела элюировали 0.1 М уксусной кислотой (pH 2.8) и нейтрализовали добавлением 1 М трис-буфера, pH 7.2. Выделенные антитела консервировали в 0.1%-ном растворе азида натрия и хранили при 4°C.

Иммуноферментный анализ. Иммуноферментный анализ на стрептавидиновых планшетах Pierce® Streptavidin Coated 96 Well Plates ("Thermo Scientific", США) проводили в соответствии с инструкцией производителя (www.thermoscintific.com/pierce) при использовании в качестве раствора для разведения реагентов и промывания планшета 0.01 М фосфатного буфера, pH 7.4, содержашего 0.137 М NaCl, 0.0027 М KCl, 0.05% твин 20 и 0.1% бычьего сывороточного альбумина (**БСА**). Биотинилированные олигосахариды абсорбировали на дне лунок (по 15 пмоль олигосахарида в 100 мкл ФСБ на одну лунку) в течение 2 ч при 22°C, затем жидкость удаляли, планшет промывали 3 раза и наносили антитела (100 мкл), которые инкубировали в течение 30 мин при 22°C. Затем жидкость удаляли, а планшет промывали 3 раза. Сорбированные антитела проявляли с использованием меченных пероксидазой хрена IgG против иммуноглобулинов кролика ("ХЕМА", Россия) и однокомпонентного хромогенного субстрата 3,3',5,5'-тетраметилбензидина (**ТМБ**). Оптическую плотность продуктов ферментативной реакции измеряли при 450 нм на "Multiskan GO" ("Thermo fisher scientific", США). Эксперименты повторяли не менее 3 раз.

РЕЗУЛЬТАТЫ И ИХ ОБСУЖДЕНИЕ

Углеводная специфичность поликлональных антител, полученных против грибов *A. fumigatus*, *A. repens* и *A. niger*, была определена методами иммуноферментного анализа с использованием библиотек синтетических олигосахаридов, отвечающих основным углеводным антигенам грибов (так называемых гликорядов, от английского GlycoArray) [22, 23]. Подобные гликоряды на основе биочипных слайдов со стрептавидиновым покрытием описаны в работе [24]. Использование для данной цели природных антигенов существенно осложняется трудностями их выделения и очистки, их высокой гетерогенностью и широким диапазоном молекулярных масс, а также сложностями их иммобилизации на поверхности пластика. Фиксация же синтетических олигосахаридов [21] на поверхности планшета из пластика осуществлялась количественно за счет сверхпрочного нековалентного взаимодействия биотиновой метки с поверхностью, модифицированной стрептавидином, при этом используемый олигоэтиленгликольный спейсер обеспечивает эффективное экспонирование углеводной части для связывания с антителами [25]. Для построения гликоряда были отобраны 8 олигосахаридов (**1–8**, рис. 1), родственных характерным антигенным структурам на поверхности клеточной стенки различных видов грибов.

Олигосахариды **1, 2** [26–28] представляют собой фрагменты галактоманнана – специфического полисахарида некоторых видов грибов из родов *Aspergillus* и *Penicillium*, синтезированные с использованием пиранозид-фуранозидной перегруппировки [29–31]. Нонасахарид **3** соответствует α-(1 → → 3)-глюкану, обнаруженному в клеточной стенке *A. fumigatus* [32, 33]. Линейные и разветвленные участки β-(1 → 3)-глюкана, являющегося общим компонентом клеточной стенки разнообразных видов грибов, представлены олигосахаридами **4** и **5** соответственно [34, 35]. Олигоманнозиды **6** и **7** [21, 36] отражают структуру полисахарида маннана, а также главную цепь галактоманнана из *A. fumigatus*. Пентасахарид **8** [37, 38] является фрагментом цепи хитина, одного из основных компонентов клеточной стенки всех грибов.

При изучении сыворотки интактных животных, которую разбавляли 1 : 100 и 1 : 500, не было обнаружено естественных антител против микоантигенов 1–8. В то же время поликлональные антитела, полученные при иммунизации препаратами грибного происхождения, специфически распознавали определенные типы лигандов.

Поликлональные антитела, полученные при иммунизации препаратами из биомассы гриба *A. fumigatus*, преимущественно распознавали антигены **1** и **2**, родственные галактоманнану, и незначительно связывались с олигосахаридами, относящимися к другим типам полисахаридов (рис. 2). Антитела, полученные при иммунизации препаратами из биомассы *A. repens*, также активно распознавали пентасахарид **2**, родственный галактоманнану, однако практически не связывались с дисахаридом **1** (рис. 2в). Это могло свидетельствовать о наличии в антигене из *A. rep-*

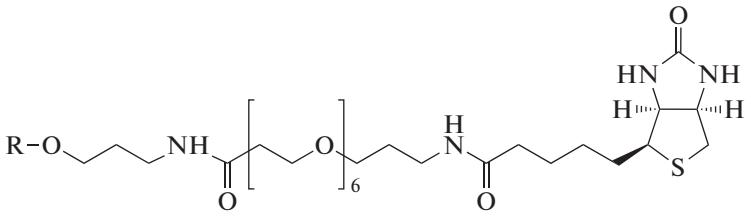

1 R = β-D-Gal*f*-(1 → 5)-β-D-Gal*f* —

2 R = [β-D-Gal*f*-(1→ 5)-β-D-Gal*f*-(1 → 6)-α-D-Man —

3 R = [α-D-Glc-(1 → 3)$_8$-α-D-Glc —

4 R = [β-D-Glc-(1 → 3)$_8$-β-D-Glc —

[β-D-Glc-(1 → 3)$_2$-β-D-Glc

1

↓

6

5 R = [β-D-Glc-(1 → 3)$_3$-β-D-Glc-(1 → 6)-β-D-Glc —

6 R = [β-D-Glc-(1 → 2)$_2$-α-D-Man —

7 R = α-D-Man-(1 → 6)-[α-D-Man-(1 → 6)]$_2$-α-D-Man —

8 R = [b-D-GlcNAc-(1 → 4)]$_4$-β-D-GlcNAc —

Рис. 1. Строение синтетических микоантигенов 1–8. Gal*f* – галактофураноза, Man – манноза, Glc – глюкоза, GlcNAc – N-ацетилглюкозамин.

ens более длинных олигогалактофуранозидных цепей, чем в антигене из *A. fumigatus.*

В отличие от поликлональных антител против *A. fumigatus* и *A. repens*, антитела против *A. niger* взаимодействовали с олигосахаридом **8**, родственным хитину (рис. 2б). Несмотря на то, что хитин входит в состав компонентов клеточной стенки всех грибов, обнаружение специфических антител к нему оказалось неожиданным, так как хитин обладает низкой иммуногенностью, представлен во внутренних слоях клеточной стенки и практически не растворим [6].

Можно предположить, что обнаруженные различия вполне закономерны и являются отражением биологической природы грибов. Для анализа углеводной специфичности антител были взяты виды крупного анаморфного рода *Aspergillus,* который традиционно по морфолого-культуральным признакам делили на группы [13], а позднее на подроды и секции [1, 14]. Хотя выбранные виды относятся к одному роду, они принадлежат к разным секциям внутри него (*A. repens* входит в секцию *Aspergillus, A. niger* – секцию *Nigri,* а *A. fumigatus* – секцию *Fumigati*) и сильно отличаются друг от друга как по морфологии и физиологии, так и генетически.

Сравнительный анализ геномных последовательностей ключевых этапов биологии аспергиллов, включая первичный и вторичный метаболизм, ответ на действие факторов стресса и трансдукцию сигналов, позволил обнаружить как некоторые общие, так и специфические черты видов этого рода. Так, для темноокрашенных аспергиллов секции *Nigri* к ключевому отличительному признаку относят наличие генов, отвечающих за синтез органических кислот [14]. Каждый из выбранных видов грибов обладает спецификой экофизиологии. Так, *A. fumigatus* и *A. repens* характеризуются устойчивостью к факторам стресса. Известны термофильные изоляты *A. fumigatus*, температурный оптимум роста которых лежит в области, близкой к температуре тела теплокровных животных и человека. Этот вид имеет много клинических изолятов [5]. *A. repens* характеризуется ксерофильными свойствами, поэтому часто приурочен к местообитаниям, где низкая активность воды лимитирует развитие других грибов. Он является причиной гниения ряда консервированных продуктов при хранении. *A. niger* относится к повсе-

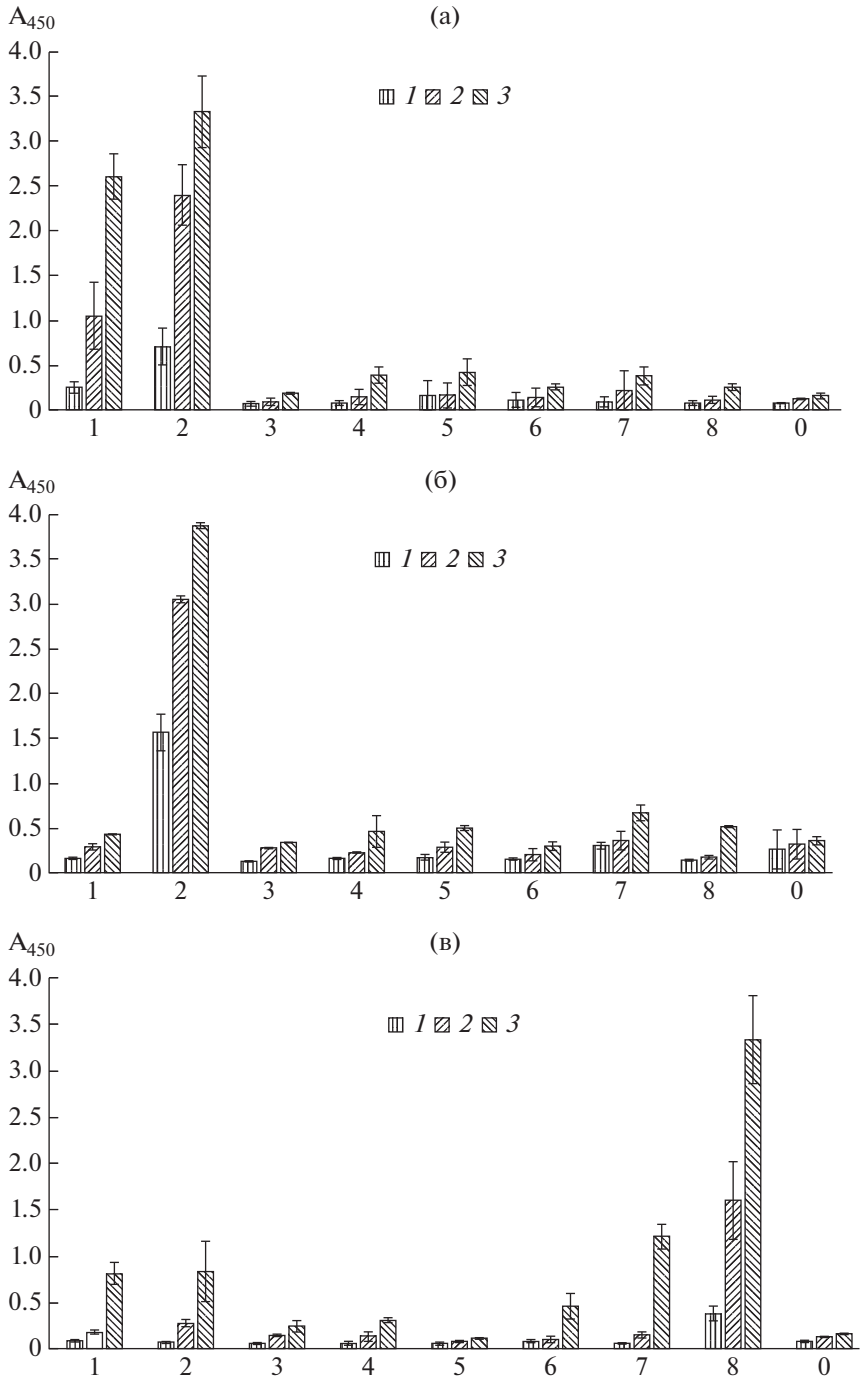

Рис. 2. Взаимодействие поликлональных антител, полученных при иммунизации препаратами из биомассы *A. fumigatus* (а), *A. repens* (б) *A. niger* (в) с синтетическими микоантигенами (1–8 на оси абсцисс, 0 – контроль, отсутствие антигена), изученное методами ИФА. Использованные концентрации антител: *1* – 1 мкг/мл, *2* – 3 мкг/мл, *3* – 9 мкг/мл.

местно распространенным видам с более широкой экологической амплитудой, чем два других вида. Он поражает различные продукты питания, орехи и сухофрукты.

Таким образом, была изучена способность поликлональных антител, полученных при иммунизации препаратами из биомассы трех разных видов грибов рода *Aspergillus*, распознавать основные углеводные микоантигены. Определены характерные особенности их специфичности. Полученные результаты позволили сформировать основы для создания диагностических тест-систем, востребованных для экологического контроля грибной контаминации продуктов питания и помещений,

а также обнаружения грибковых заболеваний человека.

Приготовление иммуногенов, работы по иммунизации лабораторных животных и выделению антител выполнены при финансовой поддержке Министерства образования и науки Российской Федерации (уникальный идентификатор проекта RFMEFI60717X0185). Получение биотинилированных олигосахаридов, создание гликорядов и анализ специфичности антител выполнены в биохимическом модуле ИОХ РАН при финансовой поддержке Российского Научного Фонда (проект № 14-50-00126).

СПИСОК ЛИТЕРАТУРЫ

1. *Samson R.A., Visagie C.M., Houbraken J., Hong S.B., Hubka V., Klaassen C.H.W., Perrone G., Seifert K.A., Susca A., Tanney J.B., Varga J., Kocsubé S., Szigeti G., Yaguchi T., Frisvad J.C.* // Stud. Mycol. 2014. V. 78. P. 141–173.
2. *Антропова А.Б., Мокеева В.Л., Биланенко Е.Н., Чекунова Л.Н., Желтикова Т.М., Петрова-Никитина А.Д.* // Микология и фитопатология. 2004. Т. 38. № 5. С. 32–41.
3. *Domsch K. H., Gams W., Anderson T-H.* Compendium of Soil Fungi. // Ed. W. Gams. Koeltz scientific Books Publishers, 2007. 672 p.
4. *Klich M.A.* // Mol. Plant Pathol. 2007. V. 8. № 6. P. 713–722.
5. *Hoog de G.S., Guarro J., Gene J., Figueras M.J.* Atlas of Clinical Fungi. 2 ed. Centraalbureau voor Schimmelcultures. Universitat Rovira i Virgili. 2000.
6. *Latgé J.P.* // Mol. Microbiol. 2007. V. 66. № 2. P. 279–290.
7. *Bongomin F., Gago S., Oladele R.O., Denning D.W.* // J. Fungi. 2017. V. 3. № 4. P. 57.
8. *Klimko N., Kozlova Y., Khostelidi S., Shadrivova O., Borzova Y., Burygina E., Vasilieva N., Denning, D. W.* // Mycoses. 2015. V. 58. № 5. P. 58–62.
9. *Groll A.H., Shah P.M., Mentzel C., Schneider M., Just-Nuebling G., Huebner K.* // J. Infect. 1996. V. 33. № 1. P. 23–32.
10. *Kohno S.* // Clin. Infect. Dis. 2008. V. 47. № 9. P. 1185–1187.
11. *Walsh T.J., Anaissie E.J., Denning D.W., Herbrecht R., Kontoyiannis D.P., Marr K.A., Patterson T.F.* // Clin. Infect. Dis. 2008. V. 46. № 3. P. 327–360.
12. *Schuster E., Dunn-Coleman N., Frisvad J.C., Van Dijck, P.* // Appl. Microbiol. Biotechn. 2002. V. 59. № 4–5. P. 426–435.
13. *Raper K.B., Fennell D.I.* The Genus *Aspergillus*. Baltimore: The Williams and Wilkins Company, 1965. 686 p.
14. *de Vries R.P., Riley R., Wiebenga A., Aguilar-Osorio G. et al.* // Genome Biol. 2017. V. 18. № 28. doi 10.1186/s13059-017-1151-0
15. *White P.L., Barnes R.A., Springer J., Klingspor L., Cuenca-Estrella M., Morton C.O.* // J. Clin. Microbiol. 2015. V. 53. № 9. P. 2832–2837.
16. *McCarthy M.W., Walsh T.J.* // Exp. Rev. Respiratory Med. 2017. V. 11. № 9. P. 739–748.
17. *Stynen D., Goris A., Sarfati J., Latge J.P.* // J. Clin. Microbiol. 1995. V. 33. № 2. P. 497–500.
18. *Held J., Schmidt T., Thornton C. R., Kotter E., Bertz H.* // Infection. 2013. V. 41. № 6. P. 1163–1169.
19. *Gustafsdottir S.M., Schallmeiner E., Fredriksson S., Gullberg M., Soderberg O., Jarvius M. Howell M., Landegren U.* // Anal. Biochem. 2005. V. 345. № 1. P. 2–9.
20. *White P.L., Parr C., Thornton C., Barnes R.A.* // J. Clin. Microbiol. 2013. V. 51. № 5. P. 1510–1516.
21. *Карелин А. А., Цветков Ю. Е., Нифантьев Н. Э.* // Успехи химии. 2017. V. 86. № 11. P. 1073–1126.
22. *Крылов В.Б., Петрук М.И., Григорьев И.В., Лебедин Ю.С., Глушко Н.И., Халдеева Е. В., Аргунов Д.А., Хатунцева Е.А., Топлишек М.В., Комарова Б.С., Карелин А.А., Юдина О.Н., Меньшов В.М., Яшунский Д.В., Цветков Ю.Е., Нифантьев Н.Э.* // Биоорган. химия. 2018. Т. 44. № 1 С. 78–86.
23. *Matveev A.L., Krylov V.B., Emelyanova L.A., Solovev A.S., Khlusevich Y.A., Baykov I.K., Fontaine T., Latgé J.-P., Tikunova N. ., Nifantiev N.E.* // PloS ONE. 2018. V. 13. e0193938 doi 10.1371/journal.pone.0193938
24. *Galanina O.E., Mecklenburg M., Nifantiev N. E., Pazynina G. V., Bovin N. V.* // Lab. Chip. 2003. V. 3. № 4. P. 260–265.
25. *Tsvetkov Y.E., Burg-Roderfeld M., Loers G., Arda A., Sukhova E.V., Khatuntseva E.A., Grachev A.A., Chizhov A.O., Siebert H.-C., Schachner M., Jimenez-Barbero J., Nifantiev N.E.* // J. Am. Chem. Soc. 2012. V. 134. № 1. P. 426–435.
26. *Argunov D.A., Krylov V.B., Nifantiev N.E.* // Org. Biomol. Chem. 2015. V. 13. № 11. P. 3255–3267.
27. *Argunov D. A., Krylov V.B., Nifantiev N.E.* // Org. Lett. 2016. V. 18. № 21. P. 5504–5507.
28. *Krylov V.B., Argunov D.A., Solovev A. S., Petruk M.I., Gerbst A.G., Dmitrenok A.S., Shashkov A.S., Latgé J.-P., Nifantiev, N.E.* // Org. Biomol. Chem. 2018. V. 16. № 7. P. 1188–1199.
29. *Krylov V.B., Argunov D.A., Vinnitskiy D.Z., Verkhnyatskaya S.A., Gerbst A.G., Ustyuzhanina N.E., Dmitrenok A.S., Huebner J., Holst O., Siebert H.-C., Nifantiev N.E.* // Chem. Eur. J. 2014.V. 20. № 50. P. 16516–16522.
30. *Krylov V.B., Kaskova Z.M., Vinnitskiy D.Z., Ustyuzhanina N.E., Grachev A.A., Chizhov A.O., Nifantiev N.E.* // Carbohydr. Res. 2011. V. 346. № 5. P. 540–550.
31. *Krylov V.B., Argunov D.A., Vinnitskiy D.Z., Gerbst A.G., Ustyuzhanina N.E., Dmitrenok A.S., Nifantiev N.E.* // Synlett 2016. V. 27. № 11. P. 1659–1664.
32. *Komarova B.S., Orekhova M.V., Tsvetkov Y.E., Beau R., Aimanianda V., Latgé J.P., Nifantiev, N.E.* // Chem. Eur. J. 2015. V. 21. № 3. P. 1029–1035.
33. *Komarova B.S., Orekhova M.V., Tsvetkov Y.E., Nifantiev N.E.* // Carbohydr. Res. 2014. V. 384. P. 70–86.
34. *Yashunsky D.V., Tsvetkov Y.E., Grachev A.A., Chizhov A.O., Nifantiev N.E.* // Carbohydr. Res. 2016. V. 419. P. 8–17.

35. *Yashunsky D.V., Tsvetkov Y.E., Nifantiev N.E.* // Carbohydr. Res. 2016. V. 436. P. 25–30.

36. *Karelin A.A., Tsvetkov, Y.E., Paulovičová, E., Paulovičová, L., Nifantiev N.E.* // Eur. J. Org. Chem. 2016. V. 2016. № 6. P. 1173–1181.

37. *Юдина О. Н., Цветков Ю. Е., Нифантьев Н. Э.* // Известия РАН Сер. Хим. 2015. V. 2015. № 12. P. 2932–2941.

38. *Юдина О. Н., Цветков Ю. Е., Нифантьев Н. Э.* // Известия РАН Сер. Хим. 2016. V. 2016. № 12. P. 2937–2942.

Study of the Carbohydrate Specificity of Antibodies against Specimens of Phytopathogenic Fungi of *Aspergillus*

V. B. Krylov[a], M. I. Petruk[a], N. I. Glushko[b], E. V. Khaldeeva[b], V. L. Mokeeva[c], E. N. Bilanenko[c], Y. S. Lebedin[d], S. A. Eremin[c], and N. E. Nifantiev[a, *]

[a]*N. D. Zelinsky Institute of Organic Chemistry, Russian Academy of Sciences, Moscow, 119991, Russia;*
[b]*Kazan Scientific Research Institute of Epidemiology and Microbiology, Kazan, 420015, Russia;*
[c]*M.V. Lomonosov Moscow State University, Moscow, 119991, Russia*
[d]*XEMA Company Limited, Moscow, 105264, Russia.*
**e-mail: nen@ioc.ac.ru*

Received December 27, 2017

Immunization of laboratory animals (brush rabbit) with the specimens prepared from the mycelium of fungi *Aspergillus fumigatus*, *Aspergillus niger* and *Aspergillus repens* was carried out. Carbohydrate specificity analysis was performed using a library of biotinylated derivatives of synthetic oligosaccharides which represent the key fragments of antigenic polysaccharides of the cell wall of named fungi -galactomannan, α- and β-glucan, mannan and chitin. It was shown that the anti-carbohydrate antibodies obtained by immunization with *A. fumigatus* and *A. repens* recognize predominantly galactofuranosyl-containing epitopes, while the antibodies against *A. niger* bind predominantly to the chitooligosaccharides. The obtained data form the basis for the detection of specific markers necessary for the development of enzyme-linked immunoassay tests.

Keywords: Aspergillus fumigatus, Aspergillus repens, Aspergillus niger, aspergillosis, antigen, antibody.

ПРИКЛАДНАЯ БИОХИМИЯ И МИКРОБИОЛОГИЯ, 2018, том 54, № 6, с. 614–618

УДК 577.114.5:616-097

УГЛЕВОДНАЯ СПЕЦИФИЧНОСТЬ АНТИТЕЛ ПРОТИВ ПРЕПАРАТОВ ДРОЖЖЕВЫХ ГРИБОВ *Saccharomyces cerevisiae* И *Candida krusei*

© 2018 г. В. Б. Крылов[1], М. И. Петрук[1], А. А. Карелин[1], Д. В. Яшунский[1], Ю. Е. Цветков[1], Н. И. Глушко[2], Е. В. Халдеева[2], В. Л. Мокеева[3], Е. Н. Биланенко[3], Ю. С. Лебедин[4], С. А. Ерёмин[3], Н. Э. Нифантьев[1, *]

[1]*Институт органической химии им. Н.Д. Зелинского РАН, Москва, 119991, Россия*

[2]*Казанский научно-исследовательский институт эпидемиологии и микробиологии, Казань, 420015, Россия*

[3]*Московский государственный университет имени М.В. Ломоносова, Москва, 119991, Россия*

[4]*ООО "ХЕМА", Москва, 105264, Россия*

**e-mail: nen@ioc.ac.ru*

Поступила в редакцию 12.01.2018 г.

Проведена иммунизация лабораторных животных (Калифорнийский кролик) природными препаратами дрожжевых грибов *Saccharomyces cerevisiae* и *Candida krusei*. Анализ полученных сывороток осуществляли с использованием библиотек лигандов, построенных из синтетических олигосахаридов, родственных основным углеводным компонентам клеточной стенки грибов. Было показано, что антитела в исследованных сыворотках распознают преимущественно фрагменты маннана, причем профиль углеводной специфичности различался для *S. cerevisiae* и *C. krusei*. Сыворотки против *S. cerevisiae* содержали антитела, распознающие β-глюкан, причем минимальный распознаваемый эпитоп – линейный трисахарид. Полученные результаты необходимы для создания востребованных иммуноферментных диагностикумов для обнаружения и видовой характеристики грибов.

Ключевые слова: Saccharomyces cerevisiae, *Candida krusei*, дрожжевые грибы, антиген, антитело

DOI: 10.1134/S0555109918060107

Дрожжи – это большая группа грибов, имеющих одноклеточную фазу в цикле развития. Некоторые из них существуют постоянно в одноклеточном состоянии, другие способны к образованию мицелия. В эту группу входят как сумчатые, так и базидиальные грибы, поэтому термин не свидетельствует о родственных связях, а лишь об их одноклеточной организации [1, 2]. Эти грибы широко распространены в природе, встречаются на сахаристых субстратах, на поверхности и внутри плодов, на поверхности растений, в почве и в пыли жилых помещений [3]. Дрожжи не только широко используются в разнообразных процессах, включая производство вина, пива, хлеба, ферментированных молочных продуктов, лекарственных препаратов, но и могут вызывать порчу продуктов питания. Некоторые виды дрожжевых грибов обладают патогенными свойствами и способны колонизировать организм человека, вызывая разнообразные заболевания, как поверхностные, так и тяжелейшие инвазивные микозы [4].

Дрожжевые грибы родов *Saccharomyces* и *Candida* относятся к порядку сахаромицетовых (*Saccharomycetales*) и представляют собой наиболее изученные роды дрожжевых грибов. У дрожжей *Saccharomyces cerevisiae* весь жизненный цикл проходит в одноклеточном состоянии. Это давно известные пекарские дрожжи, которые широко используются в пивоварении, виноделии, хлебопечении. У вида *Candida krusei* известно много клинических изолятов, вызывающих различные заболевания людей со сниженным иммунитетом [4].

Методы идентификации дрожжей на протяжении времени менялись – от определения фенотипических и физиологических признаков к молекулярно-генетическим [1, 2]. Однако увлечение последними не способно решить все проблемы, возникающие при идентификации дрожжевых грибов. Надежные методы видовой идентификации дрожжей являются крайне востребованными для промышленности, медицины и экологии. На настоящий момент описано более 1500 видов дрожжей, и для их идентификации необходим быстрый, простой и недорогой метод. Обычные системы дифференциации с использованием морфологических признаков, а также закономерностей ассимиляции и ферментации требуют высокой квалификации исследователя, трудозатрат

и отнимают много времени. Альтернативные методы, такие как анализ жирных кислот, электрофоретическое типирование, анализ ДНК, обеспечивают удовлетворительные результаты, однако трудновыполнимы на регулярной основе в лабораториях пищевой промышленности [1, 2].

В связи с этим иммунологические методы анализа являются наиболее удобными в практическом плане, однако требуют выявления специфических антигенных маркеров, представленных на поверхности клеточной стенки гриба [5]. Клеточная стенка дрожжевых грибов построена в основном из хитина, β-(1→3)-глюкана, β-(1→6)-глюкана, и маннопротеинов. Хитин и глюканы образуют жесткую трехмерную структуру, которая защищает клетку от неблагоприятных внешних воздействий. Внешняя же часть клеточной стенки обогащена высокогликозилированными белками (углеводы могут составлять до 90% их молекулярной массы), несущими полисахаридные цепи, построенные из остатков маннозы (маннаны). Именно эти маннановые цепи в значительной мере определяют антигенную специфичность дрожжевых грибов [6].

Различные структурные мотивы маннана являются антигенными факторами дрожжевых грибов [7, 8] и используются в настоящее время для обнаружения поражения грибами рода *Candida* в медицинских диагностических наборах [9]. В частности, для гриба *Candida albicans* было выявлено более десятка антигенных факторов [10], относящихся к маннану. Присутствие или отсутствие тех или иных антигенных структур в составе грибкового манана существенно зависит от вида и штамма микроорганизма [11]. Существующий на рынке диагностический набор Platelia Candida Ag Plus (“Bio-Rad”, Франция) позволяющий детектировать маннан *C. albicans*, не обнаруживает антигены продуцируемые *S. cerevisiae* и *C. krusei* [12]. Структурные особенности маннанов, продуцируемых *S. cerevisiae* и *C. krusei*, играющие критическую роль при их детектировании серологическими методами, на настоящий момент детально не изучены. В связи с этим крайне актуальной задачей является поиск как общих, так и специфических антигенных маркеров, позволяющих определять как общее грибковое загрязнение, так и содержание отдельных видов.

Цель работы – характеристика специфичности антител, продуцируемых при иммунизации препаратами *S. cerevisiae, C. krusei*, с использованием гликоряда, построенного из синтетических олигосахаридов, отвечающих основным типам природных полисахаридов грибов.

МЕТОДИКА

Получение иммуногенов. В работе использовали штаммы грибов из коллекции Санкт-Петербургской медицинской академии последипломного образования (СПбМАПО): 251 (*C.krusei*) и 56 (*S.cerevisiae*). Для получения биомассы штаммы дрожжевых грибов пересевали на жидкую питательную среду Сабуро, с расчетом получить начальную плотность культуры 5×10^7 кл./мл и выращивали в течение 48 ч при 28°C. Биомассу отделяли от питательной среды центрифугированием в течение 15 мин при 2000 *g* и дважды промывали от питательной среды 10-кратным объемом стерильного физраствора. Выход биомассы с 13 л питательной среды составил 90 г.

Биомассу заливали 90 мл глицерина, автоклавировали 45 мин при 1.5 атм и оставляли на 12 ч при 4°C. Затем экстракт отделяли от клеток центрифугированием в течение 30 мин при 8000 *g*, подкисляли уксусной кислотой до pH 4.0. К охлажденному до 4°C экстракту порциями добавляли холодный этанол при постоянном перемешивании. Для полного осаждения к 90 мл экстракта добавляли 270 мл этанола. Осадок формировался в течение 24 ч при 4°C. Через 24 ч осадок отделяли центрифугированием при 900 *g*, в течение 15 мин, промывали дважды 5-кратным объемом 96% этанола при перемешивании, затем отделяли центрифугированием при 2000 *g* 10 мин. Промытый препарат высушивали в эксикаторе под вакуумом над безводным $CaC1_2$ в течение 2 сут до постоянной массы. После высушивания было получено 1320 мг сухого иммуногена влажностью 10%.

Иммунизация. Антисыворотки против иммуногенов получали на 5 самцах кроликов породы “Калифорнийский кролик” в возрасте 4–6 мес. Животных иммунизировали 6 раз с интервалом 2 нед. свежеприготовленной эмульсией иммуногена (0.2 мг препарата по белку в 0.5 мл дистиллированной воды на кролика) с полным адъювантом Фрейнда для первой иммунизации и с неполным адъювантом Фрейнда для последующих иммунизаций. Эмульсию готовили в соотношении раствор конъюгата/адъювант – 1 : 1. В ходе иммунизации эмульсию вводили в 3–6 мест подкожно вдоль позвоночника. Забор крови проводили из краевой вены уха с помощью вакуумных пробирок Green Vac-Tube 0238 (“GC Pharma”, Республика Корея) с разделяющим гелем и активатором свертывания (SiO_2). Полученную сыворотку консервировали 0.1% азида натрия и хранили при 4°C.

Иммуноферментный анализ. Иммуноферментный анализ на стрептавидиновых планшетах Pierce® Streptavidin Coated 96 Well Plates (“Thermo

Вклейка к статье Крылова с соавт.

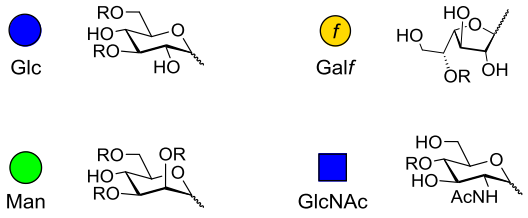

Рис. 1 Использованное графическое обозначение моносахаридных остатков, входящих в состав гликанов клеточной стенки грибов [15].

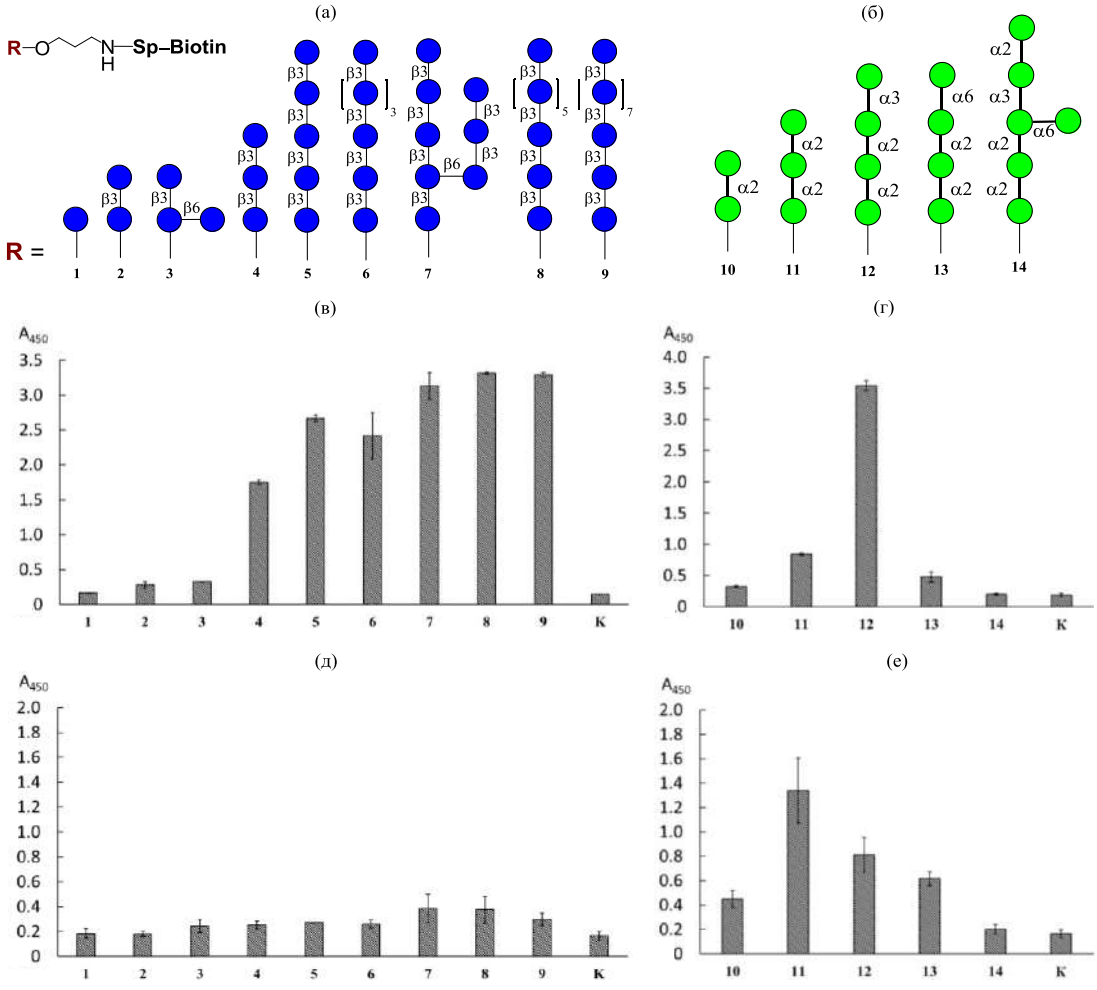

Рис. 2. Строение синтетических олигосахаридов **1-9**, родственных β-глюкану (а), и соединений **10-14**, родственных маннану (б), а также взаимодействие антител, полученных при иммунизации препаратами из *S. cerevisiae* (в, г) и *C. krusei* (д, е), с синтетическими микоантигенами **1-14** (показаны на оси абсцисс, К – контроль, отсутствие антигена), изученное методом иммуноферментного анализа (ИФА).

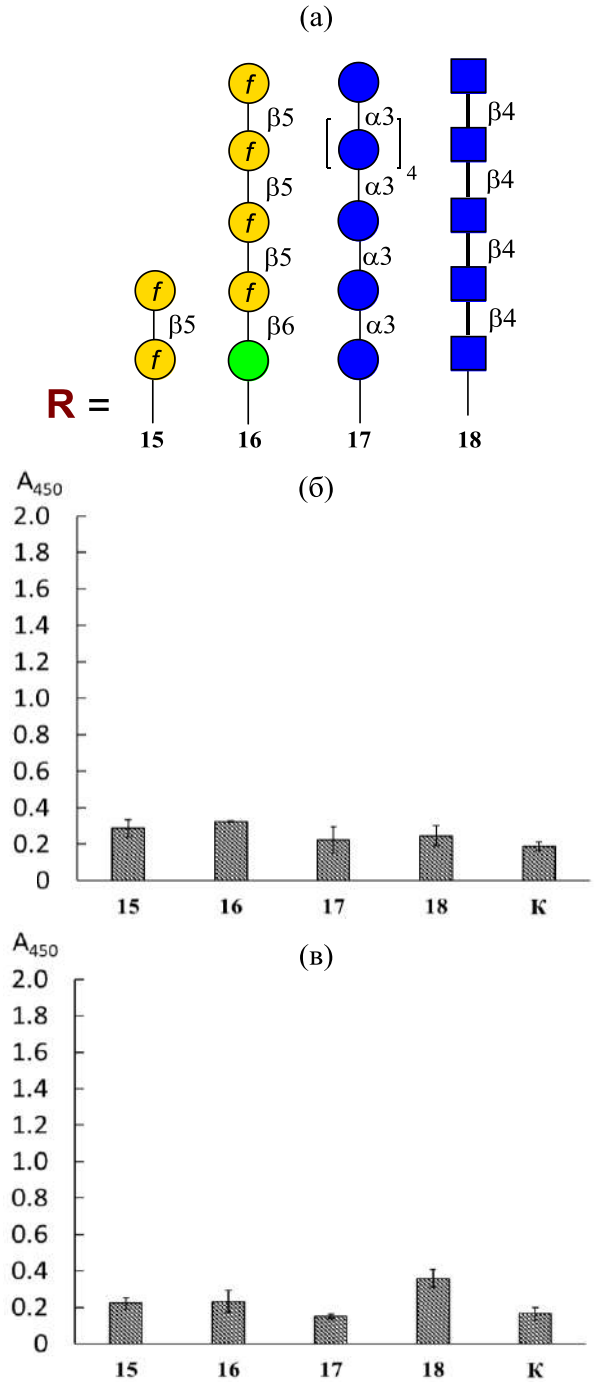

Рис. 3 Данные ИФА, полученные с использованием в качестве покрывающих антигенов синтетических олигосахаридов, родственных галактоманнану **15-16**, α-глюкану **17** и хитину **18** (а) и сывороток кроликов после иммунизации препаратами из *S. cerevisiae* (б) и *C. krusei* (в).

Scientific", США) проводили в соответствии с инструкцией производителя ("Thermo Scientific Inc.", США, www.thermoscintific.com/pierce) при использовании фосфатно-солевого буфера (**ФСБ**), содержащего 0.05% твина 20 и 0.1% бычьего сывороточного альбумина для растворения реагентов и промывания планшета. Биотинилированные олигосахариды адсорбировали на дне лунок (15 пмоль олигосахарида в 100 мкл разводящего раствора на одну лунку) в течении 2 ч при 22°C, затем содержимое планшета вытряхивали, промывали 3 раза и наносили исследуемые сыворотки (по 100 мкл, разбавление 1 : 500). Планшет инкубировали 30 мин при 22°C, после чего содержимое планшета вытряхивали, промывали 3 раза. Сорбированные антитела проявляли с использованием меченных пероксидазой хрена IgG против иммуноглобулинов кролика ("ХЕМА", Россия) и хромогенного субстрата TMB (водный раствор 3,3',5,5'-тетраметилбензидина и перекиси водорода). Оптическое поглощение продуктов ферментативной реакции измеряли на приборе "Multiskan GO" ("Thermo fisher scientific", США) при длине волны 450 нм. Эксперименты для каждой концентрации антител повторяли не менее 3 раз.

РЕЗУЛЬТАТЫ И ИХ ОБСУЖДЕНИЕ

Исследование специфичности сывороток, полученных при иммунизации различными природными препаратами грибов, позволяет установить специфические антигенные структуры на поверхности клеточной стенки. В отличие от прямого анализа строения комплексом химических и физико-химических методов при иммунологическом анализе антигенов важную роль играет не только относительное содержание, но и пространственная доступность и иммуногенность углеводных участков. Именно такие структуры являются наиболее перспективными для иммуноферментного детектирования культуры грибов.

Необходимые в данном исследовании синтетические олигосахариды были получены благодаря новым методам химии углеводов, таким как пиранозид-фуранозидная перегруппировка [13], методы регеоселективной расстановки защитных групп и стереоселективного гликозилирования [14].

Для обозначения углеводных остатков в синтетических олигосахаридах использована символьная номенклатура гликанов, рекомендованная международным гликобиологическим обществом (рис. 1) [15].

Синтез использованных в данном исследовании биотинилированных производных **1**-**18**, отвечающих основным типам грибных полисахаридов, был описан нами ранее. Олигосахариды **1**-**9** [16, 17] (рис. 2а) представляют собой линейные и разветвленные фрагменты β-глюкана различной длины. Олигоманнозиды **10**-**14** (рис. 2б) отвечают структурным элементам маннана дрожжевых грибов. Олигосахариды, относящиеся к другим типам полисахаридов, – это фрагменты галактоманнана **15**-**16** [18], линейного α-(1→3)-глюкана **17** [19] и хитина **18** [20, 21] (рис. 3а). Такие полисахариды как галактоманнан [22, 23] и α-глюкан [24] являются специфическими маркерами прежде всего для плесневых грибов [25] (например, *Aspergillus fumigatus*), однако их включение при анализе антител против дрожжевых грибов также необходимо для подтверждения специфичности данных антигенов.

Фиксация данных олигосахаридов **1**-**18** на поверхности планшета осуществлялась за счет сверхпрочного нековалентного взаимодействия биотиновой метки с поверхностью, модифицированной стрептавидином. При этом используемый олигоэтиленгликольный спейсер обеспечивает эффективное экспонирование углеводной части для связывания с антителами [26]. Образование углевод-белкового комплекса детектировалось обработкой поверхности лунки проявляющим конъюгатом вторичных антител с ферментной меткой и последующим добавлением хромогенного субстрата.

Исследование сыворотки интактных животных в разбавлении 1 : 500 не выявило фона естественных антител против исследуемых микоантигенов **1**-**18**. В то же время сыворотки животных после иммунизации препаратами грибов специфически распознавали определенные типы лигандов.

Так, антитела в сыворотке после иммунизации препаратом из *S. cerevisiae* хорошо распознавали β-(1→3)-связанные глюканы начиная с трисахарида, причем удлинение цепи усиливало наблюдаемое взаимодействие (рис. 2в). Антитела в сыворотке после иммунизации препаратом из *C. krusei*, напротив, практически не распознавали данные антигены (рис. 2д).

Антитела в сыворотке после иммунизации препаратами как из *S. cerevisiae* так и *C. krusei* распознавали олигосахариды, родственные различным структурным элементам маннана, однако профиль специфичности данных антител существенно различался (рис. 2). Так, антитела, выработанные против *S. cerevisiae*, распознавали преимущественно тетрасахарид **12**, терминированный α-(1→3)-связанным остатком маннозы. Антитела, выработанные против *C. krusei*, напро-

тив, преимущественно распознавали линейный α-(1→2)-связанный трисахарид **11**.

Важно было исследовать взаимодействие полученных сывороток с олигосахаридами, отвечающими антигенам плесневых грибов рода *Aspergillus*, изученных нами ранее [27]. Так, ни один из исследованных олигосахаридов **15**-**18** не распознавался исследуемыми сыворотками против дрожжевых грибов (рис. 3), что говорит о принципиально различной антигенной структуре клеточных стенок.

Таким образом, в ходе работы была исследована углеводная специфичность антител, вырабатываемых против препаратов дрожжевых грибов *S. cerevisiae* и *C. krusei*, и выявлены распознаваемые ими характерные углеводные эпитопы. Полученные результаты являются основанием для разработки методов иммуноферментного контроля поражения грибами, востребованных в экологии и в медицине.

Приготовление иммуногенов и работы по иммунизации лабораторных животных выполнены при финансовой поддержке Министерства образования и науки Российской Федерации (уникальный идентификатор проекта RFMEFI60717X0185). Получение биотинилированных олигосахаридов, создание гликорядов и анализ специфичности антител выполнены в биохимическом модуле ИОХ РАН при финансовой поддержке Российского научного фонда (проект № 14-50-00126).

СПИСОК ЛИТЕРАТУРЫ

1. *Barnett J.A., Payne R.W., Yarrow D.* // Yeasts: Characteristics and Identification, 2 Ed. Cambridge University Press, Cambridge: United Kingdom, 1990. 1002 p.
2. *Чернов И.Ю.* // Дрожжи в природе. Товарищество науч. изд. КМК., 2013. Москва, 336 с.
3. *Glushakova A.M., Chernov I.Y.* // Microbiology 2010. V. 79. № 6. P. 830–839.
4. *de Hoog G.S., Guarro J., Gene´J., Figueras M.J.* // Atlas of Clinical Fungi, 2 Ed. Utrecht: Centraalbureau voor Schimmelcultures, ASM Press, 2000. 1126 p.
5. *Latgé J.P.* // Mol. Microbiol. 2007. V. 66. № 2. P. 279–290.
6. *Lipke P.N., Ovalle R.* // J. Bacteriol. 1998. V. 180. № 15. P. 3735–3740.
7. *Karelin A.A., Tsvetkov Y.E, Nifantiev N.E.* // Russ. Chem. Rev. 2017. V. 86. № 11. P. 1073–1126.
8. *Krylov V.B., Paulovičová L., Paulovičová E., Tsvetkov Y.E., Nifantiev N.E.* // Pure Appl. Chem. 2017. V. 89. № 7. P. 885–898.
9. *Oliveri S., Trovato L., Betta P., Romeo M.G., Nicoletti G.* // Clin. Microbiol. Infect. 2008. V. 14. № 4. P. 391–393.
10. *Fukazawa Y., Shinoda T., Tsuchiya T.* // J. Bacteriol. 1968. V. 95. № 3. P. 754–763.
11. *Hall R.A., Gow N.A.* // Mol. Microbiol. 2013. V. 90. № 6. P. 1147–1161.
12. *Rimek D., Singh J., Kappe R.* // J. Clin. Microbiol. 2003. V. 41. № 7. P. 3395–3398.
13. *Krylov V.B., Argunov D.A., Vinnitskiy D.Z., Verkhnyatskaya S.A., Gerbst A.G., Ustyuzhanina N.E., Dmitrenok A.S., Huebner J., Holst O., Siebert H.-C., Nifantiev N.E.* // Chem. Eur. J. 2014.V. 20. № 50. P. 16516–16522.
14. *Komarova B.S., Gerbst A.G., Finogenova A.M., Dmitrenok A.S., Tsvetkov Y.E., Nifantiev N.E.* // J. Org. Chem. 2017. V. 82. № 17. P. 8897–8908.
15. *Varki A., Cummings R., Esko J., Freeze H., Hart G., Marth J.* // Essentials of glycobiology. N.Y.: Cold Spring Harbor, 1999. 823 p.
16. *Yashunsky D.V., Tsvetkov Y.E., Grachev A.A., Chizhov A.O., Nifantiev N.E.* // Carbohydr. Res. 2016. V. 419. P. 8–17.
17. *Yashunsky D.V., Tsvetkov Y.E., Nifantiev N.E.* // Carbohydr. Res. 2016. V. 436. P. 25–30.
18. *Krylov V.B., Argunov D.A., Solovev A.S., Petruk M.I., Gerbst A.G., Dmitrenok A.S., Shashkov A.S., Latgé J.-P., Nifantiev N.E.* // Org. Biomol. Chem. 2018. V. 16. № 7. P. 1188–1199.
19. *Gerbst A.G., Grachev A.A., Yashunsky D.V., Tsvetkov Y.E., Shashkov A.S., Nifantiev N.E.* // J. Carbohydr. Chem. 2013. V. 32. № 3. P. 205–221.
20. *Юдина О.Н., Цветков Ю.Е., Нифантьев Н.Э.* // Изв.РАН. Сер. хим. 2015. Т. 12. С. 2932–2941.
21. *Юдина О.Н., Цветков Ю.Е., Нифантьев Н.Э.* // Изв. РАН. Сер. хим. 2016. Т. 12. С. 2937–2942.
22. *Argunov D.A., Krylov V.B., Nifantiev N.E.* // Org. Biomol. Chem. 2015. V. 13. № 11. P. 3255–3267.
23. *Argunov D.A., Krylov V.B., Nifantiev N.E.* // Org. Lett. 2016. V. 18. № 21. P. 5504–5507.
24. *Komarova B.S., Orekhova M.V., Tsvetkov Y.E., Beau R., Aimanianda V., Latgé J.P., Nifantiev N.E.* // Chem. Eur. J. 2015. V. 21. № 3. P. 1029–1035.
25. *Крылов В.Б., Петрук М.И., Григорьев И.В., Лебедин Ю.С., Глушко Н.И., Халдеева Е.В., Аргунов Д.А., Хатунцева Е.А., Топлишек М.В., Комарова Б.С., Карелин А.А., Юдина О.Н., Меньшов В.М., Яшунский Д.В., Цветков Ю.Е., Нифантьев Н.Э.* // Биоорган. химия. 2018. Т. 44. № 1. С. 78–86.
26. *Tsvetkov Y.E., Burg-Roderfeld M., Loers G., Arda A., Sukhova E.V., Khatuntseva E.A., Grachev A.A., Chizhov A.O., Siebert H.-C., Schachner M., Jimenez-Barbero J., Nifantiev N.E.* // J. Am. Chem. Soc. 2012. V. 134. № 1. P. 426–435.
27. *Крылов В.Б., Петрук М.И., Глушко Н.И., Халдеева Е.В., Мокеева В.Л., Биланенко Е.Н., Лебедин Ю.С., Еремин С.А., Нифантьев Н. Э.* // Прикл. биохимия и микробиология. 2018. Т. 45. № 5. С. 525–531.

Carbohydrate Specificity of Antibodies Against Specimens of Yeasts *Saccharomyces cerevisiae* and *Candida krusei*

V. B. Krylov[a], M. I. Petruk[a], A. A. Karelin[a], D. V. Yashunuskii[a], Yu. E. Tsvetkov[a], N. I. Glushko[b], E. V. Khaldeeva[b], V. L. Mokeeva[c], E. N. Bilanenko[c], Y. S. Lebedin[d], S. A. Eremin[c], and N. E. Nifantiev[a, *]

[a] *Laboratory of Glycoconjugate Chemistry, Zelinsky Institute of Organic Chemistry, Russian Academy of Sciences, Moscow, 119991 Russia*

[b] *Kazan Scientific Research Institute of Epidemiology and Microbiology, Kazan, 420015 Russia*

[c] *Lomonosov Moscow State University, Moscow, 119991 Russia*

[d] *XEMA Company Limited, Moscow, 105264 Russia*

**e-mail: nen@ioc.ac.ru*

Received January 12, 2018

The immunization of laboratory animals (Brush rabbits) with natural specimens of yeasts *Saccharomyces cerevisiae* and *Candida krusei* was carried out. The analysis of the obtained sera was performed using libraries of ligands constructed from synthetic oligosaccharides related to the basic carbohydrate components of the fungal cell wall. It was shown that antibodies in the studied sera recognize predominantly mannan fragments with different specificity profile for *S. cerevisiae* and *C. krusei*. Sera against *S. cerevisiae* contained antibodies that recognize linear trisaccharide epitope of β-glucan. The obtained data are necessary for the design of the required serological EIA diagnosticums for detection and species characteristics of fungi.

Keywords: Saccharomyces cerevisiae, Candida krusei, yeast, antigen, antibody

Journal of *Fungi*

MDPI

Article

Reinvestigation of Carbohydrate Specificity of EBCA-1 Monoclonal Antibody Used for the Detection of *Candida* Mannan

Vadim B. Krylov [1], Arsenii S. Solovev [1], Ilya A. Puchkin [1], Dmitry V. Yashunsky [1], Anna V. Antonets [1,2], Olga Y. Kutsevalova [3] and Nikolay E. Nifantiev [1,*]

1 Laboratory of Glycoconjugate Chemistry, N.D. Zelinsky Institute of Organic Chemistry, Russian Academy of Sciencesa, Leninsky Prospect 47, 119991 Moscow, Russia; v_krylov@ioc.ac.ru (V.B.K.); a_solovey97@mail.ru (A.S.S.); ilya.puchkin@gmail.com (I.A.P.); yashunsky1959@yandex.ru (D.V.Y.); antnts@mail.ru (A.V.A.)

2 Medical Genetic Center, Rostov-on-Don State Medical University, Nakhichevansky, 29, 344022 Rostov-on-Don, Russia

3 National Medical Research Center of Oncology, Laboratory of Clinical Microbiology, 14 Liniya Str., 63, 344037 Rostov-on-Don, Russia; olga_kutsevalova@mail.ru

* Correspondence: nen@ioc.ac.ru; Tel.: +7-499-135-87-84

Abstract: Monoclonal antibody EBCA-1 is used in the sandwich immune assay for the detection of circulating *Candida* mannan in blood sera samples for the diagnosis of invasive candidiasis. To reinvestigate carbohydrate specificity of EBCA-1, a panel of biotinylated oligosaccharides structurally related to distinct fragments of *Candida* mannan were loaded onto a streptavidin-coated plate to form a glycoarray. Its use demonstrated that EBCA-1 recognizes the trisaccharide β-Man-(1→2)-α-Man-(1→2)-α-Man and not homo-α-(1→2)-linked pentamannoside, as was reported previously.

Keywords: *candida*; diagnosis; mannan; monoclonal antibodies; glycoarray

Citation: Krylov, V.B.; Solovev, A.S.; Puchkin, I.A.; Yashunsky, D.V.; Antonets, A.V.; Kutsevalova, O.Y.; Nifantiev, N.E. Reinvestigation of Carbohydrate Specificity of EBCA-1 Monoclonal Antibody Used for the Detection of *Candida* Mannan. *J. Fungi* **2021**, *7*, 504. https://doi.org/10.3390/jof7070504

Academic Editors: Carlos Pelleschi Taborda and Frank Ebel

Received: 12 May 2021
Accepted: 22 June 2021
Published: 24 June 2021

1. Introduction

Opportunistic yeasts of the genus *Candida* are the most common agents causing nosocomial fungal infections, and the fourth most common cause of nosocomial bloodstream infections (BSI) overall. Invasive candidiasis (IC) affects about 750,000 people worldwide with a case fatality rate of ~30–55% [1]. Growing *Candida* resistance is an urgent problem [2]. The IC diagnosis is still difficult due to the lack of specificity of the clinical symptoms and poor sensitivity of the cultural methods on blood samples up to only ~50% [3,4]. That is why the diagnosis of IC must combine direct mycological methods with other techniques. Antigen and antibody tests, β-D-glucan detection assays, *Candida* DNA detection by polymerase chain reaction (PCR), and other non-cultural tests have been entering clinical practice as additives to cultural methods for the last few decades [5]. β-D-Glucan is a common cell wall component of lots of fungi including *Candida* species. The FDA has approved a serum β-D-glucan assay (Fungitell® assay) for the diagnosis of invasive fungal infections. It helps to predict possible invasive fungal infection which, despite positive results, are not specific for *Candida* infection. The overall sensitivity and specificity of the β-D-glucan test for diagnosing IC accounted for 75–80% and 80%, respectively [6]. *Candida* PCR assays of various blood fractions help to reduce time to diagnose IC, especially compared to cultural methods. The sensitivity and specificity of PCR for suspected IC were 95% and 92%, respectively, as was shown in a recent meta-analysis [7].

Innovative nonculture molecular diagnostic assays have alternatively been developed and evaluated for the rapid identification of *Candida* species directly from clinical samples. These include the T2Candida® assay (T2Biosystems, Lexington, MA, USA) and a broad-range PCR-coupled electrospray ionization mass spectrometry platform (PCR/ESI-MS),

peptide nucleic acid-fluorescent in situ hybridization or PNA-FISH, and matrix-assisted laser desorption/ionization time-of-flight mass spectrometry or MALDI-TOF MS [8–10]. The T2Candida® assay is a molecular method that combines PCR with T2 magnetic resonance (T2MR). It is approved by the FDA for rapid diagnosis of IC caused by clinically relevant *Candida* species at minimal concentrations of 1–3 colony-forming units per milliliter (CFUs/mL) in whole-blood samples [8]. The advantages, utility, and limitations of the other cutting-edge techniques, as well as their combined use to assist in the diagnosis of this life-threatening and costly fungal infection including BSI and IC, are under discussion [10]. Nevertheless, serological methods remain significant adjunct to cultural methods.

The circulating mannan antigen in the bloodstream is considered as a diagnostic marker of invasive *Candida* infection. The commercial kit for mannan detection is the Platelia Candida Antigen Plus (Bio-Rad, France) which is based on a "sandwich"-type enzyme-linked immunosorbent assay (ELISA) and uses the monoclonal antibody EBCA-1 to the mannan from the *Candida* spp. cell wall.

This kit is characterized by moderate sensitivity (50–70%) which can be increased up to 70–100% by its use in combination with the anti-mannan antibody detection kit, the Platelia Candida Ab-Plus (Bio-Rad, France). In a meta-analysis [11] of 14 studies, the sensitivities and specificities of the mannan and anti-mannan test separately for IC were 58% and 93%, and 59% and 86%, respectively. Sensitivity and specificity for combined mannan and anti-mannan assays were 83% and 86%, respectively, with the best performance in patients with *C. albicans*, *C. glabrata*, or *C. tropicalis* infections. Significant heterogeneity of studies was noted in the meta-analysis [11].

The mannan and anti-mannan tests are employed at many European centers but are not widely used in North America, as they are not cleared by the U.S. Food and Drug Administration [12]. In addition, according to the Clinical Practice Guideline for the Management of Candidiasis of the Infectious Diseases Society of America (updated in 2016), the role of mannan and anti-mannan in detecting antibodies remains unclear [5]. In the study including patients from an intensive care unit with severe abdominal pathology, the combined determination of mannan antigen and mannan antibodies to anti-mannan was ineffective (with sensitivity at 55% and specificity at 60%). Antibodies are often present in immunocompromised patients with preexisting candidemia or severe colonization [13]. Thus, the positive predictive value of detecting antibodies with a single test in the absence of subsequent detection of their increasing concentration remains low. This observation and the unexplained variability of tests across studies is an important caution for physicians, as inaccurate laboratory results can lead to inappropriate prescription of antifungal drugs to patients who are unlikely to have IC [14,15].

Such a controversial experience in the application of existing diagnostic tests that utilize the mannan marker leads to a range of questions. There were concerns over the use of the mannan as a diagnostic tool due to its natural colonization with *Candida*. Nevertheless, under these conditions, the mannan level remains within the cut-off, while it is greatly elevated in patients with IC [16]. Consequently, mannan remains a promising biomarker in the comprehensive diagnosis of IC.

The native *Candida* mannan is a complex heterogeneous polysaccharide, comprising an α-(1→6)-mannoside backbone and α/β-(1→2)-mannoside side chains of variable lengths and structure (Figure 1). Thus, this polysaccharide may contain a number of other structural elements, including α-(1→3)-linkages, 3,6-branches, and even non-mannose carbohydrate residues. The particular structures of the mannan differ between *Candida* species and depend on a complex mannan biosynthesis network and cell wall remodeling genes [17,18]. The key point for understanding the basis of false-negative results is the elucidation of a precise chemical structure of the EBCA-1 which recognizes epitope within the mannan structure.

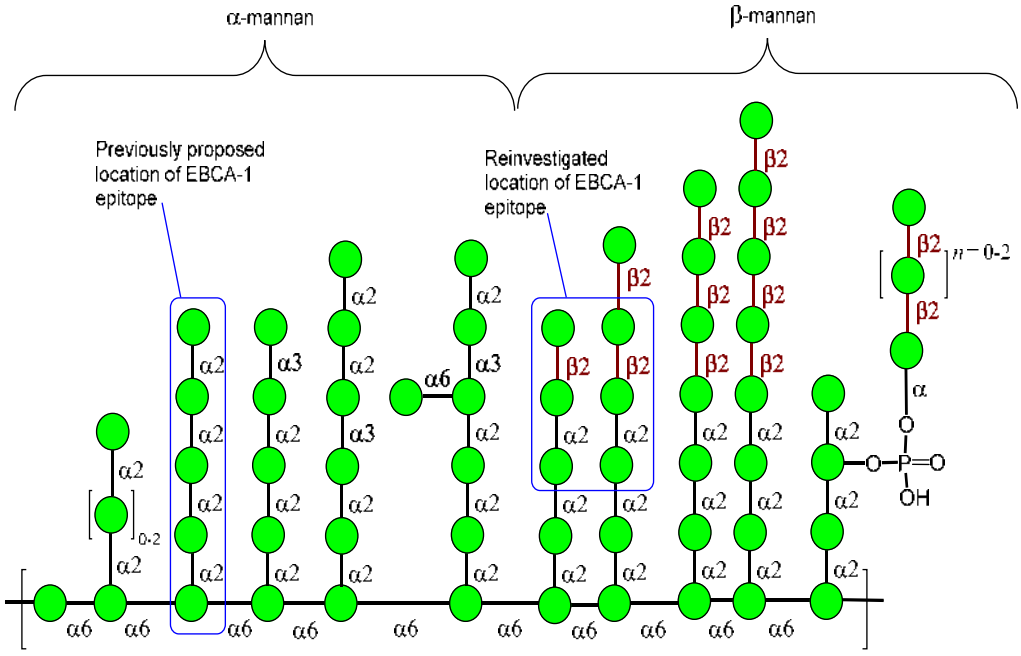

Figure 1. Key structural elements of the mannan of *C. albicans* previously proposed [14–16] and reinvestigated location of EBCA-1 epitope.

In a 1998 study that used oligomannosides prepared by depolymerization of the natural mannan, the minimal epitope of an anti-*Candida albicans* mannan monoclonal antibody EBCA-1 was claimed to be homo-α-(1→2)-mannopentaose [19–21]. Herein, we report the reinvestigation of the EBCA-1 carbohydrate specificity using the library of individual synthetic mannooligosaccharides related to the distinct fragments of the *Candida* mannan [22]. Modern methods of carbohydrate chemistry permit efficient and stereospecific assembling of complex oligosaccharide chains representing different parts of polysaccharides of the fungal cell wall [22–24]. The arrays of oligosaccharides (glycoarrays) were shown to be indispensable tools in the assessment of ligand specificity of anti-carbohydrate monoclonal antibodies [25–31] and of antibodies in the blood sera [26,32–34].

2. Materials and Methods

2.1. Biotinylated Synthetic Oligosaccharides

Biotinylated glycoconjugate ligands 1–18 (Figure 2) [22] were chemically synthesized [23,35–41] by means of coupling parent aminospacered oligosaccharides with an activated biotin derivative containing a hydrophilic hexaethylene glycol linker [42].

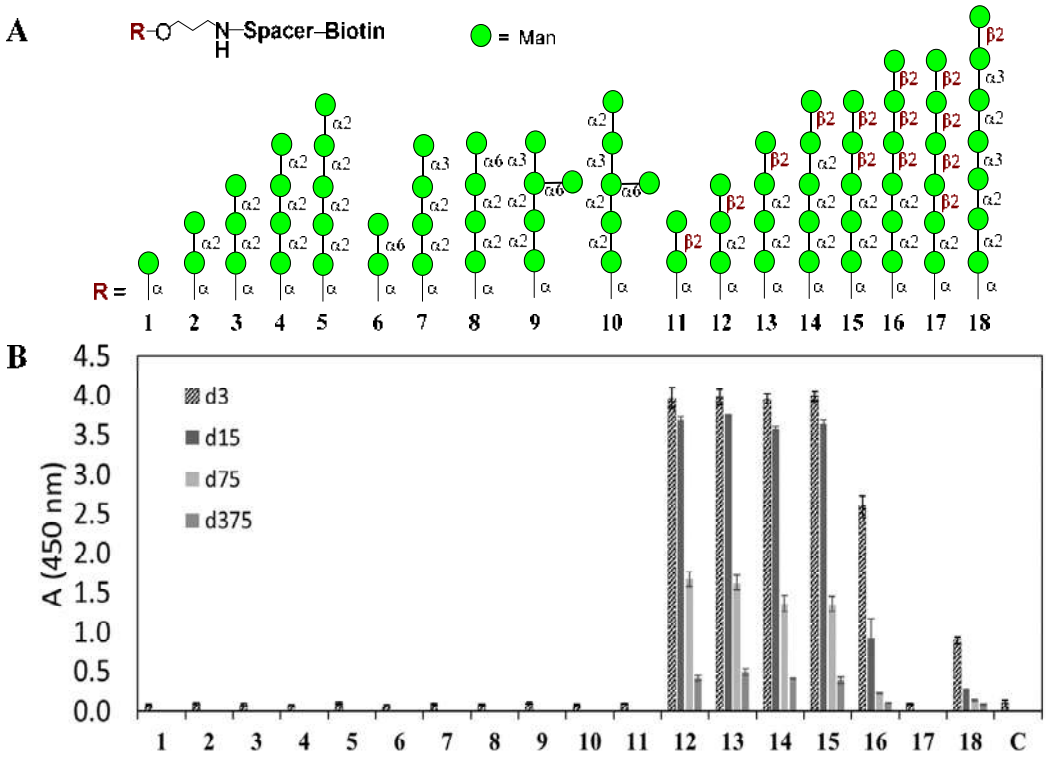

Figure 2. Investigation of oligosaccharide specificity of mAb EBCA-1. (**A**) Composition of thematic glycoarray built up of oligosaccharide ligands representing key structural elements of *C. albicans* mannan, and (**B**) the results of assaying carbohydrate specificity of EBCA-1 with the use of 3-, 15-, 75- and 375-fold dilutions of EBCA-1. C—control, absence of biotinylated ligand in the well.

2.2. Glycoarray

The wells of 96 streptavidin-coated plates (Thermo Scientific, Rockford, IL, USA.) were coated with biotin-tagged oligosaccharides 1–18 (Figure 2) (100 µL of a 15 pmol/well solution in PBS containing 0.05% Tween-20 and 0.1% BSA) and then incubated for 2 h at 37 °C. After washing, the plates were incubated with a conjugate of EBCA-1 with peroxidase (working solution from the Platelia Candida Ag Kit) in 3-, 15-, 75- and 375-fold dilution for 1 h at 37 °C. After washing five times, color was developed using a TMB monocomponent substrate (100 µL) for 15 min, and the reaction was stopped with 50 µL of 1 M sulfuric acid. Absorbance was measured at 450 nm using a MultiSkan GO plate reader (Thermo Fisher Scientific, Vantaa, Finland). All measurements were performed in triplicate.

3. Results

The selection of synthetic oligosaccharide derivatives 1–18 (Figure 2A) for this study was based on the previous structural investigations of *Candida* mannan [17]. Oligosaccharides 1–5 represent fragments of the homo-α-(1→2)-linked mannan chain which corresponds to a so-called antigenic factor 1 [43]. This structural motif is the most typical for mannans from various *Candida* species and strains, and was previously reported as recognized by monoclonal antibody EBCA-1 [19]. Oligosaccharides 6–10 are related to different antigenic factors (4, 13b, 34) present in the yeast cell wall mannan. Oligosaccharides 11–18 belong to the group of β-mannan fragments (antigenic factors 5 and 6), which are very important for host–yeast interaction and the pathogenicity of *Candida*.

The biotinylated conjugates 1–18 were immobilized on the surface of the streptavidin-coated plates to construct the thematic glycoarray. Surprisingly, its use in the reassessment of the carbohydrate specificity of the mAb EBCA-1 (Figure 2) did not detect visible binding with homo-α-(1→2)-linked pentamannoside 5, which was initially proposed by Poulain

et al. as the minimal epitope of mAb EBCA-1 [19–21]. Very recently, the same authors have reported [44] that mAb EBCA-1 has dual specificity and is able to recognize both homo-α-(1→2)-linked pentamannoside and Man-β-(1→2)-terminated α-(1→2)-linked oligomannoside chains, similar to the ones in glycoconjugates 12–15. Instead, our study only recognized oligomannosides containing a β-glycoside bond, namely compounds 12–15 (and 16 to a lesser extent). Oligosaccharides 12–15 all contain a β-Man-(1→2)-α-Man-(1→2)-α-Man trisaccharide fragment which, thus, can be assigned as a correct minimal holder of the epitope of mAb EBCA-1.

It was noticeable that the elongation of β-Man-(1→2)-α-Man-(1→2)-α-Man trisaccharide sequence from the "reducing" end by one 2)-α-Man unit (12→13) or its dimer 2)-α-Man-(1→2)-α-Man (12→14), or that elongation from the "non-reducing" end by one β-Man-(1→2)-unit (12→15) have not influenced the recognition by mAb EBCA-1. On the contrary, the elongation of the β-Man-(1→2)-α-Man-(1→2)-α-Man trisaccharide sequence from the "non-reducing" end by dimer β-Man-(1→2)-β-Man-(1→2)-(12→16) remarkably decreased the binding with mAb EBCA-1, while the attachment of one additional β-Man-(1→2)- unit (16→17) practically blocked the binding to mAb.

4. Discussion

The knowledge of fine carbohydrate specificity of the monoclonal antibody used in a diagnostic kit is important for understanding the molecular basis of observed possible false-positive and false-negative results. Previously, we reported the reinvestigation of carbohydrate specificity of EB-A2 monoclonal antibody used for the immune detection of the *Aspergillus fumigatus* galactomannan [25], where the connection between cross-reactivity, false-positive results, and the specificity of mAb EB-A2 was hypothesized. Herein, we found that the epitope-containing oligosaccharide recognized by the anti-mannan antibody EBCA-1 is the β-Man-(1→2)-α-Man-(1→2)-α-Man trisaccharide only, and not the previously proposed homo-α-(1→2)-linked pentamannoside [19–21] or both homo-α-(1→2)-linked pentamannoside and Man-β-(1→2)-terminated α-(1→2)-linked oligomannoside chains. We can only assume that the unusual duality of carbohydrate specificity reported [44] for mAb EBCA-1 could be detected because of the presence of β-Man-contamination in the used homo-α-(1→2)-linked pentamannoside that can be concluded from its published NMR spectra [45].

The reinvestigated trisaccharide epitope is abundantly present in many yeast mannans, however there are *Candida* strains lacking such fragment in the structure of their mannans [46]. This makes it impossible to detect such pathogens using this monoclonal antibody, leading to an increase in false-negative results.

Taking into account the assessed specificity of the EBCA-1 reported here, the binding of this mAb to homo-α-(1→2)-manno-fragments of *Candida* mannans reported previously (see for example papers [19–21,47] looks questionable. It should also be noted that the oligosaccharide fragment β-Man-(1→2)-α-Man-(1→2)-α-Man is not dominant in mannan of certain *Candida* strains [46]. It can be capped with two and three β-(1→2)-linked mannoside residues. Such capped sequences (for example in ligands 16 and 17 on Figure 2) have a rather low ability to bind to mAb EBCA-1 due to conformational changes and spatial loop formation reported by Bundle et al. [48].

To the best of our knowledge, there is no diagnostic antibody with an undoubtedly proven ability to recognize homo-α-(1→2)-linked oligomanoside chains. The raising of such mAbs is a rather complex task due to the tolerance of the mammalian immune system to α-mannosides, as opposed to higher immunogenicity of β-mannosides. However, antibodies against α-(1→2)-linked oligomanosides containing branch points of *Candida* mannan would be very promising for high performance diagnostics of invasive candidiasis. The generation of mAbs which are capable of recognizing such fragments are still faced with a challenge to test their applicability for clinical diagnostic needs.

Author Contributions: V.B.K., O.Y.K. and N.E.N. conceived the project, designed the experiments, and interpreted the data. A.S.S. and I.A.P. performed the experiments. D.V.Y. performed oligosaccha-

ride synthesis. V.B.K., A.V.A. and N.E.N. wrote the manuscript. All authors have read and agreed to the published version of the manuscript.

Funding: Scientific Schools Development Program of N.D. Zelinsky Institute of Organic Chemistry, RAS is gratefully acknowledged.

Institutional Review Board Statement: Not applicable.

Informed Consent Statement: Not applicable.

Acknowledgments: We thank A.G. Gerbst for critical reading this manuscript and valuable comments.

Conflicts of Interest: The authors declare no conflict of interest.

References

1. Bongomin, F.; Gago, S.; Oladele, R.O.; Denning, D.W. Global and multi-national prevalence of fungal diseases-estimate precision. *J. Fungi* **2017**, *3*, 57. [CrossRef]
2. Demin, K.A.; Refeld, A.G.; Bogdanova, A.A.; Prazdnova, E.V.; Popov, I.V.; Kutsevalova, O.Y.; Ermakov, A.M.; Bren, A.B.; Rudoy, D.V.; Chistyakov, V.A.; et al. Mechanisms of candida resistance to antimycotics and promising ways to overcome it: The role of probiotics. *Probiot. Antimicrob. Proteins* **2021**. [CrossRef]
3. Vardakas, K.Z.; Michalopoulos, A.; Kiriakidou, K.G.; Siampli, E.P.; Samonis, G.; Falagas, M.E. Candidaemia: Incidence, risk factors, characteristics and outcomes in immunocompetent critically ill patients. *Clin. Microbiol. Infect.* **2009**, *15*, 289–292. [CrossRef]
4. Clancy, C.J.; Nguyen, M.H. Finding the "missing 50%" of invasive candidiasis: How nonculture diagnostics will improve understanding of disease spectrum and transform patient care. *Clin. Infect. Dis.* **2013**, *56*, 1284–1292. [CrossRef]
5. Pappas, P.G.; Kauffman, C.A.; Andes, D.R.; Clancy, C.J.; Marr, K.A.; Ostrosky-Zeichner, L.; Reboli, A.C.; Schuster, M.G.; Vazquez, J.A.; Walsh, T.J.; et al. Clinical practice guideline for the management of candidiasis: 2016 update by the infectious diseases society of america. *Clin. Infect. Dis.* **2016**, *62*, e1–e50. [CrossRef]
6. Onishi, A.; Sugiyama, D.; Kogata, Y.; Saegusa, J.; Sugimoto, T.; Kawano, S.; Morinobu, A.; Nishimura, K.; Kumagai, S. Diagnostic accuracy of serum 1,3-β-D-glucan for pneumocystis Jiroveci pneumonia, invasive candidiasis, and invasive aspergillosis: Systematic review and meta-analysis. *J. Clin. Microbiol.* **2012**, *50*, 7–15. [CrossRef]
7. Avni, T.; Leibovici, L.; Paul, M. PCR diagnosis of invasive candidiasis: Systematic review and meta-analysis. *J. Clin. Microbiol.* **2011**, *49*, 665–670. [CrossRef]
8. Neely, L.A.; Audeh, M.; Phung, N.A.; Min, M.; Suchocki, A.; Plourde, D.; Blanco, M.; Demas, V.; Skewis, L.R.; Anagnostou, T.; et al. T2 magnetic resonance enables nanoparticle-mediated rapid detection of candidemia in whole blood. *Sci. Transl. Med.* **2013**, *5*, 182ra54. [CrossRef]
9. Jordana-Lluch, E.; Giménez, M.; Quesada, M.D.; Ausina, V.; Martró, E. Improving the diagnosis of bloodstream infections: PCR coupled with mass spectrometry. *BioMed. Res. Int.* **2014**, *2014*, 501214. [CrossRef]
10. Pitarch, A.; Nombela, C.; Gil, C. Diagnosis of invasive candidiasis: From gold standard methods to promising leading-edge technologies. *Curr. Top. Med. Chem.* **2018**, *18*, 1375–1392. [CrossRef]
11. Mikulska, M.; Calandra, T.; Sanguinetti, M.; Poulain, D.; Viscoli, C.; Third European Conference on Infections in Leukemia Group. The use of mannan antigen and anti-mannan antibodies in the diagnosis of invasive candidiasis: Recommendations from the third european conference on infections in leukemia. *Crit. Care Lond. Engl.* **2010**, *14*, R222. [CrossRef] [PubMed]
12. Clancy, C.J.; Nguyen, M.H. Diagnosing invasive candidiasis. *J. Clin. Microbiol.* **2018**, *56*. [CrossRef] [PubMed]
13. León, C.; Ruiz-Santana, S.; Saavedra, P.; Castro, C.; Loza, A.; Zakariya, I.; Úbeda, A.; Parra, M.; Macías, D.; Tomás, J.I.; et al. Contribution of candida biomarkers and DNA detection for the diagnosis of invasive candidiasis in ICU patients with severe abdominal conditions. *Crit. Care Lond. Engl.* **2016**, *20*, 149. [CrossRef]
14. Verduyn Lunel, F.M.; Donnelly, J.P.; van der Lee, H.a.L.; Blijlevens, N.M.A.; Verweij, P.E. Circulating candida-specific anti-mannan antibodies precede invasive candidiasis in patients undergoing myelo-ablative chemotherapy. *Clin. Microbiol. Infect.* **2009**, *15*, 380–386. [CrossRef]
15. Duettmann, W.; Koidl, C.; Krause, R.; Lackner, G.; Woelfler, A.; Hoenigl, M. Specificity of mannan antigen and anti-mannan antibody screening in patients with haematological malignancies at risk for fungal infection. *Mycoses* **2016**, *59*, 374–378. [CrossRef]
16. Mokaddas, E.; Burhamah, M.H.A.; Khan, Z.U.; Ahmad, S. Levels of (1→3)-β-D-glucan, candida mannan and candida DNA in serum samples of pediatric cancer patients colonized with candida species. *BMC Infect. Dis.* **2010**, *10*, 292. [CrossRef]
17. Shibata, N.; Kobayashi, H.; Suzuki, S. Immunochemistry of pathogenic yeast, candida species, focusing on mannan. *Proc. Jpn. Acad. Ser. B Phys. Biol. Sci.* **2012**, *88*, 250–265. [CrossRef] [PubMed]
18. Hall, R.A.; Gow, N.A.R. Mannosylation in Candida albicans: Role in cell wall function and immune recognition. *Mol. Microbiol.* **2013**, *90*, 1147–1161. [CrossRef]
19. Jacquinot, P.M.; Plancke, Y.; Sendid, B.; Strecker, G.; Poulain, D. Nature of Candida albicans-derived carbohydrate antigen recognized by a monoclonal antibody in patient sera and distribution over *Candida* species. *FEMS Microbiol. Lett.* **1998**, *169*, 131–138. [CrossRef]

20. Faille, C.; Mackenzie, D.W.; Michalski, J.C.; Poulain, D. Evaluation of an enzyme immunoassay using neoglycolipids constructed from *Candida albicans* oligomannosides to define the specificity of anti-mannan antibodies. *Eur. J. Clin. Microbiol. Infect. Dis.* **1992**, *11*, 438–446. [CrossRef]
21. Trinel, P.A.; Faille, C.; Jacquinot, P.M.; Cailliez, J.C.; Poulain, D. Mapping of Candida albicans oligomannosidic epitopes by using monoclonal antibodies. *Infect. Immun.* **1992**, *60*, 3845–3851. [CrossRef]
22. Krylov, V.B.; Nifantiev, N.E. Synthetic oligosaccharides mimicking fungal cell wall polysaccharides. *Curr. Top. Microbiol. Immunol.* **2020**, *425*, 1–16. [CrossRef]
23. Karelin, A.A.; Tsvetkov, Y.E.; Nifantiev, N.E. Synthesis of oligosaccharides related to polysaccharides of the cell wall of the fungi candida and aspergillus. *Russ. Chem. Rev.* **2017**, *86*, 1073–1126. [CrossRef]
24. Krylov, V.B.; Nifantiev, N.E. Synthetic carbohydrate based anti-fungal vaccines. *Drug Discov. Today Technol.* **2020**, *35–36*, 35–43. [CrossRef]
25. Krylov, V.B.; Solovev, A.S.; Argunov, D.A.; Latgé, J.-P.; Nifantiev, N.E. Reinvestigation of carbohydrate specificity of EB-A2 monoclonal antibody used in the immune detection of *Aspergillus fumigatus* galactomannan. *Heliyon* **2019**, *5*, e01173. [CrossRef]
26. Kazakova, E.D.; Yashunsky, D.V.; Krylov, V.B.; Bouchara, J.-P.; Cornet, M.; Valsecchi, I.; Fontaine, T.; Latge, J.-P.; Nifantiev, N.E. Biotinylated oligo-α-(1→4)-D-galactosamines and their N-acetylated derivatives: α-stereoselective synthesis and immunology application. *J. Am. Chem. Soc.* **2020**, *142*, 1175–1179. [CrossRef] [PubMed]
27. Schubert, M.; Xue, S.; Ebel, F.; Vaggelas, A.; Krylov, V.; Nifantiev, N.; Chudobova, I.; Schillberg, S.; Nölke, G. Monoclonal antibody AP3 binds galactomannan antigens displayed by the pathogens *Aspergillus flavus*, *A. fumigatus* and *A. parasiticus*. *Front. Cell. Infect. Microbiol.* **2019**, *9*, 234. [CrossRef] [PubMed]
28. Zheng, R.B.; Jégouzo, S.A.F.; Joe, M.; Bai, Y.; Tran, H.-A.; Shen, K.; Saupe, J.; Xia, L.; Ahmed, M.F.; Liu, Y.-H.; et al. Insights into interactions of mycobacteria with the host innate immune system from a novel array of synthetic mycobacterial glycans. *ACS Chem. Biol.* **2017**, *12*, 2990–3002. [CrossRef] [PubMed]
29. Guazzelli, L.; Crawford, C.; Ulc, R.; Bowen, A.; McCabe, O.; Jedlicka, A.J.; Wear, M.P.; Casadevall, A.; Oscarson, S. A synthetic glycan array containing *Cryptococcus neoformans* glucuronoxylomannan capsular polysaccharide fragments allows the mapping of protective epitopes. *Chem. Sci.* **2020**, *11*, 9209–9217. [CrossRef]
30. Matveev, A.L.; Krylov, V.B.; Emelyanova, L.A.; Solovev, A.S.; Khlusevich, Y.A.; Baykov, I.K.; Fontaine, T.; Latgé, J.-P.; Tikunova, N.V.; Nifantiev, N.E. Novel mouse monoclonal antibodies specifically recognize *Aspergillus fumigatus* galactomannan. *PLoS ONE* **2018**, *13*, e0193938. [CrossRef]
31. Matveev, A.L.; Krylov, V.B.; Khlusevich, Y.A.; Baykov, I.K.; Yashunsky, D.V.; Emelyanova, L.A.; Tsvetkov, Y.E.; Karelin, A.A.; Bardashova, A.V.; Wong, S.S.W.; et al. Novel mouse monoclonal antibodies specifically recognizing β-(1→3)-D-glucan antigen. *PLoS ONE* **2019**, *14*, e0215535. [CrossRef] [PubMed]
32. Komarova, B.S.; Wong, S.S.W.; Orekhova, M.V.; Tsvetkov, Y.E.; Krylov, V.B.; Beauvais, A.; Bouchara, J.-P.; Kearney, J.F.; Aimanianda, V.; Latgé, J.-P.; et al. Chemical synthesis and application of biotinylated oligo-α-(1→3)-D-glucosides to study the antibody and cytokine response against the cell wall α-(1→3)-D-glucan of *Aspergillus fumigatus*. *J. Org. Chem.* **2018**, *83*, 12965–12976. [CrossRef] [PubMed]
33. Wong, S.S.W.; Krylov, V.B.; Argunov, D.A.; Karelin, A.A.; Bouchara, J.-P.; Fontaine, T.; Latgé, J.-P.; Nifantiev, N.E. Potential of chemically synthesized oligosaccharides to define the carbohydrate moieties of the fungal cell wall responsible for the human immune response, using *Aspergillus fumigatus* galactomannan as a model. *MSphere* **2020**, *5*, e00688-19. [CrossRef] [PubMed]
34. Argunov, D.A.; Trostianetskaia, A.S.; Krylov, V.B.; Kurbatova, E.A.; Nifantiev, N.E. Convergent synthesis of oligosaccharides structurally related to Galactan I and Galactan II of *Klebsiella pneumoniae* and their use in screening of antibody specificity. *Eur. J. Org. Chem.* **2019**, *2019*, 4226–4232. [CrossRef]
35. Karelin, A.A.; Tsvetkov, Y.E.; Kogan, G.; Bystricky, S.; Nifantiev, N.E. Synthesis of oligosaccharide fragments of mannan from *Candida albicans* cell wall and their BSA conjugates. *Russ. J. Bioorg. Chem.* **2007**, *33*, 110–121. [CrossRef] [PubMed]
36. Karelin, A.A.; Tsvetkov, Y.E.; Paulovičová, L.; Bystrickỳ, S.; Paulovičová, E.; Nifantiev, N.E. Synthesis of a heptasaccharide fragment of the mannan from *Candida guilliermondii* cell wall and its conjugate with BSA. *Carbohydr. Res.* **2009**, *344*, 29–35. [CrossRef]
37. Karelin, A.A.; Tsvetkov, Y.E.; Paulovičová, L.; Bystrickỳ, S.; Paulovičová, E.; Nifantiev, N.E. Synthesis of 3, 6-branched oligomannoside fragments of the mannan from *Candida albicans* cell wall corresponding to the antigenic factor 4. *Carbohydr. Res.* **2010**, *345*, 1283–1290. [CrossRef] [PubMed]
38. Argunov, D.A.; Karelin, A.A.; Grachev, A.A.; Tsvetkov, Y.E.; Nifantiev, N.E. A new synthesis of the 3, 6-branched hexasaccharide fragment of the cell wall mannan in *Candida albicans*, corresponding to the antigenic factor 4. *Russ. Chem. Bull.* **2011**, *60*, 1004–1011. [CrossRef]
39. Karelin, A.A.; Tsvetkov, Y.E.; Paulovičová, E.; Paulovičová, L.; Nifantiev, N.E. Blockwise synthesis of a pentasaccharide structurally related to the mannan fragment from the *Candida albicans* cell wall corresponding to the antigenic factor 6. *Russ. Chem. Bull.* **2015**, *64*, 2942–2948. [CrossRef]
40. Karelin, A.A.; Tsvetkov, Y.E.; Paulovičová, E.; Paulovičová, L.; Nifantiev, N.E. A blockwise approach to the synthesis of (1→2)-linked oligosaccharides corresponding to fragments of the acid-stable β-mannan from the *Candida albicans* cell wall. *Eur. J. Org. Chem.* **2016**, *2016*, 1173–1181. [CrossRef]

41. Karelin, A.A.; Ustyuzhanina, N.E.; Tsvetkov, Y.E.; Nifantiev, N.E. Synthesis of a biotinylated probe from biotechnologically derived β-D-mannopyranosyl-(1→2)-D-mannopyranose for assessment of carbohydrate specificity of antibodies. *Carbohydr. Res.* **2019**, *471*, 39–42. [CrossRef]
42. Tsvetkov, Y.E.; Burg-Roderfeld, M.; Loers, G.; Ardá, A.; Sukhova, E.V.; Khatuntseva, E.A.; Grachev, A.A.; Chizhov, A.O.; Siebert, H.-C.; Schachner, M. Synthesis and molecular recognition studies of the HNK-1 trisaccharide and related oligosaccharides. the specificity of monoclonal anti-HNK-1 antibodies as assessed by surface plasmon resonance and STD NMR. *J. Am. Chem. Soc.* **2011**, *134*, 426–435. [CrossRef]
43. Suzuki, S. Immunochemical study on mannans of genus *Candida*. i. Structural investigation of antigenic factors 1, 4, 5, 6, 8, 9, 11, 13, 13b and 34. *Curr. Top. Med. Mycol.* **1997**, *8*, 57–70.
44. Sendid, B.; Lecointe, K.; Collot, M.; Danzé, P.-M.; Damiens, S.; Drucbert, A.-S.; Fradin, C.; Vilcot, J.-P.; Grenouillet, F.; Dubar, F.; et al. Dissection of the anti-*Candida albicans* mannan immune response using synthetic oligomannosides reveals unique properties of β-1,2 mannotriose protective epitopes. *Sci. Rep.* **2021**, *11*, 10825. [CrossRef] [PubMed]
45. Collot, M.; Sendid, B.; Fievez, A.; Savaux, C.; Standaert-Vitse, A.; Tabouret, M.; Drucbert, A.S.; Danzé, P.M.; Poulain, D.; Mallet, J.-M. Biotin sulfone as a new tool for synthetic oligosaccharide immobilization: Application to multiple analysis profiling and surface plasmonic analysis of anti-*Candida albicans* antibody reactivity against α- and β-(1→2) oligomannosides. *J. Med. Chem.* **2008**, *51*, 6201–6210. [CrossRef] [PubMed]
46. Gangneux, J.-P.; Cornet, M.; Bailly, S.; Fradin, C.; Féger, C.; Timsit, J.-F.; Leroy, O.; Sendid, B.; Bougnoux, M.-E. Clinical impact of antifungal susceptibility, biofilm formation and mannoside expression of *Candida* yeasts on the outcome of invasive candidiasis in icu: An ancillary study on the prospective AmarCAND2 cohort. *Front. Microbiol.* **2018**, *9*, 2907. [CrossRef]
47. Dalle, F.; Jouault, T.; Trinel, P.A.; Esnault, J.; Mallet, J.M.; d'Athis, P.; Poulain, D.; Bonnin, A. Beta-1,2- and alpha-1,2-linked oligomannosides mediate adherence of candida albicans blastospores to human enterocytes in vitro. *Infect. Immun.* **2003**, *71*, 7061–7068. [CrossRef] [PubMed]
48. Johnson, M.A.; Cartmell, J.; Weisser, N.E.; Woods, R.J.; Bundle, D.R. Molecular recognition of *Candida albicans* (1→2)-β-mannan oligosaccharides by a protective monoclonal antibody reveals the immunodominance of internal saccharide residues. *J. Biol. Chem.* **2012**, *287*, 18078–18090. [CrossRef]

PLOS ONE

RESEARCH ARTICLE

Novel mouse monoclonal antibodies specifically recognize *Aspergillus fumigatus* galactomannan

Andrey L. Matveev[1☯], Vadim B. Krylov[2☯], Ljudmila A. Emelyanova[1,3], Arsenii S. Solovev[2], Yana A. Khlusevich[1], Ivan K. Baykov[1], Thierry Fontaine[4], Jean-Paul Latgé[4], Nina V. Tikunova[1,3]*, Nikolay E. Nifantiev[2]*

1 Institute of Chemical Biology and Fundamental Medicine, Siberian Branch of Russian Academy of Sciences, prosp. Lavrentieva 8, Novosibirsk, Russia, **2** N.D. Zelinsky Institute of Organic Chemistry, Russian Academy of Sciences, Leninsky Prospect 47, Moscow, Russia, **3** Novosibirsk State University, Pirogova str., Novosibirsk, Russia, **4** Unité des Aspergillus, Institut Pasteur, Paris, France

☯ These authors contributed equally to this work.
* tikunova@niboch.nsc.ru (NVT); nen@ioc.ac.ru (NEN)

Citation: Matveev AL, Krylov VB, Emelyanova LA, Solovev AS, Khlusevich YA, Baykov IK, et al. (2018) Novel mouse monoclonal antibodies specifically recognize *Aspergillus fumigatus* galactomannan. PLoS ONE 13(3): e0193938. https://doi.org/10.1371/journal.pone.0193938

Editor: Joshua J. Obar, Dartmouth College, Geisel School of Medicine, UNITED STATES

Received: November 17, 2017

Accepted: February 21, 2018

Published: March 8, 2018

Data Availability Statement: All relevant data are within the paper and its Supporting Information files.

Funding: Synthesis of biotinylated oligosaccharids and of BSA-based glycoconjugate, and assaying of antibodies on glycoarray were supported by Russian Science Foundation (http://rscf.ru; grant 14-23-00199 to N.E.Nifantiev); development of mouse mAbs, SPR-study, and confocal microscopy were supported by Russian Science Foundation (http://rscf.ru; grant 16-14-00083 to N.

Abstract

A panel of specific monoclonal antibodies (mAbs) against synthetic pentasaccharide β-D-Gal*f*-(1→5)-[β-D-Gal*f*-(1→5)]$_3$-α-D-Man*p*, structurally related to *Aspergillus fumigatus* galactomannan, was generated using mice immunized with synthetic pentasaccharide-BSA conjugate and by hybridoma technology. Two selected mAbs, 7B8 and 8G4, could bind with the initial pentasaccharide with affinity constants of approximately 5.3 nM and 6.4 nM, respectively, based on surface plasmon resonance-based biosensor assay. The glycoarray, built from a series of synthetic oligosaccharide derivatives representing different galactomannan fragments, demonstrated that mAb 8G4 could effectively recognize the parental pentasaccharide while mAb 7B8 recognizes its constituting trisaccharide parts. Immunofluorescence studies showed that both 7B8 and 8G4 could stain *A. fumigatus* cells in culture efficiently, but not the mutant strain lacking galactomannan. In addition, confocal microscopy demonstrated that *Candida albicans*, *Bifidobacterium longum*, *Lactobacillus plantarum*, and numerous gram-positive and gram-negative bacteria were not labeled by mAbs 7B8 and 8G4. The generated mAbs can be considered promising for the development of a new specific enzyme-linked assay for detection of *A. fumigatus*, which is highly demanded for medical and environmental controls.

Introduction

Aspergillus fumigatus is the causative agent of a wide range of infections, the most common being allergic bronchopulmonary aspergillosis, local (non-invasive) aspergillosis, chronic pulmonary aspergillosis, as well as invasive aspergilloses [1]. In recent years, invasive pulmonary aspergillosis has been a leading cause of infection-related deaths among immunocompromised patients [2]. This infection often accompanies pulmonary tuberculosis, lung cancer, and

V/ Tikunova); microorganisms used in this work were provided by the Collection of Extremophile Microorganisms and Type Cultures (developed within Project 0309-2017-0008 granted by the Russian Federal Agency of Scientific Organizations; http://fano.gov.ru); study of the recognition of cell cultures by monoclonal antibodies was supported by The French National Research Agency (http://www.agence-nationale-recherche.fr/en/; provided support to J.-P. Latgé; there is no grant number).

Competing interests: The authors have declared that no competing interests exist.

chronic bronchitis, and may develop in transplant recipients [2–5]. The major antigenic component secreted by *A. fumigatus* into the growth medium is galactomannan–a soluble polysaccharide with molecular weight of approximately 20 kDa [6]. This polysaccharide is also present in glycoproteins as N- and O-glycan moieties and a GPI-anchored lipophosphogalactomannan [7]. Structurally, galactomannan contains a linear mannan core comprising mannotetraose repeating units connected via α-(1→2)- and partly by α-(1→6)- linkages. Some of the α-(1→2)-linked mannoside residues of a mannan backbone have side chains composed of an average of 4 to 5 β-(1→5)-galactofuranoside units attached via β-(1→6)- or β-(1→3)- linkages [6]. Recently, two new structural elements of *A. fumigatus* galactomannan have been revealed [8]. These are oligogalactofuranoside side chains containing not only β-(1→5)-linkages, but also one internal β-(1→6)-bond between galactofuranoside residues as well as oligogalactofuranoside side-chains α-(1→2)-attached to the mannan backbone (structural fragments of *A. fumigatus* galactomannan are summarized in Fig 1A).

The *A. fumigatus* antigens in biological fluids can be detected by a commercial sandwich enzyme-linked immunosorbent assay (ELISA) Platelia *Aspergillus* (Bio-Rad, Marnes-laCoquette, France) [9,10]. This diagnostic tool is widely used; however, the rate of false-positive

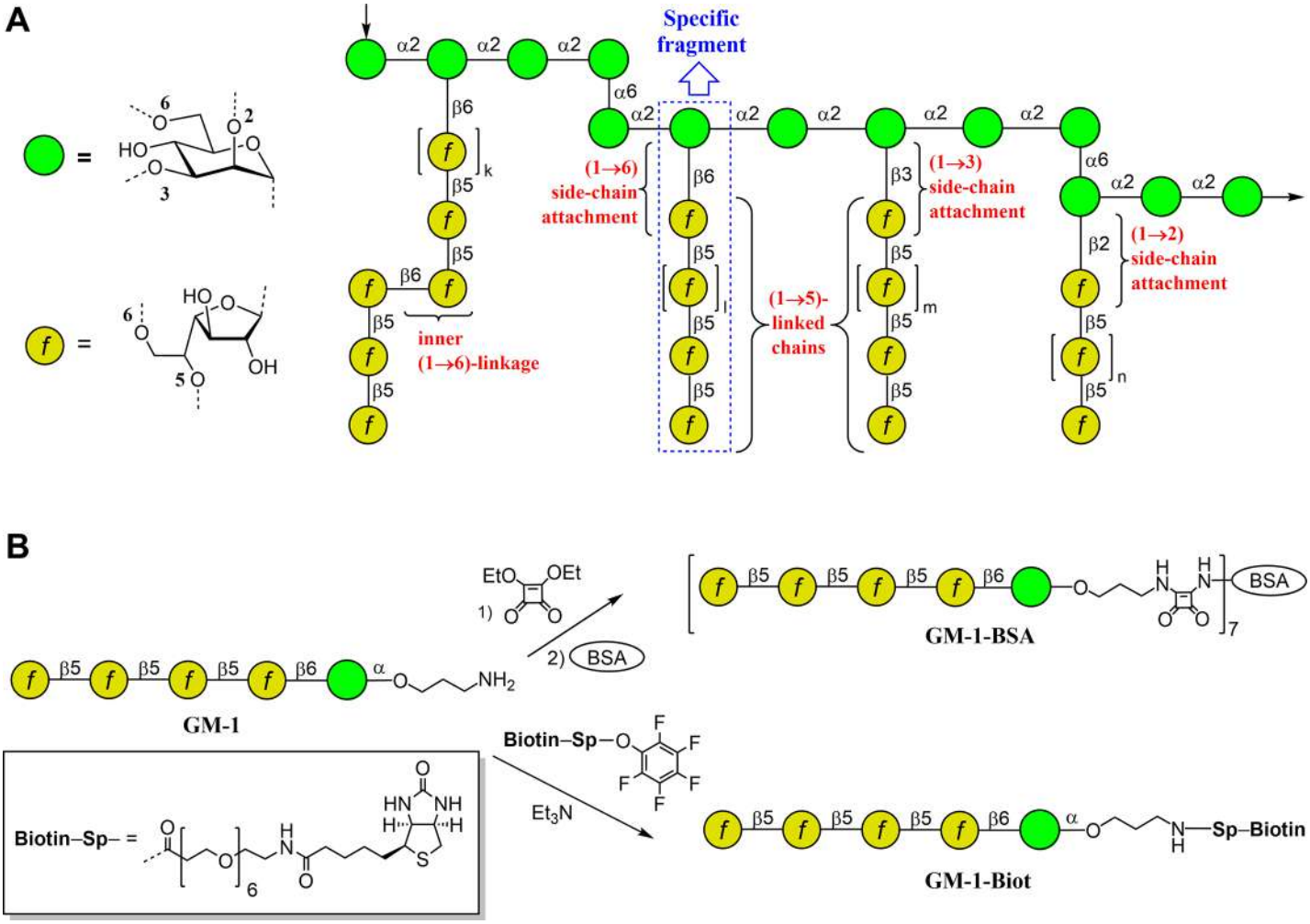

Fig 1. Structure of *Aspergillus fumigatus* galactomannan and its synthetic analogs. (A) Structural fragments of *A. fumigatus* galactomannan (summarized from refs. [6] and [8]). (B) Pentasaccharide **GM-1** and its BSA **(GM-1-BSA)** and biotinylated **(GM-1-Biot)** conjugates used in mice immunization and mAb screening. The carbohydrate sequences are represented according to symbol carbohydrate nomenclature [26].

https://doi.org/10.1371/journal.pone.0193938.g001

results for this assay is rather high, and can vary from 5% in adults to 83% in premature infants [11,12]. Other issues that interfer with the detection of galactomannan and reduce the specificity [9,13–15] of this diagnostic tool are antibiotic therapy [16] and dietary factors [17]. These false-positive results are associated with cross-reactive binding of EB-A2 monoclonal antibodies (mAbs) employed in the commercial assay with different non-*Aspergillus* fungi [18–23]. In addition, cross-reactivity with different bacteria, especially with *Bifidobacterium* spp., and members of the normal gastrointestinal microbiota of adults and infants has also been reported [24,25]. This cross-reactivity made it challenging to develop new mAb with improved specificity to be applicable in ELISA for galactomannan detection. The present study reports two new galactomannan-recognizing mAbs developed using BSA-bound (**GM-1-BSA**) and biotinylated **(GM-1-Biot)** conjugates of synthetic pentasaccharide β-D-Gal*f*-(1→5)-[β-D-Gal*f*-(1→5)]$_3$-α-D-Man*p* derivative (**GM-1**) (Fig 1B).

Materials and methods

Conjugates of synthetic oligosaccharides

The synthesis of oligosaccharides related to galactomannan fragments has been described previously [27,28]. Bovine serum albumin (BSA) conjugate **GM-1-BSA** (Fig 1B) was prepared using the squarate protocol [29]. Thus, diethyl squarate (4 μL, 0.027 mmol) was added to pentasaccharide **GM-1** solution (10.0 mg, 0.011 mmol) in 50% aqueous ethanol (1 mL). The resulting mixture was incubated for 16 h at room temperature. Then triethylamine (3 μL) was added; after 5 h, the solvents were removed. The residue was dissolved in 2 mL water and loaded onto a Sep-Pak C-18 cartridge and washed with water (10 mL). Then, the product was eluted with a gradient of methanol (5% → 20%) in water. The eluate was concentrated, and the residue was lyophilized to give a squarate intermediate (9.5 mg). A solution of this product (4.6 mg, 4.6 μmol) and BSA (15.4 mg) in 3 mL of the buffer solution (250 mL water, 8.8 g $KHCO_3$, 6.7 g $Na_2B_4O_7{\cdot}10H_2O$, pH 9) was incubated for 3 days at room temperature. The conjugate was isolated by gel chromatography on a Sephadex G-15 column in water and lyophilized to give 10 mg (50%) BSA conjugate **GM-1-BSA**. MALDI TOF mass spectrum analysis was used to identify the average presence of 8 pentasaccharide ligands per BSA molecule.

To prepare the biotinylated conjugate **GM-1-Biot**, the solution of the parent spacered pentasaccharide **GM-1** (0.116 mmol) in Et_3N (10 μL) was treated with the active ester of biotin (0.139 mmol) in DMF (0.7 mL) following the biotinylation protocol described previously [30] (as shown in Fig 1B). The mixture was incubated for 18 h at room temperature and then concentrated in vacuum, followed by gel-permeation chromatography on TSK HW-40(S) column (2 × 80 cm) in 0.1 M AcOH that formed the product **GM-1-Biot** with 75% yield. Biotinylated glycoconjugates **1–10**, **GM-2**, **GM-3** (see section «Epitope specificity of selected mAbs» below) used in the creation of glycoarrays on streptavidin-coated plates, were prepared similarly with 65–75% yields starting from the corresponding aminopropyl glycosides [27,28,31], synthesized using pyranoside-*into*-furanoside rearrangement [32,33].

Animals

Female BALB/c mice were purchased from the animal care facility in the Federal State Research Center of Virology and Biotechnology "Vector", (Koltsovo, Russia). Mice were housed in plastic cages, 800 cm^2, (6–10 animals per cage) under normal light-dark cycle. Water and food were provided *ad libitum*. All animal procedures were carried out in accordance with the recommendations for the protection of animals used for scientific purposes (EU Directive 2010/63/EU). The animals were euthanized with overdose of isoflurane (5%). Exposure of isoflurane was continued during one minute after breathing stop. All experiments

with animals were approved by the local Bioethics Committee of Institute of Chemical Biology and Fundamental Medicine, Siberian Branch of Russian Academy of Sciences, Novosibirsk, Russia.

Eukaryotic, fungal, and bacterial cells

SP2/0 myeloma cell line obtained from the EMTC collection (Institute of Chemical Biology and Fundamental Medicine, Novosibirsk, Russia) was cultured in Iscove's modified Dulbecco's medium (Invitrogen, USA) supplemented with 10% fetal bovine serum (Biolot, Russia) and antibiotics (0.1 mg/mL streptomycin and 100 IU/mL penicillin). *A. fumigatus* WT ($akuB^{Ku80}$ $pyrG^{+}$) [34] and *Δugm1* mutant [35] strains were used. Other fungal and bacterial strains were obtained from the EMTC collection. Fungal cells, *Aspergillus fumigatus*, *Aspergillus flavus*, and *Candida albicans*, were propagated in Sabouraud medium at room temperature. *Enterococcus faecalis*, *Escherichia coli*, *Proteus mirabilis*, *Pseudomonas aeruginosa*, *Salmonella enterica*, and *Staphylococcus aureus* were grown in Luria-Bertani broth at 37˚C, while *Bifidobacterium longum* and *Lactobacillus plantarum* were grown in Blaurock medium.

Mice immunization and mAbs selection

For immunization, 12–14-week-old BALB/c mice (22–28 g) were subcutaneously administered with 15 μg BSA-conjugate **GM-1-BSA** (Fig 1B) in 300 μL phosphate buffer saline (PBS), pH 7.4, emulsified with an equal volume of complete Freund's adjuvant (Sigma-Aldrich, USA). Each mouse was boosted twice at two-week and four-week intervals with equal amount of the immunogen mixed with incomplete Freund's adjuvant (Sigma-Aldrich, USA) in the same ratio. The fusion titer of anti-galactomannan antibodies in mice sera was screened using indirect ELISA. Two weeks after the third hybridization, animals were finally administered with 20 μg BSA-conjugate **GM-1-BSA** (Fig 1B) in 300 μL PBS, pH 7.4. Three days after this procedure, mice with the highest fusion titer were sacrificed, spleens were obtained, and splenocytes were fused with SP2/0 myeloma cells using PEG 2000 (Roche, Switzerland) according to the manufacturer's protocol. The level of mAbs in the supernatants was tested using indirect ELISA. Positive clones were additionally cloned two times by limiting dilution method.

Oligosaccharide-specific indirect ELISA

For indirect ELISA, the wells of 96-well Pierce™ streptavidin-coated plate were coated with 50 ng/well of biotinylated pentasaccharide **GM-1-Biot** (Fig 1B) in 25 μM Tris-HCl pH 7.5 with 150 mM NaCl, 0.5% Tween-20, and 0.3% BSA and incubated at 4˚C overnight. The supernatants from mouse experiments or mAbs in appropriate dilutions were added and incubated at 37˚C for 1 h. After washing, anti-mouse IgG alkaline phosphatase-conjugated goat IgG (Sigma Aldrich, USA) was added and incubated at 37˚C for 1 h followed by staining with 4-nitrophenyl phosphate. Absorbance was measured at 405 nm using iMark plate reader (Bio-Rad, USA). To exclude binding of mice sera and mAbs with BSA, the wells of 96-well microtiter plate were coated with control antigen, 3% BSA in PBS, pH 7.4, and after blocking, mice sera or mAbs were added and incubated at 37˚C for 1 h. Then, indirect ELISA was conducted as described above.

Purification and conjugation of mAbs

To produce mAbs, 2×10^6 selected hybridoma cells were administered intraperitoneally into 20-week-old BALB/c mice. Selected mAbs were purified by ammonium sulfate precipitation from ascitic fluids and then purified using the protein A chromatography (GE Healthcare,

USA). The purity and size of the purified IgG antibodies were examined by SDS-PAGE and western blot analyses. Purified mAbs were resolved by 12.5% SDS-PAGE under reducing conditions and transferred onto nitrocellulose membrane (Bio-Rad). After blocking by 5% dry skim milk, the membrane was incubated with anti-mouse IgG alkaline phosphatase-conjugated goat IgG (Sigma Aldrich, USA). Immune complexes were visualized by a mixture of nitro blue tetrazolium (NBT, Amresco) and 5-bromo-4-chloro-3-indolyl-phosphate (BCIP, Roche) for 20 min.

Selected mAbs were conjugated with horse-radish peroxidase (Amresco, USA) using optimized $NaIO_4$ method as described previously [36].

Affinity constant measurement

The kinetics for mAbs binding to synthetic galactomannan oligosaccharides conjugated with biotin were determined by a surface plasmon resonance (SPR) using a ProteOn XPR36 system (Bio-Rad, USA). Vertical channels L1 and L2 of GLC sensor chip were coated with streptavidin at 150–180 response unit (RU) level. Tested biotinylated oligosaccharides were immobilized onto streptavidin-coated channel L1 at 10 RU level, while L2 was used as a reference channel. Serially diluted mAb was analyzed starting from the lowest concentration at a flow rate of 25 μL/min. Chip surface was regenerated with 100 mM citric acid. Global analysis of experimental data based on a single-site or a heterogeneous analyte model was performed using the ProteOn Manager v. 3.1.0 software. Affinity constants were calculated as $K_D = k_d/k_a$ (see Fig 2).

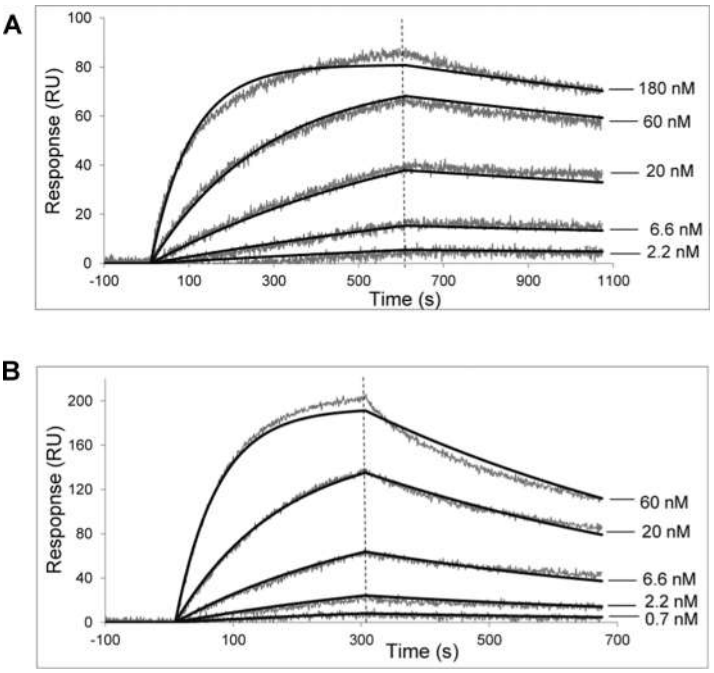

Fig 2. Binding of selected mAbs with biotinylated pentasaccharide GM-1. Serial three-fold dilutions of (A) mAb 7B8 starting from 180 nM and (B) mAb 8G4 starting from 60 nM were used as analytes. Fitted traces are depicted as smooth black lines. A global analysis of the interaction demonstrated a good quality fit and experimentally determined dissociation and association rate constants, k_d and k_a, were $(3.0 \pm 0.1) \times 10^{-4}$ s^{-1} and $(5.6 \pm 0.1) \times 10^4$ $M^{-1}s^{-1}$ for 7B8 antibody, and $(1.5 \pm 0.1) \times 10^{-3}$ s^{-1} and $(2.3 \pm 0.1) \times 10^5$ $M^{-1}s^{-1}$ for 8G4 antibody, respectively. Equilibrium constants, calculated as $K_D = k_d/k_a$, were 5.3×10^{-9} M and 6.4×10^{-9} M, respectively.

https://doi.org/10.1371/journal.pone.0193938.g002

Glycoarray

The wells of 96-well Pierce™ streptavidin-coated plates were coated with appropriate biotin-tagged oligosaccharides **1–10**, **GM-1**, **GM-2**, **GM-3** (Fig 3) (100 μL of a 20 pmol/well solution in PBS containing 0.05% Tween-20 and 0.1% BSA) and then incubated for 2 h at 37˚C. The plates were incubated with mAbs 7B8 and 8G4 serially diluted in PBS-BSA-Tween-20 buffer (two-fold, starting from 8 μg/mL concentration) for 1 h at 37˚C. After washing, anti-mouse IgG rabbit IgG-horseradish peroxidase conjugate (Imtek, Russia) was added and incubated for 1 h at 37˚C. After washing three times, color was developed using TMB mono-component substrate (100 μL) for 15 minutes and stopped with 50 μL of 1 M sulfuric acid. Absorbance was measured at 450 nm using MultiSkan GO plate reader (Thermo Fisher Scientific, USA). All measurements were done in triplicates.

Microscopy

For fluorescent microscopy, *A*. *fumigatus* WT and *Δugm1* mutant strains were grown in Sabouraud broth at 30˚C for 20 h. After fixation of the mycelium with 2.5% *p*-formaldehyde (PFA) overnight at 4˚C, immunofluorescence procedure was performed as described previously [37]. Briefly, cells were washed with PBS, incubated with 2% glycerol/PBS for 5 min and 5% goat serum in PBS for 1 h. Then, cells were incubated with mAb (2 μg/mL in 5% goat serum/PBS) for 1 h at room temperature. After washing with goat serum/PBS, cells were incubated with a goat TRITC-conjugated Ab directed against anti-mouse IgG, (Sigma) diluted 1:200 in goat serum/PBS. After washing in PBS, cells were visualized under an inverted fluorescence microscope.

For confocal microscopy, fungal and bacterial cells were fixed with 2.5% PFA overnight at 4˚C. Fixed cells were washed with PBS twice and incubated with 3% BSA in PBS for 1 h. Then, cells were washed and incubated with 5 μg/mL mAb diluted in PBS with 3% BSA for 1 h at 37˚C. After washing, cells were stained with Alexa Fluor-488-conjugated chicken anti-mouse IgG (H+L) antibodies (Life Technologies) diluted 1:500 in PBS with 3% BSA. Samples were mounted using Prolong Diamond Antifade. Images were obtained using the Carl Zeiss LSM 710 laser scanning microscope (Carl Zeiss, Germany). Observations were done using oil 63× objectives and scans were taken at 488 nm in green and differential interference contrast (DIC) channels. ZEN black edition software (Carl Zeiss, Germany) was used in the confocal microscope to visualize images. Alexa-Fluor 488 images and DIC images were obtained by excitation at 488 nm, with emission collected from 510–540 nm.

Sandwich anti-galactomannan ELISA

The wells of 96-well microtiter plates were coated with a selected 7B8 or 8G4 mAb in carbonate-bicarbonate buffer, pH 9.2 and then incubated at 37˚C for 1 h. After blocking, serially diluted (two-fold, starting from 1:100 dilution) microbial supernatants in PBS-BSA-Tween-20 buffer were added, and the plates were incubated for 1 h at 37˚C. After washing three times, indirect ELISA was performed with horseradish peroxidase-conjugated mAb (100 μL) and developed using TMB mono-component substrate (100 μL) for 15 minutes and stopped with 50 μL of 1 M sulfuric acid. Absorbance was measured at 450 nm using iMark plate reader (BioRad, USA). All microbial supernatants were tested three times and in triplicates.

Results and discussion

Production of anti-galactomannan mAbs

To generate mice mAbs specifically recognizing *A*. *fumigatus* galactomannan, the immunogen **GM-1-BSA** bearing pentasaccharide ligands comprising four (1→5)-linked galactofuranoside

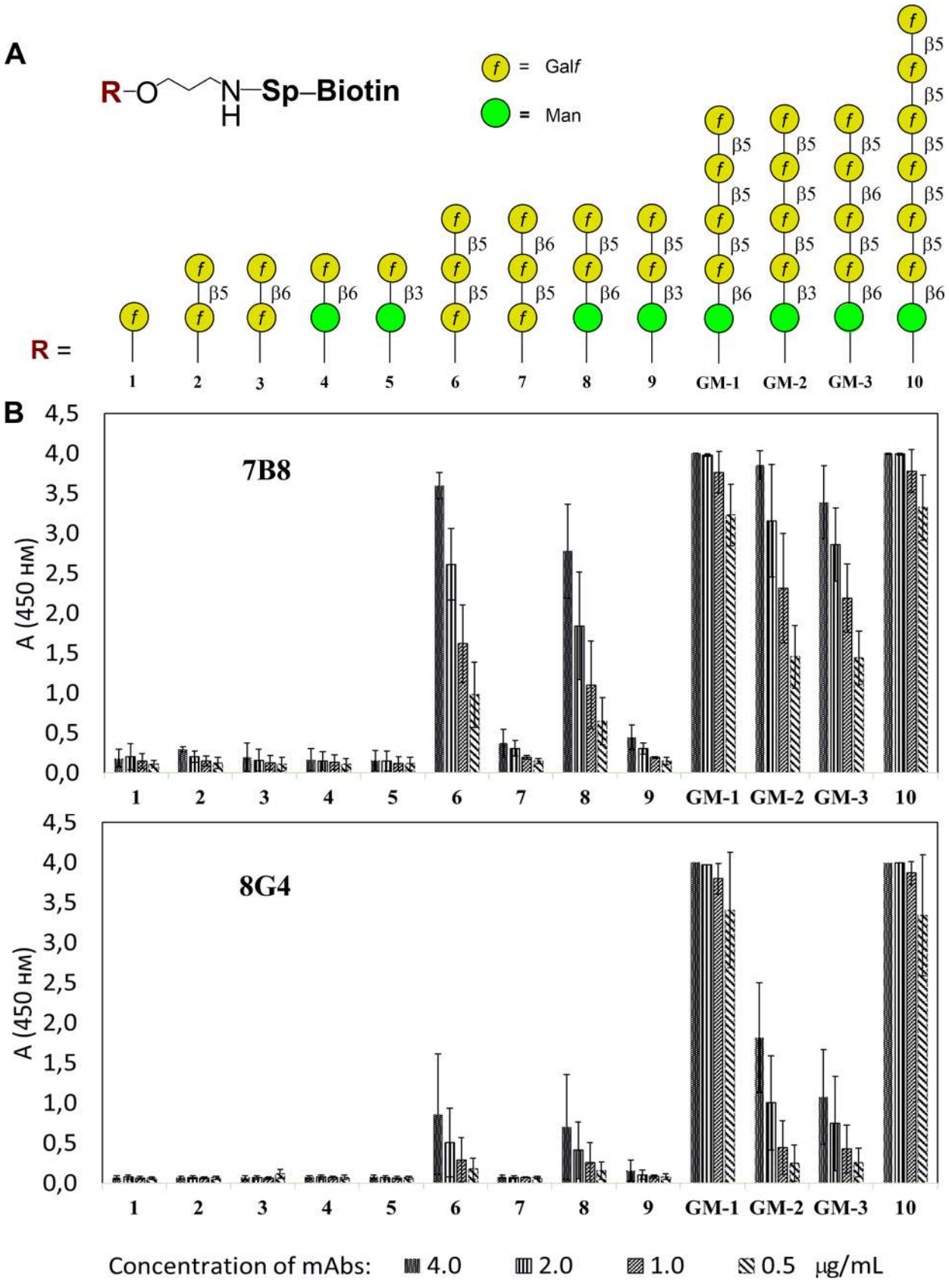
A
R–O–N–Sp–Biotin
H
f = Galf
= Man
R =
1
2
3
4
5
6
7
8
9
GM-1
GM-2
GM-3
10
B
7B8
8G4
A (450 нм)
4,5
4,0
3,5
3,0
2,5
2,0
1,5
1,0
0,5
0,0
Concentration of mAbs: 4.0 2.0 1.0 0.5 μg/mL

Fig 3. Investigation of oligosaccharide specificity of mAbs 7B8 and 8G4 using ELISA. (A) Composition of thematic glycoarray built using oligosaccharide ligands representing key structural elements of *A. fumigatus* galactomannan chain, and (B) assay for carbohydrate specificity of 7B8 and 8G4 mAbs.

https://doi.org/10.1371/journal.pone.0193938.g003

units attached via (1→6)-linkage to mannose residue was selected as a specific target fragment in the galactomannan structure (Fig 1A). The selected pentasaccharide represents characteristic fragment in the structure of *A. fumigatus* galactomannan [6,8]; it was shown that this pentasaccharide sequence can be used as a mimetic for *Aspergillus* galactomannan in immunobiological studies [38,39]. Using synthetic pentasaccharide **GM-1**, immunogen **GM-1-BSA** was prepared by conjugation of corresponding aminopropyl glycoside with BSA using the squarate protocol (Fig 1B). The biotin-tagged pentasaccharide **GM-1-Biot** required for selection of mAbs was prepared by treating amine with activated ester (Fig 1B).

To develop mAbs against galactomannan from the cell wall of *A. fumigatus*, BALB/c mice were immunized with BSA-conjugate **GM-1-BSA** four times. Four, 8, and 12 weeks after the first immunization, mice sera were screened by indirect ELISA to assess the level of anti- galactomannan IgG antibodies; biotinylated pentasaccharide **GM-1-Biot** was used as an antigen to exclude selection of anti-BSA mAbs. Final fusion titer of anti-**GM-1** antibodies in mice sera was 1:10 000 (data not shown). The binding of individual hybrid clones (n = 480) with biotinylated pentasaccharide **GM-1-Biot** was tested by indirect ELISA, and nine hybridomas were selected.

To determine IgG class of selected mAbs, a fragment of the gene encoding constant domain CH1 was amplified using the primers 5′-CTTCCGGAATTCSARGTNMAGCTGSAGSAGTC-3′ [40] and 5′-GGGAAGTAGCCTTTGACAAGGC-3′ and sequenced. Among nine selected mAbs, two belonged to the IgG3 class, while others belonged to the IgG1 class. Light chains of all the selected mAbs belonged to the kappa family.

All the selected mAbs were produced in ascitic fluids, purified using affinity chromatography, and visualized by PAAG and western blotting S1 Fig. The kinetic parameters and affinity constants for the interaction between the selected mAbs and target pentasaccharide were determined with biotinylated conjugate **GM-1-Biot** in a label-free biosensor assay using a ProteOn XPR36 system. A global analysis of interaction between the mAbs 7B8 and 8G4 and the antigen demonstrated a good quality fit and affinity constants were calculated as K_D = $(5.3 \pm 0.2) \times 10^{-9}$ M for mAb 7B8 and $K_D = (6.4 \pm 0.2) \times 10^{-9}$ M for mAb 8G4 (Fig 2). Affinity constants of other selected mAbs were $> 10^{-6}$ M, which were insufficient for the development of EIA with good sensitivity for the detection of aspergillosis; therefore, further experiments were performed with mAbs 7B8 and 8G4.

Epitope specificity of selected mAbs

The carbohydrate specificity of mAbs 7B8 and 8G4 was investigated using a library of 13 synthetic oligosaccharides representing distinct structural fragments of *A. fumigatus* galactomannan (Fig 3A). These ligands with varied size and types of inter-unit linkages represent the biotinylated conjugates, which were immobilized on the surface of the streptavidin-coated plate. mAbs were applied on glycoarrays as a series of two-fold dilutions. The highest affinity was demonstrated for the target pentasaccharide **GM-1** used in the structure of the immunogen, and in the case of elongated analog **10**, containing pentasaccharide sequence (Fig 3). Mono- and disaccharides were not recognized by both 7B8 and 8G4.

The discernible difference between mAbs 7B8 and 8G4 was revealed using the analogs of the target pentasaccharide **GM-1**. The shorter ligands, trisaccharides **6** and **8**, and ligands with changed type of linkages, **GM-2** and **GM-3**, were recognized moderately by mAb 7B8;

however, its interaction with mAb 8G4 was significantly lower (Fig 3). Notably, trisaccharides **7** and **9**, structures of which were not presented in the target pentasaccharide, were not bound by both 7B8 and 8G4 (Fig 3).

These results were additionally confirmed by SPR analysis for determining the binding of mAbs 7B8 and 8G4 with pentasaccharides **GM-2** and **GM-3**, which differed from the target pentasaccharide **GM-1** with only one glycoside bond (Fig 1C). The affinities with which mAb 7B8 bound to pentasaccharides **GM-2** and **GM-3** were $K_D = (5.9 \pm 0.2) \times 10^7\ M^{-1}$ and $K_D = (3.3 \pm 0.1) \times 10^7\ M^{-1}$, respectively, and were lower than that for the initial pentasaccharide **GM-1** (see Fig 2). Notably, binding of mAb 8G4 to pentasaccharides **GM-2** and **GM-3** were two orders lower than that with the initial pentasaccharide **GM-1**, $K_D = (6.7 \pm 0.2) \times 10^6\ M^{-1}$ and $K_D = (2.0 \pm 0.1) \times 10^6\ M^{-1}$, respectively.

Specific binding of mAbs with fungal and bacterial cells in culture

To demonstrate the ability of mAbs 7B8 and 8G4 to specifically recognize natural galactomannan, immunofluorescence experiments were performed using parental *A. fumigatus* WT and *Δugm1* mutant strains (Fig 4). Notably, previously it has been demonstrated that mycelial cell wall of *A. fumigatus Δugm1* mutant does not contain galactofuranose [35]. In this study, both 7B8 and 8G4 mAbs labeled *A. fumigatus* parental strain, while no fluorescence signal was observed for the *Δugm1* mutant (Fig 4). The lack of fluorescence signal demonstrated the involvement of galactofuranoside unit in epitopes recognized by mAbs 7B8 and 8G4.

To evaluate specificity of mAbs 7B8 and 8G4, their binding with fungi *A. fumigatus*, *A. flavus*, and *C. albicans*, as well as gram-positive and gram-negative bacterial cells, including *B. longum*, *E. faecalis*, *E. coli*, *L. plantarum*, *P. mirabilis*, *P. aeruginosa*, *S. enterica*, and *S. aureus*, was examined by confocal microscopy. Previously, it has been demonstrated that some fungal and bacterial species express polysaccharides that have structural elements similar to those from *A. fumigatus* galactomannan, while some of them do not express such polysaccharides

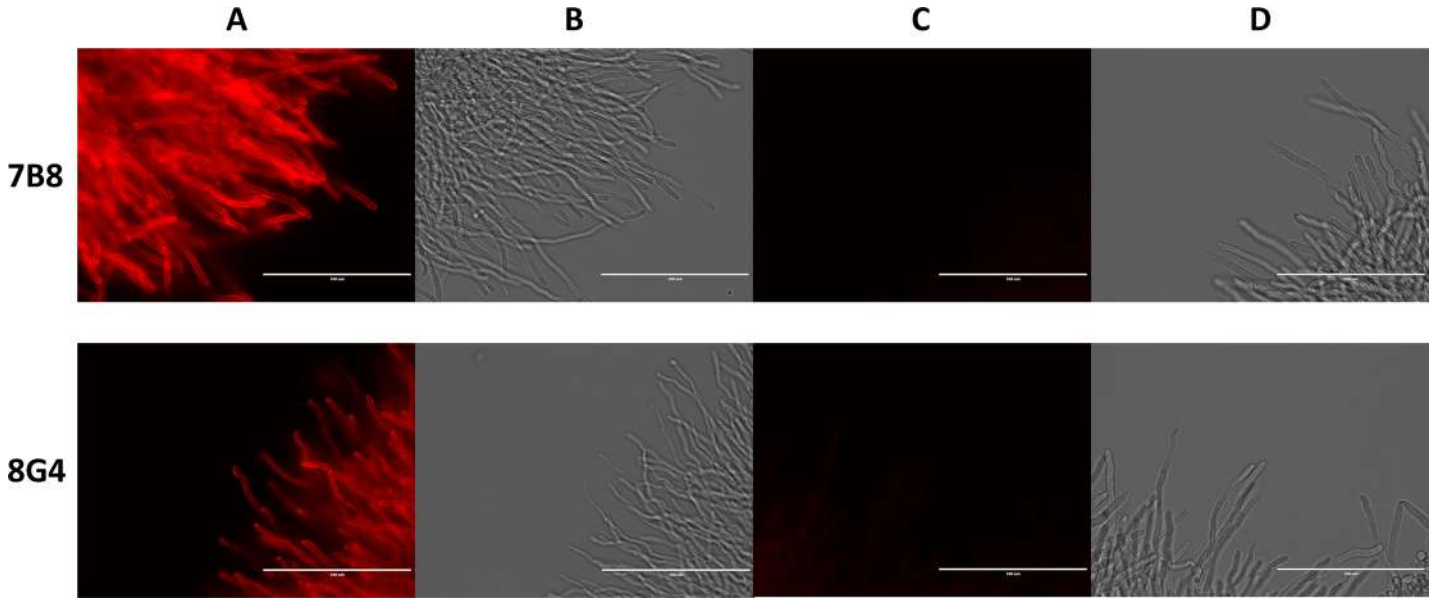

Fig 4. Immunofluorescence labeling of the *Aspergillus fumigatus* WT strain and *ΔUgm1* mutant with mAbs 7B8 and 8G4. (A, B) Wild-type parental strain of *A. fumigatus* in fluorescence microscopy and light microscopy studies, respectively. (C, D) *Ugm1* mutant of *A. fumigatus* without galactomannan in fluorescence microscopy and light microscopy studies, respectively. Binding of mAbs with Aspergillus cells was detected with goat TRITC-conjugated anti-mouse IgG antibody. Scale bar = 100 μm.

https://doi.org/10.1371/journal.pone.0193938.g004

[34,35]. In case of *A. flavus*, structure of carbohydrate antigens has not been studied in all details, however the previous immunological studies [19] suggest the presence of structures related to A. fumigatus galactomannan. The obtained images demonstrated that both 7B8 and 8G4 labeled *A. flavus* along with *A. fumigatus* (Fig 5). However, *C. albicans* (Fig 5) and all the tested bacteria (S2 Fig) were not detected by mAbs 7B8 and 8G4. Importantly, exposure time was the same in all experiments.

Specific binding of mAbs 7B8 and 8G4 with *A. fumigatus* and *A. flavus* and the lack of their binding with *C. albicans*, *B. longum*, *E. faecalis*, *E. coli*, *L. plantarum*, *P. mirabilis*, *P. aeruginosa*, *S. enterica*, and *S. aureus* were confirmed using sandwich ELISA (Fig 6). In accordance with the confocal microscopy data, supernatants of *A. fumigatus* and *A. flavus* added to mAb 7B8 were effectively bound by the same mAb (Fig 6A) or mAb 8G4 (data not shown), while supernatants of *C. albicans*, *B. longum*, and other tested bacteria were not recognized by sandwich ELISA (data for *E. faecalis*, *P. mirabilis*, *P. aeruginosa*, *S. enterica*, and *S. aureus* are not shown). The same result was demonstrated for sandwich ELISA with mAb 8G4 (Fig 6B).

Importantly, both mAb 7B8 and 8G4 could not detect *B. longum* cells either by confocal microscopy, or by sandwich ELISA. However, *Bifidobacterium* spp., including *B. longum*

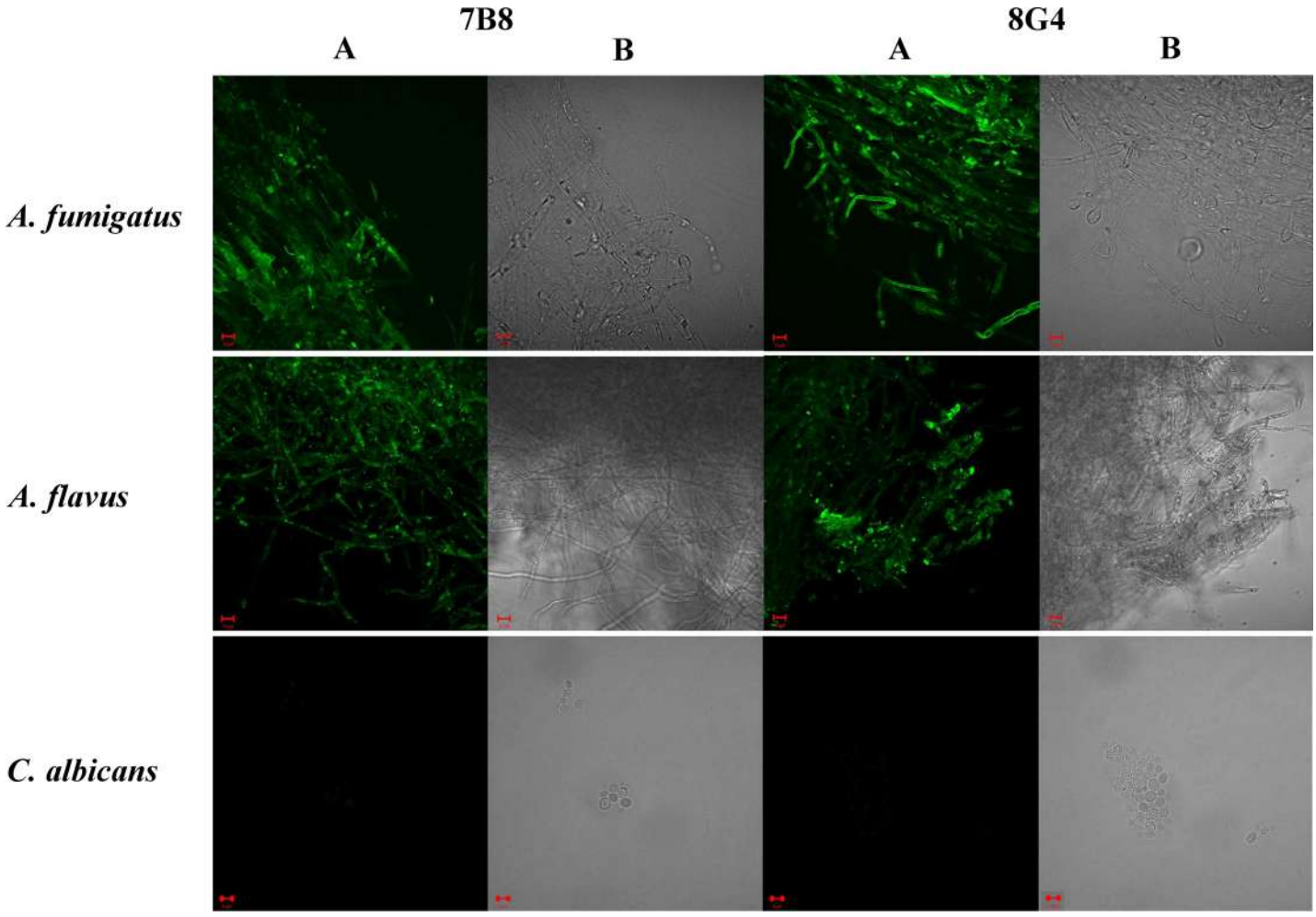

Fig 5. Specific binding of mAbs 7B8 and 8G4 with *A. fumigatus*, *A. flavus*, and *C. albicans*. Cells were grown in Sabouraud broth, fixed, and incubated with mAbs 7B8 and 8G4. Binding of mAbs with fungal cells was detected with Alexa Fluor 488-conjugated anti-mouse IgG antibody staining in (A) confocal microscopy, and (B) DIC microscopy. Scale bar = 10 μm.

https://doi.org/10.1371/journal.pone.0193938.g005

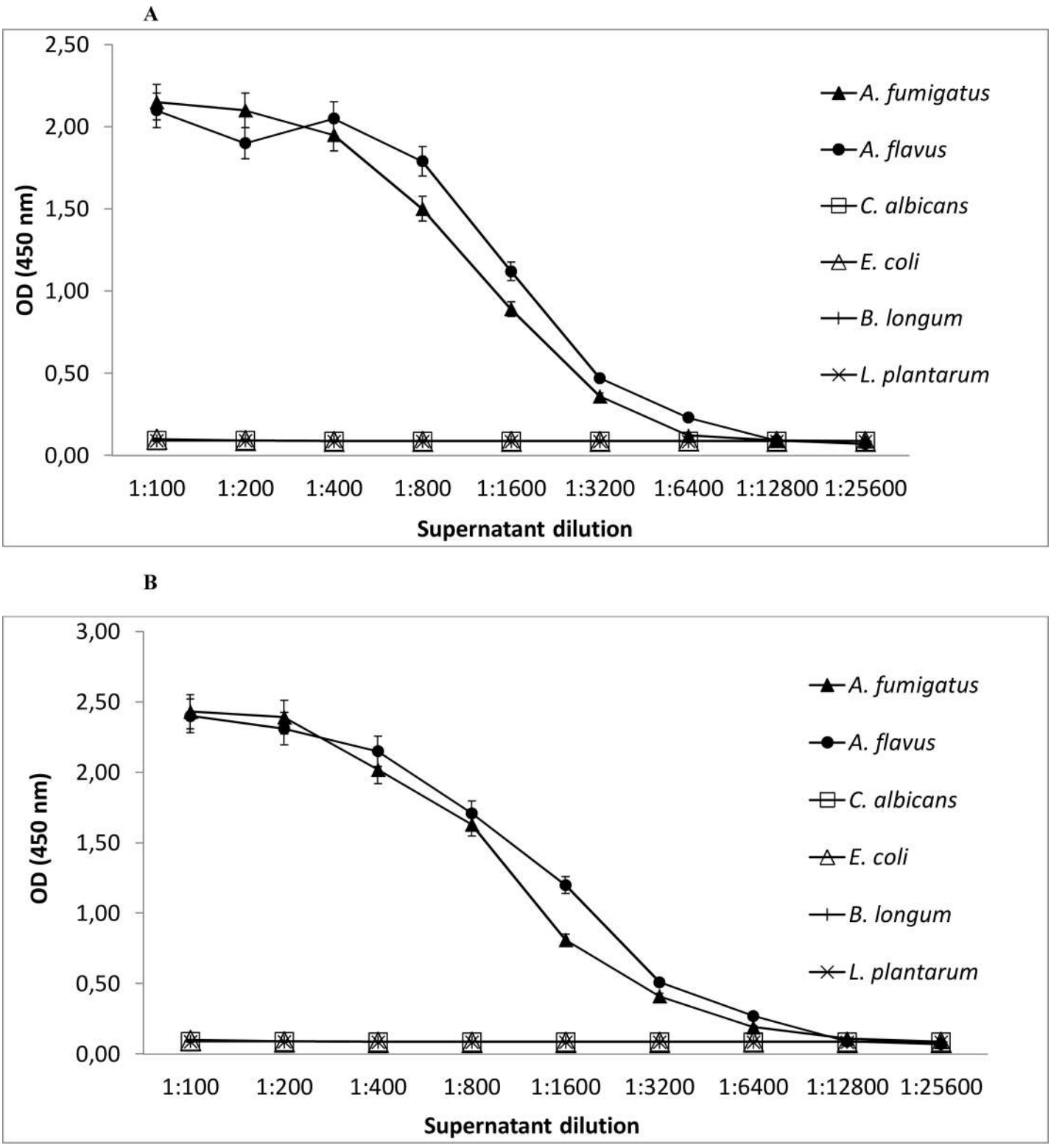

Fig 6. Binding of fungal and bacterial cultures with mAbs 7B8 and 8G4. (A) Sandwich enzyme-linked immunosorbent assay (ELISA) with 7B8 mAb: the wells of microtiter plates were coated with 7B8 mAb and incubated with serial dilutions of microbial supernatants; ELISA was performed with horseradish peroxidase-conjugated 7B8 mAb. (B) Sandwich ELISA with 8G4 mAb: the wells of microtiter plates were coated with 8G4 mAb and incubated with serial dilutions of microbial supernatants; ELISA was performed with horseradish peroxidase-conjugated 8G4 mAb.

https://doi.org/10.1371/journal.pone.0193938.g006

strains, have previously demonstrated substantial cross-reactivity with sandwich ELISA based on EB-A2 mAb [25]. *Bifidobacterium* species comprise a considerable part of the normal gastrointestinal microflora of adults and reach 90% of the total fecal microflora of infants [41,42]. Translocation of membrane-associated galactofuranoses because of the immaturity of the intestinal mucosa in neonates can explain some false-positive results [24]. The lack of binding of the mAbs 7B8 and 8G4 with *Bifidobacterium* species indicates high specificities of the studied mAbs, which could be further tested head-to-head with EB-A2 as a promising components for the development of a new specific enzyme-linked assay for detection of *A*. *fumigatus*, required for medical and environmental uses.

Conclusions

Mouse mAbs 7B8 and 8G4, which efficiently recognize galactomannan of *A*. *fumigatus*, were obtained by immunization of mice with BSA-conjugate of synthetic pentasaccharide β-D-Gal*f*-(1→5)-[β-D-Gal*f*-(1→5)]$_3$-α-D-Man*p* (**GM-1**) and hybridoma technology. The carbohydrate specificity of obtained mAbs was assessed by SPR and thematic glycoarray built using a series of synthetic oligosaccharide ligands structurally related to the characteristic galactomannan fragments. Further studies on staining of fungal and bacterial cells by mAbs confirmed good selectivity of developed mAbs suitable for detecting *A*. *fumigatus* galactomannan and made possible their use in immune diagnostics. Results showed that because of recent progress [38,43] in the synthesis of oligosaccharides related to fungal cell wall carbohydrate antigens, the synthetic oligosaccharide derivatives of distinct structure can be efficiently used for the development of mAbs as an alternative to natural polysaccharides, which are characterized by structural diversity.

Supporting information

S1 Fig. Electrophoretic and western blot analyses of monoclonal antibodies 7B8 and 8G4. (A) Coomassie blue stained 12% SDS–PAAG electrophoretic analysis of purified mAb 7B8 and mAb 8G4 in reducing conditions. (B) Western blot analysis of mAb 7B8 and mAb 8G4 fractionated by 12.5% SDS-PAAG electrophoresis in reducing conditions and developed with alkaline phosphatase conjugated anti-mouse IgG (whole molecule) goat antibody (Sigma-Aldrich, USA). Protein molecular marker masses, in kilodaltons, are shown at the left side of the gel.
(TIF)

S2 Fig. Luck of binding of monoclonal antibodies 7B8 and 8G4 to selected bacterial cells. Fixed cells were incubated with mAbs 7B8 and 8G4. (A) Bacterial DNA was stained with DAPI. (B) Binding of mAbs with bacterial cells was identified with Alexa Fluor 488 conjugated anti-mouse IgG antibodies staining in confocal microscopy. (B) Scale bar 10 μm.
(TIF)

Acknowledgments

Synthesis of biotinylated oligosaccharids and of BSA-based glycoconjugate, and assaying of antibodies on glycoarray were supported by Russian Science Foundation (grant 14-23-00199); development of mouse mAbs, SPR-study, and confocal microscopy were supported by Russian Science Foundation (grant 16-14-00083); microorganisms used in this work were provided by the Collection of Extremophile Microorganisms and Type Cultures (developed within Project 0309-2017-0008 granted by the Russian Federal Agency of Scientific Organizations); study of

the recognition of cell cultures by monoclonal antibodies was supported by the French ANR agency.

Author Contributions

Conceptualization: Nikolay E. Nifantiev.

Data curation: Nikolay E. Nifantiev.

Formal analysis: Nikolay E. Nifantiev.

Funding acquisition: Nina V. Tikunova, Nikolay E. Nifantiev.

Investigation: Andrey L. Matveev, Vadim B. Krylov, Ljudmila A. Emelyanova, Arsenii S. Solovev, Yana A. Khlusevich, Ivan K. Baykov, Thierry Fontaine.

Project administration: Nina V. Tikunova, Nikolay E. Nifantiev.

Supervision: Jean-Paul Latgé, Nikolay E. Nifantiev.

Validation: Jean-Paul Latgé, Nikolay E. Nifantiev.

Writing – original draft: Andrey L. Matveev, Vadim B. Krylov, Thierry Fontaine, Jean-Paul Latgé, Nina V. Tikunova, Nikolay E. Nifantiev.

Writing – review & editing: Andrey L. Matveev, Vadim B. Krylov, Nina V. Tikunova, Nikolay E. Nifantiev.

References

1. Brown GD, Denning DW, Gow NAR, Levitz SM, Netea MG, White TC. Hidden killers: human fungal infections. Sci Transl Med. 2012; 4: 165rv13. https://doi.org/10.1126/scitranslmed.3004404 PMID: 23253612
2. Singh N, Paterson DL. Aspergillus infections in transplant recipients. Clin Microbiol Rev. 2005; 18: 44–69. https://doi.org/10.1128/CMR.18.1.44-69.2005 PMID: 15653818
3. Latgé J-P. Aspergillus fumigatus and aspergillosis. Clin Microbiol Rev. 1999; 12: 310–350. PMID: 10194462
4. Kohno S. High mortality in invasive aspergillosis: what we need to know for determination of poor prognosis and next countermeasures. The University of Chicago Press; 2008.
5. Groll AH, Shah PM, Mentzel C, Schneider M, Just-Nuebling G, Huebner K. Trends in the postmortem epidemiology of invasive fungal infections at a university hospital. J Infect. 1996; 33: 23–32. PMID: 8842991
6. Latgé J-P, Kobayashi H, Debeaupuis J-P, Diaquin M, Sarfati J, Wieruszeski J-M, et al. Chemical and immunological characterization of the extracellular galactomannan of Aspergillus fumigatus. Infect Immun. 1994; 62: 5424–5433. PMID: 7960122
7. Latgé J-P. Galactofuranose containing molecules in Aspergillus fumigatus. Med Mycol. 2009; 47: S104–S109. https://doi.org/10.1080/13693780802258832 PMID: 18686165
8. Kudoh A, Okawa Y, Shibata N. Significant structural change in both O-and N-linked carbohydrate moieties of the antigenic galactomannan from Aspergillus fumigatus grown under different culture conditions. Glycobiology. 2015; 25: 74–87. https://doi.org/10.1093/glycob/cwu091 PMID: 25187160
9. Wheat LJ, Walsh TJ. Diagnosis of invasive aspergillosis by galactomannan antigenemia detection using an enzyme immunoassay. Eur J Clin Microbiol Infect Dis. 2008; 27: 245–251. https://doi.org/10.1007/s10096-007-0437-7 PMID: 18193305
10. Stynen D, Goris A, Sarfati J, Latge JP. A new sensitive sandwich enzyme-linked immunosorbent assay to detect galactofuran in patients with invasive aspergillosis. J Clin Microbiol. 1995; 33: 497–500. PMID: 7714217
11. Verweij PE, Mennink-Kersten MA. Issues with galactomannan testing. Med Mycol. 2006; 44: S179–S183.
12. Siemann M, Koch-Dörfler M, Gaude M. False-positive results in premature infants with the Platelia® Aspergillus sandwich enzyme-linked immunosorbent assay. Mycoses. 1998; 41: 373–377. PMID: 9916459

13. White PL, Barnes RA, Springer J, Klingspor L, Cuenca-Estrella M, Morton CO, et al. Clinical performance of Aspergillus PCR for testing serum and plasma: a study by the European Aspergillus PCR Initiative. J Clin Microbiol. 2015; 53: 2832–2837. https://doi.org/10.1128/JCM.00905-15 PMID: 26085618
14. White PL, Jones T, Whittle K, Watkins J, Barnes RA. Comparison of galactomannan enzyme immunoassay performance levels when testing serum and plasma samples. Clin Vaccine Immunol. 2013; 20: 636–638. https://doi.org/10.1128/CVI.00730-12 PMID: 23389933
15. Loeffler J, Hafner J, Mengoli C, Wirth C, Heussel CP, Löffler C, et al. Prospective biomarker screening for diagnosis of invasive aspergillosis in high-risk pediatric patients. J Clin Microbiol. 2017; 55: 101–109. https://doi.org/10.1128/JCM.01682-16 PMID: 27795339
16. Aubry A, Porcher R, Bottero J, Touratier S, Leblanc T, Brethon B, et al. Occurrence and kinetics of false-positive Aspergillus galactomannan test results following treatment with β-lactam antibiotics in patients with hematological disorders. J Clin Microbiol. 2006; 44: 389–394. https://doi.org/10.1128/JCM.44.2.389-394.2006 PMID: 16455889
17. Blijlevens NMA, Donnelly JP, Meis J, Verweij PE, De Pauw BE. Aspergillus galactomannan antigen levels in allogeneic haematopoietic stem cell transplant recipients given total parenteral nutrition. Transpl Infect Dis. 2002; 4: 64–65. PMID: 12220241
18. Bonini A, Capatti C, Parmeggiani M, Gugliotta L, Micozzi A, Gentile G, et al. Galactomannan detection in Geotrichum capitatum invasive infections: report of 2 new cases and review of diagnostic options. Diagn Microbiol Infect Dis. 2008; 62: 450–452. https://doi.org/10.1016/j.diagmicrobio.2008.08.008 PMID: 18945571
19. Kappe R, Schulze-Berge A. New cause for false-positive results with the Pastorex Aspergillus antigen latex agglutination test. J Clin Microbiol. 1993; 31: 2489–2490. PMID: 8408572
20. Stynen D, Sarfati J, Goris A, Prevost MC, Lesourd M, Kamphuis H, et al. Rat monoclonal antibodies against Aspergillus galactomannan. Infect Immun. 1992; 60: 2237–2245. PMID: 1375195
21. Swanink CM, Meis JF, Rijs AJ, Donnelly JP, Verweij PE. Specificity of a sandwich enzyme-linked immunosorbent assay for detecting Aspergillus galactomannan. J Clin Microbiol. 1997; 35: 257–260. PMID: 8968919
22. Xavier MO, Pasqualotto AC, Cardoso ICE, Severo LC. Cross-reactivity of Paracoccidioides brasiliensis, Histoplasma capsulatum, and Cryptococcus species in the commercial Platelia Aspergillus enzyme immunoassay. Clin Vaccine Immunol. 2009; 16: 132–133. https://doi.org/10.1128/CVI.00310-08 PMID: 19020109
23. Wheat LJ, Hackett E, Durkin M, Connolly P, Petraitiene R, Walsh TJ, et al. Histoplasmosis-associated cross-reactivity in the BioRad Platelia Aspergillus enzyme immunoassay. Clin Vaccine Immunol. 2007; 14: 638–640. https://doi.org/10.1128/CVI.00479-06 PMID: 17344352
24. Mennink-Kersten MA, Klont RR, Warris A, den Camp HJO, Verweij PE. Bifidobacterium lipoteichoic acid and false ELISA reactivity in aspergillus antigen detection. The Lancet. 2004; 363: 325–327.
25. Mennink-Kersten MA, Ruegebrink D, Klont RR, Warris A, Gavini F, den Camp HJO, et al. Bifidobacterial lipoglycan as a new cause for false-positive platelia Aspergillus enzyme-linked immunosorbent assay reactivity. J Clin Microbiol. 2005; 43: 3925–3931. https://doi.org/10.1128/JCM.43.8.3925-3931.2005 PMID: 16081932
26. Varki A, Cummings R, Esko J, Freeze H, Hart G, Marth J. Essentials of glycobiology. NY: Cold Spring Harbor; 1999.
27. Argunov DA, Krylov VB, Nifantiev NE. Convergent synthesis of isomeric heterosaccharides related to the fragments of galactomannan from Aspergillus fumigatus. Org Biomol Chem. 2015; 13: 3255–3267. https://doi.org/10.1039/c4ob02634a PMID: 25643073
28. Argunov DA, Krylov VB, Nifantiev NE. The Use of Pyranoside-into-Furanoside Rearrangement and Controlled O (5)→ O (6) Benzoyl Migration as the Basis of a Synthetic Strategy To Assemble (1→ 5)- and (1→ 6)-Linked Galactofuranosyl Chains. Org Lett. 2016; 18: 5504–5507. https://doi.org/10.1021/acs.orglett.6b02735 PMID: 27759393
29. Wurm FR, Klok H-A. Be squared: expanding the horizon of squaric acid-mediated conjugations. Chem Soc Rev. 2013; 42: 8220–8236. https://doi.org/10.1039/c3cs60153f PMID: 23873344
30. Tsvetkov YE, Burg-Roderfeld M, Loers G, Ardá A, Sukhova EV, Khatuntseva EA, et al. Synthesis and molecular recognition studies of the HNK-1 trisaccharide and related oligosaccharides. The specificity of monoclonal anti-HNK-1 antibodies as assessed by surface plasmon resonance and STD NMR. J Am Chem Soc. 2011; 134: 426–435. https://doi.org/10.1021/ja2083015 PMID: 22087768
31. Krylov VB, Argunov DA, Solovev AS, Petruk MI, Gerbst AG, Dmitrenok AS, et al. Synthesis of oligosaccharides related to galactomannans from Aspergillus fumigatus and their NMR spectral data. Org Biomol Chem. 2018;Advance Article https://doi.org/10.1039/C7OB02734F PMID: 29376539

32. Krylov VB, Argunov DA, Vinnitskiy DZ, Verkhnyatskaya SA, Gerbst AG, Ustyuzhanina NE, et al. Pyranoside-into-Furanoside Rearrangement: New Reaction in Carbohydrate Chemistry and Its Application in Oligosaccharide Synthesis. Chem- Eur J. 2014; 20: 16516–16522. https://doi.org/10.1002/chem.201405083 PMID: 25319316

33. Krylov VB, Argunov DA, Vinnitskiy DZ, Gerbst AG, Ustyuzhanina NE, Dmitrenok AS, et al. The pyranoside-into-furanoside rearrangement of alkyl glycosides: scope and limitations. Synlett. 2016; 27: 1659–1664.

34. da Silva Ferreira ME, Kress MR, Savoldi M, Goldman MHS, Härtl A, Heinekamp T, et al. The akuBKU80 mutant deficient for nonhomologous end joining is a powerful tool for analyzing pathogenicity in Aspergillus fumigatus. Eukaryot Cell. 2006; 5: 207–211. https://doi.org/10.1128/EC.5.1.207-211.2006 PMID: 16400184

35. Lamarre C, Beau R, Balloy V, Fontaine T, Hoi JWS, Guadagnini S, et al. Galactofuranose attenuates cellular adhesion of Aspergillus fumigatus. Cell Microbiol. 2009; 11: 1612–1623. https://doi.org/10.1111/j.1462-5822.2009.01352.x PMID: 19563461

36. Nakane PK, Kawaoi A. Peroxidase-labeled antibody a new method of conjugation. J Histochem Cytochem. 1974; 22: 1084–1091. https://doi.org/10.1177/22.12.1084 PMID: 4443551

37. Fontaine T, Delangle A, Simenel C, Coddeville B, van Vliet SJ, van Kooyk Y, et al. Galactosaminogalactan, a new immunosuppressive polysaccharide of Aspergillus fumigatus. PLoS Pathog. 2011; 7: e1002372. https://doi.org/10.1371/journal.ppat.1002372 PMID: 22102815

38. Krylov VB, Paulovičová L, Paulovičová E, Tsvetkov YE, Nifantiev NE. Recent advances in the synthesis of fungal antigenic oligosaccharides. Pure Appl Chem. 2017; 89: 885–898.

39. Paulovičová E, Paulovičová L, Hrubiško M, Krylov VB, Argunov DA, Nifantiev NE. Immunobiological Activity of Synthetically Prepared Immunodominant Galactomannosides Structurally Mimicking Aspergillus Galactomannan. Front Immunol. 2017; 8: 1273. https://doi.org/10.3389/fimmu.2017.01273 PMID: 29081774

40. Wang Z, Raifu M, Howard M, Smith L, Hansen D, Goldsby R, et al. Universal PCR amplification of mouse immunoglobulin gene variable regions: the design of degenerate primers and an assessment of the effect of DNA polymerase 3′ to 5′ exonuclease activity. J Immunol Methods. 2000; 233: 167–177. PMID: 10648866

41. Harmsen HJ, Wildeboer–Veloo AC, Raangs GC, Wagendorp AA, Klijn N, Bindels JG, et al. Analysis of intestinal flora development in breast-fed and formula-fed infants by using molecular identification and detection methods. J Pediatr Gastroenterol Nutr. 2000; 30: 61–67. PMID: 10630441

42. Requena T, Burton J, Matsuki T, Munro K, Simon MA, Tanaka R, et al. Identification, detection, and enumeration of human Bifidobacterium species by PCR targeting the transaldolase gene. Appl Environ Microbiol. 2002; 68: 2420–2427. https://doi.org/10.1128/AEM.68.5.2420-2427.2002 PMID: 11976117

43. Karelin AA, Tsvetkov YE, Nifantiev NE. Synthesis of oligosaccharides related to polysaccharides of the cell wall of the fungi Candida and Aspergillus. Russ Chem Rev. 2017; 86: 1073–1126.

frontiers in Cellular and Infection Microbiology

ORIGINAL RESEARCH
published: 16 July 2019
doi: 10.3389/fcimb.2019.00234

Monoclonal Antibody AP3 Binds Galactomannan Antigens Displayed by the Pathogens *Aspergillus flavus*, *A. fumigatus*, and *A. parasiticus*

Max Schubert[1†], *Sheng Xue*[2†], *Frank Ebel*[3], *Annegret Vaggelas*[3], *Vadim B. Krylov*[4], *Nikolay E. Nifantiev*[4], *Ivana Chudobová*[1], *Stefan Schillberg*[1,5*] *and Greta Nölke*[1]

[1] *Department of Plant Biotechnology, Fraunhofer Institute for Molecular Biology and Applied Ecology IME, Aachen, Germany,* [2] *Institute for Translational Medicine, College of Medicine, Qingdao University, Qingdao, China,* [3] *Faculty of Veterinary Medicine, Institute for Infectious Diseases and Zoonoses, Ludwig-Maximilians-University Munich, Munich, Germany,* [4] *N.D. Zelinsky Institute of Organic Chemistry, Russian Academy of Sciences, Moscow, Russia,* [5] *Institute for Phytopathology, Justus Liebig University Giessen, Giessen, Germany*

OPEN ACCESS

Edited by:
Laura Alcazar-Fuoli, Carlos III Health Institute, Spain

Reviewed by:
Michael S. Price, Liberty University, United States
Georgios Chamilos, University of Crete, Greece

***Correspondence:**
Stefan Schillberg
stefan.schillberg@ime.fraunhofer.de

[†] *These authors have contributed equally to this work and are first authors*

Specialty section:
This article was submitted to Fungal Pathogenesis, a section of the journal Frontiers in Cellular and Infection Microbiology

Received: *12 March 2019*
Accepted: *14 June 2019*
Published: *16 July 2019*

Citation:
Schubert M, Xue S, Ebel F, Vaggelas A, Krylov VB, Nifantiev NE, Chudobová I, Schillberg S and Nölke G (2019) Monoclonal Antibody AP3 Binds Galactomannan Antigens Displayed by the Pathogens Aspergillus flavus, A. fumigatus, and A. parasiticus. Front. Cell. Infect. Microbiol. 9:234. doi: 10.3389/fcimb.2019.00234

Aspergillus fumigatus and *A. flavus* are the fungal pathogens responsible for most cases of invasive aspergillosis (IA). Early detection of the circulating antigen galactomannan (GM) in serum allows the prompt application of effective antifungal therapy, thus improving the survival rate of IA patients. However, the use of monoclonal antibodies (mAbs) for the diagnosis of IA is often associated with false positives due to cross-reaction with bacterial polysaccharides. More specific antibodies are therefore needed. Here we describe the characterization of the *Aspergillus*-specific mAb AP3 (IgG1κ), including the precise identification of its corresponding antigen. The antibody was generated using *A. parasiticus* cell wall fragments and was shown to bind several *Aspergillus* species. Immunofluorescence microscopy revealed that AP3 binds a cell wall antigen, but immunoprecipitation and enzyme-linked immunosorbent assays showed that the antigen is also secreted into the culture medium. The inability of AP3 to bind the *A. fumigatus* galactofuranose (Gal*f*)-deficient mutant Δ*glfA* confirmed that Gal*f* residues are part of the epitope. Several lines of evidence strongly indicated that AP3 recognizes the Gal*f* residues of *O*-linked glycans on *Aspergillus* proteins. Glycoarray analysis revealed that AP3 recognizes oligo-[β-D-Gal*f*-1,5] sequences containing four or more residues with longer chains more efficiently. We also showed that AP3 captures GM in serum, suggesting it may be useful as a diagnostic tool for patients with IA.

Keywords: *Aspergillus* antigen, detection assay, epitope identification, galactofuranose, glycobiology

INTRODUCTION

The genus *Aspergillus* comprises 339 filamentous fungi that are ubiquitous in nature and have many potential applications in biotechnology, but some species also pose a risk to human and animal health (Samson et al., 2014). *A. niger* and *A. oryzae* are widely used for fermentation in the food industry and for the production of hydrolytic enzymes (Biesebeke and Record, 2008). In contrast, *A. fumigatus* and *A. flavus* are major pathogens responsible for allergic bronchopulmonary aspergillosis (ABPA), chronic pulmonary aspergillosis (CPA) and invasive aspergillosis (IA), which

can be fatal in immunocompromised patients, such as carriers of human immunodeficiency virus, or patients receiving transplants of allogeneic stem cells or solid organs (Singh and Paterson, 2005; Krishnan et al., 2009). The early detection of biomarkers elicited by invasive *Aspergillus* species is necessary to achieve effective antifungal therapy outcomes (Hedayati et al., 2007; Walsh et al., 2008).

A. flavus is responsible for 15–20% of reported IA cases (Perfect et al., 2001; Krishnan et al., 2009). Furthermore, *A. flavus* and *A. parasiticus* also infect plants, where they produce highly carcinogenic secondary metabolites known as aflatoxins, particularly when they grow on oil-rich staple crops under field and storage conditions (Villers, 2014). These aflatoxins are stable during food processing, and contaminated food must be discarded causing significant economic losses amounting to billions of US$ in the US alone (Robens and Cardwell, 2003).

Antibodies against different *Aspergillus* antigens have been used to track infections by staining the fungal cell wall (Ste-Marie et al., 1990; Hao et al., 2008; Kumar and Shukla, 2015; Schubert et al., 2018). Other *Aspergillus*-specific antibodies have been used to detect allergens (Kurup and Banerjee, 2000) and disease-related biomarkers (Thornton, 2010) released by pathogenic strains, and to detect aflatoxin contamination in agricultural products (Wacoo et al., 2014). Fungal-type galactomannan (GM) is a heat-stable heteropolysaccharide and a major component of *Aspergillus* cell walls. It comprises a linear mannan core and short, branched β-1,5-linked galactofuranose (Gal*f*) chains (Latge et al., 1994). Antibodies that recognize GM, the main biomarker of IA, are commercially available (Thornton, 2010). Most *Aspergillus*-specific antibodies are generated using undefined preparations, such as crude extracts, so the precise antigens are often unknown. This makes it difficult to characterize the antibodies in detail and limits their commercial applications. We have generated monoclonal antibodies (mAbs) against several different intracellular and extracellular antigens of aflatoxigenic *A. flavus* and *A. parasiticus* using crude cell wall antigen preparations (Schubert et al., 2018). Here we describe the generation and antigen-specific characterization of mAb AP3, its potential suitability for the rapid serological detection of IA, and possible further commercial applications.

MATERIALS AND METHODS

Fungal Strains

Pure cultures of *A. flavus, A. parasiticus, A. nidulans, A. niger, Fusarium oxysporum, F. culmorum, Phytophthora nicotianae, Rhizoctonia solani, Pythium ultimum, Botrytis cinerea, Cercospora nicotianae, Thielaviopsis basicola*, and *Penicillium chrysogenum* were obtained from the German Collection of Microorganisms and Cell Cultures (DSMZ, Braunschweig, Germany) and maintained on potato dextrose agar (PDA; Carl Roth, Karlsruhe, Germany), tomato agar (25% (v/v) tomato juice, 3 g/l $CaCO_3$, 15 g/l agar) or liquid potato dextrose broth medium (PDB; Carl Roth). The wild-type *A. fumigatus* strain D141 (Reichard et al., 1990) and Gal*f*-deficient mutant Δ*glfA* were cultivated as previously described (Schmalhorst et al., 2008). The *F. oxysporum* strain DSM 62316 used for immunofluorescence analysis and enzyme-linked immunosorbent assay (ELISA) experiments was cultivated and prepared as previously reported (Wiedemann et al., 2016).

Preparation of Fungal Antigens

Cell Wall Fragments and Cell Wall Proteins

Aspergillus conidia were isolated and used to inoculate liquid cultures in PDB or Czapek Dox medium. For all other fungi, an overgrown agar slice was used to inoculate liquid cultures based on the media and cultivation conditions recommended by the DSMZ. Harvested mycelia were disrupted under liquid nitrogen using a mortar and pestle to obtain cell wall fragments (CWFs) and were washed three times in 1 M NaCl to remove cytosolic antigens (Pitarch et al., 2008).

CWFs representing each fungal species listed above were resuspended in deionized water, lyophilized and weighed. Cell wall-associated proteins (CWPs) were extracted from *A. flavus* (AF-CWPs) and *A. parasiticus* CWFs (AP-CWPs) using a reducing extraction buffer (50 mM Tris-HCl pH 8.0, 0.1 M EDTA, 2% (w/v) SDS, 10 mM DTT) and resuspended in 1× phosphate-buffered saline (PBS; 137 mM NaCl, 2.7 mM KCl, 8.1 mM Na_2HPO_4, 1.5 mM KH_2PO_4, pH 7.4) as previously described (Prados-Rosales et al., 2009).

Preparation of Extracellular Aspergillus Antigens and GM Supernatants

Extracellular *Aspergillus* antigens secreted during growth were prepared by inoculating 400 ml Czapek Dox medium with 10^6 *A. flavus* conidia/ml and removing the mycelia after 7 days of growth at 28°C by filtering through three layers of Miracloth (Merck, Darmstadt, Germany). The supernatant was then precipitated in 2.5 volumes of ethanol overnight at 4°C, and the pellet was collected by centrifugation (3,000 g, 10 min, 4°C). The precipitate was washed three times with ethanol and resuspended in water, then freeze-dried and stored at −20°C. The protein content was determined using the Roti-Quant Bradford assay (Carl Roth). Supernatants from the *A. fumigatus* Δ*glfA* mutant, and GM-containing supernatants from *A. fumigatus* strain D141 (SD-Asp) and *F. oxysporum* strain DSM 62316, were prepared as previously described (Wiedemann et al., 2016).

Antibody Generation and Purification

Five 6-weeks-old female BALB/c mice (veterinary license: 9.93.2.10.54.07.044) were intraperitoneally immunized with 150 μg *A. parasiticus* CWFs in a total volume of 100 μl prepared with Gerbu Adjuvant MM (Gerbu Biotechnik, Heidelberg, Germany), and subsequent boosts were carried out at 2-weeks intervals. Five days after the final boost (boost six), B-lymphocytes were isolated from spleens and fused to myeloma cells (SP2/mIL6). The resulting hybridoma cells were cultivated

Abbreviations: 2DE, two-dimensional gel electrophoresis; ABPA, allergic bronchopulmonary aspergillosis; AF-CWP, *A. flavus* cell wall protein; CPA, chronic pulmonary aspergillosis; CWF, cell wall fragment; CWP, cell wall protein; DAS-ELISA, double antibody sandwich-ELISA; ELISA, enzyme-linked immunosorbent assay; Gal*f*, galactofuranose; GM, galactomannan; GPI, glycosylphosphatidylinositol; IA, invasive aspergillosis; Ig, immunoglobulin; mAb, monoclonal antibody; SD-Asp, *A. fumigatus* spent culture media.

in Gibco RPMI GlutaMAX medium (Thermo Fisher Scientific, Waltham, MA, USA) and the supernatants of cells producing *Aspergillus*-specific antibodies were screened by ELISA using a goat anti-mouse Fc antibody for the selection of IgG antibodies. Positive hybridoma cells were singularized by limiting dilution, and monitored using the Cellavista imaging system (Roche, Basel, Switzerland). Stable cell line AP3 (producing mAb AP3) was maintained for long-time storage by cryopreservation in liquid nitrogen. The isotype of this cell line was determined using a mouse immunoglobulin isotyping kit (BD Biosciences, San Jose, CA, USA). The cells were transferred to serum-free H5000 medium (PAN-Biotech, Aidenbach, Germany) and incubated continuously for up to 2 months at 37°C in a 5% CO_2 atmosphere in a CELLine bioreactor flask CL1000 (Sigma-Aldrich, St. Louis, MO, USA).

The AP3 antibody was purified by passing the hybridoma supernatant through MEP HyperCel resin (Pall, Port Washington, NY, USA) using the ÄKTAexplorer 10 fast protein liquid chromatography (FPLC) system (GE Healthcare, Munich, Germany). The purified antibody was dialyzed against PBS, supplemented with 0.02% (w/v) NaN_3 and stored at 4°C. Biotinylated mAb AP3 was prepared using the EZ-Link biotinylation kit (Thermo Fisher Scientific) according to the manufacturer's instructions.

Recombinant Protein Production

The cDNA coding for the *A. flavus* mycelial catalase (XP_002380889.1) was synthesized with codon optimization for *Escherichia coli* and transferred to the bacterial expression vector pET-22b(+) (Novagen, Darmstadt, Germany), providing sequences for an N-terminal signal peptide (targeting the periplasmic space) and a C-terminal His_6 tag (for affinity purification and detection). The construct was introduced into competent *E. coli* BL21(DE3) cells (New England Biolabs, Frankfurt am Main, Germany) and a positive clone of *A. flavus* mycelial catalase was selected for production and purification by Ni-NTA affinity chromatography, according to the manufacturer's instructions (Novagen).

One-Dimensional Electrophoresis (1DE) and Immunoblot

AF-CWPs and precipitated extracellular *Aspergillus* antigens were boiled in 5× reducing SDS loading buffer (62.5 mM Tris-HCl pH 6.8, 10% (v/v) 2-mercaptoethanol, 4% (w/v) SDS, 30% (w/v) glycerol, 0.05% (w/v) bromophenol blue), and separated by discontinuous SDS-PAGE using a 12% (w/v) polyacrylamide separating gel. Proteins were visualized using Coomassie Brilliant Blue (Fairbanks et al., 1971). The separated proteins were transferred to 0.45-µm nitrocellulose membranes by electroblotting, and free binding sites were blocked with 3% (w/v) milk powder in PBS containing 0.05% (v/v) Tween-20 (PBS-T). After each step, the membrane was washed with PBS-T. Proteins were detected with the purified mAb AP3 (2 µg/ml) and an alkaline phosphatase (AP)-labeled goat anti-mouse Fc (GAM^{AP} Fc, 160 ng/ml) (Jackson Immunoresearch Laboratories, West Grove, PA, USA). After washing in PBS-T and equilibrating in AP buffer (100 mM Tris-HCl pH 9.6, 100 mM NaCl, 5 mM $MgCl_2$), the signal was detected by incubating in AP buffer containing nitro-blue tetrazolium and 5-bromo-4-chloro-3-indolylphosphate (NBT/BCIP) diluted 1:100.

Two-Dimensional Electrophoresis (2DE), Immunoblot and Mass Spectrometry

Aspergillus spores were germinated in Czapek Dox medium (28°C, 16 h). Young *A. flavus* mycelia were ground to a fine powder under liquid nitrogen, and the proteins were precipitated by adding 1.8 ml ice-cold acetone containing 0.7% (v/v) 2-mercaptoethanol. The samples were incubated at −20°C for at least 1 h and then centrifuged (13,000 g, 20 min, 4°C). The pellets were resuspended in ice-cold acetone plus 0.7% (v/v) 2-mercaptoethanol followed by incubation and centrifugation as above. After the second centrifugation step, the pellets were washed twice in ice-cold acetone without 2-mercaptoethanol, dried at room temperature, and stored at −20°C. The proteins in the pellets were resolubilized overnight at room temperature in isoelectric focusing buffer (7 M urea, 2 M thiourea, 2% (w/v) CHAPS, 30 mM Tris-HCl pH 8.8), and the mixture was centrifuged as above to remove debris. The protein content of the supernatant was quantified using the 2D quant kit (GE Healthcare), and two 100-µg CWP aliquots were labeled with 200 pmol Cy3 (GE Healthcare) according to the manufacturer's instructions.

Gel electrophoresis was carried out as previously described (Horn et al., 2013). Two 2D gels were prepared under the same conditions—the first one was used for immunoblot analysis as described above, the second one as a preparative gel for the identification of proteins by mass spectrometry. After protein separation, both gels were scanned using the Ettan DIGE Imager (GE Healthcare) with the filter for Cy3 to localize all protein spots and to enable matching. Fungal proteins recognized by mAb AP3 were detected by first probing with AP3 (400 ng/ml) followed by a goat anti-mouse Cy5-labeled antibody (120 ng/ml). The membrane was then scanned twice using the Cy3 and Cy5 filters to reveal the positions of proteins bound by the AP3 antibody. The images were processed with DeCyder v7.0 (GE Healthcare). Spots of interest were marked on the preparative gel followed by blind picking. The proteins in gel spots were alkylated and digested with trypsin (Promega, Mannheim, Germany) before identification by mass spectrometry as previously described (Spiegel et al., 2015). The raw data files were evaluated using the NCBI *A. flavus* reference database (12,587 sequences; 5,779,766 residues).

Immunofluorescence Microscopy

Round glass coverslips were washed in 70% (v/v) ethanol, coated with 0.1% (v/v) poly-L-lysine and air dried. The coverslips were then washed in deionized water and deposited in 12-well cell culture plates, which were blocked with 3% (w/v) milk powder in PBS-T. Germinated *A. flavus* and *A. parasiticus* conidia (overnight incubation in RPMI medium at 37°C) were added to the wells, and the plates were centrifuged (2,000 g, 15 min, room temperature) to deposit the germlings onto the coverslips. For direct staining, mAb AP3 (2 µg/ml) was added to the wells and incubated for 2 h at room temperature.

After washing with PBS-T, AP3 binding to conidia and short hyphae was detected by adding 1.5 μg/ml GAM^{Dylight} 594 H+L (Jackson ImmunoResearch Laboratories) and incubating for 1 h at room temperature. The round coverslips were then placed upside down on a slide and sealed with nail polish to prevent desiccation. Samples were analyzed with a Leica DMR fluorescence microscope (Leica Microsystems, Wetzlar, Germany) using excitation/emission maxima of 592/617 nm. *A. fumigatus* D141, Δ*glfA* and *P. chrysogenum* were detected with mAb AP3 and suitable Cy3-labeled secondary antibodies (Jackson ImmunoResearch Laboratories). Images were captured using a Leica SP-5 confocal laser scanning microscope (Leica Microsystems) as previously described (Wiedemann et al., 2016).

Periodate Oxidation

Extracellular *Aspergillus* antigens and CWPs from *A. flavus* were immobilized on ELISA plates (40 μg/well) and treated with 200 μl sodium *meta*-periodate buffer (20 mM $NaIO_4$ in 50 mM sodium acetate buffer, pH 4.5) for 16 h in darkness at 4°C. The periodate oxidation of the SD-Asp antigen was carried out as previously described (Thornton, 2008). The binding of mAb AP3 (400 ng/ml) to the antigen after periodate treatment was measured by ELISA as described below. Untreated *Aspergillus* antigens were used as a positive control and PBS as a negative control.

Digestion of *Aspergillus* Antigens

Extracellular *Aspergillus* antigens and *A. flavus* CWPs (40 μg) were dissolved in 50 mM ammonium bicarbonate buffer supplemented with 1.5 μg trypsin protease (Promega). The solution was then incubated at 37°C overnight and the antigen (20 μg) was separated by SDS-PAGE using a 12% (w/v) polyacrylamide separating gel. The binding of AP3 to the protease-treated antigens was analyzed by immunoblot as described above.

ELISA

Quantification of mAb AP3

The concentration of AP3 was determined by sandwich ELISA using an IgG1 standard (Rasche et al., 2011) to generate a calibration curve. A high-binding microtiter plate (Greiner Bio-One, Frickenhausen, Germany) was coated with 300 ng/ml goat-Fab anti-mouse Fab in PBS (Jackson ImmunoResearch Laboratories) overnight at 4°C. After each step, the plates were washed with 200 μl PBS-T. After blocking with 200 μl 3% (w/v) skimmed milk in PBS-T for 1 h, several dilutions of AP3 (0.4–100 ng/ml) were loaded onto the ELISA plate adjacent to the calibration curve of the standard IgG1. Binding was detected by adding 160 ng/ml horseradish peroxidase (HRP)-labeled goat anti-mouse Fc antibody (Jackson ImmunoResearch Laboratories) and 2,2′-azino-*bis*(3-ethylbenzthiazoline-6-sulfonic acid) (ABTS) as the substrate. After 30 min incubation at room temperature, the absorbance was determined by spectrophotometry at 405 nm. After each incubation step, the microtiter plate was washed three times with PBS-T. All measurements were taken in triplicate.

Reactivity of mAb AP3 to Fungal Antigens

The specificity of mAb AP3 binding was measured by direct ELISA with CWFs. The prepared CWFs were used to coat high-binding microtiter plates (150 μg/ml in water) overnight at 37°C. After blocking as described above, several concentrations of AP3 (0.002–2 μg/ml) were applied as the primary antibody, followed by detection as described above. The effect of periodate oxidation was evaluated by coating high-binding microtiter plates with periodate-treated *A. flavus* CWPs (2 μg) and GM standard SD-Asp (1:100), and using untreated *Aspergillus* antigens as a control. After blocking as described above, purified AP3 (400 ng/ml) was applied as the primary antibody, followed by detection as described above.

Double antibody sandwich ELISA (DAS-ELISA) was carried out to detect CWPs and extracellular antigens secreted by *A. flavus*. High-binding microtiter plates were coated with mAb AP3 (400 ng/ml) overnight at 4°C. After blocking with 2% (w/v) biotin-free bovine serum albumin (BSA; Carl Roth), 100-μl aliquots of serially-diluted *A. flavus* antigens (0.005–25 μg/ml) were applied for 1 h and detected using biotinylated mAb AP3 (600 ng/ml) and AP-labeled streptavidin (200 ng/ml) (Jackson ImmunoResearch Laboratories), followed by detection as described above.

To analyze *Aspergillus* supernatants by direct-coating ELISA, the culture supernatants from *A. fumigatus* wild-type D141 (SD-Asp, 1:10–1:100) and Δ*glfA* (1:10) were coated onto high-binding microtiter plates for 1 h at room temperature. After blocking as described above, purified AP3 (400 ng/ml) or the GM-specific antibody IgM L10-1 (Heesemann et al., 2011) and the IgM AB135-8 (Wiedemann et al., 2016), which recognizes a novel Gal*f*-containing antigen, were applied as primary antibodies, followed by detection using a secondary HRP-labeled goat anti-mouse IgG or goat anti-mouse IgM. The signal was developed by incubating in ABTS for 20 min and detected by measuring the absorbance at 405 nm. Measurements were taken in triplicate.

Sandwich ELISA was used to detect the presence of GM in serum. Purified AP3 (400 ng/ml), L10-1, or AB135-8, were coated onto a high-binding microtiter plate at 4°C overnight. After blocking as described above, 100 μl GM-positive serum from the Platelia *Aspergillus* enzymatic immunoassay (EIA) kit (Bio-Rad, Hercules, CA, USA) was diluted 1:5,000 or 1:100,000, applied for 1 h and developed using the Gal*f*-specific EB-A2 conjugate and the detection reagents provided in the kit. The reaction was stopped after 30 min and the absorbance was measured at 450 nm. Measurements were taken in triplicate.

To investigate the cooperation of L10-1 and AP3 as capture and detection antibodies in a sandwich ELISA, purified AP3 or L10-1 (each 900 ng/ml) were coated onto a high-binding microtiter plate at 4°C overnight. After blocking as described above, serially-diluted CWPs or extracellular antigens (1:320–1:20,480) from *A. flavus* were applied for 1 h, and bound antigens were detected using the corresponding detection antibody: AP3 or L10-1 (each 900 ng/ml). Binding was detected using a secondary HRP-labeled goat anti-mouse IgG or goat anti-mouse IgM. Absorbance was measured at 405 nm after 40 min incubation in ABTS substrate. Measurements were taken in triplicate.

Glycoarray

The carbohydrate specificity of mAb AP3 was determined using a thematic glycoarray as previously described (Krylov et al., 2018b; Matveev et al., 2018). To 96-well streptavidin-coated plates (Pierce, Waltham, MA, USA), we added 20 pmol/well of the biotin-tagged oligosaccharides 1–13 (Argunov et al., 2015, 2016; Krylov et al., 2018a) in 100 µl PBS containing 0.05% (v/v) Tween-20 and 0.1% (w/v) BSA. The plates were then incubated for 2 h at 37°C before adding mAb AP3 serially diluted in the same buffer (1000, 250, 50 and 10 ng/ml) and incubating for another 1 h at 37°C. After washing, we added a rabbit anti-mouse IgG HRP conjugate (Imtek, Moscow, Russia) and incubated for 1 h at 37°C. After washing three times, color development was initiated by adding 100 µl TMB monocomponent substrate for 15 min and stopped by adding 50 µl 1 M sulfuric acid. Absorbance was measured at 450 nm using a MultiSkan GO plate reader (Thermo Fisher Scientific). Measurements were carried out twice in triplicate, and results are presented as means ± SD.

Statistical Analysis

Significant differences between the antigen-binding and control treatments in ELISAs and glycoarray experiments were determined by one way analysis of variance (ANOVA) followed by *post-hoc* Bonferroni testing using Excel software (Microsoft, Redmond, Washington, USA). Significant differences in antigen binding between ELISA experiments were confirmed by Student's *t*-test, with the significance threshold set at $p < 0.05$.

RESULTS

Characterization of the *Aspergillus*-Specific mAb AP3

Following the immunization of mice with *A. parasiticus* cell wall fragments (CWFs), seven hybridoma clones producing *Aspergillus*-specific IgG antibodies were selected by ELISA. The hybridoma clone that showed the strongest reactivity against *A. parasiticus* CWFs was selected for further analysis, and the corresponding mAb (AP3) was assigned to isotype IgG1 and κ. Because CWFs and extracted cell wall proteins (CWPs) comprise a mixture of antigens of different sizes and chemical compositions, the precise antigen bound by AP3 was initially unknown.

First we analyzed the ability of AP3 to bind to *A. flavus* CWPs by immunoblot. The CWPs were separated by SDS-PAGE (**Figure 1A**) and the proteins were transferred to a membrane and probed with AP3. The antibody bound to multiple undefined bands with molecular masses exceeding 35 kDa and was particularly reactive against *A. flavus* proteins with molecular masses exceeding 70 kDa (**Figures 1B**, **3A**). This provided the first evidence that the epitope recognized by AP3 is shared by multiple glycoproteins.

The reactivity of AP3 against *Aspergillus* antigen preparations and its cross-reactivity with other fungal plant pathogens was also tested by ELISA. The antibody bound to CWFs prepared from *A. flavus*, *A. parasiticus*, *A. nidulans* and *A. niger* (**Figure 1C**; **Table 1**), as well as CWPs extracted from *A. flavus* and *A. parasiticus*, but not to other fungal preparations (**Table 1**). This probably reflects the ability of AP3 to detect an epitope that is conserved in the genus *Aspergillus* but absent in the other fungal genera tested in this experiment (**Table 1**).

Immunofluorescence microscopy showed that the antigen recognized by AP3 is located on the *Aspergillus* cell surface (**Figure 2**), particularly the hyphal walls and tips of the germination tubes in *A. parasiticus* (**Figure 2A**), *A. flavus* (**Figure 2B**), and *A. fumigatus* (**Supplemental Figures 1A,B**) compared to control samples (**Figures 2C,D**; **Supplemental Figures 1E,F**).

We next investigated the ability of mAb AP3 to bind extracellular antigens precipitated from the *A. flavus* culture supernatant (**Figure 3B**) and *A. fumigatus* spent culture medium (SD-Asp) (**Supplemental Figure 2A**) by immunoblot and ELISA. Compared to the protein-rich cell wall fraction (**Figure 3A**), the extracellular fraction contained mainly GM and small amounts of protein, hence no distinct protein band was observed in the Coomassie-stained gel (**Figure 3B**). The low protein content of the extracellular fraction was also confirmed by Bradford assay (data not shown). However, more sensitive immunoblot analysis revealed multiple undefined bands with molecular masses exceeding 70 kDa (**Figure 3B**), indicating that glycoantigens sharing the epitope recognized by AP3 are also present in the culture supernatant. The strong binding observed by direct-coating ELISA (**Figure 3C**; **Supplemental Figure 2A**) confirmed that the antigens detected by AP3 are present in both the culture supernatant and the *Aspergillus* cell wall.

Identification of the AP3 Antigen

The *Aspergillus* glycoproteins recognized by AP3 were identified by 2DE and mass spectrometry. The separation of young *A. flavus* CWPs by 2DE (**Figure 4**) revealed a wide range of protein spots with different molecular masses and pI values. However, only a small number of these proteins were detected by immunoblot with mAb AP3 as the probe (**Figures 4C,D**).

MS/MS analysis revealed five unique proteins in nine spots, indicating that some of the identified proteins were present in multiple spots, possibly due to different forms of post-translational modification (**Table 2**). Matching the protein sequences against the *A. flavus* NRRL3357 database identified *A. flavus* mycelial catalase, Hsp70, Hsp90, an amidase family protein, and a cell wall glucanase (**Table 2**). However, these proteins do not share any peptides or sequence similarities. *In silico* analysis revealed that the detected proteins have numerous acceptor sites for *N*-linked and/or *O*-linked glycosylation (**Table 2**). We therefore tested whether protein glycosylation might be necessary for antigen recognition by mAb AP3. The gene encoding the *A. flavus* mycelial catalase (XP_002380889.1) was produced in *E. coli* BL21 (DE3) cells. Immunoblot analysis revealed that mAb AP3 failed to detect the bacterial recombinant protein, whereas a histidine-specific antibody detected a distinct band with the expected molecular mass of *A. flavus* mycelial catalase (110 kDa) (**Supplemental Figure 3**). Because *E. coli* does not synthesize eukaryotic-type *N*-linked and *O*-linked glycans, the inability of AP3 to recognize the non-glycosylated mycelial catalase suggests that it binds a carbohydrate epitope present on certain *Aspergillus* glycoproteins or associated with the

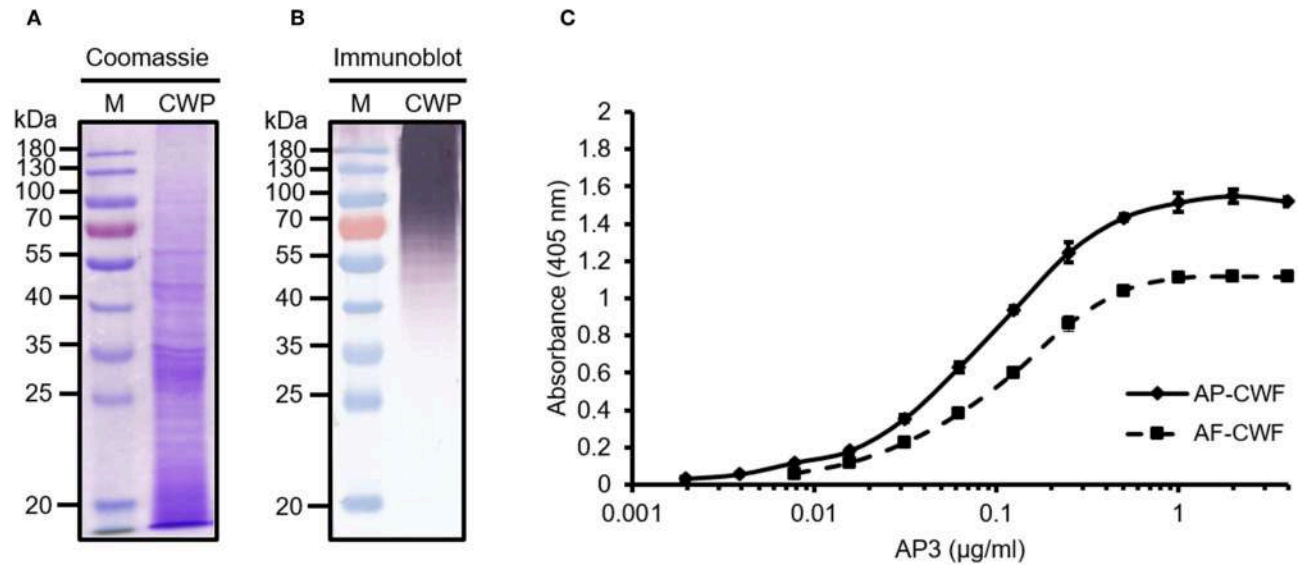

FIGURE 1 | Analysis of *A. flavus* cell wall proteins (CWPs) and the specific detection of cell wall fragments (CWFs) by ELISA using mAb AP3. Extracted CWPs were separated by SDS-PAGE and stained with **(A)** Coomassie Brilliant Blue or **(B)** transferred to a nitrocellulose membrane. Immunoblot detection was carried out using 200 µl culture supernatant from monoclonal hybridoma cell line AP3 and GAM^{AP} Fc (120 ng/ml) followed by visualization using NBT/BCIP. M: Pre-stained protein marker (Fermentas). **(C)** For the ELISA, 150 µg/ml CWFs from *A. flavus* (AF-CWF) and *A. parasiticus* (AP-CWF) were coated onto a microtiter plate. After blocking free binding sites with 3% (w/v) skimmed milk, bound antigens were detected using purified mAb AP3 (0.008–4 µg/ml) and an HRP-labeled goat anti-mouse Fc antibody (160 ng/ml). Absorbance was measured in triplicate after 15 min substrate incubation.

TABLE 1 | Cross-reactivity of mAb AP3 against CWFs from different fungal pathogens measured by ELISA.

Species	Source	Binding of mAb AP3
Aspergillus flavus Link:Fries	DSMZ 818	+++
Aspergillus parasiticus Speare	DSMZ 1300	+++
Aspergillus nidulans (Eidam) Winter	DSMZ 820	++
Aspergillus niger van Tieghem	IME	+
Fusarium oxysporum f. sp. *nicotianae*	IME	–
Fusarium culmorum W. G. Smith	IME	–
Phytophthora nicotianae	DSMZ 1828	–
Rhizoctonia solani Kühn	IME	–
Pythium ultimum Trow	DSMZ 62987	–
Botrytis cinerea Persoon:Fries	IME	–
Cercospora nicotianae	IME	–
Thielaviopsis basicola	IME	–

CWFs (150 µg/ml in water) were coated overnight at 37°C. After blocking free binding sites with 3% (w/v) skimmed milk, the bound antigen was detected using purified mAb AP3 (400 ng/ml). Antibody binding to fungal CWFs was confirmed by the addition of GAM^{HRP} Fc (1:5,000). Absorption at 405 nm was measured after 30 min incubation with the substrate ABTS. Cross-reactivity was determined based on the extinction levels after subtracting the background signal. DSMZ, German Collection of Microorganisms and Cell Cultures, Leibniz Institute, Braunschweig, Germany; IME, Fraunhofer IME, Aachen, Germany; –, $OD_{405\ nm} < 0.1$; +, $OD_{405\ nm} = 0.50–0.99$; ++, $OD_{405\ nm} = 1.00–1.49$; +++, $OD_{405\ nm} > 1.5$.

Aspergillus glycosylation pattern, as indicated by the immunoblot data (**Figures 1B**, **3**).

To determine whether AP3 recognizes a carbohydrate or a protein epitope, the CWPs and extracellular secreted antigens were treated with protease or periodate, to remove the protein component and to oxidize the glycans, respectively (**Figure 3**). No differences in immunoblot profiles were observed when we compared untreated controls with *A. flavus* CWPs (**Figure 3A**) and extracellular antigens (**Figure 3B**) digested with trypsin. This might reflect the location of trypsin cleavage sites toward the N-terminus of the target protein, resulting in minor mass changes, or proteolytic stability caused by the presence of glycans around the peptide backbone of the amino acids adjacent to the glycosylation site, thus preventing the contact between the glycoprotein surface and the protease active site (Sola and Gribenow, 2009). The epitope recognized by AP3 was found to be periodate sensitive ($p < 0.05$) and therefore most likely a carbohydrate (**Figure 3C**). Our results therefore demonstrate that AP3 recognizes an *Aspergillus* glycoantigen rather than a peptide or protein epitope. Furthermore, the smear-like staining observed for the extracellular fraction in the immunoblot suggests that most of the AP3 antigens are fragments of cell wall carbohydrate polymers.

Taken together, our data suggested that AP3 recognizes a major carbohydrate of the *Aspergillus* cell wall, which is homogenously distributed on the hyphal surface, found in a speckled pattern on swollen conidia, and not present on the surface of resting conidia. This pattern resembles that of GM (Heesemann et al., 2011) and we therefore tested the Gal*f*-deficient *A. fumigatus* mutant Δ*glfA* (Schmalhorst et al., 2008). Immunofluorescence microscopy revealed that the hyphae of the parental *A. fumigatus* strain D141 were completely stained (**Supplemental Figure 4A**), but AP3 did not bind to the Δ*glfA* mutant (**Supplemental Figures 1C,D**), indicating that Gal*f*

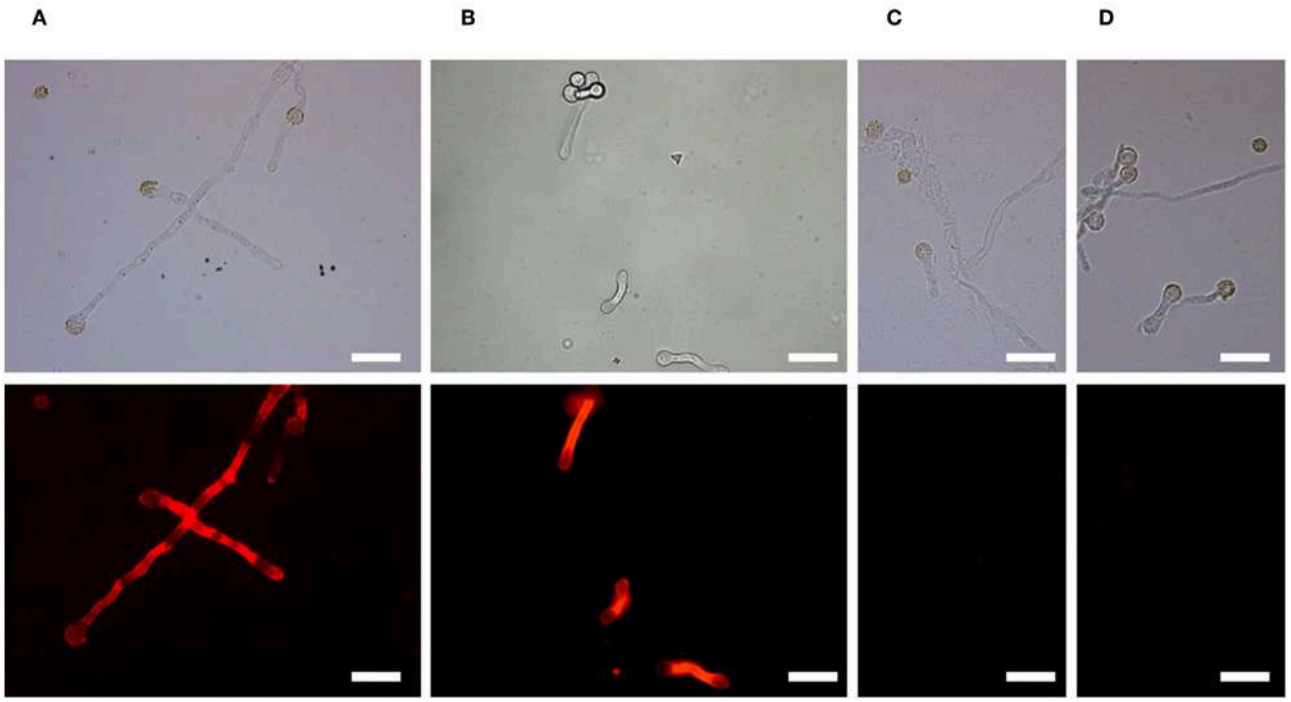

FIGURE 2 | Binding of mAb AP3 to *A. parasiticus* and *A. flavus* revealed by immunofluorescence microscopy. **(A)** *A. parasiticus*. **(B)** *A. flavus*. **(C)** *A. parasiticus* control. **(D)** *A. flavus* control. Mycelia were immobilized on glass coverslips and incubated with 200 μl hybridoma supernatant containing 25 μg/ml mAb AP3 or (Rasche et al., 2011; unrelated control). The binding of AP3 to its antigen was verified using GAM^{Dylight} 594 H + L (1.5 μg/ml). Antibody–antigen complexes were visualized under a Leica DMR fluorescence microscope. For comparison, light microscope images are shown above the immunofluorescence images. Scale bar = 50 μm.

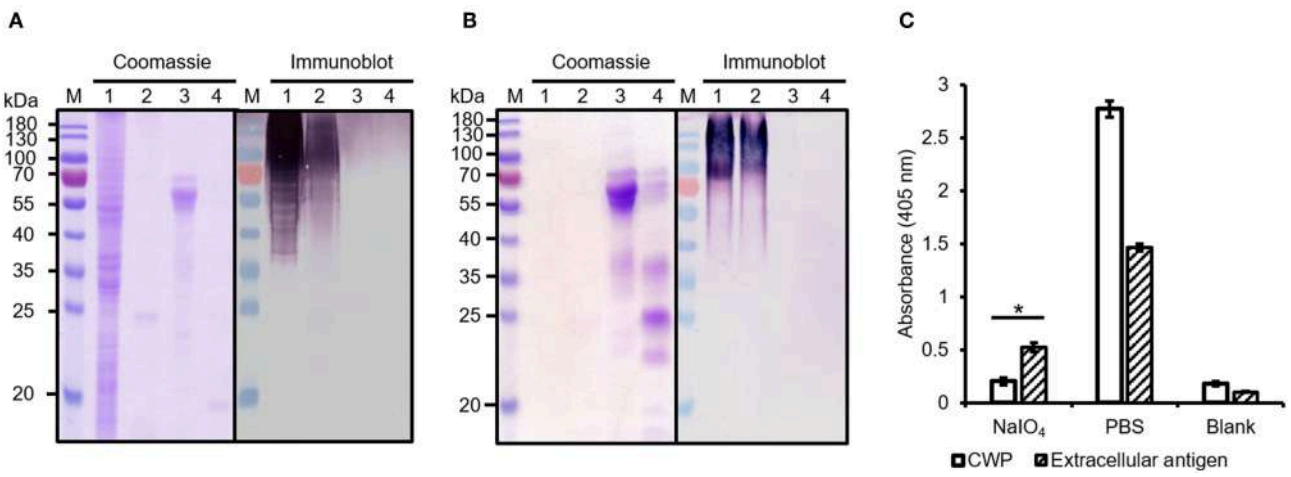

FIGURE 3 | Analysis of protease-treated and periodate-treated *Aspergillus* antigens. **(A)** Cell wall proteins and **(B)** extracellular secreted antigens of *A. flavus* were extracted and digested with trypsin. Fractions were separated by SDS-PAGE and stained with Coomassie Brilliant Blue. Proteins transferred to a nitrocellulose membrane were detected with a purified mAb AP3 (400 ng/ml) and an AP-labeled goat anti-mouse antibody (120 ng/ml) followed by NBT/BCIP substrate incubation. M: Protein marker (Fermentas); Lane 1: sample without trypsin treatment; 2: sample with trypsin; 3: control protein fetuin without trypsin treatment; 4: control protein fetuin with trypsin. **(C)** Prepared *A. flavus* cell wall proteins (CWPs) and extracellular antigens (40 μg/well) were coated onto a microtiter plate and oxidized with periodate (80 mM). Untreated preparations were used as controls. After blocking free binding sites with 3% (w/v) skimmed milk, bound antigens were detected with mAb AP3 (400 ng/ml) and an HRP-labeled goat anti-mouse Fc antibody (120 ng/ml). Absorbance was measured in triplicate after 20 min substrate incubation. Values represents means ± SD ($n = 3$) for treated ($NaIO_4$), untreated (PBS), and control (Blank). An asterisk denotes a statistically significant reduction in antigen binding between treated and untreated samples (CWF and extracellular antigen, $p < 0.05$).

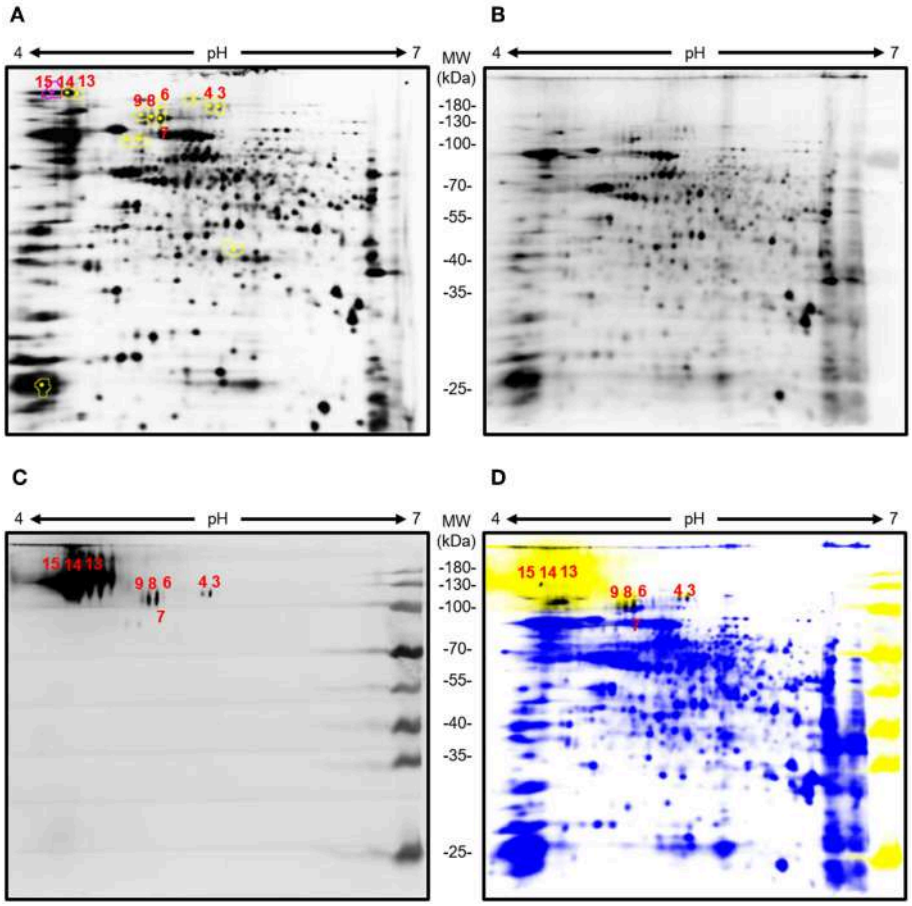

FIGURE 4 | Analysis of young *A. flavus* mycelia cell wall proteins by 2DE and immunoblot with AP3 as the detection antibody. Total *Aspergillus* mycelia and CWPs (100 μg) were labeled with Cy3 and separated in the first dimension on a 7-cm pH 4–7 immobilized pH gradient strip followed by separation in the second dimension by 12.5% (v/v) SDS-PAGE. Separated *Aspergillus* CWPs were transferred onto a nitrocellulose membrane. Immunoblot detection was carried out using purified mAb AP3 (400 ng/ml) and a goat anti-mouse Cy5-labeled antibody (120 ng/ml). Gels and membranes were scanned with an Ettan DIGE Imager equipped with appropriate filters for Cy3 and Cy5, and images were processed with DeCyder software v7.0. **(A)** Cy3 labeled 2D gel of young *A. flavus* proteins. **(B)** Cy3-labeled total CWPs blotted onto a membrane. **(C)** CWPs specifically detected by mAb AP3 visualized using a Cy5-labeled antibody. **(D)** Overlay of Cy3-labeled total CWPs (blue) and AP3-recognized CWPs (yellow). Shared protein spots are highlighted in black. Numbers indicate protein spots selected for analysis by mass spectrometry.

residues are part of the epitope. Moreover, the double-staining of *A. fumigatus* hyphae with AP3 (IgG) and the GM-specific antibody L10-1 (IgM) demonstrated that the staining patterns of both antibodies are similar (**Supplemental Figure 4**). This prompted us to analyze *Penicillium chrysogenum*, a non-pathogenic mold known to produce GM. AP3 decorated the hyphal surface of *P. chrysogenum* and additional material bound to the glass surface in close proximity to the hyphae (**Supplemental Figures 5A,B**). This staining pattern suggests that AP3 recognizes structurally identical GM antigens that are present on the surface of this fungus and partially released into the surrounding medium. We performed additional tests on culture supernatants derived from the *A. fumigatus* wild-type strain D141 and Δ*glfA* mutant for further characterization of AP3 by ELISA (**Figure 5**). Supernatants diluted 1:10 in PBS were coated onto the ELISA plate and probed with AP3, the GM-specific IgM L10-1, and AB135-8, an IgM that recognizes a Gal*f* antigen found prominently in the *Fusarium* cell wall but present in only limited amounts in the *Aspergillus* cell wall (Wiedemann et al., 2016). All three antibodies recognized their antigen in the culture supernatant of the wild-type strain, but not in the supernatant of the Δ*glfA* mutant (**Figure 5**). Similar results were observed for AP3 and L10-1 at a dilution of 1:100 (**Supplemental Figure 2A**).

Antibody-Based GM Detection and Specificity of mAb AP3

We next investigated whether AP3 and L10-1 (Heesemann et al., 2011) can cooperate to bind the soluble fungal-type GM of *A. fumigatus* (SD-Asp) (**Supplemental Figure 2B**), *A. flavus* extracellular antigens, and *A. flavus* cell wall proteins (AF-CWPs) (**Supplemental Figures 2C,D**). We therefore carried out a sandwich ELISA in which AP3 was the capture reagent and L10-1 the detection reagent or vice versa, and the detection reagent was in turn bound by an HRP-labeled anti-mouse isotype-specific secondary antibody. As shown in **Supplemental Figures 2B,D**, L10 detected all tested Gal*f*-containing antigens that were captured by AP3. Similarly, AP3 recognized CWPs immobilized

TABLE 2 | List of *Aspergillus* proteins detected by mAb AP3.

Spot no.	Short name	Protein	NCBI reference sequence	MW (kDa)	pI[a]	Score[b]	Peptides[c]	Sequence coverage (%)	Signal peptide[d]	*N*-glycan acceptor sites[e]	*O*-glycan acceptor sites[f]	Cellular localization	Function[g]
3	Catalase	Mycelial catalase cat1	XP_002380889.1	79.8	5.34	398	18 (13)	21	Yes	4	24	Extracellular (cell wall)	Cell protection (Paris et al., 2003)
4						373	14 (9)	17					
6	Hsp70	Hsp70 chaperone Hsp88	XP_002381416.1	79.8	5.02	680	32 (23)	34	No	3	3	Intracellular	Protein folding (Teutschbein et al., 2010)
8						331	16 (10)	19					
7	Hsp90	Molecular chaperone and allergen Mod-E/Hsp90/Hsp1	XP_002382894.1	79.6	4.97	405	13 (10)	20	No	4	8	Intracellular (cytosolic, cell wall)	Protein folding (Lamoth et al., 2012, 2014, 2016)
9	Amidase	Amidase family protein	XP_002377652.1	60.7	5.22	276	11 (7)	22	Yes	7	9	Extracellular	Unknown
13	Glucanase	Cell wall glucanase (Scw11), putative	XP_002372749.1	61.8	4.63	155	6 (4)	10	Yes	0	122	Extracellular (cell wall)	Cell wall remodeling (Mouyna et al., 2013)
14						262	10 (6)	15					
15						187	8 (5)	11					

Protein spots were identified by Tandem mass spectrometry and protein sequences were analyzed in silico using the A. flavus NRRL3357 reference database.

[a] *Predicted Mw and pI by ExPASy Compute pI/Mw tool.*

[b] *Protein score in Mascot Search.*

[c] *Number of total identified peptides/unique peptides.*

[d] *Predicted signal peptide (ProP 1.0).*

[e] *Predicted N-glycosylation sites (NetNGlyc1.0).*

[f] *Predicted O-glycosylation sites (NetOGlyc4.0).*

[g] *Reference.*

FIGURE 5 | Detection of *A. fumigatus* D141 GM and Δ*glfA* supernatant by ELISA. Culture supernatants from *A. fumigatus* Δ*glfA* and wild-type D141 strains were coated (1:10) onto a microtiter plate. GM was detected using 400 ng/ml purified mAb AP3 or 400 ng/ml of the IgMs L10-1 and AB135-8, which recognize distinct Gal*f*-dependent antigens, followed by isotype-specific antibodies labeled with HRP. Data are means ± SD ($n = 3$). An asterisk denotes a statistically significant difference in antigen binding between the D141 and Δ*glfA* strain ($p < 0.005$).

on the solid phase by L10-1. However, the extracellular antigens of *A. flavus* were not captured by L10-1 antigens (**Figure 2C**). Given the diverse structures of Gal*f*-antigens in *Aspergillus* species, these results provide further evidence that AP3 recognizes a defined Gal*f* epitope that may differ slightly from that recognized by L10-1. Moreover, these findings suggest that mAb AP3 detects a Gal*f* epitope that is present less frequently in extracellular *Aspergillus* antigens compared to CWPs from *A. flavus*.

GM is the most important immunological biomarker of invasive aspergillosis (IA). Therefore, the ability of AP3 to detect *Aspergillus* GM in serum was compared to the Gal*f*-specific IgM L10-1 (**Figure 6**). In a sandwich ELISA format, AP3, and L10-1 were coated onto the ELISA plate. After incubation with the positive control serum, the wells were incubated with HRP-labeled EB-A2 (a Gal*f*-specific IgM antibody) according to the procedure of the Platelia *Aspergillus* EIA. As shown in **Figure 6**, AP3 generated significantly ($p < 0.05$) stronger signals than L10-1, which demonstrates the potential of AP3 as a candidate diagnostic antibody for IA.

The epitope specificity of mAb AP3 was investigated using a library of 13 synthetic oligosaccharides representing distinct fragments of *Aspergillus* GM (Argunov et al., 2015, 2016; Krylov et al., 2018a), differing in length and in the nature of the linkages between monosaccharide residues (**Figure 7A**). AP3 showed the highest affinity ($p < 0.05$) for heptamer **13**, which contains a hexameric block of β-1,5-linked Gal*f* residues (**Figure 7B**), and lower affinity for pentamers **10** and **11**, containing four β-1,5-Gal*f*

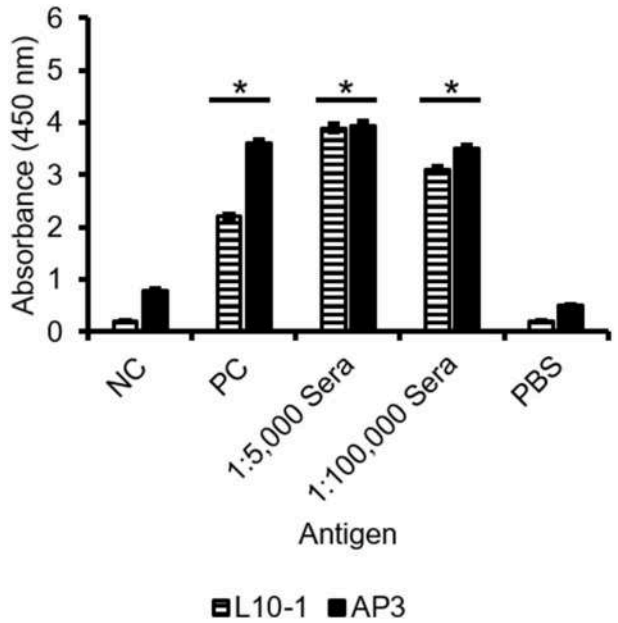

FIGURE 6 | Detection of GM in sera by sandwich ELISA using GM-specific antibodies. Microtiter plates were coated with 400 ng/ml purified mAb AP3 and L10-1. After blocking free binding sites with 3% (w/v) skimmed milk, sera diluted 1:5,000 or 1:100,000 were applied and detected using the EB-A2 conjugate. The signal was measured in triplicate at 450 nm after 20 min substrate incubation (ABTS). PC: *Aspergillus*-positive control serum from the Platelia *Aspergillus* EIA. NC: negative control serum from the Platelia *Aspergillus* EIA. PBS: negative control. An asterisk denotes a statistically significant difference in antigen binding relative to the NC control serum ($p < 0.005$).

units linked to a terminal Man*p* residue via β-1,6 or β-1,3 bonds. There was no affinity for pentamer **12** with β-1,6 linkages between Gal*f* residues, representing structures recently discovered in *A. fumigatus* GM (Kudoh et al., 2015; Krylov et al., 2018a), nor for trimer **6**, comprising three β-1,5-Gal*f* units. Taken together, these data indicate show that AP3 binds specifically to a tetramer of β-1,5-Gal*f* units present in *Aspergillus* GM and Gal*f*-containing *Aspergillus* glycoproteins. The binding of AP3 to *P. chrysogenum* indicates the presence of an identical structure in this species (**Supplemental Figure 5**).

DISCUSSION

Identification of the Epitope Recognized by mAb AP3

The fungal cell wall is a complex and dynamic structure that provides protection and mediates interactions with the environment. Detailed investigations of the composition and biosynthesis of the *A. fumigatus* cell wall have identified carbohydrates, such as chitin, glucans, and GM as major structural components. The cell wall is adorned with CWPs that can be attached to the plasma membrane by glycosylphosphatidylinositol (GPI) anchors or linked to glucan structures, thus facilitating the wall's structural organization (Bernard and Latgé, 2001; Bruneau et al., 2001).

In this study, we report the generation of mAb AP3 using *A. parasiticus* CWFs comprising a complex mixture of different antigens, and the characterization of its antigen specificity. The diversity, abundance and accessibility of potential antigens makes it challenging to identify the precise epitope (Schubert et al., 2018). The proteome and metabolome of *Aspergillus* spp. are highly dependent on the growth conditions, particularly stress-induced changes which are known to affect protein expression, cell wall composition, the production of secondary metabolites (Imanaka et al., 2010; Champer et al., 2016), and the abundance, chain length and composition of GM (Kudoh et al., 2015). The identification the epitope recognized by AP3 is also hampered by our use of different *Aspergillus* strains and cultivation conditions in different laboratory environments.

Despite the challenges described above, the specificity of mAb AP3 was confirmed in well-controlled replicate experiments using different *Aspergillus* strains and antigen compositions, leading to the successful localization and identification of the epitope. Indirect detection methods, such as ELISAs and deglycosylation assays indicated that AP3 detects substantial parts of a glycoantigen which is secreted into the culture medium, bound to the cell surface, and located on *Aspergillus* proteins. Importantly, immunofluorescence microscopy using the *Aspergillus* Δ*glfA* mutant strain, which is unable to synthesize Gal*f* residues (Schmalhorst et al., 2008), indicated that the epitope recognized by AP3 contains Gal*f* as a key constituent.

The *Aspergillus* proteins recognized by the antibody AP3 were identified by a combination of 2DE and mass spectrometry. Although we cannot be certain which of the proteins identified in the same spot was recognized by AP3, MS/MS analysis revealed that the antibody bound up to five distinct *Aspergillus* proteins that did not share any amino acid sequence similarity but carried multiple acceptor sites for *N*-linked and/or *O*-linked glycans, suggesting they are heavily glycosylated. The abundant glycosylation may explain the detection of these proteins in 2D gels at a higher molecular weights (>70 kDa) than expected. With the exception of Hsp70 and Hsp90, these glycoproteins carry a signal peptide causing them to be localized either in the cell wall (such as cell wall glucanase and amidase) or extracellular space (such as the mycelial catalase Cat1). Although Hsp90 is normally a cytosolic protein, it can travel to the fungal cell wall and regulate cell wall integrity (Lamoth et al., 2016). The lack of *N*-glycan acceptor sites and the very high number of potential *O*-glycosylation sites (122) in the cell wall glucanase, together with the strong fluorescence signal in the immunoblot (spots 13, 14, and 15) (**Figure 4C**), suggests that the AP3 antibody binds mainly to Gal*f* residues attached to *O*-linked glycan chains. Accordingly, the treatment of extracellular *Aspergillus* antigen and *A. flavus* CWPs with PNGase F did not affect the binding of mAb AP3, confirming that the signal was not associated with individual β-1,2-linked or α-1,2-linked Gal*f* residues attached to *N*-linked glycans and that AP3 binding was probably restricted to either β-1,5-linked or β-1,6-linked *O*-glycans and fungal-type GM (Komachi et al., 2013).

Finally, the direct glycoarray which uses 13 synthetic Gal*f* oligosaccharides resolved the linkage and length of the Gal*f* epitope detected by mAb AP3. These results provide a clear

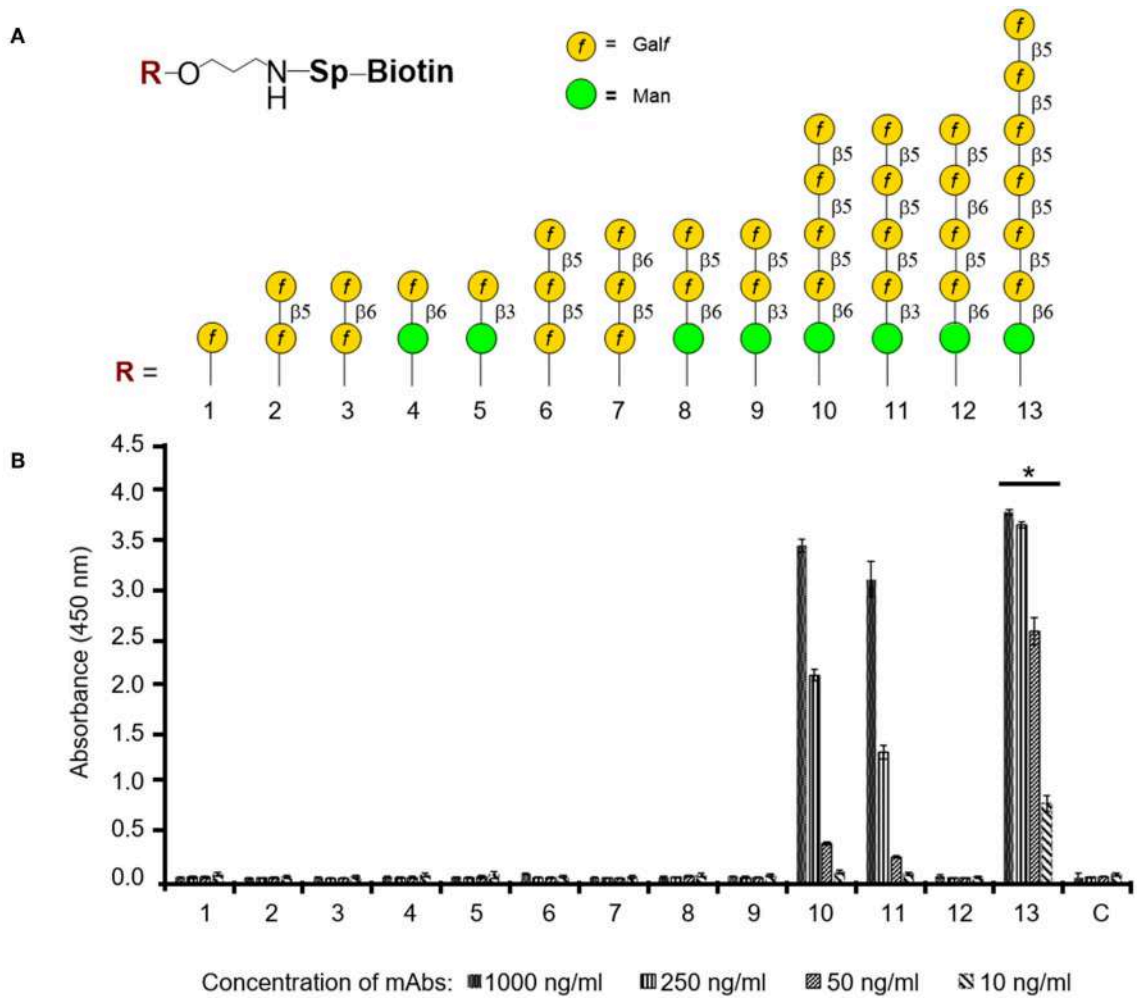

FIGURE 7 | ELISA to determine the oligosaccharide specificity of mAb AP3. **(A)** Composition of thematic glycoarray oligosaccharide ligands representing key structural elements of GM. The carbohydrate sequences are represented as previously reported (Varki et al., 2009). **(B)** Carbohydrate specificity of antibody AP3. Biotin-tagged oligosaccharides 1–13 were applied to a streptavidin-coated microtiter plate and detected with mAb AP3 (1,000, 250, 50, and 10 ng/ml) and anti-mouse IgG HRP conjugate followed by TMB substrate incubation. All measurements were taken twice in triplicate. Asterisk denotes the statistically significant difference in binding between AP3 and heptamer 13 compared to pentamers 10 and 11 ($p < 0.05$).

line of evidence that the Gal*f* pattern recognized by AP3 is characterized by a β-1,5-Gal*f* tetramer, whereas shorter oligosaccharides including a β-1,5-Gal*f* trimer are not detected. Interestingly, the replacement of the third β-1,5 Gal*f* unit with β-1,6 Gal*f* in the tetramer (oligosaccharide 12) destroys the antigen entirely. Therefore, the specificity of mAb AP3 is restricted to Gal*f*-containing structures in *Aspergillus* fungal-type GM and *O*-linked glycans ($[\beta\text{-D-Gal}f\text{-}1,5]_4$), whereas *N*-glycans containing Gal*f* (α-1,2 Gal*f*) and Gal*f*-containing glycosphingolipids (β-1,2 and or β-1,6 Gal*f*) are not detected (Latge, 2009; Tefsen et al., 2012).

Specificity of mAb AP3 Compared to Other Gal*f*-Specific Antibodies

Carbohydrates, such as GM and abundant immunodominant glycoproteins, often provide excellent biomarkers for fungal diseases because they are conserved among related species of fungi (Thornton and Wills, 2015). For example, *A. flavus* and *A. fumigatus* galactomannoproteins are recommended as biomarkers for the serological diagnosis of IA (Chan et al., 2002; Woo et al., 2003; Chong et al., 2004). Consequently, several GM-specific antibodies have already been developed for IA diagnostics, but thus far most of these antibodies belong to the IgM subclass (Thornton, 2010).

The IgM EB-A2 (Stynen et al., 1992) is the best-characterized Gal*f*-specific antibody used for the diagnosis of IA and has been regarded as the gold standard for more than 20 years. It is supplied as part of Bio-Rad's commercial Platelia *Aspergillus* EIA kit, which has been validated in several clinical studies and is approved by the FDA (Pfeiffer et al., 2006). Early epitope characterization studies suggested that EB-E2 recognized a tetramer of at least four β-1,5-linked Gal*f* moieties in *Aspergillus* GM, present in the cell wall and in glycoproteins (Stynen et al., 1992; Kudoh et al., 2015). However, a glycoarray was recently

used to reinvestigate the oligosaccharide specificity of EB-A2, revealing that it also detects dimers and trimers with β-1,6 linkages (Krylov et al., 2019). This could explain the observed cross-reactivity between EB-A2 and non-*Aspergillus* fungi, contaminating GM in β-lactam antibiotics and foodstuffs, the cancer prodrug cyclophosphamide, and several other bacterial antigens, such as *Cryptococcus* galactoxylomannan (Dalle et al., 2005), which can generate false-positive results (Viscoli et al., 2004; Aubry et al., 2006; Zandijk et al., 2008).

Both EB-A2 and AP3 can also bind *Penicillium* spp., reflecting the presence of identical Gal*f* epitopes in these species (Unkefer and Gander, 1979). Cross-reactivity has also been reported between EB-A2 and *Fusarium* GM (Tortorano et al., 2012). Interestingly, we observed no cross-reactivity between AP3 and *F. oxysporum* Gal*f*-containing antigen preparations, which comprise β-1,6-linked β-D-Gal*f* residues with multiple side chains (Chen et al., 2015). This suggests that AP3 has a greater specificity for *Aspergillus* GM than EB-A2. AP3 was unable to detect lipoteichoic acid (LTA), a bacterial membrane polysaccharide substituted with β-1,5-linked D-Gal*f* residues (data not shown). We cannot exclude the possibility that AP3 binds to other fungi and bacteria, as well as cross-reacting antigens, such as LTA from *Bifidobacter* spp., but the specificity of AP3 for longer Gal*f* chains may reduce the likelihood of cross-reaction to other epitopes.

More recently, two novel Gal*f*-specific antibodies have been generated by immunizing mice with the synthetic pentasaccharide β-D-Gal*f*-1,5-[β-D-Gal*f*-1,5]$_3$-α-D-Man*p*: mAb 7B8, which specifically recognizes the Gal*f* trimer, and mAb 8G4, which mainly detects the parental Gal*f* tetramer (Matveev et al., 2018). These are IgG antibodies like AP3 and they likewise detect defined Gal*f* epitopes located on the *Aspergillus* cell wall and glycoproteins as well as the secreted GM of several *Aspergillus* species. Neither 7B8 nor 8G4 react with *Bifidobacterium longum* and show less cross reactivity than EB-A2 (Mennink-Kersten et al., 2005). In contrast to AP3, 7B5, and 8G4 also recognize a shorter Gal*f* trimer ([β-D-Gal*f*-1,5]$_3$) and a Gal*f*-dimer with a β-1,6 Gal*f* linkage (Matveev et al., 2018).

Potential Applications of mAb AP3

In this study, we tested for the first time the potential of different Gal*f*-specific antibodies (EB-A2, L10-1, and AP3) to cooperate in the detection of Gal*f*-containing structures on AF-CWPs and *Aspergillus* GM. Interestingly, AP3 was unable to detect *Aspergillus* GM/EPS when used as the capture or detection reagent in a DAS-ELISA, whereas AF-CWPs were detected (data not shown). This is remarkable because detailed analysis of the EB-A2 antigen showed that GM contains more than 10 Gal*f* epitopes, making it possible to develop a DAS-ELISA with the GM-specific antibody acting as both the capture and detection antibodies (Stynen et al., 1992). AP3 can cooperate with L-10 and EB-A2 to detect AF-CWP and *Aspergillus* GM. However, *Aspergillus* GM could be not detected by an AP3 capture reagent with L10-1 as the detection antibody, although the reciprocal configuration was successful. The epitope detected by L10-1 has yet to be identified, so it is possible that L10-1 blocks the epitope detected by AP3 in this setup.

The glycosylation profiles of the proteins identified by 2DE were not analyzed in detail, but we speculate that the Gal*f*-epitope detected by AP3 is probably less abundant in secreted GM than CWPs, given that several such epitopes are accessible on the CWPs of *A. flavus*. The limited number of proteins specifically detected by AP3 in 2DE experiments, and the differential recognition of Gal*f*-containing epitopes by ELISA, suggest that the epitope is present on a limited number of Gal*f*-containing proteins and differs in this respect from the epitope recognized by L10-1 and EB-A2, thus making this antibody valuable for the detection of *Aspergillus* spp.

The unique ability of AP3 to bind Gal*f* oligosaccharides comprising four or more residues with β-1,5-linkages makes this antibody an ideal candidate for the detection of *Aspergillus* GM with higher sensitivity and specificity than current diagnostic reagents. It could also be used to monitor the distribution of long-chain Gal*f* oligosaccharides on fungal cell walls in combination with antibodies that recognize shorter oligosaccharide chains. Further studies are needed to validate the potential of AP3 and different Gal*f*-specific antibodies as a platform for the rapid analysis of galactofuranosylation and to distinguish between Gal*f*-containing structures on glycoproteins and fungal-type GM.

Compared to GM-specific and Gal*f*-specific IgMs, the greater stability and specificity of affinity-matured IgG antibodies, such as AP3, 7B8, and 8G4 may allow the development of novel detection assays for *Aspergillus* infections. Accordingly, the specificity of mAb AP3 for long-chain β-1,5 Gal*f* and its successful detection of GM in human serum demonstrates its value as a diagnostic tool. Although further evaluation of the AP3 sandwich assay is necessary with a larger number of patients, we have demonstrated the potential of AP3 for the rapid and sensitive diagnosis of IA.

In addition, the greater stability and reactivity of AP3 compared to IgM-based reagents could be advantageous in applications that involve the molecular imaging of *Aspergillus* infections *in vivo* (Rolle et al., 2016). The development of an IgG-based reagent could also provide therapeutic benefits (Di Mambro et al., 2019). For example, a β-glucan-specific IgG2b subtype antibody protected mice against infections with *Candida albicans*, whereas the corresponding IgM with an identical complementarity determining region did not (Torosantucci et al., 2009). The Gal*f*-specific IgM L10-1 did not confer a protective effect during an *A. fumigatus* infection (Heesemann et al., 2011). The recognition of *A. fumigatus* hyphae by the Fcγ receptor was shown to be necessary for opsonization (Gazendam et al., 2016). More recently, a humanized IgG targeting the *Crf* cell wall transglycosylase of *A. fumigatus* reduced the fungal burden in a neutropenic rat model (Chauvin et al., 2019). Therefore, mAb AP3 could also be developed as a therapeutic modality to recruit phagocytes to extracellular *Aspergillus* germ tubes, thus curing *Aspergillus* infections.

CONCLUSION

AP3 is an IgG that recognizes *Aspergillus* Gal*f*-containing epitopes of four or more residues. It was generated by the immunization of mice with *A. parasiticus* CWFs and the subsequent production of hybridoma lines. The epitope detected by mAb AP3 is present in fungal-type GM and *O*-linked glycans on several *Aspergillus* glycoproteins. The carbohydrate specificity of AP3 was assessed using a thematic glycoarray comprising a series of synthetic oligosaccharide ligands structurally related to *Aspergillus* GM. Our data suggest that AP3 recognizes a β-1,5 Gal*f* tetramer that differs from the epitopes recognized by other GM/Gal*f*-specific mAbs. However, AP3 can also cooperate with other Gal*f*-specific mAbs to identify secreted GM and cell wall-associated glycoproteins in *Aspergillus* detection assays. In this context, AP3 could be developed as a valuable tool for *Aspergillus* cell wall and protein glycosylation studies, to screen crops for *Aspergillus* infection, and to diagnose IA with a lower risk of false positives.

DATA AVAILABILITY

The raw data supporting the conclusions of this manuscript will be made available by the authors, without undue reservation, to any qualified researcher.

ETHICS STATEMENT

All animal experiments were approved by the Landesamt für Natur, Umwelt und Verbraucherschutz Nordrhein-Westfalen (LANUV), reference number 8.87.-51.05.30.10.077. All animals received humane care according to the requirements of the German Tierschutzgesetz, §8 Abs. 1 and the Guide for the Care and Use of Laboratory Animals published by the National Institutes of Health.

AUTHOR CONTRIBUTIONS

MS, SS, GN, NN, and FE contributed to the conception and design of the study. MS, SX, AV, IC, VK, and NN performed the research and analyzed data. MS, SX, and AV helped with microscopy and ELISA experiments. IC and SX contributed with the 2DE experiments and mass spectrometry. VK and NN performed the glycoarray analysis. NN, FE, GN, and SS acquired funding. MS, SX, and NN prepared the original draft. All authors contributed to manuscript revision, read, and approved the submitted version.

FUNDING

This work was funded by the Sino-German (CSC-DAAD) Postdoc Scholarship Program, Russian Science Foundation (grant 19-73-30017), and BMBF grant no. FKZ 031A284A, FKZ 50739422, and FKZ 54364828.

ACKNOWLEDGMENTS

We would like to thank Denise Herwartz, Katrin Hauten, and Dr. Nicole Raven for the production and maintenance of the hybridoma cell line AP3 and Dr. Stefan Rasche for the purification of mAb AP3. We were grateful to Marcel Houdelet, Matthias Berens, and Tannaz Goodarzi for the production of recombinant *Aspergillus* catalase and the testing of mAb AP3, Dr. Françoise Routier for the Δ*glfA* mutant, and Dr. Richard M. Twyman for editorial assistance.

SUPPLEMENTARY MATERIAL

The Supplementary Material for this article can be found online at: https://www.frontiersin.org/articles/10.3389/fcimb.2019.00234/full#supplementary-material

REFERENCES

Argunov, D. A., Krylov, V. B., and Nifantiev, N. E. (2015). Convergent synthesis of isomeric heterosaccharides related to the fragments of galactomannan from *Aspergillus fumigatus*. *Org. Biomol. Chem*. 13, 3255–3267. doi: 10.1039/c4ob02634a

Argunov, D. A., Krylov, V. B., and Nifantiev, N. E. (2016). The use of pyranoside-into-furanoside rearrangement and controlled o(5) –> o(6) benzoyl migration as the basis of a synthetic strategy to assemble (1–>5)- and (1–>6)-linked galactofuranosyl chains. *Org. Lett*. 18, 5504–5507. doi: 10.1021/acs.orglett.6b02735

Aubry, A., Porcher, R., Bottero, J., Touratier, S., Leblanc, T., Brethon, B., et al. (2006). Occurrence and kinetics of false-positive *Aspergillus* galactomannan test results following treatment with β-lactam antibiotics in patients with hematological disorders. *J. Clin. Microbiol*. 44, 389–394. doi: 10.1128/JCM.44.2.389-394.2006

Bernard, M., and Latgé, J.-P. (2001). *Aspergillus fumigatus* cell wall: composition and biosynthesis. *Med. Mycol*. 39, 9–17. doi: 10.1080/mmy.39.1.9.17

Biesebeke, R. T., and Record, E. (2008). Scientific advances with *Aspergillus* species that are used for food and biotech applications. *Microbes Environ*. 23, 177–181. doi: 10.1264/jsme2.23.177

Bruneau, J. M., Magnin, T., Tagat, E., Legrand, R., Bernard, M., Diaquin, M., et al. (2001). Proteome analysis of *Aspergillus fumigatus* identifies glycosylphosphatidylinositol-anchored proteins associated to the cell wall biosynthesis. *Electrophoresis* 22, 2812–2823. doi: 10.1002/1522-2683(200108)22:13<2812::aid-elps2812>3.0.co;2-q

Champer, J., Ito, J. I., Clemons, K. V., Stevens, D. A., and Kalkum, M. (2016). Proteomic analysis of pathogenic fungi reveals highly expressed conserved cell wall proteins. *J. Fungi* 2:6. doi: 10.3390/jof2010006

Chan, C. M., Woo, P. C., Leung, A. S., Lau, S. K., Che, X. Y., Cao, L., et al. (2002). Detection of antibodies specific to an antigenic cell wall galactomannoprotein for serodiagnosis of *Aspergillus fumigatus* aspergillosis. *J. Clin. Microbiol*. 40, 2041–2045. doi: 10.1128/JCM.40.6.2041-2045.2002

Chauvin, D., Hust, M., Schütte, M., Chesnay, A., Parent, C., Moreira, G. M. S. G., et al. (2019). Targeting *Aspergillus fumigatus* crf transglycosylases with neutralizing antibody is relevant but not sufficient to erase fungal burden in a neutropenic rat model. *Front. Microbiol*. 10:600. doi: 10.3389/fmicb.2019.00600

Chen, Y. L., Mao, W. J., Tao, H. W., Zhu, W. M., Yan, M. X., Liu, X., et al. (2015). Preparation and characterization of a novel extracellular polysaccharide with antioxidant activity, from the mangrove-associated fungus *Fusarium oxysporum*. *Mar. Biotechnol*. 17, 219–228. doi: 10.1007/s10126-015-9611-6

Chong, K. T., Woo, P. C., Lau, S. K., Huang, Y., and Yuen, K. Y. (2004). AFMP2 encodes a novel immunogenic protein of the antigenic mannoprotein superfamily in *Aspergillus fumigatus*. *J. Clin. Microbiol*. 42, 2287–2291. doi: 10.1128/JCM.42.5.2287-2291.2004

Dalle, F., Charles, P. E., Blanc, K., Caillot, D., Chavanet, P., Dromer, F., et al. (2005). *Cryptococcus neoformans* galactoxylomannan contains an epitope(s) that is cross-reactive with *Aspergillus* galactomannan. *J. Clin. Microbiol.* 43, 2929–2931. doi: 10.1128/jcm.43.6.2929-2931.2005

Di Mambro, T., Guerriero, I., Aurisicchio, L., Magnani, M., and Marra, E. (2019). The yin and yang of current antifungal therapeutic strategies: how can we harness our natural defenses? *Front. Pharmacol.* 10:80. doi: 10.3389/fphar.2019.00080

Fairbanks, G., Steck, T. L., and Wallach, D. F. H. (1971). Electrophoretic analysis of the major polypeptides of the human erythrocyte membrane. *Biochemistry* 10, 2606–2617. doi: 10.1021/bi00789a030

Gazendam, R. P., Van Hamme, J. L., Tool, A. T., Hoogenboezem, M., Van Den Berg, J. M., Prins, J. M., et al. (2016). Human neutrophils use different mechanisms to kill *Aspergillus fumigatus* conidia and hyphae: evidence from phagocyte defects. *J. Immunol.* 196, 1272–1283. doi: 10.4049/jimmunol.1501811

Hao, W., Pan, Y.-X., Ding, Y.-Q., Xiao, S., Yin, K., Wang, Y.-D., et al. (2008). Well-characterized monoclonal antibodies against cell wall antigen of *Aspergillus* species improve immunoassay specificity and sensitivity. *Clin. Vaccine Immunol.* 15, 194–202. doi: 10.1128/CVI.00362-07

Hedayati, M. T., Pasqualotto, A. C., Warn, P. A., Bowyer, P., and Denning, D. W. (2007). *Aspergillus flavus*: human pathogen, allergen and mycotoxin producer. *Microbiology* 153, 1677–1692. doi: 10.1099/mic.0.2007/007641-0

Heesemann, L., Kotz, A., Echtenacher, B., Broniszewska, M., Routier, F., Hoffmann, P., et al. (2011). Studies on galactofuranose-containing glycostructures of the pathogenic mold *Aspergillus fumigatus*. *Int. J. Med. Microbiol.* 301, 523–530. doi: 10.1016/j.ijmm.2011.02.003

Horn, R., Chudobova, I., Hansel, U., Herwartz, D., Koskull-Doring, P., and Schillberg, S. (2013). Simultaneous treatment with tebuconazole and abscisic acid induces drought and salinity stress tolerance in *Arabidopsis thaliana* by maintaining key plastid protein levels. *J. Proteome. Res.* 12, 1266–1281. doi: 10.1021/pr300931u

Imanaka, H., Tanaka, S., Feng, B., Imamura, K., and Nakanishi, K. (2010). Cultivation characteristics and gene expression profiles of *Aspergillus oryzae* by membrane-surface liquid culture, shaking-flask culture, and agar-plate culture. *J. Biosci. Bioeng.* 109, 267–273. doi: 10.1016/j.jbiosc.2009.09.004

Komachi, Y., Hatakeyama, S., Motomatsu, H., Futagami, T., Kizjakina, K., Sobrado, P., et al. (2013). GfsA encodes a novel galactofuranosyltransferase involved in biosynthesis of galactofuranose antigen of *O*-glycan in *Aspergillus nidulans* and *Aspergillus fumigatus*. *Mol. Microbiol.* 90, 1054–1073. doi: 10.1111/mmi.12416

Krishnan, S., Manavathu, E. K., and Chandrasekar, P. H. (2009). *Aspergillus flavus*: an emerging non-fumigatus *Aspergillus* species of significance. *Mycoses* 52, 206–222. doi: 10.1111/j.1439-0507.2008.01642.x

Krylov, V. B., Argunov, D. A., Solovev, A. S., Petruk, M. I., Gerbst, A. G., Dmitrenok, A. S., et al. (2018a). Synthesis of oligosaccharides related to galactomannans from *Aspergillus fumigatus* and their NMR spectral data. *Org. Biomol. Chem.* 16, 1188–1199. doi: 10.1039/c7ob02734f

Krylov, V. B., Petruk, M. I., Grigoryev, I. V., Lebedin, Y. S., Glushko, N. I., Khaldeeva, E. V., et al. (2018b). Study of the carbohydrate specificity of antibodies against *Aspergillus fumigatus* using the library of synthetic mycoantigens. *Russ. J. Bioorg. Chem.* 44, 80–89. doi: 10.1134/s1068162017060073

Krylov, V. B., Solovev, A. S., Argunov, D. A., Latgé, J.-P., and Nifantiev, N. E. (2019). Reinvestigation of carbohydrate specificity of EB-A2 monoclonal antibody used in the immune detection of *Aspergillus fumigatus* galactomannan. *Heliyon* 5:e01173. doi: 10.1016/j.heliyon.2019.e01173

Kudoh, A., Okawa, Y., and Shibata, N. (2015). Significant structural change in both *O*- and *N*-linked carbohydrate moieties of the antigenic galactomannan from *Aspergillus fumigatus* grown under different culture conditions. *Glycobiology* 25, 74–87. doi: 10.1093/glycob/cwu091

Kumar, A., and Shukla, P. K. (2015). A monoclonal antibody against glycoproteins of *Aspergillus fumigatus* shows anti-adhesive potential. *Microb. Pathog.* 79, 24–30. doi: 10.1016/j.micpath.2015.01.003

Kurup, V. P., and Banerjee, B. (2000). Fungal allergens and peptide epitopes. *Peptides* 21, 589–599. doi: 10.1016/S0196-9781(00)00181-9

Lamoth, F., Juvvadi, P. R., Fortwendel, J. R., and Steinbach, W. J. (2012). Heat shock protein 90 is required for conidiation and cell wall integrity in *Aspergillus fumigatus*. *Eukaryot. Cell.* 11, 1324–1332. doi: 10.1128/EC.00032-12

Lamoth, F., Juvvadi, P. R., Gehrke, C., Asfaw, Y. G., and Steinbach, W. J. (2014). Transcriptional activation of heat shock protein 90 mediated via a proximal promoter region as trigger of caspofungin resistance in *Aspergillus fumigatus*. *J. Infect. Dis.* 209, 473–481. doi: 10.1093/infdis/jit530

Lamoth, F., Juvvadi, P. R., and Steinbach, W. J. (2016). Heat shock protein 90 (Hsp90): a novel antifungal target against *Aspergillus fumigatus*. *Crit. Rev. Microbiol.* 42, 310–321. doi: 10.3109/1040841x.2014.947239

Latge, J. P. (2009). Galactofuranose containing molecules in *Aspergillus fumigatus*. *Med. Mycol.* 47, S104–S109. doi: 10.1080/13693780802258832

Latge, J. P., Kobayashi, H., Debeaupuis, J. P., Diaquin, M., Sarfati, J., Wieruszeski, J. M., et al. (1994). Chemical and immunological characterization of the extracellular galactomannan of *Aspergillus fumigatus*. *Infect. Immun.* 62, 5424–5433.

Matveev, A. L., Krylov, V. B., Emelyanova, L. A., Solovev, A. S., Khlusevich, Y. A., Baykov, I. K., et al. (2018). Novel mouse monoclonal antibodies specifically recognize *Aspergillus fumigatus* galactomannan. *PLoS ONE* 13:e0193938. doi: 10.1371/journal.pone.0193938

Mennink-Kersten, M. A., Ruegebrink, D., Klont, R. R., Warris, A., Gavini, F., Op den Camp, H. J., et al. (2005). Bifidobacterial lipoglycan as a new cause for false-positive platelia *Aspergillus* enzyme-linked immunosorbent assay reactivity. *J. Clin. Microbiol.* 43, 3925–3931. doi: 10.1128/jcm.43.8.3925-3931.2005

Mouyna, I., Hartl, L., and Latgé, J.-P. (2013). β-1,3-glucan modifying enzymes in *Aspergillus fumigatus*. *Front. Microbiol.* 4:81. doi: 10.3389/fmicb.2013.00081

Paris, S., Wysong, D., Debeaupuis, J.-P., Shibuya, K., Philippe, B., Diamond, R. D., et al. (2003). Catalases of *Aspergillus fumigatus*. *Infect. Immun.* 71, 3551–3562. doi: 10.1128/IAI.71.6.3551-3562.2003

Perfect, J. R., Cox, G. M., Lee, J. Y., Kauffman, C. A., De Repentigny, L., Chapman, S. W., et al. (2001). The impact of culture isolation of *Aspergillus* species: a hospital-based survey of aspergillosis. *Clin. Infect. Dis.* 33, 1824–1833. doi: 10.1086/323900

Pfeiffer, C. D., Fine, J. P., and Safdar, N. (2006). Diagnosis of invasive aspergillosis using a galactomannan assay: a meta-analysis. *Clin. Infect. Dis.* 42, 1417–1727. doi: 10.1086/503427

Pitarch, A., Nombela, C., and Gil, C. (2008). Cell wall fractionation for yeast and fungal proteomics. *Methods Mol. Biol.* 425, 217–239. doi: 10.1007/978-1-60327-210-0_19

Prados-Rosales, R., Luque-Garcia, J. L., Martinez-Lopez, R., Gil, C., and Di Pietro, A. (2009). The *Fusarium oxysporum* cell wall proteome under adhesion-inducing conditions. *Proteomics* 9, 4755–4769. doi: 10.1002/pmic.200800950

Rasche, S., Martin, A., Holzem, A., Fischer, R., Schinkel, H., and Schillberg, S. (2011). One-step protein purification: use of a novel epitope tag for highly efficient detection and purification of recombinant proteins. *Open Biotechnol. J.* 5, 1–6. doi: 10.2174/1874070701105010001

Reichard, U., Buttner, S., Eiffert, H., Staib, F., and Rüchel, R. (1990). Purification and characterisation of an extracellular serine proteinase from *Aspergillus fumigatus* and its detection in tissue. *J. Med. Microbiol.* 33, 243–251.

Robens, J., and Cardwell, K. (2003). The costs of mycotoxin management to the USA: management of aflatoxins in the United States. *Toxin Rev.* 22, 139–152. doi: 10.1081/TXR-120024089

Rolle, A.-M., Hasenberg, M., Thornton, C. R., Solouk-Saran, D., Männ, L., Weski, J., et al. (2016). ImmunoPET/MR imaging allows specific detection of *Aspergillus fumigatus* lung infection *in vivo*. *Proc. Natl Acad. Sci. U.S.A.* 113, E1026–E1033. doi: 10.1073/pnas.1518836113

Samson, R. A., Visagie, C. M., Houbraken, J., Hong, S. B., Hubka, V., Klaassen, C. H. W., et al. (2014). Phylogeny, identification and nomenclature of the genus *Aspergillus*. *Stud. Mycol.* 78, 141–173. doi: 10.1016/j.simyco.2014.07.004

Schmalhorst, P. S., Krappmann, S., Vervecken, W., Rohde, M., Muller, M., Braus, G. H., et al. (2008). Contribution of galactofuranose to the virulence of the opportunistic pathogen *Aspergillus fumigatus*. *Eukaryot. Cell* 7, 1268–1277. doi: 10.1128/ec.00109-08

Schubert, M., Spiegel, H., Schillberg, S., and Nölke, G. (2018). *Aspergillus*-specific antibodies–targets and applications. *Biotechnol. Adv.* 36, 1167–1184. doi: 10.1016/j.biotechadv.2018.03.016

Singh, N., and Paterson, D. L. (2005). *Aspergillus* infections in transplant recipients. *Clin. Microbiol. Rev.* 18, 44–69. doi: 10.1128/cmr.18.1.44-69.2005

Sola, R. J., and Gribenow, K. (2009). Effects of glycosylation on the stability of protein pharmaceuticals. *J. Pharm. Sci.* 98, 1223–1245. doi: 10.1002/jps.21504

Spiegel, H., Schinkel, H., Kastilan, R., Dahm, P., Boes, A., Scheuermayer, M., et al. (2015). Optimization of a multi-stage, multi-subunit malaria vaccine candidate for the production in *Pichia pastoris* by the identification and removal of protease cleavage sites. *Biotechnol. Bioeng.* 112, 659–667. doi: 10.1002/bit.25481

Ste-Marie, L., Senechal, S., Boushira, M., Garzon, S., Strykowski, H., Pedneault, L., et al. (1990). Production and characterization of monoclonal antibodies to cell wall antigens of *Aspergillus fumigatus*. *Infect. Immun*. 58, 2105–2114.

Stynen, D., Sarfati, J., Goris, A., Prévost, M. C., Lesourd, M., Kamphuis, H., et al. (1992). Rat monoclonal antibodies against *Aspergillus* galactomannan. *Infect. Immun*. 60, 2237–2245.

Tefsen, B., Ram, A. F., Van Die, I., and Routier, F. H. (2012). Galactofuranose in eukaryotes: aspects of biosynthesis and functional impact. *Glycobiology* 22, 456–469. doi: 10.1093/glycob/cwr144

Teutschbein, J., Albrecht, D., Potsch, M., Guthke, R., Aimanianda, V., Clavaud, C., et al. (2010). Proteome profiling and functional classification of intracellular proteins from conidia of the human-pathogenic mold *Aspergillus fumigatus*. *J. Proteome Res*. 9, 3427–3442. doi: 10.1021/pr9010684

Thornton, C. R. (2008). Development of an immunochromatographic lateral-flow device for rapid serodiagnosis of invasive aspergillosis. *Clin. Vaccine Immunol*. 15, 1095–1105. doi: 10.1128/CVI.00068-08

Thornton, C. R. (2010). Detection of invasive aspergillosis. *Adv. Appl. Microbiol*. 70, 187–216. doi: 10.1016/S0065-2164(10)70006-X

Thornton, C. R., and Wills, O. E. (2015). Immunodetection of fungal and oomycete pathogens: established and emerging threats to human health, animal welfare and global food security. *Crit. Rev. Microbiol*. 41, 27–51. doi: 10.3109/1040841x.2013.788995

Torosantucci, A., Chiani, P., Bromuro, C., De Bernardis, F., Palma, A. S., Liu, Y., et al. (2009). Protection by anti-beta-glucan antibodies is associated with restricted beta-1,3 glucan binding specificity and inhibition of fungal growth and adherence. *PLoS ONE* 4:e5392. doi: 10.1371/journal.pone.0005392

Tortorano, A. M., Esposto, M. C., Prigitano, A., Grancini, A., Ossi, C., Cavanna, C., et al. (2012). Cross-reactivity of *Fusarium* spp. in the *Aspergillus* galactomannan enzyme-linked immunosorbent assay. *J. Clin. Microbiol*. 50, 1051–1053. doi: 10.1128/JCM.05946-11

Unkefer, C. J., and Gander, J. E. (1979). The 5-O-β-D-galactofuranosyl-containing glycopeptide from *Penicillium charlesii*. Carbon 13 nuclear magnetic resonance studies. *J. Biol. Chem*. 254, 12131–12135.

Varki, A., Cummings, R. D., Esko, J. D., Freeze, H. H., Stanley, P., Bertozzi, C. R., et al. (2009). *Essentials of Glycobiology*. Cold Spring Harbor, NY: Cold Spring Harbor Laboratory Press.

Villers, P. (2014). Aflatoxins and safe storage. *Front. Microbiol* 5:158. doi: 10.3389/fmicb.2014.00158

Viscoli, C., Machetti, M., Cappellano, P., Bucci, B., Bruzzi, P., Van Lint, M. T., et al. (2004). False-positive galactomannan Platelia *Aspergillus* test results for patients receiving piperacillin-tazobactam. *Clin. Infect. Dis*. 38, 913–916. doi: 10.1086/382224

Wacoo, A. P., Wendiro, D., Vuzi, P. C., and Hawumba, J. F. (2014). Methods for detection of aflatoxins in agricultural food crops. *J. Appl. Chem*. 2014, 1–15. doi: 10.1155/2014/706291

Walsh, T. J., Anaissie, E. J., Denning, D. W., Herbrecht, R., Kontoyiannis, D. P., Marr, K. A., et al. (2008). Treatment of aspergillosis: clinical practice guidelines of the infectious diseases society of America. *Clin. Infect. Dis*. 46, 327–360. doi: 10.1086/525258

Wiedemann, A., Kakoschke, T. K., Speth, C., Rambach, G., Ensinger, C., Jensen, H. E., et al. (2016). Distinct galactofuranose antigens in the cell wall and culture supernatants as a means to differentiate *Fusarium* from *Aspergillus* species. *Int. J. Med. Microbiol.* 306, 381–390. doi: 10.1016/j.ijmm.2016.05.002

Woo, P. C., Chong, K. T., Leung, A. S., Wong, S. S., Lau, S. K., and Yuen, K. Y. (2003). AFLMP1 encodes an antigenic cel wall protein in *Aspergillus flavus*. *J. Clin. Microbiol*. 41, 845–850. doi: 10.1128/JCM.41.2.845-850.2003

Zandijk, E., Mewis, A., Magerman, K., and Cartuyvels, R. (2008). False-positive results by the Platelia *Aspergillus* galactomannan antigen test for patients treated with amoxicillin-clavulanate. *Clin. Vaccine Immunol*. 15, 1132–1133. doi: 10.1128/cvi.00022-08

Conflict of Interest Statement: The authors declare that the research was conducted in the absence of any commercial or financial relationships that could be construed as a potential conflict of interest.

PLOS ONE

RESEARCH ARTICLE

Novel mouse monoclonal antibodies specifically recognizing β-(1→3)-D-glucan antigen

Andrey L. Matveev[1☯], Vadim B. Krylov[2☯], Yana A. Khlusevich[1], Ivan K. Baykov[1], Dmitry V. Yashunsky[2], Ljudmila A. Emelyanova[1,3], Yury E. Tsvetkov[2], Alexander A. Karelin[2], Alevtina V. Bardashova[1], Sarah S. W. Wong[4,5], Vishukumar Aimanianda[4,5], Jean-Paul Latgé[4¤]*, Nina V. Tikunova[1,3]*, Nikolay E. Nifantiev[2]*

1 Institute of Chemical Biology and Fundamental Medicine, Siberian Branch of Russian Academy of Sciences, Novosibirsk, Russia, **2** N.D. Zelinsky Institute of Organic Chemistry, Russian Academy of Sciences, Moscow, Russia, **3** Novosibirsk State University, Novosibirsk, Russia, **4** Aspergillus Unit, Institut Pasteur, Paris, France, **5** Molecular Mycology Unit, Institut Pasteur, Paris, France

☯ These authors contributed equally to this work.
¤ Current address: Chinese Academy of Sciences, Beijing, China
* jplatge@pasteur.fr (JPL); tikunova@niboch.nsc.ru (NVT); nen@ioc.ac.ru (NEN).

Citation: Matveev AL, Krylov VB, Khlusevich YA, Baykov IK, Yashunsky DV, Emelyanova LA, et al. (2019) Novel mouse monoclonal antibodies specifically recognizing β-(1→3)-D-glucan antigen. PLoS ONE 14(4): e0215535. https://doi.org/10.1371/journal.pone.0215535

Editor: Joseph J. Barchi, National Cancer Institute at Frederick, UNITED STATES

Received: October 21, 2018

Accepted: April 3, 2019

Published: April 25, 2019

Data Availability Statement: All relevant data are within the paper and its Supporting Information files.

Funding: Synthesis of biotinylated oligosaccharids and of BSA-based glycoconjugate immunogen were supported by Russian Science Foundation (http://rscf.ru; grant 14-50-00126; in part to D.V. Yashunsky), assaying of antibodies on glycoarray was supported by Russian Science Foundation (http://rscf.ru; grant 14-23-00199 to N.E. Nifantiev); development of mouse mAbs, SPR-

Abstract

β-(1→3)-D-Glucan is an essential component of the fungal cell wall. Mouse monoclonal antibodies (mAbs) against synthetic nona-β-(1→3)-D-glucoside conjugated with bovine serum albumin (BSA) were generated using hybridoma technology. The affinity constants of two selected mAbs, 3G11 and 5H5, measured by a surface plasmon resonance biosensor assay using biotinylated nona-β-(1→3)-D-glucan as the ligand, were approximately 11 nM and 1.9 nM, respectively. The glycoarray, which included a series of synthetic oligosaccharide derivatives representing β-glucans with different lengths of oligo-β-(1→3)-D-glucoside chains, demonstrated that linear tri-, penta- and nonaglucoside, as well as a β-(1→6)-branched octasaccharide, were recognized by mAb 5H5. By contrast, only linear oligo-β-(1→3)-D-glucoside chains that were not shorter than pentaglucosides (but not the branched octaglucoside) were ligands for mAb 3G11. Immunolabelling indicated that 3G11 and 5H5 interact with both yeasts and filamentous fungi, including species from *Aspergillus*, *Candida*, *Penicillium* genera and *Saccharomyces cerevisiae*, but not bacteria. Both mAbs could inhibit the germination of *Aspergillus fumigatus* conidia during the initial hours and demonstrated synergy with the antifungal fluconazole in killing *C. albicans in vitro*. In addition, mAbs 3G11 and 5H5 demonstrated protective activity in *in vivo* experiments, suggesting that these β-glucan-specific mAbs could be useful in combinatorial antifungal therapy.

Introduction

The incidence of invasive fungal infections continues to increase, and successful treatment of the diseases remains a serious problem despite the development of more effective antifungal preparations with reduced toxicity [1,2]. Early detection of invasive fungal infections is

study, and confocal microscopy (in part) were supported by Russian Science Foundation (http://rscf.ru; grant 16-14-00083 to N.V. Tikunova); microorganisms used in this work were provided by the Collection of Extremophile Microorganisms and Type Cultures (developed within Project 0309-2017-0008 granted by the Russian Federal Agency of Scientific Organizations; www.fano.gov.ru); study of the recognition of cell cultures by monoclonal antibodies was supported by the Franco-German ANR-DFG (ANR-16-CE92-0031-01 AFUINTERACT to V. Kumar; (http://www.agence-nationale-recherche.fr) and the Franco-Indian CEFIPRA (Project N° 5403-1 to V. Kumar) grants.

Competing interests: The authors have declared that no competing interests exist.

extremely important for successful treatment. Invasive fungal infections in humans are caused mainly by the species from *Aspergillus*, *Candida*, *Cryptococcus*, and *Fusarium* genera. Structurally, fungal cells are protected by a cell wall composed of different polysaccharides; while establishing infection, this cell wall undergoes modification and rearrangement, during which some fragment of these polysaccharides are expected to be released [3]. One of the major and essential components of the fungal cell wall is β-(1→3)-D-glucan [4–6]. Detection and quantitative evaluation of this polysaccharide is an important challenge for clinical diagnosis, food control, and ecology monitoring. Currently, Glucatell and related kits for measurement of β-(1→3)-D-glucans with a glucan-reactive preparation of *Limulus* amebocyte lysate (LAL) [7–9] is widely used; however, it shows a high rate of false positive results for fungal infection [10]. Therefore, an antibody-based enzyme immune-assay (EIA) can be regarded as a practical alternative to the LAL-test in many cases, as it is less expensive and can be sufficiently sensitive to detect β-(1→3)-D-glucan in clinical samples [11]. Several EIAs were developed to date based on polyclonal and monoclonal antibodies [11–13] that were obtained against β-glucans and their BSA-conjugates. Their specificity was evaluated with the use of polysaccharide preparations isolated from natural sources, and therefore the tests were insufficiently characterized.

In this study, we describe selection and characterization of two anti-β-(1→3)-D-glucan monoclonal antibodies (5H5 and 3G11) that were developed with the use of nona-β-(1→3)-D-glucoside-BSA conjugate [14] **G9-BSA** (Fig 1). The nonaglucoside ligand in this preparation represents the linear fragments of β-(1→3)-D-glucan. The characterization of epitopes of mAbs 5H5 and 3G11 was performed for the first time with the use of a thematic glycoarray (Fig 2A) comprised of 13 biotinylated oligoglucoside ligands (from mono- to tridecasaccharide) representing key structural elements of linear and 3,6-branched β-(1→3)-D-glucans [15–17], which were fixed on the surface of a streptavidin-coated plate and used in an indirect ELISA. The 5H5 and 3G11 mAbs were generated with a goal to develop sandwich-like EIAs for detection of glucan in ecological, food, veterinary, and clinical samples. However, in this study, we showed the potential of these two mAbs for localizing β-(1→3)-D-glucan in the fungal cell wall, inhibiting fungal growth and in the combinatorial antifungal therapy.

Materials and methods

Biotinylated conjugates of synthetic oligosaccharides and Glc9-BSA immunogen

The synthesis of spacer-armed oligosaccharides related to β-(1→3)-D-glucan fragments has been described previously [15–17]. Bovine serum albumin (BSA) conjugate of nona-β-(1→3)-D-glucoside (**G9-BSA**) was prepared from parent aminopropyl glycoside (**G9**) using the squarate protocol [14] (Fig 1). According to MALDI TOF MS data, G9-BSA contained on average ~10 oligosaccharide chains per protein molecule.

Preparation of biotinylated conjugates from β-(1→3)-D-glucan ligands for the creation of glycoarrays (Fig 2A) was performed by treating parent aminopropyl glycosides with the active ester of biotin in dimethylformamide following the biotinylation protocol described previously [19]. Biotinylated glycoconjugates were isolated by gel-permeation chromatography on a Toyopearl HW-40(S) gel (Tosoh, Japan) column, eluted using 0.1 M acetic acid with 65–75% yields.

Animals

Female BALB/c mice were purchased from the animal care facility in the Federal State Research Center of Virology and Biotechnology "Vector" (Koltsovo, Russia). Mice were

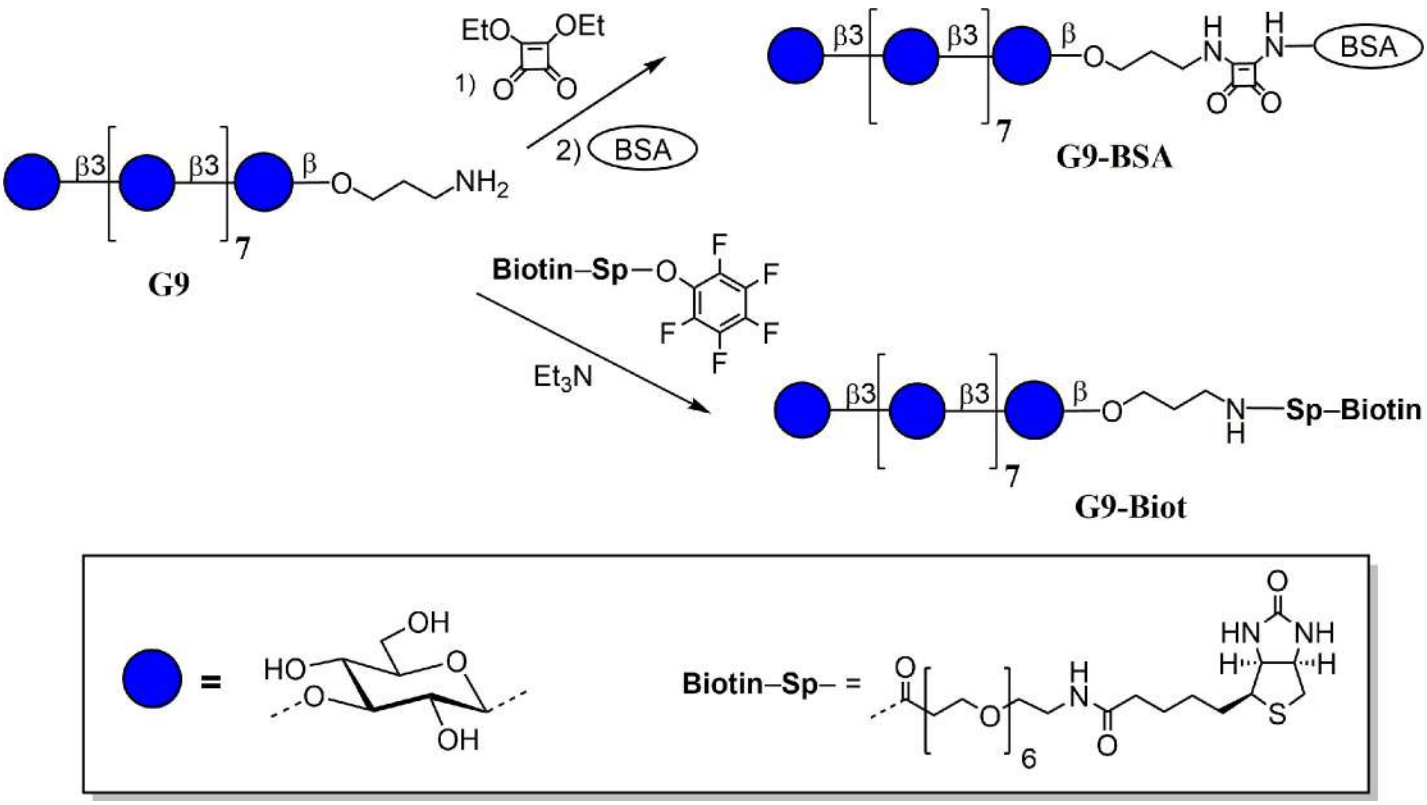

Fig 1. Structure of nonasaccharide G9 and its BSA (G9-BSA) and biotinylated (G9-Biot) conjugates used in mouse immunization and mAb screening; the carbohydrate sequences are represented according to symbol carbohydrate nomenclature [18].

https://doi.org/10.1371/journal.pone.0215535.g001

housed with a normal light-dark cycle; food and water were provided *ad libitum*. All animal procedures were carried out in accordance with the recommendations for the protection of animals used for scientific purposes (EU Directive 2010/63/EU). Immunized mice were euthanized with an overdose of isoflurane (5%). These animal experiments were approved by the local Bioethics Committee of the Institute of Chemical Biology and Fundamental Medicine, Siberian Branch of Russian Academy of Sciences (ICBFM, SB RAS), Novosibirsk, Russia.

Mouse immunization and mAbs selection

For immunization, 10 μg **G9-BSA** in 300 μL phosphate buffer saline (PBS), pH 7.4, emulsified with an equal volume of complete Freund's adjuvant (Sigma-Aldrich, St. Louis, MO) were subcutaneously administered into 12–14-week-old female BALB/c mice (22–28 g). At two and four weeks, each mouse was additionally immunized intraperitoneally with 10 μg **G9-BSA** mixed with incomplete Freund's adjuvant (Sigma-Aldrich, St. Louis, MO). Two weeks after the third immunization, mice were finally immunized with 10 μg of **G9-BSA** in 300 μL PBS, pH 7.4. After three days, antibody titer of the mice sera (obtained from orbital blood sample) against nona-β-(1→3)-D-glucoside conjugated with biotin (**G9-biot**) were checked by indirect ELISA. Those mice with the highest antibody titer were sacrificed and obtained splenocytes were fused with SP2/0 myeloma cells using PEG 2000 (Roche, Basel, Switzerland) according to the manufacturer's protocol. The SP2/0 myeloma cell line was cultured in Iscove's modified Dulbecco's medium (Invitrogen, Waltham, MA) supplemented with 10% fetal bovine serum (Biolot, Russia) and antibiotics (0.1 mg/mL streptomycin and 100 IU/mL penicillin).

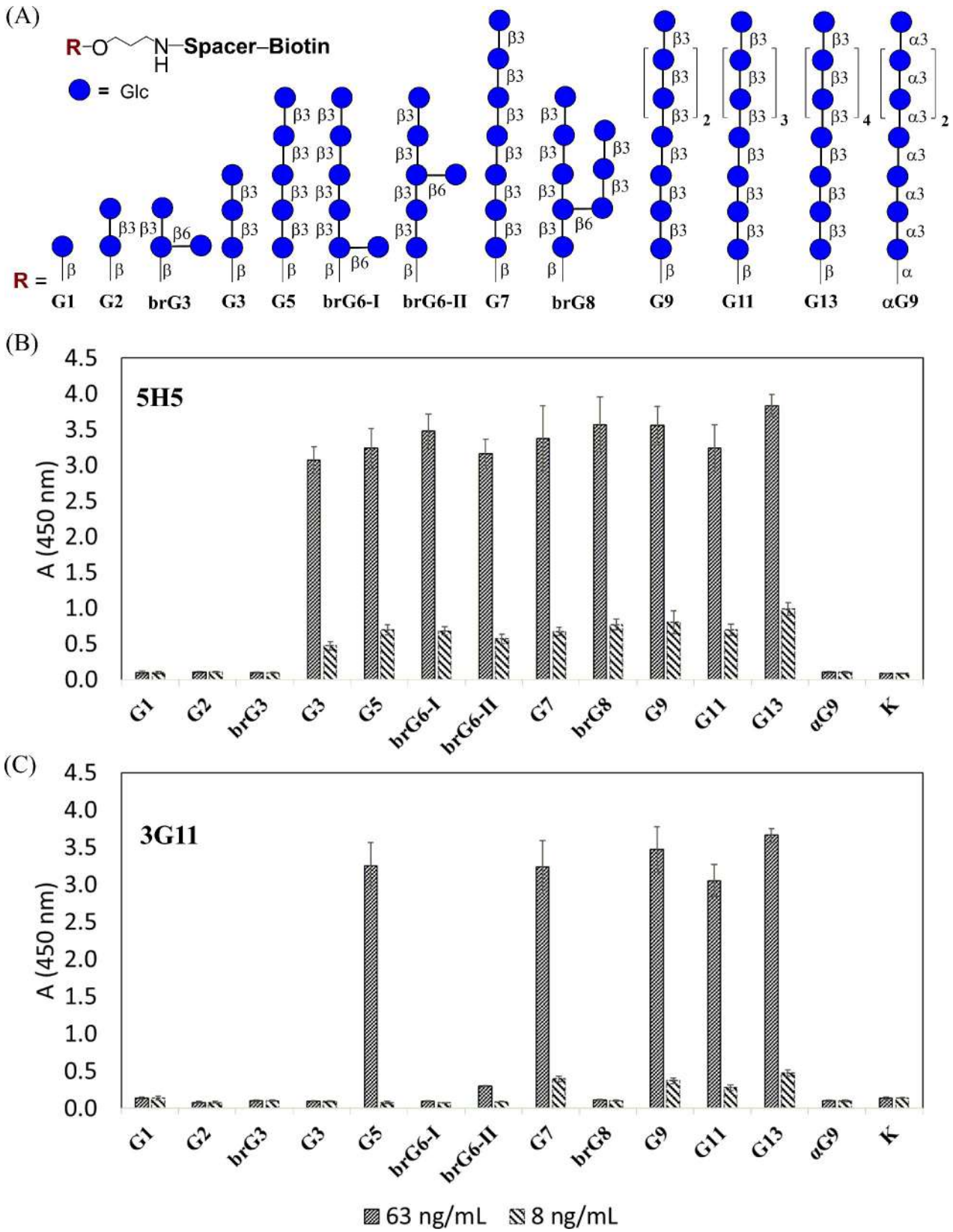
(A)
R–O–N–Spacer–Biotin
H
= Glc
R =
G1
G2
brG3
G3
G5
brG6-I
brG6-II
G7
brG8
G9
G11
G13
αG9
(B)
5H5
A (450 nm)
4.5
4.0
3.5
3.0
2.5
2.0
1.5
1.0
0.5
0.0
G1
G2
brG3
G3
G5
brG6-I
brG6-II
G7
brG8
G9
G11
G13
αG9
K
(C)
3G11
A (450 nm)
63 ng/mL
8 ng/mL

Fig 2. Investigation of oligosaccharide specificity of mAbs 3G11 and 5H5 using ELISA. (A) Composition of a thematic glycoarray built using linear (**G1**-**G13**) and branched (**brG3**, **brG6-I, brG6-II, brG8**) oligosaccharide ligands representing key structural elements of the β-(1→3)-D-glucan chain. The α-(1→3)-linked glucosaccharide **αG9** was used as a negative control. Assay for the carbohydrate specificity of 5H5 (B) and 3G11 (C) mAbs. All measurements were independently repeated twice in triplicate. The results are presented as the means ± s.d.

https://doi.org/10.1371/journal.pone.0215535.g002

Hybridomas were cultured and cloned in Iscove's modified Dulbecco's medium (Invitrogen, Waltham, MA) supplemented with 10% fetal bovine serum (Biolot, Russia), 5.7 μM azaserine (Sigma-Aldrich, St. Louis, MO), 100 μM hypoxanthine (Sigma-Aldrich, St. Louis, MO), 50 U/mL interleukin-6, and antibiotics (0.1 mg/mL streptomycin and 100 IU/mL penicillin). Hybridoma clones were selected by assaying the titer of mAbs in the supernatants by ELISA using **G9-biot**. Positive clones were additionally cloned two times by the limiting dilution method. Selected mAbs were propagated and purified using protein A chromatography (GE Healthcare, Chicago, IL), as described previously [20].

The IgG subclass determination

To determine the IgG class of a mAb produced by the selected hybridoma clone, total RNA was isolated from the appropriate hybridoma cell line using RNeasy Mini kit (Qiagen, Venlo, Netherlands). A fragment of the gene encoding constant domain CH1 was amplified by RT-PCR using the primers 5′- CTTCCGGAATTCSARGTNMAGCTGSAGSAGTC-3′ [21] and 5′-GGGAAGTAGCCTTTGACAAGGC-3′ and sequenced in both directions.

Purification and conjugation of mAbs

To obtain mAbs, 2×10^6 hybridoma cells, producing anti-**G9** antibodies, were resuspended in 0.5 mL of sterile 0.9% NaCl and administered intraperitoneally into 20-week-old BALB/c mice. Selected mAbs 3G11 and 5H5 were purified by ammonium sulfate precipitation from ascitic fluids and then purified using protein A chromatography (GE Healthcare, IL). The purity and size of the purified IgG antibodies were examined by SDS-PAGE and Western blot analyses. Purified mAbs were resolved by 12.5% SDS-PAGE under reducing conditions and transferred onto a nitrocellulose membrane (Bio-Rad, CA). After blocking with 5% casein (skim milk powder) in PBS, the membrane was incubated with anti-mouse IgG alkaline phosphatase-conjugated goat IgG (Sigma Aldrich, MO). Immune complexes were visualized by a mixture of nitro blue tetrazolium (WVR, PA) and 5-bromo-4-chloro-3-indolyl-phosphate (Roche, Germany) for 20 min. The selected mAbs 3G11 and 5H5 were conjugated with horseradish peroxidase (WVR, PA) using the optimized $NaIO_4$ method as described previously [22].

Oligosaccharide-specific indirect ELISA

For indirect ELISA, a 96-well Pierce streptavidin-coated plate was coated with 50 ng/well of **G9-biot** in 25 mM Tris-HCl, pH 7.5, with 150 mM NaCl, 0.05% Tween-20, and 0.3% BSA and incubated at 4˚C overnight. Following, the wells were washed three times with wash buffer (25 mM Tris-HCl, pH 7.5 + 150 mM NaCl + 0.05% Tween 20 + 0.3% BSA), followed by adding mouse sera, hybridoma supernatants, or mAbs in appropriate dilutions and incubating at 37˚C for 1 h. After washing three times with wash buffer, anti-mouse IgG alkaline phosphatase-conjugated goat IgG (Sigma Aldrich, USA) was added and incubated at 37˚C for 1 h, followed by washing three times with the wash buffer and then AP-buffer (100 mM Tris-HCl, pH 9.5, with 100 mM NaCl and 5 mM $MgCl_2$). The substrate 4-nitrophenyl phosphate was added, and the absorbance was measured at 405 nm using an iMark plate reader (Bio-Rad, USA).

Glycoarray

The wells of 96-well Pierce streptavidin-coated plates were coated with 20 pmol/well of appropriate linear (**G1**-**G13**) and branched (**brG3**, **brG6-I, brG6-II, brG8**) biotin-tagged oligosaccharides (Fig 2) in 100 μL of wash buffer and then incubated for 2 h at 37˚C as previously described [20,23,24]. After washing three times with wash buffer, the plates were incubated with mAbs 5H5 and 3G11 diluted in wash buffer (concentration 63, 8.0 ng/mL) for 1 h at 37˚C. After washing three times with wash buffer, anti-mouse IgG rabbit IgG-horseradish peroxidase conjugate (Imtek, Russia) was added and incubated for 1 h at 37˚C. After washing three times with wash buffer, the color was developed using TMB mono-component substrate (100 μL) for 15 minutes, and the reaction was stopped with 50 μL of 1 M sulfuric acid. The absorbance was measured at 450 nm using a MultiSkan GO plate reader (Thermo Fisher Scientific, USA). All measurements were independently repeated twice in triplicate. Results are presented as the means ± s.d.

Sandwich anti-β-glucan ELISA

For sandwich ELISA, 10^8 microbial cells were harvested by centrifugation, washed twice in 1 ml 0.9% NaCl, resuspended in 1 mL PBS, and sonicated as described previously [25] with our modifications. Sonications were done using a cell disintegrator Sonopuls Ultrasonic homogenizers HD 2070 (Bandelin, Germany) at 20 W and 20 kHz. Samples, of volumes 0.5 ml, were kept in an ice bath during cell disruption. Sonication treatments consisted of five periods of 20 sec followed by 1 min of resting to prevent overheating. In addition, supernatants of bacterial cultures were also assayed for their binding with mAbs 3G11 and 5H5 using a sandwich ELISA. The 96-well microtiter plates (Greiner, Austria) were coated with 200 ng/well mAb 3G11 or mAb 5H5 in PBS and incubated at 37˚C for 1 h. After blocking with 5% casein (skimmed milk) in PBS, coated wells were washed three times with PBS containing 0.1% Tween-20 (PBST) and three times with PBS. Then, serially diluted (five-fold) opalescent microbial cell lysates or bacterial culture supernatants were added, and the plates were incubated at 37˚C for 1 h. After subsequent washing three times with PBST and PBS, an indirect ELISA was performed with horseradish peroxidase-conjugated mAb 5H5 (100 μL). The assay was developed using 3,3',5,5'-Tetramethylbenzidine (TMB; WVR, PA) mono-component substrate (100 μL) for 15 minutes, and the reaction was stopped with 50 μL of 1 M sulfuric acid. The absorbance was measured at 450 nm using an iMark plate reader (BioRad, CA). ELISA was performed with two different preparations of microbial cell lysates, and each time in triplicate. The results are presented as the means ± s.d.

Affinity constant measurement

The affinity of mAbs to oligosaccharide antigens was determined by a Surface Plasmon Resonance-based biosensor assay (SPR) using a ProteOn XPR36 system (Bio-Rad, USA). PBS with 0.005% Tween-20 (PBSTmin) was used as a system running buffer. Vertical channels L3 and L4 of a GLC sensor chip were coated covalently with streptavidin at the 90–110 response unit (RU) level. Biotinylated oligosaccharides diluted to 3 μg/mL in PBSTmin were immobilized onto streptavidin-coated channel L3 for 50 seconds resulting in a 5 RU level, while L4 was used as a reference channel. To perform affinity measurements, three-fold dilutions of mAbs were analyzed at a flow rate of 25 μL/min. The duration of both the association and dissociation was 300 seconds. Antibody concentration ranges were determined based on data from scouting experiments, in which the starting concentration of mAbs was 180 nM. All experiments were repeated three times. The chip surface was regenerated with 100 mM citric acid. Global analysis of experimental data based on a single-site model was performed using the ProteOn Manager v. 3.1.0 software. Affinity constants were calculated as $K_D = k_d/k_a$.

Microorganisms

Fungal strains *Candida albicans* ATCC 10231 and bacterial strains *Enterococcus faecalis* ATCC 51299, *Escherichia coli* ATCC 25922, *Proteus mirabilis* ATCC 25933, *Pseudomonas aeruginosa* ATCC 27853, *Salmonella enterica* ATCC 14028, and *Staphylococcus aureus* ATCC 25923 were purchased from ATCC and maintained in the Collection of Extremophilic Microorganisms and Type Cultures (CEMTC) of ICBFM, SB RAS. Other microorganisms, including *Aspergillus fumigatus*, *Candida parapsilosis*, *Candida tropicalis*, *Candida dubliniensis*, *Debaryomyces hansenii*, *Penecillium polonicum*, *Penecillium solitum*, *Alcaligenes faecalis*, *Bifidobacterium infantis*, *Bifidobacterium longum*, and *Lactobacillus plantarum* were isolated from clinical samples or natural habitats and characterized by 16S rRNA gene sequencing and biochemical properties using a biochemical analyzer (GEN III OmniLog Combo Plus System, Biolog, USA) in CEMTC. Fungi, including *A. fumigatus*, *C. albicans*, *C. parapsilosis*, *C. tropicalis C. dubliniensis*, *D. hansenii*, *P. polonicum*, and *P. solitum*, were grown in Sabouraud Dextrose broth (SDB) at room temperature overnight (*Candida* spp.) or for 44 hrs (all other fungi). Several bacterial species, including *B. infantis*, *B. longum*, and *L. plantarum*, were cultivated in Blaurock medium, while other bacteria, namely *A. faecalis*, *E. faecalis*, *E. coli*, *P. mirabilis*, *P. aeruginosa*, *S. enterica*, and *S. aureus*, were propagated in Luria-Bertani broth at 37˚C. All these bacteria were grown in a shaken incubator for overnight and then used in experiments.

Immunolabeling and confocal microscopy

For immunolabeling, fungal and bacterial cells were allowed to adhere on slides and were then fixed with 2.5% *para*-formaldehyde overnight at 4˚C. Slides with fixed cells were washed with PBS twice and blocked with 3% BSA in PBS for 1 h. Then, cells were washed and incubated with 5 μg/mL mAb diluted in PBS with 3% BSA for 1 h at 37˚C. After washing, cells were stained with Alexa Fluor-488- or Cy5-conjugated chicken anti-mouse IgG (H+L) antibodies (Life Technologies) or FITC-conjugated anti-mouse IgG (Sigma) diluted 1:500 in PBS with 3% BSA. Samples were mounted using Prolong Diamond Antifade and examined under a Carl Zeiss LSM 710 laser scanning microscope (Carl Zeiss, Germany). Observations were performed using oil 63× objectives, and images were captured at 488 nm in green or 670 nm in red and differential interference contrast (DIC) channels. ZEN black edition software (Carl Zeiss, Germany) was used in the confocal microscope to visualize images.

Germination inhibition assay

3G11 or 5H5 (5 μl; stock solution concentration, 1 mg/mL) was added to 5×10^3 conidia in 5 μl tween-water (0.05%), and the mixture was placed on Sabouraud agar medium spread over a glass-slide. The slides were incubated at 37˚C and after 6 h, they were observed each hour for germination under the microscope. On each slide three inoculum mixtures were spotted, and at least four different positions were imaged wherein germinated and non-germinated conidia were counted. For control samples, 5×10^3 conidia in 5 μl tween-water mixed with 5 μl PBS was plated on Sabouraud agar medium, and the germination was recorded from 6 h onwards. This assay was performed in triplicate, and at least hundred conidia were counted each time.

Phagocytotic assay

A phagocytotic assay was performed for *A. fumigatus* conidia using human monocyte derived macrophages (HMDM) obtained as described previously [26,27]. *A. fumigatus* conidia were harvested from 12-15-day-old malt-agar slants using 0.05% aqueous Tween-20 and washed

twice with aqueous Tween-20. Swollen conidia were obtained by inoculating 1×10^8 conidia in 50 mL of Sabouraud liquid medium. The conidia were incubated at 37˚C in a shaken incubator (150 rpm) for 5 h, followed by harvesting of the conidia by centrifugation and washing twice with water. To label the conidia with fluorescein isothiocyanate (FITC), 1 mg/mL FITC was diluted 1:10 with carbonate buffer of pH 9.6, and 200 μl diluted FITC was then added to 1×10^8 swollen conidia. The conidia were incubated at ambient temperature for 30 min, and the supernatant was discarded after centrifugation. The pellet was washed thoroughly with carbonate buffer to remove excess of FITC and then suspended in PBS. 3G11 (5 μl; stock solution concentration, 1 mg/mL) was then added to $1x10^6$ FITC-labelled swollen conidia (wherein there is exposure of the β-(1→3)-D-glucan on the surface). The mixture was incubated for 30 min and then suspended in incomplete RPMI. These conidia were added to HMDM (obtained upon seeding $2x10^6$/well peripheral blood mononuclear cells isolated from healthy donors) adhered to culture plates and incubated at 37˚C in a CO_2 incubator for 1 h. Following, the culture supernatant was discarded, the wells were washed twice with incomplete RPMI, fixed with 2.5 μ% *para*-formaldehyde for 10 min, and washed with incomplete RPMI. Calcofluor white solution (10 μg/mL in PBS) were added to label conidia outside macrophages [26], washed with PBS, and viewed under fluorescent microscope. 3G11 untreated conidia were used as the control. The assay was performed with HMDM obtained from three different donors; for each sample, there were duplicate wells on the culture plates, and from both wells, images were taken to count at least one hundred swollen conidia.

Antifungal assays

Approximately 10^5 colony forming units/mL (CFU/mL) from the overnight *C. albicans* culture were inoculated into fresh Sabouraud dextrose broth. Fluconazole, mAb 3G11, and mAb 5H5 were diluted in 0.9% NaCl, and two-fold dilutions of mAb 3G11, mAb 5H5, or fluconazole were added to the *C. albicans* culture. The mixtures were incubated at room temperature with shaking for 18 h. Then, aliquots were withdrawn, diluted in SDB, and serial dilutions of the mixtures were plated onto Sabouraud Dextrose agar. The plates were incubated overnight at room temperature, and the number of colonies that grew on the plates was counted. When fluconazole and a mAb were added simultaneously, fluconazole was used at a concentration of 50 μg/mL, while two-fold dilutions of the mAb were used. In this experiment, fluconazole at a concentration of 100 μg/mL and sterile 0.9% NaCl were used as positive and negative controls, respectively. All experiments were carried out twice in triplicate. The limit of quantification by this method was 100 CFU/mL.

In vivo protection in mice

Protection of mAbs 3G11 and 5H5 was studied in a mouse model of systemic candidiasis, described previously [28,29] with modifications. Briefly, *C. albicans* ATCC 10231 cells, grown in SBD at 28˚C overnight, were harvested by centrifugation, washed with sterile 0.9% NaCl, and counted in a hemocytometer. Six week-old female BALB/c mice were administered intraperitoneally 0.5 mL of mAbs 3G11 or 5H5 at a dose of 150 μg/mouse; control mice received an irrelevant anti-tick-borne encephalitis mouse mAb (IgG1) [30] at the same dose or 0.5 mL 0.9% NaCl. Two hours later, all mice were infected intravenously with 0.2 mL of *C. albicans* suspension in 0.9% NaCl (5×10^6 cells per mouse). Each experimental and control group included eight mice. The mice were observed for 60 days after infection to assess the survival rate. Data were analyzed using the on-line service available at https://www.evanmiller.org/ab-testing/survival-curves.html and https://www.graphpad.com/quickcalcs.

Statistics

All measurements for oligosaccharide-specific indirect ELISA and glycoarray were independently repeated twice in triplicate. The data are presented as the mean ± standard deviation (s.d.). Statistical analysis of germination inhibition assay and phagocytotic assay was performed by one-way ANOVA; *, p<0,05 and **, p<0,005. The differences in CFU counts in antifungal *in vitro* assays were computed using a two-tailed Student's t- test; $p < 0.001$ was regarded as significant. The Fisher's exact test was used to compare the survival rates between the differently treated animal groups, whereas differences in the survival times were compared using the log-rank test.

Results and discussion

Anti-β-(1→3)-D-glucan mAbs generation and characterization

To generate mAbs specifically recognizing fungal β-(1→3)-D-glucan, the synthetic β-(1→3)-linked nonaglucoside **G9** was selected as target ligand. The conjugates of this oligosaccharide demonstrated high immunogenicity [14]. Moreover, theoretical and experimental conformational studies showed that the nonasaccharide sequence is long enough to mimic natural β-(1→3)-linked glucan [31]. Using synthetic nonasaccharide **G9**, immunogen **G9-BSA** was prepared by conjugation of corresponding aminopropyl glycoside with BSA using the squarate protocol (Fig 1). The biotin-tagged nonasaccharide **G9-Biot** required for selection of mAbs was prepared by treating amine with activated ester [19].

To select hybridomas producing mAbs against β-(1→3)-D-glucan, BALB/c mice were immunized four times with synthetic **G9-BSA**. Four, eight, and twelve weeks after the first immunization, mouse sera were screened by indirect ELISA to assess the level of anti-β-(1→3)-D-glucan antibodies. To prevent selection of anti-BSA mAbs, **G9-biot** was used as an antigen in the assay. Final titers of anti-β-(1→3)-D-glucan IgG antibodies ranged from 1:40000 to 1:200000 in the sera of different mice. Individual hybrid clones (n = 634) were screened for their binding with **G9-biot**, and ten hybridomas secreting specific mAbs were selected.

The IgG class of selected mAbs was determined as described previously [20] based on the sequences of PCR fragments encoding the constant domain CH1. Nine of the selected mAbs belonged to the IgG1 class, while mAb 5H5 was from the IgG3 class. Light chains of all the selected mAbs belonged to the kappa family.

Affinity of the purified selected mAbs was measured in a label-free SPR biosensor assay using **G9-biot** as the ligand. Two mAbs, 3G11 and 5H5, demonstrated the highest binding characteristics, while the affinity constants of the other selected mAbs were $> 10^{-6}$ M. A global analysis of the interaction between mAbs 3G11 and 5H5 and the ligand demonstrated a good quality fit (Fig 3), and affinity constants were calculated as $K_D = (1.1 \pm 0.1) \times 10^{-8}$ M for mAb 3G11 and $K_D = (1.9 \pm 0.2) \times 10^{-9}$ M for mAb 5H5. The kinetic parameters and affinity constants for binding with biotinylated **G9-biot** are indicated in Table 1. As affinity constants of other selected mAbs were not acceptable, they were not used in further experiments.

Epitope specificity of mAbs 3G11 and 5H5

The carbohydrate specificity of mAbs 3G11 and 5H5 was investigated using a library of thirteen synthetic oligosaccharides (see Fig 2B and 2C) representing distinct linear (**G1**-**G13**) and branched (**brG3**, **brG6-I, brG6-II, brG8**) structural fragments of β-(1→3)-D-glucan. These ligands as biotinylated conjugates were immobilized on the surface of the streptavidin-coated plate, and mAbs were assayed on the formed glycoarray at concentrations of 8 and 63 ng/mL.

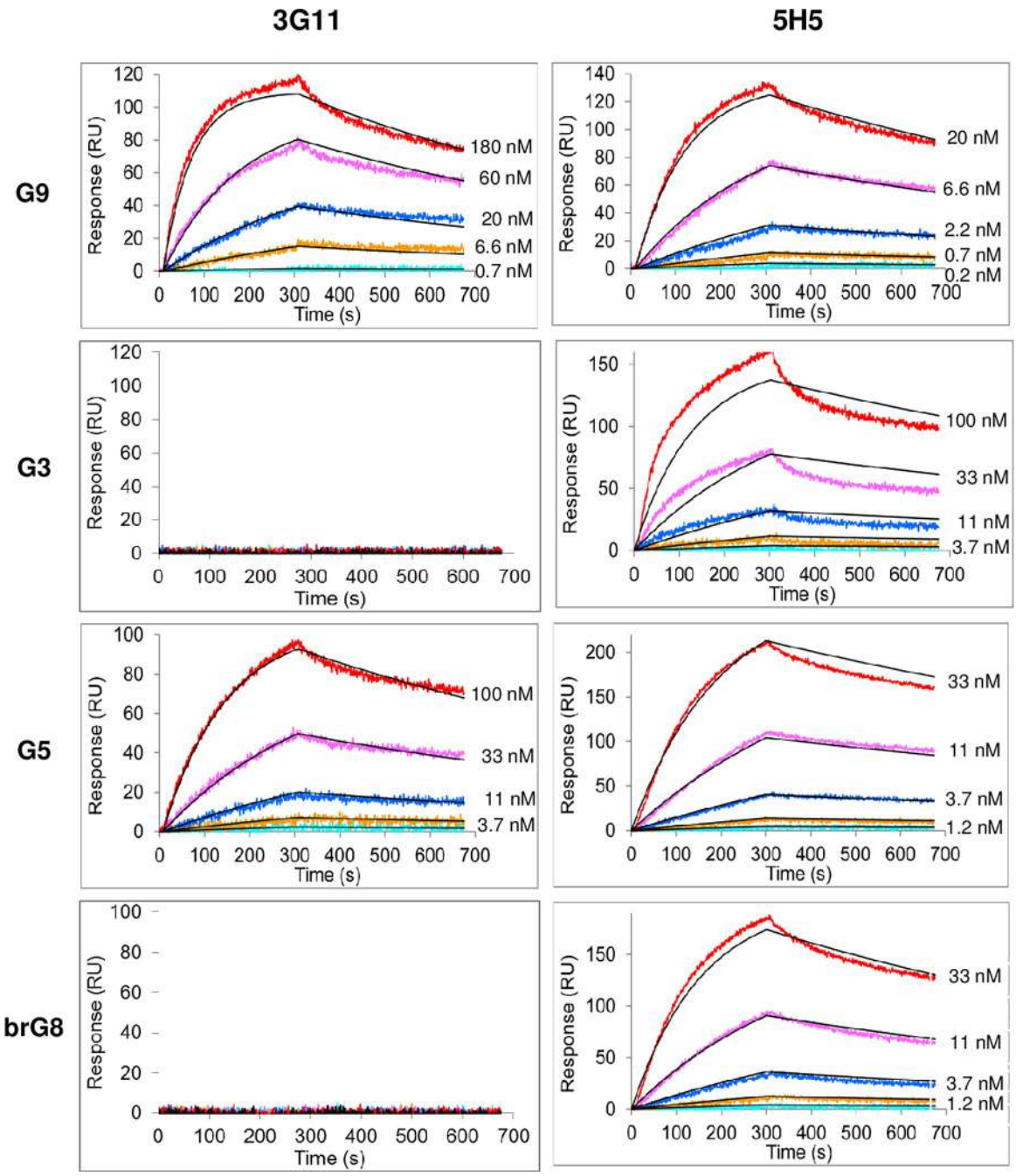

Fig 3. Binding of mAbs 3G11and 5H5 with biotinylated oligosaccharide ligands assayed by SPR. Serial three-fold dilutions of mAb 3G11 (left side) and mAb 5H5 (right side) were used as analytes. Experimental data are shown as color lines; fitted data are depicted as black curves; fitted traces are depicted as smooth black lines. Starting antibody concentrations were determined in scouting experiments.

https://doi.org/10.1371/journal.pone.0215535.g003

The antibodies demonstrated different carbohydrate specificity profiles. 5H5 was less selective and recognized all tested ligands except mono- (**G1**), diglucoside (**G2**) and branched triglucoside (**brG3**). 3G11 recognized all linear oligoglucosides longer than a pentamer (**G5**, **G7**, **G9**, **G11**), but it did not recognize branched oligoglucosides **brG6-I, brG6-II, brG8**, showing differences between the affinities of both mAbs. The mAbs did not recognize α-(1→3)-linked

Table 1. The kinetic parameters and affinity constants of mAbs 3G11 and 5H5 for binding with linear tri- (G3), penta- (G5) and nonaglucoside (G9) and branched octaglucoside brG8.

mAb	Synthetic glucosides			
	G3	**G5**	**brG8**	**G9**
3G11	$K_D > 1$ mM	$K_D = 12 \pm 1$ nM	$K_D > 1$ mM	$K_D = 11 \pm 1$ nM
		$k_a = 6.4 \times 10^4$ $M^{-1}s^{-1}$		$k_a = 8.2 \times 10^4$ $M^{-1}s^{-1}$
		$k_d = 8.5 \times 10^{-4}$ s^{-1}		$k_d = 8.8 \times 10^{-4}$ s^{-1}
5H5	$K_D = 9.0 \pm 3.0$ nM	$K_D = 4.0 \pm 0.5$ nM	$K_D = 4.5 \pm 0.5$ nM	$K_D = 1.9 \pm 0.2$ nM
	$k_a = 7.2 \times 10^4$ $M^{-1}s^{-1}$	$k_a = 1.4 \times 10^5$ $M^{-1}s^{-1}$	$k_a = 1.7 \times 10^5$ $M^{-1}s^{-1}$	$k_a = 4.2 \times 10^5$ $M^{-1}s^{-1}$
	$k_d = 6.3 \times 10^{-4}$ s^{-1}	$k_d = 5.6 \times 10^{-4}$ s^{-1}	$k_d = 7.8 \times 10^{-4}$ s^{-1}	$k_d = 8.1 \times 10^{-4}$ s^{-1}

https://doi.org/10.1371/journal.pone.0215535.t001

nonasaccharide ligand α**G9**. These results indicated that mAb 5H5 minimally recognizes the β-(1→3)-linked trisaccharide moiety, while 3G11 required the presence of a linear pentasaccharide fragment for effective binding.

These results were confirmed by SPR assays (**Fig 3**, Table 1). 5H5 recognized all tested linear antigens, though with different affinities, and the binding effectiveness increased (9 nM → 4 nM → 1,9 nM) with increasing length of the oligosaccharide **G3** → **G5** → **G9** (Table 1). By contrast, 3G11 specifically bound to penta-**G5** and nonaglucoside **G9** with almost equal affinities (Table 1). Probably, 5H5 is able to recognize a smaller fragment of β-(1→3)-D-glucan that leads to less specificity of this mAb compared to 3G11.

Immunofluorescence microscopy

The ability of mAbs 3G11 and 5H5 selected against synthetic β-glucan oligosaccharide to specifically bind with the fungal cell wall was demonstrated by immunofluorescence confocal microscopy. Both mAbs 3G11 and 5H5 recognized *Candida* species: *C. albicans*, *C. parapsilosis*, *C. tropicalis C. dubliniensis*, including medically important ones, as well as *A. fumigatus*, *P. polonicum*, *P. solitum*, *D. hansenii*, and *S. cerevisiae* (see Fig 4 and S1 File). Confocal images of *A. fumigatus*, *C. albicans* and *S. cerevisiae* are presented in Fig 4. As can be seen, there was weak binding of 5H5 with *A. fumigatus* germinating conidia, while 3G11 could bind to only the budding cell wall of *C. albicans*. 5H5 could bind the mother cell wall, and both 3G11 and 5H5 could label *S. cerevisiae*, although labeling with 5H5 was weaker. This clearly indicates differential distribution of the ligands of 3G11 and 5H5 on these fungal cell walls. Notably, the microbe-mAb interaction time was the same in experiments with all tested microorganisms.

In addition to fungal cell walls, β-glucans are also a natural component of the bacterial cell wall. To evaluate the specificity of mAbs 3G11 and 5H5, their binding with several gram-positive (*B. infantis*, *B. longum*, *E. faecalis*, *L. plantarum*, and *S. aureus*) and gram-negative (*A. faecalis*, *E. coli*, *P. mirabilis*, *P. aeruginosa*, and *S. enterica*) bacterial cells was examined by immunofluorescence confocal microscopy (S1 File). The images demonstrated that both mAbs 3G11 and 5H5 did not label all the tested bacteria. Importantly, mAbs 3G11 and 5H5 did not recognize *A. faecalis* and *P. aeruginosa*, which are known to produce β-(1→3)-D-glucan that causes a false positive detection of invasive fungal infections with the Fungitell assay [32]. The lack of recognition by mAbs 3G11 and 5H5 in the case of the bacteria could be attributed to the fact that bacterial β-(1→3)-D-glucans are mostly linear (with small amounts of 2,3-branchings) or cyclic [33], while those of fungi are partially 3,6-branched [34]. Conformational differences between bacterial cyclic or linear β-(1→3)-D-glucans (the latter may form triple helical fibrillar structures [31]) and fungal glucans can cause the observed discrimination in the recognition by the studied mAbs.

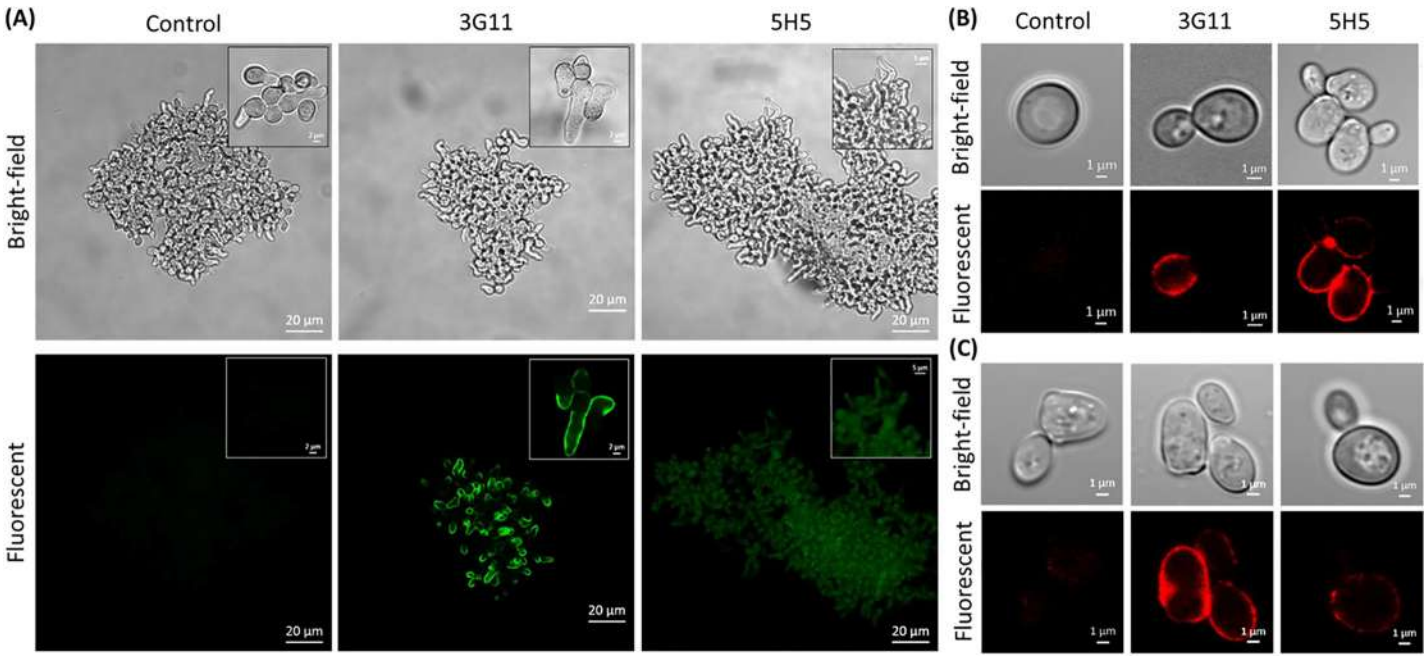

Fig 4. Immunofluorescence microscopy of different fungal species: immunolabelling for *A. fumigatus* (A), *C. albicans* (B) and *S. cerevisiae* (C) by mAbs 3G11 and 5H5.

https://doi.org/10.1371/journal.pone.0215535.g004

Sandwich anti-β-glucan ELISA

To confirm specific binding of mAbs 3G11 and 5H5 with *C. albicans*, a sandwich ELISA was performed. Sonicated suspensions of *C. albicans*, *E. coli*, or *P. aeruginosa* were serially diluted, added to mAb 3G11 or mAb 5H5 coated on ELISA plate wells, and developed using mAb 5H5 HRP-conjugate. The results showed that both mAbs did not bind *E. coli* and *P. aeruginosa* cell lysates, but they recognized sonicated suspension of *C. albicans* (Fig 5).

Since bacterial β-(1→3)-glucans were shown to be mainly secretory components of bacterial cells [35] and could be accumulated in growth medium, bacterial culture supernatants

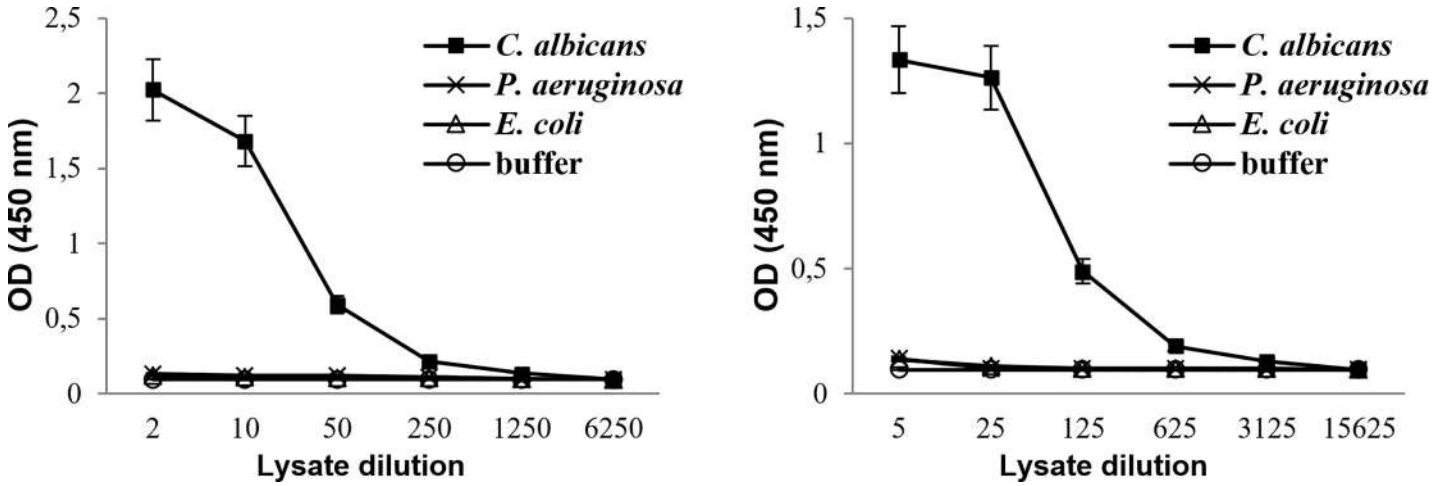

Fig 5. Binding of fungal and bacterial cell lysates with mAbs 3G11 and 5H5. Sandwich enzyme-linked immunosorbent assay (ELISA) with anti-**G9** antibodies: the wells of microtiter plates were coated with 200 ng mAb 3G11 (**A**) or mAb 5H5 (**B**) and incubated with serially diluted sonicated suspension of indicated microbial cultures; ELISA was performed with horseradish peroxidase-conjugated mAb 5H5.

https://doi.org/10.1371/journal.pone.0215535.g005

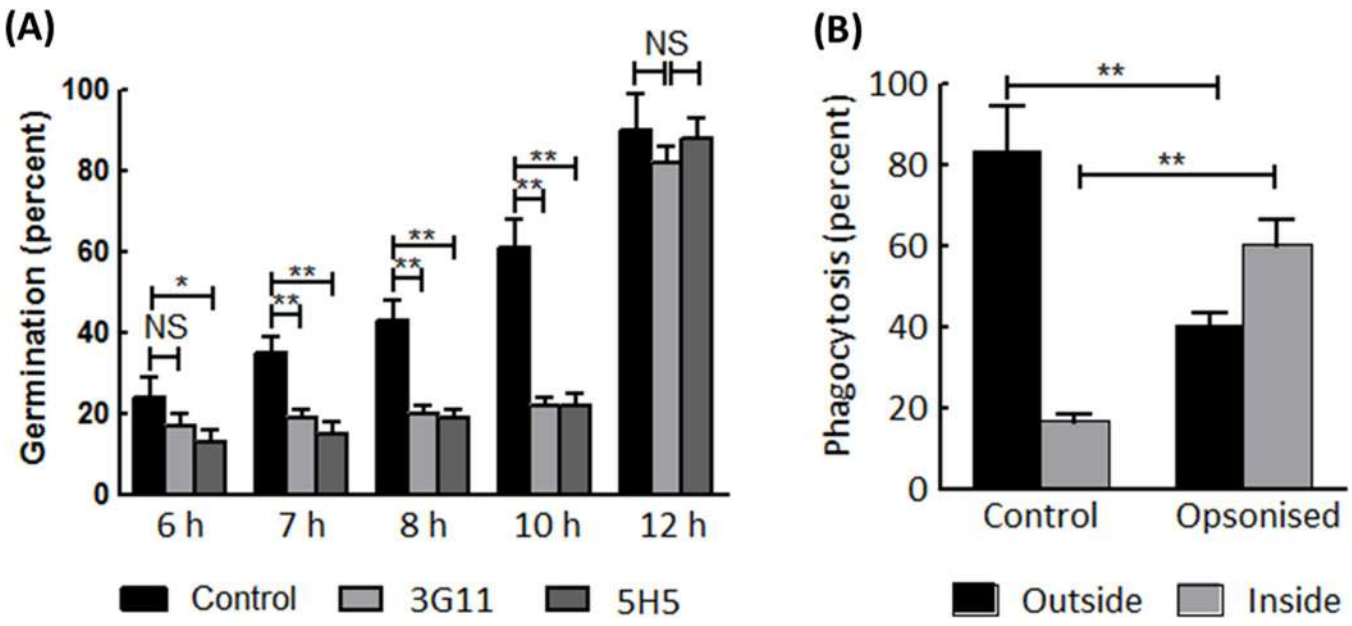

Fig 6. Antifungal activity of mAbs 3G11 and 5H5. (A) *A. fumigatus* germination inhibition assay. Conidia were treated with 3G11 or 5H5 (PBS buffer was used as a control) and placed on Sabouraud agar medium spread on a glass slide. Conidial germination was monitored after 6 h of incubation at 37˚C. The incubation time is shown on the X-axis. The assay was repeated three times, and at least hundred conidia were counted each time. **(B)** Phagocytotic assay. Swollen conidia (FITC-labelled) were treated with 3G11 for 60 min followed by feeding to human monocyte derived macrophages (HMDM). After a further 60 min of incubation at 37˚C in a CO_2 incubator, non-phagocytosed conidia were differentiated from phagocytosed FITC-labelled conidia by calcofluor white staining. Images were taken from different places to count at least one hundred swollen conidia in each experiment. Statistical analysis was performed by one-way ANOVA; *, $p<0,05$ and **, $p<0,005$.

https://doi.org/10.1371/journal.pone.0215535.g006

were additionally assayed in sandwich ELISA (S1 Fig). The data indicated that *E. coli* and *P. aeruginosa* culture supernatants were not revealed by both mAb 3G11 and mAb 5H5 and confirmed results was demonstrated by immunofluorescence confocal microscopy.

Antifungal assay

A β-(1→3)-D-glucan mAb with antifungal activity has been previously reported [28,36]. To assess possible antifungal activity, both 3G11 and 5H5 mAbs were tested *in vitro* for the inhibition of *A. fumigatus*. As shown in the Fig 6A, both 3G11 and 5H5 showed growth inhibition during the initial hours of growth, from six hours up to ten hours. We then checked the capacity of these antibodies to facility phagocytosis of *A. fumigatus* conidia by human monocyte derived macrophages. As 5H5 did not show efficient binding with *A. fumigatus* germinating conidia, we used only 3G11 for this study. Indeed, pretreatment of *A. fumigatus* conidia with 3G11 accelerated conidial phagocytosis by HMDM during the one hour of conidia-macrophage interaction (Fig 6B).

In addition, the anti-fungal activity of mAbs 3G11 and 5H5 was tested *in vitro* for the growth inhibition of *C. albicans*. An overnight *C. albicans* culture was adjusted in SDB to contain 10^5 CFU/mL, mixed with two-fold serial dilutions of mAbs 3G11 or 5H5, starting at 800 μg/mL, and cultivated for 18 h. (Fig 7A). After cultivation, aliquots were titrated and plated on Sabouraud Dextrose agar plates, and colonies were counted after overnight incubation. The results indicated that both mAbs inhibited *C. albicans* growth when they were added only at a concentration of 800 μg/mL. The addition of both mAbs at a concentration of 400 μg/mL insignificantly decreased *C. albicans* cell growth, and the other concentrations were totally

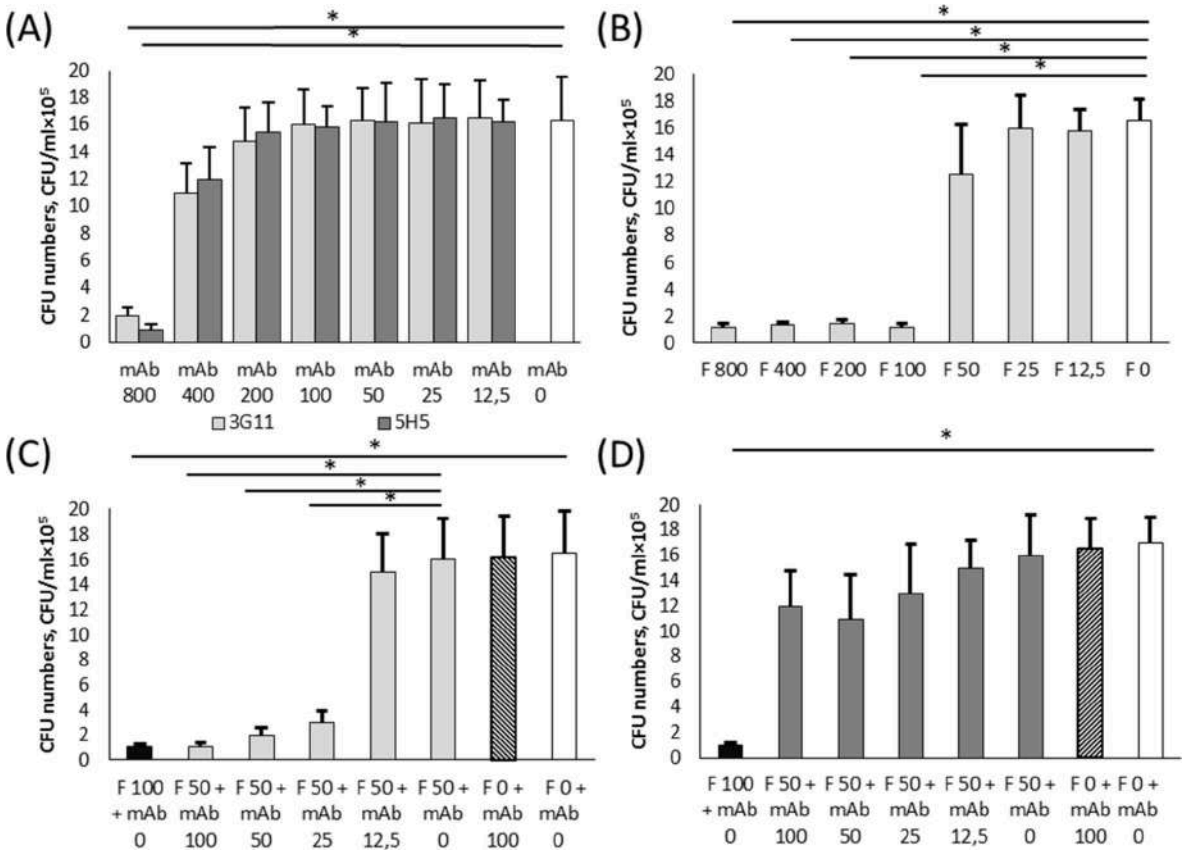

Fig 7. Antifungal activity of mAbs 3G11 and 5H5 and fluconazole. Two-fold dilutions of mAbs 3G11 or 5H5 **(A)**, fluconazole **(B)**, fluconazole with mAb 3G11 **(C)**, or fluconazole with mAb 5H5 **(D)** were added to an overnight *C. albicans* culture (10^5 CFU/mL), and the mixtures were incubated at room temperature with shaking for 18 h. After incubation, aliquots were collected, serially diluted and plated on Sabouraud Dextrose agar, and the plates were incubated overnight at room temperature. The colonies, which grew on the plates, were counted. All experiments were carried out twice in triplicate. When fluconazole and a mAb were added simultaneously, fluconazole at a concentration of 100 μg/mL and sterile 0.9% NaCl were used as positive and negative controls, respectively. The limit of quantification by this method was 100 CFU/mL. The data are indicated as a mean value ± s.d. A two-tailed Student's t- test was used to determine significance; $^*p < 0.01$. Abbreviations: F.–Fluconazole; mAb–appropriate mAb; numbers indicate fluconazole and mAbs concentrations in μg/mL.

https://doi.org/10.1371/journal.pone.0215535.g007

ineffective (Fig 7A). Next, the inhibition concentration of the well-known commercial antifungal preparation fluconazole was assessed in similar experiments (Fig 7B). *C. albicans* (10^5 CFU/mL) was grown overnight with two-fold serial dilutions of fluconazole starting at 800 μg/mL. The addition of fluconazole at concentrations of 100–800 μg/mL led to inhibition of *C. albicans* growth, whereas concentration of 50 μg/mL only insignificantly decreased cell growth (Fig 7B). Finally, the possibility of cooperative growth inhibitory activity between fluconazole and mAb 3G11 or mAb 5H5 was examined. In these experiments, 50 μg/mL of fluconazole, which was sub-inhibitory concentration, was mixed with two-fold serial dilutions of mAbs 3G11 or 5H5, starting at 100 μg/mL, and these mixtures were added to a fresh overnight *C. albicans* cultures. Fluconazole at a concentration of 100 μg/mL and 0.9% NaCl were used as the positive and negative controls. There results indicated that mAb 3G11 provided cooperative *C. albicans* growth inhibitory action with fluconazole at mAbs 3G11 concentrations of 25–100 μg/mL (Fig 7C). Unlike mAb 3G11 with fluconazole, mAb 5H5 showed a weak co-operative *C. albicans* growth inhibitory activity (Fig 7D).

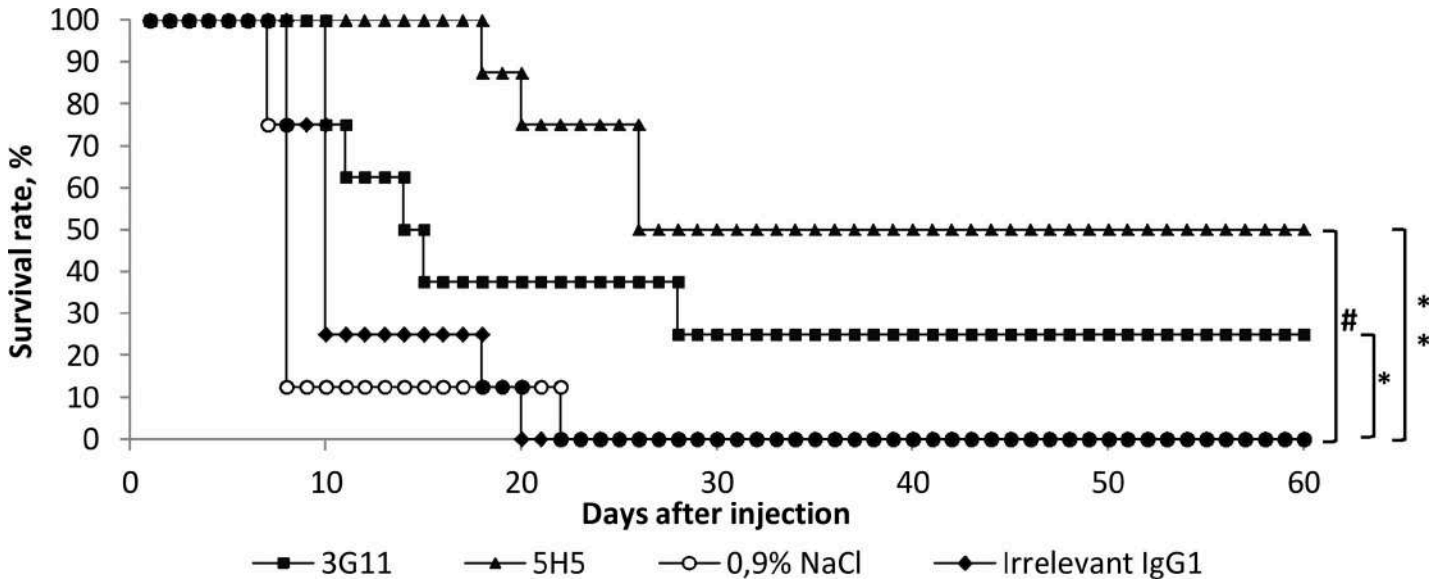

Fig 8. Protection of mice by mAbs 3G11 and 5H5 against fungal infection. BALB/c mice were administered (i.p.) once the indicated mAbs (150 μg/mouse in 0.5 mL 0.9% NaCl) or 0.5 mL 0.9% NaCl, and 2 h later, the mice received a lethal dose of *C. albicans* (5×10^6 CFU/mouse). The survival rate of mice treated with mAb 5H5 was significantly higher than that of mice injected with 0.9% NaCl or an irrelevant mAb; #$p < 0.05$. The survival time of mice passively immunized with mAb 3G11 or mAb 5H5 was significantly higher than that of mice administered with 0.9% NaCl or an irrelevant mAb; $^{*}p < 0.01$, $^{**}p < 0.001$.

https://doi.org/10.1371/journal.pone.0215535.g008

Protective efficacy of mAbs 3G11 and 5H5

To test the protective efficacy of mAbs 3G11 and 5H5, a mouse model of systemic candidiasis [28,29] was used. Four groups of female BALB/c mice received a single pre-exposure injection of mAb 3G11, mAb 5H5, irrelevant mAb (IgG1), or 0.9% NaCl and then were infected with a lethal dose of *C. albicans*. As expected, no protection was observed when mice were administered with irrelevant mAb and 0.9% NaCl (Fig 8). The survival rate of mice treated with mAb 5H5 was significantly higher than the survival rates of animals, received irrelevant mAb or 0.9% NaCl. Moreover, a single injection of mAbs 3G11 and 5H5 resulted in a significant increase in the survival times, compared to those in mice injected with irrelevant mAb or 0.9% NaCl (Fig 8). The higher protective efficacy of mAb 5H5 compared to mAb 3G11 can be explained by its higher affinity (Table 1) and broader antigenic specificity, as, in contrast to mAb 3G11, mAb 5H5 effectively bound to all linear β-(1→3)-linked oligoglucosides longer than a trimer and recognized branched oligoglucosides **brG6-I**, **brG6-II**, **brG8** (Fig 2). In addition, mAb 5H5 belongs to the IgG3 family, which is known to induce antibody-dependent cellular cytotoxicity (ADCC) and antibody-dependent cellular phagocytosis (ADCP) more effectively than IgG1 [37]. In *C. albicans* infection model 5H5 showed better protection to mice compared to 3G11, which could be related to the observation that 3G11 interacts with bud-cells (see Fig 4), whereas 5H5 could target mother cells, the main infective propagules. Immunolabelling and growth inhibition assay with A. fumigatus suggests that 3G11 and 5H5 are more specific for linear and branched β-(1→3)-glucans, respectively. Linear glucans are exposed on the germ tube, and during growth, neo-synthesis and branching of β-(1→3)-glucan, the two essential phenomena [38], are targeted by 3G11 and 5H5, respectively.

Conclusions

Several examples of anti-fungal antibodies with protective efficacy have been described [28,39–43]. Natural polysaccharides purified from fungal cells where been used to induce anti-

fungal antibodies. In this study, for the first time a synthetic oligosaccharide derivative was used successfully for the development of mAbs with protective efficacy. β-Glucan is the major component of the fungal cell wall; we developed monoclonal anti-β-(1→3)-D-glucan antibodies by immunization of mice with a BSA-conjugate of synthetic nona-β-(1→3)-D-glucoside and hybridoma technology. The carbohydrate affinity of mAbs 3G11 and 5H5 was assessed by SPR and was approximately 19 nM and 1.9 nM, respectively. In addition, the carbohydrate specificity of the mAbs was determined using a thematic glycoarray built from a series of synthetic oligosaccharide ligands structurally related to the characteristic β-(1→3)-D-glucan fragments. Immunolabelling studies confirmed the selectivity of developed mAbs in detecting β-(1→3)-D-glucan on the surface of the fungal cell wall. Further, these antibodies could inhibit fungal growth *in vitro*, facilitate fungal phagocytosis by host immune cells *in situ*, and showed efficacy in combination therapy by decreasing the required drug concentration of fluconazole compared to monotherapy. Moreover, clear protective efficacy was observed for both mAbs in *in vivo* experiments using a lethal mouse model of systemic candidiasis.

Supporting information

S1 File. Immunofluorescence microscopy of different microbial species. Immunolabelling for *C. tropicalis*, *C. parapsilosis*, *C. dubliniensis*, *D. hansenii*, gram-positive (*B. infantis*, *B. longum*, *E. faecalis*, *L. plantarum*, and *S. aureus*) and gram-negative (*A. faecalis*, *P. mirabilis*, *P. aeruginosa*, and *S. enterica*) bacterial species by mAbs 3G11 and 5H5.
(PDF)

S1 Fig. Assaying of bacterial supernatants with mAbs 3G11 and 5H5. Sandwich enzyme-linked immunosorbent assay (ELISA) with anti-**G9** antibodies: the wells of microtiter plates were coated with 200 ng mAb 3G11 (**A**) or mAb 5H5 (**B**) and incubated with serially diluted culture supernatants of indicated bacterial cultures; horseradish peroxidase-conjugated mAb 5H5 was used for sandwich ELISA.
(PDF)

Acknowledgments

The synthesis of biotinylated oligosaccharides and of BSA-based glycoconjugate immunogen was supported by Russian Science Foundation (grant 14-50-00126), assaying of antibodies on the glycoarray was supported by Russian Science Foundation (grant 14-23-00199). The development of mouse mAbs, the SPR-study, and confocal microscopy (in part) were supported by Russian Science Foundation (grant 16-14-00083). Microorganisms used in this work were provided by the Collection of Extremophile Microorganisms and Type Cultures (developed within Project 0309-2017-0008 granted by the Russian Federal Agency of Scientific Organizations). Study of the recognition of cell cultures by monoclonal antibodies was supported by the Franco-German ANR-DFG (ANR-16-CE92-0031-01 AFUINTERACT) and the Franco-Indian CEFIPRA (Project N˚ 5403–1) grants.

Author Contributions

Conceptualization: Nikolay E. Nifantiev.

Data curation: Jean-Paul Latgé, Nikolay E. Nifantiev.

Formal analysis: Vadim B. Krylov.

Funding acquisition: Dmitry V. Yashunsky, Vishukumar Aimanianda, Jean-Paul Latgé, Nina V. Tikunova, Nikolay E. Nifantiev.

Investigation: Andrey L. Matveev, Vadim B. Krylov, Yana A. Khlusevich, Ivan K. Baykov, Dmitry V. Yashunsky, Ljudmila A. Emelyanova, Yury E. Tsvetkov, Alexander A. Karelin, Alevtina V. Bardashova, Sarah S. W. Wong, Vishukumar Aimanianda.

Project administration: Nikolay E. Nifantiev.

Supervision: Nina V. Tikunova, Nikolay E. Nifantiev.

Validation: Jean-Paul Latgé.

Visualization: Vadim B. Krylov.

Writing – original draft: Andrey L. Matveev, Vadim B. Krylov, Vishukumar Aimanianda, Jean-Paul Latgé, Nina V. Tikunova, Nikolay E. Nifantiev.

Writing – review & editing: Vadim B. Krylov, Vishukumar Aimanianda, Jean-Paul Latgé, Nikolay E. Nifantiev.

References

1. Clancy CJ, Nguyen MH. Finding the "Missing 50%" of Invasive Candidiasis: How Nonculture Diagnostics Will Improve Understanding of Disease Spectrum and Transform Patient Care. Clin Infect Dis. 2013; 56: 1284–1292. https://doi.org/10.1093/cid/cit006 PMID: 23315320
2. Denning DW. Calling upon all public health mycologists. Eur J Clin Microbiol Infect Dis. 2017; 36: 923–924. https://doi.org/10.1007/s10096-017-2909-8 PMID: 28150046
3. Erwig LP, Gow NA. Interactions of fungal pathogens with phagocytes. Nat Rev Microbiol. 2016; 14: 163. https://doi.org/10.1038/nrmicro.2015.21 PMID: 26853116
4. Bacic A, Fincher GB, Stone BA. Chemistry, Biochemistry, and Biology of β-(1–3)-Glucans and Related Polysaccharides. Academic Press; 2009.
5. Karelin AA, Tsvetkov YE, Nifantiev NE. Synthesis of oligosaccharides related to polysaccharides of the cell wall of the fungi Candida and Aspergillus. Russ Chem Rev. 2017; 86: 1073–1126. https://doi.org/10.1070/RCR4750
6. Tsvetkov YE, Khatuntseva EA, Yashunsky DV, Nifantiev NE. Synthetic β-(1→3)-D-glucooligosaccharides: model compounds for the mechanistic study of β-(1→3)-D-glucan bioactivities and design of antifungal vaccines. Russ Chem Bull. 2015; 64: 990–1013. https://doi.org/10.1007/s11172-015-0969-4
7. Tamura H, Arimoto Y, Tanaka S, Yoshida M, Obayashi T, Kawai T. Automated kinetic assay for endotoxin and (1→3)-β-D-glucan in human blood. Clin Chim Acta Int J Clin Chem. 1994; 226: 109–112. https://doi.org/10.1016/0009-8981(94)90110-4
8. Mikami T, Nagase T, Matsumoto T, Suzuki S, Suzuki M. Gelation of Limulus Amoebocyte Lysate by Simple Polysaccharides. Microbiol Immunol. 1982; 26: 403–409. https://doi.org/10.1111/j.1348-0421.1982.tb00190.x PMID: 6181382
9. Tamura H, Finkelman MA. Detection and Measurement of (1→3)-β-D-Glucan with Limulus Amebocyte Lysate-Based Reagents. Toxicology of 1-3-Beta-Glucans. CRC Press; 2005. pp. 191–210.
10. Racil Z, Kocmanova I, Lengerova M, Weinbergerova B, Buresova L, Toskova M, et al. Difficulties in using 1,3-β-D-glucan as the screening test for the early diagnosis of invasive fungal infections in patients with haematological malignancies–high frequency of false-positive results and their analysis. J Med Microbiol. 2010; 59: 1016–1022. https://doi.org/10.1099/jmm.0.019299-0 PMID: 20488937
11. Douwes J, Doekes G, Montijn R, Heederik D, Brunekreef B. An immunoassay for the measurement of (1→3)-β-D-glucans in the indoor environment. Mediators Inflamm. 1997; 6: 257–262. https://doi.org/10.1080/09629359791578 PMID: 18472854
12. Noss I, Wouters IM, Bezemer G, Metwali N, Sander I, Raulf-Heimsoth M, et al. β-(1, 3)-Glucan exposure assessment by passive airborne dust sampling and new sensitive immunoassays. Appl Environ Microbiol. 2010; 76: 1158–1167. https://doi.org/10.1128/AEM.01486-09 PMID: 20038709
13. Akhapkina IG, Zheltikova TM, Antropova A., Mikhailova NA, Yashunskiy DV, Karelin AA, et al. Development of methodical approaches to creation of reagents for enzyme-linked immunosorbent detection of linear β-(1→3)-glucans and their derivatives in the environment. Immunologiya. 2015; 36: 276–279.
14. Paulovičová E, Paulovičová L, Pilišiová R, Jančinová V, Yashunsky DV, Karelin AA, et al. The evaluation of β-(1→3)-nonaglucoside as an anti-Candida albicans immune response inducer. Cell Microbiol. 2016; 18: 1294–1307. https://doi.org/10.1111/cmi.12631 PMID: 27310441

15. Yashunsky DV, Tsvetkov YE, Grachev AA, Chizhov AO, Nifantiev NE. Synthesis of 3-aminopropyl glycosides of linear β-(1→3)-D-glucooligosaccharides. Carbohydr Res. 2016; 419: 8–17. https://doi.org/10.1016/j.carres.2015.10.012 PMID: 26595660

16. Yashunsky DV, Tsvetkov YE, Nifantiev NE. Synthesis of 3-aminopropyl glycosides of branched β-(1→3)-glucooligosaccharides. Russ Chem Bull. 2015; 64: 2922–2931. https://doi.org/10.1007/s11172-015-1249-z

17. Yashunsky DV, Tsvetkov YE, Nifantiev NE. Synthesis of 3-aminopropyl glycoside of branched β-(1→3)-D-glucooctaoside. Carbohydr Res. 2016; 436: 25–30. https://doi.org/10.1016/j.carres.2016.11.005 PMID: 27846427

18. Varki A, Cummings R, Esko J, Freeze H, Hart G, Marth J. Essentials of glycobiology. NY: Cold Spring Harbor; 1999.

19. Tsvetkov YE, Burg-Roderfeld M, Loers G, Ardá A, Sukhova EV, Khatuntseva EA, et al. Synthesis and molecular recognition studies of the HNK-1 trisaccharide and related oligosaccharides. The specificity of monoclonal anti-HNK-1 antibodies as assessed by surface plasmon resonance and STD NMR. J Am Chem Soc. 2011; 134: 426–435. https://doi.org/10.1021/ja2083015 PMID: 22087768

20. Matveev AL, Krylov VB, Emelyanova LA, Solovev AS, Khlusevich YA, Baykov IK, et al. Novel mouse monoclonal antibodies specifically recognize Aspergillus fumigatus galactomannan. PloS One. 2018; 13: e0193938. https://doi.org/10.1371/journal.pone.0193938 PMID: 29518144

21. Wang Z, Raifu M, Howard M, Smith L, Hansen D, Goldsby R, et al. Universal PCR amplification of mouse immunoglobulin gene variable regions: the design of degenerate primers and an assessment of the effect of DNA polymerase 3' to 5' exonuclease activity. J Immunol Methods. 2000; 233: 167–177. PMID: 10648866

22. Nakane PK, Kawaoi A. Peroxidase-labeled antibody a new method of conjugation. J Histochem Cytochem. 1974; 22: 1084–1091. https://doi.org/10.1177/22.12.1084 PMID: 4443551

23. Krylov VB, Solovev AS, Argunov DA, Latgé J-P, Nifantiev NE. Reinvestigation of carbohydrate specificity of EB-A2 monoclonal antibody used in the immune detection of Aspergillus fumigatus galactomannan. Heliyon. 2019; 5: e01173. https://doi.org/10.1016/j.heliyon.2019.e01173 PMID: 30766929

24. Komarova BS, Wong SSW, Orekhova MV, Tsvetkov YE, Krylov VB, Beauvais A, et al. Chemical synthesis and application of biotinylated oligo-α-(1→3)-D-glucosides to study the antibody and cytokine response against the cell wall α-(1→3)-D-glucan of Aspergillus fumigatus. J Org Chem. 2018; 83: 12965–12976. https://doi.org/10.1021/acs.joc.8b01142 PMID: 30277398

25. Feliu JX, Villaverde A. An optimized ultrasonication protocol for bacterial cell disruption and recovery of β-galactosidase fusion proteins. Biotechnol Tech. 1994; 8: 509–514.

26. Shende R, Wong SSW, Rapole S, Beau R, Ibrahim-Granet O, Monod M, et al. Aspergillus fumigatus conidial metalloprotease Mep1p cleaves host complement proteins. J Biol Chem. 2018; https://doi.org/10.1074/jbc.RA117.001476 PMID: 30139746

27. Wong SSW, Rani M, Dodagatta-Marri E, Ibrahim-Granet O, Kishore U, Bayry J, et al. Fungal melanin stimulates surfactant protein D-mediated opsonization of and host immune response to Aspergillus fumigatus spores. J Biol Chem. 2018; 293: 4901–4912. https://doi.org/10.1074/jbc.M117.815852 PMID: 29414772

28. Torosantucci A, Chiani P, Bromuro C, De Bernardis F, Palma AS, Liu Y, et al. Protection by anti-β-glucan antibodies is associated with restricted β-1, 3 glucan binding specificity and inhibition of fungal growth and adherence. PLoS One. 2009; 4: e5392. https://doi.org/10.1371/journal.pone.0005392 PMID: 19399183

29. Cihlar RL, Calderone RA. Candida albicans: methods and protocols. Preface. Methods Mol Biol Clifton NJ. 2009; 499: v.

30. Baykov IK, Matveev AL, Stronin OV, Ryzhikov AB, Matveev LE, Kasakin MF, et al. A protective chimeric antibody to tick-borne encephalitis virus. Vaccine. 2014; 32: 3589–3594. https://doi.org/10.1016/j.vaccine.2014.05.012 PMID: 24837772

31. Gerbst AG, Grachev AA, Yashunsky DV, Tsvetkov YE, Shashkov AS, Nifantiev NE. Theoretical and Experimental Conformational Studies of Oligoglucosides Structurally Related to Fragments of Fungal Cell Wall β-(1→3)-D-Glucan. J Carbohydr Chem. 2013; 32: 205–221. https://doi.org/10.1080/07328303.2013.793347

32. Mennink-Kersten MASH, Ruegebrink D, Verweij PE. Pseudomonas aeruginosa as a cause of 1,3-β-D-glucan assay reactivity. Clin Infect Dis. 2008; 46: 1930–1931. https://doi.org/10.1086/588563 PMID: 18540808

33. McIntosh M, Stone BA, Stanisich VA. Curdlan and other bacterial (1→3)-β-D-glucans. Appl Microbiol Biotechnol. 2005; 68: 163–173. https://doi.org/10.1007/s00253-005-1959-5 PMID: 15818477

34. Beauvais A, Fontaine T, Aimanianda V, Latgé J-P. Aspergillus cell wall and biofilm. Mycopathologia. 2014; 178: 371–377. https://doi.org/10.1007/s11046-014-9766-0 PMID: 24947169

35. Cui J-D, Qiu JQ. Production of extracellular water-insoluble polysaccharide from Pseudomonas sp. J Agric Food Chem. 2012; 60: 4865–4871. https://doi.org/10.1021/jf3006273 PMID: 22533491

36. Pietrella D, Rachini A, Torosantucci A, Chiani P, Brown AJ, Bistoni F, et al. A β-glucan-conjugate vaccine and anti-β-glucan antibodies are effective against murine vaginal candidiasis as assessed by a novel in vivo imaging technique. Vaccine. 2010; 28: 1717–1725. https://doi.org/10.1016/j.vaccine.2009.12.021 PMID: 20038431

37. Gavin AL, Barnes N, Dijstelbloem HM, Hogarth PM. Identification of the mouse IgG3 receptor: implications for antibody effector function at the interface between innate and adaptive immunity. J Immunol Baltim Md 1950. 1998; 160: 20–23.

38. Aimanianda V, Simenel C, Garnaud C, Clavaud C, Tada R, Barbin L, et al. The Dual Activity Responsible for the Elongation and Branching of β-(1,3)-Glucan in the Fungal Cell Wall. mBio. 2017; 8. https://doi.org/10.1128/mBio.00619-17 PMID: 28634239

39. Mukherjee J, Nussbaum G, Scharff MD, Casadevall A. Protective and nonprotective monoclonal antibodies to Cryptococcus neoformans originating from one B cell. J Exp Med. 1995; 181: 405–409. PMID: 7807020

40. Yuan RR, Spira G, Oh J, Paizi M, Casadevall A, Scharff MD. Isotype switching increases efficacy of antibody protection against Cryptococcus neoformans infection in mice. Infect Immun. 1998; 66: 1057–1062. PMID: 9488395

41. Torosantucci A, Bromuro C, Chiani P, De Bernardis F, Berti F, Galli C, et al. A novel glyco-conjugate vaccine against fungal pathogens. J Exp Med. 2005; 202: 597–606. https://doi.org/10.1084/jem.20050749 PMID: 16147975

42. Rachini A, Pietrella D, Lupo P, Torosantucci A, Chiani P, Bromuro C, et al. An anti-beta-glucan monoclonal antibody inhibits growth and capsule formation of Cryptococcus neoformans in vitro and exerts therapeutic, anticryptococcal activity in vivo. Infect Immun. 2007; 75: 5085–5094. https://doi.org/10.1128/IAI.00278-07 PMID: 17606600

43. Rudkin FM, Raziunaite I, Workman H, Essono S, Belmonte R, MacCallum DM, et al. Single human B cell-derived monoclonal anti-Candida antibodies enhance phagocytosis and protect against disseminated candidiasis. Nat Commun. 2018; 9: 5288. https://doi.org/10.1038/s41467-018-07738-1 PMID: 30538246

УДК 577.114.5+616-073.55

Возможности поляризационного флуоресцентного иммуноанализа для определения галактоманнана *Aspergillus fumigatus*

В. Б. Крылов,[а] М. И. Петрук,[а,б] М. Р. Каримова,[б] Л. И. Мухаметова,[б] А. Л. Матвеев,[в] Н. В. Тикунова,[в] С. А. Еремин,[б] Н. Э. Нифантьев[а]★

[а]Институт органической химии им. Н. Д. Зелинского Российской академии наук, Российская Федерация, 119991 Москва, Ленинский просп., 47. E-mail: nen@ioc.ac.ru
[б]Московский государственный университет им. М. В. Ломоносова, Российская Федерация, 119991 Москва, Ленинские горы, 1, стр. 11
[в]Институт химической биологии и фундаментальной медицины Сибирского отделения Российской академии наук, Российская Федерация, 630090 Новосибирск, просп. Акад. Лаврентьева, 8

В данном сообщении проведена оценка аналитических возможностей метода поляризционно-флуоресцентного иммуноанализа (ПФИА) для обнаружения галактоманнана (ГМ) — специфического полисахаридного антигена условно-патогенных плесневых грибов рода *Aspergillus*. Обнаружение ГМ в биологических жидкостях пациентов является надежным критерием для диагностики опасного заболевания — инвазивного аспергиллеза легких. С использованием ПФИА показана высокая аффинность моноклонального антитела 7B8 к синтетическому олигосахариду β-D-Gal*f*-[(1→5)-β-D-Gal*f*]$_3$-(1→6)-α-D-Man*p*, родственному фрагменту галактоманнана. Константа связывания данного взаимодействия составила $(1.02\pm0.01)\cdot10^8$ л·моль$^{-1}$. Предел детектирования, определенный для данного олигосахарида методом конкурентного ПФИА, составил 3 нг·мл$^{-1}$. Полученные данные свидетельствуют о принципиальной возможности использования ПФИА для диагностики инвазивного аспергиллеза.

Ключевые слова: *Aspergillus fumigatus*, флуоресценция, антиген, антитело, галактоманнан, диагностикум.

Грибковые патогены рода *Aspergillus* (прежде всего *A. fumigatus, A. flavus* и *A. niger*) являются возбудителями различных инфекционных заболеваний, в том числе аллергического бронхолегочного аспергиллеза, местного (неинвазивного) аспергиллеза, хронического легочного аспергиллеза и наиболее тяжелого и опасного для жизни заболевания — инвазивного аспергиллеза легких (ИАЛ)[1,2]. Раннее выявление заболеваний легких, обеспечивает значительное повышение эффективности их лечения, что обусловливает необходимость разработки быстрых и удобных методов их диагностики[3,4]. На настоящий момент обнаружение циркулирующего в кровотоке галактоманнана (ГМ) является признанным критерием для диагностики инвазивного аспергиллеза[4–6]. Галактоманнан представляет собой полисахарид, построенный из α-(1→2)-/α-(1→6)-связанной маннозной основной цепи, к которой через атомы O(3) или O(6) определенных маннозных остатков присоединены короткие β-(1→5)-олигогалактофуранозидные разветвления[7]. Недавние исследования выявили дополнительные структурные фрагменты ГМ, в частности β-(1→6)-связь между галактофуранозидными остатками[8,9].

В настоящее время обнаружение ГМ основано на «сэндвич»-формате иммуноферментного анализа с использованием моноклональных антител IgM EB-A2[10,11]. Данный набор характеризуется высокой диагностической чувствительностью (85.7%)[12] и специфичностью (85.4%)[12], тем не менее вероятность ложно-положительных результатов для данной тест-системы хорошо документирована[13–16]. В связи с этим в настоящее время активно ведутся разработки новых усовершенствованных диагностикумов на основе альтернативных моноклональных антител[17–19], а также использование альтернативных физических платформ, которые позволят автоматизировать и упростить проведение анализа[20,21].

Одной из таких аналитических платформ является метод поляризционно-флуоресцентного иммуноанализа (ПФИА), который хорошо зарекомендовал себя для решения целого ряда аналитических и медицинских задач. Метод ПФИА заключается в конкуренции определяемого вещества и вещества, меченного флуоресцентной меткой (трейсера), за связывание с ограниченным количеством антител и в определении степени поляризации флуоресценции трейсера. Чем больше в образце определяемого соединения, конкурирующего с трейсером за сайты связывания, тем ниже будет поляризация флуоресценции смеси. Метод ПФИА довольно прост в постановке и заключается в добавлении к образцу (обычно 10—50 мкл) аликво-

ты трейсера и раствора антител, инкубации в течение нескольких минут и измерении поляризации флуоресценции на поляризационном флуориметре. Общее время анализа с пробоподготовкой составляет 5—20 мин. Подробно метод и примеры определения биологически-активных веществ методом ПФИА рассмотрены в обзоре[22] и наших предыдущих публикациях[23,24].

Целью настоящей работы является исследование возможности диагностики инвазивного аспергиллеза методом ПФИА с использованием высокоаффинных мышиных моноклональных антител IgG3 7B8 к галактаманнану.

Обсуждение полученных результатов

Необходимым условием для проведения поляризационного флуоресцентного иммуноанализа является выбор подходящих высокоспецифичных антител и трейсера — антигена, конъюгированного с флуоресцентной меткой. Антитела, распознающие галактоманнан, существенно различаются по строению распознаваемого ими эпитопа[13,17,19]. В данной работе в качестве антител были выбраны мышиные моноклональные антитела изотипа IgG3 7B8, для которого показана высокая специфичность по отношению к галактоманнану грибов рода *Aspergillus*[17]. В качестве трейсера был выбран флуоресцентно-меченный пентасахарид **1** (см. лит.[25,26]), являющийся иммунодетерминантным олигосахаридным фрагментом галактоманнана. Для получения трейсера **2** аминопропилгликозид **1** (см. лит.[25]) обрабатывали флуоресцеинизотиоцианатом (FITC) в присутствии Na_2CO_3 (схема 1), после чего продукт выделяли с использованием картриджа с обращенной фазой C-18. Состав продукта подтверждали данными масс-спектрометрии высокого разрешения. В качестве детектируемого вещества при количественном определении методом ПФИА использовали исходный пентасахарид **1**, являющийся низкомолекулярной моделью природного галактоманнана.

Первоначально была изучена кинетика взаимодействия антитела 7B8 и трейсера **2**. В качестве отрицательного контроля использовали нерелевантное антитело 5H5, специфичное по отношению к β-глюкану, другому полисахаридному компоненту клеточной стенки гриба[27]. Как и ожидалось, трейсер **2** хорошо связывался с изучаемым моноклональным антителом 7B8[17], что приводило к существенному росту поляризации флуоресценции (m*P*) во времени (рис. 1).

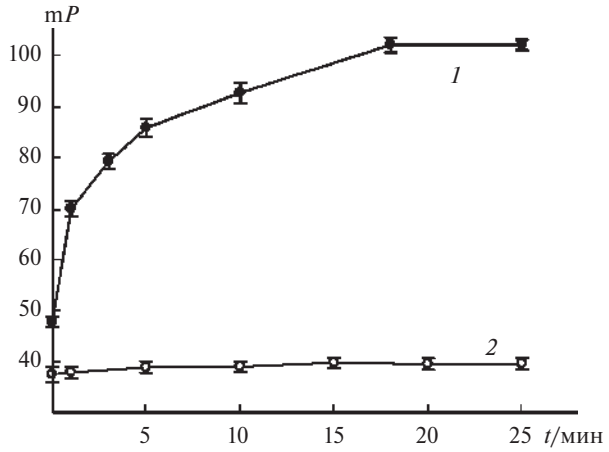

Рис. 1. Кинетика связывания трейсера **2** с антителом 7B8 (*1*) и нерелевантным антителом 5H5, использованным в качестве отрицательного контроля (*2*). Величина поляризации флуоресценции (m*P*)[22] выражена в безразмерных единицах[22]. Для каждого антитела измерения проводили трижды, результаты представлены в следующем виде: среднее значение ± стандартное отклонение.

Схема 1

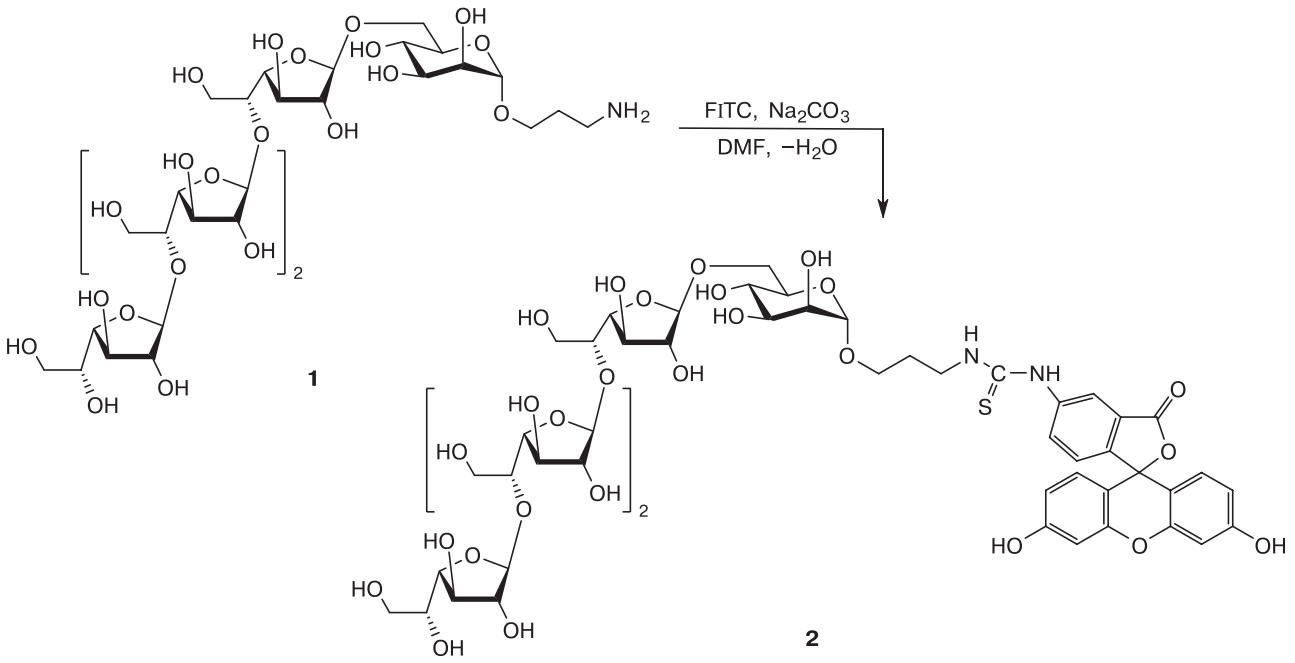

Вместе с тем добавление нерелевантного антитела 5H5 никак не изменяло поляризацию флуоресценции, что свидетельствует об отсутствии неспецифического взаимодействия между трейсером и иммуноглобулином.

Для оценки применимости ПФИА для обнаружения галактоманнана использовали метод, основанный на конкуренции определяемого антигена и антигена с флуоресцентной меткой за ограниченное число центров связывания специфических антител и измерении степени поляризации флуоресценции реакционной смеси. Полученная экспериментальная зависимость поляризации флуоресценции от концентрации антигена **1** представляла собой нелинейную зависимость (рис. 2, *a*). Диапазон концентраций, для которых наблюдается линейная зависимость (рис. 2, *b*), составил от 3 до 20 нг · мл$^{-1}$. Предел обнаружения антигена данным методом составил 3 нг · мл$^{-1}$. Данное значение было определено из расчета, что регистрируемый сигнал m*P* в присутствии пентасахарида **1** отличается на три среднеквадратичных отклонения от поляризации флуоресценции в отсутствие антигена.

Для расчета константы связывания (*K*) для области линейной зависимости строили график в координатах Скэтчарда (рис. 3), которые представляют собой зависимость отношения концентраций иммунокомплекса антиген—антитело (*B*) к концентрации антигена (**1**) в свободной форме (*F*) от концентрации иммунокомплекса (*B*), т.е. зависимость *B*/*F* от *B*. Тангенс угла наклона графика представляет собой значение константы комплексообразования[28].

Известно, что диагностическая чувствительность иммунохимических методов анализа определяется аффинностью антител, концентрацией меченого антигена и антител, а также методом проведения анализа и точностью получаемых данных. Высокая аффинность антител позволяет достичь высокой чувствительности анализа. Полученная константа связывания, рассчитанная по методу Скэтчарда из данных ПФИА, составила 1.02 · 10^8 л · моль$^{-1}$, что свидетельствует о хорошей аффинности антигена и моноклонального антитела 7B8 и, кроме того, хорошо согласуется с полученными ранее результатами. Константа связывания биотинилированного производного пентасахарида **1** с моноклональным антителом 7B8, определенная методом поверхностного плазмонного резонанса (ППР)[17], составила 1.9 · 10^8 л · моль$^{-1}$. При сравнении этих данных видно, что порядок полученных величин одинаковый, сами значения констант отличаются примерно в 2 раза, что можно считать достаточно хорошим результатом. Наблюдаемое расхождение константы связывания может быть вызвано очевидными принципиальными различиями используемых методов: во-первых, ППР является гетерогенным методом (т.е. антитела взаимодействуют с модифицированной антигеном поверхностью), а ПФИА — гомогенным (т.е. взаимодействие антитело-антиген происходит в растворе), во-вторых, в случае ППР использовали модифицированный антиген, в-третьих, использовали разные буферные растворы при разных значениях pH.

В ходе проделанной работы были выбраны трейсер и антитела, подходящие для определения галактоманнана *A. fumigatus* методами ПФИА. Высокая аффинность антитела 7B8 в условиях эксперимента была подтверждена расчетом константы связывания, кото-

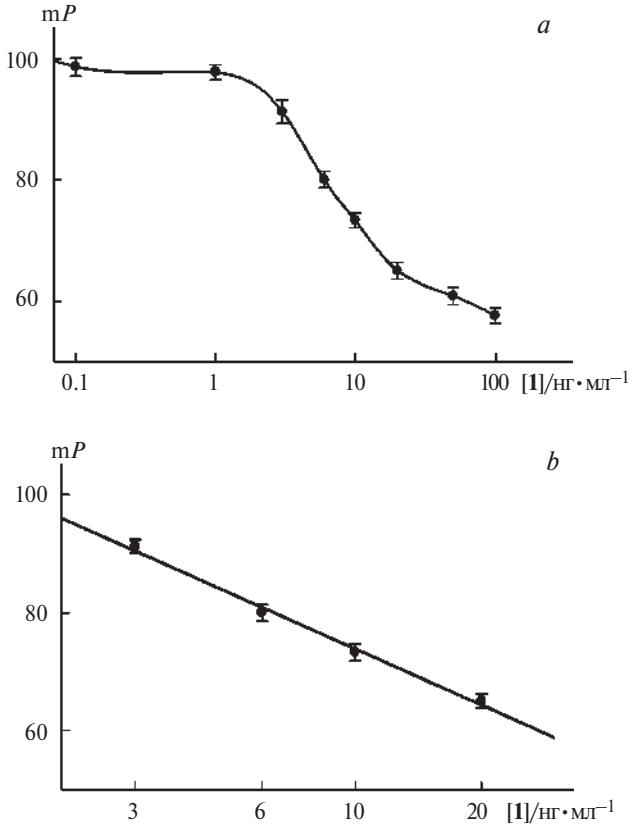

Рис. 2. Градуировочный график (*a*) и его линейный диапазон (*b*) с трейсером **2** для обнаружения пентасахарида **1**. Для каждой концентрации антигена проводили два независимых измерения по три аппаратных повторения. Результаты представлены в следующем виде: среднее значение ± стандартное отклонение.

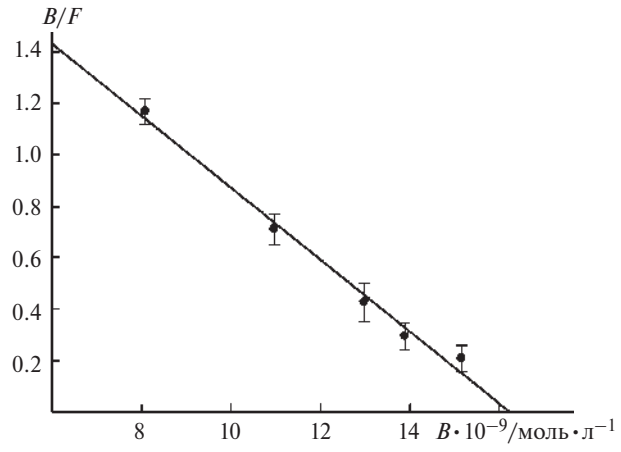

Рис. 3. Зависимость Скэтчарда для расчета константы связывания антигена **1** с антителом 7B8. Уравнение прямой: $y = (5.99\pm0.2) - (1.02\pm0.01) \cdot 10^8 x$. Рассчитанная константа связывания (*K*) составляет (1.02±0.01) · 10^8 л · моль$^{-1}$.

рая имела тот же порядок, что и константа, определенная ранее методом ППР. Предел детектирования, определенный для олигосахарида **1**, составил 3 нг · мл$^{-1}$, что сопоставимо с чувствительностью «сэндвич»-формата иммуноферментного анализа. Все это позволяет рассматривать поляризационно-флуоресцентный иммуноанализ как перспективный физический метод для разработки востребованных диагностических систем для выявления заболеваний, вызываемых грибами рода *Aspergillus*.

Экспериментальная часть

Реактивы и оборудование. В работе использовали синтетический пентасахарид **1**, родственный фрагменту галактоманнана *A. fumigatus*, полученный нами ранее[25,29] с помощью пиранозид-фуранозидной перегруппировки[30,31]. Моноклональные мышиные антитела 7B8 были получены ранее[17] с помощью синтетических иммуногенов на основе пентасахарида **1**. Использовали следующие коммерчески доступные реактивы: флуоресцеинизотиоцианат («Sigma-Aldrich»), карбонат натрия («Химмед», «х.ч.»), уксусную кислоту («Авилон-Компанихим», ледяную, «х.ч.»), диметилформамид («Sigma-Aldrich», 99.8%), таблетки для приготовления фосфатного буфера («Sigma»). Выделение конъюгатов проводили на обращенно-фазовом картридже Sep-Pak C18. Деионизованную воду получали с использованием системы для очистки воды «Simplicity Millipore» («Merck», USA). Фосфатный буфер (0.01 *M* фосфат натрия, 0.0027 *M* KCl, 0.137 *M* NaCl, pH 7.4) готовили растворением одной таблетки в 200 мл дистиллированной воды.

Масс-спектры высокого разрешения регистрировали на приборе «Bruker micrOTOF II» методом электрораспылительной ионизации (ESI). Измерения выполняли на положительных (напряжение на капилляре –4500 В) или отрицательных (напряжение на капилляре 3200 В) ионах. Диапазон сканирования масс — m/z 50 — 3000 Да, калибровка — внешняя или внутренняя («Electrospray Calibrant Solution», «Fluka»). Использовали шприцевой ввод вещества для растворов в ацетонитриле, метаноле или воде, скорость потока — 3 мкл · мин$^{-1}$. Газ-распылитель — азот (4 л · мин$^{-1}$), температура интерфейса — 180 °C.

Измерение поляризации флуоресценции проводили при комнатной температуре (20 °C) на поляризационном флуориметре «Sentry 200» («Ellie», USA). Стеклянную кювету помещали в специальную ячейку и измеряли поляризацию флуоресценции (mP) и интенсивность флуоресценции (в относительных единицах). Результаты обрабатывали по программе Sigma Plot 11 (Systat Software Inc., USA).

Синтез флуоресцеин-меченного антигена 2 (трейсер). К раствору аминопропилгликозида **1** (2.0 мг, 2.26 мкмоля) в дистиллированной воде (300 мкл) прибавляли 1 *M* водный раствор Na_2CO_3 (17 мкл) и раствор флуоресцеинизотиоцианата (1 мг, 2.57 мкмоля) в ДМФА (100 мкл), полученную реакционную смесь энергично перемешивали и выдерживали 2 ч при температуре 60 °C. Затем реакционную смесь концентрировали в вакууме, растворяли в 400 мкл воды, добавляли 0.1 *M* раствор уксусной кислоты (400 мкл) и наносили на картридж Sep-Pak C-18, предварительно промытый метанолом, а затем избытком воды. Картридж промывали порциями по 2 мл растворов метанола в воде от 0 до 55 об.% с шагом 5 об.%. Целевой продукт собирали в интервале 25—45%, упаривали на роторном испарителе и лиофильно высушивали с получением светло-оранжевого продукта. R_f 0.55 ($CHCl_3$—CH_3OH—H_2O, 10 : 5 : 1). Масс-спектр (ESI) найдено: m/z 1297.3446 $[M + Na]^+$; $C_{54}H_{70}N_2NaO_{31}S$; вычислено: 1297.3575.

Поляризационный флуоресцентный иммуноанализ. Для изучения кинетики связывания трейсера **2** с антителами 7B8 и 5H5 использовали рабочий раствор трейсера в 0.05 *M* боратном буфере (pH 8) с интенсивностью флуоресценции ~$(2.5\pm0.2) \cdot 10^5$ отн.ед. и концентрацией $7 \cdot 10^{-9}$ моль · л$^{-1}$. К 1 мл рабочего раствора трейсера добавляли раствор антител (10 мкл, 0.3 мг · мл$^{-1}$), конечная концентрация антител составляла $2 \cdot 10^{-8}$ моль · л$^{-1}$. Величину поляризации флуоресценции измеряли в течение 20—25 мин. Для каждого антитела проводили три независимых измерения.

Для построения градуировочного графика и расчета констант связывания антиген—антитело использовали рабочий раствор трейсера с интенсивностью $(4.0\pm0.2) \cdot 10^5$ отн.ед. Концентрацию рабочего раствора антитела 7B8 ($1.75 \cdot 10^{-8}$ моль · л$^{-1}$) подбирали таким образом, чтобы значение поляризации флуоресценции смеси стандартного раствора с нулевой концентрацией антигена (0.5 мл рабочего раствора трейсера + 0.5 мл рабочего раствора антитела) составляло около 70% от максимального значения mP, полученного при тестировании антител и трейсеров. Разбавлением исходного раствора пентасахарида **1** в деионизованной воде были получены стандартные растворы различных концентраций (от 0.1 до 100 нг · мл$^{-1}$).

Построение градуировочных графиков. Для построения градуировочного графика в кюветы последовательно добавляли по 10 мкл стандартных растворов различных концентраций пентасахарида **1**; 500 мкл рабочего раствора трейсера **2** и 500 мкл рабочего раствора антител 7B8. Растворы оставляли на воздухе при температуре 20 °C на 15 мин и затем измеряли степень поляризации флуоресценции растворов. На основании полученных результатов строили градуировочные графики. Для каждой концентрации антигена проводили два независимых измерения по три аппаратных повторения.

Расчет константы связывания комплекса антиген-антитело. При определении констант связывания использовали метод Скэтчарда[32]. Для этого в координатах Скэтчарда строили зависимость отношения концентраций иммунокомплекса антиген—антитело (B) к концентрации антигена в свободной форме (F) от концентрации иммунокомплекса (B), т.е. зависимость B/F от B. Тангенсы углов наклона графика представляют собой значения констант комплексообразования.

При использовании поляризационной флуоресцентной детекции определение отношения связанной и свободной форм антигена (B/F) проводили по уравнению

$$\left(\frac{B}{F}\right) = \frac{P_i - P_{\min}}{P_{\max} - P_i}, \qquad (1)$$

где B — концентрация связанной в комплекс формы антигена, F — свободная форма антигена, P_i — измеренная величина поляризации флуоресценции, $P_{\max}$ — величина поляризации флуоресценции при максимальном связывании антигена и антитела, $P_{\min}$ — величина поляризации флуоресценции при минимальном связывании антигена и антитела.

Концентрацию связанной формы антигена (B) вычисляли по уравнению

$$B = T\frac{X}{X+1}, \qquad (2)$$

где T — общее количество меченого и немеченого антигена в системе ($B + F$), X — отношения связанной и свободной форм антигена (B/F). Общая концентрация меченого

и немеченого антигена *T* при поляризационной флуоресцентной детекции, в частности при применении ПФИА, определяется как сумма концентраций свободного антигена, добавляемого в систему, и трейсера. Линейную аппроксимацию полученных данных в координатах Скэтчарда проводили с использованием программного обеспечения Sigma Plot 11 (Systat Software Inc., USA).

Работа выполнена при финансовой поддержке Российского научного фонда (проект № 19-73-30017).

Список литературы

1. G. D. Brown, D. W. Denning, N. A. R. Gow, S. M. Levitz, M. G. Netea, T. C. White, *Sci. Transl. Med.*, 2012, **4**, 165rv13.
2. J.-P. Latgé, *Clin. Microbiol. Rev.*, 1999, **12**, 310.
3. А. А. Ганеев, А. Р. Губаль, Г. Н. Лукьянов, А. И. Арсеньев, А. А. Барчук, И. Э. Джагацпанян, И. С. Горбунов, А. А. Рассадина, В. М. Немец, А. О. Нефедов, Б. А. Коротецкий, Н. Д. Соловьев, Е. Iakovleva, Н. Б. Иваненко, А. С. Кононов, M. Sillanpaa, Th. Seeger, *Успехи химии*, 2018, **87**, 904 [A. A. Ganeev, A. R. Gubal, G. N. Lukyanov, A. I. Arseniev, A. A. Barchuk, I. E. Jahatspanian, I. S. Gorbunov, A. A. Rassadina, V. M. Nemets, A. O. Nefedov, B. A. Korotetsky, N. D. Solovyev, E. Iakovleva, N. B. Ivanenko, A. S. Kononov, M. Sillanpaa, T. Seeger, *Russ. Chem. Rev.*, 2018, **87**, 904].
4. A. J. Ullmann, J. M. Aguado, S. Arikan-Akdagli, D. W. Denning, A. H. Groll, K. Lagrou, C. Lass-Flörl, R. E. Lewis, P. Munoz, P. E. Verweij, *Clin. Microbiol. Infect.*, 2018, **24**, e1.
5. T. F. Patterson, G. R. Thompson III, D. W. Denning, J. A. Fishman, S. Hadley, R. Herbrecht, D. P. Kontoyiannis, K. A. Marr, V. A. Morrison, M. H. Nguyen, *Clin. Infect. Dis.*, 2016, **63**, e1.
6. B. De Pauw, T. J. Walsh, J. P. Donnelly, D. A. Stevens, J. E. Edwards, T. Calandra, P. G. Pappas, J. Maertens, O. Lortholary, C. A. Kauffman, *Clin. Infect. Dis.*, 2008, **46**, 1813.
7. J.-P. Latgé, H. Kobayashi, J.-P. Debeaupuis, M. Diaquin, J. Sarfati, J.-M. Wieruszeski, E. Parra, J.-P. Bouchara, B. Fournet, *Infect. Immun.*, 1994, **62**, 5424.
8. V. B. Krylov, D. A. Argunov, A. S. Solovev, M. I. Petruk, A. G. Gerbst, A. S. Dmitrenok, A. S. Shashkov, J.-P. Latgé, N. E. Nifantiev, *Org. Biomol. Chem.*, 2018, **16**, 1188.
9. A. Kudoh, Y. Okawa, N. Shibata, *Glycobiology*, 2015, **25**, 74.
10. D. Stynen, A. Goris, J. Sarfati, J. P. Latge, *J. Clin. Microbiol.*, 1995, **33**, 497.
11. D. Stynen, J. Sarfati, A. Goris, M. C. Prevost, M. Lesourd, H. Kamphuis, V. Darras, J. P. Latge, *Infect. Immun.*, 1992, **60**, 2237.
12. P. L. White, T. Jones, K. Whittle, J. Watkins, R. A. Barnes, *Clin. Vaccine Immunol.*, 2013, **20**, 636.
13. V. B. Krylov, A. S. Solovev, D. A. Argunov, J.-P. Latgé, N. E. Nifantiev, *Heliyon*, 2019, **5**, e01173.
14. M. A. Mennink-Kersten, D. Ruegebrink, R. R. Klont, A. Warris, F. Gavini, H. J. O. den Camp, P. E. Verweij, *J. Clin. Microbiol.*, 2005, **43**, 3925.
15. M. A. Mennink-Kersten, R. R. Klont, A. Warris, H. J. O. den Camp, P. E. Verweij, *Lancet*, 2004, **363**, 325.
16. C. M. Swanink, J. F. Meis, A. J. Rijs, J. P. Donnelly, P. E. Verweij, *J. Clin. Microbiol.*, 1997, **35**, 257.
17. A. L. Matveev, V. B. Krylov, L. A. Emelyanova, A. S. Solovev, Y. A. Khlusevich, I. K. Baykov, T. Fontaine, J.-P. Latgé, N. V. Tikunova, N. E. Nifantiev, *PloS One*, 2018, **13**, e0193938.
18. M. Schubert, H. Spiegel, S. Schillberg, G. Nölke, *Biotechnol. Adv.*, 2018, **36**, 1167—1184.
19. M. Schubert, S. Xue, F. Ebel, A. Vaggelas, V. Krylov, N. Nifantiev, I. Chudobova, S. Schillberg, G. Nölke, *Front. Cell. Infect. Microbiol.*, 2019, **9**, 234.
20. K. M. Raval, V. Ghormade, P. R. Rajamohanan, H. Choudhary, S. M. Rudramurthy, A. Chakrabarti, K. Paknikar, *J. Med. Microbiol.*, 2019, **68**, 1341.
21. J. Held, T. Schmidt, C. R. Thornton, E. Kotter, H. Bertz, *Infection*, 2013, **41**, 1163—1169.
22. H. Zhang, S. Yang, K. De Ruyck, N. Beloglazova, S. A. Eremin, S. De Saeger, S. Zhang, J. Shen, Z. Wang, *TrAC Trends Anal. Chem.*, 2019, **114**, 293.
23. Y. Chen, Q. He, D. Shen, Z. Jiang, S. A. Eremin, S. Zhao, *Food Control*, 2019, **105**, 38.
24. E. A. Zvereva, A. V. Zherdev, A. A. Formanovsky, R. A. Abuknesha, S. A. Eremin, B. B. Dzantiev, *J. Pharm. Biomed. Anal.*, 2018, **159**, 326.
25. D. A. Argunov, V. B. Krylov, N. E. Nifantiev, *Org. Biomol. Chem.*, 2015, **13**, 3255.
26. E. Paulovičová, L. Paulovičová, M. Hrubiško, V. B. Krylov, D. A. Argunov, N. E. Nifantiev, *Front. Immunol.*, 2017, **8**, 127.
27. A. L. Matveev, V. B. Krylov, Y. A. Khlusevich, I. K. Baykov, D. V. Yashunsky, L. A. Emelyanova, Y. E. Tsvetkov, A. A. Karelin, A. V. Bardashova, S. S. W. Wong, V. Aimanianda, J.-P. Latgé, N. V. Tikunova, N. E. Nifantiev, *PloS One*, 2019, **14**, e0215535.
28. G. I. Hatzidakis, A. M. Tsatsakis, E. K. Krambovitis, A. Spyros, S. A. Eremin, *Anal. Chem.*, 2002, **74**, 2513.
29. D. A. Argunov, V. B. Krylov, N. E. Nifantiev, *Org. Lett.*, 2016, **18**, 5504.
30. V. B. Krylov, D. A. Argunov, D. Z. Vinnitskiy, S. A. Verkhnyatskaya, A. G. Gerbst, N. E. Ustyuzhanina, A. S. Dmitrenok, J. Huebner, O. Holst, H.-C. Siebert, N. E. Nifantiev, *Chem. Eur. J.*, 2014, **20**, 16516.
31. V. B. Krylov, D. A. Argunov, D. Z. Vinnitskiy, A. G. Gerbst, N. E. Ustyuzhanina, A. S. Dmitrenok, N. E. Nifantiev, *Synlett*, 2016, **27**, 1659.
32. H. Zhang, Q. Wu, M. Y. Berezin, *Expert Opin. Drug Discov.*, 2015, **10**, 1145.

Поступила в редакцию 2 октября 2019;
после доработки — 5 ноября 2019;
принята к публикации 11 ноября 2019

Sensing and Bio-Sensing Research 35 (2022) 100475

Contents lists available at ScienceDirect

Sensing and Bio-Sensing Research

journal homepage: www.elsevier.com/locate/sbsr

Nano-biosensor based on the combined use of the dynamic and static light scattering for *Aspergillus* galactomannan analysis

M.K. Alenichev [a], A.D. Levin [a,*], A.A. Yushina [a], Eu.S. Kostrikina [b], Yu.S. Lebedin [b], I. P. Andreeva [c], V.G. Grigorenko [c], V.B. Krylov [d], N.E. Nifantiev [d,*]

[a] *All-Russian Research Institute for Optical and Physical Measurements, Ozernaya st., 46, Moscow 119421, Russia*
[b] *Xema Ltd, 9 Parkovaya st., 48, Moscow 105284, Russia*
[c] *Lomonosov Moscow State University, Faculty of Chemistry, GSP-1, Leninskie Gory, Moscow 119991, Russia*
[d] *N. D. Zelinsky Institute of Organic Chemistry, Russian Academy of Sciences, Leninsky pr. 47, Moscow 119991, Russia*

ARTICLE INFO

Keywords:
Optical nanosensor
Dynamic light scattering
Elastic static light scattering
Antibodies
Aspergillus galactomannan

ABSTRACT

A biosensor based on the analyte-induced aggregation of functionalized nanoparticles recorded using two optical signals of different physical nature is developed. The hydrodynamic diameter of the conjugates, measured by the dynamic light scattering (DLS) method, and the counting rate of scattered light pulses, proportional to the elastic static scattering intensity are used together as the analytical signals. This improves the accuracy and reliability of the obtained results. Both signals are determined in one measurement on a compact DLS analyzer, specially designed as a detecting device for optical nano-biosensors. The proposed approach was used to detect *Aspergillus* galactomannan, a marker of an invasive fungal infection that poses a serious threat for the lungs. The results of the determination of galactomannan in the culture fluid of *Aspergillus* fungi, bronchoalveolar lavage (BAL) as well as in the calibration solutions, prepared on the basis of blood plasma and galactomannan calibrator are presented. A good correlation of the data obtained using nano- biosensor with the results of ELISA is shown, while the sensitivity of the analysis is not inferior to ELISA, and sample preparation is significantly simplified and accelerated by eliminating the washing stage. The detection limit for galactomannan in BAL samples was 3 ng/ml when detecting by the hydrodynamic diameter and 0.4 ng/ml when detecting by the counting rate of scattered light pulses. The total duration of sample preparation and measurements for a set of 10 samples does not exceed 100 min. The developed nano- biosensor can be used for the point of care diagnostics.

1. Introduction

Invasive pulmonary aspergillosis (IPA) is a dangerous fungal infection. *Aspergillus* spores can directly enter the tracheal bronchus and lungs, causing colonization of the airways, inflammatory granuloma of the lungs, and even more serious consequences such as necrotizing pneumonia. When spreading through the blood, spores can also infect other internal organs [1]. Initially, it was suggested that IPA occurs mainly in patients with neutrophil deficiency resulted from immunosuppressive therapy during organ transplantation, as well as the treatment of hematologic malignancies and human immunodeficiency virus (HIV) infection. IPA also poses a risk to people with pulmonary tuberculosis and chronic lung disease. Most recently, the incidence of IPA has been noted for patients with other types of severe viral infections, including COVID-19 and some forms of influenza virus [2]. In particular high incidence of IPA was reported for hospitalized patients with severe COVID-19 who were subjected to lung ventilation [3].

At the initial stages, IPA has no characteristic clinical manifestations, therefore its early diagnosis is an essential problem. The most important marker that allows this diagnosis is galactomannan (GM), a polysaccharide antigen that exists mainly in the cell wall of *Aspergillus* fungi. GM can enter the bloodstream and other body fluids already in the early stages of IPA and be present in them for a period ranging from 1 to 8 weeks. Therefore, the determination of the level of GM antigen is of considerable interest for the early diagnosis of IPA. Most often, measurements of GM level are carried out in blood plasma or and fluid secretions from the lungs, the so-called bronchoalveolar lavage (BAL). In some cases, the determination of GM is carried out in other biological fluids, for example, in urine. The physiologically relevant range of the GM concentration depends on the biological environment in which it is

* Corresponding authors.
E-mail addresses: levin-ad@vniiofi.ru (A.D. Levin), nen@ioc.ac.ru (N.E. Nifantiev).

https://doi.org/10.1016/j.sbsr.2022.100475
Received 4 November 2021; Received in revised form 26 January 2022; Accepted 1 February 2022
Available online 3 February 2022

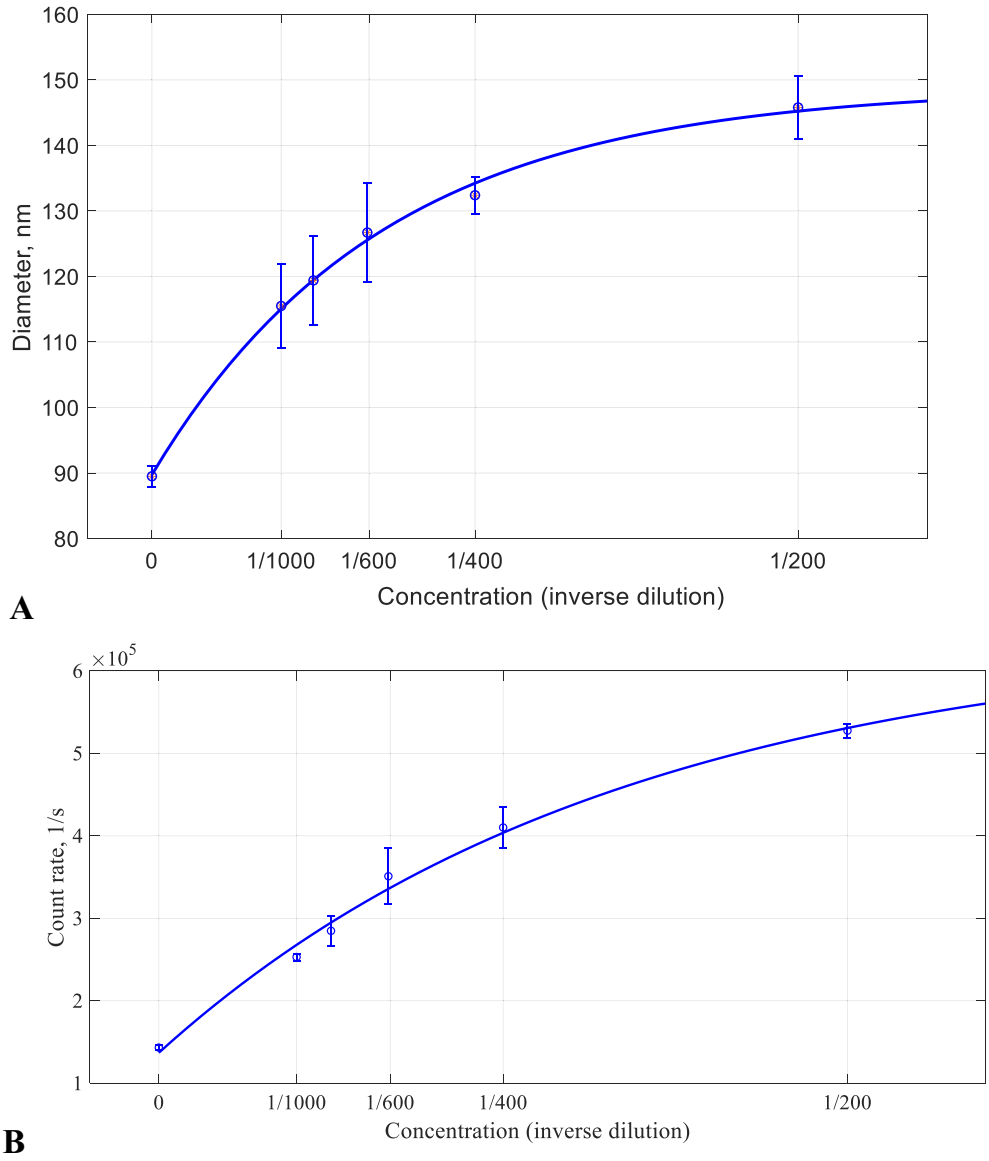

Fig. 1. Dependences of the hydrodynamic diameter of the conjugates (A) and the count rate (B) on CL concentration (reverse dilution), approximated using eq. (4). 5 replicates correspond for each point. The values of the fitting parameters are presented in tables SI-2 and SI-3.

present. For example, GM concentrations in BAL and serum of <10 ng/ml to 70 ng/ml and 10 ng/ml and 4 ng/ml respectively are regarded as positive values while 1 ng/ml as cut-off control [4,5].

Currently, the main method for GM determination in biological fluids is enzyme-linked immunosorbent assay (ELISA) [1,6]. Existing ELISA kits require rather long and laborious sample preparation, including stages of incubation with a total duration of 2.5 h and three-fold washing, while the total duration of analytical procedures is about 4 h. The analysis can be carried out only under laboratory conditions since it requires the use of washers and large fluid flow. At the same time, the analysis remains qualitative or semi-quantitative [7].

Recently, along with traditional methods of analysis, methods based on the use of biosensors have been developing. In many cases, biosensors can significantly simplify sample preparation, reduce the time of analysis, and use simple and cost-effective diagnostic devices to record the results. This permits to use of biosensors for point of care (POC) diagnostics [8,9]. Biosensors which use optical properties of nanosized particles are especially effective [10]. Such sensors are based on various physical effects, such as localized surface plasmon resonance (LSPR), surface-enhanced Raman scattering (SERS), static and dynamic light scattering, fluorescence [11,12], etc. Sensors based on dynamic light scattering (DLS) assess the presence of an analyte in solution by the detection of the aggregation of nanoparticles functionalized with receptors of the target analyte [13]. This platform is used successfully for quantitative detection of a wide range of chemical and biological targets [14,15].

DLS-based nanosensors were developed for proteins and nucleic acids [16–18], tumor markers [19–22], viruses and viral pathogens [23–25], some transgenic products [26], and toxic metal ions [27]. The use of DLS-based nanosensors for the creation of washing-free diagnostic kits is the most important and promising [28].

Monoclonal antibodies are most often used as receptors catching the analyte; recently, aptamers have also begun to be used for this purpose [15,29]. An aggregation of receptor-bearing beads with analytes forms the particles with increased size, which is determined by the DLS method, based on the measurement of intensity fluctuations of light scattered by the particles caused by their Brownian motion. The decay rate of these fluctuations, calculated from the autocorrelation function (ACF) of the scattered light intensity, allows estimation of the diffusion coefficient of particles, which, in turn, is used to calculate the

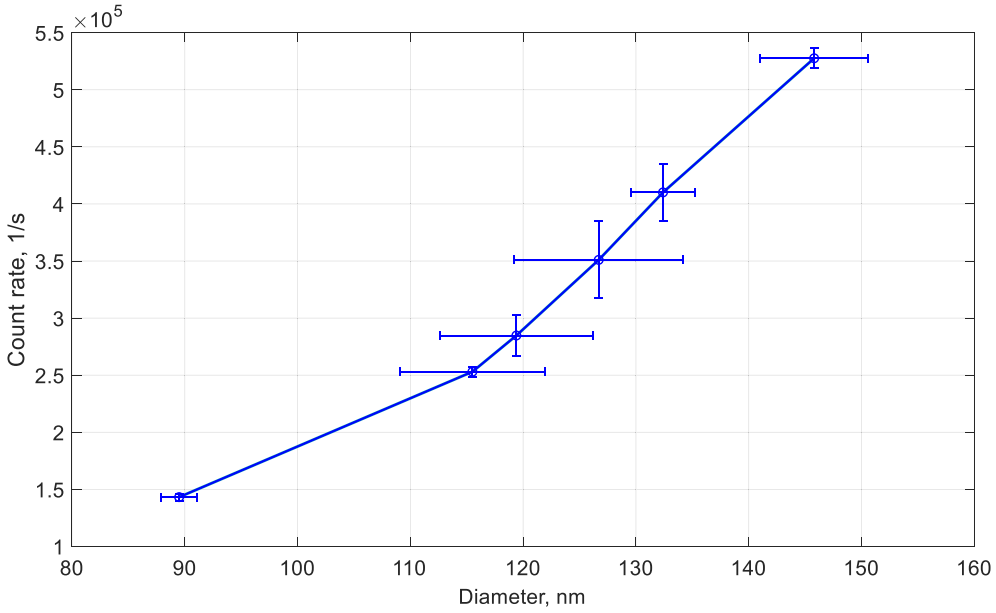

Fig. 2. Dependence of the photon count rate on the hydrodynamic diameter of the conjugates for CL samples of various degrees of dilution.

hydrodynamic diameter of these particles. In most DLS nanosensors, analyte molecules promote the aggregation of conjugates; however recently an alternative scheme was proposed based on the inhibition of this aggregation [30]. Until recently, in all DLS nanosensors, the hydrodynamic diameter of functionalized nanoparticles was used as the only analytical signal. Lately, a nanobiosensor was proposed for determining the CA 125 tumor marker via recognition of the polymerase chain reaction (PCR) product using two analytical signals – the hydrodynamic diameter of gold nanoparticle probes, measured by DLS, and the fluorescence intensity [31].

Another effective method used in optical nanobiosensors is Rayleigh light scattering (RLS), elastic scattering which intensity depends on the size and concentration of particles in the colloidal solution [32–35]. The average diameter of the particles in the solution increases with aggregation, increasing the scattered light intensity. In analytical applications of this method, scattering spectra are usually measured using a spectrofluorimeter operating in the synchronous scanning mode. In most cases, resonant RLS is used, in which the scattering wavelength is the same or close to the analyte absorption one. In some cases, an alternative approach is used, which uses scattering at a wavelength far enough from the absorption line, optimally at the red edge of the absorption band. This minimizes attenuation of the measured scattered light intensity due to the internal filter effect, as well as the formation of a thermal lens in the cuvette. Some proteins and vitamins, pesticides, and heavy metal ions were determined by the RLS method.

Thus, in the optical nanosensors discussed above, analyte-induced biospecific aggregation of nanoparticles is determined either by dynamic or by Rayleigh static light scattering. The signals recorded in this case have different physical nature. The average hydrodynamic diameter measured by DLS is determined by the diffusion motion of particles in a liquid medium and depends on its viscosity and temperature, respectively. The intensity of the scattered light, measured in static scattering, depends on the size, shape, and concentration of particles and the difference between refractive indices of these particles and the environment. The accuracy of these methods is limited by their specific sources of errors.

The work is aimed to develop an optical nanobiosensor for the determination of *Aspergillus* galactomannan in biological fluids suitable for express POC diagnostics. As compared to ELISA, this nanobiosensor should provide a simpler and faster sample preparation, washing is not needed. Also, it is necessary to provide the possibility of the quantitative determination of the analyte concentration with accuracy and reliability, not inferior to ELISA.

Gold particles functionalized with high-affinity antibodies to GM were used as probes in the biosensor. To ensure reliability and durability in the study of the aggregation of nanoparticles, these results were taken into account by two parameters - the hydrodynamic diameter of nanoparticles and intensity of their light scattering. These parameters were determined in each measurement using two independent channels. To determine the concentration of GM in clinical samples of biological fluids (BAL and blood plasma) a GM calibrator from the GalMAg-ELISA diagnostic kit was applied.

2. Materials and methods

2.1. Reagents, consumables, and accessories

2.1.1. Analytes

Serum calibrators of GM from the diagnostic test system GalMAg-ELISA (Xema Ltd., Moscow, Russia) were used in known amounts, specifically negative control – 0.0 ng/ml, Cut-Off – 0.7 ng/ml; positive control – 2.1 ng/ml. The development of the system is described [36–39].

The *Ammophilus fumigatus* strain KBP F-24 from the collection of the Department of Mycology and Algology, Faculty of Biology, M.*V.* Lomonosov Moscow State University was used to obtain a culture liquid. A *fumigatus* was grown in surface culture on a liquid Czapek medium (g/L): $NaNO_3$–2, KH_2PO_4–1, $MgSO_4$–0.5, KCl – 0.5, $FeSO_4$–0.01, sucrose – 20. The aqueous washout from a two-week culture of the fungus grown in test tubes on a slant agar medium is used as an inoculum. In shake flasks with 150 ml of medium, 107 CFU of fungal spores were added and incubated for 20 days at a temperature 26 °C. During this time, a film was formed on the surface of the liquid medium, consisting of a dense plexus of hyphae (branching filaments of fungi), and sporulation was developed on the top of the mycelium. The fungal mass was removed from the flask with the sterile spatula (or tweezers). The remaining culture fluid was centrifuged at 2000 *g* for 10 min at 4 °C, the supernatant solution was separated and treated with acetone for inactivation. The resulting solution was used as an analyte for the determination of GM.

Clinical BAL samples were collected with the written consent of the patients of the hematology department of the National Medical Research

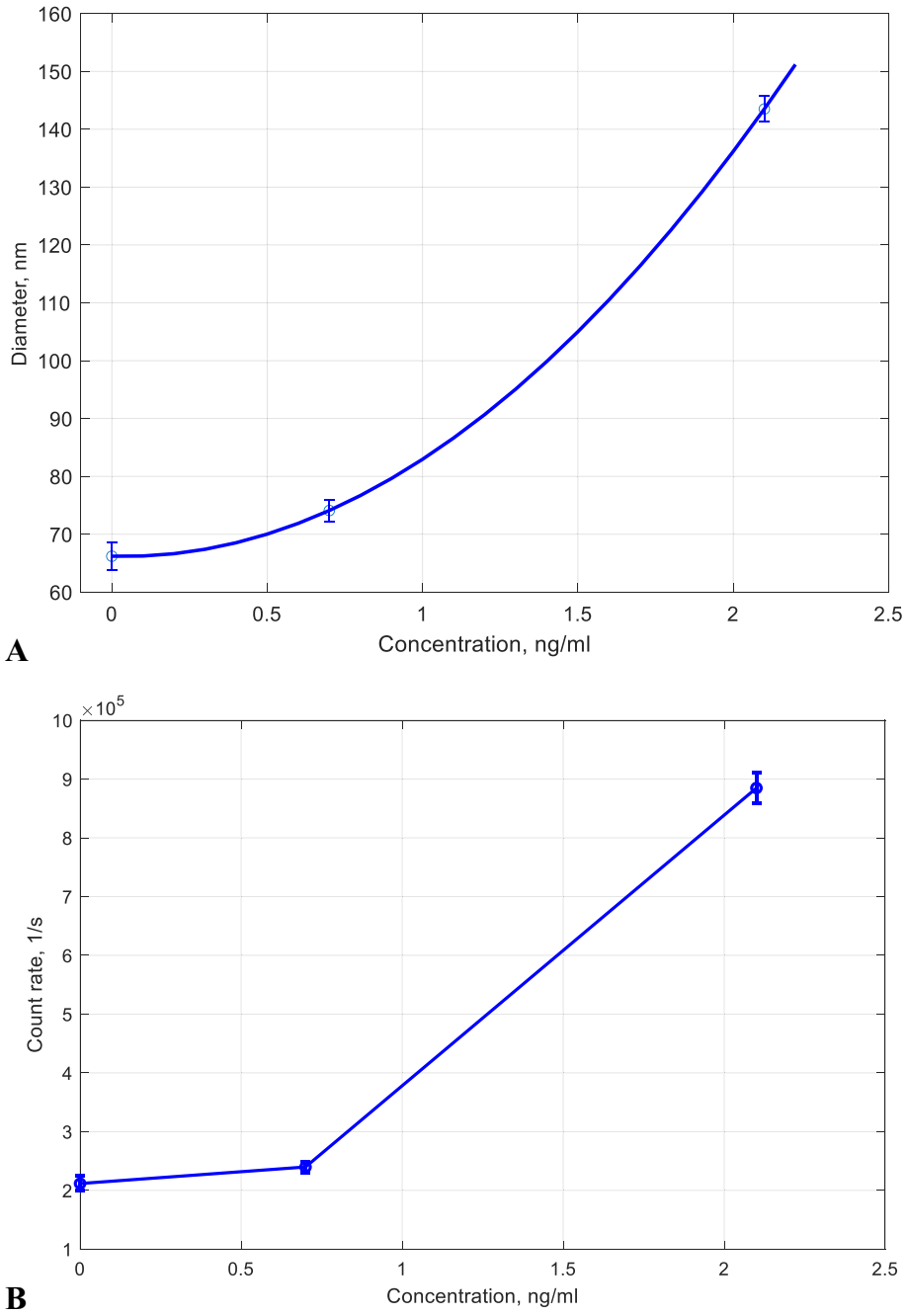

Fig. 3. Dependence of the hydrodynamic diameter of the conjugates (A) and the count rate (B) on the concentration of GM calibrator in blood plasma.

Center of Oncology (Rostov-on-Don, Russia). All obtained biological samples were examined for the content of galactomannan using the diagnostic test system GalMAg-ELISA.

Monoclonal antibody XF6 was applied in this study by using general procedures described earlier [37–39]

For comparative measurements under nanosensor performances validation, a kit GalMAg-ELISA for the enzyme immunoassay of *Aspergillus* GM antigen in blood plasma and BAL was used.

2.1.2. Equipment

Filter-based microplate photometer Multiskan FC, measurement range 0–6 Abs, Cat. № 51,119,000 (Thermo Scientific, Third Avenue 168, 02451 Waltham, MA, USA) was used as ELISA teader for comparative measurements for nanosensor's performances validation.

Electric dry-air thermostat TS-1/20 SPU, (OJSC Smolenskoe SKTB SPU, Shevchenko st. 97, 214,020 Smolensk, Russia) was used for incubation of the conjugates.

Centrifuge MiniSpin, speed range 0–13,400 rpm, Cat. № 5,452,000,010 (Eppendor AG, Barkhausenweg 1, 22,339, Hamburg, Germany) has been used to separate conjugates and natural nano-objects of biological fluids.

Reax top test tube shaker, speed range 0–2500 rpm, Cat. № 541–10,000–00-1 (Heidolph Instruments GmbH & Co. KG, Walpersdorfer Str. 12, D-91126 Schwabach, Germany) was used for mixing (vortexing) under sample preparation procedure.

Ultrapure water for sample preparation procedures was generated using Simplicity Water Purification System, a portable ultrapure water machine with a resistivity of 18.2 MΩ.cm at a temperature of 25 °C with a speed of 0.5 l per minute (Merck KGaA, Frankfurter Str. 250, 64,293 Darmstadt, Germany).

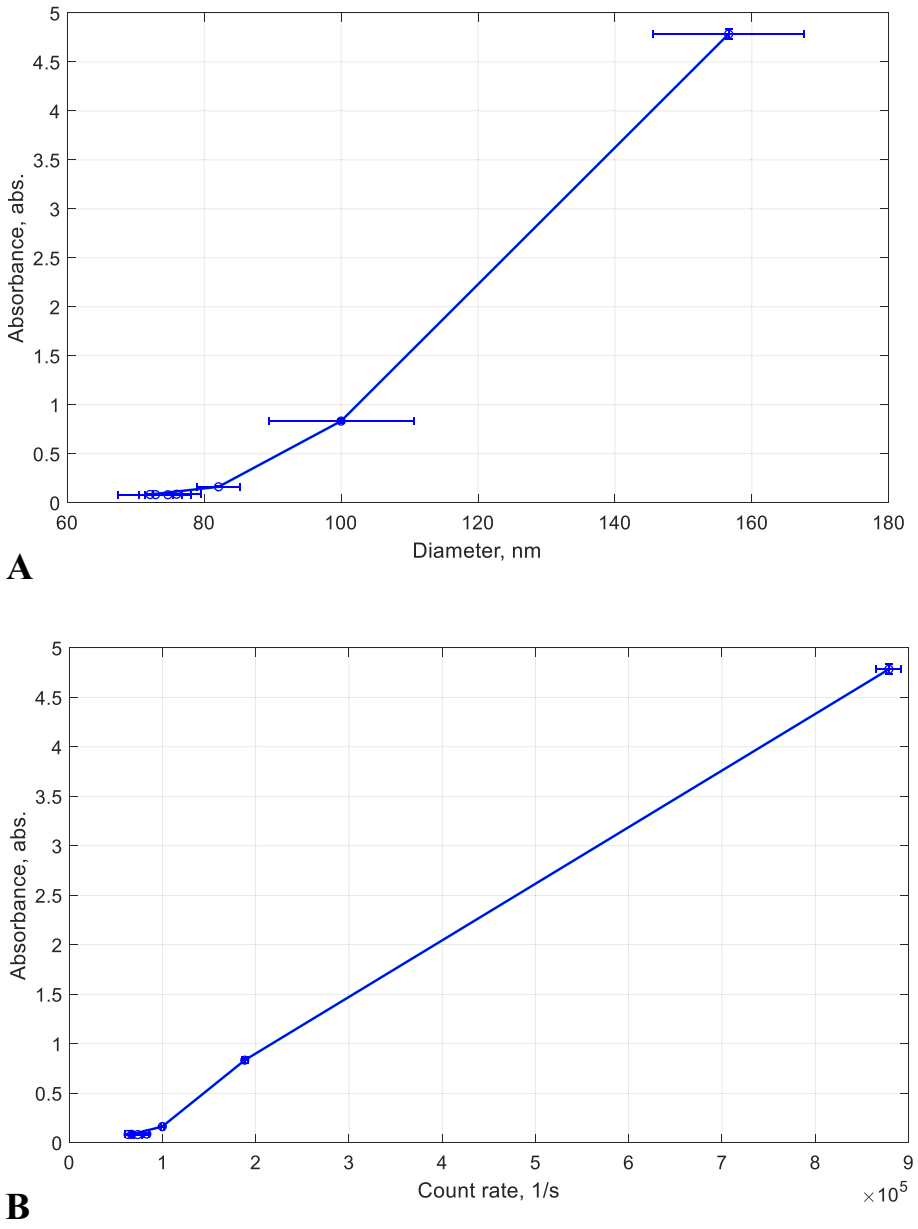

Fig. 4. Comparison of the results of determination of *Aspergillus* GM in BAL samples obtained using a nanbiosensor with the absorbance values measured using ELISA (A) hydrodynamic diameters (B) count rates.

2.1.3. Consumables

Eppendorf Safe-Lock microtubes, 2.0 ml capacity, colorless, Cat. N° 0030121023 (Eppendorf AG, Barkhausenweg 1, 22,339, Hamburg, Germany) were used as the containers for analyte samples and antibodies.

4 ml polystyrene cuvettes, 4 optically transparent walls, height 45 mm, the optical path length 10 mm, suitable for fluorescence measurements at wavelengths exceeding 330 nm, REF 67.754 (Sarstedt AG&Co. KG, Sarstedt AG & Co. KG Sarstedtstrasse 1, 51,588 Numbrecht, Germany) were used for DLS analyzer measurements

Syringe membrane filters, Chromafil Xtra PVDF, 25 mm, 0.45 μm, REF 729219.400 (Macherey-nagel GmbH & Co. KG, Neumann-Neander-Str. 6–8, 52,355 Duren, Germany) were used for conjugate solution filtering before light scattering measurements.

2.1.4. Chemicals

Ethylenediaminetetraacetic acid (EDTA): Aqueous solution of EDTA 0.1 M pH = 4 was received from Xema Ltd., 9 Parkovaya st., 48, 105,284 Moscow, Russia.

Sodium carbonate: Aqueous solution of Na_2CO_3 pH = 9, was received from Xema Ltd., 9 Parkovaya st., 48, 105,284 Moscow, Russia.

2.2. Apparatus for measuring DLS

Custom-made small-sized DLS analyzer, developed at the All-Russian Research Institute for Optical and Physical Measurements (Moscow, Russia) for using as a detecting device for POC diagnostics was applied for DLS measurements. To excite the DLS in this analyzer, we used a diode semiconductor laser with adjustable output power, the emission wavelength was 637 nm. The scattered light was collected at 90° angle, its intensity was measured using a photon-counting module SPD-100-C0A-FC from Micro Photon Devices Srl, based on an avalanche photodiode (APD) matrix, the dark current level did not exceed 250 pulses per second. The scattered light was coupled into the photon counting module using multimode optical fiber. A sequence of time intervals between adjacent one-photon pulses was used as an informative

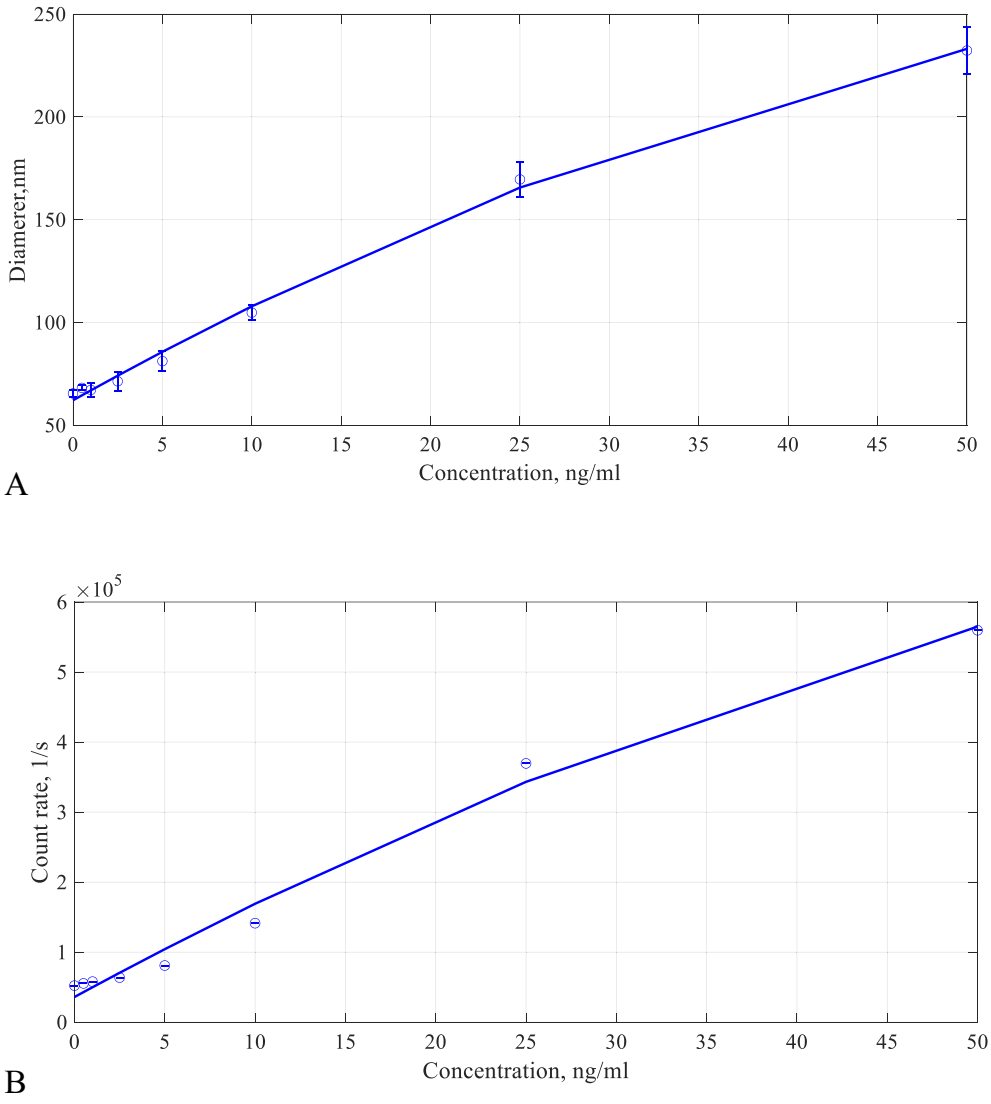

Fig. 5. Calibration curves for GM in BAL using diameter (A) and count rate (B) as analytical signals.

Table 1
Concentration values of GM in BAL obtained using diameter and count rate calibration curves/.

Nominal concentration, ng/ml.	Diameter, nm	Concentration calculated from diameter calibration, ng/ml.	Count rate, 1/s	Concentration calculated from count rate calibration, ng/mL.
0.00	66.5	0.69	52205	1.17
0.50	68.2	1.25	55430	1.40
1.00	67.2	1.04	57912	1.58
2.50	71.4	1.92	63717	2.00
5.00	81.2	4.01	80938	3.26
10.00	104.8	9.29	141370	7.83
25.00	169.6	26.17	369530	27.53
50.00	232.3	49.59	559644	49.27

The limits of detection of GM in BAL obtained from these data by the 2 sigma level are 1.9 ng/ml when assessing using the hydrodynamic diameter and 0.4 ng/ml when assessing by the count rate.

parameter processing the data of the photodetector. From these data, the autocorrelation function was calculated using the software time of the arrival correlator described [40]. The count rate of one-photon pulses *NP*, proportional to the intensity of the scattered light was also calculated from the time of arrival sequence.

Autocorrelation function was used to determine the decay rate of fluctuations Γ, which is related to the coefficient of translational diffusion of particles D by the formula

$$\Gamma = D.q^2 \tag{1}$$

where q is the wavenumber of scattered light,

$$q = \frac{4\pi n}{\lambda} \tag{2}$$

herein n is the refractive index of the liquid; λ is the wavelength of the laser that excites the scattering.

The hydrodynamic diameter of nanoparticles d_H was calculated from the determined value of D using the Stokes-Einstein formula

$$D = \frac{k_B T}{3\pi\eta d_H} \tag{3}$$

where k_B is Boltzmann constant, T is the absolute temperature, η is dynamic viscosity.

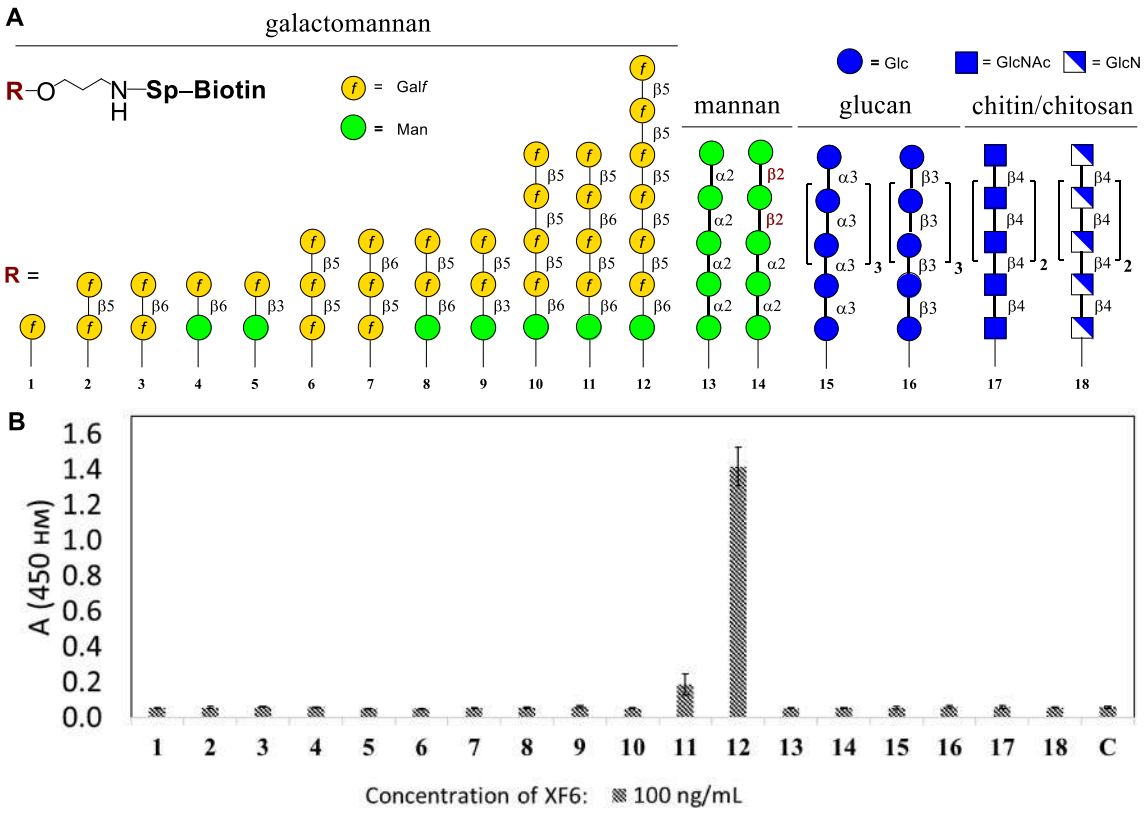

Fig. 6. Investigation of carbohydrate specificity of monoclonal antibody XF6 used in nanobiosensor. **A**: The thematic glycoarray comprising oligosaccharide ligands related fungal polysaccharides (the carbohydrate sequences are represented according to symbol carbohydrate nomenclature [53]). **B**: assay of carbohydrate specificity of antibody XF6.

2.3. Sample preparation and measurements

2.3.1. Preparation of conjugates

The preparation of conjugates based on gold nanoparticles was carried out according to the procedure described [41]. Colloidal gold particles were synthesized according to the Françs method [42]. Experimental selection of the optimal conditions for the functionalization of nanoparticles with antibodies was carried out using 96-well polystyrene plates for ELISA. Wherein, the values of the concentration of antibodies and the pH values in the wells of this plate were varied. Details of the selection of optimal conditions for preparing conjugates are presented in the Supporting Information (SI), fig. SI-1. According to the optimized procedure, 100 μl of the antibody solution in deionized water with a concentration of 0.33 mg/ml was added dropwise to 1 ml of a solution of colloidal gold at pH = 7.5 and kept for 30 min at room temperature with gentle stirring. The resulting solution was adjusted with bovine serum albumin (BSA) to a final concentration of 0.2%. Then concentrated solutions of sucrose and sodium azide were added, which volumes were selected so that the final concentration of sucrose was 10%, and sodium azide – 0.01%. The resulting solution was stored at 4 °C. To remove unbound antibodies, the conjugate solution was centrifuged at 11000 *g* for 30 min at 4 °C and resuspended in a buffer solution.

2.3.2. Preparation of culture fluid (CL) samples

50 μl of functionalized nanoparticles were mixed with 500 μl of CL, with different degrees of dilution with PBS buffer (from 200 to 1000). The resulting mixture was incubated at 37 °C for 30 min, whereupon the volume of the mixture was brought to 1 ml with PBS buffer and the average hydrodynamic diameter was measured by DLS. Pure PBS buffer was used as zero solution.

2.3.3. Preparation of BAL and blood plasma samples

During preparation, it was required to remove large particles capable of scattering light from the sample before adding conjugates. The preparation included the following stages.

A) Protein precipitation. 200 μl of EDTA solution was added to 600 μl of bioassay (BAL or blood plasma) to shift the acid-base balance to the acidic region (decrease in pH) and incubated for 5 min at 100 °C.

B) Removal of large particles by centrifugation for 10 min at a centrifugal acceleration of 10,000 *g*, followed by re-centrifugation for 3 min in a tube with a built-in membrane filter with a pore diameter of 0.21 μm in the case of BAL fluid, and by filtering through the same filter used in the form of a syringe attachment in the case of plasma blood.

C) Neutralization of EDTA solution by adding 15 μl of sodium carbonate (Na_2CO_3) to 250 μl of suppernatant followed by stirring.

D) Adding 25 or 50 μl of a solution of conjugates (functionalized nanoparticles), while a ratio of 1:10 was maintained between the volumes of the conjugates and the supernatant.

E) Incubation for 30 min at 37 °C.

F) Transferring the sample into a standard 12.5 * 12.5 * 45 mm cuvette, brought to 1 ml with PBS buffer, and measurement on DLS analyzer, both the hydrodynamic diameter of the conjugates and the pulse counting rate.

This sample preparation procedure can be used for the quantitative determination of GM in other biofluids, for example, in blood serum. In this case, for each type of biofluid, it is necessary to construct its calibration graph using solutions with known concentrations of the GM calibrator from the kit GalMAg-ELISA.

The duration of each stage of sample preparation is shown in Table SI-1. Taking into account all stages and measurements on the DLS analyzer, the total time required for the analysis of *N* samples will be $48 + 5 * N$ minutes, i.e. 10 samples will take 98 min to analyze and 5

samples will take 73 min. Thus, with a small number of samples, a significant gain in time is obtained compared to traditional ELISA, where, due to sample preparation, this time is about 4 h for any number of samples. It should be noted that in clinical practice when diagnosing aspergillosis, the number of samples in one batch usually does not exceed 5–10.

2.4. Data processing

When processing the measurement results, we used the values of the hydrodynamic diameter *dH* and the count rate of one-electron pulses *NP*, which were proportional to the intensity of the scattered light, obtained for each sample. Note that previously, in DLS instruments, the count rate was used only as an auxiliary parameter to help the selection of laser light intensity directed to the sample for scattering exciting.

In this work, the dependence of both parameters on analyte concentration and their mutual correlation was investigated. Based on the results of these studies, a two-dimensional calibration dependence can be constructed, where *dH* and *NP* are used as independent variables (predictors), and the concentration of analyte *c* is the dependent variable (response).

Thus, in the proposed nanosensor system, the analyte concentration is determined from the data of both dynamic and static light scattering. This approach permits obtaining more reliable data on conjugates aggregation correlating with analyte concentration, and, on their basis, to evaluate the results of clinical analyzes.

In a wide concentration range, the dependence of the analytical signal (the hydrodynamic diameter or the count rate) is well approximated by the equation.

$$y = A\cdot[1 - B\cdot exp.(-k\cdot c)] \quad (4)$$

where *y* is the analytical signal (the diameter or the count rate), *A, B* and *k* are fitting parameters, which were found using the nonlinear least-squares algorithm using Matlab function *lsqcurvefit.*

3. Results and discussion

3.1. Measurement results of the cultural liquid

The measurements were carried out on samples of CL of *Aspergillus* fungi at various dilutions with PBS buffer. Obtained results are shown in Fig. 1 and Table SI2 The graphs of this figure show the dependences of the hydrodynamic diameter of the conjugates and the count rate on the concentration of CL in PBS solutions, while the concentration is presented in relative units as the reciprocal of dilution.

Comparison of data for the hydrodynamic diameter and the count rate showed their good mutual correlation (see Fig. 2), the coefficient of determination for the quadratic relationship between these values is close to 1 ($R^2 = 0.9953$). Wherein, the errors in measuring the count rate are significantly less than ones in measuring the hydrodynamic diameter. Therefore, the detection limit (DL) of the analyte, estimated from the measurement results of the count rate (corresponds to the dilution of CL by a factor of 4200), turned out to be significantly lower than DL estimated from the measurements of the diameter of the conjugates (corresponds to the dilution of CL by a factor of 1620). In both cases, DL was estimated according to the 3 sigma criterion, i.e. the value of the analyte concentration, determined according to the calibration curve and corresponding to the threefold standard deviation for a solution without CL, was taken as DL.

3.2. Measurement results of blood plasma with samples of GM calibrator

Obtained results of measurements of GM calibrator in blood plasma are shown in Fig. 3 and Table S1-SI3. The detection limits for the evaluation of GM calibrator in plasma, determined by the 2 sigma level, were 0.2 ng/ml according to the hydrodynamic diameter data and 0.1 ng/ml according to the count rate data.

3.3. Measurement results with clinical BAL samples

When measuring with clinical BAL samples the obtained values of the hydrodynamic diameter and the count rate were compared with the absorbance values measured for the same samples by ELISA using a GalMAg-ELISA kit, mentioned above. The comparison results are shown in Figs. 4A, B, and Table S1- S5. In these graphs, the abscissa shows the values of the hydrodynamic diameter and the count rate of the scattered light pulses, respectively, and the ordinate shows the ELISA absorbance values.

For the whole concentration range the coefficient of determination between the values of the hydrodynamic diameter and absorbance of ELISA is $R^2 = 0.9705$, and between the values of the count rate and absorbance – $R^2 = 0.998$. For the five data points at smaller diameters (<90 nm) and lower count rates ($<1 \times 10^5$) which show ELISA absorbance <0.5, these coefficients are 0.869 and 0.760 correspondingly.

The set of experimental data with the BAL samples for the large range of quantification is presented in the table SI-6. Samples with the different analyte concentrations from 0.5 ng/mL to 50 ng/mL were prepared by adding to the GM –negative BAL samples the stock solution for positive controls of the galactomannan detecting kit GalMAg-ELISA. The calibration curves for diameter and count rate were approximated by the second order polynomial (see Fig. 5), which can be calculated by expanding the exponent in Eq. (4) for small *kc*. The calculated concentration values for each sample obtained by diameter and count rate using their corresponding calibration curves are presented in Table 1.

The accuracy of the described diagnostic system is determined by the specificity of the used monoclonal antibody XF6 used to build up the nanobiosensor. This antibody was selected for present study basing on the result of the assessment of its carbohydrate specificity on thematic glycoarray [43] buildup of synthetic oligosaccharides **1**–**18** (Fig. 6 A) related to galactomannan [44–46], α- and β-mannans [47], α-(1 → 3)-glucan [48], β-(1 → 3)-glucan [49,50], chitin and chitosan [51]. Used oligosaccharide ligands were applied in the form of biotinylated derivatives, which were immobilized on the surface of a streptavidin coated plate [43]. The highest affinity was observed for heptasaccharide **12**, containing six β-(1 → 5)-linked galactofuranoside residues (Fig. 6 B). Pentasaccharide **11**, containing four β-(1 → 5)-linked galactofuranoside units, bound significantly weaker. The oligosaccharides related to other types of fungal polysaccharides did not bind with XF6 to confirm its carbohydrate specificity towards long oligogalactofuranose containing chains of GM. Thus the specificity of XF6 resembles one of antibody AP3 which was recently described [52].

4. Conclusion

A new approach for optical nano-biosensors using aggregation of nanoparticles functionalized with antibodies to the analyte is proposed and implemented. Aggregation is assessed by two signals of different physical nature – the hydrodynamic diameter of the conjugates and the pulse counting rate (relative intensity) of the light scattered by them. Both signals are measured on conventional nanoparticle analyzers based on dynamic light scattering.

Based on the proposed approach, a nanosensor to determine the GM marker of dangerous *Aspergillus* infection was developed. A good correlation between the data obtained using the nanosensor and ELISA results for BAL samples was found. Thus the count rate in comparison with hydrodynamic diameter gives lower detection limits and a better correlation with absorbance values obtained using ELISA. At the same time, the use of the nanosensor permits to reduce significantly the labor intensity and duration of the sample preparation and excludes the washing stage. The developed nanosensors permit the provision of low values of detection limits for GM in blood plasma and BAL. The

simultaneous use of two signals of different physical nature in the developed sensor allows increasing accuracy and reliability of the results obtained without increasing the measurement time.

Comparison of the two analytical signals show that static light scattering gives lower detection limits, higher sensitivity coefficient, smaller error bars in the graphs, than dynamic light scattering. On the other hand, calibration curves constructed using dynamic light scattering allows to calculate more accurate analyte concentrations.

The possibility of using the count rate as the only analytical signal can be considered as a simplified but less accurate option. Simpler, cheaper, and more compact detecting devices could be used for such a method.

The nano-biosensor described in this article can be used for express and POC diagnostics of the marker of fungal infection *Aspergillus*, and the tested approach has the potential to develop on its basis test systems for markers of other diseases.

CRediT authorship contribution statement

M.K. Alenichev: Investigation, Methodology. **A.D. Levin:** Conceptualization, Writing – original draft. **A.A. Yushina:** Investigation. **Eu.S. Kostrikina:** Validation, Resources. **Yu.S. Lebedin:** Conceptualization, Resources. **I.P. Andreeva:** Resources. **V.G. Grigorenko:** Resources. **V. B. Krylov:** Validation. **N.E. Nifantiev:** Conceptualization, Validation.

Declaration of Competing Interest

The authors declare that they have no known competing financial interests or personal relationships that could have appeared to influence the work reported in this paper.

Acknowledgments

This work was supported in part by the Russian Science Foundation (grant № 19-73-30017).

Appendix B. Supporting Information

1. Selection of optimal conditions for the functionalization of nanoparticles (fig. SI-1).
2. Sample preparation and measurements (table SI-1).
3. Experiment results (tables SI-2 – SI-6). Supplementary data to this article can be found online at https://doi.org/10.1016/j.sbsr.2022.100475.

References

[1] K. Dichtl, U. Seybold, S. Ormanns, H. Horns, J. Wagenera, Evaluation of a novel *Aspergillus* antigen enzyme-linked immunosorbent assay, J. Clin. Microbiol. 57 (7) (2019) 1–10, https://doi.org/10.1128/JCM.00136-19.

[2] K.A. Marr, A. Platt, J.A. Tornheim, S.X. Zhang, K. Datta, C. Cardozo, C. Garcia-Vidal, Aspergillosis complicating severe coronavirus disease, Emerg. Infect. Dis. 27 (1) (2021) 18–25, https://doi.org/10.3201/eid2701.202896.

[3] A. Arastehfar, A. Carvalho, F.L. van de Veerdonk, J.D. Jenks, P. Koehler, R. Krause, O.A. Cornely, D.S. Perlin, C. Lass-Flörl, M. Hoenigl, COVID-19 associated pulmonary aspergillosis (CAPA) – from immunology to treatment, J. Fungi 6 (2) (2020) 1–17, https://doi.org/10.3390/jof6020091.

[4] A. Bhimji, A. Bhaskaran, L.G. Singer, D. Kumar, A. Humar, R. Pavan, J. Lipton, J. Kuruvilla, A. Schuh, K. Yee, M.D. Minden, A. Schimmer, C. Rotstein, S. Keshavjee, T. Mazzulli, S. Husain, Aspergillus galactomannan detection in exhaled breath condensate compared to bronchoalveolar lavage fluid for the diagnosis of invasive aspergillosis in immunocompromised patients, Clin. Microbiol. Infect. 24 (6) (2018 Jun) 640–645, https://doi.org/10.1016/j.cmi.2017.09.018.

[5] Detection of Galactomannan in Serum by PlateliaTM Aspergillus Enzyme-linked Immunosorbent Assay (BioRad Laboratories and Sanofi Diagnostics), Division of Special Pathogen and Transplant Products Biomarker Qualification Microbiology Review, https://www.fda.gov/media/90001/download, 2011.

[6] V.B. Krylov, A.S. Solovev, D.A. Argunov, J.-P. Latgé, N.E. Nifantiev, Reinvestigation of carbohydrate specificity of EB-A2 monoclonal antibody used in the immune detection of *aspergillus fumigatus* galactomannan, Heliyon. 5 (2019), e01173, https://doi.org/10.1016/j.heliyon.2019.e01173.

[7] R.L. Gorton, P.L. White, E. Bagkeris, D. Cotterall, R. Desai, T. McHugh, C. C. Kibbler, Improved standardization of the bio-rad platelia *Aspergillus* galactomannan antigen sandwich enzyme immunoassay using the DS2 (dynex) enzyme-linked immunosorbent assay (ELISA) processing system, J. Clin. Microbiol. 53 (7) (2015) 2072–2078, https://doi.org/10.1128/JCM.00157-15.

[8] V.K. Khanna, Nanosensors: Physical, Chemical, and Biological, CRC Press, 2021.

[9] T. Yang, T.V. Duncan, Challenges and potential solutions for nanosensors intended for use with foods, Nat. Nanotechnol. 16 (2021) 251–265, https://doi.org/10.1038/s41565-021-00867-7.

[10] S.M. Borisov, O.S. Wolfbeis, Optical biosensors, Chem. Rev. 108 (2) (2008) 423–461, https://doi.org/10.1021/cr068105t.

[11] V.B. Krylov, M.I. Petruk, M.P. Karimova, L.I. Mukhametova, A.L. Matveev, N. V. Tikunova, S.A. Eremin, N.E. Nifantiev, Potential of fluorescence polarization immunoassay for the detection of *Aspergillus fumigatus* galactomannan, Russ. Chem. Bull. 68 (12) (2019) 2365–2369, https://doi.org/10.1007/s11172-019-2713-y.

[12] M.T. Yaraki, Y.N. Tan, Recent advances in metallic nanobiosensors development: colorimetric, dynamic light scattering and fluorescence detection, Sensors Int. 1 (2020), 100049, https://doi.org/10.1016/j.sintl.2020.100049.

[13] A.D. Levin, M.P. Nikitin, M.K. Alenichev, E.B. Drozhzhennikova, V.G. Grigorenko, A.S. Ringaci, I.P. Andreeva, Nano-biosensors based on dynamic light scattering, in: Proc. SPIE 11060, Optical Methods for Inspection, Characterization, and Imaging of Biomaterials IV. 110600Y, 2019, https://doi.org/10.1117/12.2526055.

[14] T. Zheng, S. Bott, Q. Huo, Techniques for accurate sizing of gold nanoparticles using dynamic light scattering with particular application to chemical and biological sensing based on aggregate formation, ACS Appl. Mater. Interfaces 8 (2016) 21585–21594, https://doi.org/10.1021/acsami.6b06903.

[15] Y.H. Lai, S. Koo, S.H. Oh, E.A. Driskell, J.D. Driskell, Rapid screening of antibody–antigen binding using dynamic light scattering (DLS) and gold nanoparticles, Anal. Methods 17 (2015) 7249–7255, https://doi.org/10.1039/C5AY00674K.

[16] N. Seow, Y.N. Tan, L.-Y.L. Yung, Gold nanoparticle–dynamic light scattering tandem for the rapid and quantitative detection of the let7 microRNA family, Part. Part. Syst. Charact. 31 (2014) 1260–1268, https://doi.org/10.1002/ppsc.201400158.

[17] N. Seow, Y.N. Tan, L.-Y.L. Yung, X. Su, DNA-directed assembly of nanogold dimers: a unique dynamic light scattering sensing probe for transcription factor detection, Sci. Rep. 5 (2015) 18293, https://doi.org/10.1038/srep18293.

[18] Y. Tang, J. Zhang, D. Tang, Multifunctional magnetic bead-based dynamic light scattering aptasensor with rapid and feasible determination of disease-related biomarkers, J. Bioprocess Biotech. 6 (2016) 1–4, https://doi.org/10.4172/2155-9821.1000287.

[19] C. Li, J. Ma, Q. Fan, Y. Tao, Dynamic light scattering (DLS)-based immunoassay for ultra-sensitive detection of tumor marker protein, Chem. Commun. 52 (2016) 7850–7853, https://doi.org/10.1039/C6CC02633H.

[20] Q. Huo, S.A. Litherland, S. Sullivan, H. Hallquist, D.A. Decker, I. Rivera-Ramirez, Developing a nanoparticle test for prostate cancer scoring, J. Transl. Med. 10 (2012) 2–8, https://doi.org/10.1186/1479-5876-10-44.

[21] N. Mustafaoglua, T. Kiziltepea, B. Bilgicer, Site-specific conjugation of an antibody on a gold nanoparticle surface for one-step diagnosis of prostate specific antigen with dynamic light scattering, Nanoscale 9 (2017) 8684–8694, https://doi.org/10.1039/C7NR03096G.

[22] T. Zheng, N. Pierre-Pierre, X. Yan, Q. Huo, A. Almodovar, F. Valerio, I. Rivera-Ramirez, E. Griffith, D.D. Decker, S. Chen, N. Zhu, Gold nanoparticle-enabled blood test for early stage cancer detection and risk assessment, ACS Appl. Mater. Interfaces 7 (12) (2015) 6819–6827, https://doi.org/10.1021/acsami.5b00371.

[23] J.D. Driskell, C.A. Jones, S.M. Tompkins, R.A. Tripp, One-step assay for detecting influenza virus using dynamic light scattering and gold nanoparticles, Analyst 136 (2011) 3083–3090, https://doi.org/10.1039/C1AN15303J.

[24] X. Huang, Z. Xu, Y. Mao, Y. Ji, H. Xu, Y. Xiong, Y. Li, Gold nanoparticle-based dynamic light scattering immunoassay for ultrasensitive detection of *Listeria monocytogenes* in lettuces, Biosens. Bioelectron. 66 (2015) 184–190, https://doi.org/10.1016/j.bios.2014.11.016.

[25] T. Zheng, C. Finn, C.J. Parrett, K. Dhume, J.H. Hwang, D. Sidhom, T. Strutt, Y.Y. L. Sip, K. McKinstry, Q. Huo, A rapid blood test to determine the active status and duration of acute viral infection, ACS Infect. Dis. 3 (2017) 866–873, https://doi.org/10.1021/acsinfecdis.7b00137.

[26] D. Gao, Z. Sheng, H. Han, An ultrasensitive method for the detection of gene fragment from transgenics using label-free gold nanoparticle probe and dynamic light scattering, Anal. Chim. Acta 696 (2011) 1–5, https://doi.org/10.1016/j.aca.2011.04.001.

[27] C. Fu, H. Ma, C. Huang, N. Jia, A simple and dual functional dynamic light scattering (DLS) probe for rapid detection of mercury ions and biothiols, Anal. Methods 7 (2015) 7455–7460, https://doi.org/10.1039/C5AY01880C.

[28] X. Huang, Y. Liu, B. Yung, Y. Xiong, X. Chen, Nanotechnology-enhanced no-wash biosensors for in vitro diagnostics of cancer, ACS Nano 3 (2017) 5238–5292, https://doi.org/10.1021/acsnano.7b02618.

[29] X. Yang, J. Huang, Q. Wang, K. Wang, L. Yang, X. Huo, A one-step sensitive dynamic light scattering method for adenosine detection using split aptamer fragments, Anal. Methods 3 (2011) 59–61, https://doi.org/10.1039/C0AY00709A.

[30] A.D. Levin, A. Ringaci, M.K. Alenichev, E.B. Drozhzhennikova, K.G. Shevchenko, V. R. Cherkasov, M.P. Nikitin, P.I. Nikitin, Dynamic light scattering biosensing based on analyte-induced inhibition of nanoparticle aggregation, Anal. Bioanal. Chem. 412 (2020) 3423–3431, https://doi.org/10.1007/s00216-020-02605-9.

[31] R. Shen, J. Zhang, W. Huang, S. Wu, G. Li, S. Zou, L. Ling, Dynamic light scattering and fluorescence dual-signal sensing of cancer antigen-125 via recognition of the

polymerase chain reaction product with gold nanoparticle probe, Anal. Chim. Acta 1145 (2021) 87–94, https://doi.org/10.1016/j.aca.2020.11.005.
[32] R. El-Kurdi, D. Patra, Gold and silver nanoparticles in resonance Rayleigh scattering techniques for chemical sensing and biosensing: a review, Microchim. Acta 186 (10) (2019) 1–18, https://doi.org/10.1007/s00604-019-3755-4.
[33] W. Lu, B. Fernandez Band, Y. Yu, Q.G. Li, J.C. Shang, C. Wang, Y. Fang, R. Tian, L. P. Zhou, L.L. Sun, Y. Tang, S.H. Jing, W. Huang, J.P. Zhang, Resonance light scattering and derived techniques in analytical chemistry: past, present, and future, Microchim. Acta 158 (1–2) (2007) 29–58, https://doi.org/10.1007/s00604-006-0670-2.
[34] R.F. Pasternack, P.J. Collings, Resonance light scattering: a new technique for studying chromophore aggregation, Science 269 (5226) (1995) 935–939, https://doi.org/10.1126/science.7638615.
[35] H. Zhong, K. Wang, H.Y. Chen, Protein analysis with tetra-substituted sulfonated cobalt phthalocyanine by the technique of Rayleigh light scattering, Anal. Biochem. 330 (1) (2004) 37–42, https://doi.org/10.1016/j.ab.2004.04.006.
[36] A.A. Karelin, Y.E. Tsvetkov, N.E. Nifantiev, Synthesis of oligosaccharides related to cell wall polysaccharides of the fungi *Candida* and *Aspergillus*, Russ. Chem. Rev. 86 (11) (2017) 1073–1126, https://doi.org/10.1070/RCR4750.
[37] A.L. Matveev, V.B. Krylov, Y.A. Khlusevich, I.K. Baykov, D.V. Yashunsky, L. A. Emelyanova, A.S. Solovev, T. Fontaine, J.P. Latge, N.V. Tikunova, N. E. Nifantiev, Novel mouse monoclonal antibodies specifically recognize *aspergillus fumigatus* galactomannan, PLoS One 14 (4) (2019), e0215535, https://doi.org/10.1371/journal.pone.0193938.
[38] V.B. Krylov, M.I. Petruk, N.I. Glushko, E.V. Khaldeeva, V.L. Mokeeva, E. N. Bilanenko, Y.S. Lebedin, S.A. Eremin, N.E. Nifantiev, Carbohydrate specificity of antibodies against phytopathogenic fungi of the *Aspergillus* genus, Appl. Biochem. Microbiol. 54 (5) (2018) 522–527, https://doi.org/10.1134/S0003683818050095.
[39] V.B. Krylov, M.I. Petruk, I.V. Grigoryev, Y.S. Lebedin, N.I. Glushko, E.V. Khaldeeva, D.A. Argunov, E.A. Khatuntseva, M.V. Toplishek, B.S. Komarova, A.A. Karelin, O. N. Yudina, V.M. Menshov, D.V. Yashunskii, Y.E. Tsvetkov, N.E. Nifantiev, Study of the carbhydrate specificity of antibodies against *Aspergillus fumigatus* using the library of synthetic mycoantigens, Russ. J. Bioorg. Chem. 44 (1) (2018) 80–89, https://doi.org/10.1134/S1068162017060073.
[40] T.A. Laurence, S. Fore, T. Huser, Fast, flexible algorithm for calculating photon correlations, Opt. Lett. 31 (6) (2006) 829–831, https://doi.org/10.1364/OL.31.000829.
[41] I.P. Andreeva, V.G. Grigorenko, A.M. Egorov, A.P. Osipov, Quantitative lateral flow immunoassay for total prostate specific antigen in serum, Anal. Lett. 49 (4) (2016) 579–588, https://doi.org/10.1080/00032719.2015.1075130.
[42] G. Frens, Controlled nucleation for the regulation of the particle size in monodisperse gold suspensions, Nat. Phys. Sci. 241 (105) (1973) 20–22, https://doi.org/10.1038/physci241020a0.
[43] V.B. Krylov, N.E. Nifantiev, Synthetic oligosaccharides mimicking fungal cell wall polysaccharides, Curr. Top. Microbiol. Immunol. 425 (2020) 1–16, https://doi.org/10.1007/82_2019_187.
[44] D.A. Argunov, V.B. Krylov, N.E. Nifantiev, Convergent synthesis of isomeric heterosaccharides related to the fragments of galactomannan from *aspergillus fumigatus*, Org. Biomol. Chem. 13 (2015) 3255–3267, https://doi.org/10.1039/C4OB02634A.
[45] D.A. Argunov, V.B. Krylov, N.E. Nifantiev, The use of Pyranoside-*into*-Furanoside rearrangement and controlled O(5)→O(6) benzoyl migration as the basis of a synthetic strategy to assemble (1→5)-and (1→6)-linked galactofuranosyl chains, Org. Lett. 18 (2016) 5504–5507, https://doi.org/10.1021/acs.orglett.6b02735.
[46] V.B. Krylov, D.A. Argunov, A.S. Solovev, M.I. Petruk, A.G. Gerbst, A.S. Dmitrenok, A.S. Shashkov, J.-P. Latgé, N.E. Nifantiev, Synthesis of oligosaccharides related to galactomannans from *Aspergillus fumigatus* and their NMR spectral data, Org. Biomol. Chem. 16 (2018) 1188–1199, https://doi.org/10.1039/C7OB02734F.
[47] A.A. Karelin, Y.E. Tsvetkov, E. Paulovičová, L. Paulovičová, N.E. Nifantiev, A Blockwise approach to the synthesis of (1→2)-linked oligosaccharides corresponding to fragments of the acid-stable β-Mannan from the *Candida albicans* cell wall, Eur. J. Org. Chem. 2016 (2016) 1173–1181.
[48] B.S. Komarova, S.S.W. Wong, M.V. Orekhova, Y.E. Tsvetkov, V.B. Krylov, A. Beauvais, J.-P. Bouchara, J.F. Kearney, V. Aimanianda, J.-P. Latgé, N. E. Nifantiev, Chemical synthesis and application of biotinylated oligo-α-(1→3)-D-glucosides to study the antibody and cytokine response against the cell wall α-(1→3)-D-glucan of *Aspergillus fumigatus*, J. Org. Chem. 83 (2018) 12965–12976, https://doi.org/10.1021/acs.joc.8b01142.
[49] Y.E. Tsvetkov, E.A. Khatuntseva, D.V. Yashunsky, N.E. Nifantiev, Synthetic β-(1→3)-D-glucooligosaccharides: model compounds for the mechanistic study of β-(1→3)-D-glucan bioactivities and design of antifungal vaccines, Russ. Chem. Bull. 64 (2015) 990–1013, https://doi.org/10.1007/s11172-015-0969-4.
[50] D.V. Yashunsky, Y.E. Tsvetkov, A.A. Grachev, A.O. Chizhov, N.E. Nifantiev, Synthesis of 3-aminopropyl glycosides of linear β-(1→3)-D-glucooligosaccharides, Carbohydr. Res. 419 (2016) 8–17, https://doi.org/10.1016/j.carres.2015.10.012.
[51] Y.E. Tsvetkov, E. Paulovičová, L. Paulovičová, P. Farkaš, N.E. Nifantiev, Synthesis of biotin-tagged chitosan oligosaccharides and assessment of their immunomodulatory activity, Front. Chem. 8 (2020), 554732, https://doi.org/10.3389/fchem.2020.554732.
[52] M. Schubert, S. Xue, F. Ebel, A. Vaggelas, V.B. Krylov, N.E. Nifantiev, I. Chudobová, S. Schillberg, G. Nölke, Monoclonal Antibodyap3 binds galactomannan antigens displayed by the pathogens Aspergillus flavus, *A. fumigatus*, and *A. parasiticus*, Front. Cell. Infect. Microbiol. 9 (2019) 234, https://doi.org/10.3389/fcimb.2019.00234.
[53] A. Varki, R. Cummings, J. Esko, H. Freeze, G. Hart, J. Marth, Essentials of Glycobiology, Cold Spring Harbor, NY, 1999.

ACS APPLIED MATERIALS & INTERFACES

www.acsami.org

Research Article

Biorecognition Layer Based On Biotin-Containing [1]Benzothieno[3,2-*b*][1]benzothiophene Derivative for Biosensing by Electrolyte-Gated Organic Field-Effect Transistors

Elena Yu. Poimanova, Polina A. Shaposhnik, Daniil S. Anisimov, Elena G. Zavyalova, Askold A. Trul, Maxim S. Skorotetcky, Oleg V. Borshchev, Dmitry Z. Vinnitskiy, Marina S. Polinskaya, Vadim B. Krylov, Nikolay E. Nifantiev, Elena V. Agina, and Sergey A. Ponomarenko*

Cite This: https://doi.org/10.1021/acsami.1c24109

Read Online

ACCESS | Metrics & More | Article Recommendations | Supporting Information

ABSTRACT: Requirements of speed and simplicity in testing stimulate the development of modern biosensors. Electrolyte-gated organic field-effect transistors (EGOFETs) are a promising platform for ultrasensitive, fast, and reliable detection of biological molecules for low-cost, point-of-care bioelectronic sensing. Biosensitivity of the EGOFET devices can be achieved by modification with receptors of one of the electronic active interfaces of the transistor gate or organic semiconductor surface. Functionalization of the latter gives the advantage in the creation of a planar architecture and compact devices for lab-on-chip design. Herein, we propose a universal, fast, and simple technique based on doctor blading and Langmuir–Schaefer methods for functionalization of the semiconducting surface of C_8-BTBT-C_8, allowing the fabrication of a large-scale biorecognition layer based on the novel functional derivative of BTBT-containing biotin fragments as a foundation for further biomodification. The fabricated devices are very efficient and operate stably in phosphate-buffered saline solution with high reproducibility of electrical properties in the EGOFET regime. The development of biorecognition properties of the proposed biolayer is based on the streptavidin–biotin interactions between the consecutive layers and can be used for a wide variety of receptors. As a proof-of-concept, we demonstrate the specific response of the BTBT-based biorecognition layer in EGOFETs to influenza A virus (H7N1 strain). The elaborated approach to biorecognition layer formation is appropriate but not limited to aptamer-based receptor molecules and can be further applied for fabricating several biosensors for various analytes on one substrate and paves the way for "electronic tongue" creation.

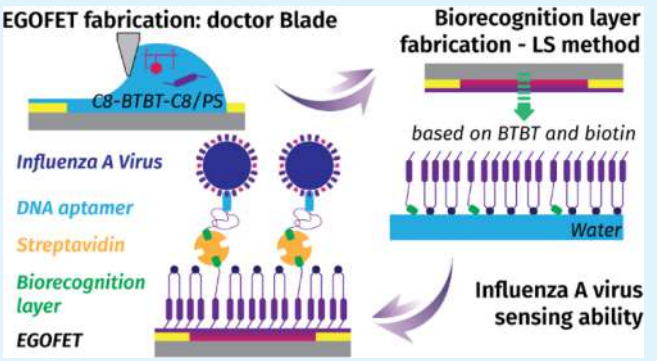

KEYWORDS: *electrolyte-gated organic field-effect transistor, biosensors, biorecognition layer, BTBT, biotin–streptavidin platform, influenza A virus*

INTRODUCTION

For healthcare system development, the progress in sensor technologies is increasingly important in applications such as biomolecule and virus detection, medical diagnostics, and environmental and food quality monitoring. Nowadays, a wide variety of gadgets being used every day contain many kinds of sensors—single devices or complex modules that detect changes in different physical quantities and subsequently convert them into signals that can be captured and analyzed.[1−4] Development of rapid and self-supported biosensors designed to provide point-of-care (POC) methods in outpatient or remote conditions can boost clinical diagnostics. Although different types of biosensors based on various combinations of receptors (enzymes, antibodies, whole cell, and aptamers), transducers (electrochemical, electronic, optical, gravimetric, and acoustic), and materials (nanoparticles, carbon nanotubes, quantum dots, dendrimers, polymers, and oligomers) were reported,[2] a lot of limitations, which hinder further development of the field and do not allow biosensors to invade the market, still remain. These limitations are associated with a number of requirements imposed on the biosensors: high selectivity and sensitivity, fast linear response, explicit accuracy of the results, reproducibility, stability, affordable manufacturing cost, and user friendliness.[1,2,5,6]

Received: December 13, 2021
Accepted: March 17, 2022

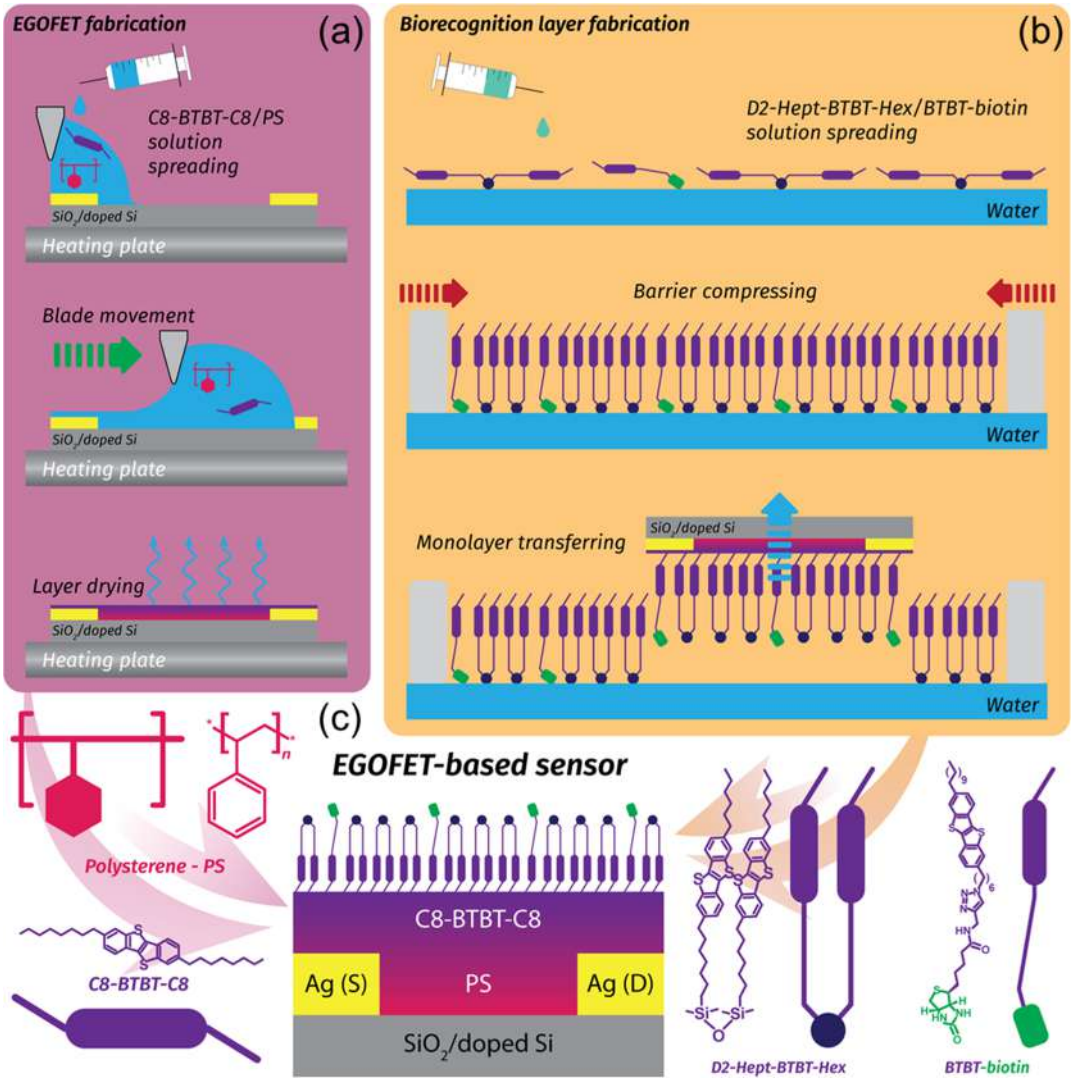

Figure 1. Illustration of the fabrication process by means of a combination of doctor blading (a) and Langmuir−Schaefer (b) techniques of the EGOFET device with **BTBT−biotin** containing a biorecognition layer (c).

Electrolyte-gated organic field-effect transistors (EGOFETs) are a promising platform for ultrasensitive, fast, and reliable detection of biological molecules by low-cost, POC bioelectronic sensors.[7,8] They attract growing attention due to their ability to transduce different sensing signals, providing direct, electronic, label-free response of biorecognition events. At the same time, they meet the requirements of device miniaturization, fast data handling, and processing. An EGOFET architecture includes an organic semiconductor (OSC) deposited between the source and drain electrodes, an electrolyte solution located on the OSC surface, and a gate electrode placed in contact with the solution.[9−11] The OSC layer works as an active channel of the device: upon application of a gate bias, electric double layers (EDLs) are formed at the OSC/electrolyte and the electrolyte/gate interfaces. Due to high capacitance of the EDLs, a significant field-effect current appears under a gate bias as low as 0.5 V,[7] allowing operations with biological molecules without their destruction. Moreover, the great advantage of EGOFETs is the possibility of biomolecular sensing in real biological liquids such as saliva, blood, serum, mucus, sweat, or urine.[7,8]

Immobilization of bioreceptors on the semiconductors or gate surfaces by anchoring biological molecules specific to appropriate bioanalytes allows specific binding with a target analyte and guarantees selectivity of the device.[7,12,13] Modern immobilization techniques include physical adsorption, covalent binding, and biochemical affinity reactions.[7] This feature paves the way to the creation of an array of EGOFET sensors with sensitivity to several biomarkers and, finally, to the elaboration of an "electronic tongue" system or to design a lab-on-chip.[14]

Despite the wide variety of possible methods for immobilization of biomolecules on metal or polymer surfaces, integration of biorecognition elements in an electronic device still remains a challenge being very significant both for fundamental issues and for the development of high-performance biosensors. An analyte dissolved in a liquid electrolyte directly contacts with a semiconductor surface that may lead to non-specific binding at the electrolyte/semiconductor interface, resulting in the semiconducting layer deterioration and device performance degradation.[15] That is why the semiconductor surface modification is considered to be a more complex approach than the gate surface modification and most of the recent papers report on EGOFET-based biosensors with recognition moieties

https://doi.org/10.1021/acsami.1c24109
ACS Appl. Mater. Interfaces XXXX, XXX, XXX−XXX

linked directly to the gate electrode usually made from gold.[16−20] EGOFETs with a modified gate have been proven to perform ultra-sensitive, label-free selective detection of different biomarkers in real biofluids[21] and could be scaled to the simultaneous detection of several analytes on one chip using a multigate architecture.[15] At the same time, such devices are rather bulkier than their analogues, which could be designed with an OSC layer modification and concede to them in planarity of the architecture and compactness. The latter is a great advantage for their further potential application in lab-on-a-chip devices.

Design and fabrication of an EGOFET bioreceptor layer include the following key issues: (1) development of novel strategies of molecular design and biomolecular grafting methods for OSCs with functional groups; (2) in-depth study on how analytes or stimuli influence the charge behavior in the conductive channel; (3) finding a balance between the device performance and its sensing capabilities; and (4) determination of the principles of the device structure to enable its adaptation to specific sensing needs.[22] A keystone for further EGOFET sensitivity and stability improvement is the strategy of bioreceptor immobilization allowing the maximization of molecular recognition and minimization of damage to the semiconducting layer.

The choice of functional materials to be used as the components of active layers in biosensors is very important and could drastically affect the performance of the target devices. First of all, smoothness and high crystallinity degree of the organic semiconducting layer,[5,23] as well as excellent electrochemical stability of the organic semiconducting material,[5] are required to achieve stable and reproducible EGOFETs with low threshold voltage and high current values that is necessary for biodetection. The low mobility of polymer chains allows the easy creation of a smooth film based on conjugated polymers:[24] the most widespread polymer used in EGOFET is poly(3-hexylthiophene) (P3HT) and its derivatives.[8,14,25−29] However, small molecules, including pentacene and some oligomers such as α-sexithiophene,[5,30−32] are also often used for highly crystalline organic semiconducting film fabrication providing high mobility for the charge carriers.[5,8,33] Another advantage of the small molecules lies in their higher material purity due to their more controllable molecular structure. One of the most widely used small-molecule OSCs is 2,7-dioctyl[1]benzothieno-[3,2-*b*]benzothiophene (C_8-BTBT-C_8). In spite of the fact that C_8-BTBT-C_8 has excellent electrochemical stability combined with high mobility of charge carriers, which make it one of the most prominent materials for EGOFETs,[15,33−35] application of BTBT-based EGOFETs as biosensors has not been reported yet.

In this paper, we propose a fast and simple technique for functionalization of the OSC surface allowing the fabrication of a large-scale biorecognition layer with a huge area of sites available for further biomodification. The biorecognition layer is based on a novel derivative of the BTBT-containing biotin fragment in the molecular structure (**BTBT−biotin**), which provides a universal anchor for bioanalytes. It can be fabricated by the Langmuir−Schaefer technique from the blend of **BTBT−biotin** with a siloxane dimer of BTBT (**D2-Hept-BTBT-Hex**)[36] on the top of a usual OSC C_8-BTBT-C_8. In order to provide the desired biorecognition properties, the fabricated biotin-containing layer can be further modified. In this work, it was modified by streptavidin (SA) followed by DNA aptamer RHA0385 to increase the specificity to influenza virus. The successful modification of the layer was proved by microscopy. The devices fabricated are very efficient and stably operate with high reproducibility of the EGOFET electrical properties. Preliminary investigations demonstrate a specific response of the BTBT-based biorecognition layer in EGOFETs to the influenza A virus (H7N1 strain, 3×10^9 virus particles per mL). The elaborated approach to biorecognition layer formation allows fabricating several biosensors for various analytes on one substrate and paves the way for "electronic tongue" creation in a manner developed by our group earlier for gas sensing applications.[37]

RESULTS AND DISCUSSION

Choice of Appropriate Materials Design, Layer Formation Strategies, and Architecture of a Biosensor. The proposed approach for fabrication of the biorecognition layer in EGOFETs exploits the bilayer structure (Figure 1) with receptors anchored to the OSC surface. Recently, we have developed a method for organic electrolytic transistor manufacturing that is based on phase microsegregation in the mixtures of an OSC, C_8-BTBT-C_8, and a dielectric polymer, polystyrene (PS).[33] This mixture in a ratio of 4:1 (C_8-BTBT-C_8/PS) was dissolved in toluene with a total concentration of 18 mg/mL and then deposited by a simple easy scalable doctor blading method at a temperature of 75 °C on highly doped silicon substrates pre-heated to 75 °C and containing a 200 nm thick layer of thermally grown silicon dioxide and 35 nm thick gold source and drain electrodes (Figure 1a). Small-molecule OSC−polymer blends are widely used for thin-film formation by solution processing.[38−40] Previously, vertical phase separation of C_8-BTBT-C_8 and PS blend solution was demonstrated, and it was shown to have a relatively good transistor performance, owing to the high intrinsic mobility of C_8-BTBT-C_8 and high viscosity of PS-added solution.[41] In our case, the addition of PS suppresses uncontrolled bulk crystallization of C_8-BTBT-C_8 molecules and promotes the formation of a smooth thin OSC film on top of the polymer dielectric layer, which is necessary for charge transport at the semiconductor−electrolyte interface. The increased substrate temperature accelerates the microsegregation process in the C_8-BTBT-C_8/PS mixture, as a result of which PS is segregated at the substrate−mixture interface, while the OSC forms the upper layer in the form of flat crystals with low roughness laying in contact with the electrolyte.[42] The desired functionality of the fabricated surface was obtained by the addition of the bioreceptor layer, which was deposited above the semiconducting layer by the Langmuir−Schaefer (LS) technique using the blend of a siloxane dimer of BTBT (**D2-Hept-BTBT-Hex**) and a specially designed biotin derivative of BTBT (**BTBT−biotin**), which contains a terminal biotin fragment in the structure to provide the anchors for bioanalytes on the surface of the OSC (Figure 1b). The siloxane dimer component of the blend is responsible for uniform Langmuir film formation on a water surface[43] and creation of a framework for biotin-containing component distributions. The packing of the siloxane dimers in the Langmuir−Schaeffer or Langmuir−Blodgett layers was discussed previously in our works,[36,43,44] where the vertical position of the molecules on the wafer was shown. This feature of siloxane dimers was used to provide the framework necessary for the distribution and keeping **BTBT−biotin** molecules in the vertical position. The presence of a non-functional alkyl terminal group (C_{11}) allows **BTBT−biotin** molecules to integrate into the Langmuir layer by co-crystallization with the siloxane dimer that results in a mixed monolayer film for selective binding with various biological

https://doi.org/10.1021/acsami.1c24109
ACS Appl. Mater. Interfaces XXXX, XXX, XXX−XXX

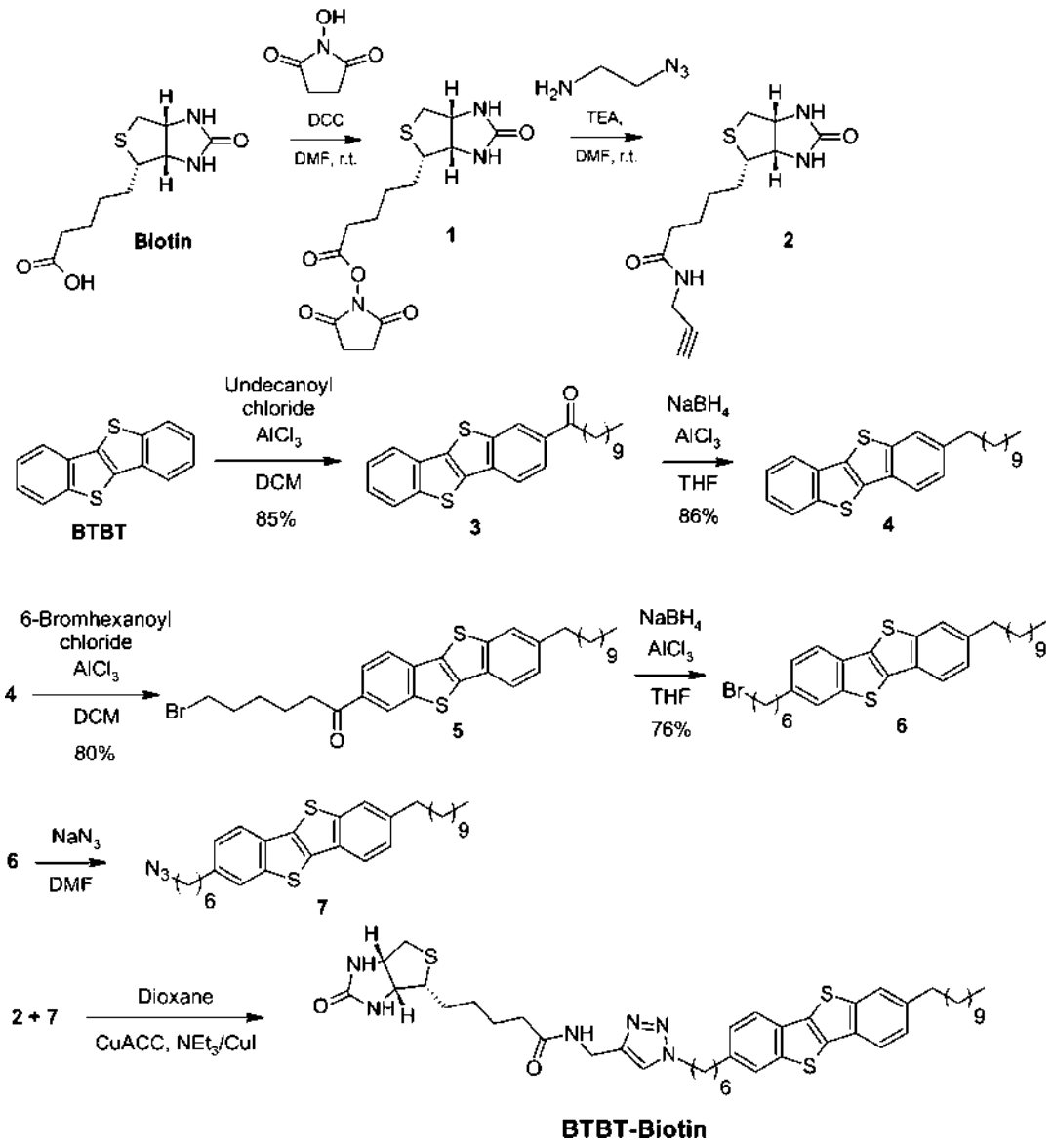

Figure 2. Scheme of the synthesis of the BTBT derivative containing biotin—**BTBT−biotin**.

target molecules. Formation of the upper lying functional monolayer film should not drastically influence the performance of EGOFETs while providing the location of biorecognition sites very close to the current-carrying layer.

Most of the OSCs are inherently hydrophobic that hinders interactions with hydrophilic biomolecules necessary for specific immobilization of biosensing layers and presents an obvious obstacle to further development of OSC surface modification.[45−48] Our approach allows overcoming this problem due to two factors. First, the LS technique of film formation is insensitive to the hydrophilic−hydrophobic balance of the substrate surface,[49] and, second, the siloxane-containing fragment of **D2-Hept-BTBT-Hex** is compatible with the hydrophobic C_8-BTBT-C_8 surface and is not prone to dewetting. The formation of the bioreceptor monolayer on top of the OSC surface is based on the dual properties of the designed **BTBT−biotin** molecule, which combines biochemical activity of a biotin fragment with strong $\pi-\pi$ interactions typical for a conjugated BTBT-fragment. Moreover, it was found that the coating of **BTBT−biotin** alone (100%, without blending with a siloxane dimer) on the OSC surface drastically decreases the electrical properties of the device. Therefore, we concluded that the presence of the siloxane dimer in the blend is essential. First of all, both molecules have the same BTBT-conjugated fragment in order to avoid phase separation between the blended components and bunching of **BTBT−biotin** islands. Second, the siloxane dimer moiety is crucial for obtaining a thermodynamically stable Langmuir−Schaefer layer in a wide range of **BTBT−biotin** concentrations. Albeit, we suppose that the other conjugated fragment could also work in such moieties, it is essential to have the same conjugated fragment in both components of the blend for a stable bioreceptor monolayer formation. We suggest that our BTBT-based bioreceptor layer might also be applied on the surface of a semiconducting layer of different chemical structures even without the BTBT conjugated core, for instance, in dialkyl-tetrathienoacene or quaterthiophene OSCs,[50,51] which requires further investigations. However, an advantage of BTBT-conjugated fragment usage in both the OSC and the biorecognition layer is its good solubility, stability, and high charge carrier mobility. On the

https://doi.org/10.1021/acsami.1c24109
ACS Appl. Mater. Interfaces XXXX, XXX, XXX−XXX

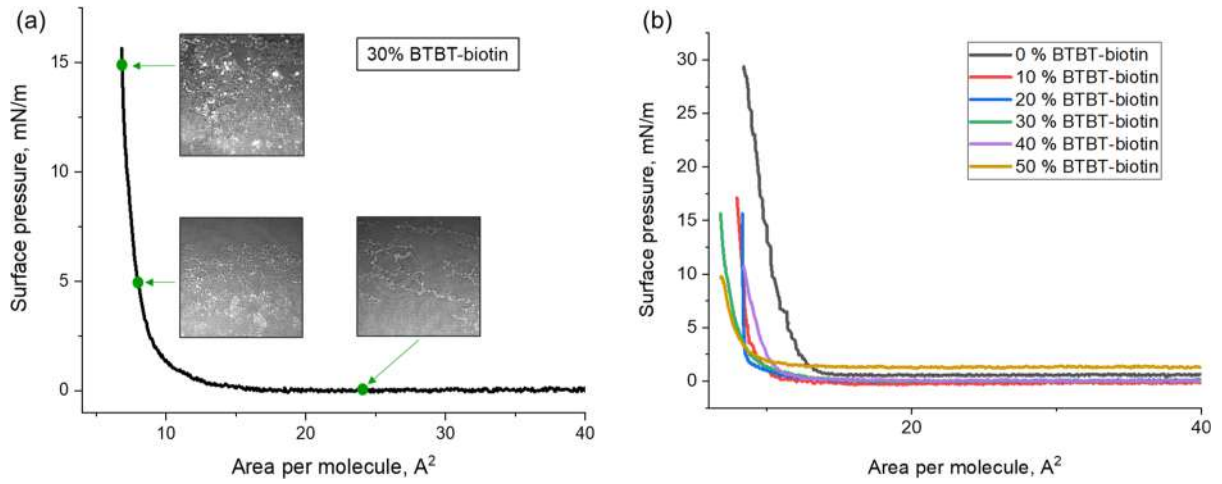

Figure 3. (a) Langmuir isotherm of 30% **BTBT−biotin** containing blend with the corresponding BAM images obtained at different surface pressures. (b) Langmuir isotherms of **D2-Hept-BTBT-Hex** and **BTBT−biotin** blends of various compositions.

contrary, usage of a siloxane dimer in the formation of the bioreceptor layer is fundamentally important because it allows creating an inert surface, which does not affect the pH of the measured solutions and makes the layer biocompatible. It should be noted that both methods used in the fabrication of the bilayer biorecognition structures—doctor blading and Langmuir−Schaefer—are rather fast, simple, and of low cost. Moreover, they are compatible with printing technologies that allow one to fabricate large-area uniform layers and can be easily scaled up to roll-to-roll technology for flexible substrates.[44,52,53]

Further development of biorecognition properties of the proposed biolayer was based on the SA−biotin interactions. SA is a tetrameric protein composed of four identical subunits each with a high-affinity ($K_d \sim 10^{-15}$ M) binding site to the biotin ligand.[54] Besides that, SA has several advantages in the biosensing model:[22] a high association rate constant, near absence of a buffer effect on the binding affinity and protein stability, wide commercial availability, and near neutral protein isoelectric point,[55] which reduces its dependence on nonspecific binding. Specificity of the biorecognition was achieved due to DNA aptamer RHA0385 to hemagglutinin (HA, surface protein of influenza virus): this aptamer binds different strains of influenza A with nearly the same affinity (K_d = 2−5 nM),[56,57] providing the possibility of strain-independent detection of the virus.[57,58]

Synthesis of Materials. **BTBT−biotin** was synthesized by the reaction of 1,3-dipolar cycloaddition (click reaction) of the azide derivative of BTBT (7) with an alkyne derivative of biotin (2)—a water soluble vitamin of B group (Figure 2). For this purpose, commercially available biotin was activated by preparation its *N*-succinimide ester (1) and then compound 2 was obtained by the amidation reaction with propargylamine.[59] The synthesis of compound 7 was based on a combination of the Friedel−Crafts acylation reaction and the reduction of the corresponding ketones. For subsequent functionalization, a non-expensive commercially available 6-bromohexanoyl chloride was used. The resulting terminal bromine was converted by nucleophilic substitution with sodium azide into the corresponding compound 7 under mild conditions. At the last stage, the precursors obtained were introduced into a click reaction in the presence of monovalent copper and a tertiary amine in dioxane to give the target compound **BTBT−biotin** (Figure 2). A detailed description of the synthetic methods and full characterization of the novel materials synthesized can be found in the Supporting Information (Figures S1−S7).

Fabrication of the Biorecognition Layer. We tuned the ratio between the components of the blend of **D2-Hept-BTBT-Hex** and **BTBT−biotin** from 1:0 (0% **BTBT−biotin**) to 1:1 (50% **BTBT−biotin**) in order to understand their mutual distribution on the surface and find optimal conditions of a uniform biorecognition layer formation. The inert nature of the deposited LS layer minimizes ionic diffusion, eventually limiting the OSC doping, while the biotinylated **BTBT−biotin** conveniently furnished the binding sites for SA proteins.

The self-assembling properties of the blends of **D2-Hept-BTBT-Hex** and **BTBT−biotin** on the water surface were investigated by the Langmuir technique. **D2-Hept-BTBT-Hex** is highly stable under normal conditions (20−25 °C, in air) and does not undergo hydrolysis or doping in water.[44] It can be easily transformed from the extended conformation into the closed one during the layer compression by Langmuir through barriers due to flexible heptylenic spacers and especially a disiloxane unit, which is able to form hydrogen bonds with water molecules as opposite to the fully hydrophobic terminal hexyl group of the dimer molecule.[36,44] Figure 3a shows a typical Langmuir isotherm of the blend of **D2-Hept-BTBT-Hex** and **BTBT−biotin** and Brewster angle microscopy (BAM) images of the water surface under different barrier pressures obtained for a 30% **BTBT−biotin** mixture. The Langmuir isotherm of the blend contains three easily distinguished regions: the first one correlates with the formation of separate non-interacting monolayer islands of the biotin-containing and disiloxane molecules in their extended conformations undergoing spontaneous gradual transformation into the closed conformation (area per molecule of ca. 60 Å^2 ÷ ca. 17 Å^2, BAM image at 0 mN/m), which leads to a constant surface pressure with the area per molecule decreasing. The second region with the slow increase of the surface pressure corresponds to the beginning of the interactions between the monolayer islands with a continuous change of the molecular conformations to a closed one (Figure 3a, BAM image at 5 mN/m) (area per molecule of ca. 17 Å^2 ÷ ca. 8 Å^2). The third region (area per molecule of ca. 8 Å^2 ÷ ca. 6 Å^2) represents a rapid increase of the surface pressure and corresponds to a fully covered monolayer formation (Figure 3a, BAM image at 15 mN/m)—all the dimer molecules completely changed their conformation to the closed one, the

https://doi.org/10.1021/acsami.1c24109
ACS Appl. Mater. Interfaces XXXX, XXX, XXX−XXX

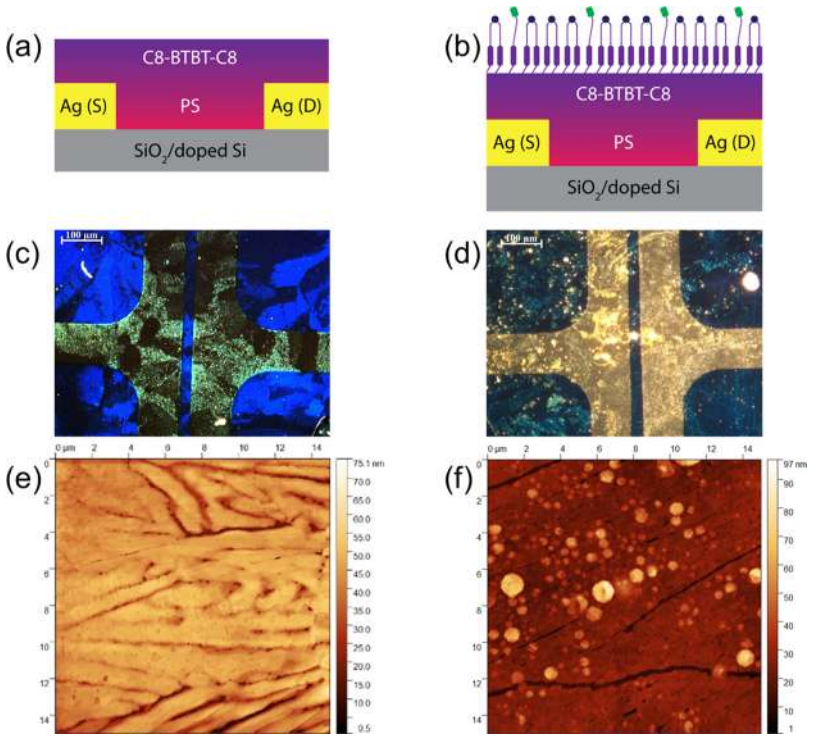

Figure 4. Layer schematics (a, b) and corresponding POM (c, d) and AFM (e, f) images for the layers without (a, c, e) and with (b, d, f) biorecognition biotin fragment.

biotin-containing molecules are embedded in the layer and co-crystallized with the siloxane-containing molecules. The anticipated decrease of the maximum pressure on the Langmuir isotherms was observed with increasing the biotin content in the blend (Figure 3b), which occurs, probably, due to the decrease of the amount of hydrogen bonds between the siloxane fragments and water molecules that leads to the lower stability of the Langmuir layer on the water surface. Based on the results obtained, we can expect that a uniform and dense monolayer of the blend containing 30% of **BTBT−biotin** is formed in the region of the areas per molecule of 17 $Å^2$ ÷ 8 $Å^2$: this region was chosen for further LS transfer of the films.

Morphology of the bioreceptor layers obtained was controlled by polarizing optical microscopy (POM) and atomic force microscopy (AFM) (Figure 4). Although the presence of the thin layer as a result of the LS deposition is obvious (Figure 4d) and corresponds to a typical Langmuir layer of the BTBT-containing siloxane dimer,[44,49] we did not find significant differences in the morphologies of the films obtained with varied amounts of biotin moieties. The main reason of this finding should be the small size of the biotin fragments, but the images observed obviously indicate that biotin-containing components of the blend do not degrade the uniform film of the siloxane dimer during the bioreceptor layer formation and do not induce any dewetting processes.

Estimation of Biotin Content on the Surface of the Biorecognition Layer. To maximize the efficiency of capturing the target bioanalyte by the biorecognition layer, an optimal coverage of the immobilized probes should be achieved. In order to solve this issue, it was necessary to correlate the **BTBT−biotin** content in the solution during the fabrication process with its deposition on the surface in the composition of the bioreceptor layer. We have used different methods of analysis to confirm the formation of a biotinylated layer on the surface of the OSC and to prove that the anchors of biotin are not hidden in the bulk of **D2-Hept-BTBT-Hex** during the Langmuir method of deposition and orient favorably on the surface to provide active binding sites for further SA immobilization. Water contact angle goniometry (WCAG) measurements revealed (Table S1, Supporting Information) an increase in the hydrophilicity of the surface upon increasing the biotin content in the layer. This observation is in a good agreement with the fact that biotin anchors are hydrophilic along with the hydrophobicity of the remaining parts of the layer formed by **D2-Hept-BTBT-Hex** showing the straight impact of biotin on the wetting properties of the surface. Due to the change in hydrophobicity, the surface covered by a drop of the reacting solution is not equable for the layers with different biotin contents correlating with the quantity of biotin anchors. In order to assess the base area of the spherical segment of the drop of volume, V, put on the surface of a biorecognition layer with contact angle, θ, calculations were conducted according to the formula shown in Figure S8, Supporting Information. It was assumed that the surface tension coefficient is large enough for the droplet shape to be considered spherical.

Estimation of the amount of biotin immobilized on the surface by the enzyme-linked immunosorbent assay (ELISA) allowed us to quantify the amount of SA attached to the surface and to estimate the distribution of biotin concentration on the surface. In order to exclude the non-specific oxidation of the 3,3′,5,5′-tetramethylbenzidine (TMB) substrate on the surface of a biorecognition layer of the sample, it was put on the surface without the HRP and SA enzymes, and no change of the color was observed. The consistent treatment of the substrates with a bioreceptor layer and control substrate by a solution of a streptavidin−horseradish peroxidase conjugate (Str−HRP) in bovine serum albumin (BSA) blocking solution and TMB substrate, resulting in the change of solution color to blue and

https://doi.org/10.1021/acsami.1c24109
ACS Appl. Mater. Interfaces XXXX, XXX, XXX−XXX

after the addition of stopping sulfuric acid solution to yellow. Therefore, we can conclude that for specific binding of the TMB substrate an enzyme is required. In addition, this experiment is evidence of biotin presence on the surface of the fabricated biorecognition layer. The quantification of the above-mentioned process was conducted by the measurement of solution absorption at a wavelength of 450 nm on a CLARIOstar (BMG) spectrophotometer (Table S1, Supporting Information).

An essential feature of the biorecognition layer is to provide a certain amount of the biotin anchors on the surface, which is able to both provide enough sites for SA binding and avoid steric hindrances for protein molecules. On the basis of the results of WCAG and ELISA, the specific concentration of biotin on the surface of the biorecognition layer with different biotin contents was evaluated considering that SA provides four binding sites for biotin. According to Figure 5, the calculated specific concentration of biotin on the surface significantly increases up to a biolayer with 30% biotin and does not meaningfully change at higher biotin contents. It should be related to the uniformity of the biolayer and hence, the **BTBT−biotin** distribution. The achieved uniformity of the biolayer correlating with enough sites for the steric placement of SA molecules is extremely significant for further immobilization of the target biomolecules, that is, antibodies, aptamers, viruses, and so forth. Therefore, on the basis of WCAG and ELISA, we conclude that the optimal concentration for the biorecognition layer is equal to 30% of **BTBT−biotin** content in the solution during the film fabrication.

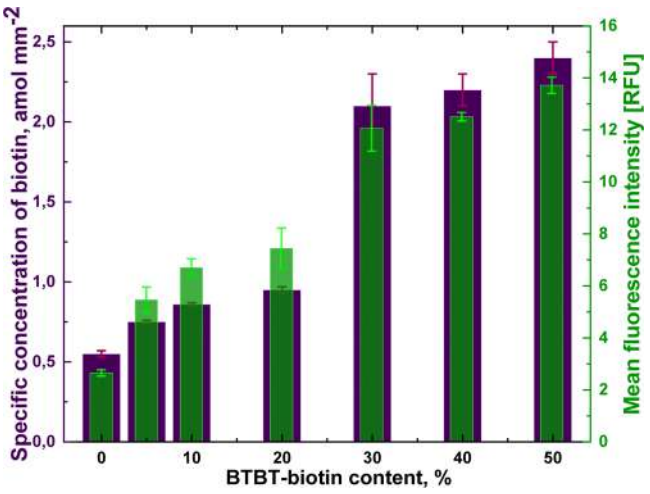

Figure 5. Change of the specific concentration of biotin on the surface of the biorecognition layer and mean fluorescence intensities (MFIs) calculated by using ImageJ software with different **BTBT−biotin** contents.

The presence of biotin and the uniformity of its distribution on the biorecognition layer surface was verified with fluorescence imaging, as shown in Figure 6a−d. Fluorescein isothiocyanate−SA (FITC−SA) was used to detect the presence and distribution of biotin in the layer. Magnification of the fluorescent area of the surface gives an understanding of the distribution of SA and as a consequence biotin on the surface distinctly correlates with the morphology of the Langmuir film of the biorecognition layer (Figure 6b). Brightness indicates the relative amount of the immobilized probes, where the fluorescent dyes emitted green light (λ = 470 nm). Overall, the biorecognition layer expressed a certain level of autofluorescence with low non-specific binding and much higher amount of FITC−SA bound to the surface than the reference sample with 0% of **BTBT−biotin** in the film composition. The brightness of the fluorescence signal was measured from the fluorescence images of the samples under the same conditions (Figure 6e). The MFIs were analyzed and calculated by using ImageJ software (Figure 5). The error bars represented one standard deviation (1σ) of MFI uncertainty measured from eight subregions of a sensing surface. As the films were fabricated with increasing concentrations of **BTBT−biotin** in the blend, the MFIs of the resulting surfaces increased proportionally. The MFIs were 2.62, 5.44, 6.68, 7.43, 12.06, 12.50, and 13.72 RFU at 0, 5, 10, 20, 30, 40, and 50% **BTBT−biotin**, respectively (Figure 5). Using fluorescent SA helps to estimate the quality of the biorecognition layer fabricated with different contents of **BTBT−biotin**. However, already a 5% containing biotin film

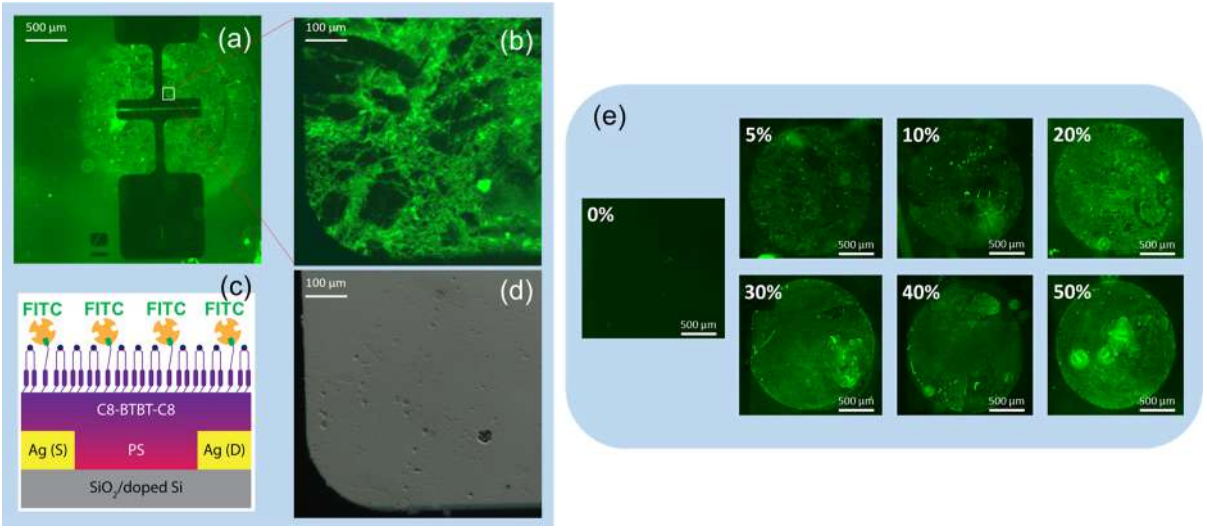

Figure 6. Fluorescence microscopy images of the sample (a,b) with 10% of **BTBT−biotin** in the biorecognition layer covered with FITC−SA (c) with correspondence to the morphology of the film on the POM image (d). Fluorescence images of the surface functionalization with a content of **BTBT−biotin** ranging from 0 to 50%, covered with FITC−SA (e).

https://doi.org/10.1021/acsami.1c24109
ACS Appl. Mater. Interfaces XXXX, XXX, XXX−XXX

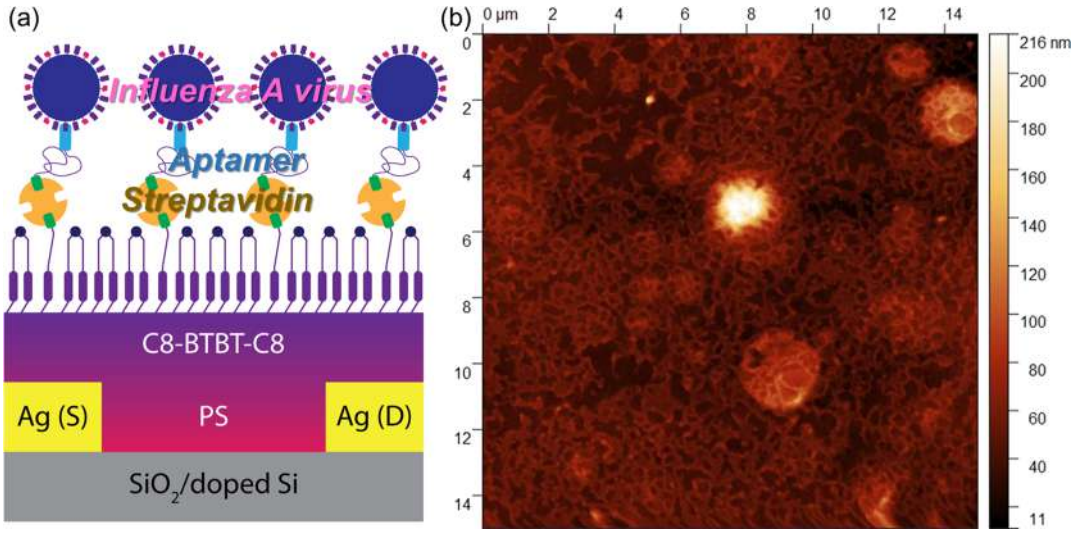

Figure 7. Virus immobilization on a surface of the biorecognition layer based on the biotin−SA interactions: (a) scheme of the sensing device with all interlayers and (b) AFM image of the device surface covered with virions of influenza A virus.

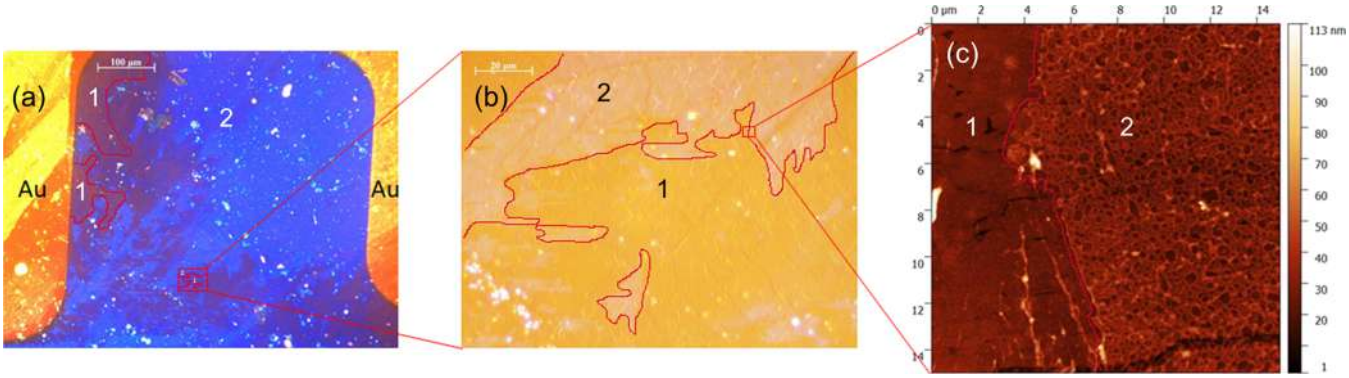

Figure 8. Influenza A virus immobilization on the surface of the biorecognition layer. Optical images with magnification ×10 (a) and ×50 (b) showing borders of the biorecognition layer film, covered with SA, aptamer, and influenza A virus (2) on the C_8-BTBT-C_8 surface (1). AFM image (c) showing the coverage of the virions.

produced perceptible fluorescence with FITC−SA, and the correlation of the uniformity of fluorescence with the morphology of the Langmuir film was achieved only at 30% of **BTBT−biotin** content. It should be noted that large-scale uniformity of the biorecognition layer was also achieved in the film with 30% **BTBT−biotin** content. This is in agreement with the data obtained on the basis of WCAG and ELISA.

When the dissolved biotin was added to the FITC−SA solution, it caused inhibition at a mass ratio of 1:10 and eventually disappearance at a ratio of 1:1 of the fluorescence of the sample surface (Figure S9, Supporting Information), which indicates that all SA binds to the dissolved biotin but does not immobilize on the surface because all sites are linked. This is also a confirmation that all interactions with SA, as a result of which we observed the contrast of fluorescence, are actually specific due to biotin anchoring on the surface.

A mixture of FITC−SA and Cy5−BSA in a mass ratio of 100:1 was used to define the distribution of biotin anchors on the surface of the bioreceptor layer (Figure S10, Supporting Information). Fluorescence images of the edge (Figure S10a) and the center (Figure S10b) of the area, treated by a mixture of SA and BSA, show that most of the surface was occupied by specific-bonded SA, while BSA immobilized non-specifically on the rest of the surface uncovered with biotin. This also indicates the selectivity of the biorecognition layer to SA regarding the other albumins.

Affinity of the Biolayer to Immobilization of Biomolecules. We chose the biorecognition layer with 30% of biotin as a uniform biorecognition layer providing enough quantity of sites for biotin−SA interactions and studied its suitability for biosensing of influenza A virus. We immobilized step-by-step SA [100 μg/mL in phosphate-buffered saline (PBS) (10 mM, pH = 7.4)], biotinylated aptamer to hemagglutinin of influenza virus (RHA0385, 2 μM solution in PBS) and influenza A virus (H7N1 strain, 3×10^9 virus particles per mL) or non-specific control virus NDV (Newcastle Disease virus, 3×10^9 virus particles per mL) on the transistor channel according to the scheme of the immobilization steps shown in Figure S11. The influenza A virus immobilizes on a surface of the biorecognition layer, forming an equable network of virions according to AFM images (Figure 7). This agrees with the morphology described in recent studies on the character of different viruses adhering to smooth surfaces.[60]

At the same time, the influenza A virus does not immobilize on breaks of the biorecognition Langmuir film (Figure 8) that is simply explained by the absence of the biotinylated aptamer at such breaks. This observation is consistent with the requirement of specific interactions with the biotinylated aptamer, SA, and

https://doi.org/10.1021/acsami.1c24109
ACS Appl. Mater. Interfaces XXXX, XXX, XXX−XXX

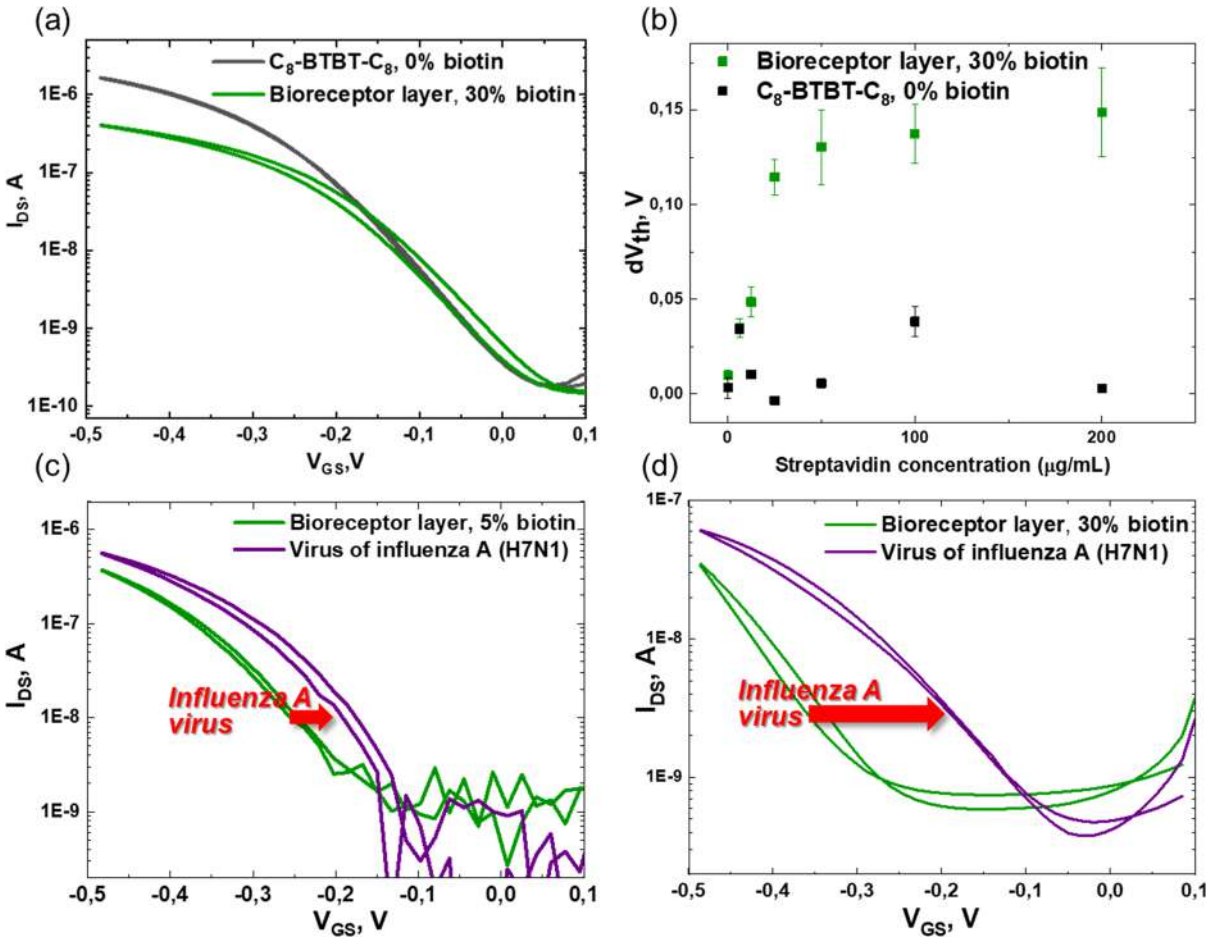

Figure 9. EGOFET transfer characteristics of the fabricated device with C_8-BTBT-C_8 and 30% **BTBT−biotin** layer (V_{DS} = −0.5 V) (a). Response to SA of the EGOFET with C_8-BTBT-C_8 and 30% **BTBT−biotin** layer (b). Response of the bioreceptor layer with 5% (c) and 30% of **BTBT−biotin** (d) to the influenza A virus.

biotin for virus immobilization and indicates the formation of a biotinylated surface by using the presented approach for biorecognition layer fabrication.

To prove the above statement, the surface treated with SA, aptamers, and viruses was investigated. Any different combinations assayed did not lead to the formation of some regular structures of the coating. However, from the AFM images, we can conclude that some small amount of bioanalytes could be immobilized non-specifically that is also in agreement with the results of fluorescence microscopy and ELISA. It is suggested[7] that the presence of an analyte dispersed in a liquid electrolyte leads to the deterioration of the layer; however, we observe that the Langmuir biolayer prevents the active layer of BTBT from dewetting under the harsh influence of biological liquids (Figure S12a−e, Supporting Information), while a bare BTBT layer collapses under such conditions (Figure S12f).

EGOFET Characteristics of the Biorecognition Layer. As the best concentrations of **BTBT−biotin**, on the basis of SA distribution, was determined to be 30% and higher, it is necessary to define an optimum between the biotin content and electrical characteristics of EGOFETs. 40 and 50% of **BTBT−biotin** significantly impair the electrical characteristics compared to the bare C_8-BTBT-C_8-based device. An EGOFET containing biorecognition layer with 30% **BTBT−biotin** retains a good electrical performance, as shown by the transfer characteristics (Figure 9a) measured in the PBS solution (10 mM, pH = 7.4) with high ionic strength (162.7 mM). The source−drain current exhibits well-shaped linear and saturation regions at the applied gate bias. On/off current ratio and threshold voltage are 1400 ± 600 and −0.13 ± 0.05 V, respectively (averaged over 20 samples). According to these data, a biorecognition layer based on **BTBT−biotin** does not dramatically affect the electrical performance of the semiconductor layer. The leakage current remains in the nanoampere range. This fact along with the very low hysteresis exhibited shows that the Langmuir−Schaefer layer efficiently acts as a barrier toward semiconductor doping. The source−drain currents decreased slightly; however, the performance of the transistor has not been impaired. The reason for the decrease in currents may be because of an increase in the surface roughness due to the presence of a receptor layer containing **BTBT−biotin**. The capacitance and the morphology of the active layer, after bioreceptor coating, changes and influences in such way that the electrical properties of the device decrease but not significantly (Figure 9a). Due to the fact that the siloxane dimer is a semiconductor, and there are several publications on its OFET properties,[36,37,44,49,52] the **BTBT−biotin**-based bioreceptor layer does not act as a dielectric. At the same time, the device with only the **BTBT−biotin**-based bioreceptor layer and without an active OSC layer shows low electrical properties with currents in the nA region and low stability as it is a monolayer,

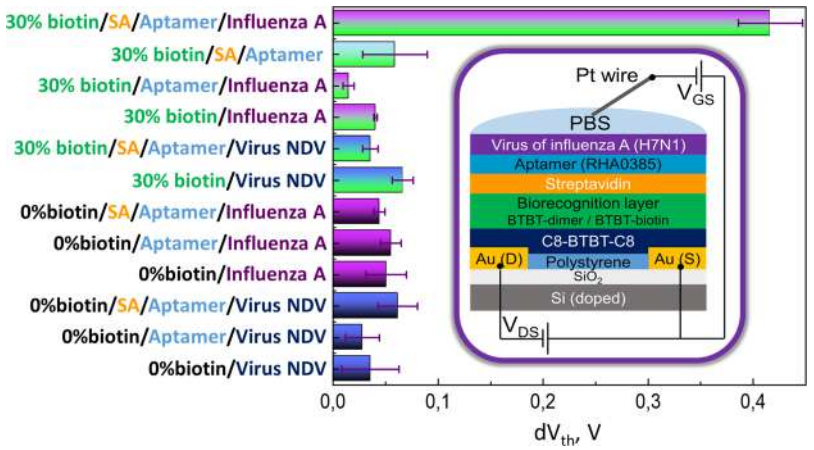

Figure 10. Shift in the threshold voltage of the fabricated EGOFET devices treated with different combinations of bioanalytes with the illustrated scheme of the **BTBT−biotin**-based device with all deposited and sensing layers.

which is not suitable for the OET sensor application (Figure S13).

The measurements of the stability of the operating devices with the bioreceptor layer in PBS solution with a 40 s delay time between the start of the consistent transfer curves show that the threshold voltage shifts during the first 20 min of the measurements which then does not undergo significant changes (the shift is about 2%) for the next 60 min of measurements (Figure S14).

Sensing Ability of the Biorecognition Layer. First of all, the performance of the fabricated bioreceptor layer was investigated for the detection of SA as a sensing model. SA was incubated on the channel and rinsed to remove unbound proteins. The measurements were performed in the PBS electrolyte before and after incubation. In Figure 9b, the responses of the sensor to different SA concentrations upon changing the threshold voltage ($dV_{th} = (V_{th} - V_{th0})/V_{th0}$) of EGOFETs with the bioreceptor layer (30% **BTBT−biotin**) and without it (0% biotin) are shown. For each concentration, measurements were performed on four different devices, and the average value and the standard deviation are presented. The absence of non-specific response of the pristine C_8-BTBT-C_8 active layer as a control is confirmed by $dV_{th} = 0.0 \pm 0.04$. The responses of the EGOFET with bioreceptor layers is linear in the region of the SA concentration from 6 to 50 μg/mL, while it levels off at the concentration of 50 to 200 μg/mL within the experimental error. The LOD of SA was estimated to be 3 times the standard deviation (over 10 replicates) of the response measured in the PBS reference solution and it was equal to 6 μg/mL. These results demonstrate the sensing ability of the layer, and for further investigations a concentration of 100 μg/mL of SA was selected to achieve the full binding of SA to all available biotin sites on the active layer of the EGOFET.

The surface above the transistor channel was modified by SA to link it to the biotin on the surface of the biorecognition layer and create sites for further immobilization of an analyte. Because nucleic acid aptamers are attractive for such applications by immobilization in a sequence-specific manner with high affinity, they are widely used in biosensing design.[58,61] As compared with antibodies and enzymes, aptamers are resilient to heat, pH variation, and chemically harsh conditions, which makes them more efficient for practical applications.[62] Moreover, typical aptamers are 10-fold smaller than, for instance, antibodies, which is expected to substantially decrease the distance between the reporter and the active layer.[58] Thus, the use of aptamers offers a method for sensitive, selective, and affordable biomolecule detection.[63] That is why we used a biotinylated aptamer to hemagglutinin of influenza virus (RHA0385) and a specific virus of influenza A for the recognition of biosensing events of the fabricated device.

Electrical measurements with PBS as the electrolyte in the saturation regime ($V_{DS} = -0.5$ V) were conducted to measure the transfer characteristics of the fabricated devices with 5 and 30% of **BTBT−biotin** in the bioreceptor layer with the layered architecture, as shown in Figure 10. After every step of incubation—with SA (100 μg/mL), the biotinylated aptamer to hemagglutinin of influenza virus (RHA0385) or influenza A virus (H7N1 strain, 3×10^9 virus particles per mL)—the device was first rinsed with PBS and deionized water to remove unbound molecules and then measurements were performed in a PBS electrolyte solution. The results are shown in Figure 9c,d for 5 and 30% of **BTBT−biotin** in the bioreceptor layer. The shift in the threshold voltage after sequential immobilization of all the components is more significant in the case of the layer with 30% of **BTBT−biotin**. This is in good agreement with the ELISA and fluorescence spectroscopy data described above showing the higher concentration of biotin and its more uniform distribution on the surface of biorecognition layer with 30% of **BTBT−biotin** and was the reason for using such a layer composition for further analysis.

To assess whether the response detected has to be ascribed to the sensing event itself instead of the other accidental phenomena (non-specific binding at the channel) that could generate false positive or negative responses, several control experiments were carried out. The devices bearing no biotin on the surface did not significantly respond to the loading with SA, aptamer, or influenza A virus (Figure 10, corresponding transfer curves are shown in Figures S15 and S16 in the Supporting Information). This rules out any contribution of non-specific binding and demonstrates that the electronic response is actually due to the immobilization of SA and other consistent components onto the bioreceptor layer. We investigated the effect of immobilization of the aptamer or influenza A virus without the SA step on the surface covered with biotin, and such EGOFETs did not significantly respond to the changes in the biolayer treatment. This also demonstrates that the transistor response is specific for the SA−biotin binding. To evaluate the selectivity, the control virus NDV was assayed in the presence of

https://doi.org/10.1021/acsami.1c24109
ACS Appl. Mater. Interfaces XXXX, XXX, XXX−XXX

the bioreceptor layer covered with SA and a biotinylated aptamer. The transfer EGOFET characteristics of the bioreceptor layer exposed to NDV were compared to the response of PBS lone, and it was found that NDV does not induce any significant threshold voltage variation. Therefore, influenza A virus-induced increase in 0.42 ± 0.03 V in dV_{th} (Figure 10) is indeed the electric transduction of highly specific interactions of each of the immobilized layers of the designed architecture of the device. All the measured devices showed reproducible electrical characteristics (Figure S17) and very low degradation during the measurements. The threshold voltage on the experiment timescale is orders of magnitude lower compared to the sensing event. Therefore, we conclude that the presented technique of the biorecognition layer fabrication on the OSC layer surface is a promising platform for biosensing based on biotin−SA interactions.

CONCLUSIONS

A fast and simple technique based on doctor blading and Langmuir−Schaefer methods for functionalization of the semiconducting surface of C_8-BTBT-C_8 is reported, which allows fabricating a large-scale biorecognition layer based on a novel functional derivative of BTBT-containing biotin fragments in the structure with a huge area of sites for further biomodification. The proposed approach to a bioreceptor layer fabrication provides the possibility of creation of a universal SA platform for further recognition of bioevents by using biotinylated aptamers or antibodies and viruses or some other biomaterials, which can bind to the biorecognition layer without significantly altering the EGOFET properties. This was achieved by a specially designed biotinylated layer anchored to the OSC surface, followed by self-assembly of SA, which can be easily further functionalized with virtually any receptors by using the well-assessed biotin−SA chemistry. The EGOFETs, with a biorecognition layer reported in this work, are very efficient in high ionic strength electrolyte solutions, providing the possibility of detection of biological objects in real samples. As a proof-of-concept, we have demonstrated a specific response of the BTBT-based biorecognition layer in EGOFETs to influenza A virus (H7N1 strain). The elaborated approach to biorecognition layer formation allows the fabrication of several biosensors for various analytes on one substrate that paves the way for an "electronic tongue" creation.

EXPERIMENTAL SECTION

Materials. Synthesis of the OSC necessary for the formation of the active layer of the device—2,7-dioctyl-benzothieno[3,2-*b*][1]-benzothiophene—was performed as described elsewhere.[64] Synthesis of the OSC required for the formation of the framework of the bioreceptor layer, which was an organosilicon derivative of dialkyl-benzothienobenzothiophene (**D2-Hept-BTBT-Hex**, **BTBT dimer**)—1,3-bis{11-(7-heptyl[1]benzothieno[3,2-*b*][1] benzothio-2-yl)hexyl}-1,1,3,3-tetramethyldisiloxane—was performed as described elsewhere.[36,65] Organic solvents (toluene and dimethylsulfoxide) were purchased from Acros Organics. PS, M_w = 280 000, was purchased from Sigma-Aldrich and used as received. Ultrapure deionized water with a resistance of 18.2 MΩ was obtained using an Akvilon deionizer D-301 (Russia). The biotinylated derivative of BTBT, applied for the formation of biotin anchors on the surface of the bioreceptor layer—**Und-BTBT-Hex-biotin** (**BTBT−biotin**), was synthesized according to the route described in the section Fabrication of the Biorecognition Layer.

Phosphate-buffered saline (PBS 10 mM, pH 7.4) tablets were procured from EcoService, Russia. The 3% H_2O_2 solution was obtained from Rosbio, Russia. Str−HRP (Lot 16731090, RPN1231, GE Healthcare, USA), 3,3′,5,5′-tetramethylbenzidine (TMB) substrate DNA oligonucleotide, and RHA0385 (5′-biotin-ttggggttattttgg-gagggcgggggtt-3′) were purchased from Sigma-Aldrich.

Influenza virus and allantoic fluid were provided by the Chumakov Federal Scientific Center for Research and Development of Immune and Biological Products of the Russian Academy of Sciences. The following influenza strains were studied: A/chicken/Rostock/45/1934(H7N1) 5th passage[66] and Newcastle disease virus (NDV). Virus stocks were propagated in the allantoic cavity of 10 day old embryonated specific pathogen-free chicken eggs. The eggs were incubated at 37 °C, cooled at 4 °C for 48 h post-infection, and harvested 16 h later. The study design was approved by the Ethics Committee of the Chumakov Institute of Poliomyelitis and Viral Encephalitides, Moscow, Russia (Approval #4 from 2 December 2014). The viruses were inactivated via the addition of 0.05% (v/v) glutaric aldehyde, preserved via the addition of 0.03% (w/v) NaN_3, and stored at +4 °C.

For proper exhibition of the functional activity, the aptamer RHA0385 was folded at 2 μM concentration in 10 mM PBS. The folding process was carried out in the following way: the solution was heated at 95 °C for 5 min and cooled to room temperature.

FITC−SA—streptavidin, modified with fluorescein-isothiocyanate containing three molecules of fluorescein per molecule of streptavidin, Cy5−BSA—bovine serum albumin, modified by cyanine containing three molecules of *N*,*N*′-(dipropyl)tetramethylindo-dicarbocyanine per molecule of BSA. The labeling was performed according to the manufacturer's protocol. The conjugates do not contain protein aggregates and free dyes.

EGOFET Architecture. A heavily doped n-type silicon wafer featuring thermal SiOx (200 nm thick) was used as the substrate for our devices; source and drain (S/D) gold-interdigitated electrodes with a channel length of 20 μm and a channel width of 4 mm were thermally evaporated through a shadow mask. For achieving better charge injection into the semiconductor, the source−drain contacts were modified by a layer of 2,3,4,5,6-pentafluorobenzothiophene (PFBT) according to the procedure, described before.[67] Deionized water was used as the electrolyte (18.2 MΩ). The gate electrode was a platinum wire immersed in the electrolyte.

Doctor Blade Films. The charge transport active layer was obtained by the doctor blading technique using a blend of BTBT and PS in a ratio of 4:1 prepared in toluene at a total concentration of 18 g L^{-1}.[33] The blend coating was realized under ambient conditions at a blade speed of 1 cm s^{-1}; the height of the blade was 650 μm; the temperature of the solution and the substrate was 75 °C.

LS Films. The spreading solution was prepared by mixing **BTBT−biotin** solution in DMSO and **BTBT dimer** solution in toluene with different weight ratios: 0:1 (0% **BTBT−biotin**), 1:99 (1% **BTBT−biotin**), 1:19 (5% **BTBT−biotin**), 1:9 (10% **BTBT−biotin**), 1:4 (20% **BTBT−biotin**), 3:7 (30% **BTBT−biotin**), 2:3 (40% **BTBT−biotin**), and 1:1 (50% **BTBT−biotin**) at a total solution concentration of 0.33 g L^{-1}. The solution was spread on a water surface and the monolayer film formed was left for 5 min to equilibrate before compression. Data were collected with a Nima 712BAM system (Nima, UK) equipped with a Brewster angle microscope MicroBAM2 (Nima, UK) using a Teflon trough and barriers at room temperature. The monolayers were compressed with a speed equal to 200 mm min^{-1}. Langmuir−Schaefer films were obtained by transfer to the silicon substrates containing a BTBT layer by the horizontal dipping method with a dipping speed of 12 mm min^{-1}.

Thin-Film Characterization. The formation of semiconducting and biorecognition layers was controlled using an NT-MDT Solver Next atomic force microscope in the tapping mode under ambient conditions using NT-MDT HA-FM silicon probes with a resonant frequency of 77 kHz and using a Carl Zeiss Axioscop A40Pol polarizing optical microscope.

Electrical Measurements. Electrical measurements were performed using a Keithley 2634B (Keithley, USA) source-meter in an ambient environment. Field-effect mobility values were extracted by fitting transfer characteristics with a Shockley's gradual-channel model in the corresponding voltage range.

https://doi.org/10.1021/acsami.1c24109
ACS Appl. Mater. Interfaces XXXX, XXX, XXX−XXX

Estimation of Biotin Immobilized on the Surface: ELISA. Silicon substrates with bioreceptor layers containing 5, 10, 20, 30, 40, or 50% of **BTBT−biotin** in the Langmuir film and a control substrate (0% **BTBT−biotin**) without **BTBT−biotin** and containing only **D2-Hept-BTBT-Hex** in the Langmuir film were treated as follows. Five drops each of 5 μL of 1/1000 (v/v) solution of Str−HRP in BSA (1 g L^{-1}) blocking buffer were distributed to cover most of the wafer surface. After 15 min of incubation at room temperature, the wafers were washed with PBS and DI water. Five drops each of 5 μL of the substrate solution (0.05 g L^{-1} of 3,3′,5,5′-tetramethylbenzidine and 0.033% H_2O_2 in 0.05 M acetate buffer, pH 4.5) were added; the peroxidase reaction was carried out for 30 min at room temperature and stopped by the addition of 100 μL of 5% (v/v) H_2SO_4. Absorption at a wavelength of 450 nm was measured with a CLARIOstar (BMG) spectrophotometer.

WCAG. WCAG was conducted using 2 μL of deionized water put on the surface of a biorecognition layer with a biotin content ranging from 0 to 50%.

Fluorescence Microscopy. The surface of substrates with a biorecognition layer containing 5, 10, 20, 30, 40, or 50% of **BTBT−biotin** in the Langmuir film and a control substrate (0% **BTBT−biotin**) without **BTBT−biotin** and containing only **D2-Hept-BTBT-Hex** in the Langmuir film were treated as follows: 5 drops each of 2.5 μL of 1/100 (v/v) solution of FITC−SA in PBS were put in different places of the substrate. After 15 min of incubation at room temperature, the wafers were washed with PBS and H_2O. The images of fluorescence of the surface were obtained using an inverted fluorescence microscope NikonECLIPSE TS2 (Japan).

EGOFET-Based Biosensor Testing. Silicon substrates with a bioreceptor layer were subsequently treated with the following reagents:

(1) Immobilization of SA (100 mg/L solution in 1 g L^{-1} BSA solution in PBS). After 15 min of incubation, it was washed with PBS and H_2O.

(2) Immobilization of biotinylated RHA0385 aptamer. After 5 min of incubation, it was washed with PBS and H_2O.

(3) Immobilization of virus: influenza A virus (H7N1 strain, 3×10^9 virus particles per mL) or a control virus (Newcastle disease virus, 3×10^9 virus particles per mL). After 30 min of incubation, it was washed with PBS and with H_2O.

The above-mentioned procedure provides specific binding of every layer. To examine non-specific interactions' influence on the biosensor work, different combinations of SA, aptamer, and virus immobilization on the surface were studied.

■ ASSOCIATED CONTENT

Supporting Information

The Supporting Information is available free of charge at https://pubs.acs.org/doi/10.1021/acsami.1c24109.

Synthesis and characterization of **BTBT−biotin** and intermediate compounds, ^1H and ^{13}C NMR spectra, mass spectrum of **BTBT−biotin**, calculation of the surface area, results of ELISA and WCAG, fluorescence images, steps of the layer immobilization on a surface of the biorecognition layer, AFM data, and electrical measurement data (PDF)

■ AUTHOR INFORMATION

Corresponding Author

Sergey A. Ponomarenko − *Enikolopov Institute of Synthetic Polymeric Materials of Russian Academy of Sciences, 117393 Moscow, Russian Federation; Chemistry Department, Lomonosov Moscow State University, 119991 Moscow, Russian Federation;* orcid.org/0000-0003-0930-7722; Email: ponomarenko@ispm.ru

Authors

Elena Yu. Poimanova − *Enikolopov Institute of Synthetic Polymeric Materials of Russian Academy of Sciences, 117393 Moscow, Russian Federation;* orcid.org/0000-0002-3026-802X

Polina A. Shaposhnik − *Enikolopov Institute of Synthetic Polymeric Materials of Russian Academy of Sciences, 117393 Moscow, Russian Federation; Chemistry Department, Lomonosov Moscow State University, 119991 Moscow, Russian Federation;* orcid.org/0000-0002-1035-5425

Daniil S. Anisimov − *Enikolopov Institute of Synthetic Polymeric Materials of Russian Academy of Sciences, 117393 Moscow, Russian Federation;* orcid.org/0000-0002-7343-2918

Elena G. Zavyalova − *Chemistry Department, Lomonosov Moscow State University, 119991 Moscow, Russian Federation;* orcid.org/0000-0001-5260-1973

Askold A. Trul − *Enikolopov Institute of Synthetic Polymeric Materials of Russian Academy of Sciences, 117393 Moscow, Russian Federation;* orcid.org/0000-0003-3969-3679

Maxim S. Skorotetcky − *Enikolopov Institute of Synthetic Polymeric Materials of Russian Academy of Sciences, 117393 Moscow, Russian Federation;* orcid.org/0000-0002-0413-0502

Oleg V. Borshchev − *Enikolopov Institute of Synthetic Polymeric Materials of Russian Academy of Sciences, 117393 Moscow, Russian Federation;* orcid.org/0000-0003-3134-9857

Dmitry Z. Vinnitskiy − *Enikolopov Institute of Synthetic Polymeric Materials of Russian Academy of Sciences, 117393 Moscow, Russian Federation;* orcid.org/0000-0003-3508-6708

Marina S. Polinskaya − *Zelinsky Institute of Organic Chemistry of Russian Academy of Sciences, 119991 Moscow, Russian Federation;* orcid.org/0000-0003-1906-6766

Vadim B. Krylov − *Zelinsky Institute of Organic Chemistry of Russian Academy of Sciences, 119991 Moscow, Russian Federation;* orcid.org/0000-0001-9477-4610

Nikolay E. Nifantiev − *Zelinsky Institute of Organic Chemistry of Russian Academy of Sciences, 119991 Moscow, Russian Federation;* orcid.org/0000-0002-0727-4050

Elena V. Agina − *Enikolopov Institute of Synthetic Polymeric Materials of Russian Academy of Sciences, 117393 Moscow, Russian Federation;* orcid.org/0000-0001-5892-6752

Complete contact information is available at: https://pubs.acs.org/10.1021/acsami.1c24109

Author Contributions

S.A.P., E.V.A., N.E.N., and E.Y.P. conceived the idea and designed the experiments. E.Y.P. and P.A.S. performed the experiments. O.V.B. designed and M.S.S. and D.Z.V. synthesized the semiconductor and biotin-containing materials. E.Y.P., P.A.S., M.S.P., and V.B.K. conducted fluorescence measurements. E.Y.P., P.A.S., and E.G.Z. conducted ELISA and biosensing experiments. E.Y.P., P.A.S., D.S.A., and A.A.T. performed data analysis and interpretation. S.A.P. supervised the project. E.Y.P., E.V.A., and S.A.P. wrote the paper. All of the authors contributed to the writing of the manuscript and have given approval to its final version.

Notes

The authors declare no competing financial interest.

https://doi.org/10.1021/acsami.1c24109
ACS Appl. Mater. Interfaces XXXX, XXX, XXX−XXX

■ ACKNOWLEDGMENTS

Synthesis of all the materials used and works on fabrication and investigation of the biorecognition layer was supported by the Russian Science Foundation (Grant 19-73-30028) and performed in ISPM RAS. Analysis of the sensor abilities of the designed devices was supported by the Ministry of Science and Higher Education of the Russian Federation (Contract FFSM-2022-0001). ^{1}H and ^{13}C NMR measurements were performed on the equipment of the Collaborative Access Center "Center for Polymer Research" of ISPM RAS. Fluorescence microscopy studies were supported by the Russian Science Foundation (Grant 19-73-30017) and performed in IOC RAS. For the samples of inactivated influenza A and Newcastle disease viruses Prof. Alexandra Gambaryan from Chumakov Federal Scientific Center for Research and Development of Immune and Biological Products RAS (Moscow, Russia) is acknowledged.

■ ABBREVIATIONS

C_8-BTBT-C_8, 2,7-dioctyl[1]benzothieno[3,2-*b*]-benzothiophene
EGOFET, electrolyte-gated organic field-effect transistor
OSC, organic semiconductor
EDL, electric double layer
PS, polystyrene
BAM, Brewster angle microscopy
WCAG, water contact angle goniometry
ELISA, enzyme-linked immunosorbent assay
TMB, 3,3′,5,5′-tetramethylbenzidine
FITC, fluorescein isothiocyanate
SA, streptavidin
Cy-5, *N*,*N*′-(dipropyl)tetramethylindo-dicarbocyanine
BSA, bovine serum albumin
NDV virus, Newcastle disease virus
PBS, phosphate-buffered saline
D2-Hept-BTBT-Hex, 1,3-bis{11-(7-heptyl[1]benzothieno-[3,2-*b*][1]benzothien-2-yl)hexyl}-1,1,3,3-tetramethyldisiloxane
BTBT−biotin, 5-[(3*aR*,4*R*,6*aS*)-2-oxohexahydro-1*H*-thieno[3,4-*d*]imidazol-4-yl]-*N*-({1-[6-(7-undecyl[1]-benzothieno[3,2-*b*][1]benzothien-2-yl)hexyl]-1*H*-1,2,3-triazol-4-yl}methyl)pentanamide
RHA0385, 5′-biotin-ttggggttattttgggagggcgggggtt-3′

■ REFERENCES

(1) Stanciu, L. A.; Wei, Q.; Barui, A. K.; Mohammad, N. Recent Advances in Aptamer-Based Biosensors for Global Health Applications. *Annu. Rev. Biomed. Eng.* **2021**, *23*, 433−459.
(2) Naresh, V.; Lee, N. A Review on Biosensors and Recent Development of Nanostructured Materials-Enabled Biosensors. *Sensors* **2021**, *21*, 1109.
(3) Flahault, A.; Geissbuhler, A.; Guessous, I.; Guérin, P. J.; Bolon, I.; Salathé, M.; Escher, G. Precision Global Health in the Digital Age. *Swiss Med. Wkly.* **2017**, *147*, w14423.
(4) Falk, M.; Psotta, C.; Cirovic, S.; Shleev, S. Non-Invasive Electrochemical Biosensors Operating in Human Physiological Fluids. *Sensors* **2020**, *20*, 6352.
(5) Wang, D.; Noël, V.; Piro, B. Electrolytic Gated Organic Field-Effect Transistors for Application in Biosensors—A Review. *Electronics* **2016**, *5*, 9.
(6) Berto, M.; Casalini, S.; Di Lauro, M.; Marasso, S. L.; Cocuzza, M.; Perrone, D.; Pinti, M.; Cossarizza, A.; Pirri, C. F.; Simon, D. T.; Berggren, M.; Zerbetto, F.; Bortolotti, C. A.; Biscarini, F. Biorecognition in Organic Field Effect Transistors Biosensors: The Role of the Density of States of the Organic Semiconductor. *Anal. Chem.* **2016**, *88*, 12330−12338.
(7) Mulla, M. Y.; Torsi, L.; Manoli, K. *Electronic Biosensors Based on EGOFETs*, 1st ed.; Elsevier Inc., 2020; Vol. *642*.
(8) Shaposhnik, P. A.; Zapunidi, S. A.; Shestakov, M. V.; Agina, E. V.; Ponomarenko, S. A. Modern Bio and Chemical Sensors and Neuromorphic Devices Based on Organic Semiconductors. *Russ. Chem. Rev.* **2020**, *89*, 1483−1506.
(9) Torsi, L.; Magliulo, M.; Manoli, K.; Palazzo, G. Organic Field-Effect Transistor Sensors: A Tutorial Review. *Chem. Soc. Rev.* **2013**, *42*, 8612−8628.
(10) Rivnay, J.; Inal, S.; Salleo, A.; Owens, R. M.; Berggren, M.; Malliaras, G. G. Organic Electrochemical Transistors. *Nat. Rev. Mater.* **2018**, *3*, 17086.
(11) Cramer, T.; Campana, A.; Leonardi, F.; Casalini, S.; Kyndiah, A.; Murgia, M.; Biscarini, F. Water-Gated Organic Field Effect Transistors-Opportunities for Biochemical Sensing and Extracellular Signal Transduction. *J. Mater. Chem. B* **2013**, *1*, 3728−3741.
(12) MacChia, E.; Picca, R. A.; Manoli, K.; Di Franco, C.; Blasi, D.; Sarcina, L.; Ditaranto, N.; Cioffi, N.; Österbacka, R.; Scamarcio, G.; Torricelli, F.; Torsi, L. About the Amplification Factors in Organic Bioelectronic Sensors. *Mater. Horiz.* **2020**, *7*, 999−1013.
(13) Manoli, K.; Magliulo, M.; Mulla, M. Y.; Singh, M.; Sabbatini, L.; Palazzo, G.; Torsi, L. Printable Bioelectronics to Investigate Functional Biological Interfaces. *Angew. Chem., Int. Ed.* **2015**, *54*, 12562−12576.
(14) Di Rosa, A. R., Leone, F.; Chiofalo, V. Electronic Noses and Tongues. *Chemical Analysis of Food: Techniques and Applications*, 2nd ed.; Elsevier Inc., 2020; pp 353−389.
(15) Parkula, V.; Berto, M.; Diacci, C.; Patrahau, B.; Di Lauro, M.; Kovtun, A.; Liscio, A.; Sensi, M.; Samorì, P.; Greco, P.; Bortolotti, C. A.; Biscarini, F. Harnessing Selectivity and Sensitivity in Electronic Biosensing: A Novel Lab-on-Chip Multigate Organic Transistor. *Anal. Chem.* **2020**, *92*, 9330−9337.
(16) Casalini, S.; Leonardi, F.; Cramer, T.; Biscarini, F. Organic Field-Effect Transistor for Label-Free Dopamine Sensing. *Org. Electron.* **2013**, *14*, 156−163.
(17) Mulla, M. Y.; Tuccori, E.; Magliulo, M.; Lattanzi, G.; Palazzo, G.; Persaud, K.; Torsi, L. Capacitance-Modulated Transistor Detects Odorant Binding Protein Chiral Interactions. *Nat. Commun.* **2015**, *6*, 6010.
(18) Macchia, E.; Manoli, K.; Holzer, B.; Di Franco, C.; Ghittorelli, M.; Torricelli, F.; Alberga, D.; Mangiatordi, G. F.; Palazzo, G.; Scamarcio, G.; Torsi, L. Single-Molecule Detection with a Millimetre-Sized Transistor. *Nat. Commun.* **2018**, *9*, 3223.
(19) Macchia, E.; Romele, P.; Manoli, K.; Ghittorelli, M.; Magliulo, M.; Kovács-Vajna, Z. M.; Torricelli, F.; Torsi, L. Ultra-Sensitive Protein Detection with Organic Electrochemical Transistors Printed on Plastic Substrates. *Flexible Printed Electron.* **2018**, *3*, 034002.
(20) Macchia, E.; Manoli, K.; Holzer, B.; Di Franco, C.; Picca, R. A.; Cioffi, N.; Scamarcio, G.; Palazzo, G.; Torsi, L. Selective Single-Molecule Analytical Detection of C-Reactive Protein in Saliva with an Organic Transistor. *Anal. Bioanal. Chem.* **2019**, *411*, 4899−4908.
(21) Macchia, E.; Manoli, K.; Di Franco, C.; Picca, R. A.; Österbacka, R.; Palazzo, G.; Torricelli, F.; Scamarcio, G.; Torsi, L. Organic Field-Effect Transistor Platform for Label-Free, Single-Molecule Detection of Genomic Biomarkers. *ACS Sens.* **2020**, *5*, 1822−1830.
(22) Li, L.; Wang, S.; Xiao, Y.; Wang, Y. Recent Advances in Immobilization Strategies for Biomolecules in Sensors Using Organic Field-Effect Transistors. *Trans. Tianjin Univ.* **2020**, *26*, 424−440.
(23) Nguy, T. P.; Hayakawa, R.; Kilinc, V.; Petit, M.; Yemineni, S. L. V. N.; Higuchi, M.; Raimundo, J.-M.; Charrier, A. M.; Wakayama, Y. Electrolyte-Gated-Organic Field Effect Transistors Functionalized by Lipid Monolayers with Tunable PH Sensitivity for Sensor Applications. *Appl. Phys. Express* **2019**, *13*, 011005.
(24) Borges-González, J.; Kousseff, C. J.; Nielsen, C. B. Organic Semiconductors for Biological Sensing. *J. Mater. Chem. C* **2019**, *7*, 1111−1130.
(25) Picca, R. A.; Manoli, K.; Macchia, E.; Sarcina, L.; Di Franco, C.; Cioffi, N.; Blasi, D.; Österbacka, R.; Torricelli, F.; Scamarcio, G.; Torsi,

L. Ultimately Sensitive Organic Bioelectronic Transistor Sensors by Materials and Device Structures' Design. *Adv. Funct. Mater.* **2019**, *30*, 1904513.
(26) Palazzo, G.; De Tullio, D.; Magliulo, M.; Mallardi, A.; Intranuovo, F.; Mulla, M. Y.; Favia, P.; Vikholm-Lundin, I.; Torsi, L. Detection beyond Debye's Length with an Electrolyte-Gated Organic Field-Effect Transistor. *Adv. Mater.* **2015**, *27*, 911−916.
(27) Knopfmacher, O.; Hammock, M. L.; Appleton, A. L.; Schwartz, G.; Mei, J.; Lei, T.; Pei, J.; Bao, Z. Highly Stable Organic Polymer Field-Effect Transistor Sensor for Selective Detection in the Marine Environment. *Nat. Commun.* **2014**, *5*, 2954.
(28) Piro, B.; Wang, D.; Benaoudia, D.; Tibaldi, A.; Anquetin, G.; Noël, V.; Reisberg, S.; Mattana, G.; Jackson, B. Versatile Transduction Scheme Based on Electrolyte-Gated Organic Field-Effect Transistor Used as Immunoassay Readout System. *Biosens. Bioelectron.* **2017**, *92*, 215−220.
(29) Schmoltner, K.; Kofler, J.; Klug, A.; List-Kratochvil, E. J. W. Electrolyte-Gated Organic Field-Effect Transistor for Selective Reversible Ion Detection. *Adv. Mater.* **2013**, *25*, 6895−6899.
(30) Alam, A. U.; Qin, Y.; Nambiar, S.; Yeow, J. T. W.; Howlader, M. M. R.; Hu, N.-X.; Deen, M. J. Polymers and Organic Materials-Based PH Sensors for Healthcare Applications. *Prog. Mater. Sci.* **2018**, *96*, 174−216.
(31) Buth, F.; Kumar, D.; Stutzmann, M.; Garrido, J. A. Electrolyte-Gated Organic Field-Effect Transistors for Sensing Applications. *Appl. Phys. Lett.* **2011**, *98*, 153302.
(32) Roberts, M. E.; Mannsfeld, S. C. B.; Tang, M. L.; Bao, Z. Influence of Molecular Structure and Film Properties on the Water-Stability and Sensor Characteristics of Organic Transistors. *Chem. Mater.* **2008**, *20*, 7332−7338.
(33) Shaposhnik, P. A.; Anisimov, D. A.; Trul, A. A.; Agina, E. V.; Ponomarenko, S. A. A Simple Approach to Fabrication of Highly Efficient Electrolyte-Gated Organic Transistors by Phase Micro-segregation of 2,7-Dioctyl [1]Benzothieno[3,2-b]Benzothiophene and Polystyrene Mixtures. *Dokl. Phys. Chem.* **2021**, *496*, 20−24.
(34) Di Lauro, M.; Berto, M.; Giordani, M.; Benaglia, S.; Schweicher, G.; Vuillaume, D.; Bortolotti, C. A.; Geerts, Y. H.; Biscarini, F. Liquid-Gated Organic Electronic Devices Based on High-Performance Solution-Processed Molecular Semiconductor. *Adv. Electron. Mater.* **2017**, *3*, 1700159.
(35) Bae, O.; Kim, F. S. Flexible Organic Electrolyte-Gated Transistors Based on Thin Polymer Blend Films of Crystalline C8-BTBT and Amorphous PTAA. *Macromol. Res.* **2020**, *28*, 677−682.
(36) Trul, A. A.; Chekusova, V. P.; Anisimov, D. S.; Borshchev, O. V.; Polinskaya, M. S.; Agina, E. V.; Ponomarenko, S. A. Operationally Stable Ultrathin Organic Field Effect Transistors Based on Siloxane Dimers of Benzothieno[3,2-b][1]Benzothiophene Suitable for Ethanethiol Detection. *Adv. Electron. Mater.* **2022**, 2101039.
(37) Anisimov, D. S.; Chekusova, V. P.; Trul, A. A.; Abramov, A. A.; Borshchev, O. V.; Agina, E. V.; Ponomarenko, S. A. Fully Integrated Ultra-Sensitive Electronic Nose Based on Organic Field-Effect Transistors. *Sci. Rep.* **2021**, *11*, 1−12.
(38) Lee, J. C.; Woo, J. H.; Lee, H. J.; Lee, M.; Woo, H.; Baek, S.; Nam, J.; Sim, J. y.; Park, S. Microfluidic Screening-Assisted Machine Learning to Investigate Vertical Phase Separation of Small Molecule:Polymer Blend. *Adv. Mater.* **2022**, *34*, 2107596.
(39) Deng, W.; Xiao, Y.; Lu, B.; Zhang, L.; Xia, Y.; Zhu, C.; Zhang, X.; Guo, J.; Zhang, X.; Jie, J. Water-Surface Drag Coating: A New Route Toward High-Quality Conjugated Small-Molecule Thin Films with Enhanced Charge Transport Properties. *Adv. Mater.* **2021**, *33*, 2005915.
(40) Wang, W.; Lu, B.; Deng, W.; Zhang, X.; Lu, Z.; Wu, D.; Jie, J.; Zhang, X. Controlled 2D growth of organic semiconductor crystals by suppressing "coffee-ring" effect. *Nano Res.* **2020**, *13*, 2478−2484.
(41) Haase, K.; Teixeira da Rocha, C.; Hauenstein, C.; Zheng, Y.; Hambsch, M.; Mannsfeld, S. C. B. High-Mobility, Solution-Processed Organic Field-Effect Transistors from C8-BTBT:Polystyrene Blends. *Adv. Electron. Mater.* **2018**, *4*, 1800076.
(42) Pérez-Rodríguez, A.; Temiño, I.; Ocal, C.; Mas-Torrent, M.; Barrena, E. Decoding the Vertical Phase Separation and Its Impact on C8-BTBT/PS Transistor Properties. *ACS Appl. Mater. Interfaces* **2018**, *10*, 7296−7303.
(43) Sizov, A. S.; Anisimov, D. S.; Agina, E. V.; Borshchev, O. V.; Bakirov, A. V.; Shcherbina, M. A.; Grigorian, S.; Bruevich, V. V.; Chvalun, S. N.; Paraschuk, D. Y.; Ponomarenko, S. A. Easily Processable Highly Ordered Langmuir-Blodgett Films of Quaterthiophene Disiloxane Dimer for Monolayer Organic Field-Effect Transistors. *Langmuir* **2014**, *30*, 15327−15334.
(44) Trul, A. A.; Sizov, A. S.; Chekusova, V. P.; Borshchev, O. V.; Agina, E. V.; Shcherbina, M. A.; Bakirov, A. V.; Chvalun, S. N.; Ponomarenko, S. A. Organosilicon Dimer of BTBT as a Perspective Semiconductor Material for Toxic Gas Detection with Monolayer Organic Field-Effect Transistors. *J. Mater. Chem. C* **2018**, *6*, 9649−9659.
(45) Buth, F.; Donner, A.; Sachsenhauser, M.; Stutzmann, M.; Garrido, J. A. Biofunctional Electrolyte-Gated Organic Field-Effect Transistors. *Adv. Mater.* **2012**, *24*, 4511−4517.
(46) Kergoat, L.; Piro, B.; Berggren, M.; Pham, M.-C.; Yassar, A.; Horowitz, G. DNA Detection with a Water-Gated Organic Field-Effect Transistor. *Org. Electron.* **2012**, *13*, 1−6.
(47) Magliulo, M.; Mallardi, A.; Mulla, M. Y.; Cotrone, S.; Pistillo, B. R.; Favia, P.; Vikholm-Lundin, I.; Palazzo, G.; Torsi, L. Electrolyte-Gated Organic Field-Effect Transistor Sensors Based on Supported Biotinylated Phospholipid Bilayer. *Adv. Mater.* **2013**, *25*, 2090−2094.
(48) Mulla, M. Y.; Seshadri, P.; Torsi, L.; Manoli, K.; Mallardi, A.; Ditaranto, N.; Santacroce, M. V.; Di Franco, C.; Scamarcio, G.; Magliulo, M. UV Crosslinked Poly(Acrylic Acid): A Simple Method to Bio-Functionalize Electrolyte-Gated OFET Biosensors. *J. Mater. Chem. B* **2015**, *3*, 5049−5057.
(49) Trul, A. A.; Chekusova, V. P.; Polinskaya, M. S.; Kiselev, A. N.; Agina, E. V.; Ponomarenko, S. A. NH3 and H2S Real-Time Detection in the Humid Air by Two-Layer Langmuir-Schaefer OFETs. *Sens. Actuators, B* **2020**, *321*, 128609.
(50) Borshchev, O. V.; Skorotetcky, M. S.; Trukhanov, V. A.; Fedorenko, R. S.; Surin, N. M.; Svidchenko, E. A.; Sosorev, A. Y.; Kazantsev, M. S.; Paraschuk, D. Y.; Ponomarenko, S. A. Synthesis, Characterization and Organic Field-Effect Transistors Applications of Novel Tetrathienoacene Derivatives. *Dyes Pigm.* **2021**, *185*, 108911.
(51) Davydok, A.; Luponosov, Y. N.; Ponomarenko, S. A.; Grigorian, S. In Situ Coupling Applied Voltage and Synchrotron Radiation: Operando Characterization of Transistors. *Nanoscale Res. Lett.* **2022**, *17*, 22.
(52) Agina, E. V.; Sizov, A. S.; Anisimov, D. S.; Trul, A. A.; Borshchev, O. V.; Paraschuk, D. Y.; Shcherbina, M. A.; Chvalun, S. N.; Ponomarenko, S. A. Thiophene-Based Monolayer OFETs Prepared by Langmuir Techniques. *Org. Field-Effect Transistors XIV; Org. Sensors Bioelectron. VIII* **2015**, *9568*, 95680Z.
(53) Zhavnerko, G.; Marletta, G. Developing Langmuir-Blodgett Strategies towards Practical Devices. *Mater. Sci. Eng., B* **2010**, *169*, 43−48.
(54) Sperling, R. A.; Parak, W. J. Surface Modification, Functionalization and Bioconjugation of Colloidal Inorganic Nanoparticles. *Philos. Trans. R. Soc., A* **2010**, *368*, 1333−1383.
(55) Magliulo, M.; Pistillo, B. R.; Mulla, M. Y.; Cotrone, S.; Ditaranto, N.; Cioffi, N.; Favia, P.; Torsi, L. PE-CVD of Hydrophilic-COOH Functionalized Coatings on Electrolyte Gated Field-Effect Transistor Electronic Layers. *Plasma Processes Polym.* **2013**, *10*, 102−109.
(56) Novoseltseva, A. A.; Ivanov, N. M.; Novikov, R. A.; Tkachev, Y. V.; Bunin, D. A.; Gambaryan, A. S.; Tashlitsky, V. N.; Arutyunyan, A. M.; Kopylov, A. M.; Zavyalova, E. G. Structural and Functional Aspects of G-Quadruplex Aptamers Which Bind a Broad Range of Influenza a Viruses. *Biomolecules* **2020**, *10*, 119.
(57) Gribanyov, D.; Zhdanov, G.; Olenin, A.; Lisichkin, G.; Gambaryan, A.; Kukushkin, V.; Zavyalova, E. SERS-Based Colloidal Aptasensors for Quantitative Determination of Influenza Virus. *Int. J. Mol. Sci.* **2021**, *22*, 1842.

https://doi.org/10.1021/acsami.1c24109
ACS Appl. Mater. Interfaces XXXX, XXX, XXX−XXX

(58) Kukushkin, V. I.; Ivanov, N. M.; Novoseltseva, A. A.; Gambaryan, A. S.; Yaminsky, I. V.; Kopylov, A. M.; Zavyalova, E. G. Highly Sensitive Detection of Influenza Virus with SERS Aptasensor. *PLoS One* **2019**, *14*, No. e0216247.
(59) Decuypere, E.; Bernard, S.; Feng, M.; Porte, K.; Riomet, M.; Thuéry, P.; Audisio, D.; Taran, F. Copper-Catalyzed Aza-Iminosydnone-Alkyne Cycloaddition Reaction Discovered by Screening. *ACS Catal.* **2018**, *8*, 11882−11888.
(60) Caldas, L. A.; Carneiro, F. A.; Higa, L. M.; Monteiro, F. L.; da Silva, G. P.; da Costa, L. J.; Durigon, E. L.; Tanuri, A.; de Souza, W. Ultrastructural Analysis of SARS-CoV-2 Interactions with the Host Cell via High Resolution Scanning Electron Microscopy. *Sci. Rep.* **2020**, *10*, 16099.
(61) Sun, H.; Zu, Y. Aptamers and Their Applications in Nanomedicine. *Small* **2015**, *11*, 2352−2364.
(62) Kubo, I.; Eguchi, T. Study on Electrochemical Insulin Sensing Utilizing a DNA Aptamer-Immobilized Gold Electrode. *Materials* **2015**, *8*, 4710−4719.
(63) Saraf, N.; Woods, E. R.; Peppler, M.; Seal, S. Highly Selective Aptamer Based Organic Electrochemical Biosensor with Pico-Level Detection. *Biosens. Bioelectron.* **2018**, *117*, 40−46.
(64) Ebata, H.; Izawa, T.; Miyazaki, E.; Takimiya, K.; Ikeda, M.; Kuwabara, H.; Yui, T. Highly Soluble [1] Benzothieno [3 , 2-b] Benzothiophene (BTBT) Derivatives For. *J. Am. Chem. Soc.* **2007**, *129*, 15732−15733.
(65) Agina, E. V.; Polinskaya, M. S.; Trul, A. A.; Chekusova, V. P.; Sizov, A. S.; Borshchev, O. V.; Ponomarenko, S. A. Organosilicon Derivatives of BTBT for Monolayer Organic Field Effect Transistors. *Organic Field-Effect Transistors XVI*. Jurchescu, O. D., Ed.; SPIE, 2017; Vol *10365*, pp 33−42.
(66) Treshchalina, A.; Postnikova, Y.; Boravleva, E.; Gambaryan, A.; Belyakova, A.; Ishmukhametov, A.; Sadykova, G.; Prilipov, A.; Lomakina, N. Substitution Arg140Gly in Hemagglutinin Reduced the Virulence of Highly Pathogenic Avian Influenza Virus H7N1. *Viruses* **2021**, *13*, 1584.
(67) Zhang, Q.; Leonardi, F.; Casalini, S.; Temiño, I.; Mas-Torrent, M. High Performing Solution-Coated Electrolyte-Gated Organic Field-Effect Transistors for Aqueous Media Operation. *Sci. Rep.* **2016**, *6*, 39623.

https://doi.org/10.1021/acsami.1c24109
ACS Appl. Mater. Interfaces XXXX, XXX, XXX−XXX